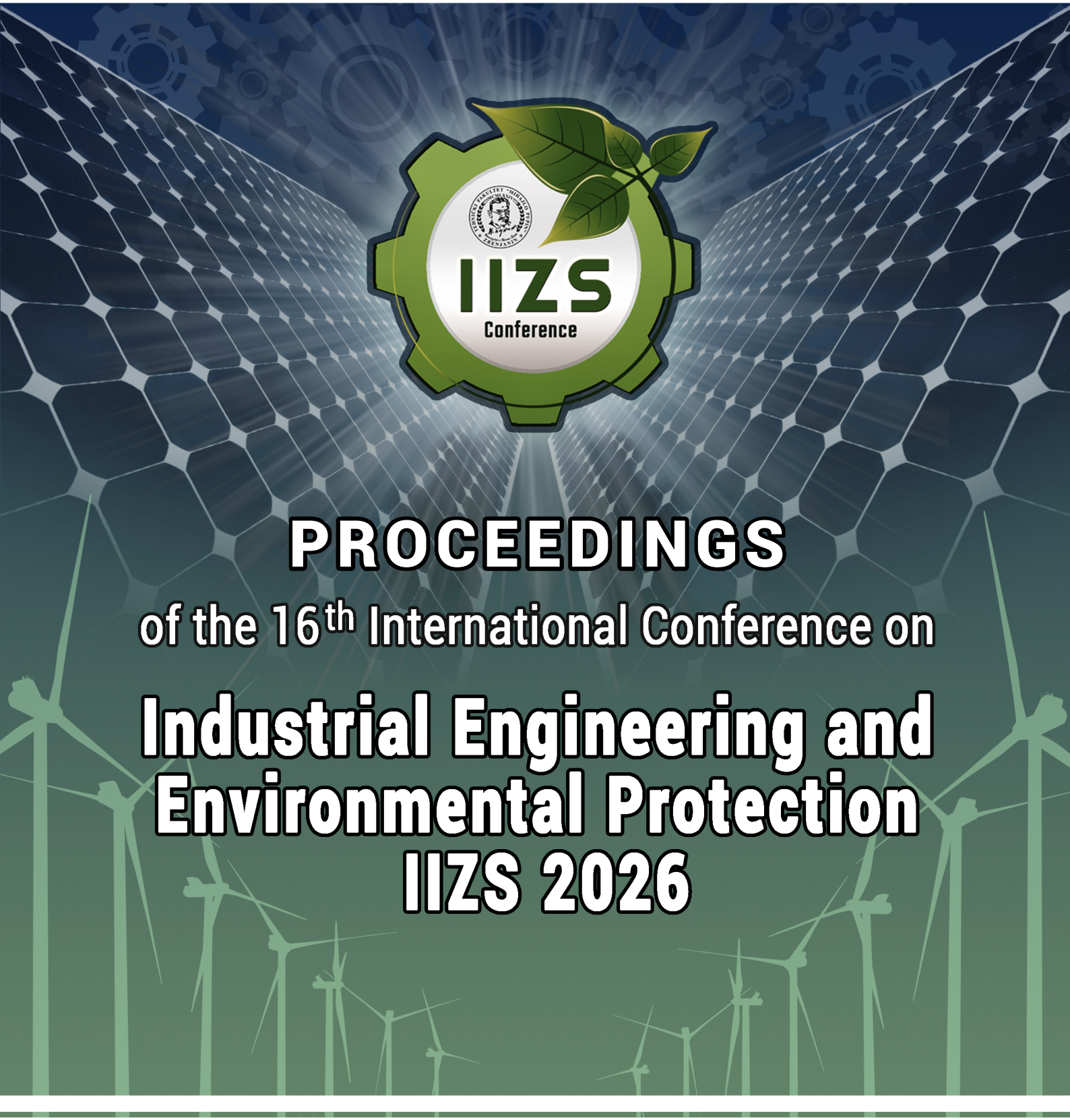
UNIVERSITY OF NOVI SAD
Technical Faculty "Mihajlo Pupin"
Zrenjanin, Republic of Serbia



PROCEEDINGS

of the 16th International Conference on

Industrial Engineering and Environmental Protection IIZS 2026

Zrenjanin, Serbia, October 1-2, 2026.

University of Novi Sad
Technical Faculty “Mihajlo Pupin”
Zrenjanin, Republic of Serbia

PROCEEDINGS

of the XVI International Conference on

Industrial Engineering and Environmental Protection IIZS 2026

Zrenjanin, October 1-2, 2026.

IN COOPERATION WITH PARTNERS:

	UNIVERSITY POLITEHNICA TIMISOARA, FACULTY OF ENGINEERING, HUNEDOARA, ROMANIA	
	UNIVERSITY «St. KLIMENT OHRIDSKI«, TECHNICAL FACULTY, BITOLA, MACEDONIA	
	„AUREL VLAICU" UNIVERSITY OF ARAD, FACULTY OF ENGINEERING, ARAD, ROMANIA	
	UNIVERSITY OF EAST SARAJEVO, FACULTY OF MECHANICAL ENGINEERING EAST SARAJEVO, REPUBLIC OF SRPSKA, B&H	
	UNIVERSITY OF GIRESUN, FACULTY OF ENGINEERING, GIRESUN, TURKEY	

Proceedings of the XVI International Conference - Industrial Engineering and Environmental Protection (IIZS 2026)

Conference organizer:

Technical Faculty “Mihajlo Pupin”, Zrenjanin, University of Novi Sad, Republic of Serbia

Reviewers:

PhD Eleonora Desnica, Technical Faculty "Mihajlo Pupin", Zrenjanin, Republic of Serbia
PhD Bogdana Vujić, Technical Faculty "Mihajlo Pupin", Zrenjanin, Republic of Serbia
PhD Slavica Prvulović, Technical Faculty "Mihajlo Pupin", Zrenjanin, Republic of Serbia
PhD Ljiljana Radovanović, Technical Faculty "Mihajlo Pupin", Zrenjanin, Republic of Serbia
PhD Jasmina Pekez, Technical Faculty "Mihajlo Pupin", Zrenjanin, Republic of Serbia
PhD Višnja Mihajlović, Technical Faculty "Mihajlo Pupin", Zrenjanin, Republic of Serbia
PhD Snežana Filip, Technical Faculty "Mihajlo Pupin", Zrenjanin, Republic of Serbia
PhD Mića Đurđev, Technical Faculty "Mihajlo Pupin", Zrenjanin, Republic of Serbia
PhD Jasna Tolmač, Technical Faculty "Mihajlo Pupin", Zrenjanin, Republic of Serbia
PhD Mihalj Bakator, Technical Faculty "Mihajlo Pupin", Zrenjanin, Republic of Serbia
PhD Ivan Palinkaš, Technical Faculty "Mihajlo Pupin", Zrenjanin, Republic of Serbia
PhD Borivoj Novaković, Technical Faculty "Mihajlo Pupin", Zrenjanin, Republic of Serbia
PhD Una Marčeta, Technical Faculty "Mihajlo Pupin", Zrenjanin, Republic of Serbia
PhD Sanja Stanisavljev, Technical Faculty "Mihajlo Pupin", Zrenjanin, Republic of Serbia
PhD Edit Terek Stojanović, Technical Faculty "Mihajlo Pupin", Zrenjanin, Republic of Serbia

Publisher:

Technical Faculty “Mihajlo Pupin”, Zrenjanin, University of Novi Sad, Đure Đakovića 1A, 23101 Zrenjanin, Republic of Serbia

For publisher:

PhD Milan Nikolić, Dean of Technical Faculty “Mihajlo Pupin”, Zrenjanin, Republic of Serbia

Technical preparation:

MSc Dejan Bajić, Technical Faculty “Mihajlo Pupin”, Zrenjanin, Republic of Serbia
MSc Jovana Čugalj, Technical Faculty “Mihajlo Pupin”, Zrenjanin, Republic of Serbia
MSc Uroš Šarenac, Technical Faculty “Mihajlo Pupin”, Zrenjanin, Republic of Serbia
MSc Branislava Radišić, Technical Faculty “Mihajlo Pupin”, Zrenjanin, Republic of Serbia
MSc Milan Marković, Technical Faculty “Mihajlo Pupin”, Zrenjanin, Republic of Serbia
BSc Dejan Landup, Technical Faculty “Mihajlo Pupin”, Zrenjanin, Republic of Serbia

ISBN 978-86-7672-401-7

CIP Classification:

CIP - Каталогизација у публикацији
Библиотека Матице српске, Нови Сад

62:005.3(082)
502/504(082)

INTERNATIONAL Conference Industrial Engineering and Environmental Protection (16 ; 2026 ; Zrenjanin)
Proceedings of the XVI International Conference on Industrial Engineering and Environmental Protection (IIZS 2026), Zrenjanin, 1-2 October 2026 [Elektronski izvor]. - Zrenjanin : Technical Faculty "Mihajlo Pupin", 2026. - 1 elektronski optički disk (CD-ROM) ; 12 cm

Nasl. sa naslovnog ekrana. - Str. [7]: Introduction / Una Marčeta. - Bibliografija uz svaki rad.

ISBN 978-86-7672-401-7

a) Индустријско инжењерство - Зборници b) Заштита животне средине - Зборници

COBISS.SR-ID 204432393

SCIENTIFIC COMMITTEE - TECHNICAL FACULTY „MIHAJLO PUPIN“

PhD Slavica Prvulović, Technical Faculty “Mihajlo Pupin”, Zrenjanin, Republic of Serbia
PhD Ljiljana Radovanović, Technical Faculty “Mihajlo Pupin”, Zrenjanin, Republic of Serbia
PhD Bogdana Vujić, Technical Faculty “Mihajlo Pupin”, Zrenjanin, Republic of Serbia
PhD Eleonora Desnica, Technical Faculty “Mihajlo Pupin”, Zrenjanin, Republic of Serbia
PhD Jasmina Pekez, Technical Faculty “Mihajlo Pupin”, Zrenjanin, Republic of Serbia
PhD Snežana Filip, Technical Faculty “Mihajlo Pupin”, Zrenjanin, Republic of Serbia
PhD Višnja Mihajlović, Technical Faculty “Mihajlo Pupin”, Zrenjanin, Republic of Serbia
PhD Jelena Stojanov, Technical Faculty “Mihajlo Pupin”, Zrenjanin, Republic of Serbia
PhD Jasna Tolmač, Technical Faculty “Mihajlo Pupin”, Zrenjanin, Republic of Serbia
PhD Mića Đurđev, Technical Faculty “Mihajlo Pupin”, Zrenjanin, Republic of Serbia
PhD Una Marčeta, Technical Faculty “Mihajlo Pupin”, Zrenjanin, Republic of Serbia
PhD Ivan Palinkaš, Technical Faculty “Mihajlo Pupin”, Zrenjanin, Republic of Serbia
PhD Borivoj Novaković, Technical Faculty “Mihajlo Pupin”, Zrenjanin, Republic of Serbia

INTERNATIONAL SCIENTIFIC COMMITTEE

PhD James G. Speight, CD&W Inc., Laramie,Wyoming, USA
PhD. dr Hosam E.A.F. Bayoumi Hamuda, Obuda Univerzity, Budapest, Hungary
PhD Svetlana Lilkova, University of Architecture, Civil Engineering and Geodesy (UACEG), Faculty of Hydraulic Engineering, Sofia, Bulgaria
PhD Dimitar G. Petrov, , Technical University Sofia, branch Plovdiv, Bulgaria
PhD Valentina Emilia Balas, „Aurel Vlaicu” University of Arad, Faculty of Engineering, Arad, Romania
PhD Imre Kiss, University Politehnica Timisoara, Faculty of engineering, Hunedoara, Romania
PhD Simona Dzitac, University of Oradea, Energy Engineering and Industrial Management Faculty, Oradea, Romania
PhD Francisc Popesku, University Politehnica Timisoara, Timisoara, Romania
PhD Mukrimin Şevket Guney, University of Giresun, Faculty of Engineering, Giresun, Turkey
PhD Muharrem Hilmi Aksoy, Selcuk University, Engineering Faculty, Konya, Turkey
PhD Alexander Salnikov, Ukhta State Technical University (USTU), Ukhta, Republic of Komi, Russia
PhD Hrvoje Glavaš, Josip Juraj Strossmayer University of Osijek, Faculty of Electrical Engineering, Computer Science and Information Technology, Osijek, Croatia
PhD Tomislav Barić, Josip Juraj Strossmayer University of Osijek, Faculty of Electrical Engineering, Computer Science and Information Technology, Osijek, Croatia
PhD Marijana Hadzima-Nyarko, Josip Juraj Strossmayer University of Osijek, Faculty of Civil Engineering,Osijek,Croatia
PhD Silva Lozančić, Josip Juraj Strossmayer University of Osijek, Faculty of Civil Engineering, Osijek, Croatia
PhD Mirko Karakašić, University of Slavonski Brod, Faculty of Mechanical Engineering Slavonski Brod, Slavonski Brod, Croatia
PhD Vangelce Mitrevski, University «sv. Kliment Ohridski«, Technical Faculty, Bitola, Macedonia
PhD Milija Kraišnik, University of East Sarajevo, Faculty of Mechanical Engineering, Republic of Srpska, Bosnia and Herzegovina
PhD Bratislav Blagojević, University of Niš, Faculty of Mechanical Engineering, Niš, Serbia
PhD Blaža Stojanović, University of Kragujevac, Faculty of Engineering, Kragujevac, Serbia
PhD Dragan D. Milanović, University of Belgrade, Faculty of Mechanical Engineering, Belgrade, Serbia
PhD Mijodrag Milošević, University of Novi Sad, Faculty of Technical Sciences, Novi Sad, Serbia

PhD Dejan Lukić, University of Novi Sad, Faculty of Technical Sciences, Novi Sad, Serbia
PhD Milan Rackov, University of Novi Sad, Faculty of Technical Sciences, Novi Sad, Serbia
PhD Jasmina Radosavljević, University of Niš, Faculty of Occupational Safety, Niš, Serbia
PhD Amelija Đorđević, University of Niš, Faculty of Occupational Safety, Niš, Serbia
PhD Snežana Dragićević, University of Kragujevac, Faculty of Technical Sciences, Čačak, Serbia
PhD Ivona Radović, University of Belgrade, Faculty of Technology and Metallurgy, Belgrade, Serbia
PhD Mirjana Kijevčanin, University of Belgrade, Faculty of Technology and Metallurgy, Belgrade, Serbia
PhD Aleksandra Sretenović, University of Belgrade, Faculty of Mechanical Engineering, Belgrade, Serbia
PhD Aleksandra Mihailović, University of Novi Sad, Faculty of Technical Sciences, Novi Sad, Serbia
PhD Nebojša Ralević, University of Novi Sad, Faculty of Technical Sciences, Novi Sad, Serbia
PhD Maja Petrović, University of Novi Sad, Faculty of Technical Sciences, Novi Sad, Serbia
PhD Zoran Čepić, University of Novi Sad, Faculty of Technical Sciences, Novi Sad, Serbia
PhD Aleksandar Ašonja, University Business Academy in Novi Sad, Faculty of Economics and Engineering Management in Novi Sad, Serbia
PhD Marina Milovanović, University “Union – Nikola Tesla“, Faculty for entrepreneurial business and real estate management, Belgrade, Serbia
PhD Jasmina Perišić, University “Union – Nikola Tesla“, Faculty for entrepreneurial business and real estate management, Belgrade, Serbia
PhD Jordana Ninkov, Senior Research Associate, Institute of Field and Vegetable Crops, Novi Sad, Serbia
PhD Marko Ristić, Research Associate, Institute Mihajlo Pupin, Belgrade, Serbia

ORGANIZING COMMITTEE

PhD Una Marčeta, Technical Faculty “Mihajlo Pupin”, Zrenjanin, Republic of Serbia, chairman
PhD Višnja Mihajlović, Technical Faculty “Mihajlo Pupin”, Zrenjanin, Republic of Serbia
PhD Ljiljana Radovanović, Technical Faculty “Mihajlo Pupin”, Zrenjanin, Republic of Serbia
PhD Slavica Prvulović, Technical Faculty “Mihajlo Pupin”, Zrenjanin, Republic of Serbia
PhD Eleonora Desnica, Technical Faculty “Mihajlo Pupin”, Zrenjanin, Republic of Serbia
PhD Bogdana Vujić, Technical Faculty “Mihajlo Pupin”, Zrenjanin, Republic of Serbia
PhD Jasmina Pekez, Technical Faculty “Mihajlo Pupin”, Zrenjanin, Republic of Serbia
PhD Snežana Filip, Technical Faculty “Mihajlo Pupin”, Zrenjanin, Republic of Serbia
PhD Zoran Čepić, Faculty of Technical Sciences, Novi Sad, Republic of Serbia
PhD Ivan Palinkaš, Technical Faculty “Mihajlo Pupin”, Zrenjanin, Republic of Serbia
PhD Mića Đurđev, Technical Faculty “Mihajlo Pupin”, Zrenjanin, Republic of Serbia
PhD Jasna Tolmač, Technical Faculty “Mihajlo Pupin”, Zrenjanin, Republic of Serbia
PhD Borivoj Novaković, Technical Faculty “Mihajlo Pupin”, Zrenjanin, Republic of Serbia
MSc Luka Đorđević, Technical Faculty “Mihajlo Pupin”, Zrenjanin, Republic of Serbia
MSc Dejan Bajić, Technical Faculty “Mihajlo Pupin”, Zrenjanin, Republic of Serbia
MSc Jovana Čugalj, Technical Faculty “Mihajlo Pupin”, Zrenjanin, Republic of Serbia
MSc Uroš Šarenac, Technical Faculty “Mihajlo Pupin”, Zrenjanin, Republic of Serbia
MSc Branislava Radišić, Technical Faculty “Mihajlo Pupin”, Zrenjanin, Republic of Serbia
MSc Milan Marković, Technical Faculty “Mihajlo Pupin”, Zrenjanin, Republic of Serbia
BSc Dejan Landup, Technical Faculty “Mihajlo Pupin”, Zrenjanin, Republic of Serbia

INTRODUCTION

The Department of Mechanical Engineering and the Department of Environmental Protection of the Technical Faculty “Mihajlo Pupin” in Zrenjanin organized the XVI International Conference on Industrial Engineering and Environmental Protection – IIZS 2026.

For sixteen years, this Conference has brought together researchers, university professors, engineers, professionals and representatives of institutions and industry. During that time, it has developed into a traditional annual gathering dedicated to the exchange of scientific knowledge, professional experience and practical solutions in the fields of industrial engineering and environmental protection.

The topics of this scientific conference cover the fields of Industrial Engineering and Environmental Protection, including: Mechanical Engineering, Energetics and Process Technique, Design and Maintenance, Oil and Gas Engineering, Health and Environmental Protection, Environmental Management, and Occupational Safety.

This year’s Conference includes 76 papers by authors from 18 countries, confirming its international character and its importance as a platform for knowledge exchange and professional cooperation. The Conference covers a wide range of topics and connects scientific research with practical work.

We would like to express our sincere gratitude to the partners of the XVI International Conference “IIZS 2026” – Aurel Vlaicu University of Arad, Faculty of Engineering, Arad, Romania; University St. Kliment Ohridski, Technical Faculty, Bitola, North Macedonia; University Politehnica Timisoara, Faculty of Engineering, Hunedoara, Romania; University of East Sarajevo, Faculty of Mechanical Engineering, East Sarajevo, Bosnia and Herzegovina, Republic of Srpska; and University of Giresun, Faculty of Engineering, Giresun, Turkey – for their support in organizing this event. We are also grateful to all authors who contributed their papers. We would also like to thank all authors who contributed their papers, the reviewers for their time and professional input, the members of the Scientific and Organizing Committees, and everyone who participated in preparing this year’s Conference. We extend our special thanks to the Ministry of Science, Technological Development and Innovation for its financial support.

The IIZS Conference has established itself as an annual meeting place for researchers from across the globe. We welcome and appreciate constructive feedback and ideas that can contribute to improving the organization and scientific program of the forthcoming XVII International Conference on Industrial Engineering and Environmental Protection.

Chairman of the Organizing Committee
Asst. Prof. Una Marčeta PhD

Zrenjanin, October 1-2, 2026.

Conference participants are from the following countries:



Serbia



Bulgaria



Bosnia and Herzegovina



Romania



Brazil



Mexico



Montenegro



North Macedonia



Portugal



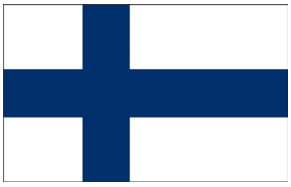
Croatia



Saudi Arabia



United Kingdom



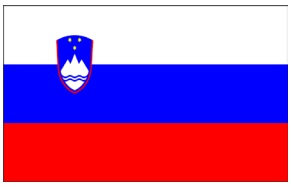
Finland



China



Russia



Slovenia



Turkey



Austria



Република Србија

Министарство просвете,
науке и технолошког развоја

XVI International Conference - Industrial Engineering and Environmental Protection (IIZS 2026) is financially supported by Ministry of Education, Science and Technological Development, Republic of Serbia

CONTENTS

PLENARY SESSION

Srđan Kovačević, Nemanja Stanisavljević, Xiaoming Wang, Galina Ilinykin:
POTENTIAL OF WASTEWATER TREATMENT SLUDGE FOR BIOGAS PRODUCTION IN THE REPUBLIC OF SERBIA 2

Dejan Bogdanović:
MULTICRITERIA ANALYSIS OF OCCUPATIONAL SAFETY MEASURES IN UNDERGROUND COAL MINES WITH METHANE 10

Session 1: Mechanical Engineering

Svetlana Lilkova-Markova, Dimitar Lolov:
DYNAMIC STABILITY OF A CONICAL PIPE RESTING ON A PASTERNAK ELASTIC FOUNDATION 17

Neagoe Andrei-Rareș, Adrian-Eugen Cioablă:
STUDIES ON THE THERMAL AND MECHANICAL BEHAVIOR OF COMPOSITE MATERIALS IN AUTOMOTIVE ELECTRONIC DEVICES 25

Sanja Simić, Mijodrag Milošević, Borislav Savković, Branko Štrbac, Dejan Božić, Dejan Lukić:
COMPARATIVE STATISTICAL ANALYSIS OF MEASUREMENT RESULTS FOR CYLINDRICAL PART CHARACTERISTICS 30

Miroslav Radomirović, Tatijana Vasiljević, Predrag Petronijević:
EVALUATING PARAMETRIC LINEAR AND INTERACTION MODELS FOR COMPRESSIVE STRENGTH ESTIMATION OF HIGH-PERFORMANCE CONCRETE 42

Vangelce Mitrevski, Cvetanka Mitrevska:
COMPARISON BETWEEN ONE AND TWO PARAMETER SORPTION ISOTHERM MODELS 50

Dragana Rodić, Dušan I. Ilić, Stevo K. Jaćimovski, Jovan P. Šetrajčić:
THE PHENOMENON OF RESONANT ABSORPTION IN MOLECULAR NANOSCOPIC FILM STRUCTURES 58

Dušan Jovanić, Aleksandar Rajić, Miodrag Kovačević, Ljubica Lazić Vulićević:
OPTIMIZATION OF PLA 3D PRINTING PARAMETERS CONSIDERING COOLING RATE AND HARDNESS 64

Haşmet Çağrı Sezgen, Abdullah Çakan:
ARTIFICIAL NEURAL NETWORK-BASED INVERSE KINEMATICS MODELING OF A 3-DOF PLANAR ROBOTIC MANIPULATOR 72

Dušan Jovanić, Spasoje Erić, Miodrag Kovačević:
TAGUCHI BASED OPTIMIZATION OF POLYETHILENE MILLING PARAMETERS BASED ON CUTTING TEMPERATURE AND SURFACE ROUGHNESS CRITERIA 82

Ivan Matin, Branko Štrbac, Miloš Ranisavljev, Đorđe Vukelić, Miodrag Hadžistević:
APPLICATION OF ADVANCED MEASUREMENT TECHNIQUES FOR DETERMINATION OF INJECTION MOLDING SHRINKAGE 90

Borivoj Novaković, Bojan Vukobrat, Luka Đorđević, Uroš Šarenac, Dejan Landup:
THE IMPACT OF LOAD-SENSING REGULATION ON THE ENERGY, ECONOMIC AND ENVIRONMENTAL EFFICIENCY OF AXIAL-PISTON PUMPS 96

Zoran Karastojković, Jasmina Pekez, Zoran Milić, Milija Kraišnik:
ADVANTAGES OF USING SOME RARE-EARTH ELEMENTS IN COPPER POWER CABLES 106

Dejan Landup, Dejan Bajić, Eleonora Desnica, Ivan Palinkaš:
INFLUENCE OF LONGITUDINAL STIFFENING RIB HEIGHT ON THE STRESS-DISPLACEMENT BEHAVIOUR OF A THIN-WALLED CONSTRUCTION OF HOUSING 113

Adam Rac, Žolt Konja, Vesna Konja, Ljiljana Radovanović:
DIGITAL TWIN-BASED TECHNICAL DIAGNOSTICS OF ROTATING MACHINERY 120

Sergiu Popa, Flavius-Maxim Petcuț, Anca-Adriana Petcuț-Lasc, Valentina-Emilia Balaș:
EVENT-TRIGGERED ADAPTIVE CONTROL AND ENERGY-EFFICIENT TRAJECTORY PLANNING FOR CARGO DRONES USING GIS AND SPIKING NEURAL NETWORKS 127

Session 2: Energetics and Process Technique

Miloš Milovančević, Ivan Kostić, Nataša Sokolov Milovančević, Vanja Stojković:
TRUE DECARBONIZATION OR CONTRACTION EFFECT? DECOMPOSING MANUFACTURING CO2 REDUCTIONS INTO ENERGY-ACTIVITY AND CARBON-FACTOR COMPONENTS ACROSS THE EUROPEAN UNION 135

Aleksandar Reljić, Saša Prodanović:
DEVELOPMENT OF DIDACTIC PLC SIMULATOR AND ITS INTEGRATION WITH A VIRTUAL 3D ENVIRONMENT 154

Snežana Dragićević, Srba Stevanović, Brankica Šutić:
POTENTIAL OF HEMP-BASED MATERIALS FOR IMPROVING THE ENERGY EFFICIENCY OF BUILDINGS 162

Marinko Barukčić, Boris Fažo, Goran Kurtović, Hrvoje Glavaš:
IMPACT OF THERMAL DYNAMICS, SOILING, AND DEGRADATION IN PHOTOVOLTAIC ENERGY YIELD ESTIMATION: A COMPARATIVE MODELING STUDY 169

Patrik Lučinger, Predrag Marić, Ružica Kljajić:
IMPACT OF PHOTOVOLTAIC GENERATION SUBSTITUTION OF CONVENTIONAL GENERATION ON ROTOR ANGLE STABILITY OF BULK POWER SYSTEM 177

Stanko P. Stankov:
CONTROL OF WASTEWATER TREATMENT AND NEUTRALIZATION IN A MINERAL WOOL PRODUCTION PLANT 186

Matthias Hauer, Ashish Srivastava, Momir Tabaković:
ROUND-TRIP EFFICIENCY (RTE) OF HOME BATTERY STORAGE SYSTEMS UNDER TROPICAL CLIMATIC CONDITIONS - A CASE STUDY OF THAILAND 194

Zorica Stojadinović, Dragana Novaković:
IMPACT OF AGRICULTURAL BIOMASS PROPERTIES ON THE ENERGY VALUE OF PELLETS: EXPERIMENTAL AND STATISTICAL ANALYSIS 201

Hristina Delibašić-Marković, Violeta Petrović, Ivan Petrović:
MONTE CARLO ANALYSIS OF RESISTOR MISMATCH IN THREE-OP-AMP INSTRUMENTATION AMPLIFIERS 209

Ionuț-Vasile Nicoraș, Flavius-Maxim Petcuț, Anca-Adriana Petcuț-Lasc, Valentina Emilia Balas:
AN INTEGRATED ENERGY AND BIOCLIMATIC SYSTEM FOR POSITIVE-ENERGY BUILDINGS: BIPV, ELECTRICAL STORAGE AND A ROOFTOP GREENHOUSE 216

Session 3: Designing and Maintenance

Peko Lakatuš, Mihalj Bakator:
STRATEGIC PROJECT MANAGEMENT IN THE ORGANIZATION OF INDUSTRIAL MAINTENANCE SYSTEMS 224

Miloš Milovančević, Ivan Kostić, Nataša Sokolov Milovančević, Vanja Stojković:
CONDITION MONITORING OF EUROPEAN INDUSTRIAL RESILIENCE: SHOCK ABSORPTION, RECOVERY TIME, AND HYSTERESIS IN EUROSTAT SHORT-TERM BUSINESS STATISTICS 235

Anita Sabo, Tibor Szakáll, Bojan Kuljić:
PROJECT MANAGEMENT APPROACH TO DRONE TECHNOLOGY IMPLEMENTATION IN CIVIL ENGINEERING 244

Anita Sabo, Bojan Kuljić, Tibor Szakáll:
QUALITY MANAGEMENT APPROACH TO INDUSTRY–EDUCATION COLLABORATION IN ENGINEERING EDUCATION 251

Marija D. Milanovic:
DEFINING A METHODOLOGY FOR IMPROVING THE PRODUCTION RESOURCE PLANNING PROCESS IN CONDITIONS OF UNCERTAINTY 258

Branislava Radu, Ljubica Kazi, Ivana Berković, Zeljko Stojanov:
APPLICATION OF LARGE LANGUAGE MODELS IN REQUIREMENTS ENGINEERING 263

Branislava Radu, Ljubica Kazi:
METRICS FOR EVALUATING SOFTWARE TESTING QUALITY 271

Dejan Igov, Duško Čučković, Verica Gluvakov, Ivana Denčić:
PROJECT PERFORMANCE MEASUREMENT: KEY PERFORMANCE INDICATORS (KPIS) AND SUCCESS METRICS FOR SUSTAINABLE INDUSTRIAL PROJECTS – A REVIEW AND CONCEPTUAL FRAMEWORK 279

Mića Đurđev, Stefan Ugrinov, Luka Đorđević, Borivoj Novaković, Dejan Bajić:
OPTIMIZATION OF VEHICLE ROUTING PROBLEM IN LOGISTICS USING GENETIC ALGORITHM 288

Milan Marković, Jasna Tolmač, Isidora Crvenkov:
FROM ENERGY MONITORING TO MAINTENANCE DECISIONS: A CONCEPTUAL FRAMEWORK FOR HYDRAULIC BLOWOUT PREVENTER CONTROL UNITS 295

Vesna Konja, Žolt Konja, Ljiljana Radovanović:
ANALYSIS OF PREVENTIVE AND CORRECTIVE MAINTENANCE PRACTICES AND MAINTENANCE DATA LIMITATIONS: A CASE STUDY 302

Session 4: Oil and gas engineering

Nikola Vojvodić, Slavica Prvulović, Jasna Tolmač, Branislava Radišić:
THE IMPACT OF POLISKREP TECHNOLOGY ON THE OPERATIONAL STABILITY OF PRODUCTION EQUIPMENT AND SAND PRODUCTION CONTROL IN OIL WELLS 311

Maja Brborić, Branka Nakomčić Smaragdakis, Sonja Dmitrašinović, Miljan Šunjević, Manu Seth:
BRIDGING MEASUREMENT AND MODELLING: HYBRID PATHWAYS FOR ACCURATE RESERVOIR GHG QUANTIFICATION 319

Branislava Radišić, Slavica Prvulović, Snežana Filip, Borivoj Novaković, Milan Marković:
FAULT TREE ANALYSIS OF A CO_2-EOR INJECTION SYSTEM 326

Session 5: Environmental management

Mirjana Dunić:
INDUSTRY 5.0 AS A DRIVER OF SUSTAINABLE INDUSTRIAL DEVELOPMENT 334

Mirjana Dunić:
ARTIFICIAL INTELLIGENCE AS AN ENABLER OF ENVIRONMENTAL SUSTAINABILITY AND THE SUSTAINABLE DEVELOPMENT GOALS 344

Alexis Toribio Dantas, Dejan Mihailović:
IS SUSTAINABILITY POSSIBLE? 353

Ankica Borota-Tišma, Draga Tišma:
FROM THE GREEN RETAIL AGENDA TO STORE-LEVEL EFFICIENCY: A DIGITAL PROGRAM FOR ENVIRONMENTAL PROTECTION IN SUSTAINABLE RETAIL 357

Jovana Čugalj, Bogdana Vujić, Dejan Ubavin, Goran Vujić:
MAPPING TEXTILE WASTE FLOWS IN SERBIA BASED ON OFFICIAL REGISTRY DATA 365

Nikola Karanović, Višnja Mihajlović:
CIRCULAR MATERIAL USE RATE INDICATOR: WHERE SERBIA AND THE EU STAND? .. 372

Ineta Nemeša, Marija Pešić, Danka Đurđić, Valentina Bozoki:
ULTRASONIC WELDING AS SUSTAINABLE TEXTILE JOINING METHOD 378

Session 6: Health and Environmental Protection

Marija Perović, Tanja Nenin, Tatjana Mitrović:
SPATIAL AND SEASONAL DISTRIBUTION OF POLYCYCLIC AROMATIC HYDROCARBONS AND TOTAL PETROLEUM HYDROCARBONS IN DANUBE RIVER SEDIMENTS (SERBIA) 386

Marija Perović, Tanja Nenin, Tatjana Mitrović:
SOURCE APPORTIONMENT AND ECOLOGICAL RISK OF PAHS IN DANUBE RIVER SEDIMENTS (SERBIA) 394

Madalina Ileana Zot, Una Marceta, Luisa Izabel Dungan, Francisc Popescu:
GREENHOUSE GAS (GHG) EMISSION TRENDS. REVIEW OF THE WORLD AND BALKAN REGION 401

Sanja Grbić, Tijana Marjanović Srebro, Maja Vujić, Jasmina Agbaba, Radivoj Tomić, Marija Maletin, Aleksandra Tubić:
REMOVAL OF MICROPLASTICS FROM NATURAL AND WASTEWATER MATRICES BY COAGULATION AND FLOCCULATON: EFFECT OF MICROSAND AND COAGULANT TYPE 407

Zoran Čepić, Julka Petrović, Višnja Mihajlović, Goran Bošković, Bogdana Vujić:
APPLICATION OF THE MONITORING, REPORTING AND VERIFICATION SYSTEM FOR GREENHOUSE GAS EMISSIONS IN THE REPUBLIC OF SERBIA: A CASE STUDY OF THE „ISTOK“ DISTRICT HEATING PLANT IN NOVI SAD 415

Jovana Čugalj, Marina Pešić, Jelena Vuković, Una Marčeta:
OVERVIEW OF ASBESTOS-CONTAINING WASTE GENERATION AND REPORTING IN THE REPUBLIC OF SERBIA 420

Stevo K. Jaćimovski, Dane Subošić, Dušan I. Ilić, Jovan P. Šetrajčić:
ANALYSIS OF AIR POLLUTION SPATIAL DISTRIBUTION: DISPERSION MODEL WITH MULTILAYER ATMOSPHERIC STRUCTURES (DMMAS) 425

Maja Brborić, Branka Nakomčić Smaragdakis, Sonja Dmitrašinović, Miljan Šunjević, Epari Ritesh Patro:
FINE-SCALE PM_1 POLLUTION DYNAMICS IN AN URBAN–SUBURBAN ENVIRONMENT ... 435

Edi Daruši:
CLIMATE CHANGE, CAPITALISM, AND THE PHILOSOPHY OF PSYCHOANALYSIS 441

Milana Drašković, Željko Eremić:
ASSESSMENT OF THE POSSIBILITIES OF ARTIFICIAL INTELLIGENCE FOR AGROCHEMICAL SOIL ANALYSIS WITH FERTILIZATION RECOMMENDATIONS 447

Nada Marković, Nebojša M. Ralević, Aleksandra Mihailović:
POTENTIALLY TOXIC ELEMENTS IN SOIL NEAR THE ALUMINUM PLANT IN PODGORICA, MONTENEGRO: A SURFACE–DEEP COMPARISON 455

Alexuță Daniel, Alexuță Ilie, Balaș M. Marius:
FUZZY SYSTEM FOR EVALUATING WATER QUALITY IN AN AQUAPONIC SYSTEM 459

Session 7: Occupational Safety

Vesna Spasojević Brkić, Mirjana Misita, Ivan Mihajlović, Martina Perišić, Iva Savić:
IN-CABIN GAS EXPOSURE IN SURFACE MINING: OCCUPATIONAL LIMITS VERSUS OPERATOR PERCEPTION 466

Aleksandra Mihailović, Robert Lakatoš, Selena Samardžić Cvijanović, Savka Adamović, Nada Marković, Ivana Lončarević:
LIGHTING CONDITIONS FOR PRACTICAL TEACHING IN A UNIVERSITY PRINTING LABORATORY 475

Cvetanka Mitrevska, Vangelce Mitrevski, Elena Milevska:
ACCIDENTS AT WORK IN THE TRANSPORT AND STORAGE SECTOR: A COMPARATIVE ANALYSIS OF THE EU-27 AND NORTH MACEDONIA 480

Goran Bošković, Marko Todorović, Nikola Karanović, Marina Bošković, Borivoj Stepanov:
FIRES IN HIGH-RISE BUILDINGS: ANALYSIS OF FIRE SAFETY AND ENGINEERING ASPECTS 489

Milana Ilić Mićunović, Borut Kosec, Zoran Čepić, Slađana Jovanović, Boris Agarski:
EDS-BASED CHARACTERIZATION OF INHALABLE METAL AEROSOLS IN OCCUPATIONAL ENVIRONMENTS 498

Leontina Pap:
SMART FACTORY, SILENT EMPLOYEES: THE HUMAN PARADOX OF DIGITAL SUSTAINABLE MANUFACTURING 504

Jelena Kiurski-Milošević, Gordana Ludajić, Iris Borjanović Trusina, Eleonora Dejanović, Miodrag Ludajić:
MODELLING OF ACCIDENTAL ETHANOL LEAKAGE FROM STORAGE TANKS 509

Ana Lončar, Mladenka Novaković Bežanović, Maja Petrović:
GENERATIVE ARTIFICIAL INTELLIGENCE AS A SUPPORT TOOL FOR HSE PROFESSIONALS IN THE ASSESSMENT OF SIMULATED INDUSTRIAL WORK SITUATIONS: A PILOT EXPLORATORY STUDY 514

Sondra Preascilla Ioana Nicorici, Mihaela Popa:
AUTOMATED IDENTIFICATION OF SAFETY-CRITICAL INCIDENTS IN AUTOMOTIVE DATABASES USING MACHINE LEARNING AND FUZZY CLUSTERING 520

Session 8: Special Session

Eleonora Desnica, Milan Nikolić:
HEISTORICAL PROJECT: FIRST STEPS TOWARDS DIGITAL MONITORING OF HISTORICAL BUILDINGS 527

Dalibor Dobrilović, Ivan Palinkaš:
LOW-COST IOT MONITORING OF HISTORICAL BUILDINGS: SENSOR SELECTION, PLACEMENT AND SYSTEM ARCHITECTURE 534

Dalibor Dobrilović, Ivan Palinkaš, Ljiljana Radovanović:
TRAINING AND FIELD DEPLOYMENT OF LOW-COST IOT SENSORS IN HISTORICAL BUILDINGS 542

Jasmina Pekez, Bogdana Vujić, Borko Bulajić:
INTEGRATING MODERN TECHNICAL STANDARDS INTO HISTORIC BUILDING EDUCATION: AN ANALYSIS OF COURSES AT SERBIAN UNIVERSITIES 549

Ștefania Ursache, Diana Nedelcu, Christiana Cazacu, Dorin Radu:
INTEGRATED SEISMIC AND ENERGY ASSESSMENT OF HISTORIC BUILDINGS IN TRANSYLVANIA REGION THROUGH NON-INVASIVE MONITORING 554

Ercan Işık, Fatih Avcil:
STRUCTURAL CHARACTERISTICS OF HISTORICAL MASONRY STRUCTURES IN BITLIS (TURKIYE) AND ITS VICINITY 562

Josip Radić, Antonija Ereš, Ivan Bandalo, Marijana Hadzima-Nyarko:
RELIABILITY OF FUNDAMENTAL PERIOD ESTIMATION FOR CONDITION ASSESSMENT AND SEISMIC EVALUATION OF RC STRUCTURES 568



XVI International Conference Industrial Engineering and Environmental Protection 2026 (IIZS 2026)
October 01-02, 2026, Zrenjanin, Serbia

Plenary Session

DOI:10.5937/IIZS26002K

POTENTIAL OF WASTEWATER TREATMENT SLUDGE FOR BIOGAS PRODUCTION IN THE REPUBLIC OF SERBIA

Keynote paper

Srđan Kovačević[1*], Nemanja Stanisavljević[2], Xiaoming Wang[3], Galina Ilinykin[4]
[1,2]University ofNoviSad,Faculty of Technical Sciences, Novi Sad, Serbia
[3]Chongqing University (CQU), Chongqing, China, Faculty of Environmental Protection and Ecology
[4]Perm National Research Polytechnic University, Environmental Protection Department, Perm, Russia

Abstract: The development of wastewater treatment infrastructure in Serbia will result in an increased amount of sewage sludge that can be used to produce energy through anaerobic digestion processes. The present work evaluates the biogas and energy-substitution potential of sludge from 11 wastewater treatment plants (WWTPs) which are planned to be upgraded in the frame of the national documents. The amount of sludge was estimated according to the design capacities of the WWTPs, while the amount of digester feed was calculated using a dry-solids mass balance, including the reduction of volatile-solids during digestion. The specific biogas yield was found to have the highest impact on the results, followed by the volatile-solids reduction. Anaerobic digestion and combined heat and power production can be considered as a viable option for sludge management in large-scale WWTPs in Serbia. The results presented in this work should be considered as the gross potential, which may not be achieved due to the specific characteristics of sludge, as well as the requirements for energy and heat in individual WWTPs.
Key words: sewage sludge; anaerobic digestion; biogas potential; lignite substitution.

INTRODUCTION

Wastewater treatment plays a crucial role in protecting the receiving surface waters and public health, yet it inevitably produces sewage sludge that requires further processing. Sewage sludge consists of organic matter, nutrients, microorganisms, and sometimes undesirable inorganic and organic constituents, which depend on the characteristics of wastewater. Anaerobic digestion is one of the most suitable routes for sludge stabilization and energy recovery at wastewater treatment plants (WWTPs). During the process, biodegradable organic matter is converted into methane-rich biogas, which can be used for combined heat and power generation. In parallel, anaerobic digestion reduces the volatile solids content and stabilizes the remaining digestate, thereby reducing the amount and environmental burden of sludge in need of subsequent treatment, transport or disposal(Appels, 2008; Cao, 2012).

The main difference between primary and waste activated sludge is that the former typically has a larger readily biodegradable fraction, while the latter is more resistant to hydrolysis due to the microbial-cell structure. As a result, methane production primarily depends on primary and waste activated sludge mass and their content of total solids (TS) and volatile solids (VS), biodegradability, retention time, temperature, organic loading rate, and the presence of inhibitory components(Carrère, 2010).

Recent studies therefore focus on improving the anaerobic digestion of sludge organic matter by means of thermal, mechanical, chemical, and biological pretreatments as well as co-digestion with complementary biodegradable feedstocks (Carrère, 2010). These approaches can enhance organic matter accessibility and thus methane yields, but their technical and economic viability needs to be evaluated in relation to the local sludge quantity, plant size and existing configuration, energy demand and logistics.

This study analyses the quantity of wastewater-treatment sludge generated at WWTPs with capacities exceeding 100,000 population equivalents, which represents the principal nationally identified feedstock for anaerobic digestion and biogas production in Serbia.

Accordingly, the present study aims to assess the potential of wastewater-treatment sludge for biogas production in the Republic of Serbia and to support the incorporation of sludge-to-

[1]Corresponding author, srdjankovacevic@uns.ac.rs, ORCID: 0000-0002-5440-8752
[2]nemanjastanisavljevic@uns.ac.rs, ORCID: 0000-0001-9484-1166
[3]wangxiaoming@cqu.edu.cn, ORCID: 0000-0002-9856-022X,
[4]galina.perm.59@yandex.ru, ORCID: 0000-0002-8829-3500

biogas systems in Serbia's future wastewater, energy and circular-economy planning.Specifically, the work is intended to: (i) compile and spatially analyze available national data on existent/expected sludge generation; (ii) identify those sludge streams and WWTP categories technically relevant for anaerobic digestion; (iii) estimate methane, biogas and energy potential under transparent scenario assumptions; and (iv) distinguish potential resources based on theoretical potential, while taking into account the impact of treatment technology, sludge characteristics and regional logistics. By this information base, the study is expected

PROJECTED SLUDGE QUANTITIES IN REPUBLIC OF SERBIA

In the Republic of Serbia, the higher wastewater-treatment levels are expected to turn sludge management into a more important environmental and resource-management issue. The national Sludge Management Programme for the Republic of Serbia for the period 2023–2032 explicitly addresses sludge as one of the by-products of municipal wastewater treatment and provides an overview of the development of treatment infrastructure and capacities for sludge management. The annual sludge generation from the existing WWTPs was estimated at approximately 11,000–15,000 t dry solids (DS). At the end of the projected infrastructure-development period, the total generation of stabilized municipal sludge is estimated at 115,390 t DS yr^{-1} under the 50th-percentile loading scenario and 135,190 t DS yr^{-1} under the 85th-percentile scenario. These values correspond to approximately 461,600–540,800 t yr^{-1} of digested and dewatered sludge at an average dry-solids content of 25%(Government of the Republic of Serbia, 2023).
The projected national volumes of sludge show the scale of the emerging situation but should not be read straight away as the quantity available for biogas generation. The Programme specifically anticipates anaerobic digestion for WWTPs with capacities over 100,000 population equivalents (PE), while the choice between aerobic and anaerobic stabilization for medium-sized plants depends on their capacity and economic viability. It also contemplates high-efficiency anaerobic digestion, energy recovery, and regional sludge-management centers for the largest plants.

ASSESSMENT OF THE WASTEWATER SLUDGE POTENTIAL BIOGAS PRODUCTION

Based on the National Sludge Management Programme for Republic of Serbia, eleven projected wastewater treatment plants with a capacity of over 100,000 PE are planned to use anaerobic digestion(Government of the Republic of Serbia, 2023). The data on the number of plants and the quantity of dry solids are available directly for Vrbas and Subotica. According to the source, these two treatment plants are expected to produce 4,200 – 5,100 t of dry solids per year. However, the total amount of sludge from all eleven projected large treatment plants is not presented. Therefore, the amount of sludge from these treatment plants should be calculated individually by using the selected specific production of sludge (40 – 45 g of dry solids per population equivalent per day).

Methodology

The analysis considered wastewater treatment plants (WWTPs) with a design capacity above 100,000 population equivalent (PE), for which the Serbian Sludge Management Programme envisages anaerobic digestion. Where plant-specific sludge quantities were unavailable, the annual production of stabilized sludge was estimated from the design capacity:

$$M_{DS,i,s} = \frac{PE_i \cdot q_S \cdot 365}{10^6} \quad (1)$$

Where:$M_{DS,i,s}$ is the annual mass of digested sludge at WWTP *i* under scenario *s;*PE_i is the design capacity of the WWTP q_S is the specific sludge-production factor (g DS $PE^{-1}d^{-1}$); *s*denotes the loading scenario.
For WWTPs above 100000 PE $q_S$was set to 40 g DS PE^{-1} $d^{-1}$for the 50th-percentile loading scenario and 45 DS PE^{-1} $d^{-1}$for the 85th-percentile scenario
Because national reports typically quantify stabilized or digested sludge rather than raw substrate, the dry-solids mass entering anaerobic digestion$M_{feed,DS}$was estimated to account for volatile solids reduction:

$$M_{feed,DS} = \frac{M_{digestate,DS}}{1 - (f_{VS} \cdot r_{VS})} \quad (2)$$

Where:$M_{\mathrm{feed,DS}}$ = estimated feed sludge entering the digester (t DS yr^{-1});$M_{\mathrm{digestate,DS}}$ = stabilised/digested sludge reported or estimated from the Programme (t DS yr^{-1});f_{VS} = volatile-solids fraction in feed sludge (kg VS kg^{-1} DS);r_{VS} = volatile-solids reduction efficiency during anaerobic digestion.

The low, reference and high scenarios applied f_{VS} values of 0.60, 0.70 and 0.80,respectively, and r_{VS}values of 0.35, 0.45 and 0.55, respectively. The selected VS range is consistent with the 60–88% VS content reported for wastewater sludge study (Milovanović, 2024), whereas the range of VS reduction reflects anaerobic-digestion performance reported in the literature (Appels, 2008; Cao, 2012; Carrère, 2010).
To express the results in terms of wet sludge supplied to the digester $M_{feed,wet}$the following conversion was applied:

$$M_{feed,wet} = \frac{M_{feed,DS}}{TS} \quad (3)$$

where TS is the total-solids fraction. A reference value of TS= 0.05 was adopted based on data from the study (Milovanović, 2024) and reported specifications for thickened sludge entering the Subotica anaerobic digestion system.
To evaluate energy recovery, a biogas factor (Y_{BG}) was derived from literature data. Data indicate that biogas yields from full-scale anaerobic digestion of municipal sewage sludge commonly range from approximately 350 to 450 Nm3 t^{-1} DS. Conventional mesophilic anaerobic digestion has been reported to produce approximately 350 Nm^3 t^{-1} DS, whereas thermal-hydrolysis- assisted configurations may achieve 387–450 Nm^3 t^{-1} DS. A full-scale survey of eight UK wastewater treatment plants reported approximately 400 Nm^3 t^{-1} DS as a typical yield, while a further WWTP case study reported an annual average of 410 Nm^3 t^{-1} DS (Gandiglio, 2017; Shen, 2015; Shana, 2016). Accordingly, a yield of 400 Nm^3 biogas t^{-1} DS was adopted as the referencescenario for municipal wastewater sludge.
The annual biogas potential was calculated from the estimated dry-solids feed to anaerobic digestion:

$$V_{BG} = M_{feed,DS} \cdot Y_{BG} \quad (4)$$

Where $V_{BG}$is the annual biogas potential (Nm^3 yr^{-1}); $M_{feed,DS}$is the estimated dry-solids mass supplied to the digester (tDS yr^{-1}) and $Y_{BG}$is the specific biogas yield ($Nm^3t^{-1}DS$).
Energy recovery was estimated from the lower heating value (LHV) of the produced biogas and the conversion efficiencies of a combined heat and power (CHP) unit:

$$LHV_{BG} = x_{methane} \cdot LHV_{methane} \quad (5)$$

$$E_{el,gross} = \frac{V_{BG} \cdot LHV_{BG} \cdot \eta_{el}}{1000} \quad (6)$$

$$E_{heat,gross} = \frac{V_{BG} \cdot LHV_{BG} \cdot \eta_{heat}}{1000} \quad (7)$$

Where:x_{methane} is the methane volume fraction in biogas;$LHV_{\mathrm{CH_4}}$ is the lower heating value of methane (9.97 kWh Nm^{-3});η_{el} and η_{th} are the electrical and thermal efficiencies of the CHP unit, respectively$E_{\mathrm{el,gross}}$ and $E_{\mathrm{heat,gross}}$ denote gross annual electricity and heat production (MWh yr^{-1}).
Gross electricity and useful-heat production were estimated using CHP conversion factors of (2.094kWh$Nm^{-3}$for biogas and 2.633kWh$Nm^{-3}$for heat, respectively.
These factors correspond to electrical and useful-heat recovery efficiencies of approximately 35% and 44%, respectively, assuming a biogas lower heating value of about 6kWh Nm^{-3}.
The selected values are consistent with reported CHP performance, according to which approximately 35% of biogas energy can be converted into electricity and a further 40–50% can be recovered as useful heat where a suitable heat demand exists(IEA, 2020).
The potential displacement of lignite was estimated under the assumption that biogas-derived electricity substitutes electricity generated in lignite-fired power plants. Electricity-related lignite displacement was calculated as:

$$M_{lignite,el} = \frac{3600 \times E_{el}}{\eta_{el} \times LHV_{lignite}} \quad (8)$$

$$M_{lignite,heat} = \frac{3600 \times E_{heat}}{\eta_{boiler} \times LHV_{lignite}} \quad (9)$$

$$M_{lignite,total} = M_{lignite,el} + M_{lignite,heat} \quad (10)$$

Where: where $M_{lignite,el}$, $M_{lignite,heat}$, and $M_{lignite,total}$ are expressed in t yr^{-1}; η_{el}=0.30) is the assumed electrical efficiency of lignite-fired power generation; η_{boiler}=0.85) is the assumed efficiency of a lignite-fired heat-only boiler; and $LHV_{lignite}$=7.85) GJ t^{-1} is the average lower heating value reported for Serbian lignite (European Association for Coal and Lignite, 2017). The factor 3600 converts energy from GWh to GJ.

Scenario-based assessment of national biogas potential

Three distinct scenarios were modeled to evaluate the biogas potential of wastewater treatment plants (WWTPs) with a design capacity exceeding 100,000 PE. These scenarios account for combined uncertainties in specific sludge production, volatile-solid (VS) content and degradation efficiency, and specific biogas yields.
The conservative scenario applies the Serbia-specific factor derived from the Sremska Mitrovica co-digestion model(Milovanović, 2024). The reference scenario uses a biogas yield of 400 Nm^3t^{-1}DS, consistent with full-scale municipal sludge digestion data. The high-potential scenario represents improved digestion performance, potentially achieved through optimized operation, a higher biodegradable organic-matter content, or pretreatment. Full-scale studies have reported typical sludge-biogas yields of approximately 350–450 Nm^3t^{-1}DS (Gandiglio, 2017; Liu, 2022; Shen, 2015).
The Sludge Management Programme identifies 11 WWTPs above 100,000 PE. Explicit capacity data were available for seven facilities, with a combined capacity of 2,819,250 PE. Since capacities were not reported for the remaining four facilities, each was conservatively assigned 100,000 PE. The resulting total capacity of 3,219,250 PE therefore represents a lower-bound estimate.
Based on the 3 scenario assumptions, the aggregated biogas potential of the 11 planned large WWTPs was estimated at 18,3 – 42,5 (million Nm^3 yr^{-1}) (with a reference value of 29, (million Nm^3 yr^{-1}).

Table 1. *Overview of Scenario Parameters*

Parameter	Conservative scenario	Reference scenario	High-potential scenario
Specific digestate production, q_S(g DS PE^{-1}d^{-1}	40.0	42.5	45.0
VS fraction in feed sludge, f_{VS}	0.60	0.70	0.80
VS reduction in anaerobic digestion, r_{VS}	0.35	0.45	0.55
Biogas yield, Y_{BG}(Nm^{3}t^{-1}DS)	308	400	450

It should be noted that the actual potential will be higher once plant-specific capacities and sludge-characterization data become available.

Table 2. *National-Level Results and Capacity Assumptions*

Indicator	Conservative scenario	Reference scenario	High-potential scenario
Digestate production (t DS yr^{-1})	47,001	49,939	52,876
Estimated digester feed (t DS yr^{-1})	59,495	72,903	94,422
Biogas potential (million Nm^3 yr^{-1})	18.32	29.16	42.49
Gross electricity potential (GWh yr^{-1})	38.37	61.05	88.96
Gross heat potential GWh yr^{-1})	48.23	76.75	111.84
Lignite displaced by electricity (10³ t yr^{-1})	58.7	93.3	136.0
Total lignite displacement with full heat utilization (10³ t yr^{-1})	84.7	134.7	196.3

Sensitivity analysis

A one-at-a-time sensitivity analysis was performed around the reference national biogas potential of 29.16 million (million Nm^3 yr^{-1}). Each parameter was varied across its defined low and high values while all other parameters were retained at their reference values. The specific biogas yield was the dominant source of uncertainty: changingY_{BG} from 400 to 308 (Nm^{3}t^{-1}DS) reduced the estimated potential by 23.0%, whereas increasing it to 450 (Nm^{3}t^{-1}DS)increased the potential by 12.5%. Volatile-solids reduction was the second most influential parameter, causing changes of −9.3% to +11.4%.
In comparison, variation in the VS fraction and specific sludge-production factor resulted in narrower ranges of −6.2% to +7.0% and ±5.9%, respectively.

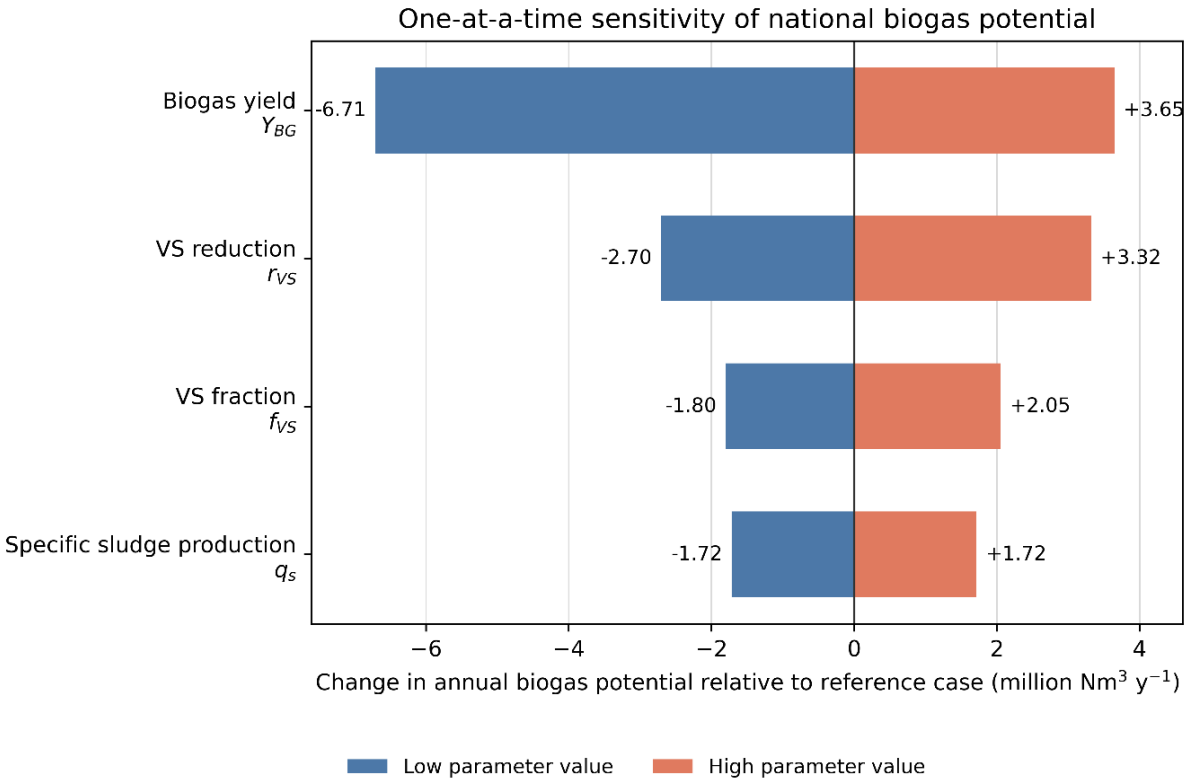


Fig. 1. *One-at-a-time sensitivity of the estimated annual biogas potential from 11 planned WWTPs above 100,000 PE. Bars indicate the absolute change relative to the reference case*

The key source of uncertainty was related to the biogas-yield factor, followed by VS reduction, VS fraction and sludge-production rate. The same parameters proportionally impact on the gross electricity and heat production. In addition, the CHP electricity and heat conversion factors should be considered when estimating energy recovery. The total-solids content was not included as a direct driver of gross biogas production since it affects wet-sludge flow and operational energy demand rather than the dry-solids based biogas yield.

These results demonstrate that reliable plant-specific measurements of sludge biodegradability, volatile-solids removal and biogas yield are more important for refining the national estimate than further refinement of the specific sludge-production factor. The uncertainty associated with the capacity of four WWTPs not explicitly specified in the Programme was treated separately: each additional 100,000 PE increases the reference biogas potential by approximately 0.91 million Nm^3 yr^{-1}.

In the reference-case scenario, biogas from sludge could provide 61.05 GWh yr $^{-1}$ of electricity and 76.75 GWh yr $^{-1}$ of useful heat. The electricity content is theoretically equivalent to 93.3 kt lignite yr $^{-1}$ of substituted emissions, and a total of 134.7 kt lignite yr $^{-1}$ if all recoverable heat energy is efficiently used.

In the different scenarios considered here, the electricity-related lignite displacement potential varies between 58.7 and 136.0 kt lignite yr $^{-1}$, while the combined electricity and heat utilization leads to a range between 84.7 and 196.3 kt lignite yr $^{-1}$.

The values are to be considered theoretical gross substitution potentials and do not necessarily imply a change in power-system operation. The electricity would substitute for on-site electrical demand at the WWTPs and, therefore, cannot necessarily be related to a particular lignite-fired electricity-generating unit. Similarly, the heat-related contribution represents a technical maximum because a continuous demand for heat is required, and the necessary infrastructure for distribution must be available. Parasitic energy consumption, biogas losses, a possible lack of combined heat and power (CHP) generation, and electricity and heat distribution losses should be accounted for if specific plant data become available.

CONCLUSION

This study provides a national level assessment of the biogas potential of the wastewater sludge of the 11 planned large WWTPs, each of which has a design capacity larger than 100,000 PE. The estimated amount of the produced stabilized sludge is between 47,001 and 52,876 t DS yr^{-1} that corresponds to 59,495–94,422 t DS yr^{-1} of the digester feed in the analyzed scenarios.The biogas potential is estimated from 18.32 to 42.49 million Nm^3 yr^{-1}, with a reference value of 29.16 million Nm^3 yr^{-1}. The corresponding amounts of electricity would be in a range from 38.37 to 88.96 GWh yr^{-1}, while the amounts of useful heat can provide from 48.23 to 111.84 GWh yr^{-1}.
The reference scenario suggests a possible total displacement of 134.7 kt lignite yr^{-1} with the caveat that the heat-related component depends on the availability of a continual local heat demand coupled with appropriate heat-distribution infrastructure.
The sensitivity analysis highlighted that the specific biogas yield and VS reduction were the primary drivers of the predicted biogas potential; consequently, the results should be considered indicative of strategic planning scenarios rather than predictors of plant-specific performance. Future project development should focus on acquiring site-specific data pertaining to actual wastewater load, primary- and waste-activated-sludge ratios, TS and VS contents, methane concentration, parasitic energy demand, CHP availability, and local heat demand.
Overall, the results suggest that anaerobic digestion and CHP technologies offer a viable opportunity for enhancing the sustainability profile of large Serbian WWTPs, facilitating the transition from conventional sludge disposal practices to those focused on resource recovery whilst simultaneously contributing to decreased reliance on fossil-fuel sources. This would enable WWTP to re-position itself as an enabler of the local production of renewable electricity and heat.

ACKNOWLEDGEMENT

This research has been supported by the Ministry of Science, Technological Development and Innovation through Contract No. 451-03-33/2026-03/ 200156.

REFERENCES

Appels, L., Baeyens, J., Degrève, J., & Dewil, R. (2008). Principles and potential of the anaerobic digestion of waste-activated sludge. Progress in Energy and Combustion Science, 34(6), 755–781. https://doi.org/10.1016/j.pecs.2008.06.002

Cao, Y., & Pawłowski, A. (2012). Sewage sludge-to-energy approaches based on anaerobic digestion and pyrolysis: Brief overview and energy efficiency assessment. Renewable and Sustainable Energy Reviews, 16(3), 1657–1665. https://doi.org/10.1016/j.rser.2011.12.014

Carrère, H., Dumas, C., Battimelli, A., Batstone, D. J., Delgenès, J.-P., Steyer, J.-P., & Ferrer, I. (2010). Pretreatment methods to improve sludge anaerobic degradability: A review. Journal of Hazardous Materials, 183(1–3), 1–15. https://doi.org/10.1016/j.jhazmat.2010.06.129

European Association for Coal and Lignite. (2017). Serbia (7th ed.): Powering transition in Europe. https://euracoal.eu/library/archive/serbia-7/

Gandiglio, M., Lanzini, A., Soto, A., Leone, P., & Santarelli, M. (2017). Enhancing the energy efficiency of wastewater treatment plants through co-digestion and fuel cell systems. Frontiers in Environmental Science, 5, Article 70. https://doi.org/10.3389/fenvs.2017.00070

Government of the Republic of Serbia. (2023). Sludge management programme in the Republic of Serbia for the period 2023–2032. Official Gazette of the Republic of Serbia, No. 84/2023.

International Energy Agency. (2020). Outlook for biogas and biomethane: Prospects for organic growth. https://www.iea.org/reports/outlook-for-biogas-and-biomethane-prospects-for-organic-growth/an-introduction-to-biogas-and-biomethane

Liu, J., & Smith, S. R. (2022). The link between organic matter composition and the biogas yield of full-scale sewage sludge anaerobic digestion. Water Science and Technology, 85(5), 1658–1672. https://doi.org/10.2166/wst.2022.058

Milovanović, R. (2024). Report on the analysis of bio-waste utilization potential: Regional solid waste management system of Sremska Mitrovica (Deliverable D3, Contract No. 10150308). UNDP Serbia.

Shana, A. (2016). Application of an innovative process for improving mesophilic anaerobic digestion of sewage sludge [Doctoral dissertation, University of Surrey]. Surrey Research Insight Open Access. https://openresearch.surrey.ac.uk/esploro/outputs/99514818002346

Shen, Y., Linville, J. L., Urgun-Demirtas, M., Mintz, M. M., & Snyder, S. W. (2015). An overview of biogas production and utilization at full-scale wastewater treatment plants in the United States. Renewable and Sustainable Energy Reviews, 50, 346–362. https://doi.org/10.1016/j.rser.2015.04.129

DOI:10.5937/IIZS26010B

MULTICRITERIA ANALYSIS OF OCCUPATIONAL SAFETY MEASURES IN UNDERGROUND COAL MINES WITH METHANE

Research paper

Dejan Bogdanović[1*]
[1]University of Belgrade, Technical Faculty in Bor, Bor, Serbia

Abstract: Underground coal mines containing methane remain among the most hazardous mining environments, exposing workers to a wide range of risks. This paper presents a systematic analysis of occupational safety measures in these mines. The Analytic Hierarchy Process (AHP), a multicriteria decision-making (MCDM) method, is used as the analytical framework. The findings identify the most critical groups of safety measures. Eight groups of occupational safety measures are analysed. The results show that these measures can be categorised into three priority levels according to the order of their application. These categories correspond to three fundamental occupational safety functions: baseline safety, explosion prevention, and life-saving response.
Key words: occupational safety measures, underground coal mines, methane, AHP

INTRODUCTION

Underground coal mining in methane-bearing seams is among the most complex and risk-intensive industrial environments, characterized by the continuous interaction of geomechanical, ventilation, and gas emission processes. Methane (CH_4), a naturally occurring by-product of coalification, presents a critical hazard due to its explosibility within a concentration range of approximately 5–15% in air, as well as its potential to displace oxygen and cause asphyxiation (ILO, 2006). Despite significant technological advancements in monitoring systems, ventilation engineering, and methane drainage techniques, methane-related incidents – often exacerbated by coal dust explosions – remain a persistent threat to occupational safety (Kissell, 2006).
The multifactorial nature of methane risk in underground coal mines requires a comprehensive analytical framework capable of integrating heterogeneous variables, including geological conditions, emission rates, ventilation performance, equipment reliability, and human factors. Effective occupational safety management depends on detection, ventilation, ignition control, and emergency preparedness (Eyüboglu, 2025; Tasoglu, 2026).
Multicriteria analysis enables the incorporation of both quantitative parameters – such as methane concentration levels, airflow rates, and system response times – and qualitative judgements related to organizational practices, worker behaviour, and safety culture (Kursunoglu, 2024; Wang & Lei, 2026; Yin et al. 2025). In this paper, the Analytic Hierarchy Process (AHP) is used as a robust MCDM technique that decomposes complex problems into hierarchical structures, allowing for pairwise comparisons of criteria and alternatives (Saaty, 1980). This paper applies AHP to develop a multicriteria analytical framework for assessing occupational safety in underground coal mines with methane, with the objective of improving risk prioritization, supporting evidence-based decision-making, and ultimately reducing the likelihood and consequences of methane-related incidents.

MATERIAL AND METHODS

The original methodology is designed to achieve optimal results. The methodology defined by the author is shown in Fig. 1.
Fig. 1 shows that the research begins with identifying groups of occupational safety measures in underground coal mines with methane. The methods were identified based on a literature review and data from underground coal mining companies in our country.
The next step involves ranking the groups of occupational safety measures in underground coal mines containing methane. The Analytic Hierarchy Process (AHP) method was employed

[1]Corresponding author, dbogdanovic@tfbor.bg.ac.rs, ORCID: 0000-0002-4871-4366

for the ranking, with scores assigned using the group decision-making method (the author, together with managers and experts from underground mines within the mining operations of our country).

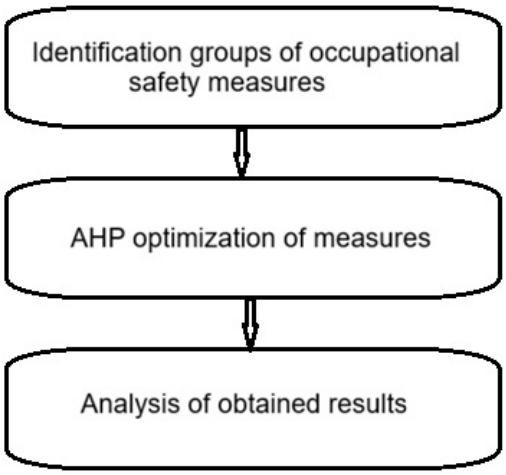


Fig. 1. *Schematic presentation of the work methodology*

Once the ranking list had been established, the results were analyzed with the aim of identifying the most significant groups of occupational safety measures in underground mining and determining general preventive measures in mining operations.

AHP METHOD

The Analytic Hierarchy Process (AHP) is a structured decision-making method that facilitates the analysis of complex decisions by decomposing them into a hierarchical framework of criteria and alternatives, followed by the determination of priorities through pairwise comparisons. The principal theoretical foundations of AHP include hierarchy construction (decomposing the decision problem into a hierarchy of objectives, criteria, sub-criteria, and alternatives), pairwise comparisons (comparing elements at each level using a 1–9 scale, as shown in Table 1), computation of priority vectors (using the eigenvector method to derive weights from the comparison matrix, thereby ensuring consistency), consistency verification (calculating the consistency ratio (CR) to assess the logical coherence of judgments, with CR < 0.1 considered acceptable), and weight aggregation (combining local priorities across the hierarchy to obtain global weights for alternatives).
AHP offers several advantages, including its ability to accommodate both qualitative and quantitative criteria, as well as providing a systematic and transparent decision-making framework.
Its main limitations are the subjectivity in pairwise comparisons and the potential complexity when a large number of criteria or alternatives are involved.
Presently, AHP is utilized in business, engineering, healthcare, and political science for multi-criteria decision analysis.

Table 1. *AHP comparison scale*

Dominance	
Description	**Mark**
Equal	1
Weak dominance	3
Strong dominance	5
Very strong dominance	7
Absolute dominance	9
2, 4, 6, 8 are intermediate values	

RESULTS AND DISCUSSION

Identification groups of occupational safety measures

Given that the research was based on the outcomes of interviews with managers and experts from mining companies, a list of occupational safety measures was compiled based on their assessments and the existing regulations pertaining to mining operations. Once an inventory of all proposed occupational safety measures had been obtained, the specified measures were analyzed, resulting in a final list comprising the essential groups of occupational safety measures in mining companies. This list includes the following measures:

- **Monitoring and detection (M1)**. This measure involves *continuous gas monitoring*, including fixed methane sensors installed at longwall faces, in return airways, and roof cavities, as well as portable detectors carried by miners, with defined *alarm thresholds* (1.0% CH_4 warning level and 1.5–2.0% CH_4 triggering power cut-off or evacuation). Modern systems incorporate real-time telemetry to surface control rooms and automated shutdown of electrical equipment.
- **Ventilation control (M2)**. The objectives of this measure are to dilute methane below its explosive limits, remove other gases (CO_2, CO), and control temperature and dust. Proper ventilation is the primary engineering control. The measures include main ventilation fans, which maintain airflow throughout the mine; auxiliary fans and ducts, which direct air to working faces; and airflow design, comprising intake airways (fresh air) and return airways (contaminated air).
- **Methane drainage (degasification) (M3)**. This comprises measures including pre-drainage (boreholes drilled before mining), post-drainage (gas captured during or after extraction), and the reduction of methane emissions at the working face. Additionally, this approach enables energy recovery through methane utilisation.
- **Explosion prevention (M4)**. This set of measures comprises three subgroups: *ignition source control* (intrinsically safe electrical equipment, explosion-proof enclosures, strict control of welding and cutting through hot work permits, and an absolute prohibition of smoking); *rock dusting* (application of inert limestone dust to prevent the propagation of coal dust explosions); and *equipment maintenance* (prevention of frictional sparks and regular inspection of machinery).
- **Worker protection and training (M5)**. The occupational safety measures mentioned include mandatory gas safety training, the use of self-rescuers (portable breathing apparatus), evacuation drills, familiarity with escape routes, and comprehensive underground communication systems.
- **Emergency preparedness (M6)**. These measures require the availability of *key systems*, including refuge chambers (sealed safe zones), emergency ventilation reversal capability, and fire suppression systems, as well as the implementation of *response plans* that include immediate evacuation protocols, isolation of affected sections, and deployment of mine rescue teams.
- **Regulatory framework and standards (M7)**. Underground coal mines with methane must implement effective regulatory frameworks and standards. These include widely recognised international frameworks such as the International Labour Organization (ILO) mining safety guidelines, Mine Safety and Health Administration (MSHA) regulations, and EU Directives on worker safety in extractive industries. Serbia aligns with EU occupational safety standards, emphasising risk assessment, preventive engineering controls, and worker training and certification.

- **Key risk control hierarchy (M8)**. The most important risk control measures include elimination through methane drainage; engineering controls such as ventilation and monitoring systems; administrative controls, including procedures and training; and personal protective equipment (PPE), such as self-rescuers, helmets, and gas detectors.

AHP optimization of measures

After identifying all groups of occupational safety measures intended to mitigate the risk of accidents in underground coal mines where methane is present, these measures were prioritized using the Analytic Hierarchy Process (AHP). As previously noted, the aim of this prioritization is to establish a ranking of the groups of occupational safety measures related to accident prevention, thereby facilitating the development of an optimal set of preventive measures against mine accidents. The ranking of the measures was carried out by managers and experts, as shown in Table 2.

Table 2. *Comparison marks of groups of occupational safety measures*

	M1	**M2**	**M3**	**M4**	**M5**	**M6**	**M7**	**M8**
M1	1	1/4	1	1/3	1/4	1/2	1	1/3
M2		1	2	2	1	2	3	1
M3			1	1/3	1/2	1	1	1/3
M4				1	1	3	2	1
M5					1	2	1	1/2
M6						1	1	1/2
M7							1	1/3
M8								1

After comparing the preventive measures, the BPMSG software (https://bpmsg.com/ahp/ahp.php) was used to obtain the ranking results. This process determined the weighting coefficients of the proposed measures, as shown in Table 3.

Table 3. *Results of measures ranking*

Nr.	**Alternative**	**Weighting coefficient**	**Rank**
1	M1	0.055	8
2	M2	0.190	1
3	M3	0.114	5
4	M4	0.167	2
5	M5	0.157	4
6	M6	0.078	6
7	M7	0.077	7
8	M8	0.161	3
Number of comparisons=28 Consistency Ratio=8.5%			

Analysis of obtained results

The results obtained (Table 3.) can be considered highly significant guidelines for mines regarding the priority in which the defined groups of occupational safety measures should be implemented.

The results show that the groups of occupational safety measures can be classified into three categories based on the priority of their application. The first group comprises measures M2 (ventilation control), M4 (explosion prevention), M8 (key risk control hierarchy), and M5 (worker protection and training). Their weight coefficients are the highest, exceeding 0.15 (15%). Ventilation control (M2) has a decisive influence on eliminating methane from mines or

maintaining its concentration at a safe level. According to expert assessment, this is the most critical occupational safety measure. Explosion prevention (M4) is in second place. Methane explosions involving coal dust have frequently caused mass casualties among miners and major material damage in mines. The key risk control hierarchy (M8) is in third place. Mining experts recognize that risk management, together with the establishment and adherence to procedures, significantly enhances workplace safety. Continuous control – both administrative and engineering – is also important here, as is the availability of self-rescuers, helmets, and gas detectors. Worker protection and training (M5) is in fourth place. Miners must be thoroughly trained in the use of all protective equipment within the mine, as well as in the rescue and evacuation plan in the event of an emergency. Rescue drills are therefore conducted at specified intervals in accordance with the rescue plan.

The second group includes only one measure, M3 (methane drainage, i.e., degasification). Its weight coefficient is 0.114, placing it in the middle among all groups of occupational safety measures. This measure aims to reduce methane concentration at underground coal mine sites. Consequently, according to mining experts, it is of great importance. This measure is applied both before and during coal extraction. Additionally, the methane obtained through this process can be used as an energy source within the mine.

The third group includes measures with weight coefficients below 0.1 (10%). These are M6 (emergency preparedness), M7 (regulatory framework and standards), and M1 (monitoring and detection). Emergency preparedness (M6) covers essential measures to ensure safe zones in the underground mine for all workers, as well as ventilation reversal capability and fire suppression systems. For the regulatory framework and standards (M7), mining experts regard these as very important, as they form a safety framework consisting of instructions, regulations, and other instruments that contribute to occupational safety in underground coal mines with methane. Mining experts ranked the final group of measures as M1 (monitoring and detection). Although these measures are crucial for occupational safety, they are included in this group because all coal mines today are equipped with real-time monitoring systems, making such measures largely taken for granted.

Based on the analysis and ranking results of the groups of occupational safety measures, it can be concluded that mining experts ranked the measures implemented within the mines themselves to be the most important, followed by other safety measures. This can be presented as follows:

1. Continuous monitoring + robust ventilation = **baseline safety**.
2. Ignition control + dust suppression = **explosion prevention**.
3. Training + emergency readiness = **life-saving response**.

CONCLUSION

In this paper, the Analytic Hierarchy Process (AHP) was used for the multicriteria analysis of groups of occupational safety measures in underground coal mines with methane. Eight groups of occupational safety measures were considered: M1 (monitoring and detection), M2 (ventilation control), M3 (methane drainage, i.e. degasification), M4 (explosion prevention), M5 (worker protection and training), M6 (emergency preparedness), M7 (regulatory framework and standards), and M8 (key risk control hierarchy).

Based on the results obtained using the AHP, the groups of occupational safety measures can be classified into three categories: the first group comprises measures implemented within the mines (M2, M4, M8, and M5); the second group consists of prevention measures (M3); and the third group includes preparedness measures as well as regulatory framework and standards (M6, M7, and M1).

All these groups of occupational safety measures in underground coal mines with methane serve three fundamental functions: baseline safety, explosion prevention, and life-saving response.

ACKNOWLEDGEMENT

The research presented in this paper was done with the financial support of the Ministry of Science, Technological Development and Innovation of the Republic of Serbia, within the funding of the scientific research work at the University of Belgrade, Technical Faculty in Bor, according to the contract with registration number 451-03-34/2026-03/200131

REFERENCES

Eyüboglu, A. K., Özfırat, M. K., & Yetkin, M. E. (2025). Methane Risk Analysis for Sustainable Occupational Safety in Underground Coal Mines. Rudarsko-geološko-naftni zbornik, 40(2), 173–184. DOI: 10.17794/rgn.2025.2.12

International Labour Organization. (2006). Safety and health in underground coalmines. Geneva: ILO.

Kissell, F. N. (2006). Handbook for methane control in mining. National Institute for Occupational Safety and Health (NIOSH).

Kursunoglu, N. (2024). Fuzzy multi-criteria decision-making framework for controlling methane explosions in coal mines. Environmental Science and Pollution Research, 31, 9045–9061. https://doi.org/10.1007/s11356-023-31782-0

Saaty, T.L.: The Analytical Hierarchy Process, McGraw-Hill, New York, 1980.

Tasoglu, G., Senol, M.E., Ozfirat, P.M. et al. (2026). Research in Underground Mining Methods Considering Rock Mechanics, Multi-Criteria Decision Making, Work Safety, and Economic Analysis. Mining, Metallurgy & Exploration, 43, 2093–2120. https://doi.org/10.1007/s42461-026-01565-5

Wang, L., Li, Y. & Lei, Y. (2026). Multi-criteria decision analysis of gas enrichment risk and land degradation in goaf areas. Scientific Reports, 16, 709. https://doi.org/10.1038/s41598-025-30390-x

Yin, Y., Li, C., Ye, Q., Wei, C., et al. (2025). Evaluating regulatory influences on coal mine accidents in China using a fuzzy multi-criteria decision-making approach. Scientific Reports, 15, 11204. https://doi.org/10.1038/s41598-024-83116-w



XVI International Conference Industrial Engineering and Environmental Protection 2026 (IIZS 2026)
October 01-02, 2026, Zrenjanin, Serbia

Session 1

Mechanical Engineering

DOI:10.5937/IIZS26017L

DYNAMIC STABILITY OF A CONICAL PIPE RESTING ON A PASTERNAK ELASTIC FOUNDATION

Research paper

Svetlana Lilkova-Markova[1*], Dimitar Lolov[2]
[1,2] University of Architecture, Civil Engineering and Geodesy, Sofia, Bulgaria

Abstract : This study employs the Generalized Differential Quadrature Method (GDQM) to analyze the stability of a fluid-conveying conical pipe, clamped at both ends and supported by a Pasternak elastic foundation. The primary objective is to assess how the foundation parameters influence the critical fluid velocity—the point at which the pipe loses stability. A numerical analysis was performed on a straight pipe with specified geometric and material properties, considering both parameters of the elastic foundation as variables. The resulting data, presented through graphical correlations between critical velocity and foundation parameters, underscore the significant influence of the Pasternak foundation on the pipe's vibrational behavior and overall stability.
Key words: Conical pipe, Fluid, Critical velocity, Dynamic stability, Pasternak elastic foundation, Generalized Differential Quadrature Method

INTRODUCTION

Fluid-conveying pipes are widely utilized across various industries, including chemical, petroleum, aviation, and nuclear sectors. Their dynamic stability has long been a subject of extensive scientific investigation.
Reference (Gaith, 2021) investigates a simply supported pipe conveying fluid, whose cross-section varies linearly along its length. The study determines the natural circular frequencies of free vibrations and the critical flow velocity.
In (Khomarian et al., 2025), fluid-conveying pipes resting on a Pasternak foundation and subjected to various boundary conditions are analyzed. The study proposes a method for identifying damage locations along the pipe by combining the finite element method with the Galerkin approach. Another recent study (Jerad et al., 2025) examines the stability of a pipe resting on a Pasternak elastic foundation. The pipe material is axially functionally graded. Hamilton's principle is employed to derive the governing differential equation for the transverse displacement of points along the pipe axis, followed by the application of the Galerkin method.
The dynamics of conical fluid-conveying pipes are examined in (Rajasekaran, 2024) and (Yan et al., 2010). In (Rajasekaran, 2024), the author investigates the free and forced oscillations of pipes with internal fluid flow. In (Yan et al., 2010), the study focuses on the oscillation characteristics of conical tubes used in heat exchangers, and the critical fluid velocity is determined.
Paper (Rahmani & Petrudi, 2020) examines the dynamics of conical pipes at the nanoscale. An analytical solution is presented for the nonlinear oscillations of a nanocomposite conical tube conveying fluid.
This research investigates a conical fluid-conveying tube supported by a Pasternak elastic foundation, employing the Generalized Differential Quadrature Method (GDQM). The study reveals the influence of foundation stiffness on the critical velocity of the internal fluid.
The structure of the paper is as follows:

- First, the pipe model is introduced, including its static configuration and the differential equation governing its natural lateral vibrations.
- Next, the GDQM is applied to solve the problem, with a detailed derivation of the system's frequency equation.
- The roots of this equation are then analyzed to assess the system's dynamic stability.
- Finally, numerical results are presented and discussed, followed by a concise summary of the main findings.

[1]Corresponding author, lilkovasvetlana@gmail.com, ORCID: 0000-0003-0582-8176
[2]dlolov@yahoo.com, ORCID: 0000-0002-8138-0265

PROBLEM FORMULATION

The differential equation governing the transverse vibrations of a straight conical pipe conveying an inviscid fluid is presented in (Yuzhen et al., 2021). When the pipe is supported by a Pasternak elastic foundation, the equation takes the following form:

$$E\frac{\partial^2}{\partial x^2}\left[I(x)\frac{\partial^2 w}{\partial x^2}\right]+\left(m_f+m_p\right)\frac{\partial^2 w}{\partial t^2}+V\frac{dm_f}{dx}\frac{\partial w}{\partial t}+2Vm_f\frac{\partial^2 w}{\partial x\,\partial t}+m_f\frac{dV}{dx}\frac{\partial w}{\partial t}+$$
$$+V^2\frac{dm_f}{dx}\frac{\partial w}{\partial x}+\left(m_fV^2-k_r\right)\frac{\partial^2 w}{\partial x^2}+\left(2m_fV\frac{dV}{dx}+k_w\right)w=0, \tag{1}$$

where E is the Young's modulus, m_f is the mass of the fluid per unit length of the pipe, m_p is the mass of the pipe per unit length, k_r and k_w are the parameters of the Pasternak elastic foundation, x is the longitudinal coordinate along the pipe axis, t is the time and l is the length of the pipe. $w(x,t)$ is the transverse displacement of the pipe's cross-section and V is the velocity of the conveyed fluid.
Figure 1 illustrates the static scheme of the pipe analyzed in this paper.

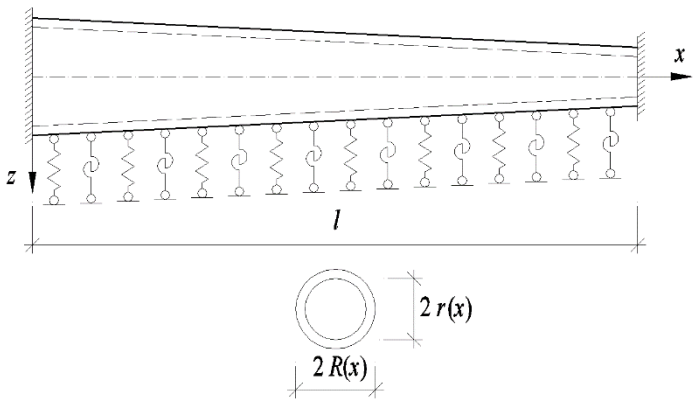


Fig. 1. *Static scheme and cross-section dimensions of the investigated pipe*

The following relation holds for the radii of an arbitrary cross-section:

$$R(x)=\left(1-\gamma\frac{x}{l}\right)R_0;\; r(x)=\left(1-\gamma\frac{x}{l}\right)r_0 \tag{2}$$

where the outer and inner radii at the inlet cross-section of the pipe are denoted by R_0 and r_0, respectively, and γ denotes the reduction coefficient.
At any given cross-section of the pipe, the fluid velocity is assumed to follow the expression below.

$$V(x)=\frac{V_0}{\left(1-\gamma\frac{x}{l}\right)^2} \tag{3}$$

with $V(0)=V_0$ representing the inlet velocity at the cross-section positioned at an abscissa of $x=0$.
At any given abscissa, the pipe's mass m_p is defined as follows.

$$m_p(x) = \left(1 - \gamma \frac{x}{l}\right)^2 \rho A(0) \tag{4}$$

Here, $A(0)$ denotes the cross-sectional area at the left end of the pipe (i.e., the section located at abscissa $x = 0$), and ρ represents the material density of the pipe.
Similarly, the fluid mass per unit length of the pipe m_f at a given position along the pipe is defined by the following relation.

$$m_f(x) = \left(1 - \gamma \frac{x}{l}\right)^2 \rho_f A_f(0) \tag{5}$$

Here, $A_f(0)$ denotes the cross-sectional area of the fluid at the left end of the pipe (i.e., the section located at abscissa $x = 0$, and ρ_f represents the density of the conveyed fluid.
The moment of inertia $I(x)$ at any cross-section of the pipe is given by the following expression.

$$I(x) = \left(1 - \gamma \frac{x}{l}\right)^4 I(0) \tag{6}$$

where $I(0)$ is the inertial moment of the cross-section at the left end of the pipe.
Differential equation (1) is solved by proposing a solution of the form:

$$w(x,t) = W(x)e^{\omega t} \tag{7}$$

In equation (7) ω denotes the circular frequency of the pipe.
Following the transformations, differential equation (1) takes the form:

$$\begin{aligned} E\frac{d^2}{dx^2}\left[I(x)\frac{d^2W}{dx^2}\right] + \left(m_f + m_p\right)\omega^2 W + V\frac{dm_f}{dx}\omega W + 2Vm_f\omega\frac{dW}{dx} + m_f\frac{dV}{dx}\omega W + \\ + V^2\frac{dm_f}{dx}\frac{dW}{dx} + \left(m_f V^2 - k_r\right)\frac{d^2W}{dx^2} + \left(2m_f V\frac{dV}{dx} + k_w\right)W = 0, \end{aligned} \tag{8}$$

Equation (8) may be reformulated as a system of algebraic equations through the application of the Generalized Differential Quadrature Method (GDQM), as presented by Soltani P. and Saadati M. (Soltani & Saadati, 2009), and Tornabene F. et al. (Tornabene et al., 2010). This method fundamentally relies on approximating the derivative of a function at any discrete point within a domain by expressing it as a weighted linear combination of the function's values at all discrete points, as described mathematically below:

$$\left.\frac{d^n W(x)}{dx^n}\right|_{x=x_i} = \sum_{j=1}^{m} \beta_{ij}^{(n)} W(x_j), \qquad i = 1, \dots, m \tag{9}$$

Here, m is the number of discrete grid points along the axis of the pipe, and $\beta_{ij}^{(n)}$ is the weighting factor for the n-th derivative evaluated at location x_i.
The Chebyshev-Gauss-Lobatto point distribution is utilized in the current work, following the approach of Tornabene F. et al. (Tornabene et al.,2010).

$$x_i = \frac{l}{2}\left[1 - cos\left(\frac{i-1}{m-1}\pi\right)\right], \qquad i = 1, \dots, m \tag{10}$$

The weighting coefficients are obtained through Lagrange interpolation functions. For the first derivative, they are calculated following the method outlined by Tornabene F. et al. (Tornabene et al., 2010):

$$\beta_{ij}^{(1)} = \frac{L^{(1)}(x_i)}{(x_i - x_j)L^{(1)}(x_j)}, \qquad i = 1, \dots, m; i \neq j \tag{11}$$

Where $L^{(1)}(x_i)$ is the first derivative of Lagrange interpolating polynomials.

$$L^{(1)}(x_k) = \prod_{l=1, l\neq k}^{m} (x_k - x_l), \qquad k = 1, \dots, m \tag{12}$$

The combination of Lagrange interpolating polynomials and Chebyshev-Gauss-Lobatto sampling points, as defined in equation (10), ensures convergence and leads to reduced error with an increasing number of sampling points.
For derivatives of higher order, the coefficients are computed through an iterative process:

$$\begin{gathered}\beta_{ij}^{(n)} = n\left(\beta_{ii}^{(n-1)}\beta_{ij}^{(1)} - \frac{\beta_{ij}^{(n-1)}}{x_i - x_j}\right), \qquad i, j = 1, \dots, m; i \neq j; n = 2, \dots, (m-1) \\ \beta_{ii}^{(n)} = -\sum_{j=1, j\neq i}^{m} \beta_{ij}^{(n)}, \qquad i, j = 1, \dots, m; n = 2, \dots, (m-1)\end{gathered} \tag{13}$$

The Generalized Differential Quadrature Method (GDQM) is applied to convert the governing equation (8) into its discrete form at specified grid points.

$$\begin{gathered}EI(x_i)\sum_{j=1}^{m}\beta_{ij}^{(4)}W(x_j) + 2E\frac{dI(x_i)}{dx}\sum_{j=1}^{m}\beta_{ij}^{(3)}W(x_j) + E\frac{d^2I(x_i)}{dx^2}\sum_{j=1}^{m}\beta_{ij}^{(2)}W(x_j) + \\ +\left[m_f(x_i) + m_p(x_i)\right]\omega^2 W(x_i) + V(x_i)\frac{dm_f(x_i)}{dx}\omega W(x_i) + \\ +2V(x_i)m_f(x_i)\omega\sum_{j=1}^{m}\beta_{ij}^{(1)}W(x_j) + m_f(x_i)\frac{dV(x_i)}{dx}\omega W(x_i) + \\ +V^2(x_i)\frac{dm_f(x_i)}{dx}\sum_{j=1}^{m}\beta_{ij}^{(1)}W(x_j) + \left[m_f(x_i)V^2(x_i) - k_r\right]\sum_{j=1}^{m}\beta_{ij}^{(2)}W(x_j) + \\ +\left(2m_f(x_i)V(x_i)\frac{dV(x_i)}{dx} + k_w\right)W(x_i) = 0,\end{gathered} \tag{14}$$

The boundary conditions at the left and right ends of the pipe (Fig. 1) are defined as follows.

$$\begin{gathered}w(0,t) = 0;\ \left.\frac{\partial w(x,t)}{\partial x}\right|_{x=0} = 0 \\ w(l,t) = 0;\ \left.\frac{\partial w(x,t)}{\partial x}\right|_{x=l} = 0\end{gathered} \tag{15}$$

Equation (16) can be expressed in matrix form as:

$$\left[B^{(4)} + B^{(3)} + B^{(2)} + B^{(1)}\right]\delta + I\delta_d = 0 \tag{16}$$

where the matrix components in Eq. (16) are given by:

$$\begin{gathered} B_{ij}^{(4)} = EI(x_i)\beta_{ij}^{(4)}; \quad B_{ij}^{(3)} = 2E\frac{dI(x_i)}{dx}\beta_{ij}^{(3)}; \\ B_{ij}^{(2)} = \left[E\frac{d^2I(x_i)}{dx^2} + m_f(x_i)V^2(x_i) - k_r\right]\beta_{ij}^{(2)}; \\ B_{ij}^{(1)} = \left[2V(x_i)m_f(x_i)\omega + V^2(x_i)\frac{dm_f(x_i)}{dx}\right]\beta_{ij}^{(1)}; \\ I_{ij} = \left[m_f(x_i) + m_p(x_i)\right]\omega^2 + V(x_i)\frac{dm_f(x_i)}{dx}\omega + m_f(x_i)\frac{dV(x_i)}{dx}\omega + \\ + \left(2m_f(x_i)V(x_i)\frac{dV(x_i)}{dx} + k_w\right); \\ i = 3,4,\dots,(m-2), \quad j = 1,\dots,m. \end{gathered} \tag{17}$$

Here, δ and δ_d are vectors of unknown displacements at the grid points, defined as:

$$\begin{gathered} \delta = \{W(x_1),\dots,W(x_m)\}^T \\ \delta_d = \{W(x_3),\dots,W(x_{m-2})\}^T \end{gathered} \tag{18}$$

Matrix representation is also applied to the four boundary conditions outlined in equation (15).

$$K_b\delta = 0 \tag{19}$$

where

$$K_b = \begin{vmatrix} 1 & 0 & 0 & \dots & 0 \\ \beta_{11}^{(1)} & \beta_{12}^{(1)} & \beta_{13}^{(1)} & \dots & \beta_{1m}^{(1)} \\ 0 & 0 & 0 & \dots & 1 \\ \beta_{m1}^{(1)} & \beta_{m2}^{(1)} & \beta_{m3}^{(1)} & \dots & \beta_{mm}^{(1)} \end{vmatrix} \tag{20}$$

The discrete formulation in equation (16), combined with the boundary conditions in (19), yields algebraic equations for the unknown nodal displacements, expressed as:

$$\begin{vmatrix} K_b \\ B^{(4)} + B^{(3)} + B^{(2)} + B^{(1)} \end{vmatrix}\delta + \begin{vmatrix} 0 \\ I\delta_d \end{vmatrix} = 0 \tag{21}$$

After transformations, Eq. (21) takes the following form:

$$\begin{vmatrix} K_{bb} & K_{bd} \\ B_{db}^{(4)} + B_{db}^{(2)} + B_{db}^{(1)} & B_{db}^{(4)} + B_{db}^{(2)} + B_{db}^{(1)} \end{vmatrix}\begin{vmatrix} \delta_b \\ \delta_d \end{vmatrix} + \begin{vmatrix} 0 & 0 \\ 0 & I \end{vmatrix}\begin{vmatrix} \delta_b \\ \delta_d \end{vmatrix} = \begin{vmatrix} 0 \\ 0 \end{vmatrix} \tag{22}$$

where:

$$\delta_b = \{W(x_1), W(x_2), W(x_{m-1}), W(x_m)\}^T \tag{23}$$

$$K_{bb} = \begin{vmatrix} 1 & 0 & 0 & 0 \\ \beta_{11}^{(1)} & \beta_{12}^{(1)} & \beta_{1(m+1)}^{(1)} & \beta_{1m}^{(1)} \\ 0 & 0 & 0 & 1 \\ \beta_{m1}^{(1)} & \beta_{m2}^{(1)} & \beta_{m(m+1)}^{(1)} & \beta_{mm}^{(1)} \end{vmatrix} \tag{24}$$

$$K_{bd} = \begin{vmatrix} 0 & 0 & 0 & \dots & 0 \\ \beta_{13}^{(1)} & \beta_{14}^{(1)} & \beta_{15}^{(1)} & \dots & \beta_{1(m-2)}^{(1)} \\ 0 & 0 & 0 & \dots & 0 \\ \beta_{m3}^{(1)} & \beta_{m4}^{(1)} & \beta_{m5}^{(1)} & \dots & \beta_{m(m-2)}^{(1)} \end{vmatrix} \tag{25}$$

$$B_{db}^{(4)} = \begin{vmatrix} B_{31}^{(4)} & B_{32}^{(4)} & B_{3(m-1)}^{(4)} & B_{3m}^{(4)} \\ B_{41}^{(4)} & B_{42}^{(4)} & B_{4(m-1)}^{(4)} & B_{4m}^{(4)} \\ \dots & \dots & \dots & \dots \\ B_{(m-2)1}^{(4)} & B_{(m-2)2}^{(4)} & B_{(m-2)(m-1)}^{(4)} & B_{(m-2)m}^{(4)} \end{vmatrix} \tag{26}$$

$$B_{dd}^{(4)} = \begin{vmatrix} B_{33}^{(4)} & B_{34}^{(4)} & \dots & B_{3(m-2)}^{(4)} \\ B_{43}^{(4)} & B_{44}^{(4)} & \dots & B_{4(m-2)}^{(4)} \\ \dots & \dots & \dots & \dots \\ B_{(m-2)3}^{(4)} & B_{(m-2)4}^{(4)} & \dots & B_{(m-2)(m-2)}^{(4)} \end{vmatrix} \tag{27}$$

It is taken into account that:

$$\delta = -K_{bb}^{-1} K_{bd} \delta_d \tag{28}$$

As a result, the following system of $(m-4)$ equations with $(m-4)$ unknowns is obtained.

$$\left(B_{dd}^{(4)} - B_{db}^{(4)} K_{bb}^{-1} K_{bd}\right)\delta_d + \left(B_{dd}^{(2)} - B_{db}^{(2)} K_{bb}^{-1} K_{bd}\right)\delta_d + \left(B_{dd}^{(1)} - B_{db}^{(1)} K_{bb}^{-1} K_{bd}\right)\delta_d + I\delta_d = 0 \tag{29}$$

For Equation (29) to have a non-trivial solution at the onset of loss of stability, the determinant of the matrix preceding the vector δ_d must equal zero. This determinant is a function of the unknown critical velocity V_0 and the unknown circular frequency ω.
The stability of the system is classified as follows:

- When $Re\omega < 0$, the system is stable.
- When $Re\omega > 0$, the system loses stability.
- If $Re\omega = 0$, the system is at the threshold of losing stability (critical state).

To determine the critical velocity, the following computational procedure is applied: a specific value is assigned to V_0, and the circular frequency ω is calculated from the condition that the determinant in Eq. (28) is zero. Based on the calculated frequency, the stability status of the system is evaluated.

RESULTS AND DISCUSSION

Numerical simulations have been conducted for the fluid-conveying pipe illustrated in Figure 1. The pipe's geometric and material properties include: the inner and outer radii of the inlet cross-section: $r = 0.022\ m; R = 0.024\ m$, the inner and outer radii of the outlet cross-section: $r = 0.012\ m; R = 0.014\ m$, Young's modulus $E = 210\ GPa$, material density $\rho_p = 7800 kg/m^3$, and the pipe length $l = 3\ m$. The analysis was performed using a specified number of sampling points $m = 21$.
For the configuration shown in Figure 1, critical inlet velocities were determined across varying parameters of the Pasternak elastic foundation, considering density of the transported fluid ($\rho_f = 1000\ kg/m^3$). The corresponding results are presented in Figure 2.

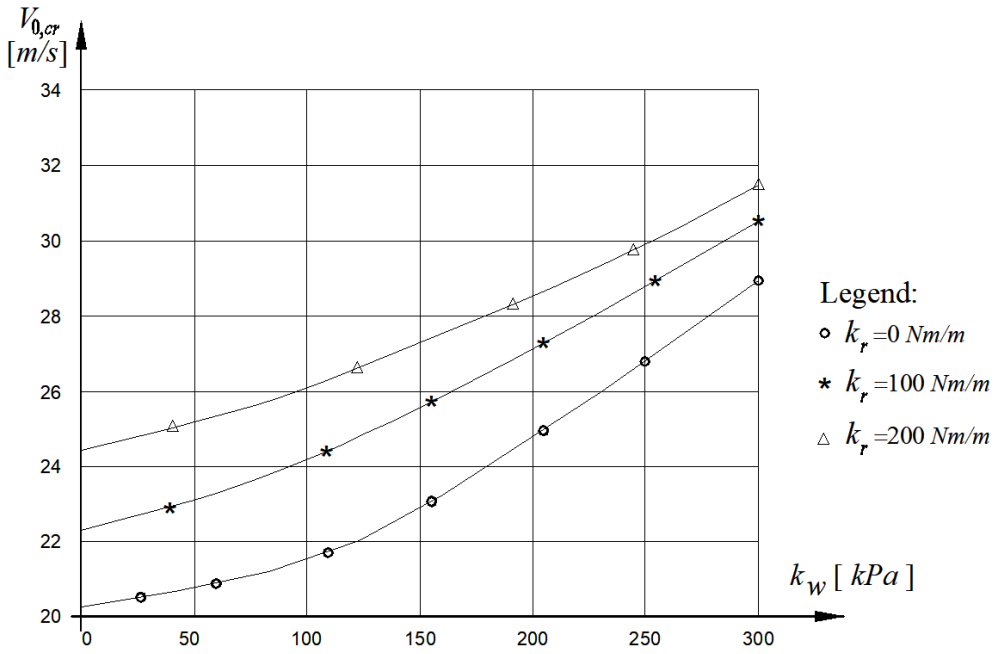


***Fig. 2**. Relationship between the critical inlet fluid velocity and the parameters of the Pasternak foundation*

CONCLUSIONS

In this paper, a conical pipe conveying fluid and resting on a Pasternak elastic foundation was investigated. The differential equation describing the lateral vibration of the pipe was solved using the Generalized Differential Quadrature Method (GDQM). A key factor in achieving a precise solution with this method is the appropriate choice of the number of sampling points. The numerical analyses presented in this article lead to several key conclusions

- The findings indicate that fluid velocity has a substantial impact on the system's dynamic behavior, which may pose risks to its structural integrity.
- Another significant observation is that increasing the parameters of the Pasternak elastic foundation leads to improved system stability.

REFERENCES

Gaith, M. (2021). The Vibration of Tubular Beam Conveying Fluid with Variable Cross Section. *Periodica Polytechnica Mechanical Engineering*, 65 (1), 56-62, https://doi.org/10.3311/PPme.17066.

Khomarian, N., et al. (2025). Damage Detection of the Pipes Conveying Fluid on the Pasternak Foundation Using the Matching Pursuit Method. *Journal of Marine Science and Application*, 24, 1-19, https://doi.org/10.1007/s11804-025-00638-z.

Jerad, Z., et al. (2025). Stability and Vibration Analysis of Porous Axially Graded Pipe Conveying-Fluid Lying on Pasternak Foundation, *International Journal of Heat and Technology*, 43 (1), pp. 361-369, https://doi.org/10.18280/ijht.430137.

Rajasekaran, S. (2024). Dynamics of Fluid Flow in Functionally Graded Tapered Pipes on Elastic Foundations. *Research Square*, 1-48, https://doi.org/10.21203/rs.3.rs-4277717/v1.

Yan, K., et al. (2010). Vibration Characteristics of Fluid-Structure Interaction of Conical Spiral Tube Bundle. *Journal of Hydrodynamics*, 22 (1), 121-128, https://doi.org/10.1016/S1001-6058(09)60036-7.

Rahmani, M., Petrudi, A. (2020). Nonlinear Vibration and Dynamic Response of Nano composite Conical Tube by Conveying Fluid Flow. International Advanced Researches and Engineering Journal, 4 (3), 180-190, https://doi.org/10.35860/iarej.750166.

Yuzhen, Z., et al. (2021). Dynamics of axially functionally graded conical pipes conveying fluid. *Journal of Mechanics*, 37, 318-326, https://doi.org/10.1093/jom/ufaa030.

Soltani, P., Saadati, M. (2009). Application of generalized quadrature rule to vibration of a curved carbon nanotube on elastic foundation. *The Sixteenth International Congress on Sound and Vibration, Krakow, 5-9 July 2009*.

Tornabene, F., et al. (2010). Critical flow speeds of pipes conveying fluid using the generalized differential quadrature method. *Advances in Theoretical and Applied Mechanics*, 3, 121-138.

DOI:10.5937/IIZS26025A

STUDIES ON THE THERMAL AND MECHANICAL BEHAVIOR OF COMPOSITE MATERIALS IN AUTOMOTIVE ELECTRONIC DEVICES

Research paper

Neagoe Andrei-Rareș[1], Adrian-Eugen Cioablă[2*]
[1,2]Politehnica University Timisoara, Mechanical Engineering Faculty, Mihai Viteazu Blv, 1, 300222, Timisoara

Abstract: The development of Advanced Driver Assistance Systems (ADAS) involves the integration of an increasing number of cameras, sensors, and electronic components into vehicle structures. Their operation under varying conditions of temperature, solar radiation, and airflow imposes specific requirements on protective housings. In this context, the present paper describes an experimental test bench designed for the study of an automotive camera located in the windshield area and investigates the potential use of composite materials as alternatives for its housing. Based on the reviewed literature, the main categories of materials with potential for this application are evaluated, with particular emphasis on carbon fiber-reinforced polymer (CFRP) composites and natural fiber-reinforced composites. Their advantages and limitations are discussed in terms of weight, mechanical and thermal properties, durability, and manufacturability. The analysis provides a basis for further research involving the simulation and experimental evaluation of the thermal and mechanical behavior of housing variants made from composite materials.
Key words: *composite materials, automotive, ADAS, housing, thermal behavior, mechanical behavior.*

INTRODUCTION

The automotive industry is undergoing a continuous development process driven by the need to increase energy efficiency, reduce vehicle weight, and integrate increasingly complex electronic functions. In this context, composite materials have become an important alternative to conventional materials due to their combination of low weight, mechanical strength, specific stiffness, corrosion resistance, and the possibility of tailoring their properties to specific application requirements (Khan et al., 2025). The literature indicates their use in body, chassis, interior, suspension, powertrain, and other automotive components.

Weight reduction represents one of the main reasons for the use of composite materials. Polymer matrix composites (PMCs), metal matrix composites, and hybrid systems offer the possibility of reducing component weight while maintaining adequate structural properties. In the case of PMCs, the use of thermoplastic or thermosetting matrices combined with different types of fibers enables the material properties to be adapted to specific operating conditions (Yan & Xu, 2025). However, their large-scale implementation is still limited by cost, recyclability, manufacturing time, and integration into multi-material structures.

In parallel with material development, Advanced Driver Assistance Systems (ADAS) have become an important component of modern vehicles. ADAS use cameras, sensors, and software to monitor the surrounding environment, detect objects, and implement functions such as lane keeping, collision avoidance, and driver monitoring (Shah & Patel, 2026). Commercial configurations may use cameras in combination with RADAR, LiDAR, and ultrasonic sensors, including architectures in which cameras play a predominant role (Kim et al., 2026).

The performance of these systems is influenced by operating conditions. Reduced visibility and adverse weather conditions can limit sensor performance and, consequently, the availability of certain ADAS functions. In the case of a camera installed in the windshield area, the assembly is additionally exposed to temperature variations and solar radiation. Consequently, the housing should be regarded not only as a protective and positioning element but also as a component that can influence the thermal and mechanical behavior of the device.

[2]Corresponding author, adrian.cioabla@upt.ro

In this context, the paper aims to identify and analyze composite materials with potential applications for automotive camera housings, with the objective of establishing design solutions that will subsequently be investigated in terms of their thermal and mechanical behavior.

DESCRIPTION OF THE EXPERIMENTAL TEST BENCH

For the analysis of the automotive camera, an experimental test bench was developed to reproduce its installation area near the windshield. The test bench is intended to enable the evaluation of the assembly under controlled conditions and to provide an experimental basis for the subsequent comparison of different materials and housing configurations.
The setup allows the reproduction of thermal factors representative of real operating conditions. The test bench is designed to generate controlled airflow, simulate heating caused by solar radiation, and measure temperature at relevant points within the assembly. In this way, the influence of external conditions on the temperature of the housing and electronic components can be evaluated.



Fig. 1. *Experimental test bench for simulation validation*

In the subsequent stages of the research, the experimental test bench will enable the comparison of the reference housing with alternative versions made from composite materials. The experimental evaluation will be correlated with numerical simulations of heat transfer and mechanical loads, allowing the influence of the material to be distinguished from that of the housing geometry. The reference configuration will provide a common basis for assessing the response of the investigated housing solutions under comparable operating conditions. This approach will make it possible to identify variations associated with the thermal and mechanical characteristics of each material and to evaluate their influence on the overall behavior of the camera assembly. The combined use of numerical and experimental methods will also support the validation of the developed models and provide a consistent methodology for the subsequent assessment of candidate materials.

ANALYSIS OF POTENTIAL COMPOSITE MATERIALS FOR THE AUTOMOTIVE CAMERA HOUSING

The automotive camera under analysis represents an electronic assembly whose operation depends on the thermal and mechanical conditions specific to its installation area. The housing constitutes a functional component of this assembly, providing both protection and support for the internal components, while also playing a role in managing heat transfer between the internal components and the external environment. In this context, the material used for the housing becomes an important design parameter, and its replacement requires an evaluation of its effects on heat transfer, stiffness, mechanical strength, dimensional stability, and the overall weight of the assembly.
The automotive camera used in the current configuration is equipped with a metal housing made of an aluminum alloy. This configuration will serve as the reference solution for subsequent research, against which housing variants made from composite materials will be evaluated.

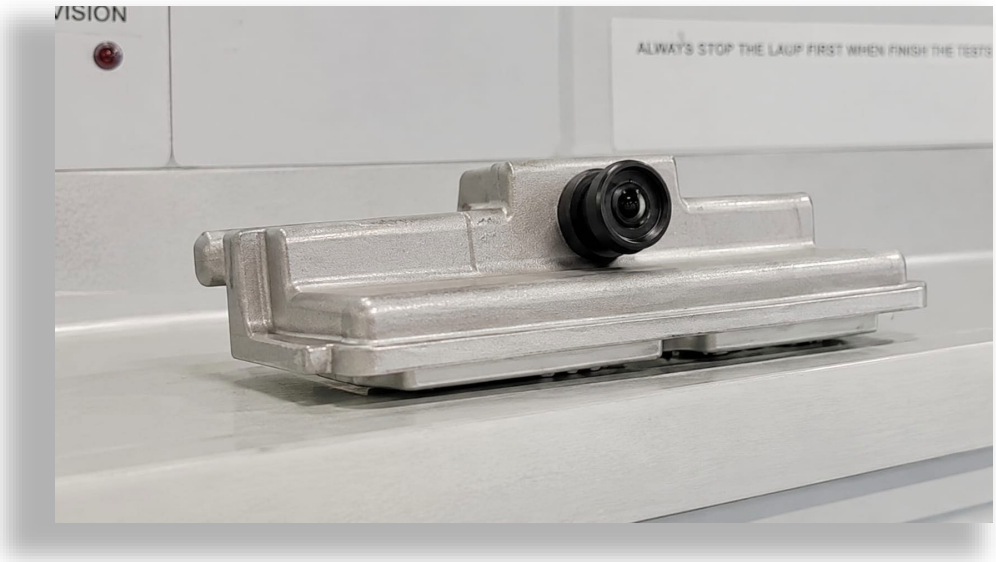


Fig. 2. *Automotive camera with the reference aluminum alloy housing*

Among the materials analyzed, carbon fiber-reinforced polymer matrix composites (CFRP) represent a category of interest for automotive applications due to their low weight and the possibility of tailoring material properties through the selection of the matrix, fiber architecture, and fiber orientation. In polymer matrix composites, the final performance is determined by the characteristics of the fibers and matrix, as well as by the interaction at the fiber–matrix interface, aspects also highlighted in studies dedicated to fiber-reinforced polymer systems (Slamnoiu-Teodorescu et al., 2026). The literature highlights several CFRP systems, including thermoplastic matrix variants, whose characteristics vary depending on the constituent materials and manufacturing technology (Fekiač et al., 2026). The selection of such a material should be based on the specific operating conditions, taking into account thermal stability, durability, manufacturability, recyclability, and cost.
For the housing of the camera under investigation, the use of CFRP is of particular interest due to the possibility of tailoring its properties and its distinct thermal behavior compared with the reference aluminum alloy solution. However, the thermal characteristics of composite systems require a dedicated evaluation under the specific operating conditions of the application. Therefore, the suitability of CFRP for the camera housing cannot be determined solely on the basis of its general material properties, but requires an assessment of its thermal and mechanical behavior.

A second category of materials with potential for the analyzed application is represented by polymer matrix composites reinforced with natural fibers. The interest in these materials within the automotive industry is mainly driven by their low density, the possibility of using renewable resources, and the advantages associated with sustainability. Natural fibers can be combined with different polymer matrices, including bio-based or recycled polymers, while the final properties of the composite are influenced by the nature of the constituents, fiber–matrix compatibility, and the manufacturing process (Saha et al., 2025; Ur Rehman & Ur Rehman, 2026). The reviewed literature highlights the potential of these materials for automotive applications, as well as the need to evaluate factors such as moisture sensitivity, thermal stability, fiber–matrix interfacial adhesion, and durability under operating conditions.
For the housing of the camera under investigation, natural fiber-reinforced composites represent a potential alternative that is worth investigating, particularly in terms of weight reduction and the use of materials with a lower environmental impact. However, the specific characteristics of these materials require an evaluation of their behavior under the thermal conditions associated with the installation area. Similar to carbon fiber-reinforced composites, their suitability for the camera housing should be determined by considering the material properties in relation to the specific thermal and mechanical requirements of the application.

CONCLUSION

The analysis carried out in this study confirms the relevance of the housing material as an important design parameter for windshield-mounted automotive camera systems. In addition to providing mechanical protection and structural support, the housing material must be selected by considering its influence on the thermal behavior, dimensional stability, weight, and overall operating conditions of the electronic assembly.
The literature analysis highlights the potential of polymer matrix composites for automotive applications and supports their investigation as possible alternatives to the reference aluminum alloy solution. Among the materials analyzed, carbon fiber-reinforced composites are of particular interest due to their low weight, mechanical properties, and the possibility of tailoring their characteristics through the selection of the matrix and reinforcement configuration. Natural fiber-reinforced composites represent an alternative direction, particularly due to their low density and sustainability-related advantages; however, their use requires additional consideration of moisture sensitivity, thermal stability, and fiber–matrix interfacial behavior.
Differences in material properties can affect heat transfer mechanisms and the mechanical behavior of the housing; therefore, material selection must be closely correlated with the actual operating conditions of the device. In this context, the developed experimental test bench enables the controlled reproduction of relevant factors, such as airflow and heating caused by solar radiation, providing a basis for the comparative evaluation of the proposed design solutions.
Future research will focus on the selection of candidate materials and the development of alternative housing configurations, followed by numerical analysis of their thermal and mechanical behavior. The simulation results will be correlated with experimental measurements performed on the test bench in order to evaluate the influence of the housing material on temperature distribution and the overall behavior of the assembly. Comparing these results with those obtained for the reference aluminum alloy housing will allow the advantages and limitations of each solution to be identified and an appropriate configuration to be established according to the specific requirements of electronic devices used in automotive applications.

REFERENCES

Fekiač, J. J., Kakošová, L., Krbata, M., Kohutiar, M., Breznická, A., Mikuš, P., Eckert, M., & Janík, R. (2026). Carbon fibre-reinforced polymer composites for automotive powertrain components: A comprehensive review of material systems, performance requirements, and functional design strategies. *Polymers, 18*(14), 1762. https://doi.org/10.3390/polym18141762

Khan, F., Hossain, N., Mim, J. J., Rahman, S. M., Iqbal, M. J., Billah, M., & Chowdhury, M. A. (2025). Advances of composite materials in automobile applications – A review. *Journal of Engineering Research, 13*(2), 1001–1023. https://doi.org/10.1016/j.jer.2024.02.017

Kim, Y., Kim, S., Kim, D., & Lee, K. (2026). Comparative review of commercialized advanced driver assistance system (ADAS) technologies. *Electronics, 15*(10), 2015. https://doi.org/10.3390/electronics15102015

Saha, A., Kulkarni, N. D., & Kumari, P. (2025). Development of Bambusa tulda-reinforced different biopolymer matrix green composites and MCDM-based sustainable material selection for automobile applications. *Environment, Development and Sustainability, 27*(5), 10655–10691. https://doi.org/10.1007/s10668-023-04327-1

Shah, V., & Patel, H. (2026). Integrating machine learning and computer vision in advanced driver assistance systems: A comprehensive review. *Augmented Human Research, 11*(1), Article 1. https://doi.org/10.1007/s41133-025-00086-y

Slamnoiu-Teodorescu, S., Olteanu, L., Ion, R. M., Gurgu, I. V., & Catangiu, A. (2026). Glass fiber-reinforced polymer matrix composites: Fibers, matrices, manufacturing and applications. *The Scientific Bulletin of VALAHIA University – Materials and Mechanics, 22*(26), 25–32. https://doi.org/10.2478/bsmm-2026-0004

Ur Rehman, S., & Ur Rehman, H. (2026). Sustainable and green composite materials. In L. Li & A. Kondratiev (Eds.), *Fiber-reinforced composites – Characteristics and emerging technologies*. IntechOpen. https://doi.org/10.5772/intechopen.1016186

Yan, L., & Xu, H. (2025). Lightweight composite materials in automotive engineering: State-of-the-art and future trends. *Alexandria Engineering Journal, 118*, 1–10. https://doi.org/10.1016/j.aej.2024.12.002

DOI:10.5937/IIZS26030S

COMPARATIVE STATISTICAL ANALYSIS OF MEASUREMENT RESULTS FOR CYLINDRICAL PART CHARACTERISTICS

Research paper

Sanja Simić[1], Mijodrag Milošević[2], Borislav Savković[3], Branko Štrbac[4], Dejan Božić[5], Dejan Lukić[6]
[1,2,3,4,5,6]University of Novi Sad, Faculty of Technical Sciences, Novi Sad, Serbia

Abstract: This paper aims to present a comparative statistical analysis conducted using two different software programs, Minitab and JASP, highlighting their capabilities, advantages, and limitations. The specific analysis was performed on cylindrical parts by measuring their characteristics with a coordinate measuring machine (CMM) and analyzing referent data using different statistical packages. The study demonstrates how the definition of the measurement task, combined with the shape of the workpiece and the choice of statistical software tool for data processing and analysis, influences the interpretation of output results and the drawing of conclusions. The contribution of this work lies in providing an applied comparative framework for evaluating statistical software in metrology, demonstrating how the choice of software tool can influence result interpretation and decision-making in engineering practice. Based on the analysis conducted, the paper can be used as a guideline for selecting appropriate software depending on the objectives of the statistical analysis.
Key words: Comparative statistical analysis, Coordinate measurement, Cylindricity tolerance, Measurement uncertainty, Design of Experiments, Statistical software tools.

INTRODUCTION

In modern manufacturing, the accuracy and precision of geometric characteristics of workpieces represent key factors for ensuring the quality and functionality of finished products (Genta, 2009; Tešić et al., 2023). The measurement of these characteristics, especially in cylindrical parts which are a common form in mechanical assemblies, requires the application of advanced measuring systems such as coordinate measuring machines (CMM), as well as appropriate statistical data processing. Statistical analysis plays a significant role in drawing conclusions about the correctness and stability of the production process. It plays a key role in detecting deviations, assessing process stability, determining the causes of variation, and validating the production process. In recent decades, there has been a growth in the use of specialized software packages for statistical analysis of measurement data. Minitab has long been used in industrial environments and is recognized for its reliability and ease of use (Pruett, 2009). In contrast, JASP is a relatively new open-source statistical software package that is gaining increasing popularity due to its user-friendly interface and support for advanced statistical analysis methods (JASP Team, 2023). Although both software tools provide similar statistical analysis capabilities, including analysis of variance, normality testing, regression analysis, and descriptive statistics, relatively few studies have focused on comparing the results obtained using these software packages (JASP Verification Project, 2023). Since different statistical packages can generate different results due to different algorithms, settings, approaches to data processing, or limitations in functionality, it is insufficiently explored how closely the results obtained in Minitab and JASP align in engineering applications. However, especially in precise technical analyses such as those in metrology, it is very important to know whether the choice of statistical software affects data interpretation.

The aim of this paper is to provide an answer to this question through the processing of results in both software packages, obtained through experimental analysis and measurements on a CMM. Special focus in the paper is placed on the influence of the software tool on the results of the analysis and the possibilities of interpreting those results. In addition to the introductory part, the following section presents the methodological part

[1]Corresponding author, ssanjaa198@gmail.com
[2]mido@uns.ac.rs
[3]savkovic@uns.ac.rs
[4]strbacb@uns.ac.rs
[5]bozic997dejan@uns.ac.rs
[6]lukicd@uns.ac.rs

which explains the details of the measurement, comparison criteria, and software capabilities. Measurements were performed on real workpieces, and statistical processing was carried out in the mentioned software tools in parallel. Differences in the interpretation of results, user interface, flexibility, and applicability in engineering practice were analyzed. The results and discussion cover a comparative analysis of the results obtained in both software packages. Finally, the conclusion chapter presents key observations, advantages and limitations of both tools, as well as recommendations for future research. The motivation is to highlight, through this paper, the potential risks in the interpretation of statistical results when relying solely on one tool, without additional verification. This emphasizes the importance of combining measurement and statistical methods, as well as the role of software tools in making technical decisions.

MATERIALS AND METHODS

Methodology of conducted research began with defining the measurement strategy and selecting workpieces on which the measurements were performed. Measurements were carried out on a coordinate measuring machine (CMM), enabling high accuracy and precision of the data. The collected measurement data were analyzed in both software packages, Minitab and JASP, using the same statistical methods to ensure a relevant comparison of the results obtained. In addition to specific differences and demonstration of the application possibilities of these programs in appropriate statistical analyses, the research methodology also included an assessment of the user experience when working with the software, as well as the applicability for engineering purposes. Such approaches are commonly applied in manufacturing engineering, where experimental design methods are used for process optimization and parameter selection (Antony, 2014; Kramar et al., 2024).

Description of Measuring Parts

The experimental part of the research was performed on eleven different workpieces shown in Figure 1. These parts were processed using various machining procedures or processed using the same machining procedure but under different machining conditions, resulting in variations in the surface roughness of the machined surfaces. In this way, diversity in the measurement samples was ensured in terms of surface finish quality, which was defined as one of the input factors in the statistical analysis and allows for a more detailed interpretation of the results.



***Fig. 1**. Workpieces used for measurement*

Surface roughness of the workpieces used in the experiment was determined by measurement with a contact measuring device, a profilometer, manufactured by Mitutoyo. This device enables the measurement of surface roughness and waviness by establishing contact between the measuring probe and the measured surface, applying a measuring force, and moving along the measured profile at a constant speed. Figure 2 shows the measured roughness profiles for a cylinder processed by grinding (cylinder 1) and rough turning (cylinder 10).

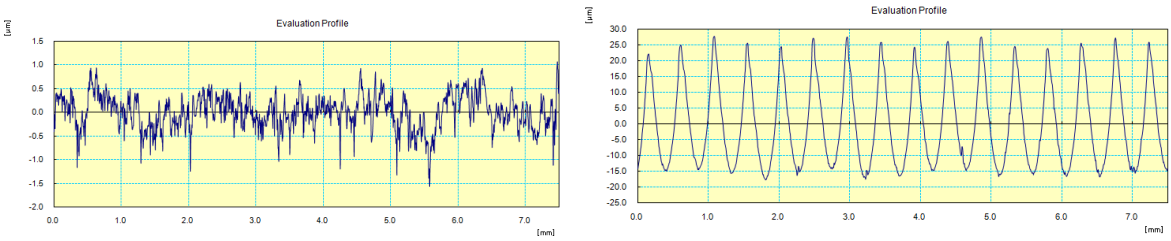


Fig. 2. *Measured surface roughness profiles of cylinders processed by grinding (cylinder 1) and rough turning (cylinder 10)*

Measuring System – CMM

Coordinate measuring systems (CMS) are highly flexible and efficient devices used to control the geometric characteristics of workpieces. Their operation is based on recording the coordinates of points on a workpiece in three-dimensional space to generate accurate measurement results. Coordinate measuring machines enable the assessment of all macro-geometric features on components of various configurations, with measurement ranges extending from micro- to nanometer scale. Due to these capabilities, coordinate measuring machines are widely used in both calibration laboratories and industrial practice (Štrbac, 2021; Hocken & Pereira, 2016; Zaimović-Uzunović et al., 2009).
For the purposes of this study, measurements were performed on a Carl Zeiss Contura RDS coordinate measuring machine. The CMM has a bridge structure. The available measuring range is 1000×1200×600 for the X, Y, and Z coordinates. The RDS head is rotary and can occupy any angle in space, and measurements can be performed in both modes: point-by-point and scanning. The CMM uses Calypso software support, which allows defining complex measurement tasks and performing analyses according to specified parameters.

Definition of the Experiment and Data Collection Strategy

When measuring cylindricity, there are several possible paths that the measuring probe can follow during point sampling, which define different measuring strategies. Among the most used are strategies based on generated lines, circular profiles, grids, point distributions, and spiral paths (Humienny et al., 2001; Weckenmann & Knauer, 1998). For this experiment, a point sampling strategy in the shape of a spiral on the outer diameter of the cylinder was selected, as shown in Figure 3.

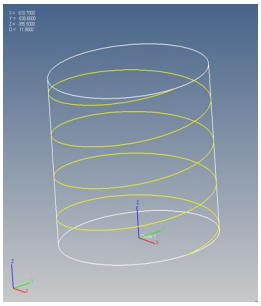


Fig. 3. *Spiral sampling strategy for cylindricity measurement*

The measurement strategy included the following parameters: scanning speed, number of points, diameter of the measuring probe tip, and the application of filters. The characteristics measured were cylindricity and center position. Measurements were performed along a spiral path at three different scanning speeds, and it was carried out both with and without filter application. In experiments where the measured data were filtered, a low-pass Gaussian filter with cutoff wavelengths of λc = 0.8 and λc = 8 was used. The least squares method was used for fitting the substitute geometry, and measurements were performed with three different probe tip diameters. The number of sampled points was also varied at three levels. Figure 4 shows the sampling of measuring points with probe tips of 1 mm and 5 mm diameter.

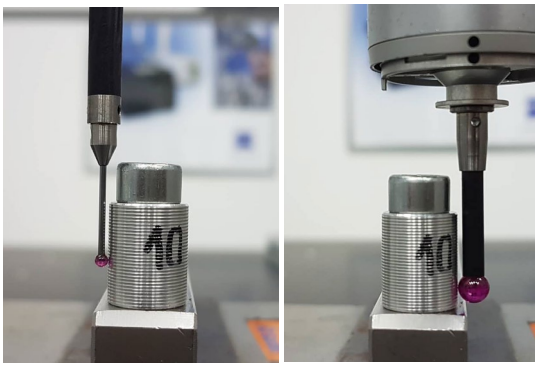


Fig. 4. *Measurement point sampling using 1 mm and 5 mm probe tips*

The Box-Behnken experimental design was used to create the experimental plan. This design was chosen for its efficiency, as it requires fewer experiments for the same number of input factors compared to the central composite design. Another reason for using the Box-Behnken design is the inability to set input parameters at a higher number of levels (Antony, 2014; Myers et al., 2016). Input factors were varied at three levels, with equal intervals between the levels. Input parameters and their levels are listed in Table 1.

Table 1. *- Input factors and their level values*

Input Factors	**Factor Level Values**		
	-1	0	1
Scanning speed - A	10	55	100
Number of points - B	25	75	125
Measuring probe tip diameter - C	1	3	5
Filter - D	no filter; 8	cut off 0.8;	cut off

Software Tools

The choice of software tools for data analysis is crucial, especially in cases where experiments and analyses involve multiple interdependent and influential variables (Kozhanov et al., 2019). In simpler analyses, differences in output results obtained using different software packages may be minimal or negligible. However, in more complex research settings, where multiple factors, interactions, and statistical relationships are considered simultaneously, software becomes the final and potentially decisive link in the data processing chain. Different software tools apply various statistical methods, data fitting models, rounding approaches, outlier handling procedures, as well as criteria for determining the significance of results. These differences, although often technical in nature, can have a significant impact on the final interpretation of results, drawing conclusions, and hypothesis validation. Therefore, software choice is not only a technical issue but also a methodological

one, which must be carefully considered in any serious research relying on statistical analysis. As the number of variables increases and analyses become more complex, differences in algorithms, statistical models, and result interpretation implemented by various software tools can substantially influence the final conclusions.
For the statistical processing of measurement data, this study employed Minitab and JASP, two software tools with differing strengths, to explore how software choice may affect data analysis and interpretation. These software tools may use different approaches for outlier handling, hypothesis testing, selection of statistical tests, and result visualization. Minitab stands out for its ease of use and specialized tools for industrial applications, while JASP, as a free and open-source software package, provides transparent insight into statistical methods but may have limitations regarding the availability of advanced options and flexibility (Alagić, 2021).

Minitab

Minitab is an example of a statistical software package developed primarily to perform statistical analysis with a high degree of numerical accuracy (Alagić, 2021). It is commercial statistical software designed mainly for industrial statistics, Six Sigma methodology, and quality control. It features an easily used interface, powerful tools for regression analysis, ANOVA tests, control charts, and design of experiments (DoE) (Ahmad, 2019). Thanks to its ease of use, Minitab is particularly suitable for users in industrial environments, as it does not require deep statistical knowledge while providing reliable data analysis. This software requires a paid license, which can be a limitation for academic and research institutions. Additionally, although it covers a wide range of standard methods, it does not include some advanced techniques offered by other software, such as Bayesian statistics.

JASP

JASP is free, open-source software developed by the University of Amsterdam with the aim of making statistical analysis more accessible and transparent, especially in academic contexts. Unlike Minitab, JASP supports Bayesian statistics, which makes it suitable for modern approaches to data analysis (van den Bergh et al., 2023; Love et al., 2019; Kelter, 2020). One of the key advantages of this software is its ability to automatically generate easy-to-read tables, charts, and analysis results, thereby significantly saving time in data processing (JASP Verification Project, 2023). JASP supports commonly used statistical methods such as t-tests, ANOVA, regression analysis, factor analysis, and correlations. However, JASP has a limited selection of methods for advanced analyses such as nonlinear regressions, structural models, and similar techniques. Additionally, JASP exhibits lower stability and longer processing times when handling large datasets, and it has certain limitations in flexibility regarding script implementation and automation of the analysis process.

Criteria for Comparative Analysis

In order to conduct a relevant comparative analysis, based on practical work with the software as well as insights from available literature, criteria were defined that include various aspects of their functionality, availability, and applicability. The analysis is based on the following criteria:

- Licensing and availability,
- Selection of statistical methods,
- User interface and accessibility,
- Data visualization,
- Flexibility of the software package.

Based on these criteria, a comparative analysis of both software packages will be presented below, with particular emphasis on their advantages and limitations in the context of application in experimental research and measurement data processing.

RESULTS AND DISCUSSION

This chapter presents and analyzes the results of statistical data processing obtained from the previously described measurements. The primary goal of the analysis is to examine the extent to which the choice of statistical software affects the interpretation of measurement results, as well as to identify potential differences in data presentation, processing, and interpretation (Wake et al., 2022). Analysis includes specific statistical methods and visualizations, such as regression analysis, residual analysis, scatter plots, Q-Q plots, and response surface diagrams.
Experiment was conducted following the Box-Behnken design, with a total of 45 measurements performed for each workpiece, covering different combinations of input factor levels. During each measurement, the cylindricity, as well as the X and Y coordinates of the workpiece center, were recorded.
Initial analysis of the results was conducted using Minitab 17, focusing on basic statistics and graphical presentations to identify potential patterns, deviations, and the influence of input parameters. Subsequently, the data were also analyzed with JASP software to enable comparison and derive fundamental statistical conclusions.

Deviation Analysis of Cylindricity

Figure 5 shows boxplot diagrams of cylindricity deviation for eleven workpieces, obtained using different software tools. The purpose of the presentation is to identify differences in the distribution of measurement data and to assess the impact of the software on the output results.
Similar distribution trend was observed in both software tools; the lowest median deviation value was identified for cylinder 1, cylinder with the finest surface finish, while the largest deviation was observed for cylinder 11, cylinder with the roughest surface. In both software packages, results indicate that increased surface roughness contributes to greater deviation from geometric tolerance. Therefore, in both cases, pronounced variability of results is visible for the cylinder with the rough surface, while data for cylinders with fine surfaces are significantly more stable. Such analysis is useful for assessing the impact of surface finish quality on measurement results, and the software tool that provides clearer and more informative visualization can play a decisive role in analyzing results and drawing conclusions.

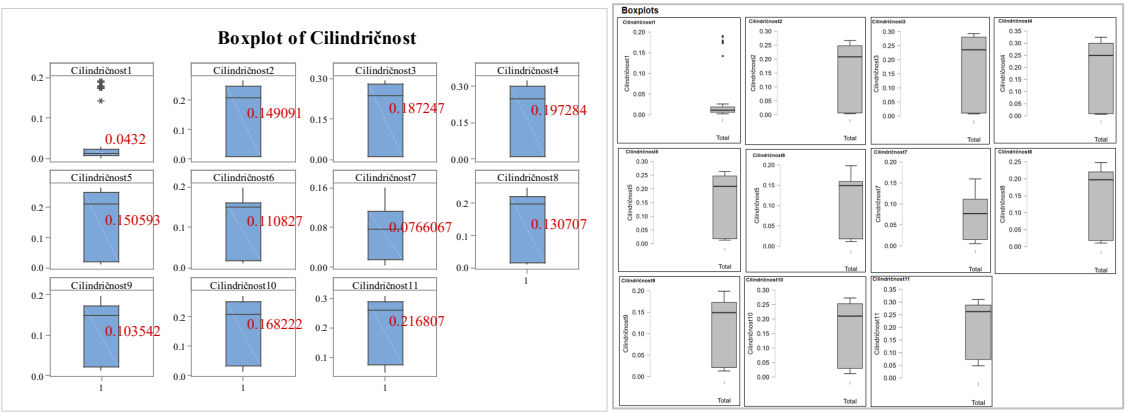


Fig. 5. *Boxplot diagram of cylindricity deviation – Minitab vs. JASP*

Visual presentations in software differ in the way of interpretation:

- Minitab provides additional information through numerical labeling of mean values directly on the diagram.
- JASP displays mean values in the tabular section, but not on the diagram itself.
- Clear depiction of isolated values (e.g., cylinder 1) is present in both software packages.
- JASP shows unique scales for each diagram, while Minitab often uses graphs with the same scale for all diagrams.

In this specific case, Minitab proved to be more suitable for visual analysis and comparison of all workpieces due to its built-in features that automatically display mean values and use a unified scale across all workpieces, which facilitates comparison. However, if a specific analysis of an individual workpiece were desired, JASP would be more appropriate.

Analysis of center position deviation

Based on the statistical analysis conducted and the results shown in Figure 6, the measured values of the center coordinates of the workpieces fall within approximately the same range, exhibiting similar deviations. This indicates that choice of software did not affect the actual output results, but only the way they were visually interpreted.

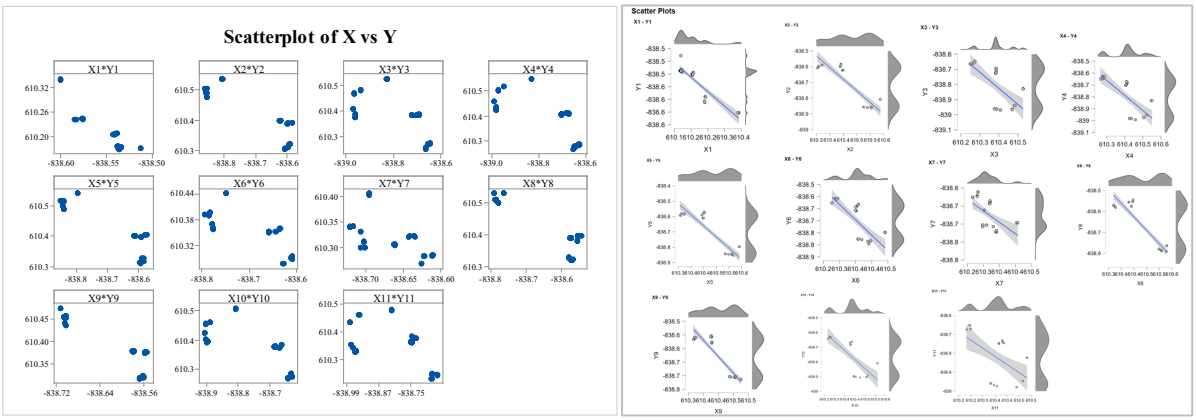


Fig. 6. *Centre position deviation – Minitab vs. JASP*

Visual presentation of data highlighted the following differences between the software:

- Minitab provides a Scatter plot display for all samples through a quick and clear visualization; however, the graphical output automatically generated by Minitab is less detailed. In addition to this basic view, Minitab allows enabling additional options for more detailed visualization.
- JASP displays individual Scatter plots with added regression lines and confidence intervals, giving a clearer picture of the strength of relationships between variables. The displays are more detailed and automatically generated, but the relationships are created and viewed individually.

Therefore, visualization generated in Minitab is suitable in cases where the goal is to present the overall relationship between variables, that is, the general structure of the data and overall correlations. However, JASP is more appropriate when a more detailed analysis of individual relationships is required, allowing for in-depth examination of the connections between specific variables.

Analysis of Results for Cylinder 1

To ensure a more concise presentation of results, this paper presents analysis for only one representative cylinder. Cylinder 1 was selected as the sample for result presentation due to its specific characteristics related to surface machining. This workpiece has the lowest arithmetic average roughness value, was finished using fine grinding, and has a surface quality grade of N5. For this reason, it is the most difficult to detect deviations and assess the influence of input factors on output characteristics. Cylinders with rougher surfaces exhibit greater deviations and wider variations in the output results. To further highlight the influence of surface roughness and machining method on the output results, this section concludes with 3D response surface diagrams for both the smoothest and the roughest cylinders. Since JASP does not directly support the generation of these diagrams, they were created using Minitab, thereby also illustrating the capabilities and limitations of both software tools in the context of this specific analysis.

Residual Analysis

To assess the accuracy of the model and identify deviations from expected values, a residual analysis was performed (Fox, 2015; Hand, 2014). This step is essential for validating the model and detecting potential imperfections. Residuals represent the differences between the actual measured values and the values predicted by the model. Figure 7 shows results of residual analysis in both software tools.

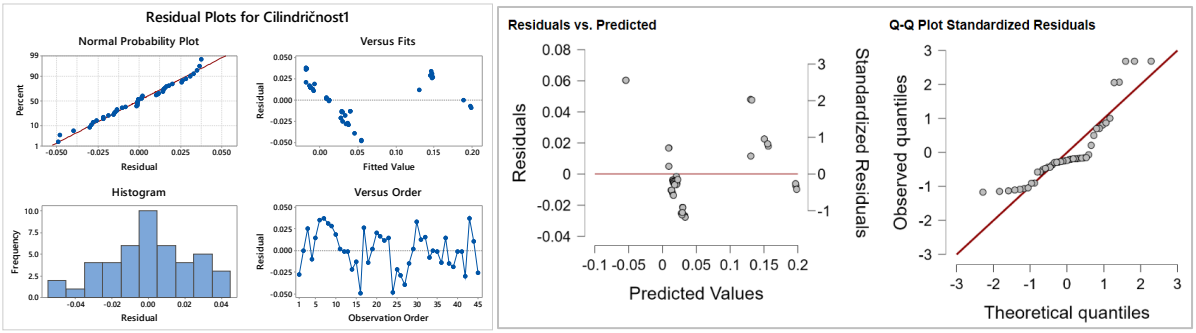


Fig. 7. *Residual analysis for Cylinder 1 – Minitab vs. JASP*

Residual analysis results indicate consistent conclusions across both software tools. The normal probability plot in Minitab shows that most of the observed values follow the expected line of normal distribution, with minor deviations at the tails of the plot, i.e., in the extreme values. A similar conclusion is supported by the Q-Q plot in JASP, where the standardized residuals largely follow the theoretical distribution line, with slight deviations at the ends. Based on this, it can be concluded that the residuals are approximately normally distributed, which confirms the validity of the applied model.

The residual histogram in Minitab further emphasizes the nearly symmetric distribution of values. The analysis in both software tools shows that most residuals fluctuate around zero, without a noticeable systematic trend, although some individual local deviations are evident. These deviations may indicate the influence of specific measurement points or machining processes.

One advantage of Minitab is its ability to display residuals in relation to the order of measurement, allowing the observation of fluctuations without a clear trend that would indicate a process error. JASP, however, offers a simpler and cleaner standardized residual plot, making it easier to detect deviations from expected values.

Overall, the results obtained in the software packages are largely consistent. Both software tools confirm that the model adequately describes the process, with Minitab allowing more

detailed analysis through a greater number of graphical outputs. Conversely, JASP provides clearer and more accessible visualizations of standardized deviations. It can be concluded that both software packages validate the reliability of the obtained results, with differing strengths in terms of visualization and analytical detail.

Analysis of the Influence of Input Parameters on Measurement Results

In this analysis, influence of four key input factors on the measurement results was examined: scanning speed, filter application, probe tip diameter, and number of points. Understanding the impact of these parameters on the output results is crucial for optimizing the measurement process and the accuracy of the obtained data. The effects of each parameter were analyzed, allowing for the identification of potential areas for improvement in the measurement process.

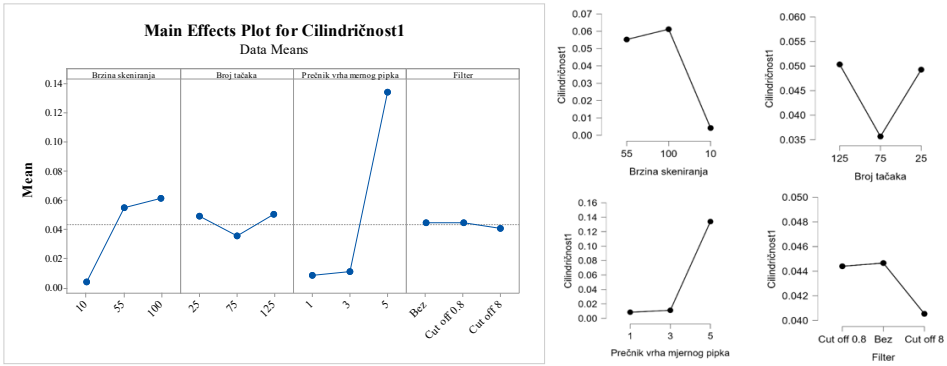


Fig. 8. *Main Effects – Minitab vs. JASP*

In Minitab, as shown in Figure 8, all main effects are presented in a single combined plot, allowing for direct comparison. Diagram indicates a pronounced influence of the probe tip diameter and scanning speed on the cylindricity tolerance. The cylindricity deviation significantly increases when using the largest probe tip diameter and the lowest scanning speed. Other factors, such as the number of points and filtering, show less significant effects. In JASP, as shown in the same picture, each factor is presented in an individual plot, which allows for better clarity when analyzing the influence of each factor separately. Observed trends are fully consistent with the results from Minitab, the cylindricity deviation increases with use of larger probe tip diameters, and greater deviation is also recorded at the lowest scanning speed. The lowest cylindricity deviation was achieved by applying a filter with a cutoff wavelength of λc = 8, while the number of points shows minimal influence, with a slight effect observed at the medium point count. Analysis identified the most dominant factors, probe tip diameter and scanning speed, leading to a more detailed analysis of their effects in the following subsection. Results obtained in both software packages are consistent, with the main difference being in the format of the visualization. Minitab allows for complete visualization of all factors and easier comparison between them, while JASP offers a more detailed display of each individual variable, which can be useful for analyzing specific effects.

3D Response Surface Plot

Response surface plots were generated to visually present the relationship between input factors and the output characteristics of the processing operation. The use of 3D visualization allows for easier observation of interactions between variables and identification of regions where optimal results are achieved (Feng et al., 2007). For the analysis, two representative samples were selected: Cylinder 1, with the finest surface finish, and Cylinder 11, with the roughest. The comparative presentation of the plots provides insight into how surface quality and changes in input factors affect the sensitivity of output parameters.

As previously noted, JASP lacks support for DoE and advanced modeling, which includes 3D response surface generation. This is consistent with previous findings indicating that, while JASP is user-friendly and transparent, its functionality remains partially limited when it comes to complex statistical methods (Love et al., 2019). Minitab is also quite a closed system regarding the analysis of data beyond the standard framework, so its use can sometimes be limited when working with non-standard data formats because it does not always allow extensibility and full control over the analysis. Similar observations regarding the advantages and limitations of statistical software tools in quality control have been noted in comparative studies of other platforms as well (Kozhanov et al., 2019).

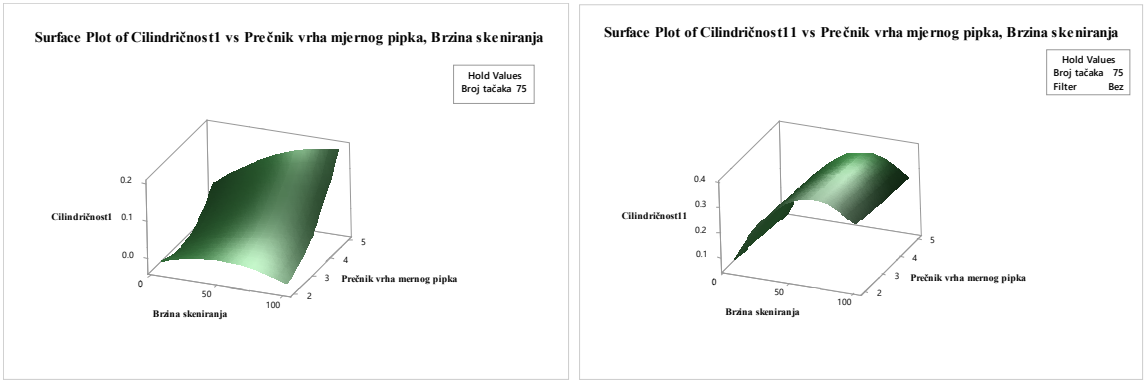


Fig. 9. *Response surface plot – Cylinder 1 vs. Cylinder 11*

In the case of Cylinder 1, the response surface shows a relatively flat trend, indicating lower sensitivity of the measurement process to changes in input parameters. The highest level of cylindricity deviation is observed at the combination of low scanning speed and large probe tip diameter, while at higher speeds and smaller diameters, the results appear more stable. These results are justified considering the more precise surface treatment method used.
For Cylinder 11, the response surface plot shows a more pronounced curvature, with higher values of cylindricity deviation and greater variability in relation to the same factors. The response surface also indicates greater system sensitivity to changes in input parameters, which aligns with the nature of rough machining such as turning. This highlights the need for more precise control of measurement parameters when assessing dimensional accuracy for such processed surfaces. While grinding results in more stable geometric accuracy and less sensitivity to measurement, rough turning exhibits greater variation requiring additional metrological attention.

CONCLUSION

This study presents a comprehensive comparison of statistical results from measurements of cylindricity deviation and center coordinates of workpieces, aiming to evaluate how the choice of software influences the interpretation of measurement data and the drawn conclusions. The results indicate that the choice of software did not affect the actual output values; key statistical results and trends showed consistency regardless of the software used. However, the manner of visual presentation, available functionalities, and the flexibility of the software environment significantly influence the analysis workflow and result interpretation. JASP does not directly support the creation of response surface models, which can be crucial for process optimization in engineering applications. Additionally, this software offers limited support for Design of Experiments (DoE), which is a significant drawback in technical research. Due to these limitations, JASP was primarily used in this work for enhanced visualization in specific areas of statistical processing, while advanced experimental modeling and analysis methods were conducted using Minitab. Otherwise, especially in the early stages of research, JASP can be more accessible in terms of usability, as it is visually adapted, accessible, and unlike Minitab, provides automatic generation of detailed analyses of individual effects through separate graphs.

In conclusion, analysis has shown that Minitab and JASP differ significantly in terms of accessibility, available features, and suitability for specific types of statistical tasks. JASP as free and open-source tool makes it more accessible for students and researchers. Its clear interface and ease of use support quick execution of basic statistical analyses and visualizations. However, its capabilities are limited when it comes to more advanced procedures, such as experimental design and response surface modeling, which reduces its usefulness in engineering contexts. Minitab, by contrast, includes a broader range of tools designed for more complex analyses. It supports experimental design, advanced visualization of residuals, and modeling of multi-factor systems, which makes it better suited for industrial and technical applications. Still, its closed system and higher learning curve can pose challenges, especially when dealing with unusual data formats or when more flexibility is needed in data handling. The comparison suggests that the choice between these programs should be guided by the specific goals of the analysis, the complexity of the data, and the user's level of experience. The combination of both tools can significantly enhance the quality of the analysis and decision-making. The combined use of both software tools in this study achieved a balance between complexity, clarity and individual analytical detail. JASP provided a basic and visually clear analysis, while Minitab enabled the execution of more advanced statistical procedures and process modeling.

Future research should include expanding the analysis through additional software tools (e.g., R, Python) to achieve greater flexibility, extensibility, and potential integration of machine learning methods.

ACKNOWLEDGEMENT

This research has been supported by the Ministry of Science, Technological Development and Innovation (Contract No. 451-03-34/2026-03/200156) and the Faculty of Technical Sciences, University of Novi Sad through project "Scientific and Artistic Research Work of Researchers in Teaching and Associate Positions at the Faculty of Technical Sciences, University of Novi Sad 2026" (No. 01-3609/1).
The paper is part of the research project of the Department of Production Engineering of the Faculty of Technical Sciences in Novi Sad for the year 2026, entitled "Trends in Production Engineering".

REFERENCES

Antony, J. (2014). Design of experiments for engineers and scientists (2nd ed.). Elsevier.

Ahmad, A. (2019). Use of Minitab statistical analysis software in engineering technology. Proceedings of the 2019 ASEE Annual Conference & Exposition.

Alagić, I. (2021). Minitab application as statistical tool for Lean Six Sigma. In I. Karabegović (Ed.), New technologies, development and application IV (Vol. 233). Springer.

Feng, C. X. J., Saal, A. L., Salsbury, J. G., Ness, A. R., & Lin, G. C. S. (2007). Design and analysis of experiments in CMM measurement uncertainty study. *Precision Engineering*, 31(2), 94-101.

Fox, J. (2015). Applied regression analysis and generalized linear models (3rd ed.). SAGE Publications.

Genta, G. (2009). Introduction to metrology. Springer.

Hand, D. J. (2014). Statistics: A very short introduction. Oxford University Press.

Hocken, R. J., & Pereira, P. H. (2016). Coordinate measuring machines and systems (2nd ed.). CRC Press.

Humienny, Z., Osanna, P. H., Tamre, M., Weckenmann, A., Blunt, L., & Jakubiec, W. (2001). Geometrical product specification. Course for Technical Universities.

JASP Team. (2023). JASP (Version 0.17.2) [Computer software]. https://jasp-stats.org

JASP Verification Project. (2023). Comparison of statistical outputs across software. https://jasp-stats.github.io

Kelter, R. (2020). Bayesian alternatives to null hypothesis significance testing in biomedical research: A non-technical introduction to Bayesian inference with JASP. *BMC Medical Research Methodology,* 20(1), 1-12. https://doi.org/10.1186/s12874-020-00980-6

Kozhanov, A., Kozhanova, A., & Sorokina, N. (2019). Comparative analysis of software for the study of statistical methods of control of product quality. IOP Conference Series: Materials Science and Engineering, 537, 042015.

Kramar, D., Sekulić, M., Rodić, D., & Pejić, V. (2024). Optimizing main cutting force in high-pressure jet-assisted turning using Taguchi method. *Journal of Production Engineering*, 27(1), 1–4. https://doi.org/10.24867/JPE-2024-01-001

Love, J., Selker, R., Marsman, M., Jamil, T., Dropmann, D., Verhagen, J., Ly, A., Gronau, Q. F., Šmíra, M., Epskamp, S., Matzke, D., Wild, A., Knight, P., Rouder, J. N., & Morey, R. D. (2019). JASP: Graphical statistical software for common statistical designs. *Journal of Statistical Software,* 88(2), 1-17. https://doi.org/10.18637/jss.v088.i02

Myers, R. H., Montgomery, D. C., & Anderson-Cook, C. M. (2016). Response surface methodology: Process and product optimization using designed experiments (4th ed.). Wiley.

Pruett, R. M. (2009). Quality improvement with Minitab. Wiley.

Štrbac, B. (2021). Procena merne nesigurnosti koordinatnih mernih mašina. Fakultet tehničkih nauka.

Tešić, S., Jotić, G., Čiča, Đ., Sredanović, B., Štrbac, B., & Ranisavljev, M. (2023). Assessing the precision of machine tools through various measurement systems. *Journal of Production Engineering, 26(2),* 18-22. https://doi.org/10.24867/JPE-2023-02-018

van den Bergh, D., Wagenmakers, E. J., Aust, F., Haaf, J. M., Hoekstra, R., & Wetzels, R. (2023). Bayesian repeated-measures analysis of variance: An updated methodology implemented in JASP. *Advances in Methods and Practices in Psychological Science,* 6(2), 1-20.

Wake, A. G., Abatan, S. M., & Olayemi, M. S. (2022). The role of statistical software in data analysis. *International Journal of Applied Research and Studies,* 3(8), 1-15.

Weckenmann, A., & Knauer, M. (1998). The influence of measurement strategy on the uncertainty of CMM measurements. CIRP Annals, 47.

Zaimović-Uzunović, N., Lemeš, Z., Denjo, D., & Softić, A. (2009). Proizvodna mjerenja. Univerzitet u Zenici.

DOI:10.5937/IIZS26042R

EVALUATING PARAMETRIC LINEAR AND INTERACTION MODELS FOR COMPRESSIVE STRENGTH ESTIMATION OF HIGH-PERFORMANCE CONCRETE

Research paper

Miroslav Radomirović[1*], Tatijana Vasiljević[2], Predrag Petronijević[3]
[1,2]Faculty of Technical Sciences, University of Pristina, Kosovska Mitrovica, Serbia,
[3]Faculty of Civil Engineering, University of Belgrade, Belgrade, Serbia

Abstract: Accurate prediction of High-Performance Concrete (HPC) compressive strength is essential for optimizing mix formulations, ensuring structural reliability, and advancing sustainable construction practices. Traditional mix design relies on exhaustive, trial-and-error laboratory testing that consumes substantial material volumes. By minimizing physical mix iterations, predictive modeling directly lowers cement consumption and reduces associated construction-related CO_2 emissions.
This paper presents a dedicated parametric linear modeling framework, evaluating Simple Linear Regression (SLR), Multiple Linear Regression (MLR), and Polynomial Interaction Models, for estimating HPC compressive strength across an experimental dataset of samples (4.10 to 291.00 MPa). Single-variable linear models demonstrate weak predictive precision ($R < 0.36$, MAPE > 35 %), underscoring that individual constituents cannot account for overall strength development. Transitioning to Multiple Linear Regression incorporates all mix ingredients simultaneously, while the introduction of multi-variable polynomial interaction terms significantly enhances precision by capturing synergistic cross-product effects between key binders, water content, and curing age.
The primary practical advantage of this linear approach lies in yielding explicit, closed-form mathematical equations. Unlike complex, non-parametric "black-box" systems, these transparent linear formulas provide structural engineers with straightforward, immediately applicable tools for site quality control, material optimization, and rapid strength estimation.
Key words: High-Performance Concrete, Compressive Strength, Parametric Linear Models, Multiple Linear Regression, Interaction Equations, Explicit Formulas.

INTRODUCTION

Concrete is the most widely consumed man-made material globally, serving as the literal foundation of modern civilization and global infrastructure. It is estimated that approximately 30 billion tons of concrete are consumed each year, nearly three times the volume used 40 years ago, highlighting its unmatched dominance in the construction sector (Monteiro et al., 2017). The scale of its usage makes the concrete industry one of the largest raw material consumers on the planet, driven by rapid urbanization, population growth, and extensive infrastructure development, particularly in developing regions and transitional societies. However, designing high-strength concretes introduces a significant environmental paradox. To achieve an extremely dense microstructure and exceptional compressive strength, these advanced cementitious mixtures require a drastically higher volume of binder compared to conventional concrete. Between 0.66 and 0.82 kg of CO_2 emissions are generated for each kilogram of cement produced, representing approximately 7% of global anthropogenic CO_2 emissions (Aprianti et al., 2015). While standard structural concrete consumes between 300 and 350 kg/m^3 of cement (Kherraf et al., 2022), high-performance mixtures demand substantially higher concentrations. This excessive cement consumption not only escalates material costs but also significantly amplifies the carbon footprint of the concrete, given that a large portion of cement grains often remains unhydrated due to low water-to-binder ratios. To address this challenge, the modern concrete industry increasingly relies on supplementary cementitious materials (SCMs), many of which are industrial and agricultural by-products. The database analyzed in this study incorporates several of these sustainable alternatives, including silica fume, fly ash, ground granulated blast-furnace slag (GGBFS), slag amount, glass powder, and rice husk ash (Malik et al., 2025). While these alternative materials have been explored in conventional concrete, their integration into explicit predictive equations

[1]Corresponding author, miroslav.radomirovic@pr.ac.rs, ORCID: 0009-0004-8623-447X
[2]tatijana.vasiljevic@pr.ac.rs, ORCID: 0009-0008-5187-1937
[3]pecap@grf.bg.ac.rs, ORCID: 0000-0002-8688-6898

specifically tailored for High-Performance Concrete (HPC) remains relatively scarce in foundational research (Chou et al., 2011; Erdal et al., 2012; Liu, 2022; Yeh, 1998). When incorporated into HPC mixtures, SCMs undergo pozzolanic reactions with calcium hydroxide, transforming it into additional strength-giving calcium silicate hydrate (C-S-H) gel. This refines the pore structure and enhances long-term compressive strength while significantly reducing ordinary Portland cement content, diverting waste from landfills and lowering manufacturing carbon emissions. While some of these supplementary materials may not individually exert a dominant simple linear influence on final compressive strength, their inclusion remains vital for overall mixture performance. In HPC, these by-products act synergistically to improve particle packing density, modify rheological properties, and enhance durability. Because these constituents interact simultaneously, capturing their combined behavior requires multi-variable linear frameworks. This paper focuses strictly on explicit parametric linear regression and polynomial interaction models. By deriving closed-form mathematical equations, this approach provides structural engineers with transparent, simple, and immediately applicable formulas for site quality control, balancing predictive transparency with sustainable industrial practice.

MATERIAL AND METHODS

Dataset and Feature Selection

The reliability and generalization capability of any data-driven predictive framework depend fundamentally on the quality, diversity, and scale of the underlying experimental dataset. In this study, a comprehensive experimental database consisting of 674 high-performance and ultra-high-performance concrete samples was utilized to calibrate and validate explicit parametric linear models. This extensive dataset was sourced from the global repository compiled by Malik et al. (2025). By aggregating records from this globally recognized database of concrete laboratory tests, the dataset captures a broad spectrum of advanced mixture designs, curing conditions, and compressive strength variations.

It is important to note that while the original repository compiled by Malik et al. (2025) contains a multi-dimensional matrix with a large number of parameters, chemical indexes, and raw experimental annotations, this study purposefully restricts the input matrix to 16 optimized physical and chemical variables. Furthermore, to eliminate specimen shape and size effects from the structural modeling process, the experimental dataset was strictly filtered to include exclusively cubic specimens with dimensions of 50 × 50 × 50 mm. By isolating this uniform geometry, geometric variability was eliminated, ensuring that variations in compressive strength reflect purely the chemical composition, mix proportions, and curing kinetics of the concrete. Incorporating an excessive number of low-impact or collinear variables can introduce multi-collinearity issues, increase matrix instability, and reduce the numerical interpretability of closed-form regression coefficients. Therefore, a feature selection process was conducted to isolate the 16 most influential descriptors that directly dictate cement hydration kinetics and strength development, aligning with established HPC modeling methodologies (Yeh, 1998; Chou et al., 2011).

This chosen subset features essential chemical admixtures, specifically superplasticizer dosage, and the structural curing timeframe, alongside primary binders, supplementary cementitious materials, sustainable fillers, and aggregates. By utilizing this refined 16-variable configuration, the formulation of explicit Simple Linear Regression (SLR), Multiple Linear Regression (MLR), and Polynomial Interaction Models is optimized, ensuring that all primary physical and chemical variables governing high-strength concrete behavior are accurately represented in clear, closed-form mathematical equations. To provide a comprehensive overview of the analytical scope, the fundamental statistical metrics for the numerical features within the refined 16-variable dataset are presented in Table 1. These metrics, including the minimum, maximum, mean, and standard deviation, define the physical limits and operational boundaries of the experimental dataset used to formulate and validate the explicit parametric regression models.

Table 1. *Statistical Metrics for Numerical Features of the Dataset*

	Max.	Min.	Mean	St. Dev.	Q1	Q2	Q3	IQR
Cement	1213.70	170.00	778.91	183.80	663.00	801.00	903.00	240.00
Silica Fume	374.00	0.00	173.58	74.58	128.00	197.10	222.75	94.75
Fly Ash	700.00	0.00	69.64	158.36	0.00	0.00	92.31	92.31
Limestone Powder	397.00	0.00	9.49	46.44	0.00	0.00	0.00	0.00
Quartz powder	302.00	0.00	42.60	89.81	0.00	0.00	0.00	0.00
Glass powder	1023.34	0.00	75.61	180.56	0.00	0.00	0.00	0.00
Rice husk ash	481.06	0.00	2.68	25.23	0.00	0.00	0.00	0.00
GGBFS	750.00	0.00	37.91	138.02	0.00	0.00	0.00	0.00
Slag Amount	1100.00	0.00	3.26	59.88	0.00	0.00	0.00	0.00
Filler	1050.00	0.00	60.10	146.60	0.00	0.00	0.00	0.00
Amount Sand	1912.00	0.00	908.98	270.85	867.10	954.50	1015.38	148.28
Quantity of Fiber	390.00	0.00	70.06	79.41	0.00	20.00	156.00	156.00
Amount water	334.00	125.00	194.45	35.32	170.00	187.00	214.85	44.85
Amount superplasticizer	96.00	2.64	28.20	16.72	13.00	22.42	44.50	31.50
Age days	90.00	1.00	28.13	22.45	7.00	28.00	28.00	21.00
Strength	291.00	4.10	142.46	47.62	114.00	142.00	171.00	57.00

To comprehensively assess the generalization characteristics and predictive accuracy of the proposed parametric linear and interaction models, the experimental dataset (N = 674) was randomly partitioned into training and testing subsets, comprising 80% and 20% of the total data, respectively. The training subset was utilized to determine the explicit regression coefficients via ordinary least squares estimation, while the independent test dataset was reserved strictly for out-of-sample validation to prevent overfitting and ensure real-world applicability.

Model Evaluation and Performance Metrics

The predictive precision of each mathematical model was systematically evaluated on the test set using a balanced combination of two absolute and two relative performance metrics. Absolute error metrics, specifically Root Mean Square Error (RMSE) and Mean Absolute Error (MAE) were employed to quantify the magnitude of prediction residuals directly in the target variable's physical units (MPa).

$$RMSE = \sqrt{\frac{1}{N}\sum_{i=1}^{N}(r_i - o_i)^2} \quad (1)$$

r_i -represents the real strength

o_i -output model strength

$$MAE = \frac{1}{N}\sum_{i=1}^{N}|r_i - o_i| \quad (2)$$

Concurrently, relative metrics namely Mean Absolute Percentage Error (MAPE) and the Pearson correlation coefficient (R) were calculated to assess percentage-based deviations and the linear strength of agreement between experimental measurements and closed-form model estimates.

$$R = \sqrt{\left[\sum_{i=1}^{N}(r_i - \bar{r})(o_i - \bar{o})\right]^2 \cdot \left[\sum_{i=1}^{N}(r_i - \bar{r})^2\,(o_i - \bar{o})^2\right]^{-1}} \quad (3)$$

R quantifies the strength of linear fit on a scale from -1 to +1.

$$MAPE = \frac{100\%}{N}\sum_{i=1}^{N}\left|\frac{r_i - o_i}{r_i}\right| \quad (4)$$

Single and Multiple Linear Regression

In its foundational form, a simple linear model assumes that the target variable is driven by only one isolated independent factor X.

$$f_c' = \beta_0 + \beta_1 X_{\,i} + \in \quad (5)$$

f_c' represents the predicted compressive strength (MPa)
β_0 is the intercept, β_1 is the regression coefficient
X_i corresponds to the specific component concentration (kg/m^3).

While highly intuitive, this approach operates under a massive oversimplification. In real-world engineering and materials science, variables never act in isolation. Trying to predict a complex property like concrete strength solely based on one component (such as water content) yields highly inaccurate results because the model is forced to lump all other critical factors into the residual error term.
To capture the true complexity of a system, the simple model is expanded into Multiple Linear Regression (MLR). Instead of looking at a single factor, the model uses an entire vector of inputs simultaneously.

$$f_c' = \beta_0 + \beta_1 X_1 + \beta_2 X_2 + \cdots + \beta_n X_n + \in \quad (6)$$

Polynomial Interaction Model

To address the inherent non-linear behavior of concrete hydration without sacrificing mathematical transparency, the Multiple Linear Regression (MLR) framework is extended into a Polynomial Interaction Model. Polynomial terms capture the non-linear response curves of individual variables (e.g., curing age or binder dosage), whereas interaction terms capture how the combined effect of two or more variables changes dynamically across different concentration levels. In High-Performance Concrete (HPC), polynomial interaction terms are essential for modeling synergistic mechanisms. To illustrate, a complete second-degree (quadratic) polynomial regression model with full interaction terms for two predictor variables (X_1 and X_2) is formulated as follows:

$$f_c' = = \beta_0 + \beta_1 X_1 + \beta_2 X_2 + \beta_3 X_1^2 + \beta_4 X_2^2 + \; + \beta_5 (X_1 \cdot X_2) + \beta_6 (X_1^2 \cdot X_2) + \epsilon \quad (7)$$

RESULTS AND DISCUSSION

To evaluate the baseline predictive capacity of individual mixture components, initial regression analyses were performed using isolated single-variable models. Specifically, Silica Fume dosage and Water content were selected for detailed single-variable evaluation because they represent opposing fundamental physical behaviors within concrete technology: Silica Fume demonstrates a overall positive correlation (Fig 1.), whereas Water content exhibits negative impact as dosage increases (Fig 2.). The individual predictive accuracy parameters for the standalone linear models of Silica Fume and Water are summarized in Table 2.

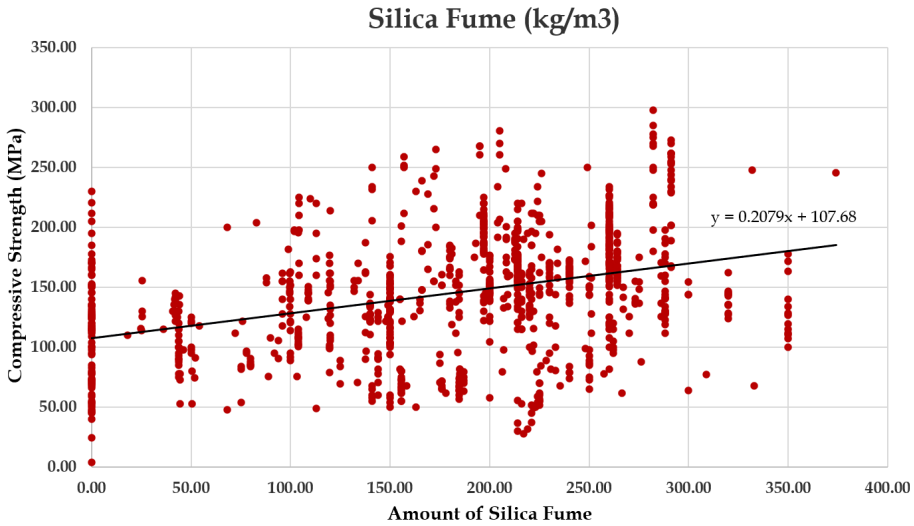


Fig. 1. *Simple Linear Regression: Compressive Strength vs. Silica Fume Content*

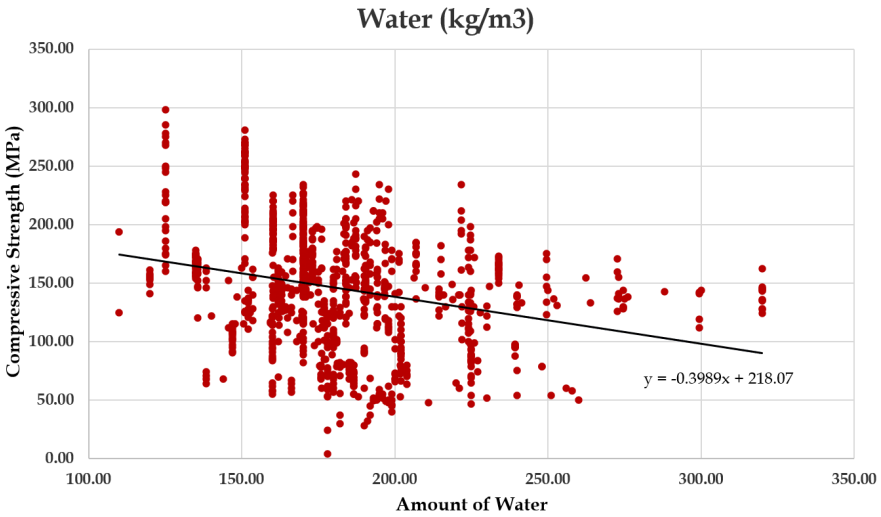


Fig. 2. *Simple Linear Regression: Compressive Strength vs. Water Content*

Table 2. *Performance Comparison of Isolated Single-Variable Regression Models*

Silica Fume		Water	
RMSE	46.55	RMSE	47.97
MAE	36.14	MAE	38.73
R	0.3587	R	0.2728
MAPE	35.66%	MAPE	39.15%

To address the limitations of standalone single-variable models, the entire 17-variable vector was integrated into a Multiple Linear Regression (MLR) framework. The predictive performance is illustrated in Fig. 3, while the quantitative evaluation metrics are detailed in Table 3. Based on the feature significance and regression sensitivity analysis, the initial set of 17 input variables was refined down to 11 statistically key predictors. Eliminating low-impact and redundant variables enhanced the stability of the model without compromising predictive accuracy. The regression coefficients corresponding, tested also with importance to the parameters are shown in Fig. 4.

Table 3. *Evaluation metrics*

RMSE	35.85
MAE	28.11
R	0.7020
MAPE	25.17%

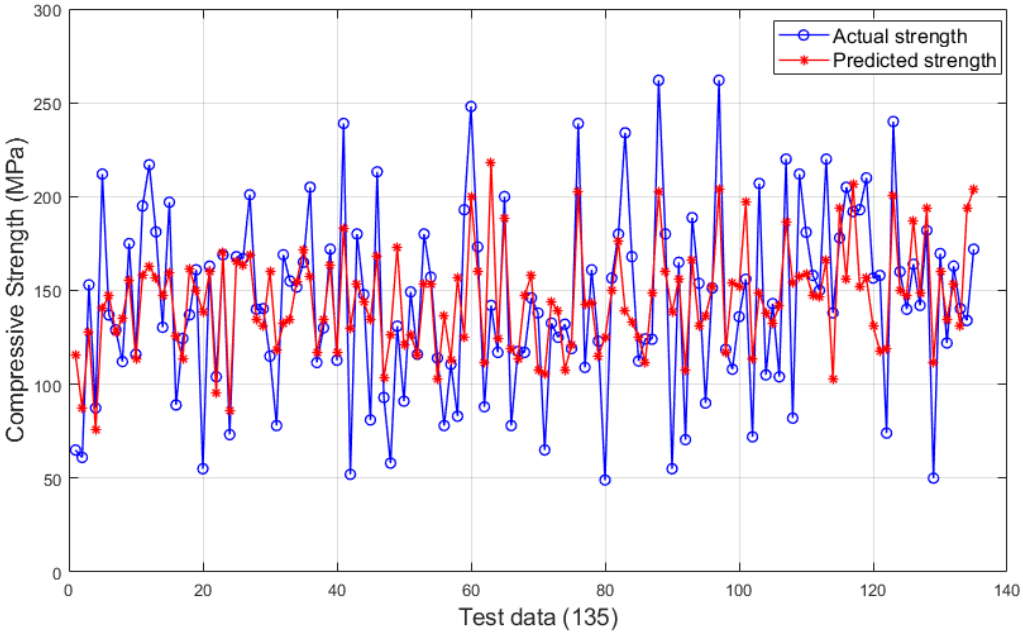


Fig. 3. *Experimental vs. Predicted Compressive Strength across Test Samples*

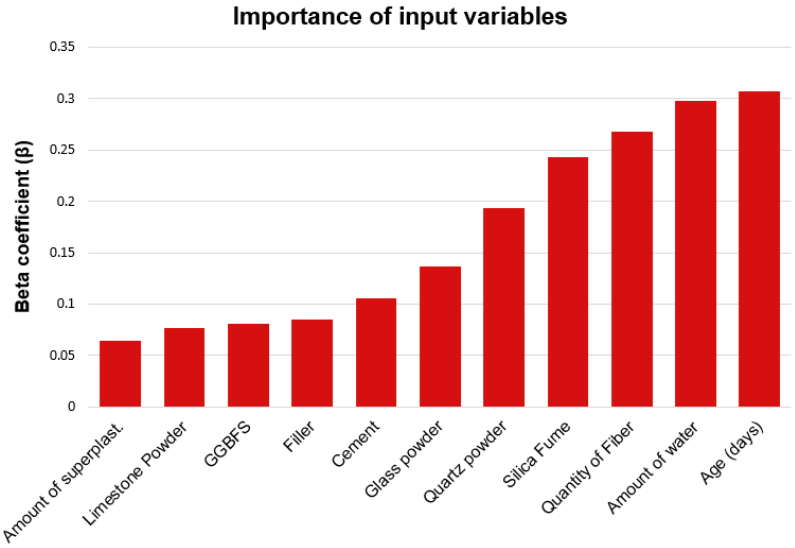


Fig. 4. *Regression coefficients beta*

To capture the complex non-linear hydration kinetics and chemical synergisms that simple linear frameworks inherently miss, the optimized 11-variable set was expanded into a Polynomial Interaction Model. The base variable for the interaction and model formulation was selected as cement, with exponents systematically varied in incremental steps based on maximizing the R coefficient ranging from 0.1 to 4. The quantitative evaluation metrics for the final polynomial interaction model are comprehensively summarized in Table 4.
To visually evaluate the model's accuracy, the relationship between experimental measurements and model predictions is illustrated in Fig. 5. The close alignment of the data points along the ideal 1:1 equivalence line demonstrates the high predictive precision and strong generalizability of the proposed interactive formulation across the full dataset spectrum. Furthermore, to quantify feature importance, the 15 most significant regression coefficients (out of 42) tested also with importance are ranked and presented in Fig. 6.

Table 4. *Evaluation metrics for polynomial interaction model*

RMSE	26.86
MAE	20.15
R	0.9069
MAPE	17.88%

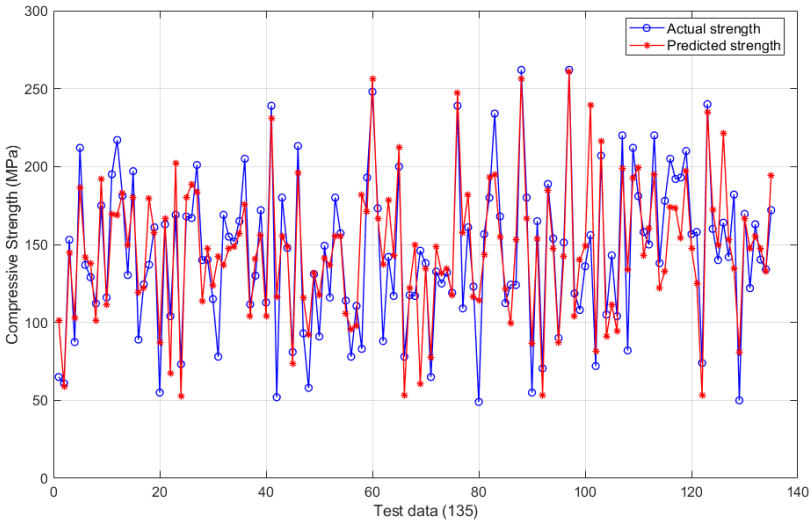


Fig. 5. *Experimental vs. Predicted Compressive Strength for polynomial interaction model*

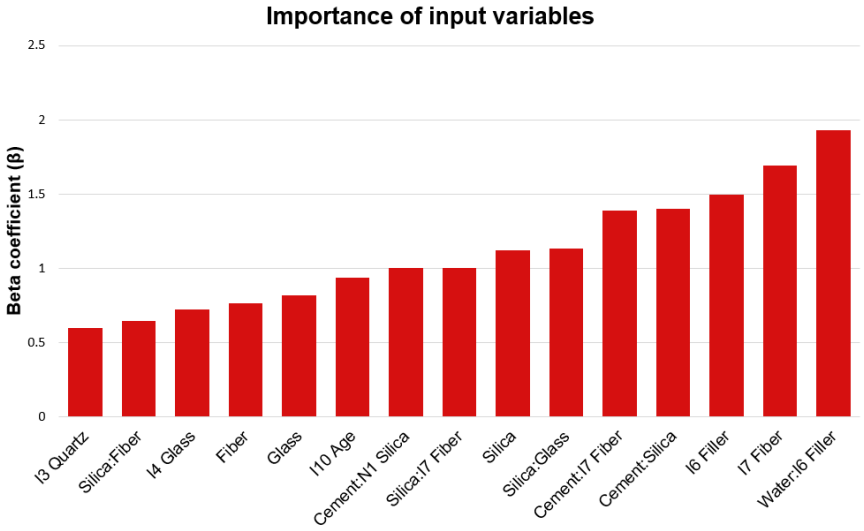


Fig. 6. *Regression coefficients beta for polynomial interaction model*

CONCLUSION

This study compared a standard multiple linear regression model with an expanded model incorporating non-linear power functions and multi-variable interaction terms to predict the compressive strength of high-performance concrete. While the standard linear model provided a baseline approximation, it failed to capture the complex, non-linear physical and chemical synergies occurring during binder hydration and microstructure development. In contrast, incorporating interaction terms, such as combined effects of cement, silica fume, fibers, and curing age, significantly enhanced predictive capability, resulting in a higher correlation coefficient R and lower prediction errors RMSE, MAE, and MAPE on the test dataset. Furthermore, combining stepwise variable selection with standardized Beta coefficient analysis allowed the model to maintain transparency, successfully ranking the most critical material interactions that govern compressive strength development.

REFERENCES

Aprianti, E., Shafigh, P., Zawawi, R., & Hassan, Z. F. A. (2015). Supplementary cementitious materials origin from agricultural wastes – A review. *Construction and Building Materials*, 74, 176–187. https://doi.org/10.1016/j.conbuildmat.2014.10.010

Chou, J.-S., Chiu, C.-K., Farfoura, M., & Altaharwa, I. (2011). Optimizing the prediction accuracy of concrete compressive strength based on a comparison of data mining techniques. *Journal of Computing in Civil Engineering*, 25(3), 242–253. https://doi.org/10.1061/(ASCE)CP.1943-5487.0000088

Erdal, H. I., Karakurt, O., & Namli, E. (2012). High performance concrete compressive strength forecasting using ensemble models based on discrete wavelet transform. *Engineering Applications of Artificial Intelligence*, 25(6), 1266–1277. https://doi.org/10.1016/j.engappai.2012.10.014

Kherraf, L., Younes, K., Abdelouahed, A., Belachia, M., & Hebhoub, H. (2022). Mechanical properties of self-compacting concrete containing fine aggregates from cement kiln dust and hardened cement waste. *SSP - Journal of Civil Engineering*, 17(1), 1–10. https://doi.org/10.2478/sspjce-2022-0004

Liu, Y. (2022). High-performance concrete strength prediction based on machine learning. Hindawi.
https://doi.org/10.1155/2022/5802217

Malik, U. J., Lee, C. K., Mohotti, D., & Mo, H. (2025). Global dataset of UHPC mix designs with supplementary cementitious materials, nano additives, and sustainable fillers. *Mendeley Data*. https://doi.org/10.17632/czb7ww5pkz.2

Monteiro, P. J. M., Miller, S. A., & Horvath, A. (2017). Towards sustainable concrete. *Nature Materials*, 16(7), 698–699. https://doi.org/10.1038/nmat4930

Yeh, I.-C. (1998). Modeling of strength of high-performance concrete using artificial neural networks. *Cement and Concrete Research*, 28(12), 1797–1808. https://doi.org/10.1016/S0008-8846(98)00165-3

DOI:10.5937/IIZS26050M

COMPARISON BETWEEN ONE AND TWO PARAMETER SORPTION ISOTHERM MODELS

Research paper

Vangelce Mitrevski[1], Cvetanka Mitrevska[2]
[1]University St.Kliment Ohridski, Faculty of Technical Sciences, Bitola, North Macedonia
[2]International Slavic University Gavrilo Romanovic Derzavin,
Faculty for Safety Engineering, Sveti Nikole, North Macedonia

Abstract: This paper presents the results of a comparative statistical analysis of five one-parameter and sixty two-parameter temperature-independent sorption isotherm models. To identify the models that provide the best fit, numerical analyses were performed using experimental equilibrium moisture content and water activity data for quince obtained at four different temperatures. For each model and data set, the coefficient of determination (R^2) was calculated, and the models were subsequently ranked according to their goodness of fit. The comparative analysis allowed the identification of the most suitable one-parameter and two-parameter models for describing the sorption behavior of quince.
Key words: sorption isotherms, one-parameter models, two-parameter models, quince.

INTRODUCTION

A food sorption isotherm describes the thermodynamic relationship between water activity, (a_w), and equilibrium moisture content, (X_e), at constant temperature and pressure. In the scientific and engineering literature, numerous mathematical models have been proposed for describing the equilibrium moisture content of food materials **(**Blahovec&Yanniotis, 2009; Mitrevski et al., 2022). Depending on the number of parameters involved, these models can be classified as one-parameter, two-parameter, three-parameter, or multi-parameter models. Sorption isotherm models can also be classified as temperature-independent or temperature-dependent, depending on whether temperature is explicitly included in the model formulation. Temperature dependent models are particularly useful for describing the effect of temperature on the equilibrium moisture content over a range of operating conditions (Popovski&Mitrevski, 2004). Popovski and Mitrevski (Popovski&Mitrevski, 2004a; Popovski&Mitrevski, 2004b; Popovski&Mitrevski, 2005; Popovski&Mitrevski, 2005a; Popovski&Mitrevski, 2005b; Popovski&Mitrevski, 2006) and Mitrevski (Mitrevski et al., 2016) proposed seven methods for generating new sorption isotherm models. In engineering applications, the simplicity of a mathematical model is an important consideration, and models with fewer parameters may offer advantages in terms of parameter estimation and practical implementation.
The objective of this paper was to perform a comparative statistical analysis of two one-parameter and sixty two-parameter temperature-independent sorption isotherm models for describing the experimental equilibrium moisture content of quince. The coefficient of determination (R^2) was used as criterion for ranking the models and identifying the best-performing model in each category. The comparison was carried out to determine the influence of the number of model parameters on the ability of the sorption isotherm models to describe the experimental data.

MATERIAL AND METHODS

The equilibrium moisture content of quince was determined at temperatures of 15, 30, 45, and 60 °C using the static gravimetric method (Mitrevski et al., 2015). Ten saturated salt solutions, LiCl, CH_3COOK, $MgCl_2$, K_2CO_3, $Mg(NO_3)_2$, NaBr, $SrCl_2$, NaCl, KCl, and $BaCl_2$, were used to establish constant equilibrium relative humidities in the glass jars, corresponding to water activity (a_w) values ranging from 0.110 to 0.920 (Mitrevski et al.,

[1]Corresponding author, vangelce.mitrevski@uklo.edu.mk, ORCID: 0000-002-638-6582-
[2]cvetanka.mitrevsk@msu.edu.mk, ORCID: 0009-0008-1417-1798

2015). Two dried quince samples were placed on a holder in each of the ten glass jars and exposed to atmospheres of different relative humidities. The sorption jars were placed in a temperature-controlled cabinet maintained at 15, 30, 45, and 60 °C with an accuracy of ±0.1 °C. Three replications were performed at each temperature and water activity level, using two samples per replication, and the average equilibrium moisture content was calculated (Mitrevski et al., 2015).
Changes in sample mass were determined every seven days using a KERN PLJ360-3M electronic balance with a precision of 0.001 g. Equilibrium between the samples and the surrounding atmosphere was considered to have been reached after 21 days, when no further change in sample mass was observed between two successive mass measurements. The equilibrium moisture content of the quince samples was determined gravimetrically by oven drying at 105 °C and atmospheric pressure for 24 h.

RESULTS AND DISCUSSION

The experimental equilibrium moisture content (X_e) data of quince slices, obtained at different water activity (a_w) and at four different temperatures (Mitrevski et al., 2015), were fitted to two one-parameter and sixty two-parameter temperature-independent sorption isotherm models, as presented in tab.1 and tab.2, respectively.

Table 1. One-parameters sorption models

Num.of model	Name of model	Model	References
M01	de Boer	$X_e = A/(1-a_w)$	de Boer, 1953
M02	Tester	$X_e = A\ a_w /(1-a_w)$	Tester, 1946

Table 2. Two-parameters sorption models

Num. model	Name of model	Model	References
M01	BET modified	$X_e = \frac{ABa_w}{[(1-a_w)(1-B\ln(1-a_w))]}$	Mitrevski et al., 2019
M02	Bradley	$X_e = A\ln(-\ln a_w) + B$	Mitrevski et al., 2019
M03	Brunauer	$X_e = \frac{Aa_w}{(1-a_w)(1-Ba_w)}$	Mitrevski et al., 2019
M04	Caurie ≡ Miniowitsch	$X_e = \exp(Aa_w + B)$	Mitrevski et al., 2019
M05	Chen and Clayton ≡ Bradley (for T=const)	$X_e = A\ln(-\ln a_w) + B$	Mitrevski et al., 2019
M06	Chung-Pfost ≡ Bradley (for T=const)	$X_e = A\ln(-\ln a_w) + B$	Mitrevski et al., 2019
M07	Chung-Pfost	$X_e = A + B(\ln a_w)$	Mitrevski et al., 2019
M08	Day-Nelson ≡ Henderson (for T = const)	$X_e = A\ln[-\ln(1-a_w)] + B$	Mitrevski et al., 2019
M09	Dubinin-Radushkevich	$X_e = \exp[A\ln(a_w^2)]B$	Mitrevski et al., 2019
M10	Freundlich ≡ McGavack-Patrick	$X_e = Ba_w^A$	Mitrevski et al., 2019
M11	Halsey	$X_e = A(-\ln a_w)^B$	Mitrevski et al., 2019

M12	Halsey modified	$X_e = A + B(\frac{a_w}{1 - Ba_w})$	Mitrevski et al., 2019
M13	Harkins-Jura	$X_e = \sqrt{\frac{A}{B - \ln a_w}}$	Mitrevski et al., 2019
M14	Henderson	$X_e = A\left[-\ln(1 - a_w)\right]^B$	Mitrevski et al., 2019
M15	Hoover-Mellon ≡ Bradley	$X_e = A\ln\left(-\ln a_w\right) + B$	Mitrevski et al., 2019
M16	Hüttig	$X_e = \frac{Aa_w(1 + a_w)}{1 - Ba_w}$	Mitrevski et al., 2019
M17	Iglesias-Chirife ≡ Halsey (for T=const)	$X_e = B(-\ln a_w)^A$	Mitrevski et al., 2019
M18	Iglesias-Chirife	$X_e = A + \frac{Ba_w}{1 - a_w}$	Mitrevski et al., 2019
M19	Isse	$X_e = \exp[\ln(\frac{A}{1 - a_w}) + B]$	Mitrevski et al., 2019
M20	Kühn	$X_e = A + B/\ln a_w$	Mitrevski et al., 2019
M21	Langumir	$X_e = \frac{Aa_w}{1 - Ba_w}$	Mitrevski et al., 2019
M22	Linear equation	$X_e = A + Ba_w$	Mitrevski et al., 2019
M23	McGavack-Partric	$X_e = Aa_w^B$	Mitrevski et al., 2019
M24	Miniowitsch	$X_e = \exp\left(Aa_w + B\right)$	Mitrevski et al., 2019
M25	Mizrahi	$X_e = \frac{A}{1 - a_w} + B$	Mitrevski et al., 2019
M26	Mizrahi modified	$X_e = A\frac{a_w}{1 - a_w} + B\frac{1}{1 - a_w}$	Mitrevski et al., 2019
M27	Oswin	$X_e = A(\frac{a_w}{1 - a_w})^B$	Mitrevski et al., 2019
M28	Pierce	$X_e = A\ln(1 - a_w) + B$	Mitrevski et al., 2019
M29	Polanyi	$X_e = A(-\ln a_w)^{-1/3} + B$	Mitrevski et al., 2019
M30	Popovski-Mitrevski	$X_e = \frac{Aa_w}{(1 - Ba_w)^2}$	Mitrevski et al., 2019
M31	Popovski-Mitrevski	$X_e = A\ln\left[-\ln(1 - a_w)\right] + B$	Mitrevski et al., 2019
M32	Popovski-Mitrevski	$X_e = A\ln\frac{a_w}{1 - a_w} + B$	Mitrevski et al., 2019
M33	Popovski-Mitrevski	$X_e = \frac{A\sin a_w}{1 - a_w} + B$	Mitrevski et al., 2019
M34	Popovski-Mitrevski	$X_e = \frac{A\cos a_w}{\sin(1 - a_w)} + B$	Mitrevski et al., 2019
M35	Popovski-Mitrevski	$X_e = \frac{Atga_w}{1 - a_w} + B$	Mitrevski et al., 2019
M36	Popovski-Mitrevski	$X_e = \exp\left[\frac{A}{\sin a_w} + B\right]$	Mitrevski et al., 2019
M37	Popovski-Mitrevski	$X_e = \exp\left[\frac{A\sin(1 - a_w)}{a_w} + B\right]$	Mitrevski et al., 2019
M38	Popovski-Mitrevski	$X_e = \exp\left(\frac{A}{tga_w} + B\right)$	Mitrevski et al., 2019

M39	Popovski-Mitrevski	$X_e = \frac{1}{\frac{A}{\sin a_w} + B}$	Mitrevski et al., 2019
M40	Popovski-Mitrevski	$X_e = \frac{a_w}{A\sin(1-a_w) + Ba_w}$	Mitrevski et al., 2019
M41	Popovski-Mitrevski	$X_e = \frac{1}{\frac{A}{tga_w} + B}$	Mitrevski et al., 2019
M42	Popovski-Mitrevski	$X_e = A\left(\frac{\sin a_w}{1-a_w}\right)^B$	Mitrevski et al., 2019
M43	Popovski-Mitrevski	$X_e = Atg^B a_w$	Mitrevski et al., 2019
M44	Popovski-Mitrevski	$X_e = A\left(\frac{tga_w}{1-a_w}\right)^B$	Mitrevski et al., 2019
M45	Popovski-Mitrevski	$X_e = \frac{A}{\arcsin(1-a_w)} + B$	Mitrevski et al., 2019
M46	Popovski-Mitrevski	$X_e = \frac{A}{\arccos a_w} + B$	Mitrevski et al., 2019
M47	Popovski-Mitrevski	$X_e = \frac{Aa_w}{arctga_w} + B$	Mitrevski et al., 2019
M48	Popovski-Mitrevski	$X_e = \exp(\frac{A}{\arcsin a_w} + B)$	Mitrevski et al., 2019
M49	Popovski-Mitrevski	$X_e = \exp\left(\frac{A}{arctga_w} + B\right)$	Mitrevski et al., 2019
M50	Popovski-Mitrevski	$X_e = \exp\left[\frac{Aarctg\ (1-a_W)}{a_W} + B\right]$	Mitrevski et al., 2019
M51	Popovski-Mitrevski	$X_e = \frac{1}{\frac{A}{\arcsin a_w} + B}$	Mitrevski et al., 2019
M52	Popovski-Mitrevski	$X_e = \frac{1}{\frac{A}{arctga_w} + B}$	Mitrevski et al., 2019
M53	Popovski-Mitrevski	$X_e = \frac{a_W}{Aarctg\cdots(1-a_W) + Ba_W}$	Mitrevski et al., 2019
M54	Popovski-Mitrevski	$X_e = A\arcsin^B a_w$	Mitrevski et al., 2019
M55	Popovski-Mitrevski	$X_e = A(\frac{a_w}{\arccos a_w})^B$	Mitrevski et al., 2019
M56	Popovski-Mitrevski	$X_e = A(\frac{a_w}{arctga_w})^B$	Mitrevski et al., 2019
M57	Posnow	$X_e = \frac{A}{B - \ln a_w}$	Mitrevski et al., 2019
M58	Smith ≡ Pierce	$X_e = A\ln(1-a_w) + B$	Mitrevski et al., 2019
M59	Thompson ≡ Henderson (for T=const)	$X_e = A\ln[-\ln(1-a_W)] + B$	Mitrevski et al., 2019
M60	White-Eyring	$X_e = \frac{A}{1 - Ba_w}$	Mitrevski et al., 2019

The suitability of each model for describing the experimental sorption data was evaluated using appropriate statistical goodness of fit criteria In scientific literature, for the goodness of fit of experimental sorption data and selection of the best isotherm model, following statistical criterions are used: coefficient of determination, R^2, root mean squared error, RMSE, and the

mean relative deviation, MRD. The selection of a sorption isotherm model with graphical evaluation of the residual randomness is also popular (Mitrevski et al., 2012). Plotting of the residuals against independent variable is a measure of distribution errors. If the sorption model is correct, then the residual should be only random independent errors with a zero mean, constant variance and arranged in a normal distribution. If the residual plots indicate a clear pattern, the model should not be accepted (Mitrevski et al., 2012). In this study the value on coefficient of determination, R^2 was the main statistical indicator for selection of the best sorption isotherm model.

The method of indirect non-linear regression analysis and estimation methods of Quasi-Newton, Simplex, Simplex and quasi-Newton, Hooke-Jeeves pattern moves, Hooke-Jeeves pattern moves and quasi-Newton, Rosenbrock pattern search, Rosenbrock pattern search and quasi-Newton, Gauss-Newton and Levenberg-Marquardt from computer software StatSoft, Inc., *STATISTICA: Data Analysis Software System*, version 10.0. USA, 2011, were used to approximate the experimental equilibrium moisture content data of quince.

For each mathematical model presented in tab.1 and tab.2, the model parameters were estimated by fitting the respective model to the experimental equilibrium moisture content (X_e) data. The goodness of fit of each model was evaluated using the coefficient of determination (R^2). Subsequently, the models were ranked according to their (R^2) values, with higher values indicating better agreement between the model predictions and the experimental data. The ranking results for the one-parameter and two-parameter sorption isotherm models are presented in tab.3 and tab.4, respectively.

Table 3. *Ranking the two-parameters models*

Model	R^2	Rank	Model	R^2	Rank
M01	**0.9897**	**1**	M02	0.9878	2

Table 4. *Ranking the two-parameters models*

Model	R^2	Rank	Model	R^2	Rank
M01	0.9897	8	M31	0.8121	59
M02	0.9278	50	M32	0.8796	55
M03	0.9867	18	M33	0.9860	21
M04	0.9855	22	M34	0.9861	20
M05	0.9278	51	M35	0.9785	32
M06	0.9278	52	M36	0.9593	47
M07	0.7251	60	M37	0.9644	43
M08	0.8121	58	M38	0.9670	41
M09	0.9749	34	M39	0.8297	57
M10	0.9749	35	M40	0.9910	3
M11	0.9853	25	M41	0.9905	7
M12	0.9088	54	M42	0.9892	15
M13	0.9375	48	M43	0.9832	31
M14	0.9897	9	M44	0.9896	12
M15	0.9280	49	M45	0.9769	33
M16	0.9907	5	M46	0.9879	17
M17	0.9853	26	M47	0.9183	53
M18	0.9844	27	M48	0.9699	40
M19	0.9702	38	M49	0.9603	46
M20	0.9854	24	M50	0.9656	42
M21	0.9911	2	M51	0.9893	14
M22	0.8593	56	**M52**	**0.9913**	**1**
M23	0.9749	36	M53	0.9908	4
M24	0.9855	23	M54	0.9841	30
M25	0.9844	28	M55	0.9907	6
M26	0.9844	29	M56	0.9880	16
M27	0.9894	13	M57	0.9866	19

M28	0.9642	44	M58	0.9642	45
M29	0.9702	39	M59	0.9897	11
M30	0.9897	10	M60	0.972	37

The comparative analysis of the one and two-parameter sorption isotherm models revealed that both model groups were capable of adequately describing the experimental equilibrium moisture content data of quince slices. Among the one-parameter models, (M01) exhibited the highest coefficient of determination (R^2 = 0.9897), whereas among the two-parameter models, the Popovski–Mitrevski model (M52) provided the highest value (R^2 = 0.9913). Although two parameter model (M52) demonstrated a slightly better fit according to the coefficient of determination, the improvement relative to the one-parameter model M01 was relatively small, with a difference of only 0.0016 between the (R^2) values of the two models.
This difference should be interpreted with consideration of model complexity. The inclusion of an additional adjustable parameter generally increases model flexibility and, consequently, may improve its ability to reproduce experimental data. Therefore, a higher (R^2) value for a two-parameter model cannot, by itself, be considered sufficient evidence of its superiority over a simpler one-parameter model. Considering model simplicity, a model with fewer adjustable parameters is generally preferred when it provides a goodness of fit comparable to that of a more complex model, as it offers a simpler mathematical structure and requires the estimation of fewer parameters.
The parameter values (A) and (B) of the Popovski–Mitrevski model (M52) were determined by fitting the model to the experimental equilibrium moisture content (X_e) data of quince slices using the quasi-Newton optimization method. The optimal parameter values were obtained by minimizing the sum of squared errors between the experimental and model-predicted (X_e) values. The resulting parameter values (A) and (B) are presented in tab.5

Table 5. *Estimated parameter values of the Popovski–Mitrevski model (M52)*

Model	A	B
$X_e = 1/[A/\arctan(a_w) + B]$	11.12	−13.72

The experimental and model-predicted equilibrium moisture content (X_e) values of quince slices at the four temperatures are presented in fig. 1a to fig1b.

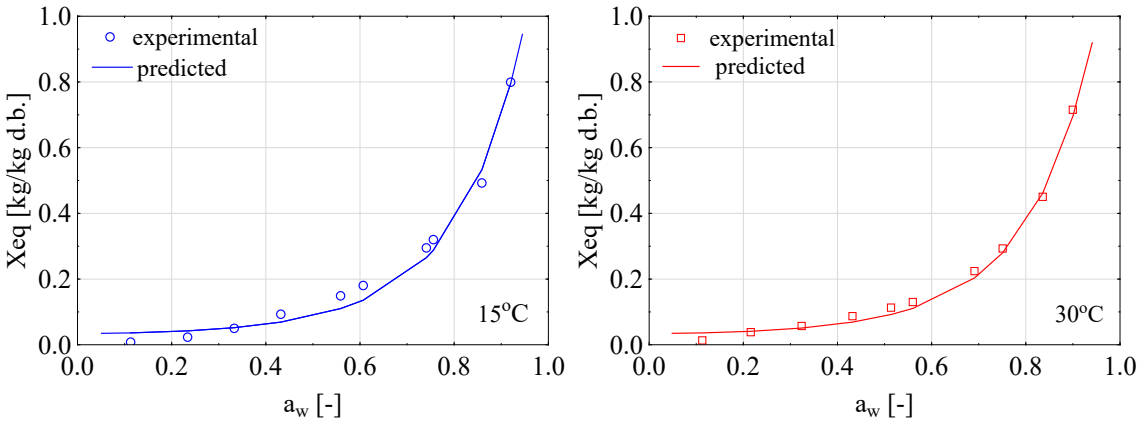


Fig. 1a. *Experimental and predicted sorption isotherms for quince at 15 and 30°C, Model M52*

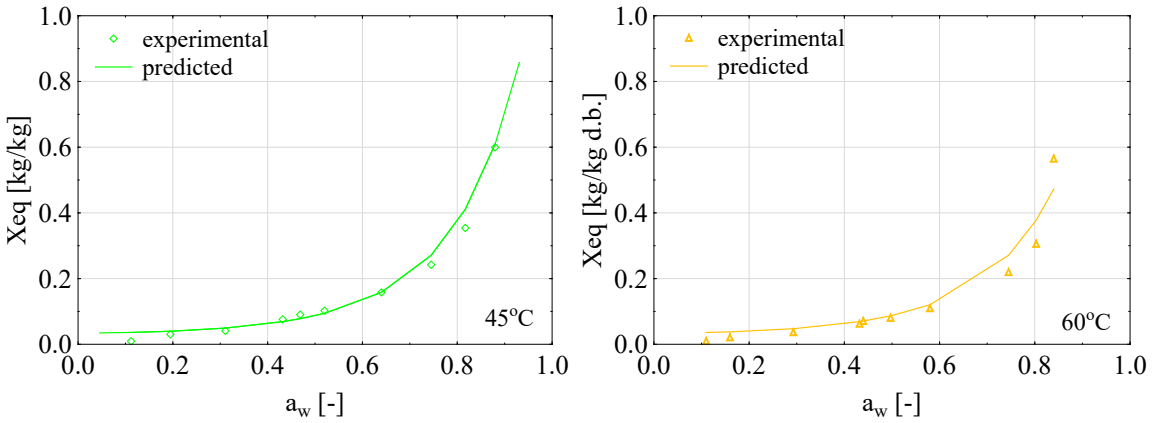


Fig. 1b. *Experimental and predicted sorption isotherms for quince at 45 and 60°C, Model M52*

As shown in Fig. 1a–b, good agreement was observed between the experimental and model-predicted equilibrium moisture content (X_e) values of quince slices over the investigated range of water activity and temperature.

CONCLUSION

The statistical evaluation performed in this paper showed that both one and two-parameter sorption isotherm models adequately described the experimental equilibrium moisture content data of quince slices. Among the models evaluated, the two-parameter Popovski–Mitrevski model (M52) provided the best overall fit, exhibiting the highest coefficient of determination. The best-performing one-parameter model (M01) also showed very good agreement with the experimental data. Although the two-parameter model provided a slightly better fit, the improvement was relatively small. Therefore, the selection of an appropriate sorption isotherm model should take into account both goodness of fit and model complexity, ensuring an appropriate balance between predictive accuracy and mathematical simplicity.

REFERENCES

J. Blahovec and S. Yanniotis, "Modified classification of sorption isotherms," *Journal of Food Engineering*, vol. 91, no. 1, pp. 72–77, 2009.
J. H. de Boer, *The Dynamical Character of Adsorption*. Oxford, UK: Clarendon Press, 239 pp., 1953.
V. Mitrevski, V. Mijakovski, T. Geramitcioski, and M. Lutovska, "Comparison between the transcendental and cyclometric sorption isotherm models," *Journal on Processing and Energy in Agriculture*, vol. 16, no. 1, pp. 1–5, 2012.
V. Mitrevski, M. Lutovska, V. Mijakovski, I. Pavkov, M. Babić, and M. Radojčin, "Adsorption isotherm of pear at several temperatures," *Thermal Science*, vol. 19, no. 3, pp. 1119–1129, 2015.
V. Mitrevski, M. Lutovska, I. Pavkov, V. Mijakovski, and F. Popovski, "The power series as water sorption isotherm models," *Journal of Food Process Engineering*, vol. 39, no. 2, pp. 178–185, 2016.
V. Mitrevski, C. Mitrevska, T. Geramitcioski, K. Popovski, and M. Babić, "Statistical evaluation of two-parameter moisture sorption isotherm models," *Journal on Processing and Energy in Agriculture*, vol. 23, no. 1, pp. 1–5, 2019.
V. Mitrevski, C. Mitrevska, Lj. Trajcevski, and B. Mitrevski, "Review models of sorption isotherms," *Journal on Processing and Energy in Agriculture*, vol. 26, no. 1, pp. 1–7, 2022.
D. Popovski and V. Mitrevski, "Temperature influence on desorption isotherms," in *Proceedings of the 14th International Drying Symposium (IDS 2004)*, São Paulo, Brazil, 22–25 August 2004, vol. A, pp. 254–257.

D. Popovski and V. Mitrevski, "Some new four-parameter models for moisture sorption isotherms," *Electronic Journal of Environmental, Agricultural and Food Chemistry*, vol. 3, no. 3, pp. 698–701, 2004.
[D. Popovski and V. Mitrevski, "A method for extension of the water sorption isotherm models," *Electronic Journal of Environmental, Agricultural and Food Chemistry*, vol. 3, no. 6, pp. 799–803, 2004.
D. Popovski and V. Mitrevski, "A method for generating water sorption isotherm models," *Electronic Journal of Environmental, Agricultural and Food Chemistry*, vol. 4, no. 3, pp. 945–948, 2005.
D. Popovski and V. Mitrevski, "A generator of water desorption isotherm models," in *Proceedings of the 11th Polish Drying Symposium*, Poznań, Poland, pp. 1–4, 2005.
D. Popovski and V. Mitrevski, "Method of free parameter for extension of the water sorption isotherm models," in *Proceedings of the 32nd International Conference of the Slovak Society of Chemical Engineering*, Tatranské Matliare, Slovakia, pp. 1–5, 2005.
D. Popovski and V. Mitrevski, "Two methods for generating new water sorption isotherm models," *Electronic Journal of Environmental, Agricultural and Food Chemistry*, vol. 5, no. 3, pp. 1407–1410, 2006.
D. A. Tester, *Journal of Polymer Science*, vol. 19, p. 535, 1946.
StatSoft, Inc., *STATISTICA: Data Analysis Software System*, version 10.0. USA: StatSoft, Inc., 2011.

DOI:10.5937/IIZS26058R

THE PHENOMENON OF RESONANT ABSORPTION IN MOLECULAR NANOSCOPIC FILM STRUCTURES

Research paper

Dragana Rodić[1], Dušan I. Ilić[2] , Stevo K. Jaćimovski[3] , Jovan P. Šetrajčić[4*]

[1]Laza Kostić High School, Novi Sad, Vojvodina – Serbia;
[2]University of Novi Sad, Technical Faculty, Novi Sad, Vojvodina – Serbia;
[3]University of Criminal Investigation and Police Studies, Zemun – Belgrade, Serbia;
[4]Academy of Sciences and Arts of the Republic of Srpska, Banja Luka, B&H

Abstract: This paper presents the results of a theoretical study on changes in optical properties caused by the presence of boundaries in molecular crystal nanofilms. The energy spectrum of Frenkel excitons and their spatial distribution along the confinement axis (across crystallographic layers) were determined using a combined analytical-numerical calculation. Subsequently, the relative permittivity and absorption index were determined, and the influence of boundary parameters on the occurrence of resonant - virtually monochromatic - absorption was analyzed.
Key words: Ultrathin films, nanostructures, Frenkel excitons, permittivity, absorption index

INTRODUCTION

Theoretical research into low-dimensional crystal systems (nanostructures such as ultrathin films, quantum wires, quantum dots, etc.) has intensified significantly, driven not only by the need to gain fundamental insights into the radically different physicochemical properties of these materials but also by their increasingly broad and high-quality practical applications in nano-, opto-, and bio-electronics (Wood K., et al., 2008). The distinctive nature of these "tiny" - i.e., ultrathin - structures lies in the fact that the presence of nearby interfaces leads to significant alterations in the materials' well-known properties and gives rise to unique phenomena - resulting from dimensional quantization effects (Tringides M.C., et al., 2007) when compared to the characteristics of corresponding "bulk" samples (Davison S.G. & Steslicka M.,1996).

Interest in studying the exciton subsystem in molecular crystals generally stems from the fact that Frenkel excitons are responsible for the dielectric, optical (absorption, light dispersion, luminescence), and photoelectric properties, as well as other physical characteristics, of these crystals (Agranovich V.M. & Ginzburg V.L., 1979). In this paper, we examine ultrathin dielectric films (characterized by a dimension not exceeding the thickness of approximately ten interatomic planes). Typical examples of such structures are molecular crystals in which elementary excitations - Frenkel excitons - arise from the interaction between an external electromagnetic field and the crystal's electrons. The relative permittivity - and through it, all the optical characteristics of the system under study - is theoretically defined using the dispersion laws and density of states of these excitons.

FRENKEL EXCITONS IN AN ULTRATHIN CRYSTALLINE FILM

The standard expression for the effective exciton Hamiltonian in the harmonic approximation - for instance, according to Ref. (Agranovich V.M. & Ginzburg V.L., 1979) - takes the form:

$$H = \sum_{\vec{n}} \Delta_{\vec{n}} B_{\vec{n}}^{+} B_{\vec{n}} + \sum_{\vec{n},\vec{m}} X_{\vec{n}\vec{m}} B_{\vec{n}}^{+} B_{\vec{m}} \ , \qquad (1)$$

where $B_{\vec{n}}^{+}$ and $B_{\vec{n}}$ are the exciton creation and annihilation operators, $\Delta_{\vec{n}}$ represents the energy of an isolated exciton at site $\vec{n}$, and $X_{\vec{n}\vec{m}}$ are the matrix elements for exciton transfer

[1] dragana.rodic@gimnazijalazakostic.edu.rs
[2] dusilic69@gmail.com, ORCID: 0000-0002-3644-1268.
[3] jacimovskis@gmail.com, ORCID: 0000-0002-4074-662X.
[4] Coresponding author, jovan.setrajcic@gmail.com, ORCID: 0000-0002-6903-2882

from site $\vec{n}$ to site $\vec{m}$. The model assumes that the exciton energy at a site is approximately 100 times greater than the exciton transfer energy (Agranovich V.M. & Ginzburg V.L., 1979). Systems bounded by two parallel surfaces are referred to as films (Cottam M.G. & Tilley D.R., 1989; Šetrajčić J.P., et al., 2008). The dimensions of the crystalline nanofilm model are such that it is infinite in the XY plane, while it has a finite thickness of $L = N\,a$ in the z-direction. We consider a dielectric nanofilm (Figure 1), which can be fabricated in practice through the controlled doping of bulk samples - matrices (Šetrajčić J.P., et al., 2008). Due to the presence of boundary surfaces, the site exciton energies and the energy transfer between the boundary planes ($n_z = 0$; $n_z = N$) and their adjacent crystallographic planes ($n_z = 1$; $n_z = N - 1$) are perturbed; this can be represented as follows (Šetrajčić J.P., et al., 2008; Pelemiš S., et al., 2008; Rodić, D., et al., 2013):

$$\Delta_{\vec{n}} \equiv \Delta\ \left[1 + d\left(\delta_{n_z,0} + \delta_{n_z,N}\right)\right];\quad X_{\vec{n},\vec{n}+\vec{\lambda}} \equiv X\ \left[1 + x\left(\delta_{n_z,0} + \delta_{n_z,N-1}\right)\right];\quad X_{\vec{n},\vec{n}-\vec{\lambda}} \equiv X\ \left[1 + x\left(\delta_{n_z,1} + \delta_{n_z,N}\right)\right], \quad (2)$$

which effectively constitute the boundary conditions, where the parameter d defines the perturbation of the exciton energy at the boundary surface sites, and the parameter x defines the perturbation of the exciton transfer energy in the boundary layers along the z-direction.

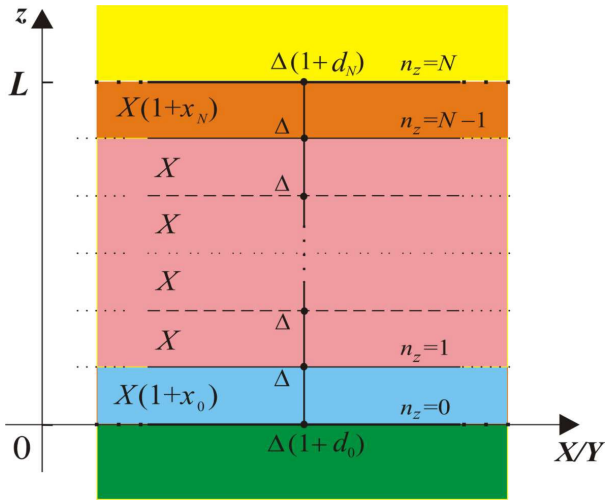


***Fig. 1**. Schematic of the ultra-thin dielectric film model*

We conduct a micro-theoretical analysis of the exciton subsystem of an ultrathin (crystalline) molecular film using the method of time- and temperature-dependent Green's functions; thus, we consider the following Green's function (Mahan G., 1990): $G_{\vec{n}\vec{m}}(t) = \left\langle\left\langle B_{\vec{n}}(t)\middle|B^{+}_{\vec{m}}(0)\right\rangle\right\rangle$, which satisfies the following equation of motion:

$$i\hbar\frac{d}{dt}G_{\vec{n}\vec{m}}(t) = i\hbar\delta(t)\delta_{\vec{n}\vec{m}} + \Delta_{\vec{n}}G_{\vec{n}\vec{m}}(t) + \sum_{\vec{l}} X_{\vec{n}\vec{l}}\,G_{\vec{l}\vec{m}}(t). \quad (3)$$

We then apply a full temporal Fourier transform, along with partial spatial Fourier transforms, to these equations, obtaining:

$$G_{n_z,m_z}\left[\rho - \frac{\Delta}{|X|}d\left(\delta_{n_z,0} + \delta_{n_z,N}\right)\right] + G_{n_z+1,m_z}\left[1 + x\left(\delta_{n_z,0} + \delta_{n_z,N-1}\right)\right] + G_{n_z+1,m_z}\left[1 + x\left(\delta_{n_z,1} + \delta_{n_z,N}\right)\right] = \frac{i\hbar}{2\pi|X|}\delta_{n_z,m_z}, \quad (4)$$

where the following notation is introduced: $\rho = \dfrac{\hbar\omega - \Delta}{|X|} + 2\left(\cos ak_x + \cos ak_y\right)$.

Equation (4) represents a system of $N+1$ inhomogeneous algebraic-difference equations for the unknown Green's functions. However, since only the poles of these functions are required to determine the dispersion law, it suffices to find the determinant of the system and set it to zero. In this way, we obtain $N+1$ solutions: $\rho \equiv \rho_\nu$; $\nu = 1, 2, 3, \ldots, N+1$.

PERMITIVITY OF NANOFILMS

To determine the occurrence probabilities and spatial distribution of exciton states in the film, it is necessary to calculate the spectral weights of the individual Green's functions. One approach is to start with the system of equations for the Green's functions (4), but written in matrix form:

$$\hat{D}_{N+1}\widetilde{G}_{N+1} = \hat{K}_{N+1}, \tag{5}$$

where $\hat{D}_{N+1}$ is the matrix corresponding to the system's determinant, and $\widetilde{G}_{N+1}$ and $\hat{K}_{N+1}$ are the vectors of the Green's functions and Kronecker deltas, respectively. By applying the inverse matrix $\hat{D}_{N+1}^{-1}$ to equation (5) from the left - and knowing that the inverse matrix can be expressed in terms of the adjugate matrix, whose entries D_{ik} are the cofactors of the elements d_{ik} of the original matrix-further calculation yields the Green's functions. The spectral weights $g_{n_z}(\rho_\nu)$ - i.e., the probabilities of finding exciton states ρ_ν (Šetrajčić J.P., et al., 2008; Pelemiš S., et al., 2008; Rodić, D., et al., 2013; Šetrajčić, I.J., 2018) - appear directly in the numerators of these functions:

$$G_{n_z} = -\frac{i\hbar}{2\pi|X|}\sum_{\nu=1}^{N+1}\frac{g_{n_z}(\rho_\nu)}{\rho-\rho_\nu}. \tag{6}$$

To determine the dynamic permittivity of the film, we will use the general expression (Dzialoshinski I.E. & Pitaevski L.P., 1959), while strictly accounting for the fact that the Green's functions - and consequently the permittivity - depend on the (number, i.e., position of) the crystallographic planes n_z of the symmetric film:

$$\varepsilon_{n_z}^{-1}(\omega) = 1 - 2\pi i\, F\,\left[G_{n_z}(\omega) + G_{n_z}(-\omega)\right], \tag{7}$$

where F is the structure factor [4,5]. Substituting the expression for the Green's functions (6) yields:

$$\varepsilon_{n_z}^{-1}(\omega) = 1 - \frac{\hbar F}{|X|}\sum_{\nu=1}^{N+1}\sum_{s=+,-}\frac{g_{n_z}^{\nu}}{\rho_s-\rho_\nu}, \tag{8}$$

where: $\rho_\pm = \frac{\mp\hbar\omega-\Delta}{|X|} + 2\left(\cos ak_x + \cos ak_y\right)$; after some analytical rearrangement, expression (8) becomes:

$$\varepsilon_{n_z}(\omega) = \left\{1 - \frac{2\hbar F}{|X|}\sum_{\nu=1}^{N+1} g_{n_z}^{\nu}\,\frac{\rho_\nu - \frac{\Delta}{|X|} - 2\left(\cos ak_x + \cos ak_y\right)}{\left(\frac{\hbar\omega}{|X|}\right)^2 - \left[\rho_\nu - \frac{\Delta}{|X|} - 2\left(\cos ak_x + \cos ak_y\right)\right]^2}\right\}^{-1}. \tag{9}$$

This expression represents the dependence of the relative dynamic permittivity on the frequency of the initial electromagnetic excitation - that is, the dielectric response of the observed symmetric molecular film to an external electromagnetic field. Figure 2 illustrates the dependence of the relative dynamic permittivity on the reduced energy of the external electromagnetic radiation for a five-layer film.

All the figures show the dependence of permittivity on the reduced frequency of the external electromagnetic field for the outer (boundary) surfaces, the first inner layers, and the central crystallographic plane. The appearance of resonant peaks is evident; their number and arrangement depend significantly on the boundary perturbation parameters.

The first image at the top, containing three graphs, shows the permittivity of an ideal ultrathin film consisting of four interatomic layers. The second and third rows of Figure 2 display the dependence of dynamic permittivity on the reduced frequency of the external electromagnetic field for a four-layer dielectric film, where the parameter Δ is varied via the perturbation d_0 (or d_N).

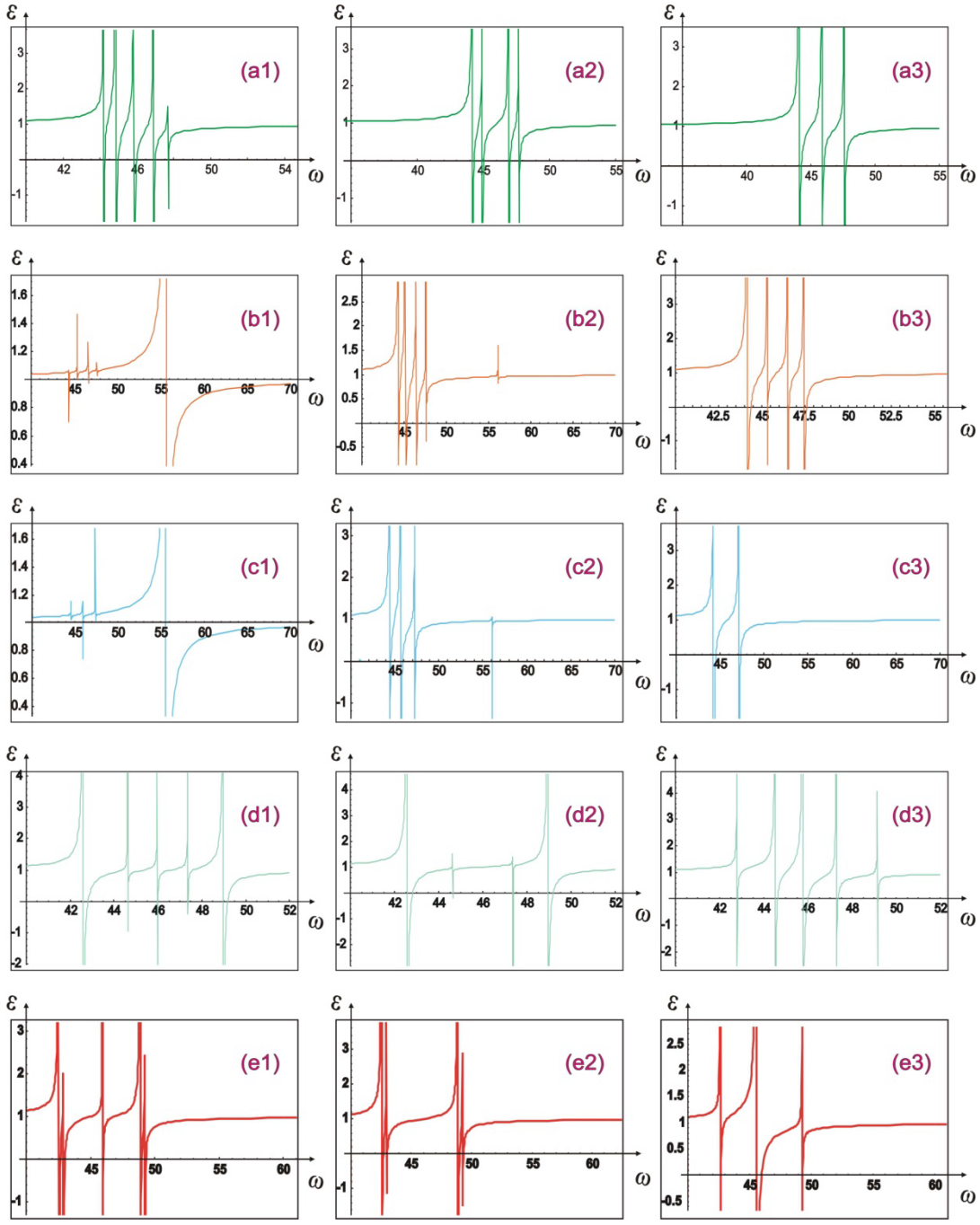


Figure 2 *– Relative permittivity ε of the perturbed film as a function of reduced frequency ω:*

HORIZONTAL (change in energy parameters):
(a1-3): $d_0 = 0{,}0$; $d_N = 0{,}0$; $x_0 = 0{,}0$; $x_N = 0{,}0$;
(b1-3): $d_0 = 0{,}2$; $d_N = 0{,}0$; $x_0 = 0{,}0$; $x_N = 0{,}0$;
(c1-3): $d_0 = 0{,}2$; $d_N = 0{,}2$; $x_0 = 0{,}0$; $x_N = 0{,}0$;
(d1-3): $d_0 = 0{,}0$; $d_N = 0{,}0$; $x_0 = 2{,}0$; $x_N = 0{,}0$;
(e1-3): $d_0 = 0{,}0$; $d_N = 0{,}0$; $x_0 = 2{,}0$; $x_N = 2{,}0$;

VERTICAL (layers/planes):
boundary (1a–e): $n_z = 0$ and 4;
inner (2a–e): $n_z = 1$ and 3;
central (3a–e): $n_z = 2$

This demonstrates that the number of resonant peaks (where $\varepsilon(\omega_r) \rightarrow \pm\infty$) depends not only on the number - or position - of the atomic plane (n_z) for which the permittivity is calculated, but also on the value of the parameter $d_{0/N}$. Increasing this parameter leads to a broadening of the absorption zone, and the dominant resonant peak is observed only at the film boundary ($n_z = 0$ or $n_z \equiv N = 4$). The fourth and fifth rows of Figure 2 show the dependence of the dynamic permittivity ε on the reduced energy of a four-layer dielectric film for a given parameter $x_{0/N}$. It is readily apparent that the number of resonant permittivity peaks differs across the layers - i.e., $\varepsilon = \varepsilon\,(n_z)$ - but also depends on the value of the parameter $x_{0/N}$.

RESULTS AND DISCUSSION

Increasing the value of this parameter results in a symmetrical broadening of the absorption zone toward higher and lower energy values across all layers, as well as the suppression of certain resonant peaks, depending on the specific location (film layer) for which the permittivity is determined. For instance, all resonant peaks are present only in the boundary planes ($n_z = 0$ and 4) and the central plane ($n_z = 2$), whereas they are suppressed in the other planes.

This demonstrates the significantly stronger influence of parameter d, which shifts the entire energy profile and determines the optical characteristics of the film structures under observation.

CONCLUSION

The results of these analyses revealed significant differences in the excitonic dielectric response between bulk and film structures, resulting exclusively from the film's confinement along the z-axis and the presence of parameter perturbations at the structure's interfaces and boundary layers.

a) The film's dielectric response exhibits selectivity - specifically, the appearance of discrete resonant absorption peaks at precise energy levels, with their number and distribution determined by the number of layers in the film and the perturbation parameters. These characteristics give films an advantage over bulk structures (which possess a continuous dielectric response across a specific energy range), as films can serve as specific filters for precise external electromagnetic radiation frequencies.

b) Compared to an asymmetric film, a symmetrically perturbed film exhibits doubled or paired effects. This implies that localization will always occur at two or four energy levels, yet single-selective absorption (an ideal filter) - which is possible with an asymmetric film - will never be achieved. In this case, the minimum configuration involves two closely spaced absorption peaks; essentially, minimum transparency occurs for a bichromatic beam (comprising two wavelengths that are not widely separated).

REFERENCES

Agranovich V.M. & Ginzburg V.L. (1979). Crystaloptics with Space Dispersion and Theory of Excitons, *Nauka*, Moskwa.

Cottam M.G., Tilley D.R., *Introduction to Surface and Superlattice Excitations,* University Press, Cambridge, 1989.

Davison S.G. & Steslicka M. (1996). *Basic* Theory of Surface States, *Clarendon Press*, Oxford.

Dzialoshinski I.E. & Pitaevski L.P. (1959). *Zh.eksper.teor. Fiz.* **36**, 1977.

Mahan G. (1990). Many Particle Physics, *Plenum Press*, New York.

Pelemiš S., Škipina B., Vučenović S.M., Mirjanić D.Lj. & Šetrajčić J.P., Selective Absorption in Symmetric Molecular Nano-Films, *Proceedings 26th MIEL* **1**, 125-128 (2008).

Rodić, D., Škipina, b., Pelemiš, S.S., Jaćimovski, S.K. & Šetrajčić J.P. (2013) Selective IR Absorption and Refraction of Symmetrical Two-Layered Molecular Nanofilms, *Optica Applicata* 43(4), 643-649; DOI: https://doi.org/10.5277/oa130402.

Šetrajčić J.P., D.Ilić D.D., Markoski B., Šetrajčić A.J., Vučenović S.M., Mirjanić D.Lj., Škipina B. & Pelemiš S. (2008). Conformation and Application of Green's Functions Method to Optical Properties of Ultrathin Molecular Films Searching, *CEWQO-08*, Belgrade.

Šetrajčić, I.J., Rodić, D., Šetrajčić, J.P., Šetrajčić-Tomić, A.J., Vučenović, S.M. (2018).

Consequences of Confinement Conditions on Absorption in Molecular Nanofilms, *Acta Phys.Pol.*A **133**/1, 129-139; DOI: https://doi.org/10.12693/APhysPolA.133.129.

Tringides M.C., Jatochawski M. & Bauer E. (April 2007). Quantum Size Effects in Metallic Nanostructures, *Physics Today*, pp.50-54.

Wood K., Hammond P., Schmidt D., Wrightman S. & Andaya B. (2008). Thin Film Delivers Drugs, Biophotonics, Cambridge (http://www.photonics.com).

DOI:10.5937/IIZS26064J

OPTIMIZATION OF PLA 3D PRINTING PARAMETERS CONSIDERING COOLING RATE AND HARDNESS

Research paper

Dušan Jovanić[1*], Aleksandar Rajić[2], Miodrag Kovačević[3], Ljubica Lazić Vulićević[4]
[1,2,3,4] Technical College of Applied Sciences, Zrenjanin, Serbia

Abstract: This paper presents the optimization of 3D printing parameters for polylactide (PLA) using the Taguchi method, aiming to investigate their influence on the cooling rate and Shore A hardness of the samples. During the 3D printing process, printing temperature, printing speed, and layer height were varied across three levels. A thermographic camera was used to measure characteristic temperatures at a point immediately behind the nozzle and after a specific period of time; these measurements were used to determine the cooling rate, which affects layer hardness. Since lower mechanical properties compared to conventional technologies represent one of the main drawbacks of 3D printing, it is essential to thoroughly investigate these properties to determine the functionality of the working parts. Hardness testing of the PLA samples was performed using an analog durometer in accordance with the EN ISO 868:2015 standard.
Key words: Optimization, Hardness testing, FDM 3D printing of PLA, Thermography, Cooling rate.

INTRODUCTION

Due to the lower surface quality and inferior mechanical properties of polylactide (PLA) parts produced by 3D printing, it is necessary to determine their mechanical characteristics: hardness, tensile strength, impact strength, compressive strength, flexural strength, fatigue strength, creep, aging, friction coefficient, shear resistance, and crack propagation in accordance with the standard ISO 17296-3: Additive manufacturing- General principles- Part 3: Main characteristics and corresponding test methods. Furthermore, this standard defines testing categories for metallic, plastic, and ceramic parts, classifying them into three groups: Group H (testing of highly safety-critical functional parts), Group M (testing of non-safety-critical functional parts), and Group L (testing of parts during design or prototype parts). For all these groups of plastic parts, hardness testing is mandatory (ISO, 2014).
The aim of this work is to determine how the cooling rate measured by a thermographic camera, i.e., the temperature homogeneity of the layers, affects the hardness of the PLA plastic workpiece depending on the 3D printing parameters (printing temperature, printing speed, and layer height), and to determine their optimal values using the Taguchi method**.**
Process parameter optimization studies, such as those published on the platform, show that layer height and printing speed have a dominant contribution of over 50–60% on hardness and dimensional accuracy (Motgi et al., 2023).
A higher extrusion temperature, between 210°C and 220°C, improves interlayer adhesion and reduces porosity, which directly increases surface hardness and shear resistance. However, excessively high temperatures without adequate cooling cause deformations and thermal degradation [Rajabi et al., 2021).
PLA is a semi-crystalline polymer. The cooling rate directly dictates the degree of crystallinity of the material. Research indicates that excessively rapid cooling (strong fans/low ambient temperature) leads to an amorphous structure, which results in lower hardness and strength but better toughness. Slower and more homogeneous cooling allows the formation of crystallites (spherulites), which dramatically increases hardness and elastic modulus (Shbanah, 2023).
The parameters were ranked by their impact on hardness as follows: Layer Thickness, Infill Density, Raster Angle, Printing Speed, and Wall Thickness, from most to least significant.Layer Thickness appears to be the second most important parameter after Infill Density. The effect on impact, hardness and surface roughness tests is significant. Increased

[1] Corresponding author, dusan.jovanic@vts-zr.edu.rs, ORCID: 0009-0001-6058-4074
[2] aleksandar.rajic@vts-zr.edu.rs, ORCID: 0000-0003-3921-1502
[3] miodrag.kovacevic@vts-zr.edu.rs, ORCID:0000-0002-1803-6816
[4] ljubica.lazic@vts-zr.edu.rs, ORCID: 0009-0002-1975-3961:

layer thickness leads to poorer adhesion between layers, resulting in diminished impact strength (Verim et al., 2025).

ADDITIVE MANUFACTURING

According to the ISO 17296-2 standard, additive manufacturing can be classified into:Vat Photopolymerization – laser stereolithography (SLA) and stereolithography based on full-layer exposure (DLP-SLA, LCD-SLA); Powder Bed Fusion – processes using a laser (SLS, SLM, DMLS) and processes using an electron beam (EBM); Material Extrusion (FFF – Fused Filament Fabrication); Material Jetting (PolyJet, PolyJet Matrix); Binder Jetting (3D Printing, Slurry-based 3D Printing); Sheet Lamination (LOM, PSL); and Directed Energy Deposition-DED(ISO, 2017).

Material extrusion process

The material extrusion process, known as FFF (Fused Filament Fabrication)orFDM (Fused Deposition Modeling) – a trademark of Stratasys (Stratasys, n.d.), utilizes a solid thermoplastic material in the form of a filament. The filament is pushed through a heated nozzle, the temperature of which depends on the type of polymer, and is deposited in a semi-molten (pasty) state onto a heated or unheated build platform, where it solidifies to form the desired part layer by layer.
The most significant adjustable parameters for FFF 3D printers include: printing speed, extrusion speed, layer height(for both shell and infill), and the temperatures of the nozzle and the build plate (bed).
In FDM printing, residual stresses occur due to the rapid and uneven cooling of the layers; therefore, temperature control is critical for interlayer bond strength. It is necessary to investigate the temperature homogeneity of the layers, as proper interlayer adhesion is essential to reduce residual stresses (B. Redwood, 2017).

POLYLACTIDE

There is a large number of polymers with various mechanical, physical, chemical, electrical, thermal, and other properties, which have a wide range of applications.Polylactide (PLA) is a thermoplastic, biodegradable plastic derived from organic sources (such as corn starch, sugarcane, or sugar beet) through the fermentation of plant starch, and it exhibits properties similar to polypropylene (PP), polyethylene (PE), or polystyrene (PS). It is used for the production of food containers, films, and medical implants, and it possesses high surface energy, making it ideal for 3D printing. The drawbacks of PLA include low heat resistance and relatively low strength. The properties of PLA are presented in Table 1 (TWI Ltd., n.d.).

Table 1. *Karakteristike Polilaktida-PLA*

The parameters	Values
Density	1,24 g/cm³
Tensile Strength EN ISO 527-1	50 MPa
Flexural Strength EN ISO 178	80 MPa
Impact Strength (IZOD) - EN ISO 180	96,1 (J/m)
Shrinkage rates	0,37-0,41%

TERMOGRAPHY

Infrared thermography (IRT), also known as thermal imaging, can be used for the identification and documentation of irregularities for the purposes of machine condition monitoring, quality control, and non-destructive testing, as well as for monitoring temperatures during various manufacturing processes, such as temperature in the cutting

zone, extrusion temperature in forming processes, casting and cooling temperatures of castings, and thermal phenomena occurring during welding.
Thermography is based on the detection and measurement of the distribution of thermal radiation emitted from the observed surface and its conversion into a representation of radiation intensity differences, i.e., a surface temperature map known as a thermogram.
A significant advantage of infrared thermometers compared to contact temperature measurement methods lies in their extremely fast response time, since the radiated energy is transferred from the object to the sensor at the speed of light, enabling an almost instantaneous response. An additional advantage of these instruments is their high sensitivity, as they are capable of detecting and displaying thermal images composed of very small temperature differences [ISO, 2008].

EXPERIMENTAL RESEARCH

In a series of experiments, a specimen with dimensions of ϕ30 x 4 mm was used as the workpiece. The 3D model of the specimen was created using the SolidWORKS 2016 software package and then converted into the corresponding STL file with the maximum resolution permitted by the software (Figure 1). Subsequently, the relevant parameters were varied according to the experimental design, and a series of specimens with identical external appearances but different properties was produced.

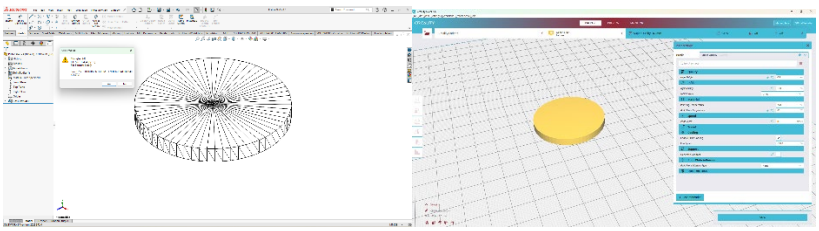


Fig. 1. *3D CAD model and STL file*

Figure 2 shows the Creality Ender-6 Core-XY 3D printer used for the experiment and the Creality CR PLA filament, while its technical specifications are given in Table 2 **(**Creality, n.d.).

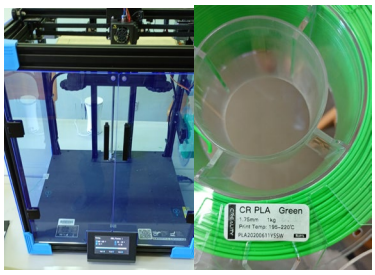


Fig. 2.*Creality Ender-6 Core-XY 3D printer and Creality CR PLA filament*

Table 2. *Technical specifications of the Creality Ender-6 Core-XY 3D printer*

The parameters	Values
Layer Height (mm)	0.1-0.4
Filament Diameter (mm)	1.75
Nozzle Diameter (mm)	0,4
Printing speed (mm/s)	30-150
Nozzle temperature (°C)	180-260
Bed Temperature (°C)	50-100

Creality CR PLA filament was used to fabricate the specimens, and its properties are presented in Table 3 (Creality, n.d.).

Table 3. *Properies of Creality CR PLA filament*

The parameters	Values
Filament Type	PLA
Diameter (mm)	1.75
Print temperature (°C)	195-220
Temperatura stola (°C)	0-60
Print speed (mm/s)	40-100

During the 3D printing of the PLA samples, the cooling rate of the layers was measured using a Testo 860i thermographic camera. The thermographic images were captured from a distance of 30 cm, at an angle of 45° to the workpiece, and with an emissivity setting of 0.95. Figure 3 shows the maximum measured temperature immediately behind the nozzle and the temperature after a time interval of 33 seconds, which were used to calculate the cooling rate (Testo SE & Co. KGaA., 2026).

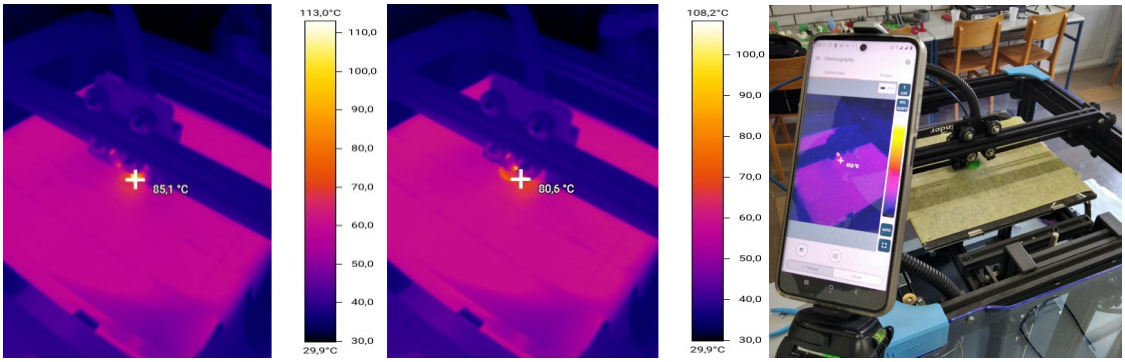


Fig. 3.*Thermograms of temperature immediately after nozzle passage and after a specific time period*

As a measuring instrument, a durometer- hardness meter Sauter A was used, following the Shore A scale, featuring a truncated cone-shaped needle with a 35° angle, requiring a minimum specimen thickness of 4 mm and possessing an accuracy of 1 HS (A) as shown in Figure 4.The test specimen was placed on a hard, horizontal, plane surface.The durometer was held in a vertical position with the point of the indenter at least 9 mm from any edge of the test specimen.The recommended mass was 1 kg for the type Adurometer.The scale of the indicating device was read after 15 s ± 1 s.Five measurements of hardness were taken at different positions on the test specimen, with a minimum separation of 6 mm, and the mean value was determined. The hardness values range from 0 (for full penetration) to 100 (for no penetration) (ISO, 2003).

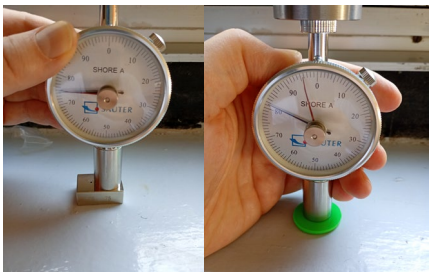


Fig. 4. *Calibration and hardness testing with a durometer*

RESULTS AND DISCUSSION

In the experiment, the values of the most significant 3D printing parameters were varied: Printing Temperature (°C), Printing Speed (mm/s), and Layer Height (mm). The values of the upper, middle, and lower levels of the 3D printing parameters are presented in Table 4. The specimens were fabricated with a 100% linear infill, a bed temperature of 60°C, and all other parameters were kept constant.

Table 4. *Values of the upper, middle, and lower levels of the PLA 3D printing parameters*

The parameters	Values		
	Level 1	Level 2	Level 3
Printing Temperature (°C)	200	210	220
Printing speed (mm/s)	40	60	80
Layer Height (mm)	0,1	0,2	0,3

The Taguchi L9 orthogonal array design of experiments was used for this study. Design of Experiments (DOE) is a systematic approach used to assess how input process parameters influence one or more output responses. By systematically varying input factors, DOE helps determine optimal process parameters and identify key factors and their best levels to meet performance targets. The Taguchi method uses the signal-to-noise (S/N) ratio to achieve the desired results. The S/N ratio method is applied when optimizing a process with multiple responses, using the "larger-the-better" criterion to maximize hardness. The mean hardness values from five measurements, as well as the cooling rate as a function of printing temperature, printing speed, and layer height, are presented in Table 5.

Table 5. *Hardness and cooling rate values for different FDM printing parameters of PLA*

Exp. no.	Printing Temperature (°C)	Printing Speed (mm/s)	Layer Height (mm)	Cooling Rate (°C/s)	Hardness (HS A)	S/N Ratio (dB)
1	200	40	0,1	0,03	88,6	38.9487
2	200	60	0,2	0,07	88,2	38.9094
3	200	80	0,3	0,11	85,6	38.6495
4	210	40	0,2	0,05	90,6	39.1426
5	210	60	0,3	0,09	88,4	38.9290
6	210	80	0,1	0,11	91,0	39.1808
7	220	40	0,3	0,22	86,5	38.7403
8	220	60	0,1	0,19	91,6	39.2379
9	220	80	0,2	0,14	88	38.8897

The mean values of hardness and S/N ratios for each individual parameter are presented in Table 6.

Table 6. *Mean hardness values and S/N ratios for each parameter*

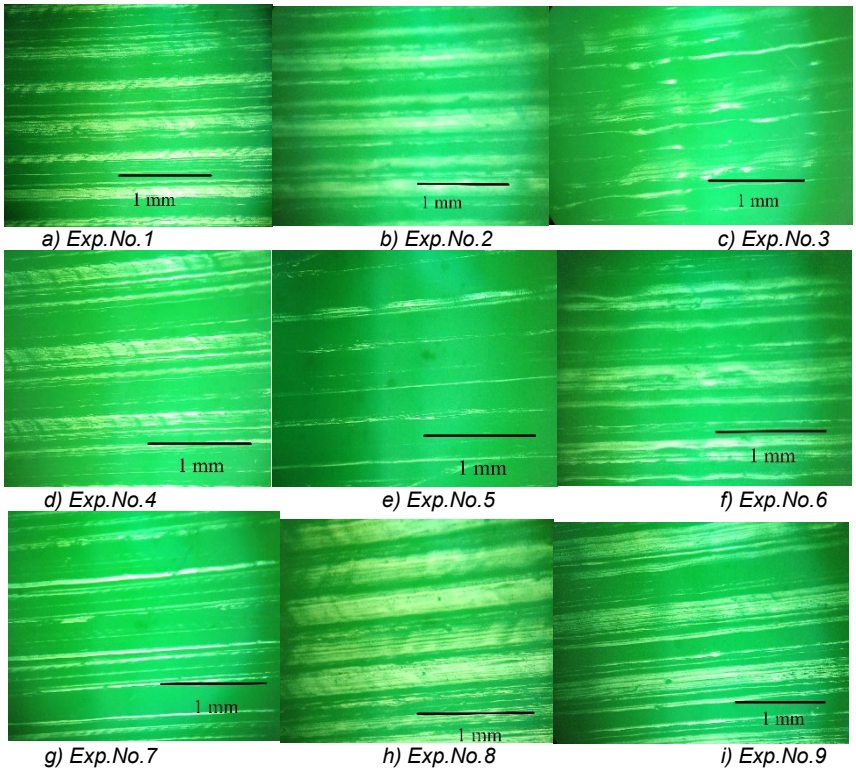
The parameters		Values	
		HS (A)	S/N ratio
Printing Temperature (°C)	200	87.47	38.84
	210	90,00	39.08
	220	88.70	38.96
Printing speed (mm/s)	40	88.57	38.94
	60	89.40	39.03
	80	88.20	38.91
Layer Height (mm)	0.1	90.40	39.12
	0.2	88.93	38.98
	0.3	86.83	38.77

Based on the S/N ratios from Table 6, it can be concluded that the optimal PLA 3D printing parameters for achieving maximum hardness are: a printing temperature of 210°C, a printing speed of 60 mm/s, and a layer height of 0.1 mm.
The influence rank is determined based on the Delta value, which represents the difference between the maximum and minimum mean values for the observed factor. A larger Delta value indicates that the factor has a stronger influence on the final response. The influence ranking for both hardness and process stability is presented in Table 7.

Table 7. *Influence ranking for hardness and process stability*

The parameters	Δ value HS (A)	Rang HS (A)	Δ value S/N	Rang S/N
Printing Temperature (°C)	2,53	2	0,24	2
Print speed (mm/s)	1,20	3	0,12	3
Layer Height (mm)	3,57	1	0,35	1

Based on the ranking of influence and process stability, it can be concluded that layer height has the greatest impact on both hardness and process stability (Rank 1), printing temperature has a moderate impact (Rank 2), and printing speed has the least impact on hardness (Rank 3). As the layer height decreases from 0.3 mm to 0.1 mm, the hardness increases significantly. A lower layer height allows for better compaction and lower material porosity, which directly enhances mechanical resistance.
Microscopic images of the PLA specimens, corresponding to the experimental design and captured at 5x magnification, are shown in Figure 5.



a) Exp.No.1 *b) Exp.No.2* *c) Exp.No.3*
d) Exp.No.4 *e) Exp.No.5* *f) Exp.No.6*
g) Exp.No.7 *h) Exp.No.8* *i) Exp.No.9*

Fig. 5*. Microscopic images of PLA specimens at 5× magnification*

In Figure 5, the darker lines represent the grooves between the layers, which act as stress concentration zones; the wider they are, the rougher the surface. Microscopic inspection revealed that the width of the deposited layer is the largest at the minimum layer height. In Figure 5a, due to the low speed, a high number of continuous lines appear, while the grooves are minimal, resulting in a homogeneous structure.

In Figure 5b, the number of visible lines decreases proportionally as the layer height doubles to 0.2 mm.
In experiment number 3, due to the combination of low printing temperature, high speed, and large layer height, the material failed to flow and fuse properly; consequently, the layer boundaries are indistinct and rough, as shown in Figure 5c.
Experiment number 4, due to the elevated temperature of 210°C and slow printing speed of 40 mm/s, enabled perfectly parallel lines with a layer height of 0.2 mm without any microscopic discontinuities, which can be seen in Figure 5d.
In Figure 5e, very wide grooves dominate, which corresponds to a layer height of 0.3 mm.
Figure 5f shows a fine structure with a high number of thin 0.1 mm layers. Here, due to the speed of 80 mm/s, a slight waviness within the lines themselves is observed compared to Figure 5a, which has the same deposited layer height.
Figure 5g displays wide grooves due to the layer height of 0.3 mm, which appear highly fused because of the high temperature of 220°C and low speed.
The structure in Figure 5h is very smooth and compact, as the high temperature allowed the thin 0.1 mm layers to achieve maximum bonding, making this surface look the most homogeneous among all the samples.
Good material cohesion due to the high printing temperature is shown in Figure 5i, but the grooves are twice as large as in the previous experiment due to the layer height of 0.2 mm and a printing speed of 80 mm/s.
The minimum layer height of 0.1 mm has a dominantly positive impact on hardness. As a rule, a lower layer height means greater compaction of the material, a lower volume of air micropores within the model, and more layer boundaries that sustain the load, which directly increases the surface hardness.

CONCLUSION

3D printing using the material extrusion process (FFF technology) results in a low surface finish quality; regarding hardness, it was determined that the 3D printing parameters—printing temperature, printing speed, and layer height—have a significant influence on this property. Based on the ranking of influence and process stability, it was confirmed that layer height has a dominant impact on both hardness and process stability, followed by printing temperature, which has a moderate impact, while printing speed has the least impact on hardness compared to these parameters. Experiments demonstrated that the highest hardness of the PLA plastic sample is achieved at the minimum layer height of 0.1 mm. A lower layer height allows for better compaction and lower material porosity, which directly enhances mechanical resistance.
A higher printing temperature enables better interlayer adhesion, while faster printing affects the cooling process. The cooling rate, measured with a thermographic camera, should not be excessively high in order to avoid residual stresses and to ensure homogeneous fusion of the layers, which leads to better mechanical properties.
Based on the optimization using the Taguchi method, the optimal PLA 3D printing parameters for maximizing hardness were determined to be: a printing temperature of 210°C, a printing speed of 60 mm/s, and a layer height of 0.1 mm. This configuration is closest to experiment number 8, which, from a microstructural standpoint, exhibits the most homogeneous structure among all samples, appearing highly smooth and compact.

ACKNOWLEDGEMENT

This paper is part of a research on the project entitled: "*Optimizacija proizvodnog procesa primenom termovizijske tehnologije*", No. *003817351 2025 09418 004 000 000 001*, supported by *Pokrajinski sekretarijat za visoko obrazovanje I naučnoistraživačku delatnost.*

REFERENCES

Creality. (n.d.). *CR-PLA*. https://wiki.creality.com/en/3d-printer-accessories/CR-PLA

Creality. (n.d.). *Ender-6 3D printer*. https://www.creality.com/products/ender-6-3d-printer

International Organization for Standardization. (2003). *Plastics and ebonite—Determination of indentation hardness by means of a durometer (Shore hardness)* (ISO Standard No. 868:2003).

International Organization for Standardization. (2008). *Condition monitoring and diagnostics of machines—Thermography—Part 1: General procedures* (ISO Standard No. 18434-1:2008).

International Organization for Standardization. (2014). *Additive manufacturing—General principles—Part 3: Main characteristics and corresponding test methods* (ISO Standard No. 17296-3:2014).

International Organization for Standardization. (2015). *Additive manufacturing—General principles—Part 2: Overview of process categories and feedstock* (ISO Standard No. 17296-2:2015).

Motgi, R. S., Mohite, S. K., Dhalait, J. G., &Patil, N. P. (2023). Optimization of 3D printing process parameters for improving hardness of PLA plastic using Taguchi method. *AIP Conference Proceedings*. https://doi.org/10.1063/5.0165714

RajabiKafshgar, A., Rostami, S., Aliha, M. R. M., &Berto, F. (2021). Optimization of properties for 3D printed PLA material using Taguchi, ANOVA and multi-objective methodologies. *Procedia Structural Integrity, 34*, 71–77. https://doi.org/10.1016/j.prostr.2021.12.011

Redwood, B., Schöffer, F., & Garret, B. (2017). *The 3D printing handbook: Technologies, design and applications*. 3D Hubs B.V.

Shbanah, M. (2024, June 15). *The effect of heat treatment on a 3D-printed PLA polymer's mechanical properties*. Thermal Processing Magazine. https://thermalprocessing.com/the-effect-of-heat-treatment-on-a-3d-printed-pla-polymers-mechanical-properties/

Stratasys. (n.d.). *FDM 3D printers*. https://www.stratasys.com/en/3d-printers/printer-catalog/fdm-printers/

Testo SE & Co. KGaA. (2026). *Testo Smart App* [Mobile app].

TWI Ltd. (n.d.). *What is PLA? (Everything you need to know)*.https://www.twi-global.com/technical-knowledge/faqs/what-is-pla

Verim, Ö., Saeed, O., Eid, M. H., Mahmoud, S. F., Saleh, D. I., &Elwakeel, A. E. (2025). Investigation of the effects of 3D printing parameters on mechanical tests of PLA parts produced by MEX 3D printing using Taguchi method. *Scientific Reports, 15*, 15008. https://doi.org/10.1038/s41598-025-98832-0

DOI:10.5937/IIZS26072C

ARTIFICIAL NEURAL NETWORK-BASED INVERSE KINEMATICS MODELING OF A 3-DOF PLANAR ROBOTIC MANIPULATOR

Research paper

Haşmet Çağrı Sezgen[1*], Abdullah Çakan[2]
[1]Department of Mechanical Engineering, Necmettin Erbakan University, Konya, Türkiye
[2]Department of Mechanical Engineering, Konya Technical University, Konya, Türkiye

Abstract: Inverse kinematics is a fundamental problem in robotic manipulator control, especially when the joint variables must be determined from a desired end-effector pose. In this study, an artificial neural network-based regression model is developed for the inverse kinematics prediction of a 3-DOF planar robotic manipulator. The model uses the end-effector position and orientation as input variables and predicts the corresponding three joint angles as output variables. The training data set was generated by considering the robot link lengths, joint constraints, reachable workspace and valid inverse kinematic solutions. A multilayer feedforward artificial neural network was trained and tested using separate training, validation and test data sets. The performance of the model was evaluated using error metrics, regression scatter diagrams, workspace-based visualization and selected target configuration tests. The results obtained indicate that the proposed ANN model can approximate the inverse kinematics mapping within the feasible workspace of the manipulator. This approach provides a simple and effective learning-based solution for joint angle estimation in planar robotic systems.
Key words: artificial neural network, inverse kinematics, planar manipulator, regression analysis, robot workspace, task space sampling.

INTRODUCTION

Artificial neural networks (ANNs) have become widely used data-driven models for approximating nonlinear input–output relationships in engineering systems. Their ability to learn from representative examples and generalize to unseen cases makes them suitable for regression, prediction, control and surrogate modeling problems (Bishop, 2006; Gurney, 2018; Haykin, 2009). In engineering applications, ANN models have been used not only in robotics but also in different physical domains where direct mathematical modeling or high-fidelity simulation can be time-consuming. For example, neural-network-based models have been investigated for thermoelectric generator performance estimation, multi-output brake disc behavior prediction based on finite element analyses CFD-based wind turbine performance and deformation prediction (Hamzah et al., 2025; Sezgen et al., 2025; Sreekala et al., 2023). These studies indicate that ANN models can serve as fast approximation tools when the underlying problem includes nonlinear relations, multiple input variables and computationally expensive conventional analyses.

Robotic manipulators are widely used in industrial automation, manufacturing, assembly, material handling, medical systems and research platforms because they can perform repetitive and precise motion tasks with high repeatability. The motion of a manipulator is commonly described through two complementary kinematic problems. Forward kinematics determines the position and orientation of the end effector from known joint variables, whereas inverse kinematics determines the required joint variables from a desired end-effector pose (Craig, 2005; Spong et al., 2006). Similar distinctions between task-space and joint-space representations are also important in movement planning studies, where target-level descriptions must be transformed into coordinated joint motion (Flash et al., 2013). For robot control and trajectory planning, inverse kinematics is particularly important because task commands are often specified in Cartesian space while the actuators are driven in joint space.

The inverse kinematics problem is generally more difficult than forward kinematics because the mapping from Cartesian space to joint space is nonlinear, may be non-unique and may include singular or infeasible configurations. Classical solution strategies such as geometric, algebraic and iterative methods are effective for certain robot structures, but they may

[1]Corresponding author, hasmetcagri.sezgen@erbakan.edu.tr, ORCID: 0000-0002-6265-4259
[2]acakan@ktun.edu.tr, ORCID: 0000-0003-3923-4069

become difficult to generalize when the manipulator geometry becomes more complex or when the number of degrees of freedom increases. Analytical research has therefore focused on deriving more efficient inverse kinematic formulations for specific robot structures, including constrained 6R robotic arms (Chen et al., 2023). In parallel, optimization-based approaches have addressed inverse kinematics by minimizing position and orientation errors through metaheuristic search strategies. Examples include beta salp swarm optimization and multi-objective modified particle swarm optimization formulations for inverse kinematics problems (Rokbani et al., 2022a, 2022b). These methods are useful alternatives, but they generally require iterative optimization for each target pose.

ANN-based inverse kinematics models have been investigated as an alternative or complementary approach to analytical, numerical and optimization-based solvers. Early studies showed that neural networks could learn the mapping between Cartesian coordinates and joint angles for robotic manipulators. Köker et al. (2004) used a neural network to solve the inverse kinematics of a three-joint robot, while Karlik and Aydin (2000) applied a structured ANN approach to the inverse kinematics of a six degree-of-freedom manipulator using end-effector position and orientation variables. Tang et al. (2014) used ANN models for predicting manipulator motion when trajectory characteristics are unknown, highlighting the ability of neural networks to approximate complex motion-related mappings. Almusawi et al. (2016) proposed an ANN-based inverse kinematics approach for a six degree-of-freedom robotic arm and showed that including the current joint configuration in the input structure can improve prediction accuracy.

Recent studies further demonstrate that ANN-based inverse kinematics remains an active research topic across different manipulator types. Comparative soft-computing studies have evaluated ANN, ANFIS and optimization-based approaches for manipulator inverse kinematics (El-Sherbiny et al., 2018). Deep artificial neural networks have been used to estimate the joint variables of serial robotic manipulators from kinematic data (Shah et al., 2020) machine-learning sequential methodologies have been proposed for inverse kinematic modelling using forward-kinematics-generated datasets (Tagliani et al., 2022). ANN and fuzzy neural network models have also been studied for serial robots with different degrees of freedom, with emphasis on learning the robot workspace rather than a single predefined trajectory (Demby's et al., 2019). In addition, ANN-based inverse kinematics has been applied to continuum robots, wrist rehabilitation robots and SCARA manipulators, showing the adaptability of neural models to different robot architectures and application requirements (Bouzid et al., 2024a; Ghoul et al., 2022; Saeedi et al., 2024). Hybrid studies combining ANN models with metaheuristic algorithms have also been reported for two- and three-degree-of-freedom manipulators, where optimization is used to improve network configuration or training performance (Bouzid et al., 2024b; Shastri et al., 2020). In this context, the use of neural networks in robotics is consistent with the broader view that neural models can support perception, control, approximation and decision-making tasks in robotic systems (Bekey & Goldberg, 2012).

Although these studies show the potential of ANN models for inverse kinematics, the reliability of such models strongly depends on how the training data are generated and how the feasible workspace is represented. In a planar three degree-of-freedom manipulator, the end-effector position alone is not sufficient to define a unique inverse kinematic solution because different joint configurations may reach the same Cartesian point. Therefore, the end-effector orientation must also be considered when constructing the input vector for a learning-based inverse kinematics model. Moreover, target configurations outside the reachable workspace or outside the joint limits should be excluded from the training and validation process in order to obtain a physically meaningful mapping.

This paper presents an ANN-based inverse kinematics model for a 3-DOF planar robotic manipulator. The model uses the end-effector position and orientation, $[x, y, \phi]^T$, as input variables and directly predicts the three joint angles, $[\theta_1, \theta_2, \theta_3]^T$, without using a sine–cosine output representation. The dataset is generated from the kinematic model by considering link lengths, joint limits, reachable workspace and valid inverse kinematic solutions. The trained model is evaluated using training and validation loss curves, joint-angle error histograms,

regression scatter diagrams and selected target configuration tests within the feasible workspace.

KINEMATIC MODEL OF THE 3-DOF PLANAR MANIPULATOR

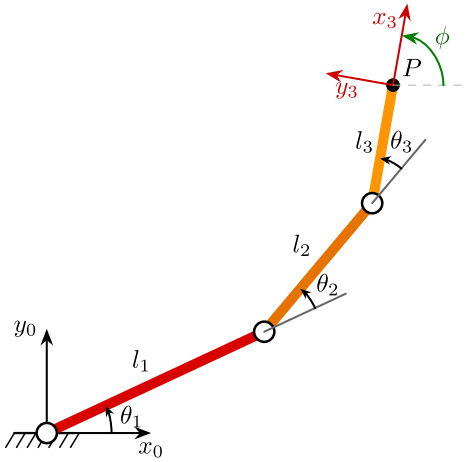


Fig. 1. *Serial 3-DOF planar robotic manipulator.*

Forward Kinematics

The studied system is a serial 3-DOF planar robotic manipulator shown in Fig. 1. The link lengths are denoted by l_1, l_2 and l_3 and the joint variables are represented by θ_1, θ_2 and θ_3. The end-effector position in the fixed Cartesian frame is defined by x and y, while the end-effector orientation is represented by the cumulative angle ϕ. The forward and inverse kinematic formulations are based on classical robotic manipulator modeling principles (Craig, 2005; Spong et al., 2006).

The forward kinematic model maps the joint variables to the end-effector pose as

$$x = l_1\cos\theta_1 + l_2\cos(\theta_1 + \theta_2) + l_3\cos(\theta_1 + \theta_2 + \theta_3) \quad (1)$$

$$y = l_1\sin\theta_1 + l_2\sin(\theta_1 + \theta_2) + l_3\sin(\theta_1 + \theta_2 + \theta_3) \quad (2)$$

and

$$\phi = \theta_1 + \theta_2 + \theta_3 \quad (3)$$

These equations were used for generating the task-space data and for checking the kinematic consistency of the ANN predictions. The robot parameters used in the MATLAB model are listed in Table 1.

Table 1. *Robot geometry and joint limits*

Parameter	Value / Minimum	Maximum
l_1	10	–
l_2	7	–
l_3	5	–
θ_1	−180°	180°
θ_2	−170°	170°
θ_3	−170°	170°

Analytical Inverse Kinematics and Feasibility Check

For a desired target pose, the wrist point is calculated by removing the contribution of the third link from the end-effector pose:

$$x_w = x - l_3 \cos\phi \tag{4}$$

$$y_w = \mathrm{y} - l_3 \sin\phi \tag{5}$$

The two-link inverse kinematics subproblem is then solved using

$$c_2 = \frac{x_w^2 + y_w^2 - l_1^2 - l_2^2}{2 l_1 l_2} \tag{6}$$

$$s_2 = b\sqrt{1 - c_2^2}, \quad b \in \{-1,1\} \tag{7}$$

where b denotes the selected inverse kinematic branch. The joint variables are obtained as

$$\theta_2 = \mathrm{atan2}(s_2, c_2) \tag{8}$$

$$\theta_1 = \mathrm{atan2}(y_w, x_w) - \mathrm{atan2}(l_2 s_2, l_1 + l_2 c_2) \tag{9}$$

$$\theta_3 = \phi - \theta_1 - \theta_2 \tag{10}$$

A target was accepted as valid only when the wrist point was reachable and all calculated joint angles satisfied the prescribed joint limits. The wrist reachability condition is

$$|l_1 - l_2| \le \sqrt{x_w^2 + y_w^2} \le l_1 + l_2 \tag{11}$$

DATA SET GENERATION AND ANN MODEL

Input and Output Definition

The inverse kinematics problem was formulated as a supervised regression task. The input vector of the ANN was defined as

$$\mathbf{p} = [x, y, \phi]^T \tag{12}$$

and the output vector was defined as

$$\mathbf{q} = [\theta_1, \theta_2, \theta_3]^T \tag{13}$$

In this implementation, the joint angles were directly used as the output variables. A sine-cosine representation of the joint angles was not used.The data set summary is presented in Table 2. The train-validation-test distribution in the reachable workspace is shown in Fig. 2.

Table 2. *Data set summary*

Quantity	Value
Total samples	71040
Training samples	49728

Quantity	Value
Validation samples	10656
Test samples	10656
Input variables	x, y, ϕ
Output variables	θ_1, θ_2, θ_3
Output representation	Direct joint angles

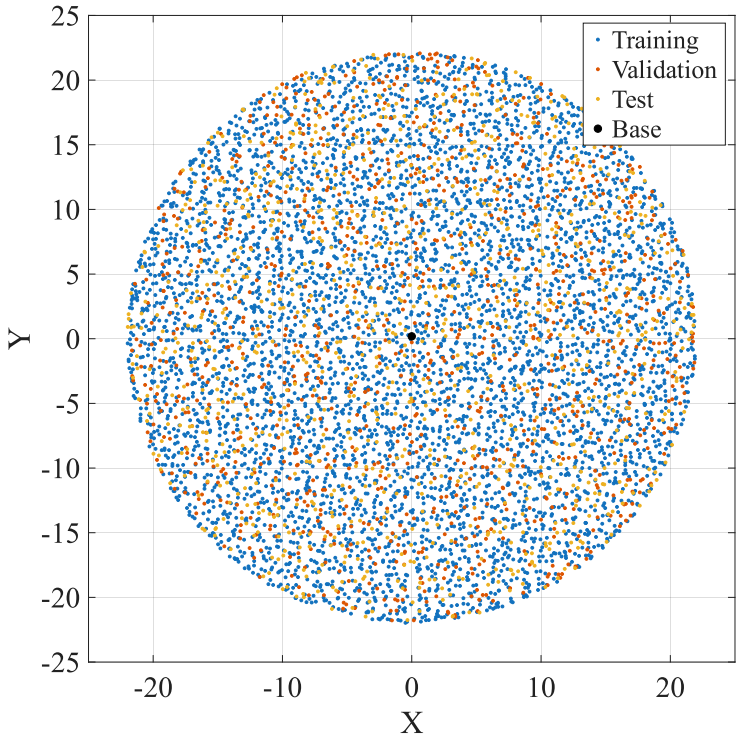


Fig.2. *Distribution of training, validation and test samples*

ANN Training

The regression model follows the general supervised learning approach used in neural network modeling (Bishop, 2006; Haykin, 2009). A feedforward ANN was used to approximate the mapping from the task-space variables to the joint variables:

$$f_{\mathrm{ANN}}: [x, y, \phi]^T \rightarrow [\theta_1, \theta_2, \theta_3]^T \tag{14}$$

The input variables were normalized using the mean and standard deviation obtained from the training subset. The same normalization parameters were then used for the validation and test subsets.

The training summary exported from MATLAB is given in Table 3. The training and validation loss histories are shown in Fig. 3.

Table 3. *Training summary*

Metric	Value
Final training loss	0.0028544
Final validation loss	0.0033002
Best validation loss	0.0031839
Learnable parameters	100998

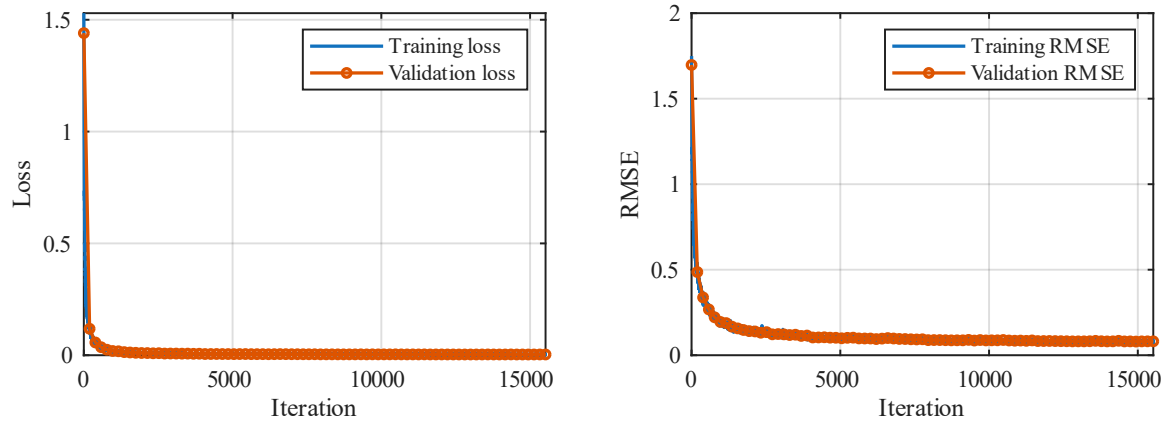


Fig. 3. *Training and validation loss histories of the ANN model*

PERFORMANCE EVALUATION

Joint Angle Error Metrics

The joint angle prediction error for each output is defined as

$$e_{\theta_i,k} = \theta_{i,k}^{\text{true}} - \theta_{i,k}^{\text{pred}} \tag{15}$$

where *i = 1, 2, 3* denotes the joint index and k denotes the sample index. The mean absolute error and root mean square error are calculated as

$$\text{MAE}_{\theta_i} = \frac{1}{N}\sum_{k=1}^{N}\left|e_{\theta_i,k}\right| \tag{16}$$

$$\text{RMSE}_{\theta_i} = \sqrt{\frac{1}{N}\sum_{k=1}^{N} e_{\theta_i,k}^2} \tag{17}$$

The error histograms for the three joint variables are shown in Fig. 4. The numerical error values exported from MATLAB are listed in Table 4.

Table 4. *Joint angle prediction error metrics in degrees*

Data set	Output	MAE	RMSE
Train	θ_1	1.4041	1.9800
Train	θ_2	1.2127	2.0099
Train	θ_3	1.9202	2.7759
Validation	θ_1	1.4427	2.0284
Validation	θ_2	1.2610	2.1270
Validation	θ_3	2.0152	2.9088
Test	θ_1	1.4475	2.0633
Test	θ_2	1.2075	2.0310
Test	θ_3	2.0343	2.9258
All	θ_1	1.4185	2.0044
All	θ_2	1.2184	2.0311
All	θ_3	1.9573	2.8266

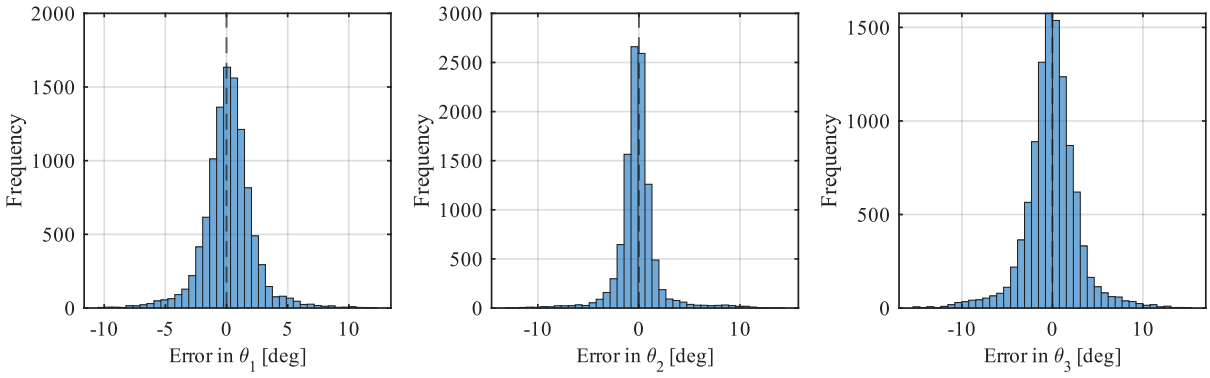


Fig. 4. *Joint angle prediction error histograms for θ_1, θ_2 and θ_3.*

Regression Scatter Analysis

Regression scatter diagrams were used to evaluate the agreement between the target joint angles and the ANN-predicted joint angles. In this paper, only the all-data regression plots are included for compact presentation. The all-data regression plots for θ_1, θ_2 and θ_3 are shown in Fig. 5. The corresponding correlation coefficients are summarized in Table 5.

Table 5. *Regression coefficients for joint angle prediction*

Output	Train	Validation	Test	All
θ_1	0.98466	0.99001	0.97786	0.98377
θ_2	0.99977	0.99975	0.99979	0.99977
θ_3	0.99914	0.99951	0.99835	0.99901

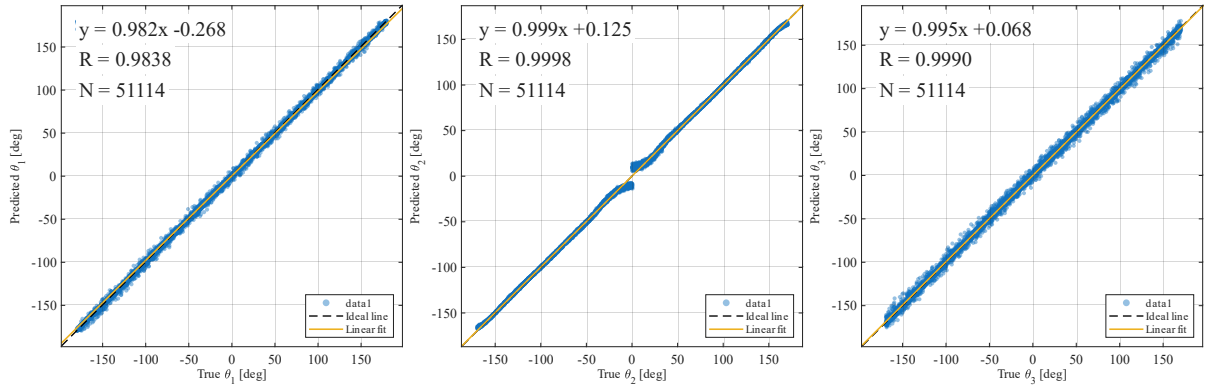


Fig. 5. *All-data regression scatter diagram for: θ_1,θ_2 andθ_3.*

TARGET-BASED VALIDATION

Selected target configurations were used for visual and numerical validation. Each target was defined by the task-space coordinates x, y and ϕ. The analytical inverse kinematics solution was calculated first and the ANN-predicted joint angles were then compared with the analytical solution.

The selected valid target configurations and the corresponding analytical inverse kinematic results are listed in Table 6. The combined robot configuration plots are given in Fig. 6. The figure is divided into three parts to improve readability.

The detailed ANN prediction errors exported for the target validation group are listed in Table 7. These values quantify the difference between the analytical inverse kinematics solution and the ANN-predicted robot posture for the reported target cases.

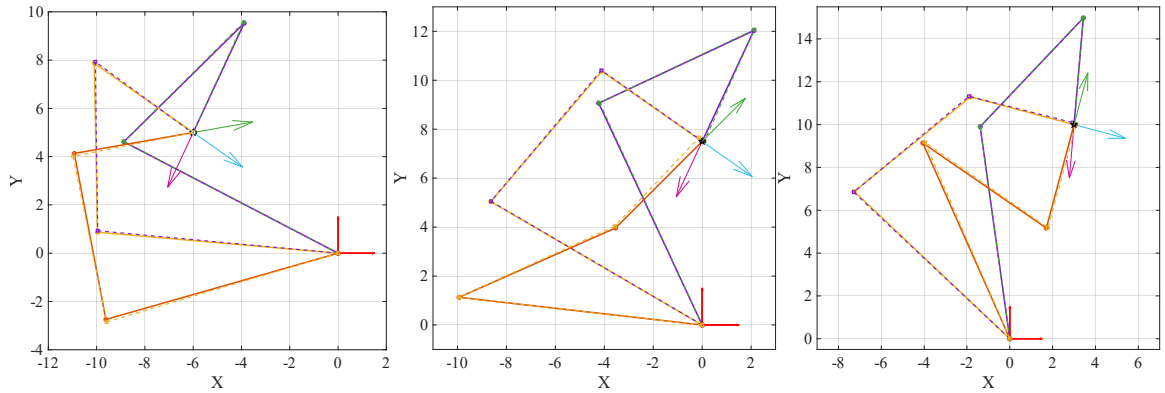


Fig. 6. *Selected target robot configurations in the reachable workspace:first target group, second target group and third target group.*

Table 6. *Selected target configurations and analytical inverse kinematic results*

Target	x	y	ϕ [deg]	θ_1 [deg]	θ_2 [deg]	θ_3 [deg]	r_w
1	−6	5	−115	152.51	−107.91	−159.60	10.294
2	−6	5	−35	175.01	−83.92	−126.09	12.800
3	−6	5	10	−164.07	−95.16	−90.77	11.679
4	0	7.5	−115	115.00	−89.91	−140.09	12.216
5	0	7.5	−35	149.73	−100.18	−84.56	11.148
6	0	7.5	45	173.51	−149.63	21.11	5.312
7	3	10	−95	97.95	−51.46	−141.49	15.370
8	3	10	−15	136.55	−97.43	−54.13	11.441
9	3	10	75	113.96	−148.49	109.53	5.445

Table 7. *ANN prediction errors for the selected target validation cases*

Target	x	y	ϕ [deg]	e_{θ_1} [deg]	e_{θ_2} [deg]	e_{θ_3} [deg]	e_p	e_ϕ [deg]
1	−6	5	−115	0.116	0.128	0.403	0.0292	0.647
2	−6	5	−35	0.258	0.697	0.005	0.0760	0.961
3	−6	5	10	1.114	0.353	0.061	0.1525	0.700
4	0	7.5	−115	0.689	0.364	0.476	0.1258	0.577
5	0	7.5	−35	0.177	0.053	0.072	0.0255	0.302
6	0	7.5	45	0.983	0.367	0.321	0.1080	0.295
7	3	10	−95	0.565	0.155	1.307	0.0164	1.717
8	3	10	−15	1.656	0.487	1.151	0.3039	0.017
9	3	10	75	2.459	0.338	1.715	0.2844	0.406

RESULTS AND DISCUSSION

The training and validation losses show that the ANN model converged during the supervised regression process. The final training loss was 0.0028544, while the final validation loss was 0.0033002. The best validation loss was 0.0031839, indicating that the validation performance remained close to training performance.

The joint angle error metrics show that the prediction error was relatively low for all three outputs. Considering the all-data results, the MAE values were 1.4185 deg, 1.2184 deg and 1.9573 deg for θ_1, θ_2 and θ_3, respectively. The corresponding RMSE values were 2.0044 deg, 2.0311 deg and 2.8266 deg.

The largest error was obtained for θ_3, which can be attributed to the cumulative nature of the planar manipulator orientation and the stronger sensitivity of the third joint in satisfying the prescribed end-effector orientation.

The regression coefficients also indicate a strong relationship between the analytical target joint angles and the ANN predictions. The all-data regression coefficients were 0.98377, 0.99977 and 0.99901 for θ_1, θ_2 and θ_3, respectively. These results show that the network

approximated the inverse kinematic mapping with high linear agreement within the feasible workspace.
The target-based validation confirms that the selected task-space points are feasible under the specified joint limits and branch selection. The combined target configuration plots in Fig. 6 provide a visual comparison of the target locations and the robot postures. The detailed target errors reported in Table 7 show that the ANN predictions remain close to the analytical solutions for the exported target cases. For the selected targets, the maximum position error was 0.3039 length units and the maximum orientation error was 1.7166 deg.

CONCLUSION

This paper presented an ANN-based inverse kinematics model for a 3-DOF planar robotic manipulator. The model uses the end-effector position and orientation as input variables and directly predicts the three joint angles. The data set was generated from the kinematic model by considering the link lengths, joint limits, feasible workspace and valid inverse kinematic solutions. The model was evaluated using selected MATLAB outputs, including train-validation-test data distribution, training and validation loss, joint error histograms, all-data regression scatter diagrams and target-based robot configuration plots.
The obtained results show that the ANN model can approximate the inverse kinematic mapping of the 3-DOF planar manipulator with satisfactory prediction accuracy in the feasible workspace. Future work may include alternative network architectures, larger and more balanced task-space data sets, branch-aware learning strategies and experimental validation on a physical robotic manipulator.

REFERENCES

Almusawi, A. R. J., Dülger, L. C., & Kapucu, S. (2016). A new artificial neural network approach in solving inverse kinematics of robotic arm (Denso VP6242). Computational Intelligence and Neuroscience, 2016, 5720163.

Bekey, G. A., & Goldberg, K. Y. (2012). Neural networks in robotics (Vol. 202). Springer Science & Business Media.

Bishop, C. M. (2006). Pattern recognition and machine learning. Springer.

Bouzid, R., Gritli, H., & Narayan, J. (2024a). ANN approach for SCARA robot inverse kinematics solutions with diverse datasets and optimisers. Applied Computer Systems, 29(1), 24–34.

Bouzid, R., Gritli, H., & Narayan, J. (2024b). Optimized inverse kinematics of a 2-DOF robotic manipulator using a hybrid approach combining an ANN with a metaheuristic algorithm. In 2024 IEEE International Conference on Artificial Intelligence & Green Energy (ICAIGE) (pp. 1–6). IEEE.

Chen, F., Ju, H., & Liu, X. (2023). Inverse kinematic formula for a new class of 6R robotic arms with simple constraints. Mechanism and Machine Theory, 179, 105118.

Craig, J. J. (2005). Introduction to robotics: Mechanics and control (3rd ed.). Pearson Prentice Hall.

Demby's, J., Gao, Y., & DeSouza, G. N. (2019). A study on solving the inverse kinematics of serial robots using artificial neural network and fuzzy neural network. In 2019 IEEE International Conference on Fuzzy Systems (FUZZ-IEEE) (pp. 1–6). IEEE.

El-Sherbiny, A., Elhosseini, M. A., & Haikal, A. Y. (2018). A comparative study of soft computing methods to solve inverse kinematics problem. Ain Shams Engineering Journal, 9(4), 2535–2548.

Flash, T., Meirovitch, Y., & Barliya, A. (2013). Models of human movement: Trajectory planning and inverse kinematics studies. Robotics and Autonomous Systems, 61(4), 330–339.

Ghoul, A., Kara, K., Djeffal, S., Benrabah, M., & Hadjili, M. L. (2022). Artificial neural network for solving the inverse kinematic model of a spatial and planar variable curvature continuum robot. Archive of Mechanical Engineering, 69(4), 595–613.

Gurney, K. (2018). An introduction to neural networks. CRC Press.

Hamzah, H., Alkhabbaz, A., Koprulu, A., Jasim, L. M., Alzubaidi, I. K., Yaseen, A. H., Yang, H.-S., & Lee, Y.-H. (2025). Integrated CFD and ANN approach for predicting blade deformation and aerodynamic response. Wind, 5(4), 33.

Haykin, S. (2009). Neural networks and learning machines (3rd ed.). Pearson.

Karlik, B., & Aydin, S. (2000). An improved approach to the solution of inverse kinematics problems for robot manipulators. Engineering Applications of Artificial Intelligence, 13(2), 159–164.

Köker, R., Öz, C., Çakar, T., & Ekiz, H. (2004). A study of neural network based inverse kinematics solution for a three-joint robot. Robotics and Autonomous Systems, 49(3–4), 227–234.

Rokbani, N., Mirjalili, S., Slim, M., & Alimi, A. M. (2022a). A beta salp swarm algorithm meta-heuristic for inverse kinematics and optimization. Applied Intelligence, 52, 10493–10518.

Rokbani, N., Neji, B., Slim, M., Mirjalili, S., & Ghandour, R. (2022b). A multi-objective modified PSO for inverse kinematics of a 5-DOF robotic arm. Applied Sciences, 12(14), 7091.

Saeedi, B., Mohammadi Moghaddam, M., & Sadedel, M. (2024). Inverse kinematics analysis of a wrist rehabilitation robot using artificial neural network and adaptive neuro-fuzzy inference system. Mechanics Based Design of Structures and Machines, 52(12), 10439–10487.

Sezgen, H. Ç., Gülbahçe, E., & Çakan, A. (2025). Prediction of brake disc mechanical behavior using artificial neural networks. In 2025 IEEE 25th International Symposium on Computational Intelligence and Informatics (CINTI) (pp. 223–228). IEEE.

Shah, S. K., Mishra, R., & Ray, L. S. (2020). Solution and validation of inverse kinematics using deep artificial neural network. Materials Today: Proceedings, 26(2), 1250–1254.

Shastri, S., Parvez, Y., & Chauhan, N. R. (2020). Inverse kinematics for a 3-R robot using artificial neural network and modified particle swarm optimization. Journal of The Institution of Engineers (India): Series C, 101(2), 355–363.

Spong, M. W., Hutchinson, S., & Vidyasagar, M. (2006). Robot modeling and control. Wiley.

Sreekala, P., Ramkumar, A., & Rajesh, K. (2023). Performance comparison and analysis of mathematical, ANSYS and neural network model of a thermo electrical generator. Measurement: Sensors, 26, 100675.

Tagliani, F. L., Pellegrini, N., & Aggogeri, F. (2022). Machine learning sequential methodology for robot inverse kinematic modelling. Applied Sciences, 12(19), 9417.

Tang, S. H., Ang, C. K., Mohd Ariffin, M. K. A., & Mashohor, S. (2014). Predicting the motion of a robot manipulator with unknown trajectories based on an artificial neural network. International Journal of Advanced Robotic Systems, 11, 176.

DOI:10.5937/IIZS26082J

TAGUCHI BASED OPTIMIZATION OF POLYETHILENE MILLING PARAMETERS BASED ON CUTTING TEMPERATURE AND SURFACE ROUGHNESS CRITERIA

Research paper

Dušan Jovanić[1], Spasoje Erić[2], Miodrag Kovačević[3]
[1,2,3]Technical College of Applied Sciences, Zrenjanin, Serbia

Abstract: This paper presents the optimization of face milling parameters for polyethylene (PE) using an end mill on an Emco 55 Mill CNC machine by applying the Taguchi method. The aim was to investigate the influence of machining parameters on cutting temperature, cooling rate, and the surface roughness of the machined surface in both the feed direction and the direction perpendicular to the feed.
During the experiment, the machining parameters: spindle speed, feed rate, and depth of cut, were varied at three levels. A thermographic camera was used to measure the characteristic temperatures at a point immediately behind the face milling cutter and after a specified time interval. Based on these measurements, the cooling rate was determined, as it influences the surface roughness of the machined surface.
The surface roughness of the polyethylene specimens was evaluated using a surface roughness tester. The measured output geometric parameters included the Arithmetic Mean Roughness (Ra), Root Mean Square Roughness (Rq), Maximum Profile Height (Rz), and Total Profile Height (Rt). In addition, the surface profile geometry, i.e., the roughness profiles, was presented both in the feed direction and perpendicular to it, in accordance with the EN ISO 4287 standard.
Key words: Optimization, Roughness, CNC milling, Polyethylene, Thermography, Cutting temperature.

INTRODUCTION

During machining by cutting, stresses are generated within the material due to plastic deformation occurring in the initial stage of chip formation, as well as due to the heat produced during the cutting process. As a result of the interaction between the cutting tool and the workpiece, in addition to thermal energy, a machined surface is created with a series of peaks and valleys, referred to as the surface roughness. In milling operations, the surface roughness is directly proportional to the square of the feed rate and inversely proportional to the cutter diameter.
The aim of this study is to investigate the influence of polyethylene milling parameters, namely spindle speed, feed rate, and depth of cut, on cutting temperature and the surface roughness of the machined surface.
Previous studies have addressed this issue to some extent. For example, one study evaluated the influence of cutting parameters, specifically cutting speed, feed per tooth, and depth of cut, on surface quality, represented by the arithmetic mean roughness (Ra) and the total profile height (Rt), as well as on productivity expressed by the material removal rate (MRR), during face milling of polyoxymethylene (POM). The results showed that feed per tooth had the greatest influence on the arithmetic mean surface roughness-Ra (Tibakh et al., 2025).
In another study, the optimal cutting conditions were determined using the desirability function approach. The results indicated that feed rate was the dominant factor contributing to the minimization of the surface roughness of high-density polyethylene (HDPE). Conversely, the cutting temperature was found to be mainly affected by cutting speed, depth of cut, and three interaction effects: cutting speed and feed rate, cutting speed and depth of cut, and feed rate and depth of cut. Finally, the optimized cutting temperatures were discussed for three target conditions: the minimum value, a target temperature of 30 °C, and the maximum allowable temperature of 32 °C (Hamlaoui et al., 2017).

[1] Corresponding author, dusan.jovanic@vts-zr.edu.rs, ORCID: 0009-0001-6058-4074
[2] spasoje.eric@vts-zr.edu.rs, ORCID: 0009-0006-0705-0635
[3] miodrag.kovacevic@vts-zr.edu.rs, ORCID:0000-0002-1803-6816

Another study applied the surface topography method to characterize four different surface roughness levels of a polyethylene liner (Pe-Lite liner) manufactured by Biomill. Three surface roughness parameters were selected for evaluation: the arithmetic mean roughness (Ra), the root mean square roughness (Rq), and the ten-point height of irregularities (Rz). The results showed that the Ra value of the conventionally manufactured liner was between the Ra values of the standard and the fast-finished surfaces (Hamzah et al., 2022).

THERMODYNAMICS OF CUTTING AND THERMOGRAPHY

Nearly all of the mechanical energy supplied during the cutting process is converted into thermal energy within the cutting zone through elastic and plastic deformation, friction at the tool–workpiece and tool–chip interfaces, and internal friction within the workpiece material. The generated heat significantly affects tool wear and tool life, machining productivity, surface roughness, and the overall quality of the machined surface [Milikić, 2003].
The temperatures generated during the cutting process include the temperature in the shear plane, which increases with increasing cutting speed; the temperature at the cutting edge and flank face of the tool, resulting from chip deformation; the temperature on the rake face, which reaches the highest value due to friction between the chip and the tool; and the temperature of the machined surface, caused by friction between the flank face of the tool and the workpiece surface.
Cutting temperature is influenced by numerous factors, the most important of which are the workpiece and tool materials, machining parameters, tool geometry, and the type of cooling and lubrication applied. The temperature of the cutting tool is generally higher than that of the chip and may reach up to twice the chip temperature [Stanković, 1967].
Infrared thermography (IRT), also referred to as thermovision, is widely used to identify and document irregularities for machine condition monitoring, quality control, and non-destructive testing, as well as for monitoring temperatures in various manufacturing processes, including the cutting zone. IRT has proven to be a highly effective method for temperature monitoring because it enables comprehensive thermal imaging of machines and their components through non-contact temperature measurement (ISO, 2008).

MACHINED SURFACE ROUGHNESS

Surface roughness is defined as the collection of surface irregularities that form the texture of a surface over a specified reference (sampling) length. The reference length is selected in accordance with the ISO 4287 standard to exclude larger waviness features and other macro-scale irregularities from the roughness evaluation.
The most commonly used surface roughness parameters are:
- Arithmetic Mean Roughness (Ra): The arithmetic mean of the absolute values of the profile deviations from the mean line over the evaluation length. It is the most widely used roughness parameter and provides an overall measure of average surface roughness.
- Root Mean Square Roughness (Rq): The root mean square (RMS) value of the profile deviations over the evaluation length. Compared with Ra, this parameter is more sensitive to pronounced surface peaks and valleys because larger deviations have a greater influence on its value.
- Maximum Height of the Profile (Rz): The arithmetic mean of the height differences between the five highest profile peaks and the five deepest profile valleys within the reference length.
- Total Profile Height (Rt): The total vertical distance between the highest profile peak and the deepest profile valley over the entire evaluation length.

In turning and planing operations, surface roughness is directly proportional to the square of the feed rate and inversely proportional to the tool nose radius. In milling, however, surface roughness is directly proportional to the square of the feed rate and inversely proportional to the cutter diameter.

POLYETHYLENE

Polyethylene is one of the most widely used thermoplastic materials in industry due to its excellent mechanical properties. In this study, polyethylene PE 500 was selected because of its good machinability, favorable mechanical properties, and excellent impact and wear resistance. However, its limitations include relatively low resistance to elevated temperatures and shear loading.The chemical formula of polyethylene-PE 500 is $(C_2H_4)_n$.

EXPERIMENTAL RESEARCH

A series of experiments was carried out on an EMCO Mill 55 CNC milling machine. Prismatic PEspecimens with dimensions of 70 × 60 × 25 mm were used as workpieces. The specimens were face milled using a high-speed steel (HSS) end mill, type B, conforming to DIN 327, with a shank diameter of 12 mm.The machining parameters, namely spindle speed (rpm), feed rate (mm/min), and depth of cut (mm), were then varied according to the experimental design, and a series of specimens was produced.Figure 1 shows the EMCO Mill 55 CNC milling machine, a simulation of the milling process, and the HSS end mill used in the experiments.

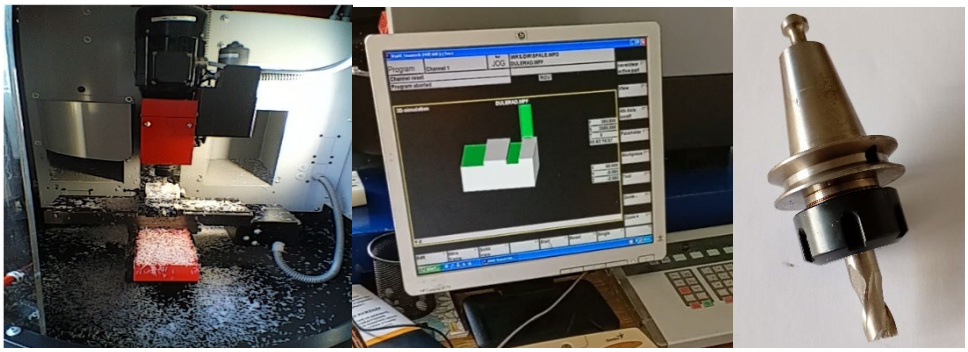


Fig. 1. *EMCO mill55 CNC milling machine, a simulation of the milling process, and the end mill*

Figure 2 also presents the cutting temperature (hot spot) measured during the face milling of PE 500 under the following machining conditions: a spindle speed of 2000 rpm, a feed rate of 200 mm/min, and a depth of cut of 4 mm. The measured cutting temperature was 35.5 °C (Testo SE & Co. KGaA, 2026).
During the face milling operation, the temperature in the cutting zone and the cooling rate were measured using a Testo 860i thermal imaging camera. The thermographic images shown in Figure 2 were captured from a distance of 50 cm, at an angle of 45° to the workpiece, with an emissivity value of 0.95.

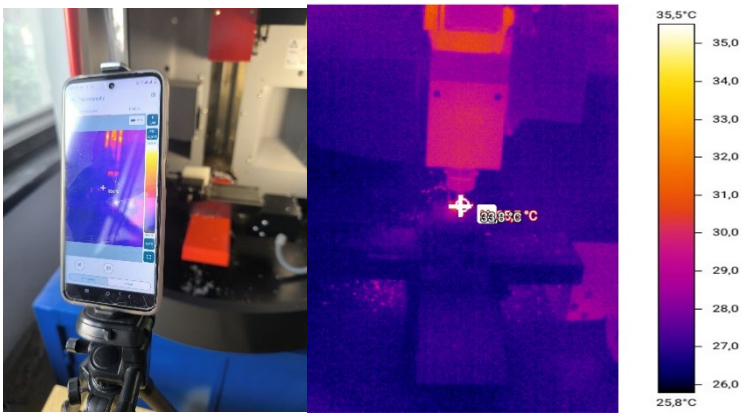


Fig. 2. *Thermography and Hot-Spot Cutting Temperature*

Figure 3 shows the maximum temperature measured immediately behind the end mill, as well as the temperature measured after a specified time interval, which were used to calculate the cooling rate.

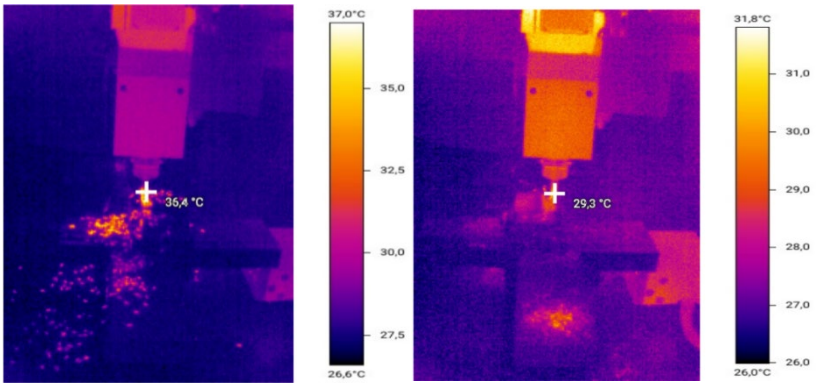


Fig. 3. *Thermograms of the temperature after the milling pass and a specified time interval*

Figure 4 shows the calibration and measurement procedure using the PCE RT 1200 surface roughness tester. In addition to the measured results, measurement units, and the Arithmetic Mean Roughness (Ra) parameter, the instrument allows the values of other surface roughness parameters to be displayed, including Root Mean Square Roughness (Rq), Maximum Height of the Profile (Rz), and Total Profile Height (Rt). The figure also shows the Gaussian filter, which is used to separate surface roughness from waviness, as well as the defined evaluation length of 2.5 mm, in accordance with EN ISO 4287 (ISO, 2025).
The instrument uses an inductive probe with a diamond stylus tip to trace the surface profile. The obtained profile data are then processed and the roughness parameters are calculated in accordance with the EN ISO 4287 standard.



Fig. 4. *Calibration and measurement procedure using the PCE RT 1200 surface roughness tester*

RESULTS AND DISCUSSION

In the experiment, the most important milling parameters were varied, namely spindle speed, feed rate, and depth of cut. The values corresponding to the upper, middle, and lower levels of the selected machining parameters for polyethylene are presented in Table 1.

Tabela 1.*Upper, middle, and lower levels of the milling parameters*

The parameters	Values		
	Level 1	Level 2	Level 3
Spindle speed (rpm)	1000	2000	3000
Feed (mm/min)	100	200	300
Depth of cut (mm)	2	3	4

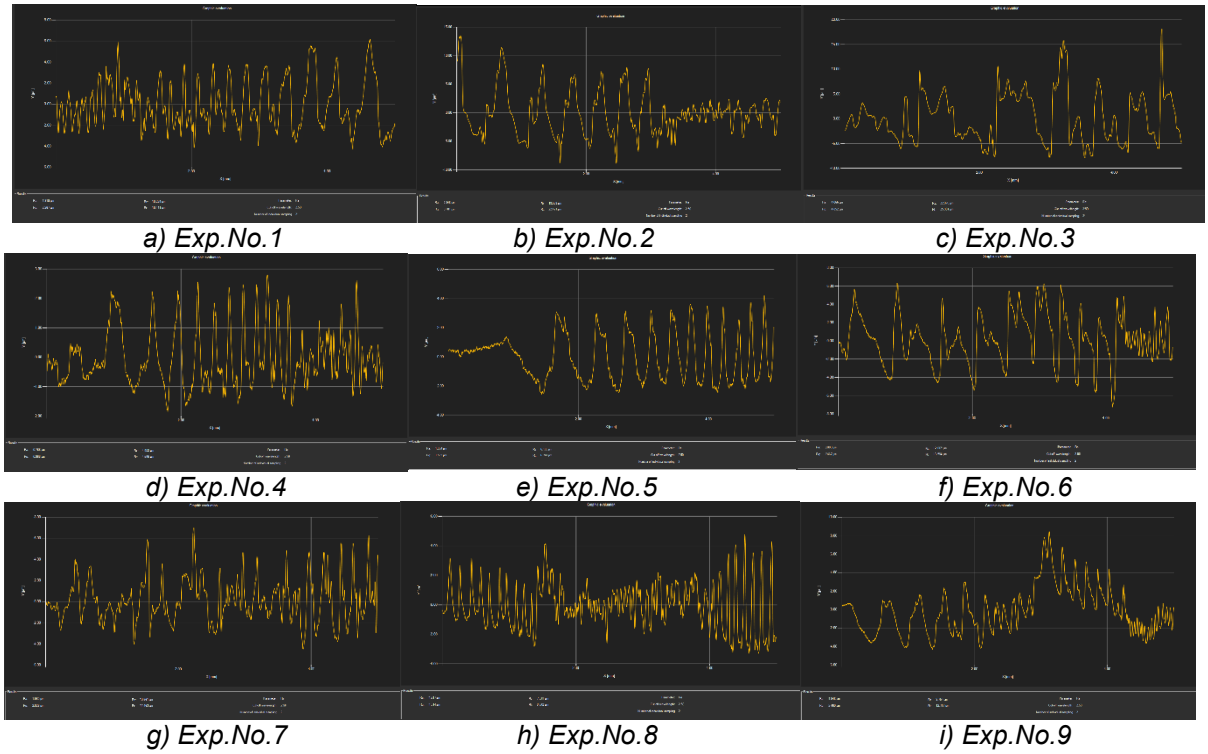
The Taguchi L9 orthogonal array was used for the experimental design. Design of Experiments(DOE) is a systematic approach used to evaluate how input process parameters affect one or more output responses. By systematically varying the input factors, DOE

enables the determination of optimal process parameters and the identification of the most influential factors and their optimal levels for achieving the desired performance targets.
The Taguchi method uses the signal-to-noise (S/N) ratio to evaluate and optimize process performance. In the present study, the S/N ratio was applied for multi-response process optimization using the Smaller-the-Better criterion to minimize surface roughness.
The measured surface roughness values, based on three measurements taken in both the longitudinal (feed) and transverse (perpendicular to the feed) directions, as well as the cooling rate as a function of spindle speed, feed rate, and depth of cut, are presented in Table 2. It can be observed that the surface roughness measured in the feed direction is higher than that measured perpendicular to the feed direction.

Table 2. *Arithmetic Mean Roughness (Ra)values and cooling rates for different milling parameters*

Exp No.	Spindle speed (rpm)	Feed (mm/ min)	Depth of cut (mm)	Cooling rate (°C/s)	Ra transverse (μm)	Ra longitud. (μm)	S/N transverse (dB)	S/N longitud. (dB)
1	1000	100	2	0,1330	2.236	2.628	-6.99	-8.39
2	1000	200	3	0,0848	3.405	3.737	-10.64	-11.45
3	1000	300	4	0,0408	3.736	4.051	-11.45	-12.15
4	2000	100	3	0,1183	1.779	0.990	-5.00	0.09
5	2000	200	4	0,0741	1.920	2.746	-5.67	-8.77
6	2000	300	2	0,0286	2.436	2.807	-7.73	-8.97
7	3000	100	4	0,1280	1.110	0.565	-0.91	4.96
8	3000	200	2	0,0667	1.804	2.889	-5.12	-9.21
9	3000	300	3	0,0283	1.739	1.822	-4.81	-5.21

The arithmetic mean roughness (Ra) profiles measured perpendicular to the feed direction, arranged according to the experimental sequence, are presented in Figure 5. In addition to the effective profile surface, the figure presents the values of the roughness parameters Ra, Rq, Rz, and Rt, as well as the cut-off wavelength, which is 2.5 mm, and the number of individual sampling lengths.



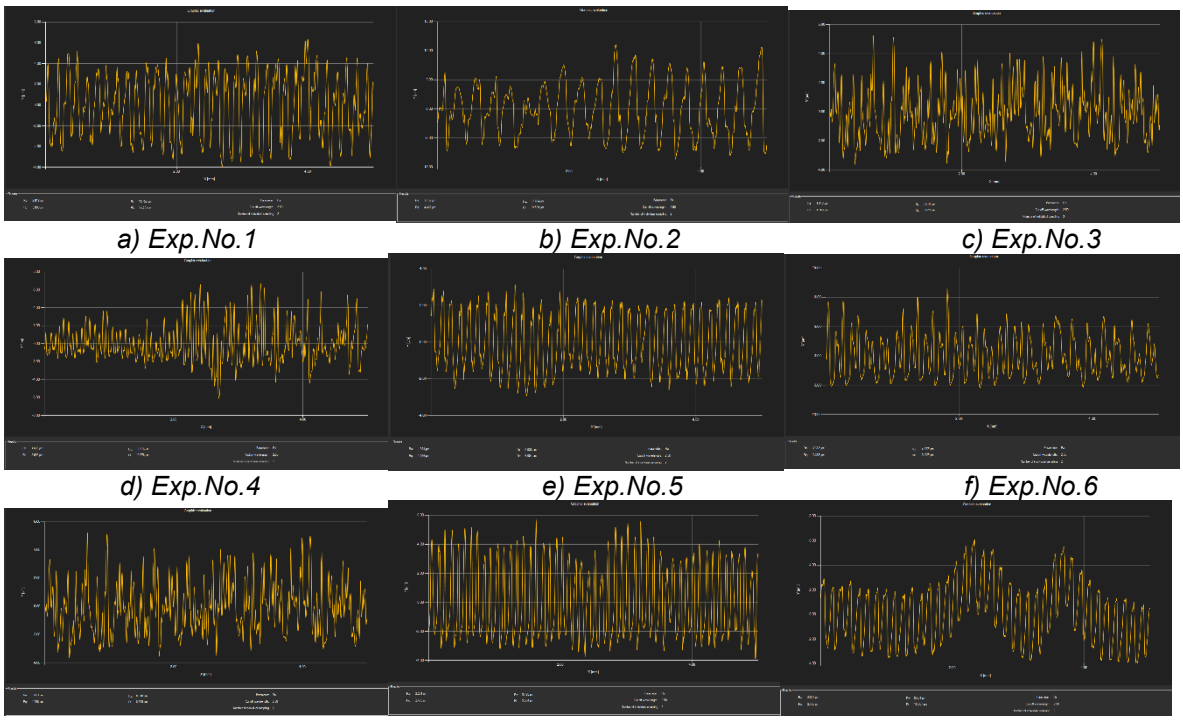
a) Exp.No.1 *b) Exp.No.2* *c) Exp.No.3*

d) Exp.No.4 *e) Exp.No.5* *f) Exp.No.6*

g) Exp.No.7 *h) Exp.No.8* *i) Exp.No.9*

Fig. 5*. The arithmetic mean roughness (Ra) profiles perpendicular to the feed direction in the experimental sequence*

Figure 6 presents the arithmetic mean roughness (Ra) profiles measured in the feed direction, arranged according to the experimental sequence.



a) Exp.No.1 *b) Exp.No.2* *c) Exp.No.3*

d) Exp.No.4 *e) Exp.No.5* *f) Exp.No.6*

g) Exp.No.7 *h) Exp.No.8* *i) Exp.No.9*

***Fig. 6**. The arithmetic mean roughness (Ra) profiles in the feed direction in the experimental sequence*

The mean Ra surface roughness values, measured both perpendicular to the feed direction and in the feed direction, together with the corresponding S/N ratios, for each machining parameter separately, are presented in Table 3.

***Table 3.** Mean Ra surface roughness values and S/N ratios for each machining parameter*

The parameters		Values			
		Ra transverse (μm)	S/N transverse Ratio	Ra longitudinal (μm)	S/N longitudinal Ratio
Spindle speed (rpm)	1000	3.126	-9.69	3.472	-10.66
	2000	2.045	-6.13	2.181	-5.88
	3000	1.551	-3.61	1.759	-3.15
Feed (mm/min)	100	1.708	-4.30	1.394	-1.11
	200	2.376	-7.14	3.124	-9.81
	300	2.637	-8.00	2.893	-8.78
Depth of cut (mm)	2	2.159	-6.61	2.775	-8.86
	3	2.308	-6.82	2.183	-5.52
	4	2.255	-6.01	2.454	-5.32

Based on the S/N ratios presented in Table 3, the optimal machining parameters for achieving minimum surface roughness in both measurement directions are a spindle speed of 3000 rpm, a feed rate of 100 mm/min, and a depth of cut of 4 mm, corresponding to Experiment No. 7**.**
This machining condition also provides the maximum cooling rate of 0.1280 °C/s, thereby reducing the risk of polyethylene melting and the formation of micro-ridges on the machined surface.

The influence ranking is determined based on the Delta value, which represents the difference between the maximum and minimum mean values for the observed factor. A larger Delta value indicates a greater influence of the corresponding factor on the final response. The influence rankings for transverse Ra,longitudinal Ra, and process stability are presented in Table 4 and Table 5.

Table 4. *Influence ranking for transverse Ra surface roughness and process stability*

The parameters	Δvalue Ra transverse	Rang Ra transverse	Δ value S/N transverse	Rang S/N transverse
Spindle speed (rpm)	1.575	1	6.08	1
Feed (mm/min)	0.929	2	3.70	2
Depth of cut (mm)	0.149	3	0.81	3

Table 5. *Influence ranking for longitudinal Ra surface roughness and process stability*

The parameters	Δ value Ra longitudinal	Rang Ra longitudinal	Δ value S/N longitudinal	Rang S/N longitudinal
Spindle speed (rpm)	1.713	2	7.51	2
Feed (mm/min)	1.730	1	8.70	1
Depth of cut (mm)	0.592	3	3.54	3

The results of the Taguchi analysis show that the lowest surface roughness during polyethylene milling is achieved at a low feed rate of 100 mm/min and a high spindle speed of 3000 rpm**.**

For surface roughness measured perpendicular to the feed direction, spindle speed has the greatest influence (Δ= 1.575 μm), followed by feed rate (Δ = 0.929 μm), while the depth of cut has a very small influence (Δ = 0.149 μm).

For surface roughness measured in the feed direction, feed rate has the greatest influence (Δ = 1.730 μm), followed closely by spindle speed (Δ = 1.713 μm), while depth of cut again has the smallest influence (Δ= 0.592 μm).

Overall, feed rate and spindle speed are the dominant factors determining the quality of the machined surface, whereas the influence of depth of cut is considerably lower within the investigated range.

CONCLUSION

The optimization of the face milling parameters for polyethylene (PE) using an end mill on an EMCO Mill 55 CNC machine, based on the Taguchi method, enabled the determination of the optimal combination of spindle speed, feed rate, and depth of cut with respect to the surface roughness measured both in the feed direction and perpendicular to it.

It was confirmed that surface roughness in the feed direction depends primarily on the feed rate, followed by spindle speed, while the depth of cut has the least influence. It was also found that the surface roughness measured in the feed direction is higher than that measured perpendicular to the feed direction.

As the spindle speed increases, the surface roughness decreases significantly. In polyethylene machining, higher cutting speeds reduce the cutting force and enable cleaner material removal without excessive plastic deformation of the machined edges.

A reduction in feed rate results in lower surface roughness in all cases. Higher feed rates leave more pronounced tool marks on the machined surface.

The depth of cut has a statistically negligible effect on surface roughness within the investigated range. This indicates that the depth of cut can primarily be selected based on

productivity requirements, as it does not significantly impair the quality of the finished surface.
Polymers such as polyethylene have a relatively low melting point and low thermal conductivity. Therefore, effective thermal management is crucial during machining. The experimental data indicate a very strong correlation between feed rate and cooling rate. At a low feed rate, the cooling rate is highest. As the feed rate increases, the cooling rate decreases significantly.

ACKNOWLEDGEMENT

This paper is part of a research on the project entitled: "*Optimizacija proizvodnog procesa primenom termovizijske tehnologije*", No. *003817351 2025 09418 004 000 000 001*, supported by *Pokrajinski sekretarijat za visoko obrazovanje i naučnoistraživačku delatnost.*

REFERENCES

EMCO GmbH. (n.d.). *Concept Mill 55*. https://www.emco-world.com/en/products/industrial-training/machines/milling/concept-mill/concept-mill-55.html

Hamlaoui, N., Azzouz, S., Chaoui, K., Mokhtar, B., &Azari, Z. (2017). Machining of tough polyethylene pipe material: Surface roughness and cutting temperature optimization. *The International Journal of Advanced Manufacturing Technology*, *92*(1), 517–527. doi.org

Hamzah, N. A., Razak, N. A. A., Karim, M. S. A., &Salleh, S. Z. (2022). Validation of a roughness parameters for defining surface roughness of prosthetic polyethylene Pe-Lite liner. *Scientific Reports*, *12*, Article 2636. doi.org

International Organization for Standardization. (2008). *Condition monitoring and diagnostics of machines — Thermography — Part 1: General procedures* (ISO Standard No. 18434-1:2008). iso.org

International Organization for Standardization. (2025). *Geometrical product specifications (GPS) — Surface texture: Profile method — Terms, definitions and surface texture parameters* (ISO Standard No. 4287:2025). iso.org

Milikić, D. (2003). *Tehnologijaobraderezanjem: Opštaiprimenjenateorija*. Fakultettehničkihnauka, Univerzitet u NovomSadu.

Stanković, P. (1967). *Mašinskaobrada: Obradametalarezanjem*. Građevinska knjiga; Mašinski fakultet, Univerzitet u Beogradu.

Testo SE & Co. KGaA. (2026). *Testo Smart App* (Version X.X) [Mobile app]. Google Play Store. google.com

Tibakh, I., Yallese, M. A., Belhadi, S., &Kaddeche, M. (2024). Multi-response optimisation during face milling of polyoxymethylene copolymer using grey relational analysis and data envelopment analysis based ranking coupled with the Taguchi approach. *Advances in Materials and Processing Technologies*, *11*(2), 681–706.
DOI:10.1080/2374068X.2024.2314838

DOI:10.5937/IIZS26090M

APPLICATION OF ADVANCED MEASUREMENT TECHNIQUES FOR DETERMINATION OF INJECTION MOLDING SHRINKAGE

Research paper

Ivan Matin[1*], Branko Štrbac[2], Miloš Ranisavljev[3], Đorđe Vukelić[4], Miodrag Hadžistević[5]
[1,2,3,4,5] University of Novi Sad, Faculty of Technical Sciences, Department of Production Engineering, Novi Sad, Serbia

Abstract: Plastic injection molding (IM) is a complex and technologically demanding process; therefore, it is characterised by IM parameters and material properties that influence the product quality. Setting satisfactory IM parameters requires knowledge of the processing properties of the material, the mold shape, and the technological capacity of the injection molding machine (IMM). Injection shrinkage causes changes in the shape and dimensions of the molded parts; therefore, it is one of the most significant problems that must be solved, both during the mold design phase and the numerical simulation phase. The paper presents determined IM parameters as well as material parameters influencing the value of the shrinkage. The conducted experimental tests were related to selected topics connected with the injection process and considered the change of the processed material characteristics, and change of certain, relatively the simplest to regulate IM parameters. Geometrical Product Specification (GPS) of the molded part was measured using two methods: Contact and Non-contact (3D scanning). The analysis of injection shrinkage illustrates that an effective influence on its value is possible by selecting appropriate IM parameters and material condition. The connection between the shrinkage and different filler concentration was established.

Key words: injection molding, shrinkage, measurement, 3D scanning, contact CMM

INTRODUCTION

Injection molding is the most widely used manufacturing process of plastic parts. There are different forms of injection and periodicity is its characteristics. Injection is used for processing almost all polymer materials, as well as rubber compounds, liquid silicon and composites. The result of injection molding is a plastic part, which depending on the type of injection and the material used, have a wide range of application possibilities, variety of shape, manufacturing accuracy and endurance properties [1-3]. Shrinkage is an extremely important parameter that must be considered during injection molding, because it affects the structural features and GPS of the molded part. It also determines the applicability and aesthetic features of the plastic part [4]. The process of IM is determined by the material type, and its IMM capacity. The IM parameters influence directly or indirectly final dimensions, the structure and the shape of the plastic parts, in accordance with the specification range established in the development process and the processing anomalies (material and surface), essential from the point of view of the user. Processing shrinkage depends on many factors, which can be grouped as follows [5]:

- material – density, structure (crystalline, semi-crystalline or amorphous),
- plastic product – shape, dimensions, dimensional accuracy,
- structure of the mold – runner system, number of cavities, shape of the cavity, cooling system, inserts, etc.
- IM parameters – melt temperature, mold temperature, holding pressure, holding time, injection pressure, cooling time, etc.

The effect of IM parameters on shrinkage and certainly sink marks has been discussed for many decades. As a matter of fact, shrinkage is an inherent property of polymer and it should be precisely handled to improve the product quality. Especially in the thick part improper setting of holding pressure, holding time and melt temperature may generate shrinkage. Therefore, satisfactory IM parameters must be carefully monitored and their impact recorded in terms of diametrical shrinkage, mass and depth of the shrinkage [6].

[1]Corresponding author, matini@uns.ac.rs, ORCID: 0000-0003-1470-5100
[2]strbacb@uns.ac.rs, ORCID: 0000-0003-3892-2767
[3]ranisavljev@uns,ac.rs, ORCID: 0000-0002-9130-5103
[4]vukelic@uns.ac.rs, ORCID: 0000-0003-2420-6778
[5]miodrags@uns.ac.rs, ORCID: 0000-0002-6753-3691

Global influence of the injection parameters according to the processing of shrinkage is presented in Fig.1.

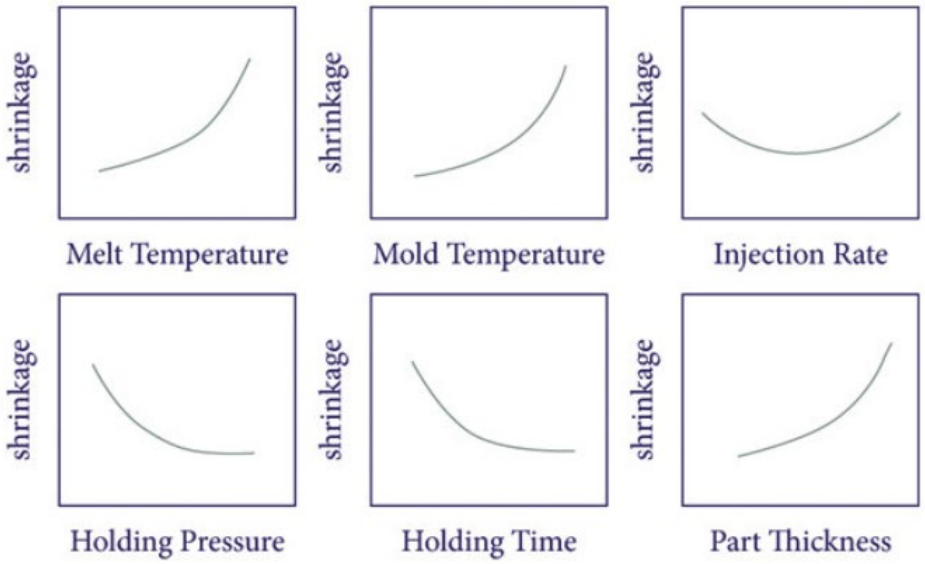


Fig. 1. *Variation of shrinkage caused by IM processing* [7-13]

Materials of greater density show greater processing shrinkage. Materials of lower density crystallise a little less because of their greater chain branching, which leads to smaller shrinkage. Processing shrinkage decreases together with an increase of the mass melt flow index. It is known that crystalline materials have greater processing shrinkage than amorphous materials. The shrinkage process should be identified based on measurements of molded part. The CAx techniques are widely used for the both mold design and IM process design. The main reason of using advanced software tools is reduction time-to-market of new product. The CAE analyses, CAM and CNC manufacturing techniques allow to faster and better fit of the design assumptions. The Reverse Engineering methods can be used to accurately reproduce free-form shapes using contact and non-contact measurement techniques. Mold design and injection molding process require a CAx programme systems and expert systems. The CAx software allows predicting of defects in early stage of the plastic part design and shrinkage elimination [14].

MATERIAL AND METHODS

The plastic parts were manufactured using a IMM called "All Rounder 270s Compact" manufactured by ARBURG company. The authors selected the previously mentioned IMM using the "SAPA" expert system. In this study, the IMM had been operated in automatic mode, and the parameters were monitored using "SELOGICA" software. The IM parameters were determined using Moldex3D/Solid Pack numerical simulation software. The widely used plastic material "Polystyrol (PS) 456M" by "BASF" was used in case study. This isotropic pure polymer has good tensile strength to weight ratio, good chemical inertness, resistance to moisture, good fatigue life, high flowability and excellent heat resistance, making it ideal for standard injection molding of parts subjected to thermal stress. The input PS granules have spherical shape with medium diameter of 4.1 mm. The composite contains the previously mentioned PS and glass fiber. The concentration of glass fiber in the composite increases in percentage. For injecting the portions of material of respectively 10 %, 20 %, 30 % and 40 % filler amounts were prepared, as well as PS without the filler. The material properties of the PS without glass fibre, and resolved injection molding parameters are both shown in Table 1.

Table 1. *Properties of PS and IM parameters determined using numerical simulation*

The parameters	**Values**
Drying Temperature (^{0}C)	75
Drying time (s)	4500
Solid density (g/cm^3)	1.05
Polymer Poisson's ratio	0.38
Max Permissible Shear Stress (MPa)	0.24
Tensile strength (MPa)	34
Mold temperature range (^{0}C)	20-60
Normal mold temperature (^{0}C)	40
Melt temperature range (^{0}C)	200-250
Normal melt temperature (°C)	225
Maximum injection pressure (MPa)	155
Maximal shear rate (1/s)	100000
Ejection temperature (^{0}C)	102
Freeze temperature (^{0}C)	122
Total Element Number of Part	96328
Total Node Number of Part	11291
Total Element Number of Part and Runner	114120
Filling time (s)	0.4
Holding time (s)	4.7
Maximal Clamping Force during holding phase (kg)	13000
Max melt front time (s)	0.2
Volumetric shrinkage (%)	1.466-2.816
Maximal shear rate (1/s)	722
Max Injection pressure	8.1MPa
Max cooling time (s)	19
Max sink marks	0.015
Flow rate (mm^3/s)	24811
Maximal bulk temperature (^{0}C)	225
Temperature of coolant liquid (°C)	20
Cooling channel diameter (mm)	8
The percentage of ethyl glycol in the cooling agent mixture (H_2O+ethylene-glycol) (%)	20

The authors used variable material options in the experimental tests. The filler was prepared and different mixtures were used. The CAD models are solid prisms with the following overall dimensions (l x b x h): l = 40 mm, b = 40 mm and, h = 3 mm. The P-V-T chart for PS without added filler is shown in Fig. 2.

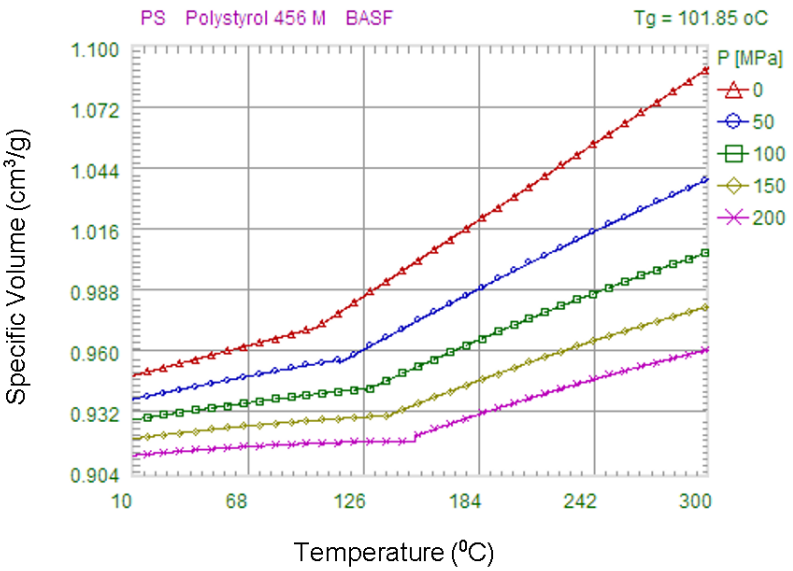


Fig. 2. *P-V-T diagram for PS*

Measurements of the geometrical dimensions of the plastic parts, achieved with identical IM parameters, were conducted using two different coordinate measurement systems:

- Coordinate measuring machine (CMM), Zeiss Contura G2 with VAST XXT tactile scanning sensor paired with a spherical probe tipand,
- Optical measuring system, 3D ATOS Compact Scan for non-contact (3D scanning) applications.

Contact measurement is suitable for applications where high accuracy and precision are required, such as dimensional inspection and quality control in manufacturing. On the other hand, non-contact measurement technologies do not require physical contact with the object and utilize optical techniques to measure surface characteristics, dimensions, or distances. While using the first measuring method, the parts were measured to an accuracy of 0.01 mm with CMM called Contura G2 by ZEISS, and in the second method particular samples were scanned with the use of 3D ATOS Compact Scan. The values of shrinkage were set according to appropriate dimensions of the mold cavity for the first method by using common mathematical dependencies presented in literature [15]. The contact CMM uses a physical stylus to measure discrete points with extreme precision, whereas ATOS utilizes non-contact blue light technology to capture full-surface 3D data instantly. The 3D ATOS scanner is a measurement system which uses the optical triangulation method. According to the measurements of the shape and dimensions of the experimental parts carried out using the 3D scanner, particular values of the shrinkage were based on comparing the results of the 3D scanning associated with the CAD model of the plastic part. It can be generated only when a CAD model is compared to a scanned part. If this condition is met, by the CAD model applied on the "stl" format, the colour visualisation of the deviation maps is obtained. The neutral format "stl" could be avoided by using Associative Topology Bus (ATB). High quality of data, a few measurement points providing information about the surface of the measured element and the direct comparison with CAD data are the main advantages when choosing the 3D scanning method. The dimensional results were inspected using GOM Inspect software. The CAD model of molded part and a CAD model of designed part both created a union, together with the map of deviations between surfaces.
Considering the assumed linear shrinkage of the mold cavity due to temperature estimated by Moldex 3D software, additionally shrinkage of the part has been corrected by PTC Wildfire Mold Design module during the mold design phase. Shrinkage arises from non-uniform cooling and insufficient holding, but it has been prevented through mold design, numerical simulation, and controlled processing.

RESULTS AND DISCUSSION

The differences in the value of shrinkage set based on the geometrical dimensions of the molded part measurements conducted with the use of the scanner and with the use of the CMM were negligible, as shown in Fig. 3.

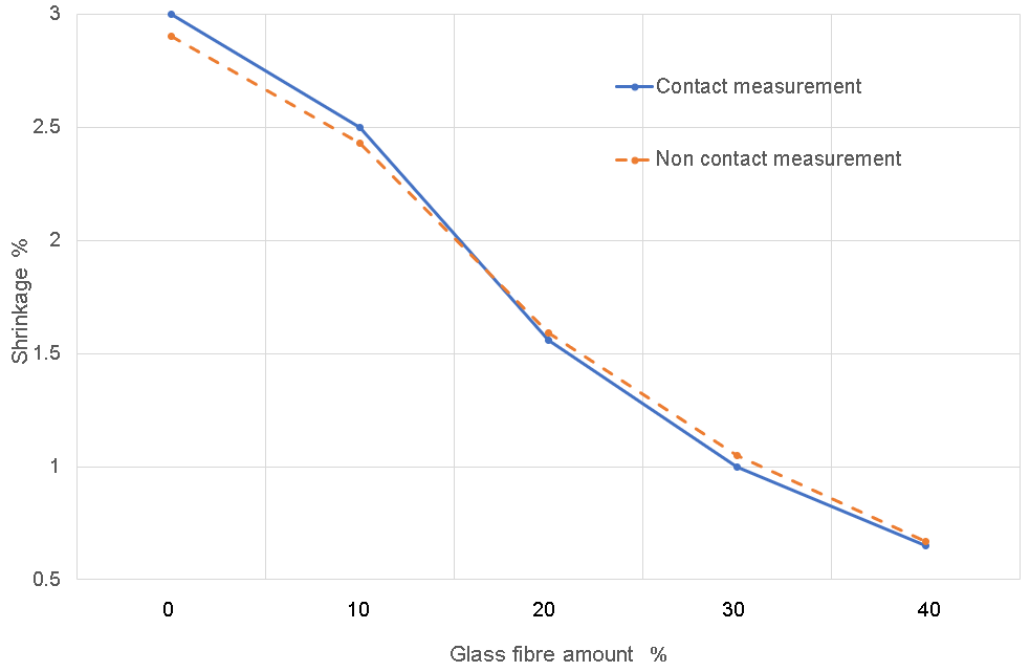


Fig. 3. *Comparison results between amount of filler and shrinkage based on both different measurement methods*

The decrease of shrinkage was visible with increase of filler from 10 % to 40 %.

CONCLUSION

The plastic injection molding is complex; therefore, it is characterised by several selected parameters. The parameters cause that setting the satisfactory injection conditions requires knowledge of the processing properties of the material, mold geometrical characteristics and the IMM parameters. With regards to the injection process, glass filler shows positive effect causing the decrease of the injection shrinkage and dimensional stabilisation of the parts. The contact (tactile) methods, such as CMM are time-consuming and need qualified operating staff. Non-contact methods, including 3D optic measurement, are an alternative. Non-contact measurement can be effectively used to object dimensioning where other techniques are ineffective or their usage is complex, time-consuming and problematic. When it comes to contact vs non-contact measurement systems, it's worth noting that contact measurements relying on tactile probes will typically be more accurate than non-contact measurement methods. Thus, contact systems are better suited for applications with high-precision requirements, especially where measurement tolerances are in the micrometrer range. Contact measurement systems often provide simpler and more cost-effective measurement solutions for more basic measurement tasks compared to more sophisticated non-contact systems. On top of everything, contact measurement systems are notably less susceptible to environmental interference, which can affect the accuracy of non-contact measurements. In the conducted case study, both previously mentioned measurements meet the requirements of the investigation. Further research should be done with an even greater increase of the percentage amount of glass fiber in composite to see if the shrinkage is still decreasing. Even further research will be based on the application and integration of benchtop tools like the Xplore IM12 Pro to visualize, quantify, and ultimately eliminate these defects early in the

development phase, ensuring that the final product is dimensionally stable and aesthetically flawless especially for micro parts.

REFERENCES

Rosato, D. V., Rosato M. G. (2000). Injection Molding Handbook. 3rd edition, Norwell, Kluwer Academic Publisher, 1640.

Suberlyak, O., Krasinskyi, V., Moravskyi, V., Gerlach, H., Jachowicz, T. (2014). Influence of aluminosilicate filler on the physico mechanical properties of polypropylene-polycaproamide composites. *Materials Science, 50, (2)*, 296–302.

Yang, S. S., Kwon, T.H. (2008). Numerical and experimental investigation of shrinkage behaviour of precision injection molded articles. *Polymer Eng& Sci*. *48, (8)*, 1569–1583.

Kwon, K. (2006). Theoretical and experimental studies of anisotropic shrinkage in injection moldings of semicrystalline polymers. *Polymer Eng.& Sci. 46, (6)*, 712–728.

Gershon, A. L., Gyger, L. S., Bruck, H. A., Gupta, S. K. (2008). Thermoplastic polymer shrinkage in emerging molding processes. *Experimental Mechanics, 48, (6)*, 789–798.

Jozwik, J., Tofil, A., Lukaszewicz, A. (2019). Application of modern measurement techniques for analysis of injection moulding shrinkage. *Engineering for rural development*, 1742–1748.

Postawa, P., Koszkul, J. (2005). Change in injection moulded parts shrinkage and weight as a function of processing conditions, *Journal of Materials Processing Technology,* 162–163, 109–115.

Matin, I., Štrbac, B., Ranisavljev, M., Hadžistević, M., Vukelić, Đ. (2024). The deviation between injected molded plastic part and FDM manufactured part. The *XIV International Conference on Industrial Engineering and Environmental Protection IIZS 2024*, Technical Faculty "Mihajlo Pupin" Zrenjanin, October 3–4, Zrenjanin, Serbia.

Fisher, J. M. (2013). Handbook of molded part shrinkage and warpage. 2nd edition, Plastic Design Library, William Andrew, 292.

Kennedy, P. K., Meijer, H. E. H., Peters, G. W. M., Anderson, P. D. (2008). Practical and Scientific Aspects of Injection Molding Simulation. Technische Universiteit Eindhoven, Eindhoven, ISBN 978-90-386-1275-1

Wang, M. W., Arifin, F., Vu, W. H. (2019). The Study of Optimal Molding of a LED Lens with Grey Relational Analysis and Molding Simulation. *Periodica Polytechnica Mechanical Engineering, 63, (4)*, 278–294.

Berihun, E., Bogale, T. (2022). Parameter Optimization of PET Plastic Preform Bottles in Injection Molding Process Using Grey-Based Taguchi Method. *Advances in Materials Science and Engineering, 5*, https://doi.org/10.1155/2022/4416602

Wen, X., Chen, C., Yang, L., Liu, T., Hao, L. (2014). Optimization of processing parameters for minimizing warpage of large thin-walled parts in whole stages of injection molding. *Chinese Journal of Polymer Science, 32, (11)*, 1535–1543.

Hodolic J., Matin I., Stevic M., Vukelic, D. Development of integrated CAD/CAE system of mold design for plastic injection molding. Materiale Plastice, 46, (3), 236–242.

Poniatowska, M., Werner, A. (2010). Fitting spatial models of geometric deviations of free-form surfaces determined in coordinate measurements. *Metrology and Measurement Systems, 17, (4)*, 599–610.

DOI:10.5937/IIZS26096N

THE IMPACT OF LOAD-SENSING REGULATION ON THE ENERGY, ECONOMIC AND ENVIRONMENTAL EFFICIENCY OF AXIAL-PISTON PUMPS

Research paper

Borivoj Novaković[1], Bojan Vukobrat[2], Luka Đorđević[3*], Uroš Šarenac[4], Dejan Landup[5]
[1,3,4,5]University of Novi Sad, Technical faculty "Mihajlo Pupin" Zrenjanin, Republic of Serbia
[2]AUMOVIO, Novi Sad, Republic of Serbia

Abstract: Modern technologies require a high level of system efficiency. In the case of hydraulic systems, this efficiency is generally considered in terms of energy, economic, and environmental performance. In the research part of the paper, the authors conducted a comparative analysis of two different designs of the same type of hydraulic pump, namely an axial piston pump: a conventional pump with a fixed displacement and a modern pump equipped with load-sensing regulation. Based on the research presented in the paper, a clear comparison was obtained showing the extent to which the application of load-sensing regulation contributes to improving system efficiency after the implementation of hydraulically regulated pumps.
Key words: hydraulic, axial-piston pump, LS regulation, efficiency.

INTRODUCTION

Fluid power is an established engineering discipline that uses pressurized fluids to transmit and control mechanical energy and perform mechanical actuation. Hydraulic systems are widely used in agriculture, construction, transportation, manufacturing, aerospace, marine, and other industrial applications. Hydraulic systems, most commonly hydraulic presses, operate under quite demanding conditions, involving variations in operating parameters such as pressure, flow rate, and temperature, as well as in the fundamental physical properties of the fluid (Novaković et al., 2026).

Axial-piston pumps are commonly applied in systems where variable pressure and flow rates are required under different operating conditions (Vacca, 2018). Their operating efficiency depends not only on the characteristics of the pump itself, but also on the way the pump output is adjusted to the actual requirements of the hydraulic system. Conventional fixed-displacement pumps provide a relatively constant flow while the pump is operating, regardless of the actual flow demand of the system (Kärnell & Ericson, 2023). When the required flow is lower than the pump output, part of the supplied hydraulic energy is lost through throttling and pressure losses (Mahato & Ghoshal, 2021). These losses increase energy consumption and can also affect the operating cost and environmental performance of the system. The use of variable-displacement axial-piston pumps with load-sensing regulation allows the pump displacement to be adjusted according to the required flow, while the pump pressure is maintained in accordance with the load demand (Axin et al., 2014; Kralev et al., 2026; Li et al., 2022).

Load-sensing regulation therefore provides a different operating principle compared with conventional fixed-displacement pump systems (Lisowski et al., 2021). The difference can be observed through changes in energy consumption, hydraulic losses, operating costs, and other parameters related to the use of the system. An analysis of these parameters can provide a more detailed comparison of conventional and load-sensing axial-piston pump configurations and can be used to assess their energy, economic, and environmental efficiency.

The energy efficiency of a hydraulic system is determined by the interaction between the pump, control valves, actuators, and the operating conditions of the system. In conventional hydraulic circuits, the difference between the flow supplied by the pump and the flow required by the actuator is often dissipated through throttling. Similar losses can occur when the pump

[1]borivoj.novakovic@uns.ac.rs, ORCID: 0000-0003-2816-3584
[2]vuki933@gmail.com
[3] Corresponding author, luka.djordjevic@uns.ac.rs, ORCID: 0000-0003-4578-9060
[4] uros.sarenac@uns.ac.rs, ORCID: 0009-0007-6619-6076
[5] dejan.landup@uns.ac.rs, ORCID: 0009-0009-3836-2182

operates at a pressure level higher than that required by the load. In load-sensing systems, the pump displacement is adjusted according to the flow demand, while the pressure is controlled based on the highest load pressure in the system. This reduces the amount of flow and pressure that needs to be dissipated compared with conventional constant-flow arrangements (Siebert et al., 2017). Load-sensing systems still contain pressure losses associated with valves, pressure compensators, flow restrictions, and the pressure margin required for stable operation. These losses can become more pronounced when several actuators operate simultaneously at different load pressures.
Energy consumption is also directly related to the economic and environmental performance of hydraulic equipment. For systems driven by an internal combustion engine, hydraulic power losses increase the required input power and can consequently increase fuel consumption and associated carbon dioxide emissions. An analysis of a mobile hydraulic system using an axial-piston pump showed that pump losses were associated with both fuel consumption and CO2 emissions, with the magnitude of these effects changing with operating pressure and rotational speed (Kapsiz, 2022). From an economic perspective, lower energy consumption can reduce operating costs during the service life of the equipment, particularly in applications with long operating cycles and high hydraulic power requirements. The relationship between operating energy use, life-cycle cost, and environmental impact has also been considered in life-cycle assessments of pumping systems, where the use phase can represent a substantial part of the total energy and environmental burden (Nault & Papa, 2015).

MATERIAL AND METHODS

The research was conducted using an empirical and analytical approach based on established equations for the analysis of hydraulic pump performance. The study focused on axial-piston pumps and included a comparative assessment of a conventional fixed-displacement pump and a variable-displacement pump with load-sensing regulation. The analysis was based on relevant input parameters obtained from manufacturer catalogues and technical documentation for axial-piston pumps. The selected parameters included pump displacement, rotational speed, operating pressure, flow rate, volumetric efficiency, and other performance characteristics required for the calculation. The experimental part of the study was performed through numerical calculations based on the selected input data and established mathematical relationships for the determination of hydraulic and energy performance. The relevant equations were used to calculate the theoretical and actual flow rate, hydraulic power, input power, energy losses, and pump efficiency under different operating conditions. The same input conditions were applied to the compared pump configurations in order to provide a consistent basis for the analysis. The load-sensing configuration was evaluated by considering the change in pump displacement and pressure according to the required system flow and load conditions. The calculated results were used to compare the operating characteristics of the fixed-displacement and load-sensing configurations. Particular attention was given to the differences in hydraulic power demand, energy consumption, and power losses under different pressure and flow conditions. The economic and environmental aspects were subsequently assessed using the calculated energy consumption as the basis for estimating the corresponding operating costs and environmental effects. This approach allowed the performance of the two pump configurations to be evaluated under comparable operating conditions using manufacturer-specified data and established calculation procedures.

COMPARISON OF REGULATED AND NON-REGULATED AXIAL-PISTON PUMPS

Axial-piston pumps can be divided according to the method used to control their displacement and output flow. In a non-regulated configuration, the pump operates with a fixed displacement, and the delivered flow is mainly determined by the pump displacement and rotational speed. The hydraulic system must therefore accommodate the difference between the flow supplied by the pump and the flow required by the load. In a regulated configuration, the pump displacement can be changed during operation, allowing the delivered flow to be adjusted

according to the operating requirements. This principle is particularly relevant in hydraulic systems with variable loads, where the required flow and pressure change during operation.
Variable-displacement axial-piston pumps are widely used in hydraulic systems where the pump output has to follow changing load requirements. The displacement is commonly controlled through the swash-plate angle, which changes the piston stroke and consequently the theoretical displacement of the pump. The control mechanism can be based on hydraulic-mechanical regulation or on an electrohydraulic control system. The use of variable displacement allows the pump to reduce its output when the required flow decreases, which can reduce the power consumed during operating conditions with low flow demand. Research on variable-displacement axial-piston pumps has shown that displacement control is closely related to pump pressure, flow rate, and the dynamic behaviour of the control system (Helian et al., 2022).
The operating characteristics of regulated and non-regulated pumps also differ with respect to their response to changes in system demand. A fixed-displacement pump can provide the required flow only when the operating conditions are compatible with its fixed displacement and rotational speed. Additional hydraulic elements are therefore required when the system demand changes significantly. In contrast, a variable-displacement pump can modify its displacement and adapt its output to the required operating point. Studies of axial-piston pump control have shown that the control of displacement has a direct effect on the dynamic response and efficiency of the hydraulic source, while the performance of the control system depends on the operating point and load conditions (Yamada et al., 2024).
The comparison of these parameters provides a basis for evaluating how changes in pump displacement and regulation affect the hydraulic power supplied by the pump and the corresponding energy requirements of the system. In Figure 1a, a pump with a fixed volume is shown, while in Figure 1b, a pump with regulation is shown.



Fig.1a. *Fixed displacement axial-piston pump (Bosch, 2026)*



Fig .1b. *Variable displacement axial-piston pump* (Parker, 2026)

Figure 2 shows the scheme of two-way load-sensing control, i.e. regulation.

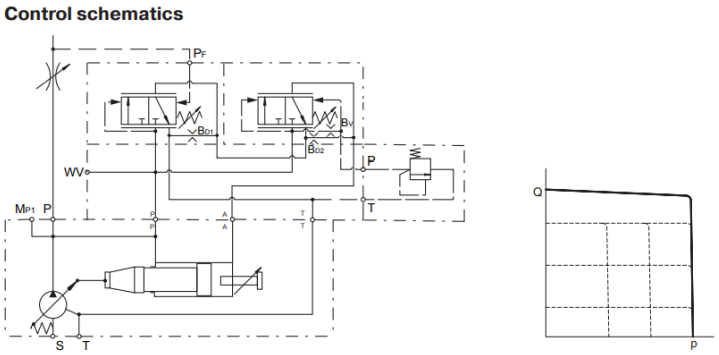


Fig 2. *Two-way load-sensing control*

ANALYTICAL AND EMPIRICAL INVESTIGATION OF AXIAL-PISTON PUMP PERFORMANCE

To assess the practical advantages and limitations of load-sensing regulated axial-piston pumps in comparison with non-regulated fixed-displacement pumps, a comparative analysis was conducted using three pump models with different operating parameters. The analysis included pumps with maximum operating pressures of 150, 250, and 300 bar, and nominal flow rates of 120, 200, and 250 L/min, respectively. For each pump type, two configurations were considered: a load-sensing regulated pump and a fixed-displacement pump. The electric motor used to drive the regulated 150 bar axial-piston pump had a rated power of 22 kW, with an estimated required active power of approximately 20 kW, whereas the corresponding fixed-displacement pump was driven by a 30 kW motor. For pump type B, the regulated configuration was driven by a 55 kW electric motor equipped with a variable frequency drive, while the fixed-displacement configuration used an 80 kW motor. For pump type C, the regulated configuration used a 77 kW electric motor, whereas the fixed-displacement pump was driven by a 120 kW motor. The main objective of the analysis was to quantify the differences between the two pump configurations in terms of energy consumption, electricity costs, carbon dioxide (CO_2) emissions, and cumulative costs over the considered service period. The analysis also included the payback period associated with the additional investment required for regulated pumps, the expected service life under ideal operating conditions, and the maintenance costs and frequency. Several assumptions were defined for the calculations, including the pump duty cycle, the efficiency of electric motors with and without a variable frequency drive, the annual operating hours, the electricity price, and the CO_2 emission factor. The selected assumptions were intended to represent typical industrial operating conditions and provide a consistent basis for the comparative calculations. The applied methodology included the calculation of annual energy consumption under the defined system load conditions, followed by a projection of cumulative costs over a twelve-year period and an estimation of the total CO_2 emissions for both pump configurations. Particular attention was given to the calculation of the simple payback period as a parameter for evaluating the economic implications of the additional investment in load-sensing regulation. The obtained results were presented in tabular and graphical form to enable a direct comparison of the analyzed pump configurations with respect to energy consumption, economic performance, and environmental impact. The calculated parameters were subsequently used to assess the differences between regulated and non-regulated axial-piston pumps under the defined operating conditions.
The power of the non-regulated pump was calculated using Equation (1):

$$P(t) = p \cdot Q(t) \tag{1}$$

For calculating the power of regulated axial-piston pumps, the time fraction of each operating condition was taken into account, as given in Equation (2):

$$P_{ls} = (1 + f_{ls}) p Q_m, Q_m = i \sum d_i \alpha_i Q_{m,max} \tag{2}$$

One of the main parameters used to compare load-sensing regulated axial-piston pumps with non-regulated pumps is electricity consumption during operation. Based on the defined operating cycle, in which the pump operates at full flow for 30% of the time, at 60% of its capacity for 50% of the time, and at 30% of its capacity for 20% of the time, the annual electricity consumption was calculated for each of the analyzed pumps. The operating time during a typical working day was also taken into account. Since the system operates continuously in three shifts, the active operating time was assumed to be approximately 18 hours per day. The annual electricity consumption was calculated using Equation (3):

$$E_{yr} = \frac{P_{el}^{F} \cdot t_{yr}}{1000}, E_{yr}^{ls} = \frac{P_{el}^{ls} \cdot t_{yr}}{1000} \quad (3)$$

The results presented in the table and graph show that load-sensing regulated pumps have lower electricity consumption compared with fixed-displacement pumps. The difference becomes more pronounced for pumps with higher power ratings and higher operating pressures. This indicates that the potential energy savings associated with load-sensing regulation increase as the power requirements of the hydraulic system increase. Table 1 shows the ratio of consumed electrical energy in three types of pumps with fixed and variable displacement.

Table 1. *Energy efficiency*

Pumps	Working pressure (bar)	Flow (l/min)	Energy consumption LS (kWh/god)	Energy consumption fixed (kWh/god)	Saving (%)
Pump A	150	120	97,631.6	145,927.5	33.07 %
Pump B	250	200	269,250.9	402,576.5	33.14 %
Pump C	300	250	385,964.9	603,864.7	36,12 %

Figure 3 graphically shows the ratio of consumed energy for pump type A, with regulation and without regulation.

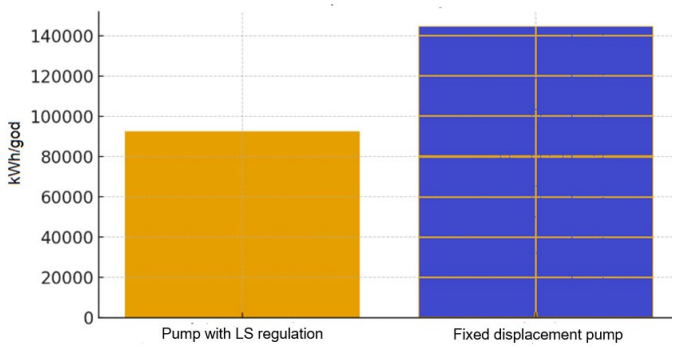


Fig. 3*. Ration of cosumed energy Pump A*

The figure 4 shows the ratio of annual energy consumption for pump B, operating parameters of pressure 250 bar and flow rate 200 l/min.

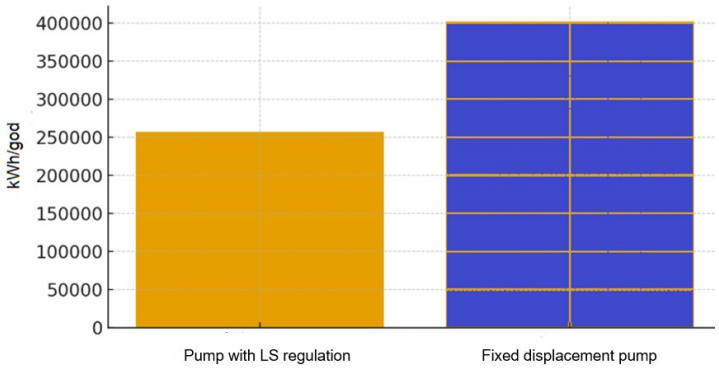


Fig. 4. *Ration of cosumed energy Pump B*

The figure 5 shows the ratio of annual energy consumption for pump type C.

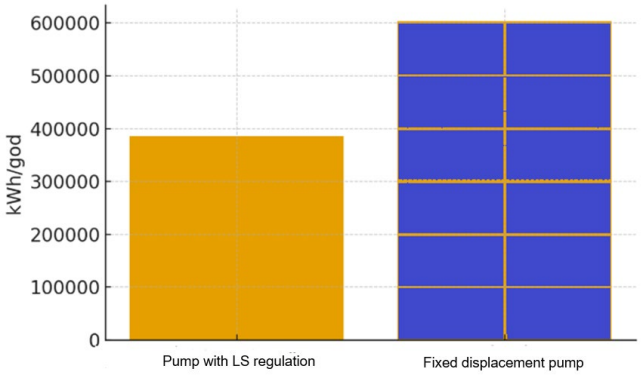


Fig. 5. *Ration of cosumed energy Pump C*

Cumulative cost analysis is a key tool in technical-economic studies of hydraulic systems because it allows making decisions that balance between initial investment, energy consumption and long-term maintenance, where LS regulation significantly contributes to reducing total costs and increasing system efficiency. Cumulative costs are calculated on an annual basis according to Equation (4):

$$Cost_{tol}^{x} = C_{cap}^{x} + \sum C_{op,t}^{x}, X \in \{F, LS\} \tag{4}$$

where is it

$$C_{op,t}^{x} = C_{el} \cdot E_{yr,t}^{x} + M_{i}^{x} \tag{5}$$

The figure 6. shows the cumulative cost analysis for the first group of pumps, i.e. for Pump A.

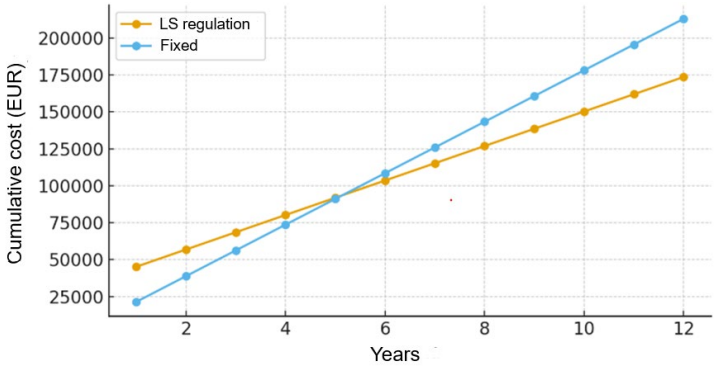


Fig. 6. *Cumulative cost analysis for. for Pump A*

The figure 7. shows the cumulative cost analysis for the Pump B.

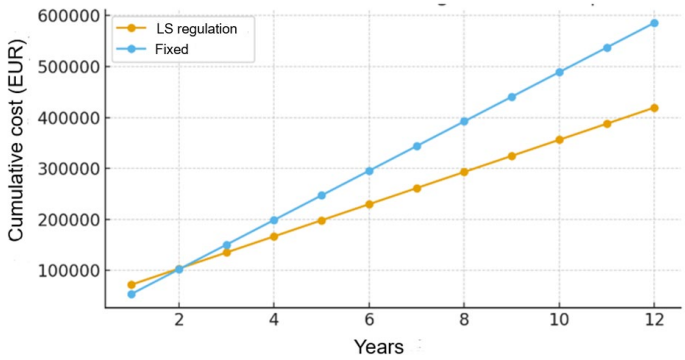


Fig. 7. *Cumulative cost analysis for. for Pump B*

The figure 8. shows the cumulative cost analysis for the Pump C.

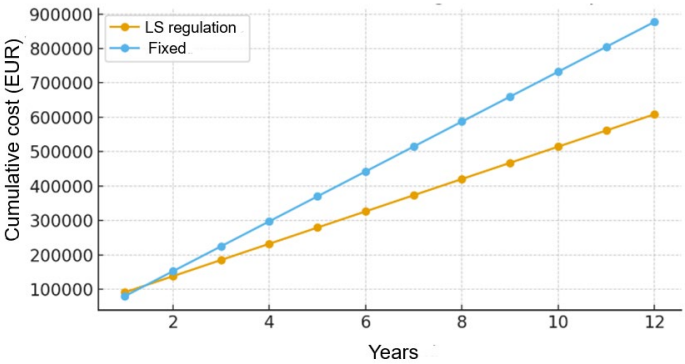


Fig. 8. *Cumulative cost analysis for. for Pump C*

The analysis of cumulative CO_2 emissions during the operational period provides a quantitative insight into the environmental impact of different types of hydraulic pumps, enabling the comparison of traditional pumps with fixed flow and pumps with Load-Sensing (LS) regulation. The presentation of these emissions through a line diagram during 12 years of operation clearly shows that pumps with LS regulation achieve significantly lower cumulative CO_2 emissions, which is a consequence of proportionally reduced electricity consumption. The figure 9 shows the cumulative emission of CO2 gases, for the period of exploitation of the pumps in the range of 12 years, on the example of Pump type A.

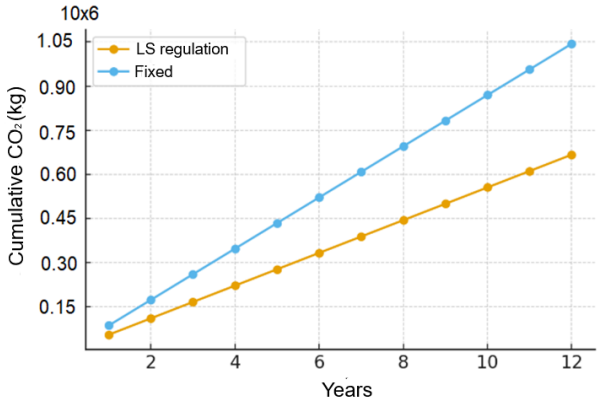


Fig.9. *The cumulative emission of CO2 gases for Pump A*

The figure 10 shows the cumulative emission of CO2 gases, for the period of exploitation of the pumps in the range of 12 years, on the example of Pump type B.

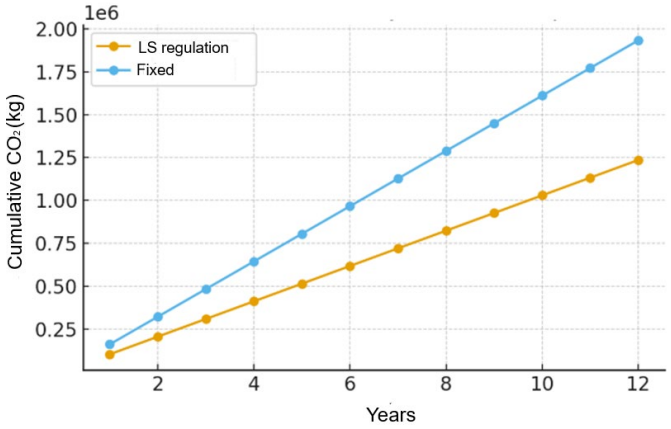


Fig.10. *The cumulative emission of CO2 gases for Pump B*

The figure 11 shows the cumulative emission of CO2 gases, for the period of exploitation of the pumps in the range of 12 years, on the example of Pump type C.

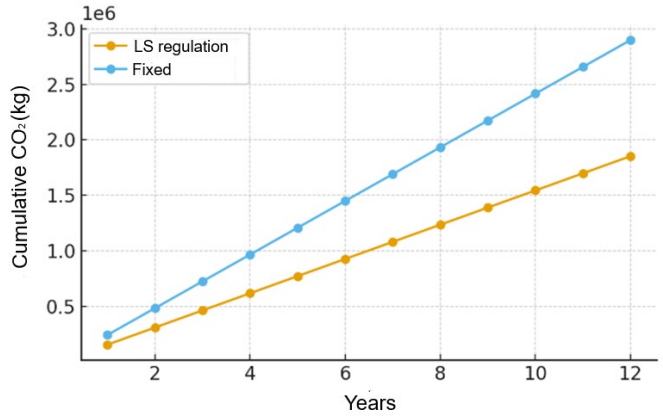


Fig.11. *The cumulative emission of CO2 gases for Pump C*

CONCLUSION

The results of the conducted analysis clearly demonstrate that the selection of pump type has a significant influence on the energy efficiency and overall operating costs of hydraulic systems. Pumps equipped with LS (Load-Sensing) regulation, owing to their ability to adjust the delivered flow rate according to the actual requirements of the consumers, achieve substantial reductions in electricity consumption compared with fixed-flow pumps. This effect becomes particularly pronounced in applications involving higher-capacity pumps and elevated operating pressures, where the difference in energy consumption increases accordingly. These findings support the initial hypothesis that the application of LS pumps enables more efficient utilization of the input power.

From an economic perspective, although LS-regulated pumps generally require higher initial capital investment, the analysis of cumulative costs indicates that the additional investment can be recovered within a relatively short operating period through the achieved energy savings. In the case of larger pump units, the payback period may be reduced to only a few years, further supporting their application in industrial environments characterized by intensive operating regimes and high energy demand. This finding highlights the importance of conducting a comprehensive life-cycle cost (LCC) analysis, as a comparison based solely on initial purchase prices does not provide a sufficiently realistic assessment of the long-term economic viability of the selected pumping solution.

The environmental aspect further supports the application of LS-regulated pumps. The analysis of cumulative CO_2 emissions over a 12-year operating period demonstrates that variable-flow regulation can substantially reduce greenhouse gas emissions. Consequently, in addition to the direct economic benefits associated with lower energy consumption, the

implementation of LS technology may contribute to broader objectives related to decarbonization and sustainable development.

Overall, the results indicate that the application of LS-regulated pumps provides significant technical, economic, and environmental advantages compared with conventional fixed-flow pump systems. Nevertheless, certain limitations should also be considered, particularly the greater complexity of the regulation system, potentially more demanding maintenance procedures, and possibly higher service costs over the long term. Despite these considerations, the overall balance between the identified benefits and limitations supports the wider implementation of LS-regulated pumps in modern hydraulic systems, particularly in applications characterized by variable load requirements and intensive operating conditions.

REFERENCES

Axin, M., Eriksson, B., & Krus, P. (2014). Flow versus pressure control of pumps in mobile hydraulic systems. *Proceedings of the Institution of Mechanical Engineers, Part I: Journal of Systems and Control Engineering*, *228*(4), 245–256. https://doi.org/10.1177/0959651813512820

Bosch, R. (2026). *Axial piston fixed pump* [Catalogue]. Bosch Company. file:///C:/Users/Administrator/Downloads/re91510_2026-07-14%20(1).pdf

Helian, B., Mustalahti, P., Mattila, J., Chen, Z., & Yao, B. (2022). Adaptive robust pressure control of variable displacement axial piston pumps with a modified reduced-order dynamic model. *Mechatronics*, *87*, 102879. https://doi.org/10.1016/j.mechatronics.2022.102879

Kapsiz, M. (2022). The efficiency of mobile hydraulic system with diesel engine and axial piston pump analysis. *Journal of Engineering Research*, *10*(4), 216–228. https://doi.org/10.36909/jer.11137

Kärnell, S., & Ericson, L. (2023). Classification and Review of Variable Displacement Fluid Power Pumps and Motors. *International Journal of Fluid Power*. https://doi.org/10.13052/ijfp1439-9776.2423

Kralev, J., Mitov, A., & Slavov, T. (2026). Approximated Adaptive Dynamic Programming Control of Axial-Piston Pump. *Mathematics*, *14*(7), 1127. https://doi.org/10.3390/math14071127

Li, R., Sun, Q., Ding, X., Zhang, Y., Yuan, W., & Wu, T. (2022). Review of Flow-Matching Technology for Hydraulic Systems. *Processes*, *10*(12), 2482. https://doi.org/10.3390/pr10122482

Lisowski, E., Filo, G., & Rajda, J. (2021). Analysis of the Energy Efficiency Improvement in a Load-Sensing Hydraulic System Built on the ISO Plate. *Energies*, *14*(20), 6735. https://doi.org/10.3390/en14206735

Mahato, A. C., & Ghoshal, S. K. (2021). Energy-saving strategies on power hydraulic system: An overview. *Proceedings of the Institution of Mechanical Engineers, Part I: Journal of Systems and Control Engineering*, *235*(2), 147–169. https://doi.org/10.1177/0959651820931627

Nault, J., & Papa, F. (2015). Lifecycle Assessment of a Water Distribution System Pump. *Journal of Water Resources Planning and Management*, *141*(12), A4015004. https://doi.org/10.1061/(ASCE)WR.1943-5452.0000546

Novaković, B. Z., Djordjević, L., & Bakator, M. (2026). Comparative study of HM and HV VG 68 oils under press-like pressure—Temperature conditions. *Results in Engineering*, *32*, 112025. https://doi.org/10.1016/j.rineng.2026.112025

Parker, H. (2026, September 17). *AXIAL PISTON PUMPS SERIES PVPLUS*. Parker-Hannifin Corporation. https://www.parker.com/content/dam/Parker-com/Literature/PMDE/Catalogs/Piston_Pumps/PV-/MSG30-3245_UK.pdf

Siebert, J., Wydra, M., & Geimer, M. (2017). Efficiency Improved Load Sensing System—Reduction of System Inherent Pressure Losses. *Energies*, *10*(7), 941. https://doi.org/10.3390/en10070941

Vacca, A. (2018). Energy Efficiency and Controllability of Fluid Power Systems. *Energies*, *11*(5), 1169. https://doi.org/10.3390/en11051169

Yamada, T., Inada, R., & Ito, K. (2024). Designing a Model Predictive Controller for Displacement Control of Axial Piston Pump. *International Journal of Automation Technology*, *18*(1), 113–127. https://doi.org/10.20965/ijat.2024.p0113

DOI:10.5937/IIZS26106K

ADVANTAGES OF USING SOME RARE-EARTH ELEMENTS IN COPPER POWER CABLES

Review paper

Zoran Karastojković[1], Jasmina Pekez[2]*, Zoran Milić[3], Milija Kraišnik[4]
[1] Society for Ethics and Evaluation in Science and Culture, Belgrade, Serbia
[2] Technical Faculty "Mihajlo Pupin", Zrenjanin, University of Novi Sad, Serbia
[3] "Milić" d.o.o., 35250 Paraćin, Glavica bb, Serbia
[4] Faculty of Mechanical Engineering, University of East Sarajevo, Bosnia and Herzegovina

Abstract: Pure copper is widely used for electrical cables because of its excellent electrical conductivity. Its relatively low mechanical strength, however, can limit applications in which higher strength and resistance to service conditions are required. Copper can be strengthened by plastic deformation and, more broadly, by alloying. Such strengthening may reduce electrical conductivity, so the addition of alloying elements must be carefully controlled. This review summarizes the principal metallurgical effects of selected rare earth elements (REEs) in copper, with emphasis on purification, grain refinement, mechanicalproperty improvement, corrosion resistance, wettability, and electrical conductivity. The reviewed literature indicates that small REE additions can promote impurity removal and microstructural refinement while maintaining high electrical conductivity when their concentration and processing conditions are appropriately controlled.
Key words: power cables, rareearth elements, lowalloyed copper

INTRODUCTION

Copper powercable producers use a relatively limited range of copper alloys, many of which belong to the group of lowalloyed copper. Classical metallurgical literature describes lowalloyed copper as a group in which small additions are used to modify selected properties while retaining the high conductivity of the copper matrix (Kočovski, 1991). The use of REEs in copper is of particular interest because these elements can influence both metallurgical quality and functional properties. From a metallurgical perspective, their effects include purification of molten copper, grain refinement during solidification, modification of inclusions, and improvement of mechanical and corrosion properties. From the electrical perspective, the main requirement is to preserve as much of copper's high electrical conductivity as possible. Recent reviews confirm that La, Ce, Y, and other REEs can act as effective microalloying elements in copper and copper alloys (Liu et al., 2025).

The available evidence suggests that the benefits of REE additions depend strongly on composition, concentration, processing route, and the impurity content of the copper matrix. Therefore, REEs should not be regarded as universally beneficial alloying additions; their effect must be evaluated for the intended copper grade and application.

Copper power cables microalloyed with selected REEs may combine high electrical conductivity with improved strength, thermal stability, corrosion resistance, and processing characteristics. REEs are also important in a wide range of modern technologies, including electronics, cleanenergy systems, automotive applications, and other high technology sectors (Natural Resources Canada, 2026).

[1]zoran.karastojkovic@gmail.com;
[2*]Corresponding author, jasmina.pekez@tfzr.uns.ac.rs, ORCID: 0000-0003-0454-5326
[3]vukasin.milic@miliccable.rs;
[4]milijakraisnik@yahoo.com, ORCID: 0000-0001-9672-7121

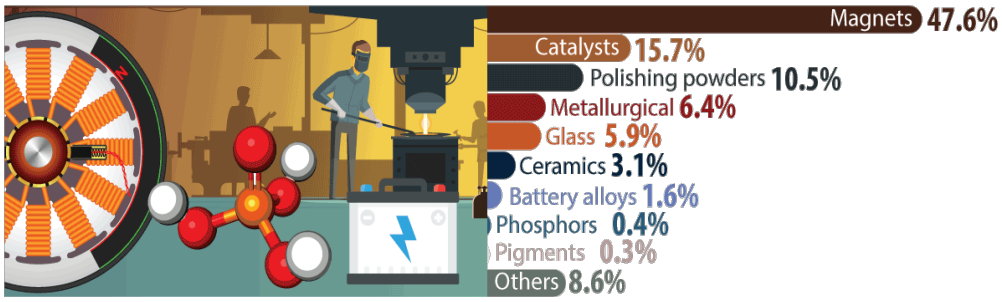


Fig. 1. *Selected application fields of rareearth elements.*
Source: Natural Resources Canada (2026).

REEs are used in electronics, automotive applications, clean energy technologies, aerospace, medical technologies, and other advanced applications. Their industrial importance is associated with their distinctive physical, chemical, magnetic, and metallurgical properties (Natural Resources Canada, 2026).

GENERAL PROPERTIES OF REEs – SHORT REVIEW

The most relevant properties of REEs are briefly considered below in terms of crystal structure, physical and chemical behavior, and metallurgical effects. These properties are important for understanding why very small REE additions can modify the behavior of copper and copper alloys (Gschneidner and Pecharsky, 2023; Liu et al., 2025).
According to their specific weight, they are classified as light and heavy REEs, and according to the geological presence at Earth's crust they are about the same as copper valid for light REEs, when heavy REEs are much more abundant than gold or molybdenum, for example.
The crystal structures of REEs include hexagonal closepacked (hcp), double hexagonal closepacked (dhcp), and facecentered cubic (fcc) structures, depending on the element and temperature. Figure 2 illustrates representative crystal structures of rareearth metals (Li Zhao, 2022).

Crystal structures

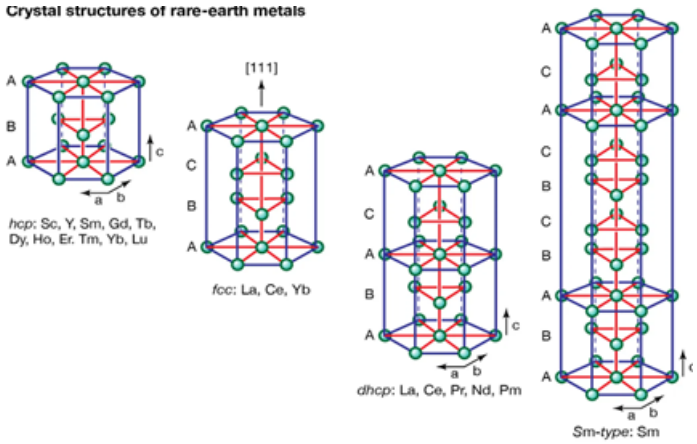


Fig. 2. *Crystal structures of representative rareearth metals.*
Source: Li and Zhao (2022).

Figure 3 shows the crystal structure of the high temperature superconductor $YBa_2Cu_3O_7$, which contains copper, yttrium, oxygen, and barium. This example illustrates the structural role that rare earth containing compounds can play in advanced functional materials (Barood et al., 2023).

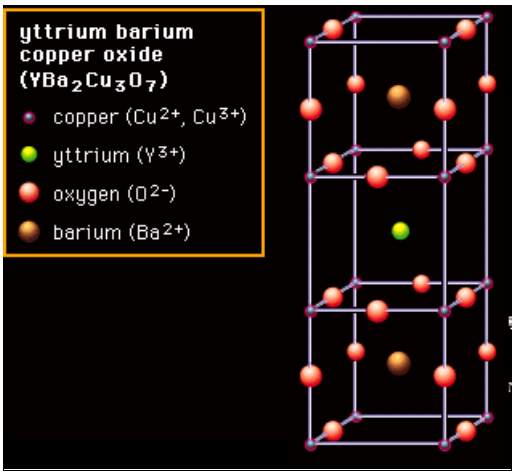


Fig. 3. *Crystal structure of $YBa_2Cu_3O_7$.*
Source: Barood et al. (2023).

Most REEs are silvery or iron gray metals and, in elemental form, are generally relatively soft, malleable, and ductile. Their mechanical properties vary substantially among individual elements and depend on purity and thermal history. For copper alloys, the more relevant effect is the response of the copper matrix to very small additions of REEs. Such additions can modify grain structure, impurity states, precipitation, and consequently the balance between strength and electrical conductivity. The development of high conductivity, high strength copper alloys like wise depends on controlling the microstructure and the distribution of strengthening phases (Gorsse et al., 2015; Liu et al., 2025).
Micro alloying copper with selected REEs can preserve high electrical conductivity while improving selected mechanical and microstructural characteristics. Here, electrical conductivity is expressed using the International Annealed Copper Standard (IACS); according to IEC 60028, 100% IACS corresponds to 58 MS/m at 20 °C (International Electrotechnical Commission, 1925). Ge et al. (2024) reported a conductivity of 103.72% IACS for a single crystal Cu–0.03Y rod, equivalent to about 60.16 MS/m and 3.72 percentage points above the 100% IACS reference. The authors attributed the increase to the interaction of Y with residual phosphorus: nanosized YP and Cu5Y precipitates reduce the amount of solute atoms dissolved in the copper matrix and thereby reduce electron scattering. This result was obtained for a specific single crystal Cu–0.03Y material and should not be interpreted as a 103.72% increase in conductivity or generalized to all copper alloys or REE concentrations.
To avoid an undesirable reduction in conductivity, REE concentrations must therefore be carefully controlled. The resulting phases may include fine precipitates or compounds formed through reactions between REEs and residual impurities. The balance between solid solution effects, precipitation, grain refinement, and impurity removal is central to the design of high strength, high conductivity copper alloys (Ge et al., 2024; Liu et al., 2025).

Chemical properties

The physical, chemical, and metallurgical behavior of REEs is strongly related to their electron configuration. Most REEs commonly occur in the +3 oxidation state, although some elements exhibit additional valence states.
REEs are chemically reactive, particularly at elevated temperatures. They readily form oxides, hydrides, nitrides, halides, and other compounds. Oxides are especially important in metallurgical processing and in the formation of stable reaction products with impurities.
Representative oxide types include:

- monoxide (lower oxide), e.g., EuO;
- dioxide, e.g., CeO_2;
- sesquioxide, R_2O_3;
- mixedvalence oxides such as R_3O_4; and

• higher oxides, e.g., Tb_4O_7 and Pr_6O_7.

REEs can also form mixed oxides such as $YAlO_3$, $LaGaO_3$, (La,M)CrO_3, and (Pr,Ca)MnO_3. Some groups have specific structural designations, including perovskites and garnets. These compounds have technologically relevant electrical, magnetic, optical, and chemical properties.

Garnet structures are substantially more complex than perovskite structures and contain several crystallographic sites occupied by oxygen and metal cations. Rare earth containing garnets are used in microwave and other electronic applications. More broadly, the diversity of REE compounds explains their importance in advanced functional materials.

Corrosion resistance

Improved corrosion resistance is another reported benefit of selected REE additions. Studies on REE containing brazing alloys show that La, Ce, and related additions can modify microstructure and improve the performance of brazed materials, while REE containing copper systems may also benefit from the formation of protective surface products (Cui et al., 2022; Duan et al., 2019; Duan et al., 2020).

Metallurgical effects

Because of their high chemical reactivity, REEs can react with impurities in molten copper and thereby contribute to a purification effect. Small additions of elements such as La and Ce can form stable compounds with impurities, while the resulting particles can act as nucleation sites during solidification. These effects may improve electrical properties, thermal stability, and microstructural uniformity when the REE addition is appropriately controlled (Karastojković et al., 2023; Liu et al., 2025).

During solidification, REE containing particles can contribute to grain refinement and modification of inclusion morphology. The literature reviewed by Liu et al. (2025) shows that REEs can reduce the size and alter the morphology of inclusions in copper, supporting a finer and more uniform microstructure.

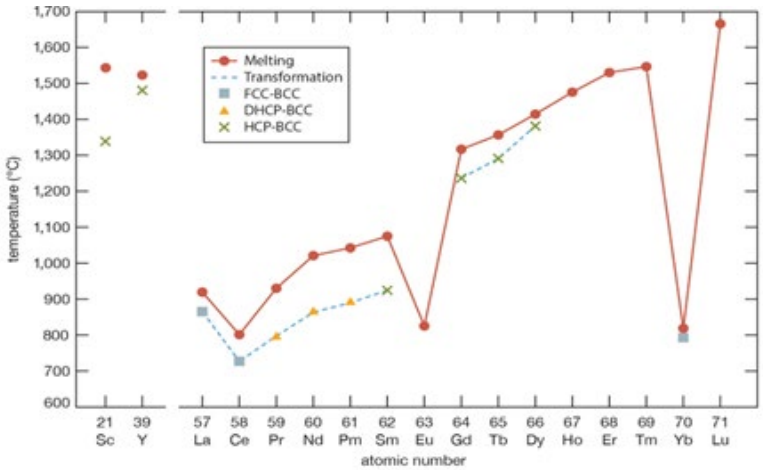


Fig. 5. *Melting and transformation temperatures of rareearth metals. Source: Gschneidner and Pecharsky (2023).*

Cerium, europium, and ytterbium have comparatively low melting temperatures among the rareearth metals. Such differences are relevant to alloy processing and the temperature range in which REEcontaining phases may form or dissolve.

COPPER – REEs AND NONMETALLIC INCLUSIONS REFINING

The effects of REEs in copper can be considered through several interconnected metallurgical mechanisms. In refining, cerium and other REEs react with harmful impurities, particularly oxygen and sulfur, producing stable compounds that can be removed from the melt or remain as finely dispersed particles. The resulting purification can reduce the concentration of detrimental impurities and modify the solidification structure.

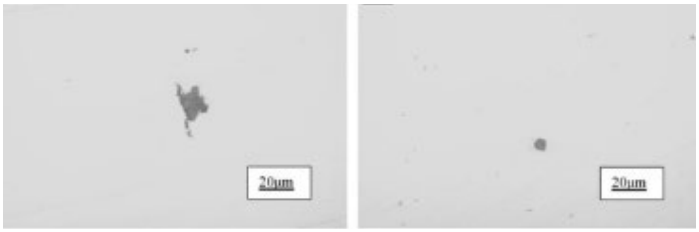
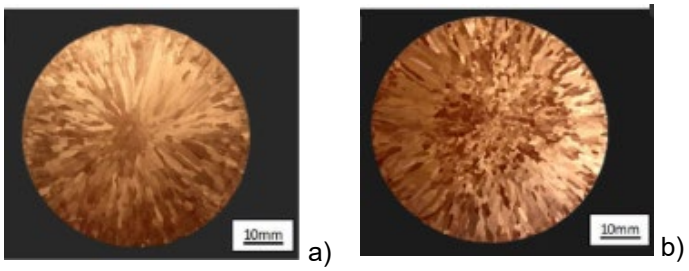


Fig. 6. *Morphology of inclusions in pure copper and copper containing 97 ppm Ce. Source: Liu et al. (2025).*

The metallographic comparison illustrates the change from larger, irregular inclusions in pure copper to finer and more uniformly distributed inclusions after the addition of a small amount of REE. This supports the interpretation that REEs can modify inclusion morphology and contribute to microstructural refinement (Liu et al., 2025).
Due to their high chemical activity, REEs can promote the formation of highmeltingpoint compounds that act as heterogeneous nucleation sites during solidification. This can reduce grain size and promote a more equiaxed structure, which is generally associated with improved strength and hardness.
The microstructural comparison indicates that REE additions can promote a finer and more equiaxed grain structure during solidification. Such refinement is consistent with the reported ability of REEs to provide heterogeneous nucleation sites and modify inclusion morphology in copper (Liu et al., 2025).



a) b)

Fig. 7. *Microstructures of crystallized pure copper and copper containing Ce. Source: Liu et al. (2025).*

REE additions can also modify the size and morphology of inclusions, promoting finer and more spheroidized particles that are more uniformly distributed in the copper matrix. Such microstructural modification can contribute to improved mechanical performance (Liu et al., 2025).
Studies of REE containing brazing alloys also report improved wettability and bonding behavior. For example, Ce additions can improve the wettability of Cu based brazing alloys and modify the interfacial microstructure, while La, Ce, Nd, and Pr additions can refine the filler metal structure and improve mechanical or wear related performance (Wu et al., 2018; Cui et al., 2022; Duan et al., 2019; Feng et al., 2023). These effects are relevant to electrical contacts, brazing, and other joining technologies.

CONCLUSION

The reviewed literature indicates that microalloying copper with small additions of selected rare earth elements (REEs) provides multifunctional benefits through several complementary metallurgical mechanisms. Primary effects include melt purification, nonmetallic inclusion modification, and grain refinement during solidification, alongside improvements in corrosion resistance and joining/brazing characteristics. When alloy composition and processing parameters are precisely controlled, these additions enhance mechanical strength and microstructural stability without causing a significant drop in electrical conductivity, making REE modified copper highly suitable for power cable applications. However, the precise effect of REE additions remains strongly concentration dependent and influenced by the copper matrix and impurity levels. Consequently, alloy design must be tailored to specific application requirements and processing routes, while balancing performance improvements with the associated material and manufacturing costs.

REFERENCES

Barood, F. A. A., Awang Kechik, M. M., Tee, T. S., Kien, C. S., Pah, L. K., Hong, K. J., Shaari, A. H., Baqiah, H., Karim, M. K. A., Shabdin, M. K., Mohd Shariff, K. K., Hashim, A., Suhaimi, N. E., Miryala, M. (2023). Orthorhombic $YBa_2Cu_3O_7-\delta$ superconductor with TiO_2 nanoparticle addition: Crystal structure, electric resistivity, and AC susceptibility. *Coatings*, 13(6), 1093. https://doi.org/10.3390/coatings13061093

Cui, B., Zhao, W., Zuo, R., Zhang, L., Cheng, Z., Jiu, Y., Qin, J., Fu, Y., Xu, D. (2022). Effect of rare earth alloy addition on the microstructure and abrasion resistance of brazed diamonds with CuSnTi filler metal. *Diamond and Related Materials*, 126, 109110. https://doi.org/10.1016/j.diamond.2022.109110

Duan, D., Li, C., Ding, J., Liu, Y., Sun, L., Lin, Q., Jiang, Z. (2020). Microstructure and performance of brazed diamond segments with NiCr–x(CuCe) composite alloys. *Ceramics International*, 46(9), 13180–13188. https://doi.org/10.1016/j.ceramint.2020.02.092

Duan, D., Sun, L., Lin, Q., Fang, X., Li, C., Jiang, Z. (2019). Effect of Cu–Ce alloy addition on the microstructure and mechanical performance of brazed diamonds with Ni–Cr alloy. *International Journal of Refractory Metals and Hard Materials*, 80, 253–258. https://doi.org/10.1016/j.ijrmhm.2019.01.022

Feng, S., Jin, T., Wang, B., Cheng, Z., Zhang, C., Zhong, S., Xu, D. (2023). Microstructure and properties of brazed diamond with Prmodified NiCr filler metals. *Diamond and Related Materials*, 138, 110224. https://doi.org/10.1016/j.diamond.2023.110224

Ge, C., Li, S., Song, K., Guo, X., Zhou, Y., Liu, H., Zhang, C., Cao, J., Cao, F., Gao, Y., Su, H. (2024). Interaction of Y and impurity P on the synergistic enhancement of elongation and electrical conductivity of single crystal copper rod. *Materials Design*, 237, 112586. https://doi.org/10.1016/j.matdes.2023.112586

Gorsse, S., Ouvrard, B., Gouné, M., PoulonQuintin, A. (2015). Microstructural design of new high conductivity high strength Cubased alloy. *Journal of Alloys and Compounds*, 633, 42–47. https://doi.org/10.1016/j.jallcom.2015.01.234

Gschneidner, K. A., Jr., Pecharsky, V. K. (2023). Rareearth element. Encyclopaedia Britannica. https://www.britannica.com/science/rareearthelement

International Electrotechnical Commission. (1925). International standard of resistance for copper (IEC 60028:1925). https://webstore.iec.ch/en/publication/98

Karastojković, Z., Bajić, N., Pekez, J., Janjušević, Z. (2023). The role of cerium as a rareearth element in a hotwork tool steel. In *Proceedings of the XIII International Conference on Industrial Engineering and Environmental Protection* (pp. 50–55). Technical Faculty "Mihajlo Pupin", University of Novi Sad.

Kočovski, B. (1991). *Bakar i bakarne legure*. Institut za bakar.

Li, R., Zhao, Y. (2022). Crystal structures and phase transitions of lanthanide metals under pressure and temperature. *Journal of Alloys and Compounds*, 895, 162810. https://doi.org/10.1016/j.jallcom.2021.162810

Liu, J.S., Yu, W.X., Chen, D.Y., Wang, S.W., Song, H.W., Zhang, S.H. (2025). A review of studies on the influence of rareearth elements on the microstructures and properties of copper and copper alloys and relevant applications. *Metals*, 15(5), 536. https://doi.org/10.3390/met15050536

Natural Resources Canada. (2026). Rare earth elements facts. Government of Canada. https://naturalresources.canada.ca/mineralsmining/miningdatastatisticsanalysis/mineralsmetalsfacts/rareearthelementsfacts

Wu, Q., Luo, Z., Wang, Y., Zhao, H., Deng, Z. (2018). Effects of rare earth Ce on the brazing performance of high energy mechanical milling Cubased alloy powder. *Metals*, 8(7), 495. https://doi.org/10.3390/met8070495

DOI:10.5937/IIZS26113L

INFLUENCE OF LONGITUDINAL STIFFENING RIB HEIGHT ON THE STRESS-DISPLACEMENT BEHAVIOUR OF A THIN-WALLED CONSTRUCTION OF HOUSING

Research paper

Dejan Landup[1*],Dejan Bajić[2], Eleonora Desnica[3], Ivan Palinkaš[4]
[1,2,3,4] University of Novi Sad Technical Faculty "Mihajlo Pupin", Zrenjanin, Serbia

Abstract: This paper presents an analysis of the influence of longitudinal stiffening rib height on the stress-displacement behaviour of a thin-walled machine housing. The analysis was carried out in SolidWorks Simulation using the finite element method within a linear static analysis. A simplified thin-walled housing model, 500 × 300 × 150 mm in size and with a wall thickness of 3 mm, was used as the reference geometry. The real functional purpose of the housing and its structural complexity were neglected, so the study focuses on the effect of rib height under a centrally applied static load on the upper plate. The housing was loaded by a force of 2000 N acting over an area of 100 × 100 mm. Five variants were compared: M0 without ribs and M1–M4 with two longitudinal ribs 20, 40, 60 and 80 mm high. For each model, von Mises stress, maximum resultant displacement and equivalent static stiffness were analysed. The results show that increasing rib height reduces displacement and increases stiffness. The most pronounced difference was obtained between M0 and M3, where displacement was reduced by 77.9%, while stiffness increased from 726.5 to 3280.8 N/mm. Further rib height increase produced a smaller stiffness gain with higher local stresses..
Key words: thin-walled housing, stiffening ribs, static stiffness, finite element method, von Mises stress

INTRODUCTION

Thin-walled structures and housings are often used in mechanical engineering practice due to their simple manufacturing process, low mass and easy adaptation to different operating and environmental requirements (Budynas & Sadegh, 2020). The drawback of thin-walled structures is reflected in increased stresses, deformations and reduced stiffness. For this reason, stiffening ribs are often applied in practice, since they contribute to the resistance of the structure without a considerable change in the overall thickness of the base wall (Jiang et al., 1997; Rezaiefar & Galal, 2022; Zou et al., 2019). The application of modern software tools represents an important part of contemporary engineering design, especially in the design and comparison of different structural and technological solutions (Desnica et al., 2025). The functionality and influence of ribs on the structure depend on their geometrical parameters, such as height, thickness, position and number of ribs. Despite their positive effects, ribs can lead to local stress concentrations, especially in the zones where the ribs are joined to the base plate and at the rib ends (Pilkey et al., 2020). In addition to deformations, it is also necessary to analyse the stress distribution in the structure. In this paper, a linear static analysis was carried out using the finite element method in SolidWorks Simulation (Bathe, 2008; Dassault Systèmes, 2026; Desnica et al., 2022; Zienkiewicz et al., 2013). Five variants of the thin-walled housing were analysed, ranging from the housing without ribs to the housing with ribs up to 80 mm high. The aim of the paper is to determine the influence of rib height on the maximum von Mises stress, maximum resultant displacement and equivalent static stiffness of the structure. For an isolated assessment of the influence of longitudinal stiffening rib height, the housing was considered as a fully idealized thin-walled structure, excluding its real functional purpose and structural details. The load position was selected at the centre of the upper plate of the structure, since this is the location where the largest bending moment and the greatest deflection of the upper plate are expected.

[1]Corresponding author, dejan.landup@tfzr.rs , ORCID: 0009-0009-3836-2182
[2] dejan.bajic@tfzr.rs , ORCID: 0000-0001-7435-9604
[3] eleonora.desnica@tfzr.rs , ORCID: 0000-0002-4724-5764
[4] ivan.palinkas@tfzr.rs , ORCID: 0000-0001-9253-1375

MATERIAL AND METHODS

The numerical analysis was carried out on a simplified model of a closed thin-walled housing supported by four feet. The foot wall thickness was the same as the wall thickness of the housing. In a real structure, the feet are represented as hollow profiles welded to the structure, while for this study an idealized case was adopted, where the feet are fully bonded to the housing. The analysis was performed through five structural variants. The reference model was M0, without ribs, while the remaining models, M1–M4, were designed with two longitudinal ribs on the outer side of the upper plate. For all variants, the ribs had the same length of 420 mm and thickness of 3 mm, while the rib height varied from 20 mm to 80 mm. The rib position, load, material, support conditions and mesh parameters were kept the same for all models, while only the rib height was changed depending on the model. Fig. 1 shows the construction of the reference model M0 without ribs and model M3 with ribs 60 mm high.

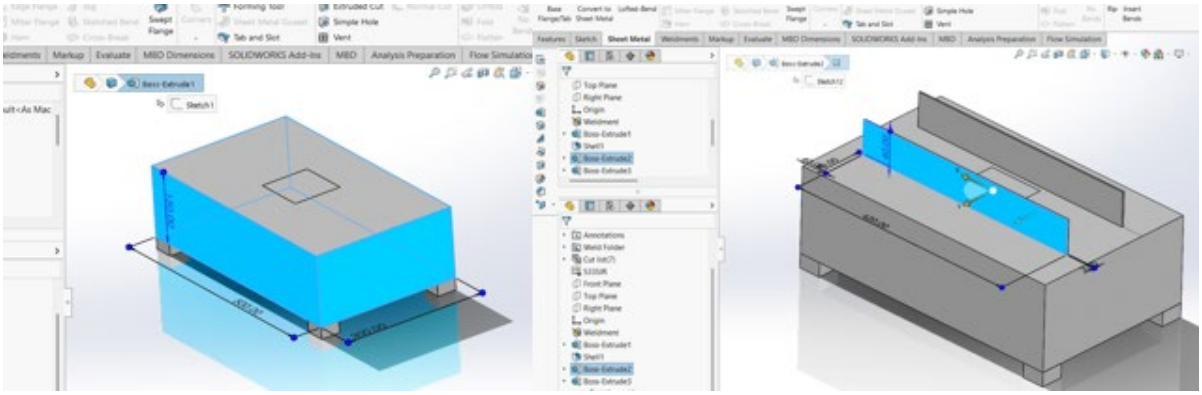


***Fig. 1**. Construction of thin walled-machine with and without rib*

The adopted housing material was S355JR steel (Institut za standardizaciju Srbije, 2020). The material specifications used in the numerical analysis were the modulus of elasticity, density, Poisson's ratio and yield strength. The simulation was performed in SolidWorks Simulation as a linear static analysis. Regarding the loading conditions, the housing was loaded on the outer side of the upper plate, where the force was applied over the defined surface. Fig. 2 shows the support conditions of the structure, defined using Fixed Geometry on the lower surface of each foot, while Fig. 3 shows the mesh generation and the action of the applied force on the thin-walled housing.

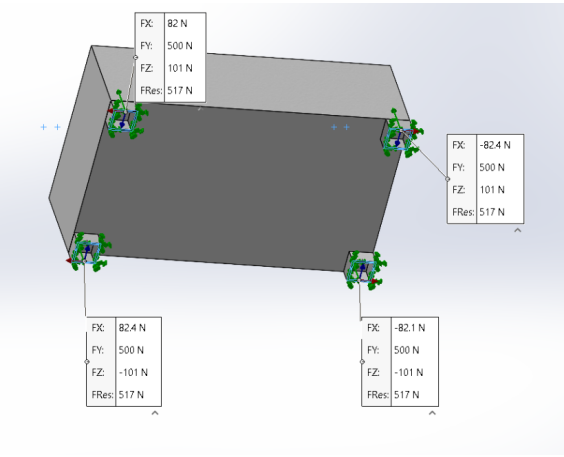


***Fig. 2**. Fixed Geometry, uniform positioning of the support*

The stress-displacement state was assessed using the maximum von Mises stress and the maximum resultant displacement. In addition, the equivalent static stiffness was calculated using the following equation:

$$k = \frac{F}{u_{max}} \tag{1}$$

In Eq. (1), *F* represents the total applied force, while u_{max} represents the maximum displacement of the model. For comparison of the models, the increase in stiffness and the reduction in displacement were evaluated relative to the reference model without ribs. Before comparing all models, mesh independence was checked on model M3, and three global element sizes were analysed: 6 mm, 4 mm and 3 mm. For the final analysis and comparison of all models, a 3 mm mesh was adopted, since the change in maximum displacement between the 4 mm and 3 mm meshes was 0,84%, while the stress changed by 4,7%. The mesh setup is shown in Fig. 3.

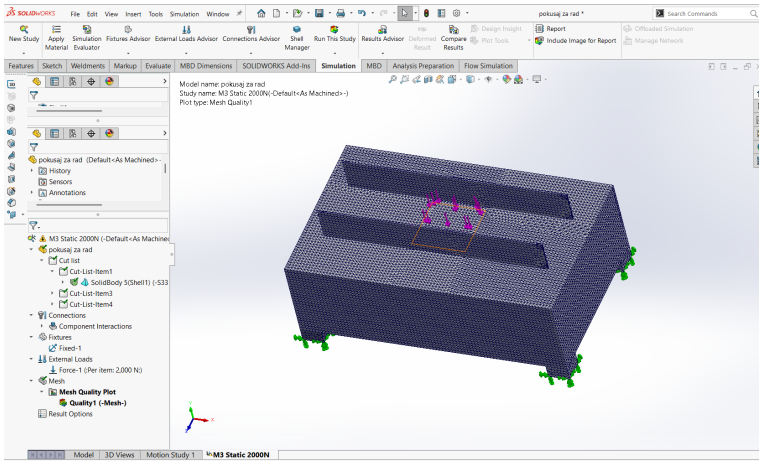


Fig. 3. *Creating mesh for construction*

Table 1. *Geometrical parameters of analysed models*

Model	Number of ribs	Rib length (mm)	Rib height (mm)	Rib thickness (mm)
M0	0	/	/	/
M1	2	420	20	3
M2	2	420	40	3
M3	2	420	60	3
M4	2	420	80	3

RESULTS AND DISCUSSION

The obtained numerical results showed that the addition of longitudinal stiffening ribs considerably reduces the displacement of the upper housing plate and increases the equivalent static stiffness of the structure (Jiang et al., 1997; Rezaiefar & Galal, 2022). Each model was analysed under the same loading conditions, support conditions, material type and mesh parameters, allowing the results to be directly compared. Table 2 presents the simulation results.

Table 2. *Numerical results from simulation*

Model	Rib height (mm)	u_{max} (mm)	K (N/mm)	$\sigma_{vM,max}$ (MPa)
M0	/	2,7530	726,5	181,8
M1	20	1,3120	1524,4	183,8
M2	40	0,7274	2749,5	317,7
M3	60	0,6096	3280,8	316,1
M4	80	0,5736	3486,8	346,6

The largest maximum displacement, shown in Fig. 4, was obtained for the housing without ribs, i.e. model M0, where the displacement was 2.7530 mm and the equivalent static stiffness was 726,5 N/mm. When the same simulation was performed on model M1, which has two longitudinal ribs 20 mm high, the maximum displacement was reduced to 1,3120 mm, while the stiffness increased to 1524,4 N/mm, as shown in Fig. 5. After comparing the first two models, it can already be concluded that even a small rib height considerably increases the resistance of the housing.

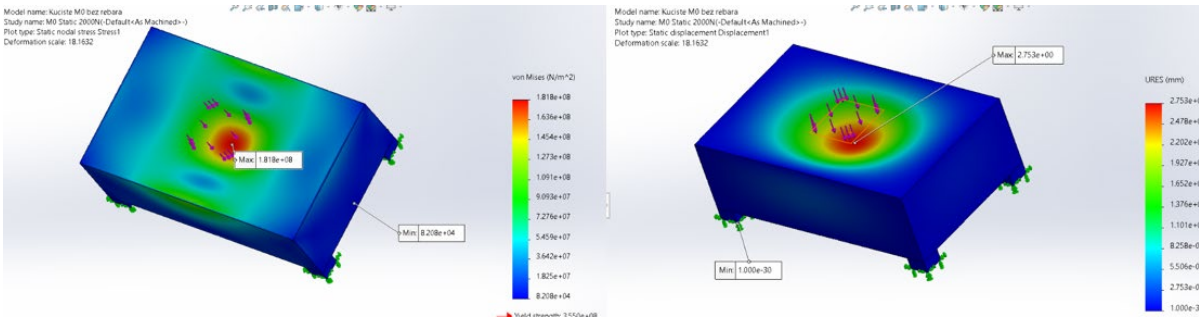


Fig. 4. *FEM results for M0: von Mises stress distribution left and resultant displacement distribution right*

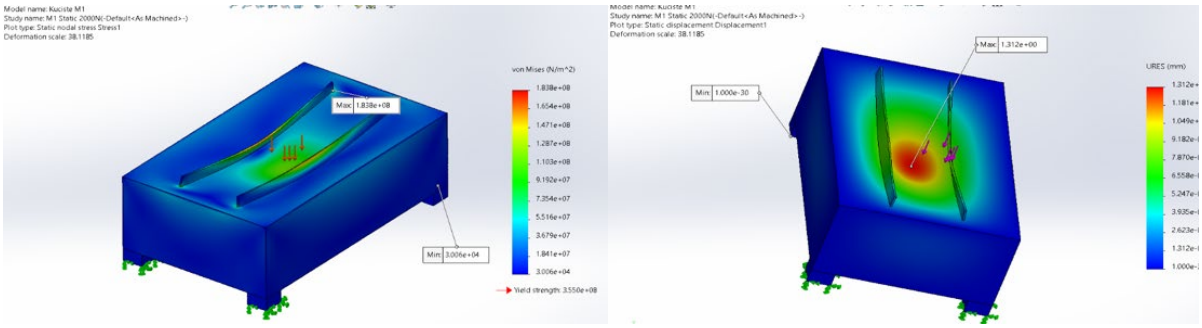


Fig. 5. *FEM results for M1: von Mises stress distribution left and resultant displacement distribution right*

For model M2, the rib height was increased to 40 mm, where the displacement decreased to 0,7274 mm, while the stiffness increased to 2749,5 N/mm, as shown in Fig. 6.

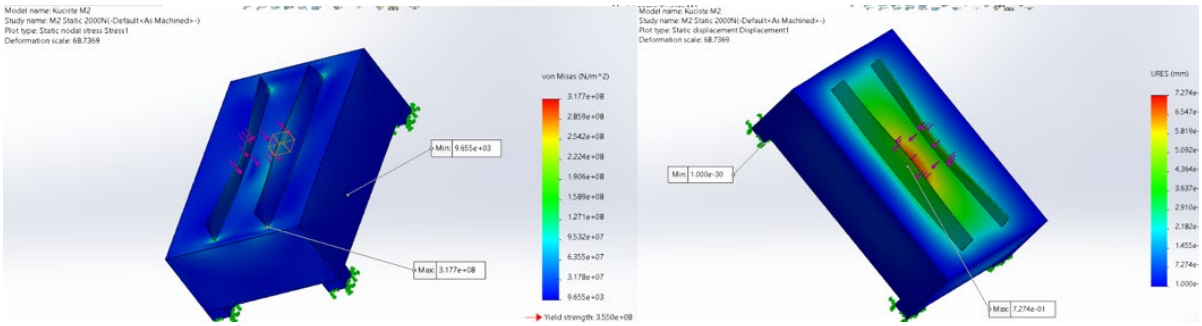


Fig. 6. *FEM results for M2: von Mises stress distribution left and resultant displacement distribution right*

With the further increase in rib height to 60 mm for model M3, the maximum displacement was 0,6096 mm, while the stiffness reached 3280,8 N/mm, as shown in Fig. 7.

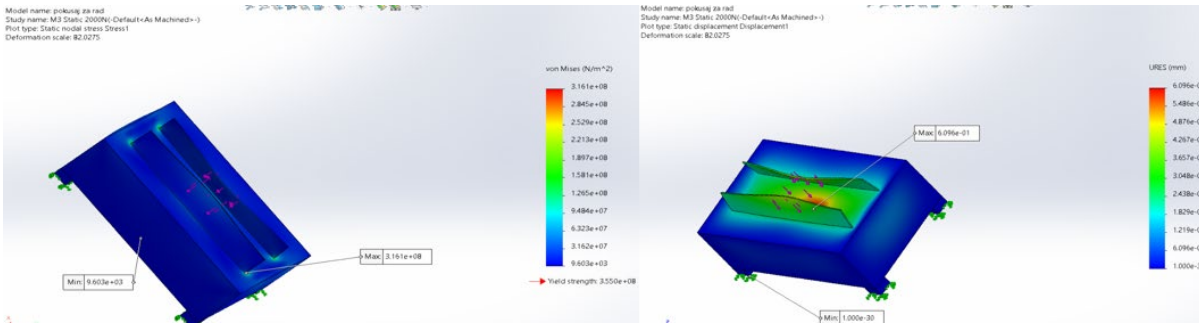


Fig. 7. *FEM results for M3: von Mises stress distribution left and resultant displacement distribution right*

The comparison of the reference model and model M3 showed a 77,9% reduction in maximum displacement, along with a 351,6% increase in stiffness. Based on the obtained results, it can be concluded that ribs with a height of 60 mm provide a pronounced stiffening effect for the thin-walled housing. The lowest maximum displacement was obtained for model M4, where the rib height was 80 mm and the displacement was 0,5736 mm. However, the stiffness increased by only slightly more than 6% compared with model M3, as shown in Fig. 8.

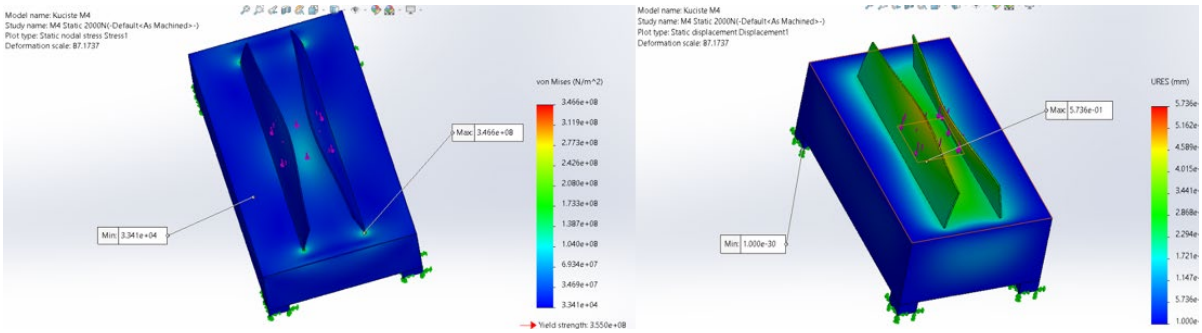


Fig. 8. *FEM results for M4: von Mises stress distribution left and resultant displacement distribution right*

The issue that appears is related to the von Mises stress, which in model M4 reaches 346,6 MPa, a value very close to the yield strength of S355JR steel, which is 355 MPa. For this reason, it can be concluded that further increasing the rib height after a certain value gives a smaller contribution to stiffness while increasing local stress concentrations (Pilkey et al., 2020). In models that contain ribs, the maximum von Mises stresses occur in the zones of rib ends and at the transitions between the ribs and the contact surface to which they are

connected, as can also be observed in the figures. This stress distribution is expected because the ribs in the numerical model were idealized with sharp transitions, without modelling fillets at the joint transition. In addition, the geometry of the welded joint that would connect the ribs to the rest of the structure was also neglected. Therefore, maximum local stresses should be interpreted together with the location where they occur, while the maximum displacement is a more suitable indicator of the structural stiffness. The graph with the obtained results is shown in Fig. 9.

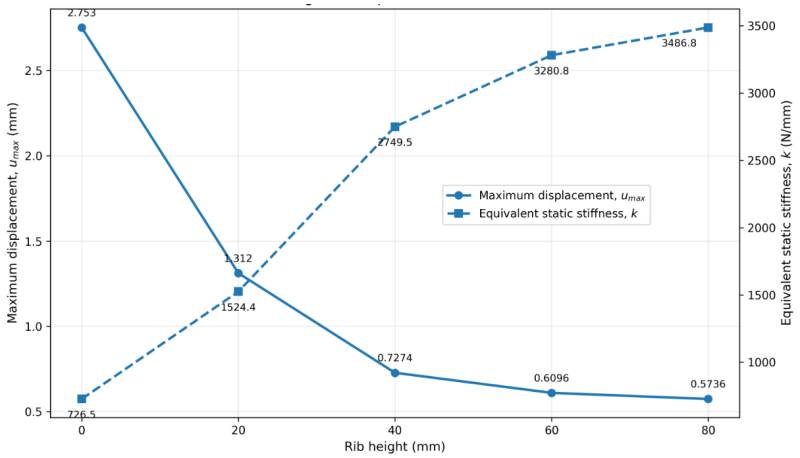


Fig. 9. *Effect of ribs height on maximum displacement and equivalent static stiffness.*

CONCLUSION

After the performed linear static FEM analysis, it can be concluded that the height of longitudinal stiffening ribs has a considerable influence on the stress-displacement behaviour of the thin-walled housing. The comparison of all models clearly shows that all models with ribs have higher equivalent static stiffness and lower maximum displacements compared with the reference model without ribs. The obtained results justify the application of ribs in thin-walled structures. The most pronounced change compared with the reference model M0 was observed for model M3 with ribs 60 mm high. This model proved to be a suitable solution, compared with the reference model, for reducing the maximum displacement and achieving a multiple increase in structural stiffness, while still remaining within the prescribed yield strength limits for S355JR steel. After model M3, one additional increase in rib height to 80 mm was analysed on model M4. However, this final increase had a very small effect on stiffness, while the structure approached the upper yield strength limit of the material. This leads to the conclusion that increasing the rib height after a certain value does not result in a proportional improvement of the entire structure. In particular, models with greater rib height showed an increase in local von Mises stresses, especially in the zones of rib ends and at the transitions to the upper surface of the structure, where the ribs are connected. An important aspect in selecting the rib geometry is to consider local stress concentrations in addition to displacement reduction. Possible directions for further research and development of this topic include the analysis of transition radii at the rib ends, more detailed modelling of the structure in terms of creating a realistic welded joint, both at the supports and on the ribs, and evaluating the achieved stiffness in relation to the increase in the mass of the structure.

REFERENCES

Bathe, K. J. (2008). Finite element method. In B. W. Wah (Ed.), *Wiley encyclopedia of computer science and engineering*. John Wiley & Sons. https://doi.org/10.1002/9780470050118.ecse159

Budynas, R. G., & Sadegh, A. M. (2020). *Roark's formulas for stress and strain* (9th ed.). McGraw Hill.

Dassault Systèmes. (2026). *Simulation verification problems*. SOLIDWORKS Design Help. Retrieved September 2, 2026, from https://help.solidworks.com/2026/english/simtutorialonline/c_simtutonline_verification_top.htm

Desnica, E., Đurđev, M., Vaščić, B., Turmanidze, R., & Dašić, P. (2022). Determination of a safety factor of a car wheel rim using finite element analysis in Solidworks. *Applied Engineering Letters, 7*(4), 163–171. https://doi.org/10.18485/aeletters.2022.7.4.4

Desnica, E., Palinkaš, I., Landup, D., Đurđev, M., Novaković, B., & Đorđević, L. (2025). Comparison of conventional and iMachining strategies using the SolidCAM software. In *Proceedings of the 11th International Scientific Conference Research and Development of Mechanical Elements and Systems IRMES 2025* (pp. 101–106). https://doi.org/10.46793/IRMES25.101D

Institut za standardizaciju Srbije. (2020). *SRPS EN 10025-2:2020: Hot rolled products of structural steels — Part 2: Technical delivery conditions for non-alloy structural steels*. Institut za standardizaciju Srbije.

Jiang, W., Bao, G., & Roberts, J. C. (1997). Finite element modeling of stiffened and unstiffened orthotropic plates. *Computers & Structures, 63*(1), 105–117. https://doi.org/10.1016/S0045-7949(96)00277-5

Pilkey, W. D., Pilkey, D. F., & Bi, Z. (2020). *Peterson's stress concentration factors* (4th ed.). John Wiley & Sons. https://doi.org/10.1002/9781119532552

Rezaiefar, A., & Galal, K. (2022). Large displacement analysis of stiffened plates with parallel ribs under lateral pressure using FE modeling with shell elements. *Engineering Structures, 259*, Article 114125. https://doi.org/10.1016/j.engstruct.2022.114125

Zienkiewicz, O. C., Taylor, R. L., & Zhu, J. Z. (2013). *The finite element method: Its basis and fundamentals* (7th ed.). Elsevier.

Zou, G., Wang, Y., Xue, Q., & Zhang, C. (2019). Buckling analysis of sandwich plate systems with stiffening ribs: Theoretical, numerical, and experimental approaches. *Advances in Civil Engineering, 2019*, Article 8737561. https://doi.org/10.1155/2019/8737561

DOI:10.5937/IIZS26120R

DIGITAL TWIN-BASED TECHNICAL DIAGNOSTICS OF ROTATING MACHINERY

Research paper

Adam Rac[1], Žolt Konja[2], Vesna Konja[3], Ljiljana Radovanović[4*]
[1,4]Technical Faculty "Mihajlo Pupin" Zrenjanin, University of Novi Sad, Serbia,
[2,3]Secondary Mechanical Engineering School, Novi Sad, Serbia

Abstract: Digital Twin technology offers new possibilities for technical diagnostics and predictive maintenance within Industry 4.0. This paper presents a simulation-based Digital Twin model for continuous diagnostics of rotating machinery using vibration monitoring. The proposed system integrates an ESP32 microcontroller, MPU6050 MEMS accelerometer, MQTT communication, and a Python-based diagnostic application for real-time data acquisition, processing, and analysis. The diagnostic method uses the root mean square (RMS) value of acceleration to detect abnormal operating conditions. The complete system was simulated in the Wokwi environment, enabling testing without expensive industrial equipment. A simulated rotor imbalance produced increased vibration levels, and when the RMS value exceeded the defined simulation threshold, the Python application generated a STOP command transmitted via MQTT to the ESP32, simulating machine shutdown. The results demonstrate the feasibility of integrating IoT, real-time analytics, and Digital Twin concepts for automated condition monitoring and prescriptive maintenance. The approach also provides a low-cost framework for testing diagnostic algorithms before implementation on real industrial systems.

Keywords: Digital Twin, technical diagnostics, predictive maintenance, Industry 4.0, IoT, ESP32, MPU6050, MQTT, vibration monitoring, RMS analysis

INTRODUCTION

High reliability, availability and safety of industrial machinery are essential for efficient production. Failures of rotating machines can cause downtime, production losses and safety risks. Traditional corrective and time-based preventive maintenance approaches do not always reflect the actual machine condition, which has increased the importance of condition-based and predictive maintenance within Industry 4.0.

This research investigates the application of the Digital Twin concept combined with Internet of Things (IoT) technologies for continuous technical diagnostics of rotating machinery. A Digital Twin is a dynamic digital representation of a physical system that is continuously updated using measurement data. In the proposed architecture, the ESP32 and MPU6050 form the sensor layer, MQTT provides data communication, and a Python application performs diagnostic analysis and control decisions.

The main objective is to develop and demonstrate a functional simulation model for real-time vibration monitoring and anomaly detection. The system was implemented in the Wokwi environment and includes:

- an ESP32–MPU6050 sensor node;
- real-time MQTT data transmission;
- Python-based RMS analysis;
- automatic generation of a STOP command when a critical condition is detected.

[1] adam20020604@gmail.com
[2] zolt.konja@gmail.com
[3] vesna.konja@gmail.com
[3] Corresponding author, ljiljana.radovanovic@tfzr.rs ORCID:0000-0002-5234-4820

The Digital Twin is implemented as a bidirectional architecture: measurement data are transmitted from the simulated physical layer to the diagnostic application, while control commands are returned to the ESP32, forming a closed feedback loop.

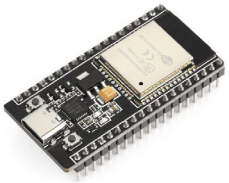


Fig.1. *ESP32 microcontroller*

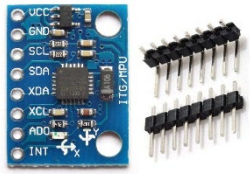


Fig.2. *MPU6050 sensor*

The paper presents the Digital Twin concept, the applied diagnostic methodology, the ESP32–MPU6050–MQTT architecture, the Wokwi simulation and the performed diagnostic test. FFT-based fault identification and Remaining Useful Life (RUL) estimation are considered advanced diagnostic functions, but are not implemented in the present prototype, which focuses on RMS-based anomaly detection and automatic feedback control.

THE CONCEPT OF THE DIGITAL TWIN IN INDUSTRY 4.0

A Digital Twin is a dynamic digital representation of a physical object, machine or process that is continuously updated using data from the monitored system. Unlike static CAD or conventional computer models, it reflects the current operational and technical condition of the physical system and enables continuous interaction between the physical and virtual domains. In technical diagnostics, Digital Twin technology combines real-time sensor data with digital models and analytical methods to support condition monitoring, anomaly detection and maintenance decision-making. The basic architecture consists of a physical system, its virtual representation and a communication infrastructure enabling bidirectional data exchange. In the proposed system, the ESP32 and MPU6050 represent the measurement layer, while the Python application represents the diagnostic layer. MQTT provides communication between these layers. This architecture enables continuous acquisition and analysis of machine-condition data and transmission of control commands back to the simulated machine. The proposed concept therefore provides a basis for real-time condition monitoring and further development towards predictive and prescriptive maintenance. Advanced functions such as FFT-based fault identification and RUL estimation can be integrated in future versions of the system.

IoT Sensor Structure and ESP32 Microcontroller

The sensor layer is based on the MPU6050 MEMS accelerometer, which provides three-axis acceleration measurements. The sensor is connected to an ESP32 microcontroller, which provides Wi-Fi communication and performs measurement acquisition and data transmission.



Fig. 3. *Three-axis accelerometer*

MQTT Communication and Data Transfer

MQTT is a lightweight publish-subscribe protocol suitable for IoT-based diagnostic systems. In the proposed architecture, the ESP32 acts as the publisher, transmitting MPU6050 measurements in JSON format to the MQTT broker, while the Python application acts as the subscriber, receiving and processing the data.

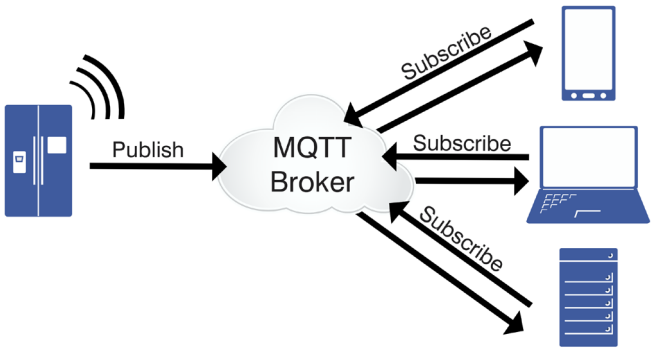


Fig. 4. *MQTT Publisher–Broker–Subscriber communication model*

Real-Time Diagnostic Analysis

The diagnostic module processes acceleration data in defined time windows and calculates the RMS value as the primary indicator of vibration level. This enables detection of deviations from normal operating conditions. More advanced methods, such as FFT-based frequency analysis and machine-learning models, can provide detailed fault identification but are not implemented in the current prototype.

APPLICATION OF THE TECHNICAL DIAGNOSTIC METHOD

Vibration-Based Condition Monitoring

Mechanical vibrations provide important information about the condition of rotating machinery. Imbalance, shaft misalignment and component wear can produce changes in vibration levels. In the proposed system, the MPU6050 continuously measures acceleration, while the

diagnostic application uses RMS analysis to detect abnormal conditions. Temperature monitoring can provide complementary information about friction and lubrication; however, it is not included in the present simulation.

Bearing Fault Diagnosis

Bearing defects can generate characteristic vibration frequencies related to bearing geometry and shaft speed. FFT analysis can be used to identify these frequencies and determine the type and location of a fault. However, FFT-based fault identification is considered only as a possible extension of the proposed system and is not implemented in the current prototype.

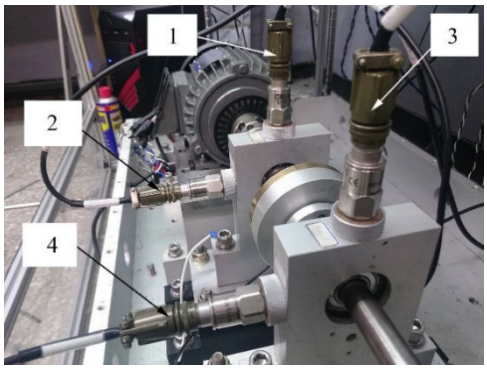


Fig. 5. *Industrial rotating machine with sensors installed to monitor bearing condition*

Remaining Useful Life Estimation

Remaining Useful Life (RUL) estimation is an advanced predictive maintenance function based on historical degradation trends. By analysing changes in vibration levels over time, a Digital Twin can potentially estimate the time remaining before a critical condition is reached. RUL estimation is not implemented in the present simulation and represents a direction for future development.

Automation and Prescriptive Feedback Control

The implemented system includes a closed feedback loop for automatic response to critical vibration levels. When the Python application detects an RMS value above the defined simulation threshold, it generates a STOP command and sends it through the MQTT broker to the ESP32. The microcontroller then changes the state of the control output, simulating machine shutdown.This architecture demonstrates the transition from condition monitoring and anomaly detection to automated prescriptive control.

PRACTICAL EXAMPLE

Simulation Model in the Wokwi Environment

The practical implementation was developed in the Wokwi environment using an ESP32 microcontroller and MPU6050 accelerometer. The ESP32 was programmed in MicroPython to acquire acceleration data, communicate via Wi-Fi and transmit measurements through MQTT to the HiveMQ broker.

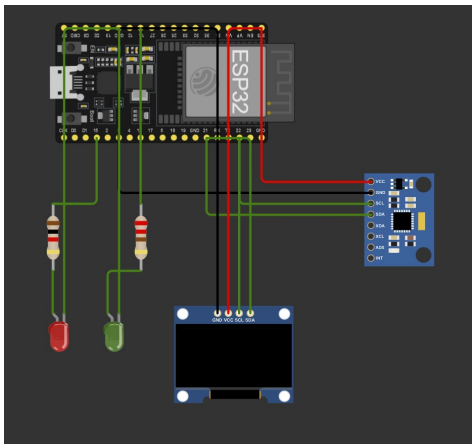


Fig. 6. *Wokwi simulation circuit with ESP32 and MPU6050*

The MPU6050 was connected to the ESP32 via I2C: VCC–3.3 V, GND–GND, SCL–GPIO 22, SDA–GPIO 21, while GPIO 15 was used as the control output for the simulated motor/relay. The Python diagnostic application, using the Paho-MQTT library, received the measurements and calculated the RMS value within defined time windows. An RMS threshold of 1.5 g was used exclusively to demonstrate anomaly detection and automatic shutdown. This value is not an ISO vibration limit; real industrial thresholds must be defined according to the machine, operating conditions, measurement method and applicable standards.

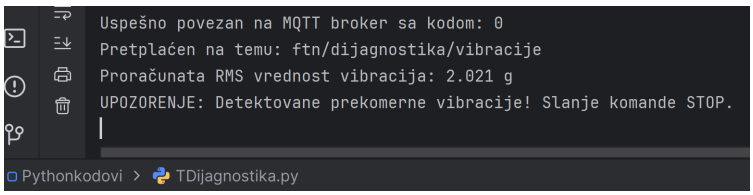


Fig. 7. *Python terminal showing RMS analysis and STOP command generation*

Simulation Test and Critical Condition Detection

The Digital Twin functionality was verified through two simulation conditions. During normal operation, the acceleration magnitude was approximately 1.0 g, primarily reflecting the gravitational component of the simulated accelerometer signal. This value should not be interpreted as vibration severity.

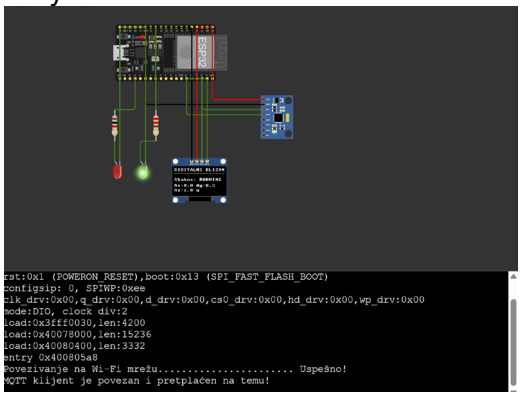


Fig. 8. *Wokwi simulation with RMS value of approximately 1.0 g*

During the second test, a simulated abnormal condition increased the RMS value to approximately 2.021 g, exceeding the 1.5 g simulation threshold.

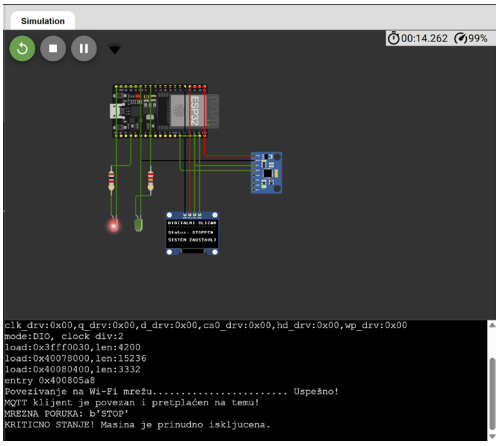


Fig. 9. *Wokwi simulation with RMS value of approximately 2.021 g*

The Python application detected the threshold exceedance and automatically generated a STOP command, which was transmitted via MQTT to the ESP32 and used to simulate machine shutdown. The test therefore demonstrated the complete closed-loop sequence:

measurement → MQTT transmission → RMS analysis → anomaly detection → STOP command → simulated shutdown.

CONCLUSION

A simulation-based Digital Twin for technical diagnostics of rotating machinery was successfully developed and demonstrated. The ESP32–MPU6050 architecture enabled data acquisition, while MQTT provided bidirectional communication with the Python diagnostic application. RMS-based analysis successfully detected the simulated abnormal condition and initiated an automatic STOP command. The Wokwi environment enabled testing of the complete diagnostic and feedback-control chain without expensive industrial equipment, providing a cost-effective basis for further development. However, experimental validation on real rotating machinery is required to assess measurement accuracy, diagnostic performance and communication reliability under real operating conditions. Future development should include FFT-based fault identification, machine-learning methods, RUL estimation, and additional sensors for temperature and electrical-current monitoring.

REFERENCES

Banks, A., Briggs, E., Borgendale, K., & Gupta, R. (2019). *MQTT version 5.0*. OASIS. https://docs.oasis-open.org/mqtt/mqtt/v5.0/os/mqtt-v5.0-os.html
Hillar, G. C. (2017). *MQTT essentials: A lightweight IoT protocol: The preferred IoT publish-subscribe lightweight messaging protocol*. Packt Publishing.
International Organization for Standardization. (2009). *ISO 10816-3:2009: Mechanical vibration—Evaluation of machine vibration by measurements on non-rotating parts—Part 3: Industrial machines with nominal power above 15 kW and nominal speeds between 120 r/min and 15 000 r/min when measured in situ* (ISO Standard No. 10816-3:2009). https://www.iso.org/standard/50528.html
International Organization for Standardization. (2016). *ISO 20816-1:2016: Mechanical vibration—Measurement and evaluation of machine vibration—Part 1: General guidelines* (ISO Standard No. 20816-1:2016).https://www.iso.org/standard/63180.html
International Organization for Standardization. (2022). *ISO 20816-3:2022: Mechanical vibration—Measurement and evaluation of machine vibration—Part 3: Industrial machinery*

with a power rating above 15 kW and operating speeds between 120 r/min and 30 000 r/min (ISO Standard No. 20816-3:2022). https://www.iso.org/standard/78311.html

Lee, J., Kao, H.-A., & Yang, S. (2014). Service innovation and smart analytics for Industry 4.0 and big data environment. *Procedia CIRP, 16*, 3–8. https://doi.org/10.1016/j.procir.2014.02.001

Ma, H., Fan, C., Zhang, Y., Wang, Q., Yu, K., & Ma, Z. (2025). Digital twin-inspired methods for rotating machinery intelligent fault diagnosis and remaining useful life prediction: A state-of-the-art review and future challenges. *Mechanical Systems and Signal Processing, 232*, 112770. https://doi.org/10.1016/j.ymssp.2025.112770

Ninković, D., & Petrović, M. (2022). *Technical diagnostics and reliability of mechanical systems*. University of Novi Sad, Faculty of Technical Sciences.

Sethi, P., & Sarangi, S. R. (2017). Internet of Things: Architectures, protocols, and applications. *Journal of Electrical and Computer Engineering, 2017*, Article 9324035. https://doi.org/10.1155/2017/9324035

Tao, F., Zhang, M., & Nee, A. Y. C. (2019). *Digital twin driven smart manufacturing*. Academic Press. https://doi.org/10.1016/C2018-0-02206-9

Wei, J., Yan, C., Liu, Y., Liu, B., & Wu, L. (2025). Digital twins assisted for fault diagnosis of rotating machinery: A review. *Measurement, 245*, 118843. https://doi.org/10.1016/j.measurement.2025.118843

DOI:10.5937/IIZS26127P

EVENT-TRIGGERED ADAPTIVE CONTROL AND ENERGY-EFFICIENT TRAJECTORY PLANNING FOR CARGO DRONES USING GIS AND SPIKING NEURAL NETWORKS

Research paper

Sergiu Popa[1*], Flavius-Maxim Petcuț[2], Anca-Adriana Petcuț-Lasc[3], Valentina-Emilia Balaș[4]

[1,3]Petroleum-Gas University of Ploiești, Doctoral School, Ploiești, Romania
[2,3,4]"Aurel Vlaicu" University of Arad, Faculty of Engineering, Arad, Romania
[4]Academy of Romanian Scientists, Bucharest, Romania

Abstract: Cargo transport with unmanned aerial vehicles (UAVs) is constrained above all by the energy stored on board, so every joule spent on propulsion, computation or communication reduces the payload and the range of the mission. This paper reviews thirteen works published between 2017 and 2025 along four directions that address this constraint: event-triggered control, trajectory planning based on geographic information systems (GIS), energy-efficient trajectory optimization, and spiking neural networks (SNNs) used as controllers. The review shows that these directions are usually treated in isolation, although they act on complementary parts of the energy budget. On this basis the paper proposes a three-layer control architecture in which a GIS layer produces an energy-aware reference trajectory, a monitoring layer evaluates a triggering condition on the state of the UAV, and an adaptive layer keeps a conventional proportional-integral-derivative (PID) controller in nominal operation and activates an SNN only when an event is detected. The architecture is presented at conceptual level; its implementation in MATLAB/Simulink and its validation on the Quanser platform of the "Aurel Vlaicu" University of Arad are the subject of further work.
Key words: *unmanned aerial vehicles, event-triggered control, spiking neural networks, GIS, energy efficiency*

INTRODUCTION

Unmanned aerial vehicles are moving from observation tasks towards the transport of goods. Cargo drones are considered today for last-mile delivery in congested cities, for medical logistics and for supplying locations that are difficult to reach by road. Compared with a van, an electric multirotor avoids road congestion and produces no local emissions during flight, which makes it attractive from the point of view of environmental protection as well. The decisive limitation, however, is not the payload the airframe can lift but the energy stored in its battery.

This limitation is more restrictive than it appears, because the energy available on board is consumed by three different processes. Propulsion consumes most of it, and it depends directly on the geometry of the flight path, on speed and on acceleration. Computation and communication consume a smaller but non-negligible share, and their contribution grows when the control law is evaluated and transmitted at a high fixed rate. Finally, part of the energy is wasted in corrections that the aircraft performs when it meets wind gusts, sensor noise or deviations that were not anticipated during planning. A solution that reduces the consumption of one of these processes while increasing that of another brings no real gain over the mission. Each of these processes has been treated in literature, but largely separately. Energy-aware trajectory planning is addressed in work on coverage path planning and on communication-oriented trajectory optimization. The cost of computation and communication is addressed in work on event-triggered control, where the control law is updated only when the tracking error leaves an admissible region. The cost of unanticipated corrections is addressed in work on adaptive and intelligent control, and more recently by spiking neural networks running on neuromorphic hardware. Geographic information systems appear in a fourth group of works, as a source of the geospatial data needed for realistic planning in urban environments.

[1]Corresponding author, sergiupopa20@yahoo.com, 0009-0006-1417-4601
[2]flavius.petcut@uav.ro, 0009-0001-6928-4019
[3]anca.petcut@uav.ro, 0009-0000-5450-5272
[4]balas@drbalas.ro, 0000-0003-0885-1283

The present paper has two objectives. The first is to review these four directions in a comparable form, with emphasis on the mechanism through which each of them saves energy and on the limitations reported by the authors. The second is to derive from this review a control architecture for cargo drones that combines them in a single structure, in which artificial intelligence is used only when the flight conditions require it rather than permanently. The main contribution of this work is the conceptual integration of GIS-based energy-aware trajectory planning, event-triggered monitoring and SNN-assisted PID adaptation within a unified architecture for cargo UAVs. The paper is the starting point of doctoral research and therefore proposes the architecture at conceptual level, without experimental validation.

MATERIAL AND METHODS

The review was carried out on thirteen works published between 2017 and 2025, selected to cover four directions relevant to the energy budget of a cargo UAV. Journal articles were taken from IEEE Transactions, from the Arabian Journal for Science and Engineering and from the journal Drones, and conference papers from four IEEE conferences (ICRA, ICTC, EIT and HPSR) and from Robotics: Science and Systems. Each work was analyzed with respect to the same three questions: which part of the energy budget it addresses, by which mechanism, and what limitations its authors report. The general state of the art on artificial intelligence applied to drone control, surveyed by Caballero-Martin et al. (2024), was used as the reference framework for this classification.

Event-triggered control of unmanned aerial vehicles

In classical digital control the control law is evaluated at fixed time instants, regardless of whether the state of the aircraft has changed. Event-triggered control replaces this fixed rhythm with a condition: the control law is recomputed only when the deviation of the current state from the state at the last update exceeds a threshold. Tian et al. (2021) apply this principle to the attitude control of a quadrotor through an event-triggered super twisting algorithm and prove, by a Lyapunov analysis, that the triggering sequence is free of Zeno behavior, that is, that the events cannot accumulate infinitely in a finite interval. Shao et al. (2021) combines the triggering mechanism with a discrete-time neural controller and a disturbance observer, treating at the same time the saturation of the inputs. Wu et al. (2024) extend the approach to the cooperative control of a group of six-rotor UAVs with prescribed finite-time performance, with the explicit aim of saving transmission resources. Cuenca et al. (2019) study the same problem from the perspective of the communication network and show, on a UAV test-bed, that periodic event-triggered sampling combined with dual-rate control reduces network utilization considerably while keeping control performance satisfactory.
The common result of these works is that a large part of the control updates performed at a fixed rate carry no useful information. The common limitation is that the triggering threshold governs a trade-off: a high threshold saves computation and transmissions but degrades tracking, and a low threshold brings the behavior back towards periodic control.

Trajectory planning based on geographic information systems

A trajectory computed in free space is of little use over a city. Rokhsaritalemi et al. (2018) plan drone trajectories for three-dimensional urban modelling starting from GIS layers, considering the visibility of the facades to be scanned and the obstacles present. Sulaiman et al. (2020) use GIS data and building models to generate automatically the flight plan of camera-equipped UAVs for fire emergency response, where the plan must be produced quickly and must avoid risk areas. In both cases the geospatial database supplies information that the aircraft cannot obtain by itself during flight: the height of buildings, the position of vegetation, restricted areas, and the shape of the terrain. The limitation reported is the dependence on the quality and the age of the geospatial data, which in a real urban environment are not always up to date.

Energy-efficient trajectory optimization

Zeng and Zhang (2017) derive a theoretical model of the propulsion energy of a fixed-wing UAV as a function of speed, direction and acceleration, and use it to optimize the trajectory jointly with the communication throughput, defining energy efficiency as the number of bits transmitted per joule consumed. The model makes explicit the fact that accelerations and changes of direction, not distance alone, dominate consumption. Shivgan and Dong (2020) exploit the same observation in coverage path planning: they formulate the problem as a travelling salesman problem, solve it with a genetic algorithm and reduce in particular the number of turns, reporting a consumption between two and five times lower than that of a greedy algorithm. Ahmed et al. (2024) extend the problem to a fleet of UAVs covering several regions, adding the management of recharging. The limitation of this direction is that the optimization is performed offline, on an assumed model of the environment; wind and the real behavior of the battery are not known at planning time.

Spiking neural networks used as controllers

Spiking neural networks process information through asynchronous impulses rather than through values updated at a fixed rate, which makes them naturally compatible with an event-driven mode of operation. Stagsted et al. (2020) implement a complete PID controller as a spiking network on a neuromorphic chip and show that the structure of the classical controller can be reproduced with spiking neurons at very low power consumption. Vitale et al. (2021) combines event-based vision with neuromorphic processing for the control of a UAV, obtaining low latency in the reaction to disturbances. Yu et al. (2025) use an SNN for fault-tolerant attitude tracking, keeping the stability of the aircraft when actuators fail. The limitations reported concern the training of such networks, which is more difficult than for conventional networks, and the availability of neuromorphic hardware qualified for flight. Table 1 summarizes the four directions.

Table 1. Summary of the reviewed research directions

Research direction	Main contribution	Reported benefit	Key references
Event-triggered control	The control law is updated only when a triggering condition on the tracking error is violated.	Fewer control updates and network transmissions at comparable tracking performance.	Tian et al. (2021); Shao et al. (2021); Wu et al. (2024); Cuenca et al. (2019)
GIS-based trajectory planning	Flight paths are generated from geospatial layers: buildings, vegetation, visibility and restricted areas.	Shorter and safer routes; automatic mission planning in dense urban areas.	Rokhsaritalemi et al. (2018); Sulaiman et al. (2020)
Energy-efficient trajectory optimization	Path and speed are optimized against an explicit propulsion-energy model.	Reported energy savings from a factor of two up to five compared with greedy planning.	Zeng & Zhang (2017); Shivgan & Dong (2020); Ahmed et al. (2024)
Spiking neural networks for control	Control and adaptation are computed with asynchronous spiking neurons on neuromorphic hardware.	Low latency and low power consumption; tolerance to sensor noise and actuator faults.	Stagsted et al. (2020); Vitale et al. (2021); Yu et al. (2025)

RESULTS AND DISCUSSION

The review shows that the four directions act on different and complementary parts of the energy budget: GIS planning and energy-aware optimization act before the flight, on the reference trajectory; event-triggered control acts during the flight, on the cost of computation and communication; spiking networks act on the quality of the reaction to disturbances and on the power consumed by the adaptation itself. None of the works reviewed combine all four. The architecture proposed below is built on this observation and is shown in Fig. 1.

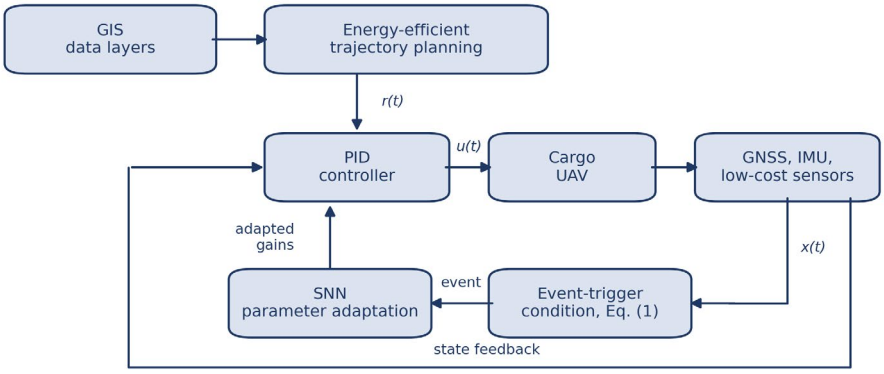


***Fig. 1**. Proposed three-layer control architecture for a cargo UAV*

Planning layer

The planning layer builds the reference trajectory *r*(*t*) from GIS layers, following Rokhsaritalemi et al. (2018) and Sulaiman et al. (2020): buildings and their heights, vegetation, restricted and risk areas, and the wind field estimated for the corridor of the mission. The route is not chosen for minimum length but for minimum energy, according to the propulsion model of Zeng and Zhang (2017), which penalizes accelerations and changes of direction. The total energy of a mission is written as

$$E_{total} = \int_0^T P_{prop}(v, a, w)\, dt + N \cdot E_{upd} \tag{1}$$

where P_{prop} is the propulsion power as a function of speed v, acceleration a and wind w, N is the number of control updates performed during the mission and E_{upd} is the energy consumed by one update, including the associated transmission. The first term is reduced by planning, the second by the mechanism described below.

Monitoring layer

During the flight, the state of the aircraft is estimated by GNSS, by the inertial measurement unit and by low-cost sensors. Following Tian et al. (2021) and Shao et al. (2021), an event is declared when the deviation between the current state and the state recorded at the last update t_k exceeds a relative threshold,

$$\|x(t) - x(t_k)\| \geq \sigma \|x(t)\| + \varepsilon \tag{2}$$

where σ is the relative threshold and ε is a strictly positive constant. The role of ε is not only numerical: as shown by Tian et al. (2021), a strictly positive term guarantees a minimum interval between two consecutive events and therefore excludes Zeno behavior. Between two consecutive events the control law is held at the value computed at t_k, so that the number of

updates follows the actual behavior of the aircraft rather than a fixed clock: a quiet flight segment produces few updates, while a wind gust produces several in quick succession.

The relative reduction in the number of control updates, with N_{ET} the number of event-triggered updates and N_P the number of periodic updates over the same interval, can be expressed as

$$\eta = 1 - N_{ET} / N_P \quad (3)$$

Adaptive control layer

In nominal conditions the aircraft is controlled by a conventional PID controller, whose parameters are those determined at commissioning. This choice is deliberate: a PID controller is predictable, inexpensive in computation and accepted in certification procedures. The SNN receives the tracking error and selected UAV state variables and provides bounded corrections to the PID gains. The SNN is therefore used as an adaptation mechanism and not as the primary controller, which keeps the behavior of the system predictable between events. Recent experimental results have also shown that intelligent adaptation of conventional PID control, such as fuzzy-PID control, can improve UAV flight stability compared with traditional PID control (Wu et al., 2025). The choice of a spiking network for this role follows from the works of Stagsted et al. (2020), Vitale et al. (2021) and Yu et al. (2025): such a network is inexpensive in energy, reacts with low latency and tolerates noisy measurements, which are exactly the properties required for an adaptation that is activated rarely and must respond quickly.
Compared with the solutions reviewed, the expected benefit of the architecture is that the three savings are cumulative rather than alternative: the trajectory is energy-aware before take-off, the control law is evaluated only when necessary, during flight, and the adaptation itself is performed on a low-power substrate. The architecture also keeps the computational load low in nominal flight, which matters for a cargo drone whose on-board computer is dimensioned for the worst case.
Several questions remain open and are assumed as such. The choice of the pair (σ, ε) is a compromise between energy saving and tracking accuracy, and it is not obvious that a single pair is suitable for the whole mission; a threshold that adapts to the flight phase is a possible development. The training of the spiking network requires representative data on disturbances, which for a cargo drone are difficult to obtain other than experimentally. Finally, the GIS layer introduces a dependence on the quality of the geospatial data, and an outdated database can produce a trajectory that is energy-optimal but unsafe. These questions can only be answered by implementation and experiment.

CONCLUSION

The energy available on board a cargo drone is consumed by propulsion, by computation and communication, and by the corrections performed in the face of unanticipated disturbances. The literature reviewed in this paper treats these three sources separately: GIS-based planning and energy-aware trajectory optimization reduce the first, event-triggered control reduces the second, and spiking neural networks act efficiently on the third. The works reviewed show that each mechanism is effective on its own, and also that each has a clear limitation when used alone.
The paper proposed a three-layer architecture that combines them: a GIS planning layer that produces an energy-aware reference trajectory, a monitoring layer that evaluates a triggering condition with a guaranteed minimum inter-event interval, and an adaptive layer in which a PID controller operates nominally and a spiking neural network intervenes only at events. The essential idea is that artificial intelligence is used when the situation requires it and not permanently, which is expected to reduce the energy consumption and the computational load in nominal flight.

The architecture is proposed here at conceptual level. The next stage of the work is its implementation in MATLAB/Simulink, for which the "Aurel Vlaicu" University of Arad holds a Campus license, followed by experimental validation on the Quanser platform available in the university laboratory. The quantities of interest for this validation are the reduction ratio defined in equation (3), the total mission energy given by equation (1) and the tracking error, measured comparatively against a conventional periodic PID controller.

ACKNOWLEDGEMENT

The authors thank the Faculty of Engineering of the "Aurel Vlaicu" University of Arad for access to the Quanser laboratory and to the MATLAB Campus license used in the continuation of this work.

REFERENCES

Ahmed, G., Sheltami, T., & Mahmoud, A. (2024). Energy-efficient multi-UAV multi-region coverage path planning approach. *Arabian Journal for Science and Engineering, 49*, 13185–13202. https://doi.org/10.1007/s13369-024-09295-w

Caballero-Martin, D., Lopez-Guede, J. M., Estevez, J., & Graña, M. (2024). Artificial intelligence applied to drone control: A state of the art. *Drones, 8*(7), Article 296. https://doi.org/10.3390/drones8070296

Cuenca, Á., Antunes, D. J., Castillo, A., García, P., Khashooei, B. A., & Heemels, W. P. M. H. (2019). Periodic event-triggered sampling and dual-rate control for a wireless networked control system with applications to UAVs. *IEEE Transactions on Industrial Electronics, 66*(4), 3157–3166. https://doi.org/10.1109/TIE.2018.2850018

Rokhsaritalemi, S., Sadeghi-Niaraki, A., & Choi, S.-M. (2018). Drone trajectory planning based on geographic information system for 3D urban modeling. In *Proceedings of the 2018 International Conference on Information and Communication Technology Convergence (ICTC)* (pp. 1080–1083). IEEE. https://doi.org/10.1109/ICTC.2018.8539556

Shao, S., Chen, M., Hou, J., & Zhao, Q. (2021). Event-triggered-based discrete-time neural control for a quadrotor UAV using disturbance observer. *IEEE/ASME Transactions on Mechatronics, 26*(2), 689–699. https://doi.org/10.1109/TMECH.2021.3051835

Shivgan, R., & Dong, Z. (2020). Energy-efficient drone coverage path planning using genetic algorithm. In *Proceedings of the 2020 IEEE 21st International Conference on High Performance Switching and Routing (HPSR)* (pp. 1–6). IEEE. https://doi.org/10.1109/HPSR48589.2020.9098989

Stagsted, R. K., Vitale, A., Binz, J., Renner, A., Larsen, L. B., & Sandamirskaya, Y. (2020). Towards neuromorphic control: A spiking neural network based PID controller for UAV. In *Robotics: Science and Systems XVI*. https://doi.org/10.15607/RSS.2020.XVI.074

Sulaiman, M., Liu, H., Binalhaj, M., Liou, W. W., & Abudayyeh, O. (2020). GIS-based automatic flight planning of camera-equipped UAVs for fire emergency response. In *Proceedings of the 2020 IEEE International Conference on Electro Information Technology (EIT)* (pp. 139–144). IEEE. https://doi.org/10.1109/EIT48999.2020.9208329

Tian, B., Cui, J., Lu, H., Liu, L., & Zong, Q. (2021). Attitude control of UAVs based on event-triggered supertwisting algorithm. *IEEE Transactions on Industrial Informatics, 17*(2), 1029–1038. https://doi.org/10.1109/TII.2020.2981367

Vitale, A., Renner, A., Nauer, C., Scaramuzza, D., & Sandamirskaya, Y. (2021). Event-driven vision and control for UAVs on a neuromorphic chip. In *Proceedings of the 2021 IEEE International Conference on Robotics and Automation (ICRA)* (pp. 103–109). IEEE. https://doi.org/10.1109/ICRA48506.2021.9560881

Wu, C.-P., Hsieh, N.-K., Chen, L.-R., & Balas, V. E. (2025). Enhancing longitudinal flight stability of electric-powered micro unmanned aerial vehicles using fuzzy proportional-integral-

derivative control. *International Journal of Control, Automation, and Systems, 23*(7), 2132–2141. https://doi.org/10.1007/s12555-024-0930-0

Wu, Y., Chen, M., Li, H., & Chadli, M. (2024). Event-triggered-based adaptive NN cooperative control of six-rotor UAVs with finite-time prescribed performance. *IEEE Transactions on Automation Science and Engineering, 21*(2), 1867–1877. https://doi.org/10.1109/TASE.2023.3241182

Yu, W., Yang, N., Wang, Z., Li, H. C., Zhang, A., Mu, C., & Pun, S. H. (2025). Fault-tolerant attitude tracking control driven by spiking NNs for unmanned aerial vehicles. *IEEE Transactions on Neural Networks and Learning Systems, 36*(2), 3773–3785. https://doi.org/10.1109/TNNLS.2023.3342078

Zeng, Y., & Zhang, R. (2017). Energy-efficient UAV communication with trajectory optimization. *IEEE Transactions on Wireless Communications, 16*(6), 3747–3760. https://doi.org/10.1109/TWC.2017.2688328



XVI International Conference Industrial Engineering and Environmental Protection 2026 (IIZS 2026)

October 01-02, 2026, Zrenjanin, Serbia

Session 2

Energetics and Process Technique

DOI:10.5937/IIZS26135M

TRUE DECARBONIZATION OR CONTRACTION EFFECT? DECOMPOSING MANUFACTURING CO_2 REDUCTIONS INTO ENERGY-ACTIVITY AND CARBON-FACTOR COMPONENTS ACROSS THE EUROPEAN UNION

Research paper

Miloš Milovančević[1]; Ivan Kostić[2]; Nataša Sokolov Milovančević[2]; Vanja Stojković[3]
[1] Faculty of Mechanical Engineering, University of Niš, Niš, Republic of Serbia
[2] University "Privredna Akademija", Brčko District, Bosnia and Herzegovina
[3] National Employment Service of the Republic of Serbia, Niš Branch, Niš, Republic of Serbia

Abstract: A decline in industrial carbon dioxide emissions is often interpreted as evidence of decarbonization, although the same aggregate outcome can arise from fundamentally different mechanisms. Emissions may fall because manufacturing uses less energy, because direct CO_2 emitted per unit of energy use declines, or because both processes occur simultaneously. This study develops a transparent two-factor decomposition framework for EU manufacturing using harmonised Eurostat Physical Energy Flow Accounts and Air Emissions Accounts. The balanced panel covers all 27 EU Member States from 2014 to 2023 (270 country-year observations; 243 annual transitions). Manufacturing CO_2 is expressed as the product of energy activity, measured by intermediate consumption of energy products, and an observed direct carbon factor, measured as tonnes of manufacturing CO_2 per terajoule. Exact additive Logarithmic Mean Divisia Index decomposition separates annual and cumulative emission changes into energy-activity and carbon-factor effects. A Decarbonization Quality Ratio (DQR) is introduced as a bounded diagnostic of the share of downward emission pressure attributable to carbon-factor improvement. EU-27 manufacturing CO_2 fell by 110.7 Mt between 2014 and 2023 (−14.4%). Country-summed endpoint decomposition attributes 48.0 Mt (43.4%) of the net reduction to lower energy activity and 62.7 Mt (56.6%) to carbon-factor improvement. Among 142 annual country-level emission reductions, 43 (30.3%; Wilson 95% CI 23.3%–38.3%) were contraction-driven, 52 combined lower energy activity with an improving carbon factor, and 47 achieved lower emissions despite stable or rising energy activity. In 2020, 16 of 24 national reductions were contraction-driven, compared with 27 of 118 reductions in all other years (odds ratio 6.74; $p < .001$). By contrast, 2022–2023 reductions were predominantly supported by carbon-factor improvement. The magnitude of a CO_2 reduction was essentially unrelated to DQR, showing that similar percentage declines can conceal opposite mechanisms. Germany and Spain, for example, both reduced manufacturing CO_2 by about 12% over 2014–2023, but their DQR values were 0 and 1, respectively. The results demonstrate that lower emissions should not automatically be equated with high-quality decarbonization and that environmental monitoring should distinguish structural carbon-factor improvement from activity contraction.
Keywords: manufacturing decarbonization; LMDI; carbon factor; energy activity; contraction effect; Eurostat; physical energy flow accounts; air emissions accounts; European Union; industrial sustainability

INTRODUCION

The European Union has made climate neutrality by 2050 legally binding and maintains an interim objective of reducing net greenhouse gas emissions by at least 55% by 2030 relative to 1990 (European Parliament & Council of the European Union, 2021). Manufacturing is central to this transition because it combines substantial direct emissions, high energy requirements, international competitiveness pressures, and large cross-country differences in industrial structure. Yet the most common indicator used in public debate—the percentage change in total emissions—does not reveal why emissions changed.

A decline in manufacturing CO_2 can arise from at least two fundamentally different processes. The first is a genuine improvement in the amount of direct CO_2 emitted per unit of manufacturing energy use. Such an improvement may reflect cleaner fuels, electrification, changes in direct process emissions, operational efficiency, or other changes in the relationship between direct emissions and energy throughput. The second is a contraction effect: manufacturing uses less energy because activity, utilisation, or energy demand falls.

[1*] Corresponding author, milos.milovancevic@gmail.com

Both processes reduce observed emissions, but they imply very different trajectories for industrial transformation.

This distinction is not semantic. A 10% decline in CO_2 produced entirely by a 10% contraction in energy use while the carbon factor is unchanged is not equivalent to a 10% decline achieved while energy activity is maintained and the carbon factor improves. The first outcome can reverse immediately with recovery; the second indicates a more durable change in the emissions-energy relationship. Aggregate emission trends therefore require decomposition before they can be interpreted as evidence of decarbonization.

Index decomposition analysis, and particularly the Logarithmic Mean Divisia Index (LMDI), is well established for separating changes in energy use or emissions into interpretable components (Ang, 2005, 2015). Earlier manufacturing applications demonstrated the value of decomposing energy-induced CO_2 emissions (Ang & Pandiyan, 1997), while later European studies applied LMDI to energy consumption, efficiency, and economy-wide emission trends (Bianco et al., 2024; Fernández González et al., 2014; Reuter et al., 2019). However, studies with many factors can become difficult to interpret operationally, and aggregate decoupling measures may still fail to distinguish whether observed emission reductions arise from lower activity or from an improved carbon-emissions relationship.

The present study addresses this problem with a deliberately parsimonious two-factor identity based on harmonised environmental-economic accounts. Eurostat Physical Energy Flow Accounts (PEFA) record energy flows in a framework compatible with national accounts, while Air Emissions Accounts (AEA) allocate emissions to resident economic activities using NACE classifications (Eurostat, 2015, 2026a, 2026b). Focusing exclusively on NACE C—Manufacturing—creates a common country-sector-year unit for comparing intermediate consumption of energy products with direct manufacturing CO_2 emissions.

The paper makes four contributions. First, it provides an exact annual and cumulative decomposition of EU-27 manufacturing CO_2 changes into an energy-activity effect and a carbon-factor effect. Second, it distinguishes four empirically observable transition mechanisms: transformative carbon-factor decarbonization, joint energy-and-carbon improvement, contraction-driven reduction, and emissions increase or rebound. Third, it proposes a bounded Decarbonization Quality Ratio (DQR) that indicates how much of the downward pressure on emissions is attributable to an improving carbon factor rather than declining energy activity. Fourth, it demonstrates that emission-reduction magnitude and decarbonization quality are empirically distinct dimensions.

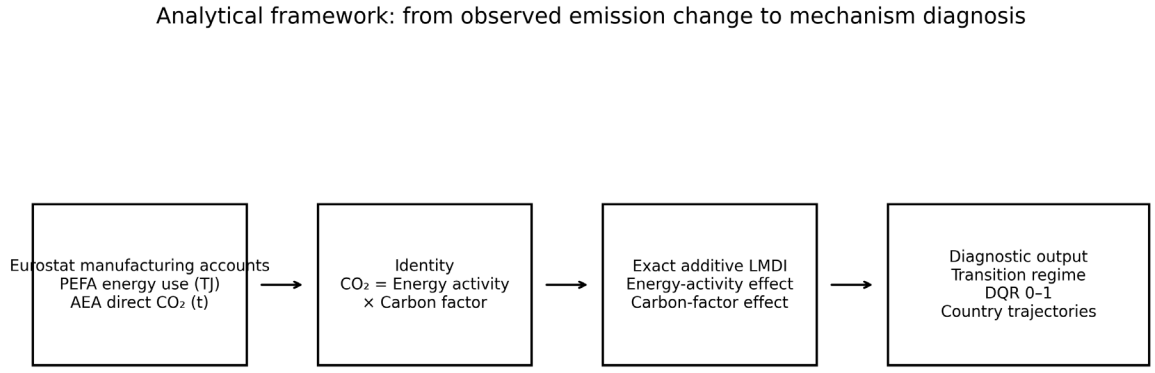


Fig. 1. *Analytical framework linking Eurostat manufacturing energy and emissions accounts to exact LMDI decomposition and mechanism diagnosis.*

LITERATURE REVIEW AND ANALYITICAL EXPECTATIONS

Why lower emissions do not necessarily imply true decarbonization

Decomposition studies are motivated by the fact that a change in an aggregate environmental outcome is rarely generated by a single process. In industry, total emissions can change because of production volume, sector composition, energy intensity, fuel mix, electricity carbon intensity, process technology, and other factors. The LMDI literature provides a flexible family of exact or near-exact identities for allocating observed change among such drivers (Ang, 2005, 2015). European evidence generally shows that technical and efficiency-related effects can contribute substantially to long-run emission reduction, while economic activity can offset those gains (Bianco et al., 2024; Fernández González et al., 2014). Reuter et al. (2019) found major energy-efficiency contributions to lower EU final energy consumption, particularly in industry. Manufacturing-focused work similarly shows that efficiency and technology can be central to climate performance, although sector-specific outcomes vary widely (Dolge & Blumberga, 2021; Dolge et al., 2021). Nevertheless, an important interpretive problem remains. When total industrial CO_2 falls during recession, pandemic restrictions, plant closures, or energy-price shocks, the decline can be counted as progress even when the emissions-energy relationship fails to improve. The present study therefore uses the term 'true decarbonization' operationally and cautiously: it refers to an observed improvement in direct manufacturing CO_2 per unit of energy activity. It does not imply proof of a specific technology, fuel substitution mechanism, or causal policy effect.

Research hypotheses

H1. Annual manufacturing CO_2 reductions across EU Member States arise from heterogeneous combinations of energy-activity and carbon-factor effects rather than from a single common decarbonization mechanism.
H2. A material share of observed annual manufacturing CO_2 reductions is contraction-driven, meaning that the downward energy-activity effect offsets a stable or worsening carbon factor.
H3. The magnitude of an observed CO_2 reduction is weakly related to its decarbonization quality; countries with similar emission declines can therefore exhibit very different DQR values.
H4. Contraction-driven reductions are disproportionately concentrated in the 2020 pandemic shock relative to other years, particularly 2022–2023.
H5. Over the full 2014–2023 period, carbon-factor improvement contributes more than half of the net EU-27 manufacturing CO_2 reduction.

DATA AND METHODS

Data sources and harmonization

The empirical analysis uses two official Eurostat datasets supplied as full-history custom CSV extracts. Manufacturing energy activity is measured with the PEFA key indicator 'intermediate consumption of energy products' (EPRD_ICNS) for NACE C, reported in terajoules. Direct manufacturing CO_2 emissions are taken from the Air Emissions Accounts for NACE C, reported in tonnes. Both environmental-economic accounting systems are aligned with the national-accounts residence principle, which improves sectoral comparability across the energy and emissions domains (Eurostat, 2015, 2026a, 2026b).
A complete balanced EU-27 panel is available from 2014 through 2023. The final dataset therefore contains 270 country-year observations and 243 annual country transitions. No missing-value imputation is used. The 2024 AEA observation is not included because the corresponding PEFA energy series in the supplied extract ends in 2023.
The PEFA energy indicator represents intermediate consumption of energy products and is broader than final energy consumption alone. The AEA CO_2 measure follows the residence

principle and records direct emissions from manufacturing resident units. Accordingly, the ratio of AEA CO_2 to PEFA energy use is interpreted as an observed direct manufacturing carbon factor, not as a pure combustion emission factor. It can change through fuel substitution, electrification, process-emission changes, operational efficiency, or other changes in the relationship between direct emissions and accounted energy use.

Table 1. *Eurostat data sources and analytical role.*

Eurostat dataset	Selected indicator	Specification	Analytical role
env_ac_pefa04	Manufacturing intermediate consumption of energy products	NACE C; EPRD_ICNS; TJ	Energy activity E
env_ac_ainah_r2	Manufacturing direct CO_2 emissions	NACE C; CO_2; tonnes	CO_2 outcome C

Table 2. *Descriptive statistics for the balanced EU-27 country-year panel, 2014–2023.*

Variable	Manufacturing energy activity (PJ)	Manufacturing CO_2 emissions (Mt)	Direct carbon factor (t/TJ)
N	270.00	270.00	270.00
Mean	1670.42	27.97	26.44
SD	2187.92	40.67	27.98
Minimum	1.37	0.07	5.94
25th percentile	231.55	4.81	13.80
Median	814.45	12.82	19.35
75th percentile	2160.50	31.90	26.48
Maximum	9639.69	207.00	169.04

Two-factor identity

For country i and year t, direct manufacturing CO_2 emissions are represented as the product of manufacturing energy activity and an observed direct carbon factor:

$$C_{\mathrm{i,t}} = E_{\mathrm{i,t}} \times F_{\mathrm{i,t}} \quad (1)$$

where $C_{i,t}$ denotes direct manufacturing CO_2 emissions in tonnes, $E_{i,t}$ denotes intermediate consumption of energy products in terajoules, and $F_{i,t}$ is the observed direct carbon factor:

$$F_{\mathrm{i,t}} = C_{\mathrm{i,t}} / E_{\mathrm{i,t}} \quad (2)$$

Exact additive LMDI decomposition

The change in CO_2 between two adjacent years is decomposed using the additive LMDI-I formulation recommended for implementation by Ang (2005, 2015). The logarithmic mean is:

$$\mathrm{L(a,b)} = (\mathrm{a} - \mathrm{b}) / [\ln(\mathrm{a}) - \ln(\mathrm{b})], \text{with } \mathrm{L(a,a)} = \mathrm{a} \quad (3)$$

The energy-activity and carbon-factor effects are:

$$\Delta C^{\mathrm{E}} = \mathrm{L}(C_{\mathrm{t}}, C_{\mathrm{t-1}}) \times \ln(E_{\mathrm{t}} / E_{\mathrm{t-1}}) \quad (4)$$

$$\Delta C^{\mathrm{f}} = \mathrm{L}(C_{\mathrm{t}}, C_{\mathrm{t-1}}) \times \ln(F_{\mathrm{t}} / F_{\mathrm{t-1}}) \quad (5)$$

The decomposition is exact at numerical precision:

$$\Delta \mathrm{C} = C_{\mathrm{t}} - C_{\mathrm{t-1}} = \Delta C^{\mathrm{E}} + \Delta C^{\mathrm{f}} \quad (6)$$

Negative contributions reduce CO_2; positive contributions increase it. The same formulation is applied directly to 2014 and 2023 endpoints for each Member State. Country endpoint effects are then summed to obtain an EU-wide decomposition that preserves country-level mechanisms.

Transition-mechanism classification

Every annual country transition is assigned to one of four mutually exclusive categories:
Transformative carbon-factor decarbonization: CO_2 falls, the carbon-factor effect is negative, and the energy-activity effect is non-negative. Emissions therefore fall despite stable or increasing energy activity.
Joint energy-and-carbon improvement: CO_2 falls and both the energy-activity and carbon-factor effects are negative.
Contraction-driven reduction: CO_2 falls because the energy-activity effect is negative while the carbon-factor effect is non-negative.
Emissions increase or rebound: total manufacturing CO_2 does not decline.

Decarbonization Quality Ratio

For every transition with falling CO_2, the Decarbonization Quality Ratio (DQR) is defined as the carbon-factor share of all downward LMDI contributions:

$$\mathrm{DQR} = \max(-\Delta C^{\mathrm{f}}, 0) \,/\, [\max(-\Delta C^{\mathrm{f}}, 0) + \max(-\Delta C^{\mathrm{E}}, 0)] \quad (7)$$

DQR is bounded between 0 and 1. A value of 0 indicates that all downward pressure on emissions comes from lower energy activity. A value of 1 indicates that all downward pressure comes from an improving carbon factor. Intermediate values indicate joint improvement.
DQR is a diagnostic indicator proposed in this study. It does not estimate causal policy effectiveness and should not be interpreted as a welfare measure. Its purpose is to distinguish the mechanism behind an observed reduction that would otherwise be hidden in the total CO_2 change.

Statistical analysis and robustness

The primary descriptive unit is the annual country transition. The prevalence of contraction-driven reductions is reported with Wilson and country-cluster bootstrap confidence intervals. Fisher's exact test compares the share of contraction-driven reductions in 2020 with other years and with the combined 2022–2023 period. Spearman rank correlations test whether DQR is associated with the magnitude of annual and cumulative CO_2 reductions.
Robustness is assessed by repeating the sign-based mechanism classification with ±0.25 and ±0.50 percentage-point neutral bands for annual changes in energy activity and the carbon factor. This tests whether the main conclusion depends on very small year-to-year movements. LMDI residuals are also verified numerically.

RESULTS

Aggregate EU-27 manufacturing trajectory

EU-27 manufacturing energy activity declined from 44,544.1 PJ in 2014 to 42,556.2 PJ in 2023, a reduction of -4.5%. Direct manufacturing CO_2 fell from 770.3 Mt to 659.6 Mt, a decline of -14.4%. Over the same period, the aggregate observed carbon factor fell from 17.29 to 15.50 t/TJ.
The trajectories diverged substantially in shock years. In 2020, energy activity contracted sharply, but the aggregate carbon factor worsened. In 2022 and 2023, by contrast, the carbon factor improved strongly and accounted for a large share of the observed emission decline. The time path therefore already suggests that equal-signed changes in total CO_2 can emerge from different combinations of energy and carbon-factor movements.

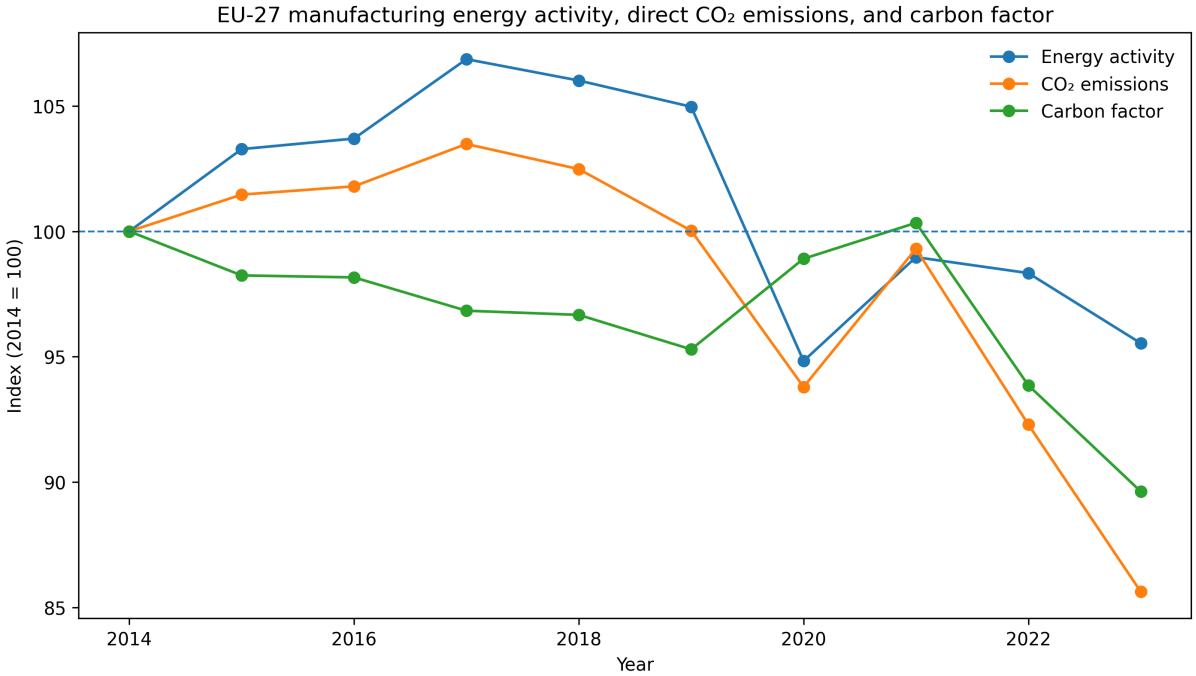


Fig. 2. *Indexed EU-27 manufacturing energy activity, direct CO_2 emissions, and observed carbon factor, 2014–2023.*

Table 3. *EU-27 aggregate manufacturing energy activity, direct CO_2 emissions, and carbon factor.*

Year	Energy activity (PJ)	CO_2 emissions (Mt)	Carbon factor (t/TJ)
2014	44544.10	770.33	17.29
2015	46005.62	781.62	16.99
2016	46192.96	784.17	16.98
2017	47604.10	797.18	16.75
2018	47224.32	789.46	16.72
2019	46758.67	770.55	16.48
2020	42239.71	722.49	17.10
2021	44085.42	764.98	17.35
2022	43802.12	710.97	16.23
2023	42556.23	659.58	15.50

Annual LMDI decomposition

The exact annual decomposition reveals three markedly different periods. From 2015 to 2017, increases in manufacturing energy activity generally pushed emissions upward, partly offset by carbon-factor improvements in 2015 and 2017. In 2018 and 2019, net emissions declined as lower energy activity and, especially in 2019, an improving carbon factor jointly reduced CO_2.
The 2020 pandemic shock produced the clearest contraction effect. EU-27 manufacturing CO_2 fell by 48.1 Mt. The energy-activity effect reduced emissions by 72.8 Mt, while the carbon-factor effect increased emissions by 24.7 Mt. In other words, the emissions decline occurred despite a deterioration in the observed direct carbon factor.
The 2021 rebound reversed both mechanisms: manufacturing CO_2 increased by 42.5 Mt, with positive contributions from both energy activity and the carbon factor. The subsequent 2022 reduction of 54.0 Mt was fundamentally different from 2020: 47.1 Mt of downward pressure came from carbon-factor improvement, compared with only 6.9 Mt from lower energy activity. In 2023, both mechanisms contributed materially.

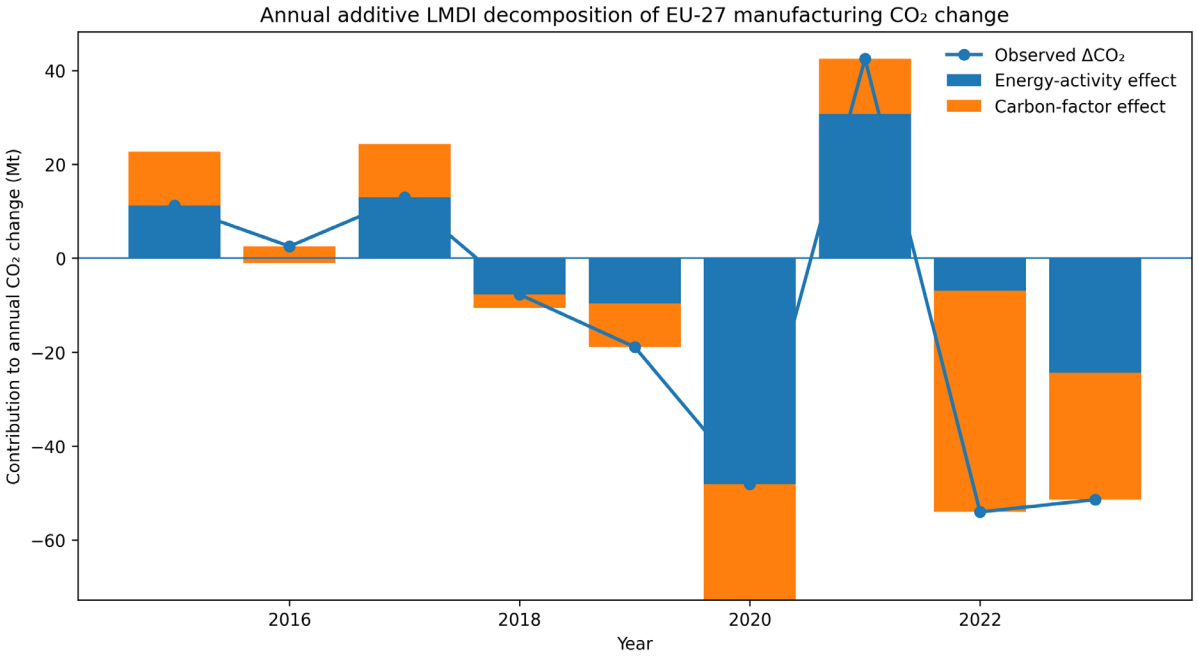


Fig. 3. *Annual additive LMDI decomposition of EU-27 manufacturing CO_2 change.*

Table 4. *Annual EU-27 LMDI decomposition.*

Year	Observed ΔCO_2 (Mt)	Energy-activity effect (Mt)	Carbon-factor effect (Mt)
2015	11.29	22.72	-11.43
2016	2.55	-1.01	3.56
2017	13.01	24.33	-11.32
2018	-7.72	-10.56	2.84
2019	-18.91	-9.57	-9.34
2020	-48.06	-72.76	24.70
2021	42.49	30.72	11.77
2022	-54.01	-6.88	-47.13

Year	Observed ΔCO_2 (Mt)	Energy-activity effect (Mt)	Carbon-factor effect (Mt)
2023	-51.39	-24.34	-27.05

How often are emission reductions contraction-driven?

Across 243 annual country transitions, 142 recorded lower manufacturing CO_2. Of these, 43 were contraction-driven, equivalent to 30.3% of all reductions. The Wilson 95% confidence interval was 23.3%–38.3%, and the country-cluster bootstrap interval was 23.6%–37.0%. The remaining reductions consisted of 52 joint energy-and-carbon improvements and 47 transformative carbon-factor decarbonization transitions.
Contraction-driven reductions accounted for 33.4% of the gross magnitude of all annual country-level CO_2 reductions. Thus, contraction effects were not only frequent; they represented a substantial share of the total downward movement observed in the panel.
H1 and H2 are therefore supported. The same headline outcome—lower CO_2—was produced by three empirically distinct mechanisms, and almost one in three reduction transitions occurred without an improving carbon factor.

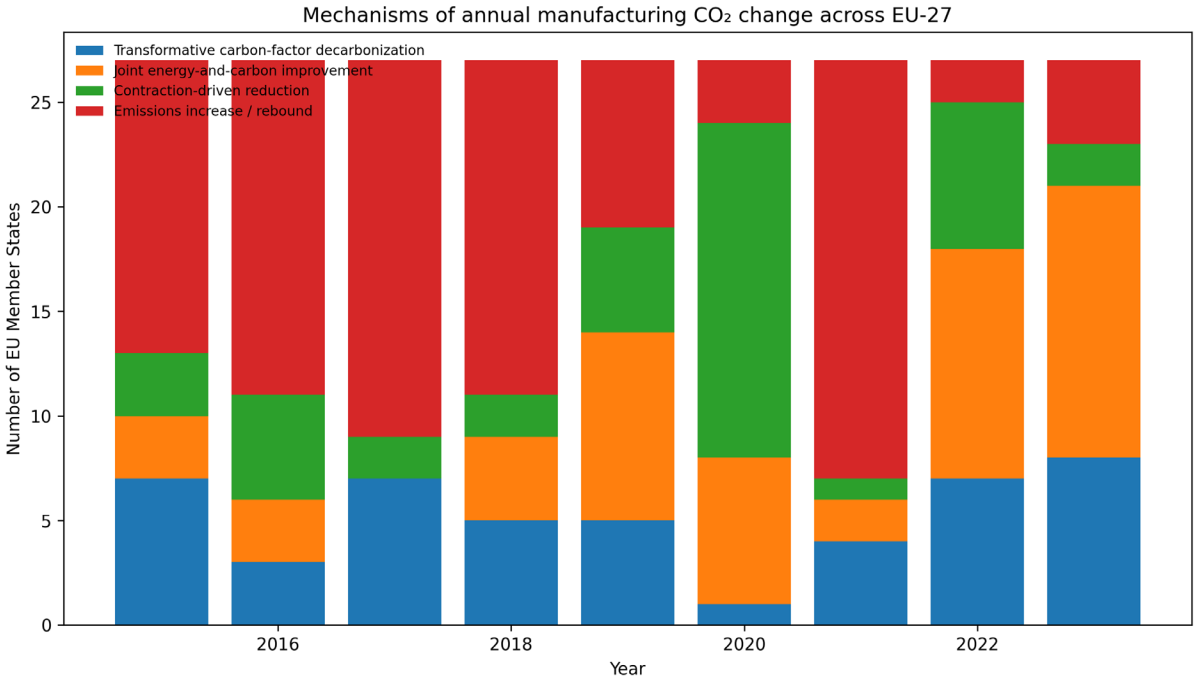


Fig. 4. *Annual distribution of manufacturing CO_2 transition mechanisms across EU-27.*

Table 5. *Number of Member States by annual transition mechanism.*

Year	Transformative CF	Joint improvement	Contraction-driven	Emissions increase
2015	7	3	3	14
2016	3	3	5	16
2017	7	0	2	18
2018	5	4	2	16
2019	5	9	5	8
2020	1	7	16	3
2021	4	2	1	20

Year	Transformative CF	Joint improvement	Contraction-driven	Emissions increase
2022	7	11	7	2
2023	8	13	2	4

Table 6. *Frequency and magnitude of the three emission-reduction mechanisms.*

Mechanism	Contraction-driven reduction	Joint energy-and-carbon improvement	Transformative carbon-factor decarbonization
N	43	52	47
Share of reduction transitions (%)	30.28	36.62	33.10
Gross CO_2 reduction (Mt)	70.71	94.30	46.59
Share of gross reduction magnitude (%)	33.42	44.57	22.02
Energy effect (Mt)	-115.15	-44.07	39.34
Carbon-factor effect (Mt)	44.44	-50.23	-85.93
Median DQR	0.00	0.56	1.00

Pandemic contraction versus later decarbonization

In 2020, 24 Member States recorded lower manufacturing CO_2, and 16 of those reductions (66.7%) were contraction-driven. Across all other years, only 27 of 118 reductions (22.9%) were contraction-driven. The odds of a contraction-driven reduction were therefore 6.74 times higher in 2020 (Fisher exact $p < .001$).

The contrast is even sharper against 2022–2023. Only 9 of 48 reductions in those two years were contraction-driven, compared with 16 of 24 in 2020 (odds ratio 8.67, $p < .001$). The DQR distribution shifted accordingly: 2020 was dominated by values near zero, whereas 2022 and especially 2023 contained substantially more joint and carbon-factor-led reductions.

These findings support H4 and show why crisis-year emission declines should not automatically be treated as evidence of durable industrial decarbonization.

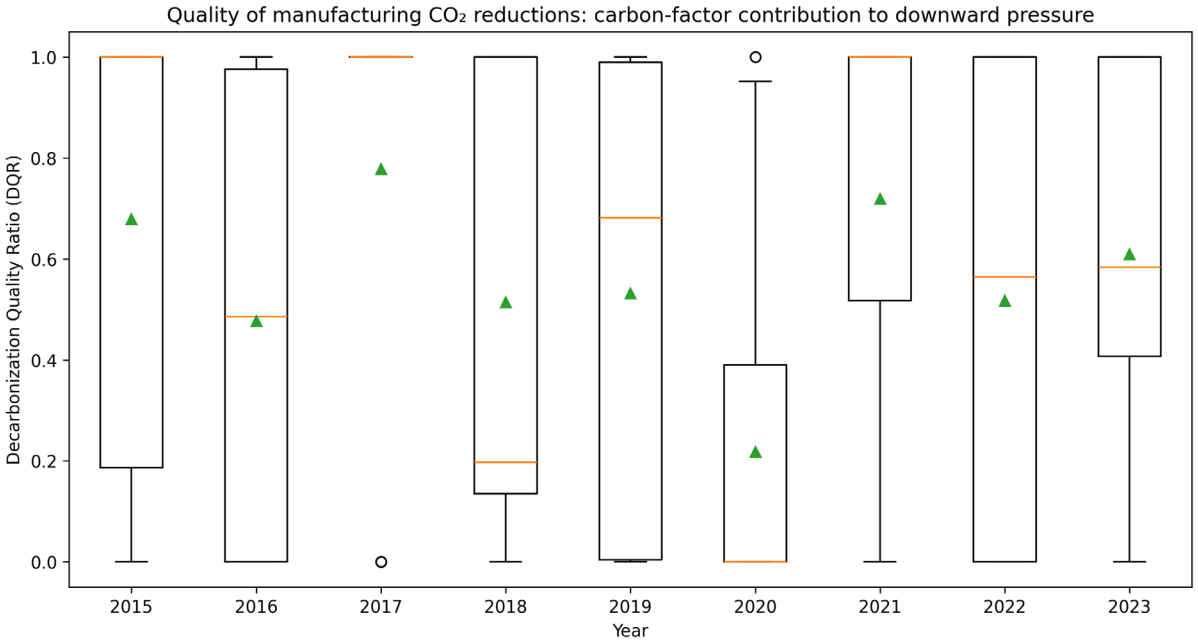


Fig. 5. *Distribution of the Decarbonization Quality Ratio among country-year emission reductions.*

Cumulative 2014–2023 decomposition

Between 2014 and 2023, EU-27 manufacturing CO_2 fell by 110.7 Mt. Summing the exact country-level endpoint decompositions attributes 48.0 Mt (43.4%) of the net reduction to lower energy activity and 62.7 Mt (56.6%) to carbon-factor improvement. H5 is therefore supported: carbon-factor improvement accounted for more than half of the net EU manufacturing CO_2 decline.

Twenty-five of the 27 Member States reduced manufacturing CO_2 over the full period. Fourteen combined lower energy activity with an improving carbon factor, eight reduced emissions despite higher or stable energy activity because the carbon factor improved sufficiently, and three—Croatia, Germany, and Slovenia—were classified as contraction-driven over the full period. Ireland and Bulgaria recorded net emission increases.

The country-level results show that large emission reductions do not map mechanically onto high-quality decarbonization. Estonia, Lithuania, Malta, Greece, Denmark, Spain, the Netherlands, and Latvia achieved transformative carbon-factor decarbonization over the cumulative period. By contrast, Germany reduced emissions almost entirely through lower energy activity while its observed carbon factor was effectively unchanged.

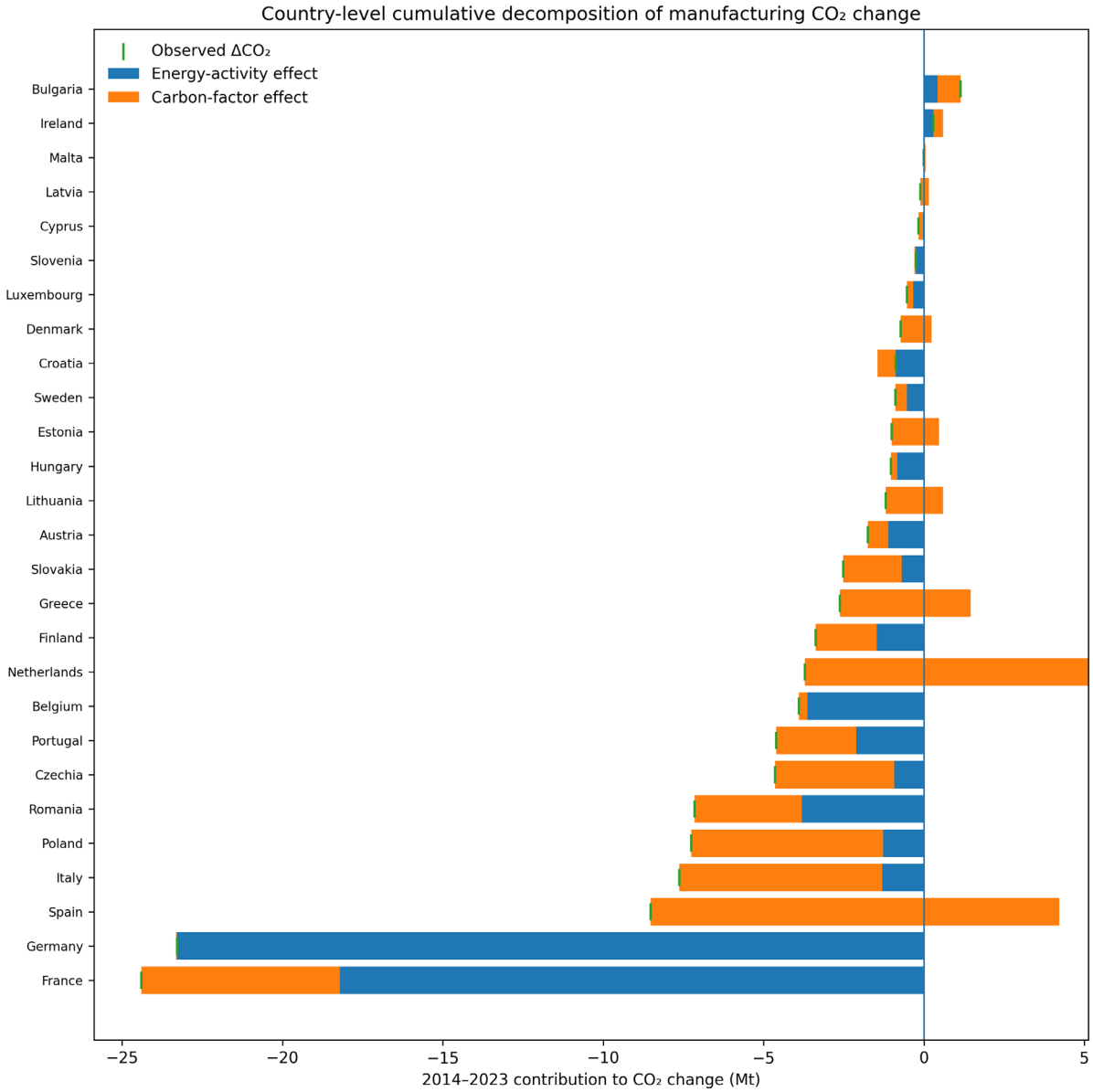


Fig. 6. *Country-level cumulative LMDI decomposition of manufacturing CO_2 change, 2014–2023.*

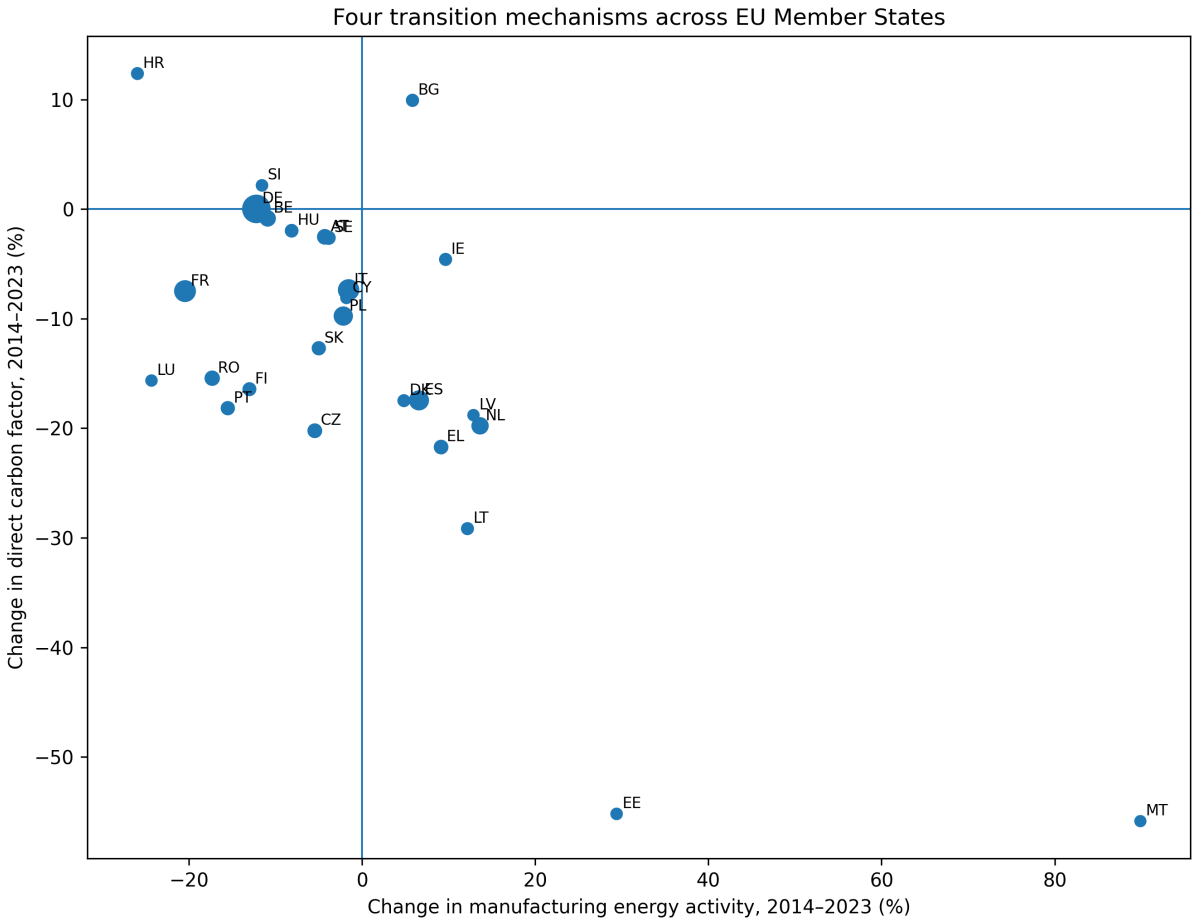


Fig. 7. *Country positioning by cumulative energy-activity and carbon-factor change. Point size reflects 2014 manufacturing CO_2 emissions*

.

Similar emission declines, opposite mechanisms

The magnitude of annual CO_2 reductions was not significantly associated with DQR (Spearman ρ = -0.063, p = 0.460). The same was true for cumulative country reductions over 2014–2023 (ρ = 0.027, p = 0.897). H3 is therefore supported.

The contrast between Germany and Spain is especially instructive. Germany reduced manufacturing CO_2 by 12.19%, while Spain reduced it by 12.03%. Yet Germany's cumulative DQR was 0 because the carbon-factor contribution was slightly positive, whereas Spain's DQR was 1 because the entire downward contribution came from carbon-factor improvement while energy activity increased. Belgium and Poland provide another example: their cumulative CO_2 reductions were nearly identical at 11.66% and 11.72%, but their DQR values were 0.07 and 0.82, respectively.

These pairs demonstrate that a ranking based only on total percentage emission decline can reverse the interpretation of transition quality.

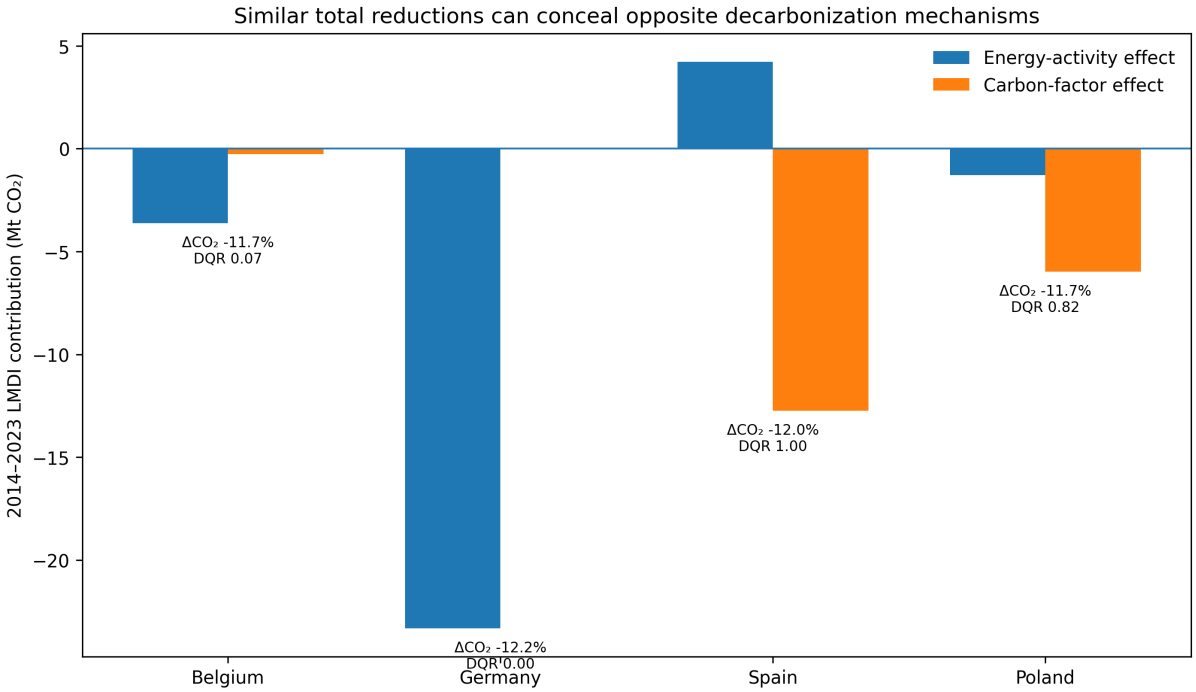


Fig. 8. *Similar cumulative CO_2 reductions with fundamentally different LMDI mechanisms.*

Robustness

The exact decomposition residual was numerically negligible, with a maximum absolute country-year residual of only 0.000001 tonnes.
The central conclusion was also robust to neutral bands around very small annual changes. With no tolerance band, 30.3% of reduction transitions were contraction-driven. The share was 31.7% with a ±0.25 percentage-point band and 35.2% with a ±0.50 percentage-point band. Treating small changes as effectively stable therefore increased rather than eliminated the estimated prevalence of contraction-driven reductions.
The country-cluster bootstrap 95% interval for mean DQR was 0.459–0.583; for the median it was 0.408–0.744. The result that decarbonization quality varies materially across country-years is therefore not driven by a small number of isolated observations.

Table 7. *Statistical diagnostics and hypothesis-relevant tests.*

Diagnostic	**Result**	**Inference**
Contraction-driven share among all reduction transitions	43/142 (30.3%)	Wilson 95% CI 23.3%–38.3%; country-cluster bootstrap 23.6%–37.0%
2020 contraction-driven share vs. all other reduction years	16/24 vs. 27/118; odds ratio 6.74	Fisher exact p = 0.000057
2020 contraction-driven share vs. 2022–2023	16/24 vs. 9/48; odds ratio 8.67	Fisher exact p = 0.000143
DQR vs. magnitude of annual CO_2 reduction	Spearman ρ = -0.063	p = 0.460
DQR vs. magnitude of cumulative 2014–2023 CO_2 reduction	Spearman ρ = 0.027	p = 0.897
LMDI exactness	Maximum annual country-transition residual = 0.000001 t	Numerically zero at reporting scale

Table 8. *Sensitivity of mechanism classification to neutral tolerance bands.*

Tolerance band (%)	Reduction transitions	Transformative CF decarbonization	Joint improvement	Contraction-driven	Contraction-driven share (%)
0.00	142.00	47.00	52.00	43.00	30.28
0.25	142.00	49.00	48.00	45.00	31.69
0.50	142.00	51.00	41.00	50.00	35.21

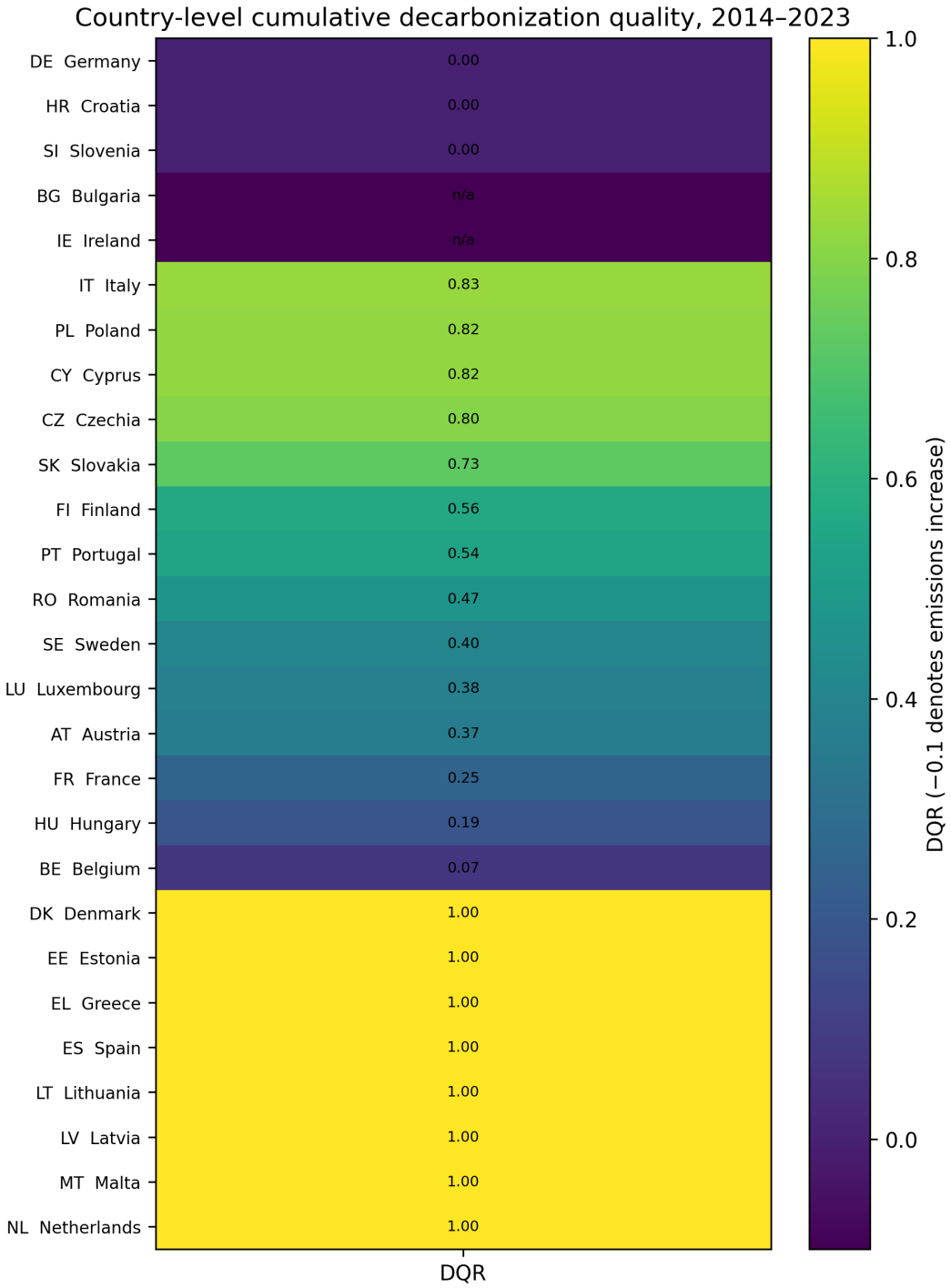


Fig. 9. *Country-level cumulative Decarbonization Quality Ratio, 2014–2023.*

DISCUSSION

The main finding is straightforward but consequential: lower manufacturing CO_2 is not a homogeneous environmental outcome. Across the EU-27 panel, almost one third of annual country-level emission reductions were contraction-driven. During those transitions, manufacturing used less energy while the observed direct carbon factor failed to improve. A conventional emissions-only dashboard would count such outcomes as progress; the decomposition framework shows that their mechanism is fundamentally different from carbon-factor-led decarbonization.

The pandemic year provides the clearest demonstration. In 2020, EU manufacturing emissions fell sharply because energy activity contracted, while the aggregate carbon factor worsened. This pattern is consistent with the exceptional disruption of production and utilisation rather than with an across-the-board technological improvement. The subsequent 2021 rebound further underlines the fragility of contraction-based reductions: both energy activity and the carbon factor pushed emissions upward.

The 2022–2023 pattern was different. Although the European energy crisis also reduced activity in parts of industry, the LMDI results show a much larger role for carbon-factor improvement than in 2020. This does not prove a single causal mechanism. The observed carbon factor can improve because of fuel substitution, direct electrification, changes in process emissions, efficiency gains, or shifts within manufacturing. Nevertheless, the key diagnostic result is robust: the emissions-energy relationship improved rather than merely benefiting from lower energy throughput.

The finding that the magnitude of a reduction is essentially unrelated to DQR has important implications for benchmarking. Germany and Spain achieved almost identical cumulative percentage emission reductions, yet the decomposition assigns them to opposite mechanisms. Similar examples appear across the panel. A league table based only on total CO_2 change therefore mixes contraction, joint improvement, and transformative decarbonization into a single ranking.

The full-period EU result is more encouraging than the annual transition count might suggest. Carbon-factor improvement accounted for 56.6% of the net 2014–2023 manufacturing CO_2 decline in the country-summed endpoint decomposition. A chain-linked sum of annual LMDI effects produced a very similar conclusion. Thus, the long-run EU reduction was not merely an artefact of declining energy activity, even though contraction effects were important in specific years and countries.

These results complement earlier LMDI research. European studies have shown substantial roles for technical and efficiency-related factors in reducing energy use and emissions (Bianco et al., 2024; Fernández González et al., 2014; Reuter et al., 2019), while manufacturing studies emphasise the importance of energy efficiency and sector-specific transition pathways (Dolge & Blumberga, 2021; Dolge et al., 2021). The present contribution is narrower but operationally transparent: it asks a first-order diagnostic question before moving to a more detailed multi-factor decomposition—did emissions fall because manufacturing used less energy, because direct CO_2 per unit of energy improved, or both?

For industrial and environmental engineering, the practical implication is that monitoring systems should display at least three indicators together: total CO_2 change, energy-activity change, and carbon-factor change. DQR can then summarise the source of downward pressure without replacing the underlying components. Such a dashboard can identify whether a nominally successful emission reduction is likely to persist if industrial energy demand recovers.

IMPLICATIONS FOR ENVIRONMENTAL AND INDUSTRIAL MONITORING

- Do not classify every fall in industrial CO_2 as equivalent decarbonization. Report the decomposition mechanism.
- Flag contraction-driven reductions separately because they can reverse with recovery in production and energy use.

• Use DQR together with total CO_2 change. A large reduction with DQR near zero and a smaller reduction with DQR near one represent different transition states.
• Track carbon-factor improvement as a persistence indicator, but investigate its underlying drivers before attributing it to technology or policy.
• Maintain sectorally aligned environmental-economic accounts. The ability to match PEFA and AEA through NACE C is a major advantage for reproducible monitoring.
• Extend the framework with manufacturing GVA, subsector structure, and energy-product mix when fully compatible data are available, allowing separation of economic activity, energy intensity, fuel mix, and direct process-emission effects.

LIMITATIONS

First, the study uses a two-factor identity. 'Energy activity' is intermediate consumption of energy products, not manufacturing gross value added. The framework therefore distinguishes lower energy throughput from an improved direct carbon factor but does not separate economic output, structural change, and energy intensity.
Second, the observed direct carbon factor is not a pure technological emissions factor. AEA direct CO_2 can include combustion and process emissions, while PEFA intermediate energy consumption includes a broad set of energy products. Changes in the ratio can therefore reflect multiple mechanisms.
Third, the AEA and PEFA residence principle improves conceptual compatibility but differs from territorial greenhouse-gas inventories. The results should not be interpreted as a decomposition of UNFCCC national inventory totals.
Fourth, the balanced period begins in 2014 because the supplied PEFA extract has complete EU-27 manufacturing coverage from that year. Longer country histories exist for only a subset of Member States.
Fifth, DQR is a descriptive diagnostic proposed for monitoring. Its thresholds are mechanically defined by the direction of LMDI contributions and do not establish causal policy effectiveness.
Sixth, country-level NACE C aggregates conceal substantial heterogeneity among manufacturing subsectors. A decline in the carbon factor can partly reflect within-manufacturing structural shifts. Detailed A*64 energy-use data would be required to separate these effects.
Finally, classifications based on signs can be sensitive to very small changes. The tolerance-band sensitivity analysis shows that the substantive conclusion is robust, but individual borderline country-year assignments should still be interpreted cautiously.

CONCLUSION

This study asked a simple question that aggregate emission statistics cannot answer: when manufacturing CO_2 falls, is the system actually decarbonizing, or is it merely using less energy?
Using a balanced EU-27 panel from 2014 to 2023 and exact additive LMDI decomposition, the analysis shows that the answer varies substantially across countries and years. EU manufacturing CO_2 fell by 110.7 Mt over the full period. Carbon-factor improvement accounted for 56.6% of the net decline, while lower energy activity accounted for 43.4%. At the annual country level, however, 30.3% of all emission-reduction transitions were contraction-driven.
The contrast between 2020 and 2022–2023 is especially important. The pandemic reduction was dominated by falling energy activity and often accompanied by a worsening carbon factor. Later reductions were much more frequently supported by carbon-factor improvement. The same total percentage decline can therefore represent either fragile contraction-based progress or a more durable change in the emissions-energy relationship.
The broader methodological conclusion is that decarbonization should be evaluated by mechanism as well as magnitude. Combining total CO_2 change, LMDI effects, transition categories, and DQR provides a transparent and reproducible way to distinguish 'less

production-related energy use' from 'less direct carbon per unit of energy use'. For industrial sustainability monitoring, that distinction is indispensable.

DATA AVAILABILITY STATEMENT

The study uses official Eurostat datasets env_ac_pefa04 and env_ac_ainah_r2. The empirical analysis reported here is based on the full-history custom CSV extracts supplied for the study and processed in July 2026. The analysis-ready country-year panel, annual LMDI transition table, country cumulative decomposition table, EU-27 aggregate series, and robustness table are included in the supplementary reproducibility package.

REPRODUCIBILITY STATEMENT

The workflow is fully deterministic: raw Eurostat filters are specified by dataset code, NACE category, indicator, unit, country, and year; all decompositions use the published LMDI formulae; the DQR and regime-classification rules are stated explicitly; and no missing-value imputation or discretionary case deletion is used within the 2014–2023 balanced panel.

CONFLICT OF INTEREST STATEMENT

The authors declare no conflict of interest.

FUNDING STATEMENT

No external funding was declared for this study.

REFERENCES

Ang, B. W. (2005). The LMDI approach to decomposition analysis: A practical guide. *Energy Policy, 33*(7), 867–871. https://doi.org/10.1016/j.enpol.2003.10.010

Ang, B. W. (2015). LMDI decomposition approach: A guide for implementation. *Energy Policy, 86*, 233–238. https://doi.org/10.1016/j.enpol.2015.07.007

Ang, B. W., & Pandiyan, G. (1997). Decomposition of energy-induced CO_2 emissions in manufacturing. *Energy Economics, 19*(3), 363–374. https://doi.org/10.1016/S0140-9883(96)01022-5

Bianco, V., Cascetta, F., & Nardini, S. (2024). Analysis of the carbon emissions trend in European Union. A decomposition and decoupling approach. *Science of the Total Environment, 909*, 168528. https://doi.org/10.1016/j.scitotenv.2023.168528

Dolge, K., Āzis, R., Lund, P. D., & Blumberga, D. (2021). Importance of energy efficiency in manufacturing industries for climate and competitiveness. *Environmental and Climate Technologies, 25*(1), 306–317. https://doi.org/10.2478/rtuect-2021-0022

Dolge, K., & Blumberga, D. (2021). Key factors influencing the achievement of climate neutrality targets in the manufacturing industry: LMDI decomposition analysis. *Energies, 14*(23), 8006. https://doi.org/10.3390/en14238006

European Parliament & Council of the European Union. (2021). Regulation (EU) 2021/1119 of the European Parliament and of the Council of 30 June 2021 establishing the framework for achieving climate neutrality and amending Regulations (EC) No 401/2009 and (EU) 2018/1999 ("European Climate Law"). *Official Journal of the European Union, L 243*, 1–17.

Eurostat. (2015). *Manual for air emissions accounts*. Publications Office of the European Union.

Eurostat. (2026a). *Air emissions accounts by NACE Rev. 2 activity* [Data set; env_ac_ainah_r2]. European Commission. https://doi.org/10.2908/env_ac_ainah_r2

Eurostat. (2026b). *Key indicators of physical energy flow accounts by NACE Rev. 2 activity* [Data set; env_ac_pefa04]. European Commission. https://doi.org/10.2908/env_ac_pefa04

Fernández González, P., Landajo, M., & Presno, M. J. (2014). Tracking European Union CO_2 emissions through LMDI (logarithmic-mean Divisia index) decomposition: The activity revaluation approach. *Energy, 73*, 741–750. https://doi.org/10.1016/j.energy.2014.06.078

Reuter, M., Patel, M. K., & Eichhammer, W. (2019). Applying ex post index decomposition analysis to final energy consumption for evaluating European energy efficiency policies and targets. *Energy Efficiency, 12*(5), 1329–1357. https://doi.org/10.1007/s12053-018-09772-w

APPENDIX A. COUNTRY-LEVEL CUMULATIVE DECOMPOSITION, 2014–2023

DQR is reported only for countries with a net decline in manufacturing CO_2. Effects are additive LMDI contributions and sum exactly to the observed change, up to numerical rounding.

Table A1. *Country-level cumulative manufacturing CO_2 decomposition and transition mechanism.*

Country	CO_2 change (%)	Energy change (%)	Carbon factor change (%)	Energy effect (Mt)	Carbon-factor effect (Mt)	DQR	Cumulative mechanism
Estonia	-42.03	29.40	-55.20	0.47	-1.47	1.00	Transformative carbon-factor decarbonization
Luxembourg	-36.17	-24.33	-15.65	-0.33	-0.20	0.38	Joint energy-and-carbon improvement
Portugal	-30.86	-15.52	-18.17	-2.11	-2.50	0.54	Joint energy-and-carbon improvement
Romania	-30.08	-17.32	-15.43	-3.80	-3.35	0.47	Joint energy-and-carbon improvement
Finland	-27.31	-13.02	-16.43	-1.48	-1.90	0.56	Joint energy-and-carbon improvement
France	-26.41	-20.46	-7.48	-18.21	-6.19	0.25	Joint energy-and-carbon improvement
Czechia	-24.59	-5.47	-20.23	-0.93	-3.72	0.80	Joint energy-and-carbon improvement
Lithuania	-20.54	12.17	-29.16	0.60	-1.79	1.00	Transformative carbon-factor decarbonization
Slovakia	-17.07	-5.00	-12.70	-0.69	-1.82	0.73	Joint energy-and-carbon improvement
Croatia	-16.79	-25.95	12.38	-1.45	0.56	0.00	Contraction-driven reduction
Malta	-16.19	89.90	-55.86	0.05	-0.06	1.00	Transformative carbon-factor decarbonization

Country	**CO_2 change (%)**	**Energy change (%)**	**Carbon factor change (%)**	**Energy effect (Mt)**	**Carbon-factor effect (Mt)**	**DQR**	**Cumulative mechanism**
Greece	-14.58	9.12	-21.72	1.45	-4.07	1.00	Transformative carbon-factor decarbonization
Denmark	-13.50	4.83	-17.48	0.24	-0.96	1.00	Transformative carbon-factor decarbonization
Germany	-12.19	-12.21	0.02	-23.32	0.04	0.00	Contraction-driven reduction
Spain	-12.03	6.57	-17.45	4.22	-12.74	1.00	Transformative carbon-factor decarbonization
Poland	-11.72	-2.17	-9.76	-1.28	-5.98	0.82	Joint energy-and-carbon improvement
Belgium	-11.66	-10.91	-0.85	-3.63	-0.27	0.07	Joint energy-and-carbon improvement
Hungary	-9.95	-8.14	-1.97	-0.84	-0.20	0.19	Joint energy-and-carbon improvement
Cyprus	-9.77	-1.82	-8.10	-0.03	-0.14	0.82	Joint energy-and-carbon improvement
Slovenia	-9.65	-11.56	2.17	-0.30	0.05	0.00	Contraction-driven reduction
Netherlands	-8.85	13.62	-19.78	5.12	-8.84	1.00	Transformative carbon-factor decarbonization
Italy	-8.82	-1.56	-7.37	-1.30	-6.33	0.83	Joint energy-and-carbon improvement
Latvia	-8.36	12.86	-18.80	0.15	-0.26	1.00	Transformative carbon-factor decarbonization
Austria	-6.73	-4.31	-2.53	-1.11	-0.64	0.37	Joint energy-and-carbon improvement
Sweden	-6.38	-3.87	-2.61	-0.53	-0.36	0.40	Joint energy-and-carbon improvement
Ireland	4.61	9.64	-4.59	0.60	-0.30	—	Emissions increase / rebound
Bulgaria	16.33	5.82	9.93	0.43	0.71	—	Emissions increase / rebound

DOI:10.5937/IIZS26154R

DEVELOPMENT OF DIDACTIC PLC SIMULATOR AND ITS INTEGRATION WITH A VIRTUAL 3D ENVIRONMENT

Research paper

Aleksandar Reljić[1*], Saša Prodanović[2]
[1,2]University in East Sarajevo, Faculty of Mechanical Engineering, East Sarajevo, Republic of Srpska, Bosnia and Herzegovina

Abstract: The paper represents the development of a didactic PLC simulator and its connection with a virtual 3D environment for educational purposes in the field of PLC programming within industrial automation and mechatronics. The developed software enables the creation, execution, and visualization of control programs in real-time based on the Ladder Diagram programming language. Bidirectional communication between the PLC simulator and the virtual 3D model was achieved, enabling continuous exchange of input and output signals, as well as synchronization of the logical control algorithm with the visual representation of the process.
Key words: PLC simulator, ladder diagram, digital twin, virtual 3D environment, industrial automation, virtual commissioning, didactic model

INTRODUCTION

In current research, significant attention has been paid to the development of Digital Twin systems in industrial automation, focusing on the possibilities of real-time synchronization between physical and virtual systems (Hrbček et al., 2026; Schamp et al., 2019). Particular emphasis has been placed on the development of architectures that enable data exchange between PLC control systems and their digital representations, utilizing standards such as IEC 61131-3 and OPC UA (Hrbček et al., 2026; Schamp et al., 2019). The field of Virtual Commissioning has also been intensively researched in recent years. Solutions have been presented that allow for the testing of PLC programs before the actual system is put into operation, thereby reducing development time, the number of errors, and implementation costs (Striffler & Voigt, 2023; Ortiz et al., 2026). Special attention has been devoted to the development of simulation models and their connection to industrial PLC devices, where the work of (Zhang, 2024) stands out. In that research, an educational PLC simulator was developed for learning programming, simulating the operation of automated systems, and performing laboratory exercises in a virtual environment without the need for expensive industrial equipment. Research has shown that Digital Twin and Virtual Commissioning represent an important direction in the development of modern industrial automation.
Starting from the actual needs in the field of student education and the idea of creating a software-based educational model, this paper represents the development of a didactic PLC simulator and its integration with a virtual 3D environment.
The objective of this work is the development of a PLC simulator with support for Ladder logic programming language and its connection to a 3D environment for visual simulation of automatic control system operations. The developed solution enables a bidirectional exchange of input-output signals between the PLC simulator and the virtual 3D model, functionally establishing a Digital Twin environment suitable for demonstrating PLC program operation and conducting laboratory exercises in the educational process.
The paper is organized into four sections. The introductory part provides a brief overview of current research in the fields of Digital Twin systems, Virtual Commissioning, and PLC simulators, as well as the objective of the work. The second chapter describes the development of the didactic PLC simulator and its connection to the virtual 3D environment. The third chapter presents an example of implementing a sorting task for objects of different lengths, an explanation of the program networks, and visualization of the operation in the 3D environment. At the end of the paper, conclusions are given regarding the achieved results and the possibilities for applying the developed system in the education process.

[1]Corresponding author, reljic94@gmail.com, ORCID: 0009-0002-3280-3724
[2]sasa.prodanovic@ues.rs.ba, ORCID: 0000-0003-2682-6022

DEVELOPMENT OF THE PLC SIMULATOR AND ITS CONNECTING WITH 3D ENVIRONMENT

With the goal of developing a didactic system for PLC control simulation, a PLC simulator was developed that allows for the creation, editing, and execution of programs in the Ladder programming language. The primary objective during the design of the simulator was to develop a modern teaching tool that would allow users to perform laboratory exercises and verify PLC logic without the need for real industrial equipment or the acquisition of software solutions that involve a significant expenditure for the user. Special attention was paid to a simple user interface, logic execution visibility, and the ability to connect to a virtual 3D model. The simulator was developed in the Python programming language, which was chosen due to the ease of creating a graphical user interface, the large number of available libraries, and good support for developing applications that require data processing and communication between different software systems. This approach enabled the development of a flexible software solution suitable for further development and adaptation to various educational tasks. The developed PLC simulator consists of several functional units. The central part of the system is the Ladder editor, which allows for the creation and modification of program networks using basic elements of PLC programming, such as normally open and normally closed contacts, output coils, memory bits, timers, counters, frequency pulse bits, and other logical functions. In addition to program creation, the simulator enables the saving and loading of projects, viewing the status of all input, output, and internal variables, contains a pre-loaded library with established basic tasks in the field of PLC programming, and the definition of tasks intended for laboratory exercises. The appearance of the PLC simulator is shown in Figure 1.

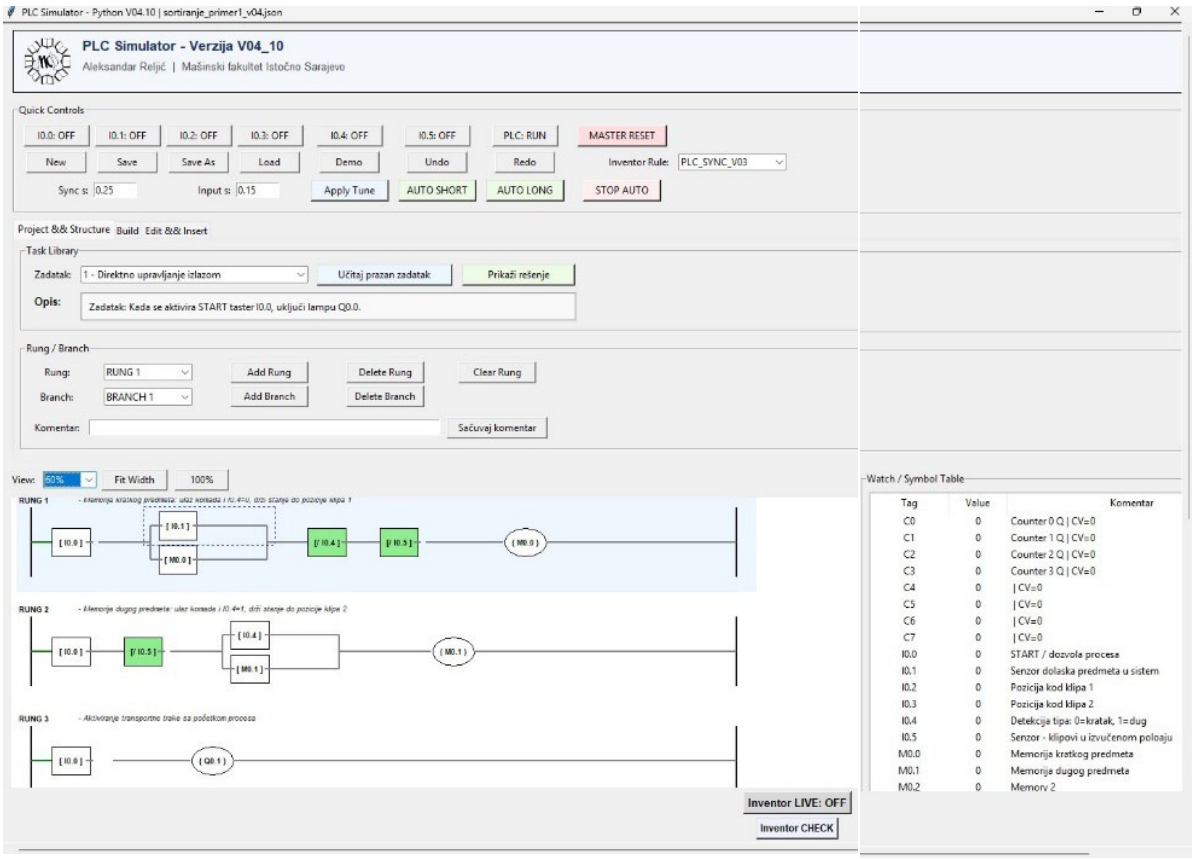


Fig. 1. *Didactic PLC simulator software*

The simulator supports two basic operating modes. In edit mode, the user creates or changes the Ladder program, adds new networks, edits comments, defines the necessary logic elements, tests the program, and so on. After finishing the program creation, code execution

mode can be accessed, where input information is activated by user clicks on corresponding buttons at the top of the window. During the execution of the logic task, active contacts, branches, and instructions are visually marked in green, allowing the user to easily follow the logic execution flow in real-time. By moving the vertical bar downwards, Global Outputs signals are accessed, where the status table for outputs, timers, counters, memory bits, and similar elements can be observed. In addition to these operating modes, the simulator has the ability to stop program operation (PLC STOP), after which the user can return to editing the logic or restarting the simulation.

In addition to the basic operating modes, the simulator includes the Inventor CHECK and Inventor LIVE functions, which enable connection to a virtual 3D environment. The Inventor CHECK function serves to verify the availability and correctness of communication between the PLC simulator and the virtual model, sending notifications in the form of messages if communication conditions are not met. The Inventor LIVE function activates bidirectional data exchange in real-time. Once communication is established, changes in the output signals of the PLC simulator are transmitted to the virtual model, while the status of the virtual sensors is automatically returned as input signals to the PLC program.

To demonstrate the operation of the PLC program, a virtual model of a didactic station with fixed mapped inputs and outputs was developed, as well as a mini-workstation for sorting objects of different lengths. The model includes a conveyor belt, input and output signals (switches/buttons and lights), and pneumatic pistons for sorting (controlled by linear actuator movement). The virtual model was developed in the Autodesk Inventor software package and serves as a digital replica of the process executed in the PLC simulator. The appearance of the virtual didactic station is shown in Figure 2.

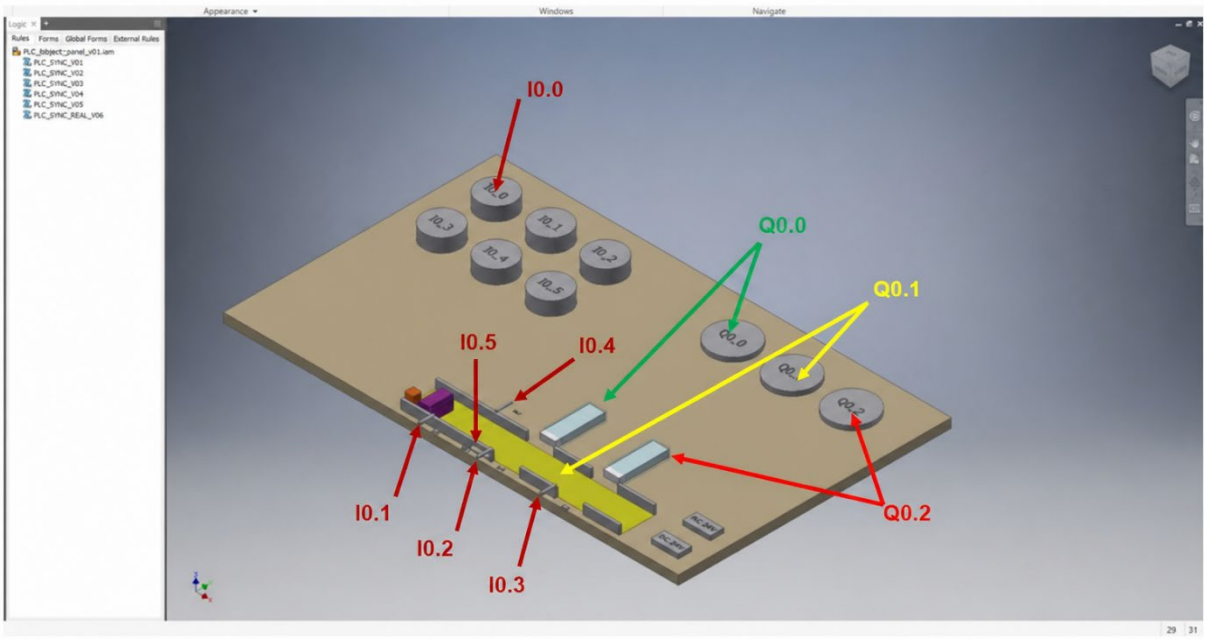


Fig. 2. *Didactic station modeled in a 3D environment*

The primary contribution of this work is the establishment of bidirectional communication between the PLC simulator and the virtual 3D environment, thereby realizing a functional Digital Twin of the system. Synchronization is achieved through a real-time data exchange mechanism using Python tools, where both software systems use a common set of input and output signals defined through user parameters.

When a user initiates the execution of a Ladder program, the PLC simulator reads the state of the input signals in each execution cycle and determines the values of the output signals based on the defined logic. The resulting values are transferred to the virtual model, where they trigger corresponding output functions, such as moving pneumatic pistons, activating lights,

and so on. Simultaneously, the virtual model continuously monitors sensor states and updates the values of the input signals. Every change of input signals in virtual model is returned to the PLC simulator. In this way, the simulator has new information about the process state in the next execution cycle, achieving continuous bidirectional data exchange between the logical and visual parts of the system.
To achieve this communication, a set of shared user parameters was defined, representing the link between the PLC simulator and the virtual model. The parameters include input and output PLC signals, as well as auxiliary parameters for controlling pneumatic pistons and other process elements. Their representation is given in Figure 3.

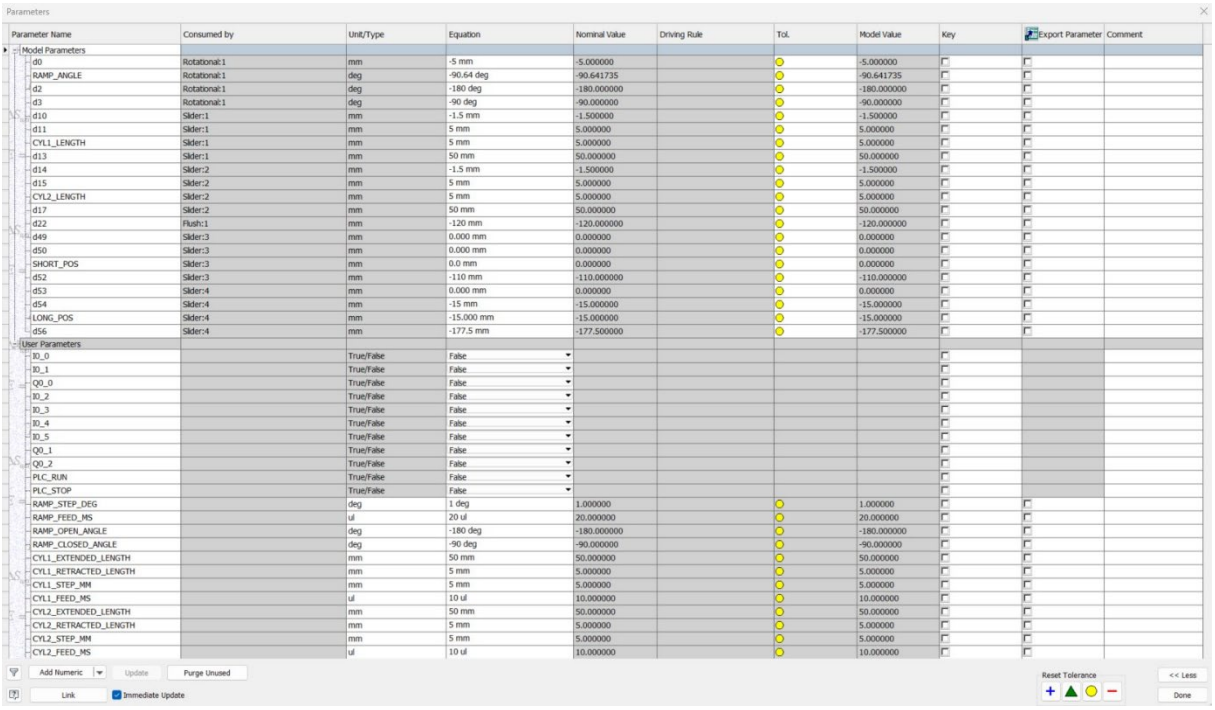


Fig. 3. *Control parameters for the synchronization process between the PLC simulator and the 3D environment*

Based on changes in the values of these parameters, corresponding iLogic procedures are executed to trigger animations, update the positions of moving elements, and change the status of virtual sensors, ensuring complete synchronization between the PLC simulator and the virtual 3D environment.
In the described manner, full synchronization between the logical and visual components of the system is achieved. Every change in the state of the PLC simulator's output signals causes a corresponding change in the 3D model. This enables real-time simulation of automated system operation, making the developed solution suitable for demonstrating PLC control principles and conducting laboratory exercises in the education system.

EXAMPLE TASK FOR SORTING OBJECTS OF DIFFERENT LENGTHS

As an example of the developed system, an automatic process for sorting objects of different lengths was implemented. The system consists of a conveyor belt, sensors for registration and determination of object length, two pistons for sorting objects, and corresponding input-output signals. After starting the process, the conveyor belt brings the object to the detection zone. Based on the signal from the sensor, it is determined whether the object is short or long, after which the PLC program activates the appropriate piston and directs the object to the designated location. Upon completion of sorting, the system returns to a state of waiting for the next object.

Input signal I0.0 represents the switch for starting the object sorting process, i.e., it represents the START switch, and its activation starts the conveyor belt that delivers items ready for sorting. Sensor I0.1 registers the presence of an object on the belt, I0.2 and I0.3 indicate object positions at piston 1 and piston 2, I0.4 serves for the detection of a longer object, while I0.5 registers the final extended position of piston 1 or piston 2. Output Q0.0 controls the extension of piston 1, Q0.1 starts the conveyor belt, and Q0.2 activates the extension of piston 2.
The process control logic was implemented using the Ladder diagram shown in Figure 4. The program is organized into multiple networks, with each network performing a specific function in the sorting process.

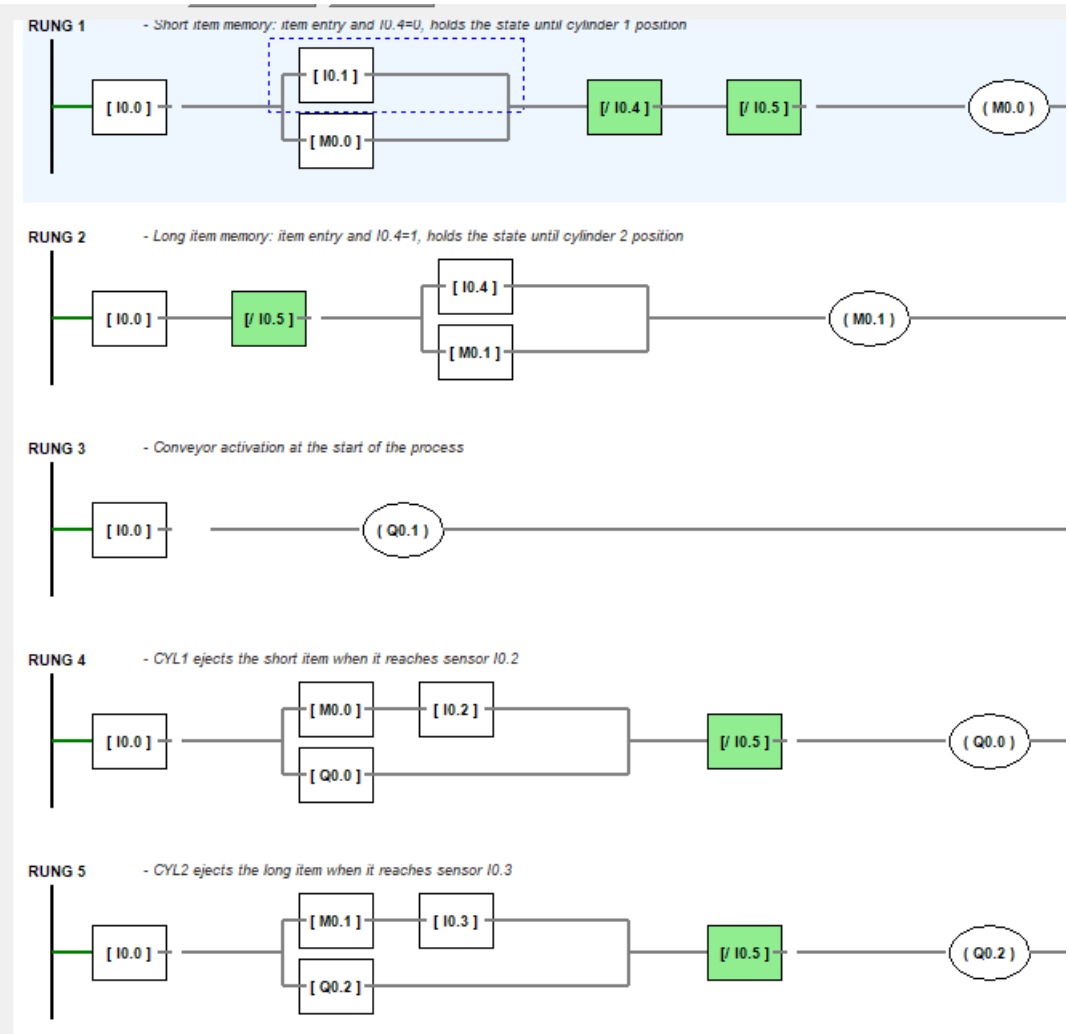


Fig. 4. *Task solution shown in the Ladder programming language*

In all networks, it is necessary for the START switch to be on for the conveyor belt to operate. Network 3 (RUNG 3) activates the conveyor belt. Network 1 registers both shorter and longer objects. Network 2 recognizes only longer objects. Network 4 defines the sorting of shorter objects with the following logic: if an object is present on the belt, if a signal for longer objects has not been registered, as soon as the object appears in front of sensor I0.2, activate output signal Q0.0 and extend piston 1, as shown in Figure 5.

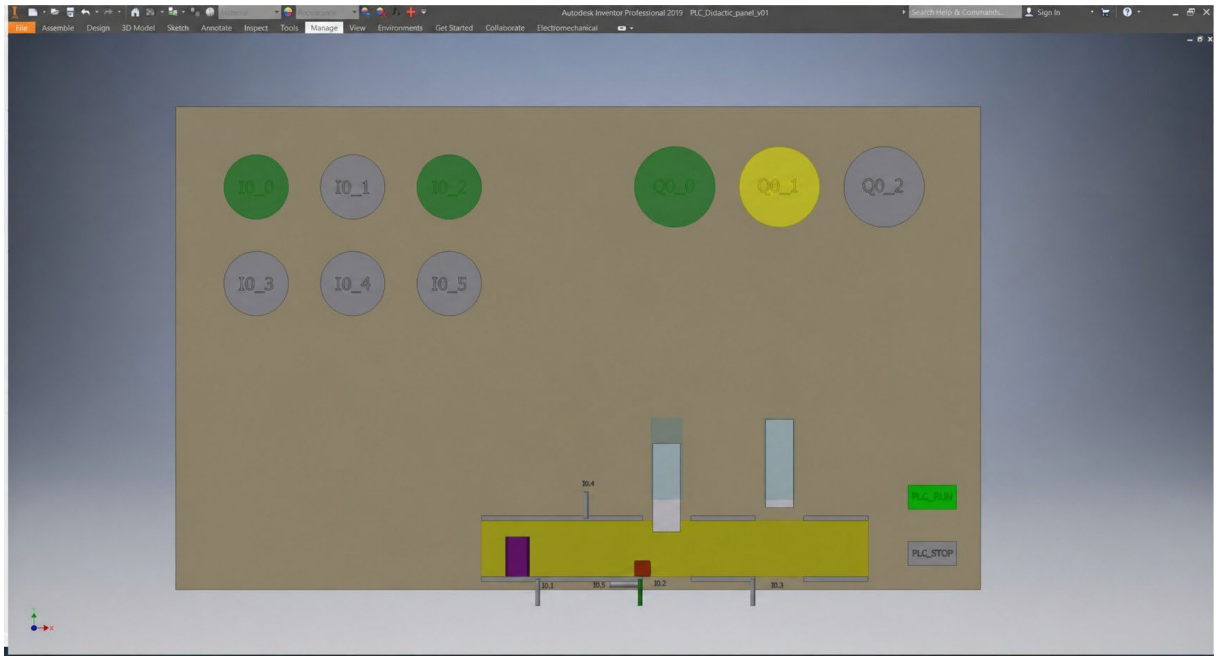


Fig. 5. *Moment of activation of piston 1 for sorting a shorter orange object*

Network 5 represents the sorting of objects of greater length. In this case, the signal from sensor I0.4 registers a longer object, and the signal from sensor I0.3 activates output signal Q0.2 and the extension of piston 2, as shown in Figure 6.

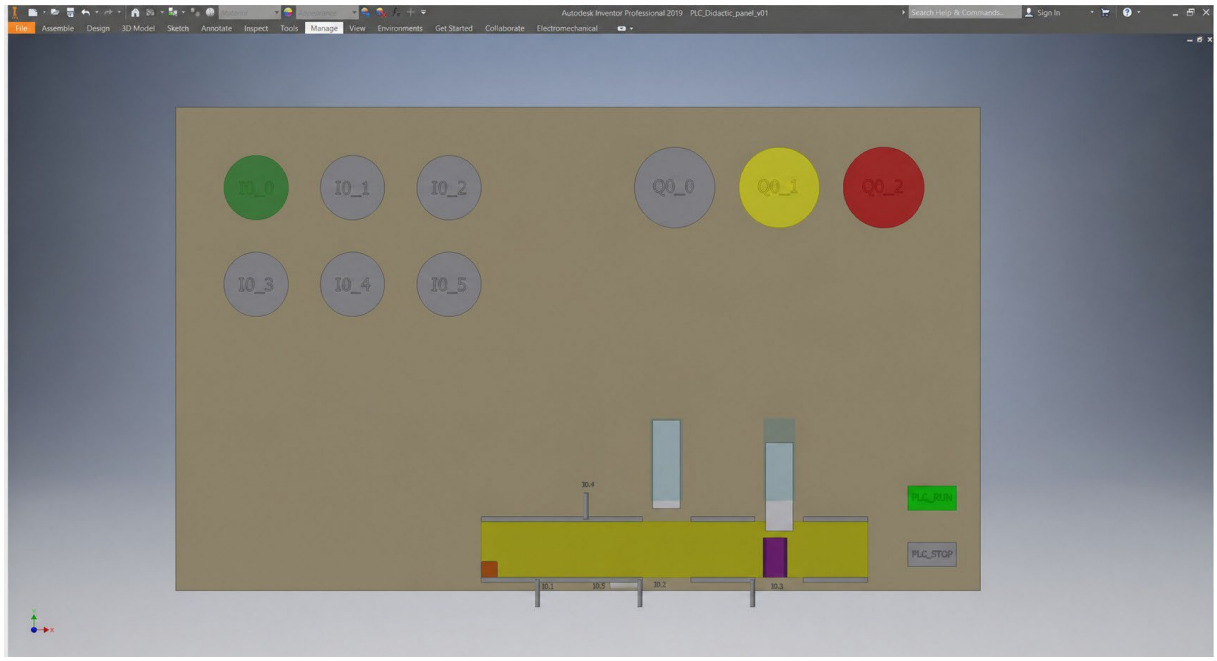


Fig. 6. *Moment of activation of piston 2 for sorting a longer purple object*

Networks 4 and 5 contain signal maintenance for the extension of the pistons due to temporary signals from sensors I0.2 and I0.3 (the object appears in front of the sensor for a short moment), as well as a normally closed contact I0.5, which serves to restart memory states and return both pistons to their initial position. The assumption is that the pneumatic pistons are single-acting and that the logistical conditions are designed so that objects on the conveyor belt arrive in an ideal arrangement.
Changes in the status of sensors I0.0, I0.1, I0.2, I0.3, I0.5 in the 3D environment are transmitted to the PLC simulator as input signals, while the output commands of the PLC

program are returned to the virtual model. This confirms the correct synchronization of the control logic and the visual model during a single object sorting cycle.

CONCLUSION

A didactic PLC simulator has been developed in this work, enabling the creation, execution, and visual monitoring of programs written in the Ladder programming language. In addition to the development of the simulator, its successful integration with a virtual 3D environment was achieved, allowing for bidirectional exchange of input-output signals between the control logic and the virtual process model. In this way, a functional system was realized that allows for simultaneous logical and visual simulation of automated process operation.
The functionality of the developed system was confirmed through the example of sorting objects of different lengths. The execution of the PLC program, the exchange of data with the virtual model, and the animation of the process occur in real-time synchronization, allowing the user to directly monitor the impact of program instructions on system behavior and more easily understand the principles of automated system operation.
A particular contribution of this work is reflected in its application in education. The developed simulator allows for the conduct of laboratory exercises without the need for real industrial equipment, providing students with the opportunity to acquire knowledge in the fields of PLC programming, automation, and mechatronics in a safe virtual environment. Simultaneously, users can monitor the execution of Ladder programs, changes in input-output signals, and the behavior of actuators in the 3D model, contributing to a better understanding of the control process. This work methodology also allows distance learning (online learning).
Beyond the costs of acquiring physical PLC devices, sensors, actuators, and didactic panels, significant financial resources are often required for the purchase of professional software tools for simulation and virtual commissioning, which are mostly licensed per user or workstation and require periodic license renewal. Furthermore, physical laboratory stations require regular maintenance, servicing and replacement of worn-out components, which further increases their cost of use. By developing a custom software solution, the possibility of performing a large number of laboratory exercises was achieved without additional license costs and without using physical equipment, resulting in significant long-term financial savings for educational institutions.
Similar advantages are cited by modern commercial systems for PLC simulation, which highlight safe testing of PLC programs, visualization of process operation, development of digital twins, support for virtual commissioning, and the conduct of laboratory exercises in a realistic virtual environment as primary benefits (MHJ Tools, n.d.).

REFERENCES

Armendia, M., Ghassempouri, M., Ozturk, E., & Peysson, F. (Eds.). (2019). Twin-Control: A Digital Twin Approach to Improve Machine Tools Lifecycle. *Springer Nature*, Cham, Switzerland.

Barale, D. (2025). Industrial Process Simulation through Digital Twin Modeling and PLC Programming. Master's thesis, *Politecnico di Torino*, Turin, Italy.

Cavalieri, S., & Scroppo, M. (2019). A CLR Virtual Machine Based Execution Framework for IEC 61131-3 Applications. *Informatica*, 43(2), 263–279.

Diekmann, M., Nitzler, J., Fischer, J., Pfisterer, H.-J., & Hartmann, D. (2026). Multi-Agent Framework Leveraging Knowledge Graphs for Virtual Commissioning Models. *arXiv preprint*, arXiv:2606.03255.

Garg, G., Kuts, V., & Anbarjafari, G. (2021). Digital Twin for FANUC Robots: Industrial Robot Programming and Simulation Using Virtual Reality. *Sustainability*, 13(18), Article 10336.

Hrbček, J., Ždánsky, J., Macko, D., & Bubeníková, E. (2026). Development of a Digital Twin Controlled by PLC in a Simulation Environment. *Transportation Research Procedia*, 93, 723–728.

Lubura, S., Mandić, Z., Prodanović, S., & Jokić, D. (2025). Procesni računari – Zbirka riješenih zadataka. *Univerzitet u Istočnom Sarajevu, Elektrotehnički fakultet Istočno Sarajevo, Akademska misao*, Beograd.

Lubura, S., & Šoja, M. (2020). Procesni računari. *Univerzitet u Istočnom Sarajevu, Elektrotehnički fakultet Istočno Sarajevo, Akademska misao*, Beograd.

Lubura, S., Šoja, M., & Ristović, M. (2013). Programabilni logički kontroleri – Zbirka riješenih zadataka. *Univerzitet u Istočnom Sarajevu, Elektrotehnički fakultet Istočno Sarajevo*.

MHJ Tools. (n.d.). PLC-Lab. Available at: *https://mhj-tools.com/products/plc-lab* (Accessed: 12 July 2026).

Ortiz, J. S., Andaluz, V. H., & Carvajal, C. P. (2026). Real-Time Digital Twin Architecture for Immersive Industrial Automation Training. *Sensors*, 26, Article 2023.

Petruzella, F. D. (2017). Programmable Logic Controllers (5th ed.). *McGraw-Hill Education*, New York, NY, USA.

Prodanović, S., & Lubura, S. (2021). Digitalno upravljanje u proizvodnji. *Univerzitet u Istočnom Sarajevu, Mašinski fakultet Istočno Sarajevo, Akademska misao*, Beograd.

Reuther, A., Plesker, C., Bassauer, D., & Schleich, B. (2026). A Digital Twin Framework for Programmable Logic Controllers in Industrial Automation Systems. *Procedia CIRP*, 139, 446–452.

Schamp, M., Van De Ginste, L., Hoedt, S., Claeys, A., Aghezzaf, E.-H., & Cottyn, J. (2019). Virtual Commissioning of Industrial Control Systems – A 3D Digital Model Approach. *Procedia Manufacturing*, 39, 66–73.

Schäfer, S., Schöttke, D., Kämpfe, T., Ralinovski, K., Tauber, B., & Lehmann, R. (2021). Design and Deployment of Digital Twins for Programmable Logic Controllers in Existing Plants. *Proceedings of the 2nd International Conference on Innovative Intelligent Industrial Production and Logistics* (*IN4PL*), 145–150.

Striffler, N., & Voigt, T. (2023). Concepts and Trends of Virtual Commissioning – A Comprehensive Review. *Journal of Manufacturing Systems*, 71, 664–680.

Zhang, W. (2024). Design of a PLC System Simulator and Application to Teaching Programmable Logic Controller Course Online. *Proceedings of the 2024 ASEE Annual Conference & Exposition*, Portland, Oregon, USA.

DOI:10.5937/IIZS26162D

POTENTIAL OF HEMP-BASED MATERIALS FOR IMPROVING THE ENERGY EFFICIENCY OF BUILDINGS

Research paper

Snežana Dragićević[1*], Srba Stevanović[2], Brankica Šutić[3]
[1,2,3]University of Kragujevac, Faculty of Technical Sciences in Čačak, Serbia

Abstract: Energy efficiency in buildings is an important aspect of reducing operational energy demand and improving the performance of the existing building stock. In parallel with conventional insulation systems, bio-based materials are increasingly considered for building-envelope applications. This study evaluates the potential of industrial hemp-based materials for improving the energy performance of an existing public building in Čačak, Serbia. Four wall-envelope scenarios were analysed in URSA Građevinska Fizika 2: the existing uninsulated wall, external insulation with 6 cm of extruded polystyrene, external insulation with 7 cm of IndiBoard hemp-fibre board, and a deep-reconstruction scenario with a 30 cm hemp-lime wall. The results indicate that hemp-fibre insulation can provide operational thermal performance comparable to extruded polystyrene at a similar insulation level, while hemp-lime achieves the lowest heating demand but requires a substantially deeper intervention. The study supports the technical potential of industrial hemp in energy renovation, while broader environmental and economic conclusions require dedicated life-cycle and techno-economic assessment.
Key words: *hemp-based materials; energy efficiency; building renovation; thermal performance*

INTRODUCTION

Energy efficiency in the building sector is one of the central challenges of contemporary energy and environmental policy. Existing buildings frequently have envelopes with insufficient thermal protection, which results in high transmission heat losses and elevated heating demand. Improvement of the building envelope is therefore among the most direct measures for reducing operational energy use. The effectiveness of such measures depends not only on insulation thickness but also on thermal conductivity, continuity of the insulation layer, moisture behaviour, construction details and the compatibility of the selected material with the existing wall system.

Conventional insulation materials such as mineral wool, expanded polystyrene (EPS) and extruded polystyrene (XPS) are widely applied because their properties are well documented and the construction industry has extensive experience with their installation. However, current research increasingly considers bio-based materials that can provide adequate thermal performance while relying partly on renewable raw materials. Industrial hemp is attracting particular attention in the construction sector because different parts of the plant can be processed into fibre insulation, hemp-lime composites, boards and other building products, supporting a broad range of potential applications in building-envelope systems, (Enarevba, 2024).

Hemp-based products are relevant to building-envelope design for two main reasons. First, fibre insulation products can reach thermal-conductivity values in the range of conventional lightweight insulation materials. Second, hemp-lime composites combine hemp shiv with a lime-based binder to form a lightweight, vapour-open material used primarily as non-load-bearing infill and thermal envelope material. Experimental studies have shown that the thermal behaviour of hemp-based materials depends strongly on density, moisture content, particle size distribution, binder type, mixing proportions and compaction level, as shown in Fig. 1, (Ahmed et al., 2022; Barbhuiya & Das, 2022; Kosiński et al., 2022; Pochwała et al., 2020).

[1]Corresponding author, snezana.dragicevic@ftn.kg.ac.rs, ORCID: 0000-0002-6244-0111
[2]srbastevanovic01@gmail.com
[3]brankica.sutic@ftn.kg.ac.rs, ORCID: 000-0001-6180-2136

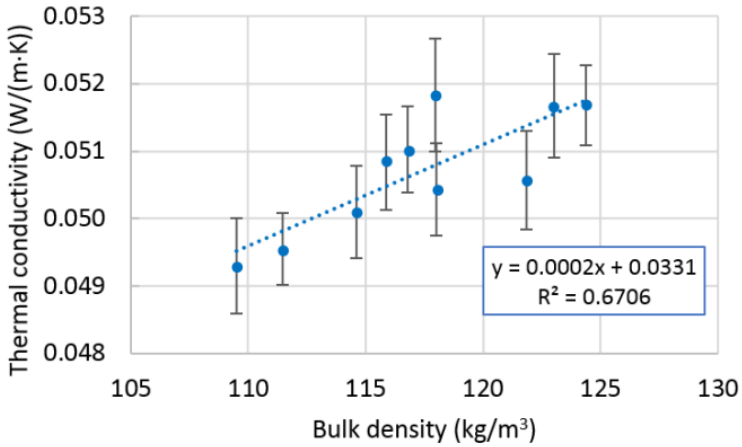


Fig. 1. *Thermal conductivity of hemp at different densities*

The environmental profile of hemp-based materials is also frequently discussed in the literature because hemp is a rapidly renewable agricultural resource and plant biomass stores biogenic carbon during growth. Nevertheless, the overall environmental performance of a construction product cannot be inferred from the raw material alone. Cultivation, processing, transport, binder production, service life, maintenance and end-of-life treatment all affect life-cycle impacts. Moreover, sustainability rankings can change substantially depending on the environmental indicators and weighting criteria included in the assessment, as demonstrated in comparative analyses of hempcrete and prefabricated wall systems, (Ošlovnik & Denac, 2025). For this reason, the present paper focuses primarily on operational energy performance and treats broader sustainability benefits as a topic requiring separate life-cycle assessment.
The objective of the study is to quantify the effect of industrial hemp-based envelope solutions on the heating performance of an existing public building and to compare the results with a conventional XPS retrofit. Four scenarios are examined: the existing wall, XPS external insulation, hemp-fibre board external insulation and a deep-reconstruction hemp-lime wall. The comparison is based on wall thermal transmittance, transmission heat losses and annual heating demand. The analysis is intended to determine whether hemp-based materials can serve as technically credible alternatives in energy renovation and to identify the limitations of a direct comparison between conventional retrofit and deep reconstruction.

MATERIALS AND METHODS

The materials considered in the study include both conventional insulation products and hemp-based alternatives. The purpose of the comparison is not to provide a comprehensive ranking of insulation materials, but rather to establish the thermal context for the simulation scenarios and to justify the selection of XPS, a hemp-fibre board, and a hemp-lime wall system for further analysis. The conventional insulation materials used as a reference for comparison are presented in Table 1. Their thermal properties provide the context for evaluating the hemp-based alternatives examined in this study.
Mineral wool products are fibrous inorganic insulations with low thermal conductivity and good fire performance. Their density varies considerably according to product type and application. Glass wool is generally lighter, while stone wool products can be manufactured at higher densities for facade, roof and fire-protection applications. Polymer-based EPS and XPS also provide low thermal conductivity at very low density. XPS has a closed-cell structure and is commonly selected where low water absorption and mechanical resistance are important. Fire behaviour of polymer insulation depends on the specific product and the complete wall assembly; therefore, simplified statements that all products behave identically should be avoided.

Table 1. *Properties and applications of conventional insulation materials*

Material	Conductivity λ [W/(mK)]	Density ρ [kg/m³]	General building use
Stone wool	0.030–0.040	40–200	Walls, roofs, ceilings; thermal and acoustic insulation
Glass wool	0.030–0.045	15–100	Lightweight insulation in walls, roofs and ceilings
EPS	0.030–0.040	15–40	Facade systems, floors and roofs
XPS	0.025–0.035	30–40	Envelope areas requiring low water absorption and higher compressive strength

The original manuscript included several broad environmental claims concerning conventional insulation. In the revised analysis these claims are treated more cautiously. Durability, recyclability, embodied energy and emissions depend on the specific product, manufacturing route and end-of-life scenario. Accordingly, conventional and bio-based materials should be compared using clearly defined performance indicators rather than by assuming environmental superiority from material origin alone.

Hemp-based insulation and hemp-lime materials

Industrial hemp can be processed into several construction products. The bast fibres are suitable for fibrous insulation mats and boards, while the woody core of the stem, commonly referred to as hemp shiv, can be combined with a mineral binder to produce hemp-lime composites. The two product groups differ significantly in density, stiffness and application. Fibre boards are installed in a manner comparable to other insulation boards, whereas hemp-lime is generally used as a non-load-bearing wall infill, cast material or block system.

One important characteristic of hemp-based materials is their porous and hygroscopic structure. This can support moisture buffering and vapour-open wall design when the complete assembly is appropriately detailed. Recent long-term in-situ monitoring combined with numerical modelling has also demonstrated the potential of hempcrete wall systems to provide satisfactory hygrothermal performance under temperate climatic conditions, (Jirgensone et al., 2024). However, hygrothermal behaviour must be evaluated at the level of the complete wall system, because the response depends on indoor and outdoor climate, coatings, render systems, air tightness and moisture loads.

The final properties of hemp-lime depend on the type and size distribution of hemp shiv, binder composition, water content, aggregate-to-binder ratio, placement method and compaction. The importance of mixture composition for the thermal conductivity of hemp-lime composites has been demonstrated in previous studies, (Pochwała et al., 2020), while low thermal conductivity has also been reported for loose hemp shiv used as an insulation material, (Kosiński et al., 2022). The literature therefore shows that a single universal thermal conductivity value cannot represent all hemp-based products. The thermal properties of selected commercially available hemp-fibre insulation products are presented in Table 2.

Table 2*. Thermal properties of selected hemp-fibre insulation products*

Product	Conductivity λ [W/(mK)]	Density ρ [kg/m³]	Specific heat c [J/(kgK)]
HempFlax Plus	0.040	35.5	1800
HempWool	0.040	45.0	-
Thermafleece / NatraHemp	0.042	28.0	1800
IndiTherm	0.039	45.0	2371
IndiBoard	0.039	130.0	2202

The values illustrate that commercial hemp-fibre products can reach thermal conductivities around 0.039–0.042 W/(mK). These values are within the range commonly associated with standard thermal-insulation products. IndiBoard was selected for the building simulation because the original model contained the required material parameters and because its thermal conductivity of 0.039 W/(mK) permits a meaningful comparison with the selected XPS layer. The thermal properties of selected commercially available hemp-lime building products are summarized in Table 3, illustrating the range of thermal conductivity and density associated with different product formulations.

Table 3. *Thermal properties of selected hemp-lime building products*

Product	Conductivity λ [W/(mK)]	Density ρ [kg/m³]	Specific heat c [J/(kgK)]	Water vapour diffusion resistance factor μ [-]
HEMPBLOCK	0.071	340	-	-
Bio Block	0.070	330	1280	4.5
Blocco Ambiente	0.044	310	1280	4.5
IsoHemp Hempblock	0.071	320	-	2.8

Compared with fibre insulation, hemp-lime products have higher density and generally higher thermal conductivity, but they can perform several envelope functions within a thicker wall system. Their low vapour-diffusion resistance in the reported product data is consistent with vapour-open construction strategies. At the same time, hemp-lime should not be treated as a direct structural substitute for conventional load-bearing masonry unless the specific system has been engineered and certified for such use. In this study it is therefore described as a hemp-lime wall or infill solution within a deep-reconstruction scenario.

Case study and simulation procedure

The energy-efficiency analysis was performed for the Home for the Blind in Čačak, Serbia, a public building constructed in 1982, shown in Fig. 2. The building has ground and first floors (P+1) and was constructed as a system of reinforced-concrete columns combined with masonry walls. The existing external wall consists of 2 cm internal plaster, 25 cm hollow clay masonry and 2 cm external perlite plaster. No additional thermal-insulation layer is present.
The gross heated volume of the building is 2424 m³, the net heated volume is 1737 m³ and the useful heated floor area is 495 m². The same geometry, orientation, heated volume and internal heat gains were retained in all simulation scenarios. Internal gains from occupants and equipment were fixed at 5207 kWh/year. The construction of floors, ceilings, windows and other envelope elements was also kept unchanged across the three renovation variants so that the effect of the external-wall modification could be isolated.



Fig. 2. *Analysed public building – Home for the Blind in Čačak*

The local climate parameters used for Čačak were a minimum outdoor design temperature of −18.3 °C and 2755 heating degree-days. The thermodynamic calculations were carried out in URSA Građevinska Fizika 2 using the calculation framework applied in Serbian building energy-efficiency practice. Transmission heat transfer through building components was calculated according to the methodology referenced in the original model, including SRPS EN ISO 6946 for building components and SRPS EN ISO 13370 for heat transfer to the ground.
Four scenarios were defined. Scenario 1 represents the existing wall and serves as the baseline. Scenario 2 adds 6 cm of XPS to the existing external wall. Scenario 3 adds 7 cm of IndiBoard hemp-fibre insulation to the same existing wall. Scenario 4 represents a fundamentally different intervention in which the existing masonry wall is replaced by a 30 cm hemp-lime wall/infill. The thicknesses used in the original model were retained so that the revised paper reports the same simulation results as the source study. The four simulation scenarios and the corresponding wall configurations and U-values are summarized in Table 4.

Table 4. *Constants and variable wall configurations used in the simulation scenarios*

Scenario	Envelope configuration	Type of intervention	Wall U-value [W/(m²K)]
1	Existing 25 cm hollow-clay wall + plaster	Baseline	1.322
2	Existing wall + 6 cm XPS	External insulation retrofit	0.397
3	Existing wall + 7 cm IndiBoard	External hemp-fibre retrofit	0.391
4	30 cm hemp-lime wall/infill	Deep reconstruction	0.219

The calculated U-value of the existing wall is 1.322 W/(m²K), confirming the limited thermal protection of the original envelope. The addition of XPS lowers the U-value to 0.397 W/(m²K), whereas the hemp-fibre board produces a slightly lower value of 0.391 W/(m²K). The 30 cm hemp-lime scenario reaches 0.219 W/(m²K). The first two renovation solutions can therefore be compared as conventional external-insulation alternatives, whereas the hemp-lime case should be interpreted as a deep-reconstruction reference.

RESULTS AND DISCUSSION

The results presented in Table 5 show a substantial reduction in transmission losses following each envelope improvement. Compared with the existing state, the transmission heat-loss coefficient H_t is reduced by approximately 68.4 % with XPS and 68.6 % with IndiBoard, while the hemp-lime scenario achieves the largest reduction, about 73.8 %. These results confirm the significant contribution of the external walls to the initial transmission losses.

Table 5. *Impact of Insulation Materials and Thicknesses on Energy Performance*

Parameter	Baseline	6 cm XPS	7 cm IndiBoard	30 cm hemp-lime
H_t [W/K]	2095.63	662.40	658.60	549.93
$Q_{H,ht}$ [kWh]	186833.88	63910.43	63659.78	56474.20
$Q_{H,sol}$ [kWh]	17839.83	12184.09	12159.85	11464.96
$Q_{H,nd}$ [kWh]	164248.12	46867.31	46640.41	40135.83
$Q_{H,nd,red}$ [kWh]	157501.33	42620.48	42403.41	36190.26
$Q_{H,an}$ [kWh/(m^{2}a)]	318.38	86.16	85.72	73.16
Energy performance rating	G	D	D	C

A similar trend is observed for the annual energy required to compensate for heat losses $Q_{H,ht}$ with reductions of approximately 65.8 % for XPS, 65.9 % for IndiBoard, and 69.8 % for hemp-lime. The annual heating demand $Q_{H,nd}$ decreases by approximately 71.5 %, 71.6 %, and 75.6

%, respectively. After application of the reduction procedure implemented in the software, the corresponding decreases in $Q_{H,nd,red}$ are approximately 72.9 %, 73.1 %, and 77.0 %.
The specific annual heating demand follows the same trend, resulting in an improvement of the building energy performance rating from class G to class D for both XPS and IndiBoard, and to class C for the hemp-lime scenario. The difference between XPS and IndiBoard is only 0.44 kWh/(m²a), or about 0.5 % of the post-renovation heating demand, indicating that their operational thermal performance is practically equivalent. Therefore, energy demand alone does not provide a sufficient basis for choosing between these two insulation materials.
Other criteria should consequently be considered, including initial investment, local availability, construction time, thermal-bridge detailing, moisture resistance, fire classification, mechanical robustness, maintenance requirements, and expected service life. For hemp-based products, reliable design also requires verified product declarations and careful consideration of moisture-sensitive thermal properties, while for XPS the fire performance of the complete facade system should be considered rather than that of the insulation material in isolation.
Although Scenario 4 achieves the greatest energy reduction, it is not directly comparable with the XPS and IndiBoard retrofit scenarios. Replacing the original masonry with a 30 cm hemp-lime wall represents a change in the construction system and should therefore be regarded as deep reconstruction rather than a conventional facade retrofit. The result demonstrates the thermal potential of a thick hemp-lime envelope but does not, by itself, establish this solution as the most practical or cost-effective option for the analysed building.
The obtained results are consistent with trends reported in previous experimental studies on hemp-based building-envelope systems. A 33 % reduction in space-heating energy use was reported after the application of hemp-lime in a full-scale renovation study, (Strandberg-de Bruijn et al., 2019). Hemp-lime renders have also been shown to substantially reduce wall thermal transmittance, (McGinn et al., 2019). Furthermore, comparative investigations indicate that hemp-lime and wood-fibre-based wall systems can achieve thermal performance comparable to conventional insulation systems when designed to similar thermal standards, (Latif et al., 2018). The greater relative reductions obtained in the present study can be attributed primarily to the poor thermal performance of the existing building envelope and the substantial improvement in wall thermal resistance introduced by the analysed retrofit measures. Recent building-scale studies also confirm that hemp-based envelope systems can achieve significant reductions in heating demand when combined with appropriate wall design and climatic conditions, (Es-sakali et al., 2023).

CONCLUSION

The performed simulation confirms that improving the external wall can substantially reduce the heating demand of the analysed public building and significantly improve its energy performance. One of the main findings is the very close thermal performance of the XPS and hemp-fibre board retrofit scenarios. Under identical building and climate assumptions, IndiBoard provides practically the same operational energy performance as conventional XPS. This indicates that hemp-based insulation can represent a technically viable alternative when thermal, moisture, fire-safety and construction requirements are adequately addressed.
The hemp-lime scenario achieves the greatest calculated energy improvement, but it involves replacement of the existing wall system and is therefore more appropriately considered a deep-reconstruction solution than a directly comparable facade retrofit. Consequently, the lowest calculated heating demand should not be regarded as the only criterion for selecting the preferred renovation option.
Future work should extend the analysis to investment and life-cycle costs, embodied energy and carbon, moisture and durability performance, construction feasibility, and sensitivity to material properties. Within the stated limitations, the results demonstrate the potential of industrial hemp-based materials for improving building-envelope energy performance and support further investigation of their application in energy-renovation practice.

ACKNOWLEDGEMENT
The authors acknowledge the financial support of the Ministry of Science, Technological Development and Innovation of the Republic of Serbia under Contract No. 451-03-34/2026-03/200132 with the Faculty of Technical Sciences in Čačak.

REFERENCES

Ahmed, A., Islam, M., Mahmud, M., Saker, M., & Islam, M. R. (2022). Hemp as a potential raw material toward a sustainable world: A review. *Heliyon, 8*(1). https://doi.org/10.1016/j.heliyon.2022.e08753

Barbhuiya, S., & Das, B. B. (2022). A comprehensive review on the use of hemp in concrete. *Construction and Building Materials, 341*, 127857. https://doi.org/10.1016/j.conbuildmat.2022.127857

Enarevba, D. R., & Haapala, K. R. (2024). The emerging hemp industry: A review of industrial hemp materials and product manufacturing. *AgriEngineering, 6*(3), 2891–2925. https://doi.org/10.3390/agriengineering6030167

Es-sakali, N., Charai, M., Kaitouni, S. I., Ait Laasri, I., Mghazli, M. O., Cherkaoui, M., Pfafferott, J., & Ukjoo, S. (2023). Energy efficiency and hygrothermal performance of hemp clay walls for Moroccan residential buildings: An integrated lab-scale, in-situ and simulation-based assessment. *Applied Energy, 352*, 121967. https://doi.org/10.1016/j.apenergy.2023.121967

Jirgensone, B., Birjukovs, M., Sinka, M., Jakovics, A., & Bajare, D. (2024). Hygrothermal performance of hempcrete in a multi-layer wall envelope. *Journal of Building Engineering, 84*, 108359. https://doi.org/10.1016/j.jobe.2023.108359

Kosiński, P., Brzyski, P., Tunkiewicz, M., Suchorab, Z., Wiśniewski, D., & Palczyński, P. (2022). Thermal properties of hemp shives used as insulation material in construction industry. *Energies, 15*(7), 2461. https://doi.org/10.3390/en15072461

Latif, E., Lawrence, R. M. H., Shea, A. D., & Walker, P. (2018). An experimental investigation into the comparative hygrothermal performance of wall panels incorporating wood fibre, mineral wool and hemp-lime. *Energy and Buildings, 165*, 76–91. https://doi.org/10.1016/j.enbuild.2018.01.028

McGinn, J., Pavia, S., & Kinnane, O. (2019). Application of hemp-lime renders to improve the insulating capacity of building walls. *Academic Journal of Civil Engineering, 37*(2), 684–689. https://doi.org/10.26168/icbbm2019.99

Ošlovnik, T., & Denac, M. (2025). How multicriteria environmental assessment alters sustainability rankings: Case study of hempcrete and prefabricated walls. *Sustainability, 17*(15), 7032. https://doi.org/10.3390/su17157032

Pochwała, S., Makiola, D., Anweiler, S., & Böhm, M. (2020). The heat conductivity properties of hemp–lime composite material used in single-family buildings. *Materials, 13*(4), 1011. https://doi.org/10.3390/ma13041011

Strandberg-de Bruijn, P., Donarelli, A., & Balksten, K. (2019). Full-scale studies of improving energy performance by renovating historic Swedish timber buildings with hemp-lime. *Applied Sciences, 9*(12), 2484. https://doi.org/10.3390/app9122484

DOI:10.5937/IIZS26169B

IMPACT OF THERMAL DYNAMICS, SOILING, AND DEGRADATION IN PHOTOVOLTAIC ENERGY YIELD ESTIMATION: A COMPARATIVE MODELING STUDY

Research paper

Marinko Barukčić[1*], Boris Fažo[2], Goran Kurtović[3], Hrvoje Glavaš[4]
[1,3,4]Faculty of Electrical Engineering, Computer Science and Information Technology Osijek, Osijek, Croatia
[2]Helmerich & Payne H&P inc., Middle East - Saudi Arabia

Abstract: Accurate estimation of annual energy yield is critical during the planning and design phase of photovoltaic (PV) power plants. However, basic mathematical models often rely solely on solar irradiance under Standard Test Conditions (STC), ignoring environmental dynamics such as operating temperature, wind cooling, dynamic soiling, and panel degradation. This paper presents a comparative analysis of five mathematical PV module models evaluating fixed-tilt and two-axis tracking configurations over a 16-year period (2005–2020) using meteorological data from Osijek, Croatia. Results demonstrate that neglecting thermal, soiling, and degradation impacts leads to an overestimation of energy production exceeding 12%, with each factor contributing approximately a 4% reduction in overall yield. Conversely, omitting wind cooling underestimates production by roughly 3.3%. Furthermore, modeling errors were found to be 1% higher in two-axis tracking systems, despite achieving ~40% higher overall yield than fixed-tilt systems. These findings emphasize the necessity of incorporating comprehensive environmental parameters into PV design models while highlighting the critical dependence of high-fidelity models on accurate meteorological input data.
Key words: Photovoltaic module modeling, Energy yield prediction, Thermal dynamics, Soiling losses

INTRODUCTION

Photovoltaic (PV) power plants are a critical component of the global transition to renewable energy. Given the rapid expansion of solar installations, this growth is expected to persist. During the planning and design phase of a PV power plant, estimating annual electricity generation is a primary performance metric. Estimating this energy yield relies on mathematical models of PV modules. Although the solar irradiance profile is the primary input parameter governing energy yield at a given location, operating temperature also significantly affects power generation efficiency.

The influence of operating temperature on PV plant productivity is widely recognized in both experimental and theoretical literature. For instance, empirical data across two consecutive years demonstrated an approximate 5% discrepancy in annual PV generation attributable to temperature variations (Nayak & Brar, 2026). Other studies, such as Dubey et al. (2013), evaluated the inverse relationship between ambient temperature and module efficiency. Furthermore, integrated modeling of dust deposition and thermal effects showed up to a 30% reduction in energy output, depending on solar irradiance levels (Zhao et al., 2025). Alaas (2024) reviewed temperature-dependent PV system performance, emphasizing the need to evaluate efficiency as a function of thermal variation. In an investigation of environmental parameters, Bamisile et al. (2025) reported a 0.4%–0.5% decline in PV efficiency for every 1°C rise in panel temperature. Additionally, modeling temperature dependencies revealed significant variations in fundamental PV cell parameters, including the fill factor, open-circuit voltage, short-circuit current, and overall conversion efficiency (Chegaar et al., 2010).

Consequently, accounting for thermal dynamics during the design and forecasting phases of a PV power plant is essential. This paper evaluates the discrepancy in projected PV energy production during the design phase by comparing mathematical models that incorporate thermal, soiling and degradation effects against temperature-independent models.

[1] Corresponding author, marinko.barukcic@ferit.hr, ORCID: 0000-0003-1703-4525
[3] ORCID: 0000-0003-1703-4525
[4] ORCID: 0000-0002-3658-0364

MATHEMATICAL MODELING OF PV MODULE PERFORMANCE

Baseline electrical model

In this study, the single-diode model is used to simulate photovoltaic (PV) system performance. The standard equivalent circuit model is shown in Fig. 1 and mathematically described by (1):

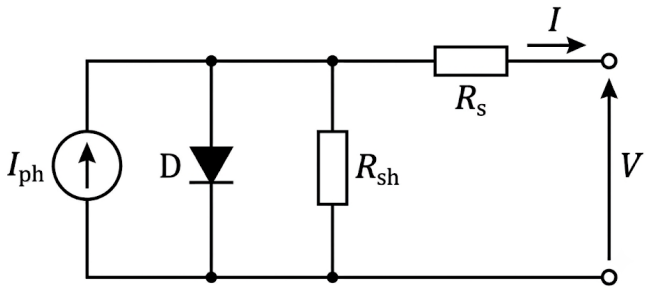


Fig. 1. *An equivalent circuit of single diode PV system model*

$$\mathrm{I} = \mathrm{I_{ph}(G,T)} - \mathrm{I_0(G,T)}\left(\exp\left(\frac{\mathrm{V}+\mathrm{IR_s}}{\mathrm{nV_t(T)}}\right)-1\right) - \frac{\mathrm{V}+\mathrm{IR_s}}{\mathrm{R_{sh}}} \tag{1}$$

where are: I cell output current (A), V cell output voltage (V), I_{ph} photocurrent, light-generated current (A), I_0 diode reverse saturation current (A), R_s equivalent series resistance (Ω), R_{sh} equivalent shunt (parallel) resistance (Ω), n diode ideality factor (typically between 1 and 2), V_t thermal voltage (V), T - operating module temperature (K) and, G - actual solar irradiance (W/m^2).
Because (1) is a nonlinear, implicit equation, numerical iterative methods are required to solve it. To avoid solving (1) directly when determining the open-circuit voltage, V_{oc} can be modeled as a function of irradiance and temperature via (2):

$$\mathrm{V_{oc}(G,\ T)} = \mathrm{V_{oc,n}} + \mathrm{K_I(T-T_n)}\ +\ \mathrm{nV_t(T)ln}\frac{G}{G_n} \tag{2}$$

where V_{oc} is open circuit voltage (V) at irradiance G, $V_{oc,n}$ – open circuit voltage (V) at Standard Test Condition (STC), K_V – open circuit voltage temperature coefficient (V/K) and G_n – irradiance at STC.
Thermal voltage is calculated from:

$$\mathrm{V_t} = \frac{\mathrm{N_s kT}}{\mathrm{q}} \tag{3}$$

where are N_s - number of series-connected cells, k - Boltzmann constant (1.380649 10^{-23} J/K), q - elementary electron charge (1.60217663 10^{-19} C)
Additional irradiance- and temperature-dependent variables are calculated according to (4) – (7):

$$\mathrm{I_{ph}} \approx I_{sc} = \left[\mathrm{I_{sc,n}} + \mathrm{K_I(T-T_n)}\right]\frac{\mathrm{G}}{\mathrm{G_n}} \tag{4}$$

where are I_{sc} – short circuit current (A), $I_{sc,n}$ – short circuit current (A) at STC, K_I - short-circuit current temperature coefficient (A/K), T_n - nominal cell junction temperature at STC (298.15 K), G_n - Nominal solar irradiance at STC (1000 W/m^2).
The fill factor also depend on temperature and irradiance what is modeled by:

$$\mathrm{FF} = \mathrm{FF_n} \cdot [1 + \mathrm{K_{FF}} \cdot (\mathrm{T} - \mathrm{T_n})] \cdot \left[\mathrm{k_1} + \mathrm{k_2}\left(\frac{\mathrm{G}}{\mathrm{G_n}}\right) + \mathrm{k_{3ln}}\left(\frac{\mathrm{G}}{\mathrm{G_n}}\right)\right] \quad (5)$$

where FF_n is the fill factor at Standard Test Conditions (STC: 1000 W/m², 298.15 K), K_{FF} is the temperature coefficient of the fill factor (%/K or 1/K), k_1, k_2, k_3 are fill factor coefficients.
The PV system power generation at the Maximum Power Point (MPP) is evaluated using *FF* via:

$$\mathrm{P}_{mpp}(G,T) = \mathrm{FF}(G,T) \cdot V_{oc}(G,T) \cdot I_{sc}(G,T)\backslash\mathrm{cdot}\mathrm{k_{DG}}(\mathrm{t}) \quad (6)$$

where V_{oc} – open circuit voltage (V), I_{sc} – short circuit current (A) and $k_{DG}(t)$ PV module generation degradation coefficient over time.
The fill factor also depends on temperature and irradiance and is modeled as:

$$\mathrm{FF} = \mathrm{FF_n} \cdot [1 + \mathrm{K_{FF}} \cdot (\mathrm{T} - \mathrm{T_n})] \cdot \left[\mathrm{k_1} + \mathrm{k_2}\left(\frac{\mathrm{G}}{\mathrm{G_n}}\right) + \mathrm{k_{3ln}}\left(\frac{\mathrm{G}}{\mathrm{G_n}}\right)\right] \quad (7)$$

where FF_n is the fill factor at Standard Test Conditions (STC: 1000 W/m², 298.15 K), K_{FF} is the temperature coefficient of the fill factor (%/K or 1/K), k_1, k_2, k_3 are fill factor coefficients.
The PV module generation degradation over time is calculated by:

$$\mathrm{k_{DG}}(\mathrm{t}) = 1 - \mathrm{c_{DG}} \cdot \frac{\mathrm{h}}{8760} \quad (8)$$

where are c_{DG} – annual degradation factor and h time in hours.
In this baseline formulation (2)–(8), maximum power output for a given solar irradiance profile is calculated by varying irradiance G while fixing the PV cell temperature at its STC value (298.15 K) and degradation coefficient (in (6)) at value 1, irrespective of actual ambient temperature fluctuations.

Dynamic module operating temperature model

The baseline model presented in the previous subsection neglects the thermal impact on key PV parameters—primarily *FF*, V_{oc}, and I_{sc}—which directly govern P_{mpp}. To account for these effects, this subsection presents a dynamic thermal model that calculates the PV module temperature and incorporates its influence on model parameters.
A transient dynamic thermal differential equation is used to estimate the PV module temperature under varying irradiance and ambient temperature conditions:

$$C_{th}\frac{dT}{dt} = \alpha G S_m - (U_0 + U_1 v_w)(T - T_a)S_m - \eta_m \mathrm{G} S_m \quad (9)$$

where are C_{th} - effective thermal capacity of the PV module (J/K), α - absorption coefficient of the module surface, S_m – PV module area (m²), U_0 - constant heat loss coefficients (W/Km²), U_1 - wind-dependent heat loss coefficients (W/Km²), v_w - instantaneous wind speed (m/s), T_a - instantaneous ambient temperature (K), η_m - electrical efficiency of the module (accounting for heat removed as electricity).
Solving (9) yields the time-dependent PV module temperature $T(t)$ under fluctuating irradiance and ambient conditions. This calculated temperature is then used to update temperature-dependent quantities—including thermal voltage, photocurrent, open-circuit voltage, fill factor, and peak power (P_{mpp})—according to (2)–(8). When wind cooling is excluded from the model, v_w is set to zero in (9).

Dynamic soiling accumulation and cleaning model

The soiling effect reduces the solar irradiance reaching the PV module surface due to the gradual deposition of dust and particulate matter over time. An effective irradiance, G_{eff}, is calculated using a soiling reduction factor t_{soil}:

$$G_{\text{eff}} = \mathrm{G} \cdot \tau_{\text{soil}} \tag{10}$$

where is τ_{soil} – soiling reduction factor.
The daily degradation of the soiling reduction factor is modeled using a linear deposition relationship:

$$\tau_{\text{soil}}(t) = \tau_{\text{soil}}(0) - \mathrm{SDR} \cdot \tag{11}$$

where are t – time in days, $\tau_{\text{soil}}(0)$ – soiling reduction factor after cleaning event (by manual or natural cleaning) and SDR – daily Soiling Deposition Rate.
The soiling reduction factor following a cleaning event is modeled as:

$$\tau_{\text{soil}}(0) \ = \mathrm{X} \cdot \tau_{\text{soil}}(t-1) \tag{12}$$

where X<1 is random number by uniform distribution $\sim \mathcal{U}(a, b)$.
Finally, the effective irradiance G_{eff} replaces the raw irradiance G in the PV module equations (2)–(9) to integrate soiling losses into the overall energy production model.

SIMULATION SETUP AND RESULTS ANALYSIS

Simulation framework and input parameters

To evaluate the influence of environmental factors on energy yield predictions, a comparative analysis was conducted using the dynamic PV models described above. Simulations were performed over a 16-year period (2005–2020) using hourly solar irradiance and meteorological data retrieved from the Photovoltaic Geographic Information System (PVGIS) for Osijek, Croatia (45.5511° N, 18.6939° E).
Ten simulation configurations were designed to isolate individual physical effects across both fixed-tilt and dual-axis tracking systems, as detailed in Table 1. The baseline system comprises a 330 Wp monocrystalline silicon PV module. Table 2 summarizes the electrical, thermal, and mechanical parameters used in the simulations.

Table 1. *The compared cases of PV module models*

Model Case	PV module model considering:	Fixed or two-axes tracking PV module
Model 1_f	irradiance only (STC T=25°C, v_w = 0 m/s, no soiling, no degradation)	Fixed (tilt = 35°, south orientation)
Model 2_f	irradiance + module temperature (v_w = 0 m/s, no soiling, no degradation)	
Model 3_f	irradiance + module temperature + wind cooling (no soiling, no degradation)	
Model 4_f	irradiance + module temperature + wind cooling + dynamic soiling (no degradation)	
Model 5_f	irradiance + module temperature + wind cooling + dynamic soiling + degradation	
Model 1_t	irradiance only (STC T=25°C, v_w = 0 m/s, no soiling, no degradation)	Two axes tracking

Model 2_t	irradiance + module temperature (v_w = 0 m/s, no soiling, no degradation)	
Model 3_t	irradiance + module temperature + wind cooling (no soiling, no degradation)	
Model 4_t	irradiance + module temperature + wind cooling + dynamic soiling (no degradation)	
Model 5_t	irradiance + module temperature + wind cooling + dynamic soiling + degradation	

Table 2. *Input data used in simulations*

Data	Value
Reference Temperature (STC)	25.0 °C (298.15 K)
Reference Irradiance (STC)	1000.0 W/m
Open-Circuit Voltage (STC)	41.5 V
Short-Circuit Current (STC)	10.2 A
Fill Factor (STC)	0.785
Peak Power Output (STC)	331.15 W
Electrical Conversion Efficiency (STC)	0.1698 (16.98%)
Number of Cells in Series	60
Diode Ideality Factor	0.9605
Module Surface Area	1.95 m²
Module Thermal Capacity	25000.0 J/K
Solar Absorptivity Coefficient	0.90
Static Heat Transfer Coefficient	25.0 W/(m²·K)
Wind Heat Transfer Coefficient	1.2 W/(m²·K·(m/s))
Current Temperature Coefficient	+0.0045 A/K
Voltage Temperature Coefficient	-0.125 V/K
Fill Factor Temperature Coefficient	-0.0015 1/K
Fill Factor Coefficient 1	0.982
Fill Factor Coefficient 2	0.018
Fill Factor Coefficient 3	0.025
Soiling Deposition Rate	0.0015 / day (0.15% / day)
Scheduled Cleaning Days per Year	Days 90, 100, 115, 160, 200, 220, 280, 330, 350
Annual degradation factor	0.005 (0.5 %)

For scheduled maintenance, module cleaning efficiency on specified operational days is modeled as a uniformly distributed random variable within the range [0.5, 0.8].

Comparative performance and energy yield analysis

Table 3 summarizes the 16-year simulation results for the five fixed-tilt PV module configurations. Excluding degradation, soiling, and temperature impacts leads to an overestimation of annual energy yield by over 12 %. Each of these three environmental factors—temperature losses, dynamic soiling, and panel degradation—accounts for approximately a 4 % reduction in overall energy production. Conversely, neglecting wind cooling overestimates thermal losses, leading to an underestimation of energy production by more than 3 % (specifically around 3.3 %) compared to models that incorporate wind speed effects.

Table 4 details the performance metrics for the two-axis tracking system models. Applying simplified mathematical models to tracking systems introduces errors over 1 % higher than those observed in fixed-tilt configurations. This indicates that comprehensive thermal and environmental modeling is even more critical when predicting energy yield for tracking PV

plants. Across all evaluated mathematical models, two-axis tracking systems produce approximately 40 % more energy than fixed-tilt systems.

Table 3. *Energy production comparison for fixed PV module*

Model Case	Total Generation (16 yrs)	Average Annual Yield	Difference vs. Baseline [%]
Model 1_f	7520.0 kWh	470.0 kWh/yr	0.00 %
Model 2_f	6918.4 kWh	432.4 kWh/yr	-8.00 %
Model 3_f	7160.0 kWh	447.5 kWh/yr	-4.79 %
Model 4_f	6852.0 kWh	428.3 kWh/yr	-8.88 %
Model 5_f	6584.0 kWh	411.5 kWh/yr	-12.45 %

Table 4. *Energy production comparison for two-axis tracking PV module*

Model Case	Total Generation (16 yrs)	Average Annual Yield	Difference vs. Baseline [%]
Model 1_t	10678.4 kWh	667.4 kWh/yr	0.00 %
Model 2_t	9685.8 kWh	605.4 kWh/yr	-9.30 %
Model 3_t	10024.0 kWh	626.5 kWh/yr	-6.13 %
Model 4_t	9592.8 kWh	599.6 kWh/yr	-10.17 %
Model 5_t	9217.6 kWh	576.1 kWh/yr	-13.68 %

Table 5. *Comparison of fixed vs two-axis tracking PV module*

Model Case	Fixed PV module Total Generation	Fixed Average Yield	Tracker PV module Total Generation	Tracker Average Yield	Tracking Yield Gain
Model 1: STC Temperature constant-Baseline	7520.0 kWh	470.0 kWh/yr	10678.4 kWh	667.4 kWh/yr	+42.00 %
Model 2: Thermal model without wind cooling	6918.4 kWh	432.4 kWh/yr	9685.8 kWh	605.4 kWh/yr	+40.00 %
Model 3: Thermal model with wind cooling	7160.0 kWh	447.5 kWh/yr	10024.0 kWh	626.5 kWh/yr	+40.00 %
Model 4: Thermal model with wind cooling and soiling	6852.0 kWh	428.3 kWh/yr	9592.8 kWh	599.6 kWh/yr	+40.00 %
Model 5: Thermal model with wind cooling, soiling and module degradation	6584.0 kWh	411.5 kWh/yr	9217.6 kWh	576.1 kWh/yr	+40.00 %

Although models incorporating full environmental dynamics (Models 4 and 5) provide the most accurate forecasts, their precision relies heavily on the availability and quality of meteorological data, particularly ambient temperature, wind speed, and local soiling profiles. Figure 2 illustrates the module temperature differential between models with and without wind cooling, which directly accounts for the 3.3 % discrepancy in energy yield shown in Tables 3 and 4.
Figure 3 compares annual production between fixed-tilt and two-axis tracking systems using Model 5 across the first and final years of the 16-year simulation period.

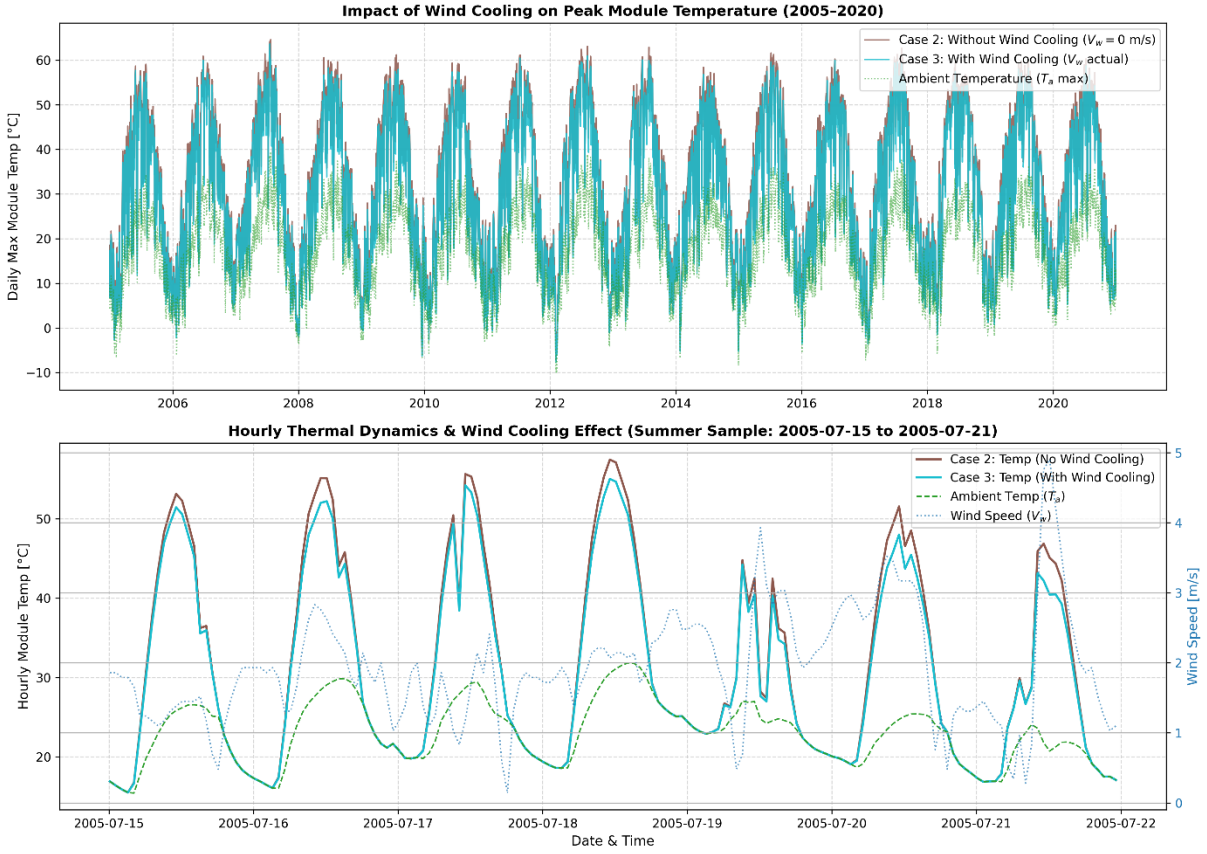


Fig. 2. *PV module temperature profiles calculated according to models 2 and 3 for fixed PV module*

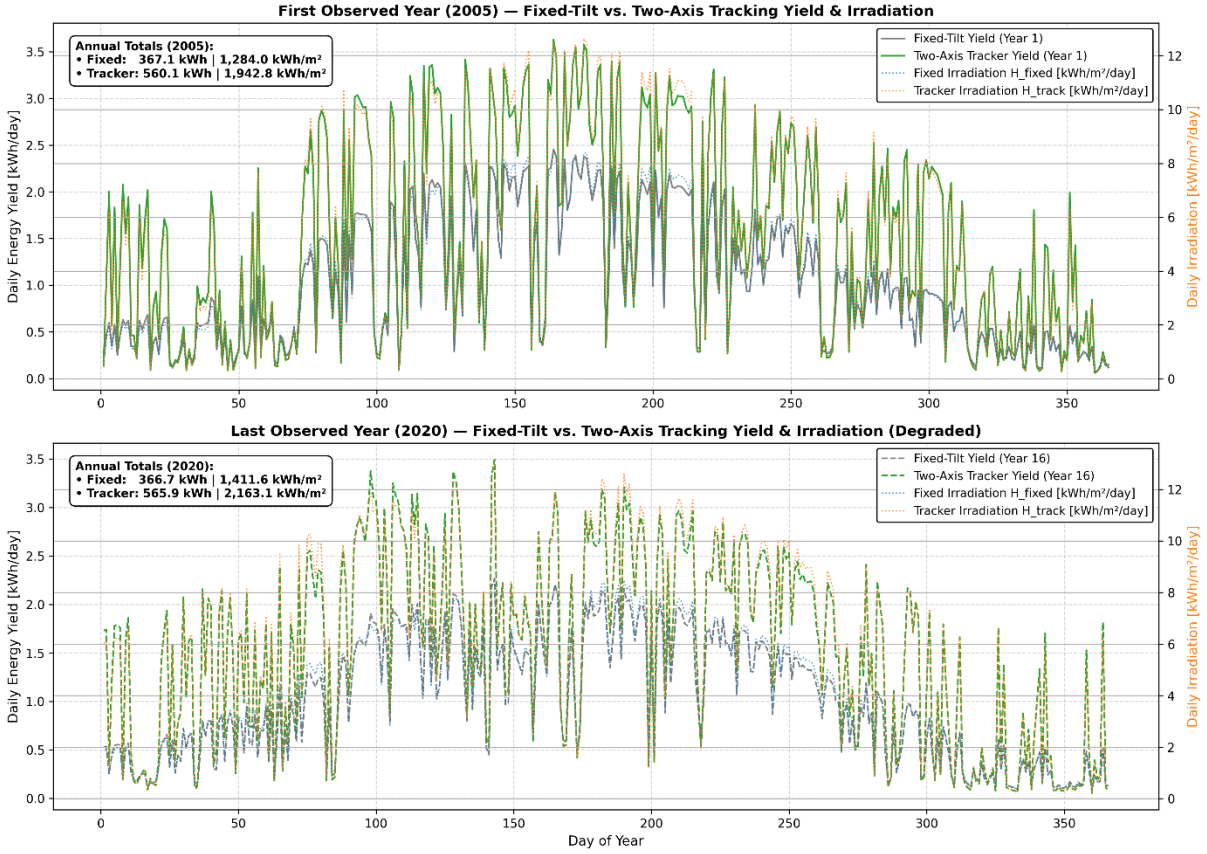


Fig. 3. *Profile of soiling reduction factor including cleaning events used in the energy calculations*

Notably, this comparison reveals that interannual increases in solar irradiance can temporarily offset long-term module degradation, resulting in higher overall energy output in the final year than in the first. Finally, while scheduled cleaning events were modeled probabilistically (as detailed in Table 2) to approximate real-world maintenance, unpredictable natural cleaning cycles from rainfall introduce additional variability that remains difficult to model over multi-year horizons.

CONCLUSION

This study evaluated the impact of incorporating thermal dynamics, wind cooling, dynamic soiling, and module degradation into mathematical models for predicting PV energy generation. Based on a 16-year simulation comparing fixed-tilt and two-axis tracking monocrystalline PV modules, several key findings emerge:

- **Yield Overestimation:** Relying strictly on STC irradiance-based models causes an overestimation of annual energy production exceeding 12%. Operating temperature, dynamic soiling, and module degradation each account for approximately 4% of energy losses.
- **Thermal Mitigation via Wind:** Incorporating wind speed mitigates predicted thermal losses, preventing an underestimation of energy production by roughly 3.3%.
- **Tracking Sensitivity:** Two-axis tracking systems generate ~40% more energy than fixed-tilt installations but exhibit ~1% higher sensitivity to mathematical modeling simplified errors, making accurate environmental modeling particularly vital for tracking plants.
- **Interannual Irradiance Effects:** Multi-year simulations reveal that interannual increases in solar irradiance can temporarily mask long-term module degradation, resulting in higher net output in later operational years despite ongoing panel aging.

Incorporating ambient temperature, wind velocity, soiling, and degradation into PV modeling significantly improves forecasting accuracy during the engineering design phase. Future research should focus on refining predictive models for stochastic natural cleaning events (e.g., rainfall) and local microclimate fluctuations.

REFERENCES

Alaas, Z. M. (2024). The Effects of Temperature on Photovoltaic and Different Mitigation Techniques: A Review. *IEEE Access, 12,* 180309-180327. https://doi.org/10.1109/ACCESS.2024.3504009

Bamisile, O., Acen, C., Cai, D., Huang, Q., & Staffell, I. (2025). The environmental factors affecting solar photovoltaic output, *Renewable and Sustainable Energy Reviews, 208*, 115073. https://doi.org/10.1016/j.rser.2024.

Chegaar, M., Bensalem, S. E., Herguth, A., & Aillerie, M. (2010). Temperature dependence of polycrystalline silicon solar cells parameters, World Renewable Energy Congress XI 25-30 September 2010, Abu Dhabi.

Nayak, A. V., & Brar, T. S. (2026). Impact of Temperature on Power Generation of Solar Photovoltaic Panels. *Journal of the Indian institute of architects, 91, (3)*, 17-22.

Dubey, S., Sarvaiya, J. N., & Seshadri, B. (2013). Temperature Dependent Photovoltaic (PV) Efficiency and Its Effect on PV Production in the World A Review. *Energy Procedia, 33*, 311 – 321.

Zhao, W., Hu, S., & Dong, Z. (2025). Impact of Multiple Factors on Temperature Distribution and Output Performance in Dusty Photovoltaic Modules, *Energies, 18,* 3411. https://doi.org/10.3390/en18133411.

DOI:10.5937/IIZS26177L

IMPACT OF PHOTOVOLTAIC GENERATION SUBSTITUTION OF CONVENTIONAL GENERATION ON ROTOR ANGLE STABILITY OF BULK POWER SYSTEM

Research paper

Patrik Lučinger[1],Predrag Marić[2*], Ružica Kljajić[3],
[1,2,3]Josip Juraj Strossmayer University of Osijek, Faculty of Electrical Engineering, Computer Science and Information Technology Osijek, Osijek, Croatia

Abstract: This paper investigates the impact of substituting part of the conventional generation in a bulk power system with large-scale photovoltaic (PV) generation on rotor angle stability. Three simulation scenarios are considered: a base case used to determine the critical fault clearing time for a three-phase short circuit on a selected transmission line for all conventional generators, and two cases in which PV generation replaces part of the conventional generation under different PV generation dispatch control modes. The electromechanical response of the synchronous generators is analyzed based on rotor speed and relative rotor-angle oscillations, as well as eigenvalue analysis. The results show that substituting conventional generation with PV generation can have opposite effects on transient and small-signal stability.
Keywords: large-scale photovoltaic generation, bulk system, rotor angle stability, critical fault clearing time

INTRODUCTION

The increasing integration of renewable energy sources (RES) and the reduction in conventional fossil-fuel generation are now common practice in power systems worldwide, aiming to reduce CO_2 emissions. A large share of RES, including PV generation, is connected to the grid via inverter interfaces. By the end of 2024, global installed PV capacity had reached approximately1,865 GW, with more than 452 GW of new capacity added during 2024 alone. PV therefore accounted for more than three-quarters of all newly installed renewable power capacity in 2024 (IRENA, 2025). In 2024, global PV generation increased by approximately 480 TWh, making PV the largest contributor to the growth of global electricity generation among all generation technologies (IEA, 2025). The reduction in conventional synchronous generation and the increasing share of converter-interfaced generation can influence electromechanical oscillations and their damping characteristics (Shah et al., 2013; Busarello & Musca, 2020; Rezaei et al., 2022). The impact of PV inverters on power system oscillatory stability has therefore become an important research topic (Nikolaev et al., 2021). PV integration can also affect transient stability by changing power flows, operating conditions, and the contribution of conventional synchronous generators. The influence of PV penetration and its location on transient stability has been investigated using critical fault-clearing time as an indicator of system stability (Kamel et al., 2024; Sampath Kumar et al., 2020; Rezaei et al., 2022). This paper demonstrates the impact of large-scale PV substitution of conventional generation on critical fault-clearing time and small-signal stability of a bulk power system based on relative rotor angle, generator speed and modal analysis following a three-phase short-circuit disturbance. The largest synchronous generator (which also has the largest inertia) has been replaced with large-scale PV converter-interfaced generation in simulation scenarios with different dispatch control of reactive power and voltage regulation of large-scale PV.

[1]patrik.lucinger@student.ferit.hr
[2] Corresponding author, predrag.maric@ferit.hr
[3] ruzica.kljajic@ferit.hr

MATERIAL AND METHODS

The paper deals with calculations and simulations of power system stability. The conventional classification of power system stability includes rotor angle stability, voltage stability, and frequency stability, as shown in Fig. 1 (Kundur, 1994).

The rotor dynamics of a synchronous generator can be described by the swing equation, which relates the changes in rotor speed and rotor angle to the difference between mechanical and electrical power. In its simplified form, the swing equation can be expressed as:

$$\frac{d^2\delta}{dt^2} = \frac{\omega_0}{2H}(P_m - P_e) \tag{1}$$

where *H* is the generator inertia constant, $P_m$is the mechanical input power, P_e is the electrical output power, and ω_0 is the synchronous angular speed. The equation indicates that a higher inertia value slows down the change in rotor speed during a disturbance (Kundur, 1994).When the mechanical power $P_m$of the generator is greater than the electric output power P_e, the generator accelerates and determines the acceleration areaA_1defined using Eq. (2), (Kundur, 1994)

$$A_1 = \int_{\delta_1}^{\delta_c} P_m d\delta \tag{2}$$

where δ_c is the critical clearing angle, δ_1 is the angle before the disturbance. Generator decelerates when the mechanical power $P_m$of the generator is lower than the electric output power P_e, and determines the decelerating area A_2defined using Eq. (3)

$$A_2 = \int_{\delta_c}^{\pi-\delta_1} (P_e(\delta) - P_m)d\delta \tag{3}$$

where $\pi - \delta_1$is the maximum allowed swing angle. Equal area criterion states that generator will remain in synchronism if acceleration and decelerating areas are equal, $A_1 = A_2$. By solving this equation, critical clearing angle can be calculated using Eq. (4)

$$\delta_c = \frac{\omega_0}{4H} P_m t_c^2 + \delta_1 \tag{4}$$

where t_c is the critical clearing time.

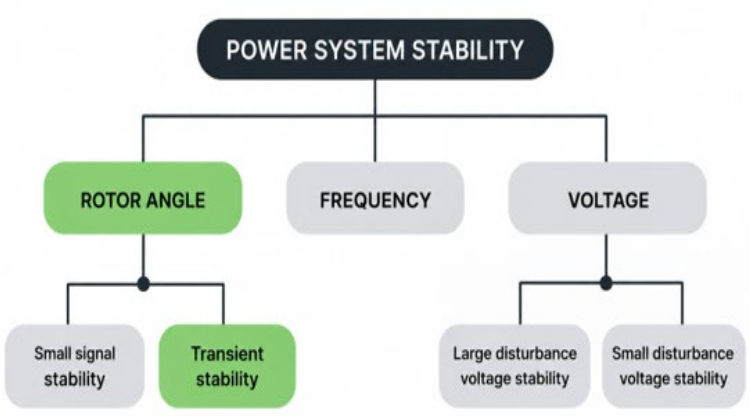


Fig. 1. *Classification of power system stability (Kundur, 1994)*

The simulations were performed using DIgSILENT PowerFactory 2025 on the IEEE 14-bus test system. In the first case, a power flow analysis was carried out on the original IEEE 14-bus system to determine the transmission line to be subjected to the subsequent short-circuit disturbance. To obtain unfavorable conditions for transient stability, line 0002_0003 was selected as the most heavily loaded line with a single connection configuration (instead of a

parallel configuration), based on the criterion of connecting two nodes with synchronous generators. A three-phase short-circuit fault was simulated at 50% of the line length. After replacing synchronous generator 1, which is the largest generator in the system and has the highest inertia, with a large-scale PV system, the generator connected to bus 2 becomes the reference machine. The subsequent cases consider different reactive power operating conditions of the large-scale PV plant in order to evaluate the influence on transient and small-signal stability.

Initial simulationscenario

A three-phase short-circuit was simulated at time *t* = 0,1 s at the midpoint of line 0002_0003. Relative rotor angle changes were observed for all synchronous generators in the system (Fig. 2), while the critical fault clearing time was determined according to the rotor angle of generator 3 (greeen line), which first reached the maximum rotor angle according to the equal-area criterion (-120.4°) (Fig. 2) during the 1,5 s simulation. The critical fault clearing time is 500 ms.

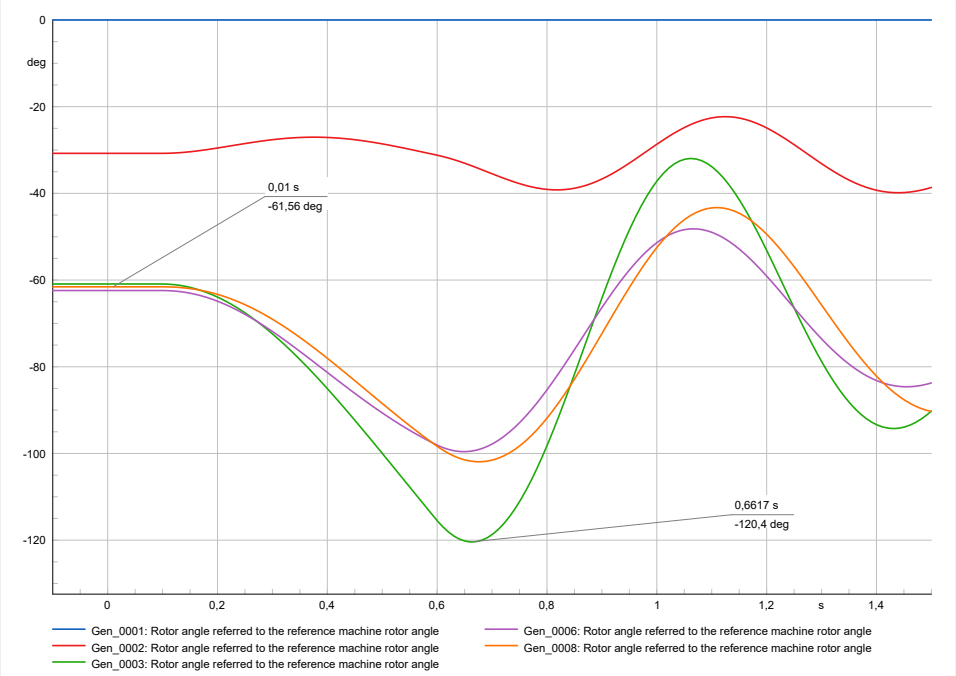


Fig. 2. *Relative rotor angles (with reference-to-reference machine) during simulation of 1,5 s*

The speeds of all synchronous generators during simulation are shown in Fig. 3, which highlights the highest speed amplitudes on generator 3 (green line). Modal analysis resulted in a total of 40 modes (eigenvalues), all located on the left side of the s-plane, indicating stable dynamic behaviour of the system. Table 1lists the first 12 modes; the dominant oscillatory modes are 00002 and 00003.

Table 1. *Eigenvalues for initial simulation scenario*

Name	Real part (1/s)	Imaginary part (rad/s)
Mode 00001	-0,081809871	0
Mode 00002	-0,134212183	0,032768836
Mode 00003	-0,134212183	-0,032768836
Mode 00004	-0,173178220	0
Mode 00005	-0,182320023	0
Mode 00006	-0,201160438	0
Mode 00007	-0,227831694	0

Mode 00008	-0,511127652	8,636216025
Mode 00009	-0,511127652	-8,636216025
Mode 00010	-0,549579886	0
Mode 00011	-0,692175668	0
Mode 00012	-0,777624472	0

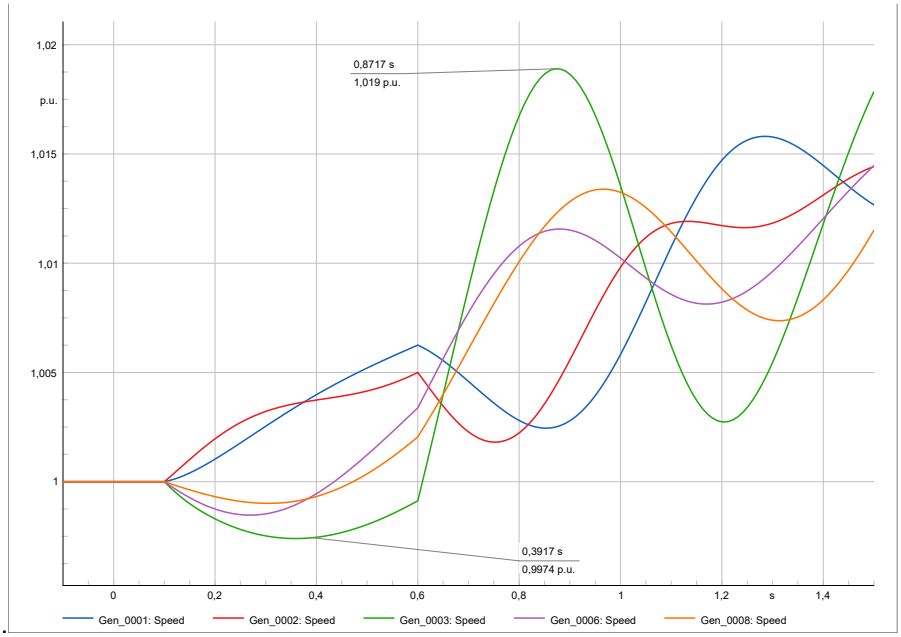


Fig. 3. *Generator speedsduring simulation of 1,5 s*

Simulation scenario 1

Synchronous generator 1 is disconnected from the system and its active power generation is replaced by the large-scale PV power connected to bus 1 (Fig. 4), without PV reactive power dispatch. Following the disconnection of synchronous generator 1, generator 2 becomes the reference machine. As in the previous scenario, a three-phase short-circuit has been simulated at time t = 0,1 s at the midpoint of line 0002_0003. Relative rotor angle changes were observed for all synchronous generators in the system (Fig. 5). The critical fault clearing time was determined, as in the previous scenario, from the rotor angle of generator 3 (green line in Fig. 5) during the 1,5 s simulation. The critical fault clearing time did not change from the previous scenario and remained 500 ms.

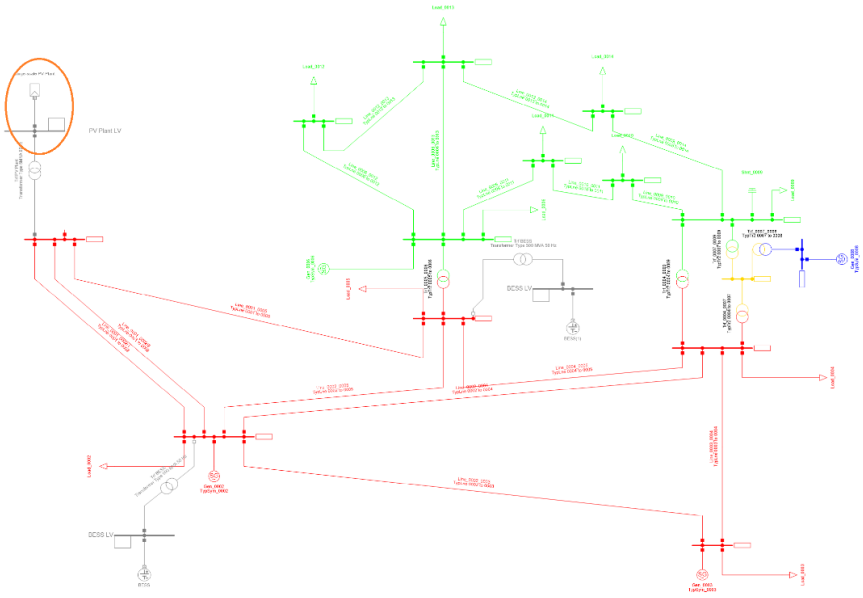


Fig. 4. *IEEE 14-bus system single-line diagram with large-scale PV connection to bus 1 (circled in the figure)*

The relative rotor angle of synchronous generator 2 remained constant during the simulation, since generator 2 is now the new reference machine in the system.

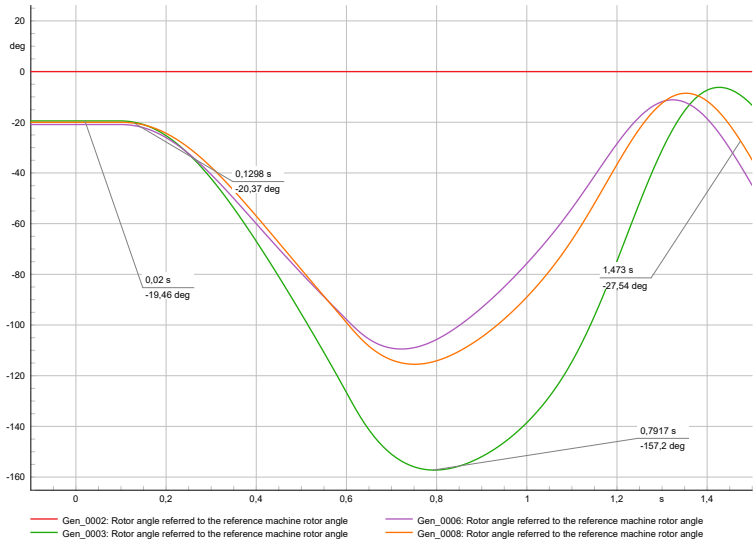


Fig. 5. *Relative rotor angles (with reference- to- reference machine) during simulation of 1,5 s*

However, the rotor speed response shown in Fig. 6 indicates a slight increase in the speed amplitude of generator 3. Although replacing synchronous generator 1 with large-scale PV does not improve the critical fault clearing time for the disturbance considered, it slightly worsens the speed magnitude.

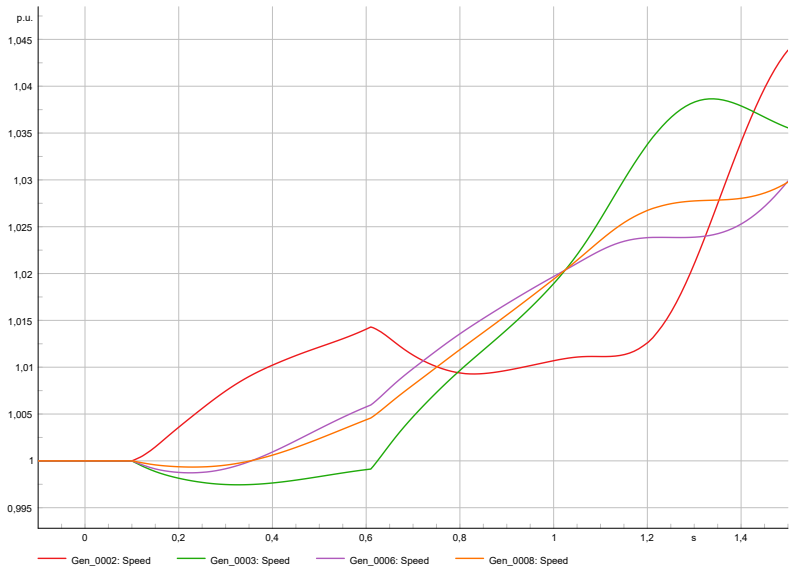


Fig. 6. *Generator speeds during simulation of 1,5 s*

Modal analysis results for the first 12 modes are presented in Table 2. Large-scale PV substitution of the largest synchronous generator in the system resulted in the appearance of an unstable monotonic mode, Mode 00001, with a positive real part of 0,0340 1/s. The dominant oscillatory mode(s) (Mode 00002 and Mode 00003) have also been shifted to the left in the s-plane.
Although replacing the largest synchronous generator in the system with large-scale PV did not affect the critical fault clearing time, it negatively affected the electromechanical response of the system.

Table 2. *Eigenvalues for simulation scenario 1*

Name	Real part (1/s)	Imaginary part (rad/s)
Mode 00001	0,034021038	0
Mode 00002	-0,052010729	0,038470748
Mode 00003	-0,052010729	-0,038470748
Mode 00004	-0,146844804	6,9144E-08
Mode 00005	-0,146844804	-6,9144E-08
Mode 00006	-0,225635412	0
Mode 00007	-0,353753649	0
Mode 00008	-0,469219267	0
Mode 00009	-0,528650650	7,06215722
Mode 00010	-0,528650650	-7,06215722
Mode 00011	-0,621837386	6,310633064
Mode 00012	-0,621837386	-6,310633064

Simulation scenario 2

The large-scale PV is now operated with a reactive power output of 16 Mvar, maintaining the voltage on its busbar at 1,06 p.u., while generator 2 remains the reference machine. The addition of PV reactive power dispatch influences the critical fault-clearing time which has increased from 500 ms to 540 ms (Fig. 7), while the amplitudes of generator speeds have slightly decreased compared with the previous simulation case (Fig.8). Both oscillograms indicate a slight improvement in transient stability.
Modal analysis for the first 12 modes (Table 3) still shows an unstable monotonic mode, Mode 0001, which is now closer to the stability margin: −0,013650664 vs −0,034021038 in

the previous simulation case, but it remains unstable. The dominant oscillatory mode(s) present in the two previous simulation cases have disappeared, or the assumptioncan be that they have been completely compensated by reactive power dispatch at large-scale PV.

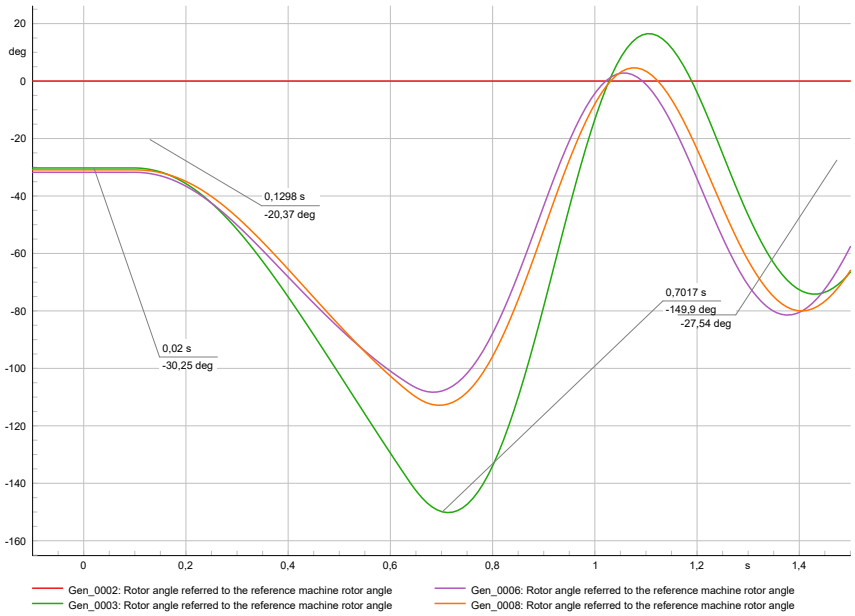


Fig.7. *Relative rotor angles (with reference to reference machine) during simulation of 1,5 s*

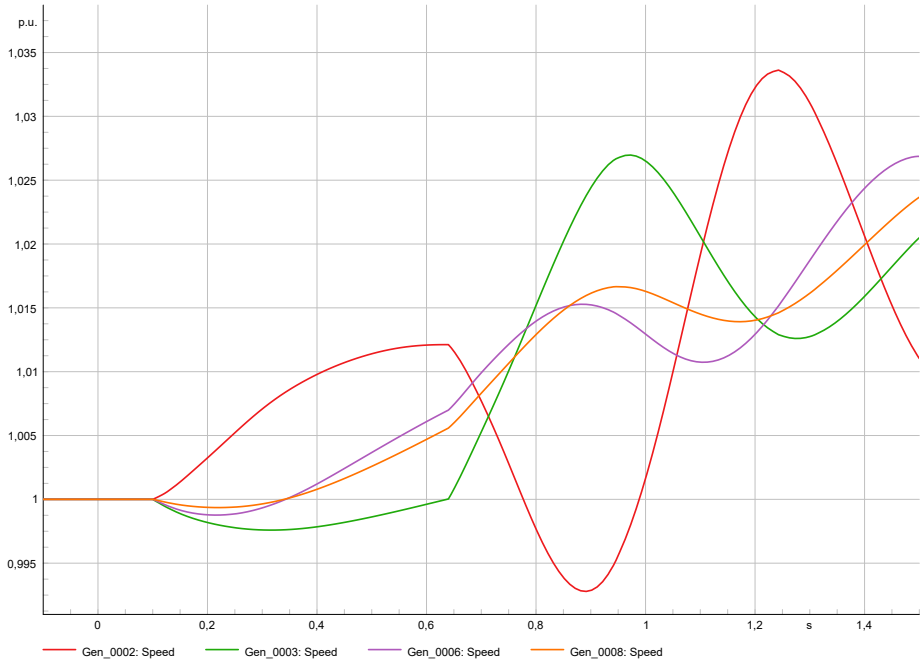


Fig. 8. *Generator speeds during simulation of 1,5 s*

Table 3. *Eigenvalues for simulation scenario 2*

Name	Real part (1/s)	Imaginary part (rad/s)
Mode 00001	0,013650664	0
Mode 00002	-0,089274483	0
Mode 00003	-0,115189082	0
Mode 00004	-0,146844804	6,9144E-08
Mode 00005	-0,146844804	-6,9144E-08
Mode 00006	-0,185270974	0

Mode 00007	-0,190845971	0
Mode 00008	-0,370681984	0
Mode 00009	-0,528851313	7,422196861
Mode 00010	-0,528851313	-7,422196861
Mode 00011	-0,642614512	0
Mode 00012	-0,706143848	8,129146415

RESULTS AND DISCUSSION

In the base study case, the critical clearing time of 500 ms in the IEEE 14-bus system was determined according to generator 3, since its relative rotor angle was the first to reach the transient stability margin during the three-phase short-circuit on line 0002_0003. The modal analysis covers all stable modes of the system. Substituting the largest generator in the system with the large-scale PV did not change the critical fault clearing time, but it worsened small-signal stability, with the appearance of an unstable monotonic mode and increased magnitudes of generator speed oscillations during and after the disturbance.
Introducing a large-scale PV reactive power output of 16 Mvar, while maintaining the voltage on the PV busbars at 1,06 p.u., corresponding to the dispatch of generator 1 (which was substituted by the large-scale PV), improved the critical fault clearing time from 500 to 540 ms, reduced the magnitudes of generator speed oscillations and completely compensated the dominant oscillatory mode(s), but did not compensate the monotonic mode (although it improved it by shifting it to the left side of the s-plane), which appeared when the largest synchronous generator in the system was replaced by the large-scale PV.

CONCLUSION

The analysis shows that the integration of PV generation changes both the transient and small-signal characteristics of the IEEE 14-bus system. Replacing generator 1 with large-scale PV generation did not change the critical clearing time of the system, but worsened the small-signal stability indices, which can also be seen in the time domain as an increase in the magnitude of speed oscillations of all generators during and after the initiated disturbance.
The addition of 16 Mvar of reactive power, while maintaining the voltage at 1,06 p.u. at the large-scale PV, produced a more favourable transient response, increasing the critical fault clearing time from 500 ms to 540 ms. Although the dominant oscillatory mode(s) have been completely compensated by the large-scale PV substitution for the largest synchronous generator in the system, the appearance of a monotonic unstable mode requires further study to determine whether such a replacement is recommended in practice, despite green policies promoting increased RES integration.

REFERENCES

Busarello, L., & Musca, R. (2020). Impact of the high share of converter-interfaced generation on electromechanical oscillations in Continental Europe power system. *IET Renewable Power Generation*, 14(19), 3918–3926. https://doi.org/10.1049/iet-rpg.2020.0489

International Energy Agency. (2025). Global energy review 2025. IEA. https://www.iea.org/reports/global-energy-review-2025

International Renewable Energy Agency. (2025). Renewable capacity statistics 2025. IRENA. https://www.irena.org/Publications/2025/Mar/Renewable-capacity-statistics-2025

Kamel, R. M., Alanzi, S. S., & Al Hashemi, Y. M. (2024.). Effect of photovoltaic penetration level and location on power system transient stability during symmetrical and unsymmetrical faults. *Sustainable Energy, Grids and Networks*, 38, 101322. https://doi.org/10.1016/j.segan.2024.101322

Kundur, P. (1994). Power system stability and control. McGraw-Hill.

Nikolaev, N., Dimitrov, K., & Rangelov, Y. (2021.). A comprehensive review of small-signal stability and power oscillation damping through photovoltaic inverters. *Energies*, 14(21), 7372. https://doi.org/10.3390/en14217372

Rezaei, J., Golshan, M. E. H., & Alhelou, H. H. (2022.). Impacts of integration of very large-scale photovoltaic power plants on rotor angle and frequency stability of power system. *IET Renewable Power Generation*, 16(11), 2384–2401. https://doi.org/10.1049/rpg2.12529

Sampath Kumar, D., Gandhi, O., Rodríguez-Gallegos, C. D., Srinivasan, D. (2020.). Review of power system impacts at high PV penetration Part II: Potential solutions and the way forward.*Solar Energy*,(210), 202-221, https://doi.org/10.1016/j.solener.2020.08.047.

Shah, R., Mithulananthan, N., Bansal, R.C. (2013.) Oscillatory stability analysis with high penetrations of large-scale photovoltaic generation. *Energy Conversion and Management*, (65), 420-429, https://doi.org/10.1016/j.enconman.2012.08.004.

DOI:10.5937/IIZS26186S

CONTROL OF WASTEWATER TREATMENT AND NEUTRALIZATION IN A MINERAL WOOL PRODUCTION PLANT

Research paper

Stanko P. Stankov[1]
[1]University of Niš, Faculty of Electronic Engineering, Niš, Serbia

Abstract: The paper discusses the automatic control system for the wastewater neutralization process in a mineral wool production plant with a capacity of 50,000 t/year. The neutralization process takes place in an equalization tank with an effective volume of 175 m^3, which, due to the specific technological procedure, is exposed to continuous changes in solution composition and occasional sharp basic and acidic disturbances. Considering the pronounced nonlinearity of the pH process around the neutral point (pH = 7.0), a comparative analysis of the dynamic response and operational stability of the final control elements was performed using two advanced methods: the classical Gain Scheduling PID controller and the Continuously Nonlinear Adaptive PID controller. Simulation results show that both approaches satisfy the process control accuracy criteria. However, by defining industrial pump response speed limitations (Rate Limiter), it is proven that the adaptive controller exhibits a significantly higher degree of robustness, eliminating the undesirable phenomenon of pump "chattering", thereby drastically reducing mechanical equipment wear and optimizing reagent consumption.
Keywords: pH value, gain scheduling, adaptive PID, robustness

INTRODUCTION

A single-line plant, whose technological scheme is shown in Fig. 1, achieves 120–170 t/day of mineral wool in a three-shift, continuous operation mode (24 h/day). The cupola furnace with a capacity of 5–7 t/h melts raw materials (basalt, diabase, dolomite), (Stankov, 2012).

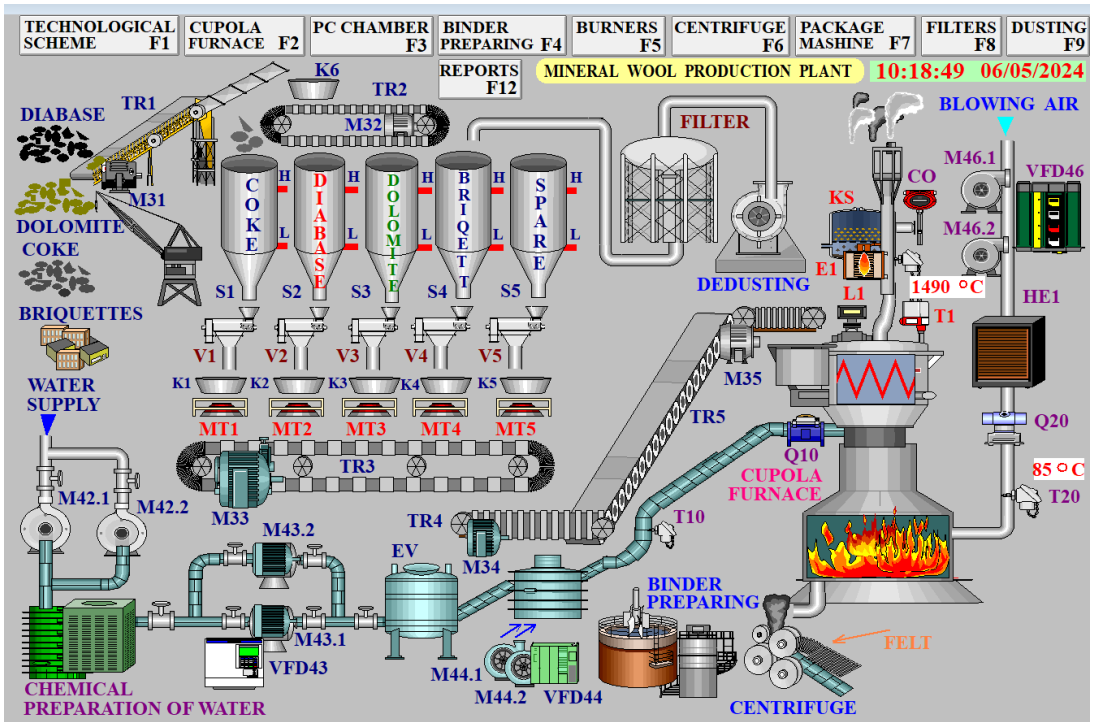


Fig. 1 *Technological process diagram of the mineral wool production plant*

A stable melt is formed after initial heating (2–4 h) and stabilization of the coke bed (2–4 h) at temperatures of 1300–1500 °C. The melt is discharged onto centrifuge wheels with the

[1]corresponding author,stanko.stankov@elfak.ni.ac.rs, ORCID: *0009-0002-4264-3111*

injection of a binder (phenol-formaldehyde resin), thereby producing a mat. Subsequently, mineral wool is formed through a polymerization process in a polycondensation chamber (PCC) and cut with saws (Stankov, 2013). With a water consumption of 0.5 to 2 m^3/t of product, 0.3–1.5 m^3 of wastewater is generated per ton, amounting to approximately 150–220 m^3/day (in practice, around 160 m^3/day). Wastewater originates from flue gas scrubbing scrubbers, fiber washing and transport systems, process condensates from the PCC, and cooling systems. The wastewater is characterized by an elevated temperature (30–50 °C) and variable composition (Stankov, 2024). Toxic substances are also present:
- suspended solids: 200–2000 mg/L (typically 800 mg/L) – fine mineral fibers, dust, and rock particles,
- toxic organic substances: phenols (1–50 mg/L) and formaldehyde (1–100 mg/L) originating from the binder,
- mineral oils and lubricants: 10–200 mg/L, alongside low concentrations of heavy metals (Al, Fe, Mn) from raw materials.
Chemical oxygen demand (COD) is ~500–5000 mg O_2/L, while biological oxygen demand (BOD) is ~100–1500 mg O_2/L. The pH value ranges from 6.5 to 9. Thanks to the treatment plant, 50–70% of the treated water (75–105 m^3/day) is returned to the gas washing, cooling, and transport systems. More efficient treatment directly ensures a higher percentage of recirculation, lower fresh water consumption, and minimal discharge into the environment.
The aim of this paper is the design and comparative analysis of advanced automatic control strategies for the wastewater pH neutralization process in a mineral wool production plant, with a special emphasis on ensuring high system stability and robustness under conditions of pronounced process nonlinearity and the presence of realistic operational disturbances. In this regard, the implementation of control algorithms for two advanced control strategies is considered:
- Gain Scheduling PID controller based on discrete error zones, and
- Continuously Nonlinear Adaptive PID controller based on smooth mathematical functions (Åström, Wittenmark, B. 2008; Visioli, A. 2006).
A simulation of system behavior was performed in MATLAB under realistic industrial environment conditions, including shock disturbances such as phenol resin breakthroughs, acid shocks from the furnace, and high-frequency noise on the sensor. Performance evaluation of pumps and mixers was carried out using a Rate Limiter and VFD regulation to prevent mechanical damage, wear, and undesirable intermittent operation (the chattering effect) of the final control elements. By comparing the efficiency of both approaches using standard integral control quality criteria IAE, ISE, ITAE, and trend analysis, the optimal technical solution for industrial application was determined (Shinskey, 1996).

CONFIGURATION OF THE NEUTRALIZATION SYSTEM AND FUNCTIONALITY MATERIAL AND METHODS

For this quantity of wastewater, given the presence of phenols, formaldehyde, fibers, and oils, a combined physicochemical and biological treatment with partial recirculation was applied (block diagram shown in Fig. 2). The wastewater treatment plant performs the following operations:
- mechanical treatment during which coarse and fibrous particles are removed using coarse screens and settling basins (sand filters).
- equalization of flow, temperature, and composition of the water. This process is carried out in an equalization basin (tank).
- coagulation and flocculation, using ferric chloride (FeC_3) lor aluminum sulfate ($Al_2(SO4)_3$) as a coagulant, and a polyelectrolyte as a flocculant. This procedure agglomerates particles, removes suspended solids and a portion of phenols absorbed by the flocs, and reduces COD.
- sedimentation, where oils, fats, and fine particles that are difficult to settle are removed.

- biological treatment, which is necessary in this case due to the presence of phenols and formaldehyde in the wastewater composition. The process takes place in an aeration basin and a secondary clarifier.

The continuous neutralization process over 24 hours (three-shift operation) takes place in a tank with a base volume of 150 m^3 increased by a 10–20% safety margin for foam and sludge, totaling 175 m^3 (vertical cylindrical tank, 8 m in diameter and 3.5 m in height). The treatment cycle consists of collection and equalization (24h), treatment/purification (8–18h), sedimentation and decantation (2–4h), and discharging (2–3h).

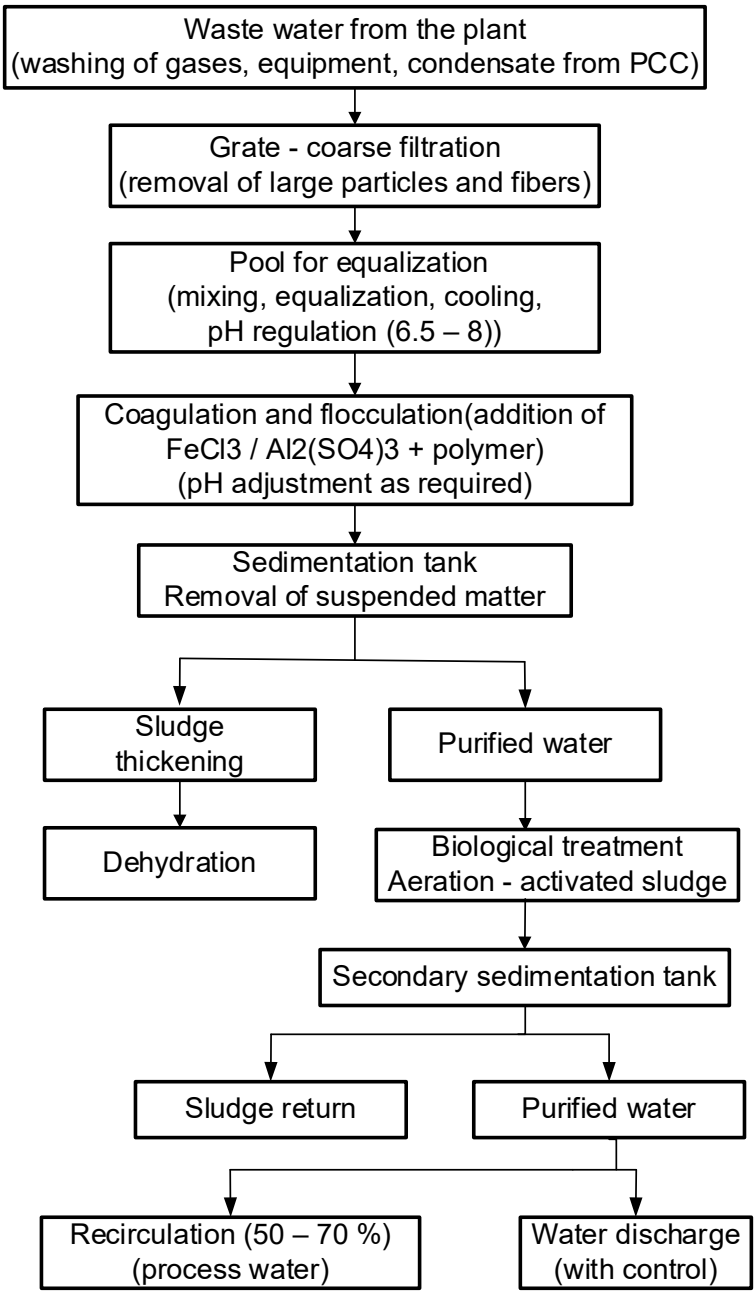


Fig. 2. *Block diagram of the wastewater treatment system in the mineral wool production plant*

Two tanks (or a dual-chamber system) are used-while the first is in the treatment and discharge cycle, the second accepts incoming wastewater. Due to the shallow and wide geometry (H/D≈0.875), 4 vertical baffles with a width of ∼1/12 of the diameter are installed every 90° to prevent rigid-body fluid rotation and the formation of a central vortex that draws in air. The mixer is a low-speed axial-turbine impeller with a diameter of 2.5–2.7 m positioned

very low (30–40 cm from the bottom) to ensure "top-to-bottom" circulation and enable mixing until the very end of discharge. For a specific power of 0.045 kW/m^3 (increased due to sticky mineral wool resins) and a volume of 175 m^3, the shaft power is ~6.75 kW.
Taking into account reserves and transmission losses, the power of the asynchronous motor with VFD is 11 kW, and the speed is 1450 rpm. The reducer is a coaxial gear reducer with a gear ratio of i≈40–45. It provides an impeller output speed of 30 to 40 rpm with a huge torque. The VFD provides an acceleration ramp (30–60 s) to eliminate mechanical shocks and protect against accumulated resin sludge. It enables dynamic speed changes (lower speeds at low levels to suppress foam, higher speeds during homogenization). Direct placement of the pH probe into the tank leads to its drying during discharge, damage to the glass membrane, and coating of the probe with resin. This effect is overcome by using an external measuring chamber. A small circulation pump takes a sample from the tank and passes it through the chamber with the sensor, while solenoid valves close the inflow and protect the probe from drying out when the main tank is empty. Wastewater from mineral wool production has an initial pH of 6.5 to 9. To neutralize 175 m^3 of water with a pH of 9 to the target pH of 7, a minimal amount of concentrated acid (e.g., 98% HCl) is required. Even in the worst-case scenario of accidental pollution, reagent consumption rarely exceeds 50–100 ml/m^3. For the treatment of the entire 175 m^3 batch, the total volume of acid/base will be a maximum of about 10–20 L per cycle. At this flow rate and an operating pressure of about 1–2 bar, the real motor power of the dosing peristaltic or diaphragm pump ranges from 0.05 to 0.18 kW (Corriou, 2018; Stankov, 2024).

NEUTRALIZATION PROCESS MODEL

Controlling wastewater pH in the process industry represents a highly nonlinear engineering problem due to the logarithmic dependence of hydrogen ion concentration. In the specific plant, round-the-clock production generates wastewater laden with toxic phenol-formaldehyde resins, surfactants, and fine mineral fibers, with an initial pH range of 6.5 to 9. To stabilize the process and prepare the water for the coagulation and flocculation stage, a vertical cylindrical tank with a shallow geometry (height 3.5 m, diameter 8 m, total working volume V=175 m^3) with four symmetrically placed baffles every 90° was applied. For solution homogenization, a centrally positioned low-speed axial-turbine mixer driven by an 11 kW asynchronous motor via a VFD and a coaxial reducer is installed, with operating speeds ranging from 20 to 45 rpm, thereby preventing foam formation caused by the presence of resins. The homogenization time constant is T_{mixing}=45 min (0.75 h), which introduces significant process inertia. The dynamics of hydrogen ion indicator change (dpH/dt) within the controlled plant are defined by the modified mass balance equation of ions in the flow:

$$\frac{dpH}{dt} = \frac{1}{\tau_{mix}} pH_{in}(t) - pH(t) + f(pH(Q_b(t) - Q_{ac}(t)k_{ef} \quad (1)$$

where $Q_b(t)$ and $Q_c(t)$ are the volumetric flow rates of the base and the acid, respectively, controlled by VFD dosing pumps sized within the optimal industrial range of 5 to 30 L/h, while f(pH) is the nonlinear function of dynamic process sensitivity that approximates the characteristic titration curve of the solution around the neutral point:

$$f(pH) = \frac{1}{1 + 9e^{-|pH(t)-7.0|}} \quad (2)$$

pH VALUE REGULATION

In the mineral wool production plant, pH regulation is performed at the beginning of the treatment in the equalization tank, where all wastewater is mixed and partially cooled. Acid or base dosing is carried out here to maintain the pH value within the 6.5 – 8 interval. The

composition of the water varies throughout the day, and maintaining the pH is necessary for the subsequent purification step – coagulation and flocculation. If the pH is high, hydrochloric acid (HCl) is dosed, while sodium hydroxide (NaOH) or calcium hydroxide ($Ca(OH)_2$) is added for low pH values. For the coagulation process, additional pH correction is sometimes required. The most favorable range is 5.5 – 7.5 (depending on the coagulant). Following biological treatment, a small additional pH correction (6.5 – 8) is often performed, e.g., for microorganism suppression. In industrial processes such as wastewater neutralization, the application of a linear controller can yield good results in one part of the operating range, but due to nonlinearity, regulation is poor in other parts of the range. Gain scheduling is a control method using linear controllers applied to nonlinear systems, where controller parameters change depending on the operating point of the system, with the plant being nonlinear across the entire range yet approximable by a linear model at specific operating points. In addition to this approach, an adaptive nonlinear PID was applied. This controller possesses self-tuning properties and the capability to independently form control protocols (Al-Dawery, et al. 2026; Chan, & Yu, 1995). Fig. 3 shows the block diagram of the control system.

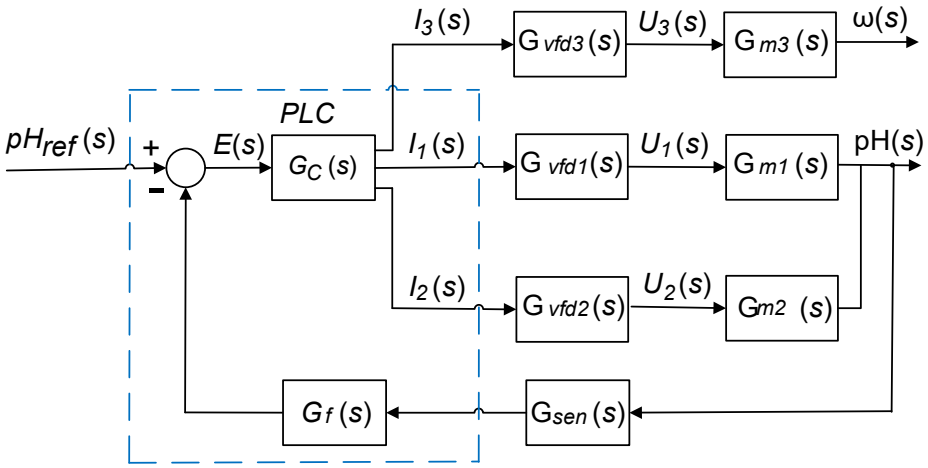


Fig. 3. *Block diagram of the control system*

Figure Labels:
pH_{ref} – reference value, pH – measured value,
G_c – controller, G_{VFD1} – VFD pump 1 (acid dosing),
G_{m1} – asynchronous motor of pump 1,
G_{VFD2} – VFD pump 2 (base dosing),
G_{sen} – pH sensor, G_f – filter,
G_{m3} – asynchronous motor of the mixer,
G_{VFD2} – mixer VFD.
An analysis of the Gain Scheduling and Adaptive nonlinear PID methods was performed in MATLAB. Graphs were generated showing the pH value, the trends of the tuning parameters K_p and T_i, the operation of the base and acid dosing pumps, as well as a quantitative evaluation of control quality.

RESULTS AND DISCUSSION

A full-day industrial cycle lasting 24 hours was simulated with a time step defined by a resolution of Δt = 1 min (Fig. 4).
Throughout the day, the baseline alkaline pH profile of the wastewater continuously oscillates, but is additionally loaded with extreme process incidents characteristic of mineral wool production: a breakthrough of basic resins between the 4th and 6th hours (+1.2 pH), a sharp acid shock due to flue gas scrubbing from the cupola furnace between the 11th and 12.5th hours (a drop of -2.5 pH), and a short-term measurement spike caused by sensor

noise in the 18th hour (+0.7 pH). For the first disturbance (resin breakthrough at the 4th hour), the input pH sharply increases.
Both methods react by activating the acid pump. Gain Scheduling instantly jumps to new fixed parameter values, causing a sharper pump reaction. The adaptive PID continuously increases K_p and decreases T_i, causing the pH to return to the value of 7 much more smoothly and with a smaller overshoot. The acid disturbance in the 11th hour causes a drastic drop in pH below normal. The system blocks the acid pump and initiates base dosing (dashed lines on the 4th graph).

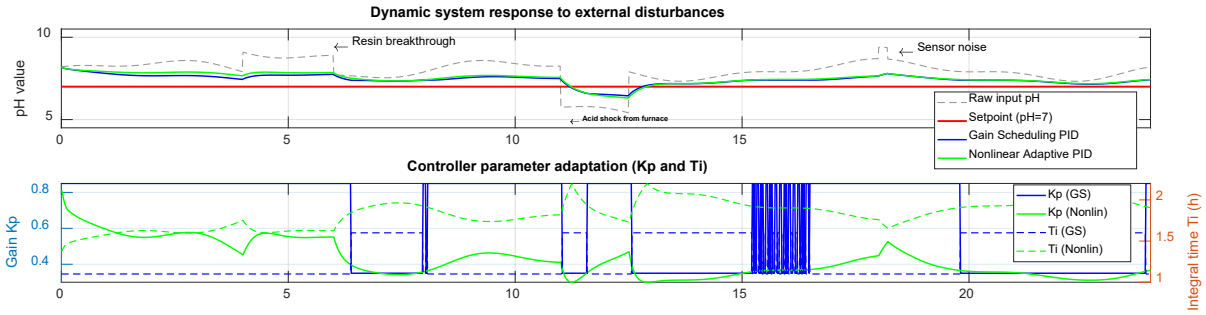


Fig. 4. *Graphical representation of the analyzed control strategies*

Given that the acid disturbance is strong, the ISE values clearly show how much faster the adaptive PID manages to stabilize the system compared to the discrete steps of Gain Scheduling. The third disturbance (sensor noise in the 18th hour) results in the nonlinear PID successfully "smoothing out" the output thanks to dynamic adaptation, whereas Gain Scheduling experiences a brief overshoot because its thresholds are rigidly defined. Quantitative evaluation of control quality was performed through the calculation of three standard statistical error indicators:
- Integral of Absolute Error (IAE), which equally weights all errors regardless of their magnitude, enabling a good balance between response speed and system stability (damping), as it does not react excessively to large initial error jumps to the extent that ISE does.
- Integral of Square Error (ISE), which quickly eliminates large deviations, but allows minor oscillations near the end of settling.
- Integral of Time-weighted Absolute Error (ITAE), which measures control quality by multiplying the absolute error by time. It is used for assessing and optimizing the quality of transient processes in automatic control systems, giving less significance to initial errors and greater weight to errors that persist for a long time.
The obtained results are presented in Table 1.

Table 1. *Control statistical evluation*

Criterion	Gain Scheduling	Nonlinear Adaptive PID
IAE (Integral Absolute Error)	11.4125	12.9916
ISE (Integral Squared Error)	6.3937	8.4354
ITAE (Integral of time-multiplied Absolute Value of Err.)	116.4867	127.6716

Analysis of the values in Table 1 reveals that both methods provide very similar performance in terms of overall accuracy. Gain Scheduling achieves a slightly lower ISE criterion value because it instantly activates maximum gains during major disturbances, whereas the nonlinear adaptive controller achieves a better result according to the ITAE criterion, indicating faster settling of the process in the steady state without prolonged oscillations. The fundamental difference in the quality of the two systems becomes clear through monitoring the operation of the final control elements (dosing pumps). Given that the input profile is predominantly alkaline throughout most of the day (pH > 7.5), the base dosing pump (Q_b) remains idle for the majority of the cycle, while acid dosing (Q_{ac}) operates continuously. The exception is the "acid shock" period when the pH drops sharply below the limit, at which point acid dosing decreases to zero and base dosing is activated. However, the trend analysis of the gain K_p in the Gain Scheduling algorithm shows the appearance of a densely packed block of high-frequency oscillations in the period after the 18th hour, even though the first graph suggests that the pH in the tank is completely stable. The cause of this phenomenon is the short-term noise of +0.7 pH, which acts as a trigger. Since Gain Scheduling is a linear system with strict, discrete zone-switching thresholds, the noise artificially pushes the controller into the zone of aggressive action. Given the mixing delay in the 175m^3 tank, a sudden parameter change introduces excess energy, causing the system to enter a so-called limit cycle. The controller begins to oscillate at high speed between discrete gain values (0.35 and 0.85), forcing the pump into sudden and intermittent operation. In real industrial practice, such operation with destructive pump "chattering" is unacceptable because it drastically shortens diaphragm lifespan, causes dangerous hydraulic shocks in the pipes, and consumes excess chemicals. By integrating an industrial rate-of-change limit (Rate Limiter) directly into the model, it is confirmed that the nonlinear adaptive PID solves this problem. Thanks to the continuous nature of the nonlinear adaptive logic, short-term measurement noise is dampened, the appearance of sharp gain peaks is prevented, and a smooth, stable, and gradual pump operation is ensured without mechanical stress on the process equipment.

CONCLUSION

In this paper, the nonlinear process of industrial wastewater treatment and neutralization in a large 175m^3 equalization tank within a mineral wool production plant was modeled and simulated. Based on the conducted research and comparative analysis of two advanced control concepts, the following conclusions are drawn: both algorithms (Gain Scheduling PID and nonlinear adaptive PID) satisfy strict environmental and technological norms by maintaining the pH value within a narrow required range around the neutral point (7.0), successfully compensating for strong periodic and incident process disturbances such as resin breakthroughs and acid shocks. Gain Scheduling PID exhibits certain systemic drawbacks in the presence of measurement noise on the pH sensor due to the destructive effect of discrete zone-switching boundaries, introducing instability into the operation of final control elements and leading to undesirable pump "chattering". The Nonlinear Adaptive PID controller demonstrates industrial robustness. Through smooth and continuous changes in the gain K_p and integral time T_i, limit cycles are eliminated and pump operation under saturation is stabilized, thereby achieving savings in chemical reagent consumption. Although sulfuric acid is often considered in wide industrial practice for correcting a high basic pH profile due to its diprotic nature and higher acidifying efficiency, hydrochloric acid is preferred in mineral wool production plants. The main reason is the high concentration of calcium ions (Ca^{++}) originating from raw materials (dolomite). The use of sulfuric acid would lead to an undesirable chemical precipitation reaction of calcium sulfate (gypsum) inside the equalization tank. The formation of solid gypsum deposits on the axial impeller of the mixer would increase mechanical resistance and motor current load, while the clogging of the external measuring chamber would prevent the proper operation of the pH sensor and destabilize the adaptive process control algorithms.

The proposed solution with an adaptive structure and implemented final control element constraints fulfills the requirements of process automation, thereby confirming its direct practical applicability and justification for introduction into actual industrial plants of this purpose.

REFERENCES

Aström, K. J., & Wittenmark, B. (2008). *Adaptive Control*. Courier Corporation.

Al-Dawery, S. K., et al. (2009/2026). *Nonlinear Adaptive Control of a pH Process*. Iraqi Journal of Chemical and Petroleum Engineering.

Chan, S. P., & Yu, C. C. (1995). *Simple adaptive pH control using gain-scheduling methods*. International Journal of Control

Corriou, J. P. (2018). *Process Control: Theory and Applications*. Springer.

Shinskey, F. G. (1996). *Process Control Systems: Application, Design, and Tuning*. McGraw-Hill.

Stankov, P. S. (2012). Monitoring and Control System of Cupola Furnace at Plant for Mineral Wool Production, *Mining engineering*, DOI: 10.5937/rudrad1203235S, vol. 5, No 3, Publisher: Mining and metallurgy institute Bor, 245 – 254.

Stankov, P. S. (2013). Savremen način upravljanja procesom proizvodnje mineralne vune, *Hemijska industrija*, vol. 67, br. 2, DOI: 10.2298/HEMIND120428069S, Izdavač: Institut SANU, Beograd, Srbija, 375 – 384.

Stankov, P. S. (2024). Modern Concepts of Supervisory Control Systems Based on PLC and SCADA Configuration, *Part of the book New Trends in Engineering Research 2024*, vol. 1216, DOI: https://doi.org/10.1007/978-3-031-78635-8_24, Springer, Cham. 289 – 313.

Stankov, P. S. (2024). Water Purification in the Process Industry, *37 međunarodni kongres o procesnoj industriji PROCESING 24*, DOI: 10.24094/ptk.024.121, SMEITS, 121 – 140.

Visioli, A. (2006). *Practical PID Control*. Springer Science & Business Media.

DOI:10.5937/IIZS26194H

ROUND-TRIP EFFICIENCY (RTE) OF HOME BATTERY STORAGE SYSTEMS UNDER TROPICAL CLIMATIC CONDITIONS - A CASE STUDY OF THAILAND

Research paper

Matthias Hauer[1]*, Ashish Srivastava[2], Momir Tabaković[3]
[1]FH Technikum Wien, Vienna, Austria

Abstract: Residential battery-storage efficiency is commonly reported under moderate reference conditions, whereas systems installed in tropical climates may experience substantially higher ambient temperatures. This paper investigates the DC-side round-trip efficiency (RTE) of a residential lithium iron phosphate ($LiFePO_4$) battery under representative Bangkok conditions using a reduced-order electro-thermal model. A constant 25 °C reference, a thermally buffered indoor case and a weather-driven outdoor case are compared. The battery is cycled between 20% and 80% state of charge at discharge rates from 0.1C to 0.6C. The model predicts only a small climate-related RTE difference: relative to the constant reference, the Bangkok outdoor case is approximately 0.16-0.28 percentage points higher. At 0.6C, modeled RTE changes from 93.94% to 94.17%, while maximum pack temperature rises from 39.06 °C to 49.95 °C. The results indicate that tropical thermal exposure affects modeled pack temperature and operating margin much more strongly than short-term battery-side RTE.

Key words: residential battery storage, round-trip efficiency, $LiFePO_4$, tropical climate, Bangkok, thermal performance

INTRODUCTION

Residential battery systems are increasingly combined with photovoltaic generation to increase self-consumption and shift locally generated electricity to later periods (Bagalini et al., 2019). Useful energy yield depends on battery-internal losses as well as converter, standby and auxiliary losses (Munzke et al., 2021).

Round-trip efficiency is therefore an important storage-performance indicator, but its interpretation depends on the selected measurement boundary. Battery-terminal DC efficiency excludes inverter and auxiliary losses included in wider system assessments (Conover et al., 2016; HTW Berlin Hochschule für Technik und Wirtschaft et al., 2019). The present work consequently uses a clearly defined battery-side DC boundary.

Temperature influences lithium-ion impedance, voltage response and degradation. Moderately higher temperature can reduce short-term resistance, whereas prolonged elevated temperature increases thermal stress and can accelerate ageing (Kucinskis et al., 2022; Liao et al., 2012; Ruiz et al., 2017). This distinction is particularly relevant in tropical installations, where batteries may operate in conditioned rooms, thermally buffered spaces or warmer outdoor environments. Studies under hot climates and Thai operating conditions likewise emphasize the importance of thermal exposure and temperature management (A'amar et al., 2025; Ketjoy et al., 2025).

Comparatively little attention has been given to short-term battery-side RTE of residential storage under representative tropical ambient conditions. This study therefore examines how Bangkok installation environments affect modeled DC-side RTE, pack temperature and operating margin while the battery configuration and cycling protocol are held constant.

[1] Corresponding author, matthias.hauer0404@gmail.com; ORCID: 0000-0000-0000-0000
[2] ashish.mexpert@gmail.com; ORCID: 0000-0000-0000-0000
[3] momir.tabakovic@technikum-wien.at; ORCID: 0000-0000-0000-0000

MATERIAL AND METHODS

Battery Model and System Boundary

A reduced-order electro-thermal battery model was implemented in Python. The nominal pack configuration is 48 V and 314 Ah. The parameter set represents a residential battery configuration for comparative simulation and is not presented as a manufacturer-specific digital twin.

The reported efficiency boundary is located at the battery DC terminals. Inverter conversion, AC-side losses, standby consumption, auxiliary loads and the energy demand of room conditioning are excluded.

A practical inverter-battery setup supported system familiarization and qualitative plausibility checks during the original study, but did not provide a controlled temperature-dependent RTE validation campaign. The numerical results are therefore interpreted as model-based comparisons.

***Table 1**. Main simulation parameters.*

Parameter	Value	Parameter	Value
Nominal voltage	48 V	Nominal capacity	314 Ah
SOC window	20-80%	Charge rate	0.30C
Discharge rates	0.1C-0.6C	Time step	5 min
Max. charge current	100 A	Max. discharge current	250 A
Reference resistance	0.012 Ω	Pack mass	130 kg
Effective c_p	950 J/(kg K)	hA	18 W/K
Model thermal cutoff	55 °C	Re-enable threshold	50 °C

The thermal parameters and reference resistance are engineering model assumptions rather than manufacturer-certified properties.

Electro-Thermal Model

Open-circuit voltage is represented as a piecewise function of SOC, consistent with the relatively flat mid-SOC behaviour of $LiFePO_4$ batteries (Roscher & Sauer, 2011; Weng et al., 2013; Zhu et al., 2015).

Internal resistance is modeled as

$$\boldsymbol{R_{\mathrm{int}} = 0.012\, F_T(T)\left[1 + 0.45(1 - \mathrm{SOC})^{1.5}\right].} \quad (1)$$

Where

$$\boldsymbol{F_T(T) = \begin{cases} \exp[0.03(25 - T)], & T < 25^{\circ}\mathrm{C}, \\ \exp[-0.01(T - 25)], & T \geq 25^{\circ}\mathrm{C}. \end{cases}} \quad (2)$$

The direction of this dependence is consistent with published temperature- and SOC-dependent $LiFePO_4$ behaviour (Liao et al., 2012; Safoutin et al., 2015). At unchanged SOC, the model resistance is approximately 9.5% lower at 35 °C and 13.9% lower at 40 °C than at 25 °C. At 50% SOC, for example, the corresponding modeled values are approximately 13.91, 12.59 and 11.97 mΩ.

Terminal voltage and DC power are calculated as

$$\boldsymbol{V_{\mathrm{term}} = V_{\mathrm{OCV}} - IR_{\mathrm{int}}, \qquad P_{\mathrm{DC}} = V_{\mathrm{term}} I.} \quad (3)$$

where positive current denotes discharge.

Pack temperature is represented by the lumped balance

$$mc_p \frac{\mathrm{d}T_{\mathrm{pack}}}{\mathrm{d}t} = I^2 R_{\mathrm{int}} - hA\left(T_{\mathrm{pack}} - T_{\mathrm{amb}}\right). \quad (4)$$

This reduced-order model does not resolve internal temperature gradients, enclosure radiation or detailed airflow (Forgez et al., 2010; Song et al., 2021). Equation (4) nevertheless captures the two effects central to this study: resistive heat generation and heat exchange with the ambient environment.

Weather Dataset and Ambient Scenarios

The outdoor scenario uses hourly air-temperature observations from Meteostat (Lamprecht, 2026). The reproducible comparison configuration uses Meteostat/WMO station 48455 (Bangkok, Thailand; approximately 13.7333° N, 100.5667° E; elevation 2 m), for which station metadata are provided by Meteostat (Meteostat, n.d.).

The weather interval is 1 March 2025 at 00:00 through 31 March 2025 at 23:00 local Bangkok time. Only hourly air temperature is used by the battery model. Missing temperature values, if present, are linearly interpolated in the hourly series. The hourly observations are subsequently expanded to the 5 min simulation grid by forward filling.

Three thermal environments are compared. The reference case uses a constant 25 °C. The outdoor case uses the Meteostat temperature series directly. The buffered indoor case is derived from the same outdoor series according to

$$T_{\mathrm{target},k} = 30 + 0.45\left(T_{\mathrm{out},k} - 30\right), \quad (5)$$

followed by

$$T_{\mathrm{in},k} = T_{\mathrm{in},k-1} + \frac{\Delta t}{12\ \mathrm{h}}\left(T_{\mathrm{target},k} - T_{\mathrm{in},k-1}\right). \quad (6)$$

The indoor case is an engineering representation of thermal buffering, not a complete building-energy model.

Cycling, Protection and RTE Averaging

Each C-rate case is simulated independently over the same monthly time window. Every run begins at the first timestamp of its ambient series with an initial SOC of 80% and an initial pack temperature equal to the corresponding ambient temperature.

The battery discharges toward 20% SOC and is subsequently charged toward 80%. Charging is requested at 0.30C, while discharge rates from 0.1C to 0.6C are evaluated. SOC is updated through Coulomb counting,

$$\mathrm{SOC}_{k+1} = \mathrm{SOC}_k - \frac{I_k \Delta t}{Q}. \quad (7)$$

A simplified supervisory layer imposes current, voltage and SOC limits. A pack temperature of 55 °C is used as a conservative model protection threshold rather than as a claimed manufacturer BMS setting. Published $LiFePO_4$ ageing research recommends substantially lower temperatures for normal operation and identifies 55 °C as an upper temperature that should not be exceeded (Xu et al., 2025). Operation is re-enabled below 50 °C, providing a 5 °C model hysteresis band. No thermal trip occurs in the reported cases.

For completed cycle j, DC-side RTE is

$$\eta_{\mathrm{RTE},j} = \frac{E_{\mathrm{dis},j}}{E_{\mathrm{ch},j}}. \quad (8)$$

The value reported as "average cycle RTE" is the arithmetic mean of all completed-cycle efficiencies within the monthly window,

$$\overline{\eta}_{\mathrm{RTE}} = \frac{1}{N}\sum_{j=1}^{N} \eta_{\mathrm{RTE},j}. \tag{9}$$

A cycle still incomplete at the end of the month is excluded. The numbers of completed cycles at 0.1C, 0.2C, 0.3C and 0.4C are 92, 146, 182 and 207, respectively, in all three scenarios. At 0.5C the reference, indoor and outdoor cases contain 270, 250 and 249 completed cycles; at 0.6C the corresponding counts are 318, 317 and 290.

SOC transitions are evaluated on the finite 5 min grid without sub-step interpolation. Differences of only a few tenths of a percentage point are therefore interpreted as comparative model trends rather than measurement-level accuracy.

RESULTS AND DISCUSSION

Table 2 summarizes modeled average cycle RTE and peak pack temperature. Increasing discharge rate decreases modeled RTE in all three environments. The climate-related separation between the three RTE series remains small.

***Table 2**. Modeled average cycle RTE and maximum pack temperature.*

C-rate	Ref. RTE [%]	Indoor RTE [%]	Outdoor RTE [%]	Ref. $T_{pack,max}$ [°C]	Indoor $T_{pack,max}$ [°C]	Outdoor $T_{pack,max}$ [°C]
0.1C	96.90	96.97	97.06	29.63	32.10	40.28
0.2C	96.20	96.28	96.39	30.40	32.86	40.94
0.3C	95.54	95.63	95.76	31.49	33.94	42.45
0.4C	94.93	95.02	95.17	34.46	36.88	45.25
0.5C	94.44	94.55	94.72	36.85	39.39	47.26
0.6C	93.94	94.06	94.17	39.06	41.79	49.95

Figure 1 shows that the effect of discharge rate is much larger than the separation between ambient scenarios.

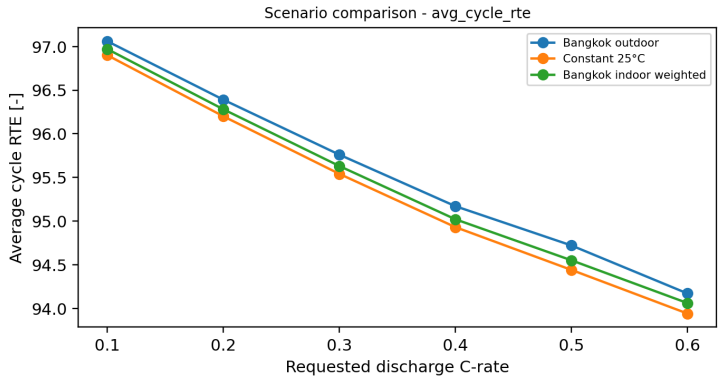


***Fig. 1**. Modeled average cycle DC-side RTE versus requested discharge C-rate.*

Within the implemented model, the Bangkok outdoor case produces an average cycle RTE approximately 0.16-0.28 percentage points above the constant-reference case. This direction follows from the modeled temperature dependence of internal resistance: higher pack temperature reduces R_{int} and therefore reduces resistive voltage loss. Because resistive loss represents only part of the battery-side energy balance, however, the resulting change in total modeled RTE remains small.

This modest electrical effect must be considered together with the substantially stronger thermal response. Across the investigated rates, peak pack temperature in the outdoor case is approximately 10 °C to 11 °C above the reference. At 0.6C, modeled RTE changes from 93.94% to 94.17%, whereas peak pack temperature increases from 39.06 °C to 49.95 °C. The latter remains below the model cutoff but leaves considerably less thermal margin.

These two observations result from the same electro-thermal model and are not contradictory. Equation (2) reduces modeled electrical resistance as temperature rises, while Eq. (4) shows that warmer ambient air simultaneously reduces the temperature difference available for heat rejection. Consequently, a warmer pack can exhibit slightly lower resistive losses while still reaching a markedly higher operating temperature.

The same resistance effect is also visible in the terminal-voltage response. At 0.3C, the minimum modeled terminal voltage is approximately 48.273 V in the reference case, 48.291 V indoors and 48.307 V outdoors. Although the warmer cases therefore show a small electrical benefit at this operating point, the magnitude of the voltage difference is minor compared with the accompanying change in thermal exposure.

Taken together, the results show why the predicted RTE increase should not be interpreted as evidence that hotter battery operation is preferable. Elevated temperature is associated with accelerated lithium-ion ageing (Ketjoy et al., 2025; Kucinskis et al., 2022; Ruiz et al., 2017). Within the scope of the present model, thermal buffering is therefore more relevant for preserving operating margin than for improving short-term battery-side RTE.

The numerical magnitude of the RTE separation remains model-dependent. The resistance relation, lumped thermal parameters, synthetic indoor temperature and finite time step introduce uncertainty, and the available practical setup did not provide controlled validation across the investigated climate cases. The sub-percentage-point differences should therefore be interpreted as trends predicted by the reduced-order model, not as experimentally established differences with two-decimal precision.

CONCLUSION

A reduced-order electro-thermal model was used to compare battery-side DC round-trip efficiency under a constant 25 °C reference and representative indoor and outdoor Bangkok conditions.

Increasing discharge rate from 0.1C to 0.6C reduces modeled RTE in all three scenarios. Within the implemented model, the Bangkok outdoor case produces an average RTE only 0.16-0.28 percentage points above the constant reference because modeled internal resistance decreases at higher pack temperature.

The thermal effect is considerably larger. At 0.6C, modeled RTE changes from 93.94% to 94.17%, while maximum pack temperature changes from 39.06 °C to 49.95 °C. The result therefore indicates greater sensitivity of thermal operating margin than of short-term battery-side RTE to tropical exposure.

Because the model has not been validated to sub-percentage-point accuracy, the small RTE difference is interpreted as a comparative model trend. For practical residential storage assessment, battery-side efficiency should be considered together with thermal exposure rather than used as an isolated indicator.

REFERENCES

A'amar, K., Sajid, M. U., Bicer, Y., & Al-Ansari, T. (2025). Thermal assessment of pole integrated LiFePO4 energy storage system for arid and non maintainable locations: A case study in Qatar. *Journal of Power Sources, 660*, 238444. https://doi.org/10.1016/j.jpowsour.2025.238444

Bagalini, V., Zhao, B. Y., Wang, R. Z., & Desideri, U. (2019). Solar PV-battery-electric grid-based energy system for residential applications: System configuration and viability. *Research, 2019*, 3838603. https://doi.org/10.34133/2019/3838603

Conover, D. R., Ferreira, S. R., Crawford, A. J., Schoenwald, D. A., Fuller, J., Rosewater, D. M., Gourisetti, S. N., & Viswanathan, V. (2016). *Protocol for uniformly measuring and expressing the performance of energy storage systems* (Tech. Rep. No. PNNL-22010 Rev. 2). Pacific Northwest National Laboratory.

Forgez, C., Do, D. V., Friedrich, G., Morcrette, M., & Delacourt, C. (2010). Thermal modeling of a cylindrical LiFePO4/graphite lithium-ion battery. *Journal of Power Sources, 195*(9), 2961-2968. https://doi.org/10.1016/j.jpowsour.2009.10.105

HTW Berlin Hochschule für Technik und Wirtschaft, BSW-Solar, & ZVEH. (2019, July). *Effizienzleitfaden für PV-Speichersysteme Version 2.0.1* (Tech. Rep.). HTW Berlin.

Ketjoy, N., Mensin, Y., Mensin, P., Kaewpanha, M., Khakhu, S., Chantarapongphan, C., & Sulaiman, S. I. (2025). Development of a degradation model for lifespan prediction: A case study on grid-scale battery energy storage systems in Thailand. *Batteries, 11*(11), 429. https://doi.org/10.3390/batteries11110429

Kucinskis, G., Bozorgchenani, M., Feinauer, M., Kasper, M., Wohlfahrt-Mehrens, M., & Waldmann, T. (2022). Arrhenius plots for Li-ion battery ageing as a function of temperature, C-rate, and ageing state - an experimental study. *Journal of Power Sources, 549*, 232129. https://doi.org/10.1016/j.jpowsour.2022.232129

Lamprecht, C. S. (2026). *Meteostat Python* [Official software documentation and citation metadata]. Meteostat.

Liao, L., Zuo, P., Ma, Y., Chen, X., An, Y., Gao, Y., & Yin, G. (2012). Effects of temperature on charge/discharge behaviors of LiFePO4 cathode for Li-ion batteries. *Electrochimica Acta, 60*, 269-273. https://doi.org/10.1016/j.electacta.2011.11.041

Meteostat. (n.d.). *Bangkok - weather station 48455* [Station metadata: 13.7333 N, 100.5667 E, elevation 2 m]. Meteostat. Retrieved September 22, 2026, from https://meteostat.net/en/station/48455

Munzke, N., Schwarz, B., Büchle, F., & Hiller, M. (2021). Evaluation of the efficiency and resulting electrical and economic losses of photovoltaic home storage systems. *Journal of Energy Storage, 33*, 101724. https://doi.org/10.1016/j.est.2020.101724

Roscher, M. A., & Sauer, D. U. (2011). Dynamic electric behavior and open-circuit-voltage modeling of LiFePO4-based lithium ion secondary batteries. *Journal of Power Sources, 196*(1), 331-336. https://doi.org/10.1016/j.jpowsour.2010.06.098

Ruiz, V., Kriston, A., Adanouj, I., Destro, M., Fontana, D., & Pfrang, A. (2017). Degradation studies on lithium iron phosphate-graphite cells. The effect of dissimilar charging-discharging temperatures. *Electrochimica Acta, 240*, 495-505. https://doi.org/10.1016/j.electacta.2017.03.126

Safoutin, M., Cherry, J., McDonald, J. F., & Lee, S. (2015). Effect of current and SOC on round-trip energy efficiency of a lithium-iron phosphate (LiFePO4) battery pack. *SAE 2015 World Congress and Exhibition*, 2015-01-1186. https://doi.org/10.4271/2015-01-1186

Song, S., Munk-Nielsen, S., Knap, V., & Uhrenfeldt, C. (2021). Performance evaluation of lithium-ion batteries (LiFePO4 cathode) from novel perspectives using a new figure of merit, temperature distribution analysis, and cell package analysis. *Journal of Energy Storage, 44*, 103413. https://doi.org/10.1016/j.est.2021.103413

Weng, C., Sun, J., & Peng, H. (2013). An open-circuit-voltage model of lithium-ion batteries for effective incremental capacity analysis. *Proceedings of the ASME 2013 Dynamic Systems and Control Conference*, V001T05A002. https://doi.org/10.1115/DSCC2013-3979

Xu, J., Li, H., Hua, S., & Wang, H. (2025). Experimental investigation of grid storage modes effect on aging of LiFePO4 battery modules. *Frontiers in Energy Research, 13*, 1528691. https://doi.org/10.3389/fenrg.2025.1528691

Zhu, L., Sun, Z., Dai, H., & Wei, X. (2015). A novel modeling methodology of open circuit voltage hysteresis for LiFePO4 batteries based on an adaptive discrete Preisach model. *Applied Energy, 155*, 91-109. https://doi.org/10.1016/j.apenergy.2015.05.103

DOI:10.5937/IIZS26201S

IMPACT OF AGRICULTURAL BIOMASS PROPERTIES ON THE ENERGY VALUE OF PELLETS: EXPERIMENTAL AND STATISTICAL ANALYSIS

Research paper

Zorica Stojadinović[1*], Dragana Novaković[2]
[1,2] University of Novi Sad, Faculty of Agricluture, Novi Sad, Republic of Serbia

Abstract: Agricultural residues represent an important renewable energy resource, and their conversion into pellets enables more efficient storage, transport, and energetic utilization of biomass. The quality and energy performance of pellets depend strongly on the properties of the raw material, particularly moisture content, ash content, and heating value. In this study, these parameters were experimentally determined for pellets produced from corn stalk, sunflower husk, wheat straw, and soybean straw. Ten independent laboratory samples of each pellet type were analyzed. Descriptive statistics were used to assess within-group variability, while one-way analysis of variance (ANOVA) and the Tukey HSD post hoc test were applied to examine differences in heating value among pellet types. Mean moisture content ranged from 7.72% in soybean straw pellets to 8.93% in sunflower husk pellets, while mean ash content ranged from 6.31% in sunflower husk pellets to 9.21% in corn stalk pellets. The highest mean heating value was recorded for sunflower husk pellets (16.59 MJ/kg), followed by soybean straw (14.94 MJ/kg), corn stalk (14.79 MJ/kg), and wheat straw pellets (14.72 MJ/kg). One-way ANOVA showed a statistically significant effect of pellet type on heating value, $F(3,36) = 399.81$, $p < 0.001$, with a very large effect size ($\omega^2 = 0.968$). Tukey HSD analysis confirmed that sunflower husk pellets had a significantly higher heating value than all other analyzed pellet types. The results demonstrate that biomass type significantly influences the energy performance of agricultural pellets and highlight sunflower husk as the most favorable raw material among the analyzed biomass types in terms of heating value and ash content.
Key words: agricultural biomass, energy pellets, moisture content, ash content, heating value

INTRODUCTION

Biomass represents an important renewable energy resource and plays a significant role in the development of sustainable energy systems, particularly in agricultural regions characterized by intensive crop production. Large quantities of agricultural residues, such as corn stalks, sunflower husks, wheat straw, and soybean straw, provide considerable potential for energy recovery, reduced dependence on conventional energy sources, and more efficient resource utilization in accordance with circular economy principles (Picchio et al., 2020). One approach to improving the energy utilization of agricultural biomass is its conversion into pellets. Pelletization transforms loose biomass into a compact and more homogeneous fuel, thereby facilitating storage, transport, handling, and utilization in different thermal energy systems (Brkić & Gluvakov, 2015). In addition to these logistical advantages, pelletization can contribute to more standardized fuel characteristics. However, the quality and energy performance of the final product remain strongly dependent on the properties of the raw material used for pellet production. The quality of energy pellets is determined by a range of physical, mechanical, and chemical-thermal characteristics, among which moisture content, ash content, and heating value are particularly important. Moisture content directly affects the amount of useful energy available during combustion, since part of the released energy is consumed in heating and evaporating water. Ash content represents the inorganic residue remaining after combustion and may influence combustion efficiency, deposit formation, equipment maintenance, and the management of combustion residues (Jach-Nocoń et al., 2021). Heating value, on the other hand, is one of the principal indicators of the energy potential of solid biofuels and provides a direct basis for comparing the energy performance of different biomass materials. Agricultural residues may differ substantially in their chemical composition, mineral content, structural characteristics, and moisture retention capacity. These differences can result in variations in the chemical-thermal properties of the pellets produced from them (Gluvakov et al., 2015). Consequently, the selection of biomass feedstock represents an important factor in determining pellet quality and energy

[1]Corresponding author, zorica.stojadinovic85@gmail.com, ORCID: 0009-0008-5445-2789
[2]dragana.tekic@polj.uns.ac.rs, ORCID: 0000-0002-1924-6196

performance. Comparative analysis of different agricultural residues is therefore necessary to identify biomass types with more favorable characteristics for solid biofuel production. The increasing role of biomass in the European energy sector is supported by the European Union regulatory framework aimed at increasing the share of renewable energy sources and promoting the decarbonization of the energy system. This framework was initially established by Directive 2009/28/EC and subsequently strengthened through Directive (EU) 2018/2001 and Directive (EU) 2023/2413. In parallel, the European Committee for Standardization developed technical specifications for solid biofuels, which were later harmonized with international ISO standards within the EN ISO 17225 series. In particular, EN ISO 17225-2 and EN ISO 17225-6 provide requirements for graded wood and non-woody pellets, respectively, and represent an important framework for evaluating the quality of pelletized solid biofuels. In addition to experimental determination of pellet quality parameters, the application of statistical methods enables an objective assessment of variability within individual pellet types and of differences among biomass sources. Descriptive statistics can be used to characterize the central tendency and dispersion of measured parameters, while analysis of variance enables testing of whether observed differences among pellet types are statistically significant. When significant overall differences are detected, post hoc procedures can further identify which specific pellet types differ from one another.
Therefore, the aim of this study was to experimentally determine the moisture content, ash content, and lower heating value of energy pellets produced from corn stalk, sunflower husk, wheat straw, and soybean straw, and to evaluate differences among the analyzed pellet types using descriptive statistics, one-way analysis of variance (ANOVA), and the Tukey HSD post hoc test.

MATERIAL AND METHODS

Pellet samples and sampling procedure

Four types of energy pellets produced from agricultural biomass were analyzed in this study: wheat straw, soybean straw, corn stalk, and sunflower husk pellets. Samples used for the determination of chemical-thermal characteristics were collected from the production facility of the pellet manufacturer. For each pellet type, ten independent laboratory samples were collected from different production batches and production cycles, thereby capturing variations associated with raw material, production date, and operating conditions. Each sample represented an independent sampling unit originating from a single package belonging to a specific production batch. The samples were randomly selected from packed and stored pellet bags after the cooling stage, following the principles of SRPS EN ISO 18135:2017 (Solid biofuels — Sampling). The mass of each laboratory sample was approximately 3 kg. After collection, the samples were hermetically sealed and stored under refrigerated conditions until laboratory analysis.

Determination of moisture content

Moisture content was determined as the loss in sample mass after drying at 105 °C to constant mass, in accordance with SRPS E.B8.012, following the principles of ISO 18134. The equipment used for moisture determination included a laboratory mill, metal drying containers, an electric drying oven with temperature control at 105 °C, a desiccator, and a laboratory balance with an accuracy of 0.1 g. Approximately 20 g of material was taken from each representative laboratory sample, ground, dried to constant mass, cooled in a desiccator, and weighed again. Moisture content was calculated according to Eq. (1):

$$\omega = \frac{(m_1 - m_2)}{m_1} * 100 \quad (1)$$

where:
ω – moisture content (%),
m_1 – sample mass before drying (g),
m_2 – sample mass after drying (g).

Determination of ash content

Ash content was determined as the mass of inorganic residue remaining after complete combustion of the sample at 575 ± 25 °C, in accordance with SRPS H.N8.136, following the principles of ISO 18122. Platinum, quartz, or porcelain crucibles, an electric muffle furnace with temperature control at 575 ± 25 °C, a laboratory grinder, and an analytical balance were used for the analysis. Approximately 20 g of material was taken from each representative laboratory sample and ground and carbonized. Following carbonization, approximately 1 g of material was subjected to ashing at 575 ± 25 °C for 3 h. After completion of the ashing procedure, the sample was cooled and weighed. Ash content was expressed as the percentage ratio of the mass of the remaining ash to the mass of the analyzed sample.

Determination of heating value

The gross heating value of the pellet samples was determined by the calorimetric method using a bomb calorimeter, following the principles of ISO 18125. Approximately 1 g of dried and homogenized sample was used for each determination. The sample was combusted in an oxygen atmosphere at a pressure of approximately 30 bar. The gross heating value was determined based on the temperature increase of the water in the calorimetric vessel. The lower heating value was subsequently calculated from the gross heating value according to Eq. (2):

$$H_d = H_g - 2500 \times (9h + w) \quad (2)$$

where:
Hg – gross heating value (kJ/kg),
Hd – lower heating value (kJ/kg),
h – hydrogen content (kg/kg),
w – moisture content (kg/kg).

Statistical analysis

Descriptive statistics were calculated separately for each pellet type and included the arithmetic mean, minimum, maximum, standard deviation, and coefficient of variation. The analyses were based on ten independent observations for each pellet type. To examine whether the lower heating value differed among pellet types, a one-way analysis of variance (ANOVA) was performed, with pellet type as the independent factor and lower heating value (MJ/kg) as the dependent variable. The assumption of homogeneity of variances was assessed using Levene's test. When the overall ANOVA indicated statistically significant differences among groups, the Tukey honestly significant difference (HSD) post hoc test was applied for pairwise comparisons. Statistical significance was evaluated at the $p < 0.05$ level. In addition to statistical significance, the magnitude of the effect of pellet type on lower heating value was assessed using omega squared (ω^2) as an effect-size measure. All statistical analyses were performed using R statistical software.

RESULTS AND DISCUSSION

The basic quality characteristics of the analyzed energy pellets were assessed based on moisture content, ash content, and lower heating value. Descriptive statistical indicators were calculated separately for each pellet type in order to evaluate the central tendency and variability of the analyzed parameters. The results are presented in Table 1.

Table 1. Descriptive statistics of the basic quality parameters of energy pellets

Parameter	Indicator	Corn stalk	Sunflower husk	Wheat straw	Soybean straw
Moisture (%)	Mean	8.10	8.93	7.74	7.72
Moisture (%)	Minimum	7.85	8.59	7.48	7.45
Moisture (%)	Maximum	8.31	9.21	7.95	7.96
Moisture (%)	Standard deviation	0.14	0.19	0.16	0.15
Moisture (%)	Coefficient of variation (%)	1.73	2.14	2.02	1.97
Ash (%)	Mean	9.21	6.31	8.40	7.73
Ash (%)	Minimum	9.05	6.05	8.12	7.41
Ash (%)	Maximum	9.45	6.62	8.72	7.98
Ash (%)	Standard deviation	0.13	0.17	0.21	0.19
Ash (%)	Coefficient of variation (%)	1.42	2.74	2.50	2.50
Heating value (MJ/kg)	Mean	14.79	16.59	14.72	14.94
Heating value (MJ/kg)	Minimum	14.68	16.29	14.52	14.68
Heating value (MJ/kg)	Maximum	14.88	16.83	14.93	15.21
Heating value (MJ/kg)	Standard deviation	0.06	0.17	0.13	0.18
Heating value (MJ/kg)	Coefficient of variation (%)	0.43	1.00	0.90	1.17

The descriptive results indicate relatively low within-group variability for all investigated pellet types. The coefficients of variation for moisture content ranged from 1.73% to 2.14%, while those for ash content ranged from 1.42% to 2.74%. The variability of lower heating value was particularly low, with coefficients of variation ranging from 0.43% to 1.17%, indicating a high degree of measurement consistency within each pellet type. The highest mean moisture content was recorded for sunflower husk pellets, at 8.93%, followed by corn stalk pellets at 8.10%. Lower mean moisture contents were observed for wheat straw and soybean straw pellets, at 7.74% and 7.72%, respectively. Moisture content represents an important parameter in the energetic utilization of agricultural biomass. High moisture levels may limit the efficiency of biomass use because they increase drying requirements and the energy needed for water evaporation during combustion. In unconditioned straw, moisture content can reach approximately 30%, which may substantially reduce its energy value and complicate efficient combustion (Gluvakov, 2012). Therefore, adequate drying of biomass represents an important prerequisite for its efficient energetic utilization. More pronounced differences among the analyzed pellet types were observed for ash content. Corn stalk pellets had the highest mean ash content, at 9.21%, followed by wheat straw pellets at 8.40% and soybean straw pellets at 7.73%. The lowest mean ash content was recorded for sunflower husk pellets, at 6.31%. Relatively high ash content is characteristic of many types of agricultural biomass and may influence the combustion process, particularly through increased deposit formation and higher maintenance requirements of combustion equipment (Jach-Nocoń et al., 2021). In addition to the natural characteristics of the raw material, ash content may also be influenced by agricultural practices and the method used for harvesting and collecting crop residues. Inadequate harvesting and collection, particularly under conditions of increased contact between biomass and soil, may result in contamination with mineral matter (Bonner et al., 2014). The presence of such impurities can increase the ash content of the final pellet product. Therefore, appropriate agricultural practices and careful

handling of crop residues are important prerequisites for improving raw-material quality and producing pellets with lower ash content. Regarding lower heating value, sunflower husk pellets showed the highest mean value, at 16.59 MJ/kg. This was followed by soybean straw pellets at 14.94 MJ/kg, corn stalk pellets at 14.79 MJ/kg, and wheat straw pellets at 14.72 MJ/kg. These results indicate the considerable energy potential of sunflower husk as a raw material for pellet production.

For a clearer visual comparison of the analyzed quality parameters, the mean values of moisture content, ash content, and lower heating value are presented in Figure 1.

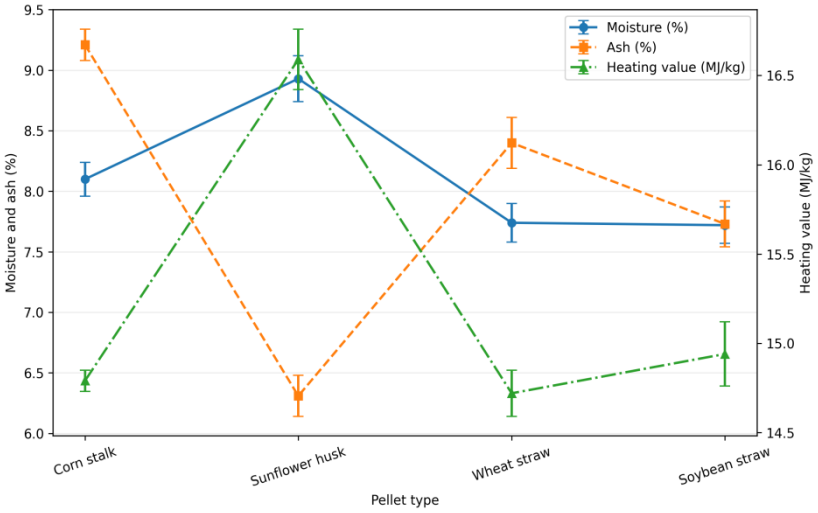


Fig. 1. *Average values of the basic quality parameters of energy pellets*

The graphical presentation confirms the differences observed through descriptive statistics. Sunflower husk pellets were characterized by the highest mean lower heating value and, at the same time, the lowest ash content among the investigated pellet types. In contrast, corn stalk pellets had the highest mean ash content, while wheat straw and soybean straw pellets showed the lowest moisture values.

The obtained results are consistent with the findings of Turzyński et al. (2021), who reported favorable energy and combustion characteristics of sunflower husk pellets. Their results indicate that sunflower husk can represent a valuable solid biofuel feedstock with favorable combustion properties. The present findings support this conclusion, particularly because sunflower husk pellets combined the highest lower heating value with the lowest ash content among the four analyzed biomass types.

Since lower heating value represents one of the key indicators of the energy performance of solid biofuels, further statistical analysis was performed to determine whether the observed differences among pellet types were statistically significant. One-way analysis of variance was applied, with pellet type as the factor and lower heating value as the dependent variable. The results are presented in Table 2.

Table 2. *Results of one-way analysis of variance for pellet heating value*

Source of variation	Sum of Squares	df	Mean Square	F	p	ω²
Pellet type	23.879	3	7.960	399.81	< 0.001	0.968
Residuals	0.717	36	0.020			

The results of the one-way ANOVA showed that pellet type had a statistically significant effect on lower heating value, $F(3,36) = 399.81$, $p < 0.001$. The null hypothesis of equal mean lower heating values among the four pellet types was therefore rejected. In addition to statistical significance, the magnitude of the observed effect was very large, as indicated by the value of $\omega^2 = 0.968$. This result shows that differences among pellet types accounted for a substantial proportion of the variability in lower heating value and confirms the importance

of raw-material type in determining the energy performance of the pellets. Because ANOVA indicates only whether an overall difference exists among group means, the Tukey HSD post hoc test was applied to identify the specific pellet types between which statistically significant differences occurred. The results are presented in Table 3.

Table 3. *Tukey HSD post hoc comparisons of heating value among different pellet types*

Comparison	Mean difference	p	Conclusion
Corn stalk – Sunflower husk	-1.803	< 0.001	significant
Corn stalk – Wheat straw	0.067	0.715	not significant
Corn stalk – Soybean straw	-0.151	0.097	not significant
Sunflower husk – Wheat straw	1.870	< 0.001	significant
Sunflower husk – Soybean straw	1.652	< 0.001	significant
Wheat straw – Soybean straw	-0.218	0.008	significant

The Tukey HSD post hoc test showed that sunflower husk pellets had a statistically significantly higher lower heating value than all other analyzed pellet types. The largest mean difference was observed between sunflower husk and wheat straw pellets, amounting to 1.870 MJ/kg ($p < 0.001$), followed by the difference between sunflower husk and corn stalk pellets, at 1.803 MJ/kg ($p < 0.001$), and between sunflower husk and soybean straw pellets, at 1.652 MJ/kg ($p < 0.001$). A statistically significant difference was also observed between soybean straw and wheat straw pellets ($p = 0.008$), with soybean straw pellets exhibiting the higher mean lower heating value. In contrast, the differences between corn stalk and wheat straw pellets ($p = 0.715$) and between corn stalk and soybean straw pellets ($p = 0.097$) were not statistically significant. These results indicate that the type of biomass significantly determines pellet energy performance, although the magnitude of the differences varies among individual biomass sources. Sunflower husk pellets were clearly distinguished by their higher lower heating value, while the energy values of corn stalk, wheat straw, and soybean straw pellets were considerably more similar. Overall, the obtained results show that the investigated agricultural biomass types differ in their chemical-thermal properties and energy performance. Among the analyzed materials, sunflower husk showed the most favorable combination of lower heating value and ash content, while corn stalk pellets were characterized by the highest ash content. At the same time, the relatively low coefficients of variation observed for all three analyzed parameters indicate good within-group uniformity of the measurements.

CONCLUSION

This study evaluated the basic chemical-thermal properties of energy pellets produced from four types of agricultural biomass: corn stalk, sunflower husk, wheat straw, and soybean straw. The results demonstrated clear differences among the analyzed pellet types in terms of moisture content, ash content, and lower heating value.

Sunflower husk pellets showed the highest mean lower heating value, at 16.59 MJ/kg, and the lowest mean ash content, at 6.31**%**, indicating the most favorable combination of energy and ash-related characteristics among the analyzed materials. In contrast, corn stalk pellets exhibited the highest mean ash content, at 9.21%, while wheat straw pellets had the lowest mean lower heating value, at 14.72 MJ/kg. The statistical analysis confirmed that pellet type had a significant effect on lower heating value, $F(3,36) = 399.81$, $p < 0.001$, with a very large effect size ($\omega^2 = 0.968$). Tukey HSD post hoc analysis further showed that sunflower husk pellets had a significantly higher lower heating value than all other investigated pellet types. The obtained results indicate that the type of agricultural biomass is an important determinant of pellet energy performance and quality. However, based on the parameters examined in this study, a complete classification of the analyzed pellets according to EN ISO

17225-6 cannot be performed, since not all parameters required by the standard were investigated.

Future research should include additional physical and mechanical pellet properties, as well as other relevant fuel-quality parameters, in order to provide a more comprehensive assessment of pellet quality and enable a more complete classification in accordance with applicable standards.

REFERENCES

Bonner, I. J., Smith, W. A., Einerson, J. J., & Kenney, K. L. (2014). Impact of harvest equipment on ash variability of baled corn stover biomass for bioenergy. *BioEnergy Research, 7*, 845–855. https://doi.org/10.1007/s12155-014-9432-x Springer

Brkić, M., & Gluvakov, Z. (2015). *Development and equipping of a biomass pelletizing and briquetting plant*. Dignet.

European Committee for Standardization. (2005). *Solid biofuels—Fuel specifications and classes (CEN/TS 14961:2005).*

European Committee for Standardization. (2021a). *Solid biofuels—Fuel specifications and classes—Part 2: Graded wood pellets (EN ISO 17225-2:2021).*

European Committee for Standardization. (2021b). *Solid biofuels—Fuel specifications and classes—Part 6: Non-woody pellets (EN ISO 17225-6:2021).*

European Parliament and Council of the European Union. (2009). Directive 2009/28/EC on the promotion of the use of energy from renewable sources. *Official Journal of the European Union, L 140*, 16–62.

European Parliament and Council of the European Union. (2018). Directive (EU) 2018/2001 on the promotion of the use of energy from renewable sources. *Official Journal of the European Union, L 328*, 82–209.

European Parliament and Council of the European Union. (2023). Directive (EU) 2023/2413 amending Directive (EU) 2018/2001, Regulation (EU) 2018/1999 and Directive 98/70/EC as regards the promotion of energy from renewable sources. *Official Journal of the European Union*.

European Pellet Council. (2022). *ENplus handbook: Quality certification scheme for wood pellets*.

Gluvakov, Z. (2012). *Methods of energy pellets from biomass* [Master's thesis, University of Novi Sad, Faculty of Agriculture].

Gluvakov, Z., Brkić, M., & Košut, Z. (2015). *Methods for determining the quality of biomass energy pellets: Laboratory manual*. Diginet.

Institute for Standardization of Serbia. (n.d.). *SRPS E.B8.012: Determination of moisture content in solid fuels*.

Institute for Standardization of Serbia. (n.d.). *SRPS H.N8.136: Determination of ash content in solid fuels*.

International Organization for Standardization. (2017). *Solid biofuels—Sampling (ISO 18135:2017).*

International Organization for Standardization. (2022). *Solid biofuels—Determination of ash content (ISO 18122:2022).* ISO trenutno vodi ISO 18122:2022 kao važeće drugo izdanje. ISO

International Organization for Standardization. (2017). *Solid biofuels—Determination of calorific value (ISO 18125:2017).* ISO potvrđuje da je ovo izdanje i dalje važeće. ISO

International Organization for Standardization. (2022). *Solid biofuels—Determination of moisture content—Part 1: Reference method (ISO 18134-1:2022).* ISO

Jach-Nocoń, M., Pełka, G., Luboń, W., Mirowski, T., Nocoń, A., & Pachytel, P. (2021). An assessment of the efficiency and emissions of a pellet boiler combusting multiple pellet types. *Energies, 14*(15), 4465. https://doi.org/10.3390/en14154465 MDPI

Picchio, R., Latterini, F., Venanzi, R., Stefanoni, W., Suardi, A., Tocci, D., & Pari, L. (2020). Pellet production from woody and non-woody feedstocks: A review on biomass quality evaluation. *Energies, 13*(11), 2937. https://doi.org/10.3390/en13112937 MDPI

Turzyński, T., Kluska, J., Ochnio, M., & Kardaś, D. (2021). Comparative analysis of pelletized and unpelletized sunflower husks combustion process in a batch-type reactor. *Materials, 14*(10), 2484. https://doi.org/10.3390/ma14102484

DOI:10.5937/IIZS26209D

MONTE CARLO ANALYSIS OF RESISTOR MISMATCH IN THREE-OP-AMP INSTRUMENTATION AMPLIFIERS

Research paper

Hristina Delibašić-Marković[1*], Violeta Petrović[2], Ivan Petrović[3]
[1,2]University of Kragujevac, Faculty of Science, Kragujevac, Serbia
[3]Academy of Professional Studies Šumadija, Department in Kragujevac, Kragujevac, Serbia

Abstract: Resistor mismatch in the output stage of an instrumentation amplifier produces a common-mode error that can limit measurement accuracy. This paper examines the effect of resistor tolerances on the DC common-mode rejection ratio (CMRR) of a three-op-amp instrumentation amplifier. A Python application was developed to perform Monte Carlo simulations with 100,000 realizations per configuration. The calculations assume ideal operational amplifiers and compare independent uniform resistor deviations with a network model containing a shared deviation and independent residual errors. For a front-stage gain of 10 and a nominal unity-gain output stage, reducing independent tolerances from $\pm 1\%$ to $\pm 0.1\%$ increased the median CMRR from 67.90 to 87.90 dB. The fraction of circuits meeting an 80 dB requirement increased from 13.28% to 91.64%. In the network model, the shared deviation cancelled from the resistance ratios, leaving the residual mismatch to determine CMRR. The calculated gains were checked against independent nodal-equation solutions. The results show how tolerance choice affects both the typical CMRR and the proportion of circuits that satisfy a design requirement under the assumed component distributions.
Key words: instrumentation amplifier; resistor tolerance; Monte Carlo simulation.

INTRODUCTION

Instrumentation amplifiers are used to measure small voltage differences in sensor interfaces, industrial monitoring and data acquisition systems. In these applications, a common-mode voltage may be much larger than the signal being measured, so even a small common-mode gain can introduce a significant error (Ren et al., 2025). In the conventional three-op-amp circuit, the first stage amplifies the differential signal, while the final stage subtracts its two outputs. The accuracy of this subtraction depends on the matching of resistor ratios. Resistor tolerances must therefore be considered when selecting components for a specified CMRR.
The effect of resistor mismatch on common-mode rejection has been studied for several decades. Pallás-Areny and Webster derived expressions for the CMRR of differential and three-op-amp instrumentation amplifiers, including the effects of finite amplifier gains, (Pallás-Areny & Webster, 1991). Later design guidance (Ahmadi et al., 2023; Carrillo et al., 2024) addressed the use of matched resistors and integrated instrumentation amplifiers in practical measurement circuits. These considerations remain relevant when choosing between discrete components and resistor networks. The present work uses the established circuit equations to compare their behavior under explicitly defined statistical assumptions. A Python application calculates CMRR distributions and the probability of meeting a specified threshold, separating a common resistance deviation from the residual mismatch between individual resistors.
The paper is organized as follows. Section 2 describes the circuit model and the statistical assumptions used for resistor deviations. Section 3 presents and discusses the Monte Carlo results, their agreement with the first-order error estimate, and the effects of resistor tolerance and front-stage gain. Section 4 gives the conclusions and the limitations of the analysis.

THEORETICAL FRAMEWORK

The input voltages of an instrumentation amplifier can be separated into differential (V_d) and common-mode (V_{cm}) components:

[1] Corresponding author, hristina.delibasic@pmf.kg.ac.rs , ORCID: 0000-0002-8391-4179
[2] violeta.petrovicpmf.kg.ac.rs, ORCID: 0000-0002-7865-523X
[3] kgivanpetrovic@gmail.com, ORCID: 0009-0003-2419-8787

$$V_d = V_2 - V_1,$$
$$V_{cm} = \frac{(V_1+V_2)}{2}. \quad (1)$$

For a linear circuit, the output voltage is:

$$V_0 = A_d V_d + A_{cm} V_{cm}. \quad (2)$$

where A_d and A_{cm} are the differential and common-mode gains, respectively. The first term represents the amplified signal, while the second is the error produced by the common-mode input. The purpose of the instrumentation amplifier is to provide a defined differential gain while keeping the common mode gain close to zero.
The circuit considered here consists of a symmetric input stage followed by a difference amplifier. All three operational amplifiers are assumed ideal. The input stage has two equal feedback resistors R_f and a gain-setting resistor R_g connecting the inverting inputs. Its differential gain is $G = 1 + 2R_f/R_g$, giving the intermediate voltages:

$$u_1 = V_{cm} - \frac{GV_d}{2},$$
$$u_2 = V_{cm} + \frac{GV_d}{2}. \quad (3)$$

Thus, the differential component is amplified by G, whereas the common-mode component passes through the first stage with unity gain. The gain G is treated as exact in this study, and component deviations are introduced only in the final stage.
The circuit analyzed in this work is shown on Fig. 1. In the output stage, R_1 connects u_1 to the inverting input of the third operational amplifier, and R_2 provides negative feedback from its output. Resistor R_3 connects u_2 to the noninverting input, while R_4 connects this input to ground. Defining $p = R_2/R_1$ and $q = R_4/R_3$, Kirchhoff's current law and the ideal operational-amplifier conditions give:

$$V_0 = -pu_1 + \left[\frac{(1+p)q}{1+q}\right] u_2 . \quad (4)$$

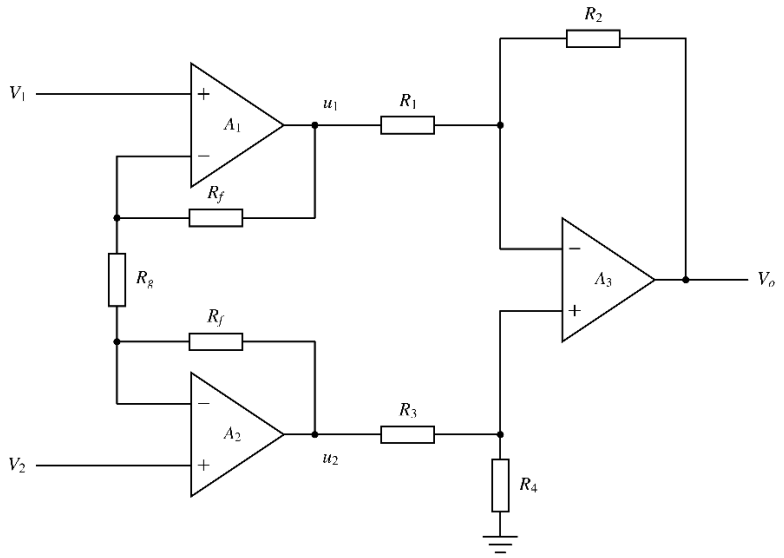


Fig. 1. *Three-op-amp instrumentation amplifier used in the analysis. The input stage has equal feedback resistors R_f and a gain-setting resistor R_g. Resistor deviations are applied only to $R_1 - R_4$ in the output stage. All operational amplifiers are assumed ideal.*

Combining Eqs. (3) and (4) gives the exact gains:

$$\begin{aligned} A_{cm} &= \frac{q-p}{1+q}, \\ A_d &= \frac{G}{2}\left[p + \frac{(1+p)q}{1+q}\right]. \end{aligned} \tag{5}$$

The common-mode gain vanishes when $p = q$. For nominal ratios $p = q = k$, the differential gain is $A_d = G_k$. Common-mode rejection therefore depends on the matching of resistance ratios rather than on the absolute resistance values, (Pallás-Areny & Webster, 1991; Sharma et al., 2023).
The CMRR and the corresponding input-referred error, e_{in}, are defined as:

$$\begin{aligned} CMRR_{\mathrm{dB}} &= 20\log_{10}\left|\frac{A_d}{A_{cm}}\right|, \\ e_{\mathrm{in}} &= \frac{V_{cm}A_{cm}}{A_d}, \end{aligned} \tag{6}$$

where e_{in} is the differential voltage that would produce the same output as the unwanted common-mode contribution. It provides a measure of the error in volts for a given common-mode input.
For the discrete-resistor configurations, the resistance values are described by:

$$\begin{aligned} R_i &= R_{i0}(1+\varepsilon_i), \\ \varepsilon_i &\sim U(-t,t), \end{aligned} \tag{7}$$

where R_{i0} is the nominal resistance and the deviations ε_i are independent. The parameter t is the relative tolerance half-width; $t = 0.01$ corresponds to $\pm 1\%$. A uniform distribution is adopted as a modeling assumption, since a specified tolerance alone does not determine the probability distribution within its bounds.
For small deviations from the nominal ratios, expansion to first order gives:

$$\begin{aligned} p &\approx k(1+\varepsilon_2-\varepsilon_1), \\ q &\approx k(1+\varepsilon_4-\varepsilon_3). \end{aligned} \tag{8}$$

The common-mode leakage referred to the differential input then becomes:

$$\frac{A_{cm}}{A_d} \approx \frac{\varepsilon_1-\varepsilon_2-\varepsilon_3+\varepsilon_4}{G(1+k)}. \tag{9}$$

Only the indicated combination of deviations contributes at first order. Equal changes in all four resistances cancel, while changes that affect the two ratios differently produce a finite error. For independent uniform deviations, each ε_i has zero mean and variance $t^2/3$. Eq. (9) therefore gives the leading-order RMS error:

$$e_{\mathrm{in},rms} \approx \frac{2|V_{cm}|t}{\sqrt{3}G(1+k)}. \tag{10}$$

This expression serves as an analytical check on the numerical results.
The resistor-network configuration is represented by a common multiplicative deviation c and independent residual deviations η_{i}:

$$\begin{aligned} R_i &= R_{i0}(1+c)(1+\eta_i), \\ c &\sim U(-a,a), \eta_{\mathrm{i}} \sim U(-m,m). \end{aligned} \tag{11}$$

The same value of c is applied to all four resistors within each realization, independently of the residual deviations. It cancels exactly from p and q, so the network's resistor-limited CMRR depends on the residual mismatch. The parameter m describes the residual deviation of each resistor and is not a specification of ratio-matching accuracy.
The Monte Carlo calculations use the exact gains in Eq. (5). For a prescribed threshold C_0, the acceptance probability is estimated as the fraction of realizations satisfying $CMRR_{\mathrm{dB}} \geq C_0$. Its sampling uncertainty is expressed using a 95% Wilson confidence interval. The analysis concerns static component variation in an ideal DC circuit. Finite amplifier CMRR, offset, temperature dependence, bandwidth and saturation are not included.

RESULTS AND DISCUSSION

The calculations were performed using CMRR Lab, a Python application with a graphical interface built with PySide6. The distributions and acceptance curves were plotted using Matplotlib (Hunter, 2007) (see Fig. 2). The user can specify resistor tolerances, front-stage gain, common-mode voltage, the number of realizations and the required CMRR. The application displays the calculated distributions and acceptance fractions and exports figures and numerical data. The source code is available on Zenodo at https://doi.org/10.5281/zenodo.22926393. Each resistor configuration was evaluated using 100,000 Monte Carlo realizations. Monte Carlo analysis has also been used in recent instrumentation-amplifier studies to assess CMRR robustness under component or device variations, although those studies consider different circuit architectures and variation models (Carrillo et al., 2024; Ahmadi et al., 2023; Raj et al., 2025). The nominal output-stage resistances were $10\ \mathrm{k\Omega}$, giving $k = 1$, and the front-stage gain was initially set to $G = 10$. Independent uniform deviations of $\pm 1\%$, $\pm 0.1\%$ and $\pm 0.01\%$ were compared with a network model containing a shared deviation of $\pm 1\%$ and independent residual deviations of $\pm 0.01\%$ per resistor. An 80 dB CMRR requirement was used to calculate the acceptance fractions. The analytical gains were checked against independent nodal-equation solutions for 500 randomly selected combinations of resistances and front-stage gains.

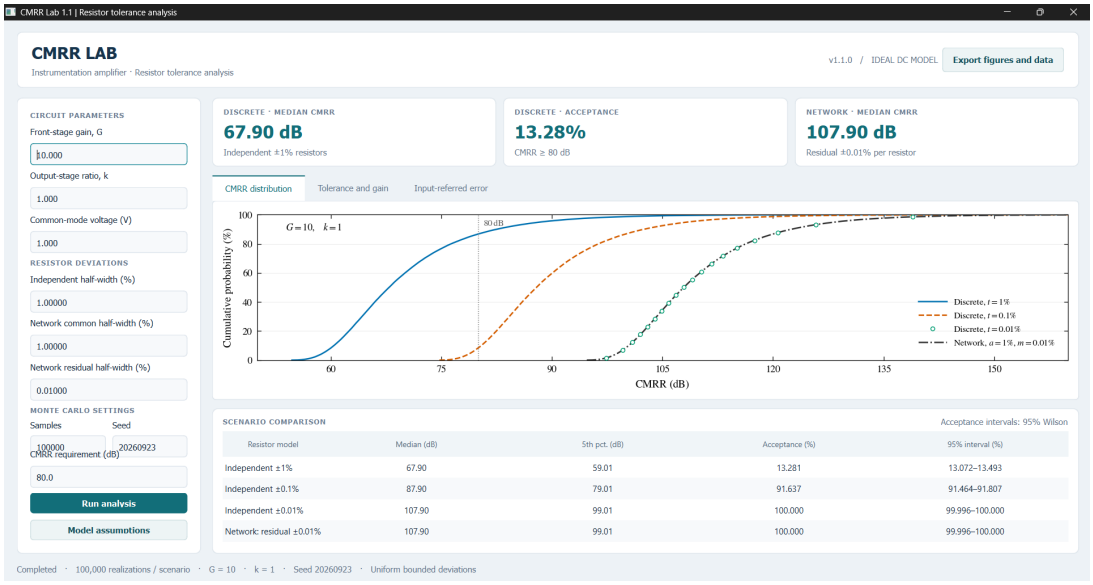


Fig. 2. *CMRR Lab interface showing the simulation parameters, CMRR distributions and acceptance fractions for the selected resistor configurations.*

The effects of resistor tolerance and front-stage gain on common-mode rejection are compared in Fig. 3. The results show both the spread of CMRR values and the fraction of simulated circuits that meet the 80 dB requirement.

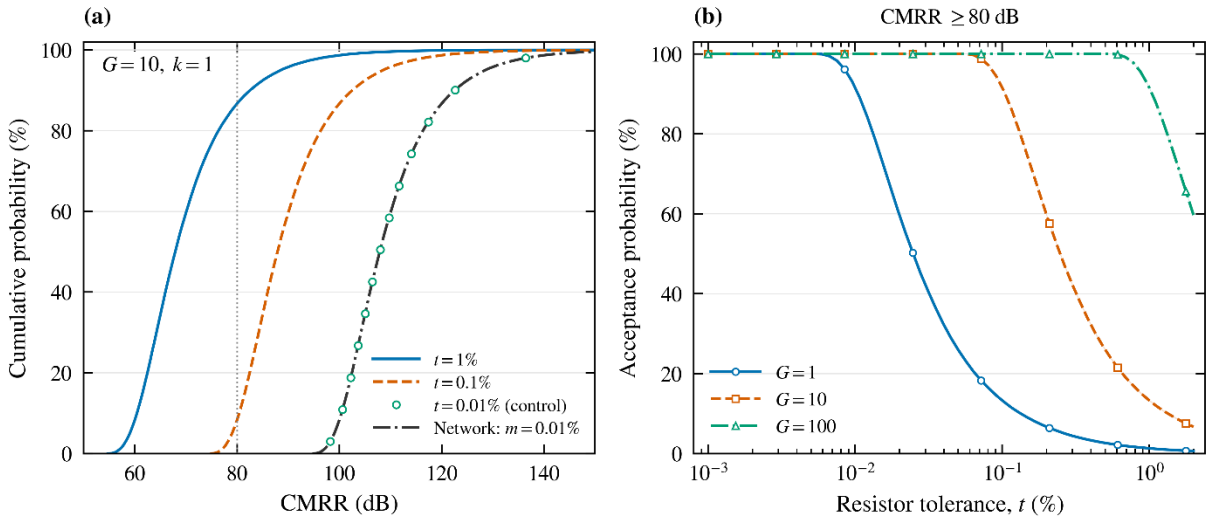


Fig. 3. *Cumulative CMRR distributions for* $G = 10$ *and* $k = 1$*. The network has a shared deviation of* $\pm 1\%$ *and independent residual deviations of* $\pm 0.01\%$ *per resistor. The dotted line marks the 80 dB requirement. (b) Probability of satisfying* $\mathrm{CMRR} \geq 80\ \mathrm{dB}$ *versus independent resistor tolerance for* $G = 1, 10$ *and* 100*. Shaded bands indicate pointwise* 95% *Wilson confidence intervals.*

Fig. 3(a) shows an approximately $20\ \mathrm{dB}$ shift towards higher CMRR for each tenfold reduction in independent resistor tolerance. The medians, obtained from the simulation data, are $67.90, 87.90$ and $107.90\ \mathrm{dB}$ for tolerances of $\pm 1\%, \pm 0.1\%$ and $\pm 0.01\%$, respectively. This trend agrees with Eq. (9), which predicts that common-mode leakage is proportional to the resistor deviations to first order. Table 1 lists the median CMRR and the percentage of realizations satisfying the 80 dB requirement for each resistor configuration.

Table 1. *CMRR statistics for 100,000 realizations per configuration, with* $G = 10$ *and* $k = 1$*.*

Resistor configuration	Median CMRR (dB)	Values
Independent, $\pm 1\%$	67.90	13.28
Independent, $\pm 0.1\%$	87.90	91.64
Independent, $\pm 0.01\%$	107.90	100.00
Network, $\pm 1\%$ shared and $\pm 0.01\%$ residual	107.90	100.00

Although the median CMRR for $\pm 0.1\%$ resistors exceed the requirement by almost $8\ \mathrm{dB}$, 8.36% of the realizations remain below the threshold. In Fig. 3(a), this fraction corresponds to the cumulative probability at $80\ \mathrm{dB}$; the acceptance fraction is its complement. The 95% Wilson confidence intervals for the acceptance fractions are $13.07 - 13.49\%$ for $\pm 1\%$ resistors and $91.46 - 91.81\%$ for $\pm 0.1\%$ resistors. These intervals describe sampling uncertainty under the assumed resistor distributions. The control markers for independent $\pm 0.01\%$ resistors overlap the network curve. This agrees with Eq. (11): the shared multiplicative deviation cancels from the resistance ratios, leaving the residual deviations to determine CMRR. The network therefore gives the same rejection distribution as independent resistors with the same residual tolerance, despite its larger shared deviation in absolute resistance. Fig. 3(b) shows that increasing the front-stage gain raises the acceptance probability at a given resistor tolerance. From Eq. (5), the differential gain is proportional to G, while the common-mode gain is independent of G. A tenfold increase in G therefore raises CMRR by $20\ \mathrm{dB}$ for a fixed realization with nonzero common-mode gain. The approximately tenfold horizontal displacement of the acceptance curves agrees with this dependence and the first-order tolerance model. The shaded confidence intervals are too narrow to distinguish clearly at the scale of the figure.
The effect of resistor mismatch on measurement accuracy is expressed as an input-referred voltage error in Fig. 4. The distributions are compared for a common-mode input of $1\ \mathrm{V}$, with $G = 10$ and $k = 1$.

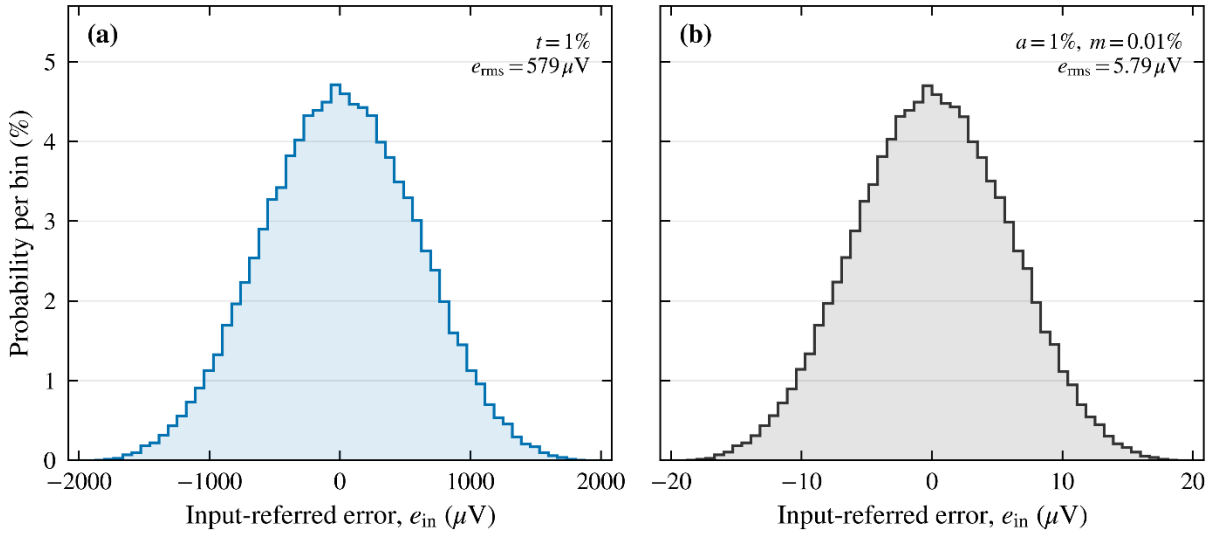


Fig. 4. *Input-referred error distributions for $V_{cm} = 1$ V, $G = 10$ and $k = 1$: (a) independent $\pm 1\%$ resistor deviations; (b) a resistor network with $\pm 1\%$ shared and $\pm 0.01\%$ residual deviations per resistor. Each histogram contains 60 bins spanning ± 3.6 times its RMS error. Note the different horizontal scales.*

Fig. 4(a) shows the input-referred error distribution for independent $\pm 1\%$ resistors, while Fig. 4(b) shows the network result with $\pm 1\%$ shared and $\pm 0.01\%$ residual deviations. The calculated RMS errors are $578.54\,\mu V$ and $5.7853\,\mu V$, respectively. This approximately hundredfold reduction follows the reduction in the independent resistor deviations that affect the resistance ratios. The first order estimates from Eq. (10), $577.35\,\mu V$ and $5.7735\,\mu V$, differ from the simulated values by approximately 0.21%. The distributions have similar shapes but substantially different voltage ranges. Each histogram uses 60 bins spanning ± 3.6 times its own RMS error, so the similar bar heights represent comparable probabilities per bin rather than comparable error magnitudes. The difference in magnitude is given by the horizontal scales and the reported RMS values. Both distributions are approximately symmetric about zero. Positive and negative errors therefore compensate across the simulated ensemble, but not within an individual circuit. For fixed resistor values and a fixed common-mode input, each circuit retains its corresponding error. The results show how residual resistor mismatch can introduce a measurable differential-input error even when the operational amplifiers themselves are ideal (Albuquerque et al., 2026).

CONCLUSION

The analysis shows that resistor selection based on median CMRR can leave a substantial fraction of circuits below the required rejection level. For $G = 10$ and $k = 1$, independent $\pm 0.1\%$ resistors produced a median CMRR of 87.90 dB, yet 8.36% of the simulated realizations failed to satisfy the 80 dB requirement. The acceptance probability therefore provides information needed to judge whether a tolerance is adequate under the assumed component distribution.

The network calculations show that the relevant quantity is the mismatch between resistance ratios. A shared multiplicative deviation cancels from these ratios, while independent residual deviations produce common-mode leakage. Increasing the front-stage gain reduces the input-referred contribution of this leakage, although the available signal range and bandwidth must also be considered in a practical design.

The Python application provides a reproducible calculation of these effects, supported by independent nodal-equation checks and agreement with the first-order RMS error estimates. Its results can inform the allocation of the resistor-mismatch contribution within a measurement error budget. They remain conditional on the adopted statistical distributions and ideal DC

assumptions; predicting complete circuit performance requires the amplifier's finite common-mode rejection, temperature dependence and frequency response to be included.

ACKNOWLEDGEMENT

Authors would like to acknowledge the support received from the Science Fund of the Republic of Serbia, #GRANT 6821, Atoms and (bio)molecules-dynamics and collisional processes on short time scale - ATMOLCOL. Our appreciation also goes to the Serbian Ministry of Education, Science and Technological Development (Agreement No. 451-03-137/2025-03/ 200122). H. Delibasic Markovic would also like to express gratitude to COST Actions CA21159 - "Understanding interaction of light with biological surfaces: possibility for new electronic materials and devices" for their support and CA22148 - "An international network for Non-linear Extreme Ultraviolet to hard X-ray techniques (NEXT)".

REFERENCES

Ahmadi, S., Mahmoudi, A., Maddipatla, D., Bazuin, B. J., Azhari, S. J., & Atashbar, M. Z. (2023). A current mode instrumentation amplifier with high common-mode rejection ratio designed using a novel fully differential second-generation current conveyor. *SN Applied Sciences, 5*, Article 34. https://doi.org/10.1007/s42452-022-05247-x

Albuquerque, L. V., dos Santos Melo, G., do Nascimento, F. B., & de Souza, C. P. (2026). An applied method based on Monte Carlo simulations to evaluate the impact of electronic component tolerance. In *2026 10th International Symposium on Instrumentation Systems, Circuits and Transducers (INSCIT)* (pp. 1-6). IEEE. https://doi.org/10.1109/INSCIT72361.2026.11707211

Carrillo, J. M., Ocampo-Hidalgo, J. J., Corbacho, I., de la Cruz-Blas, C. A., & Domínguez, M. Á. (2024). 0.6-V CMOS bulk-driven instrumentation amplifier for IoMT bioimpedance analysis. *International Journal of Circuit Theory and Applications, 52*(10), 4970-4984. https://doi.org/10.1002/cta.4008

Hunter, J. D. (2007). Matplotlib: A 2D graphics environment. *Computing in Science & Engineering, 9*(3), 90-95. https://doi.org/10.1109/MCSE.2007.55

Pallás-Areny, R., & Webster, J. G. (1991). Common mode rejection ratio in differential amplifiers. *IEEE Transactions on Instrumentation and Measurement, 40(4)*, 669-676. https://doi.org/10.1109/19.85332

Raj, N., Dutta, S., Ranjan, R. K., Das, P. K., Singh, D. K., & Kuntman, H. (2025). VDTA based transadmittance mode instrumentation amplifier with experimental results. *International Journal of Electronics, 112*(10), 2194-2211. https://doi.org/10.1080/00207217.2024.2439182

Ren, J., Niu, Y., Liu, B., Li, M., Bai, Y., & Chen, Y. (2025). Design of an SAR-assisted offset-calibrated chopper CFIA for high-precision 4-20 mA transmitter front ends. *Applied Sciences, 15*(16), Article 9084. https://doi.org/10.3390/app15169084

Sharma, D., Shylashree, N., Prasad, R., & Nath, V. (2023). Analysis of programmable gain instrumentation amplifier. *International Journal of Microsystems and IoT, 1*(1), 41-47. https://doi.org/10.5281/zenodo.8191366

DOI:10.5937/IIZS26216V

AN INTEGRATED ENERGY AND BIOCLIMATIC SYSTEM FOR POSITIVE-ENERGY BUILDINGS: BIPV, ELECTRICAL STORAGE AND A ROOFTOP GREENHOUSE

Research paper

Ionuț-Vasile Nicoraș[1*], Flavius-Maxim Petcuț[2], Anca-Adriana Petcuț-Lasc[3*], Valentina Emilia Balas[4]

[1,3]Petroleum-Gas University of Ploiești, Doctoral School, Ploiești, Romania
[1]Smart House Color, Arad, Romania
[2,3,4]"Aurel Vlaicu" University of Arad, Faculty of Engineering, Arad, Romania
[4]Academy of Romanian Scientists, Bucharest, Romania

Abstract: Highly insulated and airtight buildings reduce the heating demand, but they also retain indoors the carbon dioxide exhaled by the occupants and, in most cases, they remain simple consumers of energy. This paper proposes an integrated energy and bioclimatic system in which the envelope of a public building produces electricity through building-integrated photovoltaics (BIPV), a battery shifts this production towards the evening hours, and a rooftop bioclimatic greenhouse is coupled to the ventilation circuit so that the plants remove a part of the carbon dioxide generated indoors. A reduced-order model of the coupled building–greenhouse–photovoltaic–storage system is formulated and a preliminary annual assessment is carried out for a 600 m² office building located in Arad, western Romania. The estimated results indicate an annual energy balance ratio of 1.41, a self-sufficiency of 82% obtained with a 60 kWh battery, an indoor carbon dioxide concentration kept below 1000 ppm during the occupied period with a fresh-air flow rate reduced by 27%, and approximately 17.7 t of avoided carbon dioxide emissions per year. The paper also defines the modelling and experimental programme of ongoing doctoral research.
Key words: *BIPV, positive-energy building, energy storage, indoor air quality, rooftop greenhouse*

INTRODUCTION

The building sector is one of the main targets of the European climate policy, and photovoltaic technology is expected to provide a large share of the required on-site generation (Kougias et al., 2021). Building-integrated photovoltaics (BIPV) extend this role from the roof to the whole envelope, the modules being used at the same time as generation units and as construction elements (Biyik et al., 2017). When the photovoltaic generator is combined with electrical storage, the share of the production that is consumed on site increases substantially, typically by 13–24 percentage points for a storage capacity of 0.5–1 kWh per installed kW (Luthander et al., 2015).

At the same time, the thermal renovation of buildings has a less visible consequence. A well-insulated and airtight envelope reduces the uncontrolled air exchange, so the carbon dioxide exhaled by the occupants accumulates in the occupied rooms. Concentrations that are commonly reached in meeting rooms and classrooms have been associated with a measurable decrease of the higher-order cognitive function of office workers (Allen et al., 2016), and the reference indoor air quality categories of EN 16798-1 are defined precisely through the carbon dioxide concentration above the outdoor level (European Committee for Standardization, 2019). The conventional answer is dilution ventilation, which consumes in winter a part of the energy saved through insulation.

A third line of research, apparently unrelated, is the integration of agriculture into the building. The integrated rooftop greenhouse built on the ICTA-ICP building in Barcelona demonstrated that heat, carbon dioxide and rainwater can be exchanged between a building and the greenhouse placed on its roof, with a better environmental performance than that of a free-standing greenhouse (Nadal et al., 2017)

[1]Corresponding author, nicorasionut@gmail.com, ORCID: 0009-0001-2117-0338
[2]flavius.petcut@uav.ro, ORCID: 0009-0001-6928-4019
[3]Corresponding author, anca.petcut@uav.ro, ORCID: 0009-0000-5450-5272
[4]balas@drbalas.ro, ORCID: 0000-0003-0885-1283

The three directions are usually treated separately: the photovoltaic generator is sized by the electrical engineer, the ventilation system by the mechanical engineer and the greenhouse, when it exists, by the horticulturist. The optimum of each subsystem taken separately is not the optimum of the assembly. The aim of this paper is to describe a system in which the three subsystems are coupled and operated by a single supervisory controller, to formulate a reduced-order model suitable for control design, and to present a preliminary estimate of the energy, indoor air quality and environmental performance for a case study located in the temperate continental climate of western Romania. The work is the starting point of a doctoral research programme and continues the previous analyses of residential photovoltaic systems of the authors (Petcuț-Lasc et al., 2024).
The main contribution of this work is the integrated formulation of BIPV generation, electrical storage, indoor CO_2 management and rooftop greenhouse operation within a unified supervisory control framework for positive-energy public buildings.

THE PROPOSED SYSTEM

The structure of the proposed system is presented in Fig. 1. It contains four subsystems and two coupling loops.

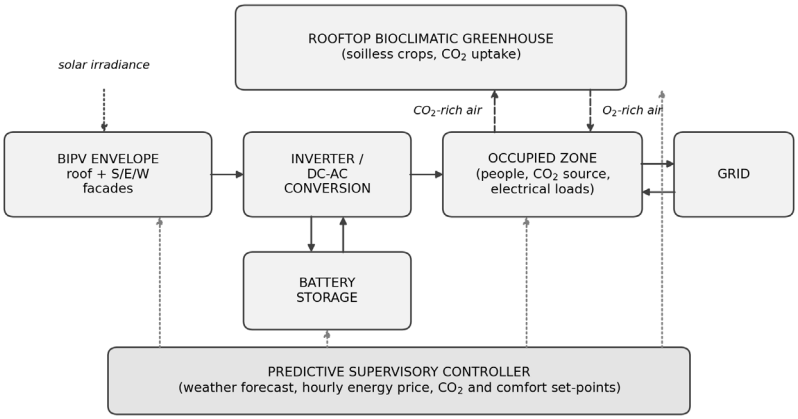


Fig. 1. *Structure of the integrated energy and bioclimatic system*

The generation subsystem consists of photovoltaic modules integrated in the roof and in the south, east and west façades. The façade modules produce less energy in summer, when the sun is high, but they compensate a part of the winter deficit, when the sun is low and the days are short, so the annual production profile becomes flatter than that of a roof-only installation.
The storage subsystem is a lithium-iron-phosphate battery. Its role is not to increase the annual production, but to move it in time: the maximum production occurs around noon, while the building consumes mainly in the morning and in the evening.
The bioclimatic subsystem is a soilless greenhouse placed on the roof. The air of the occupied zone, enriched in carbon dioxide, is transferred to the greenhouse, where a part of the carbon dioxide is consumed by photosynthesis, and the air returned to the occupied zone has a lower carbon dioxide concentration. The greenhouse therefore acts as a partial regeneration stage of the indoor air and, at the same time, as a thermal buffer above the last floor and as a source of fresh vegetables.
The fourth subsystem is the supervisory controller. It receives the weather forecast, the hourly energy price and the measured states of the building, and it computes the air flow rates, the charging and discharging power of the battery and the set-points of the heat pump. The natural formulation for such a multi-objective problem is model predictive control, whose application to buildings is now well documented (Drgoňa et al., 2020).

MATERIAL AND METHODS

Reduced-order model

The model used for control design is a lumped-parameter model. The carbon dioxide balance of the occupied zone, whose air volume is V_z and whose concentration is C_z, is written as:

$$V_z \frac{dC_z}{dt} = nG_p + q_v(C_g - C_z) \quad (1)$$

where n is the number of occupants, G_p is the carbon dioxide generation rate per person, q_v is the air flow rate exchanged with the greenhouse and C_g is the concentration in the greenhouse. The balance of the greenhouse, of volume V_g, contains in addition the infiltration term and the photosynthetic uptake:

$$V_g \frac{dC_g}{dt} = q_v(C_z - C_g) + q_i(C_o - C_g) - \Phi_p \quad (2)$$

in which q_i is the infiltration flow rate, C_o is the outdoor concentration and Φ_p is the net carbon dioxide uptake of the crop, which depends on the photosynthetically active radiation, on the leaf area and on the concentration itself. For this preliminary assessment, the photosynthetic CO_2 uptake was represented by a simplified constant uptake rate per unit leaf area. This assumption will be replaced by an experimentally identified radiation and CO_2 dependent model in the subsequent stage of the research. A net uptake rate of 5 μmol CO_2 m^{-2} s^{-1} of leaf area was applied during daylight hours, together with a leaf area index of 2.5, i.e. about 375 m² of leaf area for the 150 m² greenhouse (Table 1). The value is well below the light-saturated leaf photosynthesis rates reported for greenhouse vegetable crops (Marcelis et al., 1998) and was chosen conservatively to account for the low winter irradiance; it corresponds to about 0.3 kg of CO_2 per hour, i.e. roughly one fifth of the CO_2 generated by the 40 occupants. The state of charge of the battery follows the usual relation:

$$E_b \frac{dSOC}{dt} = \eta_c P_{ch} - \frac{P_{dis}}{\eta_d} \quad (3)$$

where E_b is the usable capacity of the battery and η_c and η_d are the charging and discharging efficiencies. Two indicators are used for the annual assessment: the energy balance ratio *EBR*, defined as the ratio between the on-site production E_{PV} and the electricity demand E_L, and the self-sufficiency *SS*, defined with the energy imported from the grid E_{imp}:

$$EBR = \frac{E_{PV}}{E_L} \quad , \quad SS = 1 - \frac{E_{imp}}{E_L} \quad (4)$$

Case study and assumptions

The reference object is an existing office building located in Arad, in the west of Romania, in a temperate continental climate. The hourly production of the photovoltaic generator was estimated for each orientation from a typical meteorological year, and the electrical demand was built from the measured load profile of a similar administrative building. The main assumptions are given in Table 1.

The typical meteorological year (TMY) used to estimate the hourly photovoltaic production was obtained from the PVGIS (Photovoltaic Geographical Information System) database, developed by the Joint Research Centre of the European Commission, for the site of Arad, Romania (46.18° N, 21.31° E). The TMY dataset, derived from multi-year climatological series

(reference period 2005–2020, depending on the SARAH-3/ERA5 solar-radiation database selected in PVGIS) following the Sandia/ISO 15927-4 methodology, provides hourly values of global horizontal and tilted irradiance, air temperature and wind speed that are statistically representative of an average climatic year rather than of an extreme year. The production of each orientation of the photovoltaic generator (roof, south façade, east and west façades) was estimated separately, applying the tilt and azimuth angles corresponding to the BIPV configuration described in the previous section, using the conversion model integrated in PVGIS (the PVGIS-CM SAF irradiance model together with the Faiman cell-temperature model).

Table 1. *Main parameters of the case study*

Parameter	**Value**
Useful floor area / occupants	600 m² / 40 persons
Occupancy schedule	08:00–18:00, working days
Annual electricity demand	34 000 kWh
BIPV roof, 30° south	28 kWp
BIPV south façade	10 kWp
BIPV east and west façades	2 × 6 kWp
Battery capacity / round-trip efficiency	60 kWh / 92 %
Greenhouse area / air volume	150 m² / 450 m³
Air flow rate between zone and greenhouse	max. 2 000 m³/h
CO_2 generation rate per person	18 l/h
Outdoor CO_2 concentration	420 ppm
Grid emission factor	0.37 kg CO_2/kWh
Leaf area index / net CO_2 uptake of the crop	2.5 / 5 μmol m^{-2} s^{-1} (daytime)

RESULTS AND DISCUSSION

The estimated monthly electricity production and consumption are presented in Fig. 2. The annual production is 47 900 kWh, for an annual demand of 34 000 kWh, which corresponds to an energy balance ratio of 1.41. During eight months of the year, from March to October, the building delivers to the grid more energy than it takes from it; the deficit remains concentrated in the four cold months, when the heating demand is maximum and the solar resource is minimum.

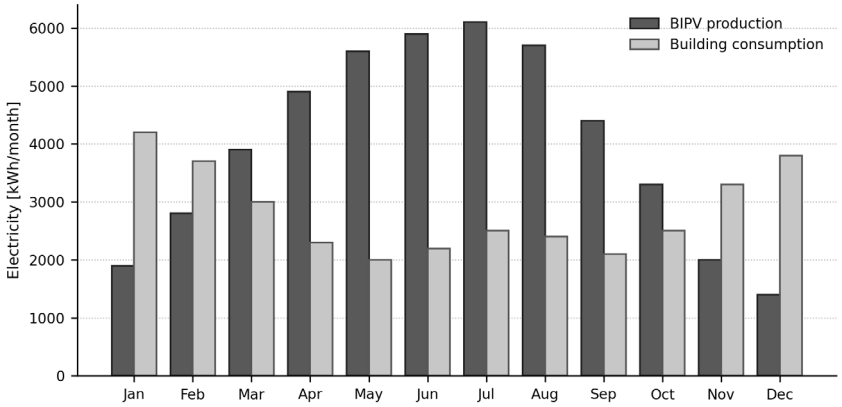


Fig. 2. *Estimated monthly electricity production and consumption*

Through the direct consumption of the photovoltaic production and the battery of 60 kWh, which shifts a part of the midday surplus towards the morning and evening hours, about 27

900 kWh per year are covered on site, so the self-sufficiency computed with relation (4) reaches 82 %, and the energy imported from the grid falls to 6 100 kWh per year. The surplus of approximately 20 000 kWh delivered to the grid is comparable with the annual consumption of ten average households.
The effect of the greenhouse loop on the indoor air quality is shown in Fig. 3, for a typical winter working day. In the reference case, with the windows closed and with the minimum mechanical ventilation, the concentration exceeds 1400 ppm after about four hours of occupancy. When a part of the air is circulated through the greenhouse, the concentration remains below 1000 ppm, which corresponds to category II of EN 16798-1, while the fresh-air flow rate taken from outside, and implicitly the energy needed to heat it, is reduced by 27 %.

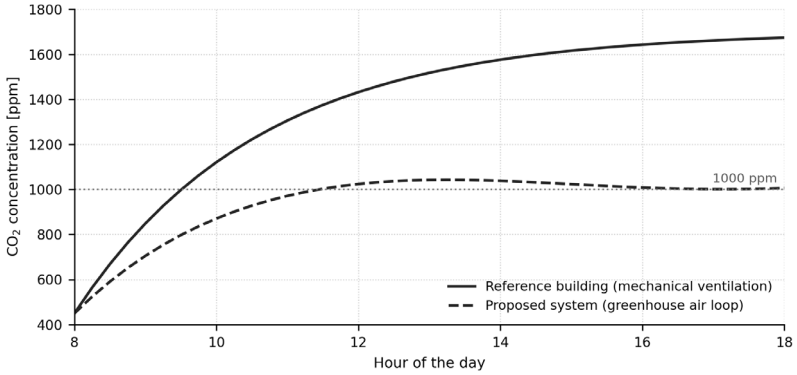


Fig. 3. *Indoor CO_2 concentration during a typical winter working day*

The comparison between the reference building and the proposed system is summarised in Table 2. Besides the energy and air quality indicators, the greenhouse produces about 3.5 t of vegetables and herbs per year on 150 m² of soilless culture, and the avoided emissions, computed with the emission factor of the Romanian grid, are of the order of 17.7 t of carbon dioxide per year.

Table 2. *Estimated annual performance, reference building and proposed system*

Indicator	Reference building	Proposed system
Electricity demand	34 000 kWh	34 000 kWh
On-site production	–	47 900 kWh
Energy balance ratio	0	1.41
Self-sufficiency	0 %	82 %
Energy imported from the grid	34 000 kWh	6 100 kWh
Energy delivered to the grid	–	20 000 kWh
Peak indoor CO_2 concentration	1 400–1 800 ppm	below 1 000 ppm
Fresh air taken from outside	reference	−27 %
Vegetables produced	–	≈ 3.5 t/year
Avoided CO_2 emissions	–	17.7 t/year

For public buildings such as schools, town halls or hospitals, the high self-sufficiency means a lower exposure to electricity price increases; a detailed economic assessment, based on actual investment costs, will be carried out in a subsequent stage of the research.

Sensitivity analysis

To assess the robustness of the preliminary results with respect to the sizing assumptions, a sensitivity analysis was performed for two parameters considered critical for the energy performance of the system: the usable battery capacity (E_b) and the annual electricity demand

(E_L). The analysis was carried out by deterministic simulation, keeping all other assumptions of Table 1 unchanged. The analysis focused on the energy balance ratio (*EBR*), while the influence of battery capacity on self-sufficiency will be quantified in a subsequent stage using the complete hourly model. Two levels were considered for the battery capacity, 40 kWh and 80 kWh, corresponding to approximately ±33% relative to the reference case and reflecting the usual commercial range of lithium-iron-phosphate modules available for a building of this size, together with a variation of ±10% in the annual electricity demand. Each scenario was obtained from a single simulation run, keeping the remaining parameters fixed (a one-factor-at-a-time design); a full factorial sensitivity analysis is left for a later stage of the research. The results are summarised in Table 3.

Table 3. *Sensitivity of the annual performance indicators to battery capacity and electricity demand*

Scenario	Battery (kWh)	Demand (kWh/year)	EBR
Reference	60	34 000	1.41
Battery −33%	40	34 000	1.41
Battery +33%	80	34 000	1.41
Demand +10%	60	37 400	1.28
Demand −10%	60	30 600	1.57

The results indicate that the energy balance ratio remains unchanged with the battery capacity, since this indicator depends only on the annual production and demand and not on the temporal distribution of the energy, and that it is, as expected, sensitive to the electricity demand, a variation of ±10% shifting it from 1.28 to 1.57. The battery capacity, by contrast, is expected to mainly affect the self-sufficiency rather than the energy balance ratio, consistent with the role of the battery as a means of shifting the energy in time rather than increasing its production, as stated in the "THE PROPOSED SYSTEM" section; quantifying this effect requires re-running the hourly model for each battery scenario and is left for a further stage of the analysis.

The results presented here are preliminary and have the value of an order of magnitude. They were obtained with a lumped-parameter model, with a constant photosynthetic uptake per unit of leaf area and with a perfect forecast of the weather and of the load. The main uncertainties concern the real uptake of the crop under variable radiation, the acceptance of a partially recirculated air by the occupants, and the behavior of the greenhouse during the summer, when it has to be protected against overheating. These aspects can be settled only by measurement, which is the reason for which the experimental validation is a central part of the research program.

CONCLUSION

The paper proposed an integrated energy and bioclimatic system in which the photovoltaic envelope, the electrical storage and a rooftop greenhouse are operated together, by a single supervisory controller, instead of being designed and operated separately. A reduced-order model of the coupled system was formulated, and a preliminary annual assessment was carried out for an office building located in western Romania.

The preliminary results suggest that the three objectives can be simultaneously pursued within the proposed integrated system: the building can produce about 41 % more electricity than it consumes over a year, it can cover 82 % of its own demand with a moderate battery, and it can keep the indoor carbon dioxide concentration below 1000 ppm with a fresh-air flow rate reduced by 27 %, while also producing fresh vegetables on the same surface.

The next stages of the research are the identification of the model parameters on measured data, the formulation of a simultaneous sizing methodology for the photovoltaic generator and the storage, and the construction of an instrumented demonstrator monitored over twelve months, so that the results are obtained in a temperate continental climate and not transferred

from the Mediterranean or northern European literature. The final objective is not a theoretical study, but a verified design methodology, applicable to the public buildings that are currently being renovated.

REFERENCES

Allen, J. G., MacNaughton, P., Satish, U., Santanam, S., Vallarino, J., & Spengler, J. D. (2016). Associations of cognitive function scores with carbon dioxide, ventilation, and volatile organic compound exposures in office workers: A controlled exposure study of green and conventional office environments. *Environmental Health Perspectives, 124*(6), 805–812. https://doi.org/10.1289/ehp.1510037

Biyik, E., Araz, M., Hepbasli, A., Shahrestani, M., Yao, R., Shao, L., Essah, E., Oliveira, A. C., del Caño, T., Rico, E., Lechón, J. L., Andrade, L., Mendes, A., & Atlı, Y. B. (2017). A key review of building integrated photovoltaic (BIPV) systems. *Engineering Science and Technology, an International Journal, 20*(3), 833–858. https://doi.org/10.1016/j.jestch.2017.01.009

Drgoňa, J., Arroyo, J., Cupeiro Figueroa, I., Blum, D., Arendt, K., Kim, D., Perarnau Ollé, E., Oravec, J., Wetter, M., Vrabie, D. L., & Helsen, L. (2020). All you need to know about model predictive control for buildings. *Annual Reviews in Control, 50*, 190–232. https://doi.org/10.1016/j.arcontrol.2020.09.001

European Committee for Standardization. (2019). *EN 16798-1:2019. Energy performance of buildings – Ventilation for buildings – Part 1: Indoor environmental input parameters for design and assessment of energy performance of buildings addressing indoor air quality, thermal environment, lighting and acoustics*. CEN.

Kougias, I., Taylor, N., Kakoulaki, G., & Jäger-Waldau, A. (2021). The role of photovoltaics for the European Green Deal and the recovery plan. *Renewable and Sustainable Energy Reviews, 144*, 111017. https://doi.org/10.1016/j.rser.2021.111017

Luthander, R., Widén, J., Nilsson, D., & Palm, J. (2015). Photovoltaic self-consumption in buildings: A review. *Applied Energy, 142*, 80–94. https://doi.org/10.1016/j.apenergy.2014.12.028

Marcelis, L. F. M., Heuvelink, E., & Goudriaan, J. (1998). Modelling biomass production and yield of horticultural crops: A review. *Scientia Horticulturae, 74*(1–2), 83–111. https://doi.org/10.1016/S0304-4238(98)00083-1

Nadal, A., Llorach-Massana, P., Cuerva, E., López-Capel, E., Montero, J. I., Josa, A., Rieradevall, J., & Royapoor, M. (2017). Building-integrated rooftop greenhouses: An energy and environmental assessment in the Mediterranean context. *Applied Energy, 187*, 338–351. https://doi.org/10.1016/j.apenergy.2016.11.051

Petcuț-Lasc, A.-A., Bălaș, V.-E., & Petcuț, F.-M. (2024). Analysis of a residential photovoltaic system. In *Proceedings of the XIV International Conference on Industrial Engineering and Environmental Protection (IIZS 2024)*. Technical Faculty "Mihajlo Pupin", Zrenjanin.



XVI International Conference Industrial Engineering and Environmental Protection 2026 (IIZS 2026)
October 01-02, 2026, Zrenjanin, Serbia

Session 3

Designing and Maintenance

DOI:10.5937/IIZS26224L

STRATEGIC PROJECT MANAGEMENT IN THE ORGANIZATION OF INDUSTRIAL MAINTENANCE SYSTEMS

Review paper

Peko Lakatuš[1], Mihalj Bakator[2]
[1,2.]University of Novi Sad, Technical Faculty "Mihajlo Pupin", Zrenjanin, Serbia

Abstract: Industry 4.0 technologies, including predictive analytics, artificial intelligence, and data-driven monitoring solutions, have significantly influenced the digital transformation of industrial maintenance systems. While these approaches improve operational efficiency and reliability, they often lack structured integration within broader organizational and strategic management frameworks. The emerging Industry 5.0 paradigm introduces a human-centric, resilient, and sustainable perspective, requiring a transition from technology-oriented maintenance models toward strategically coordinated systems.
This paper examines the transition from Industry 4.0 to Industry 5.0 within industrial maintenance organizations, with emphasis on the integration of strategic project management into digital maintenance initiatives. The review addresses three research questions concerning the integration of strategic project management into digital maintenance systems, organizational factors affecting the implementation of predictive maintenance, and the Industry 5.0 principles relevant to maintenance project management. Based on a structured review of recent literature, the study identifies a research gap concerning the alignment of predictive maintenance initiatives with strategic planning, organizational restructuring, and long-term business performance objectives.
A conceptual framework is proposed that integrates digital maintenance technologies, strategic project management, and human-centric Industry 5.0 principles. The framework distinguishes strategic project management as an integration layer that connects technological implementation with organizational objectives, resource allocation, risk management, stakeholder engagement, and performance monitoring. The paper contributes a structured perspective for coordinating digital maintenance initiatives with organizational and human factors and provides a basis for future empirical research and practical application in industrial maintenance systems.
Key words: Industry 4.0, Industry 5.0, strategic project management, industrial maintenance systems, digital transformation, human-centric management

INTRODUCTION

The rapid evolution of digital technologies has significantly transformed industrial production and maintenance systems over the past decade. Industry 4.0 has influenced maintenance practices, shifting them from reactive and preventive models toward predictive and condition-based strategies based on artificial intelligence, machine learning, and real-time data analytics (Taoufyq et al., 2025; Mallioris, 2024). These advancements have enabled organizations to reduce downtime, improve spare parts management, and improve equipment reliability.
However, despite technological progress, many industrial maintenance systems remain fragmented, lacking structured integration with strategic management and long-term business planning processes. Recent studies emphasize that predictive maintenance models frequently focus on algorithmic accuracy and technical performance, while organizational alignment and project governance structures are often neglected (Carvalho et al., 2021; Softić, 2024). In practice, this results in digital initiatives being implemented as isolated technical upgrades rather than as strategically managed transformation programs. Consequently, the expected improvements in operational efficiency and financial performance are not always fully realized.
The emerging Industry 5.0 paradigm introduces a broader perspective, highlighting human-centricity, resilience, and sustainability as key dimensions of industrial development (Benhanifia et al., 2025; Ramzan & Reforgiato, 2025). Unlike Industry 4.0, which is primarily technology-driven, Industry 5.0 promotes the integration of advanced technologies with human expertise, collaborative decision-making, and socially responsible management practices. For

[1]Corresponding author, peko.lakatus@gmail.com, ORCID: 0009-0001-1409-0065
[2]mihalj.bakator@tfzr.rs, ORCID: 0000-0001-8540-2460

industrial maintenance systems, this shift implies the need for coordinated organizational restructuring, workforce adaptation, and risk-aware planning mechanisms.

Several authors underline that digital transformation in maintenance environments requires not only advanced analytical tools but also structured governance frameworks capable of aligning technological innovation with strategic objectives (Rios et al., 2024; Achouch et al., 2022). The transition from Industry 4.0 to Industry 5.0 therefore cannot be achieved solely through technological upgrades; it demands the application of strategic project management principles to support systematic planning, stakeholder engagement, resource allocation, and performance monitoring.

Despite growing interest in Industry 5.0 concepts, there remains a limited number of studies that explicitly address the integration of predictive maintenance systems with strategic project management at the organizational level (Ali, 2024; Murtaza et al., 2024). This gap is particularly evident in industrial environments where maintenance systems represent significant assets influencing production continuity, cost efficiency, and competitive positioning.

To address this research gap, the study examines the relationship between digital maintenance technologies, strategic project management, and human-centric Industry 5.0 principles. Three research questions guide the analysis:

RQ1: How is strategic project management integrated into digital industrial maintenance systems?

RQ2: What organizational factors and barriers affect the implementation of predictive maintenance within industrial maintenance systems?

RQ3: Which Industry 5.0 principles are relevant to strategic project management of industrial maintenance initiatives?

The objective of this paper is to analyze the transition from Industry 4.0 to Industry 5.0 in industrial maintenance systems and to propose a conceptual framework that integrates digital maintenance technologies with strategic project management principles. The framework aims to support human-centric implementation, improve organizational resilience, and align maintenance activities with long-term business performance goals.

LITERATURE REVIEW

The development of industrial maintenance systems has been extensively studied in the context of predictive maintenance, machine learning applications, and digital transformation initiatives (Taoufyq et al., 2025; Mallioris, 2024; Carvalho et al., 2021). Taoufyq et al. (2025) provide a systematic evaluation of knowledge-based, physics-based, and data-driven predictive maintenance models, highlighting the need for empirical validation across industries and integration with structured project management frameworks. Similarly, Mallioris (2024) reviews state-of-the-art predictive maintenance applications across multiple sectors, pointing out insufficient integration with practical project management and organizational maintenance frameworks.

Other studies emphasize technological approaches without sufficient organizational perspective. Carvalho et al. (2021) focus on machine learning techniques applied to predictive maintenance, but the alignment with strategic project management remains underexplored. Softić (2024) demonstrates the application of survival analysis for reliability assessment; however, these methodologies have not been fully integrated into organizational maintenance systems.

The reviewed literature can be considered through three related perspectives. The first concerns the technological dimension of predictive maintenance, including machine learning, artificial intelligence, data-driven models, condition monitoring, and Industry 4.0 technologies (Taoufyq et al., 2025; Carvalho et al., 2021; Achouch et al., 2022; Benhanifia et al., 2025). These studies demonstrate the development of increasingly advanced approaches for monitoring equipment condition, predicting failures, and supporting maintenance decisions. However, the main emphasis is generally placed on technical models and their application rather than on the organizational management of their implementation.

The second perspective concerns maintenance planning and organizational integration. Rios et al. (2024) examine machine learning applications for maintenance planning and asset integrity management, while Ali (2024) discusses maintenance strategies from a broader management perspective. Bokrantz et al. (2020) and Emroozi et al. (2023) also address the integration of maintenance activities with wider production and organizational processes. These studies indicate the importance of coordinated maintenance planning, but the connection between maintenance initiatives and strategic project management remains insufficiently developed.

The third perspective is related to the transition toward human-centric Industry 5.0 maintenance systems. Ramzan and Reforgiato (2025) consider predictive maintenance in smart manufacturing with emphasis on artificial intelligence and decision-making, while Murtaza et al. (2024) examine the transition from Industry 4.0 toward Industry 5.0 and the increasing relevance of human-centric approaches. Benhanifia et al. (2025) also address predictive maintenance practices based on AI and IoT technologies. Although these studies introduce organizational and human-oriented considerations, the integration of Industry 5.0 principles with strategic project management for maintenance initiatives remains insufficiently defined.

To consolidate recent findings and identify gaps in current research, a structured overview of key studies from 2020 to 2026 is presented in Table 1. The table summarizes the main focus, limitations, and research gaps identified in the selected literature, with particular attention to predictive maintenance, industrial maintenance management, and project management.

Table 1. *Overview of Recent Literature on Predictive Maintenance, Industrial Maintenance Management, and Project Management (2020–2026)*

Author (Year)	Title	Focus	Limitation	Research Gap
Taoufyq, H. et al. (2025)	Predictive Maintenance Approaches A Systematic Literature Review	Systematic evaluation of knowledge-based, physics-based and data-driven predictive maintenance models	Limited real-world industrial validation	Need for empirical validation across industries and integration with structured project management frameworks
Mallioris, P. (2024)	Predictive Maintenance in Industry 4.0 A Systematic Multi-Sector Review	State-of-the-art predictive maintenance applications across multiple industries	Systematic review without in-depth industrial case studies	Insufficient integration with practical project management and organizational maintenance frameworks
Carvalho, T. P. et al. (2021)	A Systematic Literature Review of Machine Learning Methods Applied to Predictive Maintenance	Machine learning techniques applied to predictive maintenance	Strong technological orientation	Lack of organizational and strategic project management perspective
Softić, S. (2024)	Case Studies of Survival	Application of survival analysis	Methodological focus without	Need for application of

	Analysis for Predictive Maintenance	models for reliability assessment	integration into maintenance organization systems	survival models in strategic maintenance planning and project-based environments
Benhanifia, A. et al. (2025)	Systematic Review of Predictive Maintenance Practices in the Manufacturing Sector	Implementation of predictive maintenance using AI and IoT technologies	Predominantly technology-driven analysis	Limited connection between predictive maintenance and strategic maintenance project management
Ramzan, F. and Reforgiato, D. (2025)	A Literature Review on Enhancing Predictive Maintenance in Smart Manufacturing Industries	Comprehensive survey of AI-driven predictive maintenance and decision-making challenges	Focused on AI and data architecture	Gap in structured project management models and human-technology coordination frameworks
Rios, M. P. et al. (2024)	Optimising Maintenance Planning and Integrity in Offshore Facilities Using Machine Learning	Machine learning models for maintenance planning and asset integrity management	Sector-specific focus on offshore facilities	Need for broader industrial application within formal project management structures
Achouch, M. et al. (2022)	On Predictive Maintenance in Industry 4.0 Overview Models and Challenges	Overview of predictive maintenance models and workflows in Industry 4.0	Primarily technical and model-oriented	Lack of integration with strategic and business-oriented project management frameworks
Ali, S. (2024)	Review Optimizing Maintenance Management in Modern Industrial Facilities	Strategies for improving maintenance management performance	General management perspective without project management integration	Need for structured project-based implementation models in maintenance systems
Murtaza, A. et al. (2024)	Paradigm Shift for Predictive Maintenance and Condition Monitoring from Industry 4.0 to Industry 5.0 A Systematic	Human-centric and Industry 5.0 oriented predictive maintenance models	Conceptual and review-based orientation	Gap in project-centric execution models for predictive maintenance implementation

	Review Challenges and Case Study			
Bokrantz, J. et al. (2020)	Smart Maintenance: a research agenda for industrial maintenance management	Conceptualization of smart maintenance and future research agenda	Theoretical framework without empirical validation	Need for implementation models aligned with strategic project management and business performance objectives
Emroozi, V. B. et al. (2023)	Improving industrial maintenance efficiency a holistic approach to integrated production and maintenance planning with human error optimization	Development of integrated production and maintenance planning that incorporates human error optimization to improve overall industrial maintenance efficiency	Model-based study with simulation/analytical validation	Need for integration with strategic project management frameworks and wider empirical validation across multiple industrial contexts

The reviewed studies show that predictive maintenance research has developed substantially in terms of digital technologies, analytical models, and condition monitoring approaches. At the same time, the organizational aspects of implementing these technologies are less consistently addressed. The literature also indicates a growing interest in human-centric maintenance and Industry 5.0 principles, particularly in relation to workforce involvement, decision-making, resilience, and coordination between technological and human factors.

A further gap concerns the connection between these dimensions and strategic project management. Existing studies address predictive maintenance technologies, maintenance planning, organizational integration, and Industry 5.0 principles, but these elements are generally examined separately. The reviewed literature provides limited guidance on how strategic project management can connect technological implementation with organizational objectives, resource allocation, risk management, stakeholder engagement, and performance monitoring.

This gap provides the basis for the conceptual framework developed in this study. The proposed framework does not introduce predictive maintenance or Industry 5.0 principles as new concepts; instead, it focuses on their structured integration through strategic project management. In this perspective, strategic project management represents the connecting layer between digital maintenance technologies, organizational objectives, and human-centric Industry 5.0 requirements.

METHODOLOGICAL RESEARCH APPROACH

This study adopts a systematic literature review (SLR) approach to analyze recent research on predictive maintenance, industrial maintenance management, and strategic project management, covering publications from 2020 to 2026. The review was structured around the relationship between digital maintenance technologies, organizational management practices, and the principles of Industry 5.0.

The literature search focused on three major academic databases, Scopus, Web of Science, and Google Scholar. The search used combinations of the following keywords and related

terms: "predictive maintenance", "Industry 4.0", "Industry 5.0", "strategic project management", "industrial maintenance systems", and "human-centric maintenance". The search was limited to publications written in English and published between 2020 and 2026.

The inclusion criteria focused on peer-reviewed journal articles and high-quality research papers addressing at least one of the following areas: predictive maintenance, digital transformation of industrial maintenance, maintenance management, Industry 4.0 or Industry 5.0 applications in maintenance, or the organizational and management aspects of maintenance implementation. Studies were considered relevant when their findings provided insights applicable to the relationship between predictive maintenance, organizational management, and strategic project management.

Studies focused exclusively on technical algorithms or specific predictive maintenance models were not excluded when their findings provided relevant implications for the organizational implementation, planning, or management of maintenance systems. Publications without a relevant connection to industrial maintenance, digital maintenance technologies, organizational implementation, or the Industry 4.0 and Industry 5.0 context were not considered relevant to the research focus.

The screening process was based on the relevance of the publication to the research topic and the extent to which the reported findings could contribute to understanding the integration of digital maintenance technologies with organizational and strategic management practices. Particular attention was given to studies addressing implementation challenges, organizational requirements, human factors, maintenance planning, and project-oriented approaches.

The selected studies were analyzed according to their authors, publication year, research focus, methodological or practical limitations, and identified research gaps. These characteristics were summarized in Table 1. The analysis was used to identify recurring themes and areas in which existing research provides limited guidance, particularly regarding the integration of predictive maintenance with strategic project management.

The synthesis of the reviewed literature was structured around three interconnected dimensions. The first dimension concerns Industry 4.0 technologies and digital maintenance, including predictive maintenance, machine learning, condition monitoring, and real-time data analysis. The second dimension concerns strategic project management and its relevance to maintenance planning, resource allocation, risk management, stakeholder engagement, and performance monitoring. The third dimension concerns Industry 5.0 principles, including human-centricity, resilience, sustainability, workforce participation, and the coordination of human expertise with digital technologies.

The identified relationships between these dimensions were used as the basis for developing the conceptual framework presented in the following section. The framework connects digital maintenance technologies with strategic project management and human-centric Industry 5.0 principles, with the aim of providing a structured perspective for the implementation and management of industrial maintenance initiatives.

CONCEPTUAL FRAMEWORK / PROPOSED MODEL

The proposed conceptual framework integrates digital maintenance technologies, strategic project management, and human-centric Industry 5.0 principles into a coordinated model for industrial maintenance systems. The framework is structured around four interconnected elements: the Industry 4.0 Digital Maintenance Layer, the Strategic Project Management Layer, the Human-Centric Industry 5.0 Layer, and the Integration Mechanism. The model is intended to connect technological implementation with organizational objectives, project management practices, and human factors.

Industry 4.0 Digital Maintenance Layer

The first layer represents the technological foundation of the proposed framework. It includes predictive maintenance, machine learning, survival analysis, condition monitoring, and real-time data acquisition and analytics. These technologies provide information about equipment

condition and support maintenance decision-making based on operational data. However, technological solutions implemented as isolated tools may have limited organizational value when they are not connected with maintenance planning, resource allocation, and broader business objectives.

Strategic Project Management Layer

The second layer introduces strategic project management as a distinct organizational component of the framework. Its purpose is to align digital maintenance initiatives with organizational objectives through structured planning, resource allocation, risk management, stakeholder engagement, and performance monitoring. Maintenance digitalization is therefore considered as a managed organizational initiative rather than only a technological implementation. This layer also provides a basis for coordinating activities between maintenance, production, management, information technology, and other relevant organizational functions.

Human-Centric Industry 5.0 Layer

The third layer incorporates the human-centric principles associated with Industry 5.0. It includes workforce participation, human expertise, ergonomics, continuous learning, resilience, sustainability, and socially responsible practices. The implementation of digital maintenance technologies requires consideration of employee competencies and the interaction between workers and technological systems. Human expertise remains relevant for interpreting maintenance information, making operational decisions, and adapting maintenance practices to specific organizational conditions.

Integration Mechanism

The integration mechanism connects the three main dimensions of the framework. It links digital maintenance technologies with strategic project management and human-centric organizational requirements. The mechanism supports coordination between technological implementation, organizational planning, workforce participation, resource allocation, risk management, and performance evaluation. In this structure, strategic project management provides the organizational connection between the technological capabilities of Industry 4.0 and the human-centric requirements of Industry 5.0.

The distinguishing feature of the proposed framework is therefore not the individual use of predictive maintenance technologies or Industry 5.0 principles, which have already been addressed in previous studies. Its main contribution is the explicit positioning of strategic project management as an integration layer between digital maintenance technologies and human-centric organizational transformation. This perspective connects maintenance digitalization with project objectives, organizational resources, risks, stakeholders, workforce requirements, and long-term performance considerations. The framework consequently provides a structured view of how technological, organizational, and human dimensions can be considered within the same maintenance transformation process.

Expected Outcomes

The integration of these dimensions is expected to support improvements in maintenance efficiency, equipment reliability, resource utilization, and strategic alignment. At the organizational level, the framework also addresses resilience, sustainability, workforce participation, and the coordination of maintenance initiatives with longer-term business objectives. These expected outcomes provide a basis for further empirical examination of the proposed relationships and for the development of project-based implementation approaches in industrial maintenance systems.

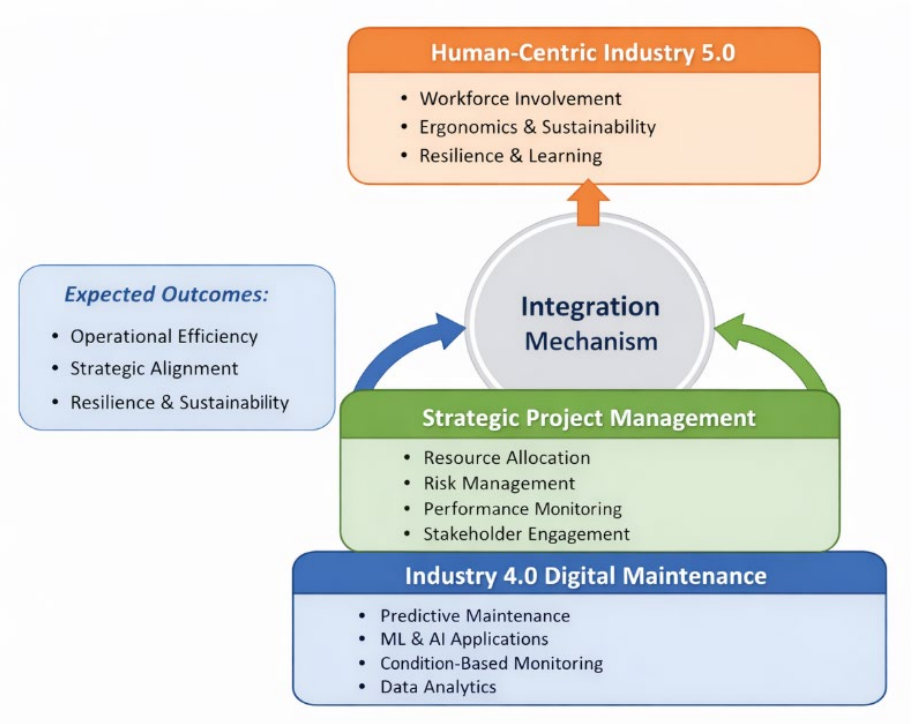


Fig. 1. *Conceptual framework linking Industry 4.0 predictive maintenance technologies, strategic project management, and human-centric Industry 5.0 principles*

RESULTS AND DISCUSSION

The reviewed literature indicates that the development of industrial maintenance systems can be considered through three interconnected dimensions: digital maintenance technologies, organizational and strategic management, and human-centric Industry 5.0 principles. The analysis of the selected studies shows that these dimensions are frequently addressed separately, while their integration within a strategic project management perspective receives less attention. The following discussion groups the main findings according to these dimensions and then considers their implications for the proposed framework.

Digitalization of Industrial Maintenance

The first group of findings concerns the application of Industry 4.0 technologies in industrial maintenance. The reviewed studies describe predictive maintenance, condition monitoring, machine learning, artificial intelligence, and real-time data analysis as important components of digital maintenance systems (Taoufyq et al., 2025; Mallioris et al., 2024). These approaches support the identification of equipment condition and maintenance requirements based on operational data and can reduce dependence on reactive maintenance practices.
Several studies also emphasize the development of analytical and predictive models for maintenance decision-making (Carvalho et al., 2021; Murtaza et al., 2024). However, the reviewed literature indicates that technical performance is often the primary focus of such approaches. Issues related to organizational integration, project planning, resource coordination, and long-term implementation are addressed less extensively. This finding supports the need to consider digital maintenance as part of a broader organizational transformation rather than as an isolated technological initiative.

Organizational and Strategic Integration

The second group of findings concerns the organizational conditions required for successful implementation of digital maintenance systems. Studies addressing maintenance

management and digital transformation emphasize the importance of planning, organizational coordination, and management practices alongside technological capabilities (Softić, 2024; Rios et al., 2024; Achouch et al., 2022).

The literature also indicates that predictive maintenance implementation requires changes in organizational processes and responsibilities. Digital maintenance initiatives may involve investments in technologies, employee competencies, data infrastructure, and coordination between different organizational functions. These requirements create a project-oriented dimension that is not fully represented when maintenance digitalization is considered only from a technological perspective.

Strategic project management provides a framework for addressing these requirements through project objectives, resource allocation, risk management, stakeholder coordination, and performance monitoring. In the context of the proposed model, these activities connect maintenance technology implementation with organizational priorities and longer-term business objectives. This represents the main link between the findings from the literature review and the proposed conceptual framework.

Industry 5.0 and Human-Centric Maintenance

The third group of findings relates to the transition from Industry 4.0 toward Industry 5.0. The reviewed literature emphasizes human-centricity, resilience, sustainability, and the interaction between people and advanced technologies (Benhanifia et al., 2025; Ramzan & Reforgiato, 2025). These principles extend the technological perspective of Industry 4.0 by placing greater attention on workforce participation, human expertise, and organizational adaptation.

For industrial maintenance, this perspective is relevant because predictive systems do not eliminate the need for human decision-making. Maintenance personnel interpret information generated by digital systems, combine it with operational experience, and make decisions according to specific equipment and production conditions. The implementation of Industry 5.0 principles therefore requires attention to employee competencies, continuous learning, ergonomics, and cooperation between workers and digital technologies.

Integration of the Main Findings

The comparison of the three groups shows a common pattern in the reviewed literature. Digital technologies provide the technical basis for predictive and condition-based maintenance, while organizational management determines how these technologies are planned, implemented, and coordinated. Industry 5.0 adds human-centricity, resilience, and sustainability to this relationship.

The proposed framework combines these dimensions by positioning strategic project management between digital maintenance capabilities and human-centric organizational transformation. This structure differs from approaches that primarily focus on predictive maintenance technologies or on individual Industry 5.0 principles. Strategic project management is used as the connecting layer through which technological initiatives can be aligned with organizational objectives, resources, risks, stakeholders, and workforce requirements.

Implications for Industrial Maintenance Management

The findings have several implications for the management of industrial maintenance systems. First, digital maintenance initiatives should be considered in relation to organizational objectives rather than only technical performance. Second, implementation requires coordination of technological investments with resources, responsibilities, employee competencies, and project risks. Third, the transition toward Industry 5.0 requires greater attention to human participation and the interaction between maintenance personnel and digital systems.

These findings support the proposed conceptual framework as a structured model for considering technological, organizational, and human dimensions together. The framework does not replace existing predictive maintenance or Industry 5.0 approaches. Instead, it provides a project management perspective for connecting these approaches within an organizational transformation process.

Research Gaps and Future Directions

The reviewed literature also identifies several areas that require further research. Empirical studies are needed to test the relationships between strategic project management practices and the performance of digital maintenance initiatives. Further research could examine project-based implementation models for predictive maintenance and investigate how organizational resources, employee competencies, stakeholder participation, and risk management affect implementation outcomes.

Another relevant area concerns human-technology interaction in Industry 5.0 maintenance environments. Future studies could examine how maintenance personnel interact with predictive systems, how digital competencies develop during implementation, and how human expertise can be incorporated into maintenance decision-making processes. Such research would provide an empirical basis for evaluating and further developing the proposed conceptual framework.

CONCLUSION

The transition from Industry 4.0 toward Industry 5.0 introduces new requirements for the management of industrial maintenance systems. The reviewed literature shows that predictive maintenance, artificial intelligence, machine learning, condition monitoring, and real-time data analytics provide important technological capabilities for digital maintenance. However, technological implementation alone does not address organizational planning, resource coordination, risk management, stakeholder engagement, and workforce requirements.

The analysis indicates that strategic project management can provide an organizational connection between digital maintenance technologies and broader business objectives. In the proposed framework, strategic project management is positioned as an integration layer connecting Industry 4.0 digital maintenance capabilities with human-centric Industry 5.0 principles. This perspective brings technological implementation, organizational requirements, and human factors into a common framework for managing maintenance transformation initiatives.

The proposed conceptual framework therefore combines three main dimensions: digital maintenance technologies, strategic project management, and human-centric Industry 5.0 principles. Its distinguishing feature is the explicit integration of strategic project management into the transition toward human-centric digital maintenance. The framework considers project objectives, resources, risks, stakeholders, performance monitoring, workforce participation, and organizational adaptation together with technological implementation.

The study contributes a structured conceptual perspective for understanding how industrial maintenance digitalization can be coordinated with organizational and human requirements. The framework can support further consideration of maintenance transformation as an organizational project rather than only as a technical implementation. It also provides a basis for developing project-based approaches to the implementation of predictive maintenance and Industry 5.0 principles.

The main limitation of the study is its conceptual nature. The proposed relationships have not been empirically tested in specific industrial organizations, and the framework therefore requires further validation. Future research should examine the framework through empirical studies and case-based applications, with particular attention to project management practices, organizational barriers, employee competencies, stakeholder participation, risk management, and maintenance performance.

Further research should also investigate how human expertise and digital technologies can be coordinated within Industry 5.0 maintenance environments. Empirical validation could provide additional evidence regarding the relationships between strategic project management, digital maintenance implementation, and organizational performance.

REFERENCES

Achouch, M., Dimitrova, M., Ziane, K., Sattarpanah Karganroudi, S., Dhouib, R., & Adda, M. (2022). On predictive maintenance in Industry 4.0: Overview models and challenges. *Applied Sciences, 12*(16), Article 8081. https://doi.org/10.3390/app12168081

Ali, S. (2024). Review: Optimizing maintenance management in modern industrial facilities. *Journal of Quality in Maintenance Engineering*. https://doi.org/10.1108/JQME-04-2022-0021

Benhanifia, A., Ben Cheikh, Z., Moura Oliveira, P., Valente, A., & Lima, J. (2025). Systematic review of predictive maintenance practices in the manufacturing sector. *Intelligent Systems with Applications, 26*, 200501. https://doi.org/10.1016/j.iswa.2025.200501

Bokrantz, J., et al. (2020). Smart maintenance: A research agenda for industrial maintenance management. *Journal of Manufacturing Systems*. https://doi.org/10.1016/j.ijpe.2019.107547

Carvalho, T. P., Soares, F. A. A. M. N., Vita, R., Francisco, R. P. D. P., Tavares Vieira Basto, J. P., & Gomes Soares Alcalá, S. (2021). A systematic literature review of machine learning methods applied to predictive maintenance. *Reliability Engineering & System Safety, 137*, 106024. https://doi.org/10.1016/j.cie.2019.106024

Emroozi, V. B., et al. (2023). Improving industrial maintenance efficiency: A holistic approach to integrated production and maintenance planning with human error optimization. *Reliability Engineering & System Safety*. https://doi.org/10.1007/s41660-023-00374-3

Mallioris, P., Aivazidou, E., & Bechtsis, D. (2024). Predictive maintenance in Industry 4.0: A systematic multi-sector mapping. *CIRP Journal of Manufacturing Science and Technology, 50*, 80–103. https://doi.org/10.1016/j.cirpj.2024.02.003

Murtaza, A., et al. (2024). Paradigm shift for predictive maintenance and condition monitoring from Industry 4.0 to Industry 5.0: A systematic review, challenges and case study. *Procedia Manufacturing*. https://doi.org/10.1016/j.rineng.2024.102935

Ramzan, F., & Reforgiato, D. (2025). A literature review on enhancing predictive maintenance in smart manufacturing industries. *Journal of Intelligent Manufacturing*. https://doi.org/10.1007/s43069-025-00584-0

Rios, M. P., et al. (2024). Optimising maintenance planning and integrity in offshore facilities using machine learning. *Ocean Engineering*. https://doi.org/10.3390/app142310902

Softić, S. (2024). Case studies of survival analysis for predictive maintenance. *International Journal of Prognostics and Health Management*. https://doi.org/10.24867/IJIEM-2024-4-366

Taoufyq, H., El Guemmat, K., Mansouri, K., & Akef, F. (2025). Predictive maintenance approaches: A systematic literature review. *Journal of Industrial Engineering and Management, 18*(3), 427–458. https://doi.org/10.3926/jiem.8537

DOI:10.5937/IIZS26235M

CONDITION MONITORING OF EUROPEAN INDUSTRIAL RESILIENCE: SHOCK ABSORPTION, RECOVERY TIME, AND HYSTERESIS IN EUROSTAT SHORT-TERM BUSINESS STATISTICS

Research paper

Miloš Milovančević[1]*, Ivan Kostić[2], Nataša Sokolov Milovančević[2], Vanja Stojković[3]
[1] Faculty of Mechanical Engineering, University of Niš, Niš, Republic of Serbia
[2] University "Privredna Akademija", Brčko District, Bosnia and Herzegovina
[3] National Employment Service of the Republic of Serbia, Niš Branch, Niš, Republic of Serbia

Abstract: Industrial resilience cannot be diagnosed from a single growth rate because abrupt shock absorption, recovery speed, nominal-value recovery, labour adjustment, and persistent output loss may move differently. This study develops a condition-monitoring framework for European industry using harmonised Eurostat short-term business statistics. A balanced panel of 4,186 country-month observations for 23 EU Member States from January 2011 to February 2026 combines industrial production and turnover, producer-price dynamics, and industrial labour input. A robust Industrial Systemic Stress Index (ISSI) identifies two dominant episodes: the pandemic collapse beginning in March 2020 and the energy-price stress episode beginning in April 2022. The pandemic shock was much deeper (median trough −23.8%) but recovered faster (Kaplan-Meier median 11 months), whereas the energy-price episode was shallower (−3.2%) but more persistent (33 months), with only 52.2% of countries restoring the pre-shock production level within 36 months. Deeper declines were associated with longer recovery in both episodes. During the energy-price episode, turnover recovered a median nine months earlier than production ($p < .001$), while industrial labour input declined substantially less than production in both shocks ($p < .001$). Two cross-shock archetypes emerged: adaptive-resilient and persistent-loss. The evidence supports multidimensional industrial monitoring that distinguishes resistance, recoverability, nominal-real divergence, labour buffering, and hysteresis.
Keywords: industrial resilience; condition monitoring; shock absorption; recovery time; hysteresis; survival analysis; Eurostat; energy-price shock

INTRODUCTION

Condition monitoring is a central engineering principle: repeated signals are used to detect abnormal system states and to distinguish transient disturbance from persistent degradation. The diagnostic question is therefore not only whether performance fell, but how deeply it fell, how long restoration required, and whether a lasting loss of capability remained (Jardine et al., 2006). Applied cautiously, the same logic is useful for national industrial systems, where production, turnover, producer prices, and labour input provide repeated measurements of a complex productive system.

Economic resilience research makes a similar distinction. Resistance captures the initial ability to absorb a shock, recoverability describes the subsequent restoration of activity, and evolutionary approaches allow for reorientation and path-dependent outcomes rather than assuming an automatic return to the previous equilibrium (Martin, 2012; Martin & Sunley, 2015; Boschma, 2015). Empirical work consequently separates the magnitude of the initial decline from the speed and completeness of recovery (Martin et al., 2016; Bristow & Healy, 2018).

Recent European disturbances illustrate why this decomposition matters. The COVID-19 pandemic caused an abrupt disruption of production, mobility, trade, and global value chains (OECD, 2021). The later energy-price shock worked through a different mechanism, with high energy costs and inflation weakening industrial competitiveness, especially in energy-intensive activities (European Central Bank, 2023). In such an environment, nominal turnover can recover because prices rise even when physical production remains depressed, while employment can remain comparatively stable if firms retain labour during temporary losses.

The study therefore asks whether a data-driven monitoring system can distinguish shock depth, recovery duration, nominal-real divergence, labour buffering, and persistent post-shock loss across European industry. Its contribution is fourfold: it detects systemic stress from joint

[1*]Corresponding author: milovancevic@masfak.ni.ac.rs

cross-country signals rather than pre-selecting crises; treats recovery as a right-censored duration process; compares production with turnover and labour signals; and identifies cross-shock resilience archetypes. The analysis is descriptive and diagnostic, not causal.

CONCEPTUAL FRAMEWORK AND HYPOTHESES

Condition-monitoring architecture

The monitoring architecture is summarized in Figure 1. Harmonised Eurostat signals are first converted into a cross-country stress measure; detected episodes are then translated into country-specific shock-response trajectories; persistence is evaluated over a common 36-month window; and the resulting resistance, recovery, and hysteresis information supports comparative diagnosis. This sequence separates systemic-stress detection from country-level diagnosis and makes the monitoring logic explicit.

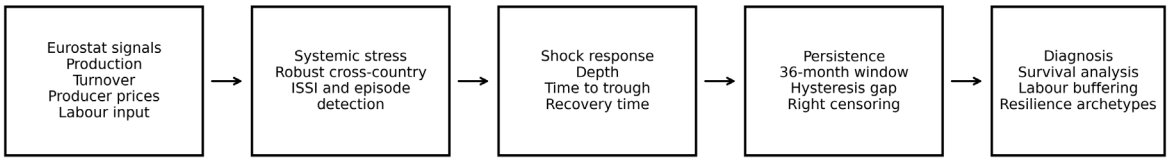


Fig. 1. *Analytical architecture of the industrial-resilience condition-monitoring framework. The sequence links Eurostat signals, systemic-stress detection, country shock trajectories, persistence assessment, and diagnostic outputs.*

Operational resilience measures

Let $P_{i,t}$ denote the seasonally and calendar-adjusted industrial production index for country i in month t. Monthly production momentum is measured as:

$$g^{P}_{i,t} = 100 \ln(P_{i,t} / P_{i,t-1}) \quad (1)$$

For systemic episode e beginning in month s_e, the pre-shock baseline is the mean production level in the three immediately preceding months:

$$B_{i,e} = (1/3) \Sigma_{k=1}^{3} P_{i,se-k} \quad (2)$$

The baseline-normalised trajectory is $Z_{i,e,h} = 100P_{i,se+h}/B_{i,e}$. Shock depth is the minimum deviation from baseline during the first 12 months:

$$D_{i,e} = \min_{0 \le h \le 11} (Z_{i,e,h} - 100) \quad (3)$$

Time to trough is the number of months from episode onset to the country-specific production minimum. Recovery is the first month after the trough in which production is at or above the baseline for three consecutive months; countries without such recovery within 36 months are right-censored. Persistent level displacement is summarized by the third-year hysteresis gap:

$$H_{i,e} = (1/12) \Sigma_{h=24}^{35} (Z_{i,e,h} - 100) \quad (4)$$

Positive $H_{i,e}$ indicates a third-year level above the immediate pre-shock baseline and negative $H_{i,e}$ indicates persistent loss. This is a transparent level-based diagnostic rather than a causal counterfactual trend estimate.

Hypotheses

H1. Shock depth, recovery time, and hysteresis vary materially across countries and shocks. **H2.** Deeper country-specific production declines are associated with longer recovery. **H3.** During high-inflation energy-price stress, nominal turnover recovers earlier than physical production. **H4.** Industrial labour input adjusts less than physical production during systemic shocks. **H5.** Joint resistance, recovery speed, and hysteresis profiles form empirically distinct cross-shock resilience archetypes.

DATA AND METHODS

Eurostat data and analytical sample

The primary balanced panel covers 23 EU Member States from January 2011 to February 2026, yielding 4,186 country-month observations: Austria, Belgium, Bulgaria, Croatia, Cyprus, Czechia, Estonia, Finland, France, Germany, Greece, Hungary, Italy, Latvia, Lithuania, Luxembourg, Malta, Poland, Romania, Slovakia, Slovenia, Spain, and Sweden. Countries were retained only when complete common coverage was available for the pre-specified harmonised series; no missing-value imputation was used. Table 1 identifies the four Eurostat datasets and explains the analytical meaning of each signal.

Table 1. *Eurostat short-term business statistics used in the monitoring system.*

Dataset	Indicator	Freq.	Selected specification	Analytical role
sts_inpr_m	Industrial production	Monthly	PRD; NACE B-D; SCA; index 2021=100	Primary physical-output trajectory
sts_intv_m	Industrial turnover	Monthly	NETTUR; NACE B-C; SCA; index 2021=100	Nominal market-side recovery signal
sts_inpp_m	Producer prices	Monthly	PRC_PRR; NACE B-D; NSA; index 2021=100	Annual price-pressure/dislocation signal
sts_inlb_q	Persons employed in industry	Quarterly	EMP; NACE B-E36; SCA; index 2021=100	Labour buffering and delayed adjustment

Data-driven systemic-stress detection

For every month, the monitoring system calculates four cross-country stress components: median monthly production growth, median monthly turnover growth, the share of countries with negative monthly production growth, and median annual producer-price inflation. Components are converted to robust z-scores using the median and the normal-consistent median absolute deviation, with only stress-increasing contributions retained:

$$\mathrm{RZ}(x_t) = [x_t - \mathrm{median}(x)] \,/\, \mathrm{MAD}^{N}(x) \tag{5}$$

The Industrial Systemic Stress Index (ISSI) is the equally weighted average of the four positive stress components—production (C^{P}), turnover (C^{T}), synchronisation (C^{s}), and price dislocation ($C\pi$):

$$\mathrm{ISSI}_t = (C^{P}{}_t + C^{T}{}_t + C^{s}{}_t + C\pi_t) \,/\, 4 \tag{6}$$

The empirical stress threshold is the 95th percentile of the ISSI distribution (2.979). Consecutive above-threshold months are grouped into one episode and the first month of each run is defined as its onset. This rule detected exactly two dominant systemic episodes over the balanced period.

Recovery, diagnostic comparisons, and archetypes

Recovery is analysed as a duration outcome. Kaplan-Meier product-limit estimates report the probability that production has not yet sustainably recovered by month h, and a log-rank test compares the two episode-specific curves (Kaplan & Meier, 1958). The same baseline and sustained-recovery rule is applied to turnover. Industrial labour input is normalised to the mean of the two quarters preceding the shock quarter; its maximum decline over the shock quarter and following three quarters is compared with the maximum 12-month production decline using paired Wilcoxon signed-rank tests. Spearman correlations assess the association between shock-depth magnitude and recovery duration. For cross-shock archetypes, country-level depth, recovery time (sign-reversed), and hysteresis scores are standardised and averaged across the two episodes. K-means solutions with two to four clusters are compared by average silhouette width (Rousseeuw, 1987).

RESULTS

Systemic-stress detection and episode contrast

Figure 2 shows the ISSI trajectory, the 95th-percentile threshold, and the two detected onsets. The first run began in March 2020 and peaked in April 2020 at ISSI = 11.532; at that peak, median monthly industrial production fell by 17.8%, turnover by 24.0%, and all 23 countries recorded negative monthly production growth. The second run began in April 2022, continued through October 2022, and peaked in June 2022 at ISSI = 3.865, when median production fell by 1.16% while median annual producer-price inflation reached 27.2%. Thus Figure 2 distinguishes an abrupt synchronised output collapse from a prolonged price-dislocation regime.

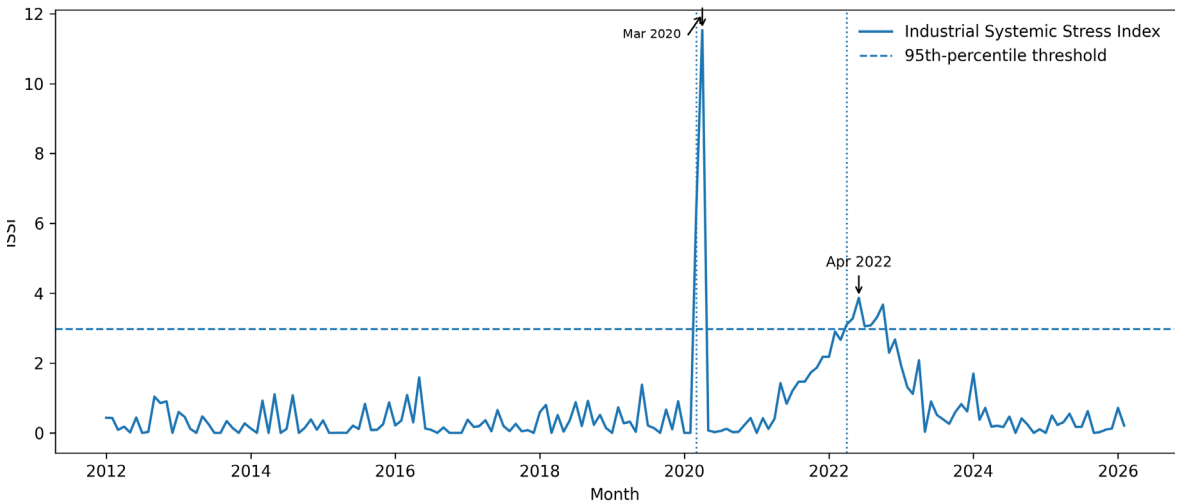


Fig. 2. *Industrial Systemic Stress Index (ISSI), 95th-percentile threshold (2.979), and detected episode onsets. Vertical dotted lines mark March 2020 and April 2022.*

Table 2 links the detected episodes to country-level resilience outcomes. The pandemic shock was far deeper, with a median trough 23.8% below baseline and a median time to trough of one month. The energy-price episode produced a smaller median trough (−3.2%) but a much slower erosion, with the median trough reached after seven months. The longer-run ranking reverses: the pandemic median hysteresis gap was +5.0%, whereas the energy-price episode

remained −3.6% below baseline in months 24–35. The paired difference in shock depth was significant ($p < .001$) and the hysteresis difference was also significant ($p = .002$), supporting H1.

Table 2. *Detected systemic episodes and core production-resilience metrics.*

Episode	Onset	Peak ISSI (month)	Median depth (%)	Median trough (m)	Recovered ≤36 m / KM median	Hysteresis 24–35 m (%)
Pandemic systemic shock	2020-03	11.53 (2020-04)	−23.83	1	82.61% / 11 m	+4.97
Energy-price systemic stress	2022-04	3.86 (2022-06)	−3.19	7	52.17% / 33 m	−3.55

Recovery as a duration process

The Kaplan-Meier curves in Figure 3 show that the probability of remaining unrecovered declined more rapidly after the pandemic shock. The KM median recovery time was 11 months after the pandemic and 33 months after the energy-price episode; 82.6% and 52.2% of countries, respectively, recovered within the 36-month window. At month 12, the unrecovered probabilities were 34.8% and 60.9%, and at month 24 they were 17.4% and 52.2%. The log-rank comparison was suggestive but did not reach the conventional 5% threshold ($\chi^2 = 3.339$, $p = .068$), so the difference in complete recovery paths should be interpreted cautiously.

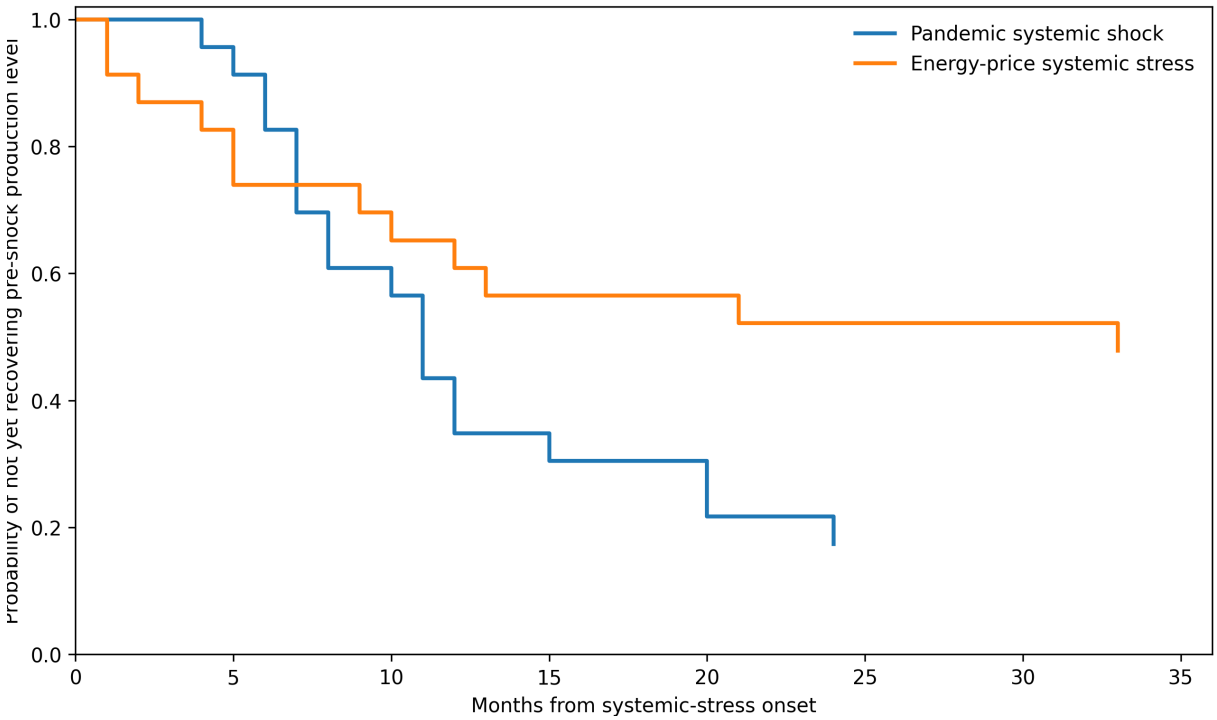


Fig. 3. *Kaplan-Meier probability that industrial production has not yet regained the pre-shock baseline. Right-censored countries remain in the risk set until the end of the common 36-month window.*

Within each episode, deeper declines were associated with longer recovery. The Spearman correlation between decline magnitude and recovery duration was $\rho = .416$ ($p = .048$) for the

pandemic and ρ = .553 (p = .006) for the energy-price episode. H2 is therefore supported within both shock regimes even though the between-episode log-rank difference is only marginal.

Nominal-real divergence and labour buffering

Production and turnover behaved similarly during the pandemic: median recovery times were 11 and 10 months and the paired difference was not significant (p = .163). Under energy-price stress, however, turnover recovered after a median five months while physical production required 33 months; the median within-country production-minus-turnover recovery gap was nine months (p < .001). This supports H3 specifically for the high-inflation episode and shows why a value-based signal can declare recovery before physical output is restored.
Labour input was more inertial than production. During the pandemic, the median production decline was 23.8% compared with 3.1% for industrial labour input, a median within-country gap of 21.47 percentage points (p < .001). During the energy-price episode, the median production decline was 3.2% while the median labour-input decline was effectively zero, again producing a significant gap (p < .001). These findings support H4 and are consistent with labour buffering or labour hoarding. Table 3 consolidates the main inferential tests so that the statistical evidence can be read directly alongside the textual interpretation.

Table 3. *Main inferential and diagnostic tests reported in the results.*

Comparison	Statistic	p	Effect / median difference
Shock depth: pandemic vs energy-price	Wilcoxon W = 6.0	< .001	−19.68 pp
Hysteresis gap: pandemic vs energy-price	Wilcoxon W = 39.0	.002	+7.66 pp
Recovery curves between episodes	Log-rank χ^2 = 3.339	.068	—
Depth vs recovery: pandemic	Spearman ρ = .416	.048	positive association
Depth vs recovery: energy-price	Spearman ρ = .553	.006	positive association
Production vs turnover recovery: energy-price	Wilcoxon W = 7.0	< .001	+9.00 months
Production vs labour decline: pandemic	Wilcoxon W = 0.0	< .001	+21.47 pp
Production vs labour decline: energy-price	Wilcoxon W = 1.0	< .001	+3.19 pp

Cross-shock resilience archetypes

The two-cluster K-means solution had the highest average silhouette width (0.344) compared with three clusters (0.287) and four clusters (0.323). Table 4 describes the retained solution. Ten countries formed an adaptive-resilient archetype with positive average standardised scores for resistance, recovery speed, and hysteresis. Thirteen countries formed a persistent-loss archetype with negative average scores on all three dimensions. The country-level median average shock depth across the two episodes was approximately −10.4% in the adaptive-resilient group and −18.9% in the persistent-loss group; corresponding median average recovery times were 14.0 and 21.5 months, and median average hysteresis gaps were +4.8% and −1.7%. The clusters summarize the two observed shocks rather than immutable national characteristics, but their multidimensional separation supports H5.

Table 4. *Cross-shock industrial resilience archetypes; higher standardized scores indicate better resilience performance.*

Archetype	Resistance	Recovery speed	Hysteresis	Composite	Countries
Adaptive-resilient	0.420	0.396	0.505	0.440	AT, BE, CZ, EL, FI, HR, LT, MT, PL, SE
Persistent-loss	−0.323	−0.305	−0.388	−0.339	BG, CY, DE, EE, ES, FR, HU, IT, LU, LV, RO, SI, SK

DISCUSSION

The central finding is that industrial resilience is not ordered by shock magnitude alone. The 2020 pandemic was an extreme but largely transient production shock, while the 2022 energy-price episode was lower in amplitude but more persistent. This result is consistent with resilience frameworks that distinguish resistance from recovery and allow shocks to alter subsequent trajectories (Martin, 2012; Martin & Sunley, 2015). A shallow decline should therefore not be interpreted as benign when it is accompanied by a long tail of incomplete recovery.

The production-turnover wedge is a second monitoring lesson. Under high producer-price inflation, nominal turnover can regain its pre-shock value long before physical output. The cross-country evidence therefore extends the ECB's discussion of energy-price pressure on European industry (European Central Bank, 2023): a monitoring dashboard should verify value-based recovery against a volume indicator before classifying the system as restored.

Third, stable industrial employment can coexist with material production loss. The smaller labour decline in both episodes is consistent with firms retaining workers because of skill specificity, adjustment costs, institutional protection, or expectations of later recovery. Regardless of the underlying mechanism, employment is a lagging signal of deterioration relative to production and should not be used alone to diagnose industrial condition.

Finally, the archetype analysis shows that multidimensional profiles contain more information than a single ranking. For operational monitoring, the minimum dashboard should report systemic stress, shock depth, time to trough, unrecovered probability, the production-turnover wedge, labour buffering, and the persistent level gap. Such a framework distinguishes resumed growth from genuine restoration and from a persistent lower-output state.

LIMITATIONS

The study has six main limitations. First, the production aggregate is NACE B-D, turnover is B-C, and labour input is B-E36; the signals are aligned as broad industrial measures but not identical in sectoral coverage. Second, the ISSI is an operational monitoring index rather than a structural causal model, and alternative weights or thresholds may shift episode boundaries. Third, hysteresis is a level gap relative to a three-month pre-shock baseline, not an estimate of the unobservable no-shock trend. Fourth, only two dominant systemic episodes are available in the common balanced period, limiting the generality of the archetypes. Fifth, the three-consecutive-month recovery rule is deliberately strict and could be varied in sensitivity analysis. Finally, the analysis identifies trajectory differences but does not establish which structural, technological, policy, or institutional mechanisms caused them.

CONCLUSION

A data-driven condition-monitoring framework applied to Eurostat short-term business statistics identifies two contrasting European industrial stress episodes. The pandemic collapse beginning in March 2020 was much deeper but generally faster to reverse; the energy-price stress beginning in April 2022 was shallower but more persistent, with a negative median third-year production gap and a substantially higher probability of incomplete recovery. Deeper country-specific declines were associated with longer restoration in both episodes.
The choice of signal materially affects diagnosis. During the energy-price episode, nominal turnover recovered well before physical production, while labour input adjusted far less than production in both shocks. Industrial resilience should therefore be monitored as a trajectory comprising resistance, time to trough, sustained recovery, nominal-real divergence, labour buffering, and hysteresis rather than as a single growth rate. This multidimensional view better distinguishes temporary disruption, genuine recovery, and persistent industrial degradation.

DATA, REPRODUCIBILITY, CONFLICT OF INTEREST, AND FUNDING

The analysis uses publicly available Eurostat datasets sts_inpr_m, sts_intv_m, sts_inpp_m, and sts_inlb_q. The workflow consists of deterministic series filtering, log-growth transformation, robust cross-country standardisation, ISSI construction, threshold-run detection, baseline normalisation, 36-month recovery tracking, Kaplan-Meier estimation, paired non-parametric tests, and silhouette-validated K-means clustering. No missing-value imputation was used in the balanced primary panel. The authors declare no conflict of interest. No external funding was received for this study.

REFERENCES

Boschma, R. (2015). Towards an evolutionary perspective on regional resilience. *Regional Studies*, 49(5), 733–751. https://doi.org/10.1080/00343404.2014.959481

Bristow, G., & Healy, A. (2018). Innovation and regional economic resilience: An exploratory analysis. *The Annals of Regional Science*, 60(2), 265–284. https://doi.org/10.1007/s00168-017-0841-6

European Central Bank. (2023). How have higher energy prices affected industrial production and imports? *Economic Bulletin*, Issue 1/2023, Box 2.

Eurostat. (2021). *European business statistics methodological manual for short-term business statistics: 2021 edition*. Publications Office of the European Union. https://doi.org/10.2785/23895

Eurostat. (2026a). Labour input in industry—Quarterly data [Data set; sts_inlb_q]. European Commission. https://doi.org/10.2908/STS_INLB_Q

Eurostat. (2026b). Producer prices in industry, total—Monthly data [Data set; sts_inpp_m]. European Commission. https://doi.org/10.2908/STS_INPP_M

Eurostat. (2026c). Production in industry—Monthly data [Data set; sts_inpr_m]. European Commission. https://doi.org/10.2908/STS_INPR_M

Eurostat. (2026d). Turnover in industry, total—Monthly data [Data set; sts_intv_m]. European Commission. https://doi.org/10.2908/STS_INTV_M

Jardine, A. K. S., Lin, D., & Banjevic, D. (2006). A review on machinery diagnostics and prognostics implementing condition-based maintenance. *Mechanical Systems and Signal Processing*, 20(7), 1483–1510. https://doi.org/10.1016/j.ymssp.2005.09.012

Kaplan, E. L., & Meier, P. (1958). Nonparametric estimation from incomplete observations. *Journal of the American Statistical Association*, 53(282), 457–481. https://doi.org/10.1080/01621459.1958.10501452

Martin, R. (2012). Regional economic resilience, hysteresis and recessionary shocks. *Journal of Economic Geography*, 12(1), 1–32. https://doi.org/10.1093/jeg/lbr019

Martin, R., & Sunley, P. (2015). On the notion of regional economic resilience: Conceptualization and explanation. *Journal of Economic Geography*, 15(1), 1–42. https://doi.org/10.1093/jeg/lbu015

Martin, R., Sunley, P., Gardiner, B., & Tyler, P. (2016). How regions react to recessions: Resilience and the role of economic structure. *Regional Studies*, 50(4), 561–585. https://doi.org/10.1080/00343404.2015.1136410

OECD. (2021). *Global value chains: Efficiency and risks in the context of COVID-19*. OECD Publishing. https://doi.org/10.1787/67c75fdc-en

Rousseeuw, P. J. (1987). Silhouettes: A graphical aid to the interpretation and validation of cluster analysis. *Journal of Computational and Applied Mathematics*, 20, 53–65. https://doi.org/10.1016/0377-0427(87)90125-7

DOI:10.5937/IIZS26244S

PROJECT MANAGEMENT APPROACH TO DRONE TECHNOLOGY IMPLEMENTATION IN CIVIL ENGINEERING

Research paper

Anita Sabo[1*], Tibor Szakáll[2], Bojan Kuljić[3]
[1,2,3]Subotica Tech, Marka Oreskovica 16, Subotica 24000, Serbia

Abstract: The increasing application of unmanned aerial vehicles (UAVs) in civil engineering provides new opportunities not only for data collection and site monitoring but also for supporting project management activities. This paper examines the implementation of drone technology in civil engineering from a project management perspective. Based on practical applications of UAVs in construction-related activities, the study analyses their potential contribution to project planning, monitoring and control, documentation, and decision-making. Particular attention is given to the integration of drone-based activities into the project workflow and to the identification of technical, operational, environmental, and organizational risks that may influence their successful implementation. The proposed approach demonstrates how drone technology can support more systematic project monitoring while providing timely visual information on project progress and site conditions. The results indicate that the effective integration of UAV technology requires not only appropriate technical solutions but also structured planning, risk management, and coordination with the overall project management process.
Key words: project management, unmanned aerial vehicles, civil engineering, project monitoring, risk management

INTRODUCTION

Unmanned aerial vehicles (UAVs) have evolved from primarily recreational devices into versatile technological tools with applications in numerous engineering fields. In civil engineering and construction, UAVs can support activities such as site observation, visual documentation, progress monitoring, inspection, and the collection of spatial information (Ahmed et al., 2022; Albeaino et al., 2019; Mohsan et al., 2022; Rachmawati & Kim, 2022). Their ability to acquire information rapidly from locations that may be difficult, time-consuming, or costly to access using conventional methods makes them particularly suitable for construction-related applications (Shakhatreh et al., 2019; Halder & Afsari, 2023).

The practical applicability of drone technology in civil engineering has already been demonstrated in different stages of the building life cycle, ranging from the observation of potential construction sites and documentation of construction activities to periodic inspections and long-term monitoring (Sabo et al., 2017). Previous practical experience has also shown that repeated aerial imaging can provide useful information about changes in the built environment over time and can therefore contribute to systematic project documentation and subsequent analysis (Sabo et al., 2017).

However, the implementation of UAV technology in construction projects should not be considered exclusively as a technical task. Drone-based activities have to be planned and coordinated with other project activities, while the required equipment, personnel, time, data processing, operational limitations, and potential risks need to be considered (Rachmawati & Kim, 2022; Molina et al., 2023). Consequently, the effective use of UAVs can also be examined from a project management perspective.

The aim of this paper is to analyse the implementation of drone technology in civil engineering within a project management framework. Based on previously demonstrated practical applications, the study focuses on the integration of UAV-supported activities into project planning, monitoring and control, documentation, and decision-making processes. Particular attention is given to the identification of relevant project resources, implementation activities, expected outputs, and technical, operational, environmental, and organizational risks. In this way, the study extends the technological perspective of UAV application by

[1]Corresponding author, saboanita@gmail.com, ORCID: 0000-0002-5737-9360
[2]szakall.tibor@gmail.com, ORCID: 0000-0003-0837-4456
[3]bojan.kuljic@gmail.com, ORCID: 0000-0003-3319-8749

examining how drone-supported activities can be systematically incorporated into the management of civil engineering projects.

PROJECT MANAGEMENT FRAMEWORK FOR DRONE IMPLEMENTATION

The implementation of drone technology in civil engineering can be considered as a set of interconnected project activities rather than as an isolated technical operation. The use of UAVs requires the definition of objectives, selection of appropriate equipment and data acquisition methods, allocation of human and technical resources, scheduling of flight and processing activities, and coordination with the overall construction project (Otto et al., 2018; Rachmawati & Kim, 2022; Molina et al., 2023). These elements make a structured project management approach particularly relevant.

The planning phase should begin with the definition of the purpose of UAV deployment and the expected project outputs. Depending on the project, drone-supported activities may include preliminary site observation, documentation of existing conditions, monitoring of construction progress, inspection of structures, or periodic recording of changes in the built environment (Albeaino et al., 2019; Halder & Afsari, 2023). Clearly defined objectives are necessary because they influence flight planning, required image quality, frequency of data acquisition, equipment selection, data processing requirements, and the allocation of project resources.

From a project management perspective, UAV implementation can be structured into five main groups of activities: planning and preparation, data acquisition, data processing, analysis and evaluation, and reporting and documentation. Planning and preparation include defining the area of interest, determining the required outputs, selecting the equipment, preparing the flight activities, and identifying operational constraints. Data acquisition covers the execution of the planned flights and collection of visual or spatial information. The collected data are subsequently processed and transformed into information suitable for engineering analysis. The results can then be evaluated and incorporated into project reports, progress documentation, or decision-making processes.

An important advantage of this structured approach is the possibility of integrating drone-based information into project monitoring and control. Repeated data acquisition can provide a visual record of project development and facilitate comparisons between different stages of construction (Rachmawati & Kim, 2022; Molina et al., 2023). Such information can support the identification of deviations, documentation of completed activities, evaluation of site conditions, and communication among project participants. The original practical application demonstrated that repeated aerial images can reveal changes in construction and urban development over time, illustrating the value of systematic visual documentation (Sabo et al., 2017).

For effective implementation, UAV activities should therefore be coordinated with the schedule and information requirements of the overall project. Drone deployment should take place when the collected information can contribute to project decisions rather than simply generate additional visual material. This requires coordination between technical personnel responsible for UAV operation and project participants responsible for planning, supervision, documentation, and decision-making.

Table 1. *Project management framework for UAV implementation in civil engineering*

Project stage	Main activities	Required resources	Expected output
Planning and preparation	Define objectives, area, flight plan and requirements	Project team, UAV operator, equipment, project documentation	UAV implementation plan
Data acquisition	Execute flights and collect data	UAV, sensors, operator	Images and spatial data
Data processing	Organize and process collected data	Software, computing resources, personnel	Processed project information
Analysis and	Compare and interpret	Engineering and project	Information for

Project stage	Main activities	Required resources	Expected output
evaluation	results	expertise	monitoring and decisions
Reporting and documentation	Integrate results into project documentation	Project management and reporting tools	Progress records and project reports

CASE STUDY AND METHODOLOGY

The case study is based on previously investigated practical applications of UAV technology in civil engineering (Sabo et al., 2017). The original application focused on the use of drones for building modelling, construction-site supervision, periodic inspection, and the documentation of changes in the built environment. In the present study, these technical activities are reconsidered from a project management perspective in order to identify how they can be planned, coordinated, monitored, and integrated into the overall project workflow.

The original contribution of the present study therefore lies not in introducing new UAV measurements, but in systematically reanalysing the previously reported technical case from a project management perspective. The activities and operational constraints described in Sabo et al. (2017) are reclassified in terms of project activities, resources, dependencies, risks, monitoring requirements, and decision-support information, providing the basis for the project management and risk management frameworks proposed in this study.

The methodology consists of three main steps. First, the UAV-supported activities identified in the practical application are classified according to their role within a civil engineering project. Second, the technical requirements and operational constraints associated with these activities are analysed as project resources, dependencies, and potential sources of risk. Finally, the information generated through UAV operations is evaluated according to its potential contribution to project monitoring, documentation, and decision-making.

For building modelling and site documentation, UAV operation requires several preparatory activities. The flight path has to be defined according to the area or structure to be recorded, while flight altitude, camera orientation, image resolution, and the required degree of image overlap have to be determined in advance. Accurate spatial positioning can be supported by GNSS data or, where necessary, by Ground Control Points (GCPs). The previous practical implementation showed that control points must be clearly identifiable in aerial images and accurately measured before data acquisition (Sabo et al., 2017).

The execution phase includes establishing communication between the UAV, flight controller, and control workstation, uploading and verifying the planned flight route, identifying possible emergency landing locations, and continuously supervising the UAV during automatic flight. Battery capacity represents an additional operational constraint. In the investigated application, the available flight duration was approximately 10–15 minutes, meaning that larger tasks could require several take-off, landing, and charging cycles (Sabo et al., 2017). These constraints directly influence activity scheduling and therefore need to be considered during project planning.

Data processing constitutes another important part of the workflow. For accurate modelling, images were acquired with substantial overlap—approximately 80% in the flight direction and 70% in the cross-flight direction (Sabo et al., 2017). This produces a large number of images that have to be stored and processed, making data processing one of the more time-consuming stages of the UAV-supported activity. From a project management perspective, processing capacity, storage requirements, and personnel time should therefore be included in resource and schedule planning rather than treating the flight itself as the complete UAV task.

The case also demonstrates the potential of UAVs for repeated construction monitoring. Drone-supported observation can be performed before construction begins, during foundation, structural, masonry, scaffolding and roofing activities, and later during periodic inspection or demolition (Sabo et al., 2017). Depending on project requirements, flights may be performed occasionally at significant project milestones or repeatedly at predefined

intervals. The resulting visual records can subsequently be organized and compared to identify changes over time.

RISK MANAGEMENT AND PROJECT CONTROL

The integration of UAV technology into civil engineering projects introduces several risks that can affect project schedule, cost, quality, safety, and the availability of information required for decision-making. Consequently, risk identification and response planning should form an integral part of UAV implementation rather than being addressed only when operational problems occur (Mohsan et al., 2023; Telli et al., 2023).

Technical risks are primarily associated with UAV equipment, communication systems, positioning accuracy, sensors, batteries, and data processing. Loss of communication, insufficient battery capacity, inaccurate positioning, or equipment failure can interrupt data acquisition and require the repetition of planned activities (Mohsan et al., 2022; Mohsan et al., 2023). The practical application showed that automatic flights require continuous supervision and predefined emergency landing locations, while limited battery capacity may necessitate several take-off, landing, and charging cycles (Sabo et al., 2017). These factors can directly influence the duration and sequencing of project activities.

Operational and environmental risks are particularly important in construction environments. Flight paths that were initially considered safe may become unsuitable as construction progresses because the position and height of site objects change. Newly constructed floors, cranes, scaffolding, and other temporary structures can therefore require modifications to previously defined flight routes (Sabo et al., 2017). Weather conditions may also influence whether planned UAV activities can be performed at the required time (Shakhatreh et al., 2019; Mohsan et al., 2023). Delayed data acquisition can consequently reduce the value of UAV information when it is needed for a specific project milestone or management decision.

Data-related risks should also be considered. High image overlap improves the availability of information for modelling but simultaneously increases the amount of data that must be transferred, stored, and processed. The analysed application demonstrated that these requirements can result in substantial data volumes and additional processing demands (Sabo et al., 2017). Insufficient processing capacity or inadequate data management may therefore create delays between data acquisition and the availability of useful project information.

From the project management perspective, these risks can be addressed through preventive planning, continuous monitoring, and predefined response measures. Table 2 summarizes the principal risk categories identified through the analysis of UAV-supported civil engineering activities.

Table 2. *Risk management framework for UAV-supported project activities*

Risk category	Example of risk	Possible project impact	Proposed response
Technical	UAV or communication failure	Interrupted activity, repeated flight, delay	Pre-flight checks, backup procedures
Energy	Insufficient battery capacity	Additional flight cycles, schedule delay	Battery planning and reserve batteries
Positioning	Inaccurate GNSS/GCP data	Reduced data quality, repeated measurement	Verification of positioning data and control points
Site conditions	New structures, cranes or scaffolding	Unsafe or unsuitable flight path	Flight-route review before each operation
Environmental	Unsuitable weather conditions	Postponed data acquisition	Flexible scheduling and weather assessment
Data management	Large volume of images	Processing and reporting delay	Adequate storage and processing capacity
Safety	Collision or emergency landing	Equipment damage, safety incident	Emergency landing plan and continuous supervision

Risk category	Example of risk	Possible project impact	Proposed response
Organizational	Poor coordination with project activities	Data collected at an inappropriate time	Integration of UAV activities into the project schedule

Project control should focus not only on whether a UAV flight has been successfully completed, but also on whether the required information has been obtained at the appropriate time and quality. This distinction is important because the flight itself represents only one activity in a broader workflow that includes preparation, data acquisition, processing, analysis, and reporting. Effective control therefore requires monitoring the entire UAV-supported process and its relationship with relevant construction milestones.
Repeated UAV operations can also contribute directly to project control. Depending on the purpose of monitoring, flights can be scheduled after important construction stages or performed at regular intervals. Systematic comparison of the resulting visual information enables changes to be identified over time and provides documented evidence of project progress (Albeaino et al., 2019; Rachmawati & Kim, 2022). In this way, UAV technology functions not only as a data acquisition tool but also as a potential information source for project monitoring and management decisions.

RESULTS AND DISCUSSION

The analysis indicates that the effective implementation of UAV technology in civil engineering depends on the integration of technical activities with project management processes. Although data acquisition is the most visible part of drone operation, the complete workflow includes planning, preparation, flight execution, data processing, analysis, reporting, and the subsequent use of the collected information (Rachmawati & Kim, 2022; Molina et al., 2023). Considering these activities as an integrated process makes it possible to identify their resource requirements, dependencies, and potential influence on project performance (Boje et al., 2020; Rasheed et al., 2020).
One of the main benefits of UAV-supported monitoring is the possibility of collecting visual information at predefined project stages. The practical application demonstrated the use of UAVs before construction, during different construction phases, during periodic inspections of completed structures, and during demolition and subsequent site observation (Sabo et al., 2017). From a project management perspective, this allows UAV activities to be associated with project milestones and control points rather than being performed as independent technical operations.
The frequency of data acquisition represents an important management decision. More frequent monitoring can provide more detailed information about project development, but it also increases flight time, data volume, processing requirements, and resource consumption. Therefore, the frequency of UAV operations should be determined according to the information needs of the project and the expected value of the collected data.
The results of the risk analysis further demonstrate that UAV implementation involves dependencies between technical and managerial factors. Technical and operational constraints identified in the analysed application can affect the schedule, resource requirements, and availability of project information. These dependencies illustrate why UAV deployment should be incorporated into resource and schedule planning rather than treated as an isolated technical activity.
Another relevant result concerns the role of UAV-generated information in project control. The comparison of images recorded at different times can reveal changes in structures, construction activities, and the surrounding built environment. In the original application, images of the same residential area recorded at different times demonstrated substantial urban development and road construction changes, illustrating the documentation potential of repeated aerial observation (Sabo et al., 2017). Within a project management framework, the same principle can be applied over shorter intervals to document progress and provide visual information for project evaluation.

For example, if UAV images acquired at a predefined project milestone indicate that the observed construction progress differs from the planned state, this information can support a project decision to review the schedule, investigate the cause of the deviation, and, where necessary, adjust subsequent activities or resource allocation. In this way, UAV-generated information becomes an input to project monitoring and control rather than serving only as visual documentation.

However, the use of UAVs should not be interpreted as a replacement for conventional project supervision or engineering assessment. The value of drone technology lies primarily in providing an additional source of timely and systematically collected information. Its effectiveness depends on whether the information is acquired at the appropriate project stage, processed within an acceptable time, and communicated to the participants responsible for project decisions (Albeaino et al., 2019; Halder & Afsari, 2023).

Based on the analysis, the proposed framework establishes a direct relationship between UAV activities and four project management functions: planning, resource management, monitoring and control, and risk management. The contribution of UAV technology is therefore not limited to improving data acquisition. When properly integrated into the project workflow, it can support a more structured documentation process and provide additional information for monitoring project progress and site conditions.

CONCLUSION

The application of UAV technology in civil engineering provides opportunities that extend beyond aerial data acquisition and visual documentation. This study examined drone implementation from a project management perspective by integrating UAV-supported activities into a structured framework covering planning and preparation, data acquisition, data processing, analysis and evaluation, and reporting and documentation.

The analysis showed that effective UAV implementation requires coordination between technical operations and the overall project workflow. Flight planning, equipment and personnel requirements, battery limitations, positioning accuracy, changing site conditions, data processing demands, and the timing of monitoring activities can all influence the successful completion of UAV-supported tasks. Consequently, these factors should be considered during project planning, resource allocation, scheduling, risk management, and project control.

The proposed risk management framework identified technical, energy-related, positioning, environmental, safety, data-management, and organizational risks that may affect UAV-supported activities. Preventive planning, verification of flight conditions and routes, adequate resource allocation, continuous supervision, and coordination with construction activities can contribute to reducing their potential impact on the project.

The results also indicate that repeated UAV-based observation can provide useful visual information for project monitoring and documentation. When data acquisition is coordinated with relevant construction stages and project milestones, the collected information can support progress assessment, documentation of site conditions, and project decision-making. However, UAV technology should be regarded as a complementary project information source rather than a substitute for engineering supervision and professional assessment.

The proposed approach demonstrates that the benefits of UAV technology depend not only on the capabilities of the technology itself but also on how effectively drone-supported activities are integrated into project management processes. The study is based on a project management reinterpretation of previously investigated practical UAV applications and does not provide new quantitative measurements of project performance. Future research could extend the framework through its application to specific construction projects and evaluate its effects on project duration, costs, information availability, and decision-making efficiency.

REFERENCES

Ahmed, M. F., Mohanta, J. C., Keshari, A., & Yadav, P. S. (2022). Recent advances in unmanned aerial vehicles: A review. Arabian Journal for Science and Engineering. https://doi.org/10.1007/s13369-022-06738-0

Albeaino, G., Gheisari, M., & Franz, B. W. (2019). A systematic review of unmanned aerial vehicle application areas and technologies in the AEC domain. Journal of Information Technology in Construction, 24, 381–405.

Boje, C., Guerriero, A., Kubicki, S., & Rezgui, Y. (2020). Towards a semantic Construction Digital Twin: Directions for future research. Automation in Construction, 114, 103179. https://doi.org/10.1016/j.autcon.2020.103179

Halder, S., & Afsari, K. (2023). Robots in inspection and monitoring of buildings and infrastructure: A systematic review. Applied Sciences, 13(4), 2304. https://doi.org/10.3390/app13042304

Mohsan, S. A. H., Khan, M. A., Noor, F., Ullah, I., & Alsharif, M. H. (2022). Towards the unmanned aerial vehicles (UAVs): A comprehensive review. Drones, 6(6), 147. https://doi.org/10.3390/drones6060147

Mohsan, S. A. H., Othman, N. Q. H., Li, Y., Alsharif, M. H., & Khan, M. A. (2023). Unmanned aerial vehicles (UAVs): Practical aspects, applications, open challenges, security issues, and future trends. Intelligent Service Robotics, 16, 109–137. https://doi.org/10.1007/s11370-022-00452-4

Molina, A. A., Huang, Y., & Jiang, Y. (2023). A review of unmanned aerial vehicle applications in construction management: 2016–2021. Standards, 3(2), 95–109. https://doi.org/10.3390/standards3020009

Otto, A., Agatz, N., Campbell, J., Golden, B., & Pesch, E. (2018). Optimization approaches for civil applications of unmanned aerial vehicles (UAVs) or aerial drones: A survey. Networks, 72(4), 411–458. https://doi.org/10.1002/net.21818

Rachmawati, T. S. N., & Kim, S. (2022). Unmanned aerial vehicles (UAV) integration with digital technologies toward Construction 4.0: A systematic literature review. Sustainability, 14(9), 5708. https://doi.org/10.3390/su14095708

Rasheed, A., San, O., & Kvamsdal, T. (2020). Digital twin: Values, challenges and enablers from a modeling perspective. IEEE Access, 8, 21980–22012. https://doi.org/10.1109/ACCESS.2020.2970143

Sabo, A., Kuljić, B., & Szakáll, T. (2017). Practical application of the drone technology in civil engineering. In Science in Practice (pp. 43–47). Pécs. ISBN 978-963-429-131-2.

Shakhatreh, H., Sawalmeh, A. H., Al-Fuqaha, A., Dou, Z., Almaita, E., Khalil, I., Othman, N. S., Khreishah, A., & Guizani, M. (2019). Unmanned aerial vehicles (UAVs): A survey on civil applications and key research challenges. IEEE Access, 7, 48572–48634. https://doi.org/10.1109/ACCESS.2019.2909530

Telli, K., Kraa, O., Himeur, Y., Ouamane, A., Boumehraz, M., Atalla, S., & Mansoor, W. (2023). A comprehensive review of recent research trends on unmanned aerial vehicles (UAVs). Systems, 11(8), 400. https://doi.org/10.3390/systems11080400

DOI:10.5937/IIZS26251S

QUALITY MANAGEMENT APPROACH TO INDUSTRY–EDUCATION COLLABORATION IN ENGINEERING EDUCATION

Research paper

Anita Sabo[1*], Bojan Kuljić[2], Tibor Szakáll[3]
[1,2,3]Subotica Tech, Marka Oreskovica 16, Subotica 24000, Serbia

Abstract: Industry–education collaboration plays an important role in improving the quality and practical relevance of engineering education, particularly in fields characterized by rapid technological development. This paper examines the integration of modern industrial measurement equipment into engineering education from a quality management perspective. The study is based on a case of cooperation between Subotica Tech and Rohde & Schwarz, in which modern measurement instruments were introduced into existing laboratory activities. Building on practical experience and comparative laboratory measurements, the collaboration is analysed in terms of stakeholder needs, educational process improvement, and the systematic integration of industrial technologies into teaching. A Plan–Do–Check–Act (PDCA) framework is used to structure the implementation and evaluation process and to identify opportunities for continual improvement. Particular attention is given to the contribution of modern equipment to measurement procedures, interpretation of results, documentation, and the alignment of practical education with current industrial practice. The analysis indicates that industry–education collaboration can contribute to educational quality not only by providing access to modern technology, but also by creating a structured feedback mechanism between industrial requirements and educational processes. The proposed approach demonstrates how such cooperation can be interpreted as a continual quality improvement process in engineering education.
Key words: quality management, industry–education collaboration, engineering education, PDCA, continual improvement

INTRODUCTION

Rapid technological development continuously changes the knowledge, skills, and practical competencies expected from engineering graduates. Higher education institutions therefore face the challenge of maintaining the relevance of their educational processes while industrial technologies, measurement systems, and professional practices evolve at an increasingly rapid pace (Sima et al., 2020; Thornhill-Miller et al., 2023). Cooperation between higher education and industry can contribute to reducing this gap by providing students and educators with access to current technologies, practical knowledge, and industrial experience (Perkmann et al., 2021; Compagnucci & Spigarelli, 2020).

In engineering education, this issue is particularly important because practical laboratory activities represent a direct connection between theoretical knowledge and its application. The quality of engineering education therefore depends not only on curriculum content but also on the availability of appropriate laboratory infrastructure, measurement equipment, and teaching methods. When educational institutions rely on equipment that no longer reflects contemporary industrial practice, students may require additional adaptation and training when entering the professional environment (Haleem et al., 2022; von Solms, 2018).

Industry–education collaboration can be interpreted from a quality management perspective as a mechanism for identifying stakeholder requirements and incorporating them into the educational process. Students, educational institutions, academic staff, and industrial partners represent stakeholders with different but interconnected expectations (Prdić et al., 2023). Industry requires graduates with relevant practical competencies, while educational institutions seek to provide learning environments that support the development of such competencies. Systematic cooperation between these stakeholders can therefore support the continual improvement of educational processes (Compagnucci & Spigarelli, 2020; International Organization for Standardization, 2015).

[1]Corresponding author, saboanita@gmail.com, ORCID: 0000-0002-5737-9360
[2]bojan.kuljic@gmail.com, ORCID: 0000-0003-3319-8749
[3]szakall.tibor@gmail.com, ORCID: 0000-0003-0837-4456

A practical example of such cooperation was previously presented through the collaboration between Subotica Tech and Rohde & Schwarz, in which modern electronic measurement equipment was integrated into existing laboratory activities (Kuljić et al., 2017). The original study focused primarily on the technical and educational advantages of modern measurement instruments and compared their application with older analogue equipment. The results demonstrated advantages related to measurement procedures, interpretation of measured values, and documentation of laboratory results (Kuljić et al., 2017).
Building on this practical case, the present study introduces a different analytical perspective. Rather than focusing primarily on the technical performance of the measurement equipment, the collaboration is examined as a quality improvement process in engineering education. The objective is to analyse how industry–education cooperation can support the identification of stakeholder needs, the integration of industrial technologies into laboratory teaching, the evaluation of practical improvements, and the continual development of educational processes. For this purpose, the Plan–Do–Check–Act (PDCA) cycle is used as a framework for structuring and interpreting the collaboration (International Organization for Standardization, 2015).

QUALITY MANAGEMENT FRAMEWORK FOR INDUSTRY–EDUCATION COLLABORATION

Industry–education collaboration can be considered a quality improvement mechanism when cooperation is systematically linked to the needs of the stakeholders involved in the educational process. In engineering education, these stakeholders include students, academic staff, higher education institutions, and industrial partners. Although their expectations differ, they are closely connected. Students require relevant knowledge and practical competencies, academic staff need appropriate resources and technologies for effective teaching, educational institutions aim to maintain the relevance and quality of their programmes, while industry requires graduates who are prepared to work with contemporary technologies and professional practices (Prdić et al., 2023; Perkmann et al., 2021).
The integration of industrial technologies into education should therefore not be considered only as an equipment upgrade. From a quality management perspective, it represents an opportunity to align educational processes with stakeholder requirements and to establish feedback between industry and higher education. Industrial partners can provide access to technologies, professional experience, and information about current industrial requirements, while educational institutions can integrate these inputs into laboratory exercises and teaching activities (Compagnucci & Spigarelli, 2020; Perkmann et al., 2021). The results of this integration can subsequently be evaluated and used to identify further opportunities for improvement. Such systematic comparison and evaluation can also be interpreted in the context of benchmarking as a tool for identifying improvement opportunities (Prdić, 2017).
The collaboration between Subotica Tech and Rohde & Schwarz provides a practical basis for this approach. Modern measurement instruments were made available for active use in the educational process, enabling students to work with technologies representative of contemporary industrial practice. Their integration into an existing laboratory exercise also made it possible to compare established teaching practices and older analogue equipment with modern digital measurement technology (Kuljić et al., 2017).
From a quality management perspective, this process can be structured according to the Plan–Do–Check–Act cycle (International Organization for Standardization, 2015). In the Plan phase, stakeholder needs and opportunities for improving practical education are identified. The Do phase includes the integration and practical use of industrial equipment in laboratory teaching. The Check phase evaluates the effects of the introduced technology on measurement procedures, interpretation of results, documentation, and practical laboratory activities. Finally, the Act phase uses the identified advantages and limitations as feedback for further development of laboratory activities and future industry–education cooperation.

Table 1. *PDCA framework for industry–education collaboration*

PDCA phase	Industry–education activity	Quality management objective
Plan	Identification of educational and industrial requirements	Alignment of stakeholder needs and educational objectives
Do	Integration of modern industrial equipment into laboratory activities	Improvement of practical teaching conditions
Check	Evaluation and comparison of laboratory procedures and results	Identification of benefits, limitations, and improvement opportunities
Act	Adaptation of laboratory activities and future cooperation	Continual improvement of engineering education

CASE STUDY AND METHODOLOGY

The practical implementation was demonstrated through an existing laboratory exercise dealing with the time and frequency response of a passive second-order RLC circuit. The same measurement task was performed using analogue and modern digital measurement equipment, which enabled a direct comparison of measurement procedures and results. The exercise included measurements at several frequencies and the determination of voltage values, phase displacement, and amplitude characteristics. The recorded results provided a practical basis for comparing the two approaches (Kuljić et al., 2017).

In the present study, this previously documented case is re-examined from a quality management perspective. The methodology does not aim to repeat the technical comparison of the measurement instruments. Instead, the practical observations and results are used as the basis for analysing how the introduction of industrial technology can contribute to the improvement of an educational process.

The analysis is conducted in three stages. First, the main stakeholders and their relevant requirements are identified in the context of industry–education collaboration. Second, the implementation of the modern measurement equipment is mapped to the Plan–Do–Check–Act cycle in order to examine the cooperation as a structured improvement process. Third, the documented differences between the analogue and digital measurement approaches are interpreted in terms of their potential contribution to educational quality, including measurement procedures, interpretation of results, documentation, and alignment with contemporary industrial practice.

The methodology therefore combines a case-study approach with a quality management reinterpretation of previously documented practical experience. This makes it possible to examine the same industry–education cooperation from a different perspective while clearly distinguishing the present analysis from the original technical comparison.

STAKEHOLDER ANALYSIS AND QUALITY IMPROVEMENT

The effectiveness of industry–education collaboration depends on the extent to which the needs and expectations of the involved stakeholders are recognized and incorporated into the educational process. In the analysed case, four main stakeholder groups can be distinguished: students, academic staff, the higher education institution, and the industrial partner. Each group contributes to the cooperation and at the same time expects specific benefits from its implementation (Prdić et al., 2023).

For students, the main benefit is access to measurement technology that reflects contemporary industrial practice. The original case demonstrated that the use of digital measurement equipment reduced the need for subjective interpretation of displayed values and enabled several parameters, including amplitude, frequency, and phase difference, to be obtained directly from the instrument (Kuljić et al., 2017). From a quality management perspective, these characteristics can support a clearer measurement procedure and allow students to focus more directly on the interpretation of the measured phenomena rather than on overcoming the technical limitations of older equipment.

For academic staff, modern measurement equipment provides additional possibilities for organizing and documenting laboratory activities. In the analysed case, measurement results could be stored digitally, including the export of measured data in CSV format, while graphical representations could be transferred directly from the oscilloscope (Kuljić et al., 2017). Such functions can facilitate the preparation, execution, and documentation of laboratory exercises and provide a more systematic basis for reviewing experimental results.
From the perspective of the higher education institution, cooperation with an industrial partner provides a mechanism for updating practical teaching without separating educational development from technological developments in industry. In the documented cooperation, the industrial partner provided modern instruments for active use in education, while the institution incorporated them into existing laboratory activities. This interaction illustrates a two-way relationship in which industrial resources and experience can contribute to educational development, while the educational environment provides a context for transferring contemporary technologies to future engineering professionals (Compagnucci & Spigarelli, 2020; Perkmann et al., 2021).
The industrial partner also represents an important stakeholder. Cooperation with educational institutions creates an opportunity to familiarize future engineers with technologies and working practices relevant to the industrial environment (Perkmann et al., 2021). However, the value of such cooperation should not be understood only in terms of equipment provision. Its broader quality-related contribution lies in establishing a connection between industrial expectations and the practical competencies developed through engineering education.
The stakeholder relationships identified in the case can be summarized as shown in Table 2.

Table 2. *Stakeholder framework for industry–education collaboration*

Stakeholder	Main need or expectation	Contribution of collaboration	Quality-related outcome
Students	Relevant practical competencies	Access to contemporary measurement technology	Improved practical learning conditions
Academic staff	Effective laboratory tools and procedures	Integration of modern measurement and documentation functions	More systematic laboratory activities
Higher education institution	Relevant and up-to-date practical education	Cooperation with industrial partners and access to technology	Better alignment with industrial practice
Industrial partner	Graduates familiar with contemporary technologies	Technology and professional input	Stronger connection with future professionals

The stakeholder analysis indicates that the quality contribution of industry–education cooperation is not limited to the technological characteristics of the equipment itself. Its value emerges from the interaction between stakeholder requirements, educational activities, and feedback from practical implementation. When these elements are systematically evaluated, the cooperation can become part of a continual improvement process rather than remain an isolated technology transfer activity (Prdić et al., 2023; International Organization for Standardization, 2015).

PDCA APPLICATION AND EVALUATION

The PDCA cycle provides a structured approach for interpreting industry–education collaboration as a continual improvement process (International Organization for Standardization, 2015). In the analysed case, the four phases can be associated with the identification of educational needs, the implementation of modern industrial equipment, the evaluation of practical experience, and the use of the obtained findings for further improvement of laboratory education.

In the Plan phase, the improvement opportunity can be identified as the need to reduce the technological gap between existing laboratory conditions and contemporary industrial measurement practice. The cooperation between Subotica Tech and Rohde & Schwarz created an opportunity to introduce modern measurement equipment into the educational environment while maintaining the existing laboratory objectives (Kuljić et al., 2017). The purpose was therefore not to replace the educational content, but to improve the technological conditions under which practical competencies were developed.
The Do phase consisted of the actual integration of the industrial measurement equipment into laboratory activities. The modern instruments were used within an existing exercise dealing with the time and frequency response of a passive second-order RLC circuit. Measurements were performed using both analogue and digital equipment, providing practical experience with the two measurement approaches and allowing their characteristics to be compared under the same laboratory task (Kuljić et al., 2017).
The Check phase is represented by the comparison of the measurement procedures, obtained results, and possibilities for documenting the experiment. The previously reported results showed that the two approaches produced comparable measurement data, while the digital equipment provided additional advantages in the measurement process. In particular, the digital oscilloscope enabled direct determination of several measured parameters and supported the storage and export of measurement results (Kuljić et al., 2017). In quality management terms, these observations provide feedback about how technological modernization can influence measurement procedures and documentation of laboratory activities.
The Act phase involves translating the identified benefits and limitations into further development of the educational process. In this context, successful practices can be incorporated into future laboratory activities, while experience gained during implementation can support decisions concerning equipment modernization, teaching procedures, and further cooperation with industrial partners. This phase is particularly important because it transforms a single collaborative activity into a potential mechanism for continual improvement (International Organization for Standardization, 2015).
The application of the PDCA cycle also demonstrates that industry–education collaboration should not end with the introduction of new technology. Equipment provision represents only one stage of the improvement process. Its educational value depends on how effectively the technology is integrated into teaching, how its effects are evaluated, and how the resulting experience is used in subsequent educational development. The cyclical nature of PDCA therefore provides a suitable framework for maintaining the connection between stakeholder requirements, industrial developments, and the continual improvement of engineering education (International Organization for Standardization, 2015).

RESULTS AND DISCUSSION

The quality management analysis of the case indicates that the main contribution of industry–education collaboration extends beyond the provision of modern laboratory equipment. The cooperation created a connection between industrial technology, practical teaching activities, and the requirements of the stakeholders involved in engineering education. When these elements are considered within a structured improvement framework, technology transfer can become part of a broader educational quality improvement process.
The comparison of analogue and digital measurement approaches provides practical evidence of how technological modernization can influence laboratory activities. The previously documented measurements showed comparable results obtained using the two approaches, while important differences were observed in the measurement procedure and documentation possibilities. With analogue equipment, some parameters required additional procedures and subjective interpretation, whereas the digital oscilloscope enabled direct measurement of several parameters and supported digital storage and export of results (Kuljić et al., 2017).

From an educational quality perspective, these differences can be interpreted at several levels. First, modern equipment can reduce the number of auxiliary operations required during laboratory measurements. Second, direct access to measured parameters and digital data can support more systematic documentation and subsequent analysis. Third, the use of equipment representative of contemporary industrial practice can improve the alignment between laboratory activities and the technological environment that engineering graduates may encounter professionally (Sima et al., 2020; Zhong et al., 2017). These benefits do not imply that traditional measurement methods have no educational value; rather, the comparison demonstrates how different technologies and technology-supported learning approaches can serve different educational objectives (Vlachopoulos & Makri, 2017).

The stakeholder analysis further shows that the benefits of collaboration are interconnected. Students gain practical experience with contemporary technology, academic staff obtain additional possibilities for organizing laboratory activities, the educational institution can strengthen the practical relevance of its programmes, and the industrial partner provides technology and professional input relevant to the development of competencies associated with current industrial practice (Perkmann et al., 2021; Prdić et al., 2023). Consequently, the value of collaboration should be evaluated as a system of stakeholder relationships rather than exclusively through the technical characteristics of the provided equipment.

The PDCA interpretation adds a continual improvement dimension to these findings. The introduction of modern equipment represents the implementation stage, while comparison of procedures and practical experience provides feedback for evaluation. The resulting information can then support decisions concerning future laboratory activities, equipment modernization, and further cooperation. In this way, the case demonstrates how an individual industry–education initiative can be transformed into a repeatable quality improvement process when implementation is followed by systematic evaluation and feedback (International Organization for Standardization, 2015).

At the same time, the analysis has limitations. The present study is based on a quality management reinterpretation of a previously documented industry–education collaboration and does not include new quantitative measurements of student learning outcomes, stakeholder satisfaction, or long-term educational performance. Therefore, the identified quality-related benefits should be interpreted primarily as case-based findings. Future research could complement the proposed framework with student and teacher feedback, stakeholder satisfaction indicators, learning outcome measures, and longitudinal evaluation of industry–education cooperation.

CONCLUSION

Industry–education collaboration can contribute to the continual improvement of engineering education when cooperation is systematically connected to stakeholder requirements, educational processes, and evaluation activities. The case analysed in this study demonstrates that the integration of modern industrial measurement equipment can be considered not only as a technological upgrade, but also as an element of a broader quality management process.

The quality management reinterpretation of the cooperation between Subotica Tech and Rohde & Schwarz identified several interconnected dimensions relevant to educational improvement. Modern measurement technology supported more direct measurement procedures, systematic documentation, and closer alignment of laboratory activities with contemporary industrial practice. At the same time, the stakeholder analysis demonstrated that the benefits of cooperation extend to students, academic staff, the higher education institution, and the industrial partner.

The proposed PDCA-based framework provides a structured approach for linking these stakeholder requirements with implementation, evaluation, feedback, and subsequent improvement. Its main value is that it shifts the focus from a one-time introduction of industrial technology towards a cyclical process in which practical experience can be used to support further development of laboratory education and future cooperation.

The study is based on a quality management reinterpretation of a previously documented industry–education collaboration and does not provide new quantitative measurements of student learning outcomes, stakeholder satisfaction, or long-term educational performance. Future research should therefore include systematic stakeholder feedback and quantitative educational indicators to evaluate the long-term effects of industry–education cooperation and to further validate the proposed quality management framework.

REFERENCES

Compagnucci, L., & Spigarelli, F. (2020). The Third Mission of the university: A systematic literature review on potentials and constraints. Technological Forecasting and Social Change, 161, 120284. https://doi.org/10.1016/j.techfore.2020.120284

Haleem, A., Javaid, M., Qadri, M. A., & Suman, R. (2022). Understanding the role of digital technologies in education: A review. Sustainable Operations and Computers, 3, 275–285. https://doi.org/10.1016/j.susoc.2022.05.004

International Organization for Standardization. (2015). ISO 9001:2015 Quality management systems — Requirements. ISO.

Kuljić, B., Sabo, A., & Szakáll, T. (2017). Bridging the gap between the industry and education. In Science in Practice (pp. 39–42). Pécs. ISBN 978-963-429-131-2.

Perkmann, M., Salandra, R., Tartari, V., McKelvey, M., & Hughes, A. (2021). Academic engagement: A review of the literature 2011–2019. Research Policy, 50(1), 104114. https://doi.org/10.1016/j.respol.2020.104114

Prdić, N. (2017). Konkurentska prednost preduzeća na osnovu benčmarking analize poslovanja. Oditor, 3(3), 107–117.

Prdić, N., Čavlin, M., & Kaiaman Nasser, K. (2023). Analysis of good practices and perceptions of stakeholders to support the development of domestic markets. Ekonomija – teorija i praksa, 16(2), 1–23.

Sima, V., Gheorghe, I. G., Subić, J., & Nancu, D. (2020). Influences of the Industry 4.0 revolution on the human capital development and consumer behavior: A systematic review. Sustainability, 12(10), 4035. https://doi.org/10.3390/su12104035

Thornhill-Miller, B., Camarda, A., Mercier, M., Burkhardt, J.-M., Morisseau, T., Bourgeois-Bougrine, S., Vinchon, F., El Hayek, S., Augereau-Landais, M., Mourey, F., Feybesse, C., Sundquist, D., & Lubart, T. (2023). Creativity, critical thinking, communication, and collaboration: Assessment, certification, and promotion of 21st century skills for the future of work and education. Journal of Intelligence, 11(3), 54. https://doi.org/10.3390/jintelligence11030054

von Solms, S. (2018). A proposed modular work integrated learning framework for South Africa. IEEE Access, 6, 71124–71135.

Zhong, R. Y., Xu, X., Klotz, E., & Newman, S. T. (2017). Intelligent manufacturing in the context of Industry 4.0: A review. Engineering, 3(5), 616–630. https://doi.org/10.1016/J.ENG.2017.05.015

Vlachopoulos, D., & Makri, A. (2017). The effect of games and simulations on higher education: A systematic literature review. International Journal of Educational Technology in Higher Education, 14, 22. https://doi.org/10.1186/s41239-017-0062-1

DOI:10.5937/IIZS26258M

DEFINING A METHODOLOGY FOR IMPROVING THE PRODUCTION RESOURCE PLANNING PROCESS IN CONDITIONS OF UNCERTAINTY

Review work

Marija D. Milanovic,[1]
[1]University of Belgrade, Innovation Center of the Faculty of Mechanical Engineering in Belgrade, 11000 Belgrade, Serbia

Abstract: The aim of this paper is to establish a theoretical framework and model for improving the process of managing production resources under conditions of uncertainty, based on the implemented quality standard, taking into account the existing production program, documentation of the selected company and key concepts, methods and techniques of modern production. In relation to the general goal, the sub-goals are: optimization of the production program, determination of the optimal series, increasing the degree of utilization of production capacities, improving product quality, reducing costs, optimizing the duration of the production cycle. Also, the proposed methodology and solutions that will be the result of this research must be simple to implement, have a universal character, i.e. they must be applicable primarily in small, and then medium-sized and large companies, as well as to achieve savings in the company. The results of this research should enable a new approach to planning and managing production resources under conditions of uncertainty with the use of application software solutions that enable management and response of the production system in real time, which will enable the rationalization of production resources and increase production efficiency.
Keywords: methodology, production resources, uncertainty, planning

INTRODUCTION

This paper will present a methodology for improving the process of planning production resources under conditions of uncertainty that can be implemented within the framework of specific research. In order to prove the set goal, the following assumptions were taken into account as guidelines for the process of generating methodological steps [1]:
- production resources in the company consist of: machine resources, material resources and human resources. The aforementioned production resources represent internal factors of the company, and the uncertainty present when planning the aforementioned production resources may originate from external factors such as the volume of demand, legal and/or statutory regulations, emergency situations, etc.
- uncertainty may be present in the planning process for one or more production resources,
- the uncertainty present in the identified production resources can be expressed in a qualitative or quantitative manner,
- the question is considered whether the uncertainty present in a particular production resource affects the uncertainty in other production resources - that is, it is necessary to identify interdependencies,
- production planning - production resource planning - define the terms,
- planning at which time level - time dimension, hierarchical level - structural dimension, horizontal/verticalintegration

RESEARCH DESCRIPTION

Given that the designed methodology for production resource planning under uncertainty provides for the definition of criteria, it is necessary to further present the criteria as objective functions, i.e. objective functions, and to consider how these functions will be represented mathematically.
The analysis of published research on the problem of improving the production resource planning process under uncertainty is very extensive and diverse. The presentation and analysis of the research is focused on uncertainty models in production plannin

[1]dmilanovic@mas.bg.ac.rs, ORCID: 0000-0001-5240-665X

In further research, the estimation of the objective function parameters is carried out using a phase matrix of pairwise comparisons (analogous to the phase analytic hierarchy process) (FAHP). The FAHP method has been widely used in various areas of research. The elements of this phase matrix are described by triangular phase numbers of type 1 (TFN). The determination of FAHP uncertainty is performed using the scope analysis method [2]. There are no research papers in the scientific literature that deal with the combination of FLP and some other methods. In practice, the values of uncertain parameters should be obtained using appropriate methods, such as expert expertise, statistical methods of FAHP, etc.
In this paper, the problem under consideration can be divided into two stages. In the first stage, the values of the objective function coefficients are determined using FAHP. In the second stage, the optimal solution of FLP is found. It can be assumed that the solution obtained, given by the application of the mentioned methods, is somewhat limited by the subjective opinions of decision makers.
Determining the material flow in different domains should be treated as an FLP problem, which is in accordance with the classification given by Ebrahimnejad, A., and Madjid Tavana, M., and which can be classified into the first five groups [3]. These problems are solved using different methods. We analyzed FFLPs with uncertain objective function coefficients and right-hand values represented by symmetric trapezoidal fuzzy numbers, while the matrix elements are described by real numbers. Each fuzzy number in the considered FLP is replaced by its equivalent. In this way, the given FLP is converted into an equivalent crisp LP. The solution of the obtained LP problem is based on the standard method. As is known, the solution of an LP problem is a crisp number. The authors used the relationship between the crisp and fuzzy problems to obtain a fuzzy solution for the considered FLP.
Jimènez et al. propose a new method for finding the optimal solution of FLP with fuzzy parameters [4]. The proposed method is implemented in two steps. In the first step, all fuzzy coefficients of the objective function are replaced by their expected values and they are crisp. The constraints of the considered FLP with the matrix of fuzzy coefficients and fuzzy right-hand sides are transformed into linear inequalities using the comparison procedure two phase numbers, as presented in the paper [5]. In this way, the considered FLP is converted into an LP with parameter α. Using the simplex method, an optimal solution with an acceptable α is found. The values of the decision variables are crisp numbers, and the value of the objective function depends on the value of α and is described by the TFN. In the second step, the degree of satisfaction of the phase goal with each optimal solution with an acceptable α is calculated. A reasonable solution is the one with the highest degree of membership in this phase subset.
Some papers introduce the assumption that all parameter and decision variables have imprecise values and that they should be described by fuzzy numbers. These problems are called full FLPs and are denoted as FFLPs, and some FFLPs will be briefly described. Lofti et al. discuss an FFLP whose parameters and decision variables are asymmetric triangular fuzzy numbers converted to crisp values by applying a special defuzzification procedure[6]. When the lexicographic rule is applied, the considered problem is transformed into two LP models. The objective function of the LP is defined as the maximization of the center of the processed FFLP. The second LP problem is formally represented as a fuzzified problem. By applying a special ranking to the fuzzy numbers, the aforementioned FFLP is transformed into a MOLP. In the paper [7], the FFLP problems, all uncertain parameters, and decision variables are described by type 1 TFNs. This model is transformed into a multi-objective linear programming (MOLP) model from the given FFLP. The constructed MOLP can serve decision makers by providing the best-fit solution for various LP models that have fuzzy numbers and decision variables in a simple and efficient way. Using the procedure, an efficient MOLP solution can be produced [8]. The author has proven in this paper that the obtained MOLP solution gives the optimal fuzzy solution for the FFLP.
The improvement of the model is based on the fact that solving real problems should be based on the creation of new approaches that combine two or more conventional or modified methods. It should be noted that the conventional AHP method is based on 4 axioms [9].

Consistency checking is performed using the eigenvector method. In the matrix phase of pairwise comparison, the elements cannot be considered reciprocals with respect to the main diagonal, nor is there a developed procedure for checking its consistency. Despite these shortcomings, when decision makers do not have enough information about the parameters under consideration, or the information changes rapidly, many authors consider the familiar FAHP framework to be very suitable for use.

RESEARCH RESULTS

The global scheme of methodological steps is given in Figure 1, which states that for planning production resources under conditions of uncertainty, it is necessary to primarily identify production resources in which uncertainty exists, and then classify production resources into those in which uncertainty must be taken into account during planning and those that do not have elements of uncertainty.
For identified production resources in which uncertainty is present in the planning process, it is necessary to define the criteria in which uncertainty is expressed.

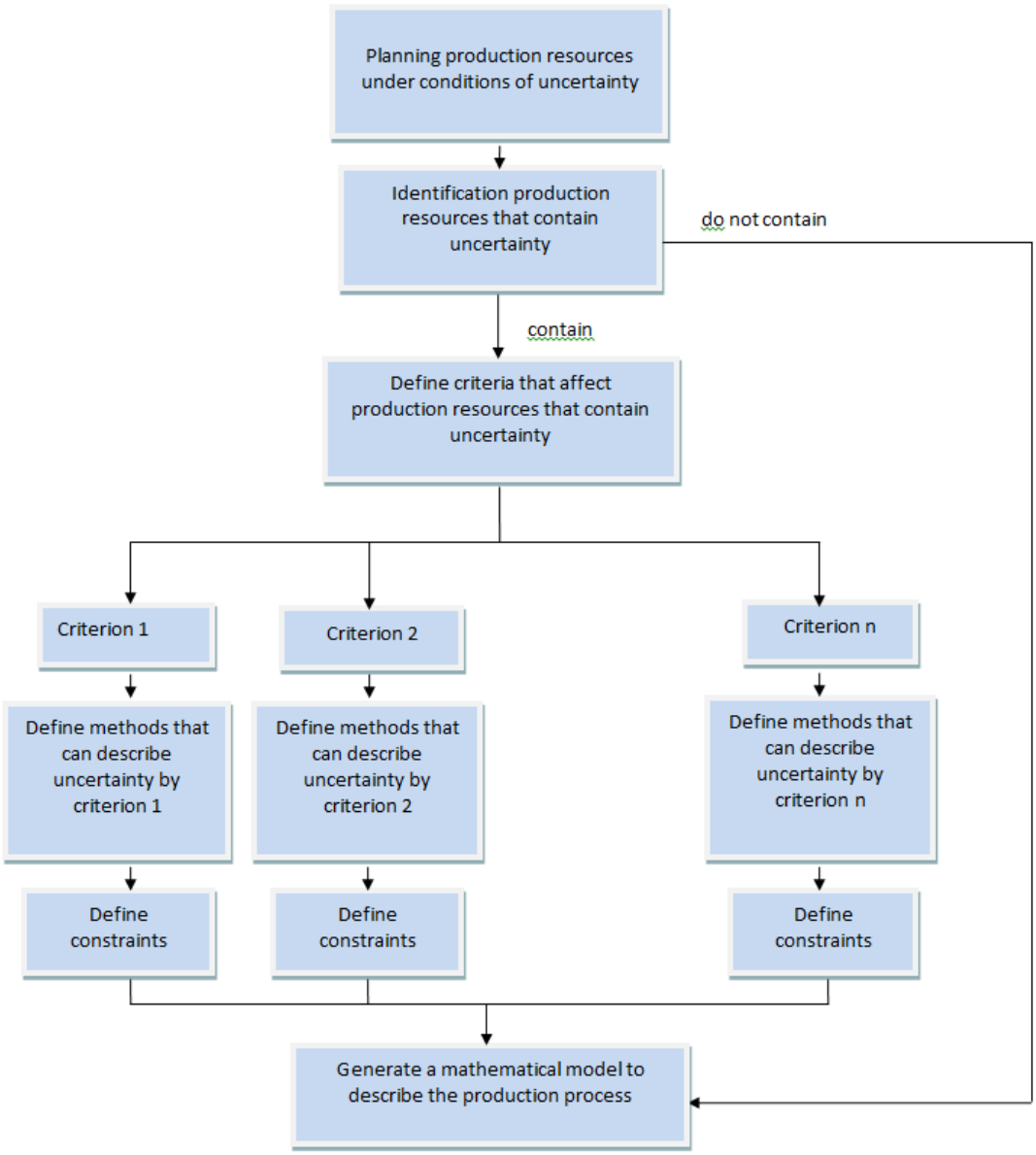


Fig 1. *Global scheme of methodological steps for production resource planning under uncertainty [1]*

This paper considers the problem of determining the optimal production quantity in an enterprise. The objective function is defined as the maximization of total profit over the considered time period. In practice, total profit depends on the value of unit profits of the considered products and their production volume. Due to rapid and frequent changes in product demand, as well as changes that develop in the enterprise, it is almost impossible to accurately determine the values of unit profits respecting the evidential data.
The available capacities of each organizational unit can be defined based on the projected number of operational production equipment and engaged workers. Based on the available data on the age of the equipment, the maintenance method of the equipment, the working environment conditions, as well as seasonal changes that may affect the workers, decision makers estimate the available production capacity.
The second group of constraints arises from the market. The demand for each type of product from the production range is monitored monthly.
Respecting all the introduced assumptions, the considered problem can be posed as an FLP problem with phase coefficients on the right side. The optimal solution to this problem is obtained using the concept of equal opportunities. By applying the proposed model, the optimal production quantity of each type of product can be determined. In this way, the production manager can monitor the change in the quantity of each type of product production over a period of time. In accordance with the results obtained, the manager should take appropriate measures to improve capacity utilization or take marketing measures that would lead to an increase in demand for the product. At the same time, such measures would lead to an increased overall profit of the manufacturing company, which is one of the most important business goals.
The results of the application of this methodology were published in a doctoral dissertation [1] and a paper published in an international journal [10] and show the concrete application of the designed methodology in the company.

CONCLUSION

The literature defines numerous methods and techniques that are used in the optimization of production resources. Planning production resources under uncertainty requires the use of the FLP (phase linear programming) and FAHP (phase analytic hierarchy process) methods to estimate the parameters of the objective function during optimization. A significant contribution to the optimization of production resources under uncertainty can be achieved by including uncertainty in the process of planning production capacities by applying the linear programming phase.
The designed methodology has been applied in research, and the obtained research results enable rational planning of production resources under uncertainty, in order to ensure optimal enterprise management. Identification of the cause-effect relationship between the values of the criteria and alternatives has enabled the design of a model for optimal enterprise management.
A scheme of methodological steps for the analysis of production resources in which uncertainty is present is proposed, which is key to optimizing the planning process. The projected production plan under conditions of uncertainty indicates the realization of higher profits if the proposed solutions are implemented.

REFERENCES

Milanović D, M., (2021). Improving the process of planning production resources under conditions of uncertainty, Doctoral dissertation, University of Belgrade, Faculty of Mechanical Engineering. Belgrade. 2021.

Chang, D., Y., (1996). Applications of the extent analysis method on fuzzy AHP. European J. of Operational Research, 95 649-655.

Ebrahimnejad, A., and Madjid Tavana, M. (2014). A novel method for solving linear programming problems with symmetric trapezoidal fuzzy numbers. Applied Mathematical Modelling , accepted for publishing.

Jiménez, M., Arenas, M., Bilbao, A., & Rodrı, M. V. (2007). Linear programming with fuzzy parameters: an interactive method resolution. European Journal of Operational Research, 177(3), 1599-1609.

Jimènez, M. (1996). Ranking fuzzy numbers through the comparison of its expected intervals. International Journal of Uncertainty, Fuzziness and Knowledge-Based Systems 4 (4), 379–388.

Lofti, H.F., Allahviranloo, T., Jondabeh, A.M., Alizadeh, L. (2009). Solving a full fuzzy linear programming using lexicography method and fuzzy approximate solution. Applied Mathematical Modelling 33, 3151–3156.

Pandian, P. (2013), Multi-objective Programming Approach for Fuzzy Linear Programming Problems. Applied Mathematical Sciences, 7 (37), 1811 – 1817.

Pandian, P. (2012). A simple approach for finding a fair solution to multiobjective programming problems. Bulletin of Mathematical Sciences & Applications, 1, 25 – 30.

Saaty TL (1990). How to Make a Decision: The Analytic Hierarchy Process. European Journal Operational Research 48: 9-26.

Milanovic D. M., Misita M., Komatina N., Determination of the Optimal Production Plan by Using Fuzzy AHP and Fuzzy Linear Programming, Journal of Intelligent and Fuzzy Systems, DOI: 10.3233/JIFS-190913, vol. 38, no 4, pp. 4315-4325, 2020, ISSN online 1875 - 89

DOI:10.5937/IIZS26263R

APPLICATION OF LARGE LANGUAGE MODELS IN REQUIREMENTS ENGINEERING

Review paper

Branislava Radu, Ljubica Kazi, Ivana Berković, Zeljko Stojanov
University of Novi Sad, Technical Faculty "Mihajlo Pupin", Zrenjanin, Serbia

Abstract: Requirements engineering plays a significant role in software development, while the development of large language models (LLMs) provides new opportunities to support and automate various activities within this process. The aim of this paper is to analyze the application of LLMs in requirements engineering, with particular focus on the tasks in which they are applied, the methods used to evaluate their outputs and the limitations of their use. Based on a review of selected literature, the applications of LLMs in requirements elicitation, specification, analysis and validation were analyzed, along with different models, prompt formulation approaches and criteria for assessing the quality of generated outputs. The analysis indicates that LLMs can contribute to the automation of certain activities, improve requirements quality and reduce the time required for their processing, while the obtained results depend on the choice of model, task characteristics, available context and prompt formulation. Key challenges include the generation of inaccurate and biased content, context-related issues, ambiguous requirements, data protection and security concerns. Further development should focus on more reliable evaluation, improved context management and more effective collaboration between LLMs and experts.
Key words: Requirements engineering, large language models, LLMs, generative artificial intelligence, evaluation

INTRODUCTION

Requirements Engineering (RE) represents one of the key phases of software development. The complexity of these activities, as well as the time and resources required to perform them, has encouraged the exploration of possibilities for their automation (Ronanki et al., 2024). The successful implementation of software projects largely depends on the quality of defined requirements, as clearly and unambiguously formulated requirements provide the foundation for the further development of a software system (Lubos et al., 2024).

The development of generative artificial intelligence, particularly large language models (LLMs), has opened new possibilities for automating and supporting Requirements Engineering activities. Owing to their ability to process natural language, LLMs are applied to various tasks, including the elicitation, analysis, specification and validation of software requirements (Arora et al., 2024). Although their application offers considerable potential for improving these activities, it is also accompanied by certain limitations. These include the possibility of generating inaccurate, fabricated and biased content, limited explainability, difficulties in handling ambiguous and complex requirements, as well as challenges related to data protection and security. Excessive reliance on these models may also lead to the neglect of the specific context and needs of stakeholders, making human verification and supervision of the obtained results necessary (Marques et al., 2024).

The aim of this paper is to analyze the application of large language models in Requirements Engineering, focusing on the tasks in which they are applied, the models used and the ways in which they are applied, approaches to evaluating their results and the limitations that arise across different activities. The paper examines various applications of LLMs in Requirements Engineering, as well as the influence of prompt formulation and model selection on the quality of the obtained results. Based on a literature review, specific models, tasks and evaluation criteria are identified with the aim of examining their capabilities and limitations, as well as identifying underexplored areas and potential directions for future research.

The paper is organized as follows. Following the introduction, the basic concepts of Requirements Engineering and large language models are presented. The applications of

[1]Corresponding author, branislava.radu@tfzr.rs, ORCID: 0009-0004-3337-8445
[2]ljubica.kazi@tfzr.rs, ORCID: 0000-0001-8089-3029
[3]ivana.berkovic@tfzr.rs, ORCID: 0000-0003-2366-3942
[4]zeljko.stojanov@uns.ac.rs, ORCID: 0000-0001-6930-5337

LLMs in Requirements Engineering are then discussed, including their use across different phases of the process and in specific tasks. This section also analyzes selected models, their input and output data and the influence of prompt formulation on performance. Furthermore, approaches to evaluating results, limitations of their application and directions for future research are discussed. Finally, the conclusions and the main findings of the research are presented.

BACKGROUND

Requirements Engineering

Requirements Engineering is a field of software engineering focused on the systematic identification, documentation, analysis and verification of system and software requirements throughout their life cycle. The process involves several interconnected activities. During requirements elicitation, information about stakeholders' needs is collected, while requirements analysis involves their assessment and the identification of shortcomings such as ambiguity, inconsistency and incompleteness. Modeling enables requirements to be represented in a structured form, while requirements management involves tracking changes and maintaining their relationships with other development artifacts. Validation and verification are used to determine whether the requirements correspond to the needs and expectations of stakeholders and whether the system specification satisfies the defined requirements. These activities are primarily based on natural language and include tasks such as classification, traceability and defect detection. A key artifact is the System/Software Requirements Specification (SRS), which defines the system's functionalities, quality attributes and constraints and serves as a basis for design, implementation and testing. In addition to the System/Software Requirements Specification, modern Requirements Engineering also uses other sources, such as user stories, user feedback and legal and regulatory documents. This increases the scope of available information but also the co (Zadenoori et al., 2025)

Large Language Models

Large Language Models (LLMs) are artificial intelligence systems that enable the processing and generation of natural language text. Their training is based on large collections of textual data, from which the models learn language patterns, meanings and relationships between words in different contexts. Most modern LLMs are based on the Transformer architecture, which uses a self-attention mechanism to efficiently process context. This structure enables the application of models to tasks such as text generation and summarization, translation and question answering, with the Generative Pre-trained Transformer (GPT) being one of the most well-known examples. Although LLMs can be used in various domains, their reliability is not always guaranteed, as they may generate inaccurate information (Zadenoori et al., 2025)

APPLICATION OF LLMs IN REQUIREMENTS ENGINEERING

Application of LLMs Across the Phases of Requirements Engineering

This section presents large language models and their application in various Requirements Engineering activities, with an overview of the tasks in which they are applied, as well as the types of input and output data.

Large language models are increasingly being applied to various Requirements Engineering activities, including requirements extraction, classification, analysis and generation, as well as tasks that connect Requirements Engineering with other software engineering activities. Large Language Models for Requirements Engineering (LLM4RE) represents a relatively new research direction that has developed more intensively since 2023, with the application

of language models expanding from predominantly analytical tasks to more complex generative activities. (Zadenoori et al., 2025)

The application of LLMs encompasses different phases of Requirements Engineering, from elicitation to validation. During elicitation, LLMs can analyze documentation, identify missing information, formulate questions and suggest requirements, as well as support virtual interviews with stakeholders. During specification, they structure information and generate user stories, functional requirements and non-functional requirements. During analysis, they assess requirements quality and identify ambiguities, incompleteness, inconsistencies and potential risks, as well as suggest additional requirements and changes. During validation, they support requirements verification, simulate different stakeholder perspectives and generate acceptance criteria and test scenarios (Arora et al., 2024).

These applications encompass numerous specific tasks, ranging from completing incomplete requirements, assessing quality and detecting ambiguities to modeling, formalization and the generation of code and test artifacts. (Hemmat et al., 2025). Prompt-based LLMs have been investigated for the automatic classification of software requirements (Binkhonain & Alfayez, 2025). For example, Bidirectional Encoder Representations from Transformers was used to complete missing parts of requirements, while Chat Generative Pre-trained Transformer (ChatGPT) and Generative Pre-trained Transformer 3 (GPT-3.5) were applied to assess quality and formulate questions for requirements elicitation (Jin et al., 2024). GPT models are primarily used for generative and analytical tasks, Bidirectional Encoder Representations from Transformers for classification and analysis, Text-to-Text Transfer Transformer and Large Language Model Meta AI 2 (Llama 2) for reformulation and summarization, while multimodal models are used to connect textual and visual information (Hemmat et al., 2025).

Depending on the task, LLMs process different types of input data and generate different outputs. The most common inputs include SRS documents, user stories, technical documentation, models and code, while outputs include structured requirements, classifications, Unified Modeling Language (UML) diagrams, formal specifications and code (Hemmat et al., 2025). Recent research has extended these applications to LLM agents and multi-agent systems for more complex activities, such as document generation, user story analysis, security requirements formulation and regulatory compliance checking (Jin et al., 2024).

Applications of LLMs in Specific Requirements Engineering Tasks

This section presents specific applications of LLMs in various Requirements Engineering tasks, as well as the influence of model selection and prompt formulation on the obtained results.

One of the tasks in which the application of LLMs has been investigated is software requirements elicitation. In one study, GPT-3.5, was used to generate questions for surveys and interviews based on short and simple prompts. The quality of the questions was evaluated according to readability, clarity, relevance and completeness. For readability, the Flesch Reading Ease, which determines how easy a text is to read and the Flesch-Kincaid Grade Level, which estimates text complexity, were used. The average Flesch score was approximately 40, while the questions were generally assessed as clear and complete. Lower readability was observed in domains with more specialized terminology, whereas questions related to clothing retail were the simplest. The findings indicate that GPT-3.5 can support initial elicitation activities, while more precise prompt formulation can contribute to more focused and specific results (Yeow et al., 2024).

LLMs can be applied to generate Software Requirements Specification (SRS) documents. In one study, Generative Pre-trained Transformer 4 (GPT-4) and CodeLlama-34b were used to generate an SRS for a university student club management portal, and their outputs were compared with a human-authored SRS. The quality of individual requirements and the overall document was evaluated. At the level of individual requirements, clarity, understandability, correctness and verifiability were assessed, while at the level of the complete SRS, internal consistency, non-redundancy, completeness and conciseness were

considered. The human-authored SRS achieved the highest overall score, while CodeLlama-34b approached or exceeded the human result in some categories. CodeLlama-34b generated a shorter document containing a larger number of requirements in most sections; however, irrelevant, generic and incorrectly classified requirements were identified, as well as cases in which multiple requirements were combined into a single requirement. These issues could negatively affect understandability and lead to ambiguity. A more detailed analysis of individual characteristics showed that the human-authored SRS achieved better results in terms of clarity and understandability, whereas the LLMs performed better in terms of correctness. ChatGPT generated fewer but more precise performance requirements, while CodeLlama-34b provided more detailed security requirements. For design constraints, the human-authored SRS received the highest evaluation, whereas CodeLlama-34b showed difficulties in transferring requirements from other sections and including irrelevant requirements. For external interfaces, both models performed worse than the human-authored SRS. During subsequent correction, ChatGPT corrected 10 out of 11 problematic requirements, while CodeLlama-34b corrected four. At the same time, the LLMs significantly reduced the time required to create the SRS. CodeLlama-34b generated more detailed, complete and consistent documents, whereas documents generated using ChatGPT were more concise and contained less repetition. During validation, ChatGPT showed smaller average deviations from the evaluations provided by human evaluators. The findings indicate the potential of LLMs for more efficient specification generation, but also reveal limitations in contextual understanding and the correct classification of requirements, making human validation necessary (Krishna et al., 2024).

LLMs are also applied to the analysis and quality assessment of software requirements. One study investigated Llama 2 with 70 billion parameters for defect detection, justification of assessments and the suggestion of improved requirement formulations. The quality of requirements was evaluated according to characteristics defined by the ISO/IEC/IEEE 29148 standard: appropriate level of abstraction, completeness, consistency, correctness, feasibility, necessity, uniqueness, unambiguity and verifiability. The results were compared with assessments provided by experienced experts. The model achieved high recall but lower precision due to the identification of problems that did not actually exist, making human verification necessary. The explanations were generally assessed as convincing, while the proposed reformulations were considered improvements. The findings indicate that LLMs can provide useful support for reviewing and improving requirements quality, but they cannot replace human judgment (Lubos et al., 2024).

In addition to model selection, the results of LLM4RE tasks are influenced by prompt formulation and temperature settings, where lower temperature values produce more stable responses, while higher values generate more diverse responses. One study examined five prompting patterns for Generative Pre-trained Transformer 3.5 Turbo (GPT-3.5-turbo) on tasks involving the classification of functional and non-functional requirements and the identification of relationships between requirements. The "Question Refinement" pattern achieved the best results for requirements traceability, while "Cognitive Verifier" and "Question Refinement" were the most successful for binary classification. The findings confirm that the choice of prompting pattern and temperature significantly affects model performance. Precision, recall, F1-score and accuracy were used to evaluate performance (Ronanki et al., 2024). In addition, model adaptation techniques such as fine-tuning, prompt and context tuning and Low-Rank Adaptation are being investigated; however, most studies still rely on pretrained models without additional tuning (Hemmat et al., 2025).

Evaluation and Limitations of LLM Applications in Requirements Engineering

This section discusses evaluation methods, limitations of LLM applications and directions for future research.

The evaluation of LLM outputs in Requirements Engineering involves quantitative, qualitative and mixed-method approaches. In the analyzed studies, quantitative and mixed-method approaches were most frequently applied, while qualitative approaches were less

represented. Quantitative evaluation most commonly uses metrics such as precision and recall, whereas qualitative evaluation is based on thematic analysis. The mixed-method approach is particularly suitable for generative tasks, such as modeling and requirements elicitation, because a single reference solution often does not exist for such tasks. Instead, multiple generated solutions may satisfy the defined criteria, making expert assessment useful for evaluating their quality, contextual appropriateness and completeness, while involving multiple evaluators can contribute to a more objective assessment. (Zadenoori et al., 2025)

Depending on the task, different metrics are used to assess the quality and reliability of the results. Correctness and completeness evaluate the accuracy and coverage of the results, while precision, recall and F1-score measure the model's performance in identifying relevant elements. Agreement and consistency metrics assess the alignment of results with human judgments or standards, as well as the stability of outputs. These measures are complemented by qualitative and expert assessments used to evaluate the relevance, clarity, understandability and usability of generated results (Hemmat et al., 2025).

Although LLMs demonstrate considerable potential for application, their use is limited by inaccurate, fabricated and biased content, limited explainability, difficulties in handling ambiguous and complex requirements, as well as data protection and security concerns. Excessive reliance on these models may lead to the neglect of context and stakeholder needs; therefore, human verification and supervision are necessary (Marques et al., 2024). Particular difficulties arise when dealing with domain-specific, ambiguous and conflicting requirements, as well as when processing large documents, where context loss and inconsistencies may occur (Arora et al., 2024).

The use of GenAI in software engineering raises concerns related to dependability, accuracy, data accessibility and transparency, while requirements engineering remains an area that requires further research (Nguyen-Duc et al., 2025).Limitations have also been identified in specific experimental studies. The reliability of results is influenced by differences among evaluators, labeling bias, data preparation and prompt formulation, while the limited range of tasks, prompting patterns and datasets, which may not be fully representative or may have been included in the data used to train GPT models, makes it difficult to generalize the results (Ronanki et al., 2024).

Several research gaps have also been identified in the literature. Certain activities, such as terminology extraction, relationship extraction and change impact analysis, remain insufficiently investigated. Regarding input data, structured documents, particularly SRS documents, predominate, while informal and dynamic sources are considerably less represented. A similar pattern can be observed in output results, which are most often focused on traditional Requirements Engineering artifacts, whereas traceability, test artifacts and other more complex outputs are less frequently addressed. This indicates a need for approaches that integrate different types of input and output data and support more comprehensive Requirements Engineering workflows. In addition, by generating explanations of their results, LLMs may facilitate the understanding of decisions in analytical tasks, including requirements classification, defect detection and other analysis activities. (Zadenoori et al., 2025)

Future research may focus on integrating LLMs with other artificial intelligence techniques, formal methods and domain-specific tools, as well as on combining Requirements Engineering knowledge with knowledge from other fields to improve requirements quality. Particular attention should be devoted to less explored activities, such as terminology extraction, relationship extraction and change impact analysis. (Zadenoori et al., 2025) Another important direction is the development of new prompting patterns and their combination to obtain more stable and reliable results, as well as the optimization of the trade-off between precision, recall and accuracy. In addition, new evaluation frameworks should be developed and the boundaries of LLM application in different Requirements Engineering activities should be more clearly established. Their application should be accompanied by an appropriate level of human oversight to ensure the reliability, quality and responsible use of generated results. (Ronanki et al., 2024)

Table 1 presents an overview of the selected LLMs and their applications in various Requirements Engineering activities.

Table 1. *Overview of LLMs and Their Applications in Requirements Engineering*

Study	Model	Specific task	Application and key findings
(Yeow et al., 2024)	**GPT-3.5**	Generation of questions for surveys and interviews in requirements elicitation	Used with short and simple prompts. The quality of the questions was assessed based on readability, clarity, relevance and completeness. The average Flesch score was approximately 40. The quality of the output depended on the use of specialized terminology and prompt formulation.
Krishna et al., 2024)	**GPT-4 / ChatGPT**	1. SRS document generation 2. Correction of problematic requirements	Used to develop an SRS for a student club management portal. It generated more concise documents with less repetition, while for performance requirements it generated fewer but more precise requirements. It was more successful in correcting problematic requirements, correcting 10 out of 11 problematic requirements and showed smaller average deviations from human evaluators' assessments. It contributed to reducing the time required to develop the SRS. Weaker results were obtained for external interfaces compared with the human-written SRS.
Krishna et al., 2024)	**CodeLlama-34b**	1. SRS document generation 2. Correction of problematic requirements	Generated shorter but more detailed, complete and consistent documents, with a larger number of requirements in most sections. It provided more detailed security requirements, while in some categories it achieved results comparable to or better than the human-written SRS. Identified problems included generic, irrelevant and misclassified requirements, copying requirements from other sections and combining multiple requirements into a single requirement, which could negatively affect understandability and lead to ambiguity. It corrected 4 out of 11 problematic requirements and contributed to reducing the time required to develop the SRS. Weaker results were obtained for external interfaces compared with the human-written SRS.
(Lubos et al., 2024)	**Llama 2 70B**	1. Defect detection, 2. Justification of assessments 3. Requirements reformulation	Requirement quality was assessed according to the criteria of the ISO/IEC/IEEE 29148 standard. The model achieved high recall but lower precision due to the identification of non-existent problems. The explanations were generally assessed as convincing, while the proposed reformulations were evaluated as improvements.

(Ronanki et al., 2024)	**GPT-3.5-turbo**	1. Classification of functional and non-functional requirements 2. Identification of relationships between requirements	Performance depended on prompt formulation and temperature. Precision, recall, F1-score and accuracy were used for evaluation. The best and most stable results for requirements traceability were achieved using the "Question Refinement" pattern, while "Cognitive Verifier" and "Question Refinement" were the most successful for requirements classification. The choice of prompt and temperature significantly affected model performance.

CONCLUSION

The aim of this paper was to analyze the application of large language models in requirements engineering, with a focus on the specific tasks in which they are applied, the models used, the methods for evaluating the results and the limitations of their use. The paper first provides an overview of the basic concepts of requirements engineering and large language models, followed by an analysis of their applications in various requirements engineering activities. The applications of LLMs in requirements elicitation, specification, analysis and validation were analyzed, as well as the applications of GPT-3.5, GPT-4, ChatGPT, CodeLlama-34b and Llama 2 70B.

The analysis showed that LLMs are applied across different phases of requirements engineering, from elicitation and specification to analysis and validation. Examples of their application in question generation, specification development, requirements classification, identification of relationships between requirements, defect detection and requirements improvement were considered. It was observed that the choice of model, prompt formulation and evaluation method can significantly affect the obtained results. LLMs can contribute to the automation of certain activities and reduce the time required for requirements processing; however, their application is limited by the possibility of generating inaccurate and biased content, difficulties in understanding context, ambiguous and conflicting requirements, as well as data protection and security concerns. Therefore, human verification and oversight are necessary.

Future research may focus on improving evaluation methods, more effective context management and the development of new prompt formulation patterns. Particular attention should be paid to the application of LLMs to domain-specific requirements, as well as to less explored activities, such as terminology extraction, relationship extraction and change impact analysis. Integrating LLMs with other artificial intelligence techniques, formal methods and domain-specific tools may further contribute to the reliability and efficiency of their application in requirements engineering. Future development should aim to establish a balance between the potential for automation and the need for human oversight in order to ensure the quality, reliability and responsible use of generated results.

ACKNOWLEDGEMENT

This research was supported by the Ministry of Science, Technological Development and Innovation of the Republic of Serbia, with a scholarship for PhD students in the year 2026.

REFERENCES

Arora, C., Grundy, J., & Abdelrazek, M. (2024). Advancing requirements engineering through generative AI: Assessing the role of LLMs. In A. Nguyen-Duc, P. Abrahamsson, & F. Khomh (Eds.), *Generative AI for effective software development* (pp. 129–148). Springer. https://doi.org/10.1007/978-3-031-55642-5_6

Binkhonain, M., & Alfayez, R. (2025). Are prompts all you need? Evaluating prompt-based large language models (LLMs) for software requirements classification. *Requirements Engineering, 30, 423–443.* https://doi.org/10.1007/s00766-025-00451-8

Hemmat, A., Sharbaf, M., Kolahdouz-Rahimi, S., Lano, K., & Tehrani, S. Y. (2025). Research directions for using LLM in software requirement engineering: A systematic review. *Frontiers in Computer Science, 7,* 1519437. https://doi.org/10.3389/fcomp.2025.1519437

Jin, H., Huang, L., Cai, H., Yan, J., Li, B., & Chen, H. (2024). From LLMs to LLM-based agents for software engineering: A survey of current, challenges and future. arXiv preprint arXiv:2408.02479. https://doi.org/10.48550/arXiv.2408.02479

Krishna, M., Gaur, B., Verma, A., & Jalote, P. (2024). Using LLMs in software requirements specifications: An empirical evaluation. *In 2024 IEEE 32nd International Requirements Engineering Conference (RE)* (pp. 475–483). IEEE. https://doi.org/10.1109/RE59067.2024.00056

Lubos, S., Felfernig, A., Tran, T. N. T., Garber, D., El Mansi, M., Erdeniz, S. P., & Le, V. M. (2024). Leveraging LLMs for the quality assurance of software requirements. *In G. Liebel, I. Hadar, & P. Spoletini (Eds.), Proceedings – 32nd IEEE International Requirements Engineering Conference, RE 2024* (pp. 389–397). IEEE. https://doi.org/10.1109/RE59067.2024.00046

Marques, N., Silva, R. R., & Bernardino, J. (2024). Using ChatGPT in software requirements engineering: A comprehensive review. *Future Internet, 16*(6), 180. https://doi.org/10.3390/fi16060180

Nguyen-Duc, A., Cabrero-Daniel, B., Przybylek, A., Arora, C., Khanna, D., Herda, T., Rafiq, U., Melegati, J., Guerra, E., Kemell, K.-K., Saari, M., Zhang, Z., Le, H., Quan, T., & Abrahamsson, P. (2025). Generative artificial intelligence for software engineering: A research agenda. *Software: Practice and Experience, 55(11),* 1806–1843. https://doi.org/10.1002/spe.70005

Ronanki, K., Cabrero-Daniel, B., Horkoff, J., & Berger, C. (2024). Requirements engineering using generative AI: Prompts and prompting patterns. In A. Nguyen-Duc, P. Abrahamsson, & F. Khomh (Eds.), *Generative AI for effective software development* (pp. 109–127). Springer. https://doi.org/10.1007/978-3-031-55642-5_5

Yeow, J. S., Rana, M. E., & Abdul Majid, N. A. (2024). An automated model of software requirement engineering using GPT-3.5. *In 2024 ASU International Conference in Emerging Technologies for Sustainability and Intelligent Systems (ICETSIS)* (pp. 1746–1755). IEEE. https://doi.org/10.1109/ICETSIS61505.2024.10459458

Zadenoori, M. A., Dąbrowski, J., Alhoshan, W., Zhao, L., & Ferrari, A. (2025). Large language models (LLMs) for requirements engineering (RE): A systematic literature review. arXiv preprint arXiv:2509.11446. https://doi.org/10.48550/arXiv.2509.11446

DOI:10.5937/IIZS26271R

METRICS FOR EVALUATING SOFTWARE TESTING QUALITY

Research paper

Branislava Radu[1], Ljubica Kazi[1]
[1]University of Novi Sad, Technical Faculty "Mihajlo Pupin", Zrenjanin, Serbia

Abstract: Software testing quality is an important aspect of developing reliable software systems and a large number of different metrics are used to evaluate it. The aim of this paper is to present a preliminary overview of metrics used to assess various aspects of testing, including the testing process, efficiency, test case quality and test code quality. Different groups of indicators are considered, with particular emphasis on coverage, defect detection and mutation testing metrics. The literature review indicates the limitations of individual metrics, particularly code coverage and highlights the need to combine multiple indicators for a more comprehensive assessment of testing quality.
Key words: testing quality, testing metrics, test case, software testing

INTRODUCTION

Software testing represents a significant part of the software development process. As software systems become increasingly large and complex, thorough testing and the application of appropriate metrics can contribute to greater confidence in software reliability, while testing metrics provide quantitative indicators for evaluating testing activities and processes(Singh et al., 2008).The development of technology has led to the increasingly widespread use of software solutions in business, prompting companies to improve development and testing processes in order to increase their efficiency and respond to increasingly complex business requirements (Barraood et al., 2023). The assessment of testing effectiveness is most commonly based on indicators such as code coverage, defect detection rate and test execution time. However, these indicators do not provide a comprehensive view of testing quality, as each addresses only a specific aspect of the process. (Do & Morales, 2026)In addition to selecting appropriate metrics, the quality of the tests themselves is an important factor in testing effectiveness, as it can affect the reliability of testing results and the quality of the final software product (Bowes et al., 2017).Testing aims to detect defects and ensure an adequate level of quality before the software product is released, but in practice it faces various challenges, including changing requirements. Under such conditions, test case quality represents an important aspect of testing effectiveness, while existing metrics for its measurement are not always sufficiently clear and do not enable a straightforward assessment of different test case quality characteristics (Barraood et al., 2023).

The aim of this paper is to present the metrics used to evaluate software testing quality and to examine them in relation to the different aspects of testing that they assess. Particular attention is given to metrics related to the testing process, efficiency and testing outcomes, as well as metrics for test case and test code quality. In addition to identifying and classifying these metrics, their limitations are also discussed, particularly regarding the extent to which an individual indicator can provide a comprehensive view of testing quality.

The paper is organized as follows. The second section presents the theoretical foundations of software testing, including basic concepts related to test cases and approaches to their identification. The third section provides an overview of related research on metrics for the testing process, efficiency and testing outcomes, as well as metrics for test case and test code quality. The fourth section discusses selected metrics identified in the reviewed studies and summarizes them according to the aspects of testing quality they assess. Finally, the paper presents conclusions and directions for future research.

[1]Corresponding author,branislava.radu@tfzr.rs, ORCID: 0009-0004-3337-8445
[2] ljubica.kazi@tfzr.rs, ORCID: 0000-0001-8089-3029

BACKGROUND

A test case represents a fundamental element of the testing process and defines how a particular functionality or property of the software is verified. Its structure includes an identifier, a description of the testing objective, preconditions, input data, expected outputs and postconditions and may also contain additional information about test execution. Particular attention should be given to expected outputs, whose precise definition can, in some cases, be complex and may require the involvement of domain experts. Test case execution involves establishing the preconditions, entering the specified input data, observing the actual results obtained and comparing them with the expected results. Based on this comparison, it is determined whether the test case has been successfully executed, after which the postconditions are checked, if necessary. Given their role in a systematic and repeatable testing process, test cases represent important work artifacts that are created, reviewed, executed, maintained and stored throughout the software life cycle(Jorgensen, 2014).
When identifying test cases, two fundamental approaches can be applied: specification-based and code-based approaches. The former is based on the expected behavior of the software and does not require knowledge of how the system is implemented. In contrast, code-based testing relies on the software implementation when selecting test cases, while coverage metrics are used to assess the extent of testing. However, neither approach alone enables complete verification of the software, because implementation-based testing cannot reveal behavior that is specified but not implemented, while specification-based testing alone cannot detect additional behavior that exists in the implementation but is not covered by the specification(Jorgensen, 2014).

METRICS FOR EVALUATING THE TESTING PROCESS AND EFFICIENCY

This section presents metrics used to evaluate different aspects of the software testing process.
Singh et al. (2008) examine various metrics for assessing the quality and effectiveness of the testing process, emphasizing that no single metric is sufficient for its comprehensive evaluation. Based on data from the NASA Metrics Data Program (MDP) repository, metrics such as Quality of Code (QC), Quality of Product (QP) and Test Effectiveness (TE) are analyzed. QC relates the number of weighted defects to the size of the product, whereas QP considers the weighted defects delivered to users in relation to the product size. The effectiveness of defect removal across different phases is determined by the ratio of defects of a particular type detected in the corresponding phase to the total number of such defects, while TE is based on the ratio of closed defects to the total number of reported defects. In this way, these metrics enable the monitoring of product quality and the effectiveness of the testing process in detecting and resolving defects (Singh et al., 2008).
In addition to the aforementioned indicators, (Singh et al., 2008)also considers metrics related to testing time, cost and efficiency, as well as measures of software size and reliability, test session efficiency, testing focus and software maturity. The study also covers metrics of subprogram complexity, test coverage, computer resource utilization and structural characteristics of modules, such as the number of procedures, conditions and loops. A specific group of indicators concerns the analysis of defects according to their cause, module, priority, type, detection method, detection phase and severity. The study also considers indicators of development efficiency, test automation and testing costs, including average testing efficiency, the contribution of requirements reviews, design reviews and program reviews, as well as the time required to verify fixes.The authors of paper also propose the Error Focus and Test Session Efficiency (TSE) metrics. Error Focus measures the proportion of reported errors that are successfully resolved and subsequently closed, while TSE relates the number of weighted defects identified during a specific testing phase to the number of added or modified lines of source code (Singh et al., 2008).

A broader overview of software metrics is presented in(Lee & Chang, 2013), where metrics are classified according to their significance, measurement method and area of application. In the context of testing, the metrics include test case development productivity, defect acceptance and rejection, defects caused by inadequate corrections, defect density in test cases, testing efficiency and effectiveness, as well as the ratio of testing time and costs to development time and costs and product size. In addition, the efficiency of individual testing phases, scripting and automation productivity and system performance expressed through response time, throughput and processor and memory utilization are considered (Lee & Chang, 2013).
The evaluation of such indicators is further addressed in (Zhang et al., 2022), which focuses not only on defining test suite effectiveness metrics but also on their reliability. The authors propose the ASSENT (evAluating teSt Suite EffectiveNess meTrics) framework for the systematic evaluation of metrics and investigate the extent to which their values correspond to the actual effectiveness of test suites. Particular attention is given to inconsistent findings in previous studies regarding the relationship between mutation score and the ability to detect real defects. The authors identify the choice of ground truth, reference test suites and agreement assessment method as possible sources of these differences (Zhang et al., 2022).
In an experiment conducted on projects from the Defects4J dataset, seven metrics were compared: statement coverage, branch coverage, mutation score, Certain Operator Selection (COS), Random Mutant Selection (RMS), Subsuming Mutation Score (SMS) and CMS (Clustering Mutation Score). A rank correlation measure was used to assess the agreement between metric values and the ground truth. When real defects were used as the ground truth, MS and SMS showed the highest accuracy in this experiment, while Statement coverage (SC), Branch Coverage (BC), COS and RMS were insensitive to improvements in test suite effectiveness in certain cases. When mutants were used as an alternative ground truth, all analyzed metrics were overestimated by more than 20% on average, with mutation score-based metrics being more overestimated than code coverage metrics. The authors therefore highlight the importance of selecting the ground truth and the method of generating test suites when evaluating metrics and recommend systematically validating new indicators within the ASSENT framework (Zhang et al., 2022).

METRICS FOR EVALUATING TEST CASE QUALITY

This section presents metrics and characteristics used to evaluate test case and test code quality.

In addition to metrics that assess the testing process as a whole, a significant body of research focuses on the quality of individual test cases and test code. The systematic review presented in research found that there is a lack of studies specifically addressing test case quality, while most of the existing literature focuses on individual characteristics, such as test case reuse, generation and selection, readability, understandability, test smells, design defect analysis and the relationship between coverage and effectiveness. Based on the analyzed studies, 16 quality characteristics were identified, including readability, understandability, simplicity or complexity, correctness, independence, reusability and maintainability (Barraood et al., 2023).
The same study identified a total of 50 metrics used to assess different aspects of test case quality. Statement coverage, code coverage and branch coverage are among the most frequently used, while mutation score appears in a smaller number of studies. Other metrics considered include modified condition coverage, Weighted Methods per Class (WMC), Depth of Inheritance Tree (DIT), Number of Children (NOC), Lack of Cohesion of a TestMethod (LCT) and the number of assertions, as well as indicators of the structural characteristics of tests, readability, execution time, cost, number of test methods and number of detected faults (Barraood et al., 2023).

Individual metrics can be associated with different quality characteristics. Code, branch and statement coverage metrics are used to assess coverage and effectiveness, while mutation score and the number of detected faults can be used to evaluate the ability of tests to detect defects. WMC, DITand NOCmetrics are related to the complexity and maintainability of test code, whereas textual metrics enable the assessment of readability and understandability. Execution time, cost and the number of test cases are associated with testing efficiency (Barraood et al., 2023).For some metrics, such as mutation score and the number of faults detected by test cases, it is not clearly specified which quality characteristics they measure. Therefore, further analysis is needed to determine their relationship with the corresponding quality characteristics.

Testing efficiency is addressed through metrics such as event-pair coverage, cost in hours, number of test methods and test case execution time. The ability to detect faults is assessed using the number of faults detected by a test case, composite code coverage, all-pairs results and mutation killing ratios. Other metrics include the number of test items, constants, variables, preceding test cases and applications that can use a test case, as well as the number of successful user acceptance tests, the total number of detected defects and the number of defects per line of code(Barraood et al., 2023).

A similar approach to test case quality is presented in (Barraood et al., 2018), in which a systematic literature review identified 30 metrics and indicators. These include test team experience, the quality of documented test cases, error and defect density, test case understandability, variability and independence, as well as test case size, similarity, cohesion and coupling. A specific group consists of coverage criteria, including method, statement, branch and condition coverage, as well as adequacy criteria based on coverage and defects. Other indicators considered include mutation analysis, historical fault detection, modified method coverage, defect detection capability and rate, defect detection time, test suite size and McCabe's cyclomatic complexity (Barraood et al., 2018).

The review in (Barraood et al., 2018) also highlights the limitations of coverage as a standalone indicator. Although different types of coverage are frequently used to assess the quality and completeness of a test suite, some of the analyzed studies do not recommend using coverage as the sole measure of test suite effectiveness. Therefore, coverage is combined with other indicators, while some studies consider mutation analysis as a complement to coverage because it enables the assessment of the ability of tests to detect changes in the program. One of the analyzed studies also considers test case quality in terms of design errors and the level of knowledge of the people who create them, indicating that insufficient understanding of relevant knowledge may limit test case quality. The identified metrics are used in various contexts, including software reliability and maintenance, productivity, reuse, test case selection, generation and prioritization, as well as test suite diagnosis (Barraood et al., 2018).

In addition to individual metrics, the quality of test code is also discussed in the literature through principles related to its structure, understandability, reliability and maintainability. Important characteristics include test simplicity, readability and understandability, clear responsibility of an individual test, focus on system behavior, test independence and maintainability. These principles can be associated with measurable characteristics of test code, such as test size, the number of `assert` statements, complexity, the amount of duplicated code, execution time and the way test dependencies are used. Particular emphasis is placed on the need for tests to cover both expected and unexpected scenarios, produce consistent results when repeatedly executed and be sufficiently simple to maintain (Bowes et al., 2017).

Test code quality is also associated with the presence of test smells, which may indicate problems in the structure, readability and maintainability of tests. Test suite quality can also be assessed by combining the number of assertions with test code structure metrics. These approaches further highlight the multidimensional nature of test quality, as different metrics and characteristics address different aspects of test code(Bowes et al., 2017).

The relationship between different characteristics of test code and its quality is also examined in (Grano et al., 2020), where unit test quality is considered in terms of behavioral,

structural and execution characteristics. Behavioral characteristics include self-validation, scope, efficiency and fault diagnosability, with code coverage and mutation score identified as important indicators. Structural characteristics include test size and design, readability, maintainability, independence and reusability, while execution characteristics include execution time, reliability and the conditions of the execution infrastructure (Grano et al., 2020).

In the second part of the study (Grano et al., 2020), the extent to which existing metrics correspond to developers' perceptions of unit test quality was examined. A total of 199 valid ratings provided by 70 developers for 10 tests were analyzed, considering mutation score, line coverage, complexity, coupling, test code size, test smells, assertion density and readability. Due to the high correlation between line coverage and mutation score, only mutation score was included in the final model. In the analyzed dataset, mutation score showed the strongest positive association with higher test quality ratings. Higher coupling between objects, the presence of the Assertion Roulette smell and a higher number of static calls (NOSI) were associated with lower ratings, whereas assertion density showed a positive association with quality ratings. Size, complexity and readability did not show a statistically significant association with developers' ratings, although readability was identified as an important characteristic of a high-quality test in the qualitative part of the study (Grano et al., 2020).

The findings of these studies particularly highlight the need to combine different indicators, which is further examined in(Jain et al., 2023).The authors analyze the limitations of using code coverage and mutation score individually to assess test suite adequacy. Coverage is a commonly used approximation of test adequacy, but it measures the execution of program code rather than necessarily the extent to which its behavior has been tested(Jain et al., 2023).

Based on an analysis of Java projects, the authors of (Jain et al., 2023) identify a positive but imperfect relationship between coverage and mutation score, with considerable variability at higher coverage levels. As an additional indicator, they propose the oracle gap, defined as the difference between source code coverage and mutation score. This approach suggests that the difference between two metrics can provide useful information about aspects of a test suite that are not visible when only one of the metrics is considered(Jain et al., 2023).

In addition to identifying potential metrics, it is important to examine whether characteristics that are commonly considered indicators of high-quality test cases are actually associated with their effectiveness. This question is addressed by the authors of (Lucrédio et al., 2023), who analyze characteristics such as size, complexity, atomicity, independence, readability, exception handling and executed code. In addition to existing metrics, such as lines of code, McCabe's cyclomatic complexity and readability, the study also uses metrics defined as part of the research, including the number of commits related to bug fixes, the number of assertions, coupling metrics and indicators of exception handling(Lucrédio et al., 2023).

The empirical analysis in (Lucrédio et al., 2023) did not confirm most of the hypotheses concerning the characteristics of high-quality test cases. The number of assertions, independence, exception handling and test case size did not show a significant relationship with test case effectiveness in detecting faults. A relationship between test case size and cyclomatic complexity was confirmed, while test case footprint and readability showed relationships contrary to expectations. Based on these findings, the authors indicate that widely accepted assumptions about test case quality are not necessarily supported by empirical data. The study identifies the selection of analyzed projects and the possibility of errors related to the implementation of metrics and the tools used as limitations, which restricts the generalizability of the findings (Lucrédio et al., 2023).

DISCUSSION

This section discusses the metrics identified in the reviewed studies for evaluating the effectiveness and efficiency of the testing process, as well as the quality of test cases and test code. Selected metrics from the analyzed studies are summarized in Tables 1 and 2.

Table 1 presents an overview of the selected metrics for evaluating testing process effectiveness and efficiency.

Table 1. *Metrics for Evaluating Testing Process Effectiveness and Efficiency*

Study	Metric	Description
Singh et al. (2008)	Test Effectiveness (TE)	Based on the ratio of closed defects to the total number of reported defects. It enables monitoring of the effectiveness of the testing process in detecting and resolving defects.
Singh et al. (2008)	Defect Removal Effectiveness	Determined by the ratio of defects of a particular type detected in the corresponding phase to the total number of such defects.
Singh et al. (2008)	Error Focus	Measures the proportion of reported errors that are successfully resolved and subsequently closed.
Singh et al. (2008)	Test Session Efficiency (TSE)	Relates the number of weighted defects identified during a specific testing phase to the number of added or modified lines of source code.

Table 2 presents an overview of the selected metrics for assessing test case and test code quality.

Table 2. *Metrics for Evaluating Test Case Quality*

Study	Quality Aspect	Metrics	Quality Aspect Assessed
Barraood et al. (2023)	Coverage and Effectiveness	Statement Coverage, Branch Coverage, Code Coverage	Coverage and effectiveness of tests.
Barraood et al. (2023)	Defect Detection	Mutation Score, Number of Detected Faults	The ability of tests to detect defects.
Barraood et al. (2018)	Test Case Characteristics	Test Case Size, Test Case Similarity, Test Case Cohesion, Test Case Coupling	Characteristics and quality of individual test cases.
Barraood et al. (2023, 2018)	Complexity and Maintainability	WMC, DIT, NOC	Complexity and maintainability of test code.

The reviewed studies indicate that a wide range of metrics has been proposed to evaluate different aspects of software testing. Coverage metrics are among the most frequently considered, while defect detection and mutation score are also widely addressed. Other metrics assess test case characteristics, as well as test code complexity and maintainability, while several studies examine the relationship between individual metrics and testing quality. However, individual metrics have limitations when used in isolation. No single metric provides a comprehensive assessment of testing quality, and code coverage alone does not fully reflect test effectiveness or quality. For some metrics, their relationship with specific quality characteristics remains unclear, while for some commonly assumed test case quality characteristics, there is insufficient consistent empirical evidence. Therefore, further research is needed to better relate individual metrics to specific quality characteristics and to examine combinations of different indicators for a more comprehensive assessment of testing quality.

CONCLUSION

This paper presents a preliminary overview of metrics used in the literature to evaluate software testing quality. Metrics related to the testing process and testing efficiency, as well as metrics for test case and test code quality, were considered. The review of the studies included indicates that testing quality can be viewed from different perspectives, including coverage, defect detection capability, mutation score, test structure and characteristics, testing time and testing costs.

It was particularly observed that no single metric can provide a complete picture of testing quality. Code coverage represents an important indicator of testing scope, but on its own, it does not provide information about the extent to which tests verify system behavior. Similar limitations were identified for other metrics, while empirical studies show that some characteristics commonly associated with test case quality are not always confirmed as indicators of their effectiveness. Therefore, a more comprehensive assessment requires consideration of multiple interconnected indicators.

Future research should focus on a more detailed analysis of the relationships between individual metrics and testing quality characteristics, as well as on examining combinations of different indicators for a more comprehensive assessment of testing quality. Particular attention could be given to combining different metrics and defining a set of indicators that would enable a more comprehensive assessment of testing quality across different software projects.

ACKNOWLEDGEMENT

This research was supported by the Ministry of Science, Technological Development and Innovation of the Republic of Serbia, with a scholarship for PhD students in the year 2026.

REFERENCES

Barraood, S. O., Mohd, H., Baharom, F., & Omar, M. (2018). Quality factors of test cases: A systematic literature review. In Knowledge Management International Conference (KMICe) 2018, 25–27 July 2018, Miri, Sarawak, Malaysia

Barraood, S. O., Mohd, H., Baharom, F., & Almogahed, A. (2023). Systematic literature review on test case quality characteristics and metrics. In *2023 3rd International Conference on Emerging Smart Technologies and Applications (eSmarTA) (pp. 1–8). IEEE. https://doi.org/10.1109/ESMARTA59349.2023.10293544

Barraood, S. O., Mohd, H., Baharom, F., & Almogahed, A. (2023). Verifying agile black-box test case quality measurements: Expert review. IEEE Access, 11, 106987–107003. https://doi.org/10.1109/ACCESS.2023.3320576

Bowes, D., Hall, T., Petrić, J., Shippey, T., & Turhan, B. (2017). How good are my tests? In 2017 IEEE/ACM 8th Workshop on Emerging Trends in Software Metrics (WETSoM) (pp. 9–14). IEEE. https://doi.org/10.1109/WETSoM.2017.2

Do, P., & Morales, E. (2026, August 6). Development of quality metrics for measuring the efficiency and reliability of automated software testing processes.

Grano, G., De Iaco, C., Palomba, F., & Gall, H. C. (2020). Pizza versus pinsa: On the perception and measurability of unit test code quality. In 2020 IEEE International Conference on Software Maintenance and Evolution (ICSME) (pp. 336–347). IEEE. https://doi.org/10.1109/ICSME46990.2020.00040

Jain, K., Kalburgi, G. T., Le Goues, C., & Groce, A. (2023). Mind the gap: The difference between coverage and mutation score can guide testing efforts. In 2023 IEEE 34th International Symposium on Software Reliability Engineering (ISSRE) (pp. 102–113). IEEE. https://doi.org/10.1109/ISSRE59848.2023.00036

Jorgensen, P. C. (2014). Software testing: A craftsman's approach (4th ed.). CRC Press.

Lee, M. C., & Chang, T. (2013). Software measurement and software metrics in software quality. International Journal of Software Engineering and Its Applications, 7(4), 15–34.

Lucrédio, D., Vincenzi, A. M. R., de Almeida, E. S., & Ahmed, I. (2023). Test case quality: An empirical study on belief and evidence. arXiv. https://doi.org/10.48550/arXiv.2307.06410

Singh, Y., Kaur, A., & Suri, B. (2008). An empirical study of product metrics in software testing. In M. Iskander (Ed.), Innovative techniques in instruction technology, e-learning, e-assessment, and education (pp. 64–72). Springer. https://doi.org/10.1007/978-1-4020-8739-4_12

Zhang, P., Wang, Y., Liu, X., Yang, Y., Li, Y., Chen, L., Wang, Z., Sun, C.-A., & Zhou, Y. (2022). Test suite effectiveness metric evaluation: What do we know and what should we do? arXiv. https://doi.org/10.48550/arXiv.2204.09165

DOI:10.5937/IIZS26279I

PROJECT PERFORMANCE MEASUREMENT: KEY PERFORMANCE INDICATORS (KPIs) AND SUCCESS METRICS FOR SUSTAINABLE INDUSTRIAL PROJECTS – A REVIEW AND CONCEPTUAL FRAMEWORK

Review paper

Dejan Igov[1*], Duško Čučković[2], Verica Gluvakov[3], Ivana Denčić[4]
[1,2] Faculty of Project and Innovation Management Prof. Dr. Petar Jovanović, Belgrade, R. of Serbia
[3,4] Technical Faculty "Mihajlo Pupin" Zrenjanin, R. of Serbia

Abstract: The growing integration of sustainability into industrial development has broadened the conventional understanding of project performance and project success. Although conventional project measurement is centered on time, cost, scope, and quality, sustainable industrial projects require a broader evaluation that also considers economic value, operational and technical outcomes, environmental effects, stakeholder and safety considerations, and longer-term benefits. This paper identifies, analyses, and classifies key performance indicators (KPIs) and success metrics relevant to sustainable industrial projects and proposes a conceptual framework for their integrated assessment. A structured literature review and qualitative content analysis were conducted using Google Scholar and ScienceDirect, with the main search period limited to 2020-2026. The synthesis distinguishes project performance, which primarily reflects execution efficiency, from broader project success, which includes benefits, stakeholder value, sustainability, and long-term outcomes. Six recurring performance dimensions were identified and organized into a three-level framework linking project delivery performance, multidimensional project outcomes, and strategic and long-term project success. The framework offers a literature-based structure for selecting project-specific indicators without imposing universal weights and provides a basis for future empirical validation in industrial project environments.
Key words: project performance, key performance indicators, project success, success metrics, sustainable industrial projects, sustainability, project management

INTRODUCTION

Measuring project performance is essential for assessing progress, detecting deviations, and supporting managerial decision-making. Conventional evaluation emphasizes time, cost, scope, and quality, although the limitations of the traditional cost-time-quality triangle were recognized early (Atkinson, 1999). De Wit (1988) distinguished project success from the success of the project-management effort. Contemporary research extends this distinction across multiple dimensions and time horizons: Ika and Pinto (2022) broaden the meaning of project success, while Korhonen et al. (2023) connect project-level measures with wider organizational success.

This distinction matters for sustainable industrial projects. In this study, sustainable industrial projects are defined as temporary initiatives in manufacturing, energy, process industries, infrastructure, and industrial construction assessed across delivery, economic/value, operational/technical, environmental, social/stakeholder/safety, and strategic or long-term sustainability dimensions. The boundary covers initiation through handover, with post-completion effects included when benefits realization is assessed. Accordingly, project-level and industrial sustainability studies combine delivery measures with financial, environmental, social, safety, governance, and resource-efficiency indicators (Bochtler et al., 2024; Contini & Peruzzini, 2022; Ibrahim et al., 2024; Mengistu & Panizzolo, 2023; Zheng et al., 2026).

The primary challenge is not a lack of indicators but their fragmentation across the project management, sustainability assessment, and industrial performance literatures. Meeting schedule and budget objectives does not guarantee environmental, stakeholder, or long-term value outcomes. Accordingly, reviews and project-level frameworks in PPP and green-

[1] Corresponding author: dejan.igov@pmc.edu.rs, ORCID: 0009-0000-7921-4527
[2] dusko.cuckovic@pmc.edu.rs, ORCID: 0000-0003-4835-2075
[3] verica.gluvakov@tfzr.rs, ORCID: 0000-0003-1083-0203
[4] ivana.dencic@tfzr.rs

building contexts call for broader indicator systems that go beyond conventional delivery criteria (Akomea-Frimpong et al., 2022; Ikudayisi et al., 2022; Shokouhi & Bachari, 2025).
The aim of this paper is to identify, analyse, and classify KPIs and success metrics relevant to sustainable project management and related industrial and engineering projects, and to organize them into a multidimensional conceptual framework. The research questions addressed are: RQ1 - Which KPIs and success metrics are used in sustainable industrial projects? RQ2 - To what extent are traditional project indicators integrated with environmental, economic, operational, and stakeholder-related sustainability dimensions? RQ3 - How can the identified indicators be structured into an integrated framework for multidimensional project performance measurement?

METHODOLOGY

This study uses a structured literature review combined with qualitative content analysis. The methodology is intentionally characterized as structured and exploratory rather than a fully systematic review, because the objective is to synthesize heterogeneous project-performance and sustainability measures into a conceptual framework. The primary publication period was 2020-2026. Seminal pre-2020 publications were used selectively to establish the conceptual background of project success and multidimensional performance measurement and were not counted in the 29-study analytical corpus.
The literature search was conducted on 11 September 2026 using Google Scholar and ScienceDirect. Three predefined Google Scholar queries were used: (1) "What key performance indicators (KPIs) and success metrics are used to measure project performance in sustainable industrial projects?"; (2) "What performance indicators and success criteria are used to evaluate sustainable project management?"; and (3) "How are project performance and project success measured using key performance indicators (KPIs) and success metrics?". The queries returned 50, 50, and 40 records, respectively. All returned records were screened, and exact-title deduplication resulted in 133 unique Google Scholar records.
ScienceDirect was searched in title, abstract, and keyword fields using three queries: "project performance" AND sustainability, "project success" AND "sustainable project management", and "industrial projects" AND sustainability. These returned 106, 5, and 38 records, respectively. After internal exact-title deduplication, 147 unique ScienceDirect records remained. Merging both sources and removing one exact-title cross-source duplicate produced 279 unique records for screening.
Records underwent combined title and abstract relevance screening, followed, where necessary, by full-text or detailed publisher-record verification. Because exclusions based solely on titles or abstracts were not prospectively logged, phase-specific exclusion counts could not be reconstructed. Of the 279 unique records, 250 were excluded as out of scope, background-only, non-project-level, duplicate/alternative versions, or insufficient for KPI extraction; 29 studies were retained (24 core project-level and five supporting industrial-sustainability studies). Grey literature and formal backward/forward snowballing were not used as separate identification streams. Eligible 2026 studies were formally published or publisher-recognized advance online/online-first by 11 September 2026.

Table 1. *Inclusion and exclusion criteria used for study screening*

Inclusion criteria	Exclusion criteria
2020–2026; earlier seminal studies only for conceptual foundations.	Organizational/product/process/technical performance without an explicit project-management perspective.
Project-level performance, project success, or project-level sustainability assessment.	Duplicate records across searches or sources.
Measurable KPIs, performance indicators, success metrics, or success criteria.	Non-academic, commercial, or insufficiently documented sources for the primary corpus.
Sustainable, industrial, infrastructure, or engineering projects; peer-reviewed sources prioritized.	No extractable project-level indicators, metrics, or criteria relevant to the research questions.

A pragmatic quality/relevance appraisal assessed each core study against four criteria: peer-reviewed and traceable source; explicit project-level performance, success or sustainability focus; transparent empirical, review, or conceptual method; and extractable indicators or success criteria supported by a measurement basis, validation procedure, or traceable evidence. Studies meeting at least three criteria were eligible for the core corpus. Because designs were heterogeneous, appraisal informed interpretive weighting rather than a single formal risk-of-bias score; systematic reviews, validated indicator systems and transparent empirical studies received greater weight.

For each retained study, information was extracted on project context, indicators or success criteria, sustainability dimension, measurement focus, evidence basis, evaluation time horizon, and the distinction between project performance and broader project success. Recurring indicators were coded into six analytical dimensions. No numerical weights were assigned because the present study does not include expert elicitation or empirical project data.

Figure 1 summarizes the literature identification, screening, and synthesis procedure used in this review. The flow diagram reports the numbers of records identified, duplicates removed, records screened, studies excluded, and studies retained for qualitative synthesis.

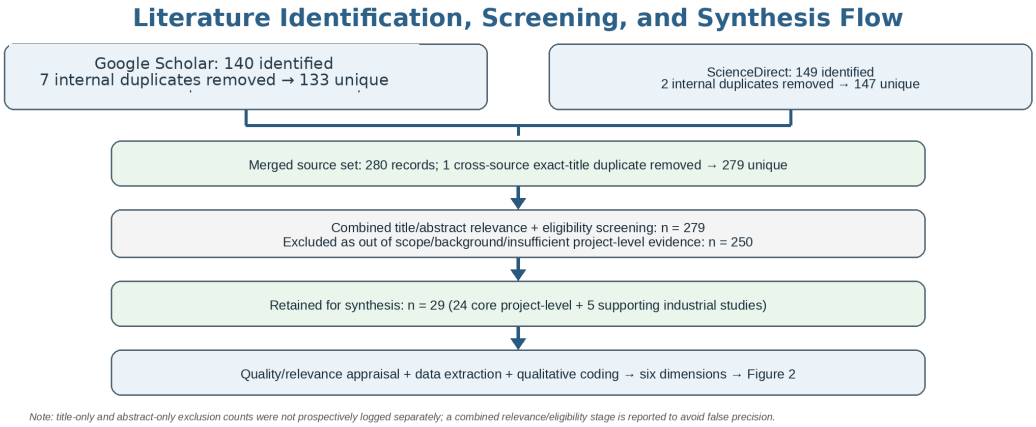


Fig.1. *Literature identification, screening, and synthesis flow*

RESULTS AND DISCUSSION

The synthesis identifies six interrelated dimensions. Non-exclusive coding of the 24 core project-level studies revealed coverage of project delivery performance (17 studies), economic and value performance (20), operational and technical performance (5), environmental performance (20), social, stakeholder, and safety performance (21), and

strategic and long-term project success (11). Individual studies could address more than one dimension. Five supporting industrial studies primarily reinforced the operational/technical and environmental indicator categories.

Addressing RQ1, traditional delivery indicators remain at the core of project performance evaluation. Time, cost, scope, and quality are consistently used to assess whether project execution conforms to planned objectives. Cruz Villazón et al. (2020) identify time, cost, resources, scope, and quality as core project-management measures, whereas Bochtler et al. (2024) describe cost, time, and scope as the dominant traditional focus. He et al. (2022) and Ibrahim et al. (2024) likewise show that project-level performance measurement increasingly supplements conventional measures with broader non-financial criteria.

Economic and value-related metrics form a second recurring group. In addition to cost performance, studies use Net Present Value (NPV), Internal Rate of Return (IRR), Life-Cycle Cost (LCC), benefit-cost measures, profitability and benefits realization. Ma et al. (2020) incorporate profitability and NPV into sustainable project selection, while Tareemi (2025) combines traditional financial metrics with LCC and a resilience benefit-cost measure. Hussain et al. (2026) further demonstrate a tri-objective structure based on NPV, environmental score, and social score, illustrating the integration of economic and sustainability objectives.

Environmental, operational, and social indicators broaden the measurement scope to energy and materials, GHG emissions, water, waste, resource efficiency, productivity, safety, stakeholder satisfaction, and community effects. Díaz Caselles and Guevara (2024) report environmental, social, and economic KPIs, while Zheng et al. (2026) include workplace safety, management efficiency, compliance, local procurement, and schedule controllability. Project applications combine schedule, cost, and carbon metrics (Kaewunruen et al., 2020), OHS and green-building performance (Iga Istri et al., 2025), and wider sustainability assessment metrics (Fallah & Moini, 2026; Ikudayisi et al., 2022). Industrial studies reinforce resource, emissions, waste, energy, and safety indicators (Iannaccone et al., 2020; Mengistu & Panizzolo, 2023; Saxena et al., 2020; Sherif et al., 2022).

An important finding in relation to RQ2 is that project performance and project success are related but not identical. Ika and Pinto (2022) distinguish performance measures associated with management processes from broader success criteria linked to project goals, benefits, stakeholder perceptions, timing, and sustainability. Korhonen et al. (2023) similarly show that the interpretation of project measures depends on their connection to wider organizational success. Consequently, sustainable project success extends beyond effective delivery to include value, stakeholder outcomes, and long-term sustainability.

The degree of integration varies by context, but the direction is consistent. Project success was already framed as a multidimensional strategic concept by Shenhar et al. (2001), while Müller and Jugdev (2012) show how success criteria and critical success factors evolved with context. Recent studies extend this logic to SDG impacts, stakeholder value, future readiness, sustainability, and value creation (Ferrarez et al., 2023; Mansell, Philbin, & Broyd, 2020; Mansell, Philbin, & Konstantinou, 2020; Moreno-Monsalve et al., 2023). Wu et al. (2023), Sanad et al. (2026), and Son et al. (2023) further demonstrate integration across construction, infrastructure, and eco-industrial projects.

Table 2. *Classification and indicative operationalization of project performance and success measures*

Performance dimension	Representative KPIs / success metrics, operationalization, data source, and timing	Representative sources
Project delivery performance	Schedule variance/SPI; cost variance/CPI; scope acceptance/change rate; defects/nonconformities. Data: schedule, cost, change, QA records. Timing: weekly/monthly; confirm at handover.	Ika & Pinto (2022); Cruz Villazón et al. (2020)
Economic and value performance	NPV; IRR; ROI; LCC; benefit-cost measures; realized financial savings/value. Data: business case, finance/ERP, benefits register. Timing: appraisal/stage gates; 6–36 months post-implementation.	Ma et al. (2020); Tareemi (2025)
Operational and technical performance	Energy intensity; productivity; availability; resource utilization; reliability. Data: SCADA/ERP/maintenance. Timing: commissioning; monthly/quarterly.	Ibrahim et al. (2024); Contini & Peruzzini (2022)
Environmental performance	Energy use; GHG emissions; water/material use; waste; recycling/resource efficiency. Data: meters, LCA, environmental logs. Timing: by phase/month; lifecycle for major impacts.	Bochtler et al. (2024); Díaz Caselles & Guevara (2024)
Social, stakeholder, and safety performance	Stakeholder satisfaction/participation; LTIFR/TRIR; incidents; local employment/community effects. Data: surveys, HSE/HR records. Timing: monthly/quarterly; handover/post-project.	Zheng et al. (2026); Wu et al. (2023)
Strategic and long-term project success	Benefits realization; strategic alignment; SDG contribution; resilience/future readiness; long-term value. Data: benefits register, strategic/SDG scorecards, post-implementation review. Timing: 6–12 months; where relevant, 2–5 years.	Ika & Pinto (2022); Moreno-Monsalve et al. (2023)

Table 2 links representative measures to indicative units, data sources, and measurement horizons. Realized financial savings/value are treated as economic outcomes, whereas benefits realization in the strategic dimension refers to broader planned business, stakeholder, and sustainability benefits achieved after handover. The specifications are guidance rather than universal thresholds and should be adapted to project type, lifecycle stage, data availability, and stakeholder priorities.

RQ3 is addressed through the three-level structure illustrated in Figure 2. The analytical core of the framework consists of the six dimensions identified in the review. Level 1 represents project delivery performance through time, cost, scope, and quality. Level 2 integrates four outcome dimensions—economic and value, operational and technical, environmental, and social, stakeholder, and safety performance. Level 3 represents strategic and long-term project success through benefits realization and sustainable value creation, strategic alignment, future readiness, and long-term societal and environmental impact. The figure translates the review findings into a progression from execution efficiency to broader project outcomes and, ultimately, to sustainable long-term success.

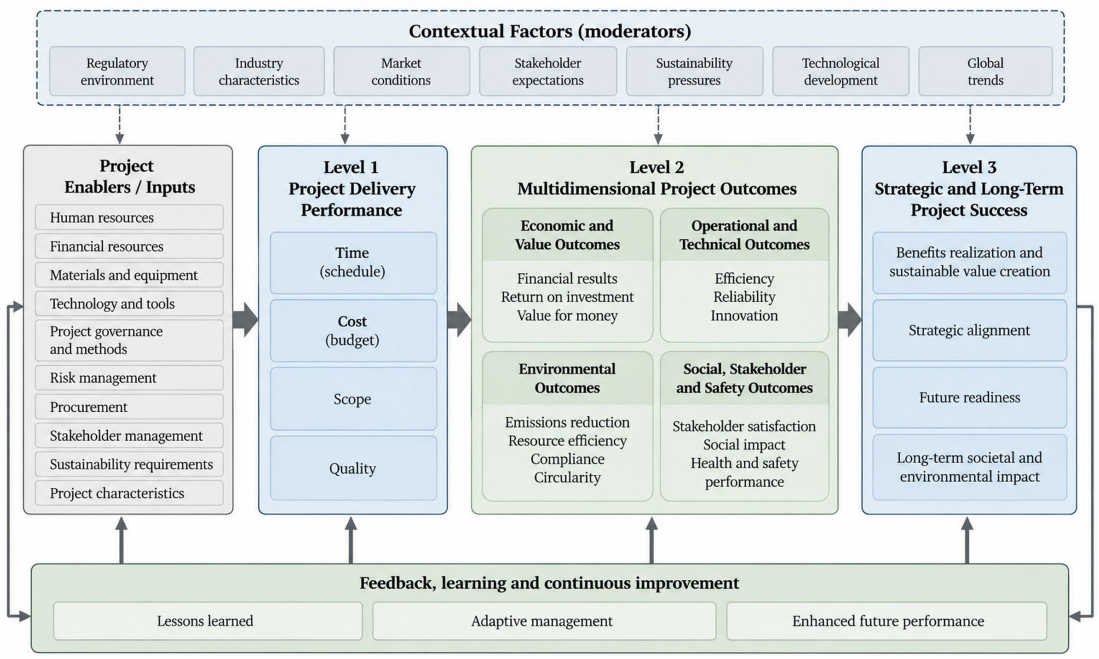


Fig. *2. Proposed multidimensional framework for project performance measurement in sustainable industrial projects*

The project enablers and contextual factors in Figure 2 are not additional outcome dimensions; they position the literature-derived framework within project-management practice. Human resources, financial resources, materials and equipment, technology and tools, project governance and methods, risk management, procurement, stakeholder management, sustainability requirements, and project characteristics enable delivery. Regulatory environment, industry characteristics, market conditions, stakeholder expectations, sustainability pressures, technological development, and global trends act as contextual moderators of outcomes. The feedback loop captures lessons learned, adaptive management, and enhanced future performance. Figure 2 should therefore be read from left to right: enablers support delivery performance; delivery contributes to multidimensional outcomes; and longer-horizon outcomes determine strategic and long-term project success.

As an example, consider a hypothetical industrial energy-efficiency retrofit. At Level 1, schedule/cost variance, scope acceptance, and commissioning defects could be used to assess project delivery. Level 2 could combine NPV/LCC, energy intensity, verified energy savings, GHG reduction, safety rates, and stakeholder acceptance. Level 3 could assess benefits realization after 6–12 months, alignment with decarbonization goals, readiness for scaling, and lifecycle value. Relevant data could be drawn from project-control systems, ERP/SCADA platforms, meters, HSE records, surveys, and post-implementation reviews.

CONCLUSION

This paper shows that time, cost, scope, and quality remain necessary measures of delivery performance but are insufficient for assessing sustainable industrial project success. The literature supports six interrelated dimensions spanning delivery, economic/value, operational/technical, environmental, social/stakeholder/safety, and strategic/long-term success.

The proposed three-level framework links project delivery performance to multidimensional outcomes and, ultimately, to broader project success. Its contribution is integrative rather than prescriptive: conventional project-control KPIs are retained while sustainability and long-term value are incorporated without imposing unsupported universal weights.

The framework is therefore a flexible classification structure whose final KPI set should be adapted to project type, lifecycle stage, stakeholder requirements, and available data.

LIMITATIONS AND FUTURE RESEARCH

Limitations include reliance on two sources rather than Scopus/Web of Science; relevance-ranked Google Scholar results; no formal citation-chasing or grey-literature stream; combined rather than prospectively separated title/abstract screening counts; and a pragmatic quality/relevance appraisal rather than a design-specific risk-of-bias tool. Table 2 and Figure 2 remain literature-based and require empirical validation.
Future research should extend searching to Scopus/Web of Science and citation chasing and validate the framework across diverse industrial sectors. A multi-case design could record Level 1 KPIs at handover and Level 2–3 outcomes at about 6–12 and 24 months, combining expert review with cross-case and longitudinal analysis. Context-specific indicator importance and integration with BIM, ERP, SCADA, and Industry 4.0 data streams could then be tested.

REFERENCES

Akomea-Frimpong, I., Jin, X., & Osei-Kyei, R. (2022). Mapping studies on sustainability in the performance measurement of public-private partnership projects: A systematic review. *Sustainability*, *14*(12), 7174. https://doi.org/10.3390/su14127174

Atkinson, R. (1999). Project management: Cost, time and quality, two best guesses and a phenomenon, its time to accept other success criteria. *International Journal of Project Management, 17*(6), 337–342. https://doi.org/10.1016/S0263-7863(98)00069-6

Bochtler, S., Misopoulos, F., Chacha, I., Suja, S., & Mutungi, D. (2024). Extending corporate sustainability reporting indicators to projects' sustainability. *Procedia Computer Science*, *239*, 346–355. https://doi.org/10.1016/j.procs.2024.06.181

Contini, G., & Peruzzini, M. (2022). Sustainability and Industry 4.0: Definition of a set of key performance indicators for manufacturing companies. *Sustainability*, *14*(17), 11004. https://doi.org/10.3390/su141711004

Cruz Villazón, C., Sastoque Pinilla, L., Otegi Olaso, J. R., Toledo Gandarias, N., & López de Lacalle, N. (2020). Identification of key performance indicators in project-based organisations through the lean approach. *Sustainability*, *12*(15), 5977. https://doi.org/10.3390/su12155977

de Wit, A. (1988). Measurement of project success. *International Journal of Project Management, 6*(3), 164–170. https://doi.org/10.1016/0263-7863(88)90043-9

Díaz Caselles, L. M., & Guevara, J. (2024). Sustainability performance in on-site construction processes: A systematic literature review. *Sustainability*, *16*(3), 1047. https://doi.org/10.3390/su16031047

Fallah, M., & Moini, A. (2026). Examining the role of sustainability metrics in advancing sustainable construction project management. *Clean Technologies and Environmental Policy*, *28*(1), 23. https://doi.org/10.1007/s10098-025-03380-w

Ferrarez, R. P. F., Valle, C. G. B. d., Alvarenga, J. C., Dias, F. d. C., Vasco, D. A., Guedes, A. L. A., Chinelli, C. K., Haddad, A. N., & Soares, C. A. P. (2023). Key practices for incorporating sustainability in project management from the perspective of Brazilian professionals. *Sustainability*, *15*(11), 8477. https://doi.org/10.3390/su15118477

He, Q., Tian, Z., & Wang, T. (2022). Performance measurement methods in megaprojects: An analytical review. *International Journal of Project Management*, *40*(6), 634–645. https://doi.org/10.1016/j.ijproman.2022.05.009

Hussain, A., Khalid, Q. S., Hussain, I., Omair, M., & Habib, M. S. (2026). A framework for project sustainability assessment and schedule optimization in multi-mode construction projects. *International Journal of Management Science and Engineering Management*. Advance online publication. https://doi.org/10.1080/17509653.2026.2706585

Iannaccone, T., Landucci, G., Tugnoli, A., Salzano, E., & Cozzani, V. (2020). Sustainability of cruise ship fuel systems: Comparison among LNG and diesel technologies. *Journal of Cleaner Production*, *260*, 121069. https://doi.org/10.1016/j.jclepro.2020.121069

Ibrahim, A., Zayed, T., & Lafhaj, Z. (2024). Enhancing construction performance: A critical review of performance measurement practices at the project level. *Buildings*, *14*(7), 1988. https://doi.org/10.3390/buildings14071988

Iga Istri, M. P., Zaika, Y., Puspa Negara, K., Solimun, & Mochamad, A. W. (2025). The effect of implementing green construction on project performance: A comprehensive study using structural equation models (SEM). *Civil and Environmental Engineering*, *21*(1), 167–181. https://doi.org/10.2478/cee-2025-0014

Ika, L. A., & Pinto, J. K. (2022). The "re-meaning" of project success: Updating and recalibrating for a modern project management. *International Journal of Project Management*, *40*(7), 835–848. https://doi.org/10.1016/j.ijproman.2022.08.001

Ikudayisi, A. E., Chan, A. P. C., Darko, A., & Adegun, O. B. (2022). Integrated design process of green building projects: A review towards assessment metrics and conceptual framework. *Journal of Building Engineering*, *50*, 104180. https://doi.org/10.1016/j.jobe.2022.104180

Kaewunruen, S., Sresakoolchai, J., & Zhou, Z. (2020). Sustainability-based lifecycle management for bridge infrastructure using 6D BIM. *Sustainability*, *12*(6), 2436. https://doi.org/10.3390/su12062436

Korhonen, T., Jääskeläinen, A., Laine, T., & Saukkonen, N. (2023). How performance measurement can support achieving success in project-based operations. *International Journal of Project Management*, *41*(1), 102429. https://doi.org/10.1016/j.ijproman.2022.11.002

Ma, J., Harstvedt, J. D., Jaradat, R., & Smith, B. (2020). Sustainability driven multi-criteria project portfolio selection under uncertain decision-making environment. *Computers & Industrial Engineering*, *140*, 106236. https://doi.org/10.1016/j.cie.2019.106236

Mansell, P., Philbin, S. P., & Broyd, T. (2020). Development of a new business model to measure organizational and project-level SDG impact—Case study of a water utility company. *Sustainability*, *12*(16), 6413. https://doi.org/10.3390/su12166413

Mansell, P., Philbin, S. P., & Konstantinou, E. (2020). Redefining the use of sustainable development goals at the organisation and project levels—A survey of engineers. *Administrative Sciences*, *10*(3), 55. https://doi.org/10.3390/admsci10030055

Mengistu, A. T., & Panizzolo, R. (2023). Analysis of indicators used for measuring industrial sustainability: A systematic review. *Environment, Development and Sustainability*, *25*(3), 1979–2005. https://doi.org/10.1007/s10668-021-02053-0

Moreno-Monsalve, N., Delgado-Ortiz, M., Rueda-Varón, M., & Fajardo-Moreno, W. S. (2023). Sustainable development and value creation, an approach from the perspective of project management. *Sustainability*, *15*(1), 472. https://doi.org/10.3390/su15010472

Müller, R., & Jugdev, K. (2012). Critical success factors in projects: Pinto, Slevin, and Prescott – the elucidation of project success. *International Journal of Managing Projects in Business, 5*(4), 757–775. https://doi.org/10.1108/17538371211269040

Sanad, H., Elbeltagi, E., Etman, E., Gaber, M., & Elkorany, T. (2026). Optimizing sustainability in infrastructure projects: A framework integrating time, economic, social and environmental perspectives. *Construction Innovation*, *26*(7), 2040–2076. https://doi.org/10.1108/CI-12-2024-0398

Saxena, P., Stavropoulos, P., Kechagias, J., & Salonitis, K. (2020). Sustainability assessment for manufacturing operations. *Energies*, *13*(11), 2730. https://doi.org/10.3390/en13112730

Shenhar, A. J., Dvir, D., Levy, O., & Maltz, A. C. (2001). Project success: A multidimensional strategic concept. *Long Range Planning, 34*(6), 699–725. https://doi.org/10.1016/S0024-6301(01)00097-8

Sherif, Z., Sarfraz, S., Jolly, M., & Salonitis, K. (2022). Identification of the right environmental KPIs for manufacturing operations: Towards a continuous sustainability framework. *Materials*, *15*(21), 7690. https://doi.org/10.3390/ma15217690

Shokouhi, M., & Bachari, M. S. (2025). An overview of the aspects of sustainability in project management. *Progress in Engineering Science*, *2*(1), 100048. https://doi.org/10.1016/j.pes.2024.100048

Son, C. H., Oh, D., & Ban, Y. U. (2023). Eco-industrial development strategies and characteristics according to the performance evaluation of eco-industrial park projects in Korea. *Journal of Cleaner Production*, *416*, 137971. https://doi.org/10.1016/j.jclepro.2023.137971

Tareemi, A. A. (2025). An integrated financial–sustainability framework for predicting green infrastructure project success. *Sustainability*, *17*(21), 9529. https://doi.org/10.3390/su17219529

Wu, S.-W., Yan, Y., Pan, J., & Wu, K.-S. (2023). Linking sustainable project management with construction project success: Moderating influence of stakeholder engagement. *Buildings*, *13*(10), 2634. https://doi.org/10.3390/buildings13102634

Zheng, Z., Zhang, N., Zhang, S., & Gao, L. (2026). Developing an indicator system for ESG performance evaluation in international construction projects. *Journal of Construction Engineering and Management*, *152*(11), 04026197. https://doi.org/10.1061/JCEMD4.COENG-17619

DOI:10.5937/IIZS26288D

OPTIMIZATION OF VEHICLE ROUTING PROBLEM IN LOGISTICS USING GENETIC ALGORITHM

Research paper

Mića Đurđev[1*], Stefan Ugrinov[2], Luka Đorđević[3], Borivoj Novaković[4], Dejan Bajić[5]
[1,2,3,4,5]University of Novi Sad, Technical Faculty "Mihajlo Pupin" Zrenjanin, Serbia

Abstract: Efficient vehicle routing is essential for reducing transportation costs and improving delivery performance in logistics. This paper presents a modified Genetic Algorithm (GA) for solving the Capacitated Vehicle Routing Problem (CVRP). The method combines tournament selection, order crossover, relocation mutation, elitism, and a best-improvement 2-opt local search procedure. The algorithm is evaluated on the E-n23-k3 benchmark instance, which consists of 22 customers, three vehicles, and a vehicle capacity of 4500. Twenty independent runs are performed, and the solutions are assessed using the best and average total distance, standard deviation, convergence behavior, and execution time. The algorithm obtained the benchmark solution in 18 of 20 runs, with an average distance of 570.74, a standard deviation of 4.44, and an average execution time of approximately 15 s. Since the study considers only one small benchmark instance, the results demonstrate the feasibility of the proposed approach but do not allow general conclusions regarding scalability. Further evaluation on larger and more diverse instances is required.
Key words: vehicle routing problem, logistics, optimization, genetic algorithm

INTRODUCTION

Supply chain management and logistics depend on efficient transportation planning to reduce costs, improve delivery reliability, and increase the responsiveness of distribution systems. Transportation planning is commonly formulated through combinatorial optimization problems such as the Traveling Salesman Problem (TSP) and the Vehicle Routing Problem (VRP). While the TSP determines a minimum-distance tour for visiting a set of locations, the VRP extends this problem to a fleet of vehicles serving multiple customers under operational constraints (Laporte, 2007; Toth & Vigo, 2014).

This study focuses on the Capacitated Vehicle Routing Problem (CVRP), in which each customer must be visited exactly once and the total demand assigned to each vehicle must not exceed its capacity. The objective is to minimize the total travel distance. Because the search space grows rapidly with the number of customers and constraints, exact methods may become impractical for larger instances. Consequently, heuristic and metaheuristic methods, including Genetic Algorithms (GAs), are frequently used to obtain high-quality solutions within acceptable computational time (Braekers et al., 2016; Zhang et al., 2022).

This paper presents a modified GA for the CVRP. The proposed method combines tournament selection, order crossover, relocation mutation, elitism, and a best-improvement 2-opt local search procedure. Its performance is evaluated on the E-n23-k3 benchmark instance using 20 independent runs. The analysis considers the best and average solution values, standard deviation, convergence behavior, and computational time.

CAPACITATED VEHICLE ROUTING PROBLEM

The classical CVRP will be presented using the mathematical model (Zhang et al., 2022). CVRP can be defined as the problem where *n* vehicles operate from a central depot (node 0) to serve *m* customers, ensuring that vehicle capacity constraints are met. The objective is to determine a set of routes that minimizes the total travel distance or cost of all vehicles, subject to the following constraints (Borčinová, 2017):

- Each route must start and end at a central depot.
- Each customer is visited exactly once.

[1]Corresponding author, mica.djurdjev@tfzr.rs, ORCID: /0000-0002-1825-2754
[2] stefan.ugrinov@tfzr.rs, ORCID: 0009-0000-7206-655X
[3] luka.djordjevic@tfzr.rs, ORCID: 0000-0003-4578-9060
[4] borivoj.novakovic@tfzr.rs,ORCID: 0000-0003-2816-3584
[4] dejan.bajic@tfzr.rs, ORCID: 0000-0001-7435-9604

- The total demand per route must not exceed the vehicle's capacity.

In the following mathematical expressions, d_i presents the demand of the customer *i*, u_s is the load of the vehicle *s*, while x_{ij}^s is the binary variable that does the following:

$$x_{ij}^s = \begin{cases} 1, vehicle\ s\ serves\ customer\ i\ followed\ by\ customer\ j \\ 0, else \end{cases}$$

The objective function is to minimize the total transportation cost for the entire fleet of vehicles which is mathematically defined as:

$$Cost = Minimize \sum_{s=1}^{n} \sum_{i,j=0}^{m} c_{ij} x_{ij}^s \quad (1)$$

where c_{ij} is the transportation cost from customer *i* to customer *j*. In other words, c_{ij} is cost or distance of travelling from node *i* to node *j* in the graph.
The objective function is followed by four different constraints that ensure the feasibility of the CVRP. The first constraint ensures that each vehicle starts from the depot and returns to the depot after delivering goods to the customers:

$$\sum_{j=0}^{m} x_{0j}^s = \sum_{j=0}^{m} x_{j0}^s = 1\,, s \in (1,2,\dots,n) \quad (2)$$

The second and third constraints are similar to one another and indicate that each customer, *i* or *j*, is visited only once. These constraints ensure vehicles do not reach a single customer twice, therefore maintaining a valid route structure:

$$\sum_{s=1}^{n} \sum_{\substack{j=0 \\ j \neq i}}^{m} x_{ij}^s = 1\,, i \in (1,2,\dots,m) \quad (3)$$

$$\sum_{s=1}^{n} \sum_{\substack{i=0 \\ i \neq j}}^{m} x_{ij}^s = 1\,, j \in (1,2,\dots,m) \quad (4)$$

This last constraint ensures that the total demand served by each vehicle does not exceed its maximum load capacity:

$$\sum_{i=1}^{m} d_i \sum_{\substack{j=0 \\ i \neq j}}^{m} x_{ij}^s \leq u_s\,, s \in (1,2,\dots,n) \quad (5)$$

METAHEURISTIC ALGORITHMS

Metaheuristics are high-level optimization methods designed to explore large and complex search spaces. They combine global exploration with local exploitation and are particularly suitable for NP-hard problems for which exact methods may require excessive computational time (Blum & Roli, 2003; Talbi, 2009). In VRP applications, frequently used metaheuristics include genetic algorithms, tabu search, simulated annealing, and ant colony optimization.
A Genetic Algorithm represents candidate solutions as chromosomes and improves a population through selection, crossover, mutation, and replacement. In this study, GA was selected because its population-based search is suitable for exploring alternative vehicle

sequences and route assignments. A 2-opt local search procedure was additionally incorporated to improve individual routes.

MATERIALS AND METHODS

To address the outlined research questions from the previous chapter and evaluate the effectiveness of the proposed genetic algorithm (GA), a structured methodological approach has been adopted. This includes selecting a representative benchmark instance of the Capacitated VRP (CVRP), implementing a modified GA with integrated local search heuristic, and systematically analyzing the algorithm's performance across multiple runs. By employing a standardized problem instance, the study ensures result comparability and allows for a precise assessment of the GA's ability to approach or reach the known global optimum. Furthermore, detailed attention is given to the algorithm's components, such as tournament selection, order crossover, relocation mutation, and 2-opt local search heuristic in order to investigate their individual and collective impact on solution quality and convergence behavior.

Benchmark problem instance

A benchmark problem instance is selected from the CVRP repository available at http://vrp.atd-lab.inf.puc-rio.br/index.php/en. This repository provides a wide range of CVRP instances, each varying in complexity based on the number of customers and vehicles. It includes benchmark sets dating from 1969 to 2011. For this study, the ***E-n23-k3*** instance from Set E (Christofides & Eilon, 1969) is used. This instance consists of 22 customers, served by three vehicles, each with a capacity of 4500. Both the customers and the depot are represented by x- and y-coordinates, enabling the calculation of Euclidean distances between locations. Their coordinates are graphically presented on the map in Figure 1. The global optimum for this instance is 569 in terms of total travel distance.

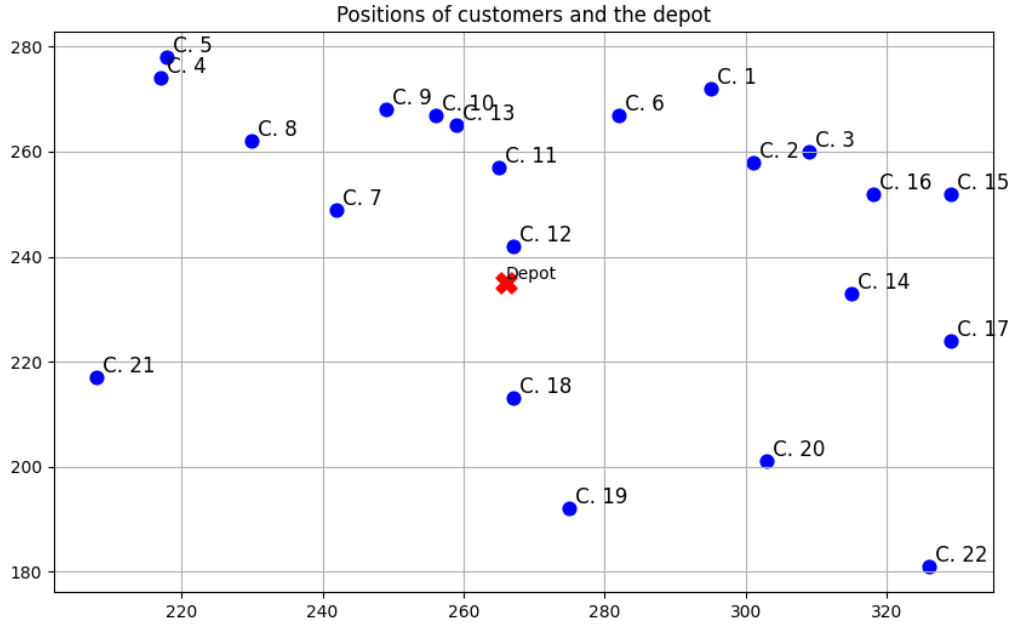


***Fig. 1**. Coordinates of customers and the depot for the instance E-n23-k3*

Genetic algorithm for CVRP

The proposed GA represents each solution as a customer sequence together with its division into vehicle routes. The initial population consists of feasible solutions. The fitness value is defined as the total Euclidean travel distance, including the return from each route to the depot.

Tournament selection with a tournament size of five is used to select parent solutions. Order crossover (OX) preserves customer uniqueness, while relocation mutation moves a customer between routes when the capacity constraint remains satisfied. A best-improvement 2-opt procedure is then applied to improve individual routes. Elitism preserves the best solutions between generations, and the algorithm is terminated after 500 generations. Infeasible solutions are repaired or rejected during the solution-generation process. The flowchart of the proposed GA for CVRP problem is given in Figure 2.

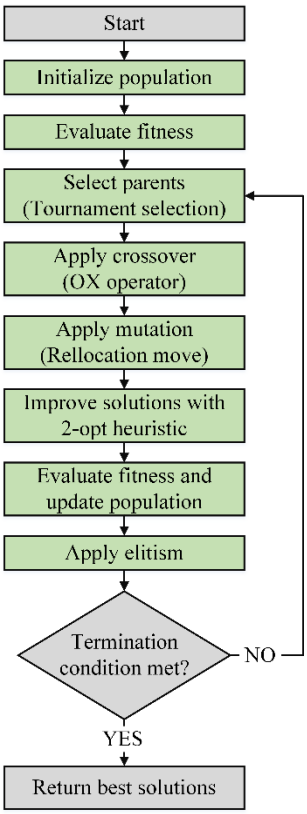


***Fig. 2**. Flowchart of GA for CVRP*

RESULTS AND DISCUSSION

The proposed GA was implemented in Python and evaluated in 20 independent runs on a laptop equipped with a 13th Generation Intel Core i7-13650HX processor and 16 GB of RAM. The best solution obtained a total distance of 569.59, while the average distance over all runs was 570.74, with a standard deviation of 4.44. The best result was obtained in 18 of the 20 runs. The average execution time was approximately 15 s per run. The optimal distance and optimal vehicle routes are presented in Tables 1 and 2. The graphical presentation of the optimal vehicle route for "E-n23-k3" CVRP problem instance is shown in Figure 3.
All three vehicle routes satisfied the capacity constraint of 4500. The loads were 4389, 4325, and 1400, respectively. The utilization of vehicles is shown in Table 3. The relatively uneven load distribution is a consequence of distance minimization and does not necessarily indicate a deficiency of the algorithm, since balanced vehicle utilization was not included as an objective.

***Table 1**. Optimal total distance with respect to capacity limit*

Optimal distance	Average distance	Standard deviation
569.59	570.74	4.44

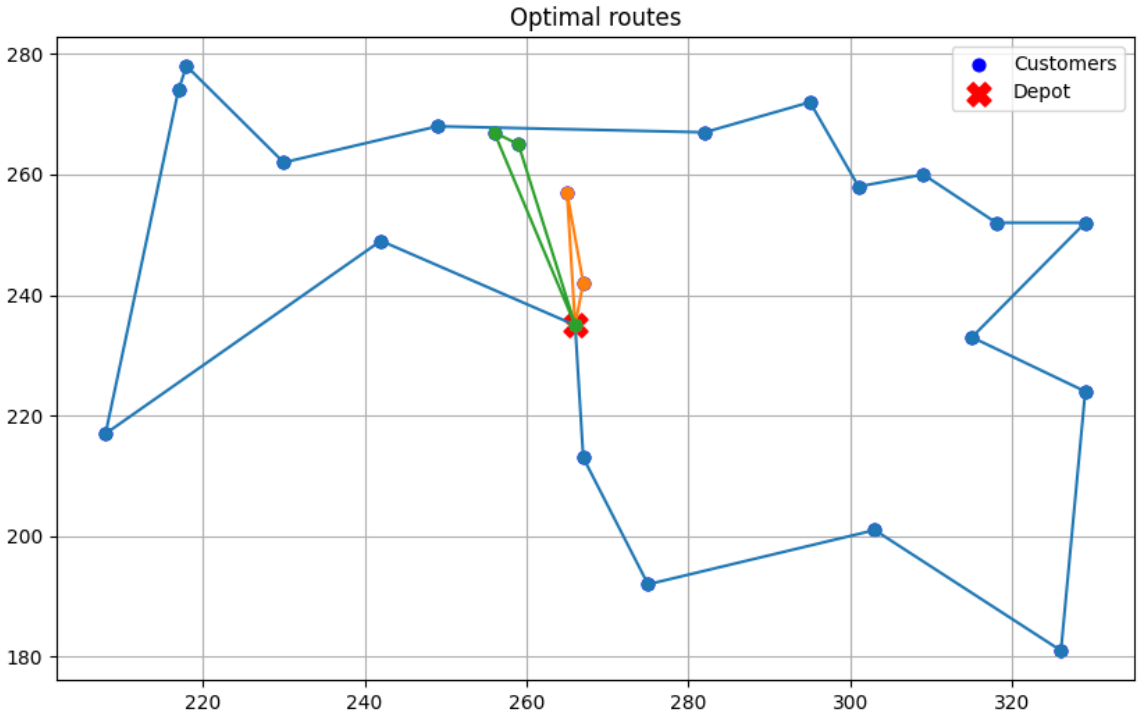


***Fig. 3**. The optimal vehicle routes for the CVRP instance E-n23-k3*

***Table 2**. The optimal vehicle routes*

Vehicles	**Optimal vehicle routes**
Vehicle 1	[0-7-21-4-5-8-9-6-1-2-3-16-15-14-17-22-20-19-18-0]
Vehicle 2	[0-11-12-0]
Vehicle 3	[0-10-13-0]

***Table 3**. Utilization of each vehicle*

Vehicle	Route load	Capacity	Utilization
Vehicle 1	4389	4500	97.53%
Vehicle 2	4325	4500	96.11%
Vehicle 3	1400	4500	31.11%

The convergence curve shows a rapid improvement during the initial generations, followed by stabilization of the best-so-far solution. Figure 4 shows the convergence curve for this problem instance. This behavior indicates that the combination of tournament selection, elitism, and 2-opt local search effectively accelerates local route improvement. However, the convergence plot represents one run and should not be interpreted as a complete statistical analysis of convergence across all 20 runs.

In the additional operator comparison, removing the 2-opt procedure increased the average distance by approximately 7% under the same experimental settings. This result suggests that local search contributes substantially to the quality of the final routes. Nevertheless, the comparison should be supported by a separate table containing the mean value, standard deviation, and number of runs for each algorithmic variant.

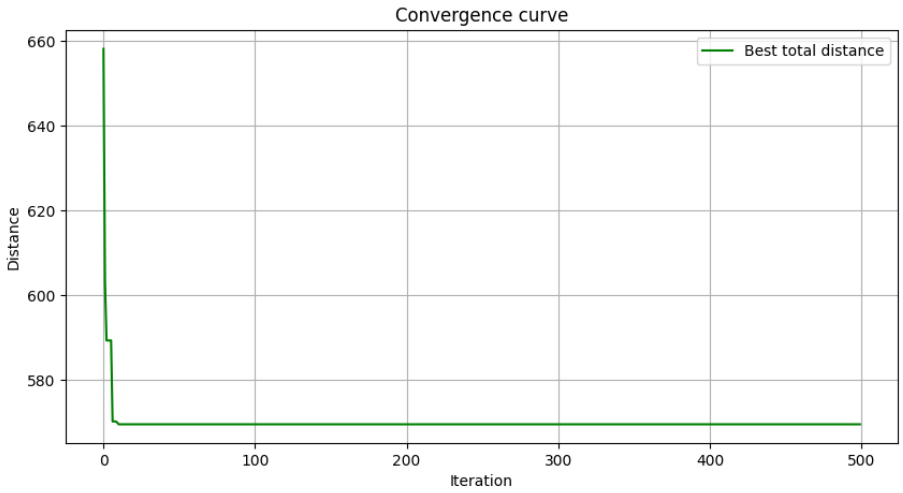


***Fig. 4**. Convergence curve of the proposed GA*

In order to evaluate the contributions of various operators within the proposed GA, controlled experiments were conducted to quantify the impact of the tournament selection OX crossover, relocation mutation, and 2-opt heuristic on the quality and stability of the obtained solutions. The results indicate that each of the analyzed operators has a specific and significant contribution, both in terms of minimizing the total distance traveled and in ensuring the robustness and stability of the algorithm across multiple runs.

The analysis of tournament selection showed that tournament size significantly influences the balance between exploitation and exploration: larger tournaments accelerate convergence but at the cost of potential premature convergence, while smaller tournaments allow diversity but with slower solution improvement. The optimal value in the study was found to be a medium-sized tournament (n=5), which provides a good compromise between solution quality and stability.

An additional operator analysis showed that the combined GA structure performed better than variants without the considered operators. Removing the 2-opt procedure increased the average distance by approximately 7%, indicating its importance for local route improvement. Tournament selection with size 5 provided a suitable balance between convergence speed and population diversity. Relocation mutation improved route flexibility by allowing customers to be reassigned between vehicles while respecting capacity constraints..

CONCLUSION

This study presented a modified Genetic Algorithm for solving the Capacitated Vehicle Routing Problem. The algorithm combines tournament selection, order crossover, relocation mutation, elitism, and a 2-opt local search procedure. Tested on the E-n23-k3 benchmark instance with 22 customers and three vehicles, the algorithm reached the known optimum of 569.59 in 18 of 20 runs. The average solution value was 570.74, with a standard deviation of 4.44 and an average execution time of approximately 15 s.

The results confirm that the proposed GA can efficiently solve the selected small CVRP instance and consistently produce high-quality solutions. However, because the evaluation was conducted on only one benchmark instance, the findings cannot be generalized to larger or more complex logistics problems. Future work should include multiple benchmark instances, real-world data, time windows, dynamic demand, heterogeneous fleets, and comparisons with other metaheuristic methods.

REFERENCES

Blum, C., & Roli, A. (2003). Metaheuristics in combinatorial optimization: Overview and conceptual comparison. *ACM Computing Surveys*, 35(3), 268-308. https://doi.org/10.1145/937503.937505

Borčinova, S. (2017). Two models of the capacitated vehicle routing problem. *Croatian Operational Research Review,* 8(2), 463-469. https://doi.org/10.17535/crorr.2017.0029

Braekers, K., Ramaekers, K., & Van Nieuwenhuyse, I. (2016). The vehicle routing problem: State of the art classification and review. *Computers & Industrial Engineering*, 99, 300–313. https://doi.org/10.1016/j.cie.2015.12.007

Christofides, N., & Eilon, S. (1969). An algorithm for the vehicle-dispatching problem. *Journal of the Operational Research Society*, *20*(3), 309-318.

Hansen, P., & Mladenović, N. (2006). First vs. best improvement: An empirical study. *Discrete Applied Mathematics, 154*(5), 802–817. https://doi.org/10.1016/j.dam.2005.05.020

Laporte, G. (2007). What you should know about the vehicle routing problem. *Naval Research Logistics*, 54(8), 811–819. https://doi.org/10.1002/nav.20261

Talbi, E.-G. (2009). *Metaheuristics: From design to implementation*. Hoboken, NJ: Wiley.

Toth, P., & Vigo, D. (2014). *Vehicle Routing: Problems, Methods, and Applications* (2nd ed.). Philadelphia, PA: Society for Industrial and Applied Mathematics (SIAM). https://doi.org/10.1137/1.9781611973594

Zhang, H., Ge, H., Yang, J., & Tong, Y. (2022). Review of vehicle routing problems: Models, classification and solving algorithms. *Archives of Computational Methods in Engineering*, 29, 1-27. https://doi.org/10.1007/s11831-021-09574-x

DOI:10.5937/IIZS26295M

FROM ENERGY MONITORING TO MAINTENANCE DECISIONS: A CONCEPTUAL FRAMEWORK FOR HYDRAULIC BLOWOUT PREVENTER CONTROL UNITS

Research paper

Milan Marković[1*], Jasna Tolmač[2], Isidora Crvenkov[3]
[1,2] Technical Faculty "Mihajlo Pupin", University of Novi Sad, Zrenjanin, Serbia
[3] Independent Researcher, Zrenjanin, Serbia

Abstract: The reliability of hydraulic blowout preventer (BOP) control units is essential for maintaining the functional capability of well-control equipment. This paper aims to develop a conceptual decision-support framework for condition-based maintenance by integrating operational monitoring, energy-performance assessment, and diagnostic evaluation into a structured procedure. The methodology is based on a synthesis of existing maintenance approaches and previously published research on the hydraulic activation of a jaw-type BOP. Five indicators are considered: operating pressure, flow rate, volumetric efficiency, clearance leakage, and required activation power. The proposed framework comprises data acquisition, comparison with documented reference conditions, deviation identification, diagnostic verification, maintenance decision-making, and subsequent monitoring. The results are presented through a decision-support flowchart and an indicator matrix linking potential deviations with diagnostic checks and maintenance-related responses. The framework emphasizes the joint interpretation of operating parameters and distinguishes changes caused by operating conditions from deviations requiring further investigation. The proposed approach provides a structured basis for organizing maintenance-related information but has not been validated using field monitoring or maintenance records. Further research is required to establish diagnostic criteria and evaluate its effectiveness under representative operating conditions.
Key words: blowout preventer, condition-based maintenance, hydraulic control unit, decision-support framework, operational monitoring, energy performance.

INTRODUCTION

Blowout preventers (BOPs) are essential safety systems in the oil and gas industry, designed to control well pressure and prevent uncontrolled fluid release during drilling operations. Their ability to perform the required safety function depends not only on the mechanical integrity of the preventer assembly but also on the reliability of the hydraulic control unit responsible for its activation. Maintaining the functional capability of BOP systems therefore requires particular attention to the condition, performance, testing, and maintenance of their components (Shafiee et al., 2020). Furthermore, the application of integrated Fault Tree Analysis (FTA) and Failure Mode and Effects Analysis (FMEA) has demonstrated the importance of identifying critical failure scenarios and assessing component-level risks in subsea BOP systems (Shafiee et al., 2019).

Conventional maintenance practices, including periodic inspections, functional testing, and corrective interventions, are essential for maintaining BOP functionality. However, periodic activities alone may provide limited information about progressive component degradation between scheduled examinations. Condition-based maintenance (CBM) and prognostic health management (PHM) offer complementary approaches by incorporating equipment condition and operational information into maintenance planning. Brandão Martins et al. (2018) examined the integration of these concepts with reliability-based approaches for BOP systems. The potential of operational monitoring has also been demonstrated through a model-based approach for detecting and identifying leakage in subsea BOP hydraulic control systems using pressure measurements and hydraulic system characteristics (Wassar et al., 2018).

The integration of condition information into reliability assessment has been investigated through several quantitative approaches. Elusakin and Shafiee (2020) developed a reliability analysis method for subsea BOP systems using stochastic Petri nets and incorporating component degradation and condition-based maintenance. In a broader safety-system

[1]Corresponding author, milan.markovic@uns.ac.rs, ORCID: 0009-0007-8130-7467
[2]jasna.tolmac@uns.ac.rs, ORCID: 0000-0003-3860-2034
[3]isidoracrvenkov@gmail.com

context, Zeng and Zio (2018) proposed a dynamic risk assessment approach that combines statistical failure data with condition-monitoring information to update reliability estimates during operation. Similarly, Cai et al. (2023) developed a data-driven approach for optimizing condition-based maintenance decisions using historical degradation and failure data. Although these studies address different systems and modelling approaches, they demonstrate the importance of incorporating operational and degradation information into reliability assessment and maintenance decision-making.

A previously published investigation of a jaw-type BOP hydraulic activation system examined the influence of operating pressure, flow rate, volumetric efficiency, and clearance leakage on the required activation power. Experimental design, regression analysis, and the Grey Wolf Optimizer (GWO) were combined to identify the influence of these parameters and determine an energy-efficient operating configuration (Marković et al., 2025). The study also introduced a deviation-based operational reliability model and discussed the potential use of operating parameters in predictive maintenance. These findings provide a basis for examining how energy-performance information could support the interpretation of hydraulic system condition.

Building on the previously published research and the identified maintenance approaches, the present paper aims to develop a conceptual decision-support framework for condition-based maintenance of hydraulic BOP control units. The proposed approach integrates operational parameter monitoring, comparison with reference conditions, deviation identification, diagnostic verification, and maintenance decision-making into a structured procedure. Particular attention is given to distinguishing changes associated with operating conditions from deviations that may require additional investigation. The framework is intended to support maintenance planning without replacing mandatory functional testing or established safety procedures. Its effectiveness remains to be evaluated using operational monitoring and maintenance data.

MATERIAL AND METHODS

Research approach

The research was conducted as a conceptual methodology development study aimed at establishing a structured procedure for supporting maintenance decisions in hydraulic blowout preventer (BOP) control units. The methodological approach integrates principles of condition-based maintenance (CBM), operational parameter monitoring, energy-performance assessment, and diagnostic evaluation.

The framework was developed through a synthesis of published research on BOP maintenance and reliability, industrial condition-monitoring practices, and maintenance decision-support methods. Brandão Martins et al. (2018) provided the theoretical basis for integrating CBM and prognostic health management (PHM) concepts into BOP management. The broader context of industrial monitoring practices was considered through the survey conducted by Higgs et al. (2004), while the integration of reliability-centered maintenance and condition monitoring into maintenance decisions was examined using the approach presented by Catelani et al. (2020).

Previously published experimental research on the hydraulic activation system of a jaw-type BOP was used as the technical basis for identifying relevant operating parameters and their relationship with energy consumption (Marković et al., 2025). The present study does not repeat the experimental design, regression modelling, or optimization procedures reported in that publication. Instead, it examines how information derived from these investigations can be organized into a conceptual maintenance decision-support procedure.

Selection of operational indicators

The selection of operational indicators was based on their physical relevance to hydraulic system performance and their potential contribution to identifying changes in operating conditions. Four parameters were considered: operating pressure, flow rate, volumetric

efficiency, and clearance leakage. The power required for BOP activation was included as a complementary energy-performance indicator.
Pressure and flow rate describe the operating conditions and hydraulic power requirements of the system. Volumetric efficiency and clearance leakage provide additional information about hydraulic losses. The relationship between these parameters and the required activation power was previously investigated by Marković et al. (2025).
Leakage was also considered because of its relevance to hydraulic system monitoring. Wassar et al. (2018) investigated a model-based approach for detecting and identifying leakage in subsea BOP control systems using pressure measurements and a hydraulic system model.
For the proposed framework, pressure and flow rate are treated as directly measurable operating variables. Volumetric efficiency, leakage, and required power may be incorporated when they are available from measurements or can be estimated using an appropriate, documented model. Their inclusion does not imply that all five indicators are continuously measured in existing BOP installations.

Deviation assessment

The assessment procedure was formulated around the comparison of available operating information with an established reference condition. Such a reference may be derived from documented functional requirements, approved operating limits, baseline measurements, or previously established operating characteristics, depending on the available information.
Previously published optimized operating parameters may provide an additional reference for evaluating energy performance (Marković et al., 2025). However, an energy-efficient configuration is not considered sufficient evidence of functional integrity or compliance with safety requirements.
The proposed assessment distinguishes changes associated with different operating conditions from deviations that may indicate a need for further investigation. Therefore, operating parameters should be compared under equivalent or appropriately documented conditions whenever possible. Changes in pressure, flow rate, and required power are interpreted jointly rather than independently.
When a deviation is identified, the procedure requires verification of measurement validity and operating conditions before a possible relationship with component degradation is considered. No universal numerical thresholds or experimentally validated fault-classification criteria are introduced in the present study.

Development of the decision-support framework

The decision-support procedure was formulated by linking operational monitoring with diagnostic verification and maintenance planning. The approach follows a sequence consisting of data acquisition, assessment of operating conditions, deviation identification, diagnostic evaluation, maintenance decision-making, and subsequent verification.
The first stage involves collecting available operating information and establishing whether the observed conditions are suitable for comparison with a defined reference. In the second stage, deviations are identified and examined to determine whether they may be explained by changes in operating conditions or measurement-related factors.
Deviations that cannot be adequately explained are directed toward further diagnostic assessment. This stage considers possible hydraulic losses, changes in component performance, and the need for additional functional checks. The resulting information is used to support the selection and prioritization of appropriate maintenance activities.
The conceptual organization of the procedure was informed by the integration of condition monitoring and maintenance decision-making discussed by Catelani et al. (2020). Unlike their application to a wind turbine yaw system, the framework proposed here is specifically directed toward interpreting the operating and energy-performance indicators of hydraulic BOP control units.

The final stage involves recording the diagnostic findings, maintenance actions, and subsequent operating conditions to support future assessments. The framework is intended to complement established maintenance practices and does not replace mandatory testing, prescribed operating limits, or safety-related decisions.
The study does not report a new experimental campaign, field implementation, or validation of maintenance effectiveness. Accordingly, the proposed procedure is presented as a conceptual framework requiring further evaluation using operational monitoring data and documented maintenance records.

RESULTS AND DISCUSSION

The main outcome of this study is a conceptual decision-support framework that organizes information from hydraulic system monitoring into a sequence of maintenance-related assessments. The framework connects five operational and energy - performance indicators — pressure, flow rate, volumetric efficiency, clearance leakage, and required activation power — with reference-condition assessment, diagnostic verification, and maintenance planning. The selection of these indicators is based on the previously published investigation of the jaw-type blowout preventer (BOP) hydraulic activation system (Marković et al., 2025).
The proposed procedure is presented in Fig. 1. Its initial stage involves collecting available operating data and checking their validity and completeness. Operating conditions are then compared with documented reference conditions, taking into account differences in the operating regime. If no relevant deviation is identified, the procedure returns to routine monitoring. Otherwise, the deviation is examined to establish whether it can be explained by measurement errors or changes in operating conditions. Unresolved deviations are subjected to additional diagnostic verification before maintenance actions are considered.

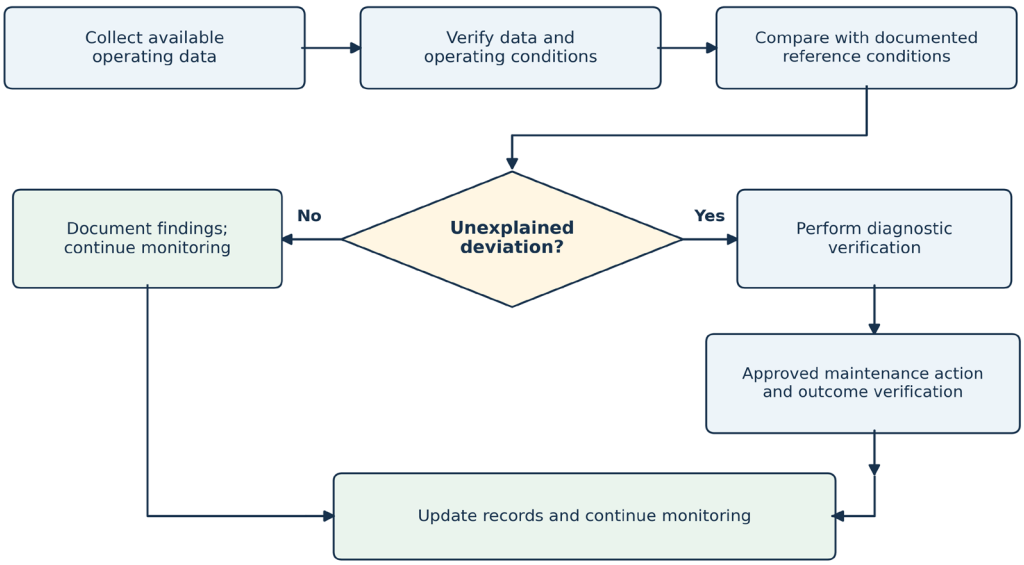


Fig. 1. *Proposed decision-support framework for condition-based maintenance of hydraulic BOP control units.*

An important feature of the framework is the separation of deviation detection from fault identification. An increase in activation power, for example, may reflect a change in operating pressure or flow rate rather than equipment degradation. Consequently, energy-performance indicators should be interpreted under comparable operating conditions and, where possible, together with additional hydraulic measurements. Previously published optimal operating parameters can support energy-performance comparisons, but they must not be treated as substitutes for approved functional requirements or safety limits (Marković et al., 2025).

Operational indicators and diagnostic interpretation

Table 1 presents the proposed relationship between selected operational indicators, possible deviations, diagnostic verification, and maintenance-related actions. The matrix is intended to guide the interpretation of monitoring data rather than provide a validated fault-diagnosis algorithm.

Table 1. *Conceptual interpretation of operational indicators and maintenance-related verification actions.*

Indicator	Deviation requiring assessment	Diagnostic verification	Maintenance-related response
Pressure	Departure from the documented reference range.	Check sensor validity, control settings, and hydraulic circuit conditions.	Investigate confirmed abnormalities and apply approved procedures.
Flow rate	Unexpected change under comparable operating conditions.	Verify flow measurement, pump operation, and possible losses.	Inspect relevant components if the deviation persists.
Volumetric efficiency	Reduction relative to a documented baseline.	Confirm the estimation method and assess possible internal losses.	Consider targeted inspection after verification.
Clearance leakage	Increase relative to the reference condition.	Verify measurement or estimation and investigate possible leakage paths.	Inspect or repair affected components as indicated by diagnosis.
Activation power	Unexpected change at comparable pressure, flow rate, and operating conditions.	Verify power data and jointly assess operating parameters and losses.	Initiate further diagnostics; do not infer a specific fault from power alone.

The matrix emphasizes the need for combined interpretation of the selected parameters. Pressure and flow rate establish the operating context, whereas changes in volumetric efficiency and clearance leakage may provide additional information about hydraulic losses. Required activation power represents an energy-performance indicator that should be assessed in relation to operating conditions. The relevance of hydraulic leakage monitoring to BOP control systems has also been addressed by Wassar et al. (2018).

The proposed framework extends the interpretation of these indicators from energy-performance assessment to maintenance decision support. Its specific contribution is the organization of monitoring, reference comparison, diagnostic verification, and maintenance planning into a single procedure for hydraulic BOP control units. The general integration of condition monitoring and maintenance decision-making is not new; for example, Catelani et al. (2020) investigated this relationship in the maintenance of a wind turbine yaw system. The present framework addresses a different application and focuses specifically on the operational indicators identified in hydraulic BOP activation research.

Applicability and limitations

The framework may provide a basis for structuring operational records and selecting additional diagnostic checks when unexplained deviations are detected. However, the present study does not demonstrate that its implementation reduces failure rates, maintenance costs, or downtime. No field data were used to establish diagnostic thresholds, validate fault identification, or quantify the effectiveness of the proposed maintenance decisions.
Future implementation would require reliable measurement or estimation of the selected indicators, documented reference conditions, maintenance and failure records, and validation under representative operating conditions. The proposed approach is supplementary to mandatory functional testing, approved maintenance procedures, and established safety requirements; any indication of compromised safety functionality must be addressed according to the applicable procedures rather than through energy-performance assessment alone.

CONCLUSION

This paper developed a conceptual decision-support framework for condition-based maintenance of hydraulic blowout preventer (BOP) control units. The proposed approach integrates operational parameter monitoring, energy-performance assessment, deviation identification, diagnostic verification, and maintenance planning into a structured procedure.
The main contribution is the organization of five operational and energy - performance indicators — pressure, flow rate, volumetric efficiency, clearance leakage, and required activation power — into a framework that links deviations from reference conditions with additional diagnostic checks and maintenance-related decisions. The developed flowchart and indicator matrix provide a systematic basis for interpreting available operating information. Particular emphasis is placed on distinguishing changes caused by different operating conditions from unexplained deviations that may require further investigation.
The framework is conceptual and has not been validated using field monitoring or maintenance records. Therefore, no conclusions can be drawn regarding its effectiveness in reducing failure rates, downtime, or maintenance costs. Future research should focus on establishing appropriate reference conditions, validating diagnostic criteria, and assessing the framework using operational and maintenance data. Its application must remain complementary to mandatory functional testing and established safety procedures.

REFERENCES

Brandão Martins, F., Cardoso, R., Tammela, I., Colombo, D., & Acioli de Matos, B. (2018). Applying CBM and PHM concepts with reliability approach for blowout preventer (BOP): A literature review. Brazilian Journal of Operations & Production Management, 15(1), 78–95. https://doi.org/10.14488/BJOPM.2018.v15.n1.a8

Cai, Y., Teunter, R. H., & de Jonge, B. (2023). A data-driven approach for condition-based maintenance optimization. European Journal of Operational Research, 311(2), 730–738. https://doi.org/10.1016/j.ejor.2023.05.002

Catelani, M., Ciani, L., Galar, D., & Patrizi, G. (2020). Optimizing maintenance policies for a yaw system using reliability-centered maintenance and data-driven condition monitoring. IEEE Transactions on Instrumentation and Measurement, 69(9), 6241–6249. https://doi.org/10.1109/TIM.2020.2968160

Elusakin, T., & Shafiee, M. (2020). Reliability analysis of subsea blowout preventers with condition-based maintenance using stochastic Petri nets. Journal of Loss Prevention in the Process Industries, 63, Article 104026. https://doi.org/10.1016/j.jlp.2019.104026

Higgs, P. A., Parkin, R. M., Jackson, M. R., Al-Habaibeh, A., Zorriassatine, F., & Coy, J. (2004). A survey on condition monitoring systems in industry. In Proceedings of the ASME 2004 7th Biennial Conference on Engineering Systems Design and Analysis (Vol. 3, pp. 163–178). American Society of Mechanical Engineers. https://doi.org/10.1115/ESDA2004-58216

Marković, M., Novaković, B., Đurđev, M., Jovanović, S., Desnica, E., Blažić, M., & Tolmač, J. (2025). Energy-efficient optimization of jaw-type blowout preventer activation using combined experimental design and metaheuristic algorithms. *Energies, 18(18), Article 4852. https://doi.org/10.3390/en18184852

Shafiee, M., Enjema, E., & Kolios, A. (2019). An integrated FTA-FMEA model for risk analysis of engineering systems: A case study of subsea blowout preventers. *Applied Sciences, 9(6), Article 1192. https://doi.org/10.3390/app9061192

Shafiee, M., Elusakin, T., & Enjema, E. (2020). Subsea blowout preventer (BOP): Design, reliability, testing, deployment, and operation and maintenance challenges. Journal of Loss Prevention in the Process Industries, 66, Article 104170. https://doi.org/10.1016/j.jlp.2020.104170

Wassar, T., Mutlu, M., Franchek, M. A., & Guiterrez, J. (2018). Leakage monitoring of subsea blowout preventer control system. In Proceedings of the Annual Offshore Technology Conference (Vol. 2, pp. 1214–1220). Offshore Technology Conference. https://doi.org/10.4043/28955-MS

Zeng, Z., & Zio, E. (2018). Dynamic risk assessment based on statistical failure data and condition-monitoring degradation data. IEEE Transactions on Reliability, 67(2), 609–622. https://doi.org/10.1109/TR.2017.2778804

DOI:10.5937/IIZS26302K

ANALYSIS OF PREVENTIVE AND CORRECTIVE MAINTENANCE PRACTICES AND MAINTENANCE DATA LIMITATIONS: A CASE STUDY

Research paper

Vesna Konja[1], Žolt Konja[2], Ljiljana Radovanović[3]*
[1,2] Secondary Mechanical Engineering School, Novi Sad, Serbia
[3]Technical Faculty "Mihajlo Pupin" Zrenjanin, University of Novi Sad, Serbia

Abstract: Maintenance is a key factor in the effective operation of industrial systems, as it is closely associated with equipment reliability, availability, and productivity. This paper analyzes preventive and corrective maintenance practices using the company "MVM Južna Bačka" as a case study. The research is based on maintenance data collected over a 12-month period, including maintenance interventions, recorded failures, failure causes, repair time, and the current level of maintenance digitalization. The results show that preventive maintenance accounted for 18 of 24 recorded maintenance interventions (75%), while corrective maintenance accounted for 6 interventions (25%). During the analyzed period, seven unplanned failures were recorded, with equipment wear and ageing identified as the most common cause. The available records did not contain sufficient operating-time and downtime data for the precise calculation of MTBF and equipment availability; therefore, these indicators were used as an analytical framework rather than calculated performance measures. The analysis also identified limitations in maintenance data collection and digital integration. Based on the findings, the paper proposes the gradual implementation of Maintenance 4.0 principles, including standardized maintenance records, CMMS/EAM implementation, condition monitoring, and data-driven predictive maintenance.
Keywords: preventive maintenance, corrective maintenance, MTBF, MTTR, availability, productivity, Maintenance 4.0

INTRODUCTION

Equipment maintenance is an important segment of the management of any industrial system in which the continuity of operation, reliability and efficiency of equipment have a direct impact on the achievement of business goals. Equipment is subject to various types of wear, degradation and failures during its life cycle, which is why it is necessary to implement an appropriate maintenance strategy. Unplanned failures can lead to downtime, increased costs, reduced productivity and delays in the implementation of business activities.Traditional maintenance can be viewed through two basic categories: preventive and corrective maintenance. Preventive maintenance involves the planned execution of activities that seek to prevent the occurrence of a failure or extend the service life of equipment. It may include inspections, cleaning, lubrication, replacement of consumable parts, adjustments and other activities that are carried out according to a predefined plan. On the other hand, corrective maintenance is carried out after the occurrence of an irregularity or failure and is aimed at returning the equipment to a functional state. (Mobley, 2002; Muchiri et al., 2011)
Although preventive maintenance is widely recognized as an important approach for reducing equipment failures, its effectiveness depends on the quality of maintenance planning, failure records, equipment condition data, and performance monitoring. In practice, organizations may perform a relatively high number of preventive interventions while still experiencing unplanned failures. This creates a need to examine not only the structure of maintenance activities but also the quality of the data used to evaluate maintenance performance. Therefore, this paper examines maintenance practices in a real industrial organization, with particular attention to the relationship between preventive and corrective interventions, recorded failures, repair time, and the level of maintenance digitalization.

[1] zolt.konja@gmail.com
[2] vesna.konja@gmail.com
[3] Corresponding author, ljiljana.radovanovic@tfzr.rs , ORCID:0000-0002-5234-4820

RESEARCH OBJECTIVE

The main objective of the research is to analyze the impact of preventive and corrective maintenance on the reliability, availability and productivity of equipment in the company "MVM Južna Bačka".

- analyze the structure of preventive and corrective maintenance interventions;
- examine the relationship between recorded maintenance interventions and failures;
- analyze the number and reported causes of failures;
- examine the reported duration of fault resolution;
- explain the role and data requirements of MTBF, MTTR and availability indicators;
- assess the availability and limitations of maintenance performance data;
- discuss the implications of the available findings for maintenance performance and future productivity assessment;
- identify shortcomings of the existing maintenance recording system;
- propose improvement opportunities through Maintenance 4.0. (Mobley, 2002; Moubray, 1997; "Preventive and Corrective Maintenance," n.d.)

Furthermore, this paper seeks to answer the following questions:

- What is the structure of preventive and corrective maintenance interventions in the analyzed company?
- What do the available failure and maintenance records indicate about current maintenance practices and data quality?
- Which improvements in maintenance data management and digitalization could support more reliable performance measurement and future quantitative assessment of reliability, availability and productivity?

RESEARCH METHOD

The research was conducted using the case study method, with the company "MVM Južna Bačka" selected as the subject of the analysis. The case study enables a detailed analysis of a specific organizational and technical system and represents an appropriate method for examining maintenance processes in real conditions. (IEC, 2015; IEC, 2016) Data for a 12-month period, from September 2024 to September 2025, were analyzed. The data include the number of preventive and corrective interventions, the number of recorded failures and unplanned failures, reported fault resolution duration, reported failure-related factors, and information on the application of digital technologies in the maintenance process. The data were obtained from internal records provided by the company's management and refer to the company as a whole rather than to individual equipment units.

For the purposes of this study, a maintenance intervention refers to a recorded maintenance activity performed on equipment, regardless of whether it was planned or initiated in response to an equipment problem. Preventive interventions are planned activities intended to prevent degradation or failure, whereas corrective interventions are activities performed to restore equipment to a functional condition following an identified problem or failure. A failure is considered an unplanned loss of the equipment's ability to perform its intended function. The available company records did not provide a one-to-one mapping between individual failures and corrective interventions. Consequently, the number of corrective interventions (6) was not treated as equivalent to the number of recorded failures (7). The available records also did not allow verification of whether one failure resulted in multiple corrective interventions or whether one corrective intervention addressed multiple failure events.

The analysis was descriptive and focused on the structure and characteristics of the available maintenance records. No statistical inference or quantitative reliability, availability or productivity assessment was performed because the available records did not contain the necessary equipment-level operating-time, failure-interval, standardized downtime and productivity data.

Standard indicators are used in this study as an analytical framework for reliability, maintainability and availability:

- MTBF - Mean Time Between Failures:
- MTBF = total operating time / number of failures

This indicator represents one of the basic measures of reliability. A higher MTBF value indicates a longer period of operation between consecutive failures and is generally associated with higher reliability. However, MTBF can only be calculated when reliable operating-time and failure-event data are available. Another important indicator is:

- MTTR – Mean Time To Repair, i.e. the mean time required for repair:
- MTTR = total time to repair / number of failures

A lower MTTR generally indicates a shorter time required to restore equipment after a failure. In this case study, however, MTTR was not calculated because individual repair records and precisely defined repair durations were not available.
Availability can be represented by the expression (1):

$$A = \frac{MTBF}{MTBF + MTTR} \times 100\% \quad (1)$$

Some of the basic parameters are presented in the Table 1.

Table 1. *Basic parameters*

KPI	Purpose	Required data
MTBF	Reliability	Operating time + failure events
MTTR	Maintainability	Individual repair durations + repair events
Availability	Operational performance	MTBF + MTTR + defined downtime
Unplanned failures	Failure monitoring	Failure records

Availability indicates the probability that equipment is in a functional state and capable of performing its intended function at a given time. (IEC, 2015; IEC, 2016) The available data are not sufficient for precise numerical calculation of MTBF and equipment availability for the analyzed equipment group. Such calculations would require equipment-level operating time, individual failure events, clearly defined time intervals between failures, and standardized downtime and repair records. The reported fault resolution duration of approximately 2–3 days cannot be used as MTTR or equipment downtime because its components are not defined in the available records. Therefore, MTBF, MTTR and availability are used in this paper as an analytical framework, while the empirical results are interpreted descriptively based on the available data. (Jardine et al., 2006)

RESEARCH RESULTS

Based on data obtained from the company "MVM Južna Bačka", an analysis of maintenance interventions and recorded failures was performed over a period of 12 months. The results are presented in Table 2.

Table 2*. maintenance interventions and recorded failures*

Indicator	Period	Value
Preventive maintenance interventions	12 months	18
Corrective maintenance interventions	12 months	6
Recorded failures	12 months	7
Unplanned failures	12 months	7
Recorded production/process downtime due to failures	12 months	No downtime recorded
Reported average fault resolution duration	12 months	Approximately 2–3 days

Preventive maintenance downtime	12 months	Not systematically recorded
Reported predominant failure-related factor	12 months	Equipment wear and ageing*

The result shows that preventive maintenance accounted for the dominant share of the recorded interventions. This structure indicates that planned maintenance activities were present in the analyzed system. However, the proportion of preventive interventions alone cannot be used to determine maintenance effectiveness or equipment reliability.
At the same time, 7 unplanned failures were recorded during the observed period. According to the company records, equipment wear and ageing were reported as the predominant failure-related factor. However, the available records did not provide a complete quantitative distribution of failure causes; therefore, this observation is treated as a reported finding rather than a statistically verified ranking of failure causes. The reported fault resolution duration of approximately 2–3 days should not be interpreted as a calculated MTTR. The available records also do not establish a one-to-one relationship between failures and corrective interventions; therefore, the 6 corrective interventions cannot be equated with the 7 recorded failures.
* The reported predominant failure-related factor is based on the company records. A complete quantitative distribution of failure causes was not available. The reported average fault resolution duration of approximately 2–3 days does not represent a calculated MTTR and cannot be interpreted as equipment downtime without additional time definitions.

Table 3. *Current State of Maintenance Digitalization in the Analyzed Company*

An element of digital maintenance	Condition
CMMS/EAM or other software	Not clearly defined
Automatic data collection from equipment	No
Sensor monitoring of equipment condition	No
Predictive maintenance	Reported by company; methodological basis not documented
Planned introduction of digital technologies	Yes

The analysis indicates a relatively low level of implementation of several elements of digital maintenance. In particular, automatic data collection from equipment and sensor-based condition monitoring were not reported. The company reported that predictive maintenance is applied and that further digital technologies are planned; however, the available data do not provide sufficient information to determine the technological or methodological basis of the reported predictive-maintenance practice. Another limitation is the absence of a clearly defined CMMS/EAM system. Such a system could consolidate data on equipment, work orders, preventive activities, failures, spare parts and maintenance costs. (Carvalho et al., 2020; Lee et al., 2015; "Maintenance Performance in the Age of Industry 4.0," 2023; "On Predictive Maintenance in Industry 4.0," 2022)
Centralized collection of this information would enable better analysis of equipment history and data-driven decision-making. (Carvalho et al., 2020; Jardine et al., 2006; Mobley, 2002; "On Predictive Maintenance in Industry 4.0," 2022) Figure 1 presents the number of preventive and corrective maintenance interventions recorded during the analyzed 12-month period, while Figure 2 presents the current level of maintenance digitalization in the case company.

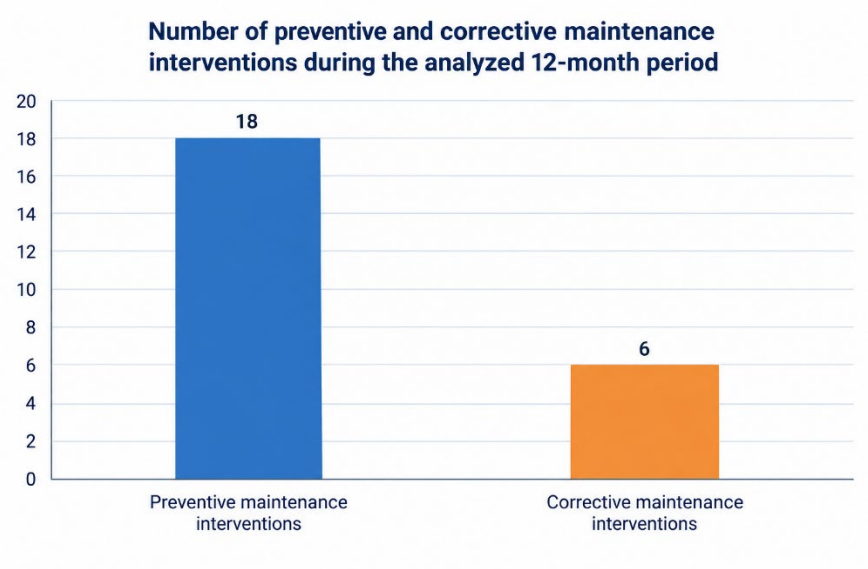


Fig. 1. *Number of Preventive and Corrective Maintenance Interventions During the Analyzed Period*

The results show that preventive maintenance accounts for three quarters of the total recorded interventions. This finding describes the structure of the recorded maintenance activities but does not by itself demonstrate higher reliability, availability or maintenance effectiveness. The presence of 7 unplanned failures during the same period confirms the need to consider failure records and data quality alongside intervention structure.

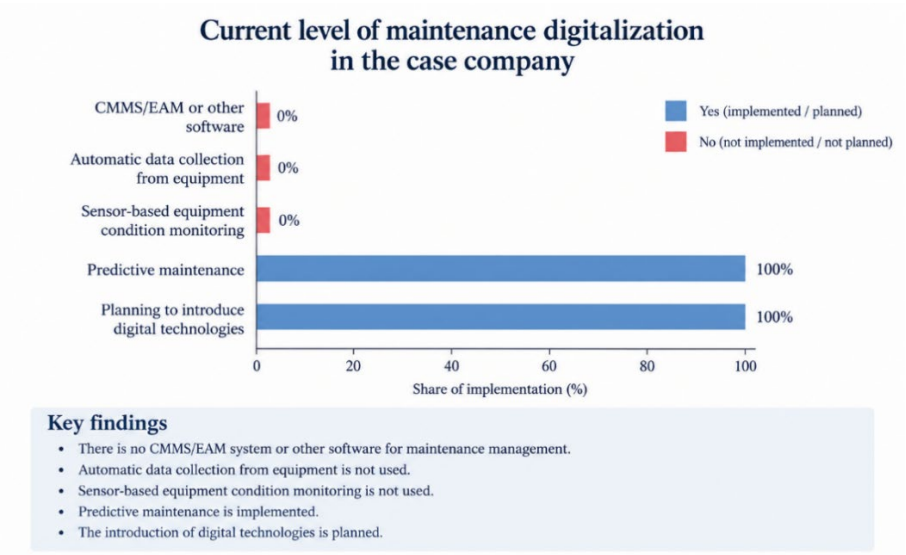


Fig. 2. Current Level of Maintenance Digitalization in the Analyzed Company

DISCUSSION

The results indicate that preventive maintenance represents a substantial share of the recorded maintenance activities in the observed system. Out of 24 recorded interventions, 18, or 75%, were preventive, while 6, or 25%, were corrective. Such a structure indicates the presence of a planned-maintenance approach. However, the frequency of preventive interventions alone is not sufficient to determine whether the maintenance system is effective, because the available data do not permit a quantitative comparison between maintenance interventions and reliability or availability outcomes.

Preventive maintenance is particularly important for equipment that is strategically important for the functioning of a system. Timely inspection and replacement of worn components can reduce the likelihood of serious failures. However, the occurrence of 7 unplanned failures during the 12-month period shows that preventive interventions did not eliminate unplanned failure events. Because operating-time data and individual failure intervals were unavailable, no quantitative conclusion about equipment reliability can be drawn. According to the company records, equipment wear and ageing were reported as the predominant failure-related factor, but a complete frequency distribution of failure causes was not available. This observation therefore should not be interpreted as a statistically verified ranking of causes. Modern maintenance systems increasingly combine preventive maintenance with monitoring of the actual condition of equipment. (ISO, 2016) In this context, MTBF and MTTR are useful performance indicators when the underlying data are collected in a standardized manner. MTBF requires reliable operating-time and failure-event data, while MTTR requires clearly defined individual repair durations. In the present case study, neither indicator could be calculated from the available records. The reported fault resolution duration of approximately 2–3 days is not treated as MTTR because its components are not sufficiently defined.

From a conceptual perspective, reducing maintenance-related delays can contribute to higher productivity by reducing the time during which equipment or maintenance personnel are unavailable for productive activities. However, productivity was not directly measured in this case study, and this relationship therefore remains a conceptual implication rather than an empirically quantified finding. The relationship is not necessarily linear, since excessive preventive maintenance can increase costs and require additional time for planned interventions. The main limitation identified in the analyzed maintenance system is therefore not the absence of preventive activities, but the limited availability, standardization and integration of maintenance performance data.

The reported absence of production/process downtime due to failures must also be distinguished from the reported 2–3-day fault resolution duration. The available records do not specify whether the latter represents active maintenance labor time, elapsed calendar time from failure detection to restoration, waiting time for spare parts or personnel, or a combination of these components. Consequently, these values cannot be used directly to calculate equipment availability. Similarly, the difference between 6 corrective interventions and 7 recorded failures indicates that the available classification does not provide a one-to-one relationship between the two categories. The records do not allow verification of whether one failure resulted in multiple corrective interventions or whether one corrective intervention addressed multiple failure events.

IMPROVEMENT OPPORTUNITIES THROUGH THE IMPLEMENTATION OF MAINTENANCE 4.0

Industry 4.0 is transforming industrial maintenance through the continuous collection, processing and use of equipment-condition data. For "MVM Južna Bačka", the first step towards Maintenance 4.0 could be the implementation of an integrated CMMS/EAM system, enabling centralized recording of equipment, failures, interventions, spare parts, costs and maintenance history. A subsequent step could involve sensor-based monitoring of critical equipment, measuring parameters such as temperature, vibration, pressure, level and flow. The collected data could support condition-based and predictive maintenance, allowing interventions to be based on the actual condition and behavior of equipment rather than only on predefined maintenance intervals. Key performance indicators should include MTBF, MTTR, equipment availability, number of unplanned failures, preventive and corrective interventions, downtime duration, maintenance costs and the percentage of implemented preventive activities. Standardized failure recording should include the date and time of failure, equipment, failure type and cause, intervention start and end times, downtime, spare parts used and the relationship between the failure event and the resulting maintenance intervention. (IEC, 2016; Muchiri et al., 2011) This would provide a reliable basis for calculating MTBF and MTTR and for monitoring maintenance performance over time. A gradual digitalization

approach is recommended, starting with data standardization and CMMS/EAM implementation, followed by condition monitoring and advanced analytics. Such an approach would support the transition towards data-driven and predictive maintenance while promoting a more systematic and objective approach to maintenance management.

LIMITATIONS OF THE STUDY

The findings of this research should be interpreted in the context of several limitations. First, the research is based on a single-company case study and a 12-month observation period, which limits the generalizability of the results. Second, the available maintenance records did not include complete equipment-level operating time, individual time intervals between failures, standardized equipment downtime, or individual repair-duration data. Consequently, MTBF, MTTR and equipment availability could not be calculated quantitatively and are used only as an analytical framework. Third, the available records indicate a discrepancy between the number of recorded failures and corrective maintenance interventions, while the relationship between individual failure events and interventions cannot be reconstructed from the available data. Fourth, the reported predominant failure-related factor could not be verified through a complete quantitative distribution of failure causes. In addition, productivity was not directly measured using a specific productivity indicator. Future research should therefore use standardized equipment-level maintenance records and longitudinal data to quantify reliability, maintainability, availability and productivity.

CONCLUSION

This case study analyzed preventive and corrective maintenance practices in "MVM Južna Bačka" over a 12-month period. Preventive maintenance accounted for 18 of 24 recorded maintenance interventions (75%), while corrective maintenance accounted for 6 interventions (25%). The dominant share of preventive activities indicates the presence of a planned-maintenance approach, but the proportion of preventive interventions alone cannot be used as a measure of maintenance effectiveness. Seven unplanned failures were recorded during the same period. According to the company records, equipment wear and ageing were reported as the predominant failure-related factor; however, a complete quantitative distribution of failure causes was not available. The reported fault resolution duration of approximately 2–3 days was not treated as a calculated MTTR because the underlying individual repair records and the components of the reported duration were not available. The available operating-time, failure-interval and standardized downtime data were insufficient for the quantitative calculation of MTBF and equipment availability. The difference between the number of recorded failures and corrective interventions also indicates a need for more consistent classification and linking of failure and maintenance events. The analysis therefore identifies maintenance data management as a key area for improvement. Standardized failure and intervention records and the gradual introduction of a CMMS/EAM system could provide a reliable basis for monitoring MTBF, MTTR, availability, downtime, maintenance costs and other performance indicators. In a subsequent stage, condition monitoring and advanced analytics could support the transition towards condition-based and predictive maintenance. Overall, the case study demonstrates the importance of combining preventive maintenance activities with systematic data collection and performance monitoring. The available evidence supports conclusions about the structure of maintenance practices and data-management limitations, but it does not permit a complete quantitative assessment of reliability, availability or productivity. Future research should therefore include a longer observation period, equipment-level operating-time data, standardized failure and downtime records, clearly defined repair-duration measures, failure-cause distributions and direct productivity indicators. Such data would enable a quantitative assessment of the relationships between maintenance strategy, reliability, availability and productivity.

Future research should include a longer observation period, equipment-level operating-time data, standardized failure and downtime records, clearly defined repair-duration measures,

failure-cause distributions, and direct productivity indicators. Such data would enable a quantitative assessment of the relationships between maintenance strategy, reliability, availability and productivity.

REFERENCES

Carvalho, T. P., et al. (2020). Predictive maintenance in the Industry 4.0: A systematic literature review. Computers & Industrial Engineering, 150, 106889. https://doi.org/10.1016/j.cie.2020.106889

IEC. (2015). IEC 60050-192:2015 – International Electrotechnical Vocabulary – Part 192: Dependability. International Electrotechnical Commission.

IEC. (2016). IEC 61703:2016 – Mathematical expressions for reliability, availability, maintainability and maintenance support terms. International Electrotechnical Commission.

ISO. (2016). ISO 14224:2016 – Petroleum, petrochemical and natural gas industries — Collection and exchange of reliability and maintenance data for equipment. ISO.

ISO. (2024). ISO 55000:2024 – Asset management — Vocabulary, overview and principles. ISO.

Jardine, A. K. S., Lin, D., & Banjevic, D. (2006). A review on machinery diagnostics and prognostics implementing condition-based maintenance. Mechanical Systems and Signal Processing, 20(7), 1483–1510. https://doi.org/10.1016/j.ymssp.2005.09.012

Lee, J., Bagheri, B., & Kao, H. A. (2015). A cyber-physical systems architecture for Industry 4.0-based manufacturing systems. Manufacturing Letters, 3, 18–23.

Maintenance performance in the age of Industry 4.0: A bibliometric performance analysis and a systematic literature review. (2023). Sensors, 23(3), 1409.

Mobley, R. K. (2002). An introduction to predictive maintenance. Butterworth-Heinemann.

Moubray, J. (1997). Reliability-centered maintenance. Industrial Press.

Muchiri, P., Pintelon, L., Gelders, L., & Martin, H. (2011). Development of maintenance function performance measurement framework and indicators. International Journal of Production Economics, 131(1), 295–302. https://doi.org/10.1016/j.ijpe.2010.04.039

On predictive maintenance in Industry 4.0: Overview, models, and challenges. (2022). Applied Sciences, 12(16), 8081.

Preventive and corrective maintenance – Cost comparison and cost–benefit analysis. (n.d.). Structure and Infrastructure Engineering, 12(5). https://doi.org/10.1080/15732479.2015.1032983

Requirements specification of a computerized maintenance management system – A case study. (2016). Procedia CIRP, 52, 268–273. https://doi.org/10.1016/j.procir.2016.07.047

The computerized maintenance management system – An essential tool for world class maintenance. (2016). Procedia Engineering, 138, 413–420. https://doi.org/10.1016/j.proeng.2016.02.100



XVI International Conference Industrial Engineering and Environmental Protection 2026 (IIZS 2026)
October 01-02, 2026, Zrenjanin, Serbia

Session 4

Oil and Gas Engineering

DOI:10.5937/IIZS26311V

THE IMPACT OF POLISKREP TECHNOLOGY ON THE OPERATIONAL STABILITY OF PRODUCTION EQUIPMENT AND SAND PRODUCTION CONTROL IN OIL WELLS

Research paper

Nikola Vojvodić[1], Slavica Prvulović[2*], Jasna Tolmač[3], Branislava Radišić[4]
[1]University of Novi Sad, Technical Faculty "Mihajlo Pupin", Djure Djakovica bb, 23000 Zrenjanin

Abstract: Sand production is a significant challenge during oil well exploitation, causing damage to production equipment, frequent workover interventions, production downtime, and increased operating costs. This paper presents the application of the organosilicate Poliskrep technology for stabilizing the near-wellbore zone and controlling sand production in the X-200 production well. The operational history of the well was analyzed, including excessive formation sand production, high water cut, and limitations of previously applied remediation methods. The Poliskrep treatment procedure is described, including preparation and injection of the organosilicate polymer, application of a flushing spacer and nitrogen, and the operating conditions during treatment. Treatment effectiveness was evaluated based on well clean-up results and subsequent monitoring of well performance. Following application of the technology, no sand production from the near-wellbore zone was recorded, enabling well completion without a gravel-pack system. During 964 days of operation, no workover interventions were required, and no mechanical impurities were detected in the produced fluid. These results indicate improved operational stability of the production equipment and reliability of the production system. The findings demonstrate that Poliskrep technology can provide an effective solution for sand production control and contribute to extending the service life of production equipment under oil well operating conditions.
Key words: poliskrep technology; sand production; near-wellbore zone; production equipment; operational stability; oil well; organosilicate polymer; production reliability.

INTRODUCTION

Sand production is one of the most significant challenges encountered during the exploitation of oil and gas wells completed in poorly consolidated reservoirs. The presence of solid particles in the produced fluid causes abrasive wear of both downhole and surface production equipment, reduces the operating efficiency of artificial lift systems, leads to the plugging of perforations and production tubing, increases the frequency of workover operations, and results in substantial economic losses (Safaei, 2023; Abass, 2002). In addition to its direct impact on production performance, sand production significantly impairs the reliability and service life of production equipment, making it an important research topic from the perspectives of mechanical engineering and the maintenance of technical systems (Talaghat, 2009; Arbadov, 2025).

A wide range of mechanical and chemical methods has been developed to control sand production. Mechanical methods, such as gravel-pack systems, wire-wrapped screens, and pre-packed screens, have demonstrated high effectiveness; however, they increase the complexity of well completion, prolong [1]workover operations, and raise capital and operating costs (Abass, 2002; Saghandali, 2022). Consequently, increasing attention has recently been devoted to the chemical consolidation of the near-wellbore zone through the application of polymeric and organosilicate systems, which promote the bonding of formation grains while minimizing the reduction in formation permeability (Safaei, 2023; Tabar, 2021; Du, 2024).

Recent studies have shown that appropriately selected chemical consolidation systems can significantly reduce sand production, improve the mechanical strength of the near-wellbore formation, and extend the service life of production equipment while reducing production downtime and the frequency of workover interventions (Du, 2024;Tabar, 2021; Mishra,

[1]nikola.vojvodic@tfzr.rs
[2] Corresponding author, slavica.prvulovic@uns.ac.rs ORCID: 0000-0001-6353-7145
[3] jasna.tolmac@uns.ac.rs ORCID: 0000-0003-3860-2034
[4] branislava.radisic@uns.ac.rs ORCID: 0009-0007-3664-2012

2015). A major challenge remains the selection of a technology capable of simultaneously providing effective formation stabilization and preserving the production potential of the well (Gelfgat, 2022; Muhammad, 2025).
This study investigates the application of the organosilicate Poliskrep technology in the X-200 production well, which was affected by severe sand production. Particular emphasis is placed on evaluating the influence of the treatment on the operational stability of production equipment, the elimination of mechanical impurities from the produced fluid, and the extension of the production period without the need for workover interventions.

MATERIAL AND METHODS

Characteristics of the Investigated Well

The study was conducted on the X-200 oil production well, which represents a typical example of a well affected by severe formation sand production and an increased water cut in the produced fluid. The well was drilled as a directional production well with a measured depth (MD) of 809 m and a true vertical depth (TVD) of 760 m. Following the completion of the final workover operations, the production interval was established between 786 and 784 m.
During its long-term operation, the well experienced numerous operational problems that adversely affected production stability and the reliability of the production equipment. The increase in formation water production was accompanied by intensive formation sand production, which caused severe abrasive wear of the downhole sucker rod pump, valves, production tubing, and other components of the production system. As a consequence, production downtime increased, and workover interventions became more frequent.
Before the application of the Poliskrep technology, several remediation methods had been implemented, including production interval cementing, water-bearing zone isolation, chemical treatments, and the installation of a gravel-pack system. However, these methods failed to provide long-term stabilization of the near-wellbore zone or a permanent solution to the sand production problem. Consequently, the X-200 well was selected for the application of the organosilicate Poliskrep chemical consolidation technology.
The main characteristics of the investigated well are summarized in Table 1.

Table 1. *Main characteristics of the investigated well*

Parameter	Value
Well designation	X-200
Well type	Directional production well
Measured depth (MD)	809 m
True vertical depth (TVD)	760 m
Production interval	786–784 m
Primary operational problem	Sand production and high water cut
Production method	Downhole sucker rod pump
Applied technology	Organosilicate Poliskrep technology

Application of the Poliskrep Technology

The Poliskrep technology is a chemical stabilization method for the near-wellbore zone based on the application of an organosilicate polymer, with the primary objective of bonding formation particles and preventing their migration during production. Unlike conventional mechanical sand control methods, chemical consolidation stabilizes the rock matrix without requiring the installation of additional mechanical components within the production interval.
Prior to the treatment, the well was prepared and the wellbore bottom was cleaned and conditioned. Subsequently, the injectivity of the production interval was evaluated to verify that the hydraulic conditions were suitable for the treatment. After confirming satisfactory

injectivity, the treatment string equipped with an operational packer was run into the well, and the target interval was isolated for the chemical treatment.
The treatment procedure began with flushing the production interval using the specialized PoliRIR-NFAS spacer fluid to remove fine particles from the pore space and improve the adhesion of the polymer to the rock matrix. This was followed by the injection of the organosilicate Poliskrep polymer. Nitrogen was subsequently used as the displacement fluid to promote uniform distribution of the polymer throughout the treated interval. After completion of the injection process, the well was shut in for the prescribed curing period to allow complete polymer hardening and the formation of a consolidated zone around the perforations.
The principal operating parameters of the Poliskrep treatment are summarized in Table 2.

Table 2. *Main operating parameters of the Poliskrep treatmen*

Parameter	Value
Volume of flushing spacer fluid	1.4 m³
Volume of Poliskrep polymer	1.25 m³
Total amount of nitrogen	Approximately 8,800 kg
Injection pressure	40–100 bar
Duration of final nitrogen injection	15 h
Well shut-in time	12 h

Research Methodology

The effectiveness of the applied technology was evaluated by comparing the operational performance of the well before and after the implementation of the Poliskrep treatment. The analysis included monitoring the key technical and production parameters that directly influence the reliability and operational performance of the production system.
The primary evaluation criteria included the occurrence of formation sand production, the presence of mechanical impurities in the produced fluid, the operational stability of the downhole sucker rod pump, the need for workover interventions, the feasibility of well operation without the installation of a gravel-pack system, and the duration of uninterrupted production following the treatment.
The results obtained during well clean-up and the subsequent production period were analyzed to assess the effectiveness of the chemical stabilization of the near-wellbore zone, the protection of production equipment against abrasive wear, and the improvement in the reliability of the production system.
To ensure an objective assessment of the treatment performance, the evaluation was based on both qualitative observations and quantitative operational indicators collected during the well clean-up stage and the subsequent production period. The comparison between the pre-treatment and post-treatment operating conditions enabled the identification of changes directly attributable to the application of the Poliskrep technology. Particular attention was given to parameters that reflect the integrity of the near-wellbore zone and the operational reliability of the production system.
The analysis also considered the continuity of well operation and the long-term behavior of the production equipment under field conditions. The absence of formation sand and mechanical impurities in the produced fluid was regarded as an indicator of successful chemical consolidation, while uninterrupted production without equipment failures or workover interventions was used to evaluate the durability of the treatment. In addition, the necessity for auxiliary sand-control measures, such as gravel-pack installation, was examined as an important practical criterion for assessing the overall effectiveness of the applied technology.
The methodological approach adopted in this study is based on field performance evaluation rather than laboratory testing, providing direct evidence of the technology under actual production conditions. Such an approach allows a realistic assessment of the operational

benefits achieved after treatment, including improved equipment reliability, reduced maintenance requirements, and enhanced production stability. The selected evaluation criteria are consistent with those commonly applied in recent studies dealing with chemical sand control technologies and production system reliability.
Figure 1 illustrates the methodology adopted for the implementation of the Poliskrep treatment and the evaluation of its effectiveness.

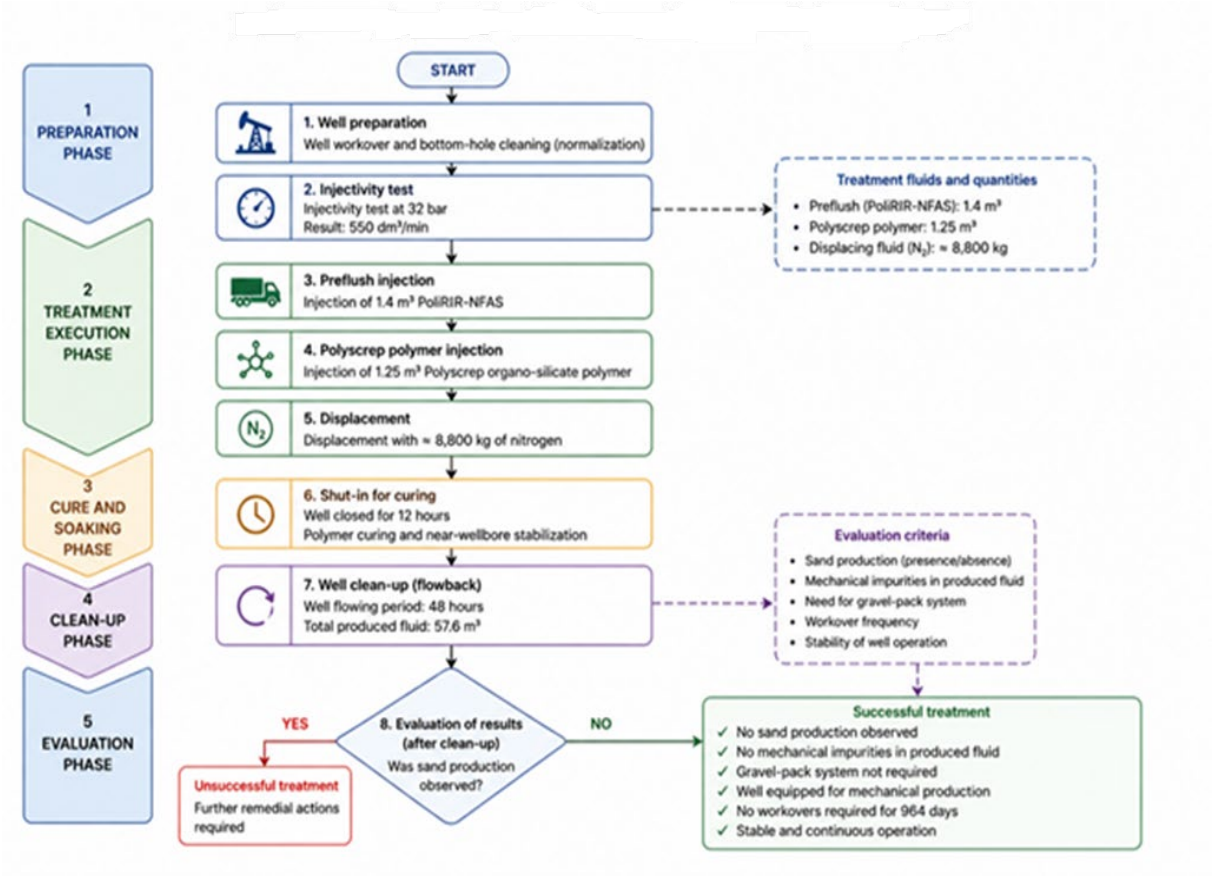


Fig. 1. *Methodology for the implementation of the Poliskrep treatment and evaluation of its effectiveness.*

RESULTS AND DISCUSSION

The analysis of production data revealed that, prior to the application of the Poliskrep technology, the X-200 well was affected by severe formation sand production and a progressive increase in water content in the produced fluid. After the well was brought into production, a fluid production rate of approximately 13 m³/day was achieved, with a water cut of about 35%. During the subsequent production period, the water cut continuously increased, reaching approximately 96% in 2018 and around 98% in 2019. At the same time, intensive migration of formation particles was observed, resulting in frequent failures of the downhole sucker rod pump, increased abrasive wear of production equipment, and a higher frequency of workover interventions.
Conventional remediation methods, including production interval cementing, reperforation, chemical treatments, and the installation of gravel-pack systems, provided only temporary improvements in production conditions. After a certain period, sand production problems reappeared, indicating that the applied methods did not provide long-term stabilization of the near-wellbore zone.
Following the implementation of the Poliskrep treatment, well clean-up operations were performed over a period of 48 h, during which a total of 57.6 m³ of fluid was produced.

Inspection of the production interval after completion of the clean-up process confirmed the absence of formation sand, representing the first indication of successful chemical consolidation of the near-wellbore zone. Based on these results, a decision was made to equip the well with an artificial lift production system without installing a gravel-pack system, which had previously been required during earlier production stages to prevent the migration of produced sand.

The most important production performance indicators after the application of the Poliskrep technology are presented in Table 3.

Table 3. *Key results after the application of the Poliskrep technology*

Parameter	Result
Well clean-up duration	48 h
Fluid produced during well clean-up	57.6 m³
Presence of sand after well clean-up	Not detected
Installation of gravel-pack (GP) system	Not required
Mechanical impurities in produced fluid	Not detected
Production period without workover intervention	964 days

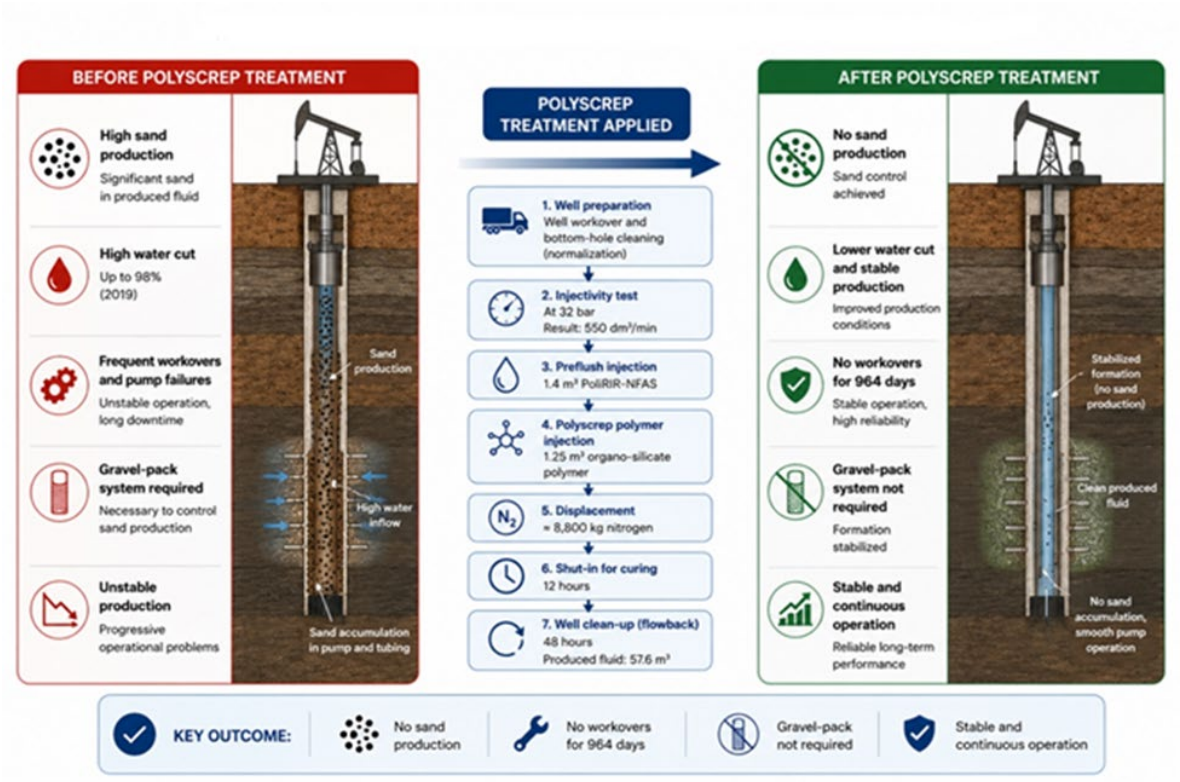


Fig.2. *Schematic representation of the well condition before and after the application of the Poliskrep technology.*

Monitoring of the well performance after returning the well to production demonstrated that, during the subsequent 964-day production period, no mechanical impurities were detected in the produced fluid, and no workover interventions were required. Compared with the previous production period, during which sand production caused frequent operational interruptions and failures of the downhole sucker rod pump, the treated well achieved continuous and stable operation of the production system. These results confirm that the chemical consolidation of the near-wellbore zone successfully prevented the migration of formation particles and ensured long-term stabilization of the production interval.

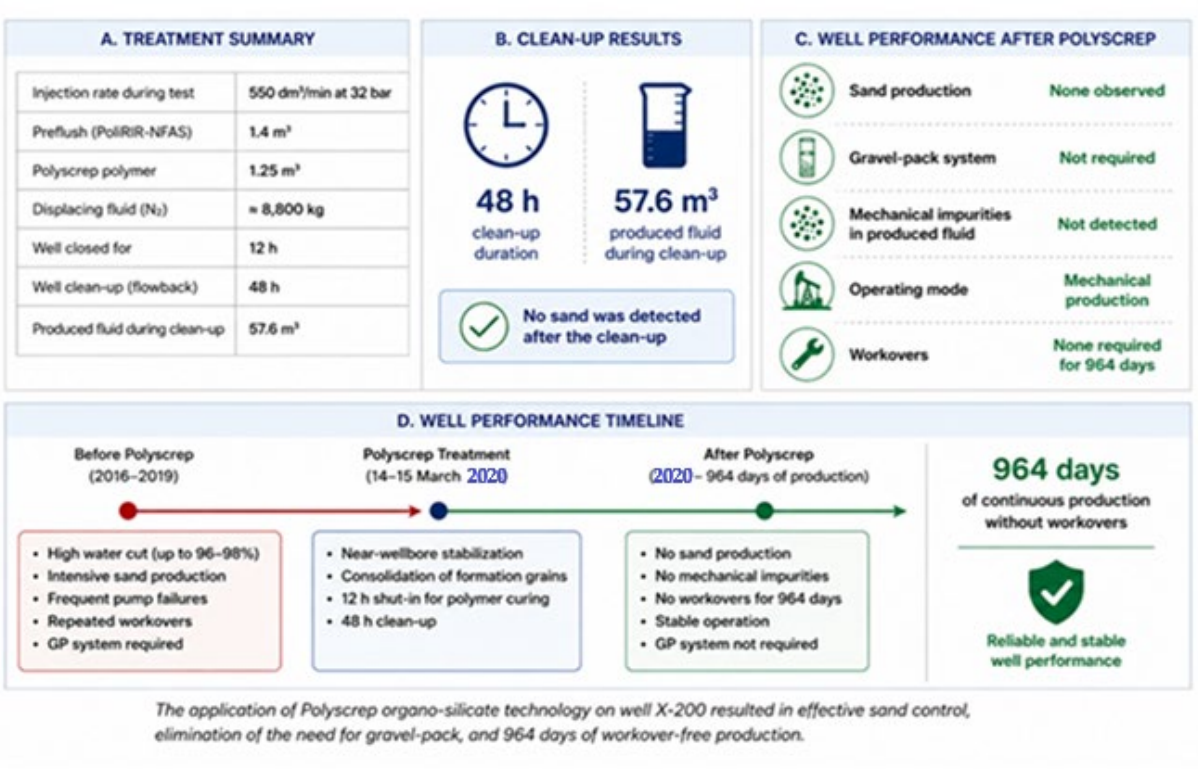


Fig. 4. *Results of the Poliskrep Treatment and Subsequent Well Performance – Well X-200*

From a mechanical engineering perspective, the elimination of sand production has multiple implications for the reliability of the production system. The presence of abrasive particles represents one of the primary causes of wear affecting pistons, valves, pump cylinders, production tubing, and other components of downhole production equipment. By stabilizing the near-wellbore zone, the detachment of rock particles and their transport through the production system were prevented, thereby significantly reducing the conditions leading to abrasive wear and mechanical damage of equipment. As a result, the availability of the production system was improved, the service life of equipment was extended, and the need for workover interventions was reduced.

A particularly important practical outcome of the achieved results is the fact that, after the application of the Poliskrep technology, there was no need for the installation of a gravel-pack system. Unlike mechanical sand control methods, chemical consolidation enabled formation stabilization without additional sand-retaining components, thereby simplifying the well completion design and reducing the complexity of future intervention operations.

The obtained results are in good agreement with findings reported in recent studies, which demonstrate that organosilicate and polymer-based chemical consolidation systems can effectively reduce sand production while preserving reservoir production characteristics. In most published studies, treatment performance is evaluated based on the reduction of sand production, extension of the period between workover interventions, and improvement of production equipment reliability. The results obtained from the X-200 well confirm these findings and demonstrate that the Poliskrep technology represents an effective alternative to conventional sand control methods, particularly in wells where previously applied mechanical methods have failed to provide satisfactory long-term results.

CONCLUSION

Based on the conducted research, it can be concluded that the application of the organosilicate Poliskrep technology represents an effective method for near-wellbore zone stabilization and sand production control in oil wells affected by severe abrasive wear of production equipment. The analysis of the X-200 well performance demonstrated that

previously applied remediation methods failed to provide long-term stability of the production system, highlighting the need for the implementation of an advanced chemical formation consolidation technology.

Following the Poliskrep treatment, no sand production was detected during the well clean-up operation, enabling the completion of the well with an artificial lift production system without the installation of a gravel-pack system. Furthermore, no mechanical impurities were identified in the produced fluid samples after the well was returned to production, confirming the successful stabilization of the production interval.

A particularly significant result is that, after the treatment, the well remained in continuous operation for 964 days without the need for workover interventions. This indicates a substantial improvement in the reliability of production equipment operation and a reduction in the adverse effects of sand production on the performance of the downhole pump and other components of the production system.

The obtained results confirm that the Poliskrep technology can represent an effective alternative to conventional mechanical sand control methods, particularly in cases where previously applied approaches have failed to achieve satisfactory long-term performance. In addition to improving production stability, the application of this technology contributes to reducing the frequency of workover interventions, increasing production equipment availability, and lowering maintenance costs.

The achieved results indicate significant potential for the application of Poliskrep technology under similar production conditions. Future research should focus on the analysis of a larger number of wells, long-term monitoring of production parameters, and comparative evaluation of performance with other sand control technologies in order to establish optimal candidate selection criteria and further improve the reliability of production systems.

REFERENCES

Abass, H. H., Nasr-El-Din, H. A., & BaTaweel, M. H. (2002). Sand control: Sand characterization, failure mechanisms, and completion methods. SPE Annual Technical Conference and Exhibition. https://doi.org/10.2118/77686-MS.

Arbadov, G., Al Shamisi, E. D., Anwar, M., et al. (2025). Unlocking Abu Dhabi's world-class unconventional energy resources in a safe, sustainable, and most economical way: Journey of well duration reduction for unconventional oil wells by 66%. ADIPEC 2025 Conference Proceedings. Society of Petroleum Engineers. https://doi.org/10.2118/229523-MS.

Du, J., Huang, Q., Liu, P., et al. (2024). Review of recent advances in chemical sand production control: Materials, methods, mechanisms, and future perspectives. *Energy & Fuels, 38(22),* 21845–21872. https://doi.org/10.1021/acs.energyfuels.4c04114.

Gelfgat, M., Geraskin, A., Perelman, O., & Fadeykin, A. (2022). Electrodrilling and new prospects in the oil & gas well construction risk reduction. *Reliability: Theory & Applications, 17, 78.*

Mishra, S., & Ojha, K. (2015). Chemical sand consolidation: An overview. *Journal of Petroleum Engineering & Technology, 5(2).* https://doi.org/10.37591/jopet.v5i2.2036.

Muhammad, M., Anugerah, A., et al. (2025). Advances and challenges of sand production and control in oilfields: A review. *Results in Engineering.* https://doi.org/10.1016/j.rineng.2025.104596.

Safaei, A., Asefi, M., Ahmadi, M., et al. (2023). Chemical treatment for sand production control: A review of materials, methods, and field operations. *Petroleum Science, 20(3),* 1640–1658. https://doi.org/10.1016/j.petsci.2023.02.013.

Saghandali, F., & Salehi, M. B. (2022). A review on chemical sand production control techniques in oil reservoirs. *Energy & Fuels, 36(10),* 5185–5208. https://doi.org/10.1021/acs.energyfuels.2c00700.

Tabar, M. A., Bagherzadeh, H., Shahrabadi, A., et al. (2021). A comprehensive research in chemical consolidator/stabilizer agents on sand production control. *Journal of Petroleum*

Exploration and Production Technology, 11, 4305–4324. https://doi.org/10.1007/s13202-021-01303-1.

Talaghat, M. R., Esmaeilzadeh, F., & Mowla, D. (2009). Sand production control by chemical consolidation. *Journal of Petroleum Science and Engineering, 67(1–2),* 34–40. https://doi.org/10.1016/j.petrol.2009.02.005.

DOI:10.5937/IIZS26319B

BRIDGING MEASUREMENT AND MODELLING: HYBRID PATHWAYS FOR ACCURATE RESERVOIR GHG QUANTIFICATION

Research paper

Maja Brborić[1], Branka Nakomčić Smaragdakis[2], Sonja Dmitrašinović[3], Miljan Šunjević[4], Manu Seth[5]

[1]University of Novi Sad, Faculty of Technical Sciences, Trg Dositeja Obradovića 6, 21000 Novi Sad, Serbia

[2]Open Hydro Ltd, 161 Gideon Road, SW11 5ER, London, United Kingdom

Abstract: Reservoir greenhouse gas (GHG) quantification remains methodologically difficult because emissions are spatially heterogeneous, temporally dynamic and distributed among diffusion, ebullition, degassing and downstream pathways. Field measurements provide indispensable process-level evidence but are difficult to extrapolate, whereas empirical and process-based models extend estimates beyond sampled locations at the cost of structural and input uncertainty. This conference paper develops a focused measurement-to-model framework for integrating these complementary information streams. Building on recent comparative evidence, the proposed pathway combines targeted field observations, Earth-observation products, reservoir and catchment descriptors, mechanistic constraints and data-driven inference within an iterative validation and uncertainty-assessment loop. Particular attention is given to pathway-specific calibration because model–measurement disagreement is not uniform: methane ebullition and carbon dioxide diffusion can be substantially less predictable than methane diffusion. A three-tier implementation strategy is proposed, progressing from low-cost screening through targeted field validation to adaptive hybrid monitoring, reporting and verification (MRV). The framework is intended to preserve site specificity where it matters while enabling spatial and temporal scaling across reservoir portfolios. Rather than replacing measurements with models, hybrid quantification uses measurements to constrain model behaviour and models to direct subsequent observations. This architecture offers a practical route toward more transparent, updateable and decision-relevant reservoir GHG estimates for hydropower sustainability assessment and climate reporting.

Key words: reservoir emissions, methane, carbon dioxide, hybrid modelling, remote sensing, machine learning, uncertainty

INTRODUCTION

Hydropower is commonly treated as a low-carbon electricity source, yet the climate performance of individual reservoir systems can differ markedly. Flooded organic matter, catchment-derived carbon and in-reservoir production are transformed under reservoir-specific thermal, redox and hydrodynamic conditions, generating carbon dioxide (CO_2) and methane (CH_4) that may reach the atmosphere through several distinct pathways. Diffusive exchange at the water surface, CH_4 ebullition, degassing at turbines and spillways, and downstream emissions operate at different spatial and temporal scales and respond differently to climate, morphology and reservoir operation. Consequently, a single emission factor or a short field campaign cannot be assumed to represent the full reservoir carbon signal (Deemer et al., 2016; Prairie et al., 2021; Seth et al., 2026).

The central methodological problem is therefore not simply how to measure reservoir emissions, but how to connect observations made at limited locations and times with models capable of representing unobserved conditions. Direct measurements remain essential because they resolve actual fluxes and provide the reference against which other methods are tested. Their spatial footprint, however, is restricted and intensive monitoring is expensive. Empirical models are readily transferable but simplify dynamic controls; process-based models preserve mechanistic relationships but require extensive parameterisation; remote sensing broadens spatial and temporal coverage but mostly observes environmental proxies rather than GHG flux directly; and machine-learning (ML) methods can learn nonlinear relationships

[1]Corresponding author, majabrboric@uns.ac.rs, ORCID: 0009-0002-7669-9033
[2]nakomcic@uns.ac.rs, ORCID: 0000-0001-5754-2669
[3]dmitrasinovic@uns.ac.rs, ORCID: 0000-0002-5686-4196
[4]msunjevic@uns.ac.rs, ORCID: 0000-0002-8125-2087
[5]mseth@openhydro.net, ORCID: 0000-0002-3997-2988

while remaining dependent on representative training data and explicit validation (Seth et al., 2026).

Recent model–measurement comparisons illustrate why integration is necessary. Across six hydropower reservoirs in the southeastern United States, Pilla et al. (2025) found that agreement depended strongly on the emission pathway: CH_4 diffusion was comparatively well constrained, whereas CH_4 ebullition and CO_2 diffusion showed substantially greater disagreement and uncertainty. At a different decision scale, Janus et al. (2025) demonstrated that incorporating reservoir-emission models into hydropower planning can alter project portfolios and reduce the carbon footprint of new development. These studies point to the same requirement: emission estimates must be sufficiently scalable for planning, but their confidence depends on observations that expose pathway-specific model weaknesses.

This paper develops a concise hybrid framework for reservoir GHG quantification designed specifically around that measurement–model interface. Unlike a broad review of available methods, the objective is to define how complementary data streams can be organised into an iterative workflow for screening, calibration, validation, spatial–temporal scaling and uncertainty reporting. The proposed architecture is intended as a practical basis for reservoir-level assessment and for monitoring, reporting and verification (MRV) systems that can be updated as new observations become available.

METHODOLOGICAL BASIS

Reservoir emission pathways and observation requirements

Reservoir GHG assessment is complicated by the fact that the principal emission pathways are not sampled in the same way. Surface diffusion is commonly quantified from floating chambers, eddy-covariance systems or dissolved-gas concentrations combined with gas-transfer formulations. Ebullition is episodic and spatially clustered and therefore requires approaches capable of resolving bubbles and sediment-associated hotspots. Degassing depends on dissolved gas concentrations and hydraulic passage through turbines or spillways, while downstream emissions require measurements below the dam and consideration of gas exchange along the receiving river. A monitoring design that resolves only one pathway may therefore provide a precise but incomplete estimate of the reservoir total.

As illustrated in Fig. 1, reservoir GHG release is the end result of interacting external drivers, biogeochemical production processes and several transport pathways. This process-oriented view is important because diffusion, ebullition and downstream degassing respond differently to environmental forcing and therefore should not be treated as interchangeable components of a single bulk flux.

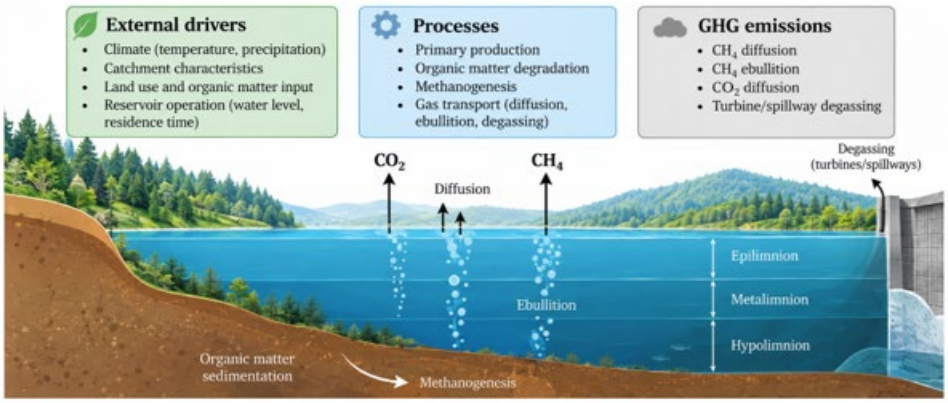


Fig. 1. *Key processes and pathways of GHG emissions from reservoirs*

From method comparison to functional integration

The value of a hybrid framework lies in assigning a specific function to each information source rather than combining methods indiscriminately. Field observations should anchor flux magnitude and pathway partitioning. Earth-observation products can characterise variables that are spatially continuous or repeatedly observable, including reservoir surface area, water-surface temperature, catchment land cover and selected optical water-quality indicators. Reservoir morphology, hydrology, meteorology and operational data provide additional explanatory variables. Process knowledge then constrains physically implausible relationships, while statistical or ML components can capture residual nonlinearities and extend inference to unsampled periods or reservoirs. This division of roles reduces the risk that a flexible model merely reproduces correlations without respecting reservoir processes.

Table 1. *Functional roles of complementary components in a hybrid reservoir GHG framework*

Component	Primary contribution	Main limitation	Best role in hybrid system	Uncertainty control
Field measurements	Observed fluxes and pathway partitioning	Sparse spatial/temporal coverage	Calibration and independent validation	Replication; seasonal coverage; QA/QC
Remote sensing	Spatially repeated environmental descriptors	Mostly indirect proxies of GHG flux	Scaling and hotspot stratification	Cloud/sensor screening; cross-validation
Empirical models	Rapid screening with limited inputs	Static relationships; domain dependence	First-pass estimates and benchmarks	Report applicability domain
Process-based models	Mechanistic and time-resolved representation	High data and calibration demand	Physical constraints and scenario analysis	Parameter sensitivity; mass-balance checks
ML / data-driven models	Nonlinear integration of heterogeneous predictors	Training bias and limited interpretability	Residual learning and spatial–temporal scaling	Independent testing; XAI; domain checks

PROPOSED HYBRID MEASUREMENT–MODEL PATHWAY

The proposed architecture is organised as a closed loop rather than a one-way progression from data collection to prediction (Figure 2). Four input groups are considered: (i) field observations of fluxes and dissolved gases; (ii) Earth-observation variables; (iii) mechanistic knowledge describing gas production, transport and exchange; and (iv) auxiliary information describing climate, catchment, morphology, hydrology and operation. These inputs converge in a hybrid inference layer in which mechanistic constraints and data-driven relationships are combined. Model outputs are then subjected to independent validation and explicit uncertainty analysis. The resulting diagnostics are used to identify where additional measurements are most informative, thereby updating the next monitoring cycle.

The integration logic shown in Fig. 2 follows this complementarity: field observations provide calibration and validation, remote sensing and auxiliary information extend spatial and temporal coverage, and empirical, process-based and machine-learning models provide alternative inference structures. Their combination is most useful when bias correction and uncertainty propagation are retained as explicit steps rather than applied only after model fitting.

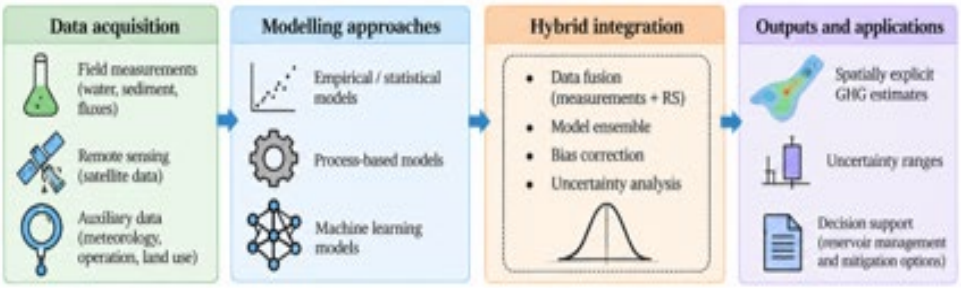


Fig. 2. *Conceptual framework for integrating measurements and modeling for reservoir GHG quantification*

Pathway-specific calibration and validation

A central design principle is that validation should be performed by emission pathway before reservoir totals are aggregated. This follows directly from empirical evidence showing that model performance can differ substantially among diffusion, ebullition and degassing. Pilla et al. (2025), for example, reported relatively low sensitivity of CH_4 diffusion to the choice of modelled versus observed data source, while CH_4 ebullition exhibited much greater variability and CO_2 diffusion showed systematic disagreement between G-res estimates and field surveys at the six reservoirs examined. Aggregating pathways too early can conceal compensating errors: an apparently plausible total may arise from overestimation of one component and underestimation of another. Hybrid calibration should therefore retain pathway-resolved outputs wherever the available data allow.

Mechanistic constraints and data-driven correction

Hybridisation can occur at several levels. In a sequential configuration, a process-based or empirical model provides a baseline estimate and ML is trained on residual errors using meteorological, hydrological, optical or operational predictors. In a constrained-learning configuration, known physical relationships or feasible ranges are incorporated into the model structure or loss function. A third option is ensemble inference, in which several models contribute to a combined estimate weighted by their validation performance and domain similarity. For reservoir applications, the first two configurations are particularly attractive because they preserve a traceable baseline while allowing the model to respond to environmental conditions not represented adequately by static emission factors.
Explainability should be treated as part of validation rather than as a cosmetic post-processing step. Feature-attribution methods can identify whether predictions are controlled by variables that are scientifically plausible, such as temperature, organic-carbon availability, water level, residence time or catchment characteristics. Such diagnostics cannot prove causality, but they can reveal unstable or non-transferable model behaviour before estimates are used for reporting or planning. The model should also report whether a prediction lies within the environmental domain represented by the training data; extrapolation to novel climates or reservoir types should carry a correspondingly larger uncertainty.

A TIERED IMPLEMENTATION STRATEGY

Not every reservoir requires the same monitoring intensity. A practical programme can therefore be organised into three tiers (Figure 3). Tier 1 uses existing reservoir descriptors, climate data and Earth observation to generate screening estimates and identify systems likely to warrant additional attention. Tier 2 adds targeted field campaigns designed around seasons, spatial zones and emission pathways that contribute most to uncertainty. Tier 3 is reserved for high-priority reservoirs, where repeated or continuous observations support adaptive model

updating and formal MRV. Movement between tiers should be driven by uncertainty and decision relevance rather than reservoir size alone.

Figure 3 is intentionally illustrative rather than a new empirical result. It summarizes two recurring features reported across the reservoir literature: pronounced seasonal variation in methane pathways and substantial between-method dispersion. The purpose is to show why temporally sparse measurements and single-model estimates can produce different reservoir-scale conclusions, thereby motivating the hybrid framework proposed here.

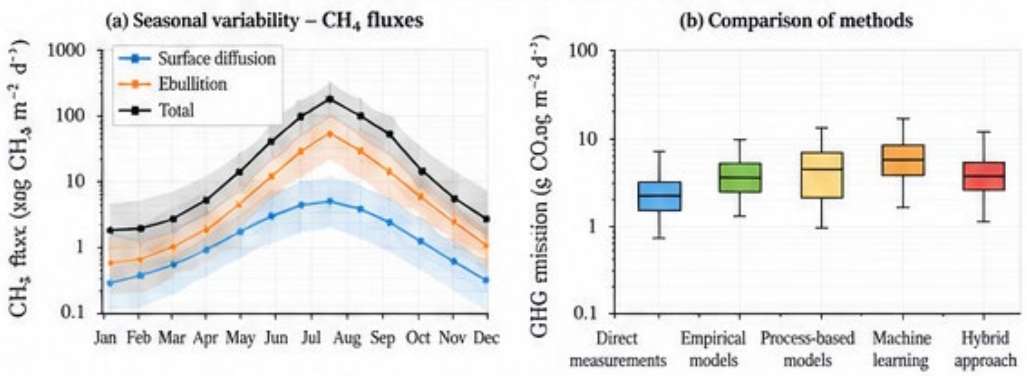


Fig. 3. *Schematic illustration of (a) seasonal variability in CH_4 emission pathways and (b) inter-method variability in reservoir GHG estimates. The graphical ranges are illustrative and are intended to represent patterns commonly reported in the literature rather than a quantitative meta-analysis*

Table 2. Suggested minimum information and outputs across implementation tiers.

Tier	Typical inputs	Field effort	Principal output	Decision use
1 Screening	Climate, morphology, catchment, operation, EO	None or legacy data	Prior emission range + hotspot/data-gap flag	Portfolio prioritisation
2 Targeted validations	Tier 1 + seasonal pathway-resolved measurements	Campaign-based	Calibrated site estimate + pathway uncertainty	Project assessment / model correction
3 Adaptive MRV	Tier 2 + repeated/continuous sensing and model updates	Long-term / adaptive	Time-resolved estimate + auditable uncertainty	Reporting, mitigation and operational management

DISCUSSION

The proposed framework differs from a conventional method-selection exercise in one important respect: it assumes from the outset that no single method should be expected to satisfy simultaneously the requirements for local accuracy, spatial representativeness, temporal resolution, interpretability and scalability. This position is consistent with the comparative synthesis of Seth et al. (2026), but the present framework translates that conclusion into an operational sequence. Measurements are not treated as an alternative to modelling; they constrain the model, test its failure modes and determine where subsequent observations should be placed. Conversely, models are not used merely to fill gaps; they organise the monitoring problem by indicating which variables, locations and periods are most informative.

The need for this iterative structure is reinforced by the magnitude and direction of model–measurement discrepancies reported in recent studies. Pilla et al. (2025) observed that the

same reservoir could appear differently depending on the emission pathway and data source, with particularly high uncertainty for ebullition and marked disagreement in CO_2 diffusion. Such results caution against validation based only on total CO_2-equivalent emissions. They also support spatially stratified sampling near inflows, shallow productive zones, deep-water areas and dam outlets, because these locations represent different biogeochemical and hydraulic controls. Long-term measurements are equally important where seasonality or episodic events dominate the annual budget.

Remote sensing and ML are valuable primarily because they can extend this sparse observational foundation. Satellite data can provide repeated information on reservoir extent, thermal conditions, catchment state and optically detectable water properties over large areas, while ML can integrate these variables with field and operational records. Nevertheless, remote sensing generally does not measure reservoir GHG flux directly, and a highly accurate statistical fit within the training dataset does not guarantee transferability to a new climatic or morphological domain. Hybrid models should therefore retain explicit provenance for every input, separate calibration from independent testing, and accompany predictions with uncertainty and applicability-domain information.

For hydropower planning, the benefit of improved quantification is not limited to more accurate inventories. Janus et al. (2025) showed that reservoir-emission modelling can be incorporated directly into project planning and portfolio optimisation, demonstrating that emissions information can influence infrastructure choices before impoundment. The same principle can be extended to existing reservoirs: pathway-resolved models can help identify whether mitigation should focus on organic-matter inputs, water-level management, turbine withdrawal depth, degassing zones or other operational controls. In this sense, a hybrid MRV system becomes not only an accounting tool but also a learning system for mitigation.

Several limitations should be recognised. First, the framework presented here is conceptual and does not prescribe a universal algorithm. The appropriate model architecture depends on the quantity and quality of available observations. Second, uncertainty cannot be eliminated through data fusion; poorly characterised inputs may instead propagate through several model layers. Third, methodological complexity must remain proportional to the decision being supported. A screening assessment for a large reservoir portfolio does not require the same monitoring density as a site-specific carbon-accounting study. The tiered structure is intended to make that distinction explicit.

CONCLUSION

Reliable reservoir GHG quantification requires a transition from isolated methods toward an integrated measurement–model system. Field observations provide the empirical anchor, mechanistic models preserve process consistency, Earth observation expands environmental coverage, and data-driven methods support nonlinear scaling across space and time. Their combination is most useful when validation remains pathway-specific, uncertainty is propagated transparently and model applicability is checked before extrapolation.

The three-tier strategy proposed here offers a practical route from broad screening to targeted validation and adaptive MRV. Its central principle is iterative: observations constrain models, model diagnostics direct new observations, and both are updated as reservoir conditions and available data evolve. Such a framework can improve the credibility of reservoir carbon accounting while keeping monitoring effort aligned with decision relevance. Future work should test the architecture across contrasting climatic regions and reservoir types using harmonised, openly documented datasets and independent validation periods.

ACKNOWLEDGEMENTS

This research has been supported by the Ministry of Science, Technological Development and Innovation (No. 451-03-33/2026-03/200156), the Faculty of Technical Sciences (No. 115001-3394/1), HORIZON-MSCA-2021-SE-01, REMARKABLE (No. 101086387), and by the

Autonomous Province of Vojvodina (No. 003870771 2025 09418 003 000 000 001 and 002497912 2026 09418 002 000 000 001 04 006).

REFERENCES

Deemer, B. R., Harrison, J. A., Li, S., Beaulieu, J. J., DelSontro, T., Barros, N., Bezerra-Neto, J. F., Powers, S. M., dos Santos, M. A., & Vonk, J. A. (2016). Greenhouse gas emissions from reservoir water surfaces: A new global synthesis. *BioScience*, 66(11), 949–964. https://doi.org/10.1093/biosci/biw117

Ion, I. V., & Ene, A. (2021). Evaluation of greenhouse gas emissions from reservoirs: A review. *Sustainability*, 13(21), 11621. https://doi.org/10.3390/su132111621

Janus, T., Barry, C., Win, S., & Kuriakose, J. (2025). Planning with emission models reduces the carbon footprint of new reservoirs. *Communications Earth & Environment*, 6, 953. https://doi.org/10.1038/s43247-025-02899-6

Pilla, R. M., Griffiths, N. A., Hansen, C., Turner, D., Fortner, A. M., Jett, R. T., Jones, M. W., Jones, N. J., & Phillips, J. R. (2025). Comparison of greenhouse gas emission estimates from six hydropower reservoirs using modeling versus field surveys. *Biogeochemistry*, 168, 28. https://doi.org/10.1007/s10533-025-01211-0

Prairie, Y. T., Mercier-Blais, S., Harrison, J. A., Soued, C., del Giorgio, P. A., Harby, A., Alm, J., Chanudet, V., & Nahas, R. (2021). A new modelling framework to assess biogenic GHG emissions from reservoirs: The G-res tool. *Environmental Modelling & Software*, 143, 105117. https://doi.org/10.1016/j.envsoft.2021.105117

Seth, M., Ubierna Aparicio, M., Nakomcic-Smaragdakis, B., Brboric, M., Calamita, E., Dasic, T., Diez Santos, C., & Patro, E. R. (2026). A review of hydropower reservoir GHG estimation methods. *Renewable and Sustainable Energy Reviews*, 233, 116859. https://doi.org/10.1016/j.rser.2026.116859

Shi, W., Wu, W., Fan, H., Sun, Q., Niu, X., Wang, S., Li, S.-L., Liang, S., & Yan, Z. (2025). Estimating CO_2 and CH_4 fluxes from reservoirs: Model development and site-level study. *Journal of Hydrology*, 132794. https://doi.org/10.1016/j.jhydrol.2025.132794

DOI:10.5937/IIZS26326R

FAULT TREE ANALYSIS OF A CO_2-EOR INJECTION SYSTEM

Review paper

Branislava Radišić[1*], Slavica Prvulović[2], Snežana Filip[3], Borivoj Novaković[4], Milan Marković[5]

[1,2,3,4,5,6]University of Novi Sad, Technical Faculty "Mihajlo Pupin", Zrenjanin, Serbia

Abstract: The application of CO_2 for enhanced oil recovery requires reliable operation of the injection system and the integrity of its technical and geological components. The aim of this study is to systematically identify potential causes and failure events that may lead to the loss of safe and effective CO_2 injection in a CO_2-EOR system. Based on a review of relevant scientific literature and the defined system boundaries, a qualitative Fault Tree Analysis (FTA) model was developed. The top event was divided into two main groups of events: loss of effective injection capability and loss of safe CO_2 containment during injection. The developed model includes surface, wellbore, reservoir, and geomechanical failure pathways, including CO_2 supply and compression problems, corrosion, loss of injectivity, loss of well barrier integrity, and unfavorable reservoir pressure response. The results show that FTA enables different failure mechanisms to be integrated into a structured cause-and-effect model and provides a basis for their further quantitative assessment and prioritization.
Key words: CO_2-EOR, Fault Tree Analysis, injection system, well integrity, failure analysis

INTRODUCTION

The application of CO_2 for enhanced oil recovery (CO_2-EOR) is based on the injection of CO_2 into an oil reservoir to improve oil mobility and increase ultimate oil recovery. In addition to its role in oil production, part of the injected CO_2 may remain stored in the reservoir, which is why CO_2-EOR is also considered in the broader context of reducing carbon dioxide emissions (Novak Mavar et al., 2021).

Safe and effective CO_2 injection depends on the reliable operation of the surface injection system, the maintenance of reservoir injectivity and injection well integrity, and an appropriate geomechanical response of the system.Maintaining the integrity of well barriers is particularly important, as they are exposed to changes in pressure and temperature, as well as chemical and mechanical effects during CO_2 injection (Iyer et al., 2022). The variety of potential failure mechanisms highlights the need for their systematic identification and cause-and-effect analysis.

Fault Tree Analysis (FTA) enables the deductive decomposition of an undesired top event into lower-level events and causes. FTA has previously been applied to identify potential CO_2 leakage pathways and mechanisms in oil reservoirs, with CO_2 leakage considered as the top event (Wang et al., 2020). However, the safe operation of a CO_2-EOR injection system depends not only on preventing leakage, but also on maintaining CO_2 supply and injection capability, reservoir injectivity, and the integrity of technical and geological barriers.

The aim of this study is to systematically identify potential causes and failure events based on published scientific literature and the defined boundaries of the CO_2-EOR injection system, and to develop a qualitative fault tree model for the top event "Loss of Safe and Effective CO_2 Injection in a CO_2-EOR System."

MATERIAL AND METHODS

CO_2-EOR System and Scope of the Analysis

CO_2-EOR is a process in which CO_2 is injected into an oil reservoir to mobilize the remaining oil and increase ultimate oil recovery. Within the broader process chain, CO_2-EOR includes CO_2 supply and preparation, injection into the reservoir, fluid production, surface separation

[1] Corresponding author, branislava.radisic@uns.ac.rs, ORCID: 0009-0007-3664-2012
[2]slavica.prvulovic@uns.ac.rs,0000-0001-6353-7145
[3]snezana.filip@uns.ac.rs, ORCID: 0000-0003-4113-9247
[4]borivoj.novanovic@uns.ac.rs, ORCID: 0000-0003-2816-3584
[5]milan.markovic@uns.ac.rs, ORCID: 0009-0007-8130-7467

and the separation and reinjection of produced CO_2. The produced gas, which mainly consists of CO_2 and associated natural gas, can be reinjected to maintain reservoir pressure, while the broader CO_2-EOR chain covers processes from CO_2 supply and transportation to oil field operations and subsequent handling of the produced oil (Jabbar et al., 2025).
For the purposes of this study, only the part of the system directly related to safe and effective CO_2 injection was analyzed. The system boundary begins with the receipt of CO_2 at the EOR site, i.e., at the end of the transportation system, followed by distribution, additional compression, measurement and control, and delivery of CO_2 to the injection wells. A typical surface injection system at a CO_2-EOR site includes a distribution manifold at the end of the transportation pipeline, distribution pipelines to the wells, additional compression, measurement and control systems, and injection wells (Novak Mavar et al., 2021). The designed injection pressure and flow rate are related to reservoir characteristics and surface facility requirements and are therefore relevant parameters in defining the injection system (Kristanto et al., 2020).
Downstream of the surface facilities, the scope of the analysis includes the injection well and its barriers, including tubing, casing, packer, and cement isolation, as well as the target reservoir and the directly relevant geological containment system. Including these elements makes it possible to consider well integrity, CO_2 injectivity into the reservoir, and the geomechanical response of the system, in addition to CO_2 supply and injection capability. Maintaining well integrity is particularly important during CO_2 injection because injection wells are exposed to changes in pressure and temperature, as well as chemical and mechanical effects that may reduce the effectiveness of well barriers. Tubing, casing, packer, and cement are important components for maintaining injection well integrity (Iyer et al., 2022).
In accordance with the aim of the study, CO_2 capture at the industrial source and the main transportation system upstream of the EOR site were excluded from the FTA, as were production wells, surface separation of produced fluids, recycling of produced CO_2, transportation and processing of crude oil, and its end use. Although these processes are part of the broader CO_2-EOR process chain, their inclusion would extend the analysis beyond the functional scope defined by the top event. Based on these boundaries, the analyzed system includes surface CO_2 supply and injection control, the injection well and its barriers, CO_2 injectivity into the target reservoir, and geomechanical containment, providing the basis for the development of the qualitative FTA model.

Fault Tree Analysis Methodology

A qualitative Fault Tree Analysis (FTA) was applied to systematically organize potential events and cause-and-effect pathways that may lead to the loss of safe and effective CO_2 injection in a CO_2-EOR system. The analysis was based on a review of relevant scientific literature and functional decomposition of the analyzed system.
FTA is a deductive approach to failure analysis that starts with a defined undesired top event and then identifies lower-level events and their logical relationships that may lead to its occurrence (Adamović&Radovanović, 2008; Wang et al., 2020).
After defining the system boundaries, the top event, "Loss of Safe and Effective CO_2 Injection in a CO_2-EOR System," was successively decomposed into lower-level events. The developed model includes the top event (T), intermediate events (G), basic events (P), and undeveloped events (S). Undeveloped events were used when an event was relevant to the analyzed system, but further decomposition was not justified by the available information or the defined scope of the analysis.
The causal relationships between events were represented using logical AND and OR gates. An OR gate was used when the occurrence of any of the input events was sufficient to cause the higher-level event, while an AND gate was used when all defined input events had to occur for the higher-level event to occur (Adamović&Radovanović, 2008). The selection of logical relationships in the developed FTA model was based on the physical meaning of the analyzed mechanisms and their cause-and-effect relationships.

The developed FTA model was used for the qualitative identification and structuring of potential failure pathways. Quantitative estimation of the probability of the top event was not included in this study.

RESULTS AND DISCUSSION

Based on the defined system boundaries and the identified potential failure pathways, a qualitative FTA model of the CO_2-EOR injection system was developed. The developed fault tree is shown in Figure 1, while the event labels and names are provided in Table 1.

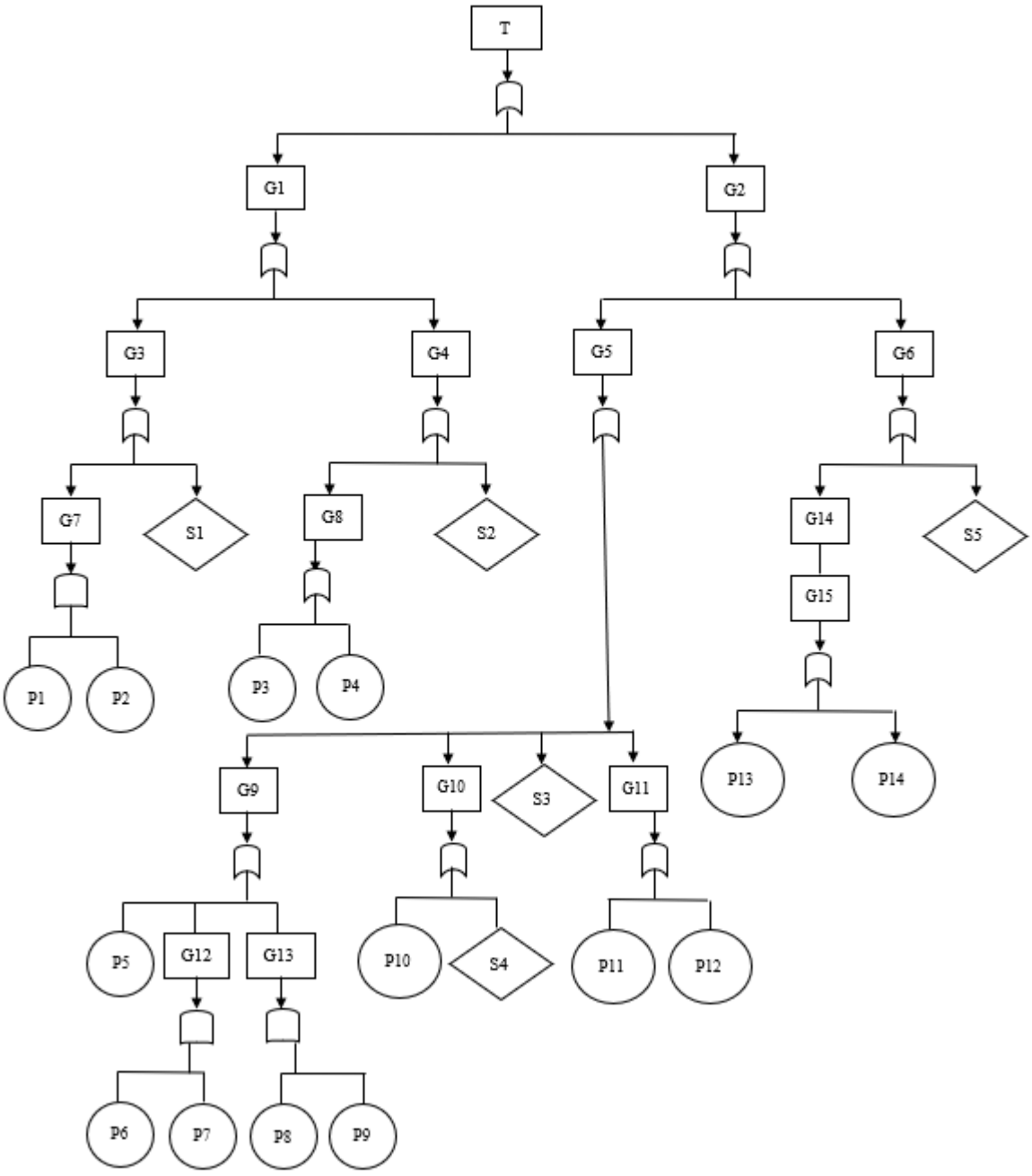


Fig. 1. *Fault tree for the loss of safe and effective CO_2 injection in a CO_2-EOR system*

Table 1. *Event labels and names in the developed FTA model*

Label	Event name
T	Loss of safe and effective CO_2 injection in a CO_2-EOR system
G1	Loss of effective CO_2 injection capability
G2	Loss of safe CO_2 containment during injection
G3	Loss of CO_2 supply / required injection pressure and flow rate
G4	Loss of reservoir injectivity
G5	Loss of injection well integrity
G6	Loss of geomechanical containment due to injection
G7	Corrosion-induced loss of integrity / flow capacity of the surface CO_2 pipeline
G8	Formation damage / near-wellbore plugging
G9	Loss of tubing integrity
G10	Loss of casing integrity
G11	Loss of cement isolation / zonal isolation
G12	Stress-corrosion cracking of tubing
G13	Tubing damage due to freezing at low temperature
G14	Hydraulic fracturing of the containment system due to injection
G15	Excessive reservoir pressure increase
P1	Presence of water / free water phase
P2	Exposure of carbon steel to CO_2-containing fluid
P3	Clay migration / geochemical fluid incompatibility
P4	Precipitate formation due to water–rock reactions / plugging
P5	Progressive CO_2 corrosion of tubing / wall thickness reduction
P6	Corrosive CO_2 environment with an aqueous phase
P7	Mechanical stress / combined loading
P8	Low-temperature CO_2 injection causing cooling below the freezing point
P9	Presence of freezable liquid in the annulus
P10	Casing corrosion progressing to wall penetration
P11	Poor cement placement / initial defects in the cement barrier
P12	Long-term CO_2 degradation of a previously compromised cement barrier
P13	Excessive / inappropriate injection pressure or flow rate
P14	Limited pressure dissipation / unfavorable reservoir pressure response
S1	Loss of compressor capability
S2	Asphaltene deposition impairing injectivity
S3	Loss of packer / annular isolation
S4	Thermomechanical casing failure at low temperature
S5	Activation / opening of existing faults or fractures due to injection-induced changes in pressure and stress state

The top event (T) was defined as the loss of safe and effective CO_2 injection in a CO_2-EOR system and was decomposed into the loss of effective injection capability (G1) and the loss of safe CO_2 containment during injection (G2). This division is based on the functional analysis performed in this study and allows separate consideration of events that affect the designed injection conditions and events that compromise CO_2 containment.

The loss of effective injection capability (G1) includes the loss of CO_2 supply and the required injection pressure and flow rate (G3), as well as the loss of reservoir injectivity (G4). The surface facilities of a typical CO_2-EOR injection system include CO_2 distribution, pipelines to injection wells, additional compression, and measurement and control systems (Novak Mavar et al., 2021), while the reliability of CO_2 infrastructure and supply is recognized as one of the technological limitations of the CO_2-EOR process (Morenov&Shchigolev, 2026). Within G3, corrosion-induced loss of integrity or flow capacity of the surface pipeline (G7) is associated with the presence of a water phase (P1) and exposure of carbon steel to

CO_2-containing fluid (P2), since the presence of water and wetting of the steel surface are key conditions for CO_2 corrosion (Wang et al., 2019). Loss of compressor capability (S1) was retained as an undeveloped event because a detailed analysis of compressor failures was outside the defined scope of this study.

The loss of reservoir injectivity (G4) is associated with formation damage and near-wellbore plugging (G8), as well as asphaltene deposition (S2). Water–rock reactions may contribute to precipitate formation and plugging (Huo et al., 2023), while formation damage and injectivity problems have also been reported from experience with geological CO_2 storage and CO_2-EOR operations (Iyer et al., 2022). Changes in pressure and system composition during contact between CO_2 and crude oil may affect asphaltene stability, and depending on the conditions, CO_2 may increase or decrease the tendency for asphaltene precipitation (Huang et al., 2026). Therefore, asphaltene deposition was treated in the model as a separate but undeveloped pathway leading to loss of injectivity.

The second main branch (G2) includes the loss of injection well integrity (G5) and the loss of geomechanical containment due to injection (G6). Well integrity involves controlled injection while preventing unwanted fluid migration. During CO_2 injection, well barriers are exposed to chemical and mechanical loads, changes in temperature and pressure, and CO_2–brine interactions with well components (Iyer et al., 2022).Therefore, in the developed model, G5 includes loss of tubing integrity (G9), casing integrity (G10), packer/annular isolation (S3), and cement or zonal isolation (G11).

For the tubing, progressive CO_2 corrosion (P5), stress-corrosion cracking (G12), and low-temperature damage (G13) were identified. The combined effect of a corrosive environment and mechanical stress provides the basis for linking a corrosive CO_2 environment with an aqueous phase (P6) and mechanical loading (P7) through an AND gate (Li et al., 2026). A separate, conditional mechanism is the freezing of liquid in the annulus during low-temperature liquid CO_2 injection, where volume expansion and the resulting frost-heave load may lead to tubing and casing failure (Chen et al., 2019). Therefore, this pathway does not represent a universal CO_2-EOR failure mechanism, but rather a scenario that depends on suitable temperature conditions and the presence of liquid that can freeze.

For the casing, corrosion progressing to wall penetration (P10) was identified in addition to low-temperature thermomechanical failure (S4). Studies from the Weyburn CO_2-EOR project reported corrosion damage ranging from small pits to complete casing wall penetration, with possible contributing factors including exposure to injected and formation fluids, CO_2, and conditions in the perforated zone (Laumb et al., 2016). These findings support the relevance of the corrosion pathway in the model but do not justify attributing all observed damage solely to CO_2. Loss of packer/annular isolation (S3) was retained as an undeveloped event, while G11 includes initial defects in the cement barrier (P11) and long-term CO_2 degradation of a previously compromised cement barrier (P12).

The geomechanical branch (G6) includes hydraulic fracturing of the containment system (G14) and the activation or opening of existing faults and fractures (S5). G14 is associated with an excessive increase in reservoir pressure (G15), which may result from inappropriate injection pressure or flow rate (P13) or limited pressure dissipation and an unfavorable reservoir pressure response (P14). Pressure changes during injection are an important factor in geomechanical stability and may be associated with the formation of new fractures or the reactivation of existing fractures and migration pathways (Wang et al., 2020; Shah et al., 2024). However, an increase in pressure does not automatically result in fracturing; geomechanical failure depends on whether the local threshold determined by the properties of the reservoir and containment system is reached.

Overall, the developed FTA shows that the loss of safe and effective CO_2 injection may occur through different but functionally related surface, wellbore, reservoir, and geomechanical pathways. The model enables their systematic identification and cause-and-effect structuring, but it does not rank the events according to risk level because quantitative failure probabilities were not determined.

CONCLUSION

A qualitative FTA model was developed to identify and systematically organize potential pathways that may lead to the loss of safe and effective CO_2 injection in a CO_2-EOR system. By defining the system boundaries and functionally decomposing the top event, two main groups of failures were identified: loss of effective injection capability and loss of safe CO_2 containment during injection.

The developed fault tree shows that the top event may occur through different surface, wellbore, reservoir, and geomechanical pathways. The identified events include problems with CO_2 supply and compression, corrosion, loss of injectivity, loss of well barrier integrity, and pressure changes that may compromise geomechanical containment. The main value of the developed model is that it integrates these different failure mechanisms into a single cause-and-effect structure focused on safe and effective CO_2 injection.

Since the analysis is qualitative, the model does not provide the probability of the top event or rank individual pathways according to risk level. However, the developed FTA structure can provide a basis for further research focused on quantitative assessment and prioritization of the identified failures.

REFERENCES

Novak Mavar, K., Gaurina-Medimurec, N., &Hrnčević, L. (2021). Significance of enhanced oil recovery in carbon dioxide emission reduction. Sustainability, 13(4), 1800. https://doi.org/10.3390/su13041800

Iyer, J., Lackey, G., Edvardsen, L., Bean, A., Carroll, S. A., Huerta, N., Smith, M. M., Torsæter, M., Dilmore, R. M., &Cerasi, P. (2022). A review of well integrity based on field experience at carbon utilization and storage sites. International Journal of Greenhouse Gas Control, 113, 103533. https://doi.org/10.1016/j.ijggc.2021.103533

Wang, Y., Zhang, L., Ren, S., Ren, B., Chen, B., & Lu, J. (2020). Identification of potential CO_2 leakage pathways and mechanisms in oil reservoirs using fault tree analysis. Greenhouse Gases: Science and Technology, 10, 331–346. https://doi.org/10.1002/ghg.1959

Jabbar, M. Y., McCoy, S. T., Masnadi, M. S., &Bergerson, J. A. (2025). Toward consistent evaluation of CO_2-EOR: A meta-analysis of life cycle assessments. International Journal of Greenhouse Gas Control, 146, 104430. https://doi.org/10.1016/j.ijggc.2025.104430

Kristanto, D., Hermawan, Y. D., Hariyadi, & Yusuf, Y. (2020). Integrated simulation system of CO_2 gas injection application for enhanced oil recovery in the oil field. Journal of Petroleum Exploration and Production Technology, 10, 3917–3923. https://doi.org/10.1007/s13202-020-00955-9

Adamović, Ž., Radovanović, Lj. (2008). Pouzdanostmašina. Univerzitet u Novom Sadu, Tehničkifakultet „Mihajlo Pupin", Zrenjanin.

Morenov, V. A., &Shchigolev, K. V. (2026). CO_2 injection for enhanced oil recovery: A review of existing methods, challenges and promising solutions. Advances in Geo-Energy Research, 20(2), 163–179. https://doi.org/10.46690/ager.2026.05.05

Wang, Z. M., Song, G.-L., & Zhang, J. (2019). Corrosion control in CO_2 enhanced oil recovery from a perspective of multiphase fluids. Frontiers in Materials, 6, 272. https://doi.org/10.3389/fmats.2019.00272

Huo, H., Liu, D., Tao, L., Wang, D., Song, C., & He, S. (2023). Integrity challenges and countermeasures of the offshore CCUS based on CO_2-EOR. Petroleum Drilling Techniques, 51(2), 74–80. https://doi.org/10.11911/syztjs.2023009

Huang, Y., Liang, Y., Tsuji, T., Cui, W., Masuda, Y., Matsuoka, T., Boek, E. S., Suzuki, T., &Takabayashi, K. (2026). Prediction of asphaltene deposition risk in CO_2-EOR using Hansen

solubility parameters by molecular dynamics simulation. Fuel, 404, 136359. https://doi.org/10.1016/j.fuel.2025.136359

Li, Q., Wang, D., Zhang, H., Li, J., Lian, W., Yang, H., & Jiang, B. (2026). Study on the stress-corrosion failure of tubing in CO_2-EOR wellbores. Engineering Failure Analysis, 185, 110369. https://doi.org/10.1016/j.engfailanal.2025.110369

Chen, S., Wang, H., Liu, Y., Lan, W., Lv, X., Sun, B., & Yuan, D. (2019). Root cause analysis of tubing and casing failures in low-temperature carbon dioxide injection well. Engineering Failure Analysis, 104, 873–886. https://doi.org/10.1016/j.engfailanal.2019.05.034

Laumb, J. D., Glazewski, K. A., Hamling, J. A., Azenkeng, A., & Watson, T. L. (2016). Wellbore corrosion and failure assessment for CO_2 EOR and storage: Two case studies in the Weyburn field. International Journal of Greenhouse Gas Control, 54, 479–489. https://doi.org/10.1016/j.ijggc.2016.08.031

Shah, M. S., Khan, F., Zendehboudi, S., &Mamudu, A. (2024). An integrated model to investigate optimized CO_2 utilization and risk mitigation in offshore hydrocarbon reservoirs. Geoenergy Science and Engineering, 234, 212589. https://doi.org/10.1016/j.geoen.2023.212589



XVI International Conference Industrial Engineering and Environmental Protection 2026 (IIZS 2026)
October 01-02, 2026, Zrenjanin, Serbia

Session 5

Engineering Management

DOI:10.5937/IIZS26334D

INDUSTRY 5.0 AS A DRIVER OF SUSTAINABLE INDUSTRIAL DEVELOPMENT

Review paper

Mirjana Dunić
Technical Faculty "Mihajlo Pupin", Zrenjanin, University of Novi Sad, Serbia

Abstract: This paper examines Industry 5.0 as a framework for sustainable industrial development, with particular emphasis on how the technological capabilities of Industry 4.0 can support human-centricity, environmental sustainability, and industrial resilience. The study adopts a literature-based evidence synthesis to examine positive and negative sustainability implications of Industry 4.0 across economic, environmental, and social dimensions and at micro, meso, and macro levels. The evidence base discussed in the paper draws, in particular, on the content-centric literature synthesis reported by Ghobakhloo et al. (2024), which identified 527 eligible articles through an initial database search and subsequent backward and forward citation screening. The present paper does not reproduce that database search or claim the 527 articles as an independently collected empirical dataset. Instead, the reported evidence is critically synthesized and interpreted in relation to the sustainability-oriented principles of Industry 5.0. The reviewed evidence highlights the potential of digital technologies to improve productivity, resource efficiency, cleaner production, circularity, innovation, and supply-chain resilience, while also identifying challenges related to energy consumption, cybersecurity, technological dependency, workforce adaptation, and social inclusion. Previous research employing Hesitant-Fuzzy Interpretive Structural Modelling (HF-ISM) and MICMAC analysis is reviewed to illustrate approaches for examining interrelationships among sustainability-oriented functions relevant to the transition toward Industry 5.0. The findings indicate that Industry 5.0 extends the technological foundations of Industry 4.0 by integrating advanced technologies with human-centric, environmental, and resilience-oriented objectives. The paper contributes to the literature by synthesizing existing evidence on the relationship between Industry 4.0 capabilities and the broader sustainability principles of Industry 5.0 and by distinguishing the literature-derived evidence and methodological approaches from the original contribution of the present review.
Key words: Industry 5.0, Industry 4.0, Sustainability, Digitalisation, Human-centricity, Resilience, Digital transformation.

INTRODUCTION

Industry 5.0 has attracted increasing attention as an emerging framework for sustainable industrial development. It builds on the technological foundations of Industry 4.0 while extending the focus of industrial transformation toward human-centricity, sustainability, and resilience (Ghobakhloo et al., 2022; Ivanov, 2023). While Industry 4.0 primarily emphasizes digitalization, automation, connectivity, and operational efficiency, Industry 5.0 integrates these technological capabilities with human, environmental, and organizational considerations. Technologies such as artificial intelligence, collaborative robotics, digital twins, and cyber-physical systems can contribute to environmental, social, and economic objectives when appropriately integrated into industrial systems (Ghobakhloo et al., 2023a; Baig & Yadegaridehkordi, 2024).

The contribution of Industry 5.0 to sustainable industrial development depends on the interaction between technological capabilities, human competencies, organizational practices, environmental objectives, and resilience. Effective governance and appropriate organizational and policy frameworks are therefore important for realizing the potential benefits of digitalization while addressing associated environmental and social risks (Ghobakhloo et al., 2022; Karmaker et al., 2023). Existing research indicates that Industry 4.0 technologies can improve productivity, resource optimization, sustainable operations, and innovation, but their effects are not exclusively positive. Digital inequality, technological dependency, cybersecurity risks, workforce adaptation, and other organizational and societal

Corresponding author, mirjana.dunic.as@gmail.com , ORCID: 0009-0003-7202-2401

challenges may influence sustainability outcomes (Yavuz et al., 2023; Ghobakhloo et al., 2024).

These considerations have contributed to the development of Industry 5.0 as a broader socio-technical perspective on industrial transformation. Rather than replacing Industry 4.0, Industry 5.0 builds upon its technological capabilities and redirects them toward human-centric, sustainable, and resilient industrial systems (Ivanov, 2023; Ghobakhloo et al., 2024). Recent studies emphasize the complementary relationship between the two paradigms and examine how advanced digital technologies can support environmental sustainability, human well-being, supply-chain resilience, and sustainable manufacturing (van Erp et al., 2024; Shabur et al., 2025).

Accordingly, this paper examines the relationship between Industry 4.0 capabilities and the sustainability-oriented principles of Industry 5.0, with emphasis on advanced technologies, human-centric approaches, environmental sustainability, and industrial resilience. The objectives are: (1) to synthesize existing evidence concerning the economic, environmental, and social implications of Industry 4.0 technologies for sustainable industrial development; and (2) to examine how sustainability-oriented functions identified in previous research relate to the human-centric, sustainable, and resilient principles of Industry 5.0.

The paper adopts a literature-based evidence synthesis and does not present a new empirical HF-ISM or MICMAC investigation. In particular, the evidence base of 527 articles discussed in this paper is derived from the content-centric literature synthesis reported by Ghobakhloo et al. (2024). That study used Scopus and Web of Science for the initial identification of relevant literature, followed by backward and forward citation screening, resulting in a final pool of 527 eligible articles. The present paper does not claim to have independently repeated that search or generated the original screening dataset. Instead, the reported evidence is used as a literature-based foundation for the present synthesis and interpretation.

The distinction between the source study and the present paper is particularly important with regard to HF-ISM. Ghobakhloo et al. (2024) independently identified sustainability functions of Industry 4.0 and subsequently applied an HF-ISM approach based on expert input to examine their interrelationships. The present paper does not reproduce that expert-based procedure, questionnaire, relationship matrix, hierarchical modelling, or MICMAC calculations. These elements are therefore treated as findings and methodological approaches reported in the existing literature rather than as original empirical results of the present study.

The contribution of the present paper therefore lies in synthesizing and interpreting existing knowledge rather than in the independent collection of expert data or the original application of HF-ISM. This distinction enables the findings discussed in the paper to be clearly separated from methodological procedures and analytical results reported in previous studies.

The paper contributes to the existing literature by bringing together evidence concerning the economic, environmental, and social dimensions of Industry 4.0 and relating these dimensions to the three central principles of Industry 5.0: human-centricity, sustainability, and resilience. Particular attention is given to the potential contribution of digital technologies to innovation, resource efficiency, supply-chain optimization, circular economy practices, risk management, and real-time communication, while also considering technological, environmental, organizational, and social challenges.

Background

Industry 5.0 represents an emerging industrial paradigm that builds on the technological foundations of Industry 4.0 while integrating advanced technologies with human capabilities, sustainability, and industrial resilience. Unlike Industry 4.0, which primarily emphasizes digitalization, automation, connectivity, and productivity, Industry 5.0 extends these technological capabilities toward environmental responsibility, human well-being, and long-term resilience (Ghobakhloo et al., 2022; Ivanov, 2023). Its emergence reflects the

recognition that technology-oriented industrial transformation alone does not fully address the social and environmental dimensions of sustainable development. Industry 5.0 therefore provides a broader socio-technical framework that combines technological advancement with sustainability, resilience, and human-centric principles (Huang et al., 2022; Baig & Yadegaridehkordi, 2024).

The European Commission conceptualizes Industry 5.0 as complementary to Industry 4.0 and emphasizes three interconnected principles: human-centricity, sustainability, and resilience. These principles extend the focus of industrial transformation beyond technological and economic performance by incorporating environmental responsibility, human well-being, social considerations, and the capacity of industrial systems to respond to disruptions and changing conditions (Renda et al., 2021). Industry 5.0 relies on Industry 4.0 technologies, including artificial intelligence, the Internet of Things, digital twins, and collaborative robotics. These technologies can support flexible production, resource optimization, predictive decision-making, human–machine collaboration, and organizational resilience. However, their contribution to sustainable industrial development depends on appropriate organizational, regulatory, and governance conditions and on their responsible integration with human and societal needs (Ghobakhloo et al., 2023; Ooi et al., 2023). Thus, Industry 5.0 extends rather than replaces Industry 4.0 by directing digital transformation toward sustainable, human-centric, and resilient industrial systems.

The present paper adopts a literature-based evidence synthesis to examine the relationship between Industry 4.0 capabilities and the sustainability-oriented principles of Industry 5.0. The synthesis draws primarily on previously published research rather than on a newly conducted independent systematic literature search. In particular, the paper uses the content-centric literature synthesis reported by Ghobakhloo et al. (2024) as an important evidence base for examining the sustainability implications of Industry 4.0. That study identified a final pool of 527 eligible articles through its own literature identification and citation-screening procedures. The present paper does not claim these 527 articles as an independently collected empirical dataset and does not reproduce the original search and screening process.

Accordingly, the search strategy, screening procedure, and article counts reported for the 527-article evidence base are attributed to the source study. The present paper uses the published evidence and findings as a basis for a further literature-based synthesis focused specifically on the relationship between Industry 4.0 capabilities and the human-centric, sustainable, and resilient principles of Industry 5.0. This distinction is important because the purpose of the present study is not to reproduce the original bibliographic search but to synthesize and interpret previously reported evidence from the perspective of Industry 5.0.

The source literature considers sustainability through economic, environmental, and social dimensions and examines the implications of Industry 4.0 at different levels of analysis. Building on these perspectives, the present synthesis considers the potential positive and negative implications of digital technologies for sustainable industrial development. Particular attention is given to resource efficiency, productivity, innovation, circularity, environmental management, supply-chain resilience, human–machine collaboration, workforce development, and social inclusion, while also considering challenges related to energy consumption, cybersecurity, technological dependency, technological obsolescence, workforce adaptation, and digital inequality.

The literature indicates that Industry 4.0 technologies may contribute to economic sustainability by improving productivity, operational efficiency, resource utilization, innovation, and supply-chain coordination. At the same time, these benefits may require substantial investment in digital infrastructure, cybersecurity, employee training, and organizational transformation. Environmental contributions include resource optimization, waste reduction, intelligent manufacturing, real-time monitoring, and improved management of material and energy flows. However, digital infrastructures and interconnected technologies may also generate additional energy requirements, electronic waste, technological complexity, and circularity challenges. Social implications include opportunities for human–machine collaboration, employee development, upskilling, reskilling, and

improved working conditions, alongside potential concerns regarding privacy, data protection, changing job requirements, and unequal digital competencies.

These dimensions are relevant to the three principles of Industry 5.0. Economic and organizational capabilities contribute to industrial resilience and adaptability; environmental efficiency and circularity support the sustainability principle; and human–machine collaboration, skills development, participation, and employee well-being contribute to human-centricity. The relationship among these dimensions is therefore considered in the present paper as an integrated socio-technical issue rather than as a purely technological transition.

The evidence synthesis reported in the source literature also provides a basis for considering sustainability functions across micro-, meso-, and macro-levels. At the micro level, digital technologies can influence organizational productivity, production processes, resource use, working conditions, and employee capabilities. At the meso level, their effects extend to supply chains, industrial networks, business models, and inter-organizational collaboration. At the macro level, digital transformation may influence industrial development, innovation ecosystems, regional competitiveness, public policy, and broader sustainability transitions. These levels are considered in the present review to provide a structured interpretation of how Industry 4.0 capabilities may contribute to Industry 5.0 objectives.

The main conceptual stages used to organize the present literature-based synthesis are illustrated in Fig. 1. The figure should be understood as a representation of the analytical organization of the literature reviewed in this paper and not as a reproduction of an independently conducted systematic-review workflow.

The literature analyzed in the present synthesis therefore serves two complementary purposes. First, it provides evidence concerning the sustainability implications of Industry 4.0 technologies. Second, it provides a conceptual basis for interpreting these implications in relation to the human-centricity, sustainability, and resilience principles of Industry 5.0. The synthesis does not claim that all identified effects are universal or automatically generated by technological adoption. Rather, the reviewed literature indicates that sustainability outcomes depend on technological choices, organizational capabilities, human competencies, infrastructure, governance, and implementation context.

Evidence Synthesis Approach

The present study is designed as a literature-based evidence synthesis rather than as an independently conducted systematic literature review or empirical investigation. Its methodological purpose is to synthesize and interpret previously published evidence concerning the sustainability implications of Industry 4.0 and their relevance to Industry 5.0.

A central source for the evidence considered in this paper is the content-centric literature synthesis reported by Ghobakhloo et al. (2024). In that study, the authors conducted the literature identification and screening process and reported a final evidence base of 527 eligible articles. The source study used database searching followed by backward and forward citation screening. Because the present paper does not independently reproduce that search, the search dates, database-specific search strings, original screening decisions, and article-level coding underlying the 527-article dataset are not presented as procedures conducted by the authors of the present paper. They are treated as methodological characteristics of the source study.

The distinction between the source study and the present review is essential. The 527 articles represent the evidence base reported by Ghobakhloo et al. (2024), whereas the present paper uses the findings reported in that literature synthesis as a foundation for a focused interpretation of Industry 4.0 capabilities in relation to Industry 5.0. Consequently, the numerical screening counts associated with the source study should not be interpreted as original screening results generated by the present research.

The present synthesis follows a structured thematic interpretation of the published evidence. The literature is organized according to three sustainability dimensions—economic, environmental, and social—and three levels of analysis—micro, meso, and macro. Within

this structure, particular attention is given to the contribution of Industry 4.0 technologies to human-centricity, environmental sustainability, and industrial resilience. Positive contributions and potential adverse implications are considered together to avoid treating digital transformation as inherently sustainable.

The synthesis focuses on recurring themes reported in the literature, including productivity, resource efficiency, innovation, circular production, environmental monitoring, energy management, supply-chain resilience, human–machine collaboration, skills development, organizational adaptation, cybersecurity, technological dependency, and social inclusion. These themes are interpreted in relation to the three principles of Industry 5.0 rather than statistically aggregated or independently validated through a new empirical dataset.

The analytical procedure can therefore be summarized in four stages: (1) identification of relevant previously published evidence, with particular reliance on the literature synthesis reported by Ghobakhloo et al. (2024); (2) organization of reported findings according to economic, environmental, and social sustainability dimensions and micro-, meso-, and macro-levels; (3) thematic interpretation of the identified sustainability-related functions of Industry 4.0; and (4) interpretation of these functions in relation to the human-centricity, sustainability, and resilience principles of Industry 5.0.

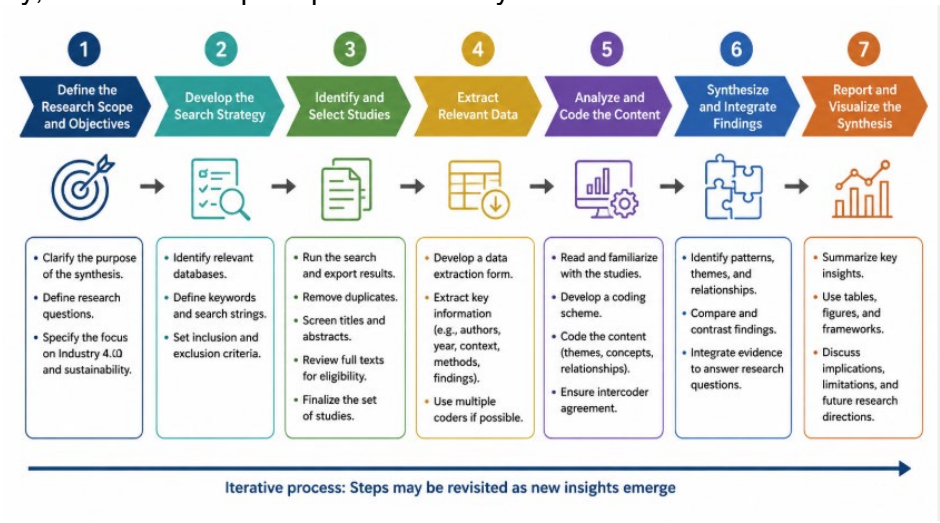


Fig. 1. *Analytical framework for the literature-based synthesis of Industry 4.0 and Industry 5.0 sustainability evidence*
Source: Authors' synthesis based on Ghobakhloo et al. (2024) and related literature

The approach adopted here does not involve independent expert elicitation, a new questionnaire, quantitative meta-analysis, or a new statistical estimation procedure. The contribution is instead interpretive and synthetic: previously published evidence is brought together to clarify how technological capabilities associated with Industry 4.0 may support or constrain the sustainability-oriented objectives of Industry 5.0.

HF-ISM Methodological Framework

Hesitant-Fuzzy Interpretive Structural Modelling (HF-ISM) represents a methodological approach that can be used to examine complex interrelationships among interconnected factors under conditions of uncertainty. Hesitant-Fuzzy sets allow decision-makers to express hesitation among several possible assessments rather than provide a single precise value (Torra, 2010). When combined with Interpretive Structural Modelling (ISM), the approach can be used to represent uncertain relationships and organize interconnected factors into a hierarchical structure.

In the context of sustainable industrial development, HF-ISM and related ISM-based approaches have been used in previous research to examine relationships among technological, environmental, economic, and human-related factors. MICMAC analysis can subsequently be used to classify factors according to their driving and dependence

characteristics. Such approaches are potentially relevant to Industry 5.0 because its sustainability functions are interconnected and may influence one another across organizational and system levels.

However, the HF-ISM and MICMAC analysis discussed in this paper was not independently conducted as part of the present study. The present paper does not report an original expert panel, questionnaire, hesitant-fuzzy assessment, relationship matrix, reachability matrix, hierarchical model, or MICMAC calculation. These methodological and analytical elements are therefore considered as findings and approaches reported in previous research, particularly the relevant work of Ghobakhloo et al. (2024), rather than as original empirical results of the present review.

Accordingly, the present paper does not reproduce the expert elicitation procedure or numerical calculations underlying the previously published HF-ISM-MICMAC analysis. The methodological framework is discussed only to explain how previous research has examined interrelationships among sustainability-oriented functions and to position those findings within the broader Industry 5.0 literature.

This distinction also determines the interpretation of the sustainability functions discussed below. They are treated as literature-derived themes and functions identified in previous research rather than as factors independently validated through an expert assessment conducted in the present study.

Identifying Sustainability Functions of Industry 4.0

The sustainability functions considered in this paper are derived from the reviewed literature and from functions reported in previous research concerning the sustainability implications of Industry 4.0. Particular attention is given to functions related to environmental efficiency, economic performance, human development, technological integration, supply-chain resilience, and organizational adaptability.

At the economic level, the literature identifies functions associated with productivity improvement, operational efficiency, innovation, resource optimization, supply-chain coordination, and new business models. At the environmental level, relevant functions include resource efficiency, waste reduction, energy management, environmental monitoring, circular production, and optimization of material flows. At the social and human-centric level, the literature highlights human–machine collaboration, employee development, upskilling, reskilling, participation, knowledge sharing, and improved working conditions.

These functions can also be interpreted according to their relevance to the three principles of Industry 5.0. Functions associated with employee participation, skills development, human–machine collaboration, and well-being are particularly relevant to human-centricity. Resource efficiency, circularity, cleaner production, and environmental monitoring are directly related to sustainability. Supply-chain visibility, adaptability, predictive decision-making, redundancy, and organizational flexibility are relevant to resilience.

The functions should nevertheless not be interpreted as independent or universally applicable determinants. Their relevance and effects may vary according to industry, organizational capabilities, technological maturity, regulatory conditions, infrastructure, workforce competencies, and broader socio-economic context.

Previous research has demonstrated the usefulness of HF-ISM-MICMAC approaches for examining relationships among such interconnected sustainability functions under conditions of uncertainty (Torra, 2010; Das et al., 2020). In the present paper, however, these approaches are discussed as methodological contributions from the existing literature. No independent expert assessment or HF-ISM-MICMAC computation was conducted.

Consequently, the identified sustainability functions represent literature-based analytical themes used to organize the discussion of Industry 4.0 and Industry 5.0 rather than a newly validated empirical factor structure. This distinction ensures that the present review does not attribute previously published empirical findings to the present study.

DISCUSSION

The reviewed literature indicates that Industry 5.0 can support sustainable industrial development by integrating advanced digital technologies with human-centricity, environmental sustainability, and industrial resilience. Rather than replacing Industry 4.0, Industry 5.0 extends its technological foundations toward broader sustainability objectives and a more balanced industrial model (Ghobakhloo et al., 2022; van Erp et al., 2024).

The evidence discussed in the reviewed literature indicates that these contributions occur at micro, meso, and macro levels. At the organizational level, Industry 5.0 can improve productivity, resource efficiency, process optimization, and employee development, while at supply-chain and industrial-ecosystem levels it can strengthen coordination, circularity, adaptability, and resilience. At the broader economic level, advanced industrial technologies can support innovation and sustainable industrial competitiveness (Ching et al., 2022). However, sustainability benefits are not automatic, as digitalization may increase energy demand, technological complexity, cybersecurity risks, and organizational challenges. Therefore, outcomes depend on the integration of technologies with organizational capabilities, sustainability strategies, and effective governance (van Erp et al., 2024).

The human-centric dimension represents an important characteristic of Industry 5.0, with human–machine collaboration supporting employee participation, skills development, knowledge sharing, and improved working conditions (Ghobakhloo et al., 2023a). Industry 5.0 can also strengthen supply-chain sustainability and resilience through real-time information exchange, improved visibility, predictive decision-making, and adaptability to disruptions. Digital technologies can support resource efficiency, waste reduction, circular production, and improved monitoring of material and energy flows (Ghobakhloo et al., 2022; Ghobakhloo et al., 2023a).

The reviewed literature further indicates that sustainability functions should not be considered as completely independent factors. Their effects may be interconnected, and their relative importance can depend on their position within a broader socio-technical system. Previous research using ISM-based and HF-ISM-MICMAC approaches has provided methodological support for examining such interrelationships (Ghobakhloo et al., 2024). In the present paper, however, these approaches are considered on the basis of previously published research and are not applied through an independent expert assessment.

Consequently, the contribution of this review lies in synthesizing and interpreting the reported relationships between Industry 4.0 capabilities, Industry 5.0 principles, and sustainable industrial development. The analysis highlights the importance of considering technological capabilities together with human competencies, environmental responsibility, organizational resilience, and effective governance. Overall, the reviewed literature supports the interpretation of Industry 5.0 as a socio-technical and strategic transformation rather than simply the next generation of industrial technologies (Ghobakhloo et al., 2022; van Erp et al., 2024).

CONCLUSION

This review examined Industry 5.0 as a driver of sustainable industrial development by synthesizing findings from the existing literature concerning advanced technologies, sustainability functions, and the economic, environmental, and social dimensions of industrial transformation. The reviewed literature indicates that Industry 5.0 builds on the technological foundations of Industry 4.0 while extending industrial transformation toward human-centricity, sustainability, and resilience.

The literature identifies several potential contributions of advanced industrial technologies, including improved resource efficiency, cleaner production, circularity, supply-chain resilience, innovation, human–machine collaboration, and employee development. At the same time, potential challenges include increased energy consumption, technological complexity, cybersecurity risks, organizational transformation, and workforce adaptation. These findings indicate that the sustainability effects of Industry 5.0 depend not only on

technological capabilities but also on organizational readiness, human competencies, governance, and sustainability-oriented practices.

The evidence base discussed in this review includes the 527-article literature synthesis reported by Ghobakhloo et al. (2024). The present paper does not claim to have independently reproduced the original database search, screening process, or evidence-mapping dataset. Instead, the previously published evidence base is synthesized and interpreted in relation to the broader sustainability principles of Industry 5.0. This distinction separates the source study's empirical and methodological procedures from the contribution of the present literature-based review.

HF-ISM and MICMAC approaches are identified in the literature as potentially useful methods for examining interrelationships among sustainability functions and classifying factors according to their driving and dependence characteristics. However, these methods were not independently applied in the present review. No original expert assessment, hesitant questionnaire, relationship matrix, hierarchical model, or MICMAC analysis was conducted as part of this study. Accordingly, the discussion of HF-ISM is limited to its role as a methodological approach and set of findings reported in previous research.

The main contribution of the present paper is therefore a literature-based synthesis of how Industry 4.0 technologies and Industry 5.0 principles are associated with sustainable industrial development. The findings support the view that Industry 5.0 represents a broader socio-technical transformation in which advanced technologies need to be integrated with human capabilities, environmental responsibility, organizational resilience, and effective governance.

Future research should empirically validate the sustainability functions identified in the literature and examine their relative importance across industries, regions, and organizational contexts. Further empirical studies could also apply HF-ISM-MICMAC or other appropriate methods to investigate the interrelationships among sustainability functions and assess their measurable effects on environmental performance, employee well-being, supply-chain resilience, and inclusive economic development.

REFERENCES

Adamik, A., & Sikora-Fernandez, D. (2021). Smart organizations as a source of competitiveness and sustainable development in the age of Industry 4.0: Integration of micro and macro perspective. *Energies, 14*(6), 1572. https://doi.org/10.3390/en14061572

Baig, M. I., & Yadegaridehkordi, E. (2024). Industry 5.0 applications for sustainability: A systematic review and future research directions. *Sustainable Development, 32*(1), 662–681. https://doi.org/10.1002/sd.2699

Bécue, A., Praça, I., & Gama, J. (2021). Artificial intelligence, cyber-threats and Industry 4.0: Challenges and opportunities. *Artificial Intelligence Review, 54*(5), 3849–3886. https://doi.org/10.1007/s10462-020-09942-2

Bolis, I., Marques, J. N., Cagno, E., & Morioka, S. N. (2025). Digital technologies, sustainability, and work: How can these themes be brought together to promote a human-centered future in Industry 5.0 implementation? *Applied Ergonomics, 125*, 104475. https://doi.org/10.1016/j.apergo.2025.104475

Chen, M., Sinha, A., Hu, K., & Shah, M. I. (2021). Impact of technological innovation on energy efficiency in Industry 4.0 era: Moderation of shadow economy in sustainable development. *Technological Forecasting and Social Change, 164*, 120521. https://doi.org/10.1016/j.techfore.2020.120521

Chiarini, A. (2021). Industry 4.0 technologies in the manufacturing sector: Are we sure they are all relevant for environmental performance? *Business Strategy and the Environment, 30*(7), 3194–3207. https://doi.org/10.1002/bse.2797

Chiarini, A., Belvedere, V., & Grando, A. (2020). Industry 4.0 strategies and technological developments: An exploratory research from Italian manufacturing companies. *Production Planning & Control, 31*(16), 1385–1398. https://doi.org/10.1080/09537287.2019.1710304

Ching, N. T., Ghobakhloo, M., Iranmanesh, M., Maroufkhani, P., & Asadi, S. (2022). Industry 4.0 applications for sustainable manufacturing: A systematic literature review and a roadmap to sustainable development. *Journal of Cleaner Production, 334*, 130133. https://doi.org/10.1016/j.jclepro.2021.130133

Dalenogare, L. S., Benitez, G. B., Ayala, N. F., & Frank, A. G. (2018). The expected contribution of Industry 4.0 technologies for industrial performance. *International Journal of Production Economics, 204*, 383–394. https://doi.org/10.1016/j.ijpe.2018.08.019

Das, S. K., Azmi, F. T., & James, P. S. (2020). Factors influencing employees' perception of human resource practice: A fuzzy interpretive structural modeling approach. *Jindal Journal of Business Research, 9*(1), 41–55. https://doi.org/10.1177/2278682120908557

Dev, N. K., Shankar, R., & Qaiser, F. H. (2020). Industry 4.0 and circular economy: Operational excellence for sustainable reverse supply chain performance. *Resources, Conservation and Recycling, 153*, 104583. https://doi.org/10.1016/j.resconrec.2019.104583

Ghobakhloo, M., Amoozad Mahdiraji, H., Iranmanesh, M., & Jafari-Sadeghi, V. (2024). From Industry 4.0 digital manufacturing to Industry 5.0 digital society: A roadmap toward human-centric, sustainable, and resilient production. *Information Systems Frontiers*. https://doi.org/10.1007/s10796-024-10476-z

Ghobakhloo, M., Iranmanesh, M., Foroughi, B., Babaee Tirkolaee, E., Asadi, S., & Amran, A. (2023a). Industry 5.0 implications for inclusive sustainable manufacturing: An evidence-knowledge-based strategic roadmap. *Journal of Cleaner Production, 417*, 138023. https://doi.org/10.1016/j.jclepro.2023.138023

Ghobakhloo, M., Iranmanesh, M., Morales, M. E., Nilashi, M., & Amran, A. (2023b). Actions and approaches for enabling Industry 5.0-driven sustainable industrial transformation: A strategy roadmap. *Corporate Social Responsibility and Environmental Management, 30*(3), 1473–1494. https://doi.org/10.1002/csr.2431

Ghobakhloo, M., Iranmanesh, M., Mubarak, M. F., Mubarik, M., Rejeb, A., & Nilashi, M. (2022). Identifying Industry 5.0 contributions to sustainable development: A strategy roadmap for delivering sustainability values. *Sustainable Production and Consumption, 33*, 716–737. https://doi.org/10.1016/j.spc.2022.08.003

Huang, S., Wang, B., Li, X., Zheng, P., Mourtzis, D., & Wang, L. (2022). Industry 5.0 and Society 5.0—Comparison, complementation and co-evolution. *Journal of Manufacturing Systems, 64*, 424–428. https://doi.org/10.1016/j.jmsy.2022.07.010

Ivanov, D. (2023). The Industry 5.0 framework: Viability-based integration of the resilience, sustainability, and human-centricity perspectives. *International Journal of Production Research, 61*(5), 1683–1695. https://doi.org/10.1080/00207543.2022.2118892

Khan, M., Haleem, A., & Javaid, M. (2023). Changes and improvements in Industry 5.0: A strategic approach to overcome the challenges of Industry 4.0. *Green Technologies and Sustainability, 1*(2), 100020. https://doi.org/10.1016/j.grets.2023.100020

Kiel, D., Müller, J. M., Arnold, C., & Voigt, K.-I. (2017). Sustainable industrial value creation: Benefits and challenges of Industry 4.0. *International Journal of Innovation Management, 21*(8), 1740015. https://doi.org/10.1142/S1363919617400151

Ma, S., Ding, W., Liu, Y., Zhang, Y., Ren, S., Kong, X., & Leng, J. (2024). Industry 4.0 and cleaner production: A comprehensive review of sustainable and intelligent manufacturing for energy-intensive manufacturing industries. *Journal of Cleaner Production, 467*, 142879. https://doi.org/10.1016/j.jclepro.2024.142879

Nara, E. O. B., da Costa, M. B., Baierle, I. C., Schaefer, J. L., Benitez, G. B., do Santos, L. M. A. L., & Benitez, L. B. (2021). Expected impact of Industry 4.0 technologies on sustainable development: A study in the context of Brazil's plastic industry. *Sustainable Production and Consumption, 25*, 102–122. https://doi.org/10.1016/j.spc.2020.07.018

Ooi, K. B., Tan, G. W. H., Al-Emran, M., Al-Sharafi, M. A., Capatina, A., Chakraborty, A., Dwivedi, Y. K., Huang, T. L., Kar, A. K., Lee, V. H., Loh, X. M., Micu, A., Mikalef, P., Mogaji, E., Pandey, N., Raman, R., Rana, N. P., Sarker, P., Sharma, A., Teng, C., Fosso Wamba, S., & Wong, L. W. (2025). The potential of generative artificial intelligence across disciplines: Perspectives and future directions. *Journal of Computer Information Systems*. https://doi.org/10.1080/08874417.2023.2261010

Pereira, C., Magalhães, M., Lopes, P., Silva, D., & Santos, M. (2025). Fostering Industry 5.0: An evidence-based framework to sustainable and human-centered technological transitions. *International Journal of Industrial Ergonomics, 110*, 103833. https://doi.org/10.1016/j.ergon.2025.103833

Renda, A., Schwaag Serger, S., Tataj, D., Morlet, A., Isaksson, D., Martins, F., Mir Roca, M., Hidalgo, C., Huang, A., Dixson-Declève, S., Balland, P.-A., Bria, F., Charveriat, C., Dunlop, K., & Giovannini, E. (2021). *Industry 5.0, a transformative vision for Europe: Governing systemic transformations towards a sustainable industry*. European Commission, Directorate-General for Research and Innovation. https://doi.org/10.2777/17322

Shabur, M. A., Shahriar, A., & Ara, M. A. (2025). From automation to collaboration: Exploring the impact of Industry 5.0 on sustainable manufacturing. *Discover Sustainability, 6*, 341. https://doi.org/10.1007/s43621-025-01201-0

Sharma, R., & Gupta, H. (2024). Harmonizing sustainability in Industry 5.0 era: Transformative strategies for cleaner production and sustainable competitive advantage. *Journal of Cleaner Production, 445*, 141118. https://doi.org/10.1016/j.jclepro.2024.141118

Strandhagen, J. W., Buer, S.-V., Semini, M., Alfnes, E., & Strandhagen, J. O. (2022). Sustainability challenges and how Industry 4.0 technologies can address them: A case study of a shipbuilding supply chain. *Production Planning & Control, 33*(9–10), 995–1010. https://doi.org/10.1080/09537287.2020.1837940

Torra, V. (2010). Hesitant fuzzy sets. *International Journal of Intelligent Systems, 25*(6), 529–539. https://doi.org/10.1002/int.20418

Toth-Peter, A., Torres de Oliveira, R., Mathews, S., Barner, L., & Figueira, S. (2023). Industry 4.0 as an enabler in transitioning to circular business models: A systematic literature review. *Journal of Cleaner Production, 393*, 136284. https://doi.org/10.1016/j.jclepro.2023.136284

van Erp, T., Carvalho, N. G. P., Gerolamo, M. C., Gonçalves, R., Rytter, N. G. M., & Gladysz, B. (2024). Industry 5.0: A new strategy framework for sustainability management and beyond. *Journal of Cleaner Production, 461*, 142271. https://doi.org/10.1016/j.jclepro.2024.142271

Yavuz, O., Uner, M. M., Okumus, F., & Karatepe, O. M. (2023). Industry 4.0 technologies, sustainable operations practices and their impacts on sustainable performance. *Journal of Cleaner Production, 387*, 135951. https://doi.org/10.1016/j.jclepro.2023.135951

DOI:10.5937/IIZS26344D

ARTIFICIAL INTELLIGENCE AS AN ENABLER OF ENVIRONMENTAL SUSTAINABILITY AND THE SUSTAINABLE DEVELOPMENT GOALS

Review paper

Mirjana Dunić[1]
[1]Technical Faculty "Mihajlo Pupin", Zrenjanin, University of Novi Sad, Serbia

Abstract: Environmental challenges have consistently stimulated discussions, debates, public concern, and awareness initiatives, generating increasing interest in innovative technologies such as Artificial Intelligence (AI). AI applications span various environmental sectors, including wildlife conservation, natural resource management, renewable energy, agriculture, energy efficiency, pollution mitigation, and waste management. In 2017, during the United Nations Artificial Intelligence Summit held in Geneva, the UN recognized that AI could serve as a catalyst for sustainable development aimed at promoting peace, prosperity, and a dignified life for humanity. The UN also proposed a renewed focus on leveraging AI to support global efforts to eradicate poverty and hunger, protect the environment, and conserve natural resources.
Addressing environmental sustainability challenges is essential; however, the rapid development of AI offers new opportunities to address environmental challenges more effectively while promoting human well-being. Sustainability encompasses the interconnected dimensions of the environment, society, and economy. The United Nations report titled "Our Common Future," often referred to as the "Brundtland Report," characterizes sustainable development as "development that fulfills the needs of the present while ensuring that future generations can also meet their own needs."
Unfortunately, the Earth is currently facing significant consequences associated with global warming and climate change, requiring urgent measures to promote environmentally friendly practices and sustainable solutions. Environmental degradation and climate change represent complex challenges that require innovative and intelligent approaches supported by AI. The body of literature on AI and environmental sustainability encompasses a wide range of fields. In particular, AI is increasingly being applied to address regional and global environmental challenges related to energy, water, biodiversity, transportation, agriculture, waste management, and pollution control.
Nevertheless, there is a pressing need to synthesize the existing literature on the application of AI to environmental sustainability, particularly regarding its contribution to key areas such as energy, water, biodiversity, transportation, and environmental health. A considerable research gap remains concerning the ways in which AI can contribute to environmental sustainability and support the achievement of the Sustainable Development Goals (SDGs). Therefore, this study aims to examine the role of AI as an enabler of environmental sustainability and to explore its potential contribution to achieving the Sustainable Development Goals.
Key words: Artificial Intelligence, Environmental Sustainability, Sustainable Development Goals, Renewable Energy.

INTRODUCTION

Recent environmental challenges have heightened public awareness and concern, leading to growing interest in innovative technologies such as Artificial Intelligence (AI). As societies confront increasingly complex environmental challenges, AI has emerged as a promising technological approach for supporting sustainable development through data-driven analysis, prediction, optimization, and decision-making (Greif et al., 2025; Gohr et al., 2025). AI has considerable potential to support the achievement of the Sustainable Development Goals (SDGs), particularly through its ability to process large and complex datasets, identify patterns, develop predictive models, and optimize environmental and energy systems (Greif et al., 2025). Furthermore, recent research indicates substantial growth in studies examining the relationship between AI and sustainable development, highlighting the potential of AI to contribute to multiple SDGs (Gohr et al., 2025). The relationship between AI and sustainability is multidimensional. AI can contribute to environmental sustainability by improving resource management, supporting energy efficiency, optimizing production and

Corresponding author, mirjana.dunic.as@gmail.com ORCID: 0009-0003-7202-2401

transportation systems, monitoring environmental conditions, and facilitating climate-related predictions (Kulkov et al., 2024). At the same time, the sustainable implementation of AI requires consideration of its energy and computational requirements and the potential environmental implications associated with the deployment of AI-based technologies. Therefore, the sustainable application of AI requires consideration not only of its potential environmental benefits but also of the resources required for its operation and implementation (Kulkov et al., 2024; Greif et al., 2025).

Achieving environmental sustainability presents a multifaceted challenge because the environmental, economic, and social dimensions of sustainability are closely interconnected. Recent research emphasizes that AI can serve as an important enabler of sustainable development by supporting organizations and industries in optimizing processes, improving decision-making, and addressing complex sustainability challenges (Kulkov et al., 2024). AI is particularly valuable because of its ability to analyze extensive datasets, identify complex relationships, generate predictions, and support the optimization of environmental systems (Greif et al., 2025; Gohr et al., 2025).

Given the threats posed by global warming and climate change, AI has increasingly been investigated as a tool for climate mitigation and adaptation. Recent research demonstrates that AI-based predictive models can support the assessment of climate change impacts, while machine learning and predictive analytics can improve the understanding and forecasting of complex climate-related processes (Ukoba et al., 2025). The application of AI is also increasingly relevant to renewable energy and energy sustainability. Recent research highlights the role of AI and machine learning in energy demand forecasting, smart-grid management, energy optimization, renewable-energy integration, and improving energy efficiency (Shahverdi et al., 2025).

The intersection of AI and environmental sustainability encompasses several important areas, including sustainable agriculture, natural-resource and biodiversity conservation, renewable energy, waste management, pollution control, and climate action. Recent research has examined AI applications across different environmental and sustainability domains, demonstrating its potential to improve prediction, monitoring, optimization, and decision-making processes (Raihan et al., 2024; Greif et al., 2025). Similarly, AI applications in sustainable energy systems have been increasingly explored as a means of improving energy efficiency, reducing waste, integrating renewable energy sources, and supporting progress toward the SDGs (Shahverdi et al., 2025).

Consequently, the sustainable and responsible use of AI has become increasingly important for achieving environmental sustainability and advancing the Sustainable Development Goals. Current research suggests that AI can act as an important enabler of sustainability; however, its benefits depend on responsible implementation, appropriate governance, data availability, transparency, and consideration of the environmental implications of AI deployment (Gohr et al., 2025; Kulkov et al., 2024).

Research on artificial intelligence for environmental sustainability spans a wide range of fields. Addressing both regional and global environmental challenges is essential, and AI is increasingly being utilized across the energy, transportation, biodiversity, and water sectors (Raihan et al., 2024; Gohr et al., 2025). These domains are continuously evolving and influencing various aspects of society. AI-based approaches can support environmental monitoring, resource optimization, climate-related analysis, sustainable infrastructure development, and the management of complex environmental systems. In particular, the application of AI to sustainable infrastructure and the construction sector provides opportunities to improve environmental performance and support more sustainable urban development (Regona et al., 2024; Debrah et al., 2022). Therefore, there is a continuing need for systematic research examining how artificial intelligence can be leveraged to advance environmental sustainability across areas such as water, energy, transportation, biodiversity, and sustainable urban development (Greif et al., 2025).

MATERIALS AND METHODS

The methodological framework of this study is based on analytical and synthesis methods used to examine the role of artificial intelligence (AI) and smart technologies in enhancing environmental sustainability in the building sector and supporting the achievement of the Sustainable Development Goals (SDGs). The research focuses on the application of AI-based models and smart technologies across the planning, design, construction, and operation stages of green buildings. Previous research has demonstrated the increasing relevance of AI for green buildings, particularly in relation to intelligent optimization, data-driven decision-making, energy efficiency, environmental performance, and the automation of building processes (Debrah et al., 2022; Rodríguez-Gracia et al., 2023).

The analytical method was applied to identify and examine the characteristics, functions, and environmental applications of AI and smart technologies used in green building practices. The synthesis method was subsequently applied to categorize and integrate the examined technologies, artificial intelligence models, information systems, and automatic control systems. This methodological approach was selected because AI applications in sustainable construction involve different technological domains, including machine learning, deep learning, artificial neural networks, Building Information Modeling (BIM), environmental monitoring, intelligent control, and optimization systems. Recent systematic research confirms that these technologies are increasingly being investigated as tools for improving the sustainability of the construction sector and supporting relevant SDGs (Regona et al., 2024; Greif et al., 2025).

The research was conducted in five sequential stages. In the first stage, the principal environmental challenges associated with construction and building operation were identified. The analysis considered atmospheric pollution, water contamination, greenhouse gas emissions, waste generation, material consumption, and energy consumption. Relevant statistical data and scientific literature were examined to identify major environmental pressures associated with the construction and building sectors. Particular attention was given to the need for technological solutions capable of monitoring environmental conditions, processing large amounts of data, optimizing resource use, and reducing the environmental impacts of buildings throughout their life cycle. The Chinese *Assessment Standard for Green Building* (GB/T 50378-2014) was also considered in order to identify the principal requirements associated with green building development. The environmental challenges identified at this stage were subsequently related to the relevant Sustainable Development Goals, particularly SDG 6 (Clean Water and Sanitation), SDG 7 (Affordable and Clean Energy), SDG 9 (Industry, Innovation and Infrastructure), SDG 11 (Sustainable Cities and Communities), SDG 12 (Responsible Consumption and Production), and SDG 13 (Climate Action) (Regona et al., 2024).

In the second stage, smart technologies used for monitoring, collecting, transmitting, and processing physical and environmental parameters associated with buildings were identified and analyzed. Particular attention was given to the integration of AI into building management and control systems. The methodological analysis included artificial neural networks, machine learning, and deep learning approaches used for prediction, classification, monitoring, optimization, and automated decision-making. The application of AI in green and smart buildings has been examined in recent literature, with applications including building performance optimization, thermal performance assessment, energy management, and environmental monitoring (Rodríguez-Gracia et al., 2023; Mahmood et al., 2024). The analysis also considered the role of AI in transforming building-related data into information that can support decision-making and automated control. Particular attention was given to applications capable of improving the operational efficiency of buildings while reducing energy consumption and environmental impacts. Recent studies on artificial intelligence across the building life cycle demonstrate that AI can be utilized during the design, construction, operation, maintenance, and retrofit phases to enhance energy efficiency (Yussuf & Asfour, 2024).

The third stage involved the synthesis and classification of technologies intended to improve the environmental and resource efficiency of construction processes. The analysis focused on reducing material consumption, energy use, waste generation, and other environmental impacts associated with construction activities. Building Information Modeling (BIM) was examined as an important digital technology for supporting sustainable building design and construction. Particular attention was given to the integration of BIM with AI-based approaches, since the combination of these technologies can support data-driven decision-making, design optimization, building performance assessment, and sustainable building management. A systematic review of BIM-AI integration in the architecture, engineering, construction, and facility management sector demonstrated that such integration is applied across the project life cycle and includes applications related to sustainable development (Zhang et al., 2022).

The environmental performance of buildings was also considered through analytical approaches for evaluating and comparing environmental and resource-efficiency parameters. The analysis included the standardization and comparison of relevant building-performance parameters, as well as consideration of environmentally appropriate construction materials. The main types of pollution associated with construction activities and the environmental protection measures required to reduce their adverse effects were also examined. Existing standards and technological approaches for green building design and construction were therefore considered as complementary elements of the methodological framework. The analyzed technologies were evaluated in relation to resource efficiency, responsible consumption and production, and sustainable urban development, corresponding primarily to SDG 11 and SDG 12.

In the fourth stage, AI models used for the collection, processing, analysis, prediction, and optimization of building design and operational parameters were examined. The analysis considered the application of AI throughout the building life cycle, including design, construction, operation, maintenance, and energy management. Particular attention was given to AI-based approaches capable of optimizing energy consumption, improving building performance, and supporting intelligent control. Recent research has demonstrated the relevance of machine learning and deep learning for improving energy efficiency and environmental sustainability in green buildings. Mahmood et al. (2024), for example, examined machine learning and deep learning approaches in green buildings and demonstrated their potential for improving energy efficiency and environmental performance. In addition, systematic research on AI and green buildings has identified intelligent optimization, automated decision-making, and data-driven building management as important areas of application (Debrah et al., 2022; Rodríguez-Gracia et al., 2023).

The methodological analysis also included waste management and the potential integration of renewable-energy and resource-recovery systems into sustainable building and energy systems. The use of intelligent control and optimization approaches for monitoring and managing energy and resource flows was considered in terms of resource efficiency and the reduction of environmental impacts. The characteristics of electricity generation and power supply systems in green buildings were also analyzed, including the challenges associated with intermittent renewable-energy generation. These aspects were considered in relation to energy efficiency and the integration of intelligent technologies for energy management These applications hold significant relevance to SDG 7 and SDG 13, as AI-driven optimization can enhance energy efficiency and facilitate the incorporation of renewable energy technologies (Yussuf & Asfour, 2024).

In the fifth and final stage, the results of the literature analysis and the examination of the identified technologies were synthesized. The analyzed AI models, smart technologies, monitoring systems, BIM-based approaches, and automatic control systems were compared according to their potential applications in the planning, design, construction, and operation of green buildings. The synthesis focused on five principal environmental dimensions: energy efficiency, resource efficiency, environmental monitoring, waste reduction, and reduction of environmental impacts. The relationship between these dimensions and the relevant SDGs was subsequently established.

The methodological framework was further informed by recent systematic reviews examining AI applications in sustainability and the SDGs. Greif et al. (2025) systematically reviewed AI techniques used in the context of the SDGs and identified supervised learning, unsupervised learning, reinforcement learning, and artificial neural networks among the principal AI approaches applied to sustainability challenges. Their analysis emphasized the relevance of AI techniques to environmental sustainability and the achievement of the SDGs. Similarly, Regona et al. (2024) specifically examined AI and the SDGs in the construction industry and identified SDGs 6–9, 11–13, 15, and 17 as relevant to the sector. Based on the five-stage methodological procedure, the study establishes an integrated framework for examining artificial intelligence as an enabling technology for environmental sustainability. The framework connects AI-based monitoring, data analysis, prediction, optimization, and automated control with sustainable building practices and the relevant SDGs. In this context, AI is considered not merely as an individual technological solution, but as an enabling technology capable of supporting more efficient resource use, energy management, environmental protection, waste reduction, and sustainable building development. The methodological framework therefore provides the basis for examining the contribution of AI-enabled technologies to environmental sustainability and their potential to support the implementation of SDG 6, SDG 7, SDG 9, SDG 11, SDG 12, and SDG 13.

The synthesis of the reviewed literature demonstrates that artificial intelligence (AI) represents an important enabling technology for enhancing environmental sustainability in the building and construction sector. AI is increasingly integrated with machine learning, deep learning, Building Information Modeling (BIM), intelligent sensing technologies, Digital Twins, and automated building management systems. These technologies enable data-driven prediction, optimization, monitoring, and decision-making throughout the building life cycle (Debrah et al., 2022; Rodríguez-Gracia et al., 2023; Mahmood et al., 2024).

A major finding of the reviewed literature concerns the contribution of AI to energy efficiency and resource management. AI-based models can predict energy demand, optimize heating, ventilation, air-conditioning, lighting, and other building systems, and support more efficient use of materials and water. AI can also assist in selecting construction materials according to environmental, technical, energy, and economic criteria, thereby supporting more sustainable design and construction decisions (Mahmood et al., 2024; Yussuf & Asfour, 2024).

Table 1. *AI-enabled technologies and their applications for environmental sustainability in buildings*

AI-enabled technology / digital approach	Main application	Environmental sustainability contribution
Artificial Intelligence and Machine Learning	Prediction, classification, monitoring, and optimization	Improved energy efficiency and resource management
Deep Learning and Artificial Neural Networks	Prediction, analysis, and automated decision-making	Improved building performance and environmental monitoring
Building Information Modeling (BIM) integrated with AI	Design optimization, performance prediction, material selection, and decision-making	Potential reduction in material consumption, construction waste, and energy demand
Intelligent sensor systems	Monitoring of temperature, humidity, air quality, occupancy, and energy consumption	Continuous environmental monitoring and improved building efficiency
AI-integrated Digital Twins	Real-time monitoring, simulation, prediction, fault detection, and optimization	Improved building performance, preventive maintenance, and resource efficiency
Intelligent building-management and control systems	Automated management of heating, cooling, ventilation, and lighting	Potential reduction in excessive energy consumption

AI for renewable-energy management	Forecasting and management of renewable-energy generation, storage, and microgrids	Improved energy efficiency and renewable-energy integration
AI for water and waste management	Monitoring, optimization, reuse, and resource recovery	Improved water efficiency and waste reduction

Source: Author's synthesis based on the reviewed literature

Table 1 summarizes the principal AI-enabled technologies and digital approaches identified in the reviewed literature, together with their main applications and contributions to environmental sustainability in buildings.

The integration of AI and BIM represents another important finding. BIM provides structured digital information about buildings, while AI enables the analysis of this information for design optimization, performance prediction, material selection, and decision-making. This integration can support the early identification of design problems and contribute to reducing material consumption, construction waste, energy demand, and environmental impacts (Zhang et al., 2022).

The reviewed studies also demonstrate the importance of intelligent monitoring and control. Sensor systems can provide continuous information on temperature, humidity, air quality, occupancy, energy consumption, and other environmental parameters. AI can analyze these data and facilitate adaptive management of heating, cooling, ventilation, and lighting systems, thereby enhancing building efficiency and potentially reducing unnecessary energy consumption (Rodríguez-Gracia et al., 2023; Yussuf & Asfour, 2024).

AI applications also extend to water and waste management and renewable-energy integration. Intelligent systems can monitor water consumption, support water optimization and reuse, improve waste-management processes, and facilitate resource recovery. AI can also support the forecasting and management of renewable-energy generation, energy storage, and microgrids, thereby contributing to more efficient and flexible building energy systems (Raihan et al., 2024; Shahverdi et al., 2025).

Digital Twins further strengthen the potential of AI-enabled sustainable buildings by integrating information from BIM, sensors, and building management systems. When combined with AI, Digital Twins can support real-time monitoring, prediction, simulation, fault detection, optimization, and preventive maintenance throughout the building life cycle (Debrah et al., 2022).

The reviewed literature indicates that substantial sustainability potential may be achieved through the integration of complementary technologies. BIM, sensors, AI, Digital Twins, renewable-energy systems, energy storage, and intelligent control can operate as an interconnected framework supporting sustainable decision-making from design and construction through operation, maintenance, and retrofit (Debrah et al., 2022; Zhang et al., 2022; Yussuf & Asfour, 2024).

The reviewed literature also identifies relevant links between AI-enabled sustainable buildings and SDG 6, SDG 7, SDG 9, SDG 11, SDG 12, and SDG 13. These relationships concern water management, energy efficiency, technological innovation, sustainable buildings and cities, resource efficiency, waste reduction, and climate action. Regona et al. (2024) additionally identified SDGs 6–9, 11–13, 15, and 17 as relevant to AI applications in the construction sector.

Table 2. *Relationship between AI-enabled environmental applications and the Sustainable Development Goals*

Environmental application	Main contribution of AI	Relevant SDG
Water management	Monitoring, optimization, and water reuse	SDG 6 – Clean Water and Sanitation
Energy efficiency	Energy-demand prediction, optimization, and intelligent	SDG 7 – Affordable and Clean Energy

	control	
Sustainable construction and technological innovation	AI-BIM integration, digital technologies, and optimization	SDG 9 – Industry, Innovation and Infrastructure
Sustainable buildings and cities	Intelligent building management and sustainable urban development	SDG 11 – Sustainable Cities and Communities
Resource efficiency and waste reduction	Optimization of material use, waste management, and resource recovery	SDG 12 – Responsible Consumption and Production
Climate action	Climate-related prediction, energy optimization, and reduction of environmental impacts	SDG 13 – Climate Action

Source: Author's synthesis based on the reviewed literature

Table 2 summarizes the relationship between the principal environmental applications of AI-enabled technologies and the relevant Sustainable Development Goals identified in the reviewed literature.

However, the results also identify several implementation challenges, including initial investment requirements, data quality, interoperability, technical expertise, cybersecurity, data privacy, organizational readiness, and regulatory conditions. In addition, AI itself requires computational resources and energy; therefore, its environmental benefits should be evaluated together with its own environmental footprint (Kulkov et al., 2024; Gohr et al., 2025; Regona et al., 2024).

Overall, the findings suggest that AI can be viewed as an enabling technology for environmental sustainability rather than as an isolated technological solution. Its integration with BIM, sensors, Digital Twins, intelligent building management systems, and renewable-energy technologies may support improvements in energy and resource efficiency, waste reduction, environmental monitoring, and building performance throughout the life cycle. These findings indicate the potential contribution of AI to environmental sustainability and, in particular, to SDG 6, SDG 7, SDG 9, SDG 11, SDG 12, and SDG 13.

CONCLUSION

Artificial intelligence (AI) has significant potential to support the transition toward environmentally sustainable buildings and construction practices. The findings of this study demonstrate that AI can improve environmental, energy, and operational performance through intelligent monitoring, prediction, optimization, and data-driven decision-making throughout the building life cycle.

The greatest potential is observed when AI is integrated with complementary digital technologies, particularly Building Information Modeling (BIM), intelligent sensor systems, Digital Twins, automated building-management systems, renewable-energy technologies, and energy-storage solutions. Such integration can improve energy efficiency, optimize the use of water and construction materials, reduce waste, strengthen environmental monitoring, and support more efficient building management.

The study also confirms the strong relevance of AI-enabled sustainable building technologies to SDG 6, SDG 7, SDG 9, SDG 11, SDG 12, and SDG 13, through improved water and energy management, technological innovation, sustainable buildings and cities, resource efficiency, waste reduction, and climate action.

However, the implementation of AI-enabled solutions is influenced by several factors, including investment requirements, data quality and availability, interoperability, technical expertise, cybersecurity, data privacy, organizational readiness, and regulatory conditions. Moreover, the environmental footprint of AI itself should be considered when evaluating its

contribution to sustainability. Therefore, AI should be implemented within an integrated framework that combines technological, environmental, economic, organizational, and regulatory considerations.

Future research should focus on developing integrated AI-based frameworks for the simultaneous assessment of environmental, energy, economic, and social performance. Further attention should be given to standardized indicators for evaluating AI contributions to the SDGs, interoperability between AI and building information systems, and the long-term environmental and economic effects of AI-enabled buildings.

In conclusion, AI should be regarded primarily as an enabling technology for environmental sustainability, rather than as an isolated technological solution. Its integration with sustainable construction principles and digital technologies can support the development of more energy-efficient, resource-efficient, adaptive, and environmentally responsible buildings and represents an important pathway toward a more sustainable built environment.

REFERENCES

Algorithmic green infrastructure optimisation: Review of artificial intelligence driven approaches for tackling climate change. (2024). *Sustainable Cities and Society, 101*, 105182. https://doi.org/10.1016/j.scs.2024.105182

Debrah, C., Chan, A. P. C., & Darko, A. (2022). Artificial intelligence in green building. *Automation in Construction, 137*, 104192. https://doi.org/10.1016/j.autcon.2022.104192

Gohr, C., Rodríguez, G., Belomestnykh, S., et al. (2025). Artificial intelligence in sustainable development research. *Nature Sustainability, 8*, 970–978. https://doi.org/10.1038/s41893-025-01598-6

Greif, L., Röckel, F., Kimmig, A., & Ovtcharova, J. (2025). A systematic review of current AI techniques used in the context of the SDGs. *International Journal of Environmental Research, 19*, 1. https://doi.org/10.1007/s41742-024-00668-5

Kulkov, I., Kulkova, J., Rohrbeck, R., Menvielle, L., Kaartemo, V., & Makkonen, H. (2024). Artificial intelligence-driven sustainable development: Examining organizational, technical, and processing approaches to achieving global goals. *Sustainable Development, 32*(3), 2253–2267. https://doi.org/10.1002/sd.2773

Mahmood, S., Sun, H., El-Kenawy, E. M., Iqbal, A., Alharbi, A. H., & Khafaga, D. S. (2024). Integrating machine and deep learning technologies in green buildings for enhanced energy efficiency and environmental sustainability. *Scientific Reports, 14*, 20331. https://doi.org/10.1038/s41598-024-70519-y

Raihan, A., Paul, A., Rahman, M. S., Islam, S., Paul, P., & Karmakar, S. (2024). Artificial Intelligence (AI) for Environmental Sustainability: A Concise Review of Technology Innovations in Energy, Transportation, Biodiversity, and Water Management. *Journal of Technology Innovations and Energy, 3*(2), 64–73. https://doi.org/10.56556/jtie.v3i2.953

Regona, M., Yigitcanlar, T., Hon, C., & Teo, M. (2024). Artificial intelligence and sustainable development goals: Systematic literature review of the construction industry. *Sustainable Cities and Society, 108*, 105499. https://doi.org/10.1016/j.scs.2024.105499

Rodríguez-Gracia, D., Capobianco-Uriarte, M. M., Terán-Yépez, E., Piedra-Fernández, J. A., Iribarne, L., & Ayala, R. (2023). Review of artificial intelligence techniques in green/smart buildings. *Sustainable Computing: Informatics and Systems, 38*, 100861. https://doi.org/10.1016/j.suscom.2023.100861

Shahverdi, N., Saffari, A., & Amiri, B. (2025). A systematic review of artificial intelligence and machine learning in energy sustainability: Research topics and trends. *Energy Reports, 13*, 5551–5578. https://doi.org/10.1016/j.egyr.2025.05.021

Ukoba, K., Onisuru, O. R., Jen, T.-C., Madyira, D. M., & Olatunji, K. O. (2025). Predictive modeling of climate change impacts using artificial intelligence: A review for equitable

governance and sustainable outcome. *Environmental Science and Pollution Research, 32*, 10705–10724. https://doi.org/10.1007/s11356-025-36356-w

Yussuf, R. O., & Asfour, O. S. (2024). Applications of artificial intelligence for energy efficiency throughout the building lifecycle: An overview. *Energy and Buildings, 305*, 113903. https://doi.org/10.1016/j.enbuild.2024.113903

Zhang, F., Chan, A. P. C., Darko, A., Chen, Z., & Li, D. (2022). Integrated applications of building information modeling and artificial intelligence techniques in the AEC/FM industry. *Automation in Construction, 139*, 104289. https://doi.org/10.1016/j.autcon.2022.104289

DOI:10.5937/IIZS26353T

IS SUSTAINABILITY POSSIBLE?

Review paper

Alexis Toribio Dantas[1], Dejan Mihailović[2*]
[1] Faculty of Economic Sciences, Rio de Janeiro State University (UERJ), Rio de Janeiro, Brazil
[2] Tecnológico de Monterrey, Mexico City, Mexico

Abstract: This paper analyses the concept of sustainable development from two perspectives: (a) differences between central and peripheral countries and (b) differences between economic structure (supply side) and consumption (demand side) in terms of long-term sustainability. Regarding sustainable development, we consider the Brundtland Commission's approach, which seeks to make economic development compatible with social and environmental concerns, not only for the present but also for future generations. The analysis suggests that existing development patterns, particularly consumption patterns in both central and peripheral countries, are no longer sustainable in the long term, even with various rationalisation efforts.
Key words: development, centre-periphery, consumption patterns

INTRODUCTION

Defining a precise concept of sustainable development is difficult, especially when considering the various qualitative dimensions involved, such as social, ecological, political, and, of course, economic issues. In this sense, the specialised literature offers hundreds of different meanings for the concept (see Jacobs, 1995). Thus, this paper first aims to define a possible concept of sustainable development that includes the most important social, economic, political, and ecological requirements, even though the result will be broad rather than precise.
After that, we discuss two important different circumstances to analyse sustainable development:
(a) differences between central and peripheral countries in relation to sustainable development, based on the theoretical framework of ECLAC (Economic Commission for Latin America and the Caribbean);
(b) differences between economic structure (supply side) and consumption (demand side) in terms of sustainability in the long run.
In the next section, we analyse key features and the conceptual foundations of sustainable development. In the final section, we present the main conclusions on the themes treated in this paper.

DISCUSSION

Sustainable development

Sustainable development is a term that gained prominence in the 1980s through the work of the Brundtland Commission, the UN World Commission on Environment and Development (Brundtland, 1991), in an attempt to integrate other key dimensions into the traditional idea of economic development: beyond the economic dimension, it is crucial to consider social and environmental issues (Estender and Pitta, 2008). In this sense, Camargo (2003, p. 43) states: "In essence, sustainable development is a process of change in which the exploitation of resources, the direction of investments, the orientation of technological development and institutional change are harmonic and enhance the present and future potential to meet the human needs and aspirations."
Nevertheless, the literature offers many definitions of sustainable development, reflecting different aspects and dimensions of this broad concept. In this sense, Ciegis et al. (2009) suggest that, given the difficulties of defining a single concept of sustainable development, it

[1] alexis.dantas@gmail.com, ORCID: 0000-0002-4742-7197
[2] Corresponding author, dmihailo@tec.mx, ORCID: 0009-0009-0355-0431

is better to adopt a broad idea and include various dimensions for analysis. In their words: "Sustainable development encompasses a very important ethical component, a manifested right of every person to the proper and fair share of the planet's resources […]. In a wider sense, sustainability is associated with the equity in distribution, i.e. the distribution of possibilities for development between the present and the future generations. Sustainable development may then be defined as a better quality of life for present and future generations. […] Because not a single reference presented a feasible definition of sustainable development which could incorporate all aspects of the concept under investigation and provide no ideal understanding of this concept, it is thought appropriate to use the definition provided in the Brundtland Commission's report […] which discloses the idea of sustainable development best. It postulates that sustainable development is the kind of development that satisfies current needs without endangering future […] generations' ability to satisfy their own. This definition of sustainable development is the most frequently cited and seems more exhaustive than most others. The essence of Brundtland's statement is the fair distribution of natural resources among different generations and among the present generation of people from the first, second, and third world, and finding a positive consensus among the environmental, social, and economic dimensions of the environment. Thus, sustainable development is not about a choice between environmental protection and social progress, but rather more about striving for economic and social development that would be compatible with environmental protection" (p. 30).

In these terms, sustainable development can be considered a way of making economic development compatible with social and environmental concerns, not only for the present but also for future generations, that is, a way of keeping development possibilities continuously viable and fair across economic, social, and ecological dimensions.

On the other hand, Young and Lustosa (2003), highlighting the importance of incorporating social justice and environmental preservation into a more precise notion of development, adopt the concept of "centre-periphery" (developed by ECLAC researchers) to emphasise specific issues concerning developing economies with respect to sustainability. Thus, they question the basic notion initially developed by Raúl Prebisch at ECLAC, arguing that "it is not 'just' that the periphery should recover trajectories of growth above the world average, it is also necessary to answer deeper questions: Where to grow? For those who grow? Why grow up? How to grow?" (p. 203).

This questioning appears in both the production and consumption dimensions. The industrialisation model adopted in the periphery, based on import-substitution dynamics, also sought to "import" the production pattern initially developed in the central countries, which was heavily dependent on natural resources and energy, with a substantial share of fossil fuels. As a consequence, environmental conditions deteriorated rapidly. Moreover, the adoption of this model was regarded as a necessary step towards a subsequent period of socioeconomic prosperity in developing countries, something like a "bill that had to be paid to get to Heaven". In this sense, the central countries, pressured by social movements to adopt cleaner technologies, could improve this aspect of their productive structure, while peripheral countries would be responsible for "dirty production".

Consumption, however, is even more complex. As Young and Lustosa point out (2003, p. 209): "The environmental issue is also related to the consumption patterns adopted by the periphery and similar to the centre. The pattern of intensive use of energy and environmental resources was widespread […]. Moreover, this pattern of consumption follows the same logic of exclusion, in which the richest consume more goods intensive in emissions and the poorest are restricted to subsistence products, which generally impose lower emissions per unit produced. If the centre has been relatively successful in dealing with industrial pollution, pollution derived from consumption is far from resolved. The increasing need for energy […] can only be met by changing the energy base. Even the adoption of alternative energy, healthier for the environment, can result in environmental damage if it does not give attention to the negative externalities they generate."

A key point emerges from this discussion. While environmental damage and inequality are more strongly felt in peripheral countries, considering the history of their integration into the

international division of labour, consumption patterns in general, even in developed countries, are highly damaging to environmental conditions – despite technological advances such as the development of electric cars. In this case, it is not possible to simply "transfer" the sustainability problem of central countries to peripheral countries – all countries remain hostages to this consumption pattern.

The current crisis experienced by most developed countries highlights this potential dilemma and, therefore, raises questions about the viability of an effective basis for sustainable development. First, a possible way out of the crisis is increasingly associated with a consistent recovery of economic growth – even considering the "obduracy" of orthodox economists who advocate austerity as a means of overcoming the crisis (support for this thesis is increasingly challenged by the facts). As Lara Resende points out (2012, p. 5): "There are only three ways to eliminate excess of debt. The first is a recession deep enough to break debtors and creditors and reset the stone. This is what happened in the 30s. The costs, as we learned, are unacceptable. The second is monetising debt. It takes time, while inflation reduces the real value of debt, but there is a risk of losing control. As in Germany in the 30s, the result can be hyperinflation, even more devastating than the worst recessions. The third is resuming growth. Because depression and inflation have unacceptable costs, the only solution is to return to growth, which reduces the debt's relative size. Growth is the only remedy, but, as Keynes taught, before growing again requires an artificial stimulus to demand through increased spending and public debt."

Decisions to stimulate growth as an alternative to overcoming the crisis, however, do not represent, in this context, any change in production patterns and, specifically, consumption patterns. Thus, referring to Paul Gilding's work, *The Great Disruption* (2011), Lara Resende indicates that "it is quite possible that today, 80 years later, the Keynesian remedy can no longer be applied" (2012, p. 5). This is the hook for a second argument. If growth is fundamental, but its current basis is virtually exhausted, what should we do, following Gilding's thesis? As explained by Lara Resende (2012, pp. 6–7): "Gilding's thesis is that the world economy will be forced to stop growing. As there was an early transition, not as we prepare for a stationary economy, we will have to face a sudden, deeply traumatic stop. The moment we become aware of the end of growth and the need for a profound reorganisation of the economy is not far away. […] The transition period will be long, hard and troubled. The reorganisation of the economy will be compulsory and deep. Entire industries will disappear. Coal, oil, and gas, well before the end of the known reserves, will be the first. The Stone Age did not end because of the lack of stones. Gilding's optimism is about the result of this procedure. The end of self-deception, the recognition of the limits of possibility, causes extraordinary technological innovations. A new reference for what it means to live better can enable a better life, permanently, for more people on Earth. A population 40 times greater than that of all times, until the beginning of the Industrial Revolution, is only possible, however, with the end of economic growth as we know it. Growth based on increased consumption of material goods is in its final chapter."

A shift in consumption patterns could increase the weight of technology, promote more rational use of natural resources, and encourage the more systematic adoption of alternative energy sources, such as solar energy for residential use or other renewables. These possible paths already exist, but they are far from dominant and, among other things, collide with the huge volume of investments still under construction or depreciation within the dominant production/consumption model. More than that, it is very difficult to create a "green pattern of consumption", as Young et al. point out (2010, p. 29): "With knowledge of the general purchasing process of green consumers, the key factors that will help green consumers purchase a more ethical technology product are: (1) the consumer's green value is strong; (2) the consumer has purchase experience; (3) the consumer has plenty of time for research and decision-making; (4) s/he has good knowledge of the relevant environmental issues; (5) green products are reasonably available and (6) the consumer can afford and is prepared for the financial costs. If any one of these criteria is a weak or negative influence, then this may water down the influence of the green criteria on the final purchase. Hence, it can be

concluded that government, company and NGO policies need to strengthen these success factors for green consumers to close the attitude–behaviour gap."
Indeed, what seems clear is that the current model is exhausted – rationalisation efforts, such as recycling and other procedures already in place, without an effective transformation of consumption patterns, can temporarily postpone the limits but do not appear sufficient to ensure a resumption of sustainable growth. Even considering existing concerns about the physical limits of the environment (and the actions implemented to slow this process), one can conclude that, without structural change, it is not possible to envisage a better future for the system.

CONCLUSION

(a) In this paper, we consider the Brundtland Commission's approach to sustainable development as a way of summarising the main features of the concept.
(b) Peripheral countries have historically faced greater obstacles to building a sustainable development trajectory, particularly considering the *modus operandi* of their industrialisation process, broadly based on import substitution. This growth dynamic implied a division of labour characterised by increasing specialisation in "dirty production".
(c) Consumption patterns, however, appear to be more "democratic" in the sense that they represent a general problem for both central and peripheral countries. Although the requirements for "green consumption" are broadly known, they are difficult to achieve because they depend on several factors, including ethical values, knowledge, purchasing experience, and economic conditions.
(d) Finally, we conclude that the current development model has reached its limits, even when various rationalisation efforts are considered. A substantial change in consumption patterns that increases the role of technology, promotes a more rational use of natural resources, and expands the use of alternative renewable energy sources is therefore crucial.

REFERENCES

Brundtland, G. H. (1991). *Nosso futuro comum: Comissão Mundial sobre Meio Ambiente e Desenvolvimento* (2nd ed.). FGV.

Camargo, A. L. de B. (2003). *Desenvolvimento sustentável: Dimensões e desafios*. Papirus.

Ciegis, R., Ramanauskiene, J., & Martinkus, B. (2009). The concept of sustainable development and its use for sustainability scenarios. *Inzinerine Ekonomika–Engineering Economics*, (2).

Estender, A. C., & Pitta, T. de T. M. (2008). O conceito do desenvolvimento sustentável. *Revista Terceiro Setor & Gestão, 2*(1), 22–28.

Gilding, P. (2011). *The great disruption: How the climate crisis will transform the global economy*. Bloomsbury.

Jacobs, M. (1995). *Sustainable development: From broad rhetoric to local reality*. Cheshire County Council.

Lara Resende, A. (2012, January 20). Os novos limites do possível. *Valor*.

Young, C. E. F., & Lustosa, M. C. J. (2003). A questão ambiental no esquema centro-periferia. *Economia, 4*(2), 201–221.

Young, W., Hwang, K., McDonald, S., & Oates, C. J. (2010). Sustainable consumption: Green consumer behaviour when purchasing products. *Sustainable Development, 18*, 20–31.

DOI:10.5937/IIZS26357B

FROM THE GREEN RETAIL AGENDA TO STORE-LEVEL EFFICIENCY: A DIGITAL PROGRAM FOR ENVIRONMENTAL PROTECTION IN SUSTAINABLE RETAIL

Review paper

Ankica Borota-Tišma[1*], Draga Tišma[2]
[1]Belgrade Business and Arts Academy of Applied Studies, Belgrade, Serbia
[2]Independent researcher, Belgrade, Serbia

Abstract: Retail sustainability has moved from peripheral corporate responsibility to an operational and competitiveness issue. Yet, a persistent implementation gap remains between high-level green retail commitments and measurable improvements at individual stores. This paper develops a multidisciplinary Green Retail Store Efficiency Program (GR-SEP) that translates the green retail agenda into store-level environmental management. The proposed program combines economic logic, environmental performance measurement and a digital engineering layer for monitoring, benchmarking and control. Based on a targeted integrative synthesis of peer-reviewed research on retail sustainability and supermarket energy performance, complemented by European Union policy documents, ISO 50001 and the Greenhouse Gas Protocol, the paper identifies six operational domains: energy and building systems, refrigeration and refrigerants, waste and circularity, water, logistics and mobility, and digital governance. A Store Green Efficiency Index is proposed to integrate normalized indicators while preserving transparent domain-level reporting. The program follows a Plan-Do-Check-Act architecture and uses sub-metering, IoT/BMS integration, rule-based alerts and analytics to connect strategic environmental objectives with daily store operations. The contribution is a practical framework that is technically implementable, economically interpretable and suitable for pilot testing across heterogeneous retail formats. Rather than claiming ex-post empirical effects, the paper specifies a validation protocol and expected performance pathways. GR-SEP is positioned as a bridge between sustainable retail strategy and environmental protection through measurable store-level efficiency.

Key words: green retail agenda, sustainable retail, store-level efficiency, environmental protection, energy management, digital monitoring

INTRODUCTION

Retail is a strategically important interface between production systems and final consumption. Its environmental relevance is therefore dual. First, retailers directly consume energy and resources through stores, warehouses, refrigeration, lighting, heating, ventilation and air-conditioning (HVAC), information technology and transport. Second, retailers influence upstream suppliers and downstream consumer choices through assortment, procurement, merchandising, packaging, product information and reverse flows. Sustainable retailing consequently extends beyond "green products" and requires environmental considerations to be embedded in retail operations and value-chain governance (Tang et al., 2016; Vadakkepatt et al., 2021). A recent systematic review further documents the breadth of the field, identifying 53 sustainable retail practices across 11 categories, including technological adoption, sustainable packaging and managerial commitment (Thakur & Budhiraja, 2026).

The policy context is moving in the same direction. The European Commission's transition pathway for retail explicitly frames the sector's future around a more resilient, digital and green retail ecosystem and calls for the co-implementation of concrete actions through 2030 and beyond (European Commission, 2024). This framing is important because the green and digital transitions are not separate managerial projects. Store-level environmental performance increasingly depends on digital measurement, interoperable data, automated control and the ability to transform large volumes of operational data into decisions.

A central problem, however, is the distance between corporate-level sustainability commitments and the operational reality of a specific store. Corporate reports may disclose total energy, carbon emissions or waste, while store managers need to know whether a

[1]Corresponding author, ankica.borota@bpa.edu.rs, ORCID: 0009-0001-5463-2885
[2] tisma.draga@gmail.com, ORCID: 0009-0002-1172-3151

refrigeration rack is drifting from expected performance, whether HVAC schedules are misaligned with opening hours, whether lighting intensity is excessive, or whether waste generation is abnormal relative to turnover and customer traffic. Naidoo and Gasparatos (2018) show that energy conservation and greenhouse-gas reduction are dominant elements of retail environmental strategies, largely because resource efficiency can simultaneously reduce environmental impacts and operating costs. This makes store-level efficiency a natural meeting point between environmental protection and retail economics.

Food retail illustrates the engineering significance of this problem particularly well. Supermarkets are energy-intensive commercial buildings in which refrigeration, HVAC and lighting interact dynamically. Earlier work showed that improved integration of refrigeration and air-conditioning systems can generate material energy savings (Cecchinato et al., 2010), while recent field-based research demonstrates substantial reductions when multiple technologies are combined, including CO2 refrigeration, heat recovery, cabinet doors, LED lighting, thermal storage, optimized ventilation and photovoltaic generation (Thanasoulas & Molinari, 2025). The environmental dimension is not limited to electricity: refrigerant leakage can create direct greenhouse-gas emissions, which makes refrigerant management an essential component of environmental protection in retail (Tassou et al., 2011).

Against this background, the objective of this paper is to develop a Green Retail Store Efficiency Program (GR-SEP) that operationalizes the green retail agenda at store level. Existing approaches address sustainable-retailing strategy, store-level energy and carbon benchmarking, sustainability-efficiency assessment, or data-driven supermarket energy analysis (Álvarez-Rodríguez et al., 2019; Ferreira et al., 2018; Uhlig et al., 2021; Vadakkepatt et al., 2021). GR-SEP integrates these strands within a single store-level architecture combining six environmental domains, a transparent communication index, explicit KPI-to-intervention logic and a digital verification loop. Its novelty lies in linking strategic environmental objectives with disaggregated KPIs, intervention selection and post-intervention verification. The paper therefore examines which domains and indicators should be managed and how digital monitoring can translate KPI deviations into prioritized and verifiable interventions.

MATERIAL AND METHODS

Research design and evidence base

The study applies a conceptual review-and-design methodology based on a targeted integrative synthesis of scientific and institutional sources. The synthesis was targeted rather than exhaustive; sources were selected for direct relevance to retail environmental operations, store energy performance and digital energy management, with priority given to peer-reviewed research and authoritative institutional guidance. First, relevant scientific literature was synthesized across three connected streams: sustainable retail and green retail operations; environmental and energy performance of retail stores, particularly supermarkets; and digital/management-system approaches to continuous performance improvement. Second, the conceptual requirements were aligned with current institutional frameworks, notably the European Commission retail transition pathway, ISO 50001 energy management principles and the Greenhouse Gas Protocol. Third, these elements were translated into an implementable program architecture and a set of store-level key performance indicators (KPIs).

The design follows four principles. The first is materiality: the program prioritizes operational domains that are significant for both environmental impact and management control. The second is normalization: absolute resource use is complemented by intensity indicators so that stores of different size and activity can be compared cautiously. The third is traceability: every composite score must remain decomposable into underlying physical indicators. The fourth is continuous improvement: the program is structured around Plan-Do-Check-Act (PDCA), consistent with the ISO 50001 energy-management framework (International

Organization for Standardization, 2018), which provides a technology-neutral framework for improving energy performance.

Operational domains of the Green Retail Store Efficiency Program

GR-SEP organizes store-level environmental protection into six domains. Domain 1 covers energy and building systems, including electricity, heating, cooling, lighting, HVAC schedules, peak demand and on-site renewable generation. Domain 2 covers refrigeration and refrigerants, including refrigeration electricity, leakage events, refrigerant global-warming potential, heat recovery and cabinet efficiency. Domain 3 covers waste and circularity, including food waste, packaging, cardboard, plastics, reverse logistics and diversion from disposal. Domain 4 covers water use and leak detection. Domain 5 covers logistics and mobility, including store deliveries, last-mile interfaces and low-emission transport options where the store can influence them. Domain 6 covers digital governance, data quality, alarms, maintenance closure, staff routines and the audit trail required to ensure that environmental KPIs correspond to actual operational behavior.

Table 1. *GR-SEP store-level environmental domains and representative indicators*

Domain	Representative KPI	Management purpose
Energy & building	EUI (kWh/m²/year); peak kW; lighting kWh/m²; renewable share	Reduce energy use, cost and indirect emissions
Refrigeration & refrigerants	Refrigeration kWh/m²; refrigerant loss (kg/year); tCO2e from leakage; heat-recovery ratio	Control major technical loads and direct climate impact
Waste & circularity	Waste kg/€1,000 sales; food waste kg/m²; diversion rate; packaging recovery	Prevent waste and improve material circularity
Water	m³/m²; anomaly/leak events; recovery/reuse share	Reduce water demand and losses
Logistics & mobility	Deliveries per €1,000 sales; load factor; low-emission delivery share	Reduce transport-related environmental burden
Digital governance	Meter coverage; data completeness; alarm closure time; verified actions/month	Convert data into accountable improvement

Performance measurement and the Store Green Efficiency Index

The core physical indicators are intentionally simple. Energy Use Intensity (EUI) is defined as annual final energy use divided by conditioned store area. Carbon intensity may be expressed as Scope 1 and Scope 2 greenhouse-gas emissions per square metre and, where appropriate, per unit of sales. Scope 1 includes direct emissions from sources owned or controlled by the retailer, whereas Scope 2 covers indirect emissions associated with purchased energy, in accordance with the GHG Protocol Corporate Standard (World Resources Institute & World Business Council for Sustainable Development, 2004). In food retail, fugitive refrigerant emissions should be tracked separately because their operational causes and mitigation actions differ from purchased-electricity emissions.

For management dashboards, the paper proposes a Store Green Efficiency Index (SGEI) as a transparent aggregation layer rather than a substitute for physical KPIs. Each domain score D_j is normalized on a 0–100 scale against a defined baseline, target trajectory or peer benchmark. Before calculation, the normalization rule, reference period and indicator directionality (lower-is-better or higher-is-better) should be predefined and applied consistently across stores.

The composite index is calculated as:

$$SGEI = \sum_{j=1}^{6} w_j D_j \,, \qquad \sum_{j=1}^{6} w_j = 1 \,\# \tag{1}$$

where w_j is the weight of domain j. For illustrative implementation purposes, the authors propose an initial weighting structure of 30% for energy and building systems, 25% for refrigeration and refrigerants, 20% for waste and circularity, 10% for water, 10% for logistics and mobility, and 5% for digital governance. These values are heuristic starting weights rather than empirically estimated parameters and should be calibrated through a retailer-specific materiality assessment, expert elicitation or an appropriate multi-criteria decision method.
The SGEI serves as a communication and benchmarking layer rather than an intervention trigger. Operational decisions are initiated from domain-level KPIs compared with a store baseline, target or peer benchmark. Material deviations initiate diagnosis, after which interventions are prioritized according to environmental benefit, lifecycle cost, operational risk and feasibility. Compliance events and confirmed refrigerant leakage require immediate corrective action. Closure is confirmed only after the relevant KPI is re-measured against the adjusted baseline.

Digital architecture

The engineering layer of GR-SEP uses a modular data architecture. At the device layer, electricity submeters, smart meters, refrigeration controllers, HVAC/BMS points, temperature sensors, water meters and waste records provide operational data. An integration layer collects these data through standard interfaces or secure APIs. A data-quality service checks timestamps, missing values, sensor plausibility and unit consistency. The analytics layer calculates KPIs, baselines and anomalies. A rules engine converts deviations into actionable alerts, while a dashboard provides store, regional and portfolio views. The final layer is the action log: every material alert is linked to a responsible person, due date, maintenance ticket or verified operational change. This closed loop is critical because monitoring without action can create a "dashboard illusion" in which environmental information increases while environmental performance does not.
The program does not require advanced artificial intelligence at the outset. A staged approach is preferable. Phase 1 establishes reliable metering, data ownership and rules. Phase 2 introduces weather normalization, store clustering and anomaly detection. Phase 3 can introduce predictive models for energy-demand forecasting, equipment-performance assessment and decision support. Data-driven building-energy research demonstrates the relevance of predictive modelling for energy management and conservation (Amasyali & El-Gohary, 2018); however, algorithmic complexity should be introduced only when data quality and operational processes are sufficiently mature to support trustworthy decisions.

RESULTS AND DISCUSSION

GR-SEP implementation cycle

The principal conceptual output of the study is a five-stage GR-SEP implementation cycle comprising baseline assessment, prioritization, intervention, verification and scaling. During baseline assessment, the retailer maps energy and environmental data, defines store boundaries, verifies meter coverage and establishes a performance baseline long enough to capture seasonal variation, preferably a full annual cycle where data are available. During prioritization, the program identifies material hotspots using engineering significance, environmental impact, operating cost and payback logic. During intervention, technical and behavioral measures are implemented. During verification, savings and environmental outcomes are evaluated against an adjusted baseline. During scaling, verified measures are standardized for stores with comparable technical characteristics.

Table 2. *KPI-to-intervention decision logic in GR-SEP*

Domain	KPI signal	Intervention	Verification
Energy & building	EUI/peak demand above baseline	Optimize schedules, set-points and controls	EUI; peak kW
Refrigeration	High intensity or leakage	Diagnose system; repair leak; optimize controls	kWh/m²; kg loss; tCO_2e
Waste	Waste above target	Category analysis; ordering/recovery measures	kg/€1,000 sales; diversion
Water	Abnormal water use	Leak inspection and corrective action	m³/m²
Logistics	High delivery intensity/low load factor	Consolidate deliveries	Deliveries/€1,000 sales; load factor
Digital governance	Incomplete data/unresolved alarms	Correct data flow and assign ownership	Data completeness; closure time

Energy efficiency as the first operational pillar

The literature strongly supports energy as the first operational pillar of a store-level green retail agenda. Previous research emphasizes both coordinated store-level energy management and the value of combined energy and carbon benchmarking for translating retail performance into actionable reference levels (Ferreira et al., 2018). Benchmarking studies consistently identify refrigeration, HVAC and lighting as major end uses in supermarkets (Tassou et al., 2011; Timma et al., 2016). The interaction between these systems means isolated optimization can be suboptimal. Bahman et al. (2012), for example, demonstrated that changes in store relative humidity affect refrigeration, defrost and anti-sweat loads, illustrating the need to treat store climate and refrigeration as an integrated system. More recent integrated designs reinforce this systems perspective. Thanasoulas and Molinari (2025) report that combining LED lighting, cabinet doors, CO2 refrigeration with heat recovery, thermal storage, ventilation optimization and photovoltaic generation can substantially reduce energy intensity relative to a baseline supermarket.

The managerial implication is that GR-SEP should sequence measures from no/low-capex operational optimization to deeper technical retrofits. Scheduling, set-points, sensor calibration and maintenance can often be addressed rapidly. Capital measures such as refrigeration replacement, heat recovery, building-envelope improvements and on-site generation should then be evaluated using lifecycle economics rather than simple first-cost comparisons. Recent real-world evidence from Swedish supermarkets shows that heat recovery from CO2 refrigeration can produce measurable operating-cost savings and that the potential increases when heat recovery is controlled to cover larger portions of heating demand (Steuer et al., 2025).

Environmental protection beyond energy

A green retail agenda that is reduced to electricity efficiency is incomplete. First, direct refrigerant emissions can be environmentally material, particularly where high-global-warming-potential refrigerants are used. Second, food and packaging waste connect store operations with circular-economy objectives. Third, logistics, mobility and omnichannel fulfillment can shift environmental burdens rather than eliminate them. Recent life-cycle research on buy-online-pick-up-in-store models shows that store energy and consumer travel can materially affect the carbon footprint of hybrid retail channels (Sun et al., 2026), illustrating why store efficiency remains relevant even as retail becomes more digital.
For these reasons, the proposed program uses a portfolio of environmental metrics but preserves economic interpretability. Waste prevention, energy efficiency and refrigerant-loss reduction often have direct cost effects. This matters for implementation because the retail sustainability literature indicates that expected economic benefits are among the strongest drivers of corporate environmental action (Naidoo & Gasparatos, 2018). GR-SEP therefore treats environmental protection and productivity as complementary when possible, while still recognizing that some measures may be justified by compliance, risk, stakeholder expectations or long-term climate targets even when short-run payback is weak.

Store benchmarking and heterogeneity

A major analytical risk in portfolio benchmarking is comparing stores that are structurally different. Store size, opening hours, climate, refrigeration intensity, customer traffic, product mix, building age and ownership arrangements can all influence performance. A retail store with a bakery, frozen-food offer and extended hours should not be compared mechanically with a small non-food store. GR-SEP therefore recommends a two-level benchmark: first compare each store against its own weather- and activity-adjusted baseline, and then compare it against a peer cluster of similar formats. Energy Use Intensity is useful, but it should be complemented by activity metrics such as kWh per transaction, kWh per €1,000 sales or refrigeration energy per metre of refrigerated display where the data are reliable.
This approach also reduces the risk of misleading composite rankings caused by structural differences among stores. A single composite ranking can reward structural advantages unrelated to management quality. The SGEI is therefore intended as a communication layer, while intervention decisions remain based on disaggregated engineering and economic evidence. The most useful benchmark is not simply the store with the lowest energy use; it is the store whose actual consumption is closest to an efficient level given its service requirements and operating context.

Pilot protocol and expected outcomes

Because GR-SEP is proposed rather than empirically implemented, no ex-post savings are claimed. Future validation should use a heterogeneous multi-store sample and a baseline sufficiently long to capture seasonal variation. Evaluation should examine data completeness, anomaly detection, verified operational savings, capital prioritization and reductions in energy use, emissions, refrigerant leakage, waste and water intensity. Both

successful and unsuccessful interventions should be recorded to support evidence-based scaling.

Managerial and engineering implications

For retail management, GR-SEP reframes sustainability as an operating system rather than a sequence of disconnected initiatives. Strategic targets are translated into store-level responsibilities, and investments are ranked by a combination of environmental materiality, controllability, risk and economic value. For engineering teams, the framework provides a structured link between building/refrigeration data and business priorities. For information technology teams, it defines a minimum viable architecture that starts with reliable data and workflow integration before moving toward advanced analytics. This sequencing is important because digitalization can otherwise increase system complexity without improving environmental outcomes.

GR-SEP is consistent with the European Union's twin green and digital transition and can generate comparable store-level evidence for benchmarking and policy evaluation, including in emerging and transition economies where empirical retail-sustainability evidence remains limited (European Commission, 2024; Naidoo & Gasparatos, 2018).

CONCLUSION

Environmental protection in retail ultimately depends on store-level operating decisions concerning energy, refrigeration, waste, water, logistics and corrective action. GR-SEP connects these decisions to strategic sustainability objectives through six operational domains, a transparent SGEI communication layer, explicit KPI-to-intervention logic and a digital monitoring-and-verification architecture. The framework is technology-neutral at the management-system level while remaining operationally specific enough to support metering, refrigeration/HVAC optimization, refrigerant management, waste analytics and data-driven maintenance.

Future research should empirically test GR-SEP across different retail formats and countries, estimate causal effects of selected interventions, compare alternative weighting schemes for the SGEI and investigate how digital maturity moderates the relationship between environmental initiatives and store efficiency. A particularly valuable direction would be a multi-store field study in Southeast Europe, where store-level evidence could connect retail competitiveness, energy efficiency and environmental policy. Such research would move sustainable retail from a broad agenda toward a measurable operational discipline.

REFERENCES

Álvarez-Rodríguez, C., Martín-Gamboa, M., & Iribarren, D. (2019). Sustainability-oriented management of retail stores through the combination of life cycle assessment and dynamic data envelopment analysis. *Science of the Total Environment, 683*, 49–60. https://doi.org/10.1016/j.scitotenv.2019.05.225

Amasyali, K., & El-Gohary, N. M. (2018). A review of data-driven building energy consumption prediction studies. *Renewable and Sustainable Energy Reviews*, *81*, 1192–1205. https://doi.org/10.1016/j.rser.2017.04.095

Bahman, A., Rosario, L., & Rahman, M. M. (2012). Analysis of energy savings in a supermarket refrigeration/HVAC system. *Applied Energy*, *98*, 11–21. https://doi.org/10.1016/j.apenergy.2012.02.043

Cecchinato, L., Corradi, M., & Minetto, S. (2010). Energy performance of supermarket refrigeration and air conditioning integrated systems. *Applied Thermal Engineering*, *30*(14–15), 1946–1958. https://doi.org/10.1016/j.applthermaleng.2010.04.019

European Commission. (2024). *A transition pathway for a more resilient, digital and green retail ecosystem*. Publications Office of the European Union. https://doi.org/10.2873/08359

Ferreira, A., Pinheiro, M. D., de Brito, J., & Mateus, R. (2018). Combined carbon and energy intensity benchmarks for sustainable retail stores. *Energy, 165*, 877–889. https://doi.org/10.1016/j.energy.2018.10.020

International Organization for Standardization. (2018). *Energy management systems—Requirements with guidance for use* (ISO Standard No. 50001:2018). https://www.iso.org/standard/69426.html

Naidoo, M., & Gasparatos, A. (2018). Corporate environmental sustainability in the retail sector: Drivers, strategies and performance measurement. *Journal of Cleaner Production*, *203*, 125–142. https://doi.org/10.1016/j.jclepro.2018.08.253

Steuer, D., Arias, J., & Sawalha, S. (2025). Techno-economic evaluation of heat recovery from supermarket refrigeration systems: A case study of four real-world installations. *Applied Thermal Engineering*, *281*, 128637. https://doi.org/10.1016/j.applthermaleng.2025.128637

Sun, L., Tian, X., & You, F. (2026). Comparative life cycle carbon footprints of buy online pick up in-store retail. *Transportation Research Part D: Transport and Environment*, *154*, 105290. https://doi.org/10.1016/j.trd.2026.105290

Tang, A. K. Y., Lai, K.-H., & Cheng, T. C. E. (2016). A multi-research-method approach to studying environmental sustainability in retail operations. *International Journal of Production Economics*, *171*, 394–404. https://doi.org/10.1016/j.ijpe.2015.09.042

Tassou, S. A., Ge, Y., Hadawey, A., & Marriott, D. (2011). Energy consumption and conservation in food retailing. *Applied Thermal Engineering, 31*(2–3), 147–156. https://doi.org/10.1016/j.applthermaleng.2010.08.023

Thakur, P., & Budhiraja, M. (2026). Revitalizing retail through sustainable retail practices: A systematic literature review. *International Journal of Retail & Distribution Management*, *54*(2), 129–146. https://doi.org/10.1108/ijrdm-08-2025-0584

Thanasoulas, S., & Molinari, M. (2025). Advancing energy efficiency and sustainability in supermarkets: A comprehensive analysis of integrated technologies and their impact on energy consumption. *Energy Reports*, *13*, 2855–2875. https://doi.org/10.1016/j.egyr.2025.02.021

Timma, L., Skudritis, R., & Blumberga, D. (2016). Benchmarking analysis of energy consumption in supermarkets. *Energy Procedia*, *95*, 435–438. https://doi.org/10.1016/j.egypro.2016.09.056

Uhlig, B., Blume, C., Thiede, S., Mennenga, M., & Herrmann, C. (2021). Data-driven energy analysis of supermarkets: A multi-level approach for different stakeholders. *Procedia CIRP, 98*, 61–66. https://doi.org/10.1016/j.procir.2021.01.006

Vadakkepatt, G. G., Winterich, K. P., Mittal, V., Zinn, W., Beitelspacher, L., Aloysius, J., Ginger, J., & Reilman, J. (2021). Sustainable retailing. *Journal of Retailing*, *97*(1), 62–80. https://doi.org/10.1016/j.jretai.2020.10.008

World Resources Institute, & World Business Council for Sustainable Development. (2004). *The greenhouse gas protocol: A corporate accounting and reporting standard* (Rev. ed.). https://ghgprotocol.org/corporate-standard

DOI:10.5937/IIZS26365C

MAPPING TEXTILE WASTE FLOWS IN SERBIA BASED ON OFFICIAL REGISTRY DATA

Research paper

Jovana Čugalj [1], Bogdana Vujić [2], Dejan Ubavin [3], Goran Vujić [4]
[1,2,]University of Novi Sad, Technical faculty „Mihajlo Pupin" Zrenjanin, Serbia
[3,4] University of Novi Sad, Faculty of Technical Sciences, Novi Sad, Serbia

Abstract: Textile waste represents a growing environmental challenge, yet reliable data on its generation and management in Serbia remains limited. This study maps and analyzes reported textile waste flows in Serbia using data from the National Registry of Pollution Sources (NRIZ) GIS portal and Serbian Environmental Protection Agency (SEPA) official reports from 2020. The analysis focuses on waste index numbers related to the textile, leather, and fur industries, primarily Waste index number 04 02 22 (waste from processed textile fibers). The findings reveal a strong regional concentration of industrial waste generation, with landfill disposal being the dominant management method, accounting for approximately 63% of the tracked waste. Treatment and export volumes are minimal, while no recorded cases of incineration with energy recovery were identified. Crucially, the registry captures only the industrial and commercial segment of the waste chain. Household textile waste remains invisible in official statistics due to legal reporting exemptions, creating a significant blind spot. Linking this data gap through direct household assessments and localized tracking is essential for developing effective recycling infrastructure and circular economy policies in Serbia.
Key words: Textile waste, Circular economy, Serbia, Waste

INTRODUCTION

The textile production industry has one of the most complex value chains in manufacturing, involving various sectors, including agriculture, chemical fiber production, textiles and apparel, retail and services. (Beton et al., 2014). The textile value chain generates significant amounts of waste, largely associated with the rapid growth of fast fashion, while also contributing to greenhouse gas emissions and high-water use (Mitsigiorgi et al., 2025). These impacts are expected to increase further, with textile production projected to generate 62% more waste, use 50% more water, and emit 63% more carbon dioxide by 2030 than in 2015 (Dragović et al., 2023).

In Serbia, textile waste generation was estimated at approximately 1 kg per person in 2022 (Kokeza et al., 2026), accounting for around 4% of municipal waste and approximately 100,000t annually (Milosevic et al., 2023). Textile waste is generated throughout the textile value chain, including both industrial processes and the post-consumer stage. Industrial textile waste arises from the production of fibers, textiles, clothing, and other textile products, while post-consumer textile waste is generated when textile products are discarded by consumers.

However, the domestic textile and clothing industry has decreased in recent years, with the largest reductions recorded in textile production in 2021 (6.5%) and clothing production in 2020 (6.9%). Leather production, in contrast, increased in 2021 and 2022 before falling by nearly 15% in 2023 (Kokeza et al., 2026)

According to Article 75 of the Law on Waste Management applicable during the 2011–2024 reporting period, households are exempt from the obligation to report waste generation, while reporting is required for legal entities, entrepreneurs, and other waste holders (Republic of Serbia, 2009). Within this reporting framework, the National Registry of Pollution Sources (NRIZ) and its GIS portal contain records covering several waste categories related to the textile sector. These include waste from textile, fur, and leather industries, classified with Waste **index number** under group 04 covering the:

- 04 02 09 (waste from mixed materials, including impregnated textiles, elastomers, and plastomers),
- 04 02 21 (waste from unprocessed textile fibers), and

[1]Corresponding author, jovana.cugalj@uns.ac.rs, ORCID: 0009-0002-7257-7936
[2]bogdana.vujic@uns.ac.rs, ORCID: 0000-0001-5249-8021
[3]una.marceta@uns.ac.rs, ORCID: 0000-0001-6664-0236
[4]dejanubavin@uns.ac.rs, ORCID: 0000-0002-2035-3554
[5]goranvujic@uns.ac.rs, ORCID: 0000-0002-3683-8986

- 04 02 22 (waste from processed textile fibers)

The registry also includes Waste index number **20 01 11**, referring to textiles from municipal sources, including household and similar commercial waste and separately collected fractions. The aim of this study is to examine what the available official data show about textile waste flows in Serbia, including where textile waste is generated and how it is managed, and to identify data gaps that limit a complete understanding of textile waste flows, particularly at the household level.To achieve this, the study analyzes the spatial distribution of reported textile waste generation and the main management pathways, including treatment, disposal, and export.

MATERIAL AND METHODS

The analysis was based on secondary data from official Serbian waste management sources. The primary source was the National Registry of Pollution Sources (NRIZ), specifically its GIS portal for waste management, supplemented by annual Waste Management Reports published by the Serbian Environmental Protection Agency (SEPA) and other available national strategic documents. Official data were accessed from the NRIZ GIS portal in August 2026. The records in the registry date from 2020, representing the most recent information available in the database at the time of the study (SEPA, 2026)
The data were extracted and filtered to include waste categories related to the textile sector and analyzed at the municipality level. The analysis covered waste generation, incineration with energy recovery, disposal treatment, and export, with the results summarized and presented in tables, charts, and maps. It is important to note that the datasets on waste generation, treatment, and disposal are not directly linked at the level of individual waste streams. Data on waste generation refer to reporting entities, while treatment and disposal data refer to waste management facilities receiving the waste. Therefore, these datasets were analyzed separately and were not used to trace individual waste streams from specific generators to specific management facilities.

RESULTS AND DISCUSSION

Based on the accessed NRIZ data, the analysis included 19 reporting companies located across 17 cities in Serbia, which generated textile waste classified under the waste index numbers identified in the registry. The majority of these companies, 13 in total, generated waste under waste index number 04 02 22, while five companies generated waste under 04 02 09 and one company under 04 02 21. Therefore, waste index number 04 02 22 represents the most widely generated and reported category among the identified textile waste streams and provides the most substantial basis for further spatial and quantitative analysis.
No records were identified for waste index number 20 01 11, corresponding to textiles from municipal sources. This absence is particularly relevant when interpreting the available data, as it indicates that no municipal textile waste was recorded in the NRIZ dataset for the period covered by the analysis.
In 2020, the total reported amount of waste generated under index number 04 02 22 (waste from processed textile fibers) was approximately 1,579 t. The largest share of waste was generated in Odžaci (759.23 t), linked to the manufacturing of automotive seating. Significant quantities were also recorded in Loznica (283.72 t), where textile waste is associated with the production of technical fabrics, and Bačka Palanka (192.82 t), where the reported activity includes the production of large industrial bags. Other cities with reported textile waste generation include Prokuplje, where activities include the production and processing of filters and the production of felt; Vranje, where activities include textile fibre preparation and spinning, as well as cut-and-sew apparel production; Prijepolje, where the main activity is the production and processing of workwear; Leskovac, where textile production includes the manufacture of hosiery, primarily stockings and socks; Niš, where the predominant activity is clothing

production; Majdanpek, where textile waste is associated with the production of upholstered furniture; and Babušnica, where garment production is recorded.
Regarding waste management, the data clearly indicate that landfill disposal remains the dominant method for handling this industrial waste. For example, the entire waste stream generated in Odžaci, as well as a large portion of waste from Prokuplje, ends up in landfills. Waste treatment (which includes recycling and other forms of recovery) is recorded in Bačka Palanka and Leskovac. Storage was recorded in several cities (Loznica, Majdanpek, Niš, Babušnica), but this represents only a temporary solution rather than a final management method. Export of textile waste is negligible, with only Prijepolje recording exports, amounting to 31.2 t. Finally, the data shows no recorded examples of this waste being directed to incineration with energy recovery, indicating that this management route is currently not utilized for processed textile waste in Serbia.
To visually map these complex flows, Figure 1 presents a Sankey diagram illustrating the movement of waste from the generation points to their final management destinations. This visualization highlights the macro-level distribution of the total tracked waste, where disposal represents the primary management route, receiving 993.17 t (approximately 63% of the total), while storage accounts for 416.71 t. Treatment captures only 60.48 t, and export remains minimal at 31.20 t. Additionally, 77.93 t are recorded as not documented, further emphasizing the tracking gaps mentioned above. The diagram also visually confirms that incineration with energy recovery is entirely absent from the management routes for this waste.

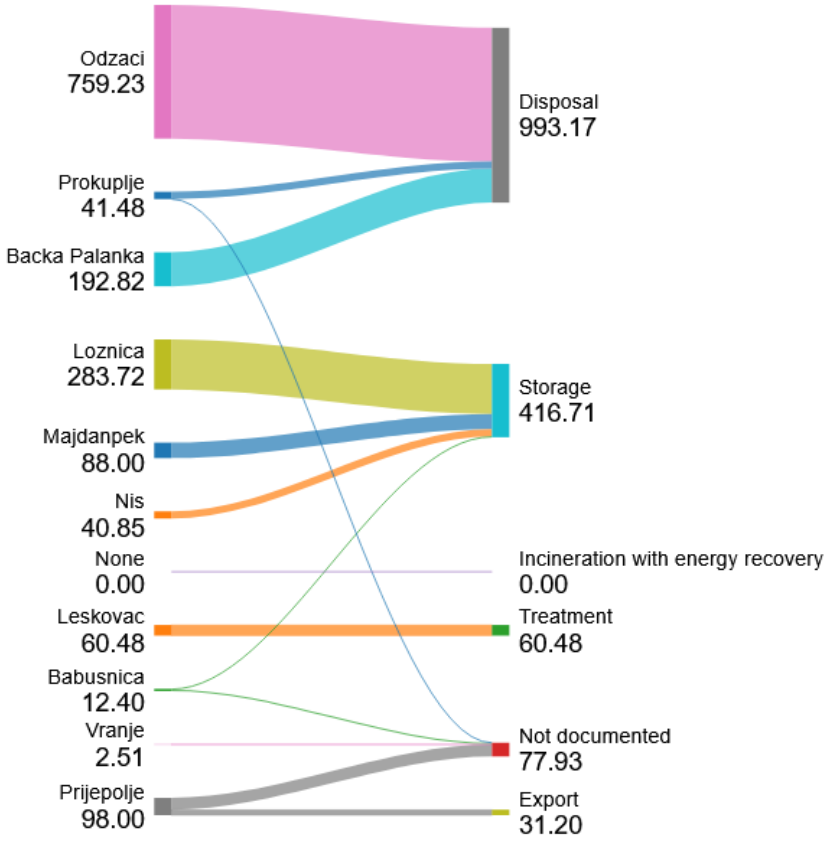


Fig. 1. *Sankey diagram of waste flows from processed textile fibers (04 02 22) from generation sites to management destinations in 2020.*

The geographical distribution of the reported textile waste generators and the corresponding quantities of generated waste is presented in Figure 2.

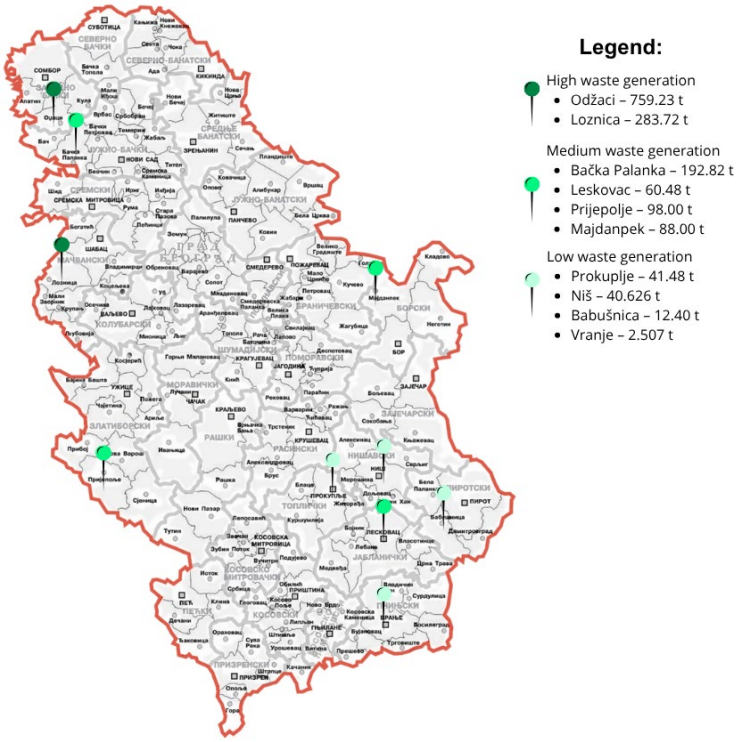


Fig. 2. *Geographical distribution of the reported textile waste generators and the corresponding quantities of generated waste*

For the **disposal** phase, the analysis will similarly focus on Waste index number 04 02 22 (waste from processed textile fibers). The data for this category are summarized and visually represented in Figure 3. In 2020, disposal of processed textile fibers was recorded at four landfill sites: Leskovac received the largest quantity (364.52 t), followed by Lapovo (253.65 t), Jagodina (101.51 t), and Kikinda (63.54 t). Beyond processed textile fibers, these landfills demonstrate varying capacities for accepting other textile waste streams. The Kikinda landfill, for instance, accepts a broader range of waste categories, including substantial quantities of mixed material waste (04 02 09), other textile wastes (04 02 99), and municipal textile waste (20 01 11). Lapovo also receives unprocessed textile fibers (04 02 21), while Pirot recorded disposal of sorted mixed material waste (19 12 08). This diversity indicates that certain facilities function as regional centralized receiving facilities for multiple waste categories, while others maintain a more specialized focus. It should be noted that the disposal data presented here are not directly linked to the previously identified waste generators, as the reporting system records quantities received at landfill facilities rather than tracing individual waste streams from their origin.

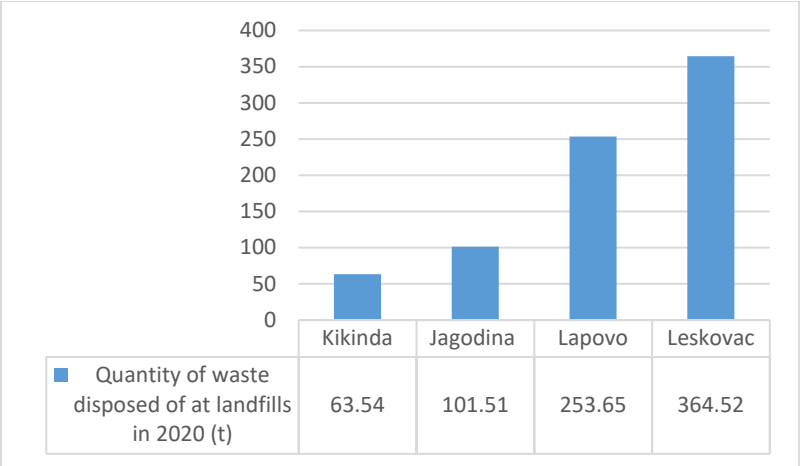


Fig. 3. *Disposal of waste from processed textile fibers (04 02 22) by landfill site in 2020*

Figure 4 presents the geographical distribution of landfill sites receiving waste from processed textile fibers (04 02 22) in 2020, with colour intensity indicating the quantity of waste received.

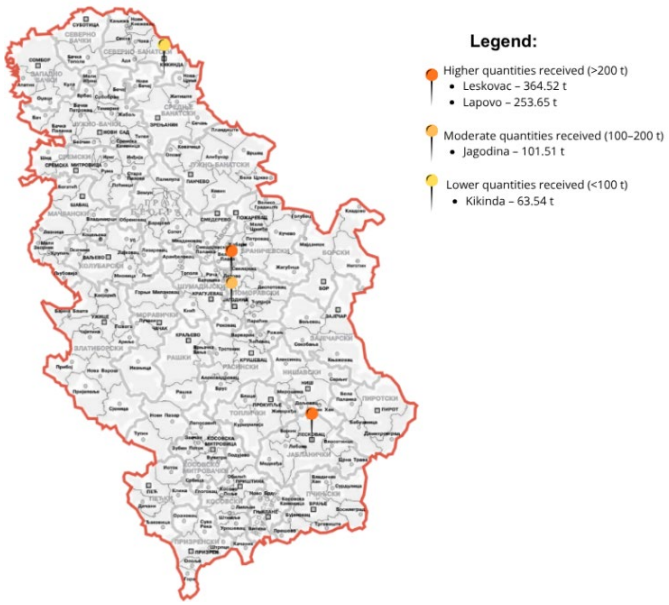


Fig. 4. *Geographical distribution of landfill sites receiving waste from processed textile fibers (04 02 22) in Serbia in 2020*

In contrast to disposal, **treatment** activities for processed textile fibers (04 02 22) are distributed across a larger number of locations, though the total quantities remain modest. The total amount of waste treated in 2020 was approximately 488.89 t. Ada recorded the highest treatment quantity (120.42 t), followed by Pančevo (80 t) and Bečej (71.79 t). Other locations with notable treatment activities include Bačka Palanka (64.1 t), Beočin (55.06 t), and Paraćin (53.12 t). Smaller quantities were treated in Varvarin (29 t) and Novi Sad (15.4 t), as illustrated in Figure 5. Importantly, the treatment data reflect the total quantities processed at each facility, which may include waste from multiple sources beyond those identified in the generation data, since the registry does not track waste streams from generator to treatment site.

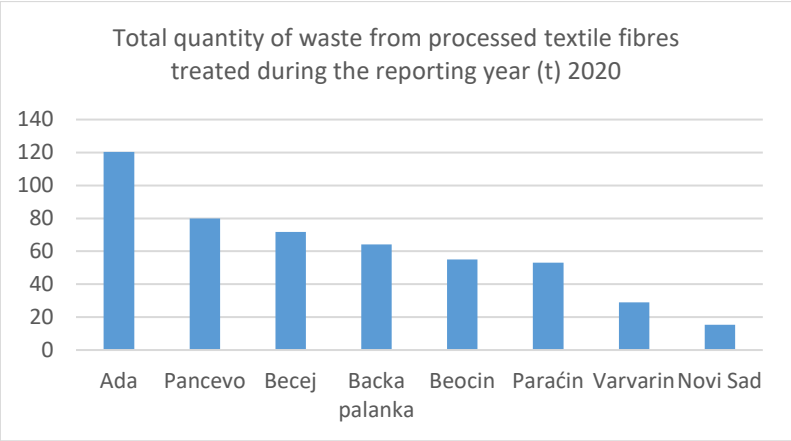


Fig. 5. *Quantities of waste from processed textile fibers (04 02 22) treated by city in 2020*

The geographical distribution of locations treating waste from processed textile fibers is presented in Figure 6, with colour intensity indicating the quantity of waste treated.

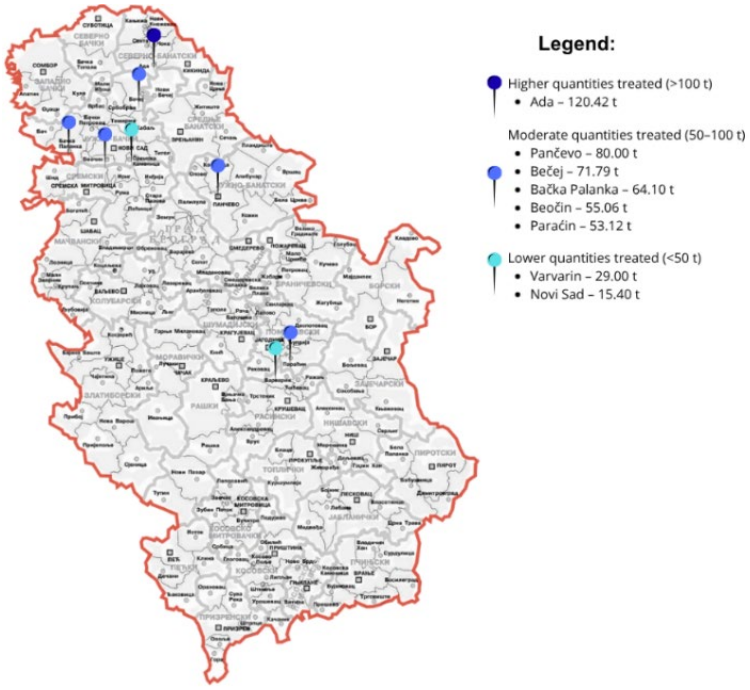


Fig. 6*. Geographical distribution of locations treating waste from processed textile fibers (04 02 22) in Serbia in 2020*

Export of processed textile fibers (04 02 22) was reported by three entities. The highest export quantity was reported in Zemun (116.834 t), with waste directed to Italy. Smaller quantities were exported from Apatin to the Czech Republic (14.58 t) and from Prijepolje to North Macedonia (31.24 t). Despite these exports, the overall volume remains minimal compared to the total waste generated, indicating that export plays a marginal role in the management of textile waste in Serbia. It should also be noted that export records identify the entities and destination countries, but do not directly trace the exported waste back to specific generators, as the system tracks these separately.

These findings indicate a significant gap in Serbia's waste tracking system, as household textile waste is not separately recorded in official statistics. Since households are not required to report textile waste, discarded textiles are generally included within mixed municipal waste, making the actual quantities difficult to determine. This lack of reliable data presents a

challenge for the planning and development of effective textile waste management and recycling systems.

CONCLUSION

Although landfill disposal accounts for the largest share, particularly for waste index number 04 02 22, some companies also use storage and treatment, while export plays only a minor role. No recorded cases of incineration with energy recovery were identified, indicating that this option for energy recovery from textile waste is currently not represented in the available data. These findings show that alternative management practices are already present, although they are used to a smaller degree, while landfill disposal remains the dominant management route. At the same time, the available data do not provide a complete picture of textile waste management in Serbia. Household textile waste is not separately recorded because households are not required to report it, and consequently, the actual amount of textile waste generated by households remains unknown. This, together with the absence of recorded incineration with energy recovery, highlights the limitations of the current waste tracking system and the need for more complete data on textile waste flows and management options in Serbia. Improving textile waste management therefore requires not only better data on industrial waste, but also suitable systems for the separate collection and monitoring of household textile waste. Future research should focus on collecting primary data on household textile waste, improving the tracking of waste flows from generation to final treatment, and assessing opportunities for textile waste recycling and reuse in Serbia. Such research could provide a more complete basis for improving textile waste management and supporting the development of circular economy practices.

REFERENCES

Beton, A., Dias, D., Farrant, L., Gibon, T., Desaxce, M., Perwueltz, A., . . . Dodd, N. (2014). *Environmental Improvement Potential of textiles (IMPRO Textiles).* Luxembourg: Publications Office of the European Union. Retrieved from https://op.europa.eu/en/publication-detail/-/publication/f8d0def8-4fd5-4d84-a308-1dfa5cf2e823/language-en

Dragović, N., Urošević, S., Vuković, M., Đorđević, D., & Stević, Z. (2023). Decrising polution in textile industry with recycled and new materials. *VI International conference „Contemporary trends and innovations in the textile industry".* Belgrade, Serbia: Union of Engineers and Textile Technicians of Serbia.

Kokeza, G., Josipović, S., & Urošević, S. (2026). New sustainable textile industry business model based on circularity and green economy. *Tekstilna industrija, 74*(2), 78-89. https://doi.org/10.5937/tekstind2004077R

Milosevic, A., Milosevic, M., Nesic, B., Bogdanovic, G., & Randjelovic, N. (2023). Testing and characterization of textile waste. *KNOWLEDGE - International Journal, 58*(3), 459-463. Retrieved from https://ojs.ikm.mk/index.php/kij/article/view/6132/5979

Mitsigiorgi, K., Stefi, A. L., & Vorgias, C. E. (2025). Recycling and valorisation of textile waste. *Serbian Journal of Engineering Management, 10*(1). https://doi.org/10.5937/SJEM2501001M

Republic of Serbia. (2009). Law on Waste Management. *Official Gazette of the Republic of Serbia*. Belgrade, Serbia: Official Gazette of the Republic of Serbia.

SEPA. (2026, August 25). Retrieved from http://77.46.150.221/nrizgis/index.html

DOI:10.5937/IIZS26372K

CIRCULAR MATERIAL USE RATE INDICATOR: WHERE SERBIA AND THE EU STAND?

Review paper

Nikola Karanović[1*], Višnja Mihajlović[2]
[1*]University of Aveiro, Aveiro, Portugal
[2]University of Novi Sad – Technical Faculty "Mihajlo Pupin", Zrenjanin, Serbia

Abstract: The transition from a linear to a circular economy requires not only improvements in waste management and recycling but also a greater substitution of primary raw materials with secondary materials. The circular material use rate (CMUR) measures the share of overall material use supplied by recycled materials and is therefore an important indicator for monitoring circularity. This paper examines CMUR trends in the European Union (EU) and Serbia, with particular attention to 2024 data and Serbia's position relative to EU Member States. The analysis uses Eurostat and European Environment Agency (EEA) data for the EU and the latest Statistical Office of the Republic of Serbia (SORS) data for Serbia. The EU CMUR increased from 10.7% in 2010 to 12.2% in 2024, whereas Serbia increased from 0.5% to 1.2% over the same period. Thus, Serbia's 2024 CMUR was 11.0 percentage points below the EU average and slightly below Romania, which recorded the lowest EU value at 1.3%. The results indicate a substantial circularity gap between Serbia and the EU and suggest that progress will require measures extending beyond recycling, including increased use of secondary raw materials, resource efficiency, reuse, industrial symbiosis and reduced dependence on primary material extraction.
Key words: circular economy, circular material use rate, material flow analysis, secondary raw materials, Serbia, European Union

INTRODUCTION

Resource use is a major driver of environmental pressure, contributing to climate change, pollution and biodiversity loss. The expansion of global resource consumption during the second half of the twentieth century was largely associated with a linear economic model based on extraction of virgin raw materials, transformation into products, consumption and disposal. This model creates continuing dependence on primary resource extraction and generates significant waste while often causing the loss of material value at the end of product life. The circular economy seeks to change this pattern by retaining the value and functionality of products, components and materials for as long as possible. Circularity therefore extends beyond waste recycling and includes product design, resource-efficient production, responsible consumption, repair, refurbishment, reuse, remanufacturing and high-quality recycling. A life-cycle perspective is required because decisions at different stages of the value chain influence material demand and the potential for material recovery (European Environment Agency, 2024). At the European Union level, the transition is supported by the Circular Economy Action Plan and the wider European Green Deal. The EU monitoring framework includes the circular material use rate (CMUR), which measures the contribution of recycled materials to total material use rather than only the proportion of waste that is recycled. The indicator therefore provides a direct link between waste management, secondary raw materials and the broader resource-use system (European Commission, 2020; Eurostat, 2018). The objective of this paper is to assess CMUR development in the EU-27 and Serbia and to position Serbia within the European context. The analysis focuses on the latest available 2024 data, examines changes since 2010, compares Serbia with the EU-27 average and individual Member States, and discusses implications for Serbia's transition towards greater material circularity.

[1]Corresponding author, nikolakaranovic@ua.pt, ORCID: 0000-0002-7498-6103
[2]visnjamihajlovic@uns.ac.rs, ORCID: 0000-0002-9750-1076

CIRCULAR ECONOMY AND MATERIAL CIRCULARITY: THEORETICAL BACKGROUND

A circular economy is an economic system that aims to reduce primary resource extraction and retain the value of products and materials through longer and repeated use cycles.
This requires changes throughout the material life cycle. At the design stage, products can be developed to support durability, repair, refurbishment, disassembly and recycling.
During production, resource efficiency and the retention of residues and by-products can reduce material losses. During use, repair, sharing, reuse and product life extension can reduce demand for new products. At end of life, effective collection, sorting and treatment systems can return materials to productive use (EEA, 2024). A distinction is therefore needed between recycling performance and material circularity. A high recycling rate does not necessarily imply a high level of circular material use if recycled materials represent only a small share of materials entering the economy. CMUR addresses this issue by relating circular use to overall material use and thereby indicating the extent to which secondary materials substitute for primary raw materials (Eurostat, 2018). The indicator is also relevant to resource security. Greater use of secondary materials can reduce pressure on natural-resource extraction and, in some circumstances, reduce dependence on imported primary resources. Circularity can therefore contribute simultaneously to environmental objectives and economic resilience. However, increasing circularity cannot be achieved through recycling alone. Reducing unnecessary material demand, extending product lifetimes and improving resource productivity are also important components of a circular economy transition (EEA, 2025). Material composition is important when interpreting CMUR. Metals can often be recovered and recycled efficiently, whereas fossil energy carriers are predominantly combusted and therefore cannot be recycled as materials. Non-metallic minerals account for a very large share of material consumption, so changes in their circular use can have a substantial influence on the aggregate indicator (EEA, 2025).

MATERIAL AND METHODS

The analysis uses secondary statistical data from Eurostat, the EEA and Statistical Office of the Republic of Serbia (SORS). For the EU-27, the principal source is the EEA indicator 'Circular material use rate in Europe', which is based on Eurostat data and provides annual values for 2010–2024 (Eurostat, 2025a). For Serbia, the latest national CMUR value is taken from the SORS Eco-bulletin 2024, while 2024 material-flow data are taken from the SORS statistical release on material flow indicators. The analysis is descriptive and comparative; it does not estimate causal relationships or forecast future CMUR values. CMUR is defined as the ratio between circular use of materials (U) and overall material use (M). Overall material use is the sum of domestic material consumption (DMC) and circular use. Circular use is approximated from waste recycled in domestic recovery operations, adjusted for imports and exports of waste destined for recycling. Eurostat includes recovery operations R2-R11 in the calculation (Eurostat, 2018, 2025b).

$$CMUR = \frac{U}{M} \times 100 \quad (1)$$

$$M = DMC + U \quad (2)$$

In which, CMUR is the circular material use rate, U is circular use of materials, M is overall material use and DMC is domestic material consumption. A higher CMUR indicates that a greater proportion of material use is supplied by secondary rather than primary materials. The Eurostat indicator is compiled from waste statistics, economy-wide material flow accounts and international trade in goods statistics (Eurostat, 2025b).

RESULTS AND DISCUSSION

EU trends

The EU CMUR increased from 10.7% in 2010 to 12.2% in 2024, an increase of 1.5 percentage points.
Despite this improvement, the share of recycled materials in total material use remains relatively low. The EEA assessment indicates that the EU is not currently on track to double the CMUR by 2030 (EEA, 2025). The EU objective is to double the circular material use rate between 2020 and 2030, reaching 22.4% by 2030 under the 8th Environment Action Programme. The Clean Industrial Deal has subsequently expressed an ambition of 24% by 2030. Starting from 12.2% in 2024, reaching 22.4% would require annual growth of more than 1.7 percentage points, greater than the total increase achieved between 2010 and 2024 (EEA, 2025). The positive trend up to 2022 was mainly associated with increased recycling while domestic material consumption remained relatively stable. Between 2022 and 2024, EU domestic material consumption fell by approximately 9%, largely reflecting reduced metal consumption. A reduction in overall material use can therefore increase CMUR even without a proportionally equivalent increase in recycled material use (EEA, 2025). Material groups show substantial differences. In 2024, CMUR was 23.4% for metal ores compared with only 3.8% for fossil energy materials. Non-metallic minerals accounted for more than half of total material consumption, making them particularly important for the aggregate indicator (EEA, 2025).

Table 1. *Circular material use rate in EU Member States, 2024.*

Country	CMUR 2024 (%)
Netherlands	32.7
Belgium	22.7
Italy	21.6
Estonia	20.5
Malta	18.6
France	17.8
Austria	15.2
Czech Republic	14.8
Germany	14.8
EU-27	12.2
Slovakia	12.2
Luxembourg	10.7
Sweden	10.4
Slovenia	10.1
Denmark	9.4
Poland	7.7
Spain	7.4
Hungary	7.3
Latvia	6.8
Croatia	5.9
Cyprus	5.5
Greece	5.2
Bulgaria	5.0
Lithuania	4.2
Portugal	3.0
Ireland	2.0
Finland	2.0
Romania	1.3

Note. Source: EEA (2025), based on Eurostat data.

The 2024 data show substantial variation across the EU. CMUR ranged from 32.7% in the Netherlands to 1.3% in Romania, a difference of 31.4 percentage points. The Netherlands, Belgium, Italy and Estonia all exceeded 20%, while Romania, Finland and Ireland recorded the lowest values (EEA, 2025; Eurostat, 2025c). Most Member States improved their CMUR since 2010: 22 of 27 recorded an increase. Malta, Estonia and Italy had the largest absolute increases, while Latvia, Croatia and Malta more than tripled their CMUR in relative terms. Finland, Romania and Luxembourg experienced decreases of more than 50% (EEA, 2025). The variation indicates that national structural conditions matter. Differences in recycling systems, material-use patterns and economic structure influence the capacity to feed secondary materials back into production. The performance of the Netherlands and Belgium, both above the EU 2030 target, demonstrates that substantially higher CMUR levels are achievable in Europe (EEA, 2025).

Serbia trends

Serbia's CMUR remains substantially below the EU average. The latest SORS data report 0.5% in 2010, 1.1% in 2015, 1.3% in 2020 and 1.2% in 2024. The long-term increase between 2010 and 2024 was therefore 0.7 percentage points, although the indicator declined slightly after 2020 (Statistical Office of the Republic of Serbia, 2025a). The latest national series should be used for the 2024 Serbia/EU comparison because it incorporates the most recent statistical information and revisions. Earlier EEA assessments reported a CMUR of 1.7% for Serbia in 2021; this historical value should not replace the revised 2024 national series when assessing current performance (EEA, 2025b; SORS, 2025a). The low Serbian CMUR occurs alongside substantial material consumption. In 2024, domestic material consumption amounted to 151453 million tonnes. Metal ores represented the largest material category at 47020 million tonnes, followed by fossil energy materials at 40952 million tonnes and non-metallic minerals at 36403 million tonnes (SORS, 2025b). This combination of high material throughput and low circular material use indicates substantial potential for increasing the role of secondary materials. Serbia's material-flow profile also highlights the need to look beyond recycling alone. Increasing CMUR requires more material to be fed back into the economy relative to overall material use. Resource efficiency, reuse, product-life extension, industrial symbiosis and reliable markets for secondary raw materials can therefore complement improvements in recycling infrastructure.

Serbia/EU comparison

In 2024, Serbia's CMUR of 1.2% was 11 percentage points below the EU average of 12.2%. The EU average was approximately 10.2 times higher than the Serbian value, meaning that Serbia's CMUR was only about 9.8% of the EU average (EEA, 2025; SORS, 2025a). The gap has existed throughout the period considered. In 2010, Serbia recorded 0.5%, compared with 10.7% for the EU. By 2024, Serbia had increased by 0.7 percentage points, while the EU had increased by 1.5 percentage points. Serbia therefore improved, but from a substantially lower starting point and at a slower absolute rate.

Table 2. *Comparison of circular material use rate in Serbia and the EU-27.*

Indicator	Serbia	EU-27
CMUR, 2010 (%)	0.5	10.7
CMUR, 2024 (%)	1.2	12.2
Change, 2010–2024 (pp)	+0.7	+1.5
Serbia relative to EU average, 2024	9.8%	100%
Gap in 2024 (pp)	11.0	—

Note. pp = percentage points. Sources: EEA (2025) and SORS (2025a).

Serbia's 1.2% in 2024 was slightly below Romania's 1.3%, the lowest value among EU Member States. Finland and Ireland each recorded 2%, while Portugal recorded 3%. At the other end of the distribution, the Netherlands reached 32.7%, Belgium 22.7% and Italy 21.6% (EEA, 2025; Eurostat, 2025c). Relative to the Netherlands, Serbia's CMUR was approximately 27 times lower in 2024; it was approximately 19 times lower than Belgium's and 18 times lower than Italy's. These ratios illustrate the scale of the gap but should be interpreted as descriptive comparisons rather than causal measures.

Implications for Serbia

The results suggest that Serbia's transition towards greater material circularity requires a systemic approach. A first priority is to increase the quantity and quality of secondary materials that can be returned to productive use. This involves improved separate collection, sorting and treatment, but also quality standards and market conditions that allow recycled materials to compete with primary raw materials.
The material composition of Serbian consumption should be considered. Metal ores and non-metallic minerals account for substantial material flows, and interventions that increase reuse and recycling of high-volume streams can have a greater effect on aggregate CMUR than interventions focused only on small waste streams. Construction and infrastructure activities are particularly relevant because they involve large quantities of mineral materials. Serbia can improve circularity by reducing overall material demand. CMUR can increase through a larger circular use component, lower overall material use, or both. Policies promoting resource productivity, product life extension, reuse, repair, remanufacturing and industrial symbiosis should therefore complement conventional recycling measures. CMUR should be interpreted alongside other indicators. It is useful for measuring the contribution of secondary materials to overall material demand, but it should be complemented by indicators on material consumption, waste generation, recycling, resource productivity and material footprints. Such a dashboard would provide a more complete assessment of Serbia's circular economy transition.

CONCLUSION

The analysis demonstrates a substantial difference in circular material use between Serbia and the EU. The EU CMUR increased from 10.7% in 2010 to 12.2% in 2024, while Serbia's CMUR increased from 0.5% to 1.2%. Although both have improved over the long term, Serbia remains at the lower end of the European distribution. In 2024, Serbia's CMUR was 11 percentage points below the EU average and slightly below Romania, which recorded the lowest EU value at 1.3%. The EU itself faces a significant challenge: at 12.2% in 2024, it is not on track to reach the 22.4% target for 2030. The performance of the Netherlands, Belgium, Italy and Estonia demonstrates that substantially higher levels of circular material use are possible. For Serbia, the findings indicate considerable potential for improvement. Increasing recycling capacity and performance is necessary but insufficient. Progress will also depend on demand for secondary raw materials, quality of recovered materials, reuse and repair, industrial symbiosis, resource productivity and reduced primary material consumption. Particular attention should be given to material-intensive sectors and high-volume material groups. Future research should investigate the structural determinants of Serbia's low CMUR and identify which material groups and economic sectors offer the greatest potential for increasing circular material use. Combining CMUR with material flow analysis, resource productivity and sector-specific circularity indicators could provide a stronger basis for policy design and monitoring Serbia's convergence with EU circular economy objectives.

REFERENCES

European Commission. (2020). A new circular economy action plan: For a cleaner and more competitive Europe (COM/2020/98 final). https://environment.ec.europa.eu/strategy/circular-economy-action-plan_en

European Environment Agency. (2024). Accelerating the circular economy in Europe: State and outlook 2024. https://www.eea.europa.eu/publications/accelerating-the-circular-economy

European Environment Agency. (2025). Circular material use rate in Europe. https://www.eea.europa.eu/en/analysis/indicators/circular-material-use-rate-in-europe

European Environment Agency. (2025). Circular material use rate: Serbia. Europe's environment 2025. https://www.eea.europa.eu/en/europe-environment-2025/countries/serbia/circular-material-use-rate

Eurostat. (2018). Circular material use rate - Calculation method - 2018 edition. Publications Office of the European Union. https://doi.org/10.2785/132630

Eurostat. (2025a). *Circular economy – material flows*. Statistics Explained. https://ec.europa.eu/eurostat/statistics-explained/index.php?title=Circular_economy_-_material_flows

Eurostat. (2025b). *Circular material use rate (env_ac_cur): Metadata*. https://ec.europa.eu/eurostat/cache/metadata/en/env_ac_cur_esms.htm

Eurostat. (2025c). *Over 12% of materials in the EU come from recycling*. https://ec.europa.eu/eurostat/web/products-eurostat-news/w/ddn-20251119-1

Statistical Office of the Republic of Serbia. (2025a). Eco-bulletin, 2024 (Bulletin 729). https://publikacije.stat.gov.rs/G2025/pdfE/G20255729.pdf

Statistical Office of the Republic of Serbia. (2025b). Material flow indicators, 2024. Statistical Release. https://publikacije.stat.gov.rs/G2025/HtmlE/G20251334.html

DOI:10.5937/IIZS26378N

ULTRASONIC WELDING AS SUSTAINABLE TEXTILE JOINING METHOD

Research paper

Ineta Nemeša[1], Marija Pešić[2], Danka Đurđić[3], Valentina Bozoki[4]
[1,2,3,4]University of Novi Sad, Technical Faculty, Zrenjanin, Serbia

Abstract: Ultrasonic technology is successfully used manufacturing wide variety of apparel and technical textile goods.It is suitable for synthetic fabrics due to their low melting points and ability to absorb ultrasonic energy efficiently. Two main types of ultrasonic textile equipment used are: roll seam machines and platen presses. Using ultrasonic technology can be performed textile seam welding, cutting, lamination, punching, embossing, lacing, riveting, inserting. Comparing with traditional sewing method ultrasonic technology can ensure several advantages: higher processing speed, higher strength of seams, and ability to create waterproof and airtight seams. Advantages that support sustainable garment manufacturing goals are: reduced waste and energy use, improved fabric recyclability, improved workplace environments for the industrial workforce.
Key words: textile joining methods, ultrasonic welding, waste reduction, textile recycling

INTRODUCTION

Ultrasonic technology has been used to weld thermoplastic materials in industrial applications since the 1950s. Since then, it is improved and has become an important and widely used industrial process. In nowadays ultrasonic technology is also successfully used manufacturing wide variety of apparel and technical textile goods (Jones, 2013; RINCO Ultrasonics, 2026. -b) (see Fig.1).
By help of ultrasonic equipment water and wind proof seams are created for outdoor and special performance wear. In lingerie, sportswear and seamless underwear this technology creates highly elastic, smooth, threadless seams that significantly improve wear comfort. Hygienic bonding and durability got by help of ultrasound are very important in medical and protective clothing (Hyusonic, 2025).
In the group of technical textile goods: filters, filtration bags, waterproof bags, canvas covers, awnings, tents, geotextiles, car interior trim components, airbags, seat covers, acoustic soundproofing materials and many others products are manufactured using ultrasound technology (Jones, 2013; RINCO Ultrasonics, 2026. -b; Hyusonic, 2025).



a **b**

Fig.1 *Jacket (a) created from textile material embossed by ultrasound (b)*

[1] Corresponding author, inetavil@gmail.com, ORCID: 0000-0003-2552-3097
[2]marija.pesic@uns.ac.rs, ORCID: 0000-0002-3745-7771
[3]danka.dordic@uns.ac.rs, ORCID: 0009-0003-4369-8306
[4]valentina.bozoki@uns.ac.rs, ORCID: 0009-0000-4045-3539

THE MAIN CHARACTERISTICS OF TEXTILE ULTRASOUND WELDING TECHNOLOGY

Ultrasonic textile welding process

Ultrasonic textile welding uses high-frequency acoustic vibrations to generate frictional heat. This heat melts synthetic origin materials, fuse and join them together at the molecular level. The welding process consists on several work steps (Jones, 2013; RINCO Ultrasonics, 2026. -d; Dizo Global, 2026. ; MURISCUT, 2026.):

- ultrasonic generator produces high-frequency sound waves typically in the range of 20–40 kHz.
- The sound waves are directed to processed material through a sonotrode, also called a horn. The sonotrode vibrates at high frequency, creates molecular friction and heat in fabric layers.
- Synthetic fibers soften and melt. The molecules from both layers of material are intermingled by the diffusion process and a weld is formed.
- When ultrasonic vibrations are stopped, the melted materials cool down and create durable bond.

Textile materials used for ultrasonic welding

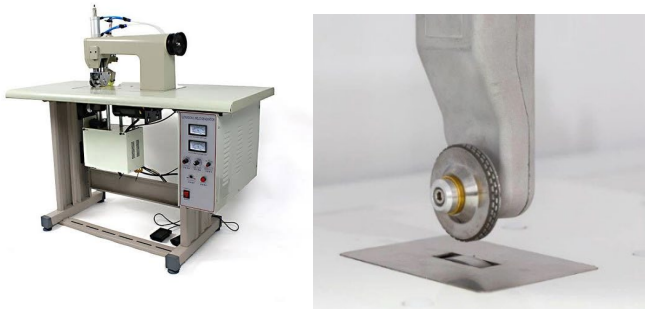
Ultrasonic welding is suitable for synthetic fabrics due to their low melting points and ability to absorb ultrasonic energy efficiently. The most commonly processed materials are: 100% synthetic origin textiles (polyester, nylon, polypropylene, polyvinylchloride, polyethylene, polyurethane, spandex/elastine) and mixed synthetic and natural origin fabrics (textiles with at least 60% synthetic fibers content). Ultrasonic welding cannot be performed for natural origin textiles, glass fibres and high-heat polymers (RINCO Ultrasonics, 2026. -d; MURISCUT, 2026.).

ULTRASOUND TEXTILE WELDING EQUIPMENT

The various types of ultrasonic textile equipment are primarily categorized by how the sonotrode moves related to the material. Two main types are: roll seam machines and platen presses (MURISCUT, 2026. ; Sonomax, 2026.).

Roll seam welding machines (ultrasonic sewing machine)

A machine operates similar to a traditional sewing machine. Continuous weld seams are created by the rotating (driven) circular sonotrode paired with an anvil roller (see Fig.2). As a processed material passes in between a sonotrode and an anvil, vibration created by ultrasonic weaves welds them together. The interchangeable sonotrodes and anvils can be differently designed and patterned to perform seaming, cutting and embossing operations (MURISCUT, 2026. ; Cheersonic, 2026. ; SONOTRONIC, 2024).



a b

Fig.2. *Roll seam welding machine (a) and a circular anvil paired with a sonotrode roller (b)*

Platen ultrasound welding presses

During the work process the textile material is held stationary on a fixed anvil (see Fig.3). The sonotrode of the machine moves downwards to apply pressure and ultrasonic energy and perform the needed operation – welding, cutting or embossing (MURISCUT, 2026. ; Sonomax, 2026.).



Fig. 3. *Platen ultrasound welding presses*

ULTRASOUND WELDING OPERATIONS

Using ultrasonic weave technology can be performed following textile treatment operations: seam welding, cutting, lamination, punching, embossing, lacing, riveting, inserting (MURISCUT, 2026. ; Raytech, 2026. ; RINCO Ultrasonics, 2026. -c).

Seam welding

Ultrasonic seam welding is used to join two or more plays of fabric together. Depending on equipment continuous welds, spot welds and seams of free geometry are created. Continuous welds are processed by roll seam machines. Spot welds and small size welds with a certain fixed geometry are created byplaten welding presses (see Fig.4).



a b

Fig.4. *Continuous welding (a) and spot weld (b)*

Cutting

Ultrasonic technology can be also used to separate thermoplastic materials. In cutting applications a shape of cutting tool is a sharp blade (for roll seam machines), guillotine, or knife-edge. When thermoplastic textiles are cut, their edges are sealed and protected against material frying (6).
Material edge cutting and joining of components can be also performed simultaneously using a roll seam welding machine with a single anvil wheel or a double tool anvil (see Fig.5).

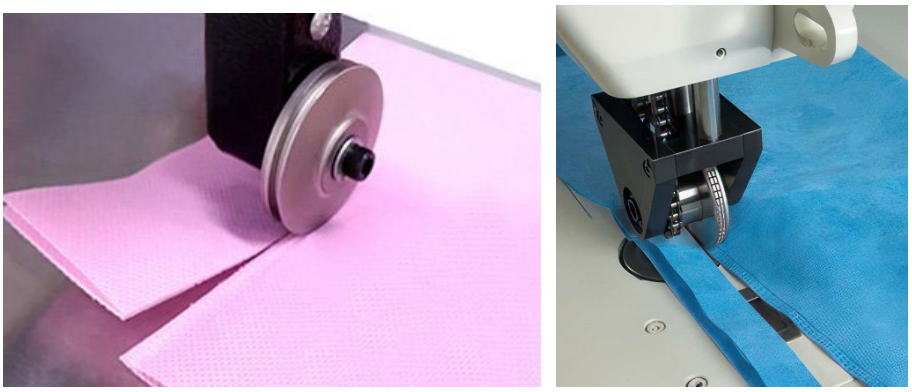


Fig. 5. *Sharp blade anvil wheel of a roll seam machine to cut and join material*

Ultrasonic lamination, embossing and quilting

All three processes refer to continuous joining of multiple flat layers of fabric together across their entire surface to create a single composite material. Often in professional literature terms lamination, embossing and quilting are used with a single meaning. However, there are three different processes.
During the lamination process two or more plays of material is joined in single one. Embossing adds texture to the material surface - three-dimensional patterns or logos. Quilting process connects three material layers - top fabric, filling, and back fabric together and creates a padded composite fabric with 3D texture (MURISCUT, 2026. ; SONOTRONIC, 2026.) (see Fig.6).



Fig.6. *Textile material with embossed pattern (a) and quilted pattern (b)*

Ultrasonic lacing

Ultrasonic textile lacing is a manufacturing process that cuts, joins, and embosses textiles (see Fig. 7). Lace machines can be designed like a traditional sewing machine or wide high productivity special purpose machines (MURISCUT, 2026. ; Alster Industry, 2025).

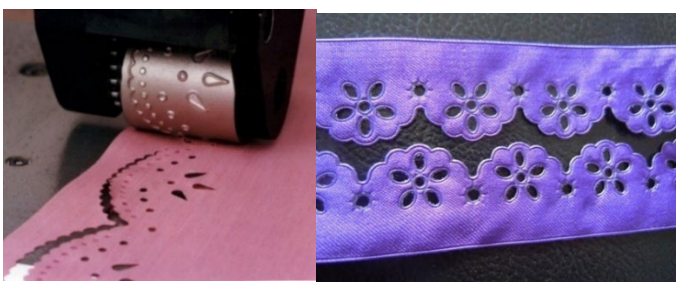


Fig. 7. *Lace formation by an ultrasonic welding machine*

SUSTAINABLE BENEFITS OF TEXTILE ULTRASOUND WELDING

Ultrasonic welding as an alternative to traditional fabric sewing method can ensure several advantages: higher processing speed, higher strength of seams, and ability to create waterproof and airtight seams (Miller Weldmaster, 2025). There are also advantages that support sustainable garment manufacturing goals - reduced waste and energy use, improved fabric recyclability, as well as, improved workplace environments for the industrial workforce (RINCO Ultrasonics, 2026. -b; Sonic Italia, 2026. ; Sonomax, 2026.).

Reduced use of raw materials and their potential waste

Reduced use of auxiliary materials

Sewing threads and chemical adhesives used by other textile joining methods are not needed performing ultrasonic welding. The components are mutually joined in molecular level by help of ultrasonic energy only.

Reduced amounts of chemical origin waste

Not using sewing threads and chemical adhesives in textile component join process, their production and further chemical waste at the end of the life cycle of textile goods is lowered.

Waterproof and airtight seams without use of auxiliary materials

By help of ultrasonic welding technology seams can be created fully waterproof and even airtight. Using traditional sewing method a needle makes holes in processed material and a seam created by threads is not air and waterproof. Additional work steps, equipment and auxiliary materials (tapes, glues, equipment, and energy) are used to create fully sealed seams (Hyusonic, 2025).

Less waste from used ultrasonic equipment

Ultrasonic welding equipment has less mechanical parts comparing with standard sewing machine. No needles, drive belts, tension mechanisms that can wear out, have to be changed and at the end of their use wasted.

Improved recyclability of textile goods

Sorting of textile waste on the bases of their fiber origin, separation of contaminants like zippers, buttons, and labels is the first and very important work step performing textile chemical recycling process. The quality of regenerated fibers obtained in chemical recycling process depends on a large extent on purity of textile waste processed.
Recycling of textile goods manufactured by ultrasonic technology (cutting and joining their components) gives higher quality regenerated raw material as they do not contain mixed origin materials - different origin thread types and glues which are used in traditional sewing process and are impossible to separate from textile goods before their recycling (Nemeša et al., 2024; Nemeša et al., 2025).

Sustainable energy practices

Only molecule frictional heat is generated

The ultrasonic technology uses high-frequency mechanical vibrations to generate localized molecular friction directly inside the synthetic fibers, meaning it does not waste energy heating the entire equipment or ambient air.

Extra work steps are eliminated

Ultrasonic welding equipment can cut, seal, and join synthetic textiles in a single work step, without need for secondary finishing or thermal sealing operations that consume extra energy.

Higher processing speed

Ultrasonic welding is up to 70–80%faster than traditional sewing. It can ensure joining of 10 to 20 meters per minute while sewing typically can reach 3 to 6 meters per minute. Reducing processing time, energy consumption spend to manufacture a single textile product is reduced too (Miller Weldmaster, 2025).

Improved workplace conditions for the workers

Work environments with reduced contaminant levels

Performing ultrasound cutting thermoplastic textiles melt and their edges are sealed. This prevents dust generation during cutting process of textile material, as well as, during other manipulations with cut components as fabric edges cannot fry anymore (Nemeša et al., 2024). The same time, there is no contamination of half-finished and ready textile goods and production premises with sewing thread ends and fried fibers of textile materials as they do not exist in the manufacturing process.

No hazardous evaporations

As processing airtight and waterproof seams chemical adhesives are not used, their evaporations cannot contaminate environment.

No temperature increase

Using ultrasound technology the heat is generated locally - only inside the processed workpieces by help of high-frequency mechanical vibrations and friction. The welding tools (a sonotrode, an anvil or others) do not heat up. Thus there is no temperature increase in environment because of heated up work process machinery.

A lower-stress work environment for machine operators

As material joining is performed without sewing threads, tapes, glues there is no needed additional attention of the operator for thread and a tape fixing, changing during the working hours. Accidental thread breakage, seam quality problems connected with of threads and their sewing parameters does not exist. Operators of welding machines work in more relaxed conditions with less mental tension.

CONCLUSION

Ultrasonic welding has become important textile goods manufacturing method that can ensure several important advantages comparing with other traditional textile joining methods, such as, sewing, fusing, thermal welding, laser cutting, others. The wide application of ultrasound technology mostly is based on its ability to ensure very high processing speeds and with it high productivity, high quality of created seams and current wide use of thermoplastic textiles in different industries.
Additionally, ultrasonic technology facilitates sustainable manufacturing practices, aligning with the heightened industrial demand seen over the last ten years – reduction of raw material use, textile waste, and energy consumption.

REFERENCES

Alster Industry. (2025). *Ultrasonic lace machine – How to attach the lace to fabrics?* https://www.alsterindustry.com/ultrasonic-lace-machine-how-to-attach-the-lace-to-fabrics/ (Accessed August 2026).

Cheersonic. *The technology of roller ultrasonic sewing machines.* https://www.cheersonic-fabric.com/the-technology-of-roller-ultrasonic-sewing-machines/ (Accessed August 2026).

Dizo Global. *How textile welding is transforming fabric manufacturing.* https://www.dizo-global.com/textiles-plastic-welding (Accessed August 2026).

Hyusonic. (2025, December 4). *Ultrasonic welding in the apparel industry: Benefits and uses.* https://hyusonics.com/ultrasonic-welding-in-apparel-industry-benefits-and-uses/ (Accessed August 2026).

Jones, I. (2013). Ultrasonic and dielectric welding of textiles. In I. Jones & G. K. Stylios (Eds.), *Joining textiles: Principles and applications* (pp. 374–397). Woodhead Publishing. https://doi.org/10.1533/9780857093967.3.374

Miller Weldmaster. (2025, June 26). *Industrial sewing vs. fabric welding: Pros, cons, and best uses of each.* https://www.weldmaster.com/blog/welding-vs-sewing-fabrics (Accessed August 2026).

MURISCUT. *Ultrasonic welding.* http://muriscut.com (Accessed August 2026).

Nemeša, I., Pešić, M., & Bozoki, V. (2024). Mechanical recycling of textile waste. *Tekstilna industrija, 72*(4), 24–28. https://doi.org/10.5937/tekstind2404024N

Nemeša, I., Pešić, M., & Bozoki, V. (2025). Chemical recycling of textile waste. *Tekstilna industrija, 73*(1), 56–61. https://doi.org/10.5937/tekstind2501056N

Raytech. *Ultrasonic technology: Cutting, welding, punching and riveting of plastics and textiles.* https://raytech.com.au/ultrasonics-cutting-welding-punching (Accessed August 2026).

RINCO Ultrasonics. (a). *Non-woven & textile.*https://www.rincoultrasonics.com/applications/non-woven-textile/ (Accessed August 2026).

RINCO Ultrasonics. (b). *Our ultrasonic expertise benefits you.* https://www.rincoultrasonics.com/ultrasonic-knowledge/ (Accessed August 2026).

RINCO Ultrasonics. (c). *Ultrasonic cutting.* https://www.rincoultrasonics.com/ultrasonic-knowledge/ultrasonic-cutting/ (Accessed August 2026).

RINCO Ultrasonics. (d). *Ultrasonic technology.* https://www.rincoultrasonics.com/ultrasonic-knowledge/ultrasonic-technology/ (Accessed August 2026).

Sonic Italia. *Ultrasonic cutting for synthetic fabrics.* https://sonicitalia.com/en/industry-specific-ultrasonic-solutions/ultrasonic-cutting-for-synthetic-fabrics/ (Accessed August 2026).

Sonomax. *Ultrasonic welding of thermoplastic materials by sector: Textile.* https://www.sonomax.it/en_gb/sector/textile-2/ (Accessed August 2026).

SONOTRONIC. (2024). *Ultrasonic roll seam module supported at both ends: Continuous ultrasonic cutting and sealing.* https://sonotronic.de/media/filer_public/0c/67/0c679ff6-b383-48a1-aaf3-41b69cd3f73f/sonotronic-rollnaht-textil-en.pdf (Accessed August 2026).

SONOTRONIC. *Ultrasonic systems for processing technical textiles.* https://sonotronic.de/media/filer_public/60/4f/604f33bb-fb24-46fd-a45e-8f5fd56be2ae/sonotronic-textilbearbeitung-en.pdf (Accessed August 2026).



XVI International Conference Industrial Engineering and Environmental Protection 2026 (IIZS 2026)
October 01-02, 2026, Zrenjanin, Serbia

Session 6

Health and Environmental Protection

DOI:10.5937/IIZS26386P

SPATIAL AND SEASONAL DISTRIBUTION OF POLYCYCLIC AROMATIC HYDROCARBONS AND TOTAL PETROLEUM HYDROCARBONS IN DANUBE RIVER SEDIMENTS (SERBIA)

Research paper

Marija Perović[1*], Tanja Nenin[2], Tatjana Mitrović[3]
[1,2] Jaroslav Černi Water Institute, Belgrade, Serbia
[3]Institute of Physics Belgrade, Serbia

Abstract: Polycyclic aromatic hydrocarbons (PAHs) and total petroleum hydrocarbons (TPH) are persistent organic pollutants widely distributed in various environmental compartments, including air, water, soil, and sediments, where they tend to accumulate due to their hydrophobic nature. This study investigates the spatial and seasonal distribution of PAHs in sediments along the Serbian sector of the Danube River based on a long-term monitoring dataset (2012–2024). Surface sediment samples were collected at seven locations during spring and autumn sampling campaigns. The total concentration of 16 priority PAHs (Σ16PAHs) was analyzed to evaluate spatial variability and seasonal differences. The results showed that PAHs were present at all sampling sites, with noticeable spatial variability reflecting differences in anthropogenic pressures and local environmental conditions. Seasonal analysis revealed higher average Σ16PAHs concentrations during the autumn period (426.3 µg/kg) compared to spring (335.9 µg/kg), indicating the influence of runoff, atmospheric deposition, and hydrological conditions on PAH accumulation. Overall, contamination levels were classified as low to moderate, suggesting that although PAHs are persistently present, pollution does not reach levels typical of heavily impacted river systems. TPH were detected in more narrow range 114 mg/kg to 235 mg/kg in both season campaign. The findings highlight the importance of long-term and seasonal monitoring for reliable assessment of sediment quality in large river basins.
Key words: Polycyclic aromatic hydrocarbons (PAHs), Danube River, sediments, spatial distribution, seasonal variability, environmental monitoring

INTRODUCTION

Polycyclic aromatic hydrocarbons (PAHs) are a group of ubiquitous organic pollutants composed of two or more fused aromatic rings, primarily generated during incomplete combustion of organic matter. Due to their persistence, hydrophobicity, and semi-volatile nature, PAHs are widely distributed across environmental compartments, including air, water, soil, and sediments (Neff, 1979; Yunker et al., 2002). Total petroleum hydrocarbons (TPH), representing a broad group of aliphatic and aromatic hydrocarbons derived mainly from crude oil and petroleum products, are also commonly detected in aquatic environments. TPH originate predominantly from oil spills, fuel leakage, industrial discharges, and urban runoff, and are frequently associated with transport and storage of petroleum-derived products. PAHs originate from both natural and anthropogenic sources. Natural inputs include forest fires, volcanic activity, and diagenetic formation of PAHs in soils and sediments, as well as transformation of natural organic matter, while anthropogenic sources are predominantly associated with fossil fuel combustion, industrial processes, vehicle emissions, domestic heating, and waste incineration (Mastral & Callén, 2000; Ravindra et al., 2008). In contrast, TPH are primarily linked to petrogenic inputs, reflecting direct contamination by petroleum and its derivatives, although some overlap exists between PAH and TPH sources. Due to their low solubility and strong affinity for organic matter, both PAHs and TPH readily adsorb onto suspended particles and accumulate in river sediments. As a result, sediments act as long-term sinks of contamination, reflecting both historical inputs and ongoing pollution processes (Karickhoff et al., 1979; Baumard et al., 1998). These characteristics make sediments a suitable matrix for assessing the distribution and variability of hydrocarbon pollution in aquatic systems. The Danube River, as one of the most important European river systems, is exposed to diverse anthropogenic pressures along its course, including urban, industrial, and transport-

[1]Corresponding author, marija.perovic@jcerni.rs, ORCID: 0000-0003-2045-001X

related activities. These influences make it a relevant system for investigating the distribution of hydrocarbons in sediments.
This study is based on a long-term monitoring dataset previously analyzed in a more comprehensive study (Nenin et al., 2026), while the present work focuses on: (a) spatial variability of PAHs along the Serbian sector of the Danube, (b) seasonal differences between sampling campaigns, and (c) complementary assessment of TPH concentrations as an indicator of petrogenic contamination.

MATERIAL AND METHODS

Study area

The study was conducted along the Serbian section of the Danube River, one of the most important transboundary river systems in Europe. Seven sampling locations (S1–S7), including Smederevo (S1), Ram (S2), Veliko Gradište (S3), Donji Milanovac (S4), Tekija (S5), Kladovo (S6), and Kusjak (S7), were selected along a longitudinal gradient between rkm 1112 and rkm 864, covering areas characterized by different environmental conditions and potential anthropogenic influences, including navigation and hydromorphological modifications. A long-term monitoring program was implemented over the period 2012–2024, during so-called spring (April–July) and autumn sampling campaigns (September–November), as described in detail in Nenin et al. (2026). This design enabled the assessment of both spatial variability and seasonal differences in hydrocarbon contamination in river sediments, with particular focus on polycyclic aromatic hydrocarbons (PAHs) and total petroleum hydrocarbons (TPH).

Sampling and sample handling

Sediment samples were collected using a Van Veen grab sampler in accordance with ISO 5667–12:2017, targeting recently deposited surface material. After collection, samples were placed in pre-cleaned glass containers, transported to the laboratory under cooled conditions (≤4 °C), and analyzed within 30 days to minimize potential changes in composition.

Sample preparation and analysis

In the laboratory, sediment samples were air-dried at room temperature, homogenized, and sieved to obtain a representative fraction for analysis. Simultaneous extraction of PAHs and TPH (C10–C40) was performed using accelerated solvent extraction (ASE) in accordance with U.S. EPA Method 3545, an organic solvent mixture suitable for hydrophobic compounds, followed by concentration and purification of extracts. Quantitative determination of 16 priority PAHs (Σ16PAHs) and TPH (C10-C40) was carried out using gas chromatography coupled with mass spectrometry (GC–MS), in accordance with standard analytical procedures for semi-volatile organic compounds in environmental samples following analytical procedures described in Nenin et al. (2026).

Quality assurance and quality control

Quality assurance and quality control (QA/QC) procedures included the use of certified reference materials, participation in proficiency testing schemes, calibration with external standards, procedural blanks, and replicate analyses. Method performance was evaluated in terms of accuracy, precision, and recovery rates, ensuring the reliability of the analytical results.

Data analysis

PAH concentrations were expressed as Σ16PAHs and TPH in range C10 – C40 and analysed to assess spatial and seasonal variability. Seasonal mean values were calculated as the

average of site-specific concentrations for spring and autumn sampling campaigns. Descriptive statistical analysis was applied to summarize PAH and TPH concentrations, including calculation of minimum, maximum, and mean values. Sampling sites represent a range of environmental conditions along the river course, enabling the assessment of spatial variability in relation to potential anthropogenic influences.

RESULTS AND DISCUSSION

Spatial distribution of PAHs

PAHs were detected at all investigated sampling sites along the Serbian sector of the Danube River, confirming their widespread occurrence in sediments of large river systems influenced by anthropogenic activities. The mean concentrations of Σ16PAHs showed clear spatial variability among the sampling locations during both the spring and autumn campaigns (Figures 1 and 2). During the spring campaign, elevated concentrations were observed at downstream locations, particularly at S5 and S7, while lower values were recorded at S2 and S4. In contrast, during the autumn campaign, the highest concentrations were detected at S1 and S2, followed by S5, whereas lower levels were observed at S4. These differences indicate a seasonal shift in the spatial distribution of PAHs, likely influenced by variations in hydrological conditions, sediment transport, and local anthropogenic inputs. Despite the observed variability between sites and seasons, the overall contamination levels can be classified as low to moderate, which is consistent with findings reported for other European river systems. This suggests that, although PAHs are persistently present, contamination does not reach levels characteristic of heavily polluted environments.

Spatial distribution of TPH

TPH were detected at all sampling sites, indicating their continuous presence in Danube River sediments throughout the monitoring period (Table 1). Compared to PAHs, TPH concentrations exhibited a narrower range of variability (114–235 mg/kg), suggesting more stable input conditions and less pronounced spatial differentiation (Table 2). In the spring campaign, slightly elevated TPH concentrations were observed at S3 and S7, while lower values were recorded at S2 and S4. This pattern is generally consistent with the distribution of PAHs at downstream locations, indicating potential accumulation processes associated with sediment transport and deposition zones. During the autumn campaign, TPH concentrations increased at most sites, particularly at S1, S3, and S6, which may be related to enhanced surface runoff and remobilization of petroleum-derived contaminants. Despite these seasonal changes, spatial differences remained less pronounced compared to PAHs, suggesting that TPH inputs are more uniform and likely associated with diffuse sources such as navigation activities, fuel handling, and urban runoff along the river corridor. The classification of TPH concentrations indicates that most samples fall within the 100–500 mg/kg range, while lower concentrations (<100 mg/kg) were primarily observed at S2 and S4. Concentrations above 500 mg/kg were rare, confirming that petroleum hydrocarbon contamination is present but does not reach levels characteristic of heavily polluted environments. Overall, the relatively moderate and spatially uniform distribution of TPH, compared to the more variable PAH patterns, suggests different dominant input mechanisms, with TPH primarily reflecting petrogenic sources and PAHs being more strongly influenced by pyrogenic inputs and localized anthropogenic pressures.

Table 1. *Seasonal variation of average Σ16PAHs and TPH concentrations in sediment samples along the Danube River (Serbia)*

Location	Ave - spring Σ16PAH (μ/kg)	Ave - autumn Σ16PAH (μg/kg)	Ave - spring TPH (C10-C40) (mg/kg)	Ave - autumn TPH (C10-C40) (mg/kg)
S1	320.66	560.81	148.83	200.25
S2	203.22	508.57	115.48	114.26
S3	324.45	367.71	211.11	235.22
S4	216.35	268.75	133.39	156.98
S5	466.87	507.37	137.42	144.62
S6	386.03	407.84	132.52	186.25
S7	434.31	363.03	154.26	159.55
Ave	335.98	426.30	147.57	171.02

Table 2. *Distribution (%) of TPH concentration classes (<100, 100–500, >500 mg/kg) across sampling sites during spring and autumn campaigns*

Location	% spring < 100	% spring 100-500	% autumns < 100	% autumn 100-500	% autumn > 500
S1	45	55	40	50	10
S2	55	45	70	30	0
S3	27	73	20	70	10
S4	64	36	40	60	0
S5	55	45	30	70	0
S6	27	73	70	20	10
S7	27	73	30	70	0
MIN	27	36	20	20	0
MAX	64	73	70	70	10

Seasonal variation

Seasonal differences in PAH concentrations were observed between the spring and autumn sampling campaigns (Figures 1 and 2; Table 1). Mean Σ16PAHs concentrations were 336.0 μg/kg in spring and 426.3 μg/kg in autumn, indicating overall higher levels during the autumn period. This pattern is particularly evident at upstream locations (S1 and S2), where a pronounced increase in concentrations was recorded in autumn compared to spring. In contrast, downstream site S7 exhibited comparable or slightly lower values in autumn, indicating spatial variability in seasonal trends.

The observed increase in autumn concentrations may be associated with enhanced surface runoff, increased atmospheric deposition, and intensified anthropogenic activities such as domestic heating during colder months. In addition, hydrological conditions likely influence the accumulation of hydrophobic compounds, as lower flow regimes and sediment deposition processes can promote the retention of PAHs. These findings highlight the importance of seasonal monitoring, as single sampling campaigns may not adequately capture the spatial and temporal variability of sediment-associated contaminants.

In contrast to PAHs, TPH concentrations exhibited less pronounced seasonal variability (Figure 3; Table 1). Mean TPH concentrations were 147.6 mg/kg in spring and 171.0 mg/kg in autumn, indicating a moderate increase during the autumn period, but without a clear and consistent seasonal pattern across all sampling sites. Slight increases were observed at several locations (e.g., S1, S3, and S6), while others showed relatively stable values between campaigns.

The weaker seasonal signal observed for TPH suggests more continuous and diffuse inputs, likely related to navigation activities, fuel handling, and urban runoff along the river corridor.

Unlike PAHs, which are strongly influenced by seasonal combustion-related emissions and atmospheric deposition, TPH appears to reflect more stable petrogenic sources, resulting in lower temporal variability.

Temporal variability

The long-term monitoring dataset (2012–2024), previously reported in Nenin et al. (2026), confirms the persistent presence of PAHs in Danube River sediments. Due to their hydrophobic nature and strong affinity for particulate matter, PAHs tend to accumulate and remain in sediments over extended periods, reflecting both historical contamination and continuous anthropogenic inputs. Despite this persistence, no pronounced long-term increasing or decreasing trend was observed, suggesting relatively stable contamination levels throughout the monitoring period. In addition to PAHs, total petroleum hydrocarbons (TPH) were evaluated to provide complementary insight into hydrocarbon contamination. TPH concentrations also indicate a continuous presence in sediments, with relatively limited temporal variability compared to PAHs. This behavior suggests stable and diffuse petrogenic inputs over time, likely associated with navigation, fuel-related activities, and urban influences along the river.
Summary statistics of Σ16PAHs and TPH concentrations, based on site-averaged values, are presented in Table 3. The obtained results indicate moderate variability within each season, with slightly higher mean concentrations observed during the autumn period for both PAHs and TPH. However, the absence of strong temporal trends highlights the importance of long-term monitoring for reliable assessment of sediment quality and contaminant persistence in large river systems.

Table 3. *Summary statistics of Σ16PAHs and TPH (C10-C40) in Danube River sediments in μg/kg and mg/kg respectively*

Season	Parameter	Units	Min	Max	Mean
Spring	Σ16PAH	(μg/kg)	203.22	466.87	~336
Autumn	Σ16PAH	(μg/kg)	268.22	560.81	~426
Spring	TPH	(mg/kg)	115.48	211.11	~148
Autumn	TPH	(mg/kg)	114.26	235.22	~171

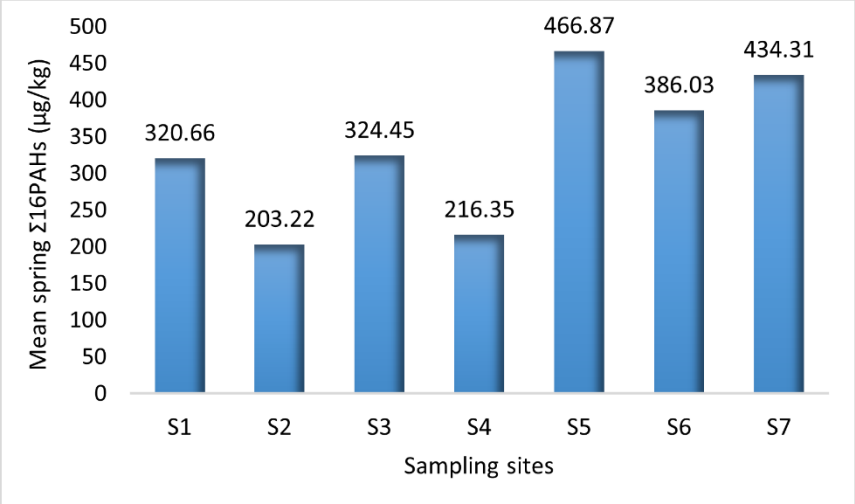


Fig. 1. *Mean Σ16PAHs concentrations along the Danube River during the spring campaign*

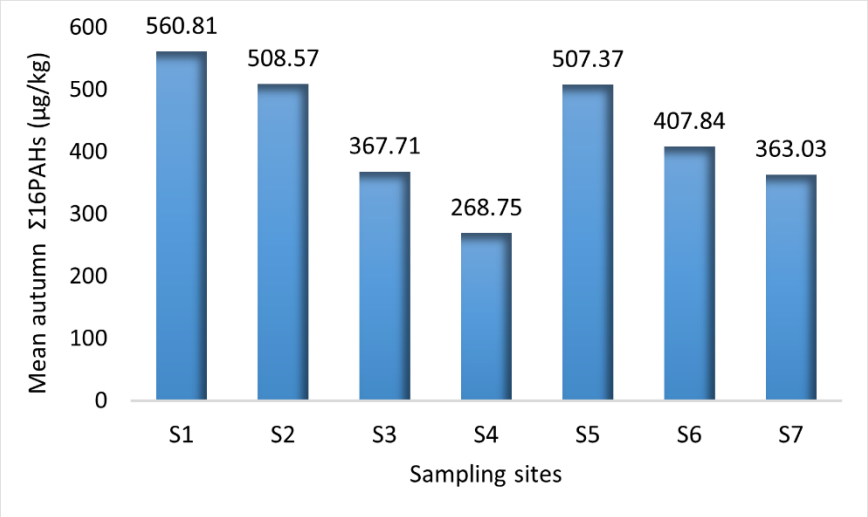


Fig. 2. *Mean Σ16PAHs concentrations along the Danube River during the autumn campaign*

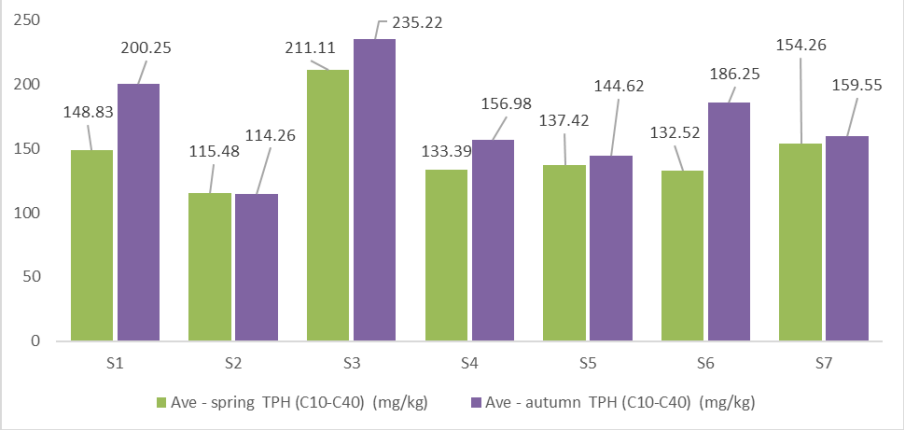


Fig. 3. *Seasonal variation of TPH (C10-C40) concentrations along the Danube River during the spring and autumn campaign*

Environmental implications

The results confirm that river sediments act as long-term sinks for hydrophobic organic pollutants such as PAHs and TPH. Due to their persistence and strong affinity for particulate matter, these compounds accumulate in sediments and may contribute to chronic exposure of benthic organisms, even at moderate concentrations. Such conditions can influence sediment quality and pose potential ecological risks over extended time scales. From a management perspective, the findings emphasize the importance of continuous monitoring programs, particularly in large transboundary river systems such as the Danube. Long-term datasets provide valuable insight into pollution dynamics, allowing for the identification of spatial patterns, temporal stability, and potential sources of contamination, while also supporting the evaluation of environmental policies and sediment management strategies. The observed spatial variability reflects differences in local environmental conditions and varying anthropogenic pressures along the river course. Variations in PAH concentrations along the longitudinal gradient suggest the influence of site-specific factors, including hydrological conditions, sediment characteristics, and localized emission sources related to urban, industrial, and transport activities. TPH concentrations were detected within a relatively narrow range (114–235 mg/kg) across both sampling campaigns, indicating moderate but consistent levels of petroleum hydrocarbons in sediments. According to Vane et al. (2018), concentrations below 100 mg/kg are typically associated with natural organic inputs (e.g., plant waxes and algal material), while values between 100 and 500 mg/kg suggest low to moderate anthropogenic petroleum influence. In this study, the dominance of the 100–500 mg/kg range

across most locations, particularly during the autumn campaign, indicates the prevalence of diffuse petrogenic inputs along the river system. In contrast, concentrations exceeding 500 mg/kg were rare and limited to isolated occurrences at specific sites (S1, S3, and S6), suggesting occasional episodic pollution events rather than persistent high-level contamination. Overall, the combined assessment of PAHs and TPH highlights the coexistence of pyrogenic and petrogenic inputs in Danube River sediments. While PAHs exhibit greater spatial and seasonal variability linked to combustion-related activities, TPH reflects more stable and diffuse sources associated with petroleum-derived contamination. This integrated approach provides a more comprehensive understanding of hydrocarbon pollution and supports informed environmental management in large river systems.

CONCLUSION

The results of this study confirm the widespread presence of PAHs in sediments along the Serbian sector of the Danube River, with clear spatial and seasonal variability. Differences among sampling locations reflect the influence of local anthropogenic pressures, hydrological conditions, and sediment dynamics. Higher Σ16PAHs concentrations observed during the autumn period indicate the role of enhanced runoff, atmospheric deposition, and accumulation processes under seasonal hydrological regimes. Despite this variability, overall contamination levels remain within the low to moderate range, suggesting that PAH pollution, although persistent, does not reach levels characteristic of heavily impacted river systems. TPH concentrations exhibited a relatively narrow range, indicating stable and generally low to moderate petroleum hydrocarbon input. The predominance of the 100–500 mg/kg fraction across most locations' points to diffuse petrogenic sources, while the limited occurrence of higher concentrations suggests occasional episodic inputs rather than widespread contamination. The combined assessment of PAHs and TPH provides a more comprehensive understanding of hydrocarbon contamination in river sediments, highlighting the coexistence of pyrogenic and petrogenic influences. These findings emphasize the importance of long-term and seasonal monitoring for reliable sediment quality assessment and provide a sound basis for future environmental management of large river systems such as the Danube.

REFERENCES

Baumard, P., Budzinski, H., Garrigues, P., Dizer, H., & Hansen, P. D. (1998). Polycyclic aromatic hydrocarbons in recent sediments and mussels (Mytilus edulis) from the Western Baltic Sea: Occurrence, bioavailability and seasonal variations. Marine Environmental Research, 47(1), 17–47. https://doi.org/10.1016/S0141-1136(98)00008-7

Karickhoff, S. W., Brown, D. S., & Scott, T. A. (1979). Sorption of hydrophobic pollutants on natural sediments. Water Research, 13(3), 241–248. https://doi.org/10.1016/0043-1354(79)90201-X

Mastral, A. M., & Callén, M. S. (2000). A review on polycyclic aromatic hydrocarbon (PAH) emissions from energy generation. Environmental Science & Technology, 34(15), 3051–3057. https://doi.org/10.1021/es001028d

Neff, J. M. (1979). Polycyclic aromatic hydrocarbons in the aquatic environment: Sources, fates and biological effects. Applied Science Publishers.

Nenin, T., Perović, M., Vuković, N., & Mitrović, T. (2026). Assessment of polycyclic aromatic hydrocarbons pollution in Danube River sediments across Serbia: Sources and ecological risk. Environmental Geochemistry and Health, 48, 56. https://doi.org/10.1007/s10653-025-02921-y

Pichler, N., de Souza, F. M., Ferreira dos Santos, V., & Martins, C. C. (2021). Polycyclic aromatic hydrocarbons (PAHs) in sediments of the Amazon coast: Evidence for localized sources in contrast to massive regional biomass burning. Environmental Pollution, 268 (Pt B), 115958. https://doi.org/10.1016/j.envpol.2020.115958.

Ravindra, K., Sokhi, R., & Van Grieken, R. (2008). Atmospheric polycyclic aromatic hydrocarbons: Source attribution, emission factors and regulation. Atmospheric Environment, 42(13), 2895–2921. https://doi.org/10.1016/j.atmosenv.2007.12.010

Vane, C. H., Lopes dos Santos, R. A., Kim, A. W., Moss-Hayes, V., Fordyce, F. M. & Bearcock, J. M. (2018). Persistent organic pollutants (PAH, PCB, TPH) in freshwater, urban tributary and estuarine surface sediments of the River Clyde, Scotland, UK. Earth and Environmental Science Transactions of the Royal Society of Edinburgh, 108(2–3), 299–313. https://doi.org/10.1017/S1755691018000294

Yunker, M. B., Macdonald, R. W., Vingarzan, R., Mitchell, R. H., Goyette, D., & Sylvestre, S. (2002). PAHs in the Fraser River basin: A critical appraisal of PAH ratios as indicators of PAH source and composition. Organic Geochemistry, 33(4), 489–515. https://doi.org/10.1016/S0146-6380(02)00002-5

DOI:10.5937/IIZS26394P

SOURCE APPORTIONMENT AND ECOLOGICAL RISK OF PAHS IN DANUBE RIVER SEDIMENTS (SERBIA)

Research paper

Marija Perović[1*], Tanja Nenin[2], Tatjana Mitrović[3]
[1,2] Jaroslav Černi Water Institute, Belgrade, Serbia
[3]Institute of Physics Belgrade, Serbia

Abstract: Polycyclic aromatic hydrocarbons (PAHs) are persistent organic pollutants widely distributed in aquatic environments, with sediments representing a major sink for their accumulation. In addition to concentration levels, the identification of pollution sources and assessment of toxic fractions are essential for understanding environmental risks. This study investigates the origin and ecological risk of PAHs in sediments of the Danube River (Serbia), based on a long-term monitoring dataset (2012–2024) previously reported in detail by Nenin et al. (2026). Source identification was performed using diagnostic ratios, particularly the low molecular weight to high molecular weight PAH ratio (LMW/HMW), while ecological relevance was evaluated through the proportion of carcinogenic PAHs (%7cPAH). Furthermore, sediment quality guidelines (SQGs), including the Threshold Effect Level (TEL) and Probable Effect Level (PEL), together with their quotient-based indices (TEL-Q and PEL-Q), were applied to assess the potential ecotoxicological risk of both individual and total PAH concentrations. The obtained LMW/HMW ratios were consistently below 1 across all sampling sites, indicating a dominant pyrogenic origin associated with combustion processes such as traffic emissions, industrial activities, and fossil fuel burning. The share of carcinogenic PAHs ranged up to 50%. According to the SQG-based assessment, ecological risk was generally classified as low (TEL level), with occasional exceedances corresponding to probable effect levels (PEL), particularly at selected locations.
Key words: PAHs, source apportionment, LMW/HMW ratio, carcinogenic PAHs, sediment quality guidelines, ecotoxicological risk, Danube River

INTRODUCTION

Polycyclic aromatic hydrocarbons (PAHs) are a group of persistent organic pollutants primarily generated during the incomplete combustion of organic matter, although they may also originate from petroleum-related sources. Due to their hydrophobic nature, low water solubility, and strong affinity for organic matter, PAHs readily associate with suspended particles and accumulate in sediments, where they can persist over long periods and reflect both historical and ongoing contamination processes (Neff, 1979; Karickhoff et al., 1979). In aquatic systems, sediments act not only as sinks but also as potential secondary sources of PAHs under changing environmental conditions, such as resuspension events or variations in redox conditions. Consequently, sediment analysis provides valuable insight into long-term pollution dynamics and the overall environmental status of river systems. Beyond concentration levels, identifying the origin of PAHs is essential for understanding pollution sources and supporting effective environmental management. Based on their formation mechanisms, PAHs are generally classified as petrogenic and pyrogenic, while biogenic and diagenetic sources are considered less significant in contamination studies. Diagnostic molecular ratios are widely applied for source apportionment, although their interpretation should be treated with caution due to potential alterations during environmental processes (Yunker et al., 2002; Tobiszewski & Namieśnik, 2012). The environmental relevance of PAHs is further emphasized by their toxic, mutagenic, and carcinogenic properties. High molecular weight PAHs are recognized as carcinogenic, and their relative contribution to total PAH concentrations is commonly used as an indicator of ecological risk (Boström et al., 2002; Nenin et al., 2026). However, concentration-based indicators alone may not fully reflect the potential biological effects of contaminants in sediments. Therefore, the application of sediment quality guidelines (SQGs), such as the Threshold Effect Level (TEL) and Probable Effect Level (PEL), provides an additional framework for evaluating the likelihood of adverse effects on benthic organisms.

[1]Corresponding author, marija.perovic@jcerni.rs, ORCID: 0000-0003-2045-001X

This study is based on a long-term monitoring dataset previously analyzed in detail by Nenin et al. (2026). The present work focuses on (i) source identification using diagnostic ratios, (ii) assessment of carcinogenic PAH fractions, and (iii) evaluation of ecological risk using a SQG-based approach (TEL/PEL and their quotient-based indices) in sediments of the Danube River (Serbia).

MATERIAL AND METHODS

Study area and sampling

The study was conducted along the Serbian sector of the Danube River. Seven sampling locations (S1–S7), including Smederevo (S1), Ram (S2), Veliko Gradište (S3), Donji Milanovac (S4), Tekija (S5), Kladovo (S6), and Kusjak (S7), were distributed along a longitudinal gradient between rkm 1112 and rkm 864. These sites represent different environmental settings along the river course. Surface sediment samples were collected within a long-term monitoring program (2012–2024), as described in detail in Nenin et al. (2026). The dataset was used for further analysis of PAH origin and ecological relevance through the application of diagnostic ratios and risk indicators.

Data analysis

To determine the origin of PAHs, diagnostic molecular ratios were applied to the long-term monitoring dataset previously described in Nenin et al. (2026). Source identification was performed using the ratio between low molecular weight (LMW) and high molecular weight (HMW) PAHs, expressed as:

$$\frac{\mathrm{LMW}}{\mathrm{HMW}} \tag{1}$$

where LMW represents the sum of low molecular weight PAHs (2–3 rings), typically including compounds such as naphthalene, acenaphthylene, acenaphthene, fluorene, phenanthrene, and anthracene, while HMW represents high molecular weight PAHs (4–6 rings), including fluoranthene, pyrene, benzo[a]pyrene, and related compounds. Values lower than 1 indicate a dominant pyrogenic origin, while values above 1 suggest petrogenic sources.

The ecological relevance of PAHs was evaluated using the proportion of carcinogenic compounds, calculated as:

$$\%7cPAH = \frac{\Sigma 7cPAH}{\Sigma 16PAH} \times 100 \tag{2}$$

where Σ7cPAH represents the sum of carcinogenic PAHs, including benzo[a]anthracene, chrysene, benzo[b]fluoranthene, benzo[k]fluoranthene, benzo[a]pyrene, indeno[1,2,3-cd] pyrene, and dibenzo[a,h]anthracene, while Σ16PAH represents the total concentration of priority PAHs.

The potential ecotoxicological risk of PAHs in sediments was assessed using SQGs, including the TEL and the PEL (Chen et al., 2015). For each individual PAH compound, the ratio between the measured concentration (Ci) and the corresponding guideline value (TELi or PELi) was calculated as TEL-Q and PEL-Q, respectively:

$$TEL\text{-}Q_i = \frac{C_i}{TEL_i} \tag{3}$$

$$PEL\text{-}Q_i = \frac{C_i}{PEL_i} \quad (4)$$

In order to evaluate the combined effect of PAH mixtures, mean quotient values (Mean TEL-Q and Mean PEL-Q) were calculated as:

$$SOG\ (TEL\ or\ PEL) = \frac{1}{n}\sum_{i=1}^{n}\frac{C_i}{PEL(or\ TEL)_i} \quad (5)$$

where C_i is the measured concentration of individual PAHs (μg/kg, dw), TEL_i and PEL_i are the corresponding guideline values, and n represents the number of detected compounds (Pichler et al., 2021). The obtained values were interpreted according to established SQG classification criteria, where lower values indicate a low probability of adverse effects, while higher values correspond to an increased likelihood of ecological risk.

TELi and PELi values were adopted from Pichler et al. (2021, Table 1). The classification criteria for SQG-TEL and SQG-PEL values, as well as the corresponding abbreviations, are presented in Table 2. Mean SQG-TEL and SQG-PEL values for Σ16PAHs were calculated according to Eq. (5). Average concentrations of individual PAHs were derived from the supplementary dataset reported by Nenin et al. (2026).

RESULTS AND DISCUSSION

Source identification

Site-averaged LMW/HMW ratios calculated over the entire monitoring period ranged from approximately 0.17 to 0.22, consistently indicating a dominant pyrogenic origin of PAHs and suggesting that combustion processes represent the primary source of contamination. (Figure 1). These sources are typically associated with traffic emissions, industrial activities, fossil fuel combustion, and atmospheric deposition of combustion-derived particles. The dominance of high molecular weight PAHs further supports the conclusion that pyrogenic inputs prevail over petrogenic sources. Similar patterns have been widely reported in large river systems, where combustion-related emissions are recognized as the dominant contributors to sediment contamination (Yunker et al., 2002).

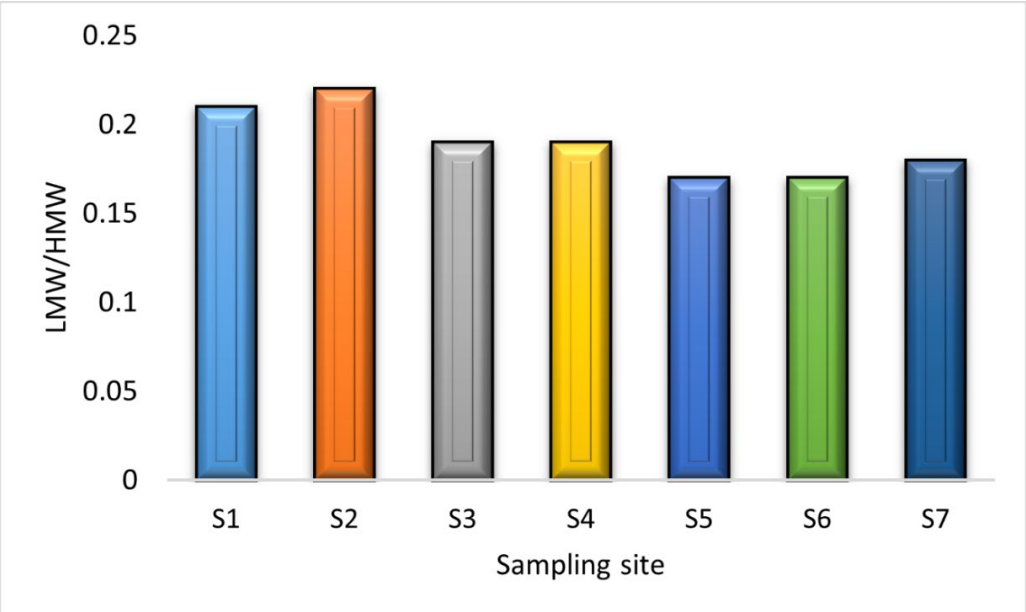


Fig. 1. *Averaged spatial variation of LMW/HMW ratios at sampling sites S1–S7*

Carcinogenic PAH fraction and ecological relevance

The proportion of carcinogenic PAHs (%7cPAH) ranged from 40% to 50%, indicating a notable contribution of toxic compounds (Figure 2). This relatively high share reflects the predominance of high molecular weight PAHs, which are typically associated with pyrogenic sources and are known for their carcinogenic properties (Boström et al., 2002). Although the overall PAH concentrations correspond to low to moderate contamination levels, the elevated proportion of carcinogenic compounds suggests that potential ecological risks should not be overlooked. This finding highlights the importance of complementing concentration-based assessments with compositional indicators that better reflect the toxicological relevance of sediment contamination. A summary of source indicators and carcinogenic PAH contributions is presented in Table 1.

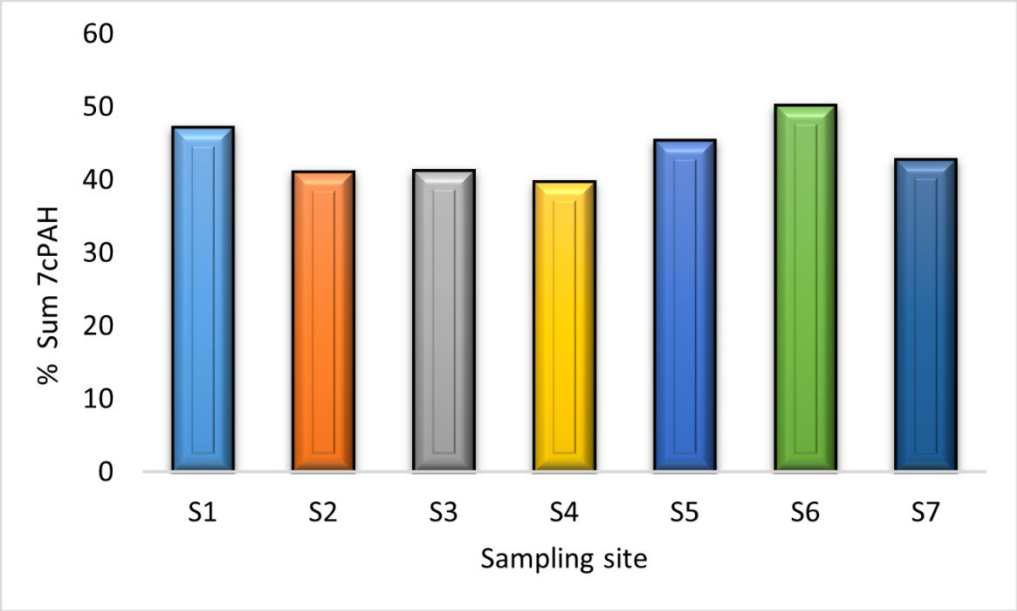


Fig. 2. *Average distribution of carcinogenic PAH fraction (%7cPAH) at sampling sites S1–S7*

Table 1. *Source identification of PAHs based on diagnostic LMW/HMW ratios and carcinogenic fraction (%7cPAH) and the Mean SQG-TEL and SQG-PEL values in Danube River sediments (2012–2024)*

Site	LMW/HMW	Source type	%7cPAH max	%7cPAH Ave (2012-2024)
S1	0.214	Pyrogenic	62.65	47.15
S2	0.217	Pyrogenic	61.54	41.07
S3	0.191	Pyrogenic	54.23	41.26
S4	0.191	Pyrogenic	57.46	39.69
S5	0.168	Pyrogenic	59.53	45.35
S6	0.168	Pyrogenic	65.90	50.15
S7	0.180	Pyrogenic	54.39	42.75

Ecotoxicological risk assessment (SQG approach)

The ecological risk of PAHs in Danube River sediments was further evaluated using SQGs, based on TEL and PEL values. The obtained SQG indices (Mean TEL-Q and Mean PEL-Q) indicate that ecological risk is predominantly low, with localized moderate risk observed at

selected sites (S1, S2 and S7) across the investigated period (Table 2). Mean TEL-Q values ranged from 0.47 to 1.56, corresponding predominantly to low to moderate risk levels, while Mean PEL-Q values remained below 0.16, indicating that adverse biological effects are unlikely under most environmental conditions (Table 3). According to the classification criteria (Table 4), most locations fall within the low-risk category, suggesting that adverse biological effects are unlikely under typical environmental conditions. However, spatial variability was observed. Location S1 showed slightly elevated SQG-PEL values, indicating occasional effects, while locations S1, S2, and S7 exhibited moderate risk levels based on SQG-TEL values (Table 3 and Table 4). These variations may reflect localized anthropogenic influences, such as urban or industrial inputs. Despite the predominantly low risk classification, the combined interpretation of SQG indices and carcinogenic PAH fractions indicates that the ecological relevance of PAHs cannot be considered negligible. The coexistence of pyrogenic sources, elevated carcinogenic fractions, and moderate risk levels at selected sites suggest persistent anthropogenic pressure on the sediment quality.

***Table 2**. Ecotoxicological risk assessment of Σ16 PAHs in Danube River sediments based on the SQG approach, using seasonal average concentrations (spring and autumn) and guideline values (TELi and PELi) (Nenin et al., 2026; Pichler et al., 2021).*

Location	Ave - spring Σ16PAH (µg/kg)	Ave - autumn Σ16PAH (µg/kg)	TEL_i	PEL_i	SQG-TEL spring	SQG-PEL - spring	SQG-TEL autumn	SQG-PEL - autumn
S1	320.66	560.81	619	5672	0.52	0.06	0.91	0.10
S2	203.22	508.57	619	5672	0.33	0.04	0.82	0.09
S3	324.45	367.71	619	5672	0.52	0.06	0.59	0.06
S4	216.35	268.75	619	5672	0.35	0.04	0.43	0.05
S5	466.87	507.37	619	5672	0.75	0.08	0.82	0.09
S6	386.03	407.84	619	5672	0.62	0.07	0.66	0.07
S7	434.31	363.03	619	5672	0.70	0.08	0.59	0.06
Average	**335.98**	**426.30**	619	5672	**0.54**	**0.06**	**0.69**	**0.08**

TELi and PELi values correspond to sediment quality guideline values for priority PAHs.
na – not available; nd – below the limit of quantification (LoQ).

***Table 3**. SQG-based ecotoxicological risk assessment of individual PAHs in Danube River sediments using average concentrations (2012–2024) and TELi/PELi guideline values (Nenin et al., 2026; Pichler et al., 2021)*

TEL_i	PEL_i	PAH (average values)	S1	S2	S3	S4	S5	S6	S7
34.6	391	Naphthalene	30.87	26.69	15.90	16.63	23.73	27.70	29.64
6.7	88.9	Acenaphthylene	nd	51.91	15.38	nd	nd	nd	10.00
5.9	128	Acenaphthene	nd	nd	nd	nd	nd	nd	23.46
21.2	144	Fluorene	17.37	67.32	16.43	12.18	18.74	16.54	19.76
86.7	544	Phenanthrene	67.42	44.64	63.20	37.88	58.30	43.77	49.14
46.9	245	Anthracene	24.39	23.22	14.34	15.94	17.83	16.32	17.16
113	1494	Fluoranthene	104.21	92.36	114.64	78.12	127.52	100.46	107.70
153	1398	Pyrene	85.89	65.97	94.02	61.69	96.70	86.32	83.31
74.8	693	Benz[a]anthracene	55.85	49.85	42.82	37.12	54.54	54.13	43.60
108	846	Chrysene	66.86	53.58	54.13	44.74	64.11	59.42	57.55
na	na	Benzo sum[b/k] fluoranthene	104.08	154.37	63.84	45.72	102.30	86.68	82.66

89	763	Benzo[a]pyrene	49.41	46.18	41.28	37.98	63.18	48.06	49.17
na	na	Indeno[1,2,3-cd] pyrene	51.61	78.44	49.26	na	na	37.75	57.24
6.22	135	Dibenzo[a,h]anthracene	33.90	nd	nd	nd	nd	nd	nd
na	na	Benzo[g,h,i] perylene	49.80	90.36	na	na	na	28.72	na
		SQG- TEL Σ16PAH*	1.19 MR	1.56 MR	0.77 Low	0.47 Low	0.71 Low	0.63 Low	1.03 MR
		SQG- PEL Σ16PAH*	0.10 OE	0.16 OE	0.08 Rare	0.06 Rare	0.08 Rare	0.07 Rare	0.09 Rare

TELi and PELi represent sediment quality guideline values for individual PAHs. SQG-TEL and SQG-PEL values for Σ16PAHs were calculated according to Eq. (5).
na – not available; nd – below the limit of quantification (LoQ). MR – moderate risk; Low – low risk; OE – occasional effects; Rare – rare effects

Table 4. *SQG-criteria for evaluating the potential eco-toxicological risks of the total PAH levels in the Danube River Sediment*

SQG-Q -TEL		**SQG-Q -PEL**	
< 0.1	No adverse effects expected	< 0.1	Rare effects- Rare
0.1 - 1.0	Low Risk - Low	0.1 - 0.5	Occasional effects- OE
1.0- 2.3	Moderate risk - MR	> 0.5	Frequent effects-Freq.E
> 2.3	High probability of toxicity -HR		

Integrated interpretation

The combined application of source identification (LMW/HMW), compositional indicators (%7cPAH), and SQG-based risk assessment provides a comprehensive understanding of PAH contamination in the Danube River sediments. While diagnostic ratios clearly indicate a dominant pyrogenic origin, and SQG values suggest generally low ecological risk, the relatively high contribution of carcinogenic PAHs highlights the importance of considering qualitative aspects of contamination. This integrated approach enables a more nuanced interpretation of sediment quality, bridging the gap between concentration-based assessments and ecotoxicological relevance, and represents a valuable tool for environmental monitoring in large river systems.

CONCLUSION

The results indicate that PAHs in Danube River sediments are predominantly of pyrogenic origin, as confirmed by consistently low LMW/HMW ratios across all sampling sites, reflecting the dominant influence of combustion-related sources such as traffic, industrial activities, and fossil fuel use. The relatively high proportion of carcinogenic PAHs (40–50%) highlights the prevalence of high molecular weight compounds and emphasizes the toxicological relevance of sediment contamination. Although total PAH concentrations correspond to low to moderate contamination levels, the application of sediment quality guidelines (SQGs) indicates that the overall ecological risk is generally low, with only occasional exceedances at the PEL level and moderate risk observed at selected locations. The combined use of source indicators, compositional metrics, and SQG-based indices demonstrates that concentration-based assessments alone may underestimate the environmental significance of PAHs. This integrated approach provides a more comprehensive evaluation of sediment quality and represents a robust framework for long-term monitoring and risk assessment in large river systems such as the Danube.

REFERENCES

Boström, C.-E., Gerde, P., Hanberg, A., Jernström, B., Johansson, C., Kyrklund, T., Rannug, A., Törnqvist, M., Victorin, K., & Westerholm, R. (2002). Cancer risk assessment, indicators,

and guidelines for polycyclic aromatic hydrocarbons in the ambient air. Environmental Health Perspectives, 110(3), 451–488. https://doi.org/10.1289/ehp.110-1241197

Chen, Y., Jia, R., Yang, S., 2015. Distribution and source of polycyclic aromatic hydrocarbons (PAHs) in water dissolved phase, suspended particulate matter and sediment from Weihe River in Northwest China. Int. J. Environ. Res. Public Health 12, 14148–14163. https://doi.org/10.3390/ijerph121114148

Karickhoff, S. W., Brown, D. S., & Scott, T. A. (1979). Sorption of hydrophobic pollutants on natural sediments. Water Research, 13(3), 241–248. https://doi.org/10.1016/0043-1354(79)90201-X

Neff, J. M. (1979). Polycyclic aromatic hydrocarbons in the aquatic environment: Sources, fates and biological effects. Applied Science Publishers.

Nenin, M., Perović, M., et al. (2026). Assessment of polycyclic aromatic hydrocarbons pollution in Danube River sediments: Spatial distribution, temporal trends and risk evaluation. Environmental Geochemistry and Health (2026) 48:56. https://doi.org/10.1007/s10653-025-02921-y .

Pichler, N., de Souza, F. M., Ferreira dos Santos, V., & Martins, C. C. (2021). Polycyclic aromatic hydrocarbons (PAHs) in sediments of the Amazon coast: Evidence for localized sources in contrast to massive regional biomass burning. Environmental Pollution, 268 (Pt B), 115958. https://doi.org/10.1016/j.envpol.2020.115958.

Tobiszewski, M., & Namieśnik, J. (2012). PAH diagnostic ratios for the identification of pollution emission sources. Environmental Pollution, 162, 110–119. https://doi.org/10.1016/j.envpol.2011.10.025

Yunker, M. B., Macdonald, R. W., Vingarzan, R., Mitchell, R. H., Goyette, D., & Sylvestre, S. (2002). PAHs in the Fraser River basin: A critical appraisal of PAH ratios as indicators of PAH source and composition. Organic Geochemistry, 33(4), 489–515. https://doi.org/10.1016/S0146-6380(02)00002-5

DOI:10.5937/IIZS26401Z

GREENHOUSE GAS (GHG) EMISSION TRENDS. REVIEW OF THE WORLD AND BALKAN REGION.

Research paper

Madalina Ileana Zot[1], Una Marceta[2], Luisa Izabel Dungan[3], Francisc Popescu[4*]
[1,3,4]University Politehnica Timisoara, Faculty of Mechanical Engineering, Timisoara, Romania
[2]Univesity of Novi Sad, Technical Faculty "Mihajlo Pupin", Zrenjanin, Serbia

Abstract: This paper investigates the emissions that contribute to global warming and climate change, with particular emphasis on carbon dioxide (CO_2) released from fossil fuel consumption and production activities. The analysis first considers CO_2 emissions from fossil fuel combustion and industrial processes separately, followed by an integrated assessment of their overall impact. In 2022, fossil fuel-derived CO_2 emissions in the Balkan region were approximately 95 Mt, representing a decline of nearly 16% relative to the 1990 baseline year. This reduction was primarily attributable to substantial decreases in emissions from the sectors with the highest contribution, notably the power generation sector and industrial combustion processes, which recorded reductions of 6% and 63%, respectively.
Key words: CO2 emission, GHG, Balkan

INTRODUCTION

Climate change represents one of the major environmental challenges of the present day, being closely associated with the intensification of anthropogenic activities and the increasing concentrations of greenhouse gases (GHGs) in the atmosphere. Carbon dioxide (CO_2), methane (CH_4), and nitrous oxide (N_2O) are among the main gases responsible for the intensification of the greenhouse effect, with their emissions primarily associated with energy production and consumption, industrial activities, transport, agriculture, and land-use changes (Crippa et al., 2021).

Over the past decades, global GHG emissions have undergone significant changes, visible on data from EDGAR (Emissions Database for Global Atmospheric Research), highlighted a substantial increase in global anthropogenic emissions since 1990, as well as considerable differences among countries and regions. These differences are determined by the level of economic development, the structure of energy systems, the degree of industrialization, and the policies implemented to reduce emissions. (Crippa et al., 2021)

A study analyzing emission trends over the period 1990–2018, showed that emissions are strongly influenced by the demand for energy, materials, mobility, and infrastructure. While some developed economies have managed to reduce emissions through improvements in energy efficiency and the expansion of renewable energy sources, in many emerging economies, increasing energy demand continues to be associated with the use of fossil fuels. (Lamb et al. 2021)

In this context, Europe shows a different trajectory compared with the global trend. Climate and energy policies, technological modernization, and the increasing use of renewable energy sources have contributed to reducing emissions in numerous European countries. Nevertheless, considerable differences remain across the regions of the continent, particularly regarding the structure of energy systems and the pace of the decarbonization process.

The Balkan region is of particular interest, as it comprises countries with different levels of economic development, distinct energy structures, and varying degrees of integration into European climate policies. Albania stands out due to the significant contribution of hydropower, whereas Serbia, Bosnia and Herzegovina, and North Macedonia exhibit a greater dependence on coal and lignite. These characteristics may lead to significant differences in GHG emission trends at the regional level. Industry, energy production, and heating represent important sources of emissions in the Western Balkans, while low energy efficiency and ageing infrastructure constitute major obstacles to the decarbonization process. (Knez et al., 2022)

[1]madalina.zot@upt.ro , ORCID: 0009-0005-7620-3159
[2]una.tasovac@tfzr.rs , ORCID: 0000-0001-6664-0236
[3]luisa.dungan@upt.ro , ORCID: 0000-0001-6114-492X
[4]Corresponding author, francisc.popescu@upt.ro , ORCID: 0000-0001-7736-0758

During the early years of the 21st century, the impacts of the greenhouse effect became increasingly apparent. By 2007, the global mean temperature of both terrestrial and oceanic environments had risen by approximately 0.8°C compared to the period between 1850 and 1900. Average land surface temperatures showed an even greater increase, reaching about 1°C above historical levels. Furthermore, the pace of global warming accelerated, with the average temperature rise increasing from roughly 0.1°C per decade during the 20th century to around 0.2°C per decade in recent decades. (Vranjanac et al., 2018)
According to the 2015 Paris Agreement, participating nations are required to periodically assess their achievements in reducing greenhouse gas emissions at five-year intervals. The principal objective of this framework is to prevent excessive increases in the global mean surface temperature by keeping warming significantly below 2°C relative to pre-industrial conditions, while also striving to restrict the temperature rise to 1.5°C

EMISSION INVENTORY AND DISSCUSSIONS

Evidence from six widely recognized global temperature datasets indicates that the average global temperature over the 2021-2025 period reached an unprecedented level, while 2024 remains the warmest individual year recorded to date. Additionally, five of these datasets rank 2025 as the third hottest year on record, with temperatures only marginally lower than those observed in 2023. Relative to the latter half of the nineteenth century, the increase in the five-year average global temperature is estimated to be between 1.3 and 1.4°C. Since the mid-1970s, the Earth's average temperature has risen by approximately 0.1°C every five years. Nevertheless, this warming trend has not occurred at a constant rate. Considerable regional and seasonal differences have been observed, reflecting the influence of multiple climatic factors. Although the persistent rise in greenhouse gas concentrations remains the dominant driver of global warming, variations in heat distribution are also governed by internal atmospheric and oceanic dynamics, as well as by the interactions between these systems, which collectively influence the spatial and temporal patterns of temperature change worldwide. (Copernicus, 2026)

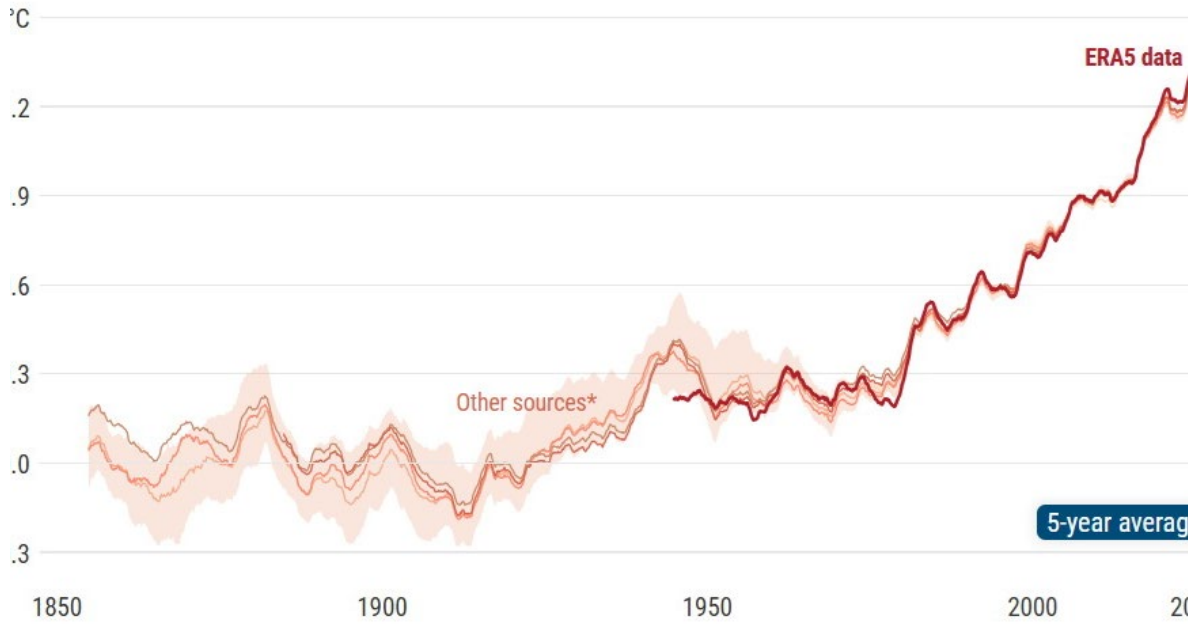


Fig. 1. *Global surface temperature increase relative to the pre-industrial baseline period (1850–1900).* (Copernicus, 2026)

The energy sector in the Balkan region has significant differences between countries but is mainly characterized by a strong dependence on fossil fuels, particularly lignite, which remains the dominant fuel for electricity generation in several countries. Serbia, for example, relies

extensively on lignite-based power production, while in most Balkan countries, fossil energy sources contribute to over 50% of total electricity generation. In contrast, Albania's power sector is largely based on hydropower, making it a notable exception within the region. (Qingsong et al., 2024) As a result of this energy profile, the production and consumption of energy represent major sources of greenhouse gas emissions. The widespread use of lignite, a highly carbon-intensive fuel, significantly influences regional emission levels and contributes to environmental degradation. Although the Balkans generally exhibit lower overall emissions than many highly industrialized European Union member states, the shift toward a low-carbon energy framework remains a complex and demanding process. One of the principal barriers is the limited availability of comprehensive emissions data and the relatively small body of scientific research addressing regional emission patterns. Consequently, the development of effective mitigation strategies, the establishment of realistic emission-reduction pathways, and the achievement of climate-related policy targets are often constrained by insufficient evidence and data-driven decision-making frameworks.

The Balkan peninsula is formed by 11 states: Greece, Albania, North Macedonia, Bulgaria, Romania, Serbia, Montenegro, Bosnia and Herzegovina, Croatia and Slovenia. To analyze the evolution of CO_2 emissions globally, at EU level and Balkan level we used the data provided by EDGAR - Emissions Database for Global Atmospheric Research. IEA-EDGAR CO_2 emissions represent the total contribution of fossil-derived carbon dioxide from a broad range of anthropogenic activities, including fossil fuel use, cement and other non-metallic mineral production, metal processing industries, urea production, agricultural liming, and solvent-related applications. Harmonization procedures are applied to global fossil CO_2 inventories to improve the consistency and reliability of emission estimates. (EDGARD, 2026)

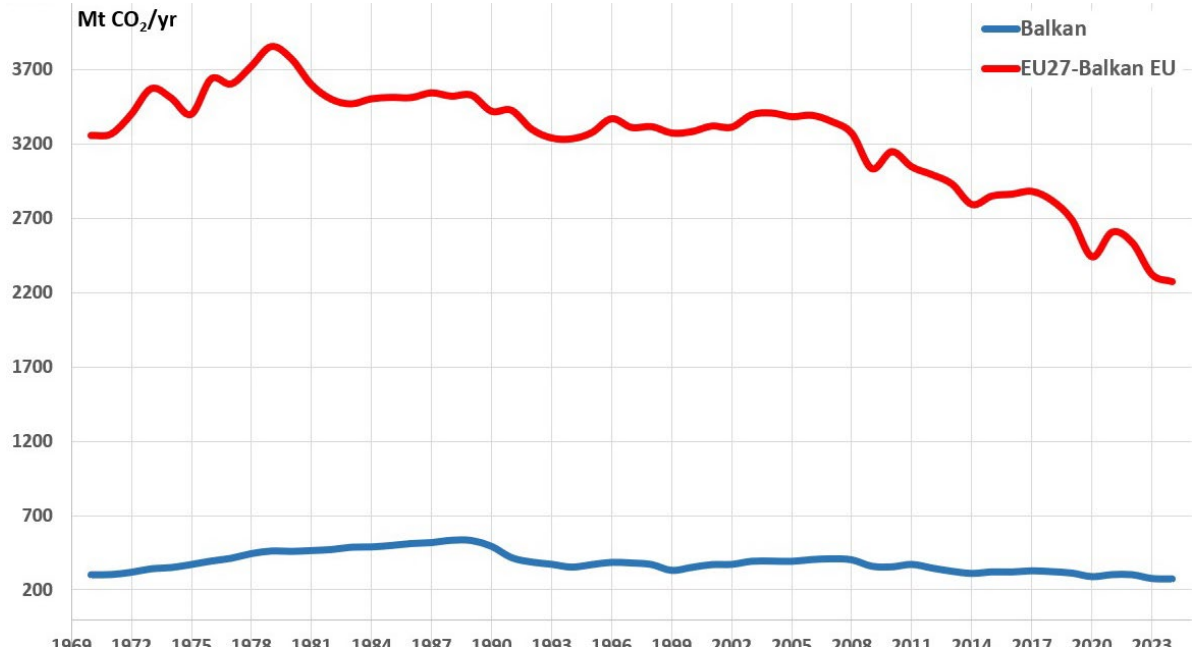


Fig. 2. *CO_2 emissions in EU (without Balkan EU states) and Balkan peninsula (1970–2024).* (data extracted from EDGAR, 2025)

Figure 2 shows the evolution of CO_2 emissions in Balkan countries and EU 27 countries (from EU27 Romania, Slovenia, Bulgaria, Croatia and Greece were extracted). It is clear from the data that green politics implemented in EU27 countries have a direct effect on CO_2 emissions while in Balkan countries the reduction of CO_2 emissions is not as rapid as expected.

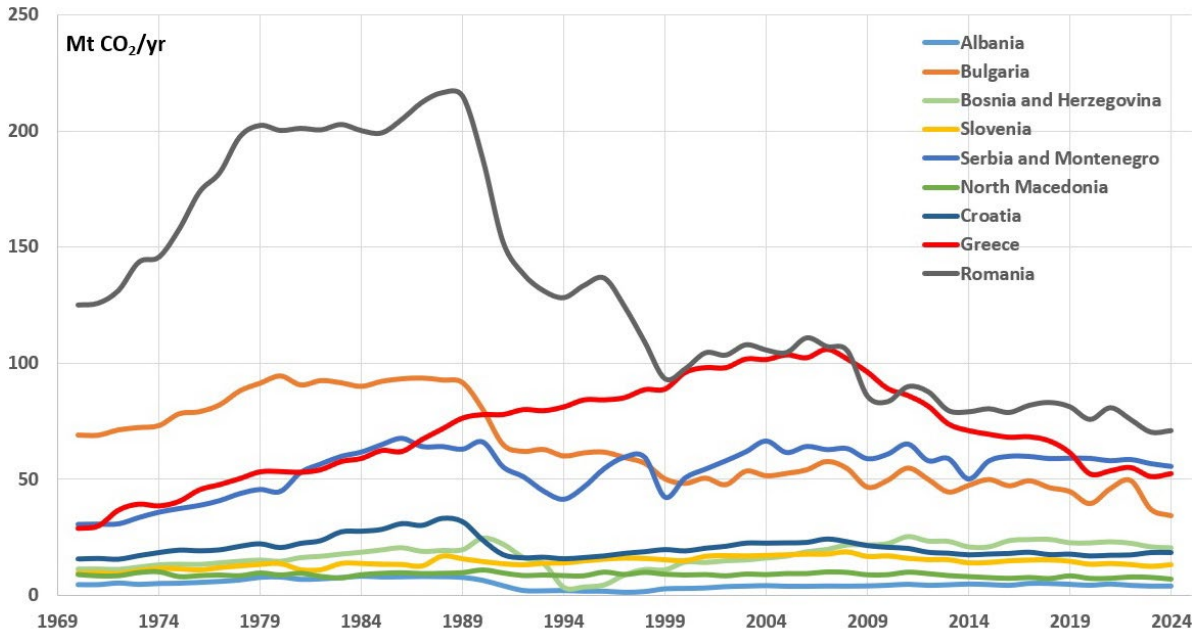


Fig. 3. *CO_2 emissions in Balkan peninsula (1970–2024).* (data extracted from EDGAR, 2025)

Figure 4 shows the evolution in time of CO_2 emissions from all Balkan countries. A significant reduction can be observed in Romania and Bulgaria in 1990, a reduction that is not due to implementation of CO_2 reduction policies but caused by the dismantle of existing large industrial complex because of communism era end. In the rest of Balkan countries, although they experience the same political change (Croatia, Serbia, Bosnia and Herzegovina), the energy intensive industry recovered, and the CO_2 emissions remained relatively constant up to present.

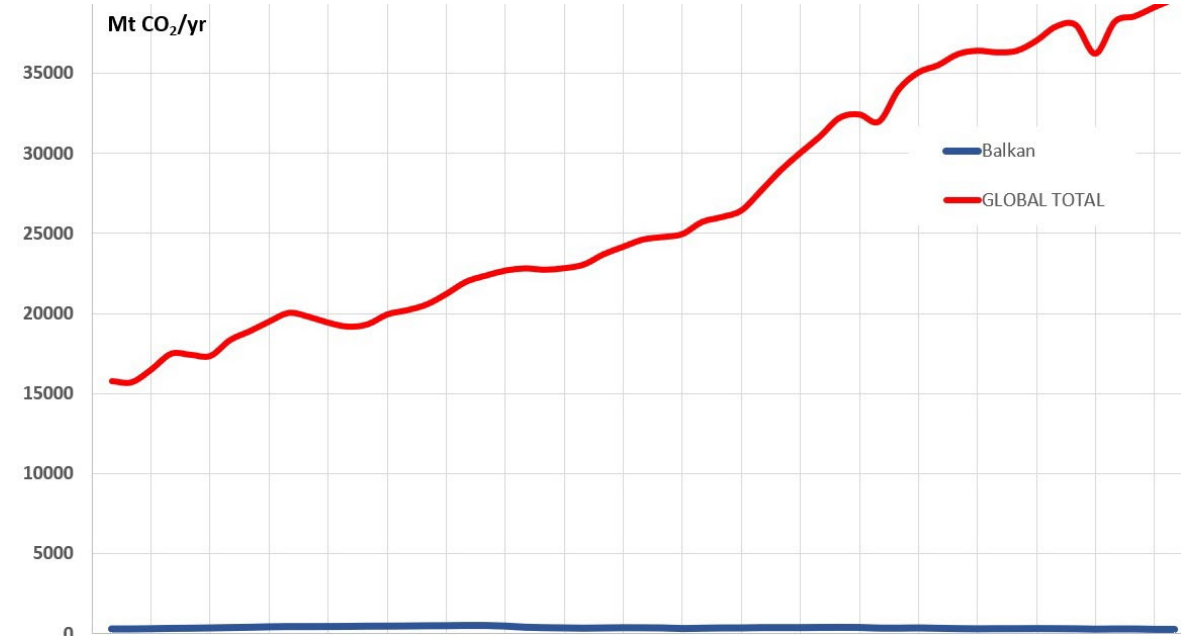


Fig. 4. *CO_2 emissions in Balkan countries and Worldwide (1970–2024).* (data extracted from EDGAR, 2025)

Figure 4 presents the evolution of Balkan and global CO_2 emissions. Net CO_2 emissions from Balkans are insignificant in relation to global CO_2 emissions, and, from figure 2, that are marginal by comparison with EU27 CO_2 emissions.

Countries in the Balkans remain comparatively underdeveloped in the field of renewable energy generation technologies. Expanding the uptake and diffusion of these technologies throughout the region has the potential to alleviate the environmental pressures resulting from the current energy consumption model. (Obradović et al., 2025)

CONCLUSION

To address the challenges posed by climate change and mitigate its adverse consequences, global leaders achieved a landmark milestone during the United Nations Climate Change Conference (COP21) held in Paris. On 12 December 2015, they adopted the historic *Paris Agreement*, establishing a comprehensive international framework for reducing greenhouse gas emissions and strengthening global climate action. Scientific evidence unequivocally indicates that avoiding the most severe consequences of climate change and maintaining conditions conducive to human well-being requires limiting the increase in global mean temperature to 1.5°C above pre-industrial levels. At present, the global average surface temperature is currently about 1.2°C than that recorded during the late nineteenth century, while greenhouse gas emissions continue to follow an upward trajectory. To achieve the temperature target established under the Paris Agreement, global emissions must decline by approximately 45% by 2030 relative to current levels and reach net-zero emissions by 2050.
The pursuit of a net-zero future constitutes a major global challenge, necessitating profound changes across all sectors of society. This transformation involves redefining the ways in which energy is generated and utilized, resources are consumed, and goods and people are transported. As the energy sector is responsible for nearly 75% of anthropogenic greenhouse gas emissions, it remains a critical component of strategies designed to reduce emissions and support the achievement of long-term climate objectives.
The key question is: will we reach net zero by 2050? The answer is simple: no! From 2015 to 2026, 195 countries (194 + EU) ratified the Parris Agreement. The combined effect of the existing national climate action plans adopted by the 195 Parties to the Paris Agreement is estimated to result in a reduction of 12% in global greenhouse gas emissions by 2035 relative to 2019 levels. Despite this projected decline, current commitments remain insufficient to meet the Paris Agreement target of limiting global temperature rise to 1.5°C. To align with this objective, global emissions must be reduced by approximately 55% by 2035, followed by the achievement of net-zero emissions by 2050.
China, the United States of America, India, the European Union, the Russian Federation, and Indonesia represent the six leading sources of greenhouse gas emissions globally. Together, the member states of the G20, comprising the world's twenty largest economies, were responsible for 77% of total global GHG emissions in 2024. (UN, 2026) In comparison, all Balkan countries (Albania, Serbia, Montenegro, Romania, Bulgaria, Slovenia, Greece and Croatia) were responsible in 2024 for 0.69 % of global CO_2 emissions.

ACKNOWLEDGEMENT

This research was partially supported by the cross-border cooperation project AEPS (http://aeps.upt.ro) "Academic Environmental Protection Studies on surface water quality in significant cross-border nature reservations Djerdap/Iron Gate national park and Carska Bara special nature reserve, with population awareness raising workshops", RORS-462, project funded by the INTERREG IPA-CBC Romania-Serbia Programme.

REFERENCES

Crippa, M., Guizzardi, D., Muntean, M., et al. (2021). Climate change in a changing world: Socio-economic and technological transitions, regulatory frameworks and trends on global greenhouse gas emissions from EDGAR v.5.0. *Global Environmental Change*, 70, 102350.

Crippa, M., Solazzo, E., Guizzardi, D., et al. (2021). Food systems are responsible for a third of global anthropogenic GHG emissions. *Nature Food*, 2, 198–209.

Copernicus. (2026), The Copernicus Climate Change Service (C3S) Climate indicators reports, https://climate.copernicus.eu/climate-indicators (accessed 09.09.2026)

EDGARD. (2026) European Commission - GHG emissions of all world countries, https://edgar.jrc.ec.europa.eu/emissions_data_and_maps#ghg (accessed 23.09.2026)

Knez, S., Štrbac, S., & Podbregar, I. (2022). Climate change in the Western Balkans and EU Green Deal: status, mitigation and challenges. *Energy, Sustainability and Society*, 12, 1.

Lamb, W.F., Wiedmann, T., Pongratz, J., et al. (2021). A review of trends and drivers of greenhouse gas emissions by sector from 1990 to 2018. *Environmental Research Letters*, 16, 073005.

Obradović, S.; Gričar, S.; Bojnec, Š.; Lojanica, N. (2025). Energy, Urbanisation and Carbon Footprint: Evidence from Western Balkan Countries, *Urban Science,* 9, no. 4: 119

Qingsong, Wang, Z., Zheng, H., Meng, J., Peng, H., Wen, Q. (2024). Uneven carbon emission distribution and its driving forces in the Balkans. *Global Environmental Change*, (Article in press), available at https://dx.doi.org/10.2139/ssrn.4846407

UN. (2026) Net-zero commitments must be backed by credible action, *Climate action*, https://www.un.org/en/climatechange/net-zero-coalition (accessed 23.09.2026)

Vranjanac, Z., Zivkovic, N., Vasovic, D., Janackovic, G., Dimitrovski, D. (2018). Comparative analysis of CO_2 emissions indicators in EU countries and Western Balkan countries – assessment of their contribution to climate change. *Journal of Environmental Protection and Ecology*, 19 (2), 453-461

DOI:10.5937/IIZS26407G

REMOVAL OF MICROPLASTICS FROM NATURAL AND WASTEWATER MATRICES BY COAGULATION AND FLOCCULATON: EFFECT OF MICROSAND AND COAGULANT TYPE

Research paper

Sanja Grbić[1*], Tijana Marjanović Srebro[2], Maja Vujić[3], Jasmina Agbaba[4], Radivoj Tomić[5], Marija Maletin[6], Aleksandra Tubić[7]
[1,2,3,4,5,6,7]University of Novi Sad, Faculty of Sciences, Department of chemistry, biochemistry and environmental protection, Novi Sad, Serbia

Abstract: Microplastics are emerging pollutants with widespread occurrence in both natural and wastewater environments, posing ecological and health risks. This study investigated the removal of powdered polyethylene (PE, 500 µm) and polyvinyl chloride (PVC, 171–279 µm) from Danube River water and municipal wastewater effluent using coagulation–flocculation processes. Ferric chloride ($FeCl_3$) and polyaluminum chloride (PACl) were applied as coagulants, and the effect of microsand addition (10 mg/L) on removal efficiency was evaluated. Jar test experiments were conducted under controlled laboratory conditions with optimal coagulant doses ranging from 20–220 mg/L for $FeCl_3$ and 10–50 mg/L for PACl. Results showed that $FeCl_3$ demonstrated broad applicability and stable performance across both water matrices, achieving high removal efficiencies for PE and PVC. PACl achieved comparable or higher efficiencies at lower doses, particularly in the presence of microsand. The addition of microsand selectively enhanced microplastic removal, improving PE sedimentation in both matrices, while its effect on PVC was limited due to higher density and weaker interactions with flocs. Optimal removal depended on the specific properties of the microplastics, the coagulant type, and the characteristics of the water matrix. These findings highlight the potential of coagulation–flocculation, with or without microsand, as an effective strategy for microplastic removal from diverse water matrices. They also emphasize the importance of process optimization considering pollutant characteristics, coagulant selection, and auxiliary agents, providing guidance for sustainable water treatment applications.
Key words: microplastics, water treatment, coagulation and flocculation, microsand

INTRODUCTION

One of the most significant challenges in environmental protection is plastic waste pollution. Due to its characteristics such as low cost, light weight, durability, and resistance to water and corrosion, plastics are widely used for commercial, industrial, and general purposes (Andrady, 2011). However, these same properties also contribute to their slow degradation. The increasing production of plastics, coupled with inadequate waste management, has resulted in the rapid accumulation of plastic waste in terrestrial and aquatic ecosystems (Bames et al., 2009; Jambeck et al., 2015). Over time, through processes such as photo-oxidative and thermo-oxidative degradation, plastics break down into smaller particles known as microplastics. Microplastics originate from various sources, including the degradation of plastic waste, the release of synthetic fibers during textile washing, plastic microbeads from personal care products, and industrial plastic pellets. Most microplastics eventually end up in the oceans, either via rivers or through direct discharge. Major sources of microplastics also include plastic products such as bags, bottles, medical devices, adhesives, and electronics (Mitrano and Wohlleben, 2020).
Wastewater treatment plants (WWTPs) can also contribute to the release of microplastics into the environment, despite retaining a certain portion of plastic fragments in oxidation basins or sewage sludge (Browne et al., 2011). Nevertheless, significant amounts of microplastics still enter aquatic systems from wastewater treatment plants consisting of primary and secondary treatment, which process water from both urban and industrial sources, thereby concentrating

[1]Corresponding author, sanjav@dh.uns.ac.rs, ORCID: 0009-0001-0263-4184,
[2]tijanam@dh.uns.ac.rs, ORCID: 0009-0006-9886-6516,
[3]maja.loncarski@dh.uns.ac.rs, ORCID: 0000-0002-0712-3199,
[4]jasmina.agbaba@dh.uns.ac.rs, ORCID: 0000-0002-9915-2885,
[5]radivoj.tomic@dh.uns.ac.rs, ORCID: 0009-0008-3630-3667,
[6]marijac@dh.uns.ac.rs, ORCID:0009-0003-7112-6954
[7]aleksandra.tubic@dh.uns.ac.rs, ORCID: 0000-0001-7503-7754

and filtering microplastics that arrive through stormwater and urban drainage. Although some studies indicate that WWTPs can remove microplastics with efficiencies of up to 99% (Lares et al., 2018; Gan et al., 2023), the fraction that is not removed is discharged into the environment.

Existing uncertainties and the limited understanding of this type of pollution highlight the need for further research, the definition of clear criteria, the improvement of existing requirements, and the development of sustainable alternatives in order to reduce microplastic pollution in the environment (Belzagui et al., 2022).

Urgent and efficient methods for removing microplastics from water are needed. Microplastics enter WWTPs from multiple sources. The most significant sources are municipal wastewater, which contains residues from personal care products, as well as wastewater generated during the production and processing of plastic materials.

It is essential to develop efficient methods for removing microplastics from water and to enable monitoring of their concentrations. Although microplastic pollution has increasingly become the focus of research, a comprehensive analysis of physical, chemical, and biological methods for microplastic removal is still lacking. This indicates the necessity of improving wastewater treatment technologies to reduce their environmental impact (Ali et al., 2021; Moteallemi et al., 2024).

Coagulation is a chemical process in which a coagulant acts on wastewater to convert dissolved pollutants into particles, which are then removed by sedimentation (Li et al., 2024). Flocculation is a physical method that is typically applied after coagulation. The combination of coagulation and flocculation has become a successful physico-chemical strategy for removing microplastics from water (Peydayesh et al., 2021). The presence of microplastics in wastewater requires certain modifications in treatment processes. Conventional methods often struggle to remove these pollutants, making it necessary to adapt treatment procedures (e.g., by adding components that can enhance the process, such as activated carbon, microsand, or similar materials). The main goal of coagulation and flocculation processes is to improve the efficiency of microplastic removal by enabling particle aggregation, followed by sedimentation or flotation (Chazovachii et al., 2021). During coagulation, particle destabilization occurs through the addition of coagulants, which neutralize their electrostatic charges. Coagulants remove the surface charges of particles, and this charge neutralization allows them to approach each other, facilitating aggregation and subsequent removal.

Studies have shown that through multiple stages of water treatment, up to 88% of microplastics can be removed, with coagulation and sedimentation contributing the most to their removal (Pivokonsky et al., 2020). Various other studies also confirm that coagulation can almost completely eliminate microplastics from water (Skaf et al., 2020; Xu et al., 2022). For this reason, coagulation is considered a sustainable technology for the complete removal of microplastics from water, and in recent years it has gained attention due to its simplicity of application, cost-effectiveness, and energy efficiency. Aluminum- and iron-based salts are most commonly used, along with coagulants such as polyacrylamide (PAM), which facilitate the aggregation of fine particles into larger groups for easier removal (Ojha et al., 2024).

Based on the above, it is necessary to conduct research on the efficiency of microplastic removal from water, with a particular focus on assessing performance in the presence of factors that influence treatment efficiency. Jar tests are used to simulate the process of floc formation during water treatment by coagulation and flocculation. In addition to their use for research purposes, these tests are essential for optimizing operational parameters in existing water treatment plants and for designing new systems.

Therefore, the aim of this study was to examine the efficiency of microplastic removal from water using coagulation and flocculation, with and without the addition of microsand.

MATERIAL AND METHODS

Coagulation experiment

The materials used in the experiments were powdered polyethylene (PE, particle size 500 μm) and powdered polyvinyl chloride (PVC, particle size 171–279 μm). Their removal by coagulation was tested in Danube River water and in the effluent of municipal wastewater from a wastewater treatment plant. The materials used (PE and PVC) are shown in Fig. 1.

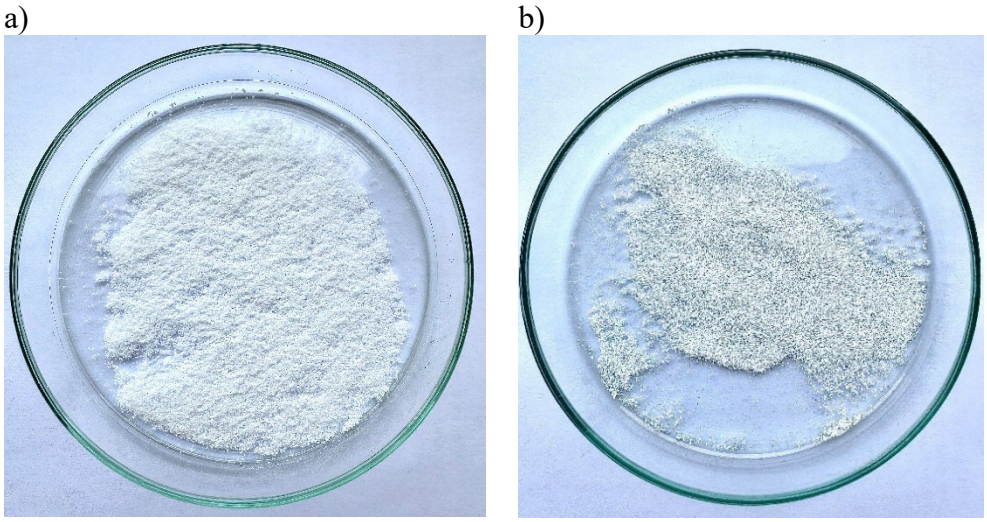


Fig. 1. *Materials used in experiment: a) PE and b) PVC*

In the experiments, ferric chloride ($FeCl_3$) and polyaluminum chloride (PACl) were applied as coagulants. Coagulation experiments were performed on a Jar test apparatus (VELP Scientifica) under laboratory conditions, at mixing speeds ranging from 10 to 300 rpm. All experiments were conducted in triplicate. Prior to the Jar test, 50 mg of plastic material was added to 0.5 L of the water matrix and left to homogenize for 24 h without mixing, before the coagulation/flocculation experiments. The coagulant concentrations used in the experiments ranged from 20 to 220 mg/L (20, 40, 60, 100, 140, 180, and 220 mg $FeCl_3$/L) for $FeCl_3$ and from 10 to 50 mg/L (10, 20, 30, 40, 50 mg Al/L) for PACl. Coagulation was performed by adding the coagulant at a mixing speed of 120 rpm for 2 min, followed by flocculant addition and continued mixing at 45 rpm for 30 min. Sedimentation was carried out for 30 min. After settling, the samples were filtered through a cellulose nitrate membrane filter with a pore size of 0.45 μm using a vacuum filtration device. The filter papers were dried in Petri dishes at room temperature for 24 h. After 24 h, the masses of the filters after coagulation, as well as the masses of the filters before filtration, were measured. Based on these data, further calculations were performed, and the microplastic removal efficiency from water was determined. Optimal coagulant doses were selected and applied in subsequent experiments.

To improve coagulation efficiency and increase the removal rate of microplastics from water matrices, treatment optimization was carried out by adding microsand as an auxiliary agent. Microsand acts as a physical support during floc formation, contributing to their stability, higher density, and faster sedimentation behavior, all of which enhance microplastic removal from solution (Su et al., 2013). In this study, microsand was used at a concentration of 10 mg/L. All experiments were performed at the previously determined optimal coagulant doses, allowing the evaluation of the effect of microsand independently from the basic coagulation parameters. This approach provided insights into the synergistic mechanisms between coagulants and microsand, as well as into the potential of this combination for application in real water treatment conditions.

RESULTS AND DISCUSSION

In this chapter, the results of the study on the effect of microsand addition on the coagulation process are presented, using the optimal doses of $FeCl_3$ and PACl coagulants. These results are discussed in more detail for each tested material in the following sections. Microsand was applied at a concentration of 10 mg/L. Fig. 2 shows the removal efficiencies of the tested materials from Danube River water by coagulation and flocculation, using the optimal doses of $FeCl_3$: 100 mg/L for PE and 20 mg/L for PVC.

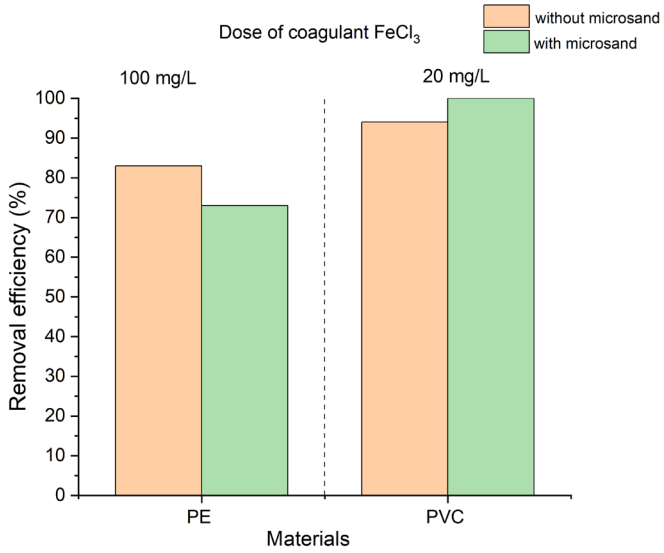


Fig. 2. *The effect of microsand addition on the efficiency of coagulation and flocculation in microplastic removal from Danube river water using $FeCl_3$ coagulant*

Fig. 2 also shows that, for effective removal of PE in the absence of microsand, a higher coagulant dose (100 mg/L) was required due to its low density and weak interaction with coagulation agents. In the presence of microsand, the removal efficiency of PE was similar (from 83% to 73%), which can be explained by possible competitive interactions between microsand and flocs, as well as the influence of interfering substances present in river water.
In contrast, the addition of microsand improved the removal of PVC from Danube river water, increasing efficiency from 94% to 100%, indicating that heavier and denser PVC particles interact more effectively with microsand in the sedimentation process. The high removal efficiency of PVC in the presence of microsand can primarily be attributed to its higher density compared to lighter polymers such as PE, which facilitates sedimentation when additional inert material is present.
The results shown in Fig. 2 confirm that under more complex conditions of a natural water matrix, the effect of microsand can be selective and dependent on the type of microplastic, as well as on the chemical composition and interfering substances in the water. The use of microsand is not always synergistic, especially when competition for interaction with flocs occurs, or when destabilization arises due to the presence of natural matter.
Fig. 3 presents the removal efficiencies of microplastics using the optimal doses of the PACl coagulant: 20 mg/L for PE and 30 mg/L for PVC.
It can be observed that the addition of microsand improved the removal of PE (82%) compared to the results without microsand (68%). In this case, a lower PACl dose (20 mg/L) was used, yet significantly higher efficiency was achieved, indicating the success of the process. In contrast, PVC showed lower removal efficiency (59%) compared to the efficiency obtained with PACl alone, without microsand addition, which was 88%.

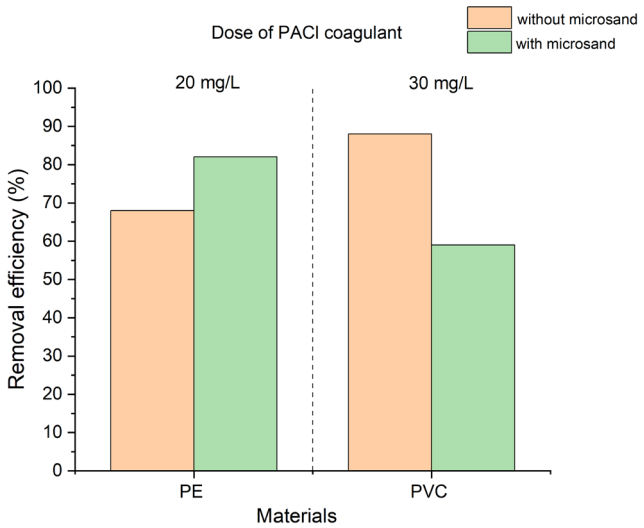


Fig. 3. *The effect of microsand addition on the efficiency of coagulation and flocculation in microplastic removal from Danube river water using PACl coagulant*

The results in Figures 2 and 3 indicate that the addition of microsand has a differentiated impact on the removal efficiency of different types of microplastics, depending on the type of coagulant and the composition of the water matrix. The best removal of PVC was achieved with $FeCl_3$ in the presence of microsand (Fig. 2), owing to its higher density, which favors sedimentation. On the other hand, PE was most effectively removed using PACl in the presence of microsand (Fig. 3), which can be attributed to its polymeric nature and greater ability to form stable flocs with this coagulant. The experimental results confirm that optimal treatment must be adapted to the specific properties of the pollutants and the chemical characteristics of the water matrix, with careful selection of coagulants and auxiliary agents.
Figures 4 and 5 show the removal efficiencies of the tested materials by coagulation from municipal wastewater effluent.

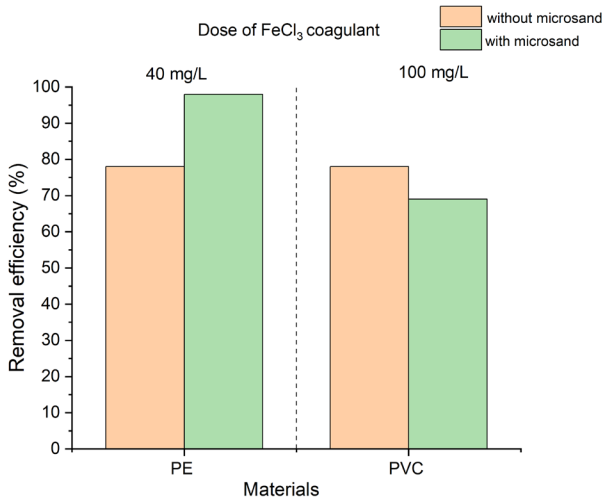


Fig. 4. *The effect of microsand addition on the efficiency of coagulation and flocculation in microplastic removal from municipal wastewater effluent using $FeCl_3$ coagulant*

Based on the results shown in Fig. 4, it can be concluded that the addition of microsand generally contributed to improving the removal efficiency of PE. Compared to the values obtained without microsand addition (78% for PE and 88% for PVC), a similar efficiency in PE removal efficiency is observed. These results indicate that microsand can play a significant role in enhancing flocculation and sedimentation of lighter materials, while for denser and less reactive materials, such as PVC, its contribution remains limited. Considering that PVC has a higher density compared to PE, it is assumed that the optimal $FeCl_3$ coagulant dose used in

this experiment (100 mg/L) was insufficient to form adequate flocs capable of incorporating PVC and microsand and promoting sedimentation. Instead, smaller or underdeveloped flocs remained suspended in the solution, reducing the efficiency of the process.
The results presented in Fig. 4 suggest that coagulation in the presence of microsand can depend on the specific properties of the microplastics, such as density and surface characteristics, as well as on the optimal coagulant dosing. Therefore, for materials like PVC, further experiments over a wider range of $FeCl_3$ doses would be necessary to determine the optimal combination for enhanced removal. These observations further emphasize the importance of fine-tuning coagulation conditions depending on the type of microplastic present in the water matrix.

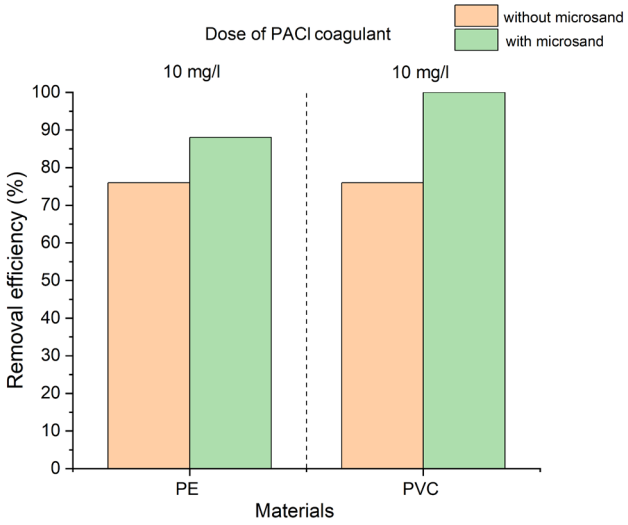


Fig. 5. *The effect of microsand addition on the efficiency of coagulation and flocculation in microplastic removal from municipal wastewater effluent using PACl coagulant*

The application of the PACl coagulant in the effluent of wastewater from a treatment plant (Fig.5) showed high microplastic removal efficiency at the applied optimal doses. Doses of 10 mg Al/L for PE and PVC proved sufficient to achieve significant particle destabilization and aggregation in the presence of organic matter typical for municipal wastewater effluent. The results presented in Figures 4 and 5 indicate that the addition of microsand can contribute to improving microplastic removal efficiency in municipal wastewater effluent, but its effect is selective and depends on the type of material, the applied coagulant, and the characteristics of the water matrix. As previously mentioned, the greatest contribution is observed for PE, whose removal is significantly enhanced due to its lower density and stronger interaction with microsand. PVC removal, due to its higher density and weaker interaction with flocs and microsand, was most effectively achieved through the application of the PACl coagulant.
The results obtained in this study confirm that the success of coagulation, with or without microsand, depends on a carefully optimized approach that considers the type of pollutants, the chemical and physical properties of microplastics and fibers, as well as the characteristics of the water matrix itself.

CONCLUSION

The results presented in this study indicate that $FeCl_3$ demonstrated broad applicability as a coagulant for microplastic removal from various water matrices, including Danube River water and municipal wastewater effluent from a treatment plant. Its efficiency under standard conditions, particularly in the presence of higher organic matter content, confirms its potential for use in real municipal wastewater treatment scenarios. Although some results showed that PACl can achieve higher efficiency at lower doses and under modified conditions (e.g., with the addition of microsand), $FeCl_3$ remains a coagulant that provides stable performance and consistent results, making it a reliable choice across different scenarios.

The addition of microsand had a selective but significant effect in certain cases. In Danube River water, microsand addition improved PE removal from 68% to 82% at a low PACl dose, while no significant changes were observed for PVC. A more pronounced effect of microsand addition was observed in municipal wastewater effluent, where PE removal reached 98%, confirming the effectiveness of coagulation in the presence of these microsand particles.
The results emphasize that coagulant selection must be based on the characteristics of the specific pollutants, the chemical properties of the water matrix, and the presence of additional agents such as microsand. An integrated approach that considers interactions between pollutants, the matrix, and coagulants is essential for optimizing treatment and developing efficient, sustainable technologies for the removal of micropollutants from water.

ACKNOWLEDGEMENT

The authors gratefully acknowledge the financial support of the Ministry of Science, Technological Development and Innovation of the Republic of Serbia (Grants No. 451-03-33/2026-03/ 200125 & 451-03-34/2026-03/ 200125).

REFERENCES

Ali, T. Ding, C. Peng, I. Naz, H. Sun, J. Li, J. Liu. (2021) Micro-and nanoplastics in wastewater treatment plants: occurrence, removal, fate, impacts and remediation technologies–a critical review, *Chem. Eng. J. 423*, 130205.

Andrady, A.L. (2011) Microplastics in the marine environment. *Mar. Pollut. Bull*. *62*, 1596-1605.

Barnes, D.K.A., Galgani F., Thompson R.C., Barlaz M. (2009) Accumulation and fragmentation of plastic debris in global environments. *Philos. Trans. R. Soc. Lond. B Biol. Sci*. *364,* 1985–1998.

Belzagui, F., Gutiérrez-Bouzán, C., & Carrillo-Navarrete, F. (2022). Novel Treatment to Immobilize and Use Textiles Microfibers Retained in Polymeric Filters through Their Incorporation in Composite Materials. *Polymers, 14(15)*, 2971.

Browne, M.A., Crump, P., Nivem, S.J., Teuten, E., Tonkin, A., Galloway, T., Thompson, R. (2011). Accumulation of microplastic on shorelines woldwide: source and sinks. *Envrion. Sci. Technol. 45*, 9175-9179.

Chazovachii, P.T., Somers, M.J., Robo, M.T. et al. (2021) Giving superabsorbent polymers a second life as pressure-sensitive adhesives. *Nat Commun 12*, 4524.

Gan, Q., Cui, J., Jin, B. (2023) Environmental microplastics: Classification, sources, fates, and effects on plants, *Chemosphere. 313*, 137559.

Jambeck, J.R., Geyer, R., Wilcox, C., Siegler, T.R., Perryman, M., Andrady, A., Narayan R.,

Lares, M.; Ncibi, M. C.; Sillanpää, M.; Sillanpää, M. (2018) Occurrence, identification and removal of microplastic particles and fibers in conventional activated sludge process and advanced MBR technology. *Water Res., 133*, 236– 246.

Law, K.L. (2015) Plastic waste inputs from land into the ocean. *Science, 347*, 768–771.

Li, W., Brunetti G., Bolshakova, A., Stumpp, C. (2024) Effect of particle density on microplastics transport in artificial and natural porous media. *Sci. Total Environ. 935*, 173429.

Mitrano, D.M., Wohlleben, W. (2020) Microplastic regulation should be more precise to incentivize both innovation and environmental safety. *Nat Commun 11*, 5324.

Moteallemi, A., Dehghani, M.H., Momeniha, F., Azizi, S. (2024) Nanoplastics as emerging contaminants: A systematic review of analytical processes, removal strategies from water environments, challenges and perspective. *Microchemical Journal, 207*, 111884.

Ojha, P.C., Satpathy, S.S., Ojha, R., Dash, J., Pradhan, D. (2024) Insight into the removal of nanoplastics and microplastics by physical, chemical, and biological techniques. *Environ Monit Assess 196*, 1055.

Peydayesh, M., Suta T., Usuelli M., Handschin S., Canelli G., Bagnani M., Mezzenga R. (2021) Sustainable Removal of Microplastics and Natural Organic Matter from Water by Coagulation–Flocculation with Protein Amyloid Fibrils, *Environ. Sci. Technol, 55*, 13.

Pivokonsky, M., Pivokonska, L., Novotna, K., Cermakova, L., Klimtova, M. (2020) Occurrence and fate of microplastics at two different drinking water treatment plants within a river catchment. *Sci. Total Environ., 741* (2020).

Skaf, D.W., Punzi, V.L., Rolle, J.T. and Kleinberg, K.A. (2020) Removal of Micron-Sized Microplastic Particles from Simulated Drinking Water via Alum Coagulation. *Chem. Eng. J, 386.*

Xu, C.; Zhou, G.; Lu, J.; Shen, C.; Dong, Z.; Yin, S.; Li, F. (2022) Spatio-vertical distribution of riverine microplastics: Impact of the textile industry. *Environ. Res. 211*, 112789.

DOI:10.5937/IIZS26415C

APPLICATION OF THE MONITORING, REPORTING AND VERIFICATION SYSTEM FOR GREENHOUSE GAS EMISSIONS IN THE REPUBLIC OF SERBIA: A CASE STUDY OF THE „ISTOK" DISTRICT HEATING PLANT IN NOVI SAD

Research paper

Zoran Čepić[1], Julka Petrović[2], Višnja Mihajlović[3], Goran Bošković[4], Bogdana Vujić[5]
[1]University of Novi Sad, Faculty of Technical Sciences, Novi Sad, Serbia
[2]Public Utility Company Novosadska toplana, Novi Sad, Serbia
[3,5]University of Novi Sad, Technical Faculty "Mihajlo Pupin", Zrenjanin, Srbija
[4]University of Kragujevac, Faculty of Mechanical and Civil Engineering, Kraljevo, Srbija

Abstract: Reliable greenhouse gas reporting requires traceable fuel consumption data, consistent calculation factors and a documented assessment of measurement uncertainty. This paper examines these elements at the „Istok" district heating plant in Novi Sad using its monitoring plan, supporting annexes and annual emission report for 2025. Carbon dioxide emissions are calculated from fuel consumption, net calorific value, emission factor and oxidation factor. Natural gas consumption amounted to 4,696,998 Nm^3, corresponding to 9,770.45 t CO_2; the reported contribution of the emergency diesel generator was 0.10 t CO_2. The combined expanded uncertainty of natural gas activity data was reproduced as 2.06%, below the 2.5% threshold of the applied tier. The turbine meter accounts for approximately 94.1% of the combined variance. The results illustrate how existing commercial and metrological documentation can support a transparent calculation, while identifying reference-condition consistency, metrological evidence and documented auxiliary-fuel estimates as practical priorities. The assessed uncertainty concerns gas quantity and does not represent the complete uncertainty of annual emissions.
Key words: MRV, district heating, carbon dioxide, activity data, measurement uncertainty

INTRODUCTION

The development of monitoring, reporting and verification (MRV) provides the data foundation for climate policy and the assessment of emissions from industrial installations. In Serbia, the framework for the first reporting cycle was established through the Law on Climate Change, the Regulation on Types of Activities and Greenhouse Gases, and the Rulebook on Monitoring and Reporting of Greenhouse Gas Emissions (Republic of Serbia, 2021, 2022, 2023). Monitoring for the first annual cycle began in 2025. The present study concerns this reporting framework and does not assess emissions trading or carbon pricing.
Čepić and Petrović (2026) discussed the introduction of MRV in Serbia and the practical difficulties encountered by operators, including data selection, calculation factors and uncertainty assessment. These issues are relevant even to conventional combustion installations. A correct emission equation alone cannot ensure reliable reporting if fuel quantities, reference conditions or supporting records are inconsistent.
The objective of this paper is to present a compact quantitative case study of the „Istok" district heating plant. The contribution is an installation-specific reconciliation of the reported emissions, reproduction of the activity data uncertainty calculation and interpretation of the relative metering contributions. The analysis uses existing documentation and requires no additional experimental programme.

DESCRIPTION OF THE INSTALLATION AND MONITORING METHODOLOGY

The „Istok" plant, operated by JKP Novosadska toplana, is located in Novi Sad and supplies heat to Podbara, Rotkvarija and part of the city centre. Its two hot-water boilers are K3 (VKLM-50, 58.15 MW) and K4 (RHV 58, 58 MW), giving a documented combined boiler capacity of 116.15 MW. Each boiler has a separate stack, designated EP1 and EP2. Natural

[1]Corresponding author, zorancepic@uns.ac.rs, ORCID: 0000-0001-5853-4767
[2]julka.petrovic@nstoplana.rs, -
[3]visnjamihajlovic@uns.ac.rs, ORCID: 0000-0002-9750-1076
[4]boskovic.g@mfkv.rs, ORCID: 0000-0002-4597-922X
[5]bogdana.vujic@tfzr.rs, ORCID: 0000-0001-5249-8021

gas is the sole boiler fuel; the boilers cannot use an alternative fuel. A separate 100 kVA diesel generator provides emergency electricity (JKP Novosadska toplana, 2026b).
The monitoring boundary includes natural gas combustion in both boilers (source stream F1) and diesel combustion in the emergency generator (F2). F1 is classified as the major source stream and F2 as de minimis. Emissions are determined by the standard calculation-based method, without continuous CO_2 measurement at the stacks. Consequently, separate stacks do not require separate fuel-based emission totals for the purpose of this installation-level assessment.
Purchased natural gas quantities are taken from JP Srbijagas invoices and equal consumption because there is no gas storage at the plant. The supplier's metering chain consists of turbine flow meter MI1 and electronic volume corrector MI2. MI1 measures gas volume and MI2 corrects it to the applicable reference conditions. They are two components of one metering chain, rather than independent supply lines. Both belong to the supplier and are subject to national legal metrological control (JKP Novosadska toplana, 2026b).
Gas net calorific value (NCV) and emission factor (EF) are based on the supplier's monthly gas-quality reports for GMRS Novi Sad, with analyses performed by its accredited gas laboratory. The monitoring methodology converts NCV from 15 °C to 0 °C at 101,325 Pa using the factor 1.0554. Gas volumes and volumetric NCV must therefore be expressed on the same basis. The annual report applies tier 3 to gas activity data, NCV and EF. The oxidation factor (OF) is 1. Diesel uses the reported estimate of 0.0313 t and default NCV and EF values (JKP Novosadska toplana, 2026a, 2026b).

METHODOLOGY FOR EMISSION CALCULATION AND UNCERTAINTY ASSESSMENT

For each fuel and reporting interval, carbon dioxide emissions are calculated as follows:

$$E = Q \times NCV \times EF \times OF \quad (1)$$

Here E is emission (t CO_2), Q is fuel quantity, NCV is expressed in TJ per quantity unit, EF in t CO_2/TJ, and OF is dimensionless. For gas quantities in Nm^3 and NCV in MJ/Nm^3, the product Q × NCV is multiplied by 10^{-6} to obtain TJ. For diesel, Q is in tonnes and NCV is 0.043 TJ/t. Annual emissions are the sum of the fuel contributions.
Monthly gas calculations retain the relevant monthly factors. For an equivalent annual calculation, NCV is weighted by gas volume and EF by the corresponding energy input. This preserves the sum of the monthly emissions; multiplying two independently calculated arithmetic averages would not generally do so. The published annual factors are used to check consistency with the annual report, while the monthly table retains the precision of the supplied methodology.
The uncertainty assessment reproduces Annex 4 of the monitoring plan. That annex applies route CT-1 to supplier-owned instruments under legal metrological control and enters 2.00% for MI1 and 0.50% for MI2 as expanded, in-service uncertainties. For uncorrelated inputs expressed at the same coverage factor, the combined relative expanded uncertainty is:

$$U(Q) = \sqrt{[U(MI1)^2 + U(MI2)^2]} \quad (2)$$

The annex reports a coverage factor k = 2; the equivalent combined standard uncertainty is obtained by dividing the result by two. The calculation assumes that the two contributions are uncorrelated. The numerical results therefore reproduce the documented assessment, rather than a new calibration-based determination. Individual certificates and their coverage assumptions were not supplied for independent examination. Maximum permissible errors and certificate uncertainties should be identified correctly and their use justified when the supporting metrological records are reviewed.
No reduction by the square root of the number of months is applied: recurring use of the same instruments does not establish independent monthly errors. The assessment covers

annual gas quantity only. Uncertainty in NCV, EF and their possible correlation is outside the quantitative scope because the required analytical uncertainty data are unavailable. A separate numerical uncertainty budget is not reported for the de minimis diesel stream.

RESULTS AND DISCUSSION

Table 1 brings together the consumption, calculation factors and emissions reported for 2025. Gas volumes refer to 0 °C and 101,325 Pa. OF is 1 for both fuels (JKP Novosadska toplana, 2026a, 2026b).

***Table 1**. Fuel consumption, calculation factors and CO2 emissions in 2025*

Period / fuel	Quantity Nm^3	NCV MJ/Nm^3	EF t CO_2/TJ	Emission t CO_2
Jan	201,310	37.379	55.6	418.4
Feb	231,933	37.391	55.6	482.2
Mar	998,873	37.380	55.6	2,076.0
Apr	708,367	37.401	55.6	1,473.0
May	0	37.686	55.7	0.0
Jun	0	37.748	55.7	0.0
Jul	0	37.788	55.7	0.0
Aug	0	37.563	55.6	0.0
Sep	243	37.694	55.7	0.5
Oct	1,068,711	37.503	55.6	2,228.4
Nov	513,665	37.406	55.5	1,066.4
Dec	973,896	37.407	55.6	2,025.5
Gas annual	4,696,998	37.42010	55.58907	9,770.45
Diesel annual	0.0313 t	43.0 MJ/kg	74.1	0.10
Total	**—**	**—**	**—**	**9,770.55**

Note. Monthly values retain source precision and sum to 9,770.4 t CO_2. Annual gas factors are weighted. The annual total is 9,770.55 t CO_2, shown as 9,770.6 in Annex 3 and rounded to 9,771 in the annual report.

The annual gas volume of 4,696,998 Nm^3 corresponds to approximately 175.76 TJ. Applying the annual NCV and EF gives 9,770.454 t CO_2, consistent with the reported 9,770.45 t CO_2. Diesel contributes approximately 0.001% of the displayed total. Its inclusion remains necessary for completeness, but gas determines the scale of the installation's emissions.
Figure 1 shows the monthly distribution of gas-related emissions. October has the highest reported value (2,228.4 t CO_2), followed by March and December. These three months account for approximately 64.8% of annual gas emissions. No gas consumption is reported from May to August. The unusually low January and February values compared with March should be checked against dispatch and operating records before attributing the distribution solely to outdoor temperature.

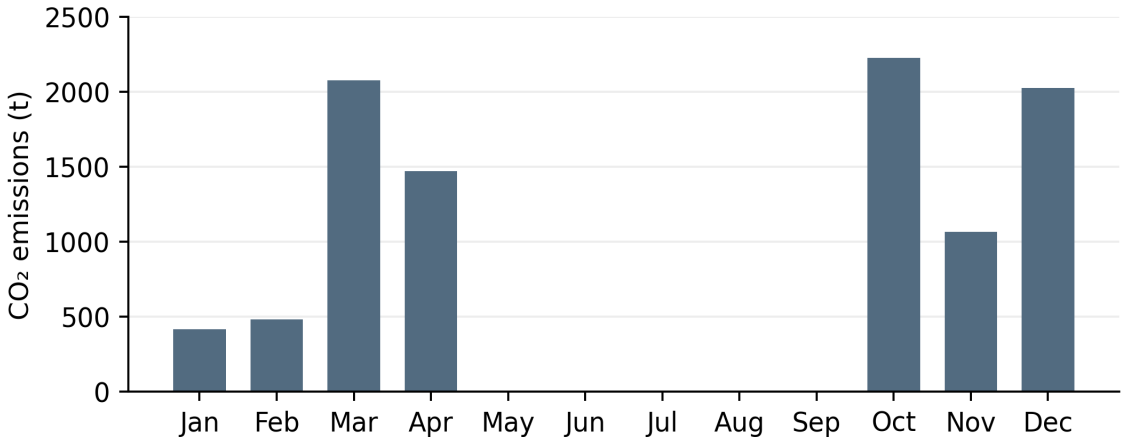


***Fig. 1**. Monthly CO_2 emissions from natural gas at „Istok" in 2025*

***Table 2**. Reproduction of the natural gas activity data uncertainty assessment*

Component / indicator	Value	Interpretation
MI1 turbine meter	2.00%	Expanded input; 94.1% of variance
MI2 volume corrector	0.50%	Expanded input; 5.9% of variance
Combined standard uncertainty	1.03%	Equivalent value at k = 1
Combined expanded uncertainty	2.06%	Result at k = 2; uncorrelated inputs
Applied tier 3 threshold	2.50%	Headroom: 0.44 percentage points

Source: Authors' calculation from Annex 4 (JKP Novosadska toplana, 2026b). Variance shares are each squared input divided by the sum of both squared inputs.

The combined result is below the 2.5% threshold for the applied activity data tier 3. The monitoring plan lists tier 2, with a 5.0% threshold, as the required tier. Thus, the documented assessment supports the higher applied tier, subject to the validity of its metrological inputs. The gas meter accounts for 94.1% of combined variance, making its documentation and performance the first priority in maintaining the metering assessment.

As a simple sensitivity interpretation, a 2.06% change in annual gas quantity would change calculated gas emissions by approximately 201 t CO_2 when all factors are held fixed. This is the emission effect of the activity data component, not a complete confidence interval for the annual emission inventory. If the two metering contributions were fully positively correlated, their combined value would be 2.50%, leaving no margin below the applied threshold. This conditional comparison shows why the correlation assumption should be documented.

Data consistency is equally important. The 15 °C to 0 °C NCV conversion changes the numerical volumetric value by 5.54%, which exceeds the assessed 2.06% metering uncertainty. Mixing gas volume and NCV reference conditions could therefore create a systematic calculation error larger than the metering component. A consistent unit convention and an independent check of spreadsheet formulas are practical controls with immediate value.

The supplied risk assessment identifies meter and corrector failures, missing calibration documentation, reading and data-entry errors, and incorrect calculation factors. It proposes checks against production records, timely acquisition of metrological documentation and review by a person independent of data entry. These measures address traceability and processing errors that are not represented by the numerical uncertainty budget (JKP Novosadska toplana, 2026b).

Two documentation issues warrant clarification. First, the supplied monitoring plan records tier 2b for gas NCV and EF, whereas the annual report records tier 3 based on laboratory analyses. This does not affect the reproduced arithmetic, but the stated tiers and supporting

evidence should be reconciled. Second, the diesel estimate uses 4.67 operating hours and 80 kW. The cited European Commission (2021) example specifies rated thermal input for this approach. Since the plant description gives a 100 kVA generator, the basis of the 80 kW value needs confirmation. If it is electrical output, fuel input cannot be established without accounting for efficiency and load. The reported 0.10 t CO_2 is retained here as a documented estimate, not independently validated fuel consumption.

CONCLUSION

The „Istok" case demonstrates a practical use of existing monitoring documentation to connect annual CO_2 emissions with activity data quality. Natural gas consumption of 4,696,998 Nm^3 yielded 9,770.45 t CO_2 in 2025. Together with the reported diesel contribution of 0.10 t CO_2, the displayed annual fuel values sum to 9,770.55 t CO_2. The calculation using the published annual gas factors reproduces the reported gas emission.
The activity data uncertainty assessment gives 2.06% at k = 2 under the documented assumption of uncorrelated meter and corrector contributions. This is below the applied 2.5% tier threshold, with the turbine meter contributing 94.1% of combined variance. The result concerns gas quantity; it should not be presented as the total uncertainty of reported emissions.
The approach is readily applicable to comparable gas-fired heating plants with supplier invoices, gas-quality data and documented metering systems. Practical priorities are to maintain metrological evidence, align gas reference conditions, reconcile factor-tier descriptions and substantiate emergency-generator fuel estimates. These targeted checks improve reporting reliability without requiring a complex additional monitoring programme.

REFERENCES

Čepić, Z., & Petrović, J. (2026). Implementation of the monitoring, reporting and verification system for greenhouse gas emissions in the Republic of Serbia: From regulatory framework to the first reporting year. *International Symposium "Engineering Management and Competitiveness" 2026*, 10–15.

European Commission. (2021). MRR guidance on uncertainty assessment – Example (MRR Guidance Document No. 4a, updated September 14, 2021). https://climate.ec.europa.eu/system/files/2021-09/ex_4a_uncertainty_en.pdf

JKP Novosadska toplana. (2026a). Annual greenhouse gas emission report for 2025: „Istok" heating plant. *eGHG export dated September 22, 2026*.

JKP Novosadska toplana. (2026b). Monitoring plan for „Istok" heating plant with Annexes 1–5, supplied documentation. *eGHG export dated September 22, 2026*.

Republic of Serbia. (2021). Law on Climate Change. *Official Gazette of the Republic of Serbia, No. 26/2021*.

Republic of Serbia. (2022). Regulation on Types of Activities and Greenhouse Gases. *Official Gazette of the Republic of Serbia, No. 13/2022*.

Republic of Serbia. (2023). Rulebook on Monitoring and Reporting of Greenhouse Gas Emissions. *Official Gazette of the Republic of Serbia, No. 118/2023*.

DOI:10.5937/IIZS26420C

OVERVIEW OF ASBESTOS-CONTAINING WASTE GENERATION AND REPORTING IN THE REPUBLIC OF SERBIA

Research paper

Jovana Čugalj [1*], Marina Pešić [2], Jelena Vuković [3], Una Marčeta [4]
[1,2,4]University of Novi Sad, Technical faculty „Mihajlo Pupin" Zrenjanin, Serbia
[2]University of East Sarajevo, Faculty of Technology Zvornik

Abstract: Asbestos-containing materials remain a waste management concern due to their continued presence in buildings and infrastructure. This study analyses reported asbestos-containing waste in Serbia using data from the Serbian Environmental Protection Agency (SEPA). Annual SEPA reports were used to examine disposed asbestos waste from 2012 to 2024, while Geographic Information System (GIS) records for 2020 were analysed to identify reported waste types, quantities, locations and management operations. The results show considerable variation in reported quantities over time, while the GIS data provide a more detailed view of their spatial distribution and management. The comparison of the two data sources also revealed differences in their coverage and level of detail. The findings highlight the need for more complete reporting and better integration of waste records to improve the assessment and management of asbestos-containing waste in Serbia.
Key words: Asbestos-containing waste, waste management, GIS, Serbia

INTRODUCTION

Asbestos refers to six naturally occurring silicate minerals with a fibrous structure, which are classified into two groups: serpentine and amphibole. Chrysotile, the main serpentine type, accounts for approximately 95% of industrial asbestos use, while the remaining types belong to the amphibole group (Pena-Castro et al., 2023). Due to its resistance to heat and fire, asbestos was widely used from the late 19th century in construction, shipbuilding, industry, and household products (Klemczak et al., 2024). However, exposure to asbestos can cause serious health effects, including asbestos-related lung diseases and cancer (Sen, 2015). In response to these health risks, Commission Directive 1999/77/EC prohibited Member States from allowing new applications of chrysotile asbestos on their territories from 1 January 2005 (European Commission, 1999). In Serbia, the production of asbestos fibres was banned in 2011, followed later by a ban on the use of asbestos-containing products (Stojšin & Ubavin, 2021). As a result, the extensive use of asbestos, particularly during the 1960s and 1970s, has led to the presence of asbestos-containing materials in many existing buildings and infrastructure. As these materials reach the end of their service life, they may become a source of asbestos-containing waste.

Under the Serbian waste classification system, asbestos-containing waste is classified according to its origin and includes several specific waste streams. These include waste containing asbestos from electrolysis (06 07 01*), waste from asbestos processing (06 13 04*), asbestos-containing waste from the production of asbestos cement (10 13 09*), metal packaging containing a hazardous porous solid matrix such as asbestos (15 01 11*), asbestos-containing brake linings (16 01 11*), discarded equipment containing free asbestos (16 02 12*), asbestos-containing insulation materials (17 06 01*) and asbestos-containing construction materials (17 06 05*). All of these waste streams are classified as hazardous waste in the Serbian Waste Catalogue (Republic of Serbia, 2010).

The management of asbestos-containing waste is additionally regulated by the Serbian Rulebook on the Management of Waste Containing Asbestos ("Official Gazette of the Republic of Serbia", No. 75/2010), which defines asbestos waste as raw asbestos, materials or products containing asbestos fibres, as well as asbestos dust generated during their processing. The Rulebook covers measures for the collection, transport, storage, treatment and final disposal of such waste, with particular emphasis on preventing the release and spread of asbestos fibres and dust into the environment. It also requires asbestos waste to be appropriately

[1*]Corresponding author, jovana.cugalj@uns.ac.rs, ORCID: 0009-0002-7257-7936
[2]marina.pesic@tfzr.rs
[4]una.marceta@uns.ac.rs, ORCID: 0000-0001-6664-0236
[3]jelena.vukovic@tfzv.ues.rs.ba , ORCID: 0000-0001-8850-1640

packaged before transport and, where applicable, treated by surface solidification, solidification or destruction of asbestos fibres before disposal (Republic of Serbia, 2010).
The aim of this study is to assess the quantities of asbestos-containing waste generated by reporting entities in Serbia. To achieve this, the research utilizes GIS records from the Serbian Environmental Protection Agency, for the year 2020. Specifically, the GIS database was queried and filtered using the waste index codes 17 06 01* (insulation materials containing asbestos) and 17 06 05* (construction materials containing asbestos). To provide a comprehensive national overview, the analysis is supplemented with data from the latest SEPA annual reports on generated waste and special waste streams.

MATERIAL AND METHODS

The methodology was based on data collected from the SEPA GIS waste management portal and SEPA reports. Reported quantities of asbestos-containing waste were analysed for the period 2012–2024 to examine changes over time. GIS records for 2020 were analysed for each reporting entity, including its location, reported waste quantity, and waste management operation (treatment or disposal). The reported quantities were then grouped by municipality to show their distribution across Serbia. The results are presented as a line graph showing the national trend, a map showing the distribution of asbestos-containing waste in Serbia, and a table with the reported quantities and management operations for each location.

RESULTS AND DISCUSSION

The available data were first examined to assess reported quantities of disposed asbestos-containing waste in Serbia between 2012 and 2024. The data show considerable variation over the observed period (Figure 1) (SEPA, 2025). The highest quantity was recorded in 2014, when 1,647 t of asbestos waste was disposed of. In the following years, the quantities decreased and remained below 1,000t. From 2018 onwards, the reported amounts were relatively similar, ranging from 201t in 2021 to 412t in 2019. In the most recent years, 253t was reported in 2022, 277t in 2023 and 278t in 2024.
The high value recorded in 2014 stands out from the quantities reported in the surrounding years. The available data do not provide an explanation for this increase which may be related to differences in demolition and reconstruction activities, the removal of asbestos-containing materials, or reporting practices. Despite the decrease compared with 2014, asbestos waste continued to be reported in Serbia in recent years, indicating that asbestos-containing materials remain present and continue to enter the waste management system.

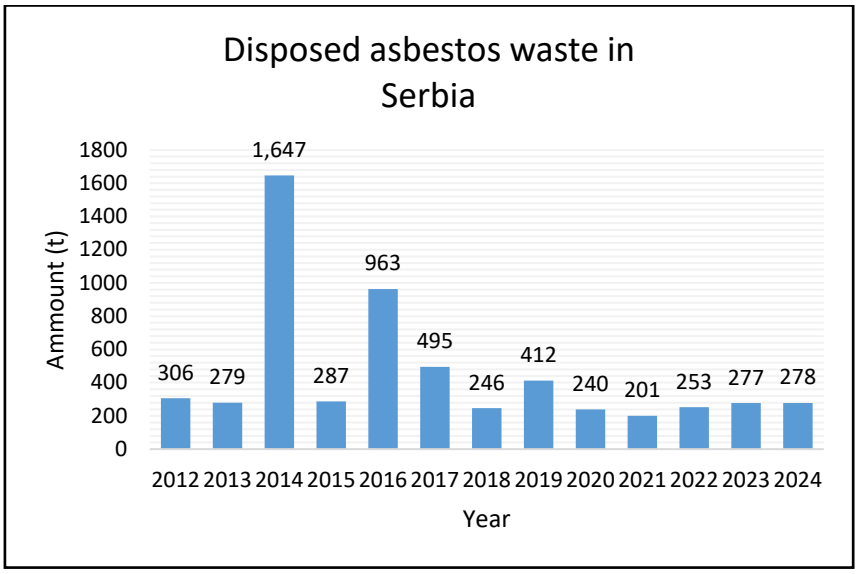


***Fig. 1.**. Reported quantities of disposed asbestos waste in Serbia, 2012–2024 (SEPA, 2025)*

To provide a more detailed view of the situation in Serbia, the available GIS data were further examined. The analysis covered the year 2020, the latest year for which data were available in the GIS database, and focused on the locations, reporting entities, waste types, and reported quantities of asbestos-containing waste. Records were available for six locations: Irig, Novi Sad, Kikinda, Kostolac, Lazarevac, and Pirot. The reported waste was classified under two waste codes, 17 06 01* and 17 06 05*. Code 17 06 01* was reported in Irig, Kikinda, and Lazarevac, while code 17 06 05* was reported in Novi Sad, Kostolac, and Pirot. The reporting entities included a waste collection and treatment company in Irig, a public utility company in Novi Sad, the Thermal Power Plant in Kostolac, a branch of the Serbian Power Utility (EPS) in Lazarevac, and an automotive tyre manufacturing company in Pirot.

A total of 21.764 t of asbestos-containing waste was reported across the six locations. The quantities varied considerably between locations, with the highest reported amount recorded in Kikinda (12.28 t), accounting for more than half of the total reported quantity. This waste was reported as sent for treatment. Lazarevac had the second-highest reported quantity, with 6.64 t, while 9.98 t was reported as sent for disposal. The remaining locations had substantially smaller reported quantities: 2.5 t in Novi Sad, 0.17 t in Pirot, 0.15 t in Kostolac, and only 0.024 t in Irig. The waste reported in Novi Sad and Pirot was sent for disposal, while the waste reported in Irig was sent for treatment. No treatment or disposal quantity was recorded for the 0.15 t reported in Kostolac.

The spatial distribution shows that the largest reported quantities were concentrated in Kikinda and Lazarevac, while substantially smaller amounts were recorded at the other four locations. These differences may reflect variations in the activities of the reporting entities and the types and quantities of asbestos-containing materials handled, rather than the overall distribution of asbestos-containing waste generated in Serbia. The spatial distribution of the reported quantities is shown in Figure 2, while the corresponding waste codes and management operations are presented in Table 2.

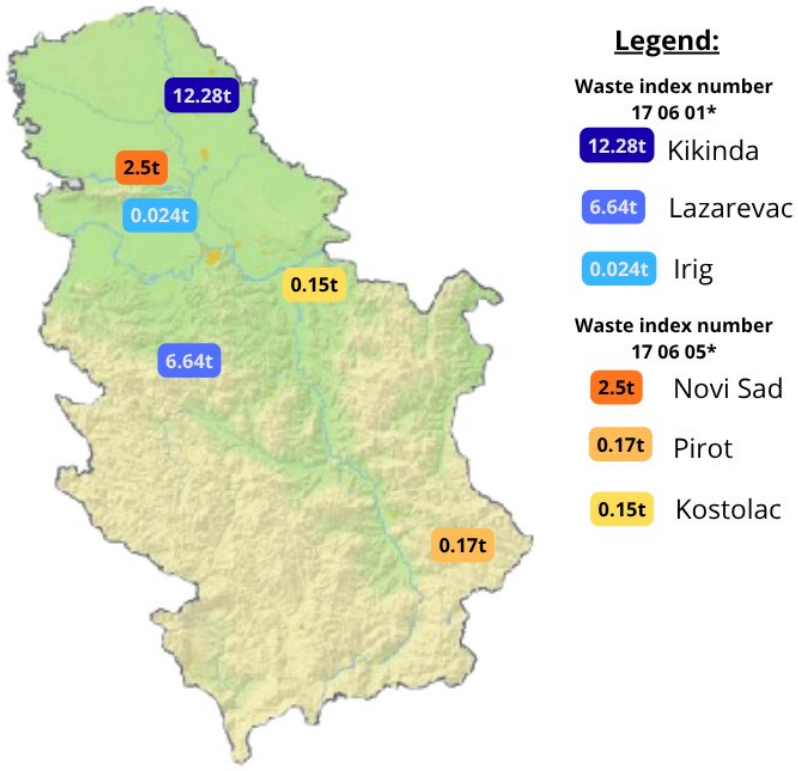


Fig. 2. *Spatial distribution of reported asbestos-containing waste in Serbia in 2020*

Table 2. *Reported quantities and management of asbestos-containing waste in Vojvodina in 2020 (SEPA, 2026)*

Location	Waste code	Waste generated in 2020 (t)	Sent for treatment (t)	Sent for disposal (t)
Irig	17 06 01*	0.024	0.024	-
Novi Sad	17 06 05*	2.5	-	2.5
Kikinda	17 06 01*	12.28	12.28	-
Kostolac	17 06 05*	0.15	-	-
Lazarevac	17 06 01*	6.64	-	9.98
Pirot	17 06 05*	0.17	-	0.17
	Total	21.764	12.304	12.65

The total quantity reported in the GIS records for 2020 was 21.764 t, compared with 240 t of asbestos-containing waste reported as disposed of in the SEPA annual report for the same year.

In comparison with EU countries, the reported quantities in Serbia are considerably lower than those reported in several European countries. Germany reported 10,860,400 t, Italy 3,650,105 t, Poland 1,647,960 t and Belgium 1,458,731 t of asbestos-containing waste for disposal. Among countries closer to Serbia, the reported quantities were 870,890 t in Austria, 98,198 t in Hungary and 68,735 t in Croatia (European Commission, 2024). Since the reporting periods are different between countries, the data are not directly comparable, but they provide an overview of the quantities of asbestos waste disposed of in Europe.

However, for Serbia, the difference between the quantities reported in the SEPA annual report and the 2020 SEPA GIS records highlights limitations in the current system of recording and integrating asbestos waste data .While the annual reports provide the total quantity disposed of, they do not indicate the quantities belonging to individual waste codes. The GIS database provides more detailed information on waste types, locations and management operations, but does not necessarily include all entities generating asbestos-containing waste and sending it for treatment or disposal. Better coordination between these data sources, together with more complete reporting and systematic integration of records, would provide a more comprehensive overview of asbestos-containing waste management in Serbia.

CONCLUSION

The analysis shows that asbestos-containing waste continues to be reported in Serbia, despite the long-standing restrictions on asbestos use. Reported quantities of disposed asbestos waste varied considerably between 2012 and 2024, with the highest quantity recorded in 2014 and relatively stable amounts in recent years. The 2020 GIS data provided more detailed information on the locations, waste types and management operations of individual reporting entities, but represented only a limited part of the total quantity reported at the national level. The comparison with SEPA annual data also revealed differences in the level of detail and coverage between the two data sources. These findings indicate a need for better coordination and integration of waste records, more complete reporting by entities generating asbestos-containing waste, and more detailed classification of reported quantities. Improving the consistency and completeness of asbestos waste data would support more reliable assessment of waste flows and provide a stronger basis for planning its safe management in Serbia.

REFERENCES

European Commission. (1999). Commission Directive 1999/77/EC. Brussels.

European Commission. (2024). Study on Asbestos Waste Management Practices and Treatment Technologies. European Commission, Directorate-General for Environment. Luxembourg: Publications Office of the European Union.

Klemczak, B., Kucharczyk-Brus , B., Sulimowska, A., & Radziewicz-Winnicki, R. (2024). Historical Evolution and Current Developments in Building Thermal Insulation Materials—A Review. Energies, 17. https://doi.org/10.3390/en17225535

Pena-Castro, M., Montero-Acosta, M., & Saba, M. (2023). A critical review of asbestos concentrations in water and air,. Heliyon, 9(5). https://doi.org/10.1016/j.heliyon.2023.e15730

Republic of Serbia. (2010). Rulebook on Categories, Examination and Classification of Waste, 56/2010. Official Gazette of the Republic of Serbia.

Republic of Serbia. (2010). Rulebook on the Management of Waste Containing Asbestos, 75/2010. Official Gazette of the Republic of Serbia.

Sen, D. (2015). Working with asbestos and the possible health risks. Occupational Medicine, 65(1). https://doi.org/10.1093/occmed/kqu175

SEPA, Serbian Environmental Protection Agency. (2025). Waste in the Republic of Serbia 2011–2024. Belgrade. https://sepa.gov.rs/wp-content/uploads/2026/04/Otpad2011-2024.pdf

SEPA, Serbian Environmental Protection Agency. (2026, September 19). Waste Management GIS Portal. http://77.46.150.221/nrizgis/index.html

Stojšin, K., & Ubavin, D. (2021). Analiza uticaja azbesta na zdravlje i mere za unapređenje uslova radne sredine. Zbornik radova Fakulteta tehničkih nauka, Novi Sad. https://doi.org/10.24867/12HZ03Stojsin

DOI:10.5937/IIZS26425J

ANALYSIS OF AIR POLLUTION SPATIAL DISTRIBUTION: DISPERSION MODEL WITH MULTILAYER ATMOSPHERIC STRUCTURES (DMMAS)

Research paper

Stevo K. Jaćimovski[1], Dane Subošić[2], Dušan I. Ilić[3], Jovan P. Šetrajčić[4,*]

[1,2]University of Criminal Investigation and Police Studies, Zemun – Belgrade, Serbia;
[3]University of Novi Sad, Technical Faculty, Novi Sad, Vojvodina – Serbia;
[4]Academy of Sciences and Arts of the Republic of Srpska, Banja Luka, B&H.

Abstract: This paper presents the results of a semi-analytical solution to the two-dimensional, time-dependent advection-diffusion equation, based on the discretization of the surface boundary layer (SBL) into *N* sub-layers. Within each sub-layer, the equation is solved using Laplace transforms, incorporating mean values for the turbulent diffusion coefficient and wind speed. The actual pollutant concentration is determined by numerically calculating the inverse Laplace transform via the Gaussian quadrature method. The pollutant concentration distributions obtained through this approach are compared with those from the Gaussian atmospheric dispersion model, as well as with available experimental results.
Key words: DMMAS model, inverse Laplace transforms, diffusion coefficient, wind speed, Gaussian quadrature, Gaussian model.

INTRODUCTION

Recently, a semi-analytical solution of the advection-diffusion equation for non-stationary conditions was obtained (Vilhena, et al. 1998). From this solution, a model named AMMD (Analytical Model of Multilayer Dispersion) was set up. The model is based on the discretization of the PBL (Planetary Boundary Layer) into *N* sub-layers, where in each sub-layer the advection-diffusion equation is solved using the Laplace transform technique, taking into account the average value of turbulence and wind speed. The main feature of this method is based on the following steps: stepwise approximation of turbulence and wind speed, double Laplace transformation for the advection-diffusion equation in *x*, *z* and *t* variables, semi-analytical solution of a set of linear ordinary equations resulting from the application of double Laplace transformation and construction of pollutant concentration using the inverse Laplace transformation using the so-called Gauss quadrature scheme (Moreira, et al., 2005). The model represents a semi-analytical solution due to the numerical inversion of the Laplace transform of the solution of the advection-diffusion equation.

DMMAS MODEL

The equation of advection and diffusion that describes the temporal evolution of the concentration of *C*, due to the release of the amount of polluting material continuously in time by an elevated source placed at (0,0,*h*), in a horizontally homogeneous atmosphere is (Tirabasi, T. et al., 2010):

$$\frac{\partial C}{\partial t} + u\,\frac{\partial C}{\partial x} = \frac{\partial}{\partial z}\left(K_z\,\frac{\partial C}{\partial z}\right). \tag{1}$$

The mathematical description of the dispersion problem represented by equation (1) is well defined when the initial and boundary conditions are provided. Indeed, it is assumed that at the beginning of the pollutant release, the dispersion region is not polluted, which means that:

[1]jacimovskis@gmail.com, ORCID No: 0000-0002-4074-662X.
[4]Corresponding author, jovan.setrajcic@gmail.com, ORCID:0000-0002-6903-2882

$$C(x,z,0) = 0, \text{ at } t = 0. \quad (2)$$

At the point (0,*z*,*t*), a continuous line source with a constant emission rate *Q* is assumed, i.e.

$$u\,C(0,z,t) = Q\,\delta(z-h), \quad \text{at } x = 0, \quad (3)$$

where *δ* is the Dirac delta function and h is the height of the source. Pollutants are also subject to zero flux boundary conditions at the ground and top of the PBL. The PBL is the boundary layer of the atmosphere (BLA), and it is covered by the inversion layer, so that within the inversion layer the atmosphere becomes extremely stable and there is no mixing of pollutants. Inverse conditions in the atmosphere (temperature inversion) represent the phenomenon when the air temperature increases with the increase in altitude, which is the opposite of the usual state in the troposphere where the temperature decreases. This condition in the atmosphere causes a stable air layer that prevents vertical mixing, which often leads to the retention of cold air, fog and pollutants in the lower layers. The inversion at the top of the PGS practically acts as an impermeable surface, and the boundary condition applies to it:

$$K_z \frac{\partial C}{\partial z} = 0, \quad \text{at } z = 0, H. \quad (4)$$

Here, *H* is the height of the boundary layer of the atmosphere. Experimental determination of the height of the boundary layer is very complex and can be carried out using radiosondes, weather balloons, towers, aircraft, radar and other methods. Given that experimental values are often unavailable, mathematical modeling is used to obtain mixing height values (Pocajt, 2018). The height of the inversion layer depends on several parameters and has different values for different conditions of atmospheric stability.

The reliability of the model largely depends on how the dispersion parameters are determined based on the structure of the (PBL) turbulence and the ability of the model to reproduce experimental diffusion data. There are a large number of formulations for the dispersion coefficient and wind speed, and the paper will use Degrazie's formulation (Degrazia, G.A. & Moraes, O.L.L., 1992; Degrazia, G.A. et al., 2001):

$$K(z) = 0{,}22\,u_*\,H\,\left(\frac{z}{H}\right)^{\frac{1}{3}}\left(1-\frac{z}{H}\right)^{\frac{1}{3}}\left[1-\exp\left(-\frac{4z}{H}\right)-0{,}0003\exp\left(\frac{8z}{H}\right)\right]; \quad (5)$$

$$u(z) = \frac{u_*}{k}\left[\ln\frac{z}{z_0} - \Psi_m\left(\frac{z}{L}\right) + \Psi_m\left(\frac{z_0}{L}\right)\right], \quad (6)$$

where is:

$$\Psi_m = 2\ln\left[\frac{1+A}{2}\right] + \ln\left[\frac{1+A^2}{2}\right] - 2\arctan A + \frac{\pi}{2};\ \ A = \left(1-16\,\frac{z}{L}\right)^{\frac{1}{4}}. \quad (7)$$

Since both mechanical and convective forces determine turbulence, Monin and Obukhov (Monin, A.S. & Obukhov, A.M., 1953) proposed a similarity theory that introduced two scaling parameters: the friction velocity u_* and the Monin-Obukhov length (*L*), which is a measure of the depth of the surface layer in which shear effects are significant under any conditions of atmospheric stability (Esmail, S.F.H., 2011), and is expressed (Ilijazi, V., 2022) as:

$$L = -\frac{u_*^3 c_p Q T}{g k G}, \tag{8}$$

where c_p is the specific heat of air at constant pressure, Q air density, k von Karman constant, T air temperature, g gravitational acceleration and G heat flux. For unstable, neutral and stable conditions, the values of L are less than zero, equal to 0 and greater than zero, respectively (Esmail, S.F.H., 2011).

Taking into account the dependence of the coefficient $K(z) \rightarrow K_z$ and the wind speed profile u on the variable z, the height of the PGS is discretized in N sub-intervals (as in the sketch from Figure 1) in such a way that within each interval K_z and u $u(z) \rightarrow u_z$ assume mean values:

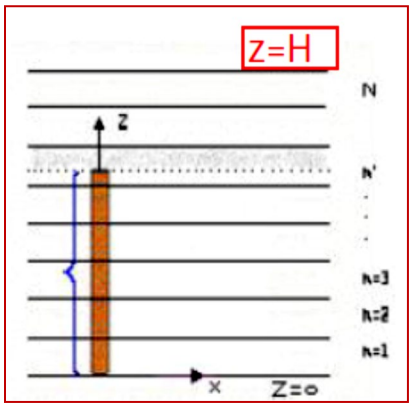


Fig. 1. *Schematic representation of the discrete layering of the dispersion coefficient and velocity along the z-direction*

$$K_n = \frac{1}{z_{n+1}-z_n} \int_{z_n}^{z_{n+1}} K_n(z)\, dz; \tag{9}$$

$$u_n = \frac{1}{z_{n+1}-z_n} \int_{z_n}^{z_{n+1}} u_n(z)\, dz. \tag{10}$$

Therefore, based on that, the solution of equation (1) is reduced to the solution of N problems of this type:

$$\frac{\partial C_n}{\partial t} + u_n \frac{\partial C_n}{\partial x} = K_n \frac{\partial^2 C_n}{\partial z^2}, \tag{11}$$

for n = 1, 2, 3, ⋯, N – 1, where C_n denotes the concentration in the nth subinterval. In order to determine the 2N integration constants, additional 2N – 2 conditions are considered, such as the continuity of concentration and flow at the boundaries in the following form:

$$C_n = C_{n+1}, \quad \text{for} \quad n = 1,2,\ldots,(N-1); \tag{12}$$

$$K_n \frac{\partial C_n}{\partial z} = K_{n+1} \frac{\partial C_{n+1}}{\partial z}, \quad \text{for} \quad n = 1,2,\ldots,(N-1). \tag{13}$$

By applying the Laplace transformation to (11), we get:

$$\frac{\partial^2 \bar{C}_n(s,z,p)}{\partial z^2} - \frac{p+su_n}{K_n} \bar{C}_n(s,z,p) = -\frac{u_n}{K_n} \bar{C}_n(0,z,p), \tag{14}$$

where: $\bar{C}_n(s,z,p) = L\{C_n(x,z,t;\ x \rightarrow s;\ t \rightarrow p\}$ – Laplace figure of concentration in sublayer n. The solution of equation (14) is known (Tošić,B.S., et al., 2018) and is expressed in the following form:

$$\bar{C}_n(s,z,p) = A_n e^{-R_n z} + B_n e^{R_n z} + \frac{Q}{2R_a}\left[e^{-R_n(z-H)} - e^{R_n(z-H)}\right], \tag{15}$$

where are:

$$R_n = \sqrt{\frac{(p+s\,u_n)}{K_n}}; \quad R_a = \sqrt{(p+s\,u_n)K_n}. \tag{16}$$

Applying the initial and boundary conditions, a system of linear algebraic equations for the integration constants A_n and B_n is obtained, as in (Essa, K.S.M. & Taha H.M.A., 2023):

$$A_n = B_n = \frac{Q\left[\mathrm{e}^{R_n(H-h)}+\mathrm{e}^{-R_n(H-h)}\right]}{2R_a(\mathrm{e}^{R_nH}-\mathrm{e}^{-R_nH})}. \tag{17}$$

After that, the concentration is obtained by numerically inverting the transformed concentration C_n using the Gauss quadrature method (Moreira, et al., 2005) in the following form:

$$C_n(x,z,t) = \sum_{i=1}^{k} w_i\left(\frac{P_i}{t}\right)\sum_{j=1}^{M} w_j\left(\frac{P_j}{t}\right)\Bigg\{A_n\,\mathrm{e}^{-\sqrt{\frac{P_j}{tK_n}+\frac{P_ju_n}{xK_n}}(z-h)} - B_n\,\mathrm{e}^{\sqrt{\frac{P_j}{tK_n}+\frac{P_ju_n}{xK_n}}(z-h)} + \\ + \frac{1}{2}\frac{Q}{2\sqrt{\frac{P_jK_n}{t}+\frac{P_ju_nK_n}{x}}}\left[\mathrm{e}^{-\sqrt{\frac{P_j}{tK_n}+\frac{P_ju_n}{xK_n}}(z-h)} - \mathrm{e}^{\sqrt{\frac{P_j}{tK_n}+\frac{P_ju_n}{xK_n}}(z-h)}\right]\theta(z-h)\Bigg\}. \tag{18}$$

Here $\theta(z-H)$ is the Heaviside function defined, e.g. as in [Tošić, B.S., et al., 2018]:

$$\theta(z-h) = \begin{cases} 1, & \text{za } z > h; \\ 0, & \text{za } z < h, \end{cases} \tag{19}$$

which indicates that the second term in (18) is added only for $z > h$.
Gauss-Lager integration (Stroud, & Secrest D., 1996) is an approximate method for finding the numerical value of the Laplace transform:

$$\int_0^\infty f(\mathrm{p})dp = \int_0^\infty \mathrm{e}^{-p}[e^p f(p)]\;dp \approx \sum_{j=1}^{n} w(p_j)\;\mathrm{e}^{p_j} f(p_j), \tag{20}$$

where p_j are the values of the roots of Lager polynomials of the appropriate degree (Tošić, B.S., et al., 2018). With this, the values of the corresponding variables, usually: $k = 2$, $M = 8$, (Stroud, & Secrest D., 1996) for the integration procedure defined in (18) are calculated and shown in Table 1. Adopted values of parameters for calculating pollutant concentration according to (Moura A.B.D., 2018) are:

L = 116 m, Q = 400 g/m2, H = 400 m, u_* = 0,31 m/s, h = 12,5 m, z_0 = 0.6 m, t = 7.200 s.

Table 1. *Values of the roots of the Lager polynomials and the corresponding weighting factors for the application of Gauss-Lager quadrature methods*

No. i	Root of a Laguerre polynomial, of order i, p_i	Weight factor $w(p_i)$	Total weight factor, $w(p_i)\;\mathrm{e}^{p_i}$
1	0,585786	0,853553	1,53333
2	3,414210	0,146447	4,45096
No. j	Root of a Laguerre polynomial, of order j, p_j	Weight factor, $w(p_j)$	Total weight factor, $w(p_j)\mathrm{e}^{p_j}$

1	0,170280	0,36918900	0,437723
2	0,903702	0,41878700	1,033870
3	2,251090	0,17579500	1,669710
4	4,266700	0,03334350	2,376920
5	7,045910	0,00279454	3,208540
6	10,758500	$9{,}07651 \cdot 10^{-5}$	4,268580
7	15,740700	$8{,}48575 \cdot 10^{-7}$	5,818080
8	22,863100	$1{,}04800 \cdot 10^{-9}$	8,906230

Based on all that, the dependence of the diffusion coefficient on the height was calculated numerically and is shown graphically in Figure 2.

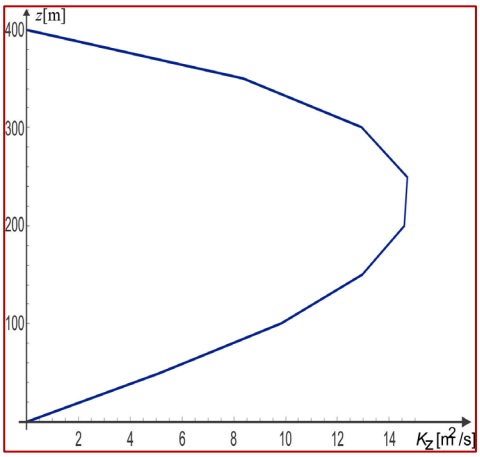


Fig. 2. *Dependence of the diffusion coefficient on the height z according to relation (5) →*

Figure 2 clearly shows the complex dependence of the diffusion coefficient with increasing distance from the earth's surface. This dependence is much more adapted to real atmospheric conditions and stability classes than the situation and the complex relationship of advective and diffuse flow.

In the Gaussian model, the diffusion coefficient is assumed to depend on x, for example, as a power function. Similar considerations apply to the dependence of wind speed u, defined by relations (6) and (7).

As an example of using the DMMAS model, it was adopted that the atmosphere from the surface to the PGS layer is divided into four layers with heights: Δz_1= 12,5 m (from the ground surface to the height of the source), Δz_2= 67,5 m; Δz_3= 120 m and Δz_4= 200 m. For those layers, according to (5), (6) and (7), and according to relation (10), the corresponding mean values of diffusion coefficients K_1, K_2, K_3, K_4 and mean values of wind speeds u_1, u_2, u_3, u_4 are found. According to (17) and the found mean values of the diffusion coefficient and the mean values of the wind speeds by layers, the values of the coefficients R_1, R_2, R_3, R_4 and R_{a1}, R_{a2}, R_{a3}, R_{a4} are found. For the given adopted parameters and for the case of a neutral or stable atmosphere and with the use of data from table 1 according to relation (18), the concentrations of air pollutants at the height z = 100 m (third layer) and z = 300 m (fourth layer) along the distance x ϵ (0, 12 km) were sought. This x-axis distance was chosen in order to be able to compare the results with the results within the Gaussian model, which gives valid results up to these distances. A graphical presentation of the results is given in Figure 3.

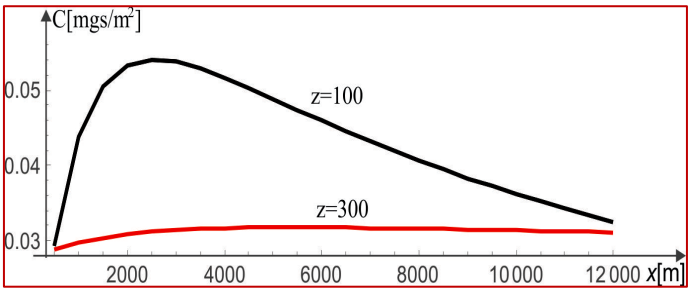


Fig. 3. *Comparative presentation of the distribution of pollutants at different heights, according to the DMMAS model*

From Fig. 3, it is noticeable that the concentration of pollutants is higher at lower altitudes and vice versa, which is again in accordance with physical laws.

GAUSS MODEL

The Gaussian model of the spatial distribution of air pollutants is the most commonly used analytical-mathematical model in environmental protection engineering and meteorology for estimating the distribution and concentration of pollutants in the atmosphere. The model observes a stationary point source (e.g. a factory chimney) from which GSAs are emitted at a constant rate. The smoke plume travels downwind, while turbulent diffusion spreads it laterally – horizontally and to the height – vertically (Nikezić, D.P., 2016), which is shown in Fig. 4.

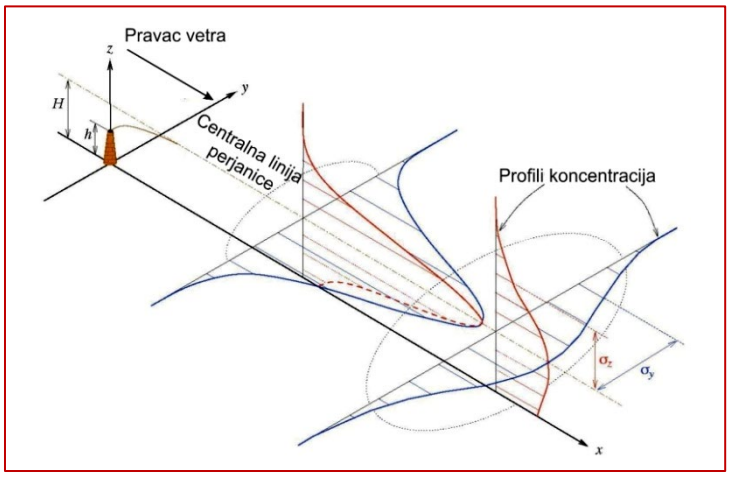


Fig. 4. *Distribution of pollutants according to the Gaussian model*

The expression for the concentration in the Gaussian model, with the reflection of pollutants from the earth's surface, according to (Vulović, A., 2022), has the following form:

$$C(t,x,z) = \frac{Q}{2\pi u \sigma_y(x)\sigma_z(x)} \exp\left(-\frac{(x-u\,t)^2}{2\sigma_x^2(x)}\right)\left\{\exp\left[-\frac{(z-l)^2}{2\sigma_z^2(x)}\right] + \exp\left[-\frac{(z+l)^2}{2\sigma_z^2(x)}\right]\right\};$$
$$\sigma_y = ax^b; \qquad \sigma_z = cx^d, \tag{21}$$

where *a*, *b*, *c*, *d* are the empirical coefficients, which depend on the stability class of the atmosphere and whose values are given in table 2. The wind speed at height l is determined by the expression:

$$\bar{u}(l) = u(z_1)\left(\frac{l}{z_1}\right)^m, \tag{22}$$

where z_1 is a fixed height, and *m* is an exponent that depends on the class of atmospheric stability (Table 2).

Table 2. *Pasquila stability classes and empirical coefficients*

	a	***b***	***c***	***d***	***m***
A	0,235	0,796	0,311	0,711	0,53
B	0,297	0,796	0,382	0,711	0,40
C	0,418	0,796	0,520	0,711	0,33

D	0,586	0,796	0,700	0,711	0,23
E	0,826	0,796	0,950	0,711	0,16
F	0,946	0,796	0,321	0,711	0,10
G	1,043	0,698	0,819	0,669	0,33

Applying relations (21) and (22), taking the points from Table 2, for the neutral atmospheric class of stability, the distribution of air pollutants at the height of z = 300 m is found, the graphic representation of which is given in Figure 5.

If we compare the obtained data on the distribution of air pollutants for the same parameter values and the same stability class in the Gaussian and DMMAS models and show it graphically (Figure 6), a drastic difference is obtained.

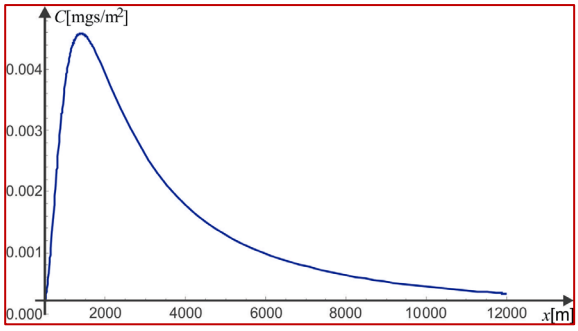


Fig. 5. *Gaussian distribution of air pollutants in space*

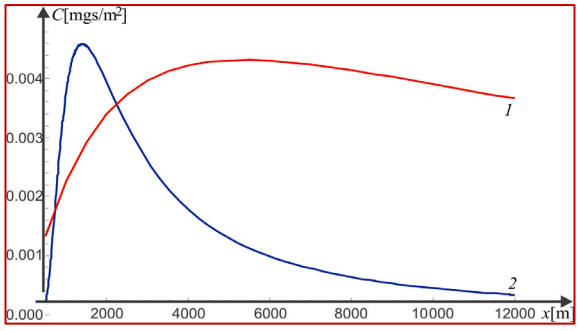


Fig. 6. *Comparative presentation of the distribution of pollutants for the same parameter values and the same class atmospheric stability: 1 – DMMAS model; 2 – Gaussian model*

From Figure 6, it can be seen that the Gaussian model gives a slightly higher maximum pollutant concentration value of 0,00455 mg/m^2 and that they are closer to the source (at 1.500 m) than the values predicted by the DMMAS model of 0,00455 mg/m^2 (at 5.500 m). At the same time, the DMMAS model indicates that pollutant concentrations do not decrease sharply with distance, after reaching the peak, i.e. maximum values.

VALIDATION OF RESULTS

Model verification is an assessment of the practical value and accuracy of the model. There is general agreement that experimental data, and especially field measurements, are the main criteria for model verification. Despite that fact, model verification is an extremely complex problem. The reasons for that are as follows (Pocajt, V. & Antanasijević D., 2018):

- The appropriate assessment method cannot be defined in a unique way, since the methods used depend on the context of application;
- Experimental field data sets for evaluation are limited and reflect only a small part of the possible scenarios. For a correct assessment of the model, it is necessary to use as many data sets as possible, with an understanding of the nature of the model;

During 1987, an experiment was conducted in Copenhagen in which SF_6 concentration values were measured in a certain period of time for different classes of atmospheric stability (Gryning, S.E., et al., 1987). This experiment serves to check the validity of DMMAS and the Gaussian model. According to Hanna (Hanna, S.R., 1989), the statistical parameters necessary for comparing the quality of the model with experimentally determined normalized concentrations are:

- Normalized mean square error: $NMSE = \frac{\overline{(C_M - C_R)^2}}{\overline{C_M}\ \overline{C_R}}$;

- Linear correlation coefficient: $R = \frac{\overline{(C_M - \overline{C_M})(C_R - \overline{C_R})}}{\sigma_{C_M}\sigma_{C_R}}$;

  (The coefficient of linear correlation (*R*) provides the least information, and thus is the least significant, of the displayed statistical indicators, because it represents the degree of linear correlation of predicted and correct values.)
- Proportion of correct predictions: $FAC2\colon\ 0{,}5 \leq \frac{C_R}{C_M} \leq 2{,}0$;

  (The proportion of correct predictions relative to the correct value. The *FA* indicator is one of the most significant statistical indicators of the model's performance, because it shows the model's ability to provide accurate predictions for a certain resolution of the error, for each individual examined case. *FAC2* shows the proportion of predictions with a relative error of less than ± 20 % allows the models to be effectively classified by performance, depending on the complexity of the problem and the required accuracy.)
- Fractional tendency: $FB = \frac{(\overline{C_M} - \overline{C_R})}{0{,}5(\overline{C_M} + \overline{C_R})}$,

  where: C_M – measured concentration and C_R – concentration calculated according to the appropriate model, and the line above the appropriate size indicates the arithmetic mean value of the given size.

If the model were perfect, i.e. if the calculated results matched the measured values, the *R* and *FAC*2 parameters would have a value of 1, and the *MNSE* and *FB* parameters would have a value of 0. Such matching is only possible in an ideal situation because no model is perfect. Table 3 shows the comparative values of the statistical parameters of the measured normalized concentrations and their values for the case when the normalized concentrations are calculated using different models.

Table 3. *Comparison of calculated values based on DMMAS and Gaussian model*

Modeli	***NMSE***	***R***	***FAC2***	***FB***
DMMAS	0,10	0,91	1,00	0,16
Gaussian	0,58	0,80	0,59	0,58

According to Table 3, it is obvious that the DMMAS model predicts the values of air pollutant concentrations significantly better than those predicted by the Gaussian model.

CONCLUSIONS

The aim of this paper was to present and discuss the results of the comparison between the Gaussian model and the DMMAS model based on the time-dependent semi-analytical solution of the advection-dispersion equation for the simulation of pollutant propagation in SBL. For a better understanding of the comparison between the two models in this paper, the focus is on the mathematical characteristics of the two approaches. Regarding the DMMAS method, it is important to emphasize that no approximation is made in this approach except the approximation of the meteorological parameters by layers and Laplace numerical inversion using the Gaussian quadrature scheme. In the DMMAS method, it is only necessary to choose the number of sublayers appropriately, taking into account the smoothness of the functions Kz and u (Moreira, D.M., et al., 2005).

The advantage of the Gaussian model lies in its exceptional computational simplicity, fast analytical results and the possibility of insight into the spatial distribution of pollution based on minimal input meteorological data. This is why it forms the basis of many modern modeling software packages (Aermod, Calpuff, ...). However, the Gaussian model does not give good results in conditions of complex topography (mountains, valleys), with extremely weak winds < 1 m/s, as well as for reactive pollutants that enter into photochemical reactions in the atmosphere (Hanna, S.R., et al., 1989).

With the same input values of the model parameters, the same atmospheric stability classes, both models give approximately the same maximum concentration values, at approximately the same distance from the source. However, the DMMAS model indicates significantly higher concentrations of air pollutants at greater distances from the source (Figure 5). In addition, according to the statistical characteristics of the validation of the DMMAS model, the model is more consistent than the Gaussian model with the experimentally measured values of air pollution.

REFERENCES

Degrazia, G.A., Moraes, O.L.L. (1992). A Model for Eddy Diffusivity in a Stable Boundary Layer, *Boundary-Layer 0 Meteorology* **58**, 205-214.

Degrazia, G.A., Moreira, D.M., Vilhena, M.T. (2001). Derivation of an Eddy Diffusivity Depending on Source Distance for Vertically Inhomogeneous Turbulence in a Convective Boundary Layer, *J. Appl. Meteor.* **40**, 1233–1240.

Essa K.S.M., Taha H.M.A. (2023). Studying the Effect of Two Analytical Solutions of Advection-Diffusion Equation on Experimental Data, *Pure Appl. Geophys*. **180**, 2407–2418.

Esmail S.F.H. (2011). Assessment of Concentration of Air Pollutants Using Analytical and Numerical Solutions of the Atmospheric Diffusion Equation, Thesis, *Faculty of Science, Zagazig University*.

Gryning S.E., Holtslag A.A.M., Irwin J.S., Siversten B., (1987). Applied Dispersion Modelling Based on Meteorological Scaling Parameters, *Atmos. Environ.* **21**/1, 79-89.

Hanna S.R. (1989). Confidence Limits for Air Quality Model Evaluations, as Estimated by Bootstrap and Jackknife Resampling Methods. *Atmos. Environ.* **23**, 1385-1398, doi: 10.1016/0004 6981(89)90161-3.

Hanna, S.R., Briggs, G.A., Jr. Hosker, R.P. (1982). Handbook on Atmospheric Diffusion. Prepared for the Office of Health and Environmental Research, office of Energy Research, *U.S. Department of Energy*, DOE/TIC 11223, J.S. Smith, Publ. Ed.

Ilijazi V. (2022), Modeling the distribution of air pollutants in accidents as a function of IT support for early response, Dissertation, *University of Criminal Investigation and Police Studies,* Zemun – Belgrade – in Serbian.

Moreira D.M., Neto P.V.F., Carvalho J.C., (2005). Analytical Solution of the Eulerian Dispersion Equation for Nonstationary Conditions: Development and Evaluation, *Environmental Modelling and Software*, **20**/9, 1159-1165.

Monin A. S., Obukhov A. M., (1953). *Doklady Akad. Nauk USSR* **93**, 2 – In Russian.

Moura, A.B.D. (1995). Analytical Solution of Turbulent Vertical Dispersion in the Stable Boundary Layer. Dissertation, *Federal University of Rio Grande do Sul*.

Nikezić, D.P. (2016). Mathematical Modeling of the Spread of Pollutants in the Air in the Vicinity of Nuclear and Industrial Facilities, Doctoral Dissertation, *Faculty of Technological Metallurgy, University of Belgrade*, Belgrade – in Serbian.

Pocajt, V., Antanasijević, D. (2018). Selected Chapters in Life Protection Engineering Environment, *Faculty of Technology and Metallurgy, University of Belgrade*, Belgrade – in Serbian.

Stroud A. H., Secrest D., (1996). Gaussian Quadrature Formulas, *Prentice-Hall*, Englewood Cliffs, p. 320.

Tirabassi T., Moreira D.M., Vilhena M.T, da Costa C.P.,(2010), Comparison between Non-Gaussian Puff Model and a Model Based on a Time-Dependent Solution of Advection-Diffusion Equation, J*. Environ. Protection* **1**, 172-178.

Tošić B.S., Šetrajčić J.P., Jaćimovski S.K., (2018). Methods of Theoretical Physics, *University of Criminal Investigation and Police Studies,* Zemun – Belgrade – in Serbian.

Vilhena, M.T., Rizza, U., Degrazia, G.A., Mangia, C., Moreira, D.M., & Tirabassi, T. (1998). An Analytical air Pollution Model: Development and Evaluation. *Contr. Atmos. Phys*. **71**/3, 315–320.

Vulović A. (2022), Analysis of the Impact of Air Pollutants on Human Health from the Aspect of Environmental Forensics, Dissertation, *University of Criminal Investigation and Police Studies,* Zemun – Belgrade – in Serbian

DOI:10.5937/IIZS26435B

FINE-SCALE PM_1 POLLUTION DYNAMICS IN AN URBAN–SUBURBAN ENVIRONMENT

Research paper

Maja Brborić[1]*, Branka Nakomčić Smaragdakis[2], Sonja Dmitrašinović[3], Miljan Šunjević[4], Epari Ritesh Patro[5]

[1,2,3,4]University of Novi Sad, Faculty of Technical Sciences, Trg Dositeja Obradovića 6, 21000 Novi Sad, Serbia

[5]Water, Energy and Environmental Engineering Research Unit, University of Oulu, Oulu FI-90014, Finland

Abstract: Submicron particulate matter (PM_1) is not routinely regulated as a separate ambient-air fraction, yet its spatial behavior can provide useful information on combustion-related aerosol and neighborhood-scale exposure contrasts. This study examined one complete heating/non-heating cycle (16 April 2024-15 April 2025) at five monitoring locations in the Novi Sad urban-suburban system, Serbia: Novi Sad, Sremska Kamenica, Sremski Karlovci, Ledinci and Beočin. Daily PM_1 observations from a community sensor network were evaluated using descriptive statistics, seasonal contrasts, inter-site correlations and a parsimonious cross-site regression model. Median PM_1 concentrations over the study window ranged from 8 to 14 μg m^{-3}. Heating-season medians were 2.2–3.2times higher than non-heating medians, with the largest absolute winter burden observed in Novi Sad. Daily concentrations were strongly correlated across the suburban sites (r = 0.80-0.90 for most pairs), indicating coherent regional forcing, while the weaker association between Novi Sad and Beočin (r = 0.66) pointed to local modulation. A linear model using the four surrounding sites reproduced daily PM_1 at the urban site with R^2 = 0.72 on a chronologically independent test period. The combined results show that a compact five-site network can resolve both shared pollution episodes and site-specific amplification without requiring a geographically extensive monitoring design.

Key words: PM_1, submicron particles, urban-suburban gradient, low-cost sensors, seasonal variability

INTRODUCTION

Ambient particulate matter remains a major environmental determinant of population health. Current air-quality regulation and health-based guidance are centered on $PM_{2.5}$ and PM_{10}, while PM_1 is generally not treated as a separate regulatory mass fraction. Nevertheless, particles below 1 μm account for an important component of combustion-derived and secondary aerosol, and their temporal behavior may differ from that of the coarser particle fractions. The World Health Organization (2021) therefore provides a useful health context for particulate pollution as a whole, but it does not define a specific ambient guideline value for PM_1.

European observations indicate that submicron aerosol is strongly seasonal. In a Central European urban area, Samek et al. (2018) reported daily mean PM_1 concentrations of 6.9 μg m^{-3} in summer and 17.3 μg m^{-3} in winter, with combustion and secondary aerosol making larger contributions during the cold season. Long-term measurements in Warsaw likewise demonstrated pronounced seasonal changes in PM_1 concentration and composition (Majewski et al., 2018). Such evidence is particularly relevant to continental urban areas where residential heating coincides with weak winter dispersion.

A second difficulty is spatial representativeness. Regulatory stations provide high-quality measurements but cannot resolve every neighborhood-scale gradient. Low-cost optical sensors can complement reference networks by increasing spatial density, provided that their limitations are recognized. Plantower sensors have shown good ability to track temporal PM variability, but their response can vary with season, humidity, aerosol type and sensor age (Sayahi et al., 2019). Laboratory and field evaluations have also shown that Plantower performance depends on particle size and relative humidity (Zamora et al., 2019).

[1]Corresponding author: majabrboric@uns.ac.rs; ORCID: 0009-0002-7669-9033
[2]nakomcic@uns.ac.rs; ORCID: 0000-0001-5754-2669
[3]dmitrasinovic@uns.ac.rs; ORCID: 0000-0002-5686-4196
[4]msunjevic@uns.ac.rs; ORCID: 0000-0002-8125-2087
[5]Ritesh.Patro@oulu.fi; ORCID: 0000-0003-0714-6582

Consequently, dense sensor networks are most defensible when used for comparative patterns and screening rather than as substitutes for regulatory measurements.
The present study focuses on a deliberately compact urban-suburban transect rather than the full regional monitoring network. Five locations were selected around Novi Sad to test whether a one-year record is sufficient to resolve seasonal amplification, spatial coherence and local departures within a geographically compact system. The objective was to quantify (i) site-level PM_1 distributions, (ii) heating versus non-heating differences, (iii) inter-site correlation structure and (iv) the extent to which daily PM_1 at the urban site can be reconstructed from simultaneous observations at four surrounding locations. This scope provides a focused assessment of fine-scale dynamics without attempting source apportionment or long-term trend attribution.

MATERIAL AND METHODS

Study area and monitoring design

The study domain comprised Novi Sad (D1) and four surrounding settlements: Sremska Kamenica (D2), Sremski Karlovci (D3), Ledinci (D4) and Beočin (D5). The five sites form a compact urban-suburban system within the wider Novi Sad area and represent different combinations of urban density, traffic, residential heating and local land use. Restricting the analysis to these locations was intentional: the objective was to examine short-range spatial coherence around the urban center rather than to characterize the entire regional network.
PM data were obtained from the Klimerko community monitoring network, which uses Plantower PMS7003 optical particle sensors. The devices report PM_1, $PM_{2.5}$and PM_{10}, but only PM_1 was used here. The measurements were treated as indicative, comparative observations. No claim of regulatory equivalence was made, consistent with published evaluations showing that low-cost optical PM sensors require careful interpretation under varying aerosol and meteorological conditions (Sayahi et al., 2019; Zamora et al., 2019).

Study period, preprocessing and seasonal definition

The analytical window extended from 16 April 2024 through 15 April 2025 and therefore contained one complete non-heating period and one complete heating season. The heating season was defined as 15 October-15 April and the non-heating period as 16 April-14 October. Daily observations were analyzed as provided in the research dataset; missing days were not interpolated. Valid PM_1 coverage was 364 days at D1, 358 at D2, 356 at D3, 327 at D4 and 335 at D5. The shorter record at D5 ended on 21 March 2025 and this limitation was considered when interpreting the seasonal comparison.

Statistical analysis and cross-site model

For each site, the number of valid days, arithmetic mean, median, 95th percentile (P95), maximum and seasonal medians were calculated. Pearson correlation coefficients were computed from pairwise-overlapping daily observations and displayed as a correlation heatmap. Because the distributions were right-skewed and episodic, the median and P95 were emphasized in the descriptive interpretation.
A simple linear regression was used as an exploratory test of network coherence. Daily PM_1 at Novi Sad (D1) was modeled from simultaneous PM_1 observations at D2-D5. Only dates with complete observations at all five sites were used (n = 299). To avoid evaluating the model on the same days used for fitting, the data were ordered chronologically: the first 70% (n = 209) formed the training period and the final 30% (n = 90) formed an independent test period. Performance was summarized by R^2, root mean square error (RMSE) and mean absolute error (MAE). The model was not intended as a forecasting system or source model; it was used only to quantify how much of the urban day-to-day variability was shared with the surrounding network.

RESULTS AND DISCUSSION

Spatial distribution of PM_1

PM_1 concentrations differed across the five sites despite their relatively short geographic separation (Table 1). The annual-window median was highest in Novi Sad (14 μg m^{-3}) and lowest at Sremska Kamenica, Sremski Karlovci, Ledinci and Beočin (8 μg m^{-3} at each site). The contrast became more pronounced toward the upper tail: D1 reached a P95 of 38.8 μg m^{-3}, compared with 29.1-33.0 μg m^{-3} at the surrounding sites. This indicates that the urban location differed not only in central tendency but also in the magnitude of high-concentration days.

Table 1. *Descriptive PM_1 statistics and seasonal medians for the five monitoring sites.*

Site	N	Mean	Median	P95	Max	NH med.	H med.	H/NH
D1	364	16.9	14.0	38.8	57	10.0	22.0	2.20
D2	358	11.2	8.0	29.1	53	6.0	14.0	2.33
D3	356	11.8	9.0	33.0	45	5.0	16.0	3.20
D4	327	11.9	9.0	32.0	54	5.0	15.0	3.00
D5	335	12.0	9.0	29.3	62	6.0	16.0	2.67

Concentrations in μg m^{-3}; NH = non-heating period; H = heating season.

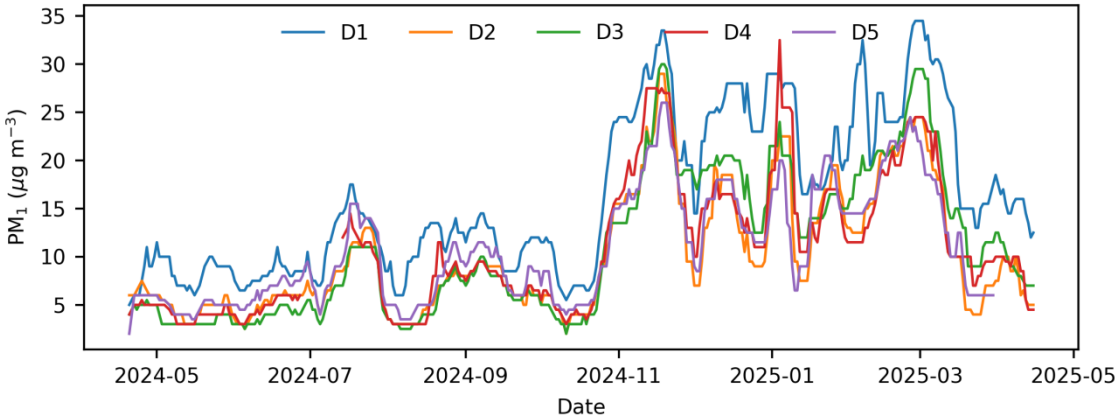


Fig. 1. *Fourteen-day rolling median PM_1 concentrations at the five monitoring sites during the study period. Gaps represent missing observations.*

The temporal profiles in Figure 1 show a common seasonal envelope, with lower concentrations during the warm period and repeated increases during winter. The broad synchrony is consistent with the role of regional meteorology in controlling dispersion and accumulation. At the same time, the amplitude of individual episodes was not identical among sites, indicating that common atmospheric forcing was superimposed on local differences in emission intensity and site surroundings. Comparable cold-season enhancement has been reported in Central European PM_1 studies; Samek et al. (2018), for example, observed a winter/summer mean ratio of approximately 2.5 in an urban Polish setting. The magnitude in the present dataset was site-dependent rather than uniform, which is expected where heating structure and local source density vary over short distances.

Inter-site correlation structure

Daily PM_1 concentrations were positively correlated throughout the network (Figure 2). The strongest relationships occurred among several suburban pairs, including D2-D4 (r = 0.90), D2-D5 (r = 0.88) and D3-D4 (r = 0.86). Novi Sad was most strongly associated with Sremski

Karlovci (D1-D3, r = 0.90), whereas its correlation with Beočin was lower (D1-D5, r = 0.66). The generally high correlations indicate that major concentration changes were not purely local events. Rather, the five sites responded to a shared regional component, while the variation in r values indicates differing local modulation.

This interpretation is compatible with the behavior expected in compact urban sensor networks: common meteorological conditions can synchronize temporal variability, whereas traffic, domestic heating and other local sources modify concentration amplitude. Dense low-cost networks are particularly useful for resolving this combination of regional coherence and local heterogeneity, although sensor-specific uncertainty remains important (Sayahi et al., 2019).

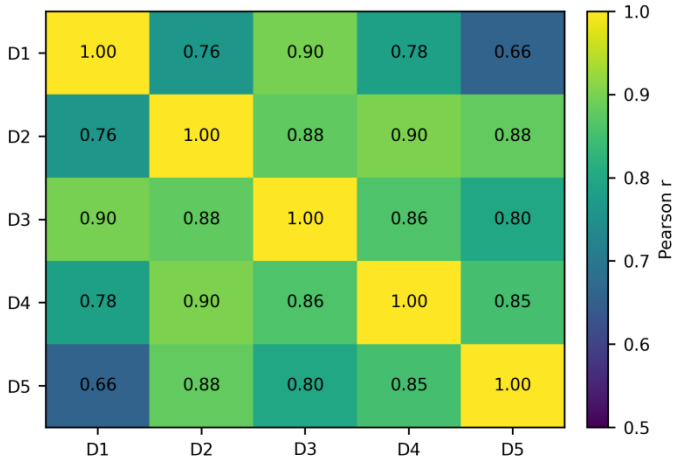


Fig. 2. *Pearson correlation matrix for daily PM_1 concentrations. Coefficients are based on pairwise-overlapping observations.*

Heating-season amplification

All five locations showed higher median PM_1 during the heating season (Figure 3). The heating/non-heating median ratios were D1: 2.20, D2: 2.33, D3: 3.20, D4: 3.00, D5: 2.67. The strongest relative amplification occurred at Sremski Karlovci, while Novi Sad retained the highest absolute heating-season median (22.0 μg m^{-3}). These results support a spatially widespread cold-season effect rather than an isolated urban-core phenomenon.

The seasonal contrast should not be attributed to residential heating alone. Heating activity increases during the same period in which lower mixing heights, calm conditions and temperature inversions favor particle accumulation; secondary aerosol formation and regional transport can also contribute. The Central European source-apportionment study of Samek et al. (2018) similarly found that both combustion and secondary aerosol contributions to PM_1 increased in winter. The present analysis does not contain chemical tracers and therefore identifies seasonal amplification rather than its causal partitioning.

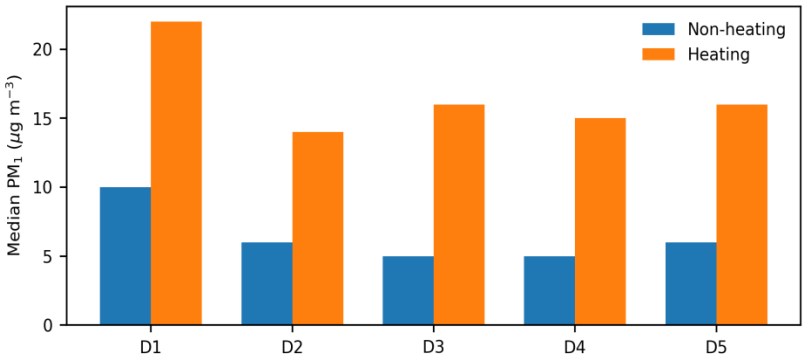


Fig. 3. *Median PM_1 concentrations during the non-heating and heating periods at the five sites.*

Cross-site reconstruction of urban PM_1

The exploratory cross-site model reproduced a substantial part of the day-to-day PM_1 variability at Novi Sad. On the independent final 30% of the complete-case record, the model achieved $R^2 = 0.72$, RMSE = 6.4 μg m^{-3} and MAE = 4.7 μg m^{-3} (Figure 4). This level of performance is notable because the model used no meteorological variables and no measurements from the target site as predictors. It therefore provides an additional quantitative indication that much of the temporal signal was shared across the compact monitoring domain.
The model should not be interpreted as a calibrated prediction tool. Its coefficients are conditional on one year, one sensor network and the selected locations; multicollinearity among the surrounding sites also limits physical interpretation of individual regression coefficients. A stronger predictive framework would require meteorological covariates, longer temporal validation and explicit sensor calibration. Here, the regression serves a narrower purpose: it demonstrates that the urban signal contains a strong network-wide component while leaving a residual fraction attributable to local processes, measurement uncertainty and unmodeled atmospheric effects.

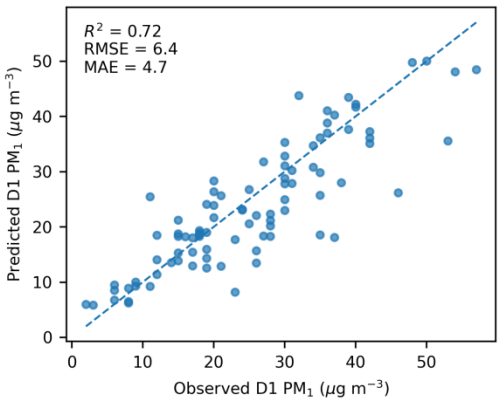


Figure 4. *Observed and regression-predicted daily PM_1 at Novi Sad (D1) for the chronologically independent test period.*

Limitations and implications

Three limitations are particularly relevant. First, optical low-cost sensors can be affected by humidity, aerosol composition and sensor aging. Sayahi et al. (2019) documented seasonal differences and drift in Plantower sensors, while Zamora et al. (2019) found particle-size- and humidity-dependent accuracy. Second, the five records were not perfectly complete, especially at Ledinci and Beočin, although no gap filling was used. Third, the study did not include chemical composition or source tracers and therefore cannot distinguish residential combustion from traffic, secondary aerosol or transported pollution. These limitations argue for conservative interpretation of absolute concentrations, but they do not negate the value of the network for comparing observed temporal and spatial patterns.
From a monitoring perspective, the five-site design appears sufficient to demonstrate fine-scale structure around Novi Sad without extending the analysis to the full regional network. This is important methodologically: a compact network can identify shared pollution episodes, quantify urban-suburban contrasts and flag locations or periods that warrant more intensive reference-grade measurements. The present results therefore support a tiered monitoring strategy in which dense indicative sensing is used for spatial screening and targeted deployment, while regulatory and source-specific conclusions remain anchored to reference instrumentation and dedicated chemical analyses.

CONCLUSION

One complete heating/non-heating cycle across Novi Sad and four nearby settlements revealed a coherent but spatially non-uniform PM_1 field. Median concentrations were highest at the urban site, all locations showed cold-season amplification, and daily concentrations were strongly correlated across the network. The correlation structure and the cross-site regression both indicate a substantial shared regional component, whereas differences in episode magnitude and weaker correlations for selected pairs point to local modulation. A five-site urban-suburban design therefore provides sufficient spatial resolution for a focused conference-level assessment while avoiding unnecessary use of the broader multi-year regional dataset. The results should be interpreted as comparative and indicative because the measurements originate from low-cost optical sensors and no source-apportionment data were available.

ACKNOWLEDGEMENTS

This research has been supported by the Ministry of Science, Technological Development and Innovation (No. 451-03-33/2026-03/200156), the Faculty of Technical Sciences (No. 115001-3394/1), HORIZON-MSCA-2021-SE-01, REMARKABLE (No. 101086387), and by the Autonomous Province of Vojvodina (No. 003870771 2025 09418 003 000 000 001 and 002497912 2026 09418 002 000 000 001 04 006).

REFERENCES

Majewski, G., Rogula-Kozłowska, W., Rozbicka, K., Rogula-Kopiec, P., Mathews, B., & Brandy, A. (2018). Concentration, chemical composition and origin of PM1: Results from the first long-term measurement campaign in Warsaw (Poland). *Aerosol and Air Quality Research*, 18, 636-654. https://doi.org/10.4209/aaqr.2017.06.0221

Morawska, L., Thai, P. K., Liu, X., Asumadu-Sakyi, A., Ayoko, G., Bartonova, A., Bedini, A., Chai, F., Christensen, B., Dunbabin, M., Gao, J., Hagler, G. S. W., Jayaratne, R., Kumar, P., Lau, A. K. H., Louie, P. K. K., Mazaheri, M., Ning, Z., Motta, N., ... Williams, R. (2018). Applications of low-cost sensing technologies for air quality monitoring and exposure assessment: How far have they gone? *Environment International*, 116, 286-299. https://doi.org/10.1016/j.envint.2018.04.018

Samek, L., Stegowski, Z., Styszko, K., Furman, L., & Fiedor, J. (2018). Seasonal contribution of assessed sources to submicron and fine particulate matter in a Central European urban area. *Environmental Pollution*, 241, 406-411. https://doi.org/10.1016/j.envpol.2018.05.082

Sayahi, T., Butterfield, A., & Kelly, K. E. (2019). Long-term field evaluation of the Plantower PMS low-cost particulate matter sensors. *Environmental Pollution*, 245, 932-940. https://doi.org/10.1016/j.envpol.2018.11.065

World Health Organization. (2021). WHO global air quality guidelines: Particulate matter (PM2.5 and PM10), ozone, nitrogen dioxide, sulfur dioxide and carbon monoxide. World Health Organization. https://www.who.int/publications/i/item/9789240034228

Zamora, M. L., Xiong, F., Gentner, D., Kerkez, B., Kohrman-Glaser, J., & Koehler, K. (2019). Field and laboratory evaluations of the low-cost Plantower particulate matter sensor. *Environmental Science & Technology*, 53(2), 838-849. https://doi.org/10.1021/acs.est.8b05174.

DOI:10.5937/IIZS26441D

CLIMATE CHANGE, CAPITALISM, AND THE PHILOSOPHY OF PSYCHOANALYSIS

Review paper

Edi Daruši[1]
[1]Zrenjanin Gymnasium, Zrenjanin, Serbia

Abstract: Capital expands its flow through growth alone: the greater the number of biophysical resources that can be converted into commodities and sold, the greater the profit, and with greater profit even more resources can be acquired — and so the cycle continues. Given that large-scale Capital has extended its market to cosmic proportions, the only avenue remaining for further expansion of production is the artificial multiplication of one-dimensional human desires. The contemporary capitalist cult of consumption, free enjoyment, and the satisfaction of desires does not, therefore, represent a natural expression of desire, but rather a cultural organisation of our *desiring forces*.
Key words*: capitalism, Nature, psychoanalysis, desires, ideology*

INTRODUCTION

"That's not us. We are worse. We are watching a horrible story unfold, much more terrible than Auschwitz, and we must ask ourselves the cashier's question: What did I do? What did I fail to do? Future generations — if there are any — will ask that of us." — Noam Chomsky (Chomsky & Waterston, 2022)
According to French philosopher Félix Guattari, the capitalist system does not merely intervene ruthlessly in Nature and social reality — it also penetrates us at an unconscious level, communicating with the "key components of integrated world capitalism with unprecedented and uncharted invasiveness" (Guattari, 2016). Walter Benjamin likewise draws an analogy between repressed imagination and capital, for which "the hell of the unconscious must pay interest" (Benjamin, 1921).
When we focus on the subjective violence produced by social agents — fanatical crowds and malevolent individuals — we conceal the core of the problem. According to philosopher Slavoj Žižek, at the root of violence one must recognise the metaphysical dance of Capital, which follows the *logic of profit*, its unstoppable circulation that conditions the repressive structure of material social processes, and is entirely indifferent to how its movement will affect reality as a whole. As Žižek writes: "This is the fundamental systemic violence of capitalism, more uncanny than any direct socio-ideological violence… this violence can no longer be attributed to concrete individuals and their "evil" intentions, for it is entirely "objective", systemic, anonymous" (Žižek, 2008). For Walter Benjamin as well, the historical specificity of capitalism lies in its tendency to conquer the world gripped by despair. Building on Marx's analysis of the fetish character of the commodity in *Capital*, Benjamin holds that at the root of capitalism as a religious movement lies the drive toward the *total destruction of everything that exists*. Or, as Benjamin writes in Fragment 74: "The historical specificity of capitalism lies in the fact that religion is no longer the reform of being but rather its complete destruction" (Benjamin, 1921).

MATERIAL AND METHODS

The primary question addressed in this paper is the role and significance of insights from the philosophy of psychoanalysis in confronting the problem of climate change. Resolving this problem demands a fundamental transformation in approaches to ecological policy, together with the mobilisation of anti-capitalist efforts in order to secure a sustainable future. In light of the identified problem, the following research objectives have been formulated:

[1]Corresponding author, edidarusi@gmail.com

- To critically assess the neoliberal capitalist ideological system and its destructive relationship with Nature.
- To expose the methods of affective engineering and the role of unconscious formations in perpetuating capitalism.
- To propose comprehensive strategies and policies aimed at ideological transformation toward sustainable practices, by promoting innovative solutions, swarms of alternative experiences that focus on respect for singularity and autonomous creative subjectivity.

ACCUMULATION OF POWER

"Accumulate, accumulate! That is Moses and the prophets!… Accumulation for the sake of accumulation, production for the sake of production!" — Karl Marx (Marx, 1978)

Recalling Marx's concept of primitive accumulation of capital, Andreas Malm underscores the well-known fact that capital expands its flow through growth alone: the greater the number of biophysical resources that can be converted into commodities and sold, the greater the profit, and with greater profit even more resources can be acquired — and so the cycle continues. Hannah Arendt, in her book *The Origins of Totalitarianism*, refines Marx's insights by arguing that primitive accumulation of capital is a cyclical phenomenon: capital, whenever it encounters a new living space, transforms it into a resource. In *Dialectic of Enlightenment*, Max Horkheimer and Theodor Adorno argue that the Enlightenment — understood in the broadest sense as progressive thinking — has always pursued the goal of freeing human beings from fear and of installing them as masters. Yet the fully enlightened world "beams with triumphant disaster… Human beings pay for the increase of their power with alienation from that over which they exercise their power. The Enlightenment treats things as a dictator treats people. He knows them in so far as he can manipulate them" (Horkheimer & Adorno, 1989). Horkheimer does not, however, claim that greed is innate to the human race; rather, it arises within the ideological matrix of capitalist society: "The greed of men to extend their power into two infinities, the microcosm and the universe, does not proceed immediately from their own nature but from the structure of society… the totalitarian attack of the human race on everything it excludes from itself arises more from inter-human relations than from innate human qualities" (Horkheimer & Adorno, 1989).

Through the growth of technological power to transform the Nature around us, we have in fact arrived at the "point of destabilising the basic geological foundations of life" (Žižek, 2019).

AFFECTIVE ENGINEERING OF CAPITALISM

"Ask yourself, what do we want most of all in this country? People want to be happy, don't they? Isn't that why we keep them moving? So they're always happy to see a new diversion come along? We have our finger in the dike. Hold it! Don't let the torrent of melancholy and drear philosophy drown our world." — Ray Bradbury, *Fahrenheit 451* (Bradbury, 2015)
"The superego is the imperative of jouissance — Enjoy!" — Jacques Lacan (Lacan, 1998)
The totality of repressive capitalist society, despite its enormous wealth, is expressed in the *surplus-repression* of drives that are socially conditioned and, as such, historically unjustified and unnecessary. Herbert Marcuse identifies the primary reason why regressive surplus-repression of drives is enforced in contemporary society as the performance principle upon which capitalist reality rests — the imperative of efficiency and uncompromising profit. Given that large-scale Capital has extended its market to cosmic proportions, the only remaining avenue for further expansion of production is the artificial multiplication of one-dimensional human desires. As Yanis Varoufakis writes: "Capitalism has now skillfully produced desires as well" (Varoufakis, 2015). The individual thus becomes easy prey for media manipulation — a mere medium for implanting stereotypical "material and cultural needs that perpetuate

obsolete forms of the struggle for existence" (Marcuse, 1968). In this context, what is at work is a directed mechanism for managing the drive-structure of contemporary human beings; "marketing is now an instrument of social control", argues Gilles Deleuze (Deleuze, 2010). Thus, despite the apparent liberalisation of human desires and pleasures, what is actually taking place is a mass-media enslavement of intimate life. Edward Bernays writes that human desires are the steam that drives the social machinery: "Only by understanding the true desires of the public can the propagandist control that vast, loose-jointed mechanism which is modern society" (Bernays, 2019).

The contemporary capitalist cult of consumption, free enjoyment, and the satisfaction of desires does not, therefore, represent a natural expression of desire, but rather a cultural organisation of our *desiring forces*, which in turn bind us to our most reactive tendencies, **since the dynamic foundation of capitalism is: affective enslavement**. In the contemporary postmodern world, the imperative that governs our daily lives is "Enjoy!" — and in every possible way, writes Žižek: "from intense sexual pleasures to success in society to spiritual self-fulfilment" (Žižek, 2011). In other words, the superego has now been harnessed by hyper-commercialised capitalist machinery, compelling us to enjoy. As Lacan argues: "The superego is the imperative of *jouissance* — Enjoy" (Lacan, 1998).

LIBIDINAL DESIRING MACHINES

"The unconscious functions like a factory, not a theatre." — Gilles Deleuze and Félix Guattari, *Anti-Oedipus: Capitalism and Schizophrenia* (Deleuze & Guattari, 1995)

Re-examining Wilhelm Reich's dualistic position — libidinal economy versus political economy — Gilles Deleuze and Félix Guattari reject interiorised sexual repressions and, through a structural revision of Freud's concept of the unconscious while following Marx's thought, offer the concept of the **libidinal desiring machine that operates on the basis of alignment with capitalist machines**.

Although Michel Foucault maintains that psychoanalysis remains deaf to the voice of unreason, Deleuze and Guattari acknowledge that psychoanalysis has "discovered" desires — the desiring machines that the unconscious creates and that whirr, grind, and flutter in the depths of the unconscious.

These authors have allowed us finally to grasp the ever-present social engineering and, seemingly paradoxically, the artificial nature of desires. The unconscious is the space of eruptive expansion of *'desiring machines'*; that is, the unconscious is an unbounded production of desires: "*if desire produces, its product is real*" — reality is the reality of the object produced by desire (Deleuze & Guattari, 1995). Desire is thus created unconsciously and freely conquers social and political space. **As producer, desire can only produce reality.** For Deleuze and Guattari, social assemblages — such as capitalist ones — are an act of desire from the depths of the unconscious. Desiring machines operate within the microphysics of the unconscious, which now belongs to, or rather constitutes the foundation of, the infrastructure of society.

Desire, as the internal principle of the capitalist system, is discovered by Deleuze at the very foundation of capitalist production (Deleuze & Parnet, 2009). In their nature, desires rely on needs, and capitalism both supports and satisfies desires but also produces them. Capitalism is repressive precisely in the sense that it uncontrollably imposes and accumulates desires.

According to Deleuze and Guattari, capitalist reality is incorporated into the drive-structure of the contemporary human being. The founders of schizoanalysis interpret Capital as the body-without-organs of the capitalist, which appropriates individual desiring machines for its own ends (Deleuze, 2010) and triggers the existence of desire (Deleuze & Parnet, 2009). The production of desire is the defining concept of capitalism, for capitalist society creates desires oriented toward the growth of capital. ***Capitalism is not outside us — we are capitalism!***

RESULTS AND DISCUSSION

Despite the urgent need for immediate measures regarding climate change, alternative ideologies remain largely marginalised in the absence of a globally coordinated strategy. Equally absent is a genealogy of repressive social mechanisms that would allow us to confront the damage inflicted by capitalism.

Th philosophy of psychoanalysis — from Freud and Reich through Marcuse, Deleuze, and Guattari — reveals that capitalist ideology does not merely constrain consciousness from without but is embedded within the very drive-structure of the individual. This insight is crucial for any ecological politics that aspires to be more than technocratic management: it demands that we confront not only structural contradictions of the capitalist economy but also the unconscious formations that reproduce our complicity in the commodification of Nature.

The manufactured desires analysed above are not peripheral to the ecological crisis — they are constitutive of it. Affective engineering sustains overconsumption; superego imperatives of enjoyment undermine restraint; the libidinal alignment of desiring machines with capitalist assemblages makes ecological subjectivities appear alien or ascetic. Any viable ecological strategy must therefore operate simultaneously at the level of policy and at the level of desire.

CONCLUSION

"…political failure must never be explained by the strength of the adversary, but always by the weakness of our own project… weakness is always, when all is said and done — a weakness of thought." — Alain Badiou (Badiou, 2019)

Karl Marx and, after him, Wilhelm Reich, Erich Fromm, and other thinkers revealed that the social field of human freedom, the mechanism of the unconscious, and the entire character-structure of individuals and masses are all subject to the repressive commodification that lies at the core of the logic of Capital. Capitalism shapes the drive-structure which then, in a feedback loop, services the capitalist machinery.

Hence Branko Milanović can conclude that the extraordinary success of capitalism lies precisely in having successfully implanted its own goals within every individual. By leading global humanity to accept capitalism's goals as its own, dominant social values have been aligned with its economic and political objectives. Global humanity willingly participates in the commodification of Nature, thanks precisely to the process of socialisation in capitalist societies, which transforms people into capitalist calculating machines "endowed with limitless needs". Milanović writes in this vein that the capitalist mode of production is no longer even necessary for us to live in capitalism, for each of us has become "a small centre of capitalist production" (Milanović, 2021). The extension of commodification to the private sphere is a process in which people participate by their own free will.

Althusser pointed out that capitalist ideology is not a symbolic matrix imposed on reality from outside, but rather our interpretation of reality. The reproduction of contemporary capitalist society in its totality — and the reproduction of the conditions of production — encompasses, according to Althusser, the educational system, culture, science, and a consumerist mentality (Althusser, 2009). State mechanisms are at the very foundation of the reproduction of capital, securing through educational, ecological, social, economic, legal, and other mechanisms its unimpeded accumulation by dispossession; hence resistance to global neoliberal capitalism cannot occur from within the existing late-capitalist consumer culture.

A massive reconstruction of social mechanisms is therefore necessary if we are to confront the damage inflicted by capitalism. According to Guattari, reforms will not come "from the top" through laws and decrees or bureaucratic programmes, but through the promotion of innovative practices, swarms of alternative experiences focused on respect for singularity and autonomous creative subjectivity that connects appropriately with the rest of society (Guattari, 2021). Žižek likewise agrees that cooperation between different human communities is necessary, even as it becomes increasingly difficult in the face of rising

"sectarian, religious, and ethnic violence and the willingness to sacrifice even the world for one's particular goal" (Žižek, 2019).
Marx had that image of the old mole burrowing just beneath the surface — the image of a revolutionary spirit that says: I actually do **not want** this. And not much is needed for that current to break the surface when the right situation arrives, through globally networked anti-capitalist ecological activism and engagement — and then those changes come that move society forward. As Félix Guattari reminds us: "there can be no revolution… until desire itself takes on a revolutionary orientation that actively brings unconscious formations into play" (Deleuze & Guattari, 1972). The desire for revolutionary change, as an incorporated **power of desire**, can transcend the manufactured desires of capitalism and restore to people their lives — lives held captive by the capitalist formations of power.
But the question is, of course, what do we **want**?!

REFERENCES

Althusser, L. (2009). *Ideology and ideological state apparatuses*. Karpos.

Badiou, A. (2019). *A pocket panopticon*. Karpos.

Benjamin, W. (1921). *Capitalism as religion*. Retrieved March 2, 2026, from https://anarhisticka-biblioteka.net/library/walter-benjamin-kapitalizam-kao-religija

Bernays, E. (2019). *Propaganda*. Ammonite.

Bradbury, R. (2015). *Fahrenheit 451*. Laguna.

Chomsky, N., & Waterston, M. (2022). *The consequences of capitalism*. Akademska knjiga.

Deleuze, G. (2010). *Negotiations*. Karpos.

Deleuze, G., & Guattari, F. (1972). On Anti-Oedipus. Retrieved February 2, 2026, from http://www.womenngo.org.rs/sajt/sajt/izdanja/zenske_studije/zs_s4/aedip.html

Deleuze, G., & Guattari, F. (1995). *What is philosophy?*. Izdavačka knjižarnica Zorana Stojanovića.

Deleuze, G., & Guattari, F. (2010). *Anti-Oedipus: Capitalism and schizophrenia*. University of Minnesota Press.

Deleuze, G., & Parnet, C. (2009). *Dialogues*. Fedon.

Deleuze, G. (2010). Societies of control. Retrieved April 2, 2025, from https://pescanik.net/drustva-kontrole/

Guattari, F. (2016). Integrated world capitalism and molecular revolution. Retrieved March 2, 2026, from https://atkingsmith.com/wp-content/uploads/2016/10/integrated-world-capitalism-and-molecular-revolution.pdf

Guattari, F. (2021). *The three ecologies*. FMK.

Horkheimer, M., & Adorno, T. W. (1989). *Dialectic of enlightenment*. Logos.

Lacan, J. (1998). *On feminine sexuality: The limits of love and knowledge (The Seminar, Book XX)*. Norton.

Marcuse, H. (1968). *One-dimensional man*. Logos.

Marx, K. (1978). *Capital. In K. Marx & F. Engels, Works*, Vol. 21. Prosveta.

Milanović, B. (2021). *Capitalism alone*. Akademska knjiga.

Varoufakis, Y. (2015). *Technofeudalism*. Publikpraktikum.

Žižek, S. (2008). *Violence*. Ljevak.

Žižek, S. (2011). *In defence of lost causes*. Akademska knjiga.

Žižek, S. (2019). *Like a thief in broad daylight*. Laguna.

DOI:10.5937/IIZS26447D

ASSESSMENT OF THE POSSIBILITIES OF ARTIFICIAL INTELLIGENCE FOR AGROCHEMICAL SOIL ANALYSIS WITH FERTILIZATION RECOMMENDATIONS

Research paper

Milana Drašković[1*], Željko Eremić[2]
[1,2]Technical College of Applied Sciences, Zrenjanin, Serbia

Abstract: Various artificial intelligence models exist today. This paper examines the capabilities these models offer in the field of agrochemical soil analysis and fertilizer recommendations. We leveraged internet technologies to evaluate the potential of several artificial intelligence models within agricultural technology. The outputs obtained were compared against official recommendations. The paper presents a comparison between soil fertilization recommendations based on agrochemical analysis results provided by professional services and those generated by various artificial intelligence models. The results of this comparison and the associated conclusions are presented and subsequently discussed in terms of the reliability of the tested models.
Key words: AI models, Internet technologies, Agrochemical soil analysis, fertilization

INTRODUCTION

Agrochemical soil analysis is a basic prerequisite for successful agricultural production in vegetable, arable and fruit growing (Dinkins & Jones, 2013; Varga, 2015). Every year, plants take out a certain type and amount of nutrients from the soil, which must be returned to the soil by fertilizing (Kızılkay,et al. 2022; Paolo &Rinaldi, 2008).
Agrochemical soil analysis is a key step for achieving high and stable yields in agriculture. It provides a precise insight into the current state of nutrients in the soil.
The main benefits of regular soil testing include:

- **Economic savings:** Fertilizer is introduced specifically and in the correct quantities, which avoids unnecessary expenditure on nutrients that are already in abundance.
- **Environmental protection:** Prevents excessive fertilization that can lead to groundwater pollution and soil structure degradation.
- **Proper plant development:** Plants receive balanced nutrition, which directly affects better fruit quality and greater resistance to diseases and drought.
- **Long-term planning:** The received recommendation for fertilization is valid for the next four years, which enables optimal planning of crop rotation and investments.

Hazelnut plantations in Serbia(Fig.1.) are becoming more and more important, primarily because of the price that hazelnuts have reached on the market. Hazelnuts represent a very important type of stone fruit whose fruits are highly valued on the domestic and world markets.
Good yields of hazelnuts can be expected on soils of medium fertility, light, sandy loam, humus-carbonate and moderately moist. According to the reaction of the soil, hazelnut is tolerant, because it thrives well on soil with a pH value of 5 to 8.
Mineral nutrition of young trees should be in accordance with their development. As the tree grows, so do the fertilizer rates, (Korać M., et al. 2020). If necessary, other corrections are made during this period, such as correction of the pH value, because the hazelnut root absorbs nutrients more easily when the pH is from 6.8 to 7.3.

[1]Corresponding author, milana.draskovic@gmail.com., ORCID: 0009-0002-2085-4356
[2]zeljko.eremic@gmail.com, ORCID: 0009-0003-3310-3081



Fig.1 *Hazelnut plantations*

Different AI models have different capabilities. We have decided on several of the most popular free versions of the model. We asked each of them the same question, gave them the same input data set, and the same desired output format. These results are compared and discussed.This paper examines what recommendations for soil fertilization are provided by the AI models used based on the results of agrochemical analysis of soil under hazelnut plantations.

MATERIAL AND METHODS

Agrochemical soil analysis

Average soil samples, consisting of an appropriate number of individual samples (20-25), were taken from a plot of land with an area of 1.7 ha. The depth from which samples are taken for the purpose of soil fertility control for fruit species is 0-30 cm, and 30-60 cm. The samples were taken using hand-held soil sampling probes. Agrochemical soil analysis was performed in the accredited laboratory of the Agricultural Expert Service (PSS) in Zrenjanin.

AI models

In our research, we used several artificial intelligence models, providing them with the same input data and the same question. The desired response format was also specified within the question. The models are listed:

- GPT, Version GPT-5.6, https://chatgpt.com
- Google Gemini, Version 3, https://gemini.google.com
- Perplexity, N/A, https://www.perplexity.ai
- DeepSeek, DeepSeek-V3, https://chat.deepseek.com
- Meta, Spark 1.1., https://www.meta.ai
- Claude, Claude Sonnet 5, https://claude.ai

The question sent to each of the models is: Based on the results of the agrochemical analysis of the soil in the hazelnut orchard, provide a recommendation regarding fertilization for the next 4 years. The soil analysis results are presented in Tables 1 and 2. The recommendation should be provided in the format of Table 3. Can I send you Tables 1 and 2 in the first image as input data, and then Table 3—which you need to fill out—in the second image?Each of the models then asked to load the first image with tables 1 and 2 (input data), and then the second image with table 3 (desired output format). These images have been loaded successfully in each model.

Our research is a continuation and extension of research (Drašković&Eremić, 2024) where the same input data were used, but the communication channel was textual and only one artificial intelligence model was used.
Results of agrochemical analysis of the soil under hazelnut planting with fertilization recommendation for cadastral plot number 2348, cadastral municipality of Žitište, area of 1.7 ha.The results of testing the agrochemical properties of the soil for the average sample taken at a depth of 0-30 cm are shown in Table 1.

Table 1. *Results of agrochemical soil analysis for an average sample taken from a depth of 0-30cm*

Parameter	Unit	Value	Method
Soil reaction (pH) in 1M KCl		7,70	SRPS ISO 10390:2007
Soil reaction (pH) in water		8,41	SRPS ISO 10390:2007
$CaCO_3$ content	%	9,72	SRPS ISO 10693:2005
Easily accessible phosphorus as P_2O_5	mg/100 gr	67,21	MZ 10 05
Easily accessible potassium as K_2O	mg/100 gr	36,60	MZ 10 06
Humus content	%	2,93	MZ 10 04
Total nitrogen content$_{(calculation)^*}$	%	0,15	

($Note^*$:refers to the requested part of the examination that is not in the scope of accreditation)

The results of testing the agrochemical properties of the soil for the average sample taken at a depth of 30-60 cm are shown in Table 2.

Table 2.*Results of agrochemical soil analysis for an average sample taken from a depth of 30-60cm*

Parameter	Unit	Value	Method
Soil reaction (pH) in 1M KCl		7,91	SRPS ISO 10390:2007
Soil reaction (pH) in water		8,56	SRPS ISO 10390:2007
$CaCO_3$ content	%	12,52	SRPS ISO 10693:2005
Easily accessible phosphorus as P_2O_5	mg/100 gr	48,98	MZ 10 05
Easily accessible potassium as K_2O	mg/100 gr	25,20	MZ 10 06
Humus content	%	1,95	MZ 10 04
Total nitrogen content$_{(calculation)^*}$	%	0,10	

($Note^*$: refers to the requested part of the examination that is not in the scope of accreditation)

The soil contains excessive amounts of phosphorus and optimal amounts of potassium, so it is not recommended to introduce fertilizers containing phosphorus into the soil in the next four years.

Template for the desired response format is shown in Table 3

Table 3. *Template for the desired response format*

Year	Basic fertilization (until December 15)		1. Nitrogen supplementation (in the middle of January)		2.Nitrogen supplementation (in the middle of March)	
	Type of fertilizer	Quantity per hectare	Type of fertilizer	Quantity per hectare	Type of fertilizer	Quantity per hectare

RESULTS AND DISCUSSION

The recommendation for the introduction of nutrients based on the results of the agrochemical properties of the soil under the hazelnut plantation is shown in Table 4.andTables 5-10 show the responses of different artificial intelligence models.

Table 4. *Fertilization recommendation for hazelnut (13 years old)*

Year	Basic fertilization (until December 15)		1. Nitrogen supplementation (in the middle of January)		2.Nitrogen supplementation (in the middle of March)	
	Type of fertilizer	Quantity per hectare	Type of fertilizer	Quantity per hectare	Type of fertilizer	Quantity per hectare
Year 1	SOP-51%+18% potassium sulfate-200kg/ha		UREA 46%	150 kg/ha	AN 33%	150 kg/ha
Year 2	SOP-51%+18% potassium sulfate-200kg/ha		UREA 46%	150 kg/ha	AN 33%	150 kg/ha
Year 3	SOP-51%+18% potassium sulfate-200kg/ha		UREA 46%	150 kg/ha	AN 33%	150 kg/ha
Year 4	SOP-51%+18% potassium sulfate-200kg/ha		UREA 46%	150 kg/ha	AN 33%	150 kg/ha

Table 5. *Model response: GPT*

Year	Basic fertilization (until December 15)		1. Nitrogen supplementation (in the middle of January)		2.Nitrogen supplementation (in the middle of March)	
	Type of fertilizer	Quantity per hectare	Type of fertilizer	Quantity per hectare	Type of fertilizer	Quantity per hectare
Year 1	No mineral fertilizer required	0	CAN (27% N)	185	CAN (27% N)	185
Year 2	No mineral fertilizer required	0	CAN (27% N)	185	CAN (27% N)	185
Year 3	No mineral fertilizer required	0	CAN (27% N)	185	CAN (27% N)	185
Year 4	No mineral fertilizer required	0	CAN (27% N)	185	CAN (27% N)	185

Table 6. *Model response: Google Gemini*

Year	Basic fertilization (until December 15)		1. Nitrogen supplementation (in the middle of January)		2.Nitrogen supplementation (in the middle of March)	
	Type of fertilizer	Quantity per hectare	Type of fertilizer	Quantity per hectare	Type of fertilizer	Quantity per hectare
Year 1	/ (Not required due to extremely high P_2O_2 and K_2O)	0 kg/ha	Ammonium Sulfate (21% N)	150 kg/ha	KAN (27% N)	150 kg/ha
Year 2	/ (Not required)	0 kg/ha	Ammonium Sulfate (21% N)	150 kg/ha	KAN (27% N)	150 kg/ha
Year 3	Organic fertilizer (Manure / Compost)*	15–20 t/ha	Ammonium Sulfate (21% N)	150 kg/ha	KAN (27% N)	150 kg/ha
Year 4	/ (Not required)	0 kg/ha	Ammonium Sulfate (21% N)	150 kg/ha	KAN (27% N)	150 kg/ha

*Note: Applying well-rotted organic manure in Year 3 will help preserve soil structure, lower active pH slightly, and improve micronutrient availability (especially Iron/Zinc) in alkaline soils without over-supplying phosphorus.

Table 7. *Model response: Perplexity*

Year	Basic fertilization (until December 15)		1. Nitrogen supplementation (in the middle of January)		2.Nitrogen supplementation (in the middle of March)	
	Type of fertilizer	Quantity per hectare	Type of fertilizer	Quantity per hectare	Type of fertilizer	Quantity per hectare
1	No phosphorus or potassium fertilizer; optional mature compost/manure	10–15 t/ha*	Ammonium sulfate (21% N)	180 kg/ha	Ammonium sulfate (21% N)	180 kg/ha
2	No phosphorus or potassium fertilizer; optional mature compost/manure	10–15 t/ha*	Ammonium sulfate (21% N)	180 kg/ha	Ammonium sulfate (21% N)	180 kg/ha
3	No phosphorus or potassium fertilizer; optional mature compost/manure	10–15 t/ha*	Ammonium sulfate (21% N)	180 kg/ha	Ammonium sulfate (21% N)	180 kg/ha
4	No phosphorus or potassium fertilizer; optional mature compost/manure	10–15 t/ha*	Ammonium sulfate (21% N)	180 kg/ha	Ammonium sulfate (21% N)	180 kg/ha

*Apply compost or well-rotted manure only if available and if the orchard's organic-matter management requires it; do not treat this as a substitute for a measured mineral-N requirement

Table 8. *Model response: DeepSeek*

Year	Basic fertilization (until December 15)		1. Nitrogen supplementation (in the middle of January)		2.Nitrogen supplementation (in the middle of March)	
	Type of fertilizer	Quantity per hectare	Type of fertilizer	Quantity per hectare	Type of fertilizer	Quantity per hectare
Year 1	Mature compost/manure[1]	20–30 t/ha	KAN (27% N)[2]	150 kg/ha	KAN (27% N)	150 kg/ha
Year 2	Mature compost/manure	20–30 t/ha	KAN (27% N)	150 kg/ha	KAN (27% N)	150 kg/ha
Year 3	Mature compost/manure + K_2SO_4[3]	20–30 t/ha + 100 kg/ha	KAN (27% N)	150 kg/ha	KAN (27% N)	150 kg/ha
Year 4	Mature compost/manure + K_2SO_4	20–30 t/ha + 100 kg/ha	KAN (27% N)	150 kg/ha	KAN (27% N)	150 kg/ha

Table 9. *Model response: Meta*

Year	Basic fertilization (until December 15)		1. Nitrogen supplementation (in the middle of January)		2.Nitrogen supplementation (in the middle of March)	
	Type of fertilizer	**Quantity per hectare**	**Type of fertilizer**	**Quantity per hectare**	**Type of fertilizer**	**Quantity per hectare**
1	Well-rotted cattle manure (no mineral P,K)	20 t/ha	Ammonium sulfate 21% N	250 kg/ha = 52.5 kg N	KAN 27% N	250 kg/ha = 67.5 kg N
2	**SKIP** - No basic (P,K extremely high)	0	Ammonium sulfate 21% N	200 kg/ha = 42 kg N	KAN 27% N	200 kg/ha = 54 kg N
3	Well-rotted cattle manure	20 t/ha	Ammonium sulfate 21% N	250 kg/ha = 52.5 kg N	KAN 27% N	250 kg/ha = 67.5 kg N
4	**SKIP** - Repeat soil analysis	0	Ammonium sulfate 21% N	200 kg/ha = 42 kg N	KAN 27% N	200 kg/ha = 54 kg N

Table 10. *Model* response*: Claude*

Year	Basic fertilization (until December 15)		1. Nitrogen supplementation (in the middle of January)		2.Nitrogen supplementation (in the middle of March)	
	Type of fertilizer	**Quantity per hectare**	**Type of fertilizer**	**Quantity per hectare**	**Type of fertilizer**	**Quantity per hectare**
1	Well-rotted farmyard manure	30 t/ha	Urea (46% N)	90 kg/ha	Urea (46% N)	130 kg/ha
2	Not required (P, K reserves very high)	-	Urea (46% N)	90 kg/ha	Urea (46% N)	130 kg/ha
3	Not required (P, K reserves very high)	-	Urea (46% N)	90 kg/ha	Urea (46% N)	130 kg/ha
4	Well-rotted farmyard manure	30 t/ha	Urea (46% N)	90 kg/ha	Urea (46% N)	130 kg/ha

None of the used artificial intelligence models gave an adequate recommendation for fertilizing a plot of 1.7 ha under hazelnut planting in relation to the agrochemical analysis of the soil. Deviations are significant both in the recommended amount of mineral fertilizers and in the selection of the type of fertilizer.The most similar fertilization recommendations to those obtained from PSS, only for Nitrogen supplementation(in the middle of January)were given by the artificial intelligence model Claude.

CONCLUSION

In our work, we showed one application of the artificial intelligence model in the field of agrochemical soil analysis with fertilization recommendations. Several free versions of artificial intelligence models were used. Models were sent questions, input data, and output format. Later, the results of the model were discussed. The conclusion is that all the used models are not reliable to give recommendations for fertilizing hazelnut plantations, based on the given results of agrochemical soil analysis.
Directions for further research refer to the possibility of using some other models, new versions of existing models when they become available, as well as application in some other areas.

REFERENCES

Dinkins, C.P., & Jones, C.(2013). Interpretation of soil test results for agriculture, Montana State University Extension, Mont Guide, Publication no. MT200702AG.

Korać M., Cerović S., Korać J., Gološin B., Todorović –Ninić J.,(2000). Proizvodnja lešnika, Zbornik naučnih radova Instituta PKB Agroekonomik. Vol. 6, br. 2, str 19-26

Paolo, E.D., Rinaldi, M.(2008).Yield response of corn to irrigation and nitrogen fertilization in a Mediterranean environment, Field Crops Research, Vol.105, 202-210.

Varga, D.(2015). Priručnik za đubrenje ratarskih i povrtarskih kultura, PSS Subotica AD.Kızılkaya, R. Dumbadze, G. Gülser, C. Jgenti, L.(2022) Impact of NPK fertilization on hazelnut yield and soil chemical-microbiological properties of Hazelnut Orchards in Western Georgia, Eurasian Journal of Soil Science, 11(3), 206 – 215.

Drašković, M., & Eremić, Ž. (2024). Testing the capabilites of CHATGPT 4.0 for agrochemical soil analysis with fertilization recommendations. Book of proceedings. Vol 3 / International Multidisciplinary Conference "Challenges of Contemporary Higher Education" - CCHE 2024, Kopaonik January 29th - February 3rd 2024, 487-492.

DOI:10.5937/IIZS26455M

POTENTIALLY TOXIC ELEMENTS IN SOIL NEAR THE ALUMINUM PLANT IN PODGORICA, MONTENEGRO: A SURFACE–DEEP COMPARISON

Research paper

Nada Marković[1], Nebojša M. Ralević[2], Aleksandra Mihailović[3*]
[1]Ministry of Energy and Mining of Montenegro, Podgorica, Montenegro
[2,3]University of Novi Sad, Faculty of Technical Sciences, Novi Sad, Serbia

Abstract: Potentially toxic elements (PTEs) in soils affected by industrial activities may accumulate over time, with their concentrations varying with soil depth. This study assessed concentrations of As, Hg, Cd, Zn, Pb, Cu, Ni, and Cr in soil collected near the Aluminium Plant in Podgorica, Montenegro, at two depth intervals: 0–40 cm and 1–4 m. All analysed elements were more concentrated in the surface soil than in the deep soil sample. The greatest relative differences between the two depth intervals were observed for Zn and Pb, with surface-to-deep concentration ratios of 6.31 and 5.33, respectively. In the surface soil, Cr (112 mg/kg), Ni (125 mg/kg), and Pb (80 mg/kg) exceeded the maximum permitted concentrations prescribed by Montenegrin soil-quality regulations. In comparison, Cr (55 mg/kg) slightly exceeded the permitted value in the deep soil. We compared the results with published data from other industrially affected areas to provide wider context for the measured concentrations. The results show marked differences between surface and deep soil and emphasise the importance of site-specific monitoring to assess soil contamination in industrial areas.
Key words: potentially toxic elements, industrial soil, soil contamination, sampling depth

INTRODUCTION

Potentially toxic elements (PTEs) occur naturally in the environment but may also originate from anthropogenic activities. Their natural concentrations in soil are influenced by the geological origin and mineral composition of the parent material, as well as by weathering and other geochemical processes. Anthropogenic inputs may arise from mining and metallurgical activities, industrial emissions, fossil fuel combustion, traffic, wastewater and sludge, waste disposal, and the application of certain fertilisers and pesticides. Unlike many organic pollutants, PTEs do not degrade and may persist in soil for long periods, while their chemical forms and mobility can change depending on environmental conditions (Alloway, 2013; Kabata-Pendias, 2011).

Areas affected by long-term industrial, mining, and energy-related activities are of particular interest in Montenegro. In such areas, PTE accumulation in soil may reflect the combined influence of industrial inputs, local geological conditions, and soil properties. The vicinity of the Aluminium Plant in Podgorica therefore represents a relevant area for assessing PTE occurrence in soil and differences in their concentrations between surface and deeper soil.

This study aimed to determine the concentrations of selected PTEs (As, Hg, Cd, Zn, Pb, Cu, Ni, and Cr) in soil collected near the Aluminium Plant in Podgorica at two different depths, to compare their concentrations with the maximum permitted values prescribed by Montenegrin regulations, and to place the obtained results in the context of data reported for other industrially affected areas.

MATERIAL AND METHODS

The study was based on laboratory results from composite soil samples collected near the Aluminium Plant in Podgorica, Montenegro. The samples represented two depth intervals: surface soil (0–40 cm) and deep soil (1–4 m). Before analysis, the soil samples were air-dried under laboratory conditions, homogenised, and sieved through a 2 mm sieve. The prepared samples were then subjected to instrumental analysis to determine potentially toxic elements.

[1]nada.markovic.nk@gmail.com, ORCID: 0009-0009-8483-5622
[2]nralevic@uns.ac.rs, ORCID: 0000-0002-3825-9822
[3]Corresponding author, zandra@uns.ac.rs, ORCID: 0000-0002-8965-1226

We determined the concentrations of Pb, Cd, Cr, Ni, Cu, and Zn by inductively coupled plasma mass spectrometry (ICP-MS) using an Agilent 7700X instrument (Agilent Technologies, Santa Clara, CA, USA), according to ISO 17294-2. For analysis, 0.2 g of homogenised soil was digested with a mixture of concentrated $HF/HNO_3/HCl$ (5:5:2) and diluted with deionised water to a final volume of 10 mL before instrumental determination. Arsenic (As) and mercury (Hg) were determined by atomic absorption spectrometry (AAS). The concentrations of all analysed elements were expressed as mg/kg of dry soil. Quality assurance and quality control (QA/QC) included reagent blanks, replicate analyses, and standard reference materials (GBW07403, GBW07407, and GBW07429). Reported recoveries for the analysed elements ranged from 95% to 120%.

RESULTS AND DISCUSSION

Table 1 presents concentrations of the analysed potentially toxic elements in the surface and deep soil. All analysed elements showed higher concentrations in surface soil than in deep soil.

Table 1. *Concentrations of potentially toxic elements in surface and deep soil, maximum permitted concentrations (MPC), and surface-to-deep concentration ratios*

Element	0–40 cm (mg/kg)	1–4 m (mg/kg)	MPC (mg/kg)	Surface/deep ratio
As	13	3	20	4.33
Hg	0.040	0.019	1.5	2.11
Cd	1.1	0.48	2	2.29
Zn	202	32	300	6.31
Pb	80	15	50	5.33
Cu	83	22	100	3.77
Ni	125	34	50	3.68
Cr	112	55	50	2.04

Comparison with the maximum permitted concentrations (MPC) prescribed by Montenegrin soil-quality regulations (Rulebook, 1997) showed that Cr, Ni, and Pb exceeded the corresponding limits in the surface soil. The concentrations of Cr and Ni were approximately 2.2 and 2.5 times higher than their respective MPC values, while Pb exceeded the limit by approximately 60%. In the deep soil, most analysed elements were below the prescribed limits, except Cr (55 mg/kg), which slightly exceeded the MPC of 50 mg/kg. The concentrations of As, Hg, Cd, Zn, and Cu remained below the corresponding MPC values at both investigated depth intervals.

We further evaluated differences between the two depth intervals using surface-to-deep concentration ratios (Table 1). The most pronounced differences were observed for Zn and Pb, with concentrations in the surface soil approximately 6.3 and 5.3 times higher, respectively, than those in the deep soil. As, Cu, and Ni also showed marked surface enrichment, with concentration ratios ranging from 3.68 to 4.33. The smallest differences were observed for Cr and Hg, with ratios of approximately 2.0 and 2.1, respectively. These results indicate higher concentrations of all analysed elements in the surface soil. However, because the two broad and non-contiguous sampling intervals are separated, these differences should not be interpreted as direct evidence of metal migration through the soil profile.

We compared the surface-soil concentrations descriptively with values reported for selected urban and industrially affected soils (Table 2). Considerable variability among published data is expected due to differences in industrial activities, local geological and soil conditions, sampling depths, and analytical approaches. Therefore, we used the literature data primarily to provide general context for the measured concentrations rather than for direct statistical comparison.

Table 2. *Comparison of PTE concentrations (mg/kg) in the present study with values reported for selected urban and industrially affected soils*

R*	SA**	Sampling depth (cm)	As	Cd	Cr	Cu	Ni	Pb	Zn	Hg
R1	*SA1*	0-40	13	1.1	112	83	125	80	202	0.04
R2	SA2	Surface soil	-	2.8	-	52.9	-	85.91	112.5	-
R3	SA3	Surface soil	20.49	0.44	40	46.98	33.65	43.85	119.8	0.12
R4	SA4	0-20	-	5.93	-	60.2	71.4	41.31	115.8	-
R5	SA5	0-15	18.6	13.2	545.8	334.6	30.9	571.3	908.6	10.4

R* (Reference)	SA** Study area / industrial activity
R1 Present study	SA1 Podgorica, Montenegro / aluminum industry
R2 (Mugoša et al., 2015)	SA2 Podgorica, Montenegro / urban soil
R3 (Su et al., 2022)	SA3 South China / intensive industrial area
R4 (Zhang et al., 2024)	SA4 Henan, China / area downstream of battery industry
R5 (Kodom et al., 2012)	SA5 Kumasi, Ghana / industrial cluster

The comparison with published data shows a wide range of PTE concentrations among the selected study areas. Overall, the values obtained in the present study fall within the broad ranges reported in the literature. Some highly industrialised sites, such as the industrial area in Kumasi, reported higher concentrations of several elements, particularly Cd, Pb, Zn, and Cu. In contrast, concentrations reported for some other study areas were lower or comparable to those measured in the surface soil near the Aluminium Plant in Podgorica. These differences emphasise the importance of considering specific industrial activity, sampling depth, and local soil and geological characteristics when comparing PTE concentrations across study areas.

The observed surface enrichment of PTEs may reflect long-term external inputs, including atmospheric deposition from industrial and other anthropogenic activities. However, soil properties such as pH, organic matter content, particle-size distribution, mineralogical composition, and the presence of Fe and Mn oxides also strongly influence element distribution, affecting metal retention and mobility (Alloway, 2013; Kabata-Pendias, 2011).

We did not determine soil properties in the present study; therefore, we cannot directly identify the processes responsible for the observed differences between the surface and deep soil. Furthermore, using two broad, non-contiguous depth intervals does not allow a detailed assessment of the vertical distribution or migration of PTEs through the soil profile. Distinguishing between geogenic and anthropogenic contributions would require additional information on local geological and geochemical background, soil physicochemical properties, and potential emission sources. Nevertheless, the consistently higher concentrations observed in the surface soil, together with the exceedances of the Montenegrin MPC values for Cr, Ni, and Pb, indicate that further site-specific investigation

and monitoring would be useful for a more comprehensive assessment of soil contamination in the area.

CONCLUSION

The results showed consistently higher concentrations of all analysed potentially toxic elements in the surface soil (0–40 cm) than in the deep soil (1–4 m) near the Aluminum Plant in Podgorica. The largest surface-to-deep concentration ratios were observed for Zn and Pb. In the surface soil, Cr, Ni, and Pb exceeded the maximum permitted concentrations prescribed by Montenegrin soil-quality regulations, while Cr marginally exceeded the permitted value in the deep soil. The measured concentrations generally fell within the broad ranges reported for selected industrially affected soils. However, differences in industrial activities, sampling depths, and local soil and geologic conditions limit direct comparisons across study areas. The observed surface enrichment alone cannot establish the origin or migration pathways of the analysed elements. Further site-specific investigations, including additional sampling depths and relevant soil physicochemical properties, would allow a more thorough assessment of PTE distribution and possible contamination in the investigated area.

ACKNOWLEDGEMENT

This research has been supported by the Ministry of Science, Technological Development and Innovation (Contract No. 451-03-34/2026-03/200156) and the Faculty of Technical Sciences, University of Novi Sad through the project "Scientific and Artistic Research Work of Researchers in Teaching and Associate Positions at the Faculty of Technical Sciences, University of Novi Sad" (No. 01-3609/1).

REFERENCES

Alloway, B. J. (Ed.). (2013). Heavy metals in soils: Trace metals and metalloids in soils and their bioavailability (3rd ed.). Springer. https://doi.org/10.1007/978-94-007-4470-7

Kabata-Pendias, A. (2011). Trace elements in soils and plants (4th ed.). CRC Press.

Kodom, K., Preko, K., & Boamah, D. (2012). X-ray fluorescence (XRF) analysis of soil heavy metal pollution from an industrial area in Kumasi, Ghana. *Soil and Sediment Contamination*, 21(8), 1006–1021. https://doi.org/10.1080/15320383.2012.712073

Mugoša, B., Đurović, D., Pirnat, S., Bulat, P., & Barjaktarović-Labović, S. (2015). Children's health risk assessment based on the content of toxic metals Pb, Cd, Cu and Zn in urban soil samples of Podgorica, Montenegro. *Vojnosanitetski pregled*, 72(9), 807–812. https://doi.org/10.2298/VSP130716062M

Su, C., Meng, J., Zhou, Y., Bi, R., Chen, Z., Diao, J., Huang, Z., Kan, Z., & Wang, T. (2022). Heavy metals in soils from intense industrial areas in South China: Spatial distribution, source apportionment, and risk assessment. *Frontiers in Environmental Science*, 10, 820536. https://doi.org/10.3389/fenvs.2022.820536

Zhang, J., Jiao, Q., Wu, Y., Liu, H., Yu, P., Liu, D., Hua, D., & Song, J. (2024). Evaluation of heavy metal contamination and associated human health risk in soils around a battery industrial zone in Henan Province, Central China. *Agriculture*, 14(6), 804. https://doi.org/10.3390/agriculture14060804

Rulebook (1997, Rulebook on permitted amounts of dangerous and harmful substances in soil and methods for their examination. *Official Gazette of the Republic of Montenegro*, No. 18/97.

DOI:10.5937/IIZS26459D

FUZZY SYSTEM FOR EVALUATING WATER QUALITY IN AN AQUAPONIC SYSTEM

Research paper

Alexuță Daniel[1*], Alexuță Ilie[2], Balaș M. Marius[3],
[1,2,3] Aurel Vlaicu University of Arad, Faculty of Engineering, Arad, Romania

Abstract (10 pt): The paper presents the implementation of a fuzzy logic-based system in the MATLAB environment, designed to evaluate environmental conditions in a fish tank and assess water quality. The system uses three main water parameters: temperature, pH, and dissolved oxygen concentration. For each parameter, membership functions are defined using three linguistic terms: Low, Optimal, and High. Based on these input variables, a fuzzy rule base is developed to evaluate the general state of the aquatic environment and provide an output value representing the suitability of the water quality conditions. The model is implemented and tested in MATLAB using fuzzy logic tools, and the obtained results allow the analysis of system behavior as the input parameters vary. The proposed approach provides a simple and flexible method for integrating multiple environmental parameters into a single assessment system.a
Key words: fuzzy logic, aquaponics, water quality, aquaculture, MATLAB.

INTRODUCTION

Fish farming in controlled systems involves monitoring the physicochemical parameters of the water. Their variations can influence the development and condition of aquatic organisms. In the case of carp, water temperature, pH and dissolved oxygen concentration are important parameters for evaluating the rearing conditions.
Fuzzy logic is suitable for evaluating such systems, as it allows the use of intermediate values and linguistic terms such as "low", "optimal" and "high". In contrast to methods based on fixed thresholds, it allows for a gradual transition between different states and the simultaneous integration of several parameters.
A fuzzy system is proposed to evaluate the environmental conditions necessary for carp farming. The model uses temperature, pH and dissolved oxygen as input variables, and the result is expressed as a level of adequacy of environmental conditions. The system is implemented and simulated in MATLAB, using membership functions and "If–Then" rules.

MATERIAL AND METHODS

Implementing and Simulating the Fuzzy System in MATLAB

For the evaluation of water quality in the aquaponic system, a system based on fuzzy logic was developed, implemented and tested in the MATLAB environment. The use of fuzzy logic is suitable for the analysis of systems in which the input parameters show continuous variations and in which the boundaries between the different states of the system cannot always be defined by fixed thresholds.
By using membership functions, the numerical values of the parameters can be represented by linguistic terms and subsequently combined by means of fuzzy rules (Rad et al., 2022).
In aquaculture systems, water quality is influenced by several physicochemical parameters, including temperature, dissolved oxygen, pH, ammonia, nitrates, and salinity. Monitoring these parameters is important because variations in environmental conditions can influence the health of aquatic organisms, feeding efficiency, growth rate, and system productivity (Abul Kashem et al., 2026).
Within the model proposed in this paper, three input parameters considered representative for evaluating the environmental conditions in the basin were selected: water temperature, pH and dissolved oxygen (DO). The reduction in the number of variables allows obtaining a fuzzy

[1]Corresponding author, alexutadaniel@yahoo.com

model that is simpler and easier to interpret, while maintaining the main information necessary for the evaluation of the water status.

Studies dedicated to aquaponic systems highlight the need for automatic monitoring and control of water quality parameters to maintain proper system operating conditions (Mustika et al., 2023).

For each input variable, three membership functions have been defined, corresponding to the linguistic terms 'Low', 'Optimal' and 'High'. The use of linguistic terms allows the numerical values of the parameters to be transformed into information that can be processed by the fuzzy system. In the case of systems based on fuzzy logic, this representation is especially useful when the input information presents uncertainty or imprecision and when it is necessary to construct a relationship between several input variables and an output variable (Rad et al., 2022).

Membership functions were entered into MATLAB for each of the three input variables. For temperature, the range of analysis was set between 0 and 35 °C, for pH between 0 and 14, and for dissolved oxygen between 0 and 15 mg/L. The partial overlap of the membership functions allows a value between two linguistic states to contribute to several fuzzy rules simultaneously, leading to a gradual transition of the system's response.

The structure of the fuzzy system is built on the basis of an "IF–THEN" rule base. The rules establish the relationship between the state of temperature, pH and dissolved oxygen and the resulting level of water quality (Bautista et al., 2022; Gustilo et al., 2014). Such an approach allows the combination of information from several inputs into a single decision.

In fuzzy control applications, the rules and control structure can be adapted to changing operating conditions, and the behavior of the system can be verified by simulation (Popa et al., 2022).

An example of a rule used in the model is: "IF temperature is Optimal AND pH is Optimal AND dissolved oxygen is Optimal THEN water quality is Optimal". Similarly, rules can be defined for situations where one or more parameters are in the low or high range. Thus, the system can provide an overall assessment of water quality based on the combination of the monitored parameters. The fuzzy model is then simulated in MATLAB for different combinations of input parameters.

The simulation allows the observation of the change in the system output when the temperature, pH or concentration of dissolved oxygen are changed. The use of simulation is an important step in verifying the behavior of a fuzzy system before an eventual practical implementation, a method also used in the development of fuzzy control systems for engineering applications (Popa et al., 2022).

The graphical representation of the response surfaces allows the simultaneous influence of two input variables on the output variable to be analyzed. In the case of the proposed system, these representations can highlight how the combination of temperature and dissolved oxygen or that of pH and dissolved oxygen influences the final assessment of water quality. This approach facilitates the interpretation of the model's behavior and the identification of areas where changing parameters causes significant changes in the fuzzy output. In a practical application, the fuzzy system can represent an intermediate step between the acquisition of data from the sensors and the automatic control system.

The measured data in real time can be transmitted to the fuzzy model, and its result can be used to signal an improper condition or to control equipment such as pumps and aeration systems. In intelligent aquaponics systems, automating the control of water parameters can help to manage operating conditions more efficiently (Mustika et al., 2023; You et al., 2021).

The choice of parameters used in the model is also supported by previous studies on aquaponic systems. The analysis of the water parameters in an aquaponic system highlights the importance of monitoring the characteristics of the water for maintaining the proper operating conditions of the system (Alexuță & Bălaș, 2023). In this context, the integration of the monitored parameters into a fuzzy model allows the transition from the simple measurement of the values to an automatic and interpretable assessment of the state of the system.

Therefore, the implementation in MATLAB provides the possibility to experimentally verify the fuzzy system structure, membership functions, and rule base before integration into a real aquaponics system. The model can later be extended by introducing additional parameters, modifying membership functions, or connecting to data from sensors. The use of computational models for water quality analysis and classification is also a current direction in the development of modern aquaculture monitoring systems (Abul Kashem et al., 2026).

Definition of Input and Output Variables

Table 1. *Parameters and linguistic levels of the fuzzy system.*

Parameter (Unit)	Domain	Low(L)	Optimal(O)	High(H)
Water temperature (°C)	0–35	0–22	14–30	22–35
pH	0–14	0–7	5–9	7–14
Dissolved oxygen (mg/L)	0–15	0–5	2–8	5–15
Water Quality (%)	0–100	0–50	25–75	50–100

The fuzzy system uses three input parameters: water temperature, pH, and dissolved oxygen (DO). Each parameter is described by three linguistic levels: Low, Optimal, and High. The output variable, Water Quality, is also divided into three linguistic levels. The parameter ranges were chosen so that the membership functions overlap, with adjacent linguistic sets intersecting at a membership degree of 0.5. This approach ensures a gradual transition between linguistic levels and avoids sudden changes in the fuzzy system's response. The defined ranges were later implemented in MATLAB using triangular and trapezoidal membership functions.

In aquaponic systems, maintaining water parameters at appropriate intervals is an important condition for the proper development of aquatic organisms and plants. pH control can be achieved through systems based on fuzzy logic, which allow control actions to be adapted to continuous variations in environmental parameters. Rahayu et al. (2021) presented a pH control and water recirculation system in an aquaponic system, using a Mamdani-type fuzzy regulator. The results of this type of approach highlight the possibility of using fuzzy logic for the automatic management of water quality parameters in aquaponic systems.

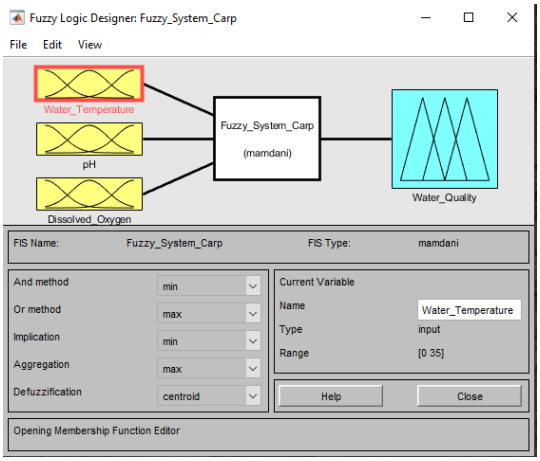


Fig. 1. *Fuzzy System Interface*

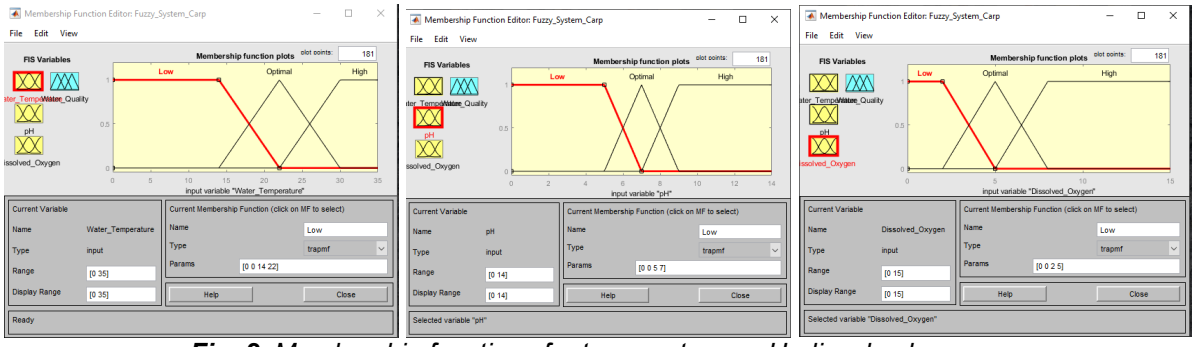


Fig. 2. *Membership functions for temperatures, pH, dissolved oxygen*

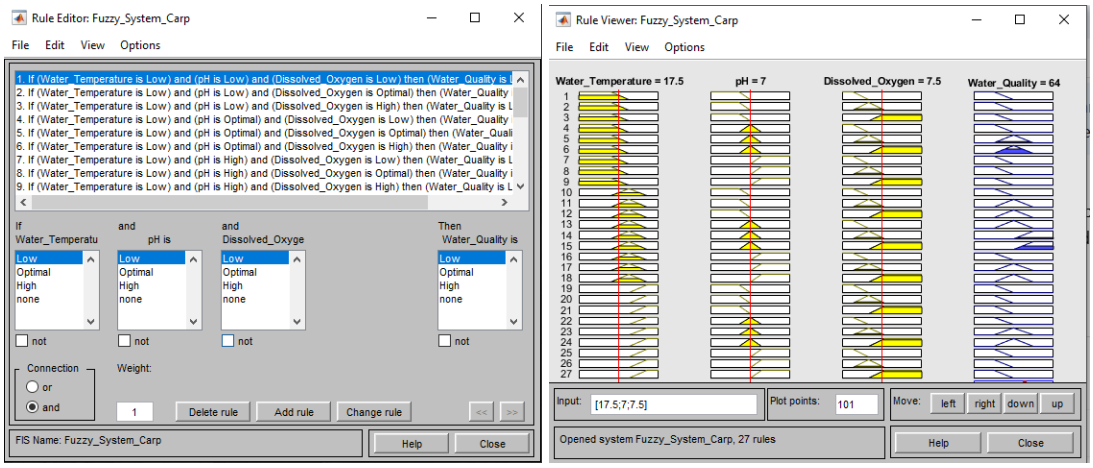


Fig. 3. *Rule base, graphical visualization of the rule base*

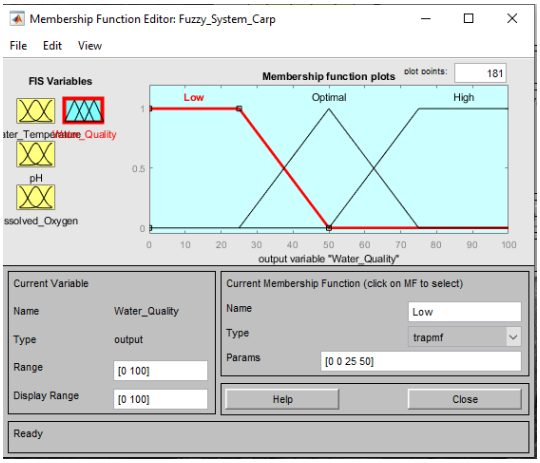


Fig. 4. *Interpretation of water quality in percentages*

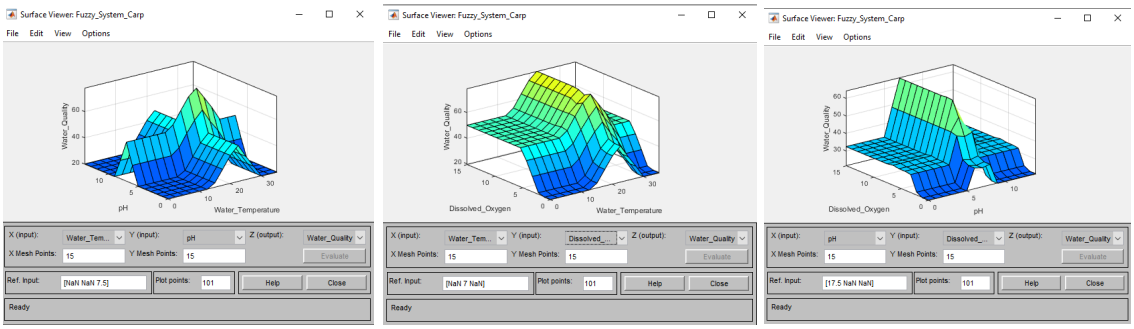


Fig. 5. *Visualization of the control surface according to selected parameters.*

RESULTS AND DISCUSSION

The simulation of the fuzzy system performed in MATLAB demonstrated the possibility of automatic evaluation of the water quality in an aquaponic system based on important physicochemical parameters. The system uses three input variables, namely water temperature, pH and dissolved oxygen concentration, and the result is expressed by the output variable Water Quality, defined on a scale from 0 to 100.

The system was tested using a water temperature of 22 °C, a pH of 7.2, and a dissolved oxygen concentration of 6 mg/L. These values are processed by the membership functions defined for each variable and are then evaluated via the fuzzy rule base. Since the input values can belong to several fuzzy sets simultaneously, the system allows for a gradual interpretation of the water status, as opposed to a strict classification based on fixed limits.

The Water Quality result should be interpreted as a fuzzy index: values close to 0 indicate low water quality, values in the central area indicate an intermediate or optimal state, and values close to 100 indicate high quality according to the rules defined in the model. Thus, the output is not a direct physical measurement, but an estimate obtained by combining the input parameters.

The simulation confirms that the fuzzy system can simultaneously integrate several parameters and transform the numerical information into an easy-to-interpret assessment of the water status. The model can form the basis for the further development of a real-time monitoring system, by connecting temperature, pH and dissolved oxygen sensors to an acquisition and control system.

The proposed fuzzy model can be further extended by integrating sensors for real-time measurement of water parameters and using an IoT-like platform for data transmission and processing. Such a development would allow the transition from simulation performed in MATLAB to a real-time monitoring and control system. Nagothu et al. (2025) presented an approach based on fuzzy logic and IoT technologies for monitoring and maintaining water quality parameters in aquaculture, using parameters such as temperature, pH, and dissolved oxygen, and allowing automatic control of some equipment, such as aerators and pumps. This approach supports the possibility of further developing the proposed model towards a practical automatic monitoring and control application (Nagothu et al., 2025).

CONCLUSION

The present study demonstrated the development and simulation of a fuzzy logic system for evaluating water quality in an aquaponic system intended for carp farming. The proposed model uses three main water quality parameters as inputs: water temperature, pH, and dissolved oxygen concentration. Each input variable was represented by three linguistic levels, namely Low, Optimal, and High, using triangular and trapezoidal membership functions with overlapping regions. The fuzzy inference system was implemented in MATLAB using a Mamdani-type architecture and a rule base designed to combine the three input parameters into a single Water Quality output. The overlapping membership functions, with adjacent sets intersecting at a membership degree of 0.5, provide a gradual transition between different water quality conditions and reduce abrupt changes in the system response.

The simulation demonstrated that the proposed approach can combine several water parameters and provide an easily interpretable assessment of the overall condition of the aquatic environment. The response surfaces generated in MATLAB also allow the influence of different combinations of input parameters on the final output to be analyzed.

The proposed model represents a preliminary computational solution that can be further developed by incorporating additional parameters, such as ammonia, nitrite, turbidity, or salinity, and by connecting the fuzzy system to real-time sensor measurements. In a practical implementation, the resulting assessment could also be used as an input for automatic control of aeration, water circulation, or other equipment. Therefore, the developed fuzzy model

provides a flexible basis for future development of intelligent monitoring and control systems for aquaponic and aquaculture applications.

REFERENCES

Abul Kashem, M., Hasan Shuvo, M., Mustary, S., Mithun Ali, M., Ullah, N., Delwar Hossain, M., ... and Uddin, J. (2026). A Fuzzy-Logic and Machine Learning-Based Framework for Water Quality Index Classification in Extensive and Intensive Aquaculture Systems. Engineering Reports, 8(6), e70839.

Alexuță, D., & Bălaș, M. M. (2023). The Study of Water Parameters in an Aquaponic System. In XIII International Conference – Industrial Engineering and Environmental Protection (IIZS 2023), p. 468.

Bautista, M. G. A. C., Palconit, M. G. B., Rosales, M. A., Concepcion II, R. S., Bandala, A. A., Dadios, E. P., & Duarte, B. (2022). Fuzzy logic-based adaptive aquaculture water monitoring system based on instantaneous limnological parameters. *Journal of Advanced Computational Intelligence and Intelligent Informatics*, *26*(6), 937-943.

Gustilo, R. C., Dadios, E. P., Calilung, E., & Lim, L. A. G. (2014). Neuro-fuzzy control techniques for optimal water quality index in a small scale Tiger prawn aquaculture setup. *Journal of Advanced Computational Intelligence and Intelligent Informatics*, *18*(5), 805-811.

Mustika, I. W., Najib, F., & Yusriadi, Y. (2023, August). Fuzzy Logic-Based Automatic Water Quality Control System in Smart Aquaponics. In 2023 10th International Conference on Information Technology, Computer, and Electrical Engineering (ICITACEE) (pp. 425–430). IEEE.

Nagothu, S. K., Bindu Sri, P., Anitha, G., Vincent, S., & Kumar, O. P. (2025). Advancing aquaculture: fuzzy logic-based water quality monitoring and maintenance system for precision aquaculture. *Aquaculture International*, *33*(1), 32.

Popa, M., Alexuta, D., & Balas, V. E. (2022). Fuzzy-Interpolative Control of Temperatures for the Intelligent Rooftop Greenhouse. Journal of Intelligent & Fuzzy Systems, 43(2), 1793–1797.

Rad, D., Rad, G., Maier, R., Demeter, E., Dicu, A., Popa, M., ... Mărineanu, V. D. (2022). A Fuzzy Logic Modelling Approach on Psychological Data. Journal of Intelligent & Fuzzy Systems, 43(2), 1727–1737.

Rahayu, L. P., Al Kindhi, B., Pradika, C. D., Adhim, F. I., Priananda, C. W., Musthofa, A., ... and Istiqomah, F. (2021, December). Design of pH control system and water recirculation in aquaponic cultivation using Mamdani fuzzy logic control. In 2021 International Conference on Advanced Mechatronics, Intelligent Manufacture and Industrial Automation (ICAMIMIA) (pp. 287-292). IEEE.

You, G., Xu, B., Su, H., Zhang, S., Pan, J., Hou, X., ... and Ding, R. (2021). Evaluation of aquaculture water quality based on improved fuzzy comprehensive evaluation method. *Water*, *13*(8), 1019.



XVI International Conference Industrial Engineering and Environmental Protection 2026 (IIZS 2026)
October 01-02, 2026, Zrenjanin, Serbia

Session 7

Environmental Management

DOI:10.5937/IIZS26466S

IN-CABIN GAS EXPOSURE IN SURFACE MINING: OCCUPATIONAL LIMITS VERSUS OPERATOR PERCEPTION

Research paper

Vesna Spasojević Brkić[1*], Mirjana Misita[2], Ivan Mihajlović[3], Martina Perišić[4], Iva Savić[5]
[1,2,3,4,5]University of Belgrade – Faculty of Mechanical Engineering, Belgrade, Serbia

Abstract: Heavy surface-mining machinery operators are frequently exposed to gaseous pollutants that accumulate inside vehicle cabins. This study investigates in-cabin concentrations of carbon dioxide CO_2, sulphur dioxide SO_2, and nitrogen dioxide NO_2 monitored across 32 machine workplaces at ten surface mines in Serbia and Montenegro, factoring in local atmospheric pressure (856–1020 mbar) as a proxy for site altitude. The instrumentally recorded data were evaluated against mandatory national occupational exposure limits (OELs) and benchmarked against a subjective operator perception survey. Descriptive and non-parametric statistical analyses revealed that while CO_2 levels remained within safe boundaries, SO_2 exceeded the OEL at one workplace (3.1%), and NO_2 breached the threshold at four workplaces (12.5%, reaching up to 144.5% of the limit). Notably, in-cabin gas concentrations showed no significant statistical dependence on machine category, vehicle age, or engine emission stages ($p > 0.05$) while critical NO_2 exceedances occurred even within brand-new Stage V machines. However, a significant negative correlation was discovered between CO_2 levels and atmospheric pressure (Spearman $\rho = -0.547$, $p = 0.001$), indicating higher CO_2 accumulation at lower-pressure, higher-altitude sites due to altered ventilation dynamics. Furthermore, a severe misalignment was identified between empirical measurements and worker awareness: operators reported minimal subjective disturbance, failing to recognize hazardous exposures even when experiencing acute symptoms like coughing or headaches. The findings demonstrate that in-cabin exposure is governed by geographic site elevation and cabin integrity rather than engine emission technology. Consequently, relying on operator perception under-detects real occupational hazards, making continuous instrumental monitoring mandatory for effective health protection.
Key words: *surface mining, cabin air quality, gaseous pollutants, occupational exposure limits, operator perception*

INTRODUCTION

Mining is both an economically significant sector and one of the riskiest, owing to inherent features such as humidity, dust and gaseous-pollutant exposure and the risk of falling rocks and related injuries (Baghaei Naeini & Badri, 2024). Surface mining machinery is designed for 40 to 50 years of operation (Czmochowski & Pietrusiak, 2012), while operating heavy machinery still carries significant risks even under current regulations (Saleh & Cummings, 2011; Spasojević Brkić et al., 2026a).

Mining machinery workplaces are recognised as physically and mentally demanding (Matamala Pizarro & Aguayo Fuenzalida, 2021; Horberry et al., 2016). The operator must be perceptive, precise and continuously focused, while working in conditions with noise, vibration, pollutant gases and air dust, and the risk of explosion, fire and electric shock (Bęś et al., 2025), while the work is also linked to musculoskeletal disorders (Weston et al., 2016; Spasojević Brkić et al., 2024; Perišić et al., 2024). Spasojević Brkić et al. (2023) emphasize that mitigating operational risks in open-pit mining requires a data-driven approach that integrates failure analysis with reliability-based assessments to minimize downtime and optimize maintenance strategies. Korshunov et al. (2025) also add that addressing health hazards in surface mining requires integrated, risk-based frameworks that evaluate occupational exposures directly during the project design phase to proactively mitigate long-term respiratory diseases.

Non-road mobile machinery is one of the main causes of air pollution (Pradhan et al., 2025; Waluś et al., 2018), yet the emission characteristics of these mobile sources have not been fully studied (Li et al., 2023). Recent studies have also employed neural-network models to predict and forecast particulate-matter emissions of loading machinery at mining sites (Janev

[1]* Corresponding author: vspasojevic@mas.bg.ac.rs, ORCID: 0000-0003-4642-3482
[2] mmisita@mas.bg.ac.rs, ORCID: 0000-0002-7039-0783
[3] imihajlovic@mas.bg.ac.rs, ORCID: 0000-0002-9489-8207
[4] mperisic@mas.bg.ac.rs, ORCID: 0000-0002-8385-1593
[5] isavic@mas.bg.ac.rs, ORCID: 0009-0002-9517-7986

et al., 2026). Most studies focus on what machines release into the environment; far less is known about what accumulates inside the operator's cabin, where exposure is continuous throughout an eight-hour shift (Pradhan et al., 2025). Elevated in-cabin CO_2, SO_2 and NO_2 are important indicators of air quality: NO_2 in particular acts as a respiratory-tract irritant and, in enclosed or poorly ventilated spaces such as a cabin, is associated with airway irritation, coughing, chest tightness and shortness of breath (Sharma, 2025; Szczurek et al., 2020). A recent comparison of outside-cabin gaseous pollutants between backhoe and loader excavators found significant differences between machine types and recommended, as future work, a correlation analysis between operators' responses and measured values (Spasojević Brkić et al., 2026b). The present paper takes up that recommendation, shifting the focus to in-cabin exposure, testing whether concentrations depend on machine category, emission stage or age, and confronting the measurements with operators' own perception.

MATERIAL AND METHODS

Measuring instrument and sample

Measurements were carried out at ten surface mines in Serbia and Montenegro on 32 machines operating under real exploitation conditions. In-cabin concentrations of CO_2, SO_2 and NO_2 were recorded with an ALMEMO 2590-2A/4AS multi-channel data-acquisition system fitted with compatible ALMEMO® sensors; the instrument operates in the −10 °C to +50 °C range, stores all readings in internal memory, and was calibrated before measurement in line with the recommended procedure. Atmospheric pressure was logged as an accompanying variable. The investigated sample covers hydraulic excavators, loaders, bulldozers, dumpers and two electrically driven rotor (bucket-wheel) excavators from several manufacturers, with installed power from approximately 120 kW to 630 kW, years of manufacture from 1995 to 2024, and emission stages III to V. These emission stages are defined by the European regulatory framework for non-road mobile machinery (Directive 97/68/EC – Measures against the emission of gaseous and particulate pollutants from internal combustion engines to be installed in non-road mobile machinery; The Non-Road Mobile Machinery (Emission of Gaseous and Particulate Pollutants) Regulations 1999; Regulation (EU) 2019/1242 setting CO_2 emission performance standards for new heavy-duty vehicles and amending Regulations (EC) No 595/2009 and (EU) 2018/956 of the European Parliament and of the Council). The sample structure is given in Table 1.

Table 1. *Structure of the sample of measured operators' workplaces (N = 32 valid).*

Machine category	N	Installed power (kW)	Year of manufacture
Excavator (hydraulic)	9	128–370	2011–2024
Loader	8	129–251	2001–2020
Bulldozer	7	120–406	2011–2024
Dumper	6	246–386	2008–2011
Rotor excavator (electric)	2	630	1995–2000

Occupational exposure limits

Measured values were compared with the mandatory occupational exposure limit values (OELs) for the workplace defined by the Rulebook on preventive measures for safe and healthy work during exposure to chemical substances (Official Gazette of the Republic of Serbia, No. 106/2009, 117/2017 and 107/2021). The OEL is the time-weighted concentration of a hazardous substance in the breathing zone over a standard eight-hour shift below which exposure is not considered a health risk while short-term limit values (STLVs) of the Rulebook 1 ppm for both SO_2 and NO_2 were used only as a reference for peak concentrations. The relevant limits are given in Table 2.

Table 2. *Mandatory occupational exposure limit values for the measured gases.*

Substance	CAS number	mg/m³	ppm
Carbon dioxide (CO_2)	124-38-9	9000	5000
Sulphur dioxide (SO_2)	7446-09-5	1.3	0.5
Nitrogen dioxide (NO_2)	10102-44-0	0.96	0.5

Statistical analysis

All measured variables were first checked for normality using skewness and kurtosis. As none of the variables were normally distributed, non-parametric Kruskal–Wallis H test compared the four main machine categories and the three emission stages, and the Spearman rank correlation related each gas to year of manufacture and installed power. In parallel, all operators were surveyed on a five-point Likert scale (1 = strongly disagree, 5 = strongly agree) regarding perceived pollutant gases, operational disturbance and symptoms, so that subjective perception could be confronted with the instrumental results.

RESULTS AND DISCUSSION

Descriptive statistics for the three gases across the 32 valid workplaces are given in Table 3. All three distributions are right-skewed with coefficients of variation (CV) above 50%, confirming high variability and departure from normality and justifying non-parametric tests. CO_2 remained well below its maximal prescribed limit everywhere, reaching at most 59.3% of the OEL. SO_2 was near zero at most workplaces but exceeded its limit once (121.8% of the OEL). NO_2 was the most critical gas which exceeded the OEL at four workplaces (12.5%), reaching 144.5% of the limit, with a fifth workplace essentially at the threshold (0.497 ppm). Although the 8-hour OEL for NO_2 was exceeded, the highest recorded values (SO_2 0.61 ppm, NO_2 0.72 ppm) stayed below the short-term limit value of 1 ppm, indicating that the exceedances concern average rather than acute short-term exposure. The distributions by workplace are shown in Fig. 1 and Fig. 2.

Table 3. *Descriptive statistics of measured in-cabin concentrations and exceedance of OELs (N = 32).*

Statistic	CO_2 (ppm)	SO_2 (ppm)	NO_2 (ppm)
Minimum	474.06	0.0000	0.0000
Maximum	2964.90	0.6088	0.7226
Mean	1273.44	0.0715	0.2436
Median	1057.37	0.0083	0.2124
Std. deviation	693.63	0.1398	0.2065
CV (%)	54.5	195.5	84.8
Skewness	1.17	2.54	0.67
Exceedances of OEL	0 (0%)	1 (3.1%)	4 (12.5%)
Maximum, % of OEL	59.3%	121.8%	144.5%

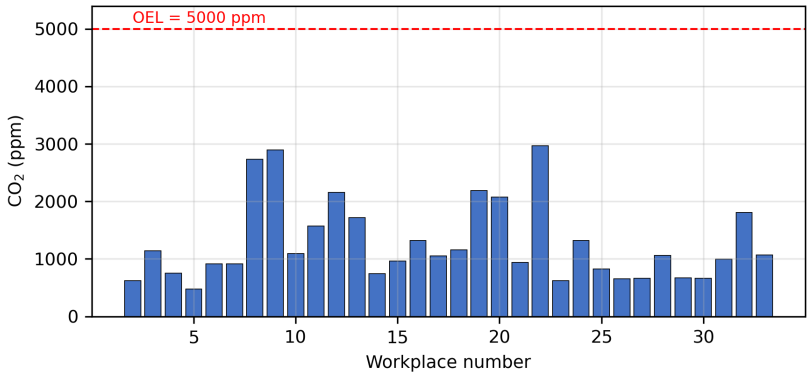


Fig. 1. *Measured in-cabin CO_2 concentrations by workplace (ppm), with the OEL of 5000 ppm.*

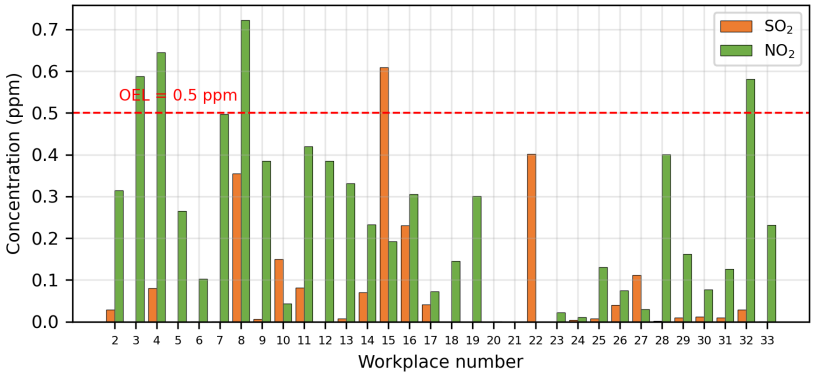


Fig. 2. *Measured in-cabin SO_2 and NO_2 concentrations by workplace (ppm) relative to the OEL of 0.5 ppm.*

To test whether the gases depend on the type of machine, the four main categories were compared with the Kruskal–Wallis test (Table 4). None of the three gases differed significantly between excavators, loaders, bulldozers and dumpers (all $p > 0.05$). The distribution of NO_2 across categories (Fig. 3) confirms the absence of any category effect.

Table 4. *Non-parametric comparison of gases between machine categories and emission stages (p-values).*

Test	CO_2	SO_2	NO_2
Kruskal–Wallis (4 categories)	0.613	0.523	0.983
Kruskal–Wallis (emission stage III/IV/V)	0.613	0.151	0.239

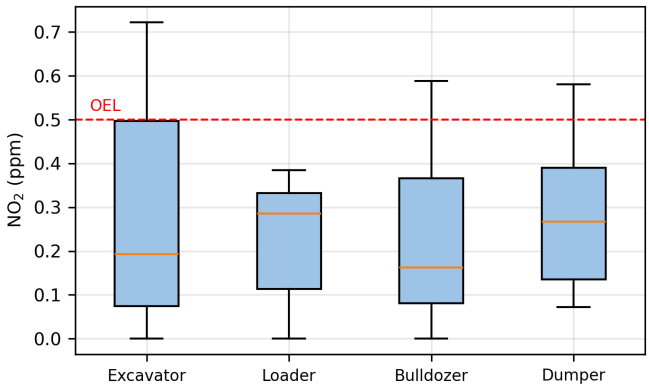


Fig. 3. *Distribution of in-cabin NO_2 by machine category; the dashed line marks the OEL.*

The same picture emerges for emission technology and machine age. Grouping by emission stage (III, IV, V) produced no significant differences for any gas (NO_2 p = 0.239), and Spearman correlations of NO_2 with year of manufacture (ρ = 0.11, p = 0.540) and installed power (ρ = −0.07, p = 0.686) were negligible. Newer, higher-stage machines therefore did not exhibit lower in-cabin NO_2; indeed, one of the four exceedances occurred on a Stage V excavator manufactured in 2024 (Fig. 4). The only significant correlation was a moderate positive association between SO_2 and year of manufacture (ρ = 0.47, p = 0.007), driven by the large number of near-zero SO_2 readings and interpreted with caution.
Atmospheric pressure, logged as a proxy for site altitude, ranged from 856 to 1020 mbar across the ten mines. CO_2 correlated significantly and negatively with atmospheric pressure (Spearman ρ = −0.547, p = 0.001), i.e. higher CO_2 at lower-pressure, higher-altitude sites, whereas SO_2 (ρ = 0.23, p = 0.207) and NO_2 (ρ = −0.12, p = 0.519) showed no significant association, suggesting that in-cabin CO_2 build-up is partly conditioned by site elevation and ventilation rather than by the machine itself.

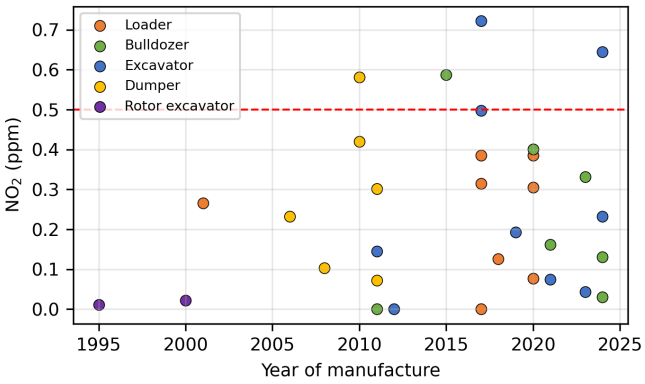


Fig. 4. *In-cabin NO_2 versus year of manufacture by machine category; no downward trend with newer machines.*

Operators' perception was then confronted with the measurements. Averaged over all respondents, agreement with "Exhaust gases in the cabin bother me" was very low (mean 1.19), as was agreement with statements on operational disturbance (1.74) and symptoms such as coughing, headache and breathing difficulty (1.87); dust was perceived as a somewhat greater nuisance (2.16) than exhaust gases, and the use of personal protective equipment scored high (4.29). Mean perception scores are shown in Fig. 5. This low perceived disturbance persisted even among operators of machines on which NO_2 exceedances were instrumentally recorded, so subjective perception did not coincide with the measured exceedances.

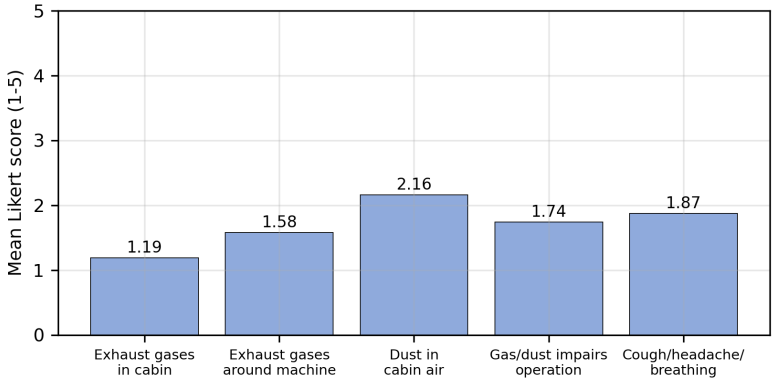


Fig. 5. *Mean operator perception scores (1–5 scale) for cabin air-quality statements across all respondents.*

The corresponding descriptive statistics of the perception items are summarised in Table 5. Agreement was consistently low for the gas- and symptom-related statements, with mean scores between 1.19 and 2.16 on the five-point scale, whereas the use of personal protective equipment scored highest (mean 4.29). The coefficient of variation exceeded 30% for every item except protective-equipment use, confirming high variability and departure from normality and thus supporting the non-parametric approach adopted above.

Table 5. *Descriptive statistics of operators' perception (Likert scale 1–5; N = 31).*

Survey item	N	Min	Max	Mean	Std. Dev.	CV%
Exhaust gases in cabin bother me	31	1	5	1.19	0.75	62.8
Exhaust gases around machine bother me	31	1	5	1.58	1.15	72.6
Dust in cabin air bothers me	31	1	5	2.16	1.42	65.5
Gas/dust sometimes impairs operation	31	1	5	1.74	1.26	72.6
Cough / headache / breathing difficulty	31	1	5	1.87	1.26	67.2
Use of PPE as supplementary measure	31	1	5	4.29	1.22	28.4

The discordance is most striking at the five workplaces where NO_2 reached or exceeded the OEL (Table 6): the two operators exposed to the highest NO_2 (workplaces 8 and 7) reported pronounced symptoms of coughing, headache and breathing difficulty (scores 4 and 5), yet none of the five operators attributed any disturbance to cabin gases (scores 1–2).

Table 6. *Measured NO_2 versus operators' perception at the five workplaces with NO_2 exceedances or threshold values.*

Workplace	Machine	NO_2 (ppm)	"Gases bother me" (1–5)	"Cough/headache" (1–5)
3	Bulldozer	0.59	1	1
4	Excavator	0.64	1	1
7	Excavator	0.50	1	5
8	Excavator	0.72	1	4
32	Dumper	0.58	2	2

Two findings stand out. First, in-cabin NO_2 is the critical parameter, exceeding the mandatory limit in one workplace out of eight, whereas CO_2 never approached its limit and SO_2 exceeded it only once. Second, and in contrast to outside-cabin comparisons that found significant differences between machine types (Spasojević Brkić et al., 2026b), in-cabin concentrations did not vary significantly with machine category, emission stage or age. Because exceedances appeared across all categories and even on a brand-new Stage V machine, the accumulation of NO_2 in the cabin is best explained by factors specific to the cabin and the operating situation – cabin sealing and ventilation, filtration state, the machine's position relative to exhaust sources, and the organisation of operations, rather than by the engine emission technology, which governs what is released outside the machine, not what reaches the breathing zone inside. The perception survey reinforces that operators largely did not report exhaust gases as a disturbance even where measurements showed exceedances, consistent with the physiology of these gases, since NO_2 near the limit is hard to identify by smell, SO_2 odour is an unreliable exposure indicator under simultaneous dust exposure, and CO_2 is odourless. Reliance on operators' perception therefore under-detects real exposure. In practice, operator

cabins should be fitted with filtered, positive-pressure ventilation meeting recognised cabin air-filtration categories (e.g. EN 15695), and cabin air quality should be verified through routine instrumental monitoring rather than through operator perception.

CONCLUSION

In-cabin CO_2, SO_2 and NO_2 were measured on 32 surface-mining machines and compared with mandatory occupational exposure limits. CO_2 never exceeded its limit, SO_2 exceeded it at one workplace (3.1%), and NO_2 at four workplaces (12.5%, up to 144.5% of the limit), making NO_2 the critical in-cabin pollutant. Non-parametric testing showed no significant dependence of any gas on machine category, emission stage or machine age, and Spearman correlations of NO_2 with year of manufacture and power were negligible; an exceedance occurred even on a 2024 Stage V machine. Crucially, empirical data revealed a strong and statistically significant negative correlation between in-cabin CO_2 accumulation and local atmospheric pressure (Spearman $\rho = -0.547$, $p = 0.001$), proving that carbon dioxide build-up is significantly aggravated at lower-pressure, higher-altitude mine sites due to compromised baseline ventilation dynamics. Conversely, the dispersion and entrapment patterns of SO_2 and NO_2 within the cabins demonstrated complete independence from geographical site elevation. Simultaneously, the subjective survey data indicated that operators' perception of toxic cabin gases was uniformly deficient and completely uncoupled from the objectively recorded exceedances. Taken together, these findings conclusively demonstrate that real occupational exposure is driven by cabin structural sealing, ventilation functionality, and specific micro-operational regimes rather than by external engine emission technology. Consequently, relying on worker perception is deeply unsafe, and continuous instrumental monitoring, rather than subjective evaluation, is an absolute requirement to guarantee operator health. Future work should enlarge the active research sample, incorporate short-term exposure limit values, and deploy multivariate modelling frameworks to map the intersecting dynamics of cabin, machine, and operational variables. Additionally, future studies must explicitly focus on modelling the pressure-drop across varied site elevations and directly quantify the micro-level mitigation effects of positive-pressure cabin ventilation and specialized chemical filtration systems on in-cabin NO_2 degradation.

ACKNOWLEDGEMENT

This research was supported by the Ministry of Science, Technological Development and Innovation of the Republic of Serbia under the Agreement on Financing Scientific Research Work of Teaching Staff at Accredited Higher Education Institutions No. 451-03-34/2026-03/200105, and Eureka project No. 20495 - SMARTMEN.

REFERENCES

Baghaei Naeini, S. A., & Badri, A. (2024). Identification and categorization of hazards in the mining industry: A systematic review of the literature. *International Review of Applied Sciences and Engineering*, *15*(1), 1–19. https://doi.org/10.1556/1848.2023.00621

Bęś, P., Strzałkowski, P., Górniak-Zimroz, J., Szóstak, M., & Janiszewski, M. (2025). Innovative technologies to improve occupational safety in mining and construction industries Part I. *Sensors*, *25*(16), 5201. https://doi.org/10.3390/s25165201

Czmochowski, J., & Pietrusiak, D. (2012). Selected problems in designing and constructing surface mining machinery. *FME Transactions*, *40*, 153-164.

Directive 97/68/EC of the European Parliament and of the Council on measures against the emission of gaseous and particulate pollutants from internal combustion engines to be installed in non-road mobile machinery. (1998). *Official Journal of the European Communities*.

Horberry, T., Burgess-Limerick, R., & Steiner, L. J. (2016). *Human factors for the design, operation, and maintenance of mining equipment*. CRC Press. https://doi.org/10.1201/9781439802335

Janev, N., Spasojević Brkić, V., Perišić, M., & Savić, I. (2026). Neural network modeling and forecasting of particulate matter of wheel loaders at mining site. *Manufacturing Innovation as a Driver of the Future 2025*, *1*, 14-20.

Korshunov, G., Iliashenko, I., & Kovshov, S. (2025). An Integrated Risk-Based Method for Assessment of Occupational Exposures in Surface Mining. *Mining*, *5*(4), 85. https://doi.org/10.3390/mining5040085

Li, X., Yang, L., Liu, Y., Zhang, C., Xu, X., Mao, H., & Jin, T. (2023). Emissions of air pollutants from non-road construction machinery in Beijing from 2015 to 2019. *Environmental Pollution*, *317*, 120729. https://doi.org/10.1016/j.envpol.2022.120729

Matamala Pizarro, J., & Aguayo Fuenzalida, F. (2021). Mental health in mine workers: A literature review. *Industrial Health*, *59*(6), 343–370. https://doi.org/10.2486/indhealth.2020-0178

Perišić, M., Spasojević Brkić, V., Mihajlović, I., Brkić, A., & Janev, N. (2024). *Excavators' cabins ergonomic design influential factors modelling: Preliminary study*. 15th International Conference on Applied Human Factors and Ergonomics (AHFE 2024). https://doi.org/10.54941/ahfe1005351

Pradhan, D. S., Patra, A. K., Santra, S., Penchala, A., Sahu, S. P., & Nazneen. (2025). In-cabin particulate matter exposure of heavy earth moving machinery operators in Indian opencast coal mine. *Aerosol Science and Engineering*, *9*(2), 259–276. https://doi.org/10.1007/s41810-024-00258-0

Regulation (EU) 2019/1242 of the European Parliament and of the Council setting CO_2 emission performance standards for new heavy-duty vehicles and amending Regulations (EC) No 595/2009 and (EU) 2018/956. (2019). *Official Journal of the European Union*.

Rulebook on preventive measures for safe and healthy work during exposure to chemical substances. (2009, 2017, 2021). Official Gazette of the Republic of Serbia, Nos. 106/2009, 117/2017 and 107/2021.

Saleh, J. H., & Cummings, A. M. (2011). Safety in the mining industry and the unfinished legacy of mining accidents: Safety levers and defense-in-depth for addressing mining hazards. *Safety Science*, *49*(6), 764–777. https://doi.org/10.1016/j.ssci.2011.02.017

Sharma, S. (2025). *Enhancing cabin air quality: Challenges, impact and advanced climate control solutions.* SAENIS TTTMS Thermal Management Systems Conference. https://doi.org/10.4271/2025-28-0433.

Spasojević Brkić, V., Misita, M., Mihajlović, I., & Janev, N. (2026a). Dumper and excavator operator's workplace risks and ergonomic issues. In *Modern Technologies in Ergonomics and Workplace Safety*, 98-125.

Spasojević Brkić, V., Misita, M., Papić, N., Brkić, A., & Perišić, M. (2024). Ergonomic adjustment needs of transport and mining machines: A preliminary study of operators' attitudes in Serbia. *Human Factors and Systems Interaction*. https://doi.org/10.54941/ahfe1005347

Spasojević Brkić, V., Mihajlović, I., Janev, N., Perišić, M., & Alsharif, A. M. (2026b). Backhoe and loader excavator operators' workplace health and safety and gaseous pollutants. AHFE International, accepted for publication, 1–10. https://doi.org/10.54941/AHFE-Paper-0022

Spasojević Brkić, V., Petrović, N., & Bugarić, U. (2023). *Reliability-based risk assessment of auxiliary machinery in open-pit mines: Case study of a hydraulic excavator*. In *Proceedings of the XIII International Conference on Industrial Engineering and Environmental Protection (IIZS 2023)* (Vol. 13, pp. 200–207). Technical Faculty "Mihajlo Pupin", University of Novi Sad.

Szczurek, A., Maciejewska, M., Przybyła, M., & Szetelnicki, W. (2020). Improving air quality for operators of mobile machines in underground mines. *Atmosphere*, *11*(12), 1372. https://doi.org/10.3390/atmos11121372

The Non-Road Mobile Machinery (Emission of Gaseous and Particulate Pollutants) Regulations 1999 (SI 1999/1053). (1999). The Stationery Office.

Waluś, K. J., Warguła, Ł., Krawiec, P., & Adamiec, J. M. (2018). Legal regulations of restrictions of air pollution made by non-road mobile machinery—the case study for Europe: A review. *Environmental Science and Pollution Research*, *25*(4), 3243–3259. https://doi.org/10.1007/s11356-017-0847-8

Weston, E., Nasarwanji, M. F., & Pollard, J. P. (2016). Identification of work-related musculoskeletal disorders in mining. *Journal of Safety, Health and Environmental Research*, *12*(1), 274–283.

DOI:10.5937/IIZS26475M

LIGHTING CONDITIONS FOR PRACTICAL TEACHING IN A UNIVERSITY PRINTING LABORATORY

Research paper

Aleksandra Mihailović[1], Robert Lakatoš[2*], Selena Samardžić Cvijanović[3], Savka Adamović[4], Nada Marković[5], Ivana Lončarević[6]

[1,2,3,4,6] Faculty of Technical Sciences, University of Novi Sad, Novi Sad, Serbia,
[5] Ministry of Energy and Mining of Montenegro, Podgorica, Montenegro

Abstract: University printing laboratories constitute a specific educational and working environment where practical teaching activities are carried out alongside the Faculty's printing and publishing activities. This study aimed to assess the lighting conditions in a university digital printing laboratory used for both purposes. Illuminance measurements were performed at nine representative student and employee workstations using a digital lux meter, and the measured values were compared with the recommended illuminance level of 300 lx for educational facilities. The results showed that illuminance was not uniformly distributed throughout the laboratory. While the employee workstations generally satisfied or closely approached the recommended illuminance level, illuminance at the student workstations ranged from approximately 142 to 236 lx, indicating insufficient lighting conditions for practical teaching activities.

Keywords: *illuminance; lighting assessment; printing laboratory; practical teaching; visual comfort.*

INTRODUCTION

The quality of the indoor environment has become an increasingly important aspect of modern educational facilities, particularly in university laboratories where theoretical instruction is complemented by practical training. Indoor Environmental Quality (IEQ) encompasses several physical factors, including thermal comfort, air quality, acoustics, and lighting, all of which contribute to occupants' comfort, health, and work efficiency (Brink et al., 2021). Among these factors, lighting is a key prerequisite for performing visual tasks safely and accurately, especially in laboratories where students work with technical equipment and printed materials.

Adequate lighting conditions directly affect visual comfort, concentration, learning performance, and task accuracy (Katabaro & Yan, 2019; Qu et al., 2024). Insufficient illuminance may increase visual fatigue, reduce productivity, and impair the recognition of fine details, while excessive brightness or glare can also negatively affect visual comfort and task performance. Consequently, international standards and national regulations prescribe recommended illuminance levels for educational facilities, including laboratories, to ensure safe, comfortable, and productive learning and working conditions (CEN, 2021).

Numerous studies have investigated different aspects of the indoor environment in schools, universities, offices, and industrial workplaces (Castillo-Martinez et al., 2018; Noor et al., 2021). However, considerably less attention has been devoted to specialised university laboratories equipped with printing machinery, where educational activities are carried out alongside printing and publishing. Such facilities offer a unique educational and working environment, as students and employees share the same space while performing tasks that require appropriate visual conditions.

Creating healthy learning environments has therefore become an important objective of universities, not only to ensure compliance with technical standards but also to support students' well-being, learning performance, and long-term occupational health (Heschong et al., 2013). Regular assessment of lighting conditions in educational laboratories provides an important basis for identifying lighting deficiencies, improving visual comfort, optimising workplace design, and supporting both teaching activities and occupational safety.

[1]zandra@uns.ac.rs, ORCID: 0000-0002-8965-1226
[2*] Corresponding author,. laki@uns.ac.rs, ORCID: 0000-0002-8206-7692
[3]selena@uns.ac.rs, ORCID: 0000-0003-2578-7412
[4]adamovicsavka@uns.ac.rs, ORCID: 0000-0003-1649-4482
[5]nadamarkovic71@t-com.me, ORCID: 0009-0009-8483-5622
[6]ivanalon@uns.ac.rs, ORCID: 0000-0001-5028-8514

The digital printing laboratory investigated in this study is used for practical teaching and for the Faculty's printing and publishing activities. Students attend laboratory teaching activities while employees operate digital printing and finishing equipment, making appropriate lighting conditions essential for both educational and professional tasks. In our previous study, the indoor environmental conditions of this laboratory were comprehensively evaluated through measurements of several physical factors and subjective assessment by laboratory users. The obtained results indicated that illuminance levels at several workstations did not fully comply with the recommended illuminance levels for educational facilities, suggesting the need for a more detailed evaluation of lighting conditions (Samardžić et al., 2023).
The present study focuses on assessing lighting conditions in the university printing laboratory. Illuminance measurements were performed at representative student and employee workstations and compared with the recommended lighting requirements for educational facilities. The study aimed to identify locations with insufficient illumination and to provide recommendations for improving visual conditions during practical teaching activities.

MATERIALS AND METHODS

Printing laboratory

The study was conducted in the Digital Printing Laboratory of the Department of Graphic Engineering and Design, Faculty of Technical Sciences, University of Novi Sad, Serbia. The laboratory is used for both practical teaching and the Faculty's printing and publishing activities. During laboratory classes, students participate in digital printing and finishing processes under the supervision of teaching staff and laboratory technicians who operate the equipment. The laboratory consists of two working areas equipped with digital printing and finishing machines, workstations, and student desks. A detailed description of the laboratory layout, equipment, and measurement locations has been presented in our previous publication (Samardžić et al., 2023) and is therefore not repeated in this paper.

Lighting measurements

Illuminance measurements were performed using a PeachTech 5025 Compact Digital Lux Meter with a measurement accuracy of ±(5% + 10 digits) and measurement ranges of 20, 200, 2000, and 20000 lx. The instrument incorporates an integrated spectral filter to ensure accurate measurements within the visible light spectrum.
Measurements were conducted at nine representative student and employee workstations within the laboratory. Each measurement location was divided into four equal sections. Illuminance was measured with the sensor placed horizontally over the centre of each section, and the average of the four measurements was used as the representative illuminance value for each workstation. Measurement locations were situated opposite the windows in both laboratory rooms, with a distance exceeding 4 m from the nearest windows, thus minimising the influence of daylight. The measurements were performed under normal operating conditions, using the laboratory's existing lighting system. The measured illuminance values were compared with the recommended maintained illuminance level of 300 lx in accordance with EN 12464-1:2021 (CEN, 2021). Since the evaluated laboratory is predominantly used for practical teaching activities, computer-based work, and routine printing tasks rather than high-precision visual inspection or colour matching, this value was adopted as the reference illuminance level for assessing the adequacy of lighting conditions.

Data analysis

The measured illuminance values were analysed using descriptive statistics and evaluated against the recommended illuminance level for educational facilities. The analysis focused on identifying workstations that did not satisfy the recommended requirements and assessing the adequacy of lighting conditions for practical teaching activities. The results were

subsequently interpreted to identify potential improvements that could enhance visual comfort and create a higher-quality learning environment in the university printing laboratory.

RESULTS AND DISCUSSION

The measured illuminance levels at the evaluated workstations are summarised in Tables 1 and 2, while Figure 1 provides an overview of deviations from the recommended illuminance level of 300 lx, allowing a direct assessment of lighting adequacy at all evaluated workstations. Measurements were performed at nine workstations, including three employee workstations in Room 1 and six student workstations in Room 2. Overall, the results indicate that the lighting conditions were not uniform throughout the laboratory, with larger deviations from the recommended illuminance level observed at most student workstations. For clarity, the results obtained for employee and student workstations are discussed separately below.
Among the three evaluated employee workstations, one (A2) met the recommended illuminance level, while workstation A1 was within the measurement uncertainty of the recommended value. In contrast, workstation A3 exhibited a considerably lower illuminance level, indicating that the available lighting was not uniformly distributed throughout the employee work area. Nevertheless, the overall lighting conditions in Room 1 were generally more favourable than those in the area intended for practical teaching activities, where substantially larger deviations from the recommended illuminance level were observed.

Table 1. *Illuminance levels at employee workstations (Room 1)*

Workstation	Natural illuminance (lx)	Combined illuminance (lx)	Compliance*
A1	37.6 ± 1.9	303.1 ± 15.2	Compliant
A2	29.7 ± 1.1	393.8 ± 19.7	Compliant
A3	31.5 ± 1.4	206.5 ± 10.3	Non-compliant

**Compliance with the recommended illuminance level of 300 lx for educational facilities (CEN, 2021)*

The lighting conditions at the student workstations in Room 2 were considerably less favourable than those observed at the employee workstations. Of the six evaluated workstations, only B1 was considered acceptable, as the measured illuminance differed from the recommended value by only 3.0 lx, which falls within the measurement uncertainty. The remaining five workstations exhibited illuminance levels below the recommended threshold, indicating that the existing lighting system did not provide adequate lighting throughout the area intended for practical teaching activities.

Table 2. *Illuminance levels at student workstations (Room 2)*

Workstation	Natural illuminance (lx)	Combined illuminance (lx)	Compliance*
B1	17.0 ± 0.9	297.0 ± 14.8	Compliant**
B2	12.9 ± 0.7	232.3 ± 11.6	Non-compliant
B3	14.9 ± 0.8	157.8 ± 7.9	Non-compliant
B4	11.0 ± 0.6	145.3 ± 7.3	Non-compliant
B5	7.9 ± 0.4	236.5 ± 11.8	Non-compliant
B6	14.3 ± 0.7	141.8 ± 7.1	Non-compliant

**Compliance with the recommended illuminance level of 300 lx for educational facilities (CEN, 2021)*

Since this part of the laboratory is primarily used for practical teaching activities, students spend considerable time performing visually demanding tasks, including reading, writing, examining printed materials, and following practical demonstrations. Under such conditions, insufficient illuminance may reduce visual comfort, increase visual fatigue, and adversely affect their performance during prolonged visual tasks (Qu et al., 2024). Workstations A1 and B1 were classified separately because their measured illuminance levels differed from the

recommended value by only +3.1 lx and −3.0 lx, respectively, which is within the measurement uncertainty.

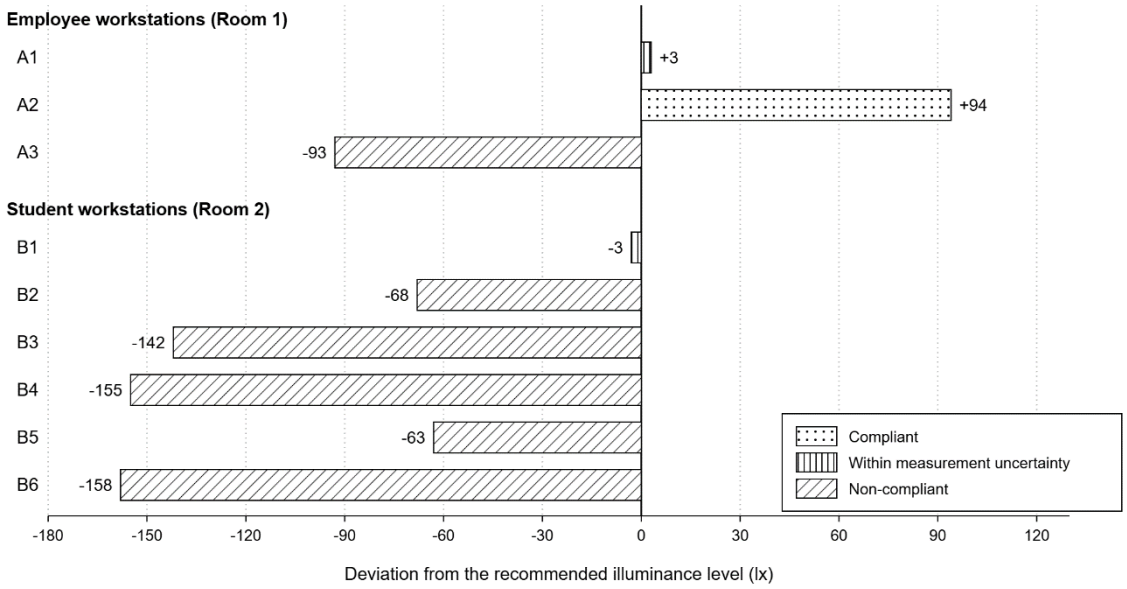


Fig. 1. *Deviation of illuminance levels at employee and student workstations from the recommended value of 300 lx.*

The overall distribution of deviations from the recommended illuminance level is presented in Figure 1. The figure clearly shows that the largest negative deviations were recorded at the student workstations, whereas employee workstations generally exhibited more favourable lighting conditions. These findings indicate that the existing lighting system provides uneven illuminance throughout the laboratory. Therefore, the identified lighting deficiencies should be taken into account when planning future improvements to the laboratory lighting system to provide more uniform illuminance and enhance the visual environment for practical teaching activities.

CONCLUSION

The present study demonstrated that lighting conditions in the investigated university digital printing laboratory were not uniform. While the employee workstations generally satisfied or closely approached the recommended illuminance level, most student workstations exhibited illuminance levels substantially below the recommended requirements for educational facilities. Since practical teaching activities involve prolonged, visually demanding tasks, improving lighting conditions at student workstations would enhance visual comfort, reduce visual fatigue, and create a more favourable visual environment for practical teaching. The findings of this study provide a useful basis for planning future improvements to the laboratory lighting system. The proposed approach may also serve as a practical framework for assessing and improving lighting conditions in similar university laboratories.

ACKNOWLEDGEMENT

This research has been supported by the Ministry of Science, Technological Development and Innovation (Contract No. 451-03-34/2026-03/200156) and the Faculty of Technical Sciences, University of Novi Sad through project "Scientific and Artistic Research Work of Researchers in Teaching and Associate Positions at the Faculty of Technical Sciences, University of Novi Sad 2026" (No. 01-3609/1).

REFERENCES

Brink, H. W., Loomans, M. G. L. C., Mobach, M. P., & Kort, H. S. M. (2021). Classrooms' indoor environmental conditions affecting the academic achievement of students and teachers in higher education: A systematic literature review. *Indoor Air*, 31(2), 405–425.

Castillo-Martinez, A., Medina-Merodio, J.-A., Gutierrez-Martinez, J.-M., Aguado-Delgado, J., De-Pablos-Heredero, C., & Otón, S. (2018). Evaluation and improvement of lighting efficiency in working spaces. *Sustainability*, 10, 1110.

European Committee for Standardization (CEN). (2021). *Light and lighting — Lighting of work places — Part 1: Indoor work places (EN 12464-1:2021).* Brussels, Belgium: CEN.

Heschong, L., Wright, R., & Okura, S. (2013). Daylighting impacts on human performance in school. *Journal of the Illuminating Engineering Society*, 31, 101–114.

Katabaro, J. M., & Yan, Y. (2019). Effects of lighting quality on working efficiency of workers in office building in Tanzania. *Journal of Environmental and Public Health*, 2019, Article 3476490.

Noor, S. N. A. M., Ding, H. H., Saharuddin, S., Yusof, N. F. M., Roshdi, F. R. M., & Namandadin, N. A. (2021). Indoor environment quality (IEQ): Lighting and acoustics factors toward occupants satisfaction. *AIP Conference Proceedings*, 2347, 020004.

Qu, G., Ren, L., Liu, G., Zhang, Y., Lau, S.-K., Zhan, M., & Yan, M. (2024). The best college classroom light environments have changed: Attributed to the public health issue of decreased sensitivity to students' eyesight. *Energy and Buildings*, 307, 113948.

Samardžić, S., Mihailović, A., Adamović, S., Adamović, D., Banjanin, B., Rajs, V., & Lakatoš, R. (2023). Noise and lighting as physical stressors in a printing laboratory – A case study. *Environmental Engineering and Management Journal*, 22(3), 595–604.

DOI:10.5937/IIZS26480M

ACCIDENTS AT WORK IN THE TRANSPORT AND STORAGE SECTOR: A COMPARATIVE ANALYSIS OF THE EU-27 AND NORTH MACEDONIA

Review paper

Cvetanka Mitrevska[1], Vangelce Mitrevski[2], Elena Milevska[3]
[1]International Slavic University Gavrilo Romanovic Derzavin,
Faculty for Safety Engineering, Sveti Nikole
[2]University St.Kliment Ohridski, Faculty of Technical Sciences, Bitola
[3]Public Health Institution "Dr. Haim Abravanel" Health Center, Bitola

Abstract: This paper examines non-fatal and fatal accidents at work in the transport and storage sector (NACE Rev. 2, Section H) in the EU-27 and the Republic of North Macedonia during 2018–2023. A comparative descriptive analysis was conducted using Eurostat data and national occupational safety and health data from North Macedonia. In the EU-27, accident incidence rates generally declined over the study period, although the transport and storage sector consistently recorded higher rates than those observed across all NACE activities, particularly for fatal accidents. In North Macedonia, non-fatal accident incidence remained relatively low, whereas fatal accident incidence was comparatively high and showed considerable variation over the study period
Key words: transport and storage sector, non-fatal accidents, fatal accidents, incidence rate.

INTRODUCTION

Work processes within the transport and storage sector encompass a broad range of activities, including: the transportation, loading, unloading, handling, and storage of goods, as well as the operation of various types of vehicles, machinery, and material-handling equipment. These activities are typically performed in dynamic and time-sensitive working environments characterized by intensive material flows, continuous movement of vehicles and cargo-handling equipment, and the simultaneous coordination of multiple operational processes. Workers in the transportation and storage sector are exposed to several general Occupational Safety and Health (OSH) risks and hazards that may cause wear and tear on the body and can cause injury (Snijders et.al., 2024). According to the ESENER 2019 results for the EU-27, workers in the transportation and storage sector are particularly exposed to four musculoskeletal disorders risk factors, namely, prolonged sitting (81%), repetitive hand or arm movements (62%), risk of accidents with machines (60%), and lifting or moving heavy loads (55%) (Snijders et.al., 2024). In the case of prolonged sitting, this is significantly more frequent than when compared to the rest of the total economy (61%) (Snijders et.al., 2024) The comparison with all sectors shows that workers in the transportation and storage sector are less exposed to certain OSH risks, such as chemical or biological substances, increased risk of slips, trips and falls, and loud noises (Snijders et.al., 2024). In 2023, four economic sectors, construction, transport and storage, manufacturing, and agriculture, forestry and fishing accounted for 66.8% of all fatal and 44.8% of all non-fatal accidents at work in the EU-27. In 2023, transport and storage accounted for the second-highest share of fatal accidents at work in the EU-27 (16.4%), following construction (24.0%) (Eurostat, n.d). In 2023, accidents at work in North Macedonia were concentrated primarily in several economic sectors. Transport and storage accounted for the largest share of fatal occupational accidents (46.7%), followed by manufacturing (13.3%). In terms of non-fatal accidents, at work manufacturing recorded the highest share (29.0%), followed by public administration and defence (22.6%) and transport and storage (16.1%). Transport and storage accounted for 5.4% of all non-fatal occupational accidents, while no fatal accidents were recorded in this sector (Macedonian Occupational Safety and Health Association, 2023).
This paper presents selected statistical indicators of accidents at work in the transport and storage sector, including the number of non-fatal and fatal accidents at work and their corresponding incidence rates, in EU-27 and North Macedonia during the period 2018–2023.

[1] cvetanka.mitrevsk@msu.edu.mk; ORCID: 0009-0008-1417-1798
[2] Corresponding author, vangelce.mitrevski@uklo.edu.mk; ORCID: 0000-0002-6838-6582
[3] emitrevska7@gmail.com; ORCID: 0009-0002-0917-9337

MATERIAL AND METHODS

In this paper, two main types of statistical indicators are used to assess accidents at work in the transport and storage sector: the absolute number of non-fatal and fatal accidents at work and the corresponding incidence rates. The analysis covers EU-27 and the Republic of North Macedonia during the period 2018–2023, thereby enabling a comparative assessment of occupational accident trends between the two observed areas. Data on the number of non-fatal and fatal accidents at work in the EU-27 were obtained from the official Eurostat databases, whereas the corresponding data for North Macedonia were collected from the relevant national institutions responsible for recording and reporting occupational accidents. For the calculation of the values of the incidence rate the methodology of the European Statistics on Accidents at Work (ESAW), (European Commission & Eurostat, 2013).
This papaer uses data from the European Statistics on Accidents at Work (ESAW), Eurostat's framework for collecting comparable data on accidents that occur during work and cause physical or mental harm. Its published data distinguish non-fatal accidents that result in at least four full calendar days of absence from work from fatal accidents, defined as those that lead to death within one year of the accident. The data can be examined by year, country and economic activity. In this study, transport and storage is identified as Section H of the NACE Rev. 2 classification.
Two indicators are used: the non-fatal accident incidence rate and the fatal accident incidence rate. Each expresses the number of recorded accidents per 100,000 employed persons in the population covered by the selected series:

Incidence rate = (number of accidents at work/ number of employed persons) x 100000

The non-fatal and fatal rates show how often work accidents result in at least four days of absence or death, respectively. Rates account for differences in workforce size, making them more useful than accident counts alone when comparing countries, sectors or years. They measure recorded accident frequency, however, and do not describe the severity of individual non-fatal injuries or the total burden of shorter absences. Counts and rates should therefore be identified separately in tables and figures. Every reported rate should be labelled with its year, geography, economic activity, accident outcome and unit (accidents per 100000 employed persons). In particular, an EU-27 rate for all economic activities must not be presented as a rate for Section H.

RESULTS AND DISCISSION

Statistical indicators for non-fatal and fatal accidents at work in the European Union

Analysis of accident at work data for the EU-27 indicates that the transport and storage sector (NACE Rev. 2, Section H) maintained a substantial contribution to the overall burden of work-related accidents during 2018–2023 (Table 1) (Eurostat, n.d). In 2023, the sector recorded 263,000 non-fatal accidents at involving at least four calendar days of absence from work, accounting for 9.31% of the 2,824,711 non-fatal accidents reported across all NACE activities. This represents a decrease of 17,000 cases (6.07%) compared with 2018, when 280,000 non-fatal accidents were recorded. However, the temporal pattern was non-linear: the number declined to a six-year minimum of 231,000 in 2020, subsequently increased to 265,000 in 2021, and remained comparatively stable in 2022–2023. Accordingly, the sector's share of all non-fatal accidents at work remained relatively stable over the study period, ranging from 8.43% in 2020 to a maximum of 9.31% in 2023, compared with 8.96% in 2018, 8.98% in 2019, 9.16% in 2021, and 8.81% in 2022. Thus, although the absolute number of non-fatal accidents at work decreased between the beginning and end of the observation period, the relative contribution of transport and storage to EU-27 total increased by 0.35 percentage points.

The sector-specific disparity was considerably more pronounced for fatal accidents at work. In 2023, 541 fatalities were recorded in transport and storage, corresponding to 16.40% of the 3,298 fatal occupational accidents across all NACE activities (Eurostat, n.d). Compared with 2018, when the sector recorded 557 fatalities (16.72% of the EU-27 total), this represents a modest absolute reduction of 16 deaths (2.87%). Fatalities reached their lowest level in 2020 (482; 14.35% of all fatal accidents), followed by a marked increase to 552 in 2021 (16.29%); the corresponding proportions were 14.99% in 2019 and 15.64% in 2022. Importantly, throughout the entire study period, the sector's proportional contribution to fatal accidents (14.35–16.72%) was substantially greater than its contribution to non-fatal accidents (8.43–9.31%). In 2023, the share of fatal accidents was approximately 1.76 times the corresponding share of non-fatal accidents (16.40% vs. 9.31%). Collectively these descriptive findings demonstrate a persistent disproportion in the distribution of fatal versus non-fatal accidents at work in the transport and storage sector. Although these data do not allow causal inference or direct estimation of individual-level accident risk, the consistently elevated share of fatal accidents highlights the need for further sector-specific investigation of occupational safety outcomes and their determinants.

Table 1. *Total number of non-fatal and fatal accidents at work in transport and storage sector, EU-27, 2018-2023 (persons)*

Transport and storage (NACE Rev. 2, Section H)						
	2018	2019	2020	2021	2022	2023
Non-fatal accidents	280000	282000	231000	265000	262000	262616
Total all NACE activities	3124828	3140952	2741574	2892329	2973646	2824711
Fatal accidents	557	511	482	552	514	541
Total all NACE activities	3332	3408	3358	3389	3286	3298

Source of data: Eurostat
update: 21/08/2026

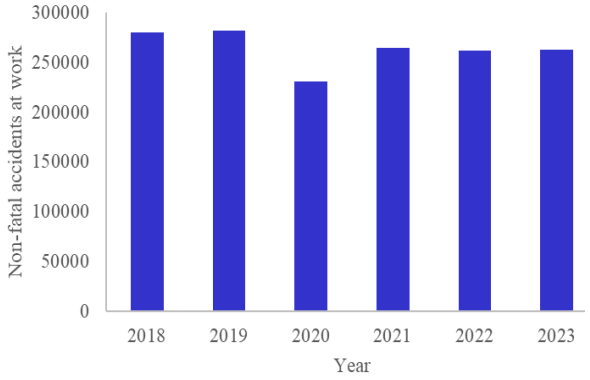


Fig.1. *Non-fatal accidents at work, 2018-2023*

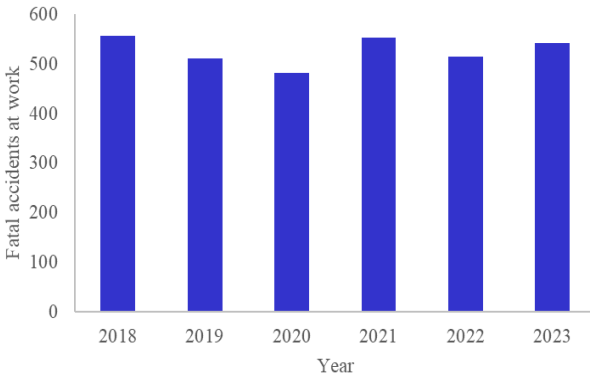


Fig.2. *Fatal accidents at work, 2018-2023*

Substantial between EU-27 country variation was observed in the absolute number of accidents at work in the EU-27 transport and storage sector in 2023 (Table 2), (Eurostat, n.d).

In 2023 the 262,616 non-fatal accidents recorded across EU-27, Germany accounted for the largest proportion (82,972; 31.6%), followed by France (53,946; 20.5%) and Spain (35,253; 13.4%). Together, these three EU Member States contributed 65.6% of all non-fatal accidents in the sector, indicating a marked concentration of reported cases. At the opposite end of the distribution, Cyprus (101), Malta (181), and Romania (269) recorded the lowest absolute numbers of non-fatal accidents at work.

A similarly heterogeneous although less concentrated, distribution was observed for fatal occupational accidents. Of the 541 fatalities recorded in EU-27, France accounted for the largest share (120; 22.2%), followed by Germany (79; 14.6%) and Spain (75; 13.9%), with these three countries collectively representing 50.6% of all sector-related fatalities. No fatal accidents at work were reported in Cyprus or Sweden, while Croatia and Malta each recorded one fatality (Eurostat, n.d). Importantly, the geographical distribution of fatal accidents did not fully correspond to that of non-fatal accidents: Germany contributed the largest share of non-fatal cases, whereas France accounted for the largest share of fatalities. This divergence highlights the importance of distinguishing between the absolute frequency and severity profile of occupational accidents when characterizing their geographical distribution. Nevertheless, these country-level differences should not be interpreted as direct evidence of differences in occupational risk, since absolute accident counts are inherently influenced by the size of the national workforce and the magnitude of occupational exposure. Consequently, standardized incidence measures are required for valid cross-country comparisons of occupational safety outcomes.

Table 3 summarizes the incidence rates of non-fatal and fatal accidents at work in EU-27 transport and storage sector (NACE Rev. 2, Section H) during 2018–2023 (Eurostat, n.d). Over the study period, the incidence rate of non-fatal accidents decreased from 2,789 to 2,366 per 100,000 persons employed, corresponding to an overall reduction of 15.17%. The temporal trend was characterized by a marked decline to a minimum of 2,218 in 2020, followed by a rebound to 2,625 in 2021 and a subsequent decrease to 2,366 in 2023. Despite the overall downward trend, the sector consistently exhibited substantially higher incidence rates than those observed across all NACE activities. In 2023, the non-fatal accident incidence rate in transport and storage exceeded the corresponding all-NACE rate by 69.85% (2,366 vs. 1,393 per 100,000 persons employed), compared with a 67.01% difference in 2018 (2,789 vs. 1,670), (Eurostat, n.d).

Table 2. Number of non-fatal and fatal accidents at work in transport and storage sector, EU-27, 2023

persons

	Accidents at work involving at four calendar days absence from work	**Fatal accidents at work**
	Total	Total
European Union - 27 countries (from 2020)	262 616	541
Belgium	7 064	14
Bulgaria	286	24
Czechia	3 216	16
Denmark	3 820	3
Germany	82 972	79
Estonia	351	3
Ireland	1 526	2
Greece	422 p	6
Spain	35 253	75
France	53 946	120
Croatia	624	1
Italy	29 383	56

Cyprus	101	0
Latvia	313	13
Lithuania	564	10
Luxembourg	503	4
Hungary	3 514	13
Malta	181	1
Netherlands	12 006	6
Austria	3 225	4
Poland	5 883	29
Portugal	7 637	17
Romania	269	23
Slovenia	1 033	3
Slovakia	772	5
Finland	2 988	5
Sweden	4 763	0
Iceland	168	9
Norway	1 272 b	0
Switzerland	7 088	11b

Source of data: Eurostat
update: 21/08/2026

A more pronounced sectoral disparity was observed for fatal occupational accidents. The incidence rate in transport and storage decreased from 5.5 per 100,000 persons employed in 2018 to 4.9 in 2023, representing an overall reduction of 10.91%. Following a decline to the period minimum of 4.6 in 2020, the rate increased to 5.5 in 2021 and subsequently decreased to 4.8 in 2022, with a slight increase to 4.9 in 2023. By comparison, the fatal accident incidence rate across all NACE activities decreased from 1.8 to 1.6 per 100,000 persons employed between 2018 and 2023Consequently, in 2023, the incidence rate of fatal occupational accidents in the transport and storage sector was approximately 3.06 times higher than the corresponding rate across all NACE sectors. Collectively, these findings indicate that, although both non-fatal and fatal accident incidence rates declined over the study period, the relative disparity between transport and storage and the overall EU-27 economy persisted.

Table 3. Incidence rates for non-fatal and fatal accidents at work in transport and storage sector, EU-27, 2018-2023

Transport and storage (NACE Rev. 2, Section H)						
	2018	2019	2020	2021	2022	2023
Non-fatal accidents	2789	2663	2218	2625	2445	2366
Total all NACE activities	1670	1616	1447	1519	1507	1393
Fatal accidents	5.5	4.8	4.6	5.5	4.8	4.9
Total all NACE activities	1.8	1.8	1.8	1.8	1.7	1.6

Source of data: Eurostat
update: 21/08/2026

Figure 3 presents the incidence rates of non-fatal accidents at work in the transport and storage sector in 2023, expressed as the number of accidents per 100,000 persons employed. Considerable variation was observed across the countries included in the analysis, with incidence rates ranging from 60 per 100,000 persons employed in Romania to 2,724 per 100,000 in France. Compared with the EU-27 rate of 1,392 per 100,000 persons employed, the highest incidence rates were recorded in France (2,724), Portugal (2,494), Switzerland (2,345), and Spain (2,320), whereas the lowest rates were observed in Romania (60), Bulgaria (86), and Greece (115).

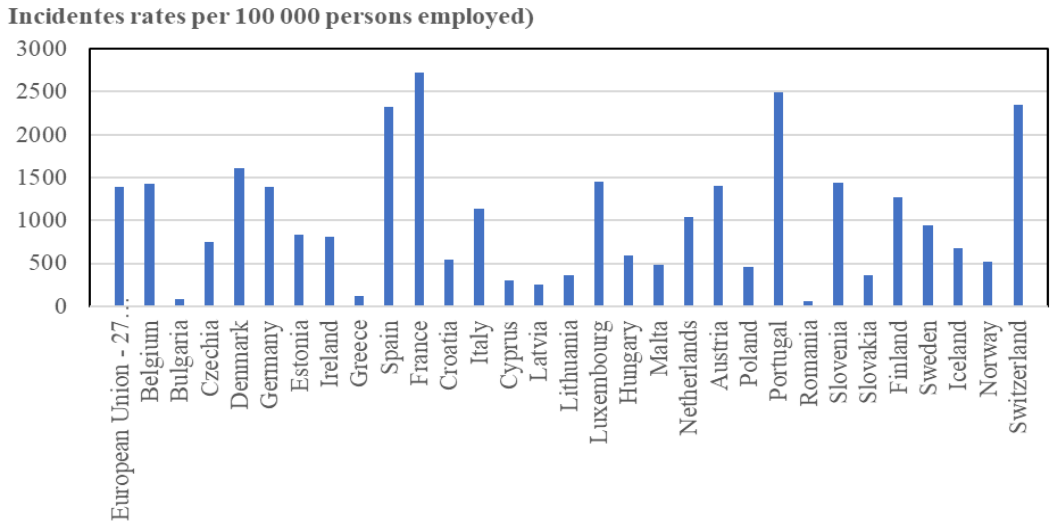


Fig 3. *Non-fatal accidents at work in transport and storage sector, 2023 (incidence rates per 100000 persons employed)*

Figure 4 presents the incidence rates of fatal accidents at work in the transport and storage sector in 2023, expressed per 100,000 persons employed. Considerable variation was observed across the countries included in the analysis, with rates ranging from 0.38 per 100,000 persons employed in the Netherlands to 3.60 per 100,000 in France. Compared with the EU-27 rate of 1.64, the highest incidence rates were recorded in France (3.60), Bulgaria (3.51), Cyprus (3.24), Latvia (3.21), and Austria (3.00), whereas the lowest were observed in the Netherlands (0.38), Iceland (0.45), and Germany (0.71).

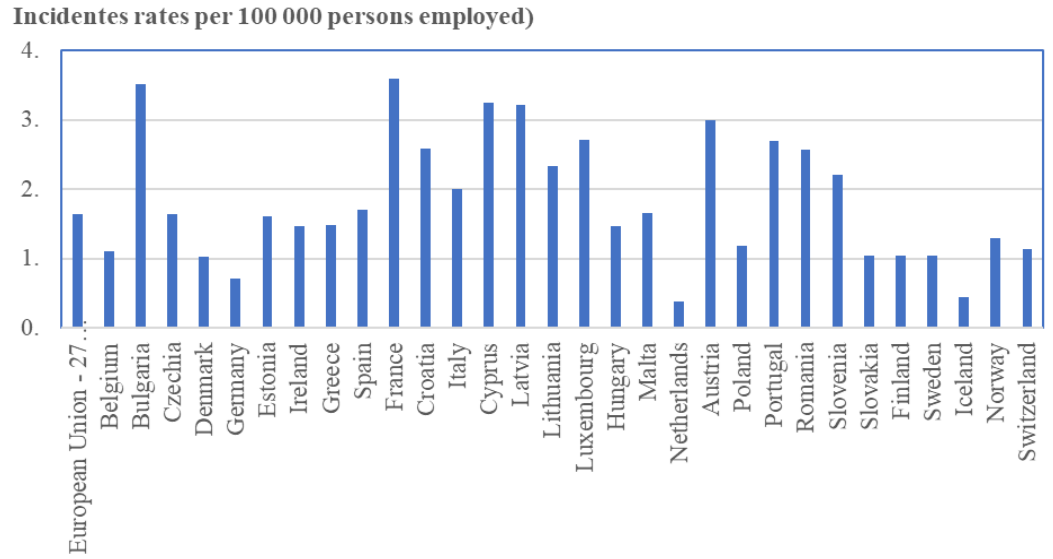


Fig 4. *Fatal accidents at work in transport and storage sector, 2023 (incidence rates per 100000 persons employed)*

Statistical indicators for non-fatal and fatal accidents at work in North Macedonia

In North Macedonia there are several organizations and institutions dealing exclusively with working conditions. These include State statistical office, the Labour inspectorate, Institute for public health, the Macedonian Occupational Safety and Health Association, Organization of the employers of Republic of Macedonia and the Trade unions. The data on the number of accidents at work in the Republic of North Macedonia is not confidential for the reason that

different relevant institutions published various statistical data (Mitrevska et al., 2019; Mitrevska et al., 2022).

In this paper, the statistical indicators related to the number of non-fatal and fatal accidents at work in transport and storage sector in the period 2018÷2023 are based on the data of the Macedonian Occupational Safety and Health Association (Macedonian Occupational Safety and Health Association, 2018, 2019, 2020, 2021, 2022, 2023). The reason for that is what in the statistical reports of the other relevant institutions that register accidents at work no distinction is made between the number of non-fatal and fatal accidents at the workplace. As shown in Table 4, 14 non-fatal and 5 fatal accidents at work were recorded in the transport and storage sector in 2018. During the 2018–2023 period, the number of non-fatal accidents showed an overall decline, decreasing from 14 cases in 2018 to 5 in 2023, corresponding to a reduction of 64.3%. The lowest number of non-fatal accidents was recorded in 2020 (4 cases), followed by a temporary increase to 11 cases in 2022. Fatal accidents fluctuated throughout the study period, with no fatalities recorded in 2020 and the highest number observed in both 2018 and 2023 (5 cases each). In 2023, the transport and storage sector accounted for 5.4% of all non-fatal accidents (5 of 93) and 33.3% of all fatal accidents (5 of 15) recorded across all NACE activities in North Macedonia.

Table 4. Total number of non-fatal and fatal accidents at work in transport and storage sector, Republic North Macedonia, 2018-2023 (persons)

Transport and storage (H)						
	2018	2019	2020	2021	2022	2023
Non-fatal accidents	14	13	4	7	11	5
Total all NACE activities	124	153	127	135	147	93
Fatal accidents	5	4	0	4	2	5
Total all NACE activities	33	25	25	30	22	15

Source of data: Macedonian Occupational Safety and Health Association

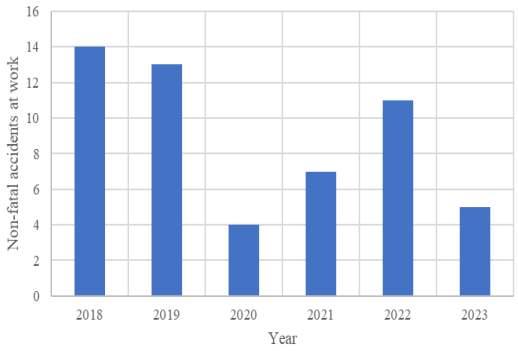


Fig.5. *Non-fatal accidents at work, 2018-2023*

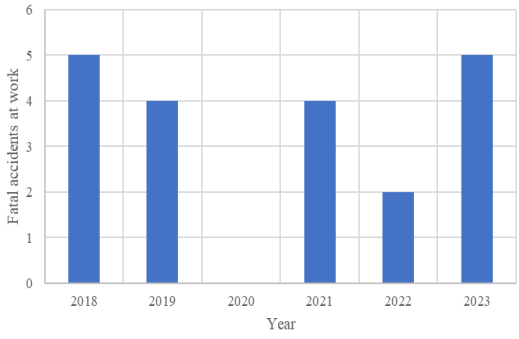


Fig.6. *Fatal accidents at work, 2018-2023*

Comparison with the EU-27 revealed a more pronounced relative contribution of fatal than non-fatal occupational accidents in the transport and storage sector in North Macedonia. In 2023, the sector accounted for 33.3% of all fatal accidents and 5.4% of all non-fatal

accidents recorded across all NACE activities in North Macedonia, indicating that its proportional contribution to fatal accidents was approximately 6.2 times that to non-fatal accidents. A similar, although less pronounced, pattern was observed in the EU-27, where the incidence rates for transport and storage were approximately 3.06 and 1.70 times the corresponding all-NACE rates for fatal and non-fatal accidents, respectively. These findings suggest that fatal occupational accidents represent a disproportionately greater safety burden in the transport and storage sector in both North Macedonia and the EU-27. This comparison should, however, be interpreted with caution because differences in national reporting systems, coverage, and reference populations may affect the comparability of occupational accident statistics across countries.
In Table 5 the incidence rates for non-fatal and fatal accidents at work in period from 2018 to 2023 in transport and storage sector are given (Macedonian Occupational Safety and Health Association, 2018, 2019, 2020, 2021, 2022, 2023). During 2018–2023, the incidence rates of accidents at work in the transport and storage sector in North Macedonia showed considerable year-to-year variability. The non-fatal accident incidence rate decreased from 35.77 per 100,000 persons employed in 2018 to 13.64 in 2023, representing an overall reduction of 61.9%, with the lowest rate recorded in 2020 (9.23). The incidence rate of fatal accidents showed substantial year-to-year variability, ranging from 0.00 per 100,000 persons employed in 2020 to 13.64 in 2023. Notably, in 2023, fatal and non-fatal accidents exhibited identical incidence rates of 13.64 per 100,000 persons employed, with five cases recorded in each category.

Table 5. Incidence rates for non-fatal and fatal accidents at work in transport and storage sector, Republic of North Macedonia, 2018-2023

Transport and storage (H)						
	2018	2019	2020	2021	2022	2023
Non-fatal accidents	35.77	29.27	9.23	17.04	31.29	13.64
Total all NACE activities	124	153	127	135	147	93
Fatal accidents	12.78	9.01	0	9.74	5.69	13.64
Total all NACE activities	33	25	25	30	22	15

Source: Macedonian Occupational Safety and Health Association

Comparison with the EU-27 revealed a contrasting pattern in occupational accident incidence in the transport and storage sector. In 2023, the calculated incidence rate of non-fatal accidents in North Macedonia was 13.64 per 100,000 persons employed, markedly lower than the EU-27 rate of 2,366 per 100,000. Conversely, the fatal accident incidence rate in North Macedonia was 13.64 per 100,000 persons employed, approximately 2.8 times the EU-27 rate of 4.9 per 100,000. This pronounced contrast between the relatively low reported incidence of non-fatal accidents and the comparatively high incidence of fatal accidents suggests that the occupational accident profile of the transport and storage sector in North Macedonia differs substantially from that observed in the EU-27. However, the exceptionally large difference in non-fatal accident rates should be interpreted with caution, as differences in reporting practices, statistical coverage, data sources, and the small number of recorded cases in North Macedonia may affect direct comparability. Accordingly, the low reported incidence of non-fatal accidents should not necessarily be interpreted as evidence of a lower underlying occupational accident risk.

CONCLUSION

The present results of this paper indicate that accidents at work remain an important safety concern in the transport and storage sector in both the EU-27 and North Macedonia. Despite the overall decline in occupational accident incidence across the EU-27 during 2018–2023, the consistently higher rates observed in the transport and storage sector, particularly for fatal accidents, indicate that occupational safety remains a significant concern in this sector. In North Macedonia, the low reported incidence of non-fatal accidents contrasted with a

comparatively high incidence of fatal accidents, although this pattern should be interpreted cautiously due to differences in reporting practices, statistical coverage, and the relatively small number of recorded cases. These findings underscore the importance of strengthening occupational accident surveillance, harmonizing reporting systems, and implementing evidence-based, sector-specific preventive measures.

REFERENCES

European Commission, Eurostat. (2013). European Statistics on Accidents at Work (ESAW): Summary Methodology. Publications Office of the European Union, Luxembourg.

Eurostat. (n.d.). Accidents at work – statistics by economic activity. Statistics Explained. https://ec.europa.eu/eurostat/statistics-explained/index.php?title=Accidents_at_work_-_statistics_by_economic_activity (accessed September 22, 2026).

Macedonian Occupational Safety and Health Association. (2018). Annual Report for Fatalities, Injuries and Accidents at Work 2018.

Macedonian Occupational Safety and Health Association. (2019). Annual Report for Fatalities, Injuries and Accidents at Work 2019.

Macedonian Occupational Safety and Health Association. (2020). Annual Report for Fatalities, Injuries and Accidents at Work 2020.

Macedonian Occupational Safety and Health Association. (2021). Annual Report for Fatalities, Injuries and Accidents at Work 2021.

Macedonian Occupational Safety and Health Association. (2022). Annual Report for Fatalities, Injuries and Accidents at Work 2022.

Macedonian Occupational Safety and Health Association. (2023). Annual Report for Fatalities, Injuries and Accidents at Work 2023.

Mitrevska, C., Mitrevska, E., & Mitrevski, V. (2022). Statistical indicators for accidents at work in the transport and storage sector. Annals of the Faculty of Engineering Hunedoara – International Journal of Engineering, 20(1), 87–90.

Mitrevska, C., Mitrevska, E., Mitrevski, B., Geramitcioski, T., Mijakovski, V., & Mitrevski, V. (2019). Analysis of non-fatal and fatal accidents at work by economic activities in the European Union and the Republic of North Macedonia. In Proceedings of the IX International Conference Industrial Engineering and Environmental Protection (IIZS 2019) (pp. 244–252). Zrenjanin, Serbia, October 3–4, 2019.

Snijders, J., Clarke, M., de Kok, J., Vroonhof, P., Isusi, I., Durán, J., & Kudász, F. (2024). Transportation and Storage Activities – Evidence from the European Survey of Enterprises on New and Emerging Risks (ESENER). European Agency for Safety and Health at Work.

DOI:10.5937/IIZS26489B

FIRES IN HIGH-RISE BUILDINGS: ANALYSIS OF FIRE SAFETY AND ENGINEERING ASPECTS

Review paper

Goran Bošković[1*], Marko Todorović[1], Nikola Karanović[2], Marina Bošković[1], Borivoj Stepanov[3]

[1]Faculty of Mechanical and Civil Engineering in Kraljevo, University of Kragujevac, Kraljevo, Serbia
[2]University of Aveiro, Portugal
[3]Faculty of Technical Sciences, University of Novi Sad, Novi Sad, Serbia

Abstract: Fires in high-rise buildings represent complex engineering problems due to the interaction between fire development, smoke movement, building geometry, ventilation, façade systems, structural response, and fire protection measures. The increased height of buildings limits the effectiveness of external firefighting and creates conditions for vertical smoke and fire spread through stairwells, elevator shafts, ventilation systems, and façade cavities. This paper reviews the principal fire safety and engineering aspects of high-rise building fires, with emphasis on fire dynamics, smoke and heat transport, internal and external fire spread, passive and active protection systems, evacuation and firefighting conditions, and engineering approaches to fire risk assessment. Particular attention is given to computational fluid dynamics (CFD), Fire Dynamics Simulator (FDS), travelling-fire scenarios, and performance-based fire safety engineering. The reviewed literature indicates that conventional prescriptive approaches may be insufficient for complex high-rise configurations and that reliable fire safety assessment requires an integrated consideration of realistic fire scenarios, smoke movement, protection systems, structural response, and firefighting conditions.
Key words: high-rise buildings; fire dynamics; smoke movement; fire spread; fire safety engineering; evacuation; CFD

INTRODUCTION

The rapid development of urban areas has resulted in an increasing number of high-rise buildings with complex structural, architectural, and mechanical systems. Although high-rise construction provides an efficient response to limited urban space, the vertical configuration of such buildings introduces specific challenges for fire safety. Building height, compartmentation, vertical shafts, façade systems, ventilation networks, and limited accessibility for external firefighting can significantly influence fire development and its consequences.

High-rise fires differ from fires in low-rise buildings because the vertical dimension creates long travel paths for smoke and hot gases and increases the importance of buoyancy-driven flow. Stairwells, elevator shafts, service ducts, and other vertical openings may provide pathways for rapid smoke transport, while façade systems may facilitate external vertical fire spread. Previous research has identified façade flame and plume behaviour, flame spread over façade materials, and buoyancy-driven smoke transport through long vertical channels as key aspects of high-rise fire dynamics (Alianto et al., 2022). The stack effect can further intensify vertical smoke movement as building height increases (Cho et al., 2025).

The engineering assessment of high-rise fires therefore requires consideration of several mutually dependent phenomena. Fire development determines the heat release rate and thermal environment, while ventilation, wind, and building geometry influence fire growth and smoke movement. The resulting thermal and smoke exposure affects occupants, firefighters, and structural elements, whereas the performance of compartmentation, detection, suppression, and smoke-control systems determines the extent to which fire development can be controlled.

The present review was based on relevant peer-reviewed and technical literature addressing high-rise fire dynamics, fire spread, smoke movement, fire protection, structural fire engineering, evacuation, and risk assessment. Particular attention was given to studies

[1]Corresponding author, boskovic.g@mfkv.kg.ac.rs, ORCID: 0000-0002-4597-922X
[2]todorovic.m@mfkv.kg.ac.rs, ORCID: 0000-0003-3684-2819
[3]nikola.karanovic83@yahoo.com, ORCID: 0000-0002-7498-6103
[4]boskovic.m@mfkv.kg.ac.rs, ORCID:0000-0002-3637-2741
[5]bstep@uns.ac.rs, ORCID:0000-0002-0193-8231

involving numerical modelling, experimental observations, realistic fire scenarios, and performance-based engineering approaches.
The objective of this paper is to provide an engineering-oriented review of fire safety in high-rise buildings, focusing on fire development and spread, protection systems, evacuation and firefighting conditions, and engineering methods for fire risk assessment.

FIRE DEVELOPMENT AND FIRE SPREAD IN HIGH-RISE BUILDINGS

Ecological aspects

Fire development is primarily determined by the available combustible materials, their distribution, ventilation conditions, and characteristics of the enclosure. Fire load is therefore one of the fundamental parameters influencing the potential heat release and duration of burning. A study of 50 high-rise residential buildings in Istanbul demonstrated considerable variation in fire-load density between different rooms and used FDS simulations to estimate fire growth and spread times. The study reported compartment peak heat release rates in the range of approximately 8–25 MW and fire spread times of approximately 1–11 min, depending on the compartment configuration (Dai et al., 2017).
The heat release rate (HRR) is particularly important because it determines the intensity of the thermal environment and strongly influences buoyant flow and smoke production. In high-rise buildings, these effects can be amplified by vertical communication paths and building-induced airflow.
Recent numerical research has also demonstrated that fire development can vary considerably depending on the position of a fire within a high-rise building and on the configuration of windows and doors. (Vovk et al., 2025) investigated a residential apartment on the 20th floor of a 22-storey building using FDS and found that openings and external wind affected fire development, airflow, the distribution of hazardous fire factors, and fire-detector response (Dundar & Selamet, 2023). These results demonstrate that fire development cannot always be adequately represented by a single simplified fire scenario.

Smoke movement and stack effect

Smoke movement is one of the most critical aspects of high-rise fire safety. Hot gases generated by a fire rise due to buoyancy and may rapidly enter vertical shafts and communication spaces. Stairwells, elevator shafts, ventilation ducts, and service shafts can therefore become important pathways for smoke propagation.
A field experiment conducted in the basement of a high-rise building demonstrated rapid vertical smoke transport through a stairwell. For a 0.125 MW fire scenario, smoke reached areas associated with the fourth or fifth floor within approximately 300 s, while the smoke-layer height at the stairwell corner decreased to approximately 2.0 m (Escrig et al., 2026). Such observations demonstrate the importance of considering actual vertical flow paths when evaluating smoke-control strategies.
The stack effect further contributes to smoke propagation. The pressure difference between the interior and exterior of a tall building is influenced by building height and temperature differences. During a fire, buoyancy-driven flow can increase vertical air movement and accelerate smoke transport. Cho and coauthors (2025) investigated a 49-storey residential building using CFD and System Dynamics and reported that the stack effect associated with building height can accelerate smoke propagation and increase risks during firefighting and rescue operations.
External wind represents an additional source of uncertainty. Recent research using CFD-generated wind-field data demonstrated that high-rise fire scenarios can involve complex airflow patterns, including changes in wind speed, direction, and vertical velocity (Fischer et al., 2022). Consequently, wind and fire-induced buoyancy should be considered as interacting phenomena when assessing high-rise fire behaviour.

The principal engineering factors affecting fire development and fire spread are summarized in Table 1.

Table 1. *Principal engineering factors affecting high-rise building fire development and spread*

Factor	Engineering effect	Values
Fire load	Determines potential heat release and fire duration	Increased fire severity
Ventilation	Controls oxygen supply and fire growth	Changes HRR and smoke production
Building height	Increases vertical pressure differences	Enhanced smoke movement
Vertical shafts	Provide low-resistance flow paths	Rapid vertical smoke spread
External wind	Modifies airflow and flame trajectory	Increased uncertainty in fire spread
Façade configuration	May provide vertical fire pathways	External fire spread
Compartmentation	Limits fire and smoke propagation	Reduced fire spread
Structural system	Determines response to thermal exposure	Loss of load-bearing capacity

Internal and external fire spread

Fire spread within high-rise buildings can occur horizontally between adjacent compartments and vertically through openings, shafts, façades, and other building elements. Effective compartmentation is therefore a fundamental passive fire protection measure.
External fire spread represents an additional risk because flames emerging from windows can impinge on façades and subsequently spread towards upper floors. This problem becomes particularly significant when combustible façade materials or inadequately protected cavities are present.
A recent review of existing high-rise residential buildings with combustible façades emphasized that façade systems, construction details, cavity barriers, joints, and seams must be considered when evaluating the potential for vertical external fire spread (Li et al., 2018). The authors also highlighted limitations of conventional façade fire testing in representing complex real-world fire scenarios.
The interaction between internal fire, façade geometry, cavity configuration, and external wind makes predicting façade fire spread particularly difficult. Therefore, façade fire safety should be considered as an integral component of the overall building fire safety strategy.

Internal and external fire spread

An additional engineering issue concerns the applicability of conventional design fire curves to large high-rise compartments. Traditional structural fire design commonly assumes relatively uniform burning and homogeneous temperature conditions within a compartment. However, research on large compartments indicates that fire may remain localized and move across a floor plate as combustible materials are consumed (Rein et al., 2007).
This phenomenon, known as a travelling fire, can produce substantially different thermal exposure than a uniform compartment fire. Rein et al. proposed an engineering methodology for defining realistic fire environments in complex multi-storey buildings, demonstrating the potential importance of non-uniform fire development for structural engineering (Ronchi & Nilsson, 2013).
Subsequent research has emphasized both the potential value and the limitations of travelling-fire models. Paper (Dai et al., 2017). identified the lack of sufficiently detailed large-scale experimental data as an important limitation for further development and validation of such models (Stern-Gottfried & Rein, 2012). Nevertheless, travelling-fire scenarios provide

an important basis for performance-based structural fire assessment in large open-plan compartments.

FIRE SAFETY AND ENGINEERING PROTECTION MEASURES

High-rise fire safety depends on the combined performance of passive and active protection systems. Because no individual measure can reliably control every possible fire scenario, these systems should be designed as complementary components of an integrated fire safety strategy.

Passive fire protection

Passive fire protection aims to limit fire development and propagation without requiring active intervention. Principal measures include fire-resistant structural elements, compartmentation, fire-rated walls and floors, fire doors, and fire stopping of service penetrations.
Compartmentation is particularly important because it limits horizontal and vertical fire spread and helps maintain protected circulation and escape routes. The effectiveness of compartmentation depends not only on the nominal fire resistance of individual elements but also on the continuity and integrity of the overall barrier system.
Façade protection should similarly be considered as part of passive fire safety. Appropriate material classification, cavity barriers, fire-resistant construction details, and control of joints and penetrations can reduce the probability of rapid external fire spread (Li et al., 2018).

Active fire protection

Active systems include automatic detection, alarm systems, sprinklers, and other suppression technologies. Early detection is particularly important in high-rise buildings because the vertical distance and complexity of evacuation and firefighting operations can increase response times.
The FDS investigation by Vovk and coauthors (2025) demonstrated that detector performance can be influenced by airflow and external wind conditions. In the investigated scenarios, wind and openings modified the airflow field and affected detector response (Dundar & Selamet, 2023). This indicates that detector performance should be evaluated not only on the basis of nominal spacing but also with consideration of airflow conditions where these are critical to system performance.
Automatic sprinkler systems can limit fire growth and heat release and consequently reduce the potential for fire spread. Their effectiveness, however, depends on appropriate design, maintenance, water supply, and compatibility with the fire scenario.

Smoke-control systems

Smoke-control systems are particularly important because smoke can propagate through vertical pathways considerably faster than the fire itself. Mechanical smoke extraction, stairwell pressurization, and protected elevator lobbies are among the principal engineering measures used to control smoke movement.
Alianto and coauthors (2022) reviewed 163 publications on smoke management in high-rise buildings. They emphasized the importance of smoke movement through elevator shafts, ventilation shafts, and stairwells, as well as the application of pressurization and extraction systems (Sun et al., 2013). Their review also supports performance-based approaches when prescriptive requirements cannot adequately describe actual building and fire conditions.
The effectiveness of smoke-control systems depends on building geometry, pressure differences, leakage characteristics, shaft configuration, and the interaction between natural and mechanical airflow. Consequently, smoke-control systems for complex high-rise buildings should preferably be evaluated under representative fire and environmental scenarios.

Figure 1 illustrates the principal sequence from fire ignition and growth to smoke movement, vertical and façade fire spread, and structural exposure. The schematic emphasizes the coupled nature of the physical processes rather than representing a single specific fire scenario.

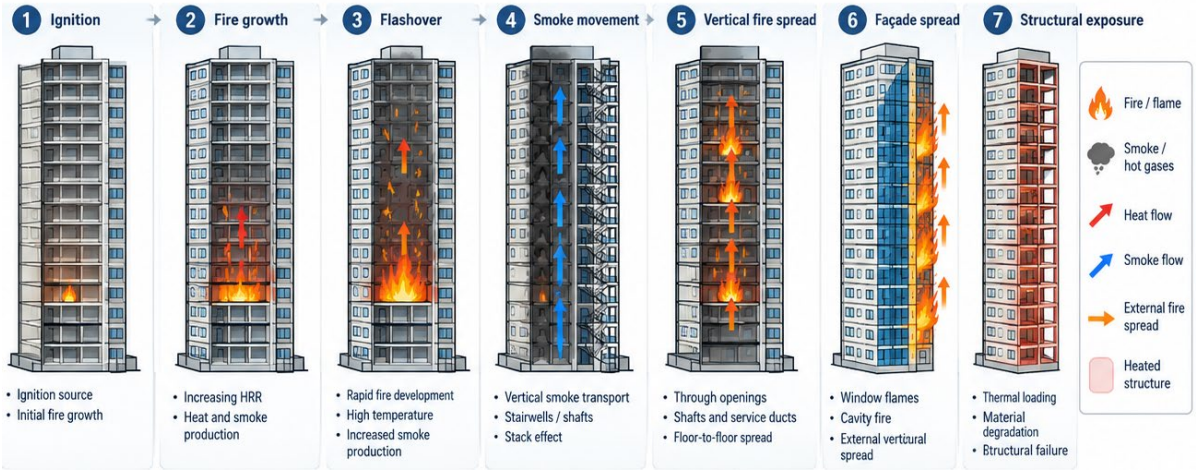


Fig. 1. *Schematic representation of fire development and fire spread mechanisms in a high-rise building.*

EVACUATION, FIREFIGHTING AND HUMAN SAFETY

Although the main focus of this review is engineering, evacuation and firefighting cannot be separated from the physical development of a high-rise fire. The available time for safe evacuation is directly influenced by smoke movement, temperature, toxic gases, and the performance of fire protection systems.

The concept of Available Safe Egress Time (ASET) provides an engineering framework for comparing the time before untenable conditions develop with the Required Safe Egress Time (RSET). In high-rise buildings, smoke propagation through stairwells and other vertical pathways can substantially reduce available evacuation time. Evacuation modelling research has demonstrated that high-rise evacuation is influenced by the configuration of stairs and elevators, occupant distribution, building use, and evacuation strategies (Vovk et al., 2025).

Firefighting operations are similarly constrained by the physical characteristics of high-rise buildings. Cho and colleagues (2025) discussed the limited operational reach of aerial ladder equipment and the need for firefighters to enter buildings through protected internal routes when fires occur above the practical reach of external equipment.

The same study linked CFD-based smoke propagation with a System Dynamics model to examine how smoke spread interacts with firefighting and evacuation operations (Cho et al., 2025). This type of coupled modelling illustrates the potential benefit of integrating physical fire phenomena with operational risk assessment.

FIRE RISK ASSESSMENT AND ENGINEERING ANALYSIS

The complexity of high-rise fires makes engineering analysis an essential component of both new building design and assessment of existing buildings. Risk assessment should consider not only the probability of fire initiation but also the consequences associated with different fire-development and fire-spread scenarios.

A basic risk formulation can be expressed as:

$$R = P \times C \tag{1}$$

where (R) is the risk, (P) is the probability of occurrence, and (C) represents the potential consequence. Although simple qualitative and semi-quantitative approaches are useful for

screening and prioritization, complex high-rise buildings increasingly require more advanced engineering methods.

CFD and FDS-based analysis

Computational Fluid Dynamics (CFD), including FDS, enables detailed investigation of fire-induced flow, temperature, smoke concentration, and pressure fields. The reviewed studies demonstrate applications of CFD to smoke movement, stack effect, detector response, wind–fire interactions, and firefighting risk (Cho et al., 2025; Dundar & Selamet, 2023; Fischer et al., 2022). The principal advantage of CFD is its ability to resolve spatially distributed physical phenomena that are difficult to represent using simplified calculations.
The study by Fischer and co-authors (2022) also demonstrates the possibility of combining CFD-generated data with machine-learning methods to obtain faster predictions of complex wind fields. Such approaches may become useful for repeated engineering analyses, although they should currently be regarded as complementary to physically based simulation.

Structural fire engineering

Structural response represents another important component of high-rise fire safety. Elevated temperatures can reduce the strength and stiffness of structural materials, cause thermal expansion and deformation, and potentially contribute to local or progressive structural failure.
For steel structures, the spatial and temporal distribution of fire exposure is particularly important. Research on travelling fires has shown that localized and moving fire scenarios can generate thermal exposures substantially different from those predicted by uniform standard-fire assumptions (Rein et al., 2007; Stern-Gottfried & Rein, 2012; Wu et al., 2025).
Fischer et al. demonstrated the relevance of travelling-fire modelling for performance-based structural fire engineering of steel-frame buildings, highlighting the importance of realistic fire scenarios where uniform fire assumptions may be inappropriate (Wu et al., 2025).

Performance-based fire safety engineering

Performance-based fire safety engineering provides a framework for integrating fire dynamics, smoke movement, evacuation, protection systems, and structural response. Instead of relying exclusively on prescriptive requirements, performance-based approaches evaluate whether defined safety objectives are achieved under specified fire scenarios.
Li and coauthors (2018) identified performance-based design as an important direction in modern fire safety engineering for high-rise buildings and emphasized the importance of defining fire scenarios, performance objectives, and appropriate engineering criteria.

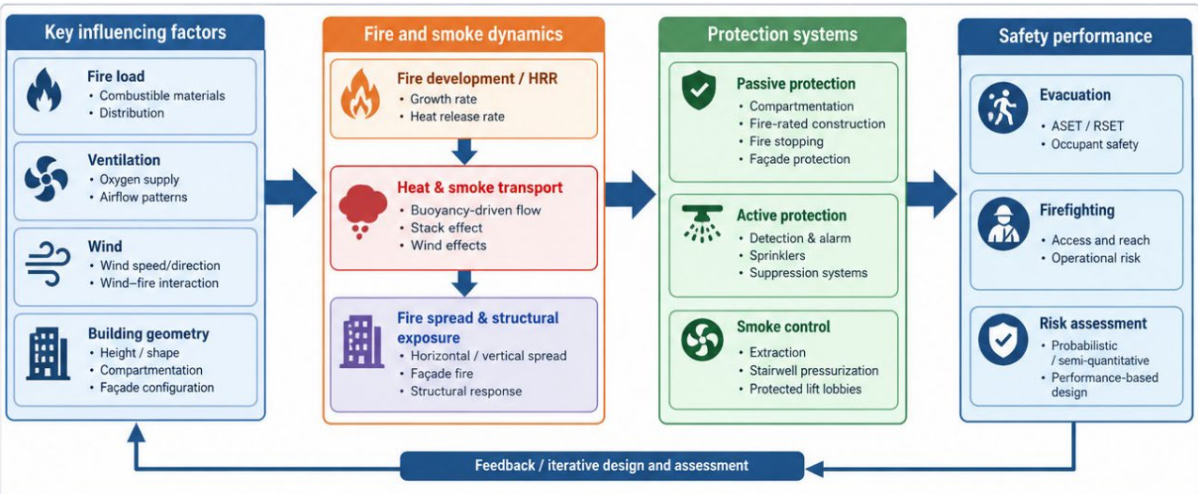


Fig. 2. *Schematic representation of fire development and fire spread mechanisms in a high-rise building.*

Figure 2 provides an overview of the engineering interactions among fire load, ventilation, wind, and building geometry, as well as fire development and heat release, smoke and heat transport, fire spread and structural exposure, and passive and active fire protection measures.

DISCUSSION

The reviewed literature demonstrates that fire safety in high-rise buildings is a coupled engineering problem in which fire development, smoke movement, fire spread, protection systems, structural response, evacuation, and firefighting are strongly interconnected.

Several dominant engineering factors can be identified. First, fire development is strongly influenced by fire load, ventilation, openings, and compartment characteristics. Second, vertical shafts and the stack effect can substantially accelerate smoke propagation. Third, façade systems may provide an important pathway for vertical external fire spread, particularly when combustible materials or inadequately protected cavities are present. Fourth, conventional uniform fire scenarios may not adequately represent all realistic high-rise fires, particularly in large open-plan compartments where travelling fires may develop.

The performance of passive and active protection systems is therefore critical. Compartmentation, fire-resistant construction, detection, sprinklers, and smoke-control systems should be considered as interacting components of a common fire safety strategy. Their performance may also depend on wind, ventilation, building geometry, and the specific fire scenario.

Modern computational methods provide increasingly powerful tools for high-rise fire assessment. CFD and FDS can be used to investigate fire development, smoke movement, airflow, and wind–fire interactions, while structural fire models can evaluate the thermal and mechanical response of load-bearing systems. Risk-based and performance-based approaches can then integrate these results into an overall assessment.

Nevertheless, important limitations remain. Advanced models depend on assumptions concerning fire growth, ventilation, material properties, and boundary conditions, while experimental data for realistic large-scale high-rise fire scenarios remain limited. Further research should therefore focus on validation of coupled fire–smoke–structure models, realistic façade-fire scenarios, travelling fires, wind effects, and integrated performance-based assessment of existing high-rise buildings.

CONCLUSIONS

High-rise building fire safety cannot be reliably addressed by considering individual protection measures in isolation. The reviewed studies indicate that fire development, smoke

and heat transport, internal and external fire spread, structural response, evacuation, and firefighting are closely interconnected and should therefore be considered within an integrated engineering framework.

The assessment of high-rise fire safety should combine realistic fire scenarios with appropriate passive and active protection measures, smoke-control analysis, structural fire engineering, evacuation assessment, and risk-based evaluation. Advanced computational approaches, including CFD/FDS and performance-based fire safety engineering, provide valuable tools for analysing these interactions and supporting engineering decisions.

At the same time, the reliability of such assessments depends on the quality of input assumptions, model validation, and the availability of realistic experimental data. Future research should therefore emphasize validation of coupled fire–smoke–structure models, realistic façade-fire and travelling-fire scenarios, wind effects, and integrated assessment of existing high-rise buildings.

Overall, an integrated engineering approach combining realistic fire scenarios, smoke and heat transport analysis, passive and active protection, structural fire engineering, and risk assessment provides a more reliable basis for high-rise fire safety design and evaluation.

ACKNOWLEDGEMENT

This work has been supported by the Ministry of Science, Technological Development, and Innovation of the Republic of Serbia, through the Contract for the scientific research financing in 2026, 451-03- 34/2026-03/200108 to build resilient infrastructure, promote inclusive and sustainable industrialization, and foster innovation, which is the ninth goal of the UN's 2030 Agenda for Sustainable Development.

REFERENCES

Alianto, B., Nasruddin, N., & Nugroho, Y. S. (2022). High-rise building fire safety using mechanical ventilation and stairwell pressurization: A review. *Journal of Building Engineering*, *50*, 104224. https://doi.org/10.1016/j.jobe.2022.104224

Cho, M., Song, M., Yun, H., Kim, J., & Yoon, J. (2025). Risk Analysis of Firefighting and Rescue Operations in High-Rise Buildings: An Exploratory Study Utilising a System Dynamics Approach. *Fire*, *9*(1), 25. https://doi.org/10.3390/fire9010025

Dai, X., Welch, S., & Usmani, A. (2017). A critical review of "travelling fire" scenarios for performance-based structural engineering. *Fire Safety Journal*, *91*, 568–578. https://doi.org/10.1016/j.firesaf.2017.04.001

Dundar, U., & Selamet, S. (2023). Fire load and fire growth characteristics in modern high-rise buildings. *Fire Safety Journal*, *135*, 103710. https://doi.org/10.1016/j.firesaf.2022.103710

Escrig, T., Soto, T., Serrano-Lanzarote, B., & Ruiz, A. G.-P. (2026). Preliminary Study on Measures to Improve Fire Safety in Existing High-Rise Residential Buildings with Combustible Façades. *Buildings*, *16*(6), 1196. https://doi.org/10.3390/buildings16061196

Fischer, E. C., Varma, A. H., & Gordon, J. A. (2022). Performance-Based Structural Fire Engineering of Steel Building Structures: Traveling Fires. *Frontiers in Built Environment*, *8*, 907237. https://doi.org/10.3389/fbuil.2022.907237

Li, G.-Q., Zhang, C., & Jiang, J. (2018). A Review on Fire Safety Engineering: Key Issues for High-Rise Buildings. *International Journal of High-Rise Buildings*, *7*(4), 265–285. https://doi.org/10.21022/IJHRB.2018.7.4.265

Rein, G., Zhang, X., Williams, P., Hume, B., Heise, A., Jowsey, A., Lane, B., & Torero, J. (2007). *Multi-story Fire Analysis for High-Rise Buildings*.

Ronchi, E., & Nilsson, D. (2013). Fire evacuation in high-rise buildings: A review of human behaviour and modelling research. *Fire Science Reviews*, *2*(1), 7. https://doi.org/10.1186/2193-0414-2-7

Stern-Gottfried, J., & Rein, G. (2012). Travelling fires for structural design–Part I: Literature review. *Fire Safety Journal*, *54*, 74–85. https://doi.org/10.1016/j.firesaf.2012.06.003

Sun, J., Hu, L., & Zhang, Y. (2013). A review on research of fire dynamics in high-rise buildings. *Theoretical and Applied Mechanics Letters*, *3*(4), 042001. https://doi.org/10.1063/2.1304201

Vovk, S., Kopchak, B., Kushnir, A., Shapovalov, O., & Ferents, N. (2025). Research Into the Dynamics of Fire Development and the Efficiency of the Fire Alarm System in a High-Rise Building. *Proceedings of the Latvian Academy of Sciences. Section B. Natural, Exact, and Applied Sciences.*, *79*(5–6), 289–301. https://doi.org/10.2478/prolas-2025-0024

Wu, L., Yue, S., Cheng, H., & Zhong, M. (2025). Fire smoke spread experiment in the basement of high-rise buildings. *Journal of Tsinghua University (Science and Technology)*, *65*, 469–478. https://doi.org/10.16511/j.cnki.qhdxxb.2025.26.001

Zhang, S., Xu, Z., & Wei, J. (2026). Channel–Spatial Fusion Attention for Wind Field Prediction in High-Rise Building Fire Scenarios. *Sensors*, *26*(9), 2666. https://doi.org/10.3390/s26092666

DOI:10.5937/IIZS26498I

EDS-BASED CHARACTERIZATION OF INHALABLE METAL AEROSOLS IN OCCUPATIONAL ENVIRONMENTS

Research paper

Milana Ilić Mićunović[1*], Borut Kosec[2], Zoran Čepić[3], Slađana Jovanović[4], Boris Agarski[5]

[1,3,4,5]University of Novi Sad, Faculty of Technical sciences, Novi Sad, Serbia
[2]University of Ljubljana, Faculty of Natural Sciences and Engineering, Ljubljana, Slovenia

Abstract: Workplace exposure to airborne metallic aerosols during thermal joining processes represents significant occupational health risks. This study presents a comparative microstructural and elemental characterization of inhalable welding aerosols generated during Metal Active Gas (MAG) and Tungsten Inert Gas (TIG) processing of structural steels. Personal aerosol sampling was conducted in the operator's breathing zone using mixed cellulose ester (MCE) filters at a flow rate of 3.5 L/min. Microchemical analysis was performed using Field Emission Scanning Electron Microscopy with Energy-Dispersive X-ray Spectroscopy (FEG-SEM/EDS), utilizing both point-spectrum acquisition and EDS Layered Imaging for spatial mapping. The results revealed distinct chemical signatures between the two processes: TIG-generated particles were dominantly composed of iron oxides (79–83 wt% Fe) with trace amounts of Ni and Cr, whereas MAG aerosols mainly contained manganese (31.37–42.28 wt% Mn) and silicon (0.45–7.29 wt% Si) due to the intense vaporization and condensation of filler wire deoxidizers. EDS elemental mapping confirmed the co-localization of Mn, Si, and O within complex spherical submicron aggregates. These findings highlight the efficacy of SEM-EDS in resolving single-particle chemical heterogeneity and providing process-specific elemental profiles essential for targeted occupational health risk assessments and exposure control strategies.
Key words: EDS, welding aerosols, occupational exposure

INTRODUCTION

Measurement and characterization of airborne particulate matter in the occupational environment are of critical importance for the prevention of occupational respiratory diseases. Particle size directly determines the site of deposition within the respiratory tract, which is why a standardized classification into inhalable and respirable fractions is applied in industrial hygiene (ISO 7708, SRPS EN 481).

Inhalable fraction includes particles with an aerodynamic diameter of up to 100 μm that are inhaled through the nose and mouth. The primary site of deposition is the upper respiratory tract (nasal cavity, pharynx, and trachea). This fraction is predominant in processes such as grinding, stone processing, and bulk material handling (Ilic Micunovic, 2024, SRPS EN 481).

Thoracic fraction consists of particles with an aerodynamic diameter of less than 10μm (with a 50% collection efficiency cut-point at 10μm) that pass through the larynx and penetrate into the conducting airways of the lungs, the tracheobronchial tree. These particles primarily deposit in the trachea, main bronchi, and bronchioles, causing localized inflammatory responses, bronchospasms, and exacerbation of pre-existing airway conditions such as asthma and chronic bronchitis (Brown, 2013).

Respirable fraction consists of particles with an aerodynamic diameter of less than 2.5 μm (with a 50% collection efficiency cut-point at 4 μm) that penetrate deep into the respiratory bronchioles and alveoli. Due to their size, these particles bypass the respiratory tract's natural clearance mechanisms and remain permanently deposited in the lung tissue or enter systemic circulation (Ribalta, 2019, Brown, 2013).

Monitoring fractions enables accurate risk assessment and comparison with occupational exposure limits (OELs), as coarser particles cause local irritation and mucosal damage, whereas respirable particles lead to chronic fibrotic and systemic diseases (Ribalta, 2019).

Transition metals present in industrial aerosols, during welding, casting, thermal cutting and electroplating, exhibit high toxicity, primarily through the generation of reactive oxygen species

[1] Corresponding author, milanai@uns.ac.rs, ORCID: 0000-0002-5673-4690
[2]borut.kosec@ntf.uni-lj.si, ORCID: 0009-0001-8117-9721
[3]zorancepic@uns.ac.rs, ORCID: 0000-0001-5853-4767
[4]sladjana.jovanovic@uns.ac.rs, ORCID: 0009-0001-2226-1645
[5] agarski@uns.ac.rs , ORCID: 0000-0002-7206-5714

through Fenton and Fenton-like reactions, leading to oxidative stress, DNA damage, and cellular inflammation. Chronic inhalation of iron oxides leads to siderosis ("welder's lung"). Although siderosis was traditionally considered a benign pneumoconiosis, contemporary research indicates that the presence of respirable iron causes persistent tissue inflammation and synergistically increases the risk of chronic obstructive pulmonary disease (COPD) (Liu, 2025). Respirable manganese aerosols cross the alveolar-capillary membrane and reach the central nervous system via retrograde axonal transport along the olfactory nerve. Chronic exposure to manganese causes an irreversible neurodegenerative disorder that clinically mimics Parkinson's disease. Hexavalent chromium is a potent mutagen and Group 1 carcinogen (IARC). It readily crosses cell membranes, where it is reduced, generating ROS and DNA adducts/crosslinks, leading to lung cancer, nasal ulcerations, and chronic asthmatic bronchitis. Inhalation of nickel compounds (particularly nickel subsulfide and nickel oxide) is associated with a high risk of developing lung and nasal cavity cancers. Nickel inhibits DNA repair mechanisms and acts as a strong allergen, causing occupational asthma and contact dermatitis (Khoshnaw, 2023). Titanium is predominantly present in the form of titanium dioxide (TiO_2). While bulk particles are considered less toxic, ultrafine and nano-sized TiO_2 particles possess high surface reactivity, inducing alveolar inflammatory responses and pulmonary fibrosis, and are classified as possibly carcinogenic to humans (IARC Group 2B) (Rahul, 2021). Standard gravimetric and bulk chemical analyses of airborne particulate matter provide essential data on total mass concentration, but they often mask the intrinsic heterogeneity of complex industrial aerosols. Advanced microanalytical techniques such as Scanning Electron Microscopy coupled with Energy-Dispersive X-ray Spectroscopy (SEM-EDS), Transmission Electron Microscopy (TEM), and automated digital image analysis offer single-particle resolution that is indispensable for comprehensive occupational health risk assessment.

SEM-EDS mapping allows for the identification of specific toxic elements (e.g., transition metals like Cr, Ni, Mn, Fe) within individual particles. Microanalysis distinguishes between externally mixed aerosols where distinct chemical species exist as separate particles, and internally mixed aerosols where heterogeneous agglomerates containing multiple elements. This distinction is critical because internal chemical interactions can significantly alter particle solubility, bio accessibility, and toxicity (Stefaniak, 2010).

The main objective of this study is to perform a comparative chemical and microstructural characterization of workplace metallic aerosols generated during MAG and TIG material processing. Utilizing Energy-Dispersive X-ray Spectroscopy (EDS) via point-spectrum analysis and elemental mapping, the study aims to identify the primary elemental composition (wt%) of inhalable particles produced under different process conditions, specifically comparing aerosol characteristics generated during MAG welding with Mn and Si containing filler wire and TIG welding under an argon shielding atmosphere. Furthermore, it seeks to determine the spatial distribution and localization of key alloying and deoxidizing elements such as Fe, Mn, Si, Cr, Ni, and O within individual particles and agglomerates. Ultimately, this approach establishes a clear spectroscopic correlation between processing parameters and process-specific elemental signatures relevant to occupational exposure assessment, thereby providing concise data for workplace risk assessment.

MATERIAL AND METHODS

Aerosol Sampling and Preparation

Workplace aerosol particles generated during MAG and TIG metal processing were collected to evaluate the operator's direct exposure to airborne emissions. Sampling was conducted using a ZAMBELLI EGO PLUS TT personal air sampler equipped with a 25 mm mixed cellulose ester (MCE) filter. The device was calibrated prior to each experimental run and operated at a constant flow rate of 3.5 L/min with a conical inlet, specifically chosen for capturing the inhalable aerosol fraction. To capture representative breathing-zone samples, the filter inlet was secured near the operator's clavicle, approximately 30 cm from the breathing area.

The sampled particulate matter originated from the thermal joining of structural and tool steel specimens. Aerosol generation was evaluated across two distinct process configurations: Metal Active Gas (MAG) welding using solid wire filler materials rich in manganese (Mn) and silicon (Si) deoxidizers, and Tungsten Inert Gas (TIG) welding conducted under a protective argon atmosphere. The collected airborne samples thus represent a mix of condensed metallic vapors, oxidized fumes, and micro-particles emitted directly into the breathing zone during the melting and solidification of the base and filler metals.

Scanning Electron Microscopy (SEM)

Microstructural and morphological evaluations of the collected airborne particles were conducted using a Field Emission Scanning Electron Microscope (FEG-SEM, Thermo Fisher Scientific Quattro S). The instrument is equipped with multiple imaging modes, including Secondary Electron Imaging (SEI) for high-resolution surface topography and Backscattered Electron Imaging (BEI) for compositional contrast. High-magnification micrographs (ranging from 1 to 10 μm scale bars) were acquired to evaluate individual particle geometries, sphericity, and agglomeration phenomena across the MCE filter matrix.
For elemental and microchemical analysis, the FEG-SEM system is integrated with an Energy-Dispersive X-ray Spectroscopy (EDXS) detector (Ultim® Max). Microchemical characterization was performed using both localized point-spectrum acquisition and EDS elemental mapping (EDS Layered Imaging). Accelerating voltages and acquisition parameters were optimized to capture characteristic Kα and Lα emission lines for key metallic species specifically Fe, Mn, Si, Cr, Ni, and Ti as well as light elements (O, C) originating from the substrate and oxidized phases. Spatial element distribution maps were generated to evaluate element co-localization within individual micro-spheres and complex particle aggregates.

RESULTS AND DISCUSSION

Elemental Composition of TIG and MAG Aerosols

The EDS point-spectrum analysis revealed distinct chemical profiles for aerosol particles generated by the two investigated processes (Table 1.). Particles captured during TIG processing (without additives) are characterized by a high iron content ranging from 79 to 83 wt% Fe alongside oxygen, indicating the formation of primary iron oxides (Fig. 1.). Minor trace amounts of nickel (up to 3.63 wt% Ni) were also detected, closely reflecting the base and filler metal compositions. Conversely, MAG aerosols generated with additives exhibit a strong enrichment in manganese, reaching 31.37 to 42.28 wt% Mn, and silicon between 0.45 and 7.29 wt% Si, together with moderate amounts of chromium (up to 3.89 wt% Cr). This chemical signature confirms the intense evaporation and condensation of Mn-Si deoxidizing agents and alloying elements present in the MAG wire. Additionally, minor aluminum signals (0.18–0.49 wt% Al) observed across both process conditions likely originate from background scatter or trace constituents in the sampling setup. Furthermore, high carbon and nitrogen contents detected in certain area spectra, such as Spectrum 2, originate from the underlying mixed cellulose ester filter matrix rather than the metallic particles themselves (Fig. 2.).

Table 1. Elemental composition of representative aerosol particles derived from EDS point spectra.

Process Condition	Spectrum Label	Fe (wt%)	Mn (wt%)	Si (wt%)	Ni (wt%)	Cr (wt%)	O (wt%)	Al (wt%)
TIG (without additives)	Spectrum 7	79.24	—	—	—	—	20.76	-
TIG (without additives)	Spectrum 3	62.01	—	—	3.63	—	34.09	0.26
MAG (with additives)	Spectrum 2	16.21	31.37	6.92	—	3.61	41.40	0.49
MAG (with additives)	Spectrum 3	14.50	42.28	7.29	—	3.89	31.86	0.18

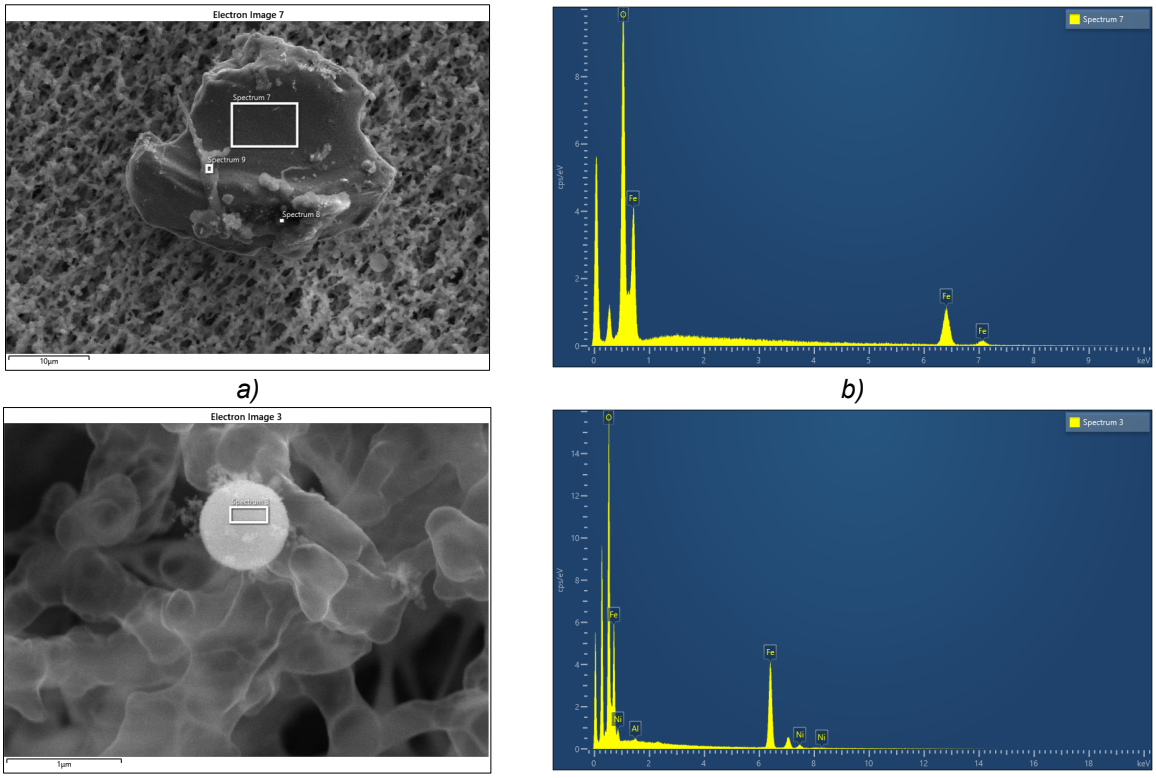


Fig. 1. *Representative SEM micrographs and corresponding EDS point spectra of TIG aerosol particles: (a, c) particle morphology, and (b, d) their elemental composition.*

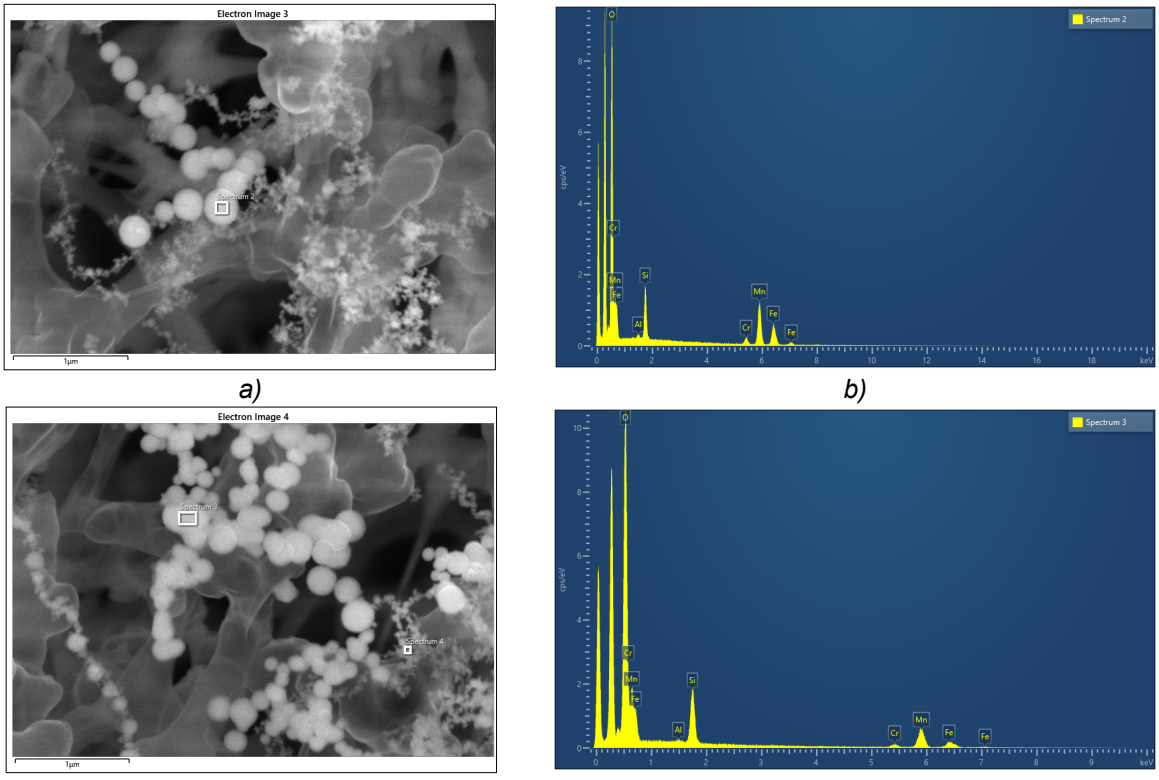
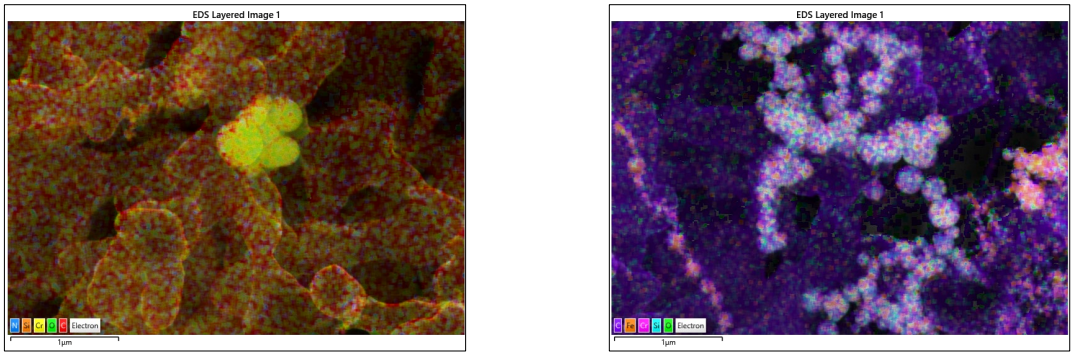


Fig. 2. *Representative SEM micrographs and corresponding EDS point spectra of MAG aerosol particles: (a, c) particle morphology, and (b, d) their elemental composition.*

Elemental mapping via EDS Layered Imaging confirmed the localization of key elements within individual particles across the investigated process conditions. In MAG aerosols, the spatial signals for manganese, silicon, and oxygen overlap directly over the spherical particles, confirming the formation of complex mixed Mn-Si-Fe oxides resulting from vapor condensation (Fig. 3a). Conversely, larger and more irregularly shaped particles exhibit a distinctly heterogeneous element distribution, characterized by iron-rich cores surrounded by localized surface oxidation (Fig. 3b).



a) *b)*

***Fig. 3**. Representative EDS elemental mapping (Layered Imaging) showing the spatial distribution and co-localization of key elements (Fe, Mn, Si, O, Cr) in: (a) MAG spherical aerosols, and (b) irregular TIG particles.*

These findings demonstrate the value of combining SEM morphology, EDS point spectra, and elemental mapping for characterizing the chemical heterogeneity of individual airborne particles. From an occupational exposure perspective, the pronounced manganese enrichment observed in MAG particles is particularly relevant due to associated inhalation risks. However, EDS weight percentages describe comparative, process-specific elemental profiles rather than absolute airborne concentrations or inhaled doses. The semi-quantitative nature of EDS, as well as substrate interaction with the MCE filter, should be considered during interpretation.

CONCLUSION

This study demonstrates that Energy-Dispersive X-ray Spectroscopy EDS provides a rapid and spatially resolved approach for characterizing and differentiating airborne metallic particles generated during welding processes. The elemental analysis clearly distinguished the physical and chemical mechanisms of two distinct operations: MAG processing produces aerosols heavily enriched in manganese (up to 42.28 wt% Mn) and silicon from filler wire vaporization, whereas TIG processing yields predominantly iron rich oxide particles. Recognizing these distinct chemical profiles is vital for assessing process-specific occupational health risks and implementing targeted exposure controls. While EDS provides exceptional speed and spatial precision for elemental identification, future research should incorporate complementary analytical techniques such as X-ray Diffraction (XRD), X-ray Photoelectron Spectroscopy (XPS), or Transmission Electron Microscopy (TEM) to precisely determine the underlying crystal structures, phase transformations, and oxidation states of the collected airborne particulates.

ACKNOWLEDGEMENT

This research has been supported by the Ministry of Science, Technological Development and Innovation (Contract No. 451-03-34/2026-03/200156) and the Faculty of Technical Sciences, University of Novi Sad through project "Scientific and Artistic Research Work of Researchers in Teaching and Associate Positions at the Faculty of Technical Sciences, University of Novi Sad 2026" (No. 01-3609/1).

REFERENCES

ISO 7708 (1995): Air quality — Particle size fraction definitions for health-related sampling.

SRPS EN 481 (2010): Vazduh na radnom mestu - Definisanje veličine frakcija čestica za merenje u vazduhu.

Ilic Micunovic, M., Budak, I., Vukelic, D., Djurovic Koprivica, D., Kuzmanovic, M., Agarski, B., Puskar, T (2024). Investigation of the Geometric Characteristics of Inhalable Particles Emitted from the Process of Grinding Dental Restorations. *Applied Sciences*, 14, 5169.

Brown, J.S., Gordon, T., Price, O. (2013). Thoracic and respirable particle definitions for human health risk assessment. *Particle and Fibre Toxicology,* 10, 12.

Ribalta, C., López-Lilao, A., Estupiñá, S., Fonseca, A.S., Tobías, A., García-Cobos, A., Minguillón, M.C., Monfort, E., Viana, M. (2019). Health risk assessment from exposure to particles during packing in working environments, *Science of the Total Environment*, 671, 474-487.

Liu, Y., Yang, R., Chai, Y., Wang, Y., (2025). Welding and burnishing dusts' exposure characteristics and health risk assessment in electromechanical processing workshop: Based on oxidation potential and EPA, *Building and Environment*, 279, 112971.

Khoshnaw, F., (2023). Chapter 1 - An introduction to welding of metallic materials, Editor(s): Fuad Khoshnaw, *Welding of Metallic Materials*, Elsevier, 1-35.

Rahul, M., Sivapirakasam, S.P., Vishnu, B.R., (2021). Health issue owing to exposure with welding fumes and their control strategies at the source–a review, *Materials Today*, Proceed., 46, 9239-9245

Stefaniak, A. B., Virji, M. A., & Day, G. A. (2010). Characterization of chemical and physical properties of airborne particles to inform exposure and risk assessment. *Inhalation Toxicology*, 22(S2), 19–38.

DOI:10.5937/IIZS26504P

SMART FACTORY, SILENT EMPLOYEES: THE HUMAN PARADOX OF DIGITAL SUSTAINABLE MANUFACTURING

Research paper

Leontina Pap[1]

[1]University of Novi Sad, Technical faculty "Mihajlo Pupin", Zrenjanin, Serbia

Abstract: Smart factories integrate cyber-physical systems, the Internet of Things, artificial intelligence and advanced data analytics to improve operational efficiency and environmental performance. While these technologies offer clear benefits, their implementation without corresponding updates to job roles, training systems and organizational practices creates a socio-technical imbalance. Employees risk becoming "silent employees" remaining physically present yet functionally muted, with their tacit knowledge underutilized. This paper reviews Industry 4.0, Industry 5.0, socio-technical systems and sustainable manufacturing research to identify the main factors behind the disconnect between technology, organization and human capability, and its implications for environmental performance.

Key words: smart factories, socio-technical imbalance, silent employees, human-centric approach, environmental performance

INTRODUCTION

Digital technologies are increasingly transforming manufacturing systems by changing the way production processes are designed, monitored and managed. Smart factories integrate cyber-physical systems, the Internet of Things, artificial intelligence, collaborative robotics and advanced data analytics to improve operational efficiency, production flexibility, process quality and resource utilization (Zhang et al., 2023). Recent research indicates that the application of these technologies can contribute to improved energy efficiency, reduced material consumption and enhanced process performance, positioning digitalization as an important component of contemporary manufacturing development (Ghobakhloo et al., 2025). The increasing integration of digital technologies also has important implications for the organization of the human work. It is altering existing job requirements and employee responsibilities by automation of routine activities, with introduction of data - driven decision making and the growing autonomy of production systems. As new technology arrives, employees face significant challenges, including a gap in their technical skills and a shift from physical labor to heavier mental workloads. (Mukhuty et al., 2022; Callari et al., 2025,; Lim & Hwang, 2026) The biggest shift is for the employees that are no longer working in line crafting products, instead their job has evolved into supervising automated systems and processes. This means that they only step in when something breaks down or an error occurs. These developments indicate that technological transformation affects not only production processes, but also the structure of work and the competencies required within manufacturing organizations. Modern manufacturing performance relies on a balance of three elements. These elements are technology or technological infrastructure, organizational processes and human capabilities (Frank et al., 2021; Tortorella et al., 2021). The implementation of advanced tools and technologies requires constant update of the job roles, training and development, management styles and work organization. Insufficient alignment between technological development and workforce capabilities may limit the effective utilization of employee knowledge and experience and may reduce opportunities for employee involvement in operational decision-making. This issue has gained importance with the shift from Industry 4.0 to Industry 5.0. While Industry 4.0 focusses almost entirely on digitalization and automation, Industry 5.0 brings a broader focus on human centricity, long-term resilience and environmental sustainability (Zhang et al., 2023). Within this context employees are considered as essential components of advanced production systems rather than users or operators of digital technologies.

[1] Corresponding author, leontinapap@gmail.com

Nevertheless, existing research indicates that the implementation of digital transformation may continue to place greater emphasis on technological deployment and operational efficiency than on the organizational and human requirements associated with these changes (Callari et al., 2025).

METHODOLOGY

The subject and the problem of research

The subject of this research is the human paradox in digital sustainable manufacturing and its implications for environmental performance. The core problem is that smart factories increasingly introduce advanced digital technologies to improve resource efficiency, reduce emissions and support environmental goals. However, when these technologies are implemented without corresponding updates in job roles, training systems and organizational practices, a socio-technical imbalance occurs. Employees become less involved in decision-making processes, their practical knowledge remains underutilized, and the potential environmental benefits of digitalization are only partially realized.

Research goal

The goal of this research is to examine, through a structured review of recent academic literature, how the imbalance between digital technologies, organizational processes and human capability affects the environmental performance of smart factories. The study aims to identify the main causes of this disconnect and to highlight approaches that can better align technological, organizational and human factors in order to strengthen the contribution of smart factories to environmental protection and sustainable manufacturing.

Research questions

RQ1: What are the main factors that create a disconnect between digital technologies, organizational processes and human capability in smart factories, and how does this disconnect affect environmental performance?
RQ2: What approaches can help better align technology, organization and human capability in smart factories in order to improve both operational efficiency and environmental outcomes?

Research method

This study uses a theoretical research approach based on literature review, analysis, synthesis and deduction. Peer-reviewed scientific papers that address Industry 4.0, smart factories, socio-technical systems, sustainable manufacturing and environmental performance were analyses. The findings of different authors were compared and synthesized in order to draw conclusions relevant to the relationship between human factors in digital manufacturing and environmental protection.

SOCIO-TECHNICAL SYSTEMS AND ENVIRONMENTAL PERFORMANCE IN SMART FACTORIES

Manufacturing systems are recognized as socio-technical systems where optimization of technology, organizations' processes and human capacity has to be optimized simultaneously (Cimini et al., 2020; Neumann et al., 2021; Marcon et al., 2021). In accordance with socio-technical systems theory, optimization of only one aspect will not lead to sustainable performance. The best possible outcome is achieved if the technical system (machines, digital technologies, information systems), the organizational system (processes,

structure, management practices) and the human system (skills, roles, involvement) are designed and developed at the same time. (Clegg, 2000; Neumann et al., 2021). The beginning of Industry 4.0 and appearance of Industry 5.0 resulted in numerous advanced digital technologies. They include cyber-physical systems, IoT, AI, digital twins and data analytics. Such technologies possess significant potential of improving resource efficiency, reducing energy use and greenhouse gases emissions and developing the circular economy (Zhang et al. 2023; Ghobakhloo et al. 2025). On the other hand, recent studies indicate that mere investments into technology are not sufficient. Introduction of new digital instruments without corresponding innovations in organization of work, learning, decision-making and management systems leads to socio-technical misbalance (Mukhuty et al., 2022; Marcon et al., 2021; Callari et al., 2025). Employees are deprived of opportunities to use their tacit knowledge, their involvement in problem solving and learning diminishes, and companies become increasingly dependent on automated systems. In this way, the potential of digitalization for the environment is accomplished. The concept of paradox theory adds another perspective. Companies strive for both automation (due to efficiency, consistency and good environmental performance) and human augmentation (in order to be flexible, have good judgment and innovate). They are interdependent, but often contradictory (Callari et al., 2025). If the automation pole prevails without enough regard for human capabilities and organizational redesign, there is a risk of decreasing the overall resilience of the system and its capacity to continuously improve environmental performance. Industry 5.0 literature responds to this challenge by placing human-centricity, sustainability and resilience on equal footing (Zhang et al., 2023; Ghobakhloo et al., 2025). It argues that digital manufacturing can contribute to environmental performance of the company only through active participation of employees in this process. In this way, skills development, redesigned jobs, participation and learning become crucial conditions for reaching environmental performance in smart factories rather than human-resource issues. The accomplishment of environmental performance in digital manufacturing is possible due to development of three balanced interdependent elements. As previously mentioned, these elements include advanced technology, organizational processes and human capabilities. Neglecting any of these elements weakens the overall socio-technical system and limits the contribution of smart factories to environmental protection and sustainable industrial development.

DISCUSSION

Examining the operational realities of smart manufacturing companies reveals that digital transformation extends far beyond a purely technical infrastructure upgrade. It is functioning instead as a profound socio-technical reorganization. While early Industry 4.0 paradigms frequently prioritized hardware optimization and automated data throughput, empirical evidence from leading production sites demonstrates a fundamentally more nuanced dynamic. The industrial cases of the Ericsson 5G Smart Factory in Lewisville, Texas, and Schneider Electric's facilities in Wuxi, China, and Lexington, Kentucky provides profound insights into this dynamic. Rather than corroborating deterministic narratives of total human displacement, these cases demonstrate that advanced automation alters, rather than eliminates, the human contribution.

At the Ericsson Lewisville plant, the integration of private 5G, autonomous guided vehicles, and machine learning yielded a 120% increase in output per employee alongside a 65% reduction in manual material handling (Ericsson, 2021). Crucially, this technological leap was coupled with organizational restructuring. They did not solve this by removing workers, Ericsson developed specialized training pathways for over 200 graduates to handle advanced, digitally oriented manufacturing roles (World Economic Forum, 2026). Similarly, Schneider Electric's Wuxi company recognized as a Global Sustainability Lighthouse after achieving net-zero Scope 1 and Scope 2 emissions ahead of schedule, demonstrates that breakthrough environmental gains (such as a 90% reduction in direct emissions and a 32% boost in ventilation energy efficiency via digital twins) rely heavily on human agency (World Economic Forum, 2025; Schneider Electric, 2021). Schneider Electric explicitly emphasizes

that technology serves as an enabler, while employees remain the central drivers who leverage digital tools through continuous skill development and expertise (Schneider Electric, 2021).

These industrial examples underscore the fundamental divergence between possessing raw technological capability and effectively translating it into organizational learning. As highlighted by Marcon et al. (2021), advanced manufacturing adoption is closely bound to the simultaneous co-development of social, technical, work-organization, and environmental factors. Furthermore, Tortorella et al. (2023) empirically demonstrate that Industry 4.0 technologies fundamentally modify the relationship between socio-technical practices and worker performance, proving that the outcomes of digital transformation depend heavily on how work is structured around new tools. When organizations fail to establish this alignment, they risk generating an operational disconnect. This gap gives rise to the concept of the "silent employee" a phenomenon wherein operators remain physically present on the shop floor yet functionally muted, as their tacit knowledge and practical problem-solving capabilities find fewer formal pathways into decision-making structures (D'Antonio & Chiabert, 2018). When automated systems independently dictate monitoring priorities, deviation alerts, and prescribed interventions, human operators and employees risk being downgraded from active contributors of continuous improvement to passive supervisors of automated instructions. Although this imbalance may not instantly impair short-term operational output, it introduces a severe long-term vulnerability. That can be explained as a systemic erosion of organizational learning, cognitive adaptability, and innovation potential (Bainbridge, 1983; D'Antonio & Chiabert, 2018). As demonstrated by the Ericsson and Schneider Electric cases, overcoming this risk requires an intentional organizational model that equips employees with the skills, contextual information, and institutional authority needed to interpret digital outputs and feed their experiential insights back into the system. The key issue is therefore not whether automation exists, but whether organizations create mechanisms through which human experience and machine-generated information can be combined.

CONCLUSION

The study examined the human paradox that is embedded in digital sustainable manufacturing that technological sophistication is increasing but so is the importance of human capabilities. As per RQ1, the findings indicate a significant social-technical imbalance due to the gap between digital technologies, organizational processes and human capabilities. When smart factories focus on the technological automation of production facilities, structures, and decision-making processes without ensuring the same for their work structures and decision-making processes, their employees become,"silent employees". As a result of this, while they may be present in the organization physically, their practical and tacit knowledge are not deployed to the extent it could have been. This may not affect operational efficiency immediately; however, it could lead to risks to learning, adaptability and continuous improvement in a longer time frame. Addressing RQ2, findings indicate that addressing this gap necessitates improved coordination between technology, organizational structures and people and the principles of Industry 5.0. For this reason, digitalization is not the replacement of work but rather an enhancement and empowerment of employees.

Businesses must redesign work roles, encourage participatory decision-making, and establish linkages between machine-produced data and workers' experiential knowledge. Examples from the likes of Ericsson and Schneider Electric show how the combination of the development of technology with investments in human capabilities and organizational adaptation is made. Overall, sustainability and resilience of smart manufacturing systems depend not only on technological sophistication, but also on the ability of organizations to integrate digital technologies with human knowledge and decision-making.

REFFERENCES

Bainbridge, L. (1983). Ironies of automation. Automatica, 19(6), 775–779.

Callari, T. C., Curzi, Y., & Lohse, N. (2025). Realising human-robot collaboration in manufacturing? A journey towards Industry 5.0 amid organisational paradoxical tensions. Technological Forecasting and Social Change, 219, Article 124249.

Cimini, C., Pirola, F., Pinto, R., & Cavalieri, S. (2020). A human-in-the-loop manufacturing control architecture for the next generation of production systems. Journal of Manufacturing Systems, 54, 258–271.

Clegg, C. W. (2000). Sociotechnical principles for system design. Applied Ergonomics, 31(5), 463–477.

D'Antonio, G., & Chiabert, P. (2018). How to manage people underutilization in an Industry 4.0 environment? In Product lifecycle management to support Industry 4.0 (pp. 455–464). Springer.

Ericsson. (2021). Ericsson USA 5G Smart Factory recognized as Global Lighthouse by the World Economic Forum.

Frank, A. G., Marcon, E., Soliman, M., & Gerstlberger, W. (2021). Sociotechnical factors and Industry 4.0: An integrative perspective for the adoption of smart manufacturing technologies. Journal of Manufacturing Technology Management, 33(2), 259–286.

Ghobakhloo, M., Fathi, M., Okwir, S., Al-Emran, M., & Ivanov, D. (2025). Adaptive social manufacturing: A human-centric, resilient, and sustainable framework for advancing Industry 5.0. International Journal of Production Research. Advance online publication.

Lim, J., & Hwang, J. (2026). Exploring knowledge management technologies to enhance sustainability and mitigate technostress from a collaborative perspective. Journal of Knowledge Management,

Mukhuty, S., Upadhyay, A., & Rothwell, H. (2022). Strategic sustainable development of Industry 4.0 through the lens of social responsibility: The role of human resource practices. Business Strategy and the Environment, 31(5), 2068–2081.

Neumann, W. P., Winkelhaus, S., Grosse, E. H., & Glock, C. H. (2021). Industry 4.0 and the human factor – A systems framework and analysis methodology for successful development. International Journal of Production Economics, 233, Article 107992.

Schneider Electric. (2021). World Economic Forum awards Schneider Electric Lexington, Kentucky Sustainability Lighthouse recognition and Wuxi, China Smart Factory Advanced Lighthouse status.

Tortorella, G., Fogliatto, F. S., Kumar, M., Gonzalez, V., & Pepper, M. (2023). Effect of Industry 4.0 on the relationship between socio-technical practices and workers' performance. Journal of Manufacturing Technology Management, 34(1), 44–66.

Tortorella, G., Miorando, R., Caiado, R., Nascimento, D., & Portioli Staudacher, A. (2021). The mediating effect of employees' involvement on the relationship between Industry 4.0 and operational performance improvement. Total Quality Management & Business Excellence, 32(1-2), 119–133

Zhang, C., Wang, Z., Zhou, G., Chang, F., Ma, D., Jing, Y., Cheng, W., Ding, K., & Zhao, D. (2023). Towards new-generation human-centric smart manufacturing in Industry 5.0: A systematic review. Advanced Engineering Informatics, 57, Article 102121.

DOI:10.5937/IIZS26509K

MODELLING OF ACCIDENTAL ETHANOL LEAKAGE FROM STORAGE TANKS

Research paper

Jelena Kiurski-Milošević[1*], Gordana Ludajić[2], Iris Borjanović Trusina[3], Eleonora Dejanović[4], Miodrag Ludajić[5]

[1,2,3,4]Techical college of applied sciences in Zrenjanin, Serbia
[5]Amelo doo Šid, Serbia

Abstract: Chemical leakage from storage tanks pose a significant threat to the occupational safety at first, as well as to air quality and people living nearby. Therefore, the most important issue in environmental protection and process safety is to prevent such accidents. This research will model how vapors of ethanol leakage behave in the atmosphere. it will be shown how far a vapor cloud of an easily volatile liquid can move, according to its physicochemical properties. All calculations were made for the assumption that there was an ethanol leakage in the secondary containment in which 6 storage tanks are located. The results show that the concentration of concerns for people are estimated till 31m from the tanks. So, the biggest negative impact of the accident itself is on the workers in the plant.
Key words: ethanol, leakage, modeling, vapor cloud

INTRODUCTION

The storage of flammable liquids such as ethanol entails the implementation of appropriate technical and organizational measures to ensure the safety of workers, equipment, and the environment. The possibility of accidental release cannot be entirely ruled out. A significant hazard associated with ethanol storage systems is its uncontrolled release resulting from a loss of integrity of the storage tank or associated equipment.
Evaluating fluid behavior and environmental dispersion is critical for determining the maximum safe radius during toxic leaks. These calculations directly enhance crisis management and minimize civilian and first-responder injuries. When dealing with ethanol—a highly flammable, volatile, and colorless organic compound widely used across industrial, pharmaceutical, and consumer sectors storage tank incidents carry severe risks. Its dangerous characteristics are flammability and irritation and adverse effects (NCBI,2026).
While ethanol is primarily managed as a flammable hazard, massive spills create heavy vapor clouds evaluated using Acute Exposure Guideline Levels (AEGL) or Emergency Response Planning Guidelines (ERPG) (Doğan and Ensari Özay, 2024):

- ERPG 1: Mild Impact (1,800 ppm – 3390 mg/m^3): Causes transient eye irritation and mild respiratory discomfort in the general population.
- ERPG 2: Critical Evacuation Limit (3,300 ppm – 6220 mg/m^3): The maximum threshold for safe escape without suffering irreversible health effects or impaired judgment.
- ERPG 3: Life-Threatening Threshold: Not applicable (AIHA, 2022).

The purpose of this research is to simulate the threat zones in case of ethanol leakage from storage tank in secondary containment as a case study.

MATERIAL AND METHODS

Modelling of accidental ethanol leakage from storage tanks

This paper presents the modeling of ethanol leakage vapors from storage tanks—specifically, from the secondary containment. Secondary containment is an engineered backup system designed to catch and hold 100% hazardous liquids if the primary storage tank leaks or ruptures. Their use aims to prevent the uncontrolled spread of ethanol beyond the storage area, thereby reducing the risk of fire, explosion and environmental pollution.

[1]Corresponding author, jelena.kiurski@vts-zr.edu.rs

Secondary containment is constructed as reinforced concrete structures with an impermeable lining. The structure must be liquid-tight and designed to withstand the hydrostatic and hydrodynamic loads that may result from a sudden release of liquid from the tank (Lees, 2012). Modeling was performed for a secondary containment with an area of 440.2 m² housing six stainless-steel ethanol tanks: three with a volume of 90 m³ and three with a volume of 130 m³. The tanks are cylindrical, with a radius of 3.5 m and a height of 14.86 m.
Based on an assumed quantity of released liquid (ethanol), it is assumed that the liquid forms a pool, and the evaporation rate from that pool—within the bund or containment basin—is calculated. Passive protection measures are taken into account when estimating the release rate. Passive protection consists of embankments and channels. Active protection measures aimed at reducing the evaporation rate from the pool within the bund include foam or impregnated covers, as well as water- or chemical-based spray jets.
The evaporation rate for liquids at ambient temperature is calculated according to the following formula (Braun and Caplan, 1989):

$$QR = \left(0{,}284 \cdot 2{,}4 \cdot MW^{2/3} \cdot P_L \cdot NP\right)/(82{,}05 \cdot T) \quad (1)$$

where:
QR = evaporation rate (lb/min);
2.4 = wind speed factor = $3.0^{0.78}$, where 3.0 m/s is the wind speed;
MW = molecular weight (lb/mol);
PL= surface area of the puddle-tank resulting from the amount of discharged liquid (ft^2);
NP = vapor pressure (mm Hg);
T = temperature of released matter (K); temperature in °C+273.

Figure 1 represents dependence of the vapor pressure and temperature of ethanol (NIST, 2023).

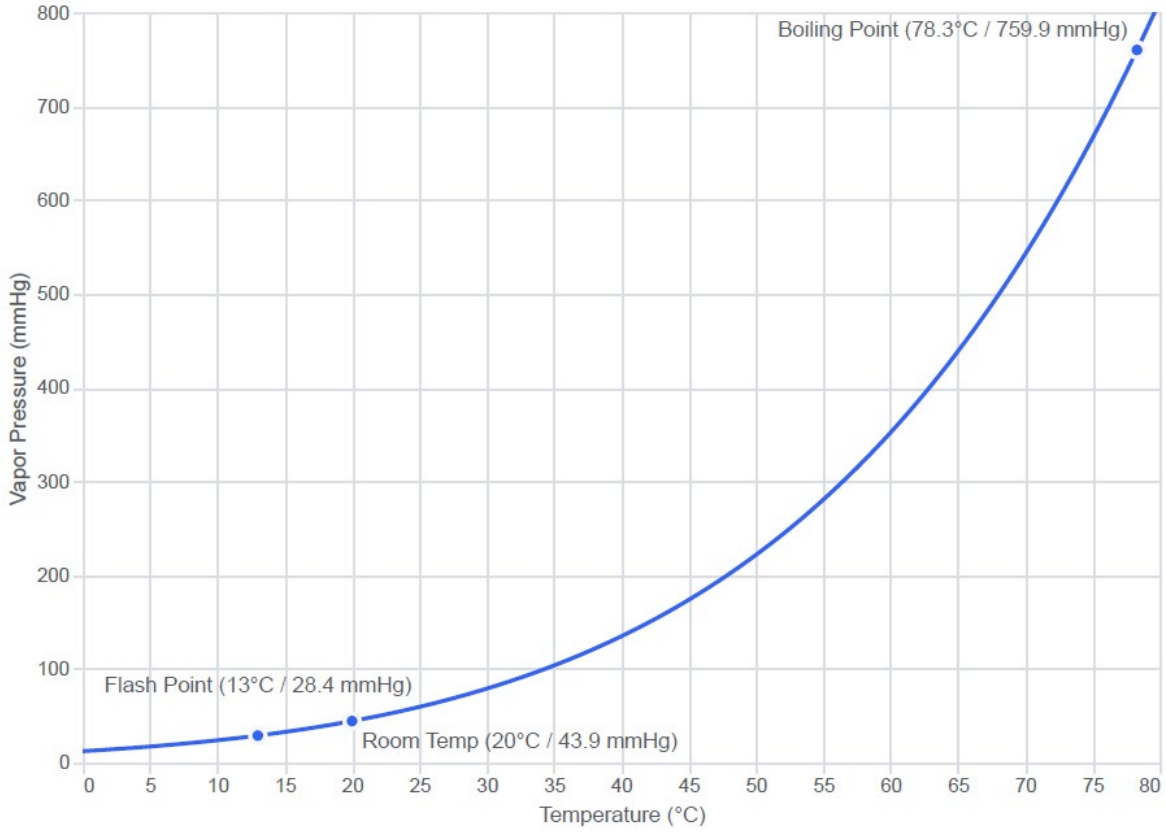


Fig. 1. *Ethanol Vapor Pressure vs. Temperature*

The Gaussian dispersion model is used to describe how the concentration of vaporized ethanol in the air changes with distance from the release point. The Gaussian model is based on describing the substance concentration distribution and dispersion within the atmospheric air release from the source. In its general form, the model defines concentration as a function of source location and spatial coordinates, with the concentration determined by source strength, air flow velocity, and substance dispersion characteristics. The Gaussian straight-line model is presented using coordinates x, y and z, where x represents the distance in the downwind direction, while y and z represent the lateral and vertical distances from the source (Nikezić, 2016). In this paper, the model calculates only the x-coordinate which represents the change in ethanol concentration with distance from the source in the direction of airflow (Kumar et al.,2025):

$$C(x,0,0) = \frac{Q}{\pi u \sigma_y \sigma_z} exp\left(\frac{H^2}{2{\sigma_z}^2}\right) \quad (2)$$

where:
C - concentration of pollutants at a given point downwind from the source;
Q - emission rate;
u - wind speed;
σy and σz - dispersion coefficients in the horizontal and vertical directions;
H - effective stack height.

RESULTS AND DISCUSSION

Based on formula 1. the evaporation rate will be calculated for the given assumption:

$$QR = \left(0{,}284 \cdot 2{,}4 \cdot 0{,}1^{2/3} \cdot 4113{,}97 \cdot 43{,}9\right)/(82{,}05 \cdot 293) = 1{,}095\ lb/min \quad (1)$$

Converting the units, we get evaporation rate of 8280 g/s of ethanol from source. This evaporation rate represents an exceptionally large-scale, catastrophic release scenario. In consequence modeling, a mass release rate of this magnitude typically indicates a massive pool fire, a severe tank shell rupture, or a catastrophic failure within a large secondary containment basin during high-temperature conditions. The vapor cloud expands rapidly downwind.
Now it will be shown how the concentration of ethanol will move with the distance from the source using Gaussian model. The concentrations will be represented in the Table 1.

Table 1. *Ethanol concentration vs. distance from the source*

Distance from source (m)	10	20	30	40	50	60	70	80	90	100
Ethanol concentration (mg/m^3)	60206	7811	3527	1976	1256	866	632	481	378	304

Data for the calculations: atmospheric stability class III/2, Q=8280 g/s, u=3m/s, H=2m.

Based on the data from Table 1, a graph of the change in ethanol concentration with the distance from the source will be created.

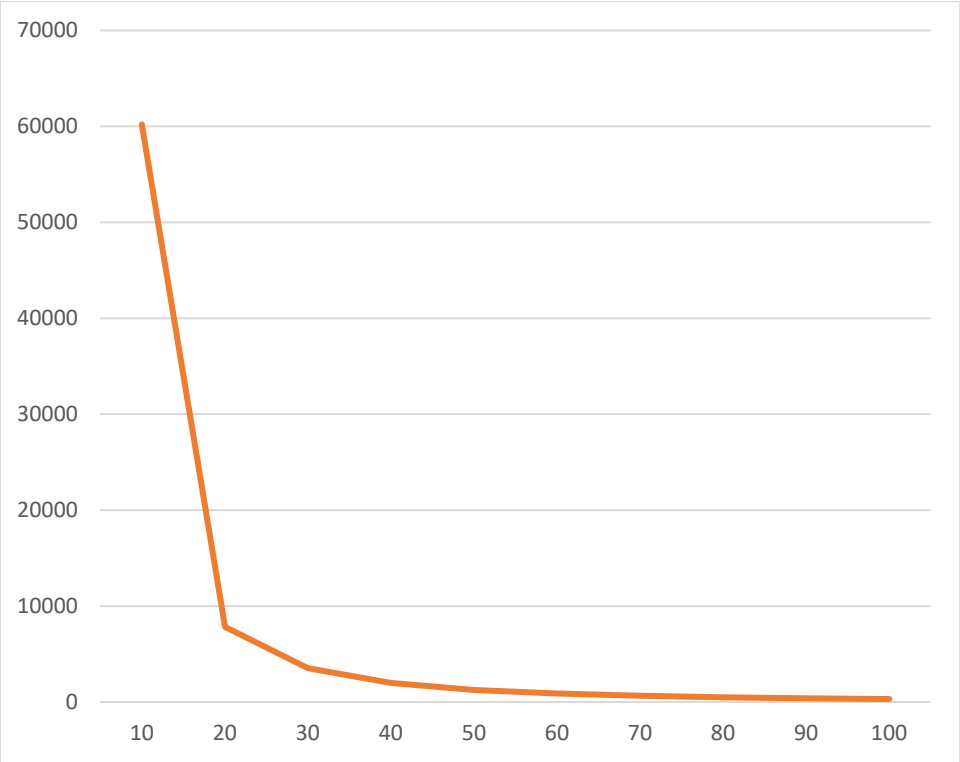


Fig. 2. *Ethanol concentration vs. distance from source*

This graph illustrates a rapid, exponential decay of ethanol concentration as distance from the source increases, characteristic of atmospheric gas dispersion behavior following an accidental chemical release. Starting at a peak of 60,000 units at a 10-meter distance, the concentration drops dramatically to less than 10,000 units by 20 meters, after which the curve asymptotically flattens toward zero.

The ERPG-2 area is about approximately 22 meters from the source, where the plume dilutes past the Emergency Response Planning Guideline-2 (6,220 mg/m^3, 3,300ppm). Thermodynamically, this marks the boundary where the vapor concentration no longer poses an immediate threat of irreversible neurological depression or severe lacrimation that would inhibit self-evacuation (NIOSH, 2014).

The ERPG-1 area is from 22 to 31 m from the source. At 31 meters, the concentration crosses the ERPG-1 threshold (3,390 mg/m^3, 1,800 ppm). At 31 meters, that initial force is completely gone. The chemical is now light enough that the natural swirling motion of the wind takes over, breaking the cloud apart and diluting it into the atmosphere.

So, the main thing is to prevent such accidental situations by implementing technical and organizational protective measures. The integrity of the tank and associated equipment, level control and overfill prevention systems, pressure and vacuum relief systems, proper maintenance, grounding, detection systems, and fire protection constitute important elements of the preventive system. The secondary containment is of particular importance, as it enables the retention of spilled ethanol in the event of a loss of tank integrity and limits its spread beyond the storage area.

CONCLUSION

As a result of the research, the consequences of ethanol leakage from storage tanks are summarized in Table 1. The data from table gives the potential treat distance.

The Red Zone covers the area from 0 to 22 meters from source. This radius defines the immediate danger zone where vapor concentrations pose severe, life-threatening health risks, including fatal asphyxiation or irreversible injury. Beyond toxicological exposure, this 22-meter

boundary maps the exact physical envelope of the flammable vapor cloud, where concentrations hover near or above the Lower Explosive Limit (LEL). Consequently, to prevent catastrophic casualties from a potential flash fire or vapor cloud explosion (VCE), all emergency response and command operations must be staged and executed strictly outside this perimeter.

The Orange Zone covers the area from 22 to 31 meters from source. Within this narrow 9-meter outer band, atmospheric dispersion rapidly dilutes the chemical plume. While the direct threat to human life drops to zero, the airborne concentration remains high enough to cause acute, temporary physical discomfort. Individuals entering this zone will experience pronounced lacrimation (eye irritation), nasal discomfort, and respiratory tract irritation, accompanied by a strong, distinct alcohol odor.

The safety of ethanol storage cannot be ensured through the application of a single measure or protection system alone. The highest level of safety is achieved through the continuous operation of all protection layers—ranging from proper design and equipment selection, through system monitoring and maintenance, to employee training and effective emergency response. This approach minimizes the probability of an accidental leak and, if should one occur, limits its spread and consequences to the absolute minimum.

REFERENCES

AIHA Guideline Foundation. (2022). Emergency response planning guidelines (ERPG) and workplace environmental exposure levels (WEEL) handbook. American Industrial Hygiene Association.

Braun, K. O., Caplan, K. J. (1989), Evaporation rate of volatile liquids. Final report, Second Edition, U.S. Environmental Protection Agency.

Doğan S., Ensari Özay M. (2024). Consequence modeling and analysis of ethanol leakage from storage tank using the ALOHA program, *Journal of Amasya University the Institute of Sciences and Technology 5(1),* 49-59.

Kumar Sinha S., Franklin R., Preeti Pradhan P., Noor Shah U., Ahmad F., Aneja A. (2025). Application of the Gaussian Plume Model to Simulate Industrial Air Pollutant Dispersion, *NESciences 10 (3),* 222-233. doi: 10.28978/nesciences.1811119.

Lees, F. (2012). Loss Prevention, 4th Edition: Hazard Identification, Assessment and Control, Butterworth-Heinemann, ISBN-13 978-0123971890.

National Center for Biotechnology Information (2026). PubChem Compound Summary for CID 702, Ethanol. Retrieved September 20, 2026 from https://pubchem.ncbi.nlm.nih.gov/compound/Ethanol.

National Institute for Occupational Safety and Health (NIOSH). (2014). Ethanol: Immediately Dangerous to Life or Health (IDLH) values. U.S. Department of Health and Human Services.

National Institute of Standards and Technology (NIST). (2023). Ethanol: Antoine equation parameters. NIST Chemistry WebBook.

Nikezić, D. P., (2016). Mathematical modeling of atmospheric air pollutant dispersion in the environment of nuclear and industrial facilities. Doctoral dissertation, Faculty of Technology and Metallurgy, University of Belgrade.

DOI:10.5937/IIZS26514L

GENERATIVE ARTIFICIAL INTELLIGENCE AS A SUPPORT TOOL FOR HSE PROFESSIONALS IN THE ASSESSMENT OF SIMULATED INDUSTRIAL WORK SITUATIONS: A PILOT EXPLORATORY STUDY

Research paper

Ana Lončar[1*], Mladenka Novaković Bežanović[2], Maja Petrović[3]
[1,2,3] University of Novi Sad, Faculty of Technical Sciences, Novi Sad, Serbia

Abstract: This pilot exploratory study investigates the use of generative artificial intelligence (AI) as support for HSE professionals in the assessment of simulated industrial work situations. Five professionals with industrial HSE experience assessed six scenarios each, resulting in 30 assessments, of which 15 were completed independently and 15 with standardized AI-generated support. The assessments were evaluated in terms of recognition of key HSE aspects, identification of additional information requirements, adequacy and specificity of control measures, unsupported assumptions, final decisions, and confidence in the assessment. Descriptive results showed slightly higher average values with AI support for recognition of key HSE aspects (85.0% vs. 80.0%), identification of additional information requirements (60.0% vs. 53.3%), and adequacy of control measures (75.0% vs. 70.0%). The specificity and applicability of proposed measures remained unchanged, while confidence was slightly higher in the AI-supported condition. Participants also supplemented AI-generated content with additional professional considerations. The findings suggest that generative AI may provide useful complementary support in HSE assessment, while professional experience and expert judgment remain essential for evaluating and contextualizing AI-generated recommendations.
Key words: generative artificial intelligence, HSE, occupational safety, risk assessment, professional judgment, decision support

INTRODUCTION

Occupational health and safety (OHS) risk assessment is a fundamental component of preventive safety management, requiring hazard identification, recognition of relevant risk factors, and selection of appropriate control measures. At the same time, industrial work environments are continuously changing due to technological development, new work processes, and increasingly complex interactions between people, equipment, and organizational systems. The International Labour Organization therefore emphasizes the importance of research addressing emerging occupational risks and the impact of new technologies on safety and health at work (International Labour Organization, 2023).

Recent developments in generative artificial intelligence (AI), particularly large language models (LLMs), have created new opportunities for supporting professional analysis and decision-making. In safety-related applications, LLMs may assist in identifying potential hazards, proposing risk-control measures, generating alternative perspectives, and structuring complex information. Previous research suggests that generative AI has potential to support selected risk assessment and safety analysis tasks, including the generation of possible failure modes and risk-mitigation options, as well as the development of initial safety-analysis models and alternative perspectives (Collier et al., 2025; Sujan et al., 2025). However, these studies also indicate important limitations. AI-generated outputs may be generic, incomplete, inconsistent, or occasionally incorrect, making expert review particularly important in safety-critical contexts (Collier et al., 2025; Oviedo-Trespalacios et al., 2023).

Consequently, generative AI in safety assessment may be more appropriately considered as a decision-support tool rather than a replacement for professional expertise. Sujan et al. (2025) showed that LLMs can provide useful starting points and alternative perspectives in safety analysis, while emphasizing that domain expertise remains necessary to identify gaps and validate AI-generated outputs. This issue is particularly relevant in industrial HSE practice, where professional judgment is influenced not only by formal knowledge but also by practical experience and understanding of actual work conditions. However, empirical evidence on the

[1*]Corresponding author, email: loncar.anaa05@gmail.com, ORCID: 0009-0002-1463-5624
[2]majadjogo@uns.ac.rs, ORCID: 0000-0003-3423-6559
[3]email:mladenkanovakovic@uns.ac.rs, ORCID: 0000-0001-5036-6682

effectiveness of AI-supported approaches in occupational safety practice remains limited. A recent systematic review concluded that the field is still at an early stage and that further research is required before widespread use of AI in OHS practice can be supported by strong evidence (Jetha et al., 2025).

Therefore, this study explores the use of generative AI as a support tool for experienced HSE professionals when assessing simulated industrial work situations. A pilot within-subject design was applied in which five HSE professionals each assessed six industrial scenarios, completing three assessments independently and three with standardized AI-generated support, resulting in a total of 30 assessments. The study compares recognition of key HSE aspects, identification of additional information requirements, adequacy and specificity of control measures, final safety decisions, and confidence in the assessment. In AI-supported tasks, perceived AI usefulness and participants' reactions to AI-generated content were also examined. The objective was to explore whether and how standardized AI-generated support may influence selected characteristics of professional HSE assessment, while retaining professional judgment as the basis for the final assessment.

MATERIAL AND METHODS

Participants and study design

A pilot exploratory study was conducted with five professionals working in occupational health, safety, and environmental (HSE) roles in industrial settings. Participants were selected purposively to include professionals with practical experience in industrial HSE contexts. Purposive sampling is commonly applied when participants are selected on the basis of specific knowledge or experience relevant to the research question (Palinkas et al., 2015). Their HSE experience ranged from 2 to 25 years, while total industrial experience ranged from 10 to 31 years. Four participants reported no previous professional use of generative artificial intelligence, while one participant reported rare professional use. Participation was voluntary, and the responses were analyzed without personal identifiers.

A within-subject design was applied. Each participant assessed six simulated industrial work situations covering typical HSE challenges: maintenance of a process pump, opening of a process pipeline, hot work in a process area, simultaneous activities in the same work zone, chemical transfer, and confined-space entry. Each participant completed three scenarios independently and three scenarios with standardized generative AI support. The allocation of AI-supported and independent scenarios was varied across participants to reduce the potential influence of scenario-specific characteristics on the comparison between the two conditions.

Procedure

For each scenario, participants were asked to identify relevant hazards and risk factors, specify additional information required before making a final HSE assessment, propose appropriate control measures, identify up to three priority measures, and provide a final recommendation regarding whether the activity could proceed. Participants also rated their confidence in their assessment on a five-point scale.

For AI-supported scenarios, participants were provided with standardized AI-generated analyses prepared using the free version of ChatGPT (OpenAI) prior to data collection. A predefined prompt structure was used to generate the analysis for each scenario. The AI-generated analyses were prepared once prior to data collection and were used without substantive modification. They remained unchanged throughout participant assessment. Free interaction with the AI system was not allowed; participants assessing the same scenario with AI support received the same predefined AI-generated content. Participants were additionally asked to rate the usefulness of the AI analysis on a five-point scale and indicate whether they accepted, supplemented, modified, or rejected parts of the AI-generated content. The final HSE assessment remained the responsibility of the participant.

Coding and data analysis

Responses were evaluated by a single HSE expert using a predefined coding framework. The coding framework was established prior to the analysis and applied to all 30 assessments using the same predefined criteria. Each complete expert response to one scenario represented one unit of analysis, resulting in 30 assessments in total.
The analysis included recognition of key HSE aspects (HRC), identification of additional information requirements (IGR), adequacy of control measures (CA), specificity and applicability of proposed measures (MSS), unsupported assumptions (UA), and self-reported confidence.
For each scenario, four reference elements were predefined for each of three assessment dimensions: key HSE aspects (HRC), additional information requirements (IGR), and adequacy of control measures (CA). HRC, IGR, and CA scores represented the percentage of these four reference elements identified or adequately addressed in each participant response. MSS was rated on a three-level scale from 0 to 2, while UA represented the number of unsupported assumptions identified in the response.
For AI-supported assessments, additional indicators included perceived AI usefulness, participants' reaction to AI-generated content, the number of expert-added relevant elements not included in the AI analysis, and the number of relevant elements overlapping with the AI-generated support.
Due to the exploratory nature of the study and the small sample size, the analysis was descriptive. Pilot studies are primarily intended to explore procedures, patterns, and feasibility rather than to provide statistically generalizable conclusions (Thabane et al., 2010). Descriptive summaries of assessments performed with and without AI support were compared using mean values and frequency distributions. No inferential statistical testing was performed, and no claims of statistical generalizability were made.

RESULTS AND DISCUSSION

A total of 30 HSE assessments were analyzed, including 15 assessments performed independently and 15 assessments performed with standardized generative AI support. The comparison focused on recognition of key HSE aspects, identification of additional information requirements, adequacy and specificity of control measures, unsupported assumptions, and participants' confidence in their assessments

Table 1. *Comparison of HSE assessment indicators with and without AI support*

Indicator	Without AI	With AI	Difference
Recognition of key HSE aspects	80.0%	85.0%	+5.0 pp
Identification of additional information requirements	53.3%	60.0%	+6.7 pp
Adequacy of control measures	70.0%	75.0%	+5.0 pp
Specificity and applicability of proposed measures (0–2)	1.73	1.73	0.00
Unsupported assumptions (count)	0	0	0
Confidence in assessment (1–5)	4.27	4.47	+0.20

The descriptive results indicate slightly higher values in the AI-supported condition for recognition of key HSE aspects, identification of additional information requirements, and adequacy of control measures. The largest difference was observed for identification of additional information requirements, increasing from 53.3% without AI support to 60.0% with AI support. Recognition of key HSE aspects increased from 80.0% to 85.0%, while adequacy of control measures increased from 70.0% to 75.0%. No difference was observed in the specificity and applicability of proposed measures, with an average MSS score of 1.73 in both

conditions. No unsupported assumptions were identified in either condition. Participants also reported slightly higher confidence in their assessments when AI support was available, with an average score of 4.47 compared with 4.27 without AI support.

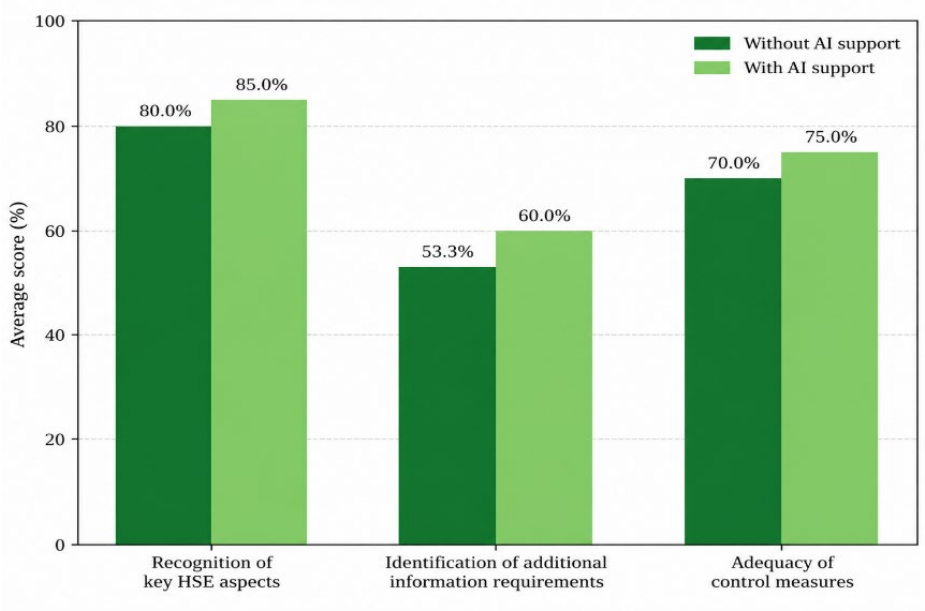


***Fig. 1**. Comparison of HSE assessment indicators with and without AI support*

In addition to the comparison between the two assessment conditions, participants' interaction with the AI-generated support was analyzed separately. Across the 15 AI-supported assessments, the mean perceived usefulness of AI was 2.60 on a five-point scale. In seven assessments, participants reported that they did not modify or supplement the AI-generated content, while in five assessments the AI output was supplemented with additional professional considerations. In three assessments, participants indicated that the AI content had been changed, supplemented, or rejected, but the exact type of reaction could not be reliably determined from the completed form.

***Table 2.** Participants' interaction with AI-generated support*

Indicator	Result
Mean perceived AI usefulness (1–5)	2.60
AI content not modified/supplemented	7/15
AI content supplemented	5/15
Reaction could not be classified reliably	3/15
Mean number of expert-added relevant elements per AI-supported assessment	1.87
Mean number of relevant elements overlapping with AI support per AI-supported assessment	3.73

The results indicate that the AI-generated analysis was not simply accepted as a final assessment in all cases. Participants frequently added professional considerations that were not included in the standardized AI support, with an average of 1.87 additional relevant elements per AI-supported assessment. At the same time, an average of 3.73 relevant elements overlapped with the AI-generated content. The results indicate that participants did not rely exclusively on the AI-generated analysis in all AI-supported assessments. Participants added an average of 1.87 relevant elements that were not included in the standardized AI support, while an average of 3.73 relevant elements overlapped with the AI-generated content.

This pattern suggests that AI-generated support was used alongside participants' own professional judgment.

The observed descriptive differences suggest that generative AI may provide support in selected components of HSE assessment. Slightly higher average values were observed in the AI-supported condition for recognition of key HSE aspects, identification of additional information requirements, and adequacy of control measures. However, these differences were relatively small, and no difference was observed in the specificity and applicability of proposed measures. This pattern is consistent with Collier et al. (2025), who reported that large language models performed relatively well in generating potential hazards and risk-mitigation ideas, while also noting that their outputs could be generic and did not reflect the depth of knowledge of experienced safety professionals.

Notably, the mean perceived usefulness of the AI-generated support was 2.60 on a five-point scale, despite the slightly higher descriptive values observed for several assessment indicators. This suggests that differences in selected assessment indicators do not necessarily correspond to professionals' subjective perception of AI usefulness.

The AI-specific results also highlight the role of professional judgment in interpreting and supplementing AI-generated content. Similar conclusions were reported by Sujan et al. (2025), who found that large language models can provide useful starting points and alternative perspectives in safety analysis, while human expertise remains essential for validating and interpreting AI-generated outputs. This is particularly important in safety-critical applications, since previous research has demonstrated that generative AI may also produce incomplete, incorrect, or potentially harmful safety-related information (Oviedo-Trespalacios et al., 2023).

The study has several limitations. The small purposively selected sample and the use of simulated industrial scenarios limit the generalizability of the findings. In addition, all responses were evaluated by a single HSE expert using a predefined researcher-developed coding framework. Although predefined criteria were applied consistently across all assessments, the absence of independent coding may have introduced interpretative bias. The results should therefore be considered descriptive and exploratory. Future studies should include larger samples, additional industrial scenarios, and independent coders, and should further evaluate the reliability of the assessment framework.

CONCLUSION

This pilot study explored the use of generative artificial intelligence as support for HSE professionals in the assessment of simulated industrial work situations. Descriptive results showed slightly higher average values in the AI-supported condition for recognition of key HSE aspects, identification of additional information requirements, adequacy of control measures, and confidence in the assessment. No difference was observed in the specificity and applicability of proposed measures.

The findings also indicate that participants used their own professional judgment alongside the AI-generated support, supplementing the AI output in several assessments with additional considerations based on their knowledge and experience. The results suggest that generative AI may have potential as a complementary decision-support tool in HSE assessment, while professional judgment remains essential for evaluating and contextualizing AI-generated content.

Due to the small purposively selected sample of five professionals, the findings should be interpreted as exploratory. Future research should include larger samples, additional industrial scenarios, independent coders, and further evaluation of how professional experience influences the use and validation of AI-generated HSE recommendations.

ACKNOWLEDGEMENT

Funded by the European Union. Views and opinions expressed are however those of the author(s) only and do not necessarily reflect those of the European Union or European Education and Culture Executive Agency (EACEA). Neither the European Union nor the

granting authority can be held responsible for them. Grant agreement number 101179757. The authors would like to thank the HSE professionals who participated in the pilot study and contributed their time and professional experience.

REFERENCES

Collier, Z. A., Gruss, R. J., & Abrahams, A. S. (2025). How good are large language models at product risk assessment? *Risk Analysis, 45*(4), 766–789. https://doi.org/10.1111/risa.14351

International Labour Organization. (2023). *Global strategy on occupational safety and health 2024–30 and plan of action for its implementation* (GB.349/INS/8).

Jetha, A., Bakhtari, H., Irvin, E., Biswas, A., Smith, M. J., Mustard, C., Arrandale, V. H., Dennerlein, J. T., & Smith, P. M. (2025). Do occupational health and safety tools that utilize artificial intelligence have a measurable impact on worker injury or illness? Findings from a systematic review. *Systematic Reviews, 14*, 146. https://doi.org/10.1186/s13643-025-02869-1

Oviedo-Trespalacios, O., Peden, A. E., Cole-Hunter, T., Costantini, A., Haghani, M., Rod, J. E., Kelly, S., Torkamaan, H., Tariq, A., Newton, J. D. A., Gallagher, T., Steinert, S., Filtness, A. J., & Reniers, G. (2023). The risks of using ChatGPT to obtain common safety-related information and advice. *Safety Science, 167*, 106244. https://doi.org/10.1016/j.ssci.2023.106244

Palinkas, L. A., Horwitz, S. M., Green, C. A., Wisdom, J. P., Duan, N., & Hoagwood, K. (2015). Purposeful sampling for qualitative data collection and analysis in mixed method implementation research. *Administration and Policy in Mental Health and Mental Health Services Research, 42*(5), 533–544. https://doi.org/10.1007/s10488-013-0528-y

Sujan, M., Slater, D., & Crumpton, E. (2025). How can large language models assist with a FRAM analysis? *Safety Science, 181*, 106695. https://doi.org/10.1016/j.ssci.2024.106695

Thabane, L., Ma, J., Chu, R., Cheng, J., Ismaila, A., Rios, L. P., Robson, R., Thabane, M., Giangregorio, L., & Goldsmith, C. H. (2010). A tutorial on pilot studies: The what, why and how. *BMC Medical Research Methodology, 10*, 1. https://doi.org/10.1186/1471-2288-10-1

DOI:10.5937/IIZS26520N

AUTOMATED IDENTIFICATION OF SAFETY-CRITICAL INCIDENTS IN AUTOMOTIVE DATABASES USING MACHINE LEARNING AND FUZZY CLUSTERING

Research paper

Sondra Preascilla Ioana Nicorici[1,2*], Mihaela Popa[3]
[1]Petroleum-Gas University of Ploiesti, Romania
[2]S.C.Aumovio Technologies Romania
[3]Aurel Vlaicu University of Arad, Romania

Abstract*:* This study explores the efficacy of supervised and unsupervised machine learning techniques in identifying vehicle accidents within large-scale, unstructured consumer complaint databases. Using data from the National Highway Traffic Safety Administration (NHTSA), we implemented a comparative analysis between Logistic Regression and Support Vector Machines (SVM), supplemented by Fuzzy C-Means (FCM) clustering. Textual descriptions were processed using TF-IDF vectorization, focusing on the top 200 significant terms. Our results demonstrate that both Logistic Regression and Linear SVM achieved a high recall rate of 0.93 for the accident class. Although precision remained at 0.18, reflecting a conservative risk-management strategy that prioritizes safety, the high sensitivity is vital for safety-critical systems. The application of Fuzzy C-Means clustering further highlighted the inherent ambiguity between technical defects and crash-related incidents.
KeyWords: Machine Learning, NHTSA, Predictive Modeling, Fuzzy C-Means.

INTRODUCTION

Modern vehicle safety management relies heavily on the analysis of field data to identify emerging risks. The National Highway Traffic Safety Administration (NHTSA) maintains extensive databases of consumer complaints, which serve as a primary source for identifying potential safety defects. However, the sheer volume and unstructured nature of these reports make manual review inefficient.
The objective of this research is to develop an automated framework capable of distinguishing between general technical complaints and high-risk incidents involving crashes. By leveraging supervised learning and fuzzy clustering, we aim to provide a scalable solution for prioritizing safety investigations, moving from reactive responses to proactive risk mitigation.

MATERIAL AND METHODS

Data Processing and Inputs

The dataset consists of safety-related complaints extracted from the NHTSA database. The core of the analysis is the "CDESCR" column, which contains narrative descriptions of the incidents. To transform the unstructured narratives into a machine-readable format, we applied TF-IDF vectorization, a method proven effective in similar automated vehicle safety analysis (Nayak, 2019). Furthermore, we limited the vocabulary to the top 200 terms to ensure model generalizability, as recommended for large-scale consumer databases (NHTSA, 2022).
Secondary Features: In addition to text, vehicle mileage and age (derived from YEARTXT) were integrated to provide context regarding the operational state of the vehicle at the time of the incident.

[1] Corresponding author, priscilla.vacarescu@yahoo.com, ORCID: 0009-0005-8050-8932

Supervised Learning Architecture

Two primary classification algorithms were implemented and compared:

Logistic Regression: Employed as a baseline probabilistic model to establish linear relationships between specific keywords (e.g., "brake failure," "crash," "deployed") and the occurrence of an accident.
Support Vector Machine (SVM): Utilized with a linear kernel to find the optimal hyperplane for class separation in the high-dimensional TF-IDF space.

To compensate for the rarity of crashes compared to general defects, we utilized a balanced class weight strategy (Pedrogosa, 2011). This approach ensures that the high-risk minority class is prioritized, which is essential when secondary features like vehicle age are integrated into the predictive model (Brown, 2021).

Detailed Explanation of the Models

A. Logistic Regression (Baseline Model)
Logistic Regression was implemented with a balanced class weight strategy.
- Purpose: It serves as a probabilistic baseline to determine the linear relationship between specific keywords in a complaint and the likelihood of a crash.
- Mechanism: It uses the sigmoid function to map the TF-IDF vectors into a probability range [0, 1].

B. Support Vector Machine (SVM)
SVM was utilized to find the optimal hyperplane that separates crash-related complaints from non-crash reports.
- Kernel Selection: We employed a linear kernel (as evidenced by the identical results with Logistic Regression), which suggests that in the high-dimensional space created by TF-IDF, the data points are linearly separable.
- Optimization: Like the Logit model, SVM used a cost-sensitive learning approach (class_weight='balanced') to compensate for the fact that crashes are much rarer than simple defects.

C. Analysis of the Confusion Matrix
To further evaluate the predictive capabilities of the models, a confusion matrix was generated. The matrix provides a granular view of how the classifier handles the significant class imbalance between non-accident reports and actual crashes.

D. To uncover hidden patterns within the NHTSA dataset without relying on predefined labels, a Fuzzy C-Means (FCM) clustering algorithm was applied. Unlike hard clustering methods, FCM provides a probabilistic membership degree for each incident, which is particularly useful for handling the linguistic ambiguity found in consumer complaints. The use of fuzzy logic allows for a nuanced interpretation of consumer reports that often contain overlapping technical and safety-critical descriptions, following the principles of intelligent fuzzy systems (Balas, 2020).

Recent advancements in automotive Quality 4.0 demonstrate a growing trend toward bridging machine learning algorithms with standard industrial quality tools. Building upon the core Quality 4.0 applications introduced by the author (Vacarescu, 2025), this work extends the deployment of Artificial Intelligence to raw, unstructured field defect descriptions. While preliminary strategies for automated decision support in automotive quality engineering were established in (Vacarescu, 2023), the current study introduces a hybrid decision model capable of real-time multi-dimensional risk scoring. Furthermore, in line with the framework proposed

by the author (Nicorici, 2025) for integrating quality management with machine intelligence, this architecture closes the operational loop by automatically mapping prediction outputs to PFMEA updates and CAPA actions.

Analysis and Results

Based on the results obtained (*Recall: 0.93, Precision: 0.18*), the following conclusions can be drawn in this paper:

1. High Sensitivity for Safety Criticality: The exceptionally high Recall *(0.93*) indicates that the models are highly effective at "flagging" potential accidents. In the context of automotive safety research, this is the most vital metric, as the cost of missing a real accident (False Negative) is significantly higher than investigating a false alarm.
2. Impact of Class Imbalance: The low Precision (*0.18*) is a direct consequence of the dataset's nature. Since non-crash complaints vastly outnumber actual crashes, the models adopt a "conservative" stance, over-predicting the risk to ensure safety.
3. Model Convergence: The identical performance of SVM and Logistic Regression suggests that for this specific subset of NHTSA data (5,000 samples), the textual features are the primary drivers of the classification, and a linear boundary is sufficient to capture the risk patterns (Figure 1).

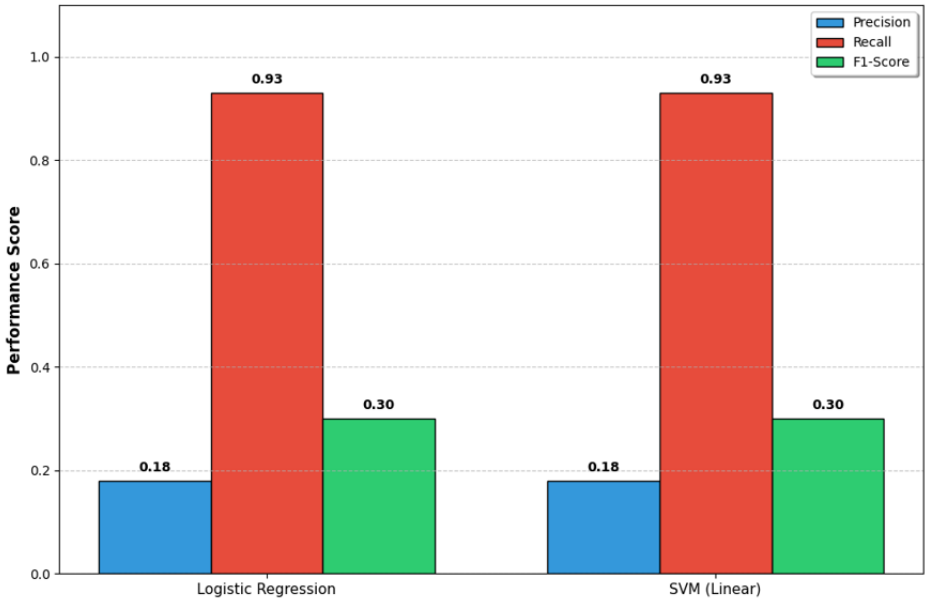


Fig. 1. *Comparative Analysis of Classification Metrics (NHTSA Dataset)*

The performance analysis reveals several critical insights regarding the model's decision-making process as presented in Figure 2:

True Positives (185): The model successfully identified 185 actual accidents out of the 199 present in the test set. This high detection rate is the primary goal of the system, ensuring that most critical events are not overlooked.

Type II Error - Missed Crashes (14): Only 14 accidents were misclassified as non-accidents. In safety-critical engineering, minimizing these "False Negatives" is crucial, as an undetected crash represents a direct failure of the monitoring system to flag a high-risk scenario.

Type I Error - False Alarms (851): There is a high volume of non-accident cases (851) classified as accidents. While this leads to low precision, it confirms the "conservative" bias of the model. From an automotive safety perspective, investigating a false alarm is a manageable operational cost, whereas ignoring a real crash is a catastrophic failure.

True Negatives (200): The model correctly identified 200 non-accident reports. The relatively low number here, compared to the false alarms, indicates that the TF-IDF features of many

technical complaints share high similarity with actual crash descriptions, causing the model to default to a "high-risk" classification for safety.

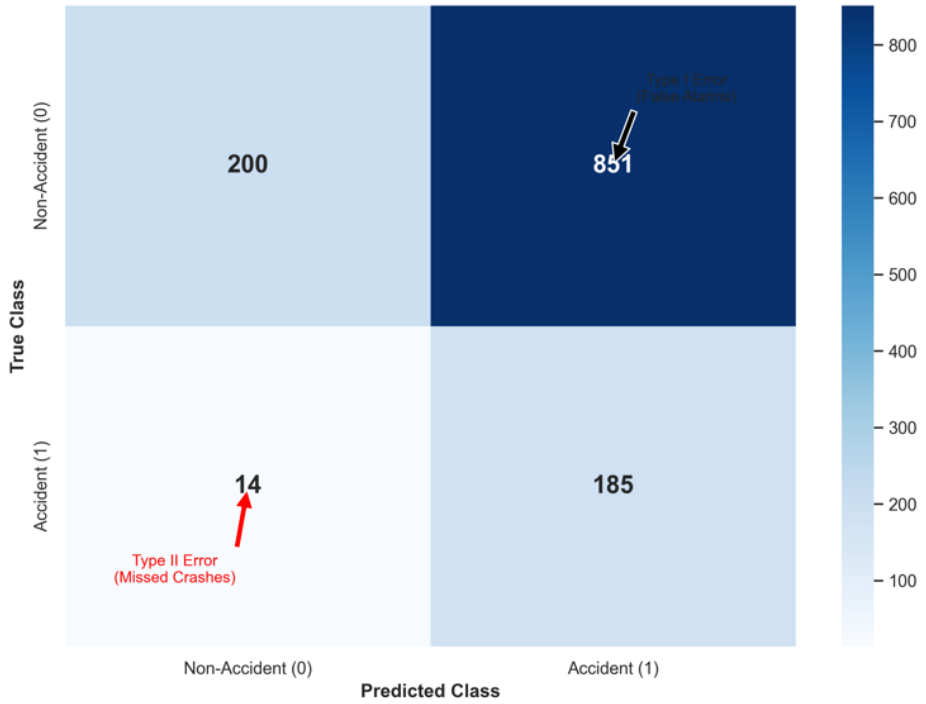


Fig. 2. *Confusion Matrix: Accident Prediction Model*

As illustrated in Figure 3, the data points are distributed across two principal standardized dimensions: Vehicle Age/Year (Feature 1) and Text Sentiment/Frequency (Feature 2). The visualization reveals several key insights:

Cluster Centroids: The black "X" markers represent the mathematical centers of the identified clusters. These centroids signify the "typical" incident profile for each group, ranging from new vehicle technical glitches to older vehicle safety failures.

Cluster Overlap: The transition of colors between the groups highlights the "fuzzy" nature of the data. This overlap suggests that many safety incidents do not belong exclusively to one category (e.g., "mechanical failure" vs. "crash"), but rather exist on a spectrum of risk.

Cluster Overlap: The transition of colors between the groups highlights the "fuzzy" nature of the data. This overlap suggests that many safety incidents do not belong exclusively to one category (e.g., "mechanical failure" vs. "crash"), but rather exist on a spectrum of risk.

Data Distribution: The clusters on the right side of the plot (positive values on Feature 1) represent incidents involving newer vehicle models, whereas the clusters on the left represent older vehicles. The vertical axis (Feature 2) effectively separates reports with high-intensity safety keywords from those with more neutral technical descriptions.

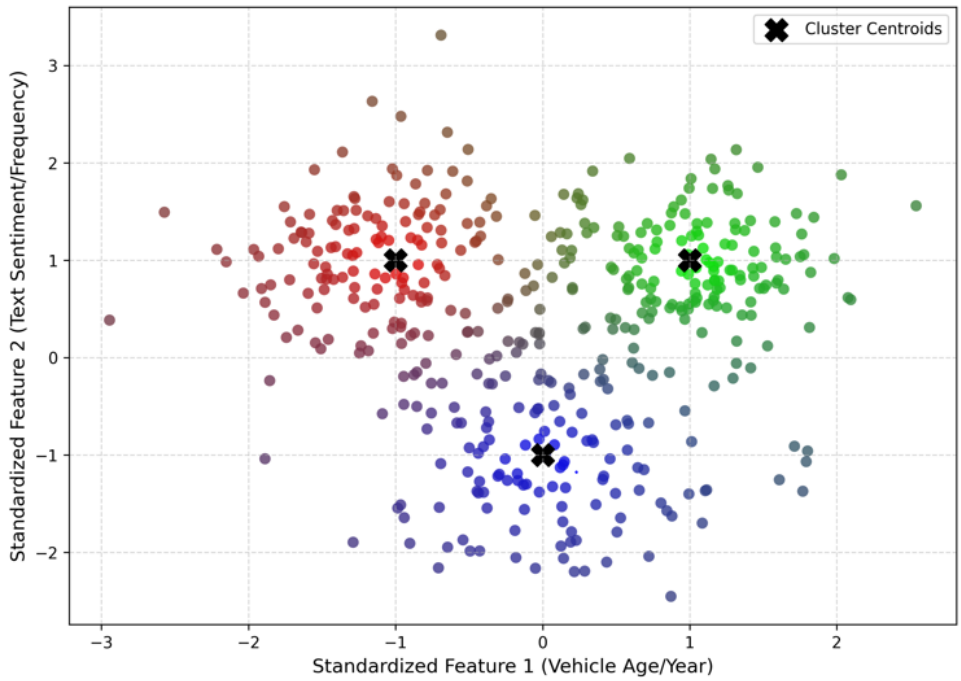


Fig. 3. *Fuzzy C-Means Clustering of NHTSA Incident Data*

Practical Significance for Safety Engineers:
The application of FCM clustering demonstrates that automated tools can group similar safety concerns even when the explicit "accident" label is missing. By identifying these natural groupings, safety oversight agencies can detect emerging trends—such as a specific sensor failure appearing across a particular vehicle age group—before they escalate into a high volume of crashes. This unsupervised approach complements the supervised models (SVM and Logistic Regression) by providing a broader context of the overall safety landscape.

CONCLUSION

The integration of advanced Machine Learning (ML) and Natural Language Processing (NLP) techniques represents a significant paradigm shift in automotive safety monitoring. This research successfully demonstrated that automated frameworks can effectively parse and categorize unstructured consumer complaints from the NHTSA database to identify safety-critical incidents.
The comparative analysis between Logistic Regression and Linear Support Vector Machines (SVM) revealed that both models, when optimized with TF-IDF vectorization and balanced class weights, achieved a remarkable recall rate of 0.93. From a safety-engineering perspective, this high sensitivity is the most critical metric, as it ensures that 93% of actual accidents are flagged for manual review, thereby minimizing the risk of undetected systemic vehicle defects. Although the precision remained relatively low (0.18), this conservative bias is intentionally aligned with "safety-first" principles, where the operational cost of reviewing false alarms is secondary to the catastrophic risk of missing a life-threatening incident.
Furthermore, the application of Fuzzy C-Means (FCM) clustering provided a deeper understanding of the inherent ambiguity within incident reporting. By visualizing the data through fuzzy membership, we observed that technical failures and crash-related incidents often share overlapping linguistic patterns. This unsupervised approach proves that AI can detect emerging safety trends even in the absence of explicit labels, offering a proactive tool for oversight agencies to identify risks before they escalate into large-scale recalls.
In conclusion, the proposed methodology offers a scalable and reliable solution for prioritizing safety investigations. Future research will explore the use of Deep Learning architectures, such as BERT or Long Short-Term Memory (LSTM) networks, to further improve precision by

capturing the complex temporal and contextual nuances of consumer narratives without compromising the essential high recall required for automotive safety-critical systems.

REFERENCES

Balas, V. E. (2020). Fuzzy Logic and Intelligent Systems. Springer Publishing.

Brown, M., & Smith, J. (2021). Predictive Analytics in Automotive Safety: A Machine Learning Approach. Automotive Engineering International, 12(4), 110–118.

Nayak, A., et al. (2019). Automated analysis of vehicle safety reports using Natural Language Processing. Journal of Safety Research, 71, 25–34.

NHTSA Data Standards. (2022). Analytical Methods for the Consumer Complaint Database. National Highway Traffic Safety Administration, Report No. DOT-HS-812.

Nicorici, S. P. I., & Balas, V. E. (2025). Integrating Quality Management and Artificial Intelligence in Automated Decision Support. In A. K. S. Pundir, A. Yadav, R. M. R. Domínguez, & S. Das (Eds.), Recent Trends in Communication and Intelligent Systems: Proceedings of ICRTCIS 2025 (pp. 105–116). Springer. https://doi.org/10.1007/978-3-032-09832-0_9

Pedregosa, F., et al. (2011). Scikit-learn: Machine Learning in Python. Journal of Machine Learning Research, 12, 2825–2830.

Vacarescu, S. P. I., Paraschiv, N., & Balas, V. E. (2023). Automated Decision Support Systems Using Artificial Intelligence in Quality Engineering within the Automotive Industry. XIII International Conference on Industrial Engineering and Environmental Protection (IIZS 2023), Zrenjanin, Serbia, October 5–6, 2023, p. 462.

Vacarescu, S. P. I., Balas, V. E., & Paraschiv, N. (2025). Artificial Intelligence in Quality Management within the Automotive Industry 4.0: Real Life Applications. In 2025 IEEE 29th International Conference on Intelligent Engineering Systems (INES), Palermo, Italy. https://doi.org/10.1109/INES67149.2025.110782



XVI International Conference Industrial Engineering and Environmental Protection 2026 (IIZS 2026)
October 01-02, 2026, Zrenjanin, Serbia

Session 8

Special Session

within the Erasmus+ project "Strengthening green and digital capacities in higher education through collaboration in integrating historical buildings into a sustainable and digital future – HEIstorical", Project No. 2025-1-RO01-KA220-HED-000364478, co-funded by the European Union.

DOI:10.5937/IIZS26527D

HEISTORICAL PROJECT: FIRST STEPS TOWARDS DIGITAL MONITORING OF HISTORICAL BUILDINGS

Research paper

Eleonora Desnica[1*], Milan Nikolić[2]
[1,2]University of Novi Sad, Technical faculty „Mihajlo Pupin" Zrenjanin, Serbia

Abstract: The HEIstorical project – Strengthening green and digital capacities in higher education through collaboration in integrating historical buildings into a sustainable and digital future – focuses on the application of modern digital technologies and sustainable approaches to the preservation and monitoring of historical buildings. This paper presents the activities carried out during the first year of the project at the University of Novi Sad, with particular emphasis on the selection and initial field investigation of historical buildings in the Vojvodina region. Four representative buildings located in Zrenjanin and Ečka were selected: the National Museum of Zrenjanin, the Secondary Music School "Josif Marinković", the Historical Archive of Zrenjanin, and the gallery section within the Kaštel Castle in Ečka. Field investigations were conducted on November 20 and December 5, 2025, during which relevant measurement and construction-related data were collected. A total of 37 students participated in the field activities under the supervision of project team members. The selected buildings differ in their architectural characteristics, construction periods, functions, and preservation requirements, providing a suitable basis for subsequent monitoring activities and the application of digital technologies for sustainable cultural heritage preservation.
Key words: HEIstorical project, historical buildings, cultural heritage, digital monitoring, field investigation, Vojvodina

INTRODUCTION

The project Strengthening green and digital capacities in higher education through collaboration in integrating historical buildings into a sustainable and digital future – HEIstorical is being implemented within the Erasmus+ KA220-HED – Cooperation Partnerships in Higher Education programme, under project number 2025-1-RO01-KA220-HED-000364478. The project started on September 1, 2025, and is planned to run for three years, until August 31, 2028. The project is coordinated by Transilvania University of Brașov, Romania, with Dorin Radu serving as the project coordinator. In addition to the coordinating institution, the consortium includes Josip Juraj Strossmayer University of Osijek, Croatia; Bitlis Eren University, Türkiye; Politehnica University Timișoara, Romania; and the University of Novi Sad, Serbia.

The main objective of the project is to strengthen the green and digital capacities of higher education institutions through the development and application of modern approaches to the preservation, monitoring, and sustainable renovation of historical buildings. Particular emphasis is placed on the application of digital tools, IoT-based sensor systems, machine learning methods, and artificial intelligence-supported data analysis. In this way, the project aims to establish a basis for assessing the condition of historical buildings and predicting potential damage, while simultaneously considering their energy efficiency, seismic performance, and microclimatic conditions. In addition to its research component, the project has a strong educational dimension, involving students and academic staff in field and research activities, the development of new teaching content, and the strengthening of interdisciplinary and international cooperation.

The project activities are organized into four work packages. In addition to project management, they include international cooperation among higher education institutions in analyzing the current condition of historical buildings and the possibilities for integrating modern standards, the application of advanced digital technologies to the energy, seismic, and microclimatic aspects of historical building renovation as well as the strengthening of educational capacities through knowledge exchange, improvement of existing and development of new teaching content, and transnational teaching activities. The overall project

[1]Corresponding author, eleonora.desnica@tfzr.rs, ORCID:0000-0002-4724-5764
[2]milan.nikolic@tfzr.rs, ORCID:0000-0001-6643-1442

approach is based on linking field-collected data with digital monitoring and modern analytical methods in order to develop methodologies that simultaneously address the energy, seismic, and microclimatic aspects of historical building preservation.
One of the first research and fieldwork steps in the implementation of the project was the selection of representative historical buildings in the partner regions, which will be included in subsequent measurements and monitoring activities. The project envisages the monitoring of a total of 20 historical buildings across five transnational regions, with data collection related to their energy efficiency, microclimatic conditions, and structural dynamic characteristics. Within Work Package 2 and Activity 2.8, the University of Novi Sad ,Technical faculty „Mihajlo Pupin" Zrenjanin was responsible for selecting four historical buildings in the Vojvodina region, collecting initial field data, and involving students in the implementation of the activity. The project documentation for Activity 2.8 specifically defines the selection of four buildings, the subsequent installation of sensors in the selected buildings, the collection of data on their most important dynamic characteristics, and the participation of students and professors from the University of Novi Sad (UNS TFMP 2026).
Accordingly, this paper presents the activities carried out during the first year of the HEIstorical project at the University of Novi Sad, with particular emphasis on the selection of historical buildings in Zrenjanin and Ečka and the initial field activities conducted as a basis for their further monitoring. The selected buildings differ in terms of construction period, architectural and structural characteristics, and present-day function, allowing the digital monitoring approaches and methodologies developed in subsequent project phases to be examined under different conditions of use and cultural heritage preservation.

STUDY AREA – THE REGION OF VOJVODINA AND THE CITY OF ZRENJANIN

Vojvodina is an autonomous province of the Republic of Serbia characterized by a rich and diverse cultural and architectural heritage shaped by different historical periods and cultural influences. A significant part of its historical urban fabric dates from the 18th, 19th, and early 20th centuries and includes buildings constructed in Baroque, Classicist, Secession, and Academic styles.
Vojvodina is also characterized by a well-preserved tradition of multilingualism, multiconfessionalism, and coexistence of diverse cultures. In addition to its cultural significance, the region represents an important educational and research center, with the University of Novi Sad playing a significant role in contemporary research, innovation, and interdisciplinary cooperation. The combination of rich cultural heritage and academic capacities makes Vojvodina a suitable framework for projects addressing digital, sustainable, and interdisciplinary approaches to the monitoring, protection, and preservation of historical buildings.
Zrenjanin, one of the major cities of Vojvodina and the administrative center of the Central Banat region, has preserved numerous historically and architecturally significant buildings that continue to serve public, cultural, and educational functions. Within the HEIstorical project, four representative buildings were selected: the National Museum of Zrenjanin, the Secondary Music School "Josif Marinković," the Historical Archive of Zrenjanin, and the gallery section within the Kaštel Castle in Ečka. These buildings represent different architectural typologies, construction periods, materials, and contemporary functions, making them suitable for investigating the application of digital monitoring and sustainable approaches to cultural heritage preservation.
The relevance of the selected study area was additionally emphasized by Zrenjanin's designation as the Serbian Capital of Culture in 2025, which highlighted the importance of preserving, promoting, and revitalizing the city's cultural heritage.
The geographical location of the study area, including the position of Vojvodina within the Republic of Serbia and the city of Zrenjanin, is presented in Fig. 1.



a) b)

Fig. 1. *Territory of the Republic of Serbia (a), Vojvodina and the city of Zrenjanin (b)*

Building of the National Museum

The National Museum of Zrenjanin (Fig. 2a), formerly the Palace of Finance, is one of the most significant examples of historic architecture in the city and is protected as a cultural monument of great importance. The building was constructed in 1893 for the Ministry of Finance of the Austro-Hungarian Monarchy, according to the design of Budapest architect István Kiss. It was built in the academic style with distinctive Neo-Renaissance elements and has largely preserved its original appearance. Since 1966, it has housed the permanent exhibition of the National Museum.

The building is distinguished by its carefully composed façades, with the main façade oriented toward today's Liberty Square, contributing significantly to the architectural identity of the city center. It has a complex and irregular ground plan resembling the Cyrillic letter "П", which forms an inner courtyard—an atrium. As a late 19th-century building constructed using traditional materials and techniques, it represents a characteristic example of the historical architectural heritage of Zrenjanin.

The National Museum was selected for the HEIstorical project due to its cultural significance and the specific environmental conditions required for the preservation of more than 49,000 museum artefacts. Monitoring of temperature, humidity, vibrations, and other relevant parameters can provide important information for assessing microclimatic conditions, structural stability, and the preservation of sensitive exhibits. Therefore, the Museum represents an important case study for the application of digital monitoring technologies in historical buildings.

Building of the Secondary Music School "Josif Marinković"

The building of the Secondary Music School "Josif Marinković" (Fig. 2b) represents a significant example of preserved Classicist architecture in Zrenjanin. It was constructed in the mid-19th century, while the courtyard wing was most likely added at the beginning of the 20th century. Reliable information about the original owner and architect has not been preserved, reflecting the building's long and multilayered historical development.

The single-storey building has an elongated L-shaped floor plan and has largely preserved its original Classicist façade, making it one of the few remaining examples of this architectural style in Zrenjanin. Archival records indicate that the building housed the city police at the beginning of the 20th century. The courtyard wing was probably added during this period, as indicated by the presence of a Prussian vault in the intermediate floor structure, characteristic of construction from the late 19th and early 20th centuries.

Since November 1949, the building has housed the Secondary Music School "Josif Marinković". Its interior was subsequently adapted for educational purposes, including the

conversion of the attic into classrooms. The gables were also redesigned with vertical elements symbolically resembling musical notes and a staff, giving the building a distinctive architectural identity related to its contemporary function.
The building was selected for the HEIstorical project as a valuable example of 19th-century architecture constructed using traditional materials and techniques. Its current educational function also requires stable microclimatic conditions, particularly with regard to temperature and humidity, which are important for the preservation of musical instruments and appropriate teaching conditions. Sensor-based monitoring can therefore provide relevant data for the maintenance and long-term preservation of both the building and its specific cultural and educational function.

Historical Archive of Zrenjanin

The Historical Archive of Zrenjanin (Fig. 2c) is located within the City Hall building, formerly the Torontal County Palace, in the historic center of Zrenjanin. As a regional cultural institution, the Archive is responsible for the protection, collection, processing, and permanent preservation of archival material related to the Central Banat region.
The City Hall building is one of the most representative architectural landmarks of Zrenjanin and is protected as a cultural monument of great importance. It was originally constructed between 1816 and 1820 according to the design of architect Josif Fischer. Between 1885 and 1887, the building was extensively reconstructed and enlarged according to the plans of Budapest architects Ödön Lechner and Gyula Pártos, acquiring its present neo-Baroque appearance. The building has preserved its administrative function and a highly representative interior, including a marble double-flight staircase, the Baroque Hall, and stained-glass windows created by Eduard Kratzmann.
The archival repositories cover approximately 584 m² and contain several hundred archival fonds and more than 5,000 linear meters of records dating from 1765 to the present. Among them, 67 fonds are designated as cultural heritage of exceptional importance and 66 as cultural heritage of great importance. The Archive also maintains a substantial library collection, while digitization and microfilming activities have been carried out since 2003 to improve the protection and accessibility of archival materials.
Due to the high sensitivity of paper-based materials to temperature, humidity, and other microclimatic variations, the Historical Archive represents an important case study within the HEIstorical project. Continuous monitoring of environmental conditions can support the long-term preservation of archival collections, improve the management of storage conditions, and contribute to the protection of both documentary heritage and the historic building in which it is preserved.

Gallery Section within the Kaštel Castle in Ečka

Kaštel Castle in Ečka (Fig. 2d) represents one of the most valuable architectural and landscape ensembles of the Central Banat region. It was built in the second decade of the 19th century as the residence of the noble Lazar family. The complex developed throughout the 19th century and acquired an elongated L-shaped layout, characterized by modest but recognizable elements of Classicism. The castle and its surroundings were declared a cultural monument in 2001, and subsequent conservation and restoration works contributed to the preservation and revitalization of the complex.
An important part of the complex is the gallery space, located in a building that originally served as the estate's laundry facility. It was later adapted for cultural purposes and became associated with the Contemporary Gallery of Zrenjanin and the Ečka Art Colony. The Art Colony was founded in 1956, followed by the establishment of the Contemporary Gallery in 1958, with the aim of preserving, studying, and exhibiting artworks created within the colony.
Over the decades, numerous Yugoslav, Serbian, and international artists have contributed to the development of a valuable contemporary art collection comprising paintings, watercolors, sculptures, prints, installations, and video works. The presence of sensitive artworks creates

specific requirements regarding stable microclimatic conditions, particularly temperature and humidity.
Within the HEIstorical project, the gallery section represents a valuable case study combining historical architecture with contemporary cultural use. Continuous monitoring of environmental conditions can contribute to the preservation of both the historic building and the artworks housed within it.



Fig. 2. *Selected historical buildings within the HEIstorical project: (a) National Museum of Zrenjanin, (b) Secondary Music School "Josif Marinković", (c) Historical Archive of Zrenjanin, and (d) Contemporary Gallery within the Kaštel Castle in Ečka.*

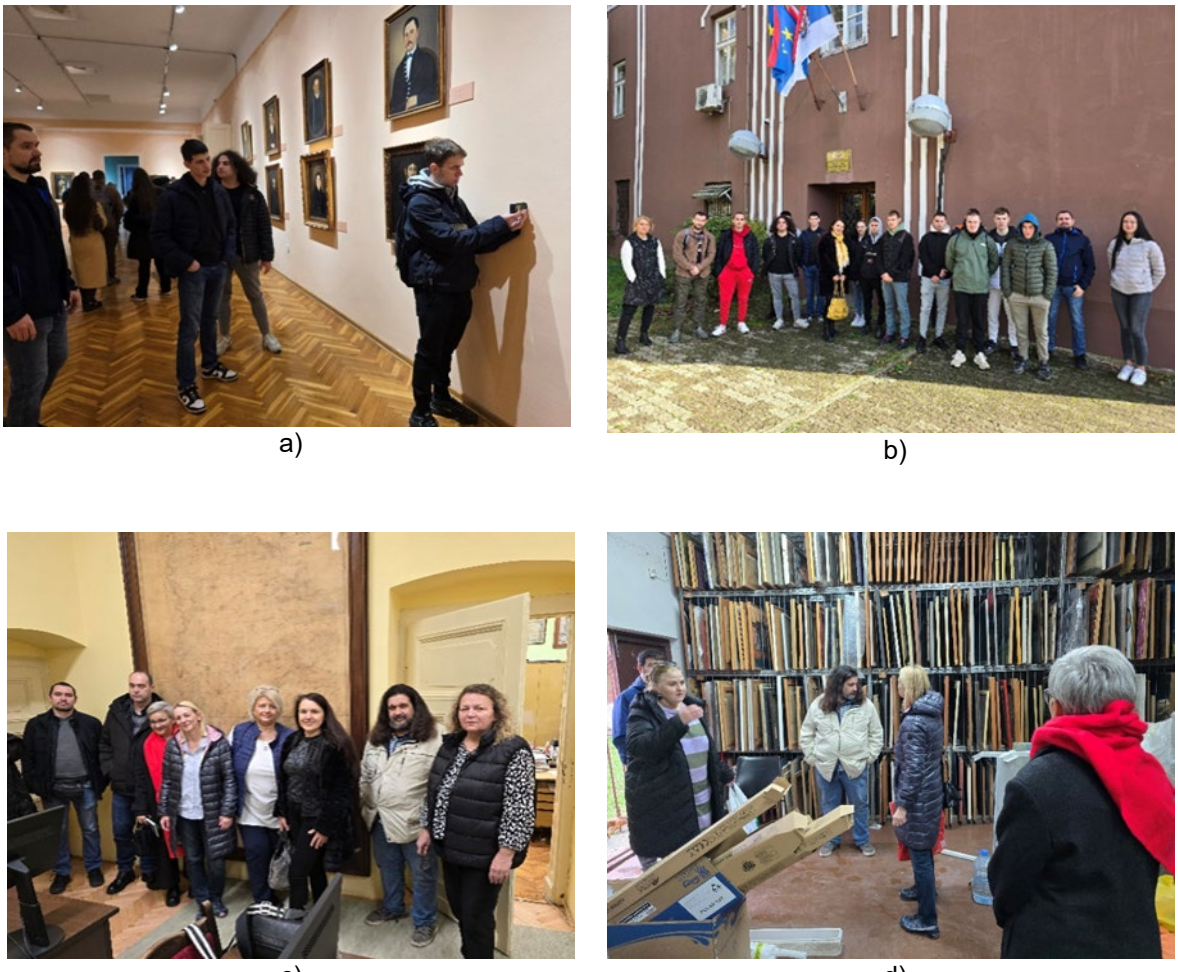
FIELD DATA COLLECTION

As part of the HEIstorical project activities in Vojvodina, field investigations were conducted to identify suitable historical buildings and obtain the data required for their subsequent monitoring. Four representative buildings located in Zrenjanin and Ečka were selected and included in this phase of the project. Field visits were carried out on November 20 and December 5, 2025, during which relevant measurements and construction-related information were collected directly on site. The collected data provided an initial basis for further assessment and monitoring of the selected buildings. All four buildings represent significant elements of the cultural heritage of Zrenjanin and the wider Vojvodina region.
Another important outcome of the field activities was the involvement of students from the Technical Faculty "Mihajlo Pupin" in Zrenjanin, University of Novi Sad. A total of 37 students from the Engineering Management and Mechanical Engineering study programs participated in the investigation and data collection process. The dynamic characteristics of the selected historical buildings were examined, while the fieldwork was conducted under the guidance of professors from the Technical Faculty "Mihajlo Pupin" who are members of the HEIstorical project team.

The field activities enabled the collection of the necessary on-site information for all four selected buildings and established a foundation for their further monitoring within the HEIstorical project. At the same time, the participation of students provided practical experience in field investigation of historical buildings and supported the educational dimension of the project.

The field investigation also highlighted the diversity of preservation requirements among the selected buildings. While the National Museum and the gallery section require stable environmental conditions for the protection of artworks and museum collections, the Historical Archive places particular emphasis on the preservation of paper-based materials. The Music School, on the other hand, combines the preservation requirements of a historical building with specific conditions related to musical instruments and educational activities. This diversity confirms the suitability of the selected buildings as representative case studies for the further development and application of digital monitoring approaches within the HEIstorical project.

Selected photographs illustrating the field investigation and data collection activities at the four historical buildings are presented in Fig. 3.



a) b) c) d)

Fig. 3*. Field investigation and data collection activities at the selected historical buildings: a) visit to the National Museum of Zrenjanin, b) visit to the Secondary Music School "Josif Marinković", c) visit to the Historical Archive of Zrenjanin, and d) visit to the gallery section within the Kaštel Castle in Ečka.*

CONCLUSION

Participation in the project Strengthening green and digital capacities in higher education through collaboration in integrating historical buildings into a sustainable and digital future – HEIstorical represents an important contribution to contemporary approaches to cultural heritage preservation. Through interdisciplinary cooperation among higher education

institutions, the application of modern digital technologies, and the active involvement of students in research activities, the project supports the development of sustainable and technologically advanced approaches to the protection of historical buildings.
The selection of four historical buildings in Zrenjanin and Ečka—the National Museum of Zrenjanin, the Secondary Music School "Josif Marinković," the Historical Archive of Zrenjanin, and the gallery section within the Kaštel Castle—provides an opportunity to examine different architectural typologies, functional uses, structural characteristics, and microclimatic requirements. At the same time, the project creates a basis for assessing how modern sensor systems and digital tools can support the identification of potential risks, optimization of indoor conditions, planning of conservation and restoration activities, and more sustainable management of cultural heritage buildings.
The establishment of continuous monitoring in the selected buildings is expected to contribute not only to their long-term preservation, but also to the development of educational practices that enable students to gain practical experience and a better understanding of the behavior and monitoring of historical structures.
The implementation of HEIstorical project activities in Zrenjanin has additional significance in the context of the city's designation as the Serbian Capital of Culture 2025. In this way, the project contributes to the visibility, valorization, and contemporary presentation of Zrenjanin's cultural heritage while supporting its long-term preservation through digital and sustainable approaches.

ACKNOWLEDGEMENT

This paper was developed within the Erasmus+ project "Strengthening green and digital capacities in higher education through collaboration in integrating historical buildings into a sustainable and digital future – HEIstorical", Project No. 2025-1-RO01-KA220-HED-000364478, co-funded by the European Union. The authors thank the The National Museum of Zrenjanin, the Secondary Music School "Josif Marinković" Zrenjanin, the Historical Archive of Zrenjanin and the gallery section within the Kaštel Castle in Ečka for hosting the sensors.
The information on the selected historic buildings was obtained from the official websites of the respective institutions. These online sources were used for basic descriptive and contextual information and are therefore listed in the References section without individual in-text citations.

REFERENCES

University of Novi Sad, Technical faculty „Mihajlo Pupin" Zrenjanin. (2026). Selection and detailed measurements of historical buildings monitored in the region Vojvodina (HEIstorical Project Report, Activity 2.8).
https://heistorical.unitbv.ro/
https://www.zrenjaninheritage.com/
https://www.vojvodina.gov.rs/vojvodina/o-vojvodini
https://znamenitostivojvodine.rs/gradovi-vojvodine/zrenjanin/
https://muzejzrenjanin.org.rs/
https://www.josif.edu.rs/
https://arhivzrenjanin.rs/
https://kastelecka.com/

DOI:10.5937/IIZS26534D

LOW-COST IOT MONITORING OF HISTORICAL BUILDINGS: SENSOR SELECTION, PLACEMENT AND SYSTEM ARCHITECTURE

Research paper

Dalibor Dobrilović[1]*, Ivan Palinkaš[2]
[1,2]University of Novi Sad, Technical faculty „Mihajlo Pupin" Zrenjanin, Serbia

Abstract: Historical buildings require monitoring systems that can record environmental and structural conditions without damaging protected materials or architectural elements. This paper proposes an IoT-based monitoring approach that combines building-specific sensor placement, hardware selection, parameter coverage analysis, and cloud-based data management. Twelve monitoring parameters are considered within four groups related to structural stability, material degradation, microclimate, and additional environmental information. Five ESP8266- and ESP32-compatible sensor configurations are compared according to the number of parameters covered and practical deployment requirements. The basic PMS7003 and BME280 configuration covers 41.67% of the defined parameters, while the addition of an MPU6050 increases coverage to 58.33%. A broader low-cost configuration reaches 91.67% coverage, with displacement remaining outside the proposed setup. Sensor positions are determined according to building function, sensitive materials, air circulation, structural characteristics, human activity, and conservation restrictions. The proposed architecture connects distributed sensor nodes through local Wi-Fi networks to a cloud platform for data storage, visualization, alerts, and export. The resulting approach provides a practical basis for scalable and non-invasive monitoring of historical buildings under financial and conservation constraints.
Key words: historical buildings, IoT monitoring, sensor placement, structural health monitoring, microclimate, low-cost sensors, cloud monitoring

INTRODUCTION

Historical buildings require continuous observation because aging materials, environmental exposure, structural loads, and human activity can gradually affect their condition. Museums, archives, libraries, religious buildings, theatres, schools, and other heritage structures often combine cultural value with active use, which creates specific requirements for preservation and user safety. Structural health monitoring and environmental monitoring can provide information on changes that are difficult to detect through occasional visual inspection alone (Rossi & Bournas, 2023). Previous research has examined monitoring systems for architectural heritage, including structural assessment, wireless sensing, and long-term condition tracking (Clementi et al., 2021). Internet of Things technologies have also been applied to distributed monitoring because several sensor nodes can collect data from different locations and transmit measurements to a common digital platform (Mecocci & Abrardo, 2014). Monitoring requirements differ according to building function, materials, construction characteristics, occupancy, and environmental exposure. Temperature and relative humidity are relevant for archives and collections containing paper, wood, textiles, instruments, artworks, and other materials sensitive to environmental fluctuations. Particulate matter can contribute to surface contamination and degradation, while moisture can indicate conditions associated with deterioration of masonry and other materials (Karoglou et al., 2025). Vibration, tilt, strain, cracks, and displacement provide information on structural behavior and can be particularly relevant in buildings exposed to traffic, seismic activity, wind, or other mechanical influences. Research on cultural heritage therefore increasingly combines microclimate monitoring with structural condition monitoring instead of treating these requirements as unrelated tasks (Mitro et al., 2022). Sensor placement is closely connected with the usefulness of the collected measurements. Devices should be positioned where they can represent the conditions affecting sensitive materials and where structural response can be recorded with acceptable reliability.

[1]Corresponding author, dalibor.dobrilovic@uns.ac.rs, ORCID: 0000-0002-3083-5725
[2]ivan.palinkas@uns.ac.rs , ORCID: 0000-0001-9253-1375

Storage rooms, exhibition areas, zones with stronger air circulation, frequently occupied rooms, and structurally relevant elements may require different positions. Elevated architectural elements can also provide information on exposure to wind, temperature variation, and vibration. Recent work on heritage buildings confirms that sensor position can be evaluated through both model-based and data-driven approaches. Installation methods require additional attention because drilling, cutting, or permanent alteration may not be permitted in protected structures. Existing fixtures, independent supports, reversible adhesive solutions, and other minimally intrusive mounting methods can therefore be required. Non-intrusive monitoring has also been considered in research on heritage structures where the installation method must respect the physical condition of the building.
Hardware selection introduces a second design problem because broader parameter coverage generally requires additional sensors, power connections, communication capacity, and financial resources. Low-cost sensors have been examined as an option for building monitoring when a larger number of nodes must be deployed (Mobaraki et al., 2021). Open-source hardware and wireless sensor networks have also been used in heritage buildings, showing that modular systems can support monitoring without relying only on specialized commercial platforms. Cloud-based systems extend this approach through centralized storage and remote access to measurements from several locations. The design problem is therefore not limited to choosing individual sensors. It also includes the relationship between monitored parameters, sensor-node cost, installation restrictions, connectivity, and the intended use of the collected data.

INTEGRATED MONITORING CONCEPT

Building function and monitoring priorities

The selection of buildings and measurement locations is based on both functional significance and vulnerability to environmental or structural risks. Buildings containing paper-based archival materials require particular attention to temperature, relative humidity, and dew point. Museums, galleries, and facilities containing instruments or delicate artifacts additionally require monitoring of particulate pollution because deposited particles can contribute to contamination and surface degradation. Buildings used for education, worship, or public activities introduce an additional safety dimension, for which air quality (particulate matter only) and, where appropriate, vibration monitoring become relevant (UNS TFMP 2026a).

Table 1. *Building categories and monitoring priorities*

Building context	Main monitoring concerns	Parameters highlighted in the report
Archives / paper collections	Humidity- and temperature-related material degradation	Temperature, relative humidity, dew point
Museums / galleries / collections	Microclimate and particulate contamination	Temperature, relative humidity, dew point, particulate matter
Schools / cultural facilities	Indoor environmental quality and structural response	Temperature, humidity, particulate matter, air quality (particulate matter only), vibration where required
Monumental structures / elevated elements	Environmental exposure and structural response	Microclimate, vibration, tilt and related structural indicators

Monitoring parameters

The monitored variables into structural stability, material degradation, microclimate, and additional contextual parameters. The defined set includes temperature, relative humidity, dew point, moisture in materials, vibration, tilt, strain, displacement, cracks, pressure/height, air quality (particulate matter only), and light level. Relative humidity appears in both the material-degradation and microclimate categories in the source report, but it is counted once in the

coverage calculation. The same calculation treats atmospheric pressure (with derived altitude/relative height where appropriate) as a combined monitoring item.

Table 2. *Monitoring parameter structure used for the sensor coverage analysis*

Category	Parameters included in the project analysis
Structural stability	Vibration, tilt, strain, displacement, strain; crack-related deformation with appropriate transducer/mounting
Material degradation	Relative humidity, moisture in materials, air quality (particulate matter only), light level
Microclimate	Temperature, relative humidity, dew point
Additional/contextual	Atmospheric pressure (with derived altitude/relative height where appropriate)

SENSOR PLACEMENT STRATEGY

Location selection inside historical buildings

the exact sensor position should be established on site rather than fixed in advance. Placement should consider building geometry, accessibility, conservation restrictions, available mounting points, indoor air circulation, environmental gradients, human activity, and the presence of structurally significant elements. For material preservation, the sensor should represent the microclimate experienced by the relevant collection or surface. For structural monitoring, the selected position should provide meaningful information about the behaviour of the element or zone under observation.
Particular attention is given to elevated architectural elements such as minarets. Their height and exposure can make them sensitive to wind, thermal variations, and vibration, so they may provide useful reference information when structural stability is part of the monitoring objective. The report also identifies storage rooms, exhibition areas, and other zones with significant material or human activity as potential locations.

Installation constraints

Heritage conservation places direct constraints on the physical installation of monitoring devices. Drilling and permanent modification of protected surfaces are generally unsuitable. The proposed alternatives are attachment to existing fixtures, tripods or independent stands, and high-quality double-sided adhesive mounting where appropriate. Standalone supports can protect the building fabric but may affect vibration measurements, which means that the installation method should be considered when interpreting vibration data.
The deployment plan specifies two sensors per building, corresponding to eight sensors per project partner in the reported project configuration. The exact height and position are intentionally left for on-site determination because the appropriate location depends on the geometry and conservation conditions of each building.

Indoor and outdoor deployment

Outdoor deployment may be possible when the sensor node is installed in a suitable weather-protected enclosure while maintaining adequate airflow for environmental and particulate measurements. Protected and discreet locations are recommended to reduce the possibility of vandalism, theft, or accidental damage. Indoor deployment generally offers greater protection, while outdoor or elevated placement may be required when the monitored phenomenon is directly associated with the exterior envelope or exposed structural elements.

LOW-COST SENSOR NODE CONFIGURATION

Hardware selection

Proposes an ESP8266-based monitoring platform, with ESP32-class platforms also considered compatible with the general concept. The basic configuration combines a BME280 environmental sensor and a PMS7003 particulate matter sensor. Additional low-cost modules are introduced to increase functional coverage: MPU6050 for vibration and tilt, a capacitive moisture sensor for material moisture, BH1750 for light level, and HX711 with a strain gauge for basic strain/crack monitoring (UNS TFMP 2026b).

Table 3. *Candidate low-cost sensing elements*

Sensor / module	Main measured or derived variables	Integration described in the report
BME280	Temperature, relative humidity, pressure; dew point calculated in software	I²C
PMS7003	PM1.0, PM2.5, PM10	Particulate-matter interface
MPU6050	Vibration and tilt	I²C
Capacitive moisture sensor	Moisture in materials	Analog input
BH1750	Light level	I²C
HX711 + strain gauge	Basic strain and crack-related measurement	Digital/analog interface

Coverage methodology

The report evaluates sensor configurations against 12 monitoring parameters. Equal weighting is applied, so each fully covered parameter contributes approximately 8.33 percentage points. Dew point is considered covered when it is calculated from temperature and relative humidity. The methodology explicitly notes that displacement is not covered by the low-cost modules and would require a specialized sensor such as an LVDT or laser-based device.

Table 4. *Sensor configuration coverage values*

Configuration	Sensor set	Covered parameters	Coverage
Base	PMS7003 + BME280	Temperature, RH, dew point, air quality (particulate matter only), pressure/height	41.67%
Base without BME280	PMS7003	Air quality (particulate matter only)	8.33%
Base + MPU6050	PMS7003 + BME280 + MPU6050	Base variables + vibration + tilt	58.33%
Expanded without MPU6050	PMS7003 + BME280 + moisture + BH1750 + HX711	Base variables + moisture + light + strain/cracks	75.00%
Expanded + MPU6050	PMS7003 + BME280 + MPU6050 + moisture + BH1750 + HX711	All above except displacement	91.67%

Figure 1 shows the monitoring device parameter coverage in the perecent.

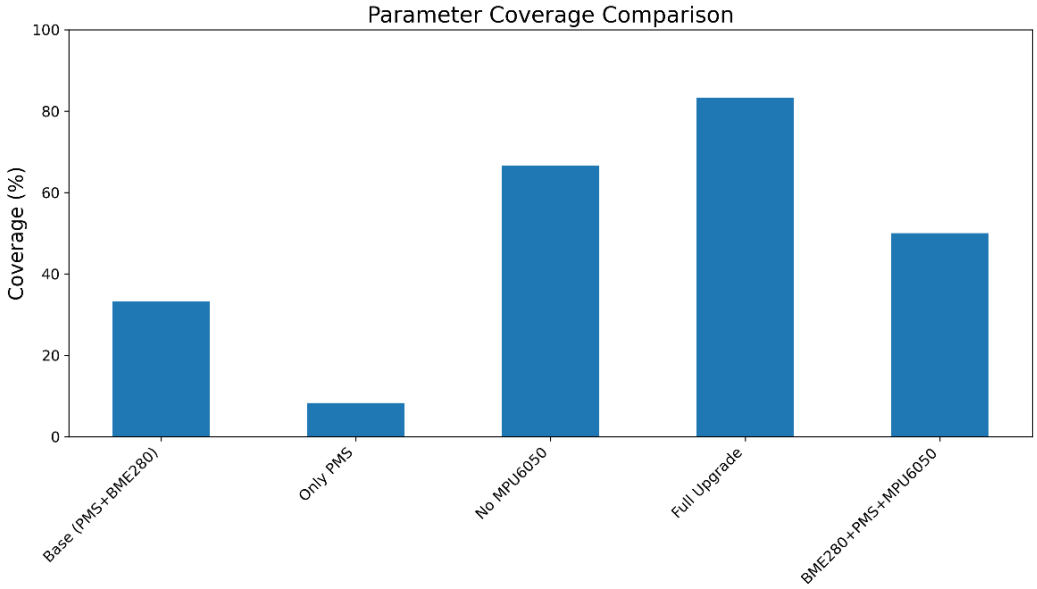


Fig. 1. *Monitoring device parameter coverage (%)*

Figure 2. shown Coverage versus estimated cost per sensor node.

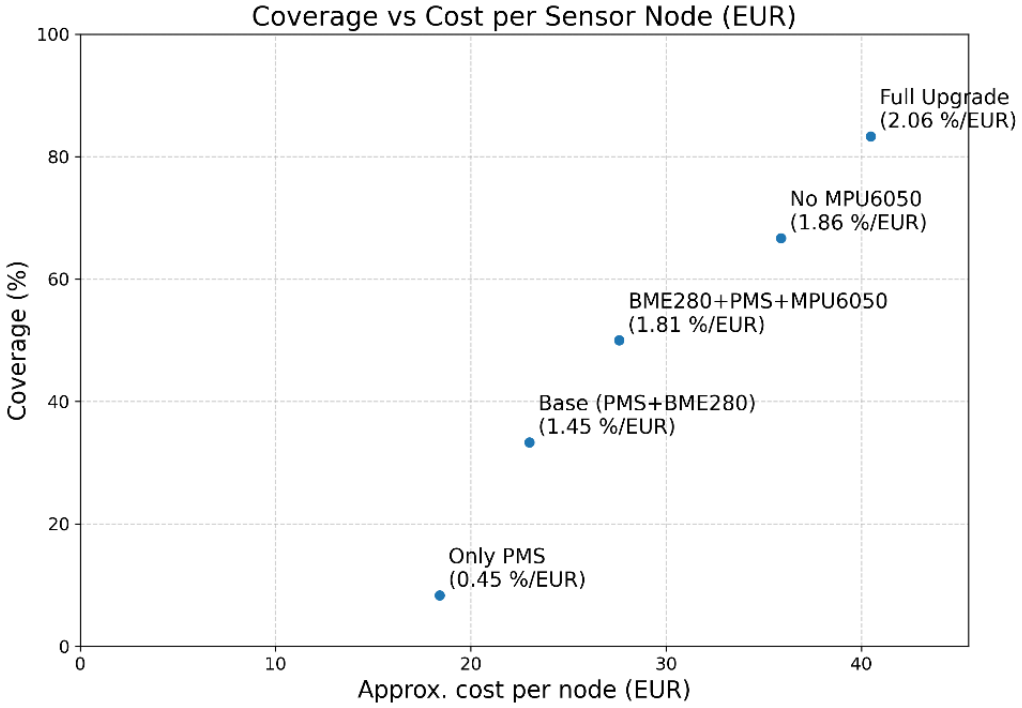


Fig 2. *Coverage versus estimated cost per sensor node*

The coverage analysis shows a progressive increase in monitored functionality as sensors are added. The Base configuration provides a compact solution for environmental and particulate monitoring, while the addition of the MPU6050 introduces basic structural indicators without substantially changing the overall architecture. The expanded configuration provides broader coverage of material degradation and structural variables. According to the source analysis, the expanded configuration with MPU6050 reaches 91.67% coverage, while displacement remains the principal uncovered parameter

COMMUNICATION ARCHITECTURE AND SOFTWARE ENVIRONMENT

Distributed IoT architecture

The proposed monitoring architecture is distributed: each sensor node acquires measurements locally and transfers the data through the building's Wi-Fi infrastructure to an Internet-connected cloud platform. This arrangement avoids the need for a dedicated local server at every historical building and allows centralized access to measurements from multiple institutions. Figure 3 shows Proposed ESP8266-based sensor node and cloud communication architecture (UNS TFMP 2026b).

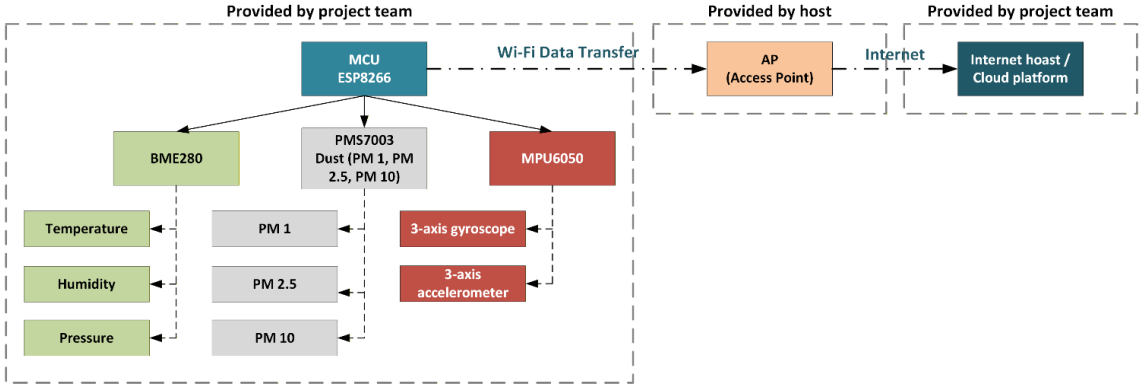


Fig. 3. *Proposed ESP8266-based sensor node and cloud communication architecture*

The architecture links the ESP8266 microcontroller with BME280, PMS7003, and MPU6050 sensing elements. The resulting measurements are transferred through a Wi-Fi access point and then to an Internet host or cloud platform. Wi-Fi as the preferred communication method. Where a building lacks suitable Wi-Fi infrastructure, a 4G/5G mobile Wi-Fi router with a SIM card is proposed.

Cloud interface and data access

The cloud-based architecture addresses the need to collect measurements from buildings located at different institutions. Previous research has already shown the use of public cloud infrastructure for indoor environmental monitoring in historic buildings, while IoT research on cultural heritage supports distributed sensing and remote access to monitoring information. The architecture proposed in the project follows the same general direction but connects it directly with the selected low-cost sensor nodes and the planned multi-building deployment. Local Wi-Fi reduces the amount of additional network hardware where Internet access is already available, while a mobile router can provide a practical alternative in buildings without suitable infrastructure.

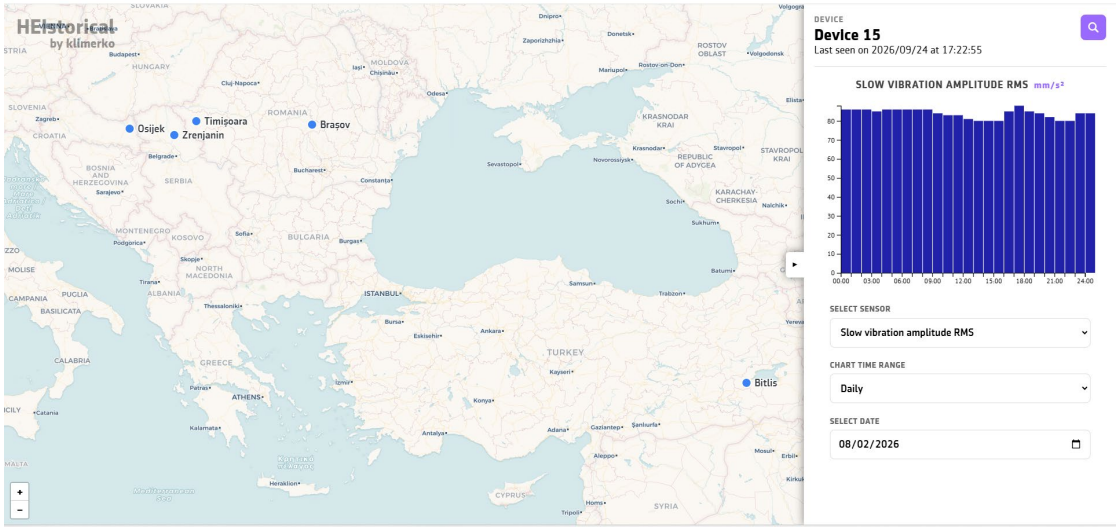


Fig. 4. *Proposed map-based software interface for multi-building monitoring*

DISCUSSION

The proposed approach has several practical implications for heritage institutions and project teams. First, the parameter list provides a structured way to match monitoring needs with the function of each building. Second, the configuration comparison allows hardware decisions to be made according to measurable parameter coverage instead of selecting components only on the basis of unit price. Third, the placement procedure acknowledges that conservation restrictions can determine whether a technically suitable sensor can be used in a particular location. Fourth, the shared cloud platform allows institutions to review data from multiple buildings without installing local servers at every site. The same architecture can also support later analysis of long-term trends when a sufficient amount of historical data has been collected.

The analysis also identifies limitations that should be addressed in later work. The equal weighting of all twelve parameters is useful for comparison but does not reflect differences in risk between building types. For an archive, humidity stability may be more important than light or vibration, while a structure exposed to traffic or seismic activity may require a different weighting system. Future testing should therefore compare parameter weights according to building function and documented risks. The proposed low-cost sensors should also be tested against reference instruments to determine measurement accuracy under real operating conditions. Long-term field deployment is needed to assess Wi-Fi reliability, sensor drift, maintenance needs, power interruptions, and the effect of different mounting methods on vibration and structural measurements. The software layer can later be extended with automated threshold alerts and analytical methods once stable datasets are available.

The combined analysis of monitoring requirements, sensor configurations, placement restrictions, and data architecture provides a coherent basis for an IoT monitoring system intended for historical buildings. The results show that low-cost hardware can cover a substantial part of the environmental and structural parameters identified in the project, but the most suitable configuration depends on the monitored building and the intended use of the data. A configuration with PMS7003, BME280, and MPU6050 provides a practical balance for combined environmental and basic structural monitoring, while broader sensor sets can be reserved for locations where material moisture, light, cracks, or strain must also be recorded.

Non-invasive installation and site-specific positioning remain necessary because the value of the measurements depends on both sensor capability and the location in which the device is installed. Connecting the nodes through local Wi-Fi to a common cloud platform allows measurements from several institutions to be stored and reviewed within one system

The proposed concept can therefore support planned monitoring across different categories of historical buildings while keeping hardware modular, installation reversible, and data access centralized. Field validation across the selected buildings can provide the next basis for refining sensor configurations, placement rules, and data interpretation procedures.

ACKNOWLEDGEMENT
This paper was developed within the Erasmus+ project "Strengthening green and digital capacities in higher education through collaboration in integrating historical buildings into a sustainable and digital future – HEIstorical", Project No. 2025-1-RO01-KA220-HED-000364478, co-funded by the European Union. The authors thank the The National Museum of Zrenjanin, the Secondary Music School "Josif Marinković" Zrenjanin, the Historical Archive of Zrenjanin and the gallery section within the Kaštel Castle in Ečka for hosting the sensors.

REFERENCES

Clementi, F., Formisano, A., Milani, G., & Ubertini, F. (2021). Structural Health Monitoring of Architectural Heritage: From the past to the Future Advances. *International Journal of Architectural Heritage*, *15*(1), 1–4. https://doi.org/10.1080/15583058.2021.1879499

Karoglou, M., Moropoulou, A., Mouzakis, Ch., & Asimakopoulos, S. (2025). Monitoring of a historic building's masonry moisture content. *Journal of Building Engineering*, *104*, 112313. https://doi.org/10.1016/j.jobe.2025.112313

Mecocci, A., & Abrardo, A. (2014). Monitoring Architectural Heritage by Wireless Sensors Networks: San Gimignano — A Case Study. *Sensors*, *14*(1), 770–778. https://doi.org/10.3390/s140100770

Mitro, N., Krommyda, M., & Amditis, A. (2022). Smart Tags: IoT Sensors for Monitoring the Micro-Climate of Cultural Heritage Monuments. *Applied Sciences*, *12*(5), 2315. https://doi.org/10.3390/app12052315

Mobaraki, B., Lozano-Galant, F., Soriano, R., & Castilla Pascual, F. (2021). Application of Low-Cost Sensors for Building Monitoring: A Systematic Literature Review. *Buildings*, *11*(8), 336. https://doi.org/10.3390/buildings11080336

Rossi, M., & Bournas, D. (2023). Structural Health Monitoring and Management of Cultural Heritage Structures: A State-of-the-Art Review. *Applied Sciences*, *13*(11), 6450. https://doi.org/10.3390/app13116450

University of Novi Sad, Technical faculty „Mihajlo Pupin" Zrenjanin. (2026a). Analysis of building interiors to determine the optimal positions for sensors (HEIstorical Project Report, Activity 2.10).

University of Novi Sad, Technical faculty „Mihajlo Pupin" Zrenjanin. (2026b). Specification and selection of sensor solution tailored for installation in historic buildings (hardware and software system specification) (HEIstorical Project Report, Activity 3.1).

DOI:10.5937/IIZS26542D

TRAINING AND FIELD DEPLOYMENT OF LOW-COST IOT SENSORS IN HISTORICAL BUILDINGS

Research paper

Dalibor Dobrilović[1]*, Ivan Palinkaš[2], Ljiljana Radovanović[3]
[1,2,3]University of Novi Sad, Technical faculty „Mihajlo Pupin" Zrenjanin, Serbia

Abstract: Low-cost Internet of Things systems offer a practical option for continuous environmental monitoring with basic vibration sensing in historical buildings, but their successful use depends on device configuration, wireless connectivity, non-invasive installation and staff competence. This paper presents a case study of a two-day Training of Trainers activity followed by field deployment of low-cost monitoring nodes at four historical sites in Vojvodina, Serbia. The training covered the hardware and wireless configuration of the Klimerko KU7V device, which combines particulate-matter, temperature, humidity, pressure and vibration sensing with Wi-Fi data transmission. Participants applied the configuration procedure during field installation and verified each device through the HEIstorical monitoring portal. Eight sensor nodes were installed at the National Museum, Art Colony Ečka, Historical Archive and Secondary Music School "Josif Marinković". The activity demonstrated the practical feasibility of using a short training format to support supervised device configuration and field deployment across different heritage environments. The case also identifies practical issues related to sensor placement, local Wi-Fi access, installation restrictions and on-site verification. The documented procedure provides a basis for replication in similar deployments in historical buildings.
Key words: historical buildings, IoT monitoring, sensor deployment, Training of Trainers, low-cost sensors, cultural heritage

INTRODUCTION

Historical buildings are exposed to environmental changes, material aging, structural movement and human activity that can affect both preservation and safe use. Continuous monitoring can provide information on indoor microclimate and structural response that is not available through occasional visual inspection alone. Structural health monitoring has therefore become an established research area for architectural heritage, with recent work addressing sensor networks, low-cost devices and Internet of Things solutions for long-term data collection Wireless monitoring is particularly relevant where repeated access is difficult or where several buildings must be observed through a common digital platform.

Heritage monitoring differs from conventional building monitoring because installation methods are restricted by conservation requirements. Sensor nodes should be compact, removable and positioned without permanent alteration of original surfaces whenever possible. Previous studies have examined wireless sensor networks in heritage sites and low-cost building-monitoring systems, showing that distributed nodes can support environmental and structural measurements while reducing installation complexity. IoT-based approaches also allow measurements from different locations to be transferred to remote platforms for storage and review.

Technical suitability alone does not determine whether such systems can be deployed consistently. Personnel must understand device configuration, network connection, placement requirements and basic verification procedures. This is relevant in international projects where several institutions may later repeat the same installation procedure in different buildings and countries. A training format that combines short theoretical instruction with immediate field work can provide a common installation procedure and allow technical issues to be identified while the devices are being configured.

This paper presents a case study of a Training of Trainers activity and subsequent field installation of low-cost IoT monitoring nodes in four historical buildings in Vojvodina, Serbia. The activity was conducted within the HEIstorical project and hosted by the University of Novi

[1]Corresponding author, dalibor.dobrilovic@uns.ac.rs, ORCID: 0000-0002-3083-5725
[2]ivan.palinkas@uns.ac.rs , ORCID: 0000-0001-9253-1375
[3]ljiljana.radovanovic@uns.ac.rs , ORCID: 0000-0002-5234-4820

Sad. The analysis focuses on the training procedure, sensor-node configuration, field deployment, Wi-Fi connection and verification of active data transmission. Particular attention is given to the practical transfer from classroom configuration to installation in different heritage environments. The paper also discusses the limits of the activity, including the absence of a formal pre-training and post-training assessment and the dependence of field deployment on site-specific connectivity and mounting conditions (UNS TFMP 2026).

METHODOLOGICAL APPROACH

The study uses a descriptive case-study approach based on the implementation records of Activity 2.11 of the HEIstorical project. The activity combined technical training with supervised field installation. It was organized over two days at the University of Novi Sad, Technical Faculty "Mihajlo Pupin" in Zrenjanin. Three professors from the host institution conducted the Training of Trainers activity. Eight academic staff members from partner institutions in Romania, Croatia and Türkiye participated together with students from the University of Novi Sad. The project record reports 20 participating students. The activity was designed so that the same configuration procedure presented during training was used directly at the selected historical sites.

The monitored device was the Klimerko KU7V, an ESP8266-based node developed for the HEIstorical platform. The device integrates a Plantower PMS7003 sensor for PM1, PM2.5 and PM10, a Bosch BME280 sensor for temperature, relative humidity and atmospheric pressure, and a Gravity LIS2DW12 three-axis accelerometer for vibration measurements. Data are transmitted through a 2.4 GHz Wi-Fi connection to the HEIstorical portal. The portal provides time-series data, geographic device locations and an indication of the most recent data transmission. These functions were used during field verification after installation.

Table 1. *Main components and monitored parameters of the KU7V sensor node*

Component	Function	Recorded parameters
PMS7003	Particulate-matter sensing	PM1, PM2.5, PM10
BME280	Environmental sensing	Temperature, relative humidity, atmospheric pressure
LIS2DW12	Three-axis acceleration sensing	Three-axis acceleration; vibration RMS and peak amplitude derived in software
ESP8266	Processing and wireless communication	2.4 GHz Wi-Fi data transfer

The training content covered device architecture, sensor functions, Wi-Fi provisioning, LED status indicators and portal-based verification. Participants were instructed to activate the device access-point mode, connect to the temporary device network, open the configuration interface at 192.168.4.1, enter the target Wi-Fi credentials and save the settings. Successful connection was then checked through the monitoring portal. The same sequence was used during field deployment. This approach allowed the technical procedure to be observed under actual site conditions rather than only in a classroom environment.

TRAINING AND FIELD DEPLOYMENT

The training was delivered over two days, with approximately three hours of instruction per day. The classroom component introduced the hardware configuration and the relation between individual sensors and heritage-building monitoring. Participants also reviewed common connectivity problems, device status information and the steps required to confirm that a node was actively sending data. The training therefore concentrated on the actions required for installation and routine verification rather than on sensor design or advanced signal processing.

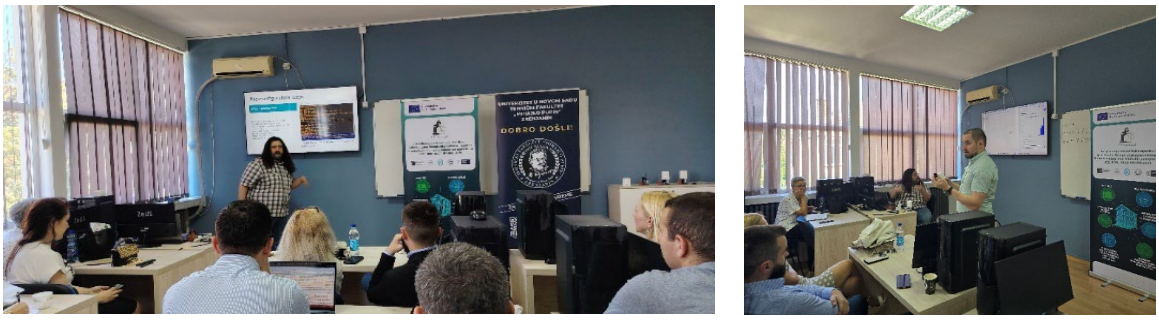


Fig. 1. *Classroom training and device-configuration activities at the Technical Faculty "Mihajlo Pupin"*

After the training component, participants moved to selected sites and repeated the configuration procedure during installation. Eight nodes were deployed at four historical locations. Three sensors were installed in the National Museum, one in the Art Colony in Ečka, two in the Historical Archive and two in the Secondary Music School "Josif Marinković". The distribution reflected the installation plan for the activity rather than an attempt to provide equal coverage at every building.

Table 2. *Field deployment during the Training of Trainers activity*

Day	Historical site	Sensor nodes	Field verification
Day 1	National Museum, Zrenjanin	3	Portal connection checked on site
Day 1	Art Colony, Ečka	1	Portal connection checked on site
Day 2	Historical Archive, Zrenjanin	2	Portal connection checked on site
Day 2	Secondary Music School "Josif Marinković", Zrenjanin	2	Portal connection checked on site

Field installation required adaptation to the physical conditions of each building. The source activity records show deployment in museum, archive, art and educational environments, which differ in room use, furnishings, visitor movement and available network infrastructure. The practical procedure therefore included selecting an installation point, providing electrical power where required, connecting the node to the available Wi-Fi network and checking whether measurements were received by the portal. This sequence is consistent with earlier work showing that wireless monitoring systems in heritage buildings require site-specific decisions even when the hardware platform is standardized.

The four locations also represent different operational settings. Museum spaces contain collections and visitor areas where equipment should remain unobtrusive and should not interfere with movement. Archive spaces contain stored documentary material and usually require stable indoor conditions together with predictable access for staff. The art-colony setting introduces a different combination of collections, working areas and visitor use, while the music school represents an educational environment with regular occupancy and acoustic activity. These differences do not change the basic configuration procedure, but they affect the selection of a suitable point for installation and the later interpretation of measurements.

Non-invasive placement is particularly relevant in protected buildings. The activity records do not describe permanent modification of historic surfaces, and the photographs show compact nodes installed at accessible interior positions. This is consistent with the general requirement that monitoring equipment in heritage settings should be removable and should avoid unnecessary intervention in original materials. Low-cost systems can be useful in this context because individual nodes are small and can be relocated when a position is unsuitable. At the

same time, relocation changes the local measurement environment, so every movement should be documented if long-term datasets are compared.

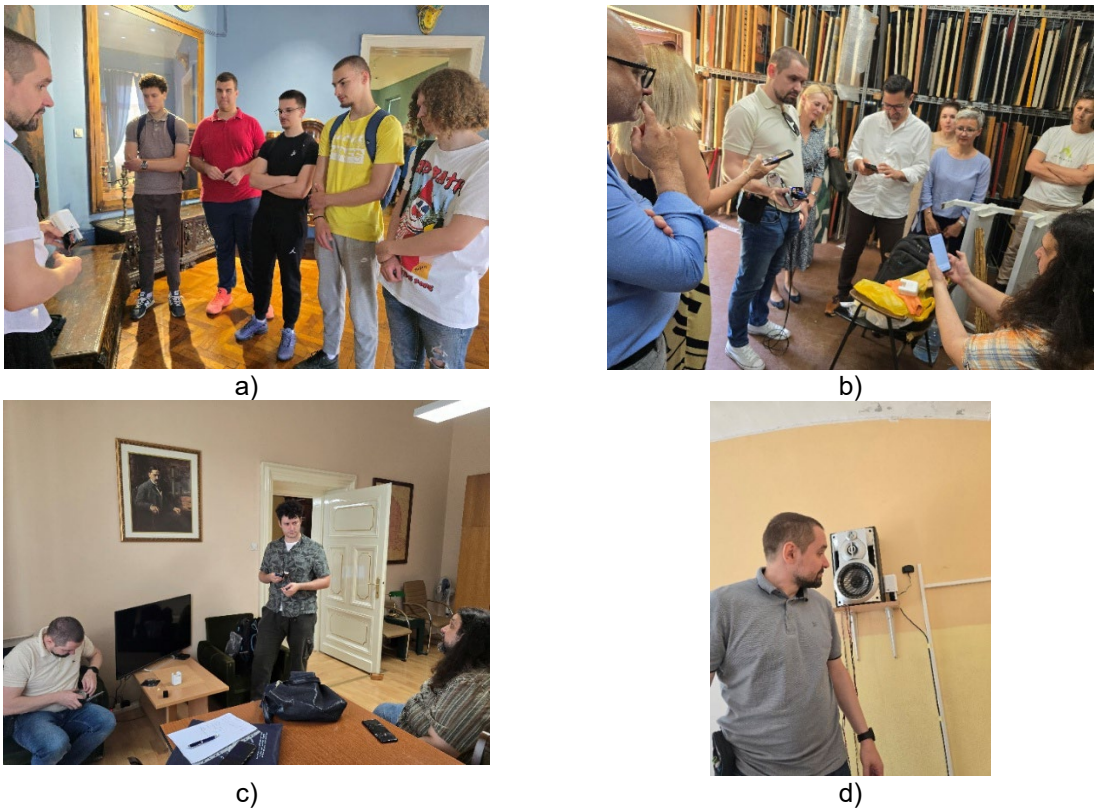


Fig. 2. *Examples of sensor installation at the a) National Museum, b) Art Colony Ečka, c) Historical Archive, d) Secondary Music School "Josif Marinković"*

The installation photographs also show why on-site instruction was useful. Participants had to work around existing furniture, display areas, wall finishes and available power points rather than follow one fixed mounting arrangement. The same hardware can therefore require a different practical solution from one room to another. For training purposes, this variation exposes participants to decisions that are difficult to reproduce in a laboratory setting. It also provides an opportunity to check whether the selected location allows stable power and wireless communication before the installation is treated as complete.

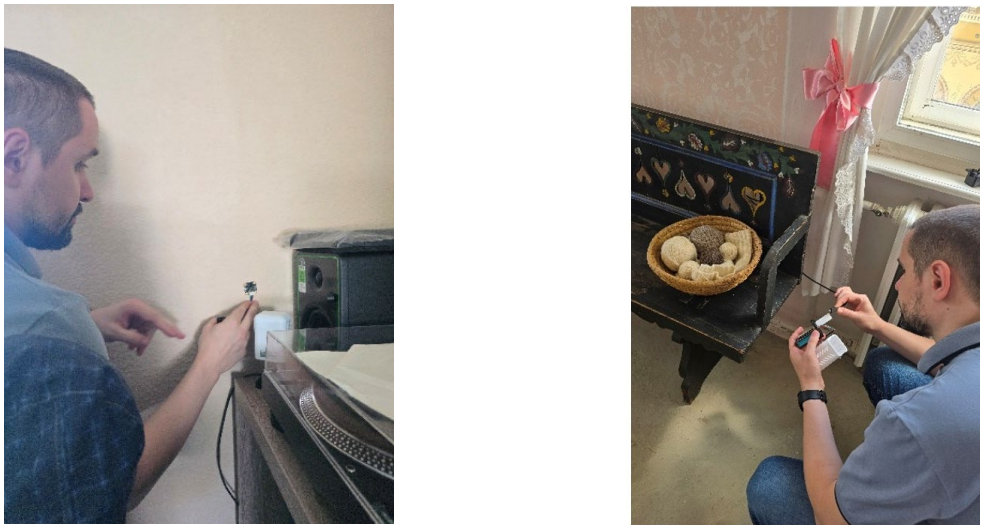


Fig. 3. *Close-up examples of sensor placement and connection at selected historical sites*

All eight installations were followed by portal verification. The device status and the "Last seen" timestamp were checked to confirm that the node had joined the selected Wi-Fi network and was transmitting recent measurements. This step was important because successful local configuration does not necessarily confirm end-to-end data delivery. The verification procedure connected installation work with the cloud-based monitoring interface and gave participants a direct method for identifying configuration or network problems before leaving the site.

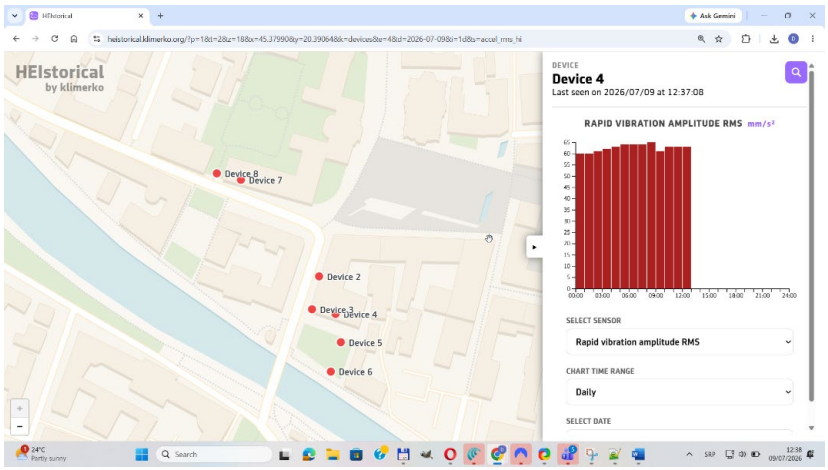


Fig. 4. *HEIstorical monitoring portal used for device-location and data-transmission verification*

RESULTS AND DISCUSSION

The activity resulted in the configuration and field installation of eight monitoring nodes across four historical sites. Each device was connected to the local wireless network and checked through the HEIstorical portal after installation. The completed deployments show that the same basic configuration sequence can be applied across several types of heritage buildings when local network access and suitable installation points are available. The procedure also demonstrates the practical value of combining training and deployment within the same activity because participants move directly from guided configuration to work under actual building conditions.

The selected hardware supports simultaneous environmental and vibration monitoring. The PMS7003 provides particulate-matter measurements, the BME280 provides temperature, relative humidity and pressure, and the LIS2DW12 provides vibration information. This combination does not cover every parameter that may be required for structural vibration monitoring, but it provides a compact set of measurements suitable for distributed low-cost nodes. Research on low-cost building sensors and IoT structural monitoring has similarly reported the usefulness of modular sensor nodes where large numbers of measurement points or limited budgets make specialized systems difficult to deploy.

The field work also identified practical conditions that influence repeatability. Wireless credentials must be available at the installation location, signal quality must be sufficient for stable transmission, and installation points must meet heritage-protection requirements. A configuration that works in a training room may therefore require additional adjustment at a historical site. Remote data access reduces the need for repeated manual collection, but reliable monitoring still depends on local power, network stability and maintenance access. Similar operational issues are reported in IoT and vibration-monitoring research, where communication reliability and sensor placement remain important parts of system design.

Connectivity was a central part of the exercise because each installation depended on access to a local 2.4 GHz Wi-Fi network. The training procedure separated device setup into a temporary access-point stage and a station-mode stage. This sequence gave participants a direct way to distinguish between problems in the local configuration interface and problems related to the destination network. The portal check then added a third verification point because it confirmed communication beyond the local connection. Treating these checks as

separate steps reduces ambiguity during troubleshooting and makes the procedure easier to repeat at another location.

The combination of staff and student participation added another practical dimension. Academic staff from partner institutions were the intended future multipliers of the procedure, while students received direct exposure to IoT configuration and heritage-monitoring applications. The available project records confirm participation and successful supervised installation, but they do not contain individual performance measures. For that reason, the activity can be described as a completed training and deployment exercise rather than as a controlled educational experiment. A later study could use structured observation sheets, task-completion times and error counts to measure learning outcomes more directly.

The portal interface also supports future use of the installed system beyond the training event. Location information and time-series measurements allow users to review whether devices remain active and whether environmental or vibration values change over time. The present paper does not analyze the recorded measurements because the source activity focused on installation and verification. Longitudinal analysis could compare patterns among the four buildings, but such work would require a defined observation period, data-quality screening and information about changes in device position or network availability. Keeping installation documentation together with sensor data would improve later interpretation.

The Training of Trainers format can support later replication because partner staff complete the same procedure they are expected to repeat independently. The project record also reports the issue of digital credentials to participating academic staff and students, providing formal documentation of participation. However, the present case does not contain a pre-training and post-training knowledge test, a structured competency score or long-term follow-up data on independent installations. It is therefore not possible to quantify learning gains from the available records. The successful completion of supervised installations indicates procedural usability, while the effectiveness of knowledge transfer over a longer period requires separate evaluation.

Another limitation concerns the monitoring period. The activity confirms initial connectivity and recent data transmission, but it does not provide a long-term comparison of sensor uptime, calibration drift, network interruptions or differences between the four buildings. Future work can use the deployed nodes to examine data continuity, seasonal environmental variation and vibration patterns over longer periods. A later assessment could also compare installation time, error frequency and independent task completion across partner institutions. Such data would allow the training procedure and the technical deployment model to be assessed separately.

CONCLUSION

This case study documents a two-day training and field-deployment procedure for low-cost IoT monitoring in historical buildings. The activity combined classroom instruction on the Klimerko KU7V node with direct installation at four sites in Vojvodina. Eight nodes were installed and verified through the HEIstorical portal. The same five-step Wi-Fi configuration process was used during training and field work, which provided a consistent procedure for connecting the devices and confirming data transmission.

The case also shows that training material for heritage-monitoring systems should include both configuration steps and site decisions. Participants need to understand how to connect the node, but they also need to recognize when a proposed position creates problems related to access, power, wireless signal or protected surfaces. Immediate verification through the portal provides a simple final check before a team leaves the site.

The experience shows that deployment in heritage buildings depends on more than sensor hardware. Installation points, access to power, Wi-Fi availability, reversible mounting and immediate portal verification must be considered together. The activity provides a practical procedure that partner institutions can adapt for similar deployments. Further evaluation should examine long-term device performance and measure whether participants can repeat the installation independently after the training period.

ACKNOWLEDGEMENT

This paper was developed within the Erasmus+ project "Strengthening green and digital capacities in higher education through collaboration in integrating historical buildings into a sustainable and digital future – HEIstorical", Project No. 2025-1-RO01-KA220-HED-000364478, co-funded by the European Union. The authors thank the The National Museum of Zrenjanin, the Secondary Music School "Josif Marinković" Zrenjanin, the Historical Archive of Zrenjanin and the gallery section within the Kaštel Castle in Ečka for hosting the sensors.

REFERENCES

University of Novi Sad, Technical faculty „Mihajlo Pupin" Zrenjanin. (2026). Installation of sensors in historical buildings in the region Vojvodina and ToT (Training of Trainers) (HEIstorical Project Report, Activity 2.11)

Lecture presentation - Klimerko_KU7V_WiFi_Configuration_Slides_v2.pdf

https://heistorical.klimerko.org/

DOI:10.5937/IIZS26549P

INTEGRATING MODERN TECHNICAL STANDARDS INTO HISTORIC BUILDING EDUCATION: AN ANALYSIS OF COURSES AT SERBIAN UNIVERSITIES

Research paper

Jasmina Pekez[1]*, Bogdana Vujić[2], Borko Bulajić[3]

[1,2]University of Novi Sad, Technical faculty „Mihajlo Pupin" Zrenjanin, Serbia
[3]University of Novi Sad, Faculty of technical sciences, Novi Sad, Serbia

Abstract: This paper analyses nine courses in architecture and risk management at three Serbian universities to examine how contemporary technical standards are taught alongside the conservation of historic structures. Course content, teaching methods and stated learning outcomes were compared across bachelor's, master's and doctoral levels. Undergraduate teaching establishes a strong foundation in architectural history and heritage values, while seismic safety, structural assessment, fire protection and energy efficiency receive limited systematic coverage. Applied methods are developed most fully at doctoral level, with weak transfer to earlier study cycles. The analysis identifies the need for progressively linked curricula, practical interdisciplinary modules, and case studies that integrate technical performance with the cultural integrity of heritage buildings.
Key words: architectural heritage, higher education, modern standards, historic structures, curriculum analysis

INTRODUCTION

Existing higher education courses must address modern engineering, architectural and conservation standards in work on historic structures while safeguarding their cultural, structural and aesthetic integrity. This analysis forms part of WP4 of the HEIstorical project, which aims to strengthen institutional capacity by improving existing courses, developing new learning opportunities and supporting hybrid transnational teaching.
The study identifies curricular content concerning conservation, structural rehabilitation, the history of architecture in Serbia and heritage protection; assesses the coverage of contemporary technical standards; and identifies gaps and overlaps that can guide future courses. It also considers ways to improve cooperation among partner institutions and build capacity over the longer term (UNS TFMP 2026).

MATERIAL AND METHODS

Nine courses from the University of Novi Sad (UNS), the University of Belgrade (UBG) and the University of Priština (UP) were examined: six at bachelor's level, one at master's level and two at doctoral level. The sample includes architecture and risk-management curricula. Publicly available programme pages and course books were used as source documents.
The courses were compared in terms of thematic content, teaching methods and stated learning outcomes. The assessment considered structural safety, seismic resistance, fire protection, energy efficiency, digital tools and risk-based approaches alongside the preservation of architectural, historical and cultural value. Qualitative ratings such as "low" or "high" summarise the reviewed course descriptions; they are comparative interpretations rather than measured performance indicators.

RESULTS AND DISCUSSION

Courses and study levels

Table 1 summarises the nine courses, the extent to which they address modern standards, and their attention to historic integrity. The detailed patterns by study level are discussed below.

[1] Corresponding author, pekezjasmina@gmail.com, ORCID: 0000-0003-0454-5326
[2]bogdana.vujić@tfzr.rs, ORCID: 0000-0001-5249-8021
[3]borkobulajic@yahoo.com ORCID: 0000-0002-9241-1469

***Table 1**. Courses included in the curriculum analysis*

Univ.	Course (level)	Standards / heritage	Course focus
UNS	Architectural Heritage, Renewal and Protection 1 (BSc)	Medium / High	Provides a theoretical foundation in heritage protection, with an emphasis on architectural, cultural, and urban-planning aspects.
UNS	Architectural Heritage, Renewal and Protection 2 (BSc)	Medium–High / High	Combines practical exercises and case studies with an introduction to energy efficiency and structural strengthening.
UP	Protection of Architectural Heritage (BSc)	Medium / Medium–High	Covers the basic principles of heritage conservation and regional approaches.
UP	Urban Renewal (BSc)	– / Medium	Provides a theoretical overview of urban regeneration in historic settings.
UBG	History of architecture in Serbia (BSc)	High / High	Provides a comprehensive theoretical foundation in heritage protection.
UBG	Protection and Revitalization of Architectural Heritage (BSc)	Medium–High / High	Examines the integration of old and new architectural elements and the application of conservation strategies.
UNS	Cultural Heritage in Urban and Regional Development (MSc)	Medium–High / High	Connects theoretical foundations in regional development with the principles of heritage protection.
UNS	Selected Topics in Seismic Risk Assessment (DAS)	High / Medium	Covers practical methods for seismic risk assessment and safety evaluation.
UNS	Seismic Risk Assessment of High-Risk Buildings (DAS)	High / Medium	Provides in-depth technical content on assessing the structural safety of high-risk heritage buildings.

UNS bachelor's courses provide a grounding in architectural history, urban heritage, typology, traditional materials and cultural identity. Their technical standards are largely implicit, and the links to structural safety, seismic resistance and energy efficiency remain limited. The teaching described in the curricula is predominantly theoretical. These courses therefore develop heritage knowledge more strongly than the technical application of contemporary standards.

At UBG, students encounter architectural heritage, conservation and revitalisation, international charters, legal frameworks and case-study learning. Seismic safety, fire protection and energy efficiency are generally treated descriptively rather than through quantitative or performance-based analysis. Coordination with structural engineering and building physics is limited. UP courses emphasise local and regional heritage, historical identity and traditional construction. They offer less exposure to contemporary technical standards, risk assessment and performance-oriented rehabilitation.

The UNS master's curriculum connects heritage theory with applied technical understanding and introduces regulatory considerations and interdisciplinary perspectives. Structural and safety issues, however, are addressed mainly at a conceptual level. Dedicated teaching on seismic strengthening, energy upgrades in protected buildings and fire safety in historic settings is lacking, while GIS and modelling receive limited attention. Heritage protection is present, but it is often considered as context rather than incorporated into technical optimisation.

The analysed UNS doctoral curricula have the most advanced technical and methodological content. They cover seismic hazard and vulnerability, performance-based approaches, probabilistic and analytical modelling, and the structural safety of existing buildings, including heritage structures. Historic buildings are explicitly recognised as requiring tailored assessment. This knowledge remains concentrated at doctoral level, with limited transfer to earlier cycles and weak links to architectural conservation decisions at those stages.

Table 2. *Comparative overview across study levels and institutions*

Study Level	Institution	Heritage Knowledge	Modern Standards Integration	Technical Depth
PhD	UNS	High	Very high	Very high
Master	UNS	Medium–High	Medium	Medium
BSc	UNS	High	Low	Low
BSc	UBG	High	Low–Medium	Low
BSc	UP	Medium–High	Very low	Very low

Across the sample, cultural and architectural heritage is established most clearly in undergraduate teaching, whereas advanced technical methods are developed chiefly at doctoral level. Integration among architecture, engineering and fire protection remains limited. Opportunities for cooperation across institutions and countries, as well as hybrid and blended teaching, are scarce in the curricula reviewed.

Competencies and teaching methods

Existing learning outcomes encompass three groups of competencies. Knowledge-based competencies include the history and theory of architectural heritage, conservation principles and, at doctoral level, risk and vulnerability. Analytical competencies cover heritage assessment, interpretation of previous interventions and advanced seismic-risk methods, including GIS-supported analysis. Practical skills include reasoning from case studies, awareness of professional roles and communication of research or project findings.

Historical and theoretical knowledge enables students to understand how architectural and urban heritage has developed, including its typologies, construction systems, materials and values in Serbia and wider contexts. Conservation teaching covers the principles of protection, valuation methods, legal frameworks, international charters and national regulations. In the doctoral courses, this foundation is supplemented by advanced knowledge of seismic hazard, exposure and vulnerability as they relate to cultural and historical buildings.

In analytical work, students learn to identify cultural, historical, architectural and spatial values and to evaluate precedents and contemporary interventions in protected settings. More advanced courses introduce empirical, analytical and hybrid methods of vulnerability and risk assessment, sometimes supported by GIS. Case-study reasoning draws on examples such as monasteries, historic urban centres, residential buildings and industrial heritage. Other transferable outcomes include understanding the architect's role within professional and legal settings and presenting research findings and project proposals in writing and orally.

The main gaps concern the limited integration of seismic safety, fire protection and energy efficiency at bachelor's and master's levels; insufficient design work that combines conservation with technical upgrades; and weak continuity between study cycles. Students also have limited opportunities to work in teams spanning architecture, engineering and risk management during the earlier stages of study.

Proposed competencies include applying contemporary standards to heritage buildings without diminishing their cultural value, assessing structural and environmental performance, and developing integrated solutions with engineers, conservators and risk specialists. Students should be able to use disaster-risk evidence when selecting conservation or reuse strategies, compare interventions by risk, cost and heritage impact, and apply legal and ethical requirements. Attention to local communities and the translation of research into practical guidance are also needed.

The technical and heritage strands should be developed together. Students should be able to incorporate measures for seismic resistance, fire safety and energy efficiency into a protected building and evaluate structural, environmental and safety performance using current methods. This work calls for cooperation with structural engineers, conservators and risk-management specialists when identifying feasible interventions.

Risk-informed decisions should draw on seismic and other disaster-risk assessments when planning conservation, adaptation or reuse. Students can compare minimal intervention, strengthening and adaptive reuse in terms of risk, cost and effects on heritage values. The professional dimension includes the ethical and regulatory responsibilities involved in work on protected buildings, consideration of community needs, and translation of research into practical guidance, design proposals and policy recommendations.

***Table 3**. Mapping competencies to teaching methods*

Teaching Method	Existing Focus	Proposed Enhancement
Lectures	Historical/theoretical knowledge	Integration of standards and risk-based approaches
Case studies	Descriptive and analytical work	Comparative, performance-based, and risk-based analysis
Fieldwork	Documentation and observation	Risk screening and rapid vulnerability assessment
Project work	Limited or elective use	Mandatory interdisciplinary design projects
IT/GIS tools	Used mainly at the doctoral level	Gradual introduction from the bachelor's level

Curricula can be linked more clearly across bachelor's, master's and doctoral study so that technical skills develop progressively alongside conservation knowledge. Practical modules in structural safety, seismic resistance, energy efficiency and fire protection can be introduced earlier. Comparative case studies, fieldwork, joint design projects and GIS-based exercises would connect disciplinary knowledge with decisions about interventions in historic buildings. Hybrid and transnational formats could support exchange between institutions and expose students to approaches used in different settings.

CONCLUSION

The reviewed courses provide a solid theoretical foundation in architectural history, conservation and restoration, particularly at bachelor's and master's levels. Coverage of seismic resilience, structural safety, energy efficiency and fire protection is less systematic and progressive, with the most comprehensive technical methods concentrated at doctoral level.
Better alignment across study levels and more applied, interdisciplinary teaching would help students use contemporary standards in work on historic structures while preserving their authenticity and cultural value. The identified gaps provide a basis for developing practical modules, cross-institutional case studies and hybrid teaching within the HEIstorical project.

ACKNOWLEDGEMENT

This paper was developed within the Erasmus+ project "Strengthening green and digital capacities in higher education through collaboration in integrating historical buildings into a sustainable and digital future – HEIstorical", Project No. 2025-1-RO01-KA220-HED-000364478, co-funded by the European Union.
The study programs' curricula were analyzed in the paper; for this reason, it was impossible to cite them according to APA style.

REFERENCES

University of Novi Sad, Technical faculty „Mihajlo Pupin" Zrenjanin. (2026). Analysis of existing courses for integrating modern standards without compromising the integrity of historical structures - Serbia (HEIstorical Project Report, Activity 4.3).

University of Belgrade Faculty of Architecture. (2021). Course book for undergraduate academic studies in architecture [PDF]. https://www.arh.bg.ac.rs/wp-content/uploads/2021/06/OASA-Knjiga-predmeta-2021.pdf

University of Belgrade Faculty of Architecture. Undergraduate academic studies in architecture. https://www.arh.bg.ac.rs/programi/osnovne-akademske-studije-arhitektura/

University of Novi Sad Faculty of Technical Sciences. Course book. https://ftn.uns.ac.rs/knjiga-predmeta/

University of Novi Sad Faculty of Technical Sciences. Course book for first-cycle studies [PDF]. https://ftn.uns.ac.rs/wp-content/uploads/2024/04/Knjiga_predmeta_I_stepen.pdf

University of Novi Sad Faculty of Technical Sciences. Course book for second-cycle studies [PDF]. https://ftn.uns.ac.rs/wp-content/uploads/2024/04/Knjiga_predmeta_II_stepen.pdf

University of Novi Sad, Technical faculty „Mihajlo Pupin" Zrenjanin. (2026). Analysis of existing courses for integrating modern standards without compromising the integrity of historical structures - Serbia (HEIstorical Project Report, Activity 4.3).

University of Priština Faculty of Technical Sciences. Architecture: Undergraduate academic studies. https://ftn.pr.ac.rs/studije/oas/a_o/

University of Priština Faculty of Technical Sciences. Architecture course book [PDF]. https://ftn.pr.ac.rs/wp-content/uploads/2022/09/Arhitektura_knjiga_predmeta.pdf

DOI:10.5937/IIZS26554U

INTEGRATED SEISMIC AND ENERGY ASSESSMENT OF HISTORIC BUILDINGS IN TRANSYLVANIA REGION THROUGH NON-INVASIVE MONITORING

Research paper

Ștefania Ursache[1], Diana Nedelcu[2], Christiana Cazacu[3], Dorin Radu[4*]
[1,2,3,4]Transilvania University of Brașov, Faculty of Civil Engineering, Brașov, Romania

Abstract: Historic buildings in Romania are both energy-deficient and seismically vulnerable, yet energy retrofitting and structural strengthening are regulated, funded and designed as separate problems. This paper presents an integrated assessment approach developed within the Erasmus+ project HEIstorical and its first application to four listed buildings in the Brașov area of Transylvania: the Härman fortified church, Saint Martin Church, the Obere Vorstadt Evangelical Church and the Apollonia Cultural Center. The approach combines a review of the Romanian evidence and regulations, a survey of building custodians, dimensional surveys and continuous non-invasive monitoring. Eight low-cost IoT nodes were installed without any intervention on the historic fabric. Each node records temperature, relative humidity, dew point, pressure, particulate matter, vibration and tilt; the two nodes of a building are identical and differ only in position, one at interior occupied level and one at an elevated position such as a tower or upper hall. The review shows that thermal rehabilitation is frequently carried out without structural strengthening, while the heritage exemption in national energy law leaves protected buildings without energy data. Interim survey responses confirm missing seismic assessments and energy data and support integrated planning. The first monitoring records confirm a working data pipeline and identify processing needs, including removal of the static gravity component and characterisation of the accelerometer noise floor. Coupled microclimate and structural records are proposed as the basis for sequencing interventions.
Key words: *historic buildings, seismic vulnerability, energy retrofitting, non-invasive monitoring, IoT sensors, microclimate*

INTRODUCTION

Romania's built heritage is exposed to two distinct seismic sources: intermediate-depth earthquakes in the Vrancea zone, which produce long-duration motion over large parts of the country, and shallow events in the Banat region, which produce short, high-acceleration pulses. An updated probabilistic hazard assessment indicates peak ground accelerations above 0.3 g in the areas influenced by the Vrancea source (Pavel et al., 2016). Historic masonry buildings were designed for gravity loads; churches develop characteristic block-rotation mechanisms around openings, towers and vaults (Mosoarca & Gioncu, 2013), and vaulted elements are sensitive to the vertical component of ground motion (Chieffo et al., 2021).

The same buildings perform poorly in energy terms. Solid masonry walls 0.40–0.75 m thick typically have thermal transmittances of 1.0–1.6 W/(m^{2}K), while single-glazed timber windows and uninsulated attics dominate heat losses (Transilvania University of Brașov [UNITBV], 2026d). Low-impact measures can still deliver substantial savings: for the Câmpulung Town Hall, window upgrading, attic insulation and photovoltaics were estimated to save up to 47.5% of energy without altering the façade (Șerban et al., 2024). Internal wall insulation, which addresses the largest heat-loss surface, carries the highest hygrothermal risk, governed mainly by render absorptivity and wind-driven rain (Zhou et al., 2022), and no universal retrofit solution exists for heritage buildings (Nair et al., 2022).

The regulatory framework separates the two problems. The recast Energy Performance of Buildings Directive allows Member States not to apply minimum requirements to protected buildings (Directive (EU) 2024/1275, 2024). Romanian Law No. 372/2005 exempts protected monuments and places of worship and also removes the obligation to issue an energy performance certificate, so that for much of the protected stock no energy data exist (Law No. 372/2005, 2020).

[1]Corresponding author, dorin.radu@unitbv.ro, ORCID: 0000-0001-5043-2723

The methodology approved by Order No. 3568/2022 defines a non-invasive approach to energy efficiency in buildings with historical value (Order No. 3568/2022, 2022), but it does not address structural safety, which remains under the seismic code and the technical expertise regime (UNITBV, 2026e). EN 16883 recommends a multi-criteria selection of measures, but its use is voluntary (CEN, 2017).
In practice, thermal rehabilitation is often performed without structural strengthening. Added mass without added lateral capacity increases seismic demand, new renders conceal the crack patterns on which visual assessment depends, and the scaffolding and disruption common to both types of work are duplicated (UNITBV, 2026d). Combined seismic–energy retrofitting is technically feasible for existing European buildings (Menna et al., 2021), but for heritage structures the decision requires data that are rarely available. The Romanian literature is concentrated on Banat and Bucharest, Transylvania is under-represented, and very few historic buildings have long-term records combining structural, thermal and microclimatic variables, which are needed for data-driven damage assessment (Mishra, 2021; Soleymani et al., 2023).
This paper addresses that gap. It presents the integrated assessment approach adopted by Transilvania University of Brașov within the Erasmus+ project HEIstorical (HEIstorical, n.d.) and reports its first application: the selection, survey and non-invasive instrumentation of four listed buildings in the Brașov area, together with interim findings from the regulatory analysis and a survey of custodians.

MATERIAL AND METHODS

Integrated assessment framework

The approach treats seismic safety, energy performance and microclimate as a single decision problem and organises the work in four stages (Fig. 1). Diagnosis combines a literature review of the Romanian historic stock, an analysis of heritage and energy regulations, a questionnaire for owners and managers, and dimensional surveys. Monitoring records microclimatic and structural variables simultaneously, with identical nodes placed at two levels in each building. Interpretation derives coupled indicators and normalises structural indicators for environmental effects. The last stage selects and sequences interventions, feeds an open-access database and transfers the method into teaching (UNITBV, 2026a, 2026b). Monitoring continued after an intervention verifies its actual performance.

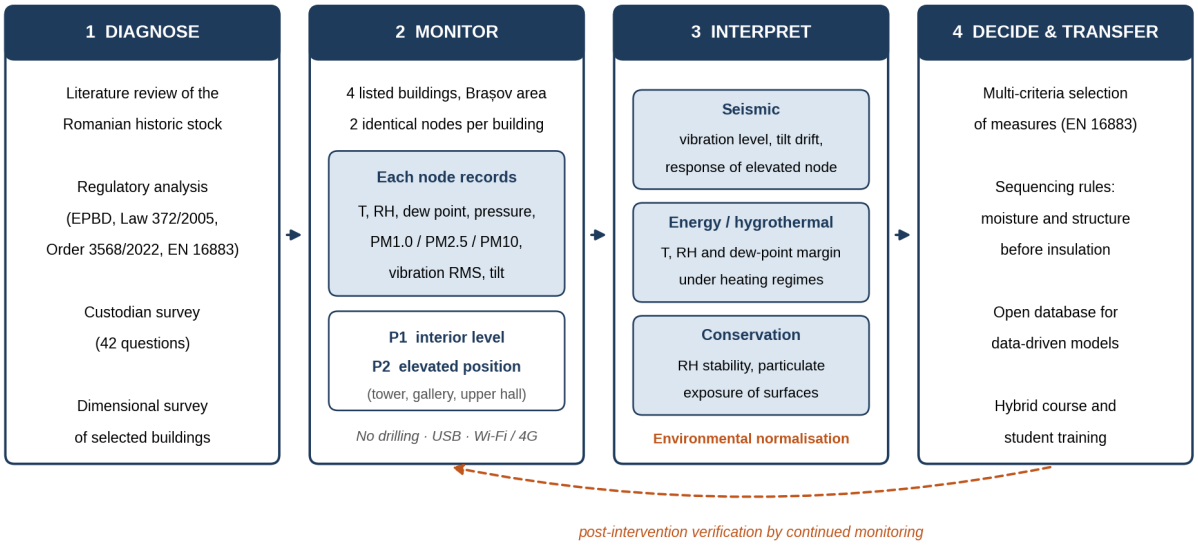


Fig. 1. *Integrated seismic, energy and microclimate assessment framework*

Custodian survey

The questionnaire has 42 questions in eight sections: building identification, structural and seismic status, energy status, interventions carried out, barriers, public support, competing priorities and open feedback. Most items are single-choice questions or 1-to-5 rating scales. It was distributed online in Romanian and English with identical numbering, so that responses can be pooled across partner countries. At the cut-off date of the interim analysis, two valid Romanian responses had been received, together with 38 responses from Türkiye and Serbia (UNITBV, 2026g). Only the Romanian responses are discussed here, as qualitative evidence.

Selection of buildings

Buildings were selected using five criteria: heritage significance, typological diversity, vulnerability to seismic, microclimatic and moisture risks, use pattern, and feasibility of access formalised in a partnership agreement with the owner or manager (UNITBV, 2026f). The four buildings (Table 1) comprise a rural fortified church, a medieval urban hall church, a suburban Lutheran parish church and an early twentieth-century Jugendstil public building. Hărman, with an inner defensive wall about 12 m high and a total wall circumference of about 430 m, is one of the largest Transylvanian Saxon fortified churches. Saint Martin, dated to around 1235 and enlarged in 1792, has a heterogeneous fabric that records nearly eight centuries of damage and repair. Apollonia, built in 1906–1908 as the Burzenland Bank, reopened in 2022 as a cultural venue. The three churches are heated intermittently under a conservation-driven regime, whereas Apollonia is heated for occupant comfort and houses artworks. Students carried out dimensional surveys with laser distance meters to produce measured layouts and to identify sensor positions.

Table 1. *Selected buildings and sensor positions*

Building	Typology and period	Use regime	Node P1 (interior level)	Node P2 (elevated position)
Hărman (Honigberg) fortified church	Basilica (by 1240) within a 15th–17th c. fortified enclosure	Religious, intermittent heating	Nave	Bell-tower base
Saint Martin Church, Brașov	Buttressed hall church, c. 1235, enlarged 1792	Religious, intermittent heating	Nave	Western tower
Obere Vorstadt Evangelical Church, Brașov	Hall church with western tower and apse	Religious, intermittent heating	Nave	Tower / gallery
Apollonia Cultural Center, Brașov	Jugendstil former bank, 1906–1908	Cultural venue, continuous use	Ground-floor exhibition hall	Upper hall

Monitoring system

All nodes use the same configuration, chosen by comparing the coverage of twelve target parameters against cost (UNITBV, 2026c). Each node combines an ESP8266/ESP32 microcontroller with a Bosch BME280 environmental sensor (temperature ±0.5 °C, relative humidity ±3%, pressure 300–1100 hPa), a Plantower PMS7003 laser-scattering particulate sensor (PM1.0, PM2.5 and PM10) and an InvenSense MPU6050 three-axis accelerometer and gyroscope with ranges from ±2 g to ±16 g. The configuration covers about 58% of the twelve parameters; strain, crack width, displacement and moisture in materials are not measured. Nodes are USB-powered and transmit over Wi-Fi or, where no network exists, through a 4G/5G mobile router to a cloud platform with dashboards and CSV export.
Two nodes were installed in each building. Both are identical and record the same parameters; they differ only in position. Node P1 is placed at interior occupied level, in the nave or exhibition hall, where it represents the microclimate acting on sensitive materials. Node P2 is placed at an elevated position, on a tower, gallery or upper hall, where height and exposure make it most

responsive to vibration and to thermal variation. Recording the full parameter set at both levels allows vertical differences in temperature, humidity and vibration within the same building to be compared directly, and provides a second record of each quantity. Installation is strictly non-invasive: nodes are mounted on existing fixtures, on stands or with removable adhesive pads, with no drilling and in positions agreed with the custodians (Fig. 2). The eight nodes were installed in May–June 2026 by twenty students supervised by three staff members, for a minimum recording period of six months (UNITBV, 2026c).



Fig. 2. *Sensor nodes before installation (left) and an installed node with the project information poster (right)*

Derived indicators

Dew point is derived from air temperature T (°C) and relative humidity RH (%) using the Magnus approximation (Alduchov & Eskridge, 1996):

$$\gamma = \ln\left(\frac{\mathrm{RH}}{100}\right) + \frac{aT}{b+T} \tag{1}$$

$$T_\mathrm{d} = \frac{b\gamma}{a-\gamma} \tag{2}$$

where a = 17.625 and b = 243.04 °C. The margin $\Delta T_\mathrm{d} = T - T_\mathrm{d}$ is used to screen for condensation risk. Because the nodes measure air rather than surface temperature, the margin at cold wall surfaces is smaller than the recorded value. Vibration is characterised by the root-mean-square acceleration over a window of N samples:

$$a_\mathrm{RMS} = \sqrt{\frac{1}{N}\sum_{i=1}^{N}(a_i - \bar{a})^2} \tag{3}$$

where a_i is the measured acceleration and $\bar{a}$ is the window mean, which removes the static gravity component and slow tilt drift. Tilt is tracked separately from changes in the mean orientation of the accelerometer axes.

RESULTS AND DISCUSSION

Decoupling of seismic and energy interventions

The review found a mature, case-rich seismic literature on Romanian historic buildings and a thin energy literature, dominated by single case studies and largely disconnected from the structural work (UNITBV, 2026d). Policy pressure and funding, however, are concentrated on energy, and no national instrument requires energy, structural and conservation assessments to be carried out together (UNITBV, 2026e). Table 2 summarises how energy measures interact with seismic and conservation performance, and the indicator through which each interaction can be observed with the deployed system.

Table 2. *Interactions between energy retrofitting, seismic performance and conservation, with monitoring indicators*

Mechanism	Consequence	Monitoring indicator
Added mass (roof covering, floors, renders) without added lateral capacity	Higher seismic demand on an unstrengthened structure	Change in vibration response at both levels before and after works
New render or insulation over cracked masonry	Diagnostic surface concealed; damage progresses unseen	Archived baseline of vibration and tilt drift
Internal insulation and increased airtightness	Reduced drying, interstitial condensation, decay of embedded timber	RH and dew-point margin ΔT_d at both levels
Intermittent full-volume heating of churches	Rapid RH cycling in murals, timber and organs	Hourly rate of change of RH (node P1)
Urban traffic and air pollution	Soiling and chemical weathering of brick and painted surfaces	PM2.5 and PM10 exposure; vibration
Wind and thermal loading on towers	Cumulative cracking at tower base and openings	Vibration and tilt of node P2 versus pressure and temperature

Three sequencing rules follow from these interactions (UNITBV, 2026b, 2026d):

- structural repair of cracks, foundations and rainwater disposal precedes any insulation, because insulation over an active moisture path accelerates and hides decay;
- any measure that adds mass or changes the load path is checked against the seismic model before installation;
- the diagnostic record, including the crack survey, material data and a monitoring baseline, is completed and archived before surfaces are covered.

Custodian perspective

The two interim Romanian responses come from contrasting custodians: the owner-architect of an 80–100-year-old residential building in the protected centre of Brașov, and the administrator of an individually listed rural church more than 150 years old. Neither building has a seismic assessment, neither custodian could report annual energy consumption, and the only energy measure in either building was partial window work, carried out as thermopane replacement in one case and as conservation-led restoration of the original joinery in the other (UNITBV, 2026g). Economic and institutional barriers, such as insufficient grants and slow permitting, were rated highest, and technical consultancy and faster permits were the most requested forms of support. Both respondents favoured authenticity over energy saving and safety over comfort, and both rated integrated planning of seismic and energy works at 4 on a 5-point scale. The owner-architect also reported a shortage of specialists and a tendency toward invasive, concrete-based structural solutions. Two responses cannot be generalised, but they are consistent with the literature and regulatory findings and provide hypotheses for the growing sample.

Deployment and first monitoring records

All eight nodes were installed without drilling or permanent alteration and transmit to the common platform. Fig. 3 shows dashboard outputs for one of the nodes in Brașov. Over the displayed 24-hour period, air temperature remained between about 25 and 26 °C. PM10 concentrations varied between about 6 and 9.5 μg/m^3, rising in the morning and peaking around midday. Particulate exposure is relevant because pollutants and weathering compounds have been identified on medieval bricks of historic buildings in Brașov (Bogdan et al., 2024). The hourly RMS of rapid vibration ranged from about 30 to 37 mm/s^2, without a clear day–night contrast.

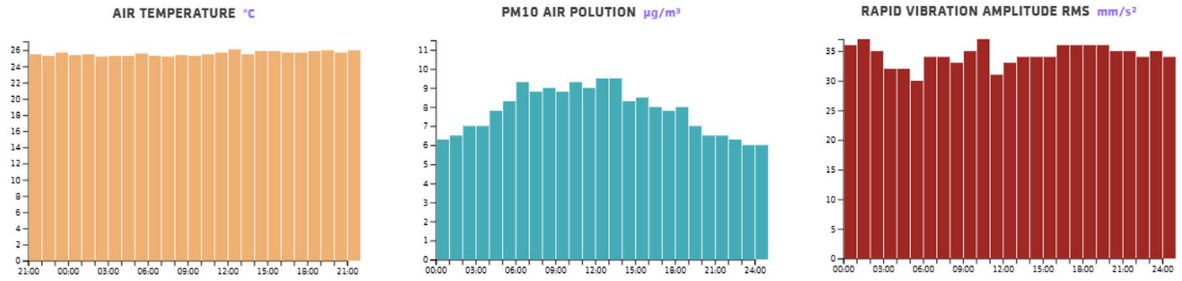


Fig. 3. *First dashboard records: air temperature (last 24 h), PM10 concentration and rapid vibration RMS (28 June 2026)*

Two processing requirements emerge from these records. First, the vibration levels are of the same order as the noise expected from a consumer-grade MEMS accelerometer, whose noise density is specified at 400 µg/√Hz (InvenSense, 2013), integrated over a bandwidth of several tens of hertz. The absence of a day–night pattern supports this reading, so the noise floor must be established, for example with a co-located reference accelerometer, before ambient or traffic-induced vibration is interpreted. Second, the peak-acceleration channel returned values close to 10,000 mm/s^2, approximately the gravitational acceleration, which indicates that the static component is included and must be removed as in Eq. (3).
These first records are illustrative and do not yet support conclusions about building condition. Their value lies in confirming that microclimate and structural response are recorded simultaneously on the same buildings, which is the precondition for environmental normalisation. The dynamic properties of masonry vary with temperature and humidity, and this variation can exceed the effect of genuine damage (UNITBV, 2026d); a structural-only deployment could not separate the two. Because a damaging earthquake is unlikely within six months, the most useful near-term data are environmental: RH stability and dew-point margins under different heating regimes, and the response of towers to wind and temperature. The main limitations are partial parameter coverage, the use of air rather than surface temperature, the short recording period and the small number of buildings. Decisions on internal insulation would additionally require surface temperature and interface humidity sensors at critical details such as timber beam ends. The approach is nevertheless transferable: the hardware is low-cost, installation requires no intervention on protected fabric, and the method has been built into a ten-lecture hybrid transnational course (UNITBV, 2026a).

CONCLUSION

An integrated approach to the seismic and energy assessment of historic buildings was developed and applied to four listed buildings in the Brașov area of Transylvania. The review and regulatory analysis show that, in Romania, the seismic and energy performance of historic buildings are assessed, regulated and funded separately. Thermal rehabilitation without structural strengthening adds mass, hides damage and duplicates costly works, while the heritage exemption in national energy law leaves protected buildings without energy data. Interim custodian responses confirm the lack of basic seismic and energy information and support integrated planning.
A low-cost configuration of two identical nodes per building, each recording microclimate, particulate matter, vibration and tilt, one at interior occupied level and one at an elevated position, was installed in eight positions without any intervention on the historic fabric. The first records confirm a working data pipeline and show that the static gravity component must be removed and the accelerometer noise floor characterised before structural interpretation.
Coupled microclimate and structural records allow structural indicators to be normalised for environmental effects and energy measures to be checked for hygrothermal and conservation risk. Together with the three sequencing rules, they provide a basis for evidence-based intervention decisions.

Two outcomes extend beyond the four buildings. The records feed an open-access database that, combined with the characteristics collected for the regional building stock, supplies the continuous long-term data required for data-driven models, which the literature identifies as the main constraint in this field. The same workflow is transferred to education: the twenty students who installed the nodes carried out the complete non-invasive procedure as field training, and the integrated methodology is taught in a hybrid transnational course, addressing the shortage of specialists reported by the custodians (UNITBV, 2026a).
Future work will analyse the full six-month records, extend the survey sample and compare the Transylvanian buildings with those monitored by the partner institutions.

ACKNOWLEDGEMENT

This paper is part of a research on the project entitled: "*Strengthening green and digital capacities in higher education through collaboration in integrating historical buildings into a sustainable and digital future (HEIstorical)*", No. *2025-1-RO01-KA220-HED-000364478*, supported by *the Erasmus+ Programme of the European Union*. The authors thank the Evangelical Church of the Augsburg Confession (Hărman and Brașov parishes) and the Apollonia Hirscher Cultural Center for hosting the sensors, and the Technical Faculty "Mihajlo Pupin" Zrenjanin, University of Novi Sad, for the specification of the monitoring system.

REFERENCES

Alduchov, O. A., & Eskridge, R. E. (1996). Improved Magnus form approximation of saturation vapor pressure. *Journal of Applied Meteorology, 35*(4), 601–609.

Bogdan, A., Cioban, L. A., Copolovici, D. M., Chambre, D., & Copolovici, L. (2024). Pollutants and weathering compounds on medieval bricks of historic buildings from Brasov (Transylvania, Romania). *Urban Climate, 55*, 101930. https://doi.org/10.1016/j.uclim.2024.101930

CEN. (2017). *Conservation of cultural heritage – Guidelines for improving the energy performance of historic buildings* (EN 16883:2017). European Committee for Standardization.

Chieffo, N., Mosoarca, M., Formisano, A., Lourenço, P. B., & Milani, G. (2021). The effect of ground motion vertical component on the seismic response of historical masonry buildings: The case study of the Banloc Castle in Romania. *Engineering Structures, 249*, 113346. https://doi.org/10.1016/j.engstruct.2021.113346

Directive (EU) 2024/1275 of the European Parliament and of the Council of 24 April 2024 on the energy performance of buildings (recast). (2024). *Official Journal of the European Union*, L 2024/1275. https://eur-lex.europa.eu/eli/dir/2024/1275/oj

HEIstorical. (n.d.). *AI-driven green retrofitting for seismic-safe historic buildings*. Transilvania University of Brașov. Retrieved September 11, 2026, from https://heistorical.unitbv.ro/

InvenSense. (2013). *MPU-6000 and MPU-6050 product specification* (Revision 3.4). InvenSense Inc.

Law No. 372/2005 on the energy performance of buildings, republished. (2020). *Monitorul Oficial al României*, Part I, No. 579.

Menna, C., Del Vecchio, C., Di Ludovico, M., Mauro, G. M., Ascione, F., & Prota, A. (2021). Review of methods for the combined assessment of seismic resilience and energy efficiency towards sustainable retrofitting of existing European buildings. *Sustainable Cities and Society, 72*, 103052. https://doi.org/10.1016/j.scs.2021.103052

Mishra, M. (2021). Machine learning techniques for structural health monitoring of heritage buildings: A state-of-the-art review and case studies. *Journal of Cultural Heritage, 47*, 227–245.

Mosoarca, M., & Gioncu, V. (2013). Failure mechanisms for historical religious buildings in Romanian seismic areas. *Journal of Cultural Heritage, 14*(3, Suppl.), e65–e72.

Nair, G., Verde, L., & Olofsson, T. (2022). A review on technical challenges and possibilities on energy efficient retrofit measures in heritage buildings. *Energies, 15*(20), 7472. https://doi.org/10.3390/en15207472

Order No. 3568/2022 of the Minister of Culture approving the methodology of intervention for the non-invasive approach to energy efficiency in buildings with historical and architectural value. (2022). *Monitorul Oficial al României*, Part I, No. 1260 bis.

Pavel, F., Vacareanu, R., Douglas, J., Radulian, M., Cioflan, C., & Barbat, A. (2016). An updated probabilistic seismic hazard assessment for Romania and comparison with the approach and outcomes of the SHARE project. *Pure and Applied Geophysics, 173*(6), 1881–1905. https://doi.org/10.1007/s00024-015-1223-6

Șerban, S. E., Catalina, T., Popescu, R., & Popescu, L. (2024). The intersection of architectural conservation and energy efficiency: A case study of Romanian heritage buildings. *Applied Sciences, 14*(11), 4835. https://doi.org/10.3390/app14114835

Soleymani, A., Jahangir, H., & Nehdi, M. L. (2023). Damage detection and monitoring in heritage masonry structures: Systematic review. *Construction and Building Materials, 397*, 132402.

Transilvania University of Brașov. (2026a). *Content of a hybrid transnational course on a methodology integrating energy, seismic and microclimatic aspects in the restoration of historical buildings* (HEIstorical Project Report, Activity 4.4).

Transilvania University of Brașov. (2026b). *Existing methods for integrating modern standards without jeopardizing the historical value of the building* (HEIstorical Project Report, Activity 2.4).

Transilvania University of Brașov. (2026c). *Installation of sensors in historical buildings in the Transylvania region* (HEIstorical Project Report, Activity 2.13).

Transilvania University of Brașov. (2026d). *Literature overview and analysis of the condition of historical buildings in Romania regarding energy efficiency and seismic vulnerability* (HEIstorical Project Report, Activity 2.1).

Transilvania University of Brașov. (2026e). *Regulations related to the energy restoration of historical buildings and protected cultural heritage sites in Romania* (HEIstorical Project Report, Activity 2.2).

Transilvania University of Brașov. (2026f). *Selection and detailed measurements of historical buildings monitored in the Transylvania region* (HEIstorical Project Report, Activity 2.5).

Transilvania University of Brașov. (2026g). *Survey of owners and managers on aligning historical buildings with modern standards of energy efficiency and seismic vulnerability in Romania: Interim report* (HEIstorical Project Report, Activity 2.3).

Zhou, X., Derome, D., & Carmeliet, J. (2022). Analysis of moisture risk in internally insulated masonry walls. *Building and Environment, 212*, 108734. https://doi.org/10.1016/j.buildenv.2021.108734

DOI:10.5937/IIZS26562I

STRUCTURAL CHARACTERISTICS OF HISTORICAL MASONRY STRUCTURES IN BITLIS (TURKIYE) AND ITS VICINITY

Research paper

Ercan Işık[1], Fatih Avcil [2]
[1,2]Bitlis Eren University, Faculty of Engineeringand Architecture, Bitlis, Türkiye

Abstract: Bitlis, as one of the oldest settlements in Eastern Anatolia, is located on a strategic corridor along the Silk Road and has been a cradle of many different civilizations for centuries. Numerous historical structures built by various civilizations have survived to the present day and make significant contributions to the region's cultural heritage. During the first round of fieldwork conducted as part of the project, 50 historical masonry structures representing the region's historical fabric such as conical-roofed tombs, mausoleums, mosques, bathhouses, caravanserais, and fortresses were documented in detail and converted into an empirical dataset. Analysis of the obtained data indicates that all the buildings examined were constructed using local natural stone as the primary structural material and a stone masonry load-bearing system. Regarding the distribution of the structures by intended use, religious and monumental buildings predominate, followed by historic buildings serving tourism and commercial functions. Structural assessments revealed that the vast majority (96%) of the buildings examined were maintained in a good general state of preservation; however, all structures exhibited exposure to external rainwater and moisture at the foundation and façade levels. Additionally, microscopic hairline cracks were observed in the masonry walls, while significant structural deformations such as bowing and bulging were identified in 4% of the walls. The study not only presents an inventory of the current condition of the historic masonry building stock in the Bitlis region but also establishes a fundamental basis for future restoration and strengthening interventions by revealing the long-term effects of climatic and environmental factors on masonry structures.
Key words: historic buildings, seismic vulnerability, monitoring, microclimate

INTRODUCTION

Historical monuments are tangible embodiments of collective memory that carry the architectural philosophy, construction techniques, aesthetic values, and socio-cultural characteristics of their respective eras into the present. Safely transmitting this heritage to future generations in high-seismic-risk regions is an imperative necessity not only for societies to maintain the link to their past and ensure cultural continuity, but also to preserve engineering knowledge and local craftsmanship through a sustainable approach. Safeguarding these heritage structures in earthquake-prone areas is only possible by scientifically identifying their structural load-transfer capacities and existing geometric deficiencies. The insights gained from these evaluations serve as a crucial support tool for decision-makers, ultimately providing the highest academic and technical contribution to maximizing life safety while preserving the original fabric of these ancient monuments (ICOMOS, 2003; Işık et al, 2024; Colace et al., 2025; Formisano and Longobardi, 2025; Puppio et al., 2025; Jadallah et al., 2025; Bilgin et al., 2025; Radić et al., 2025; Işık et al., 2021).
Historical and cultural heritage is among the most vital tangible assets that convey the lifestyles, engineering knowledge, and aesthetic concepts of past societies into the present day. Situated strategically along the Silk Road in the Eastern Anatolia Region, the province of Bitlis and its district Ahlat host a rich architectural legacy, owing to their location at the crossroads of Eastern and Western civilizations. Spanning from the Middle Ages to the Ottoman period, this region synthesizes Seljuk, Ilkhanate, Akkoyunlu, and Ottoman architectural schools, housing numerous monumental masonry structures such as domed tombs, mausoleums, mosques, inns (khans), bridges, and castle fortifications. Bitlis is an ancient settlement located on the Silk Road in the Eastern Anatolia Region, serving as a crossroads of civilizations with its strategic location and millennia-old history. This deep-rooted historical legacy comes to life in the historic Bitlis houses, which stand as one of the most unique examples of civil architecture. Expertly crafted from locally quarried Bitlis stone, these

[1]Corresponding author,ercanbitliseren@gmail.com, ORCID: 0000-0001-8057-065X
[2]avcilfatih@gmail.com, ORCID: 0000-0001-6550-550X

structures not only fulfill basic shelter needs but also symbolize a tailored adaptation to the region's climatic conditions and cultural identity. However, safely transferring these heritag structures to the future within an earthquake-prone region necessitates analyzing their existing geometric and mechanical irregularities through scientific methods and retrofitting them while preserving their original authenticity. The location of the study area is shown in Figure 1.

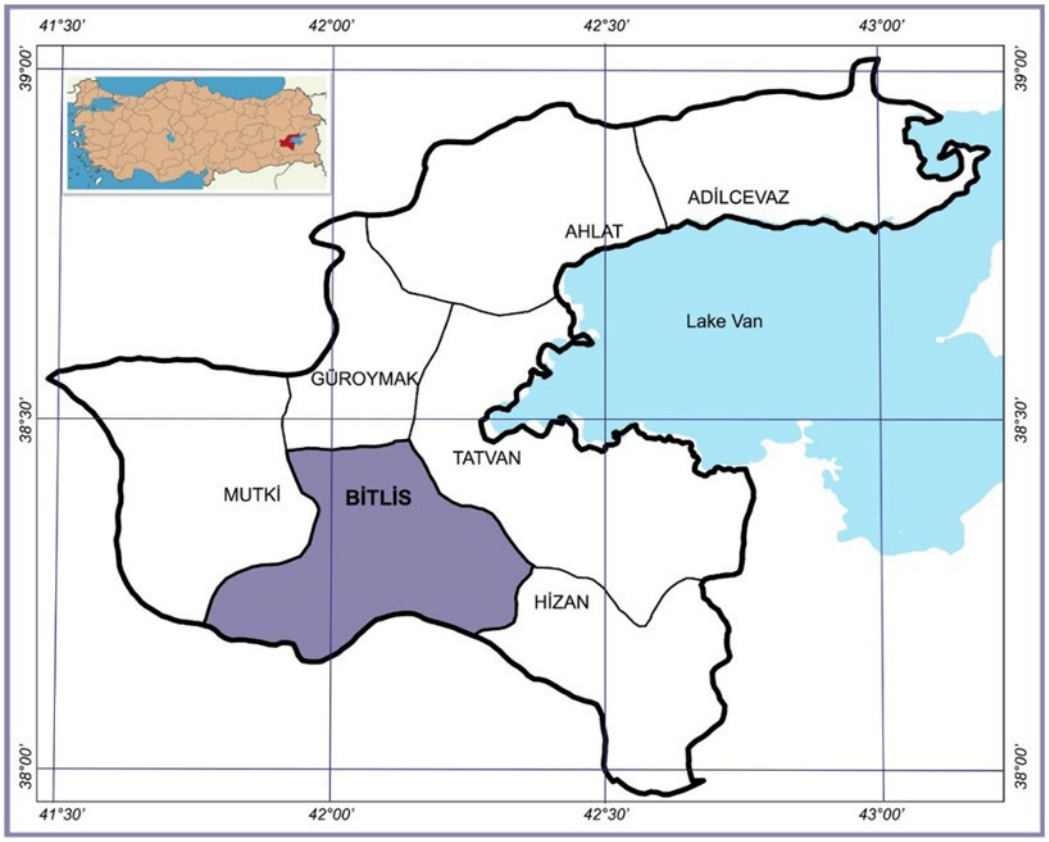


Fig. 1. *Bitlis Province and its location in Türkiye*

The primary components that govern the structural performance, strength, and lifespan of load-bearing systems in historical masonry buildings are the physical and mechanical properties of the materials used, construction techniques, structural geometry, and environmental factors. Historically, local natural stones of volcanic origin specifically Ahlat stone (ignimbrite) along with lime mortar, have served as the principal building materials in the Bitlis region. Characterized by its ease of workability, porous nature, and high thermal insulation value, this stone type has defined the unique architectural identity of the area. However, due to their low tensile strength and limited ductility, masonry structures remain highly vulnerable to external actions such as earthquakes, foundation settlements, thermal fluctuations, and exposure to moisture and water (Arkan et al., 2026; Işık et al., 2016; Işık et al., 2022; Işık et al., 2026; Avcil et al., 2026).

Field investigations and structural inventory surveys constitute the primary and most critical phase of heritage conservation strategies. Within the scope of this project, 50 historical masonry buildings in and around Bitlis were documented in detail, and their structural typologies, construction periods, geometric parameters, conservation states, and existing damage indicators were systematized into a comprehensive dataset. This study aims to analyze the structural characteristics of the historical masonry building stock in the Bitlis region through the lens of material and construction technology, quantitatively evaluate structural degradation mechanisms (micro cracks, shape deformations, moisture/water actions), and establish an empirical database for future restoration efforts, engineering interventions, and preservation strategies.

MATERIAL AND METHODS

Study Area and Data Collection Procedure

The dataset utilized in this study was acquired through field surveys and engineering observations conducted on 50 registered historical masonry structures located in the city center of Bitlis and the Ahlat region. The investigated buildings comprise monumental religious structures (domed tombs, mausoleums, mosques), touristic and cultural sites, as well as commercial and social structures. Images of some of the historical buildings examined are shown in Figure 2.



Fig. 2. *Images of some of the historical buildings*

During the field investigations, a standardized evaluation form was prepared for each building, categorizing the following main parameters:

- Identity and Location Data: Building ID, building name, geographic coordinates, year of construction.
- Geometric and Typological Characteristics: Number of stories, story height (m), location within the block (detached, corner, etc.), primary usage.
- Structural and Material Properties: Structural system type, primary construction material, floor system, roof geometry, and roof covering material.
- Damage and Environmental Exposure Parameters: Overall conservation status (good/poor), plan and vertical irregularities, exposure to rainwater and moisture at the foundation level, presence of external cracks in masonry walls, wall deformations (out-of-plane tilting, bulging), and indoor climate control/occupancy status.

The collected field data were evaluated using statistical and qualitative analysis methods. The historical distribution of the structures, the frequencies of materials and structural typologies,

and the relationships between floor and roof systems and damage parameters were established using percentage distributions and descriptive statistics.

RESULTS AND DISCUSSION

The empirical data obtained from the 50 historical masonry structures examined during the field investigations were analyzed under the categories of historical distribution, geometric and typological characteristics, material and structural conditions, and physical/structural degradation mechanisms.
The construction dates of the 50 analyzed historical structures range between 1100 and 1836, with a mean construction year calculated at approximately 1500 (late 15th century). An examination of the chronological distribution reveals 3 structures dating back to the 12th century, 11 to the 13th-14th centuries (Seljuk and Ilkhanate periods), 20 to the 15th-16th centuries (Akkoyunlu and Early Ottoman periods), and 16 to the 17th–19th centuries (Ottoman period). Regarding their intended functions (functional classification), monumental religious structures (domed tombs/kümbets, mausoleums, mosques) represent 88% (44 buildings) of the total building stock. Of the remaining structures, 10% (5 buildings) comprise touristic and cultural facilities (caravanserais, castles, historical monuments), while 2% (1 building) serves a commercial purpose. This distribution demonstrates that the historical masonry stock in and around Bitlis consists predominantly of monumental religious architecture. The general typological, geometric, and functional characteristics of the 50 analyzed historical masonry structures are summarized in Table 1.

Table 1. *General typological characteristics of the analyzed historical masonry structures*

Parameter	Category	Number of structures	Percentage (%)
Purpose of Use	Religious / Monumental (Religious)	44	88%
	Tourism / Cultural (Tourism)	5	10%
	Commercial	1	2%
Number of Floors	1 Story	27	54%
	2 Stories	23	46%
Roof Type	Gable Roof	29	58%
	Flat Roof	17	34%
	No Roof / Missing (Nothing)	4	8%
Occupancy Status	Uninhabited	28	56%
	Inhabited	22	44%

All analyzed buildings possess a load-bearing masonry system constructed using dressed (ashlar) and rubble natural stone. An evaluation of the geometric parameters yields the following findings:

- **Block Position and Geometry:** All of the structures (100%) are detached, isolated buildings.
- **Number of Stories and Height:** 54% of the buildings (27 units) are single-story, while 46% (23 units) are two-story structures. Total structural heights range from 2.00m to 14.50m, with a mean story/building height of 7.55m.
- **Roofing and Floor Systems:** Masonry vaults and domes were utilized as the load-bearing floor and superstructure systems across all buildings (100%). Regarding roof forms, gable/hipped roofs were observed in 58% of the cases and flat roofs in 34%, whereas the roofing system was found to be completely destroyed in 8% of the structures.

- **Regularity:** All structures feature a symmetric and regular mass geometry both in plan and vertical elevation (regularity in plan and height).

Field evaluations regarding the current state of the structures, moisture/water exposure, and structural damage indicators yielded the following findings:

- **Conservation Status:** Overall maintenance and preservation levels (good maintenance) were found to be satisfactory in 48 of the 50 analyzed structures (96%), whereas only 2 structures (4%) exhibited neglect and severe deterioration (bad maintenance).
- **Water and Moisture Exposure:** All evaluated structures (100%) showed evidence of exterior rainwater and moisture exposure at the foundation and ground levels. The harsh climatic conditions and snow accumulation in the region cause moisture rise within stone surfaces and lead to surface flaking due to freeze-thaw cycles.
- **Cracks and Deformations:** Micro/hairline exterior surface cracks were present on all examined masonry wall surfaces (100%). Conversely, while 96% of the structures (48 buildings) exhibited no out-of-plane tilting, leaning, or bulging in their load-bearing walls, distinct structural wall deformations (leaning/bulging walls) were recorded in 4% of the sample (2 buildings).
- **Interior Space and Occupancy:** Currently, 56% of the structures (28 buildings) are uninhabited, whereas 44% (22 buildings) are occupied. Natural ventilation via window openings was observed in 98% of the interior spaces.

CONCLUSION

This study, conducted on 50 historical masonry structures in and around Bitlis, demonstrates the overall condition of the region's architectural and structural heritage through quantitative data. The main conclusions drawn from the evaluation are summarized below:

- **Material and Structural Integrity:** The entire masonry building stock in the region was constructed using natural stone and vaulted transition systems, with a significant majority (96%) preserving its original structural form to the present day.
- **Environmental Risk Factors:** Rainwater and moisture exposure identified at the foundation level in 100% of the examined buildings constitutes the primary long-term risk factor for these masonry structures. Moisture action coupled with freeze-thaw cycles leads to the deepening of capillary micro cracks and strength degradation in the stone units.
- **Intervention Recommendations:** Effective drainage and waterproofing systems must be established around building foundations to prevent capillary moisture rise. Microcracks on external walls should be injected with lime-based mortars compatible with the original fabric, and pointing repair works should be completed. Immediate structural shoring (propping) and comprehensive restoration projects must be implemented for the 4% segment exhibiting out-of-plane wall deformations such as bulging and leaning.

ACKNOWLEDGEMENT

This paper is part of a research on the project entitled: "Strengthening green and digital capacities in higher education through collaboration in integrating historical buildings into a sustainable and digital future (HEIstorical)", No. 2025-1-RO01-KA220-HED-000364478, supported by the Erasmus+ Programme of the European Union.

REFERENCES

Arkan, E., Avcil, F., Işık, E., Radu, D., & Hadzima-Nyarko, M. (2026) Tarihi Bitlis evlerinin yapısal düzensizlikler açısından değerlendirilmesi ve güçlendirme önerileri. *Harran Üniversitesi Fen Bilimleri Dergisi,* 1(1), 16-29.

Avcil, F., Yılmaz, A., Işık, E., & Büyüksaraç, A. (2026). Material characterization and seismic assessment of the historic Pamukçular Masonry Bridge. *Applied Sciences*, 16(11), 5721.

Bilgin, H., Biglari, M., & Hysenlliu, M. (2025). Seismic fragility of masonry building stock in the Southwestern Balkans. *Bulletin of Earthquake Engineering*, 1-35.

Colace, F., Gaeta, R., Lorusso, A., Pellegrino, M., & Santaniello, D. (2025). New AI challenges for cultural heritage protection: A general overview. *Journal of Cultural Heritage*, 75, 168-193.

Formisano, A., & Longobardi, G. (2025). Seismic assessment and restoration strategies for cultural heritage buildings in the Neapolitan area: the case of Villa Vannucchi. *Heritage,* 8(4), 143.

ICOMOS., (2003), "Principles for the Analysis, Conservation and Structural Restoration of Architectural Heritage", *Victoria Falls: ICOMOS*.

Işık, E., Bilgin, H., Avcil, F., İzol, R., Arkan, E., Büyüksaraç, A., ... & Hysenlliu, M. (2024). Seismic performances of masonry educational buildings during the 2023 Türkiye (Kahramanmaraş) Earthquakes. *GeoHazards,* 5(3), 700-731.

Işık, M., Işık, E., & Haricihian, E. (2021). Application of IOS/Android rapid evaluation of postearthquake damages in masonry buildings. *Gazi Mühendislik Bilimleri Dergisi*, 7(1), 3650.

Işık, E., Öztürk, G., & Velioğlu, E. (2016). Bitlis ilinde bulunan tarihî bir yığma yapının deprem güvenliğinin belirlenmesi. *Bitlis Eren Üniversitesi Fen Bilimleri Dergisi*, 5(1).

Işık, E., Harirchian, E., Arkan, E., Avcil, F., & Günay, M. (2022). Structural analysis of five historical minarets in Bitlis (Turkey). *Buildings,* 12(2), 159.

Işık, E., Arkan, E., Avcil, F., Mişe, O., & Yuzbasi, J. (2026). Seismic behavior and failure assessment of historical masonry minarets in the Bitlis urban conservation area with numerical analysis. *Scientific Reports.*

Jadallah, M., Alghamri, R., & Doğangün, A. (2025). Seismic retrofitting of the historic Şirvani Mosque using fiber-reinforced polymer (FRP): A case study. *Engineering Failure Analysis*, 109898.

Puppio, M. L., Ariu, M., Deligia, M., Doveri, F., Ferrini, M., & Sassu, M. (2025). Evaluation of the seismic capacity of cultural heritage in case of aggregate buildings: the Castle of Rosignano Marittimo. *Bulletin of Earthquake Engineering*, 23(1), 553-578.

Radić, J., Işik, E., & Hadzima-Nyarko, M. (2025). Evaluation of different rapid assessment approaches for seismic risk evaluation of masonry structures. *Civil Engineering Journal*, 11(10).

DOI:10.5937/IIZS26568R

RELIABILITY OF FUNDAMENTAL PERIOD ESTIMATION FOR CONDITION ASSESSMENT AND SEISMIC EVALUATION OF RC STRUCTURES

Research paper

Josip Radić[1*], Antonija Ereš[2], Ivan Bandalo[3], Marijana Hadzima-Nyarko[4]
[1,2,3,4]Josip Juraj Strossmayer University of Osijek,
Faculty of Civil Engineering and Architecture, Osijek, Croatia

Abstract: The fundamental vibration period is a key global dynamic parameter for characterizing the structural response and condition of existing reinforced concrete buildings. Its reliable estimation is particularly important because changes in structural stiffness, damage, nonstructural components, and other building characteristics can significantly affect the dynamic properties of a structure. This study evaluates the reliability of commonly used expressions for estimating the fundamental period of RC buildings, including formulations prescribed by international seismic design codes and empirical models proposed in the literature. A database of experimentally measured fundamental periods of existing RC buildings is used as a reference for evaluating the predictive performance of the selected expressions. The comparison reveals considerable discrepancies between experimentally identified and empirically estimated periods, with simplified formulations frequently resulting in overestimation or underestimation of the actual dynamic response. The results indicate that expressions based primarily on building height may not adequately represent the influence of structural configuration, nonstructural elements, local construction characteristics, and structural condition. These findings highlight the importance of experimentally informed fundamental period estimation for reliable condition assessment and seismic evaluation of existing RC structures and emphasize the need for models that better account for parameters affecting their actual dynamic behavior
Key words: fundamental period, reinforced concrete, condition assessment, seismic evaluation

INTRODUCTION

The dynamic characteristics of a building provide valuable information about its structural behavior and existing condition. Among them, the fundamental vibration period is an important global parameter closely related to structural mass and stiffness. Structural damage and associated stiffness degradation can alter dynamic properties, generally resulting in an increase in the fundamental period. Reliable identification or estimation of this parameter is therefore relevant not only for seismic analysis but also for condition assessment of existing Reinforced Concrete (RC) structures (Ditommaso et al., 2013; Masi & Vona, 2010). In engineering practice, the fundamental period is commonly estimated using simplified empirical expressions prescribed by seismic design codes, such as EN 1998-1 (CEN, 2004), which are primarily based on building height. Although convenient for preliminary analysis, such expressions cannot fully account for characteristics influencing the actual dynamic response of existing structures. In particular, masonry infill walls can significantly increase structural stiffness and reduce vibration periods, while their neglect may lead to considerable errors in period estimation (Sofi et al., 2015; Asteris et al., 2019; Furtado et al., 2021). Experimental and numerical studies have demonstrated considerable differences between measured fundamental periods and predictions obtained from simplified expressions. Building height and number of stories are important parameters, but regional construction characteristics, masonry infill, soil–structure interaction, and structural system can substantially affect the dynamic response. Consequently, expressions relying predominantly on building geometry may not adequately represent the actual dynamic properties of existing RC structures (Lee et al., 2000; Oliveira & Navarro, 2010; Hatzigeorgiou & Kanapitsas, 2013). From the perspective of condition assessment, dynamic properties may also change during the service life of a structure. Experimental and numerical investigations have shown that structural damage and stiffness degradation can increase the fundamental period.

[1]Corresponding author, jradic@gfos.hr, ORCID: 0009-0009-0787-8020
[2]aeres@gfos.hr, ORCID:0009-0009-8799-2375
[3]ibandalo@gfos.hr
[4]mhadzima@gfos.hr, ORCID: 0000-0002-9500-7285

Post-earthquake investigations have similarly identified changes in the dynamic characteristics of damaged RC buildings, demonstrating that the measured period depends not only on the original structural configuration but also on the actual condition of the building (Masi & Vona, 2010; Ditommaso et al., 2013; Asteris et al., 2019). Experimental identification therefore provides an important reference for evaluating simplified estimation methods. More recently, machine-learning and Artificial Neural Network (ANN) approaches have also demonstrated potential for improving period prediction by incorporating parameters commonly omitted from conventional expressions (Elgohary, 2025; Kumar et al., 2025). Despite extensive research, significant discrepancies remain between periods obtained from code expressions, empirical formulations, numerical models, and experimental measurements. This uncertainty is particularly relevant for existing RC buildings, where structural and nonstructural characteristics and the current structural condition may differ from the assumptions underlying simplified expressions. Reliable period estimation is also important for seismic evaluation because the fundamental period directly influences spectral demand and the resulting structural response. Therefore, this study evaluates the reliability of commonly used code-based and empirical expressions by comparing their predictions with experimentally identified periods of existing RC buildings. Particular attention is given to systematic overestimation and underestimation and their implications for condition assessment and seismic evaluation.

FUNDAMENTAL PERIOD AS A PARAMETER FOR CONDITION ASSESSMENT AND SEISMIC EVALUATION

The fundamental vibration period is a key global dynamic property related to the mass and lateral stiffness of a building. Changes in structural stiffness may alter the fundamental period, making its experimental identification useful for assessing the actual dynamic condition of existing RC structures. However, the period is also influenced by structural configuration, nonstructural components, and soil–structure interaction, and its variation cannot be attributed exclusively to structural damage. The fundamental period also plays an important role in seismic evaluation, as it affects the spectral demand used in commonly applied linear-elastic analysis procedures. Consequently, reliable representation of the fundamental period is important for estimating seismic response. When experimental or numerical dynamic properties are unavailable, seismic design codes provide simplified empirical expressions for period estimation. However, their applicability to existing buildings may be limited by differences in structural characteristics and construction practices from those represented in the datasets used for their calibration. According to EN 1998-1 (CEN, 2004), the fundamental period of vibration may be estimated using the following expression:

$$T = C_t \cdot H^{\frac{3}{4}} \tag{1}$$

where H is the total building height in meters and C_t is a coefficient depending on the structural type, taken as 0.085 for steel moment-resisting frames, 0.075 for reinforced concrete moment-resisting frames and steel eccentrically braced frames, and 0.050 for all other structures. For structures incorporating concrete or masonry shear walls, the coefficient C_t can be determined using the corresponding expression:

$$C_t = \frac{0.075}{\sqrt{\sum A_i \cdot \left(0.2 + \left(\frac{l_{w,i}}{H}\right)^2\right)}} \tag{2}$$

where A_i is the effective cross sectional area of the shear wall in the direction considered at the first story (m²), and $l_{w,i}$ is the length of the shear wall at the first story measured parallel to the applied seismic forces, provided that $l_{w,i}/H \leq 0.9$. Although such expressions are practical for engineering applications, they provide a simplified representation of structural dynamic

behavior. Period–height relationships cannot fully account for the actual stiffness, nonstructural components, damage, or other characteristics affecting the response of existing buildings. In contrast, an experimentally identified period more directly reflects the current global dynamic behavior of the structure. Therefore, comparison of empirical estimates with experimentally identified periods is important for assessing their reliability and limitations.

EXPERIMENTAL IDENTIFICATION OF FUNDAMENTAL PERIOD IN EXISTING RC BUILDINGS

A database of experimentally identified fundamental vibration periods was compiled from published studies on existing Reinforced Concrete (RC) buildings to evaluate commonly used empirical period-estimation expressions (Bandalo, 2025). The reviewed studies include controlled and forced vibration testing, ambient vibration measurements, and strong-motion system identification, providing information on the dynamic characteristics of buildings under different excitation levels and structural conditions. Controlled and forced vibration tests have shown that experimentally identified periods may differ considerably from geometry-based estimates and that stiffness degradation associated with damage can result in increased fundamental periods (Sachanski, 1964; Goksu et al., 2017). Ambient vibration testing provides a practical non-destructive approach and has demonstrated the influence of structural configuration, masonry infill, and construction characteristics on measured periods (Güler et al., 2008; Al-Nimry et al., 2014). Strong-motion measurements provide additional information on the dynamic properties of buildings subjected to seismic excitation and have contributed to the development and evaluation of empirical period expressions (Farsi, 1996). Overall, experimental investigations demonstrate that measured periods may differ substantially from standardized predictions due to variations in effective stiffness, structural configuration, nonstructural components, damage, and local construction characteristics. Experimental identification therefore provides an important reference for evaluating the reliability of empirical period-estimation methods and their applicability to condition assessment and seismic evaluation of existing RC structures.

EXPERIMENTAL DATABASE AND RELIABILITY ASSESSMENT OF FUNDAMENTAL PERIOD ESTIMATION

Experimental database of RC buildings

A database comprising 40 existing RC buildings with experimentally identified fundamental vibration periods was compiled from the studies discussed in the previous section, and are shown in Figure 1.

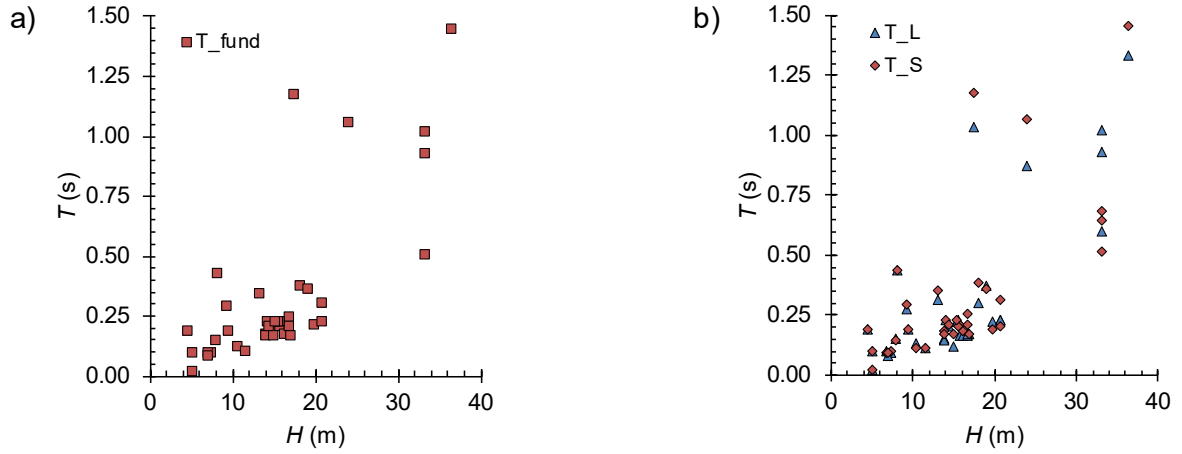


Fig. 1. *Fundamental period as a function of building height: a) fundamental period of the structure; b) directional periods in the longitudinal (T_L) and transverse (T_S) directions*

Most periods were obtained from ambient vibration measurements and include overall, longitudinal, and transverse values for buildings with different geometric and structural characteristics. Building height was selected as the principal comparison parameter, showing a general increase in fundamental period, although considerable scatter indicates the influence of other structural characteristics.

Code-based and empirical period estimation methods

To evaluate the reliability of simplified fundamental period estimation, the experimental database was compared with selected code-based and empirical expressions. Most expressions rely primarily on building height as the main predictor and are summarized in Table 1 and Table 2.

Table 1. *Seismic design code expressions for estimating the fundamental period of RC structures*

Source	Expression	Note
EN 1998-1 (CEN, 2004)	$T = C_t \cdot H^{3/4}$	$C_t = 0.075$
ASCE 7-10 (ASCE, 2010)	$T = C_r \cdot h_n^x$	$C_r = 0.047$, x = 0.9

Table 2. *Considered empirical expressions for estimating the fundamental period of RC structures*

Source	Expression
(Aničić, 2002)	$T = N/10$
(Farsi, 1996)	$T = 0.009 \cdot H^{1.11}$
(Güler et al., 2008)	$T = 0.026 \cdot H^{0.9}$
(Urlich & Carder, 1952)	$T = 0.019 \cdot H$
(Korchynski, 1965)	$T = H/150$

The selected methods represent different levels of simplification and were developed using different structural datasets and assumptions. Consequently, direct comparison with experimentally identified periods provides a basis for assessing their applicability to existing RC buildings. Particular attention is given to systematic tendencies toward overestimation or underestimation and to the variation of prediction accuracy with building height.

RESULTS AND DISCUSSION

Comparison of experimentally identified and estimated periods

The experimentally identified periods were compared with the period–height relationships prescribed by EN 1998-1 and the Croatian National Annex, as shown in Figure 2.

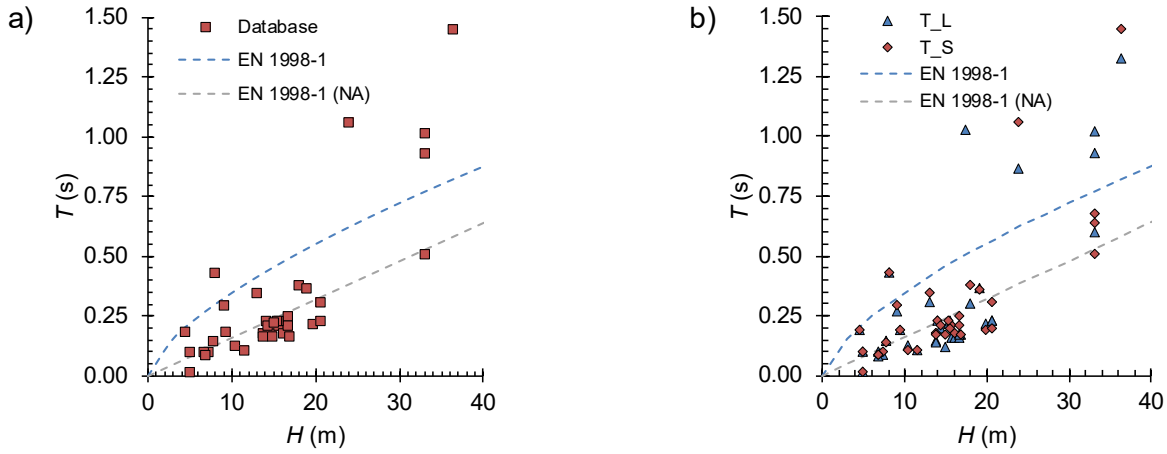


Fig. 2. *Comparison of: a) measured fundamental periods, and b) directional periods with EN 1998-1 and the Croatian National Annex*

A broader comparison was subsequently performed using all selected code-based and empirical expressions. Figure 3 presents the experimentally identified periods as discrete data points, while the estimated period–height relationships are represented by continuous curves. This representation enables direct identification of systematic differences among the selected methods and their tendencies to overestimate or underestimate the measured fundamental periods.

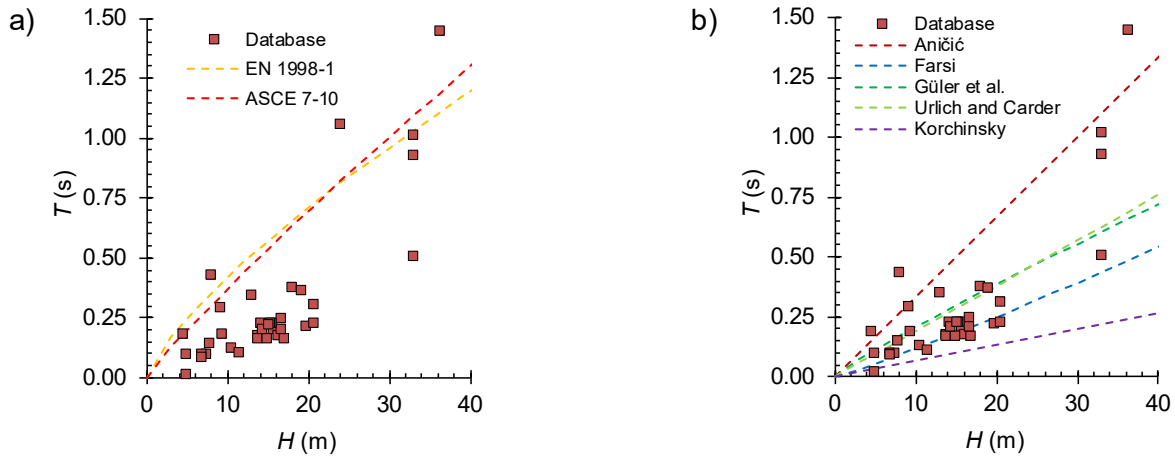


Fig. 3. *Comparison of measured fundamental vibration periods from the database with: a) periods predicted by international seismic design codes, and b) empirical expressions proposed by various researchers*

Reliability assessment and implications for condition assessment

Reliability of the selected estimation methods was evaluated based on their agreement with experimentally identified fundamental periods. For each building and estimation method, the period ratio R_T was calculated as:

$$R_T = \frac{T_{est}}{T_{exp}} \tag{3}$$

where T_{est} is the fundamental period obtained using the considered empirical or code-based expression and T_{exp} is the experimentally identified fundamental period. A value of R_T=1.0 indicates perfect agreement between the estimated and experimental values, whereas R_T<1.0 indicates underestimation and R_T>1.0 indicates overestimation of the experimentally identified period. To characterize the overall tendency of each estimation method, the median value of R_T was determined for the analyzed building database. The median was selected because it is less sensitive to individual extreme values and therefore provides a representative indication of systematic overestimation or underestimation within the heterogeneous experimental dataset. The resulting median R_T values and the number of underestimations and overestimations for each method are summarized in Table 3.

Table 3. *Reliability assessment of fundamental period estimation based on the period ratio R_T*

Source	No. of buildings	Median R_T	No. of buildings with:	
			R_T < 1.0	R_T > 1.0
EN 1998-1 (CEN, 2004)	40	2.48	7	33
ASCE 7-10 (ASCE, 2010)	40	2.33	8	32
(Aničić, 2002)	15	0.96	8	7
(Farsi, 1996)	40	0.80	33	7
(Güler et al., 2008)	40	1.29	14	26
(Urlich & Carder, 1952)	40	1.25	17	23
(Korchynski, 1965)	40	0.44	39	1

The distribution of R_T values for individual buildings is presented in Figure 4, providing a visual comparison of the overestimation and underestimation tendencies of the selected methods.

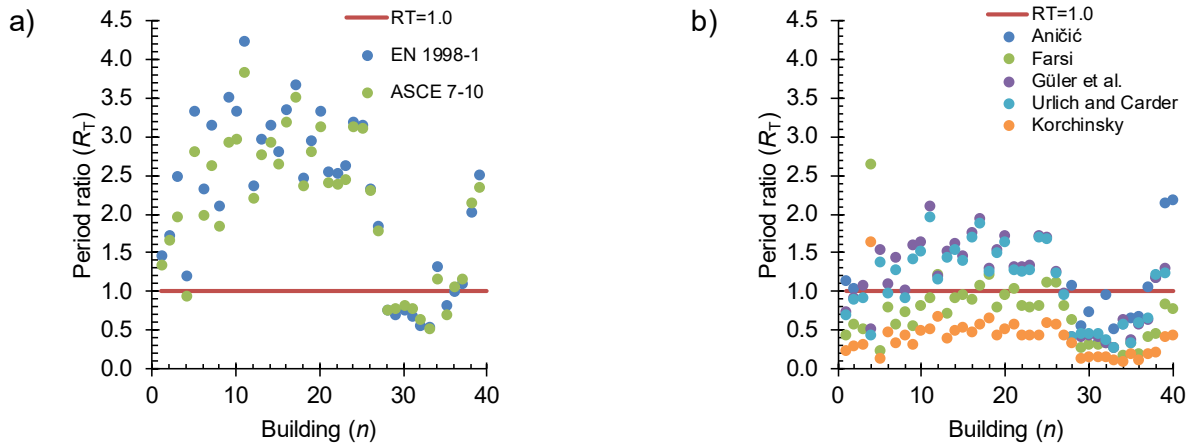


Fig. 4. *Period ratio R_T for individual buildings: a) code-based expressions; b) empirical expressions.*

The calculated R_T values reveal considerable differences among the investigated estimation methods. EN 1998-1 and ASCE 7-10 show a pronounced tendency to overestimate the experimentally identified fundamental periods, with median R_T values of 2.48 and 2.33, respectively. EN 1998-1 overestimates the experimental period in 33 of the 40 analyzed buildings, while ASCE 7-10 does so in 32 cases. In contrast, the Farsi and Korchinsky expressions predominantly underestimate the measured periods, with median R_T values of 0.80 and 0.44, respectively. The Korchinsky expression shows the strongest tendency toward underestimation, with R_T<1.0 for 39 of the 40 buildings. The expressions proposed by Güler et al. and Urlich and Carder exhibit intermediate behavior, with median R_T values of 1.29 and 1.25, respectively. The Aničić expression, evaluated for the 15 buildings for which the required number of stories was available, provides a median R_T of 0.96 and therefore shows the closest overall agreement with unity.

For condition assessment, experimentally identified fundamental periods can provide valuable information on the actual dynamic state of existing RC buildings. Since the fundamental period is closely related to global structural stiffness, its variation over time may indicate changes in structural behavior and can therefore support periodic condition monitoring. However, differences between measured and estimated periods, or changes observed between successive measurements, should not be interpreted independently as direct evidence of structural damage. Such variations may also result from structural configuration, masonry infill, construction characteristics, environmental conditions, or other factors affecting the dynamic response. Experimental identification should therefore be considered a complementary diagnostic tool that, together with visual inspections and other assessment methods, can support the identification of structures requiring more detailed investigation.

From a maintenance perspective, periodic monitoring of dynamic characteristics may provide useful information for tracking changes in structural behavior throughout the service life of a building. Establishing reliable reference values and recognizing significant changes in the fundamental period can support maintenance planning and help prioritize further inspections or interventions. This can contribute to a more condition-based approach to maintenance, in which detailed assessment and intervention are directed toward structures showing relevant changes in their dynamic characteristics. At the same time, reliable fundamental period estimation remains important for seismic evaluation, since differences in period may affect spectral demand and consequently the calculated seismic forces and structural response. The combined use of experimentally identified dynamic properties and appropriate estimation methods can therefore contribute to condition assessment, maintenance decision-making, and more reliable seismic evaluation of existing RC buildings.

CONCLUSION

This study evaluated the reliability of commonly used code-based and empirical expressions for estimating the fundamental vibration period of existing reinforced concrete buildings. A database of 40 buildings with experimentally identified fundamental periods was used as a reference, while the period ratio, R_T was introduced to evaluate the agreement between estimated and measured values. The results revealed considerable differences among the investigated methods. EN 1998-1 and ASCE 7-10 showed a pronounced tendency to overestimate experimentally identified periods, with median R_T values of 2.48 and 2.33, respectively. In contrast, the Farsi and Korchinsky expressions predominantly underestimated the measured periods, with median values of 0.80 and 0.44. The expressions proposed by Güler et al. and Urlich and Carder showed intermediate behavior, while the Aničić expression provided a median R_T of 0.96 for the smaller subset of buildings for which the required number of stories was available. These results demonstrate that the selected estimation method can significantly influence the predicted fundamental period and that simplified expressions cannot consistently reproduce the experimentally observed dynamic behavior of existing RC buildings. Experimentally identified fundamental periods can provide valuable information for condition assessment, as changes in dynamic characteristics may indicate variations in global structural stiffness. However, such changes should not be interpreted independently as evidence of damage, since other structural and environmental factors may also affect the measured response. Periodic monitoring can therefore complement conventional inspections and support condition-based maintenance by identifying structures requiring further assessment.
Reliable fundamental period estimation is also important for seismic evaluation because it directly affects spectral demand and structural response. Overall, experimentally informed dynamic characterization can contribute to more reliable condition assessment, maintenance planning, and seismic evaluation of existing RC structures.

ACKNOWLEDGEMENT

The results presented in this scientific paper have been obtained through the research activities within the projects: 2023-1-HR01-KA220-HED-000165929 "Intelligent Methods for Structures, Elements and Materials" [https://im4stem.eu/en/home/], co-funded by the European Union under the program Erasmus+ KA220-HED—Cooperation partnerships in higher education.
This research was supported by the Croatian Science Foundation (HRZZ) through the projects DOK-NPOO-2023-10-2448 and DOK-2025-02-9828 under the "Young Researchers' Career Development Project – Training of Doctoral Students" programme.

REFERENCES

Al-Nimry, H., Resheidat, M., & Al-Jamal, M. (2014). Ambient vibration testing of low and medium rise infilled RC frame buildings in Jordan. *Soil Dynamics and Earthquake Engineering*, *59*, 21–29. https://doi.org/10.1016/j.soildyn.2014.01.002
Aničić, D. (2002). *Ispitivanje konstrukcija*. Građevinski fakultet Osijek Sveučilišta Josipa Jurja Strossmayera u Osijeku.
ASCE. (2010). *Minimum Design Loads for Buildings and Other Structures*.
Asteris, P. G., Armaghani, D. J., Hatzigeorgiou, G. D., Karayannis, C. G., & Pilakoutas, K. (2019). Predicting the shear strength of reinforced concrete beams using Artificial Neural Networks. *Computers and Concrete*, *24*(5), 469–488. https://doi.org/10.12989/CAC.2019.24.5.469
Bandalo, I. (2025). *Comparative Analysis of Mathematical Formulations for Estimating the Fundamental Period of Reinforced Concrete Structures* [Master's thesis]. Josip Juraj Strossmayer University of Osijek.
CEN. (2004). *EN 1998-1: Eurocode 8: Design of structures for earthquake resistance – Part 1: General rules, seismic actions and rules for buildings*.

Ditommaso, R., Vona, M., Gallipoli, M. R., & Mucciarelli, M. (2013). Evaluation and considerations about fundamental periods of damaged reinforced concrete buildings. *Natural Hazards and Earth System Sciences*, *13*(7), 1903–1912. https://doi.org/10.5194/nhess-13-1903-2013

Elgohary, H. A. (2025). A comprehensive review and ANN analysis of empirical formulae for determining the fundamental period of Multi-Story RC moment resisting frames. *Journal of Umm Al-Qura University for Engineering and Architecture*, *16*(4), 1519–1526. https://doi.org/10.1007/s43995-025-00192-3

Farsi, M. N. (1996). *Identification des structures de Génie Civiles à partir de leurs réponses vibratoires. Vulnérabilité du bâti existant, disertacija i dodatni rad: Dynamic characteristics of common buildings under strong shaking: A statistical study through system identification from CSMIP data*. Université Joseph Fourier – Grenoble I, Grenoble.

Furtado, A., Rodrigues, H., Arêde, A., & Varum, H. (2021). A Review of the Performance of Infilled RC Structures in Recent Earthquakes. *Applied Sciences*, *11*(13), 5889. https://doi.org/10.3390/app11135889

Goksu, C., Inci, P., Demir, U., Yazgan, U., & Ilki, A. (2017). Field testing of substandard RC buildings through forced vibration tests. *Bulletin of Earthquake Engineering*, *15*(8), 3245–3263. https://doi.org/10.1007/s10518-015-9799-x

Güler, K., Yuksel, E., & Kocak, A. (2008). Estimation of the Fundamental Vibration Period of Existing RC Buildings in Turkey Utilizing Ambient Vibration Records. *Journal of Earthquake Engineering*, *12*(sup2), 140–150. https://doi.org/10.1080/13632460802013909

Hatzigeorgiou, G. D., & Kanapitsas, G. (2013). Evaluation of fundamental period of low-rise and mid-rise reinforced concrete buildings. *Earthquake Engineering & Structural Dynamics*, *42*(11), 1599–1616. https://doi.org/10.1002/eqe.2289

Korchynski, I. L. (1965). *Seismic Resistivity of Extended Structures*. Proceedings of the Third World Conference on Earthquake Engineering New Zealand.

Kumar, P., Gogineni, A., Kumar, A., & Modi, P. (2025). A Comparative Analysis of Machine Learning Algorithms for Predicting Fundamental Periods in Reinforced Concrete Frame Buildings. *Iranian Journal of Science and Technology, Transactions of Civil Engineering*, *49*(3), 2257–2276. https://doi.org/10.1007/s40996-024-01560-0

Lee, L.-H., Chang, K.-K., & Chun, Y.-S. (2000). Experimental formula for the fundamental period of RC buildings with shear-wall dominant systems. *The Structural Design of Tall Buildings*, *9*(4), 295–307.

Masi, A., & Vona, M. (2010). Experimental and numerical evaluation of the fundamental period of undamaged and damaged RC framed buildings. *Bulletin of Earthquake Engineering*, *8*(3), 643–656. https://doi.org/10.1007/s10518-009-9136-3

Oliveira, C. S., & Navarro, M. (2010). Fundamental periods of vibration of RC buildings in Portugal from in-situ experimental and numerical techniques. *Bulletin of Earthquake Engineering*, *8*(3), 609–642. https://doi.org/10.1007/s10518-009-9162-1

Sachanski, S. (1964). *Experimental determination of the periods of natural frequencies of buildings and equipment*. *9*, 1–6.

Sofi, M., Hutchinson, G. L., & Duffield, C. (2015). Review of Techniques for Predicting the Fundamental Period of Multi-Storey Buildings: Effects of Nonstructural Components. *International Journal of Structural Stability and Dynamics*, *15*(02), 1450039. https://doi.org/10.1142/S0219455414500394

Urlich, F. P., & Carder, D. S. (1952). *On Vibration of Structures, Properties of Structures nad Materials*. Symposium on the Earthquake and Blast Effects on Structures.